INTEGRATED APPROACHES TO THE RECONSTRUCTION OF EARLY LAND VEGETATION AND ENVIRONMENTS FROM LOWER DEVONIAN STRATA, CENTRAL-SOUTH WALES

VOLUME I OF II

TEXT, FIGURES AND REFERENCES

A THESIS SUBMITTED TO CARDIFF UNIVERSITY FOR THE DEGREE OF DOCTOR OF PHILOSOPHY BY

JENNIFER LOUISE MORRIS MSCI

SCHOOL OF EARTH AND OCEAN SCIENCES

CARDIFF UNIVERSITY

AUGUST 2009

ProQuest LLC
789 East Eisenhower Parkway
P.O. Box 1346
Ann Arbor, MI 48106-1346

DECLARATION

This work has not previously been accepted in substance for any degree and is not concurrently submitted in candidature for any degree.

Signed .....J.Morris..... (candidate) Date ....15/01/10.....

STATEMENT 1

This thesis is being submitted in partial fulfillment of the requirements for the degree of PhD.

Signed .....J.Morris.....(candidate) Date ....15/01/10.....

STATEMENT 2

This thesis is the result of my own independent work/investigation, except where otherwise stated. Other sources are acknowledged by explicit references.

Signed .....J.Morris..... (candidate) Date .....15/01/10.....

STATEMENT 3

I hereby give consent for my thesis, if accepted, to be available for photocopying and for inter-library loan, and for the title and summary to be made available to outside organisations.

Signed ....J.Morris..... (candidate) Date ...15/01/10.....

STATEMENT 4:

I hereby give consent for my thesis, if accepted, to be available for photocopying and for inter-library loans after expiry of a bar on access previously approved by the Graduate Development Committee.

Signed .....J.Morris..... (candidate) Date ...15/01/10.....

ABSTRACT

Integrated approaches to the reconstruction of Lower Devonian vegetation and environments are presented, combining palaeobotanical, palynological and sedimentological evidence from Old Red Sandstone strata of the Anglo-Welsh Basin.

A new lower Lochkovian plant assemblage from central-south Wales is similar in diversity to contemporaneous assemblages along the southern margins of Laurussia. Coalified megafossils of rhyniophytes and rhyniophytoids e.g. *Cooksonia hemisphaerica*, represent basal embryophytes. Geometric morphometric analysis of sporangial morphology revealed a strong taphonomic control on shape. Newly discovered highly-branched mesofossils are synonymous with published charcoalified specimens from lower Přídolí and middle Lochkovian localities, and represent stem-group embryophytes with bryophytic characters. The non-embryophytes, with the largest biomass, include the fungal-like *Prototaxites* and associated mycelia, *Pachytheca*, and evidence for microbial biofilms.

Several new dispersed palynomorph taxa are described, assemblages dominated by cryptospores. With additional published palynomorph and sedimentological data, broad palynofacies are constructed to reveal some information regarding lower Lochkovian habitats.

Using core data from this locality, lower strata are correlated to the Raglan Mudstone Formation, and a two-stage, ephemeral, mud-dominated, dryland river system is envisaged. The appearance of sandier, meandering channel deposits in upper strata are correlated to the St. Maughans Formation, which suggests either a change in fluvial morphology or the switching-on of trunk channels, the causes for which are discussed.

By combining palaeobotanical and sedimentological data, several plant taphofacies are recognised and a taphofacies model envisaged, the most significant taphonomic constraint on palaeoecological studies being the stratinomic partitioning of vegetation prior to burial by fluvial hydraulic sorting. Plant material is restricted to channel elements with low preservational potential, therefore the extent of phytoterrestrialisation and soil productivity may have previously been underestimated. Indirect evidence for significant soil productivity, which may have increased chemical weathering, potentially altering atmospheric ρCO_2 levels, is calculated from the stable carbon isotopic values of pedogenic carbonate nodules.

ACKNOWLEDGEMENTS

I would firstly like to thank my official supervisors, Dianne Edwards and Paul Wright for their guidance, enthusiasm and inspiration through the last few years. Many thanks also goes to John Richardson from the Natural History Museum (London), for experienced guidance in the identification of Lower Devonian sporomorphs and helpful discussions on Anglo-Welsh Basin biostratigraphy and palynofacies.

I would like to thank all technicians at the School of Earth and Ocean Sciences, in particular Lindsey Axe, not only for experienced knowledge in macerations, palaeobotanical techniques, SEM and light microscopy, but also for general support and a friendly ear; Pete Fisher for his technical aid in SEM microscopy and together with Tony Oldroyd, transportation of the core to and from BGS; Lawrence Badham for the preparation of thin sections; and Julia Becker for preparation of the mass spectrometer and processing pedogenic carbonate samples for isotopic analysis. Thanks to Geoff Abbott and Iso-Analytical Ltd for processing fossilised organic matter samples for isotopic analysis.

Thanks to Keith Jones, Tredomen Quarry manager for access and information on quarry history. Thanks to Rhian Hicks for sharing preliminary observations and photographs of some specimens. For discussions on the Old Red Sandstone in the field, thanks go to Sue Marriott, Rob Hillier and Bill Barclay. Thanks to David Marshall from the School of Computer Science, Cardiff University, for discussion on geometric morphometrics and MATLAB. Thanks to Claudia Mora and Tim Kearsey for discussions and sharing frustration of the palaeo-CO_2 barometer equation.

Thanks to members of LEBARG (Kathryn Amos, Carmen Krapf, Rachel Nanson, Marianne Sandstrom) for inviting me to the Channel Country, and together with Steve Hasiotis and Joanna Morris for campsite discussions and sharing the wonders of the outback, making the trip very enjoyable.

Thanks to fellow postgraduates at Cardiff University with whom I have shared many tea breaks and problems, in particular Martin Wolstencroft, Tracy Aze, Heather Birch, Heather Price, Sarah Dare and Catherine Burgess. Thanks to Alan Channing and family, for being a great office mate and friend. Thanks to long standing friends who have supported me particularly Marianne, Sarah, Rick and Suzie. Thanks to Anna and Pete for taking me in and sharing your home and cats. Thanks to Paul Cornish, for supporting and looking after me through stressful times, and reminding me that I am not Superman.

Finally, thanks to Mum and Dad for continual support and interest in everything I do, and encouraging an early interest in geology and palaeontology by allowing me to collect pebbles and shells from the beach and field questions like 'What do stones eat?' This thesis is dedicated to you.

CONTENTS

VOLUME I OF II

TEXT, FIGURES AND REFERENCES

CHAPTERS

Chapter 1: INTRODUCTION

1.1: Introduction p1-1

1.1.1: *Rationale* p1-1

1.1.2: *Aims and objectives* p1-3

1.1.3: *Layout of thesis* p1-5

1.2: Geological background: The Old Red Sandstone Continent p1-6

1.2.1: *Palaeozoic palaeogeography and formation of the ORS continent* p1-6

1.2.2: *Formation of the Anglo-Welsh Basin* p1-8

1.2.3: *Stratigraphy and Anglo-Welsh Basin strata* p1-11

1.2.4: *Provenance and topography* p1-22

1.2.5: *Late Silurian to Early Devonian climate* p1-24

1.2.6: *Flora and fauna of the Old Red Sandstone Continent* p1-25

Chapter 2: METHODS AND LOCALITIES

2.1: Methods p2-1

2.1.1: *Palynological techniques* p2-1

2.1.2: *Palaeobotanical techniques* p2-4

2.1.3: *Sedimentological techniques* p2-5

2.2: Localities p2-7

2.2.1: *Tredomen Quarry* p2-7

2.2.2: *Targrove Quarry* p2-9

Chapter 3: RECONSTRUCTING VEGETATION FROM OLD RED SANDSTONE STRATA

3.1: Introduction p3-1

3.2: Systematic descriptions p3-3

3.2.1: *Early embryophyte megafossils* p3-3

3.2.2: *Early embryophyte mesofossils* p3-30

3.2.3: *Non-embryophytes and non-vegetative fossils* p3-46

3.3: Chapter discussion and summary.....p3-52

Chapter 4: GEOMETRIC MORPHOMETRICS OF EARLY EMBRYOPHYTES

4.1: Introduction.....p4-1

4.2: Methods.....p4-3

4.3: Results.....p4-8

4.3.1: *All megafossils*.....p4-8

4.3.2: *Megafossil intra-species variation*.....p4-12

4.3.3: *Three-dimensional principal components plots*.....p4-30

4.4: Chapter summary and assessment.....p4-43

Chapter 5: THE DISPERSED SPORE RECORD

5.1: Introduction.....p5-1

5.2: Tredomen Quarry spore assemblages.....p5-3

5.3: Systematic descriptions.....p5-12

5.3.1: *Cryptospores*.....p5-12

5.3.2: *Triletes*.....p5-45

5.4: Assemblage characteristics and age of Tredomen Quarry strata.....p5-60

5.4.1: *Assemblage characteristics*.....p5-60

5.4.2: *Age of Tredomen Quarry strata*.....p5-71

5.4.3: *Comparisons with other Late Silurian - Early Devonian assemblages*.....p5-71

5.5: Palaeoecological tool: comparisons with published *in situ* spores.....p5-74

5.6: Palynofacies.....p5-78

5.7: Chapter summary.....p5-85

Chapter 6: LOWER DEVONIAN OLD RED SANDSTONE DEPOSITIONAL ENVIRONMENTS

6.1: Introduction.....p6-1

6.2: Lithofacies descriptions of Tredomen Quarry strata and core.....p6-1

6.2.1: *Intraformational conglomerates*.....p6-18

6.2.2: *Sandstones*.....p6-19

6.2.3: *Siltstones*.....p6-21

6.2.4: *Heterolithics*.....p6-22

6.2.5: *Mudstones*.....p6-23

6.3: Lithofacies descriptions of Targrove Quarry strata..... p6-26
6.3.1: *Intraformational conglomerates*..... p6-28
6.3.2: *Medium-grained sandstones*..... p6-32
6.3.3: *Very-fine-grained sandstones and siltstones*..... p6-33
6.3.4: *Mudstones*..... p6-34
6.4: Lithofacies interpretations..... p6-35
6.4.1: *Intraformational conglomerates*..... p6-35
6.4.2: *Sandstones*..... p6-38
6.4.3: *Siltstones*..... p6-39
6.4.4: *Heterolithics*..... p6-41
6.4.5: *Mudstones*..... p6-42
6.5: Markov Chain Analysis of Tredomen Quarry strata..... p6-45
6.6: Geomorphic models..... p6-50
6.6.1: *Geomorphic model 1: Two-stage, ephemeral mud-dominated dryland river system*..... p6-50
6.6.2: *Geomorphic model 2: Two-stage, sand-dominated meandering river system*..... p6-53
6.6.3: *Geomorphic model 3: Interfluvial drainage and trunk channel model*.... p6-55
6.7: Regional comparisons..... p6-58
6.8: Chapter summary..... p6-60

Chapter 7: TAPHOFACIES AND TAPHONOMIC CONSTRAINTS ON PALAEOECOLOGICAL INTERPRETATIONS

7.1: Introduction..... p7-1
7.2: Taphofacies..... p7-2
7.2.1: *Taphofacies descriptions*..... p7-2
7.2.2: *Taphofacies interpretations*..... p7-9
7.2.3: *Taphofacies model*..... p7-17
7.3: Taphonomic constraints on understanding palaeoecology..... p7-20
7.4: Chapter summary..... p7-21

Chapter 8: ESTIMATING THE ATMOSPHERIC ρCO_2 LEVEL DURING THE EARLY DEVONIAN USING STABLE ISOTOPIC ANALYSIS

8.1: Introduction p8-1

8.2: Using stable carbon isotopes from pedogenic carbonate to estimate palaeo-ρCO_2 levels p8-4

8.2.1: *Carbon dioxide in soils* p8-5

8.2.2: *Stable carbon isotopes of soil* CO_2 ..... p8-7

8.2.3: *Soil carbonate* ρCO_2 *barometer equation* p8-8

8.3: Results p8-16

8.3.1: *Selection of carbonate nodules* p8-16

8.3.2: *Organic matter used for stable isotope analysis* p8-19

8.3.3: *Stable carbon and oxygen isotopic composition of pedogenic carbonate and organic matter* p8-19

8.4: Inferred ρCO_2 levels for the earliest Devonian p8-22

8.5: Chapter summary p8-29

Chapter 9: RECONSTRUCTING LOWER DEVONIAN VEGETATION AND HABITATS FROM OLD RED SANDSTONE STRATA FROM THE ANGLO-WELSH BASIN

9.1: Early land plant habitats and possible causes for a change at the Downtonian (Přídolí) - Dittonian (Lochkovian) boundary p9-2

9.2: Evidence of broad basin-wide habitats using palynofacies p9-7

9.3: Taphonomic constraints on palaeoecological studies of Lower Devonian vegetation p9-8

9.4: Seasonal controls on Lower Devonian vegetative growth p9-12

9.5: Soil productivity and climate feedback as a result of Lower Devonian phytoterrestrialisation p9-13

CONCLUSIONS pC-1

REFERENCES pR-1

FIGURES

Chapter 1: INTRODUCTION

Figure 1.1: *a*: Palaeogeographic reconstruction for the Early Ordovician (modified after Ron Blakey)..... p1-7

Figure 1.1: *b*: Palaeogeographic reconstruction for the Early Devonian (modified after Ron Blakey)..... p1-7

Figure 1.2: Silurian and Lower Devonian outcrops of the Anglo-Welsh Basin (modified after Edwards and Richardson 2004 and Woodcock and Gibbons 1988) p1-10

Figure 1.3: *a*: Palaeogeography of the Anglo-Welsh Basin during the lower Downtonian (modified after Barclay et al. 2005)..... p1-23

Figure 1.3: *b*: Palaeogeography of the Anglo-Welsh Basin during the upper Downtonian, (modified after Barclay et al. 2005).....p1-23

Figure 1.3: *c*: Palaeogeography of the Anglo-Welsh Basin during the Dittonian (modified after Barclay et al. 2005).....p1-23

Chapter 2: METHODS AND LOCALITIES

Figure 2.1: *a*: Regional geological map around Tredomen Quarry (BGS sheet 214, Talgarth, scale 1:50000)..... p2-8

Figure 2.1: *b*: Geological map of Tredomen Quarry..... p2-8

Figure 2.2: *a*: Regional geological map around Targrove Quarry (BGS sheet 181, Ludlow, scale 1:50000)..... p2-10

Figure 2.2: *b*: Sketch of the main lithological units at Targrove Quarry.....p2-10

Chapter 3: RECONSTRUCTING VEGETATION FROM OLD RED SANDSTONE STRATA

Figure 3.1: Terminology and measurements taken for the analysis of megafossils and mesofossils from Tredomen Quarry..... p3-2

Figure 3.2: Outlines of cf. *Cooksonia caledonica* specimens from Tredomen Quarry..... p3-4

Figure 3.3: Outlines of *Cooksonia hemisphaerica* specimens from Tredomen Quarry..... p3-8

Figure 3.4: Outlines of *Cooksonia* cf. *cambrensis* specimens from Tredomen Quarry.....p3-14

Figure 3.5: Outlines of cf. *Uskiella reticulata / Tarrentia salopensis* specimens from Tredomen Quarry p3-17
Figure 3.6: Outlines of *Salopella allenii* specimens from Tredomen Quarry..... p3-20
Figure 3.7: Outlines of *Salopella* cf. *marcensis* specimens from Tredomen Quarry.....p3-25
Figure 3.8: Outlines of elongate club-shaped specimens from Tredomen Quarry...p3-28
Figure 3.9: *a*: Comparisons between the size and branching patterns of the mesofossils and megafossils from Tredomen Quarry.....p3-32
Figure 3.9: *b*: Typical examples of the six main types of mesofossil.....p3-32
Figure 3.10: Outlines of mesofossil type A specimens from Tredomen Quarry.....p3-34
Figure 3.11: Reconstruction of mesofossil type A p3-35
Figure 3.12: Outlines of mesofossil type B specimens from Tredomen Quarry.....p3-37
Figure 3.13: Outlines of mesofossil type C specimens from Tredomen Quarry.....p3-39
Figure 3.14: Outlines of mesofossil type D specimens from Tredomen Quarry.....p3-42
Figure 3.15: Outlines of *Tortilicaulis* cf. *offaeus* specimens from Tredomen Quarry p3-44
Figure 3.16: Outlines of other mesofossils with elongate sporangia from Tredomen Quarry..... p3-47
Figure 3.17: Comparison between a) Tredomen Quarry and b) Targrove Quarry palaeobotanical collections..... p3-61
Figure 3.18:a: Distribution of megafossil assemblages during the Ludlow to Přídolí.p3-63
Figure 3.18:b: Distribution of megafossil assemblages during the Lochkovian.....p3-63

Chapter 4: GEOMETRIC MORPHOMETRICS OF EARLY EMBRYOPHYTES

Figure 4.1: AAMToolbox methods:
a: Template Creator.....p4-4
b: Template Editor Tool..... p4-4
c: Point Model Editor..... p4-4
Figure 4.2: AAMToolbox methods:
a: Statistical Model Generator Tool..... p4-6
b: PCA walks..... p4-6
Figure 4.3: AAMToolbox methods: Point Model Plots in Shape Space Viewer..... p4-7
Figure 4.4: Sporangial shape variation of all specimens from an allometric model.....p4-9

Figure 4.5: Sporangial shape variation of all specimens from a non-allometric model.....p4-11
Figure 4.6: Point model templates used for each species model.....p4-13
Figure 4.7: *a*: Sporangial shape variation for cf. *Cooksonia caledonica* / *Renalia* sp. from an allometric model.....p4-15
Figure 4.7: *b*: Sporangial shape variation for cf. *Cooksonia caledonica* / *Renalia* sp. from a non-allometric model.....p4-15
Figure 4.8: *a*: Sporangial shape variation for *Cooksonia* cf. *cambrensis* from an allometric model.....p4-19
Figure 4.8: *b*: Sporangial shape variation for *Cooksonia* cf. *cambrensis* from a non-allometric model.....p4-19
Figure 4.9: *a*: Sporangial shape variation for *Cooksonia hemisphaerica* from an allometric model.....p4-21
Figure 4.9: *b*: Sporangial shape variation for *Cooksonia hemisphaerica* from a non-allometric model.....p4-21
Figure 4.10: *a*: Sporangial shape variation for cf. *Uskiella reticulata* / *Tarrantia salopensis* from an allometric model.....p4-23
Figure 4.10: *b*: Sporangial shape variation for cf. *Uskiella reticulata* / *Tarrantia salopensis* from a non-allometric model.....p4-23
Figure 4.11: *a*: Sporangial shape variation for elongate club-shaped sporangia from an allometric model.....p4-25
Figure 4.11: *b*: Sporangial shape variation for elongate club-shaped sporangia from a non-allometric model.....p4-25
Figure 4.12: *a*: Sporangial shape variation for *Salopella allenii* from an allometric model.....p4-27
Figure 4.12: *b*: Sporangial shape variation for *Salopella allenii* from a non-allometric model.....p4-27
Figure 4.13: *a*: Sporangial shape variation for *Salopella* cf. *marcensis* from an allometric model.....p4-29
Figure 4.13: *b*: Sporangial shape variation for *Salopella* cf. *marcensis* from a non-allometric model.....p4-29
Figure 4.14: Three-dimensional plot showing morphospace of cf. *Cooksonia caledonica* / *Renalia* sp. using PC2, PC3 and PC4.....p4-31

Figure 4.15: Three-dimensional plot showing morphospace of *Cooksonia* cf. *cambrensis* using PC2, PC3 and PC4..... p4-33
Figure 4.16: Three-dimensional plot showing morphospace of *Cooksonia hemisphaerica* using PC1, PC3 and PC4..... p4-34
Figure 4.17: Three-dimensional plot showing morphospace of cf. *Uskiella reticulata / Tarrantia salopensis* using PC1, PC3 and PC4..... p4-36
Figure 4.18: Three-dimensional plot showing morphospace of elongate club-shaped sporangia using PC1, PC3 and PC5..... p4-37
Figure 4.19: Three-dimensional plot showing morphospace of *Salopella allenii* using PC1, PC3 and PC5..... p4-39
Figure 4.20: Three-dimensional plot showing morphospace of *Salopella* cf. *marcensis* using PC2, PC3 and PC4..... p4-40
Figure 4.21: *a*: All megafossils plotted on 3D plot, without species identification..... p4-42
Figure 4.21: *b*: All megafossils plotted on 3D plot, with species identification and 2 standard deviation ellipses..... p4-42
Figure 4.21: *c*: All megafossils plotted on 2D plot (PC1 vs. PC3), with species identification and 2 standard deviation ellipses..... p4-42
Figure 4.21: *d*: All megafossils plotted on 2D plot (PC1 vs. PC4), with species identification and 2 standard deviation ellipses..... p4-42
Figure 4.21: *e*: All megafossils plotted on 2D plot (PC3 vs. PC4), with species identification and 2 standard deviation ellipses..... p4-42

Chapter 5: THE DISPERSED SPORE RECORD

Figure 5.1: Cumulative graphs for each palynological assemblage..... p5-4
Figure 5.2: Sporomorph terminology and measurements..... p5-10
Figure 5.3: Pie charts showing proportions of spore morphotypes in each assemblage
a: Assemblage 5..... p5-61
b: Assemblage 4..... p5-61
c: Assemblage 3..... p5-61
d: Assemblage 2..... p5-61
e: Assemblage 1..... p5-61
Figure 5.4: Distribution of sporomorph diameter ranges through time..... p5-63

Figure 5.5: Relative abundance of palynomorph morphotypes from the latest Přídolí to the early Lochkovian across the Anglo-Welsh Basin (modified after Richardson 2007)..... p5-79
Figure 5.6: Palaeogeography for the upper Downtonian (directly below the Bishop's Frome Limestone, uppermost Přídolí to lowermost Lochkovian) based on palynofacies..... p5-82
Figure 5.7: Palaeogeography for the lowermost Dittonian (Lochkovian) based on palynofacies..... p5-83
Figure 5.8: Palaeogeography for the lower Dittonian (Lochkovian) based on palynofacies..... p5-84

Chapter 6: LOWER DEVONIAN OLD RED SANDSTONE DEPOSITIONAL ENVIRONMENTS

Figure 6.1: Tredomen Quarry log A..... p6-2
Figure 6.2: Tredomen Quarry log B..... p6-3
Figure 6.3: *a*: Tredomen Quarry Borehole 1, beds 1 to 25..... p6-4
Figure 6.3: *b*: Tredomen Quarry Borehole 1, beds 25 to 51..... p6-5
Figure 6.3: *c*: Tredomen Quarry Borehole 1, beds 52 to 74..... p6-6
Figure 6.3: *d*: Tredomen Quarry Borehole 1, beds 74 to 82..... p6-7
Figure 6.4: *a*: Tredomen Quarry Borehole 2, beds 1 to 62..... p6-8
Figure 6.4: *b*: Tredomen Quarry Borehole 2, beds 63 to 118..... p6-9
Figure 6.4: *c*: Tredomen Quarry Borehole 2, beds 119 to 152..... p6-10
Figure 6.4: *d*: Tredomen Quarry Borehole 2, beds 153 to 180..... p6-11
Figure 6.4: *e*: Tredomen Quarry Borehole 2, beds 181 to 199..... p6-12
Figure 6.4: *f*: Tredomen Quarry Borehole 2, bed 199..... p6-13
Figure 6.5: Tredomen Quarry correlated logs..... p6-14
Figure 6.6: *a*: Proportions of Tredomen Quarry lithofacies by number of beds..... p6-17
Figure 6.6: *b*: Proportions of Tredomen Quarry lithofacies by lithofacies thickness. p6-17
Figure 6.7: Targrove Quarry log..... p6-27
Figure 6.8: *a*: Proportions of Targrove Quarry lithofacies by number of beds..... p6-31
Figure 6.8: *b*: Proportions of Targrove Quarry lithofacies by lithofacies thickness... p6-31
Figure 6.9: *a*: Most common lithofacies transitions in Tredomen Quarry sequence.. p6-49
Figure 6.9: *b*: Schematic log based on the most common lithofacies transitions from the upper sequence of Tredomen Quarry core..... p6-49

Figure 6.10: Geomorphic model 1: Two-stage, ephemeral mud-dominated river system..... p6-51
Figure 6.11: Geomorphic model 2: Two-stage, sand-dominated, meandering river system..... p6-54
Figure 6.12: Geomorphic model 3: Interfluvial drainage and trunk channel model...p6-57

Chapter 7: TAPHOFACIES AND TAPHONOMIC CONSTRAINTS ON PALAEOECOLOGICAL INTERPRETATIONS
Figure 7.1: Taphofacies model for the Lower Devonian St. Maughans Formation p7-18

Chapter 8: ESTIMATING THE ATMOSPHERIC ρCO_2 LEVEL DURING THE EARLY DEVONIAN USING STABLE ISOTOPIC ANALYSIS
Figure 8.1: Estimates of Phanerozoic atmospheric ρCO_2 levels from geochemical models GEOCARB III and GEOCARBSULF (modified after Berner 2006)..... p8-2
Figure 8.2: *a*: Model of the concentration of soil CO_2 with depth, based on modern soils (modified from Cerling 1999)..... p8-6
Figure 8.2: *b*: Variation in CO_2 concentration with depth, for soils of differing respiration rates (modified from Cerling 1999).....p8-6
Figure 8.2: *c*: Variation in CO_2 concentration with depth, for soils of differing porosities (modified from Cerling1999)..... p8-6
Figure 8.2: *d*: Variation in CO_2 concentration with depth, for soils of differing depths of production (modified from Cerling 1999).....p8-6
Figure 8.3: The distribution of $\delta^{13}C$ through the soil profile (modified from Cerling 1991a)..... p8-9
Figure 8.4: The variation in $\delta^{13}C$ ratios for the different chemical components of modern plants compared with the average bulk value of -27‰ (modified from Gröcke 2002).....p8-14
Figure 8.5: Cross plots of $\delta^{13}C$ and $\delta^{13}O$ values from Tredomen Quarry pedogenic carbonate nodules..... p8-21
Figure 8.6: Cross plots of $\delta^{13}C$ and $\delta^{13}O$ values extracted from pedogenic carbonate nodules from across the Anglo-Welsh Basin, additional data from Eden (2007) and Jenkins (1998)..... p8-21

Figure 8.7: Estimates of atmospheric ρCO_2 levels of the Palaeozoic, from geochemical model GEOCARBSULF, and the palaeosol record from this study and Mora et al. (1996)..... p8-28

Chapter 9: RECONSTRUCTING LOWER DEVONIAN VEGETATION AND HABITATS FROM OLD RED SANDSTONE STRATA FROM THE ANGLO-WELSH BASIN

Figure 9.1: Percentages of Old Red Sandstone lithofacies from different Lochkovian localities across the Anglo-Welsh Basin.....p9-11

TABLES

Chapter 1: INTRODUCTION

Table 1.1: Stratigraphy of the Anglo-Welsh Basin (after Barclay et al. 2005).....p1-12

Table 1.2: Lithostratigraphy and environmental interpretations for the main formations in the Anglo-Welsh Basin, from the Late Silurian to the Early Devonian p1-13

Table 1.3: Miospore assemblages for the Late Silurian to Early Devonian (modified after Richardson and McGregor 1986)..... p1-21

Table 1.4: Early land plants from the Late Silurian to Early Devonian of the Anglo-Welsh Basin.....p1-26

Table 1.5: International spore assemblage biozones for the Silurian and Devonian (modified after Richardson and McGregor 1986)..... p1-33

Table 1.6: Sporomorph evolutionary stages (modified after Richardson 1996).... p1-36

Chapter 3: RECONSTRUCTING VEGETATION FROM OLD RED SANDSTONE STRATA

Table 3.1: Comparison of rhyniophyte and rhyniophytoid dimensions between Tredomen Quarry, other Anglo-Welsh Basin and global occurrences.. p3-54

Chapter 4: GEOMETRIC MORPHOMETRICS OF EARLY EMBRYOPHYTES

Table 4.1: Proportions and controls on shape variance represented by each principal component (PC) for each species, using allometric models..... p4-14

Table 4.2: Proportions and controls on shape variance represented by each principal component (PC) for each species, using non-allometric models..... p4-17

Chapter 5: THE DISPERSED SPORE RECORD

Table 5.1:*a*: Sporomorph taxa from Tredomen Quarry and their distribution, arranged taxonomically..... p5-6

Table 5.1:*b*: Sporomorph taxa from Tredomen Quarry and their distribution, arranged in order of appearance.....p5-8

Table 5.2: Cryptospore classification scheme (after Richardson 1996a)..... p5-11

Table 5.3: Comparisons between Tredomen Quarry assemblages and published *in situ* spores..... p5-75

Chapter 6: LOWER DEVONIAN OLD RED SANDSTONE DEPOSITIONAL ENVIRONMENTS

Table 6.1: Lithofacies descriptions for Tredomen Quarry strata and core..... p6-15

Table 6.2: Lithofacies descriptions for Targrove Quarry strata..... p6-29

Table 6.3: Lithofacies interpretations for Tredomen Quarry and Targrove Quarry..... p6-36

Table 6.4: *a*: Observed transition matrix for Markov Chain Analysis of Tredomen Quarry sequence..... p6-47

Table 6.4: *b*: Observed transition matrix for Embedded Markov Chain Analysis of the Tredomen Quarry sequence..... p6-47

Table 6.4: *c*: Summary of Markov Chain Analysis and Embedded Markov Chain Analysis of Tredomen Quarry sequence..... p6-47

Chapter 7: TAPHOFACIES AND TAPHONOMIC CONSTRAINTS ON PALAEOECOLOGICAL INTERPRETATIONS

Table 7.1: Taphofacies and their interpretations..... p7-3

Chapter 8: ESTIMATING THE ATMOSPHERIC ρCO_2 LEVEL DURING THE EARLY DEVONIAN USING STABLE ISOTOPIC ANALYSIS

Table 8.1: Stable carbon and oxygen isotopic values extracted from pedogenic carbonate nodules from Tredomen Quarry core..... p8-20

Table 8.2: Stable carbon isotopic values extracted from fossilised organic matter from Tredomen Quarry..... p8-20

Table 8.3: All estimates of atmospheric ρCO_2 levels for the Late Silurian to Early Devonian..... p8-23

Table 8.4: Stable carbon and oxygen isotopic valves extracted from pedogenic carbonate nodules from Llansteffan and Freshwater West, by Eden (2007)..... p8-26

Table 8.5: Stable carbon and oxygen isotopic values extracted from pedogenic carbonate nodules from Lydney, Manobiėr and Gardners Bank, by Jenkins (1998)..... p8-26

CHAPTER 1 : INTRODUCTION

1.1: INTRODUCTION

1.1.1: *Rationale*

The evolution and diversification of terrestrial vegetation during the Late Silurian and Devonian was a key event in Earth history. Phytoterrestrialisation had a global impact, altering not only the terrestrial realm, but also the oceans and atmosphere. The evolution of large roots in the Mid to Late Devonian resulted in increased rates of chemical and physical weathering, soil development, stabilisation of terrestrial landscapes, changes to hydrological systems, and changes to the carbon cycle (Retallack 1997, Algeo et al. 2001). Land plants became the primary producers of terrestrial ecosystems, providing habitats and nutrition for the diversification of terrestrial faunas (Beerbower 1985). It has been hypothesised that this increase in nutrient supply from the terrestrial realm to the oceans resulted in marine anoxia and extinctions during the Late Devonian (Algeo et al. 1995). The increase in silicate weathering, together with an increase in organic carbon burial, has been cited as the cause for the dramatic drop in atmospheric CO_2 levels during the Devonian (Berner 1997, 1998). This was the likely cause of global cooling and icehouse conditions towards the end of the Devonian (Caputo 1985). The increase in organic carbon burial has also been hypothesised as the cause of a rise in atmospheric oxygen levels during the Late Palaeozoic and Mesozoic (Berner 2006).

The Late Silurian to Early Devonian was a critical time period for the adaptation and diversification of terrestrial vegetation. Much of our understanding of the earliest land plants is from studying coalified compression or charcoalified body fossils, as well as the spores they contain and those dispersed within the surrounding strata. Palaeobotanical and palynological studies of fossils from the terrestrial Old Red Sandstone magnafacies of the Anglo-Welsh Basin have contributed much to the understanding of early land plant evolution (Edwards et al. 1986, Edwards et al. 1992, Edwards and Axe 1992, Edwards and Richardson 1996, 2004). Despite the exceptional anatomical preservation of some specimens (Edwards 1996), relatively few plant fossil assemblages have been discovered from Old Red Sandstone strata. Not only faced with a small number of specimens, anatomical details are often poorly preserved in coalified compression fossils, hindering interpretations regarding affinity. *In situ*

spores are rare, with a bias towards vegetation with a high preservation potential, whilst the dispersed spore record is a more accurate reflection on diversity, with many sporomorph taxa described (Richardson and Lister 1969, Burgess and Richardson 1995, Richardson 1996a), although often their parent plants are unknown. Fossil assemblages are commonly allochthonous, with fossils occurring potentially some distance from their original growth position, complicating any palaeoecological interpretations.

To understand these early terrestrial vegetative ecosystems, an assessment must therefore be made regarding the taphonomic effects on the preservation and distribution of fossil material, and the constraints that taphonomy has on palaeoecological interpretations. To achieve this, any relationships between fossilised material and sedimentary features and the processes that lead to these relationships, must be recognised.

An understanding of the landscapes and environments which these early land plants inhabited is also essential for any palaeoecological interpretations. During the Lower Devonian, the Anglo-Welsh Basin sat at the edge of the Old Red Sandstone Continent, approximately 17° south of the equator (Scotese 2003), and therefore likely to have experienced a semi-arid to arid climate. This creates something of a paradox, as to how these small, shallow rooting plants were able to survive on land in such harsh environments. The study of the possible geomorphic features and habitats of these early landscapes may provide the answers to these questions.

Palaeobotanical and palynological studies provide information regarding the diversity, physiology and affinity of early terrestrial vegetation. When considering palaeoecology however, these studies provide little evidence of the nature and possible metabolic pathways of the main components of the vegetative ecosystem. Stable carbon isotopes extracted from fossilised organic matter can be compared with values from extant plants to hypothesise the likely nature and metabolic pathways of the fossilised vegetation. This may highlight any trophic relationships between different components of the ecosystem. In conjunction with stable carbon isotope values extracted from pedogenic carbonates, an assessment of the degree of soil productivity may also be made, as well as estimates for the levels of ρCO_2 in the atmosphere during the Early Devonian.

This thesis aims to investigate early terrestrial plant ecosystems of the Anglo-Welsh Basin during the Early Devonian, involving the taxonomy, physiology and affinity of the vegetation, the depositional settings, environments and landscapes for phytoterrestrialisation, and the taphonomic constraints on reconstructing palaeoecological interpretations.

1.1.2: *Aims and objectives*

There are 5 main objectives:

1. To expand the palaeobotanical and palynological record of the Early Devonian, and to contribute to the understanding of early land plant evolution and diversification across the Anglo-Welsh Basin.
2. To envisage the environments of deposition in which phytoterrestrialisation are recorded, via sedimentological analysis and interpretation of Old Red Sandstone strata.
3. To identify any relationship between fossil plant assemblages and strata of the Old Red Sandstone, to understand the role of taphonomy in the distribution of plant material, and its constraints on palaeoecological interpretations.
4. To use stable carbon isotopes to determine if biological productivity within Old Red Sandstone soils was significant, and to estimate atmospheric CO_2 levels during the Early Devonian, as well as investigating the trophic relationships between different vegetative components of the ecosystem.
5. To synthesise the data of objectives 1 to 4 in an attempt to understand Early Devonian vegetative ecosystems across the Anglo-Welsh Basin.

The following aims are to be considered:

The palaeobotanical and palynological record

1. Contribute to the database of early embryophyte diversity during the Early Devonian, including the description and analysis of specimen morphology, and the description of any *in situ* sporomorphs, to be compared with the published dispersed spore record.
2. Describe any dispersed sporomorphs, and compare with the published dispersed spore record, to assess local and regional variations in diversity and to develop broad palynofacies useful for palaeoenvironmental interpretations. In association with the published *in situ* spore record, non-fossilised components of the palaeo-ecosystem may also be recognised.
3. Contribute to the continuous enhancement of the international palynological biozones, particularly for the Late Silurian and Early Devonian.

Lower Devonian depositional environments

4. Identify and interpret the main lithofacies of Lower Old Red Sandstone strata that contain significant palaeobotanical content.
5. Assess the degree of cyclicity of the strata using statistical analysis, to enhance an understanding in the nature of deposition.
6. Envisage geomorphic models and the environments of deposition for the strata analysed, and make regional comparisons across the Anglo-Welsh Basin using published data.

Taphonomy

7. Determine the preservation type and distribution of plant fossils within Old Red Sandstone strata, and recognise any relationship between fossil assemblage and lithofacies, and describe these as taphofacies.
8. Interpret taphofacies, to understand the taphonomic and stratinomic controls on plant preservation and distribution.
9. Incorporate the taphonomic data into the geomorphic models, to envisage a taphonomic model, to assess the taphonomic constraints on understanding palaeoecology.

Isotopic analysis

10. Extract stable carbon and oxygen isotopes from pedogenic carbonate and fossilised organic matter, to calculate the atmospheric carbon dioxide levels during the Early Devonian.
11. Assess the degree of soil productivity in Early Devonian soils using stable carbon isotopes.
12. Investigate the trophic relationships between different components of early land vegetation using stable carbon isotopes.

Synthesis

13. Envisage the possible vegetative palaeo-ecosystems of the Early Devonian, by synthesising the palaeobotanical, palynological and geochemical data with the taphonomic and geomorphic models.

1.1.3: *Layout of thesis*

The layout of the thesis is as follows. In Chapter 2, the palynological, palaeobotanical, sedimentological and geochemical methods used, and the localities from which fossilised material and strata were analysis are described. In Chapter 3, the fossilised plant assemblages are described and interpreted. In Chapter 4, the diversity of sporangial shapes of the early embryophyte fossils collected are analysed, using geometric morphometrics. In Chapter 5, the dispersed palynological assemblages are described and interpreted. In Chapter 6, Old Red Sandstone strata from which the fossils were extracted are described and interpreted, and the environments of deposition and geomorphic landscapes during the Early Devonian are envisaged. Chapter 7 investigates the relationships between fossilised material and sedimentology, and interprets the taphonomic constraints on interpreting palaeoecology. Chapter 8 discusses the use of stable carbon isotopes from organic matter and pedogenic carbonates in calculating carbon dioxide levels in the atmosphere, assessing soil productivity during the Early Devonian and nature of the main vegetative components of the ecosystems. In Chapter 9, all data are considered in an attempt to envisage the plant ecosystems of the Lower Devonian across the Anglo-Welsh Basin.

All stratigraphy and timescales used are based on the International Stratigraphic Chart 2008 including Global Standard Section and Points (GSSPs), complied by the International Commission on Stratigraphy, part of the International Union of Geological Sciences.

All figures and tables can be found in volume I, on the consecutive page after appearance in the text. Plates and plate captions can be found in volume II. A content page can be found at the front of this thesis, pages vi-xviii. References can be found at the back of volume I. Appendices II to IX can be found in the back of volume II. Appendix I and part *d* of appendix V can be found on the DVD provided.

1.2: GEOLOGICAL BACKGROUND: THE OLD RED SANDSTONE CONTINENT

1.2.1: *Palaeozoic palaeogeography and formation of the ORS continent*

The Old Red Sandstone continent (also known as Laurussia) was an amalgamation of three separate landmasses: Laurentia (North America, Greenland, Scotland and northwest Ireland); Baltica (northern Europe); and Avalonia (Belgium, northern France, England, Wales and southeast Ireland) (Figure 1.1*b*). These landmasses were brought together by the closure of the Iapetus Ocean between the Late Ordovician and the Early Devonian. During the Early Ordovician (Figure 1.1*a*), Laurentia was equatorial, and remained so for the majority of the Lower Palaeozoic. The large Iapetus Ocean separated Baltica to the east of the Laurentian margin. Avalonia, originally an arc attached to Gondwana, drifted north during the Late Cambrian to Early Ordovician to sit south of Laurentia and to the west of Baltica. Around 490Ma, the Iapetus Ocean began to close and Avalonia, Baltica and Laurentia were brought together by sinistral, oblique plate convergence. The timing and nature of these continental collisions that gave rise to the extensive landmass of the Old Red Sandstone continent are under debate.

One of the main uncertainties is the position and tectonics of Avalonia. Most are in agreement over a Gondwana origin, but the relationship with Baltica is still under debate. Trench and Torsvik (1992) and Torsvik et al. (1996) use palaeomagnetic data and faunal distributions to suggest a collision of eastern Avalonia with Baltica during the Mid to Late Ordovician. Trench and Torsvik (1992) considered the collision as one of dextral amalgamation rather than hard continent-continent collision. By the Late Silurian (425Ma), Avalonia-Baltica had collided with Laurentia.

Dewey and Strachan (2003) accepted Trench and Torsvik's notion of the Avalonia-Baltica collision in the Late Ordovician, but considered the collision to be "soft". They also developed a tectonic framework and timing of collisions, with particular significance to basin formation. Using palaeomagnetic and structural data from Laurentia and Baltica, Dewey and Strachan (2003) identified three main tectonic regimes associated with the final stages of the Caledonian Orogeny.

1. Between 435 and 425 Ma, sinistral transpression resulted in the Scandian Orogeny, with the collision of Baltica and Laurentia, and hence the deformation of rocks across northwest Scotland, Scandinavia, east Greenland and Svalbard. Around 425Ma a

Figure 1.1a: Palaeogeographic reconstruction during the Early Ordovician, 1.1b: during the Early Devonian, modified after reconstructions by Ron Blakey.

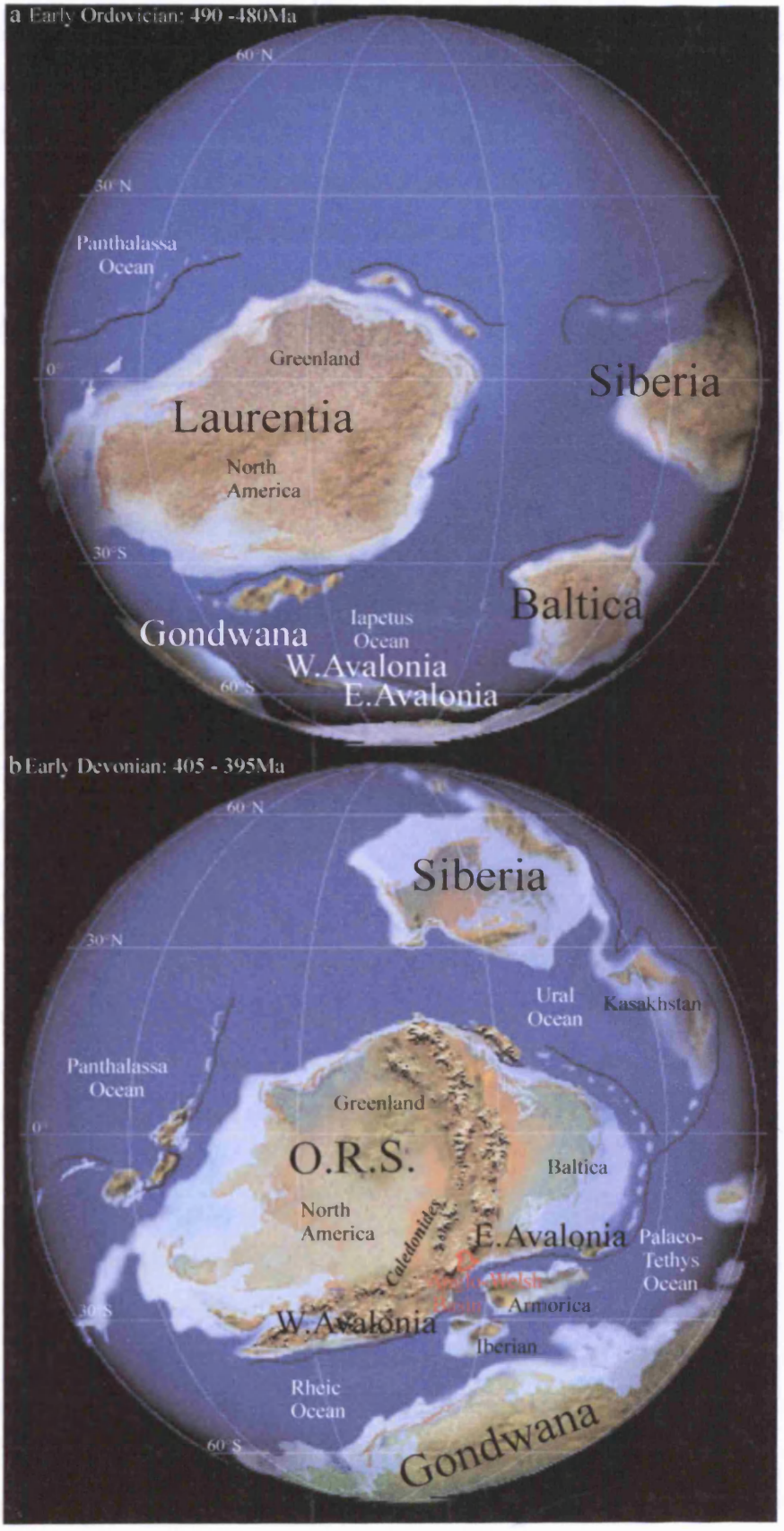

softer, sinistral oblique collision occurred between Avalonia and Laurentia, with deformation of rocks in the southern Uplands and Lake District.

2. Between 425 and 410Ma, the Scandian Orogeny climaxed, and the tectonic regime altered from transpressional to orogen-parallel, sinistral strike-slip, particularly along the Great Glen Fault Zone.
3. Between 410 to 395Ma, sinistral transtension occurred, with the formation of pull-apart basins and continental sedimentary successions such as the Orcadian Basin in the Shetlands. The period of transtension was halted by the compression regime of the Acadian Orogeny, at approximately 395Ma.

Dewey and Strachan (2003) therefore recognised a significant time gap between the closure of the Iapetus Ocean and the Acadian Orogeny, during which tectonics were dominated by strike-slip and transtensional regimes.

Despite this model fitting the stratigraphy of Laurentia and Baltica, the successions of the Anglo-Welsh Basin and others of Avalonia do not match the timings proposed. Using evidence from Avalonian deposits, Soper and Woodcock (2003) propose that:

1. A structurally separate Avalonia collided with Laurentia by oblique sinistral convergence from the Early Silurian to c.420Ma.
2. Between 420 and 400Ma, convergence ceased and a transtensional regime dominated Avalonia. Pull-apart basins formed, either infilling with fluvial sediments or lamprophyre emplacement.
3. Around 400Ma, sediment infill of basins halted with the start of transpressive shortening brought on by the Acadian Orogeny.

Despite differences in timing, both models recognise that there is a significant time gap between the Iapetus closure and the Acadian Orogeny, and during this period the basins of the Old Red Sandstone formed. The mechanisms for basin formation will be discussed in section 1.2.2.

1.2.2: *Formation of the Anglo-Welsh Basin*

Between the closure of the Iapetus Ocean and the onset of the Acadian Orogeny (Late Silurian to Early Devonian) a number of sedimentary basins were created across the Old Red Sandstone Continent: the Orcadian Basin in the Shetlands, the Midland Valley of Scotland, the Scottish Border Basin, Mell Fell Trough in southern Lake District and the Anglo-Welsh Basin. The mechanisms of how these basins formed are under debate.

Sedimentary successions of Late Silurian to Early Devonian age can be found in south and central Wales, southwest Wales (Pembrokeshire) and the Welsh Borderland (Figure 1.2). The successions are typical of the Lower Old Red Sandstone: coarsening upwards basin infill, with a marine to terrestrial transition. The Welsh Borderland Fault System defines the northern margin of the outcrop (Figure 1.2), although outliers on Anglesey and Clun Forest suggest a wider extension of the basin (Barclay et al. 2005). The basin may also have extended into southeast England. On the whole, sedimentation began in the Přídolí (419Ma), although Wenlock to Ludlow terrestrial deposits do outcrop in Pembrokeshire. Changes in local subsidence patterns across the basin were likely caused by extension and transtensional synsedimentation (Barclay et al. 2005).

James (1987) and King (1994) first discussed the mechanism of basin formation, and used subsidence analysis to determine basin history. Backstripped subsidence curves from the Welsh Borderland and South Wales were concave, which was interpretated as load-generated flexural subsidence in a foreland basin setting. This may have been caused by the continuation of oblique subduction of Avalonia beneath Laurentia after Iapetus closure (Friend et al. 2000, Soper and Woodcock 2003).

However, Dewey and Strachan (2003) as discussed in section 1.2.1, modelled a period of sinistral transtension between the closure of the Iapetus (410Ma) and the Acadian Orogeny (395Ma). A number of pull-apart basins developed in Laurentia and Baltica, and were either infilled with sediments (central-east Greenland, north-central Svalbard, Orcadian Basin) or emplaced with lamprophyres (southern Uplands, eastern Ireland).

Soper and Woodcock (2003) recognised a significant overburden of now lost Old Red Sandstone (evidence from illite crystallinity of mudrocks), which would not be supported by the flexural subsidence model. A calculated minimum thickness of 3.4km of Lower Old Red Sandstone has been lost from the Lake District, as well as a comparable amount from North Wales. Soper and Woodcock (2003) expanded on the transtensional model of Dewey and Strachan (2003) based on the evidence from the Avalonian outcrops, and concluded that pull-apart basins developed between 420 and 400Ma. Hillier and Williams (2004) suggest that the transtensional model is only applicable to the basins of the north, and that the Anglo-Welsh Basin was more affected by flexural subsidence or extensional tectonics associated with rifting on the southern side of Avalonia, with the opening of the Rheic Ocean.

Figure 1.2: Silurian and Devonian outcrops of the Anglo-Welsh Basin (modified after Edwards and Richardson 2004 and Woodcock and Gibbons 1988)

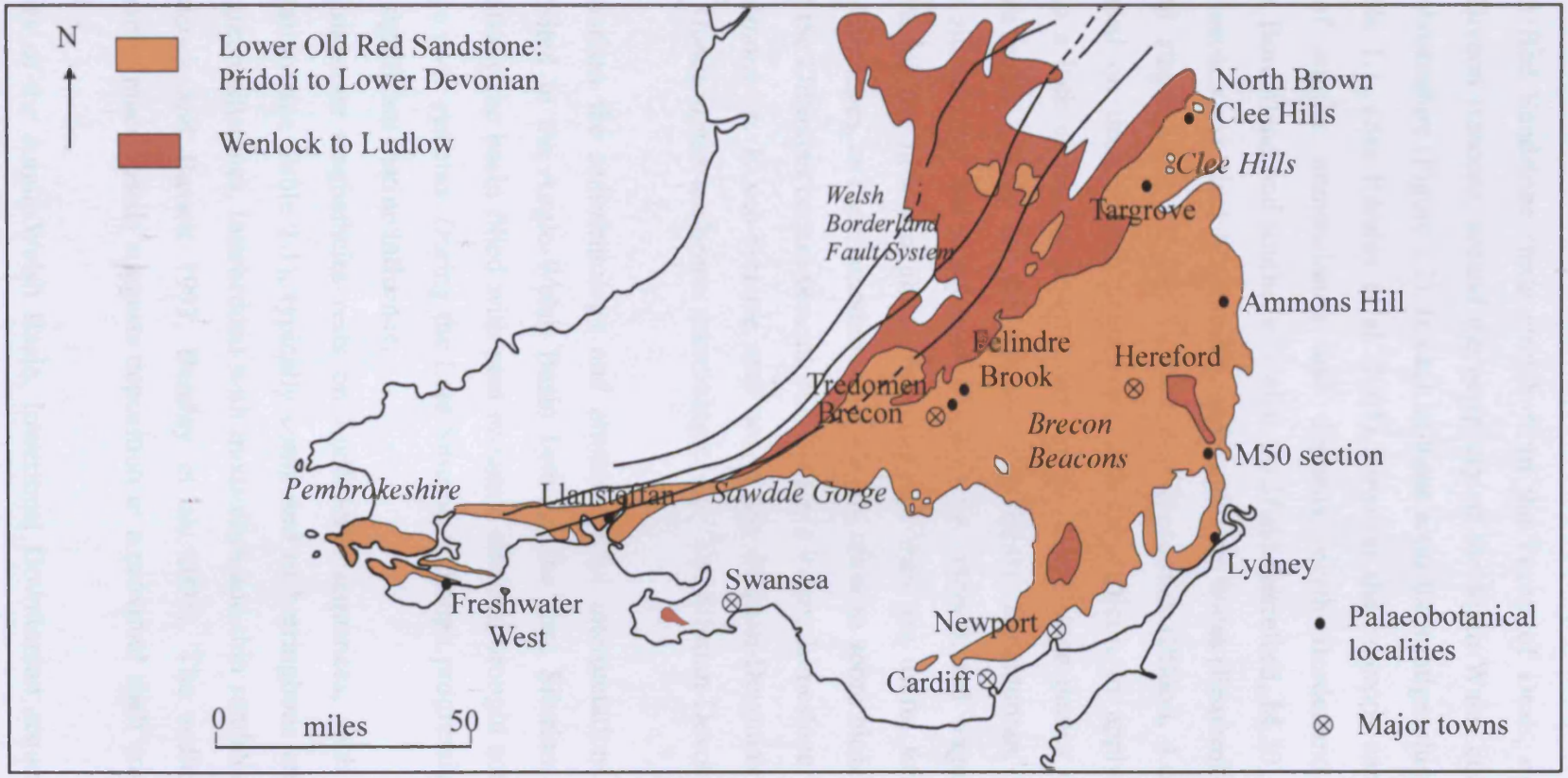

1.2.3: *Stratigraphy and Anglo-Welsh Basin strata*

Outcrops of Old Red Sandstone strata stretch from the Forest of Dean, over the Black Mountains and Brecon Beacons, around the periphery of the south Wales coalfield, and to some extent Pembrokeshire (Figure 1.2). In each of these areas the stratigraphic nomenclature is different (Table 1.1, after Barclay et al. 2005), however the outcrops can be split into general areas of similar nomenclature and deposits: north Borderland (Clee Hills, Shropshire), east Borderland and southeast Welsh Coalfield (Hereford, M.50), south-central Wales (Brecon Beacons and Black Mountains), and southwest Wales (Pembrokeshire).

The international stages used for the Silurian and Devonian (Přídolí, Lochkovian and Pragian) are based on deep marine sequences, and are difficult to apply to terrestrial sequences due to a lack of marine invertebrate fossils. Local stage names were therefore devised by Allen et al. (1977) for the Anglo-Welsh Basin: Downtonian, Dittonian and Breconian, with similar, but not exact boundaries to the international stages (Table 1.1). Although these terms are now thought to be out-dated, they are useful when discussing palynological assemblages, as their boundaries are closely relate to spore biozone boundaries (e.g. the base of the Dittonian occurs beneath the Bishop's Frome Limestone, at the base of the *Apiculiretusispora* sp. E sub-biozone and not at the Silurian-Devonian boundary, as correlated with *Monograptus uniformis* assemblage (see 'The Silurian-Devonian boundary' section, p1-20).

Table 1.2 summarises the sedimentology and environmental interpretations for the main formations deposited in the Anglo-Welsh Basin between the Late Silurian and the Early Devonian. Essentially the basin filled with post orogenic detritus, brought southward to the coastline by large river systems. During the Late Silurian, although progressively retreating, there was still a significant marine influence.

The Old Red Sandstone magnafacies rests on Ludfordian sequences, such as the Upper Whitcliffe Formation (see Table 1.1), typically composed of herringbone and hummocky-bedded grey to green siltstones, interbedded with mudstones and thin sandstones (Bassett et al. 1982, Woodcock and Bassett 1993, Barclay et al. 2005). The sedimentology and abundance of marine macrofossils suggests deposition in a proximal shelf environment (see Table 1.2).

Over the majority of the Anglo-Welsh Basin, lowermost Downtonian sequences represent deposition in intertidal areas such as shallow marine, shoreface or back-barrier lagoonal deposits (Table 1.2). The base of the Old Red Sandstone, defined as the Ludlow Bone Bed,

Table 1.1: Stratigraphy of the Anglo- Welsh Basin (modified after Edwards and Richardson 2004, Barclay et al. 2005, Hillier and Williams 2007)

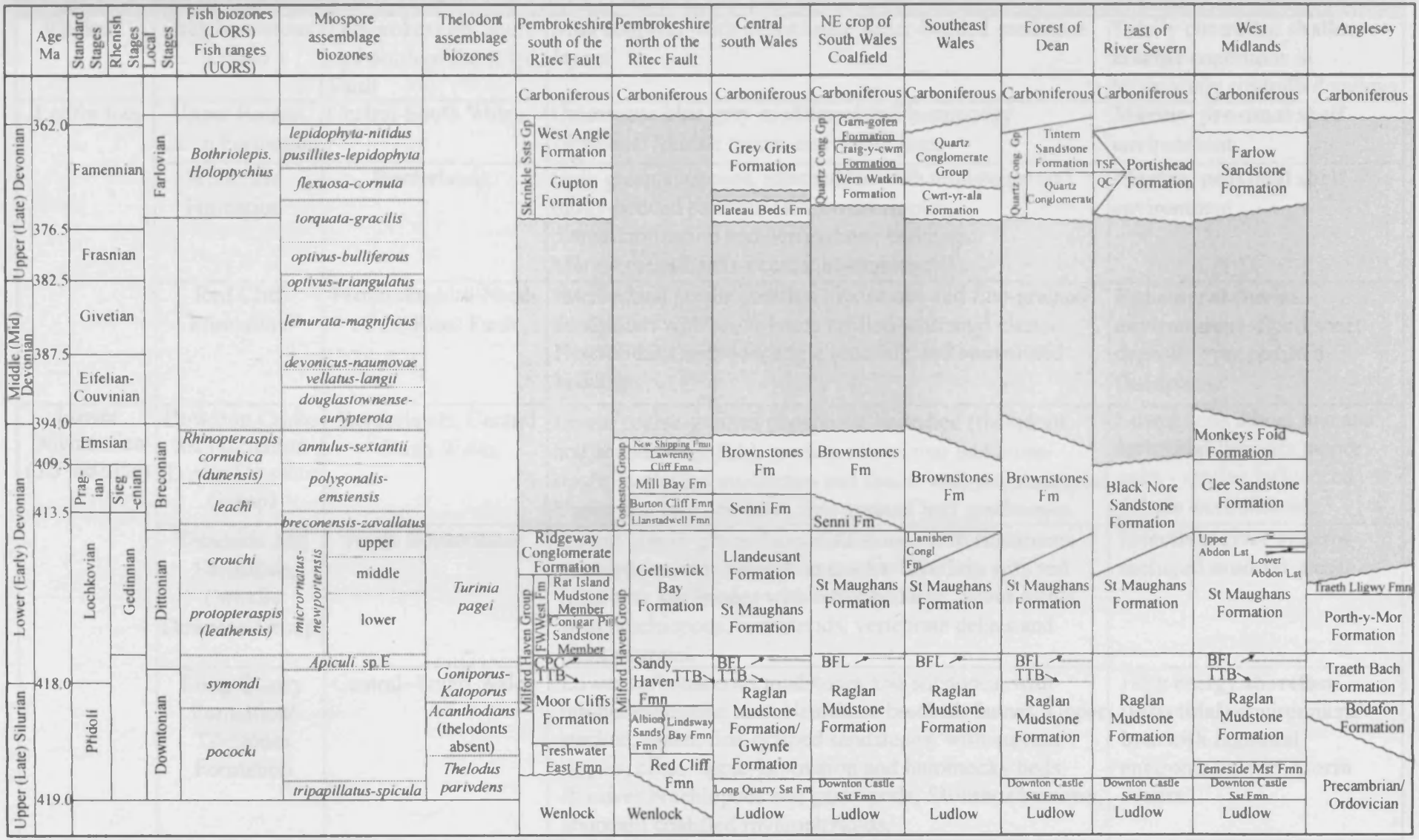

Table 1.2: Lithostratigraphy and environmental interpretations for the main formations deposited in the Anglo-Welsh Basin, from the Late Silurian and the Early Devonian.

Age	Formation	Area	Rocks	Interpretations
Wenlock	Grey Sandstone Group	Pembrokeshire- south and north of the Ritec Fault	Mud couplets, with subordinate flaser-bedded sandstone layers.	Tidally controlled **shallow marine** conditions in tectonically controlled valleys.
Ludfordian	Upper Roman Camp Formation	Central-South Wales	Calcareous blue grey mudstones and hummocky siltstones. Marine faunas and shelly lags.	**Marine proximal shelf** environment
	Whitcliffe Formation	Borderlands	Grey green siltstones, interbedded with mudstones and thinly-bedded sandstones. Current ripples, planar-lamination and herringbone bedding. Marine megafossils-benthic assemblages.	**Marine proximal shelf** environment
	Red Cliff Formation	Pembrokeshire-North of the Ritec Fault	Interbedded purple pedified mudstones and fine-grained sandstones with scour bases infilled with mud clasts. Heterolithics with low angle scouring and convoluted bedding.	**Ephemeral fluvial environment** -flood sheet deposits over pedified floodplains.
Lower Downtonian (TS biozone)	Downton Castle Sst Formation (Lower Downton Group)	Borderlands, Central South Wales	Lower coarse-grained phosphatic bone bed (thelodont and acanthodian fish), grading into planar and cross-ripple-laminated mudstones and shales with plant material. Upper unit cross-bedded, fine-grained buff sandstones.	Lower units strand line and **intertidal** deposits; upper units - marine influenced **deltaic** environment.
	Temeside Mst Formation (Middle Downton Group)	North Borderlands	Lower coarse-grained green siltstones with calcareous concretions and desiccation cracks. Overlain with red mica-rich sandstones with cross-bedding. Scour infills with brachiopods, eurypterids, vertebrate debris and plant material.	**Intertidal river** systems sheltered **mudflat** areas.
	Long Quarry Formation/ Tilestones Formation	Central- South Wales	Lower carbonaceous mudstones and siltstones, with thinner sandstone lens. Nearshore brackish faunas. Upper stacked, green, fine-grained sandstones, with current ripples, cross-ripple-lamination and hummocky beds. Bivalves,brachiopods and gastropods, *Skolithos* burrows, abundant coalified rhyniophytoids.	High energy **shoreface (intertidal)** environment/ **brackish lagoonal** environment with **storm events.**

Table 1.2: Lithostratigraphy and environmental interpretations for the main formations deposited in the Anglo-Welsh Basin, from the Late Silurian and the Early Devonian (continued).

Age Ma	Formation	Area	Rocks	Interpretations
Lower Downtonian (TS biozone)	Freshwater East Fmn (Lower Milford Haven Group)	Pembrokeshire, south of Ritec Fault	Basal beds of grey-green pebble conglomerate, with exotic clasts. Marine-influenced, medium-grained grey sandstones sheets are interbedded with green siltstones, heterolithics and lesser red mud-cracked mudstones. Plant debris, lingulids and ostracods and phosphatic nodules are present.	**Coastal mudflats** or floodplains with a **tidal influence.**
	Albion Sands Formation	Pembrokeshire, north of the Ritec Fault	Thick, buff-coloured and quartz-rich sandstone units, stacked with erosive extra- and intraconglomeratic bases. Subordinate red mudstones.	**Braided river systems**
	Lindsway Bay Formation	Pembrokeshire, north of the Ritec Fault	Conglomeratic with pebbles composed of igneous material, quartz and epidotic rocks, as well as local mudstone clasts. Beds with scour bases and sharp tops. Subordinate mudstones and calcretes.	**Alluvial fan** setting, with subordinate **channel and floodplain deposition**
Middle to Upper Downtonian	Raglan Mudstone Formation/ Ledbury Formation	Central South Wales, Borderlands	Cyclothems of thick, pedified red mudstones and siltstones interbedded with thinner, laterally discontinuous beds of coarse-grained, planar and cross-bedding, siltstones and sandstones with scour bases. Fauna includes fish specimens, plant debris, bivalves and ostracods.	**Estuarine/ tidal mudflats, brackish** and **ephemeral** high velocity rivers, and prolonged **periods of exposure**.
	Gwynfe Formation	Central- South Wales	Lower green micaceous, fine to medium-grained sandstones and heterolithics. Upper pedified red calcareous mudstones (see Raglan Mudstone description).	Basal **floodsheet deposits** by **ephemeral** river systems on **tidal mudflats**.
	Moor Cliff Formation	Pembrokeshire, south of the Ritec Fault	Bright pedified red micaceous siltstones and mudstones and mud aggregates (80%), with subordinate intraformational conglomerates, multi-storey sandstones and heterolithics.	Broad **alluvial dryland floodplains** with **ephemeral river systems.**

Table 1.2: Lithostratigraphy and environmental interpretations for the main formations deposited in the Anglo-Welsh Basin, from the Late Silurian and the Early Devonian (continued).

Age Ma	Formation	Area	Rocks	Interpretations
Middle to Upper Downtonian	Sandy Haven Formation	Pembrokeshire; north of the Ritec Fault	Thick, pedified and fine-grained red siltstones and mudstones, with subordinate purple-grey sandstones and extra- and intraformational conglomerates.	Major broad **tidal mudflats** - periods of geomorphic stability and pedogenesis interrupted by high velocity ephemeral flood events.
Dittonian (MN biozone)	Ditton Group	Borderlands	Cyclothems of grey-green fine to medium-grained sandstones with basal conglomerates, including well-preserved plant megafossils, fining up into heterolithic siltstones and fine-grained red siltstones and finally pedified red mudstones.	**Perennial - ephemeral** complex **fluvial** channel system, with **overbank flood sheet** and broad **floodplains** deposits.
	St Maughans Fm	South Borderlands, Central-South Wales		
	Llanddeusant Fm	Central-South Wales		
	Freshwater West Formation	Pembrokeshire; south of the Ritec Fault	Lower sandstone member fine to medium-grained green multi-storey sandstones and heterolithics with subordinate mudstones. Upper mudstone member pedified mudstones with subordinate green sandstones.	Lower fmn: **perennial ephemeral channels**, point bar + crevasse splay deposits. Upper fmn: distal **ephemeral** river system.
	Gelliswick Bay Formation	Pembrokeshire; north of the Ritec Fault	Cyclothems, with basal channel sandstones with extra-formational conglomerates, heterolithics and pedified mudstones.	**Perennial fluvial** channel system, **overbank flood sheet** + broad **floodplains** deposits.
Lower Breconian (BZ - PE biozones)	Clee Sandstone Formation	Borderlands	Olive green, medium-grained, cross-bedded and planar-laminated ssts, (plus well-preserved plant fossils), with erosive intraformational conglomeratic bases. Interbedded structureless, mud-cracked siltsts and mudsts.	Large medial **braided river systems,** with low sinuosity.
	Senni Formation	Central-South Wales		
	Cosheston Formation	Pembrokeshire; north of the Ritec Fault	Lower, thick green sandstones, with finer-grained subordinate green and red siltstones. Upper sequences of coarse-grained red brown breccias and conglomerates.	Lower: **meandering and braided** river systems. Upper: **Braided** river system
Upper Breconian (AS biozone)	Woodbank Formation	North Borderlands	Coarse-grained red multi-storey sandstones, with interbedded green mudstones and siltstones. Interlocking lenticular internal structure, with cross bed sets, trough and sigmoidal cross and planar-lamination.	Low sinuosity, **proximal braided river system**
	Brownstones Formation	South Borderlands, Central-South Wales		

represents the transition from open marine conditions to near-shore depositional environments. The Ludlow Bone Bed (base of the Downton Castle Sandstone Formation), consisting of lenticular and ripple-laminated coarse-grained beds with phosphatic vertebrate remains, has been interpreted as strand line deposits (Bassett et al. 1982). The overlying *Platyschisma* Shale Member, containing the gastropod *Platyschisma*, lingulids, ostracods, eurypterids and plant material, was likely deposited in the near-shore intertidal zone. The strata of the equivalent Long Quarry Sandstone Formation (Table 1.2) have been interpretated as deposition in a high-energy shoreface environment (Woodcock and Bassett 1993).

The Downton Castle Sandstone Member, with evidence of sub-aerial exposure (calcareous concretions and desiccation cracks) and plant remains, suggests near shore deposition, possibly in a deltaic environment (Table 1.2) (Bassett 1982). The strata of the overlying Temeside Mudstone Formation are composed of coarse-grained green siltstones with calcareous concretions and desiccation cracks, overlain with cross-bedded, mica-rich sandstones, with scour-and-fill structures and current ripple lamination (Allen and Tarlo 1963, Bassett 1982). These sequences have been interpreted as marine influenced deltaic channels, where sandy channels have eroded into previously sheltered, partially pedified mudflat areas (Bassett 1982).

Across the majority of the Anglo-Welsh Basin, the Raglan Mudstone Formation is thought to be mid to upper Downtonian in age (Late Přídolí) (see Table 1.1), and represents a change in facies and environmental settings. The Raglan Mudstone Formation consists of massive to thickly-bedded mudstones, predominately pedified with significant calcium carbonate horizons, and interbedded siltstones and sandstones (Allen and Dineley 1976) (see Table 1.2). At some localities, bivalves and ostracods are present, suggesting a marine influence (Barclay et al. 1994). It has been suggested that deposition occurred on estuarine or tidal mudflats, with periods of ephemeral, high velocity waters, followed by prolonged periods of dryness and non-deposition (Allen and Tarlo 1963, Barclay et al. 2005).

Due to the lack of good palynological material from the Late Silurian, a regional marker horizon, the Townsend Tuff Bed, is often used for correlation (Table 1.1). The Townsend Tuff is a cumulative bed of volcanic ash falls, and is thought to be sourced from a large, but distant Plinian eruption, which was responsible for numerous, yet less voluminous tuff falls across the Anglo-Welsh Basin during the late Přídolí and early Devonian. It is widespread throughout the basin, approximately 100m below the top of the Raglan Formation. It is typically a very-fine-grained, brittle and siliceous mottled-green muddy tuff, ranging from 1.5

to 4m thick (Allen and Williams 1981, 1982). It can have a sharp contact with pedified mudstones beneath, or a more gradational zone of green-red mottling. It often has a fine cleavage and may be weathered to porcellanite. Palaeontological features such as coprolites, tracks and burrows have been preserved at the base of the tuff (Allen and Williams 1981, Marriott et al. 2009).

A second regional marker horizon, the Bishop's Frome Limestone (previously known as the *Psammosteus* Limestone, and known as the Chapel Point Calcrete where overlying the Moor Cliff Formation, south of the Ritec Fault), occurs at the top of the Raglan Mudstone Formation (Table 1.1). This well-developed palaeosol horizon of calcium carbonate nodules has been interpreted as a cumulative, stage IV-V C-horizon of palaeo-calcic-Vertisols. This horizon forms a mappable escarpment across most of the Anglo-Welsh Basin, and represents a significant period of geomorphic stability (estimated from 10,000 to 100,000 years) (Wright and Marriott 1996), where large quantities of carbonate production indicate a period of non-deposition or sediment starvation in the basin. It is also coincident with a facies change from marine-influenced to continental fluvial-dominant deposits, and a change in flora and fauna (coincident with fish and spore assemblage biozones boundaries). It is therefore often taken as the stratotype for the Silurian-Devonian boundary, despite its lateral discontinuous and possible diachronous nature.

Above the Bishop's Frome Limestone, strata have been dated as the Early Devonian (Lochkovian or locally known as the Dittonian), based on palynological assemblages belonging to the *micrornatus-newportensis* biozone (see Table 1.1). The St. Maughans Formation overlies the Bishop's Frome Limestone across the majority of the Welsh Basin. The St. Maughans Formation can be recognised from previous formations by an increase in the proportion of sandstone bodies, characterised by patterns of grey-green fine to medium-grained sandstones with basal conglomerates, fining up into heterolithics and fine-grained siltstones and finally pedified mudstones (Allen and Tarlo 1963, Allen 1964, Barclay et al. 2005) (Table 1.2). These sandstones represent perennial and complex river channel deposits (Allen 1964). Sandstone units often grade up into planar-bedded, fine-grained heterolithics and thought to represent overbank flood sheet deposits or deposition in a lacustrine setting (Table 1.2). Heterolithics grade up into red fine siltstones and mudstones typically pedified and lack distinct bedding. Calcium carbonate nodule-rich horizons, pseudo-anticlinal slicken-sided slip planes, burrows, desiccation cracks and drab haloes are all common within these palaeosols. These rocks were originally deposited on broad floodplains that were subjected to prolonged periods of exposure.

Palynological assemblages from sequences directly overlying the St. Maughans Formation belong to the biozone *breconensis-zavallatus*, and therefore are Breconian in age (late Lochkovian) (see Table 1.1). In south-central Wales sequences belong to the Senni Formation, overlain by the Brownstones Formation (see Table 1.2). The Senni Formation of the lower Breconian consists of channelised intraformational conglomerates, cross-bedded pebbly sandstones, planar-laminated fine-grained sandstones and interbedded cross-ripple-laminated siltstones. Owen (1995) interpreted these deposits as high-energy floods, either from widespread channelised floods, or overbank floods such as crevasse splays. Structureless siltstones were interpreted as abandoned channel infill. Owen (1995) hypothesised that deposition occurred in large, low sinuosity, medial braided river systems.

The Brownstones Formation of the lower to upper Breconian, lies directly above the St. Maughans Formation across most of the basin, and consists of fine to coarse-grained red multi-storey sandstones, with interbedded green mudstones and siltstones (Allen 1983). Allen (1983) discovered an interlocking lenticular internal structure within the sandstone units that represents gravel-sand bar deposits. Interbedded mudstones represent abandoned channel infill that may have been subjected to a period of exposure.

Although the sequences of Old Red Sandstone are similar in southwest Wales, local tectonic controls or climatic differences may have resulted in different sedimentology observed (see Table 1.2). North of the Ritec Fault, the Red Cliff Formation has been interpreted as fluvial deposition by ephemeral river systems (Hillier and Williams 2004). Terrestrial environments were therefore first present in this part of the Anglo-Welsh Basin as early as the Ludfordian. The overlying Albion Sands Formation is composed of stacked, cross-bedded sandstone units, with erosive extra- and intra-conglomeratic bases (Allen and Williams 1978, Hillier and Williams 2004). Within the Marloes Inlier, the Lindsay Bay Formation interfingers with the Albion Sands Formation, consisting of conglomerates of exotic source, and likely to have been deposited in an alluvial fan setting (Hillier and Williams 2004).

The Sandy Haven Formation, Gelliswick Formation and Cosheston Formation are the lateral equivalent of the Raglan Mudstone Formation, St. Maughans Formation and Senni Formation, respectively (Table 1.2) (Allen et al. 1977, Allen and Williams 1978, Allen et al. 1982, Barclay et al. 2005). Lithologies are similar with the exception that basal conglomerates of the Gelliswick Formation contain exotic clasts (Allen et al. 1982), and the upper sequences of the Cosheston Formation consist of coarse-grained red brown breccias and exotic conglomerates (Thomas et al. 2006). The Cosheston Formation likely represents

deposition in braided river system, which occurred during active tectonism along the Benton Fault (Thomas et al. 2006).

South of the Ritec Fault, the Freshwater East Formation of the lower Downtonian is more similar in lithology to the upper Downtonian Raglan Mudstone Formation, representing deposition in a tidal flat environment. In the upper Downtonian, the Moor Cliff Formation is lithological similar to the Raglan Mudstone Formation (Marriott and Wright 1993, Wright and Marriott 1996, Marriott and Wright 2004). The Chapel Point Calcrete is the lateral equivalent of the Bishops Frome Limestone, and also signifies a change in facies and biota in this region.

The Freshwater West Formation is separated into the lower Conigar Pit Sandstone Member and the upper Rat Island Mudstone Member. The Conigar Pit Sandstone is lithologically similar to the St. Maughans Formation (Table 1.2). Deposition of this sequence likely occurred within perennial-ephemeral river systems. The overlying Rat Island Mudstone Formation is more similar to the Raglan Mudstone Formation, mainly consisting of mudstones with clear pedogenic features, and subordinate current-rippled sandstone beds, representing deposition in an ephemeral river system. Floodplain sediments experienced prolonged periods of surface exposure.

The Ridgeway Conglomerate Formation, previously thought to have been Eifelian in age (Allen 1977), is now thought to lie conformably above the Rat Island Mudstone Formation and therefore Early Devonian in age (Hillier and Williams 2007). Sequences consist mainly of conglomerates containing exotic pebbles with clast imbrication, interbedded with parallel-laminated sandstones or pedified mudstones, plus sheet sandstones, inclined and non-inclined heterolithics and finely laminated siltstones, all interpreted as alluvial fan with axial-fluvial deposits (Hillier and Williams 2007). There are no Middle Devonian sequences in the Anglo-Welsh Basin.

Dating and correlation methods

The Anglo-Welsh Basin sequences are dated using spore and fish biozones (see Table 1.2). Although there is a general dearth of fish in the Anglo-Welsh Basin, those that have been discovered are important for correlation between the terrestrial Old Red Sandstone facies with equivalent Rhenish and Bohemian deposits (shoreface and deep marine facies, respectively).

White (1950) first described fish specimens from the Anglo-Welsh Basin, and devised fish biozones for the Downtonian, Dittonian and Breconian (see Table 1.1), which correlated with

the Clee Hills stratigraphy (Ball and Dineley 1961, White 1961). Spore biozones are more commonly used however to date and correlate Upper Silurian to Lower Devonian rocks. Spores have a high preservational potential, due to their chemically resistant exospore. Spores are widely distributed, and are abundant over a range of facies, allowing correlation of the terrestrial deposits of the Old Red Sandstone in Britain with the Rhenish and Bohemian deposits of Europe. Within the near-shore to deep marine facies spores are found in association with other palynomorphs such as acritarchs, chitinozoans and parsinophycean cysts, which increases their correlation potential (Richardson 1984). Relationships between spores and these other palynomorphs can also indicate transgressive or regressive sequences, using the marine influence index and the inshore index (Richardson and Rasul 1990). Spores are also particularly useful due to their morphological variability, and as a result spore biozones have been successfully constructed (Richardson and McGregor 1986). Morphological variability also reflects evolution, and together with the study of *in situ* spores can help reconstruct early land plant diversity and biogeography.

Richardson and co-workers have been collating data on the dispersed spore record from the Anglo-Welsh Basin and related marine deposits for over 40 years. Initial studies (Richardson 1967, Richardson and Lister 1969, Richardson 1974, Richardson et al. 1982) culminated in the construction of 19 international spore assemblage biozones for the Silurian and Devonian (Richardson and McGregor 1986) (see Table 1.3). Each biozone is defined by the arrival of two distinct spore species, from which the biozone takes its name, as well as an associated spore assemblage.

The Silurian-Devonian boundary

Early workers on the stratigraphy in the Anglo-Welsh Basin agreed that the Silurian-Devonian boundary should be placed at the base of the Ludlow Bone Bed (White 1950). This placed all Old Red Sandstone facies in the Devonian. In 1972 an international agreement at the Montreal Devonian Symposium repositioned the Silurian-Devonian boundary at the appearance of *Monograptus uniformis* from the deep marine Klonk succession, Czech Republic. The equivalent rocks in the Old Red Sandstone are difficult to correlate due to their terrestrial origins. Richardson and co-workers have attempted to correlate Old Red Sandstone sequences from the British Isles with Libyan, Estonian and Podolian (Richardson et al. 1981) and Cantabrian sequences (Richardson et al. 2000) using palynomorphs. It was discovered that the base of the *micrornatus-newportensis* spore biozone, which is well defined in the Anglo-Welsh Basin, is close to the Silurian-Devonian boundary in these European

Table 1.3: Miospore assemblages for the Upper Silurian to Lower Devonian (modified after Richardson and McGregor 1986).

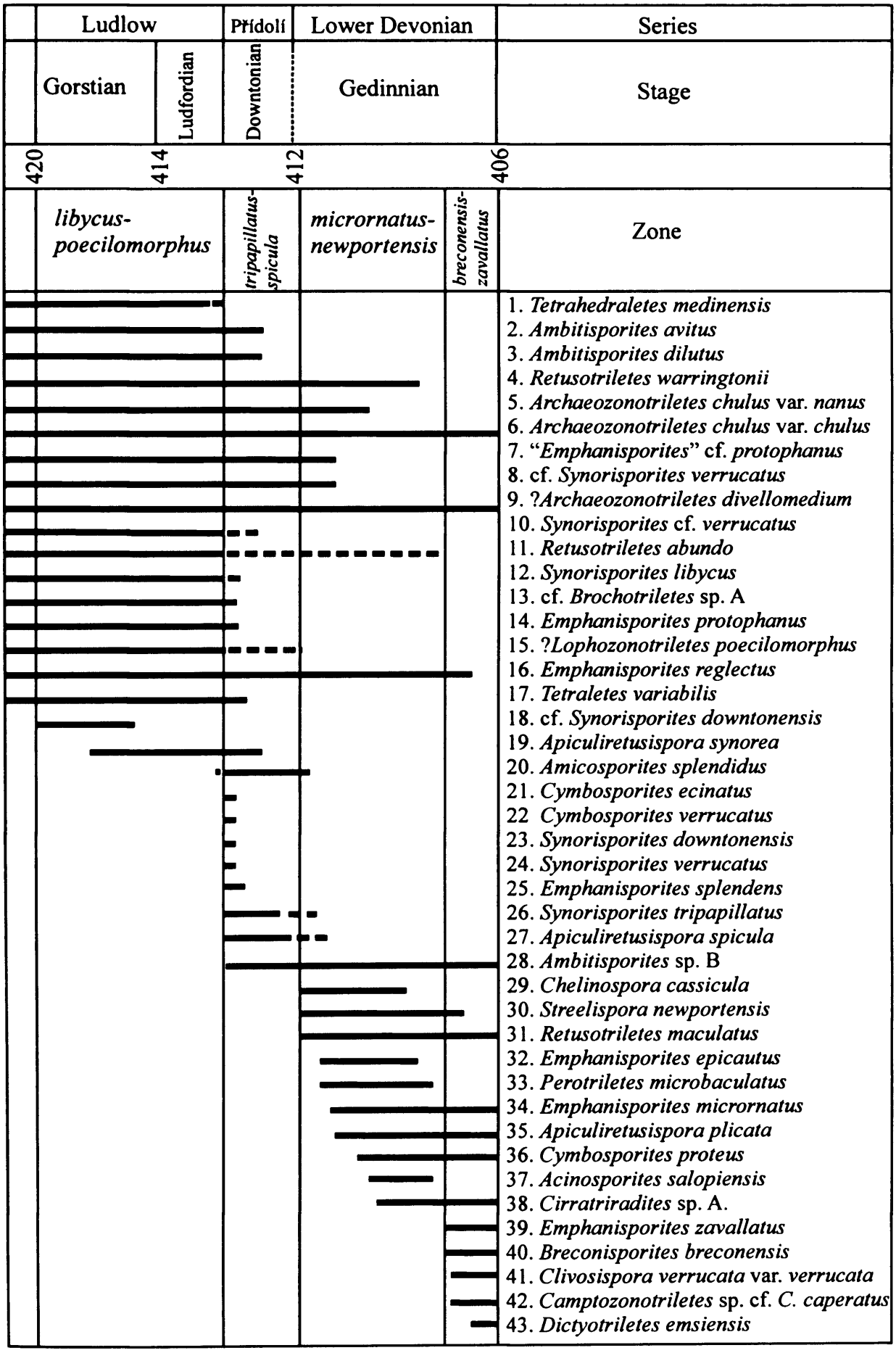

successions. The Downtonian sequences (the lowest Old Red Sandstone deposits) were therefore placed in the Silurian (see Table 1.1). The base of the MN biozone in Wales is close to the Bishop's Frome Limestone, which is found across the Anglo-Welsh Basin, making it an appropriate marker horizon. Allen and Williams (1981) argued that the Townsend Tuff Bed, that lies up to 100m below the Bishop's Frome Limestone, is more appropriate as a marker horizon, due to its instant and widespread deposition and distinct lithology. Although the Bishop's Frome Limestone may be diachronous and laterally discontinuous, it does however mark a boundary of facies change from marine to fluvial influenced deposition and hence is more significant in terms of environmental interpretation.

1.2.4: *Provenance and topography*

The Anglo-Welsh Basin was an extramontane and coastal basin, distal to the Caledonian mountain range to the northwest (Friend et al. 2000). Strata of the Upper Silurian Old RedSandstone contain plentiful mica grains, as well as staurolite and kyanite (Allen and Crowley 1983), sourced from weathered metamorphic strata. Simon and Bluck (1982) hypothesised that sediment was sourced from the newly-formed Caledonian mountains, and transported in a south-easterly direction by large fluvial systems to the coastal margins of the Old Red Sandstone Continent, infilling tectonically active basins. These rivers, approximately 500km in length, are thought to have connected the Anglo-Welsh Basin with other Lower Old Red Sandstone basins.

Allen and Crowley (1983) hypothesised a different scenario for the dispersal systems infilling the Anglo-Welsh Basin. As hypothesised by Simon and Bluck (1982), during the Late Silurian (Downtonian), the distal areas of the Old Red Sandstone continent were low-lying, marine-influence, mud dominated landscapes, with broad fluvial systems (Figure 1.3*a* and *b*). Sediments were rich in heavy minerals and mica, likely sourced from metamorphic terranes of the Caledonides to the northwest.

A significant change in facies type and sedimentary style occurred however in the Early Devonian (Dittonian), from the Raglan Mudstone Formation to the St. Maughans Formation, and their equivalents. This may be due to local tectonic uplift (Allen and Crowley 1983). There is little evidence for any marine influence, and it has been hypothesised that broad fluvial channels occupied low-lying, muddy floodplains (Figure 1.3*c*). The rocks are less micaceous, suggesting a halt to dispersal from the distant Caledonides (Allen and Crowley 1983). A greater proportion of igneous debris has been recorded, potentially transported from

Figure 1.3: Palaegeography of the Anglo-Welsh Basin during a: the lower Downtonian, b: the upper Downtonian, c: the Dittonian. Modified after Barclay et al. 2005.

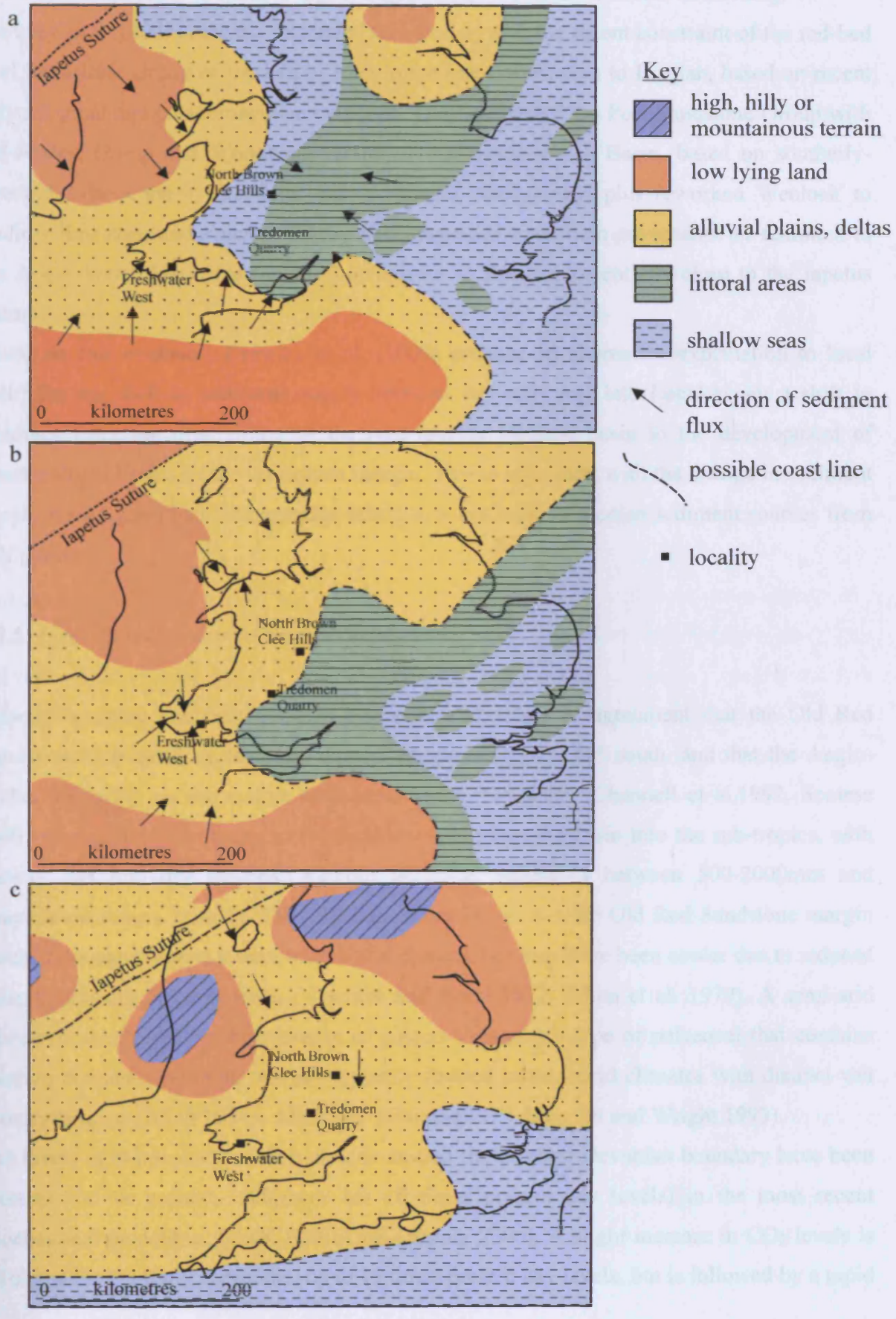

a more local source, such as the Irish Sea High or Bristol Landmass (Figure 1.3*c*) (Allen and Crowley 1983). There was also a higher degree of intra-basinal sediment re-working.

Crowley et al. (2008) recently expanded this model, with the recent constraint of the red-bed Peel Sandstone Group of the Isle of Man to the late Lochkovian to Pragian, based on recent palynological and palaeomagnetic evidence. They correlated the Peel Sandstone Group with the Abdon Group and Woodbank Group of the Anglo-Welsh Basin, based on southerly-directed palaeocurrent directions, heavy mineral petrography, plus reworked Wenlock to Ludlow limestone and volcanic clasts. This suggested a northern provenance of sediment to the Anglo-Welsh Basin for the late Lochkovian to Pragian, potentially close to the Iapetus Suture.

Based on this evidence, Crowley et al. (2009) propose an alternative explanation to local uplift for the shift in sediment supply between the early and late Lochkovian: a shift in tectonics from the final filling of the post-Iapetus foreland basin to the development of transtensional basins on the Avalonian margin. This is consistent with the change in sediment supply from Laurentian metamorphic debris to more local Avalonian sediment sources from half grabens.

1.2.5: *Late Silurian to Early Devonian climate*

Palaeogeographic and palaeomagnetic reconstructions are in agreement that the Old Red Sandstone Continent lay from the equator to approximately 30° south, and that the Anglo-Welsh Basin lay on the margin at approximately 17° south (Channell et al.1992, Scotese 2003) (Figure 1.1*b*). In today's climate this would place the basin into the sub-tropics, with distinct wet and dry seasons. Rainfall in these regions is between 500-2000mm and temperature ranges from 16-20°C. It is therefore likely that the Old Red Sandstone margin would have experienced a semi-arid to arid climate, but may have been cooler due to reduced solar luminosity of early Earth (Newman and Rood 1977, Owen et al. 1979). A semi-arid climate is confirmed by the presence of palaeo-Vertisols, a type of palaeosol that contains calcium carbonate horizons that are typically formed in semi-arid climates with distinct wet and dry seasons (Allen 1974a, Allen and Williams 1979, Marriott and Wright 1993).

The levels of atmospheric carbon dioxide around the Silurian-Devonian boundary have been estimated to be around 3000ppmV (or 10 times present day levels) in the most recent geochemical modelling, GEOCARBSULF (Berner 2006). A slight increase in CO_2 levels is predicted for the Early Devonian, up to 15 times present day levels, but is followed by a rapid

decline in CO_2 levels from the Mid Devonian onwards, reaching a low at the Carboniferous-Permian boundary.

Oxygen levels at the Silurian-Devonian boundary have been estimated to be around 25% of atmospheric composition (Berner 2006). In the Early Devonian, a significant drop to 13% has been modelled. From the Mid Devonian onwards, O_2 levels rise to a maximum of 30% at the Carboniferous-Permian boundary (Berner 2006).

1.2.6: *Flora and fauna of the Old Red Sandstone Continent*

Flora of the Upper Silurian and Lower Devonian Anglo-Welsh Basin

Brief descriptions and average measurements of the floral taxa known from Late Silurian to Early Devonian strata of the Anglo-Welsh Basin are shown in Table 1.4. The ancestors of early land plants are thought to originate from green algae (Charophyta), possessing similar biochemistry (chlorophyll, starch and cellulose), ultrastructure and cell division (Kenrick and Crane 1997, Bhattacharya and Medlin 1998, Graham and Gray 2001). It has been hypothesised that during the Precambrian encrusting prokaryotic mats and fungi also appeared on the land (Edwards and Selden 1993). It is thought that from green algae, stem group embryophytes with bryophytic characters emerged, and are hypothesised from molecular studies to be close to extant mosses, hornworts and in particular liverworts (Malek et al. 1996, Qiu et al. 1998, Renzaglia et al. 2001). The early ancestors of vascular plants may have possesses thalli, water conducting tissue, and erect sub-aerial portions, composed of parenchyma tissue capable of surviving desiccation in terrestrial environments (Kenrick and Crane 1997, Edwards and Wellman 2001, Raven and Edwards 2004). The main adaptation was the development of a reproductive organ carrying asexually reproductive cells (spores). There is no direct fossil evidence for these pioneers, except for the spores, and therefore the nature and extent of the spore producing generation (sporophyte) is unknown. Extant mosses, liverworts and hornworts lack the biopolymers that strengthen plant tissue (lignin), and it is likely that the stem group embryophytes were also composed of non-resistant tissue, resulting in the low preservational potential for this group. Due to these gaps in the fossil record, the relationship between algae, stem group embryophytes and early vascular plants (in particular the rhyniophytes) is presently unknown.

Unequivocal dispersed cryptospores can be found as far back as the Llanvirn (Darriwilian, Mid Ordovician) (Strother et al. 1996), although equivocal non-marine cryptospore-like palynomorphs have been found as far back as the Middle Cambrian (Strother 1998, Taylor

Table 1.4: Early land plants from the Late Silurian and Early Devonian of the Anglo-Welsh Basin.

Plant genus	Plant species	Description	SH mm	SW mm	AW mm	Reference
Rhyniophytes and Rhyniophytoids						
Genus *Cooksonia* sporangia height: sporangia width ratio equal to or less than 1	*Cooksonia hemispherica*	Smooth, dichotomously branched naked axes, gradually thickening towards terminal, hemispherical sporangia, with straight sporangial-axial junctions. Narrow sporangial border in some specimens. *In situ* spores *Ambitisporites*.	0·68-2·08	0·83-3·25	0·27-1·07	Lang 1937, Edwards and Fanning 1985, Fanning et al. 1992.
			0·20-2·00	0·30-2·00	0·25-1·60	Edwards 1979.
	Cooksonia pertoni	Smooth, dichotomously branched naked axes, gradually thickening towards terminal flattened, discoidal sporangia, with broad, straight sporangial-axial junctions. Evidence of stoma, sterome and tracheids.	0·17-0·27	0·63-1·56	0·31-0·41	Lang 1937, Edwards and Fanning 1985, Edwards et al. 1986, Edwards et al. 1992
	ssp. apiculispora	*In situ* spores *Streelispora newportensis/ Aneurospora* sp.	/	/	/	Fanning et al. 1988
	ssp. pertoni	*In situ* spores *Ambitisporites* sp.	/	/	/	Fanning et al. 1988
	ssp. synorispora	*In situ* spores *Synorisporites verrucatus*	/	/	/	Fanning et al. 1988
	ssp. reticulispora	*In situ* spores *Synorisporites* sp.	0·20-0·25	0·77	0·18	Habgood et al. 2002.
	Cooksonia cambrensis	Smooth, dichotomously branched naked parallel-sided axes, terminated by subspherical (forma α) to transversely elliptical (forma β) sporangia, with slightly concave sporangial-axial junctions. *In situ* spores *Ambitisporites* sp.	0·50-0·95	0·40-0·90	0·06-0·50	Edwards 1979, Edwards and Fanning 1985, Fanning et al. 1991.
			0·30-1·30	0·35-1·77	0·06-0·50	
	cf. *Cooksonia caledonica*	Smooth, dichotomously branched naked axes, gradually tapering towards terminal reniform sporangia, with slightly convex sporangial-axial junctions. Distinctive sporangial border. *In situ* spores smooth, granulose triletes.	0·80-1·70	0·40-1·70	0·10-0·45	Edwards 1970a, 1979, Edwards and Fanning 1985 Fanning et al. 1992.
	Cooksonia banksii	Smooth, dichotomously branched naked axes, gradually tapering towards terminal discoidal sporangia, with a distinctive concave sporangial-axial junctions, protruding into subtending axes. *In situ* spores *Ambitisporites avitus*.	0·41-0·76	0·28-0·39	0·07-0·18	Habgood et al. 2002
Genus *Uskiella* sporangia height: sporangia width ratio equal to or no more than 2	*Uskiella spargens*	Smooth, dichotomously branched naked axes, gradually tapering towards terminal, vertically elliptical sporangia, with distinctive diamond shaped cells on the sporangial wall. Tracheids present. Dehiscence along sporangial border.	3·00-5·30	2·00-4·00	c.0·93	Shute and Edwards 1989
			1·40-4·44	1·00-3·50	c.0·7	
	Uskiella reticulata	Smooth, dichotomously branched naked axes, gradually tapering towards terminal, vertically elliptical sporangia, with distinctive reticulate pattern on the sporangial wall. Dehiscence along sporangial border.	0·53-2·00	0·38-1·50	0·05-0·50	Fanning et al. 1992

Table 1.4: Early land plants from the Late Silurian and Early Devonian of the Anglo-Welsh Basin (continued)

Plant genus	Plant species	Description	SH mm	SW mm	AW mm	Reference
Rhyniophytes and Rhyniophytoids (continued)						
Genus *Tarrantia*	*Tarrantia salopensis*	Smooth, dichotomously branched naked axes, gradually tapering towards terminal, vertically elliptical sporangia, similar to *Uskiella reticulata*, but lacking the distinctive reticulate pattern on the sporangial wall.	0·38-2·63	0·25-2·00	0·13-0·88	Fanning et al. 1992
Genus *Salopella* sporangia height: sporangia width ratio more than 2	*Salopella allenii*	Smooth, dichotomously branched naked axes terminated by vertically elongate, fusiform sporangia. Constriction at sporangial-axial junction. Sporangial tips rounded, blunt or pointed.	2·00	9·00	1·10-2·00	Edwards and Richardson 1974
	Salopella marcensis	Smooth, dichotomously, branched naked axes terminated by vertically elongate, fusiform sporangia. Constriction at sporangial-axial junction. Sporangia smaller than *Salopella allenii*. Sporangial tips rounded or blunt.	0·75-3·38	0·25-0·88	0·05-0·50	Fanning et al. 1992
Genus *Tortilicaulis*	*Tortilicaulis transwalliensis*	Short and small naked axes, gradually tapering towards terminal, vertically elongate, fusiform sporangia. Subtending axes and cells on the sporangial wall are twisted. *In situ* spores *Apiculiretusispora*.	1·10-3·90	0·38-1·30	0·10-0·40	Edwards 1979
			1·63-7·17	0·63-1·81	0·30	Fanning et al. 1992
	Tortilicaulis offaeus	Short and small, dichotomously branched naked axes, tapering towards terminal,vertically elongate, fusiform sporangia. Sporangia may bifurcate. Subtending axes and cells on the sporangial wall are twisted.	0·31-0·89	0·19-0·54	0·06-0·14	Edwards et al. 1994
Genus *Caia*	*Caia langii*	Smooth, dichotomously branched and unbranched naked axes, gradually tapering towards terminal elongate sporangia with parallel sides and obtuse apices. Small projections on the top-third of sporangia. *In situ* spores *Retusotriletes* sp.	1·38-3·13	0·58-1·25	0·18-0·75	Fanning et al. 1990
Genus *Pertonella*	*Pertonella dactylethra*	Smooth, dichotomously branched naked axes, gradually tapering towards terminal horizontally elliptical, discoidal sporangia. Small sporangial projections with rounded tips. *In situ* spores *Apiculiretusispora arcidecus*.	0·20-0·40	0·62-1·69	0·16-0·42	Fanning et al. 1991a Richardson, Rodriguez and Sutherland et al. 2001
Genus *Hollandophyton*	*Hollandophyton colliculum*	Dichotomously branching naked axes with striations, terminating with reniform sporangia. Sporangial cell walls swollen and framboidal, with an uneven surface. Dehiscence along margin.	0·50-0·80	1·00-1·60	0·33-0·68	Rogerson et al. 2002
Genus *Steganotheca*	*Steganotheca striata*	Smooth, parallel-sided unbranched axes, terminated by elongate funnel-shaped sporangia. Sporangia have truncated tips, with oblique striations on the basal section of the sporangia.	1·80-2·70	1·00-1·50	0·40-0·80	Edwards 1970a Edwards and Rogerson 1979

Table 1.4: Early land plants from the Late Silurian and Early Devonian of the Anglo-Welsh Basin (continued)

Plant genus	Plant species	Description	SH mm	SW mm	AW mm	Reference
Rhyniophytes and Rhyniophytoids (continued)						
Genus *Resilitheca*	*Resilitheca salopensis*	Dichotomously branched smooth, naked axes with some evidence of overtopping, terminated by ellipsoidal or reniform sporangia. Dehiscence splits values equally. *In situ* spores ?*Apiculiretusispora* or *Retusotriletes*	1·07-2·07	1·17-4·21	0·18-0·91	Edwards et al. 1995a
Genus *Sporathylacium*	*Sporathylacium salopense*	Smooth, naked unbranched subtending axes terminated by ellipsoidal to circular sporangia, with an unclear junction. Distinctive thick border, composed of smooth elongate cells, 90° to the distal margin. Multi-layered sporangial wall.	1·15-1·25	1·14-2·00	0·25	Edwards et al. 2001b
Genus *Horneophyton*	cf. *Horneophyton* sp.	Smooth, naked, parallel-sided, dichotomously branched cylindrical sporangia, with truncated flat tips. *In situ* triletes *Emphanisporites* cf. *micrornatus*.	1·50	0·24	0·25	Edwards and Richardson 2000.
Genus *Taeniocrada*	*Taeniocrada* sp.	Sterile, naked dichotomously or laterally branching, ribbon like axes	/	/	2·00-8.00	Croft and Lang 1942
Genus *Sennicaulis*	*Sennicaulis hippocrepiformis*	Smooth, naked, parallel-sided branched sterile axes, with terete xylem, including tracheids with annular or helical secondary thickenings (S type).	/	/	6·00	Edwards 1981
Genus *Psilophytites*	*Psilophytites* sp.	Fragmentary sterile axes, with spreading, undivided enations, interpreted as spines, occurring along the axes. Spines short and triangular.	/	/	0·20-1·00	Edwards 1979
Cryptospore-producers						
Genus *Cululitheca*	*Cululitheca richardsonii*	Minute elongate parallel-sided, beaker-shaped sporangium, with truncated tip, connected to smooth rapidly tapering subtending axis. *In situ* cryptospore unfused dyad *Dyadospora murusdensa*.	0·86	0·40	0·10	Wellman et al. 1998a
Genus *Fusitheca*	*Fusitheca fanningiae*	Minute smooth, naked dichotomously branched axes, terminated by elongate, fusiform sporangia, tapering to a pointed tip. *In situ* fused dyad cryptospores *Pseudodyadospora petasus*.	0·89	0·18	0·11	Wellman et al. 1998a
Genus *Grisellatheca*	*Grisellatheca salopensis*	Smooth, naked, dichotomously branched axis, terminated by elongate, bilobed sporangium, with maximum width at base, tapering upwards to a point. *In situ* cryptospore unfused dyads *Dyadospora murusdensa*.	1·54	0·27	0·12	Edwards et al. 1999

Table 1.4: Early land plants from the Late Silurian and Early Devonian of the Anglo-Welsh Basin (continued)

Plant genus	Plant species	Description	SH mm	SW mm	AW mm	Reference
Bryophytes?						
Genus *Sporogonites*	*Sporogonites exuberans*	Short, straight length of slender axis, terminated by vertically elongate sporangium, with parallel sides and bluntly rounded at the tip. Ridged texture at the sterile, basal region of the sporangium. Stomata present on subtending axis.	3·50	7·00	1·00	Croft and Lang 1942
	cf. *Sporogonites* sp.	Short, straight length of slender axis, terminated by vertically elongate sporangium, with maximum width in the lower third. Tapering, but bluntly rounded sporangium tip. Striated vertical texture on sporangial wall. Stomata present on subtending axis.	0·54	0·45	0·15	Edwards and Axe 1992 Edwards 1996
Zosterophylls						
Genus *Zosterophyllum*	*Zosterophyllum* cf. *fertile*	Dichotomously branched axes, with terminal fructifications, composed of two rows of laterally borne sporangia, attached to the main axes by short stalks. Two rows inserted spirally. Xylem strand visible, with scalariform tracheid thickenings. *In situ Retusotriletes*.	1·70-2·50	1·60-2·00	0·80-2·50	Edwards 1969a (Leclercq 1942)
	Zosterophyllum llanoveranum	Infrequent dichotomously branched axes, with terminal fructifications, composed of one or two rows of laterally borne, reniform sporangia, attached to the main axes by short stalks, along one plane. Xylem strand visible, with scalariform tracheid thickenings.	c.2·50	5·00-6·00	1·00-2·50	Croft and Lang 1942
			c.4·00	c.3·50	0·80-2·20	Edwards 1969b
	Zosterophyllum cf. *australianum*	Short unbranched axes, terminated by a number of spikes, with laterally borne, spirally arranged, overlapping sporangia. Sporangia reniform in shape and decrease in size towards the tip of the axes.	c.4·00	3·60-5·00	3·00	Croft and Lang 1942
Genus *Deheubarthia*	*Deheubarthia splendens*	Pseudomonopodially and dichotomously branched axes, with circinate vernation. Reniform sporangia are laterally borne, arranged in two opposite or sub-opposite rows, in a well defined distal fertile zone. Xylem composed of tracheids with annular thickenings. Small spines present on all axes.	2·90-5·80	c.5·00	1·20-11·00	Edwards et al. 1989
Genus *Gosslingia*	*Gosslingia breconensis*	Pseudomonopodially or dichotomously branched naked axes. Circinately coiled in apical regions, and axillary tubercles below branching points. Xylem composed of tracheids with scalariform thickenings and reticulate pitting (G type). Oval to reniform sporangia laterally borne on short sporangial stalks, occurring on both sides of the axes.	1·70-2·50	0·90-2·20	0·50-4·00	Heard 1927 emend. Edwards 1970b

Table 1.4: Early land plants from the Late Silurian and Early Devonian of the Anglo-Welsh Basin (continued)

Plant genus	Plant species	Description	SH mm	SW mm	AW mm	Reference
Zosterophylls (continued)						
Genus *Thrinkophyton*	*Thrinkophyton formosum*	Pseudomonopodially and dichotomously branched axes with circinate tips. Large axillary tubercles may occur below branching points. Laterally borne sporangia arranged in one or two rows on opposite sides of the axis. Sporangia are reniform, attached to a curved sporangial stalk.	1·30	2·20	0·50-2·80	Kenrick and Edwards 1988 Kenrick 1988
Genus *Tarella*	*Tarella trowenii*	Isotomously branched axes with circinate tips, with broad based projections of variable shape and size scattered over the sterile and fertile regions. Reniform sporangia laterally attached to main axes by stalks, positioned in two opposite vertical rows.	1·50-3·00	2·20-4·00	2·80-8·20	Edwards and Kenrick 1986 Kenrick 1988
Trimeophytes						
Genus *Dawsonites*	*Dawsonites* sp.	Naked pseudomonopodially and dichotomously branched axes with distinct fertile distal regions, with terminal sporangia arranged in pendent trusses. Fertile branches arise laterally and are helically arranged on broader axes. Sporangia fusiform in shape with curved tips. Preservation of a vascular strand in some specimens.	1·50-4·00	0·50-1·00	3·00-5·00	Croft and Lang 1942
Lycopsids						
Genus *Krithodeophyton*	*Krithodeophyton croftii*	Pseudomonopodially branched naked axes, with dichotomously branched axes in distal part. Protostele composed of tracheids with scalariform and reticulate thickenings. (G-type). Sporangia in terminal spikes. Oval, sessile sporangia borne in two rows, one on either side of the axis. Sterile appendages alternate with sporangia. *In situ* spores *Apiculiretusispora*.	1·25-1·50	0·80-1·00	1·50-4·30	Edwards 1968
Genus *Drepanophycus*	*Drepanophycus spinaeformis*	Fertile shoots; wide axes with widely spaced, short spike like leaves, indicated by scars or pits. Narrow strand of vascular tissue, composed of tracheids with annular thickenings (G type). Sporangia associated with the leaves. Lateral branching or H-shaped type branching.	4·00-7·00	4·00-7·00	5·00-25·0	Göppert 1852 Croft and Lang 1942

and Strother 2008). Rare fragmentary mesofossils have been found to contain cryptospores from the Caradoc (Katian, Late Ordovician) (Wellman et al. 2003). Previously, the oldest record of dispersed triletes came from strata of Ashgill age (Hirnantian, Late Ordovician) from Turkey (Steemans et al. 1996). However, both laevigate and ornamented triletes have been found as far back as the Caradoc (mid Katian, Late Ordovician) from a locality in Oman (Steemans et al. 2009). However the gap between the arrival of cryptospores and triletes suggests the presence of bryophytic-like land plants prior to the arrival of rhyniophytes, of which the first megafossil remains have been discovered from the late Wenlock (Edwards and Feehan 1980).

Rhyniophytes may have evolved from bryophyte-like stem group embryophytes or from a separate lineage of green algae. The rhyniophytes are plants with simple, naked dichotomously branched axes with terminal sporangia bearing triletes, (see Table 1.4) and possess a number of characteristics thought to be adaptations to terrestrial environments. Firstly trilete exospores are composed of resistant polymer sporopollenin, suggesting sub-aerial distribution. Tissues are strengthened by the biopolymer lignin, which allows plant portions to be erect, as well as increasing preservational potential. Cuticle covers sub-aerial portions of the plant, providing protection from desiccation and harmful UV radiation. To control water loss and gas exchange, pores or stomata occur on the stems or sporangia. Another feature that confirms adaptation to land is the presence of vascular tissue. Xylem or water conducting cells and strands are represented by tubes with secondary thickenings, or tracheids. Taxa with evidence of tracheids and hence vascular tissue are classed as rhyniophytes, and are considered the first true land plants. The remaining species that resemble rhyniophytes, including features such as stomata and cuticle, but lack vascular tissue, are classed as rhyniophytoids.

Zosterophylls evolved in the Late Silurian (Kotyk et al. 2002), but began to diversify across the Anglo-Welsh Basin from the Early Devonian, extending into the Late Devonian. The zosterophylls are similar to rhyniophytes, but differ in the position of the sporangia, which are attached laterally to either dichotomously or pseudomonopodially branched axes (Table 1.4). Sporangia are reniform to globular in shape, and split into two valves marginally. Zosterophylls are generally larger plants than rhyniophytes, reaching up to 50cm in height (Edwards 1970b). Although axes are leafless, zosterophylls often have spines (or enations). There is unequivocal evidence of tracheids and vascular tissues within the axes, and tracheids with annular, spiral or G-type thickenings have been discovered.

Trimerophytes are a class of early vascular plants that also evolved in the Early Devonian. They characteristically have a main axis that branched pseudomonopodially or dichotomously in the distal regions. Clusters of sporangia terminate the distal branches, forming pendant trusses (Table 1.4). Sporangia are commonly fusiform in shape. These characteristics are similar to rhyniophytes, which are thought to be ancestral to the trimerophytes.

Lycopsida first evolved in the Devonian, but diversified to be an important class in the Carboniferous. Similar to the zosterophylls, sporangia are attached to the axes laterally, but are associated with microphylls (small leaf structures that are vascularised) and are adaxial (see Table 1.4). Lycopods are thought to have been herbaceous and bushy in growth habit. There are examples of transitional plants between zosterophylls and lycopods (that possess non-vascularised leaf like projections in association with sporangia) suggesting that the former were ancestral (e.g. *Asteroxylon*).

The dispersed spore record

Over the last 40 years work by Richardson and co-workers on the dispersed spore record from Old Red Sandstone has resulted in a detailed database of known spores and the construction of international biostratigraphical assemblage zones (Richardson 1967, Richardson and Lister 1969, Richardson 1974, Richardson et al. 1982). Richardson and McGregor (1986) contains a full description of the spore assemblage biozones used to date the Silurian and Devonian, with many reference sections from the Anglo-Welsh Basin. Table 1.5 shows the main spore species used for each spore zone and their ranges for the Late Silurian and Early Devonian. Major evolutionary events in the morphology of spores are also shown. The following summary is based on the full descriptions of Richardson and McGregor 1986.

1. *Ambitisporites avitus - Ambitisporites dilutus*

The majority of spores from the Lower Silurian are cryptospores (permanent dyads, dyads and monads). Until recently the earliest record of spores with trilete marks came from an assemblage of Ashgill age (Steemans et al. 1996), and became one of the definitions for the base of the *avitus-dilutus* assemblage zone (Richardson and McGregor 1986) (Table 1.5). Recently trilete spores (both laevigate and ornamented) have been recorded as far back as the Caradoc (Steemans et al. 2009). Triletes from the Aeronian stage (Early Silurian) are

Table 1.5: International spore assemblage biozones for the Silurian and Devonian (modified after Richardson and McGregor 1986)

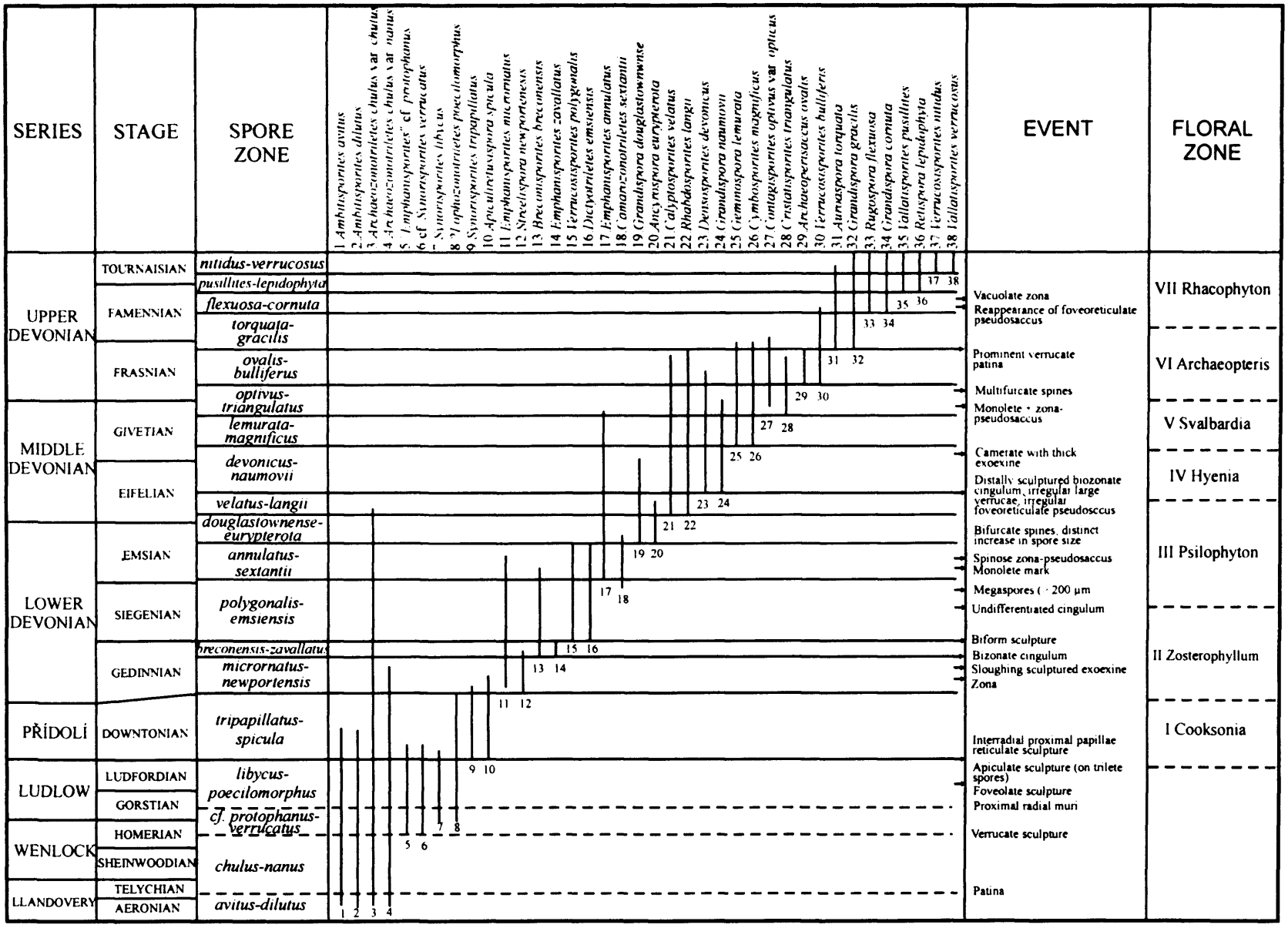

laevigate with equatorial crassitudes (e.g. *Ambitisporites avitus*), in association with sculptured cryptospores.

2. *Archaeozonotriletes chulus* var. *chulus* - *Archaeozonotriletes chulus* var. *nanus*

By the Telychian, laevigate trilete spores developed patina (e.g. *Archaeozonotriletes chulus* var. *chulus*).

3. *Emphanisporites* cf. *protophanus* - cf. *Synorisporites verrucatus*

Until recently, the first appearance of sculptured triletes occurred in the upper Homerian (the murornate sculpture of "*Emphanisporites*" cf. *protophanus*, and the verrucate sculpture typical of cf. *Synorisporites verrucatus*) (although this is now continuous with the discovery of ornamented triletes from the Caradoc (Steemans et al 2009)).

4. *Synorisporites libycus* - ?*Lophozonotriletes poecilomorphus*

The murornate sculpture developed further, with proximal radial muri on trilete spores from the Gorstian onwards (e.g. "*Emphanisporites*" *protophanus*) and distally murornate *Lophozonotriletes poecilomorphus*.

5. *Synorisporites tripapillatus* - *Apiculiretusispora spicula*

Towards the end of the Ludfordian, triletes and cryptospores with apiculate sculpture began to appear. An undoubted apiculate sculpture can be found on retusoid trilete *Apiculiretusispora spicula*, which is found at the base of the *tripapillatus-spicula* assemblage zone, which defines the base of the Downtonian. As well as being an important evolutionary event in the morphology of triletes and cryptospores, it coincides with the change in sedimentary facies from open marine (Ludfordian) to near shore (Downtonian) and the base of the Old Red Sandstone deposits. This assemblage also marks the appearance of spores that have developed proximal inter-radial papillae (e.g. *Synorisporites tripapillatus*).

6. *Emphanisporites micrornatus* - *Streelispora newportensis*

The base of the *micrornatus-newportensis* assemblage zone occurs slightly above the Silurian-Devonian boundary, which is taken approximately at the Bishop's Frome Limestone horizon in the Anglo-Welsh Basin. This also marks the Downtonian-Dittonian boundary. This assemblage is characterised by distally sculptured *Emphanisporites* taxa (e.g. *Emphanisporites micrornatus*) and proximally tripapillate distally granulate-apiculate triletes.

Spores with prominent zona make their first appearance in this assemblage. Spores with reticulate sculpture, such as *Chelinospora* are more abundant in this assemblage.

7. *Breconisporites breconensis - Emphanisporites zavallatus*

The final assemblage that can be found in the Anglo-Welsh Basin is the *brecon ensis-zavallatus* zone, of which the base is placed at the incoming of bizonate spores (*Breconisporites breconensis*). *Emphanisporites* with distal echinate sculpture are found in association.

Richardson (1996b) arranged the appearance and evolution of triletes and cryptospores stratigraphically, and set up stages for sporomorph evolution (Table 1.6). Unequivocal cryptospores first appeared in the Llanvirn (Strother et al. 1996), namely enveloped, laevigate permanent tetrads, pseudodyads and monads, and define the base of Phase 2 (Table 1.6). The first unequivocal cryptospores from the Anglo-Welsh Basin have been reported from the Caradoc. True dyads appeared and pseudodyads began to diversify during the Ashgill and Early Silurian.

The base of Phase 3 (Table 1.6) was defined by the appearance of the first triletes during the late Aeronian, initially laevigate and crassitate e.g. *Ambitisporites*. However this is now contentious, as trilete spores have been recorded from the Caradoc (Steemans et al. 2009). During phase 3 laevigate triletes diversified, developing patinate in the Telychian e.g. *Archaeozonotriletes*. Despite the diversification of laevigate triletes, cryptospores were still dominant. Hilate monads first appear at the end of the Telychian e.g. *Laevolancis*. This phase continues until the upper Homerian (late Wenlock), where triletes have evolved sculpture (Phase 4, Table 1.6). Initially triletes developed a distal murornate to verrucate sculpture (e.g. *Synorisporites*). Hilate monads also developed a distal verrucate sculpture during this phase. By the early Ludlow, triletes had developed proximal radial muri (e.g. *Emphanisporites*).

During the upper Ludfordian, retusoid triletes appeared with apiculate sculpture (e.g. *Apiculiretusispora*) (Phase 5A, Table 1.6). Patinate triletes with distal radial muri also appeared. By the lower Přídolí, triletes had developed proximal, inter-radial tripapillae (*Synorisporites tripapillatus*) (Phase 5B, Table 1.6). Spore assemblages from the upper Přídolí are very poorly preserved and sparse, and therefore no evolutionary stage has been assigned to this time period.

By the lower Gedinnian (lowermost Devonian), distally apiculate crassitate triletes appeared (e.g. *Aneurospora*) and dyads and hilate monads developed reticulate distal sculpture (Phase

Table 1.6: Sporomorph evolutionary stages (modified after Richardson 1996b)

SYSTEM	STAGE/ SERIES	PHASE/ SUBPHASE		
SILURIAN	lower Homerian	PHASE 3 LAEVIGATE MIOSPORES	C	Incoming of hilate monads
	Sheinwoodian			Incoming of trilete patinate, laevigate miospores; persistence of cryptospores
	Telychian		B	
	Aeronian		A	Incoming of trilete, crassitate laevigate, miospores
	Rhuddanian	PHASE 2 CRYPTO-SPORES	C	Appearance of true dyads; pseudodyads with narrow convolute muri
ORDOVICIAN	Ashgill		B	Incoming of pseudodyads with broad convolute muri
	Caradoc		A	Permanent tetrads, pseudodyads and monads; some with rugulate envelopes
	Llandelio			?
	Llanvirn			?
	Arenig	PHASE 1 PRE-CRYPTO SPORES		Monads, laevigate or with murornate sculpture; occasional loose tetrads
	Tremadoc			
CAMBRIAN				
Pre-C	Vendian			*Ambiguaspora*

SYSTEM	STAGE	PHASE/ SUB-PHASE	
DEVONIAN	uppermost Gedinnian	7A	Incoming of bizonate miospores (*Breconisporites*) and coarsely echinate *E. cavallatus*; waning and disappearance of *Aneurospora - Streelispora* complex; incoming of retusoid miospores with verrucate or murornate sculpture
	upper Gedinnian	6D	Diversification of distally apiculate *Emphanisporites*
	middle Gedinnian	6C	Incoming of *Emphanisporites micrornatus*; persistence of hilate cryptospore monads and permanent dyads; appearance of proximally monopapillate monads, diversification of apiculate monad cryptospores, persistence of laevigate and apiculate permanent tetrads.
	lower Gedinnian	6B	Incoming of *Streelispora* s.s., prolification of patinate miospores with distal reticulum; profilication of hilate and non-hilate cryptospores with verrucate and apiculate sculpture
	lowermost Gedinnian	6A	Incoming of equatorially crassitate miospores with prominent distal coni; cryptospores dominated by laevigate pseudodyads and monads, often bilate permanent tetrads persist.
SILURIAN	upper Přídolí	?	
	lower Přídolí	5B	Incoming of tripapillate miospores; abundance of equatorially crassitate murornate miospores; incoming of distally patinate and apiculate miospores and hilate apiculate dyads.
	Ludfordian	5A	Incoming of retusoid apiculate miospores, persistence of distally radially ribbed patinate miospores, hilate monads, persistence of permanent tetrads.
	Gorstian	4A	Proliferation of distally murornate miospores; incoming of distally radially ribbed patinate miospores; persistence of hilate cryptospores and permanent tetrads
	upper Homerian		Incoming of murornate and emphanoid sculpture in monad cryptospores and trilete miospores.

6A, Table 1.6). Throughout the Gedinnian, crassitate, proximally tripapillate and distally apiculate-granulate triletes diversified further e.g. *Streelispora, Emphanisporites micrornatus* (Phases 6B, 6C and 6D, Table 1.6). The final sporomorph evolutionary stage occurs in the uppermost Gedinnian, with the appearance of bizonate triletes (e.g. *Breconisporites*) (Phase 7A, Table 1.6).

Early fauna

The first unequivocal evidence for terrestrial fauna in the Anglo-Welsh Basin comes from late Silurian intertidal deposits of the Downton Castle Sandstone Formation, known as the Ludford Lane biota. The base of the Downton Castle Sandstone Formation is defined by a series of bone beds, which contain acanthodian, eurypterid and invertebrate remains. Associated with these bone beds and siltstone lenses contain arthropod cuticles, fragments of myriapods, aquatic scorpions, trigonotarbid arachnids, and appendages thought to be centipede (Jeram et al. 1990). Rhyniophytoids have been found in association with these faunas, and it has been proposed that the Ludford Lane biota inhabited a rhyniophytoid-rich saltmarsh (Edwards and Selden 1993).

Other body fossils from Lower Devonian Anglo-Welsh Basin strata have been discovered, including a trigonotarbid specimen from Tredomen Quarry, Brecon Beacons (Dunlop and Selden 2004). As body fossils are very rare, studies have focused on plant-biota interactions. These interactions include feeding, shelter, transport, reproduction and co-evolution (Shear and Selden 2001). Early plant morphology suggests these interactions, including spines and enations on plant axes designed for defence, whilst biota adapted feeding organs for piercing and sucking. Coprolites show direct evidence of plant-animal interactions. Spore walls were composed of resilient polymers that are indigestible, and therefore the plants that these early faunas were consuming might be identified.

These coprolite-producing faunas may have either been herbivores (directly feeding on living plant material) or detritivores (feeding on dead litter) (Edwards et al. 1995a). Feeding on sporangia would have certainly been advantageous, as spores would have been high in energy. Detritivores such as millipedes may have fed on plant litter rich in sporangial material. The predominance of spores in coprolites however may be the result of the inability to digest sporopollenin.

CHAPTER 2 : METHODS AND LOCALITIES

2.1: METHODS

2.1.1: *Palynological techniques*

Acid maceration

To extract the organic fractions from rock samples (including palynomorphs, mesofossils and phytodebris), the following acid maceration procedure was performed. All steps were performed in a fume cupboard under COSHH standards.

1. Specimens were first cleaned to restrict modern contamination, by the removal of any adherent mud, modern plant life or iron-oxide patches, using a knife or wet brush. Hard rock samples were then crushed into gravel-sized fragments using a pestle and mortar or hammer, while soft, friable samples were disintegrated using water. Approximately the same amount of each sample (~30g) was placed as a layer at the bottom of individual 1 litre plastic beakers.
2. To digest the carbonate fraction, the rock samples were first washed in cold 40% HCl. Only enough acid to immerse the rock samples was used (no more than 400ml). The samples were stirred gently with a plastic rod and left for 2 to 3 hours, before placing lids over the top of the beakers and left for 24hrs. The amount of carbonate in each sample was estimated by the amount of effervescence caused by the reactions. When the reaction was strongly effervescent, the samples were washed in HCl again to ensure that all carbonate had been removed.
3. Once all carbonate had been removed, the HCl was decanted and replaced with 1 litre of distilled water in each beaker. The samples were stirred gently, covered and left for 24hrs.
4. To digest the silicate fraction, the rock samples were subjected to a HF wash. The distilled water was decanted, and carefully replaced with 40% HF, just so that the samples were immersed in the acid. After the initial reactions, which sometimes produced violent effervescence, the samples were stirred gently 2-3 times a day, covered and left for 24hrs.

5. The next day, the HF was decanted, and the samples diluted with 1 litre of distilled water, stirred gently, covered and left for 24hrs. This step was repeated until the solutions reached pH 5, which took between 4 and 5 days.
6. The samples were then split into two fractions by sieving through 100μm filter meshes to separate any large organic fragments and undissolved rock from the palynological fraction. The palynological samples were further filtered through a 10μm mesh, the product of which was disgarded. When the rock samples were particularly fine or clay-rich, this process was aided by a small amount of detergent.
7. Any large organic fragments such as mesofossils from the +250μm fraction were observed under light microscopy. If any grains were still attached the fragments were washed in a small amount of 40% HF to remove any silicates, or with a small amount of boiling 40% HCl to remove carbonate and any calcium fluoride. The fragments were then removed from the solution, diluted, and left to dry on filter paper in a fume cupboard. Once dried, fragments were stored in covered Petri dishes.
8. At this stage, the palynological samples were observed on water slides under a light microscope to determine the quality of the samples. When silicates or carbonate grains were identified, the samples were washed again in a small amount of 40% HF or boiling 40% HCl and re-sieved. When heavy minerals were identified, a heavy mineral separation technique was employed. This was either done using a panning dish, or using a heavy solution. In the former, samples were placed in centrifuge tubes and additional water separated by centrifuge and pipette. Approximately 20ml of sodium polytungstate was then added and stirred into each sample. The samples were then centrifuged for 30 minutes at ~1500rpm, or until separation had occurred. The organic fractions were then removed using a pipette, rinsed through 10μm meshes using distilled water. The quality of each sample was then checked again to ensure all additional minerals had been removed. At this stage, each sample was split into two, dried and stored in vials with 5-10% HCl.

Examination of the palynological samples

The prepared palynological samples were observed under light microscopy and SEM. All counts and observations, including measurements, were recorded in a database and spreadsheets (see Appendices I and V). The slides and stubs were prepared by the following procedures.

Light microscopy

1. It was often the case that organic material was too dark to be examined using light microscope. To avoid this, one of the two fractions from each palynological sample was oxidised, which has a bleaching effect on the palynomorphs. This process is delicate, as too much oxidation can destroy the palynomorphs. Samples were therefore placed in a watch-glass, and small amounts of the oxidant were added a few drops at a time, until the palynomorphs were sufficiently oxidised, at which point the reaction was stopped by adding a few drops of distilled water. Schulze's solution was used as the oxidant; prepared by one part potassium chlorate ($KClO_{3(aq)}$) and two parts concentrated HNO_3. Firstly $KClO_3$ is added to the sample, followed by the careful addition of HNO_3 by a few drops at a time. In some cases, the palynomorphs were less readily oxidizable, and so were left in the solution for up to 20 minutes, or treated with a stronger Schulze solution (1:3 part HNO_3).
2. Before placing the samples on glass slides (or stubs for SEM), the concentration of palynomorphs per sample was adjusted so that a sufficient number of specimens was present on each slide, by adding distilled water or pipetting the sample through a 10μm mesh to remove water.
3. Slides were prepared using two methods:

   i.) *Using an UV adhesive*: a drop of PVA glue was added to each sample. A cover slip for each sample was placed onto a hot plate, and identification numbers scratched onto clean glass slides. Drops of each sample were then placed onto the cover slips using a pipette, starting at one corner to the next, covering the whole slip evenly. Whilst the cover slips were left to dry on the hot plate, a drop of UV adhesive was placed onto each glass slide. The glass slides were then 'dropped' on the cover slips, making sure that the cover slip was not stuck to the hot plate, and turned over quickly. Placing pressure onto cover slip ensured that the adhesive spread to the corners. The slides were then placed under UV light for 30 seconds to set the adhesive.

   ii.) *Using glycerine jelly*: The glycerine jelly was melted on a hot plate, and using a plastic pipette with the tip cut off, a drop of jelly was placed onto each clean labelled glass slide. Three drops of the sample were then dropped into the jelly and mixed gently on the slide. Once the water had evaporated off (checked for condensation with a cover slip) the slides were removed from the hot plate, and a cover slip lower on the glass slide using a steel needle, and adding pressure to ensure an even spread

of the sample across the slide. The slides were then left to dry, and the sides cleaned up using a scalpel and wiped with acetone.

4. The slides were then observed using transmitted and reflected light microscopy, using a Leica Mircosystems DMR-X microscope. In transmitted light, to get the optimum image, Köhler illumination was used. Digital photography of specimens was obtained using Leica Microsystems DFC480 digital camera and Leica IM1000 imaging program.

Scanning Electron Microscope

1. Palynological stubs for the SEM were prepared by sticking a cover slip to a stub using circular black adhesive, and then strewing the sample across the cover slip, and leaving to dry naturally.
2. The stubs were then splutter gold coated before placing in the SEM chamber. The SEM at Cardiff University is a FEI Systems XL30 ESEM FEG, and stubs were observed in high vacuum.

2.1.2: *Palaeobotanical techniques*

Collection

The plant fossils from Tredomen Quarry (see section 2.2.1) were discovered within fossiliferous-rich horizons of fine-grained sandstones and siltstones. These rock layers were particularly friable in nature, and contained extremely delicate fossils, and so care was taken to remove rock pieces using a geological hammer and chisel. Blocks were then wrapped up in newspaper to be transported back to Cardiff University. Any rock fragments thought to contain fossils within were collected, for sorting and splitting open in the lab. Once in the lab, all fragments were cleaned and observed under a dissecting light microscope. Large pieces were split open carefully to reveal the fossils within. Fossils of particular interest were then labelled, described and identified in a database (see Appendix I) and subsequently stored. Fossils of particular interest were selected for photography and further analysis.

Photography and images

Before any work was conducted on the fossils, those of interest were photographed using a Leica Microsystems MZ16 Stereomicroscope, DFC480 digital camera and IM1000 imaging program. Specimens were photographed using low polarised light from lamps and from a

polarised filter on the microscope, which reduced the glare from minerals such as mica, as well as improving the contrast between the fossil and the host rock. Images were taken in monochrome, which could be subsequently digitally altered. Larger specimens were photographed using a FinePix camera under polarised light. Once photographed, those specimens that were analysed were traced and outlines created, allowing for easier comparison between specimens.

Dégagement

Once all specimens of interest had been photographed and initially documented, the method of dégagement was used to reveal more of the compression fossils, by removal of the surrounding rock. This step is important, as removal of individual grains can alter the perceived morphology of the particularly small fossils. Most of the fossil specimens observed occurred oblique to the plane in which they were observed, with additional material hidden at depth. This method revealed those features, including additional sporangia. The removal of grains or flakes was achieved using a sharp tungsten needle under the microscope, or if larger fragments needed to be removed, a small chisel and toffee hammer were used. Once this method was complete, the specimens that had been developed were re-photographed, measured and collated in spreadsheets (see Appendix II and III).

Isolation of coalified material

The plant fossils collected from Tredomen Quarry are preserved either as coalified compressions or as impressions. Where coalified films had been preserved, some of the material was removed either for the possible extraction of *in situ* spores (by isolating sporangia), or for stable carbon isotope analysis (see section 2.1.3 and Chapter 8). The coaly material was removed using a tungsten needle and small paintbrush. For the extraction of *in situ* spores, the sporangia were treated with Schulze's solution, by adding potassium chlorate ($KClO_{3(aq)}$) to the specimen in a watch glass, and adding, drop-by-drop, fuming nitric acid (100%) to oxidise the organic matter. The reaction was stopped using distilled water.

2.1.3: *Sedimentological techniques*

Core preparation and imaging

Two cores were drilled at Tredomen Quarry (see section 2.2.1), one reaching a depth of 66.3m from the top quarry surface and another to 103.0m from bottom quarry surface. The

British Geological Survey split the 7cm diameter cores, and half is stored in the BGS core store, whilst the other half is stored at Cardiff University. Initially the core was cleaned and transferred into labelled one metre cardboard boxes. Before sedimentological logging was conducted, the cut surface was polished, by grinding the surface on a glass plate using a silicon carbide grit and water. Interesting portions of the core were scanned using an Epson Perfection V100 photo scanner.

Thin sections

Thin sections of carbonate nodules were taken to assess the degree of diagenetic overprinting. Carbonate nodules were extracted from the core, and blocks were cut using a rock saw. Uncovered thin sections were prepared at Cardiff University by Lawrence Badham. Thin sections were then partially stained with Alizarin Red S and Potassium Ferricyanide Blue, to determine if these nodules were composed of ferroan or non-ferroan calcite.

Stable carbon and oxygen isotopes

Stable carbon and oxygen isotopes were extracted from carbonate nodules and organic material (see chapter 8). For the carbon isotopic values from organic material, coaly material was removed from a variety of fossil compressions using a tungsten needle (see section 2.1.2). To remove any adherent grains, the samples were washed in a small amount of HF, rinsed and sieved. Once dry, the coaly material was also treated in boiling HCl (40%) to remove any carbonate grains, which may contaminate the sample. The samples were sent to Newcastle University and Iso-Analytical Ltd for analysis.

Iso-Analytical Ltd employed the following techniques. The samples were tested for carbon content, and treated to HCl (10%) washes, rinsed in distilled water and oven dried for 24 hours. The samples were then analysed by elemental-analyser-isotope-ratio-mass-spectrometry (EA-IRMS). Samples and references were sealed into tin capsules and loaded into a Europa Scientific elemental analyser. The samples were then transferred into a furnace at 1000°C and combusted in the presence of oxygen. The temperature in the furnace rose to a temperature of 1700°C, due to the combustion of the tin capsules in which the samples were held. The combusted gases produced were then carried over copper oxide wires that oxidized the hydrocarbons, and across silver wool to remove sulphur and halides, leaving N_2, NO_x, H_2O, O_2, and CO_2 remaining. These gases were then reduced over pure copper wires at a temperature of 600°C (removing O_2 and converting NO_x to N_2). Magnesium perchlorate was used to remove the water. To separate the N_2 and CO_2 a packed column gas chromatograph at

100°C was used. The resultant CO_2 was then ionised and accelerated by the Europa Scientific 20-20 IRMS (ion source). Different masses were separated by a magnetic field, and then measured using a Faraday cup collector array.

As a standard, a number of known reference material were used by Iso-Analytical: IA-R001 (Iso-Analytical working standard flour, $*^{13}C_{VPDB}$ = -26.43 ‰); IAEA-CH-6 (IAEA sucrose standard, $*^{13}C_{VPDB}$ = -10.43 ‰), which is an inter-laboratory comparison standard distributed by the International Atomic Energy Agency (IAEA), and is calibrated against IA-R005 (Iso-Analytical working standard beet sugar standard, $*^{13}C_{VPDB}$ = -26.03). The results were calibrated to the PDB scale.

Carbonate from pedogenically-formed calcium carbonate nodules were also analysed for stable carbon and oxygen isotopes. Samples were collected and powdered from nodules with primary carbonate by a microdrill. Analysis was performed using a Finnigan MAT252 mass spectrometer with automated carbonate preparation device at Cardiff University. Stable isotope results were calibrated to the PDB scale by international standard NBS19.

2.2: LOCALITIES

2.2.1: *Tredomen Quarry*

Located five miles northeast of Brecon, Tredomen Quarry (SO 116304) provides a rare opportunity to study extensive inland outcrops of Old Red Sandstone (Figure 1.2, Chapter 1 and Figure 2.1). With an area of approximately 22,500m^2 and a maximum depth of 14m, it is one of the largest outcrops of Lower Old Red Sandstone strata in southeast Wales. This working quarry, with numerous recent palaeobotanical discoveries (see Chapter 3), trace fossils (fish trails, arthropod trackways and *Beaconites* burrows) (Morrissey et al. 2004) and animal body fossils (cephalapsids and a trigonotarbid) (Dunlop and Selden 2004), provides a unique opportunity for an integrated case study of an early terrestrial ecosystem.

Based on regional geological mapping, the quarry outcrops have been assigned to the St. Maughans Formation (Lochkovian, Lower Devonian) (see Table 1.1, Chapter 1) by the British Geological Survey (Barclay and Wilby 2003). *Beaconites* burrows are present (see Chapter 6), and are known regionally only above the Bishop's Frome Limestone (Morrissey et al. 2004). The Bishop's Frome Limestone is equivalent to the Chapel Point Calcrete in Pembrokeshire, and was previously known as the *Psammosteus* Limestone. This regional

Figure 2.1a: Regional geological map around Tredomen Quarry (taken from BGS sheet 214 Talgarth, scale 1:50000.

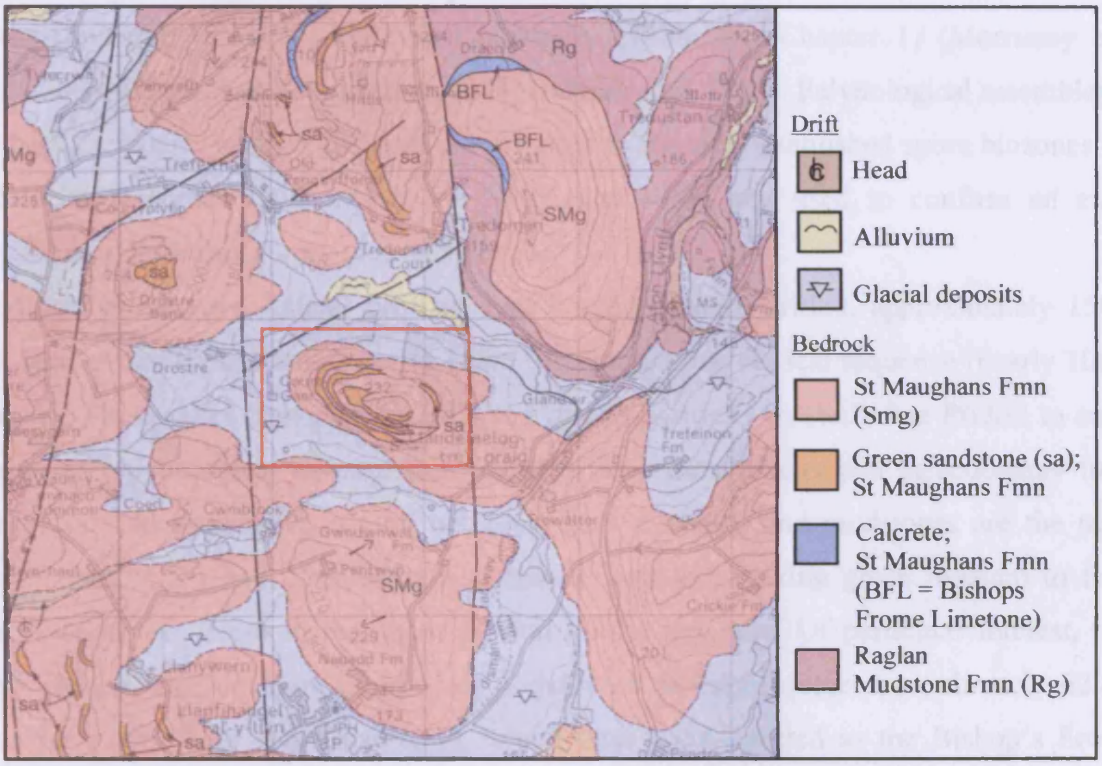

Figure 2.1b: Geological map of Tredomen Quarry - mapped 19.06.06

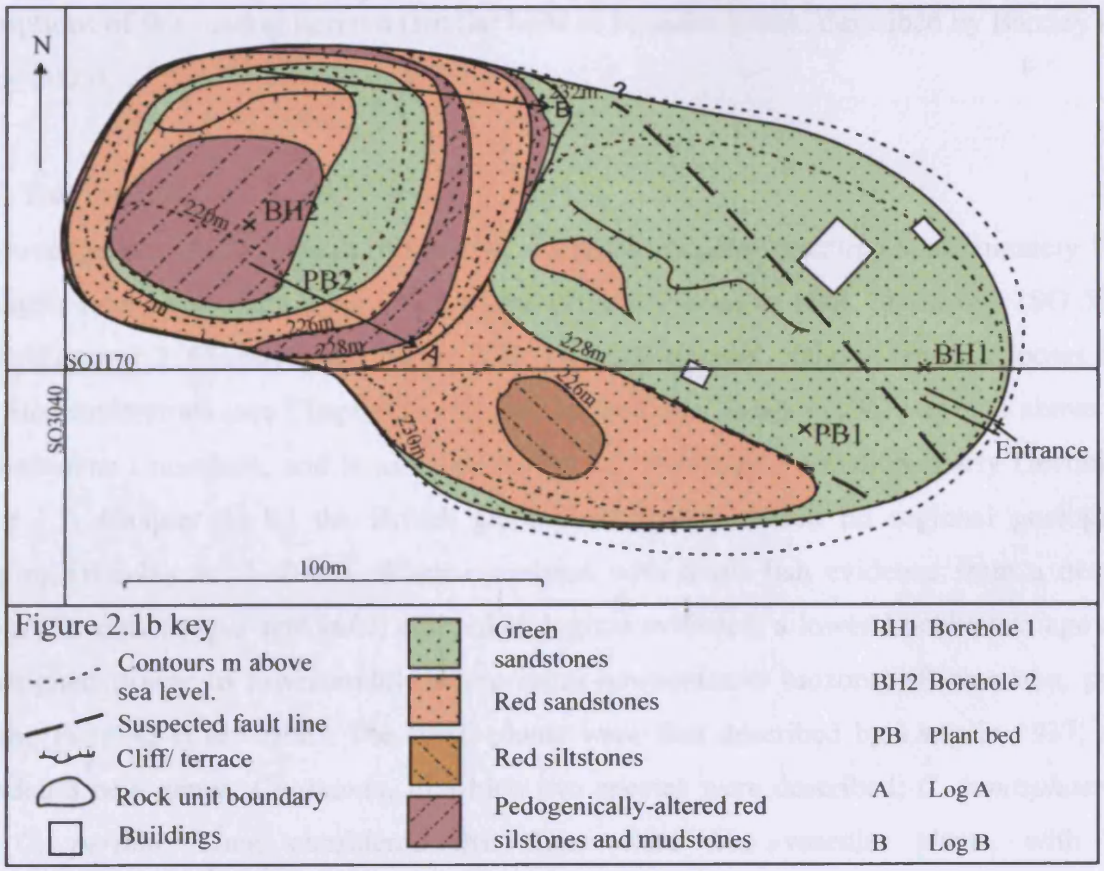

marker horizon separating the Downtonian Raglan Mudstone Formation and the Dittonian St. Maughans Formation in east and southeast Wales occurs approximately 33m above the Silurian-Devonian (Přídolí-Lochkovian) boundary (Table 1.1, Chapter 1) (Morrissey and Braddy 2004, Edwards and Richardson 2004, Barclay et al. 2005). Palynological assemblages from both the quarry surface and core are assigned to the well-established spore biozones for the Silurian-Devonian (Richardson and McGregor 1986) and used to confirm an early Lochkovian age for this quarry (see Chapter 5).

In addition to extensive lateral profiles, two boreholes were drilled, approximately 150m apart, 7cm in diameter, culminating in 118m of a continuous vertical sequence (nearly 100% recovery). These cores provided not only the rare opportunity to study late Přídolí to early Lochkovian palynological assemblages, but also the sedimentology and palaeobotany from an area that lacks extensive natural outcrops. Red siltstones and mudstones are the most common rock types, and often contain carbonate nodules. Striking green medium to fine-grained sandstones occur in the upper portion of the sequence. Of particular interest, two closely spaced, well-developed carbonate nodule-rich horizons occur approximately 62.8m below the quarry floor (see Chapter 6), which have been inferred as the Bishop's Frome Limestone, based on carbonate nodule development, thickness and similarity to regional descriptions of this marker horizon (similar beds in Felindre Brook, described by Barclay and Wilby 2003).

2.2.2: *Targrove Quarry*

Targrove Quarry, 3km northeast of Ludlow, is a small overgrown cutting approximately 10m in height, located on the northern side of the drive to Downton Hall, Shropshire (SO 5254 7799) (Figure 1.2, Chapter 1 and Figure 2.2). This cutting, only 100m in length, exposes Old Red Sandstone strata (see Chapter 5), mapped by Ball and Dineley (1961) as 60m above the *Psammosteus* Limestone, and is assigned to the St. Maughans Formation (Early Devonian, Table 1.1, Chapter 1) by the British Geological Survey, based on regional geological mapping (Barclay et al. 2005). When correlated with fossil fish evidence from a nearby stream (*Taraquairaspis symondsi*) and palynological evidence, a lower Lochkovian age can be assigned (lower to lower-middle *micrornatus-newportensis* biozone) (Richardson, pers. comm., Fanning et al. 1992.) The fossil plants were first described by Lang in 1937, and included a new genus, *Cooksonia*, of which two species were described; *C. hemisphaerica* and *C. pertoni*. Lang considered that these were true vascular plants, with the

Figure 2.2a: Regional geological map around Targrove Quarry (taken from BGS sheet 181, Ludlow, scale 1:50,000)

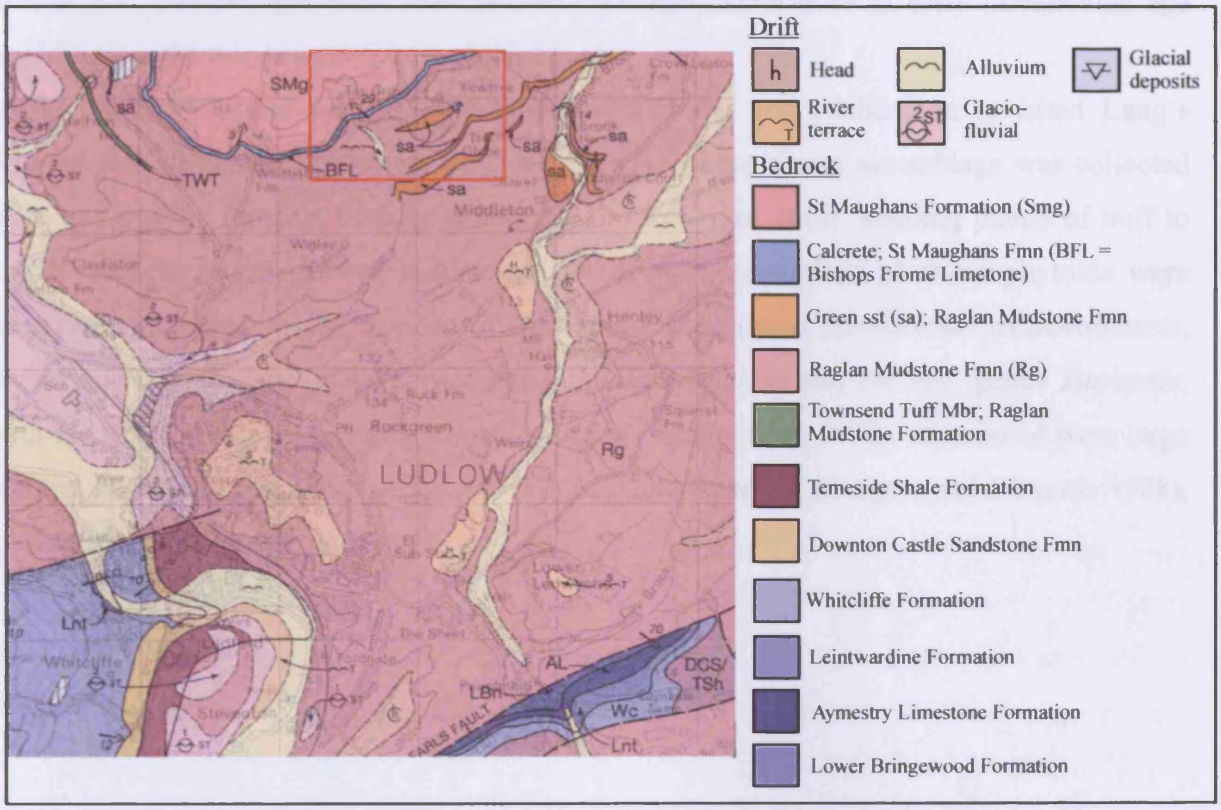

Figure 2.2b: Sketch of main lithological units at Targrove Quarry.

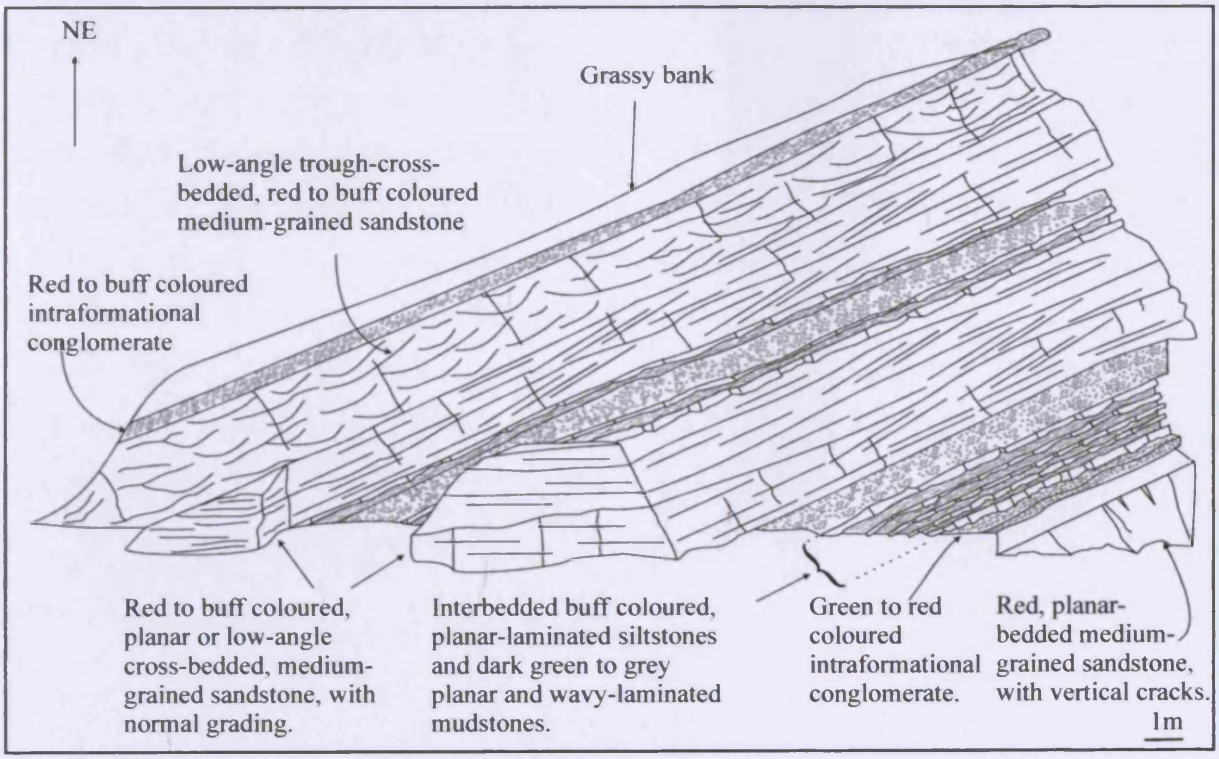

discovery of *in situ* tracheids occurring within an associated axis. This was not confirmed however until 1992, when Edwards et al. discovered *in situ* tracheids within the subtending axis of a *C. pertoni* specimen, from Brown Clee Hill, Shropshire of early Lochkovian age (middle *micrornatus-newportensis* sub-biozone).

In the mid 1980s and early 1990s, Edwards, Fanning and Richardson revisited Lang's original field localities, including Targrove Quarry, where a new assemblage was collected from this prolific locality, both axial and thalloid in nature, from 'bedding planes of buff to green, micaceous fine-grained sandstones'. A diverse assemblage of rhyniophytoids were described, including several species of *Cooksonia*, the minute *Tortilicaulis transwalliensis*, the new species *Salopella marcensis* and *Uskiella reticulata* and the new genus *Tarrantia*, with the type species being *Tarrantia salopensis* (Fanning et al. 1992). Also noted were large amount of thalloid fragments of *Prototaxites* or *Nematasketum* (Burgess and Edwards 1988), *Pachytheca* and *Nematothallus*.

CHAPTER 3 : RECONSTRUCTING VEGETATION FROM OLD RED SANDSTONE STRATA

3.1: INTRODUCTION

The following chapter describes and analyses the palaeobotanical collection from Tredomen Quarry. The fossils were discovered by Keith Jones (Tredomen Quarry Manager) and collected by Dianne Edwards and other members of the Palaeobiology Research Group, Cardiff University. Compressed coalified remains of dichotomously branched axes, some with terminal sporangia were found from a small outcrop on the top surface of the quarry (PB1 in Figure 2.1, Chapter 2). Palynological evidence places Tredomen Quarry strata in the lower Lochkovian, specifically the lower *micrornatus-newportensis* sub-biozone (see assemblage 1, Chapter 5). All fossils in the collection have been recorded and briefly described in a database (Appendix I*a*). A subset of well-preserved fossils were selected for further analysis, and were photographed, prepared by the dégagement method, measured and recorded in spreadsheets (see Appendices II and III). This collection can be split into two main categories, primarily based on size, but also related to the lithofacies in which they were found. Green, trough-cross-bedded sandstones encase well-preserved, fertile megafossils, defined by the minimum height of sporangia reaching at least 1mm. Interbedded with the sandstones, planar to wavy and cross-ripple-laminated green siltstones are packed full of minute-sized dichotomously branched axes, some with sporangia below 1mm in maximum height, and will be referred to as mesofossils. In section 3.2, the megafossils and the previously undescribed mesofossils are systematically described and identified. Section 3.2.3 briefly describes some of the non-embryophytic fossils found within a second plant bed at Tredomen Quarry (PB2, Figure 2.1, Chapter 2), namely *Prototaxites* / *Nematasketum* and *Pachytheca*. Terminology used is illustrated in Figure 3.1. Measurements taken are also illustrated in Figure 3.1 on an example specimen.

Figure 3.1: Terminology and measurements taken for the analysis of megafossils and mesofossils from Tredomen Quarry

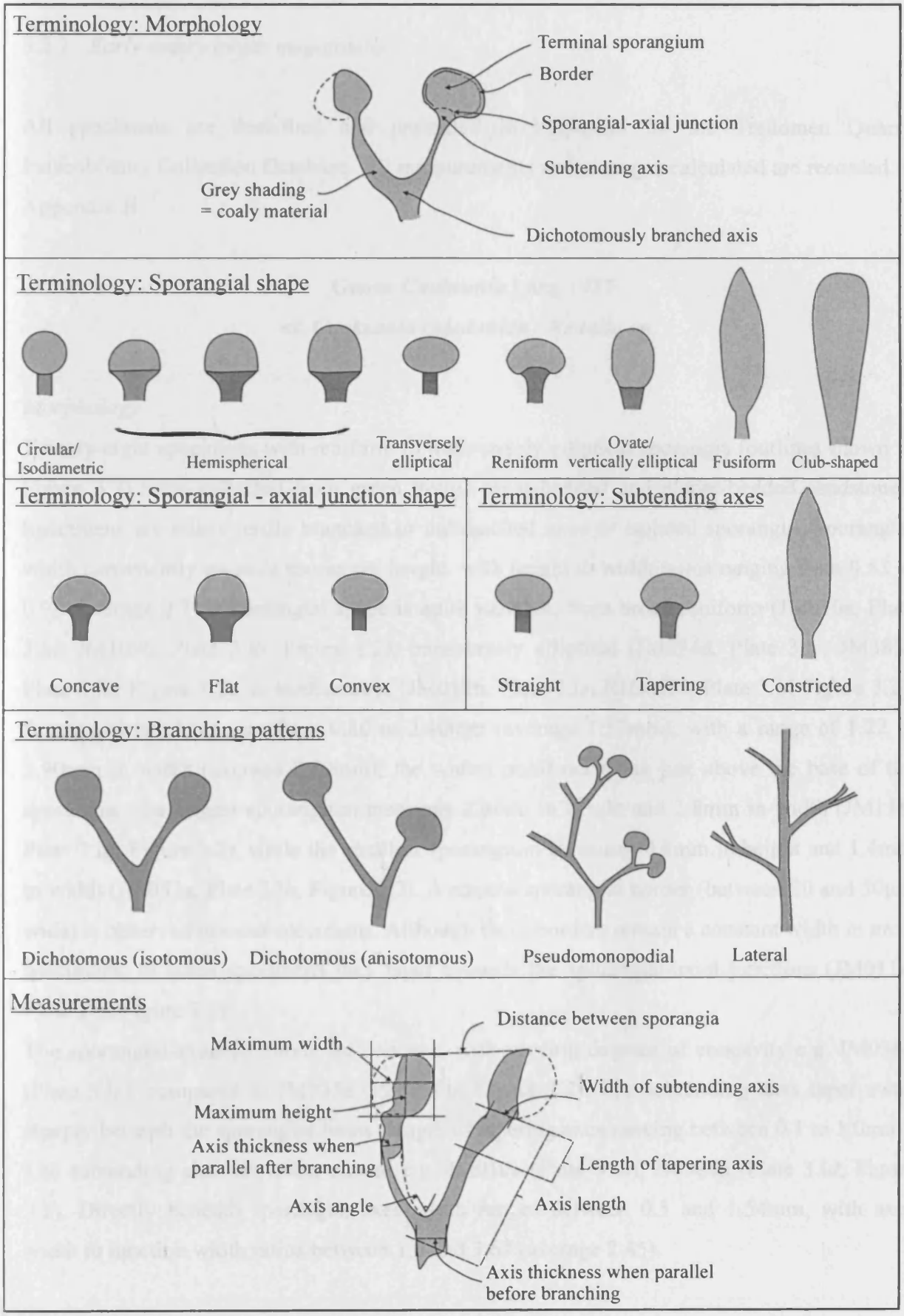

3.2: SYSTEMATIC DESCRIPTIONS

3.2.1: *Early embryophyte megafossils*

All specimens are described and presented in Appendix I*a*, the Tredomen Quarry Palaeobotany Collection Database. All measurements and averages calculated are recorded in Appendix II.

Genus *Cooksonia* Lang 1937

cf. *Cooksonia caledonica / Renalia* sp.

Morphology

Twenty-eight specimens with reniform to transversely elliptical sporangia (outlines shown in Figure 3.2) were collected from green trough-cross-bedded and planar-bedded sandstones. Specimens are either fertile branched or unbranched axes or isolated sporangia. Sporangial width consistently exceeds sporangial height, with height to width ratios ranging from 0.53 to 0.98 (average 0.71). Sporangial shape is quite variable, from broad reniform (JM010a, Plate 3.1*a*; JM109b, Plate 3.1*b*; Figure 3.2), transversely elliptical (JM034d, Plate 3.1*c*; JM385a Plate 3.1*d*; Figure 3.2), to isodiametric (JM012b, Plate 3.1*e*; RHJM04, Plate 3.1*f*; Figure 3.2). Sporangial height ranges from 0.80 to 2.40mm (average 1.57mm), with a range of 1.22 to 2.90mm in width (average 2.20mm), the widest point occurring just above the base of the sporangia. The largest sporangium measures 2.4mm in height and 2.8mm in width (JM118, Plate 3.1*g*; Figure 3.2), while the smallest sporangium measures 0.8mm in height and 1.4mm in width (JM053a, Plate 3.1*h*; Figure 3.2). A narrow sporangial border (between 20 and 50μm wide) is observed in most specimens. Although these borders remain a constant width in most specimens, in some specimens they taper towards the sporangial-axial junctions (JM011a, Plate 3.1*i*; Figure 3.2).

The sporangial-axial junctions are concave, with varying degrees of concavity e.g. JM034d (Plate 3.1*c*), compared to JM035a (Plate 3.1*j*; Figure 3.2). The subtending axes taper away sharply beneath the sporangial bases (length of tapering axes ranging between 0.1 to 1.0mm). The subtending axes are often curved e.g. JM010a (Plate 3.1*a*), JM385a (Plate 3.1*d*; Figure 3.2). Directly beneath sporangia, axes width ranges between 0.5 and 1.54mm, with axes width to junction width ratios between 1.6 and 3.67 (average 2.45).

Figure 3.2: Outlines of cf. *Cooksonia caledonica* specimens from Tredomen Quarry.
Scale bar = 1mm

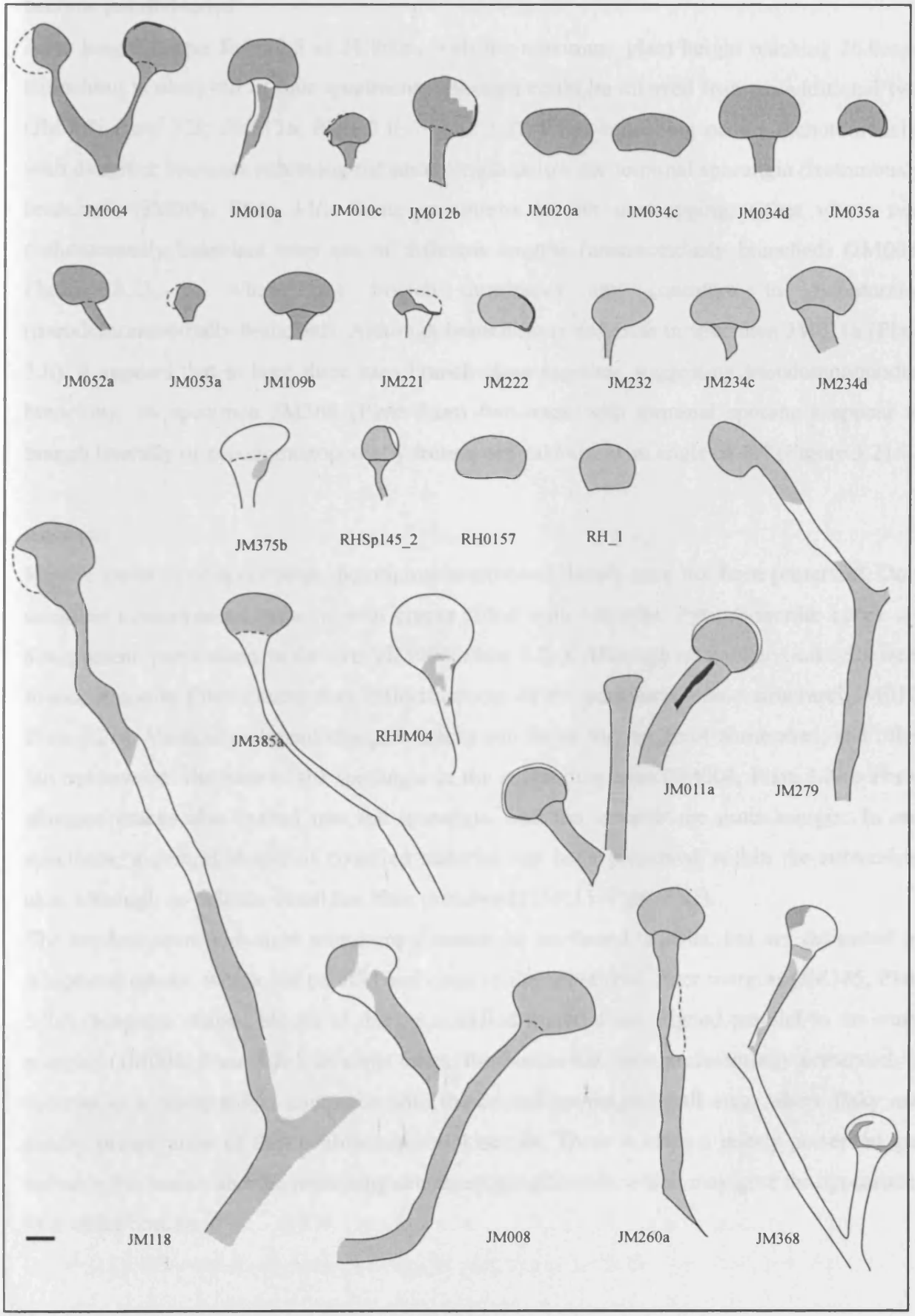

Axes width then tapers to between 0.2 and 1.0mm (average 0.6mm), and eventually axes become parallel-sided.

Axes length ranges from 0.5 to 21.0mm, with the maximum plant height reaching 26.0mm. Branching is observed in four specimens, although could be inferred from an additional two (JM008, Plate 3.1*k*; JM011a, Plate 3.1*i*; Figure 3.2). Some branching occurs dichotomously, with daughter branches achieving the same length below the terminal sporangia (isotomously branched) (JM004, Plate 3.1*l*). Some specimens exhibit overtopping, either where two dichotomously branched axes are of different lengths (anisotomously branched) (JM008, Figure 3.2), or where one branch dominates and continues to dichotomise (pseudomonopodially branched). Although branching is not clear in specimen JM011a (Plate 3.1*i*), it appears that at least three axes branch close together, suggesting pseudomonopodial branching. In specimen JM368 (Plate 3.1*m*) two axes with terminal sporangia appear to branch laterally or pseudomonopodially from a central axis, at an angle of 40° (Figure 3.2).

Anatomy

For the majority of specimens, the original anatomical details have not been preserved. Only coalified compressions remain, with cracks filled with limonite. Pyrite-limonite cubes are also present, particularly in the axes (JM004, Plate 3.2*a*). Although no unequivocal cells were found, limonite filled cracks may reflect aspects of the peripheral tissue structure (JM010, Plate 3.2*b*). Vertically aligned elongate cracks run down the length of some axes, and often fan out towards the base of the sporangia in the subtending axes (JM004, Plate 3.2*a*). These elongate cracks also extend into the sporangia, and fan towards the outer margin. In one specimen, a central strand of coalified material has been preserved within the subtending axis, although no cellular detail has been preserved (JM011, Plate 3.2*c*).

The borders seen with light microscopy cannot be attributed to cells, but are delimited by peripheral cracks, which run parallel and close to the sporangial outer margins (JM385, Plate 3.2*d*). Irregular shaped blocks of thicker coalified material are aligned parallel to the outer margins (JM004, Plate 3.2*e*). In some cases, the border has been preferentially preserved, or appears as a raised ridge, compared with the central sporangial wall area, where flaky and patchy preservation of thin coalified material occurs. There is often a poorly preserved gap between the border and the remaining central sporangial wall, which may give the appearance of a wider border.

A few questionable spores were found on the surface of the coalified material, but as pyritisation has caused distortion, they can only be described as trilete spores with circular ambs, equatorial crassitudes and laevigate proximal exines (JM368, Plate 3.2*f*).

Discussion

As some of these specimens are isotomously branched naked axes terminated by sporangia that are wider than high, they are placed in the genus *Cooksonia* Lang 1937. Within the genus *Cooksonia*, the most similar species is *Cooksonia caledonica*, which was erected by Edwards 1970a, for Dittonian (Lochkovian) impression specimens from Scotland. The latter specimens have dichotomously branched axes at an angle of 55 to 60°, with terminal oval, spherical to reniform sporangia, which possess borders. The sporangial to axial junctions are curved, and the subtending axes tapers away from the base of the sporangia (Plate 3.2*g*) (Edwards 1970a). Despite similarities to *Cooksonia caledonica*, a few Tredomen Quarry specimens show a branching habit that is more complex than simply isotomous, with overtopping and lateral insertion of daughter axes at an angle of around 40°. Similar specimens were discovered from Targrove Quarry, Welsh Borderlands, which is contemporaneous to Tredomen Quarry (Fanning, unpublished thesis 1987, Fanning et al. 1992). The branching habits of the Targrove Quarry specimens were not clear, but suggested more complexity than simply isotomous, and therefore were named cf. *Cooksonia caledonica / Renalia* sp.. Complex branching with reniform sporangia is also observed in *Renalia hueberi* Gensel (1976), from the Emsian Battery Point Formation, Gaspé Bay. Compressions show dichotomously branched daughter axes terminating in reniform sporangia, which are laterally inserted on a main axis (Plate 3.2*h*). Dehiscence was observed along the border, and *in situ* spores were trilete, circular with smooth to granulose ornament.

Similar reniform sporangia with narrow borders, terminating isotomously branched axes, were described by Edwards et al. (2001a), from the Late Silurian Lipeón Formation, southern Bolivia. Like the Tredomen Quarry and Targrove specimens, they are poorly preserved coalified compressions, and do not always show a curved sporangial to axial junction. Additionally, branching angles are larger. These specimens were therefore placed in *Cooksonia* cf. *caledonica* (Edwards et al. 2001a).

Other species with reniform, bivalved sporangia have been described from the middle Dittonian (Lochkovian) Welsh Borderlands, where exceptionally preserved specimens allowed for detailed anatomical descriptions and spore identification. *Resilitheca salopensis* Edwards et al. (1995a) has been described as being synonymous with *Cooksonia caledonica*.

A number of reniform isolated sporangia exhibit dehiscence along the distal margin, but do not possess a thick border, although this may be due to a preservational loss. *In situ* spores closely resemble *Apiculiretusispora*. Additionally, the species *Sporathylacium salopense* Edwards et al. (2001b) describes isolated, bivalved, circular to elliptical sporangia, with multilayered sporangial walls and borders at least 160μm wide. However, *in situ* spores have an equatorial crassitude unlike those seen in *Resilitheca salopensis* or *Renalia* sp. (Edwards et al. 2001b).

As the majority of the Tredomen Quarry specimens are poorly preserved compressions of isolated sporangia, it is not possible to come to a conclusion on typical branching habit and therefore to assign a definite species name. Little anatomical information has been preserved, no spores were extracted and dehiscence has not been observed, although the border may indicate the presence of cells adapted for dehiscence along the distal margin. The Tredomen Quarry specimens can therefore be known only as cf. *Cooksonia caledonica/ Renalia* sp.

Cooksonia hemisphaerica Lang 1937

Morphology

One hundred and twenty-three coalified compressions of dichotomously branched and unbranched naked axes, terminating in sporangia of variable shape, were found in green, trough-cross-bedded sandstones. Sporangia are variable in shape from hemispherical, circular to vertically elliptical (examples of the variety of sporangial shape and size are shown in the outlines of Figure 3.3). Height to width ratio ranges from 0.75 to 1.5 (average 1.05), with the majority of sporangia hemispherical in shape (e.g. JM367, Plate 3.3*a*; JM133a, Plate 3.3*b*; and RH015, Plate 3.3*c*), with a few isodiametric (e.g. JM228a, Plate 3.3*d* and JM112a, Plate 3.3*e*), and some sporangia where height slightly exceeds width (e.g. JM374, Plate 3.3*f*). Hemispherical sporangia have rounded or flattened apices (e.g. JM121c, Plate 3.3*g*), with maximum width in the top third of the sporangia. Circular and elliptical sporangia have a maximum width at mid-length (e.g. JM121b, Plate 3.3*h*). Sporangial height ranges from 0.89mm to 2.8mm (average 1.86mm), while width ranges from 0.7mm to 3.1mm (average 1.79mm). The largest sporangium measures 2.8mm in height and 2.6mm in width (JM312b, Plate 3.3*i*).

The peripheral margins of the sporangia are slightly raised in some specimens, whilst in others it often is the only coalified material remaining, which may reflect the presence of a

Figure 3.3: Outlines of *Cooksonia hemisphaerica* specimens from Tredomen Quarry.
Scale bar = 1mm

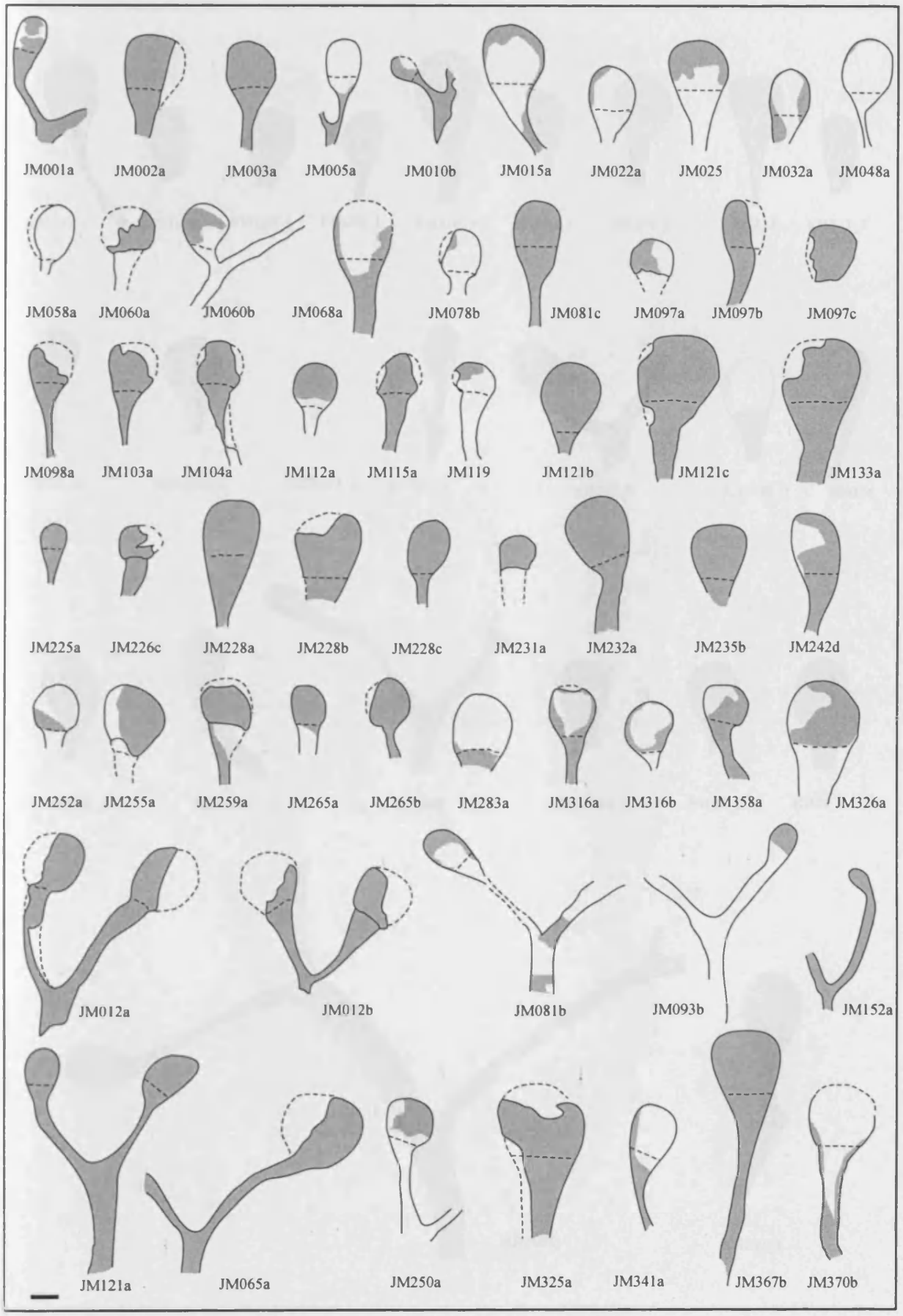

Figure 3.3: Outlines of *Cooksonia hemisphaerica* specimens from Tredomen Quarry (continued). Scale bar = 1mm

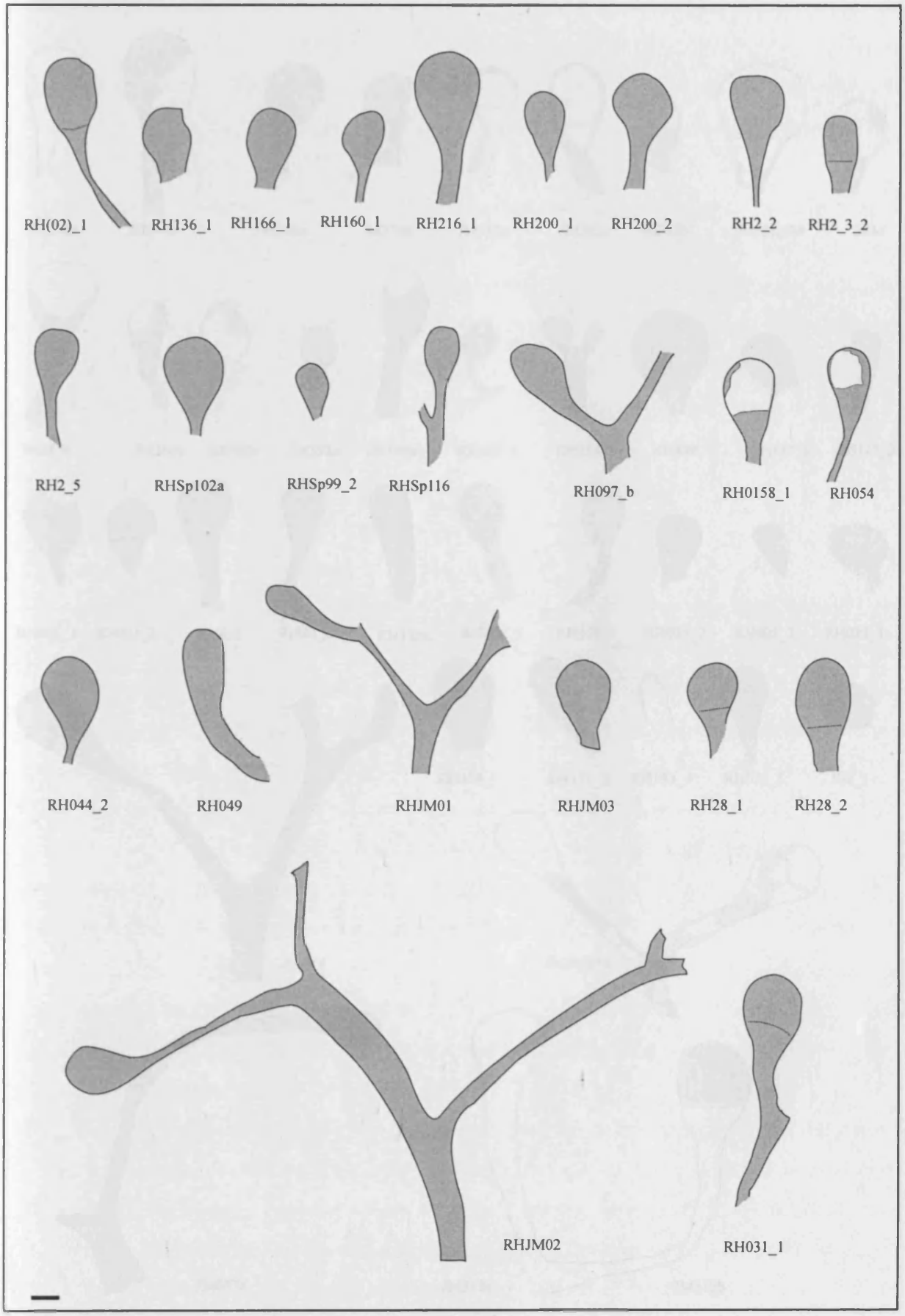

Figure 3.3: Outlines of *Cooksonia hemisphaerica* specimens from Tredomen Quarry. (continued). Scale bar = 1mm

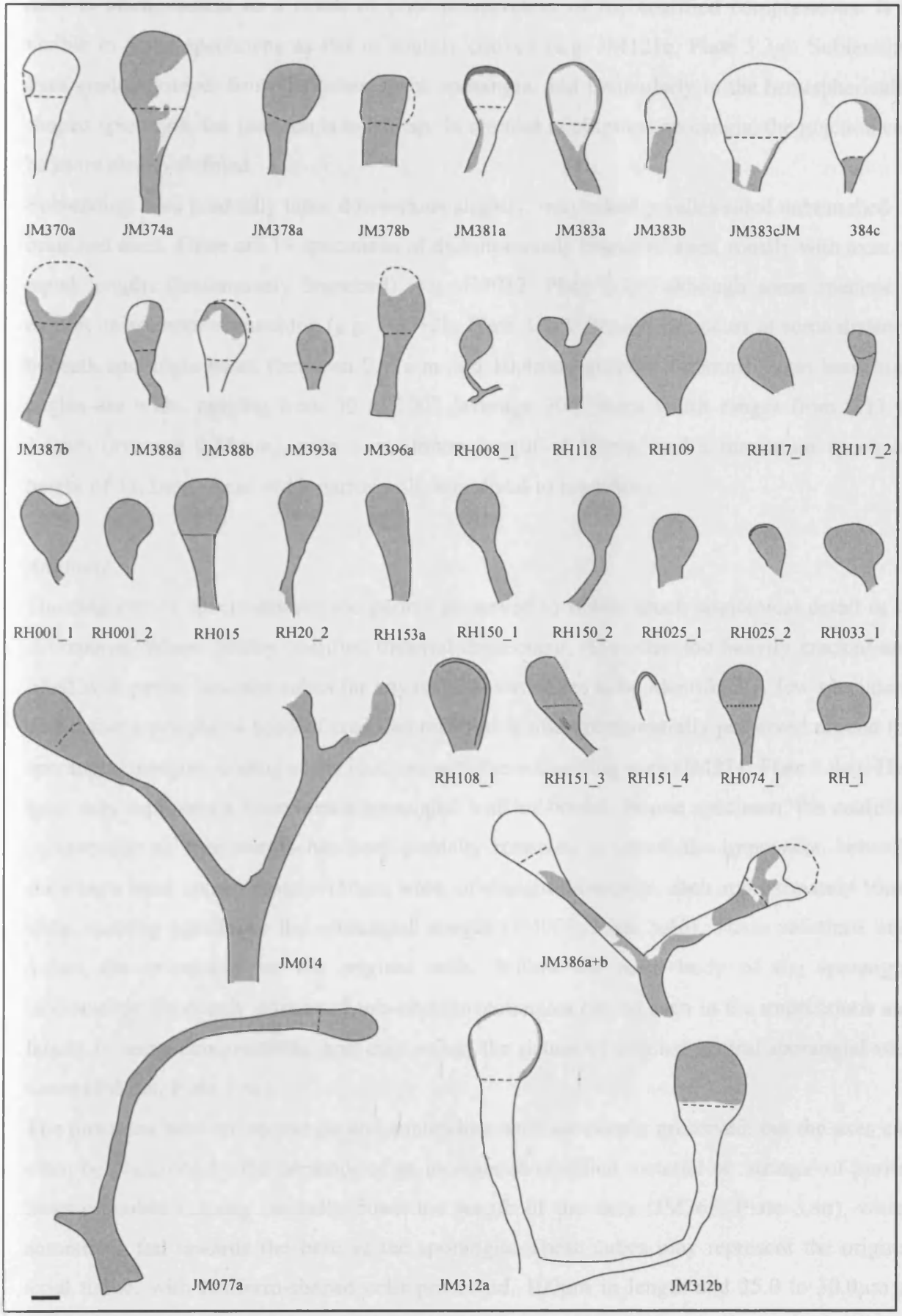

narrow border (e.g. JM374, Plate 3.3*f*). The junction between sporangia and the subtending axes is often unclear as a result of poor preservation of the coalified compressions. It is visible in some specimens as flat to slightly convex (e.g. JM121c, Plate 3.3*g*). Subtending axes gradually taper from the bases of the sporangia, and particularly in the hemispherically shaped sporangia, the junction is indistinct. In circular to elliptical sporangia, the junction can be more clearly defined.

Subtending axes gradually taper downwards slightly, into naked parallel-sided unbranched or branched axes. There are 19 specimens of dichotomously branched axes, mostly with axes of equal lengths (isotomously branched) (e.g. JM012, Plate 3.3*j*), although some specimens exhibit anisotomous branching (e.g. JM312b, Plate 3.3*k*). Branching occurs at some distance beneath sporangia bases (between 0.67mm and 10.4mm, average 4.05mm). Axes branching angles are wide, ranging from 30 to 100° (average 70°). Axes width ranges from 0.13 to 1.4mm (average 0.58mm), with a maximum length of 16mm, and a maximum specimen height of 11.2mm. Axis width narrows slightly distal to branching.

Anatomy

The majority of specimens are too poorly preserved to obtain much anatomical detail or *in situ* spores. Where patchy coalified material does occur, it is often too heavily cracked and filled with pyrite-limonite cubes for any original structures to be identified. A few specimens reveal that a peripheral band of coalified material is often preferentially preserved around the sporangial margins, ending at the junction with the subtending axes (JM374, Plate 3.4*a*). This band may represent a compressed sporangial wall or border. In one specimen, the coalified compression of this margin has been partially removed to reveal the impression beneath, showing a band approximately 150μm wide, of elongate striations, each approximately 10μm wide, running parallel to the sporangial margin (JM003, Plate 3.4*b*). These striations may reflect the orientation of the original cells. Within the main body of the sporangia, isodiametric, randomly orientated sub-circular rectangles can be seen in the impressions and faintly in some compressions, and may reflect the nature of original central sporangial wall tissue (JM020, Plate 3.4*c*).

The junctions between sporangia and subtending axes are poorly preserved, but the axes can often be discerned by the presence of an increase in coalified material or 'strings' of pyrite-limonite cubes running centrally down the length of the axes (JM367, Plate 3.4*d*), which sometimes fan towards the base of the sporangia. These cubes may represent the original axial tissue, with fusiform-shaped cells preserved, 100μm in length and 25.0 to 30.0μm at

maximum width. These crystals are rare within the sporangia, but where they do occur, larger crystals are randomly orientated.

Discussion

These specimens most closely resemble *Cooksonia hemisphaerica*; a species erected by Lang in 1937 for smooth, dichotomously branched naked axes, gradually thickening towards terminal, hemispherical sporangia, with flat sporangial-axial junctions. In Lang's specimens from Targrove Quarry, Shropshire (lower Lochkovian), sporangia width slightly exceeds sporangia height. An investigation into a larger collection of *Cooksonia hemisphaerica* from the same locality, Fanning et al. (1992) revealed that sporangia shape and size range is quite variable (from hemispherical, spherical to elliptical in shape and from 0.68 to 2.08mm in height, and 0.83 to 3.25mm in width). It was also observed that in some sporangia height exceeds width, but never more than 1.5 times. These differences were noted by Edwards (1979) for *Cooksonia hemisphaerica* specimens from Freshwater West, Pembrokeshire (lower Přídolí).

The Tredomen Quarry specimens are similar, with variable sporangial shape and a large size range. The maximum sporangial height (2.8mm) exceeds that of the known ranges (2.08mm), but this may be a result of the poor preservation of sporangial to axial junctions, and therefore undistinguishable sporangia bases. Like the Targrove Quarry specimens, sporangial height to width ratios never exceeds 1.5.

Fanning et al. (1992) describes a narrow peripheral band around the margin of the *Cooksonia hemisphaerica* sporangia, which tapers towards the base and may represent a compressed sporangia wall, which is also seen in some of the Tredomen Quarry specimens. This marginal band surrounds a central zone of isodiametric cells of the central sporangial wall. Although no unequivocal anatomical evidence can be taken from these specimens, the presence of elongate, cell-like striations parallel to the margin, and the preferential preservation of this marginal band, suggests that these cells differ from those in the central wall zone. These cells may have been adapted for dehiscence, which has been observed to occur marginally into two valves from the Targrove Quarry specimens (Fanning et al. 1992). Unfortunately no spores were extracted from the Tredomen Quarry specimens for comparison.

Fanning et al. (1992) describe the Targrove Quarry specimens as isotomously branched axes, with no indication of a more complex branching pattern for *Cooksonia hemisphaerica*. This is also the case with most Tredomen Quarry specimens, with axes branching at similar angles (45 to 100°) at some distance from the sporangia bases. There is however some evidence of anistomous branching in the Tredomen Quarry specimens.

Lang (1937) and Fanning et al. (1992) both noted the presence of central strands running down the axes of *Cooksonia hemisphaerica*, but no tracheids have been discovered in fertile axes. The fusiform-shaped and string-like nature of the pyrite-limonite cubes seen in some of the Tredomen Quarry specimens suggest the presence of vascular tissue, where after burial, pyrite precipitation occurred.

An investigation into previous assigned *Cooksonia* sp. (Croft and Lang 1942) specimens with sporangia that are greater in height than width, resulted in the formation of the genus *Uskiella*, for isotomously branched axes with elongate ellipsoidal sporangia that "split longitudinally around the longest dimension into two valves", with a height to width ratio no more than 2 (Shute and Edwards 1989). The type species *Uskiella spargens* is based on detailed information on the sporangial wall organisation, particularly the presence of diamond-shaped cells in the peripheral wall, plus a significant border, which is not seen in these Tredomen Quarry specimens. The sporangia of *Uskiella spargens* are described as oval in shape, with the maximum width at mid-length, compared with the top-third of the sporangia often seen in *Cooksonia hemisphaerica.*

Fanning et al. (1992) introduced a second species to the genus, *Uskiella reticulata*, describing isotomously branched axes, with parallel-sided subtending axes and terminal, vertically elongate, ellipsoidal sporangia, but possessing a prominent reticulate texture, representing thick isodiametric cells of the peripheral sporangial wall, not present in the Tredomen Quarry specimens.

The sporangia from Tredomen Quarry, that have height: width ratios between 1.01 and 1.5 and do not have any features similar to *Uskiella*, have been placed (with similar specimens that have a height: width ratio below 1) in the species *Cooksonia hemisphaerica.*

Cooksonia* cf. *cambrensis

Morphology

Seven poorly preserved specimens of circular to transversely ellipsoidal sporangia terminating parallel-sided, naked unbranching axes, similar to *Cooksonia hemisphaerica,* were discovered from the green trough-cross-bedded sandstones (see Figure 3.4). Unlike *Cooksonia hemisphaerica*, subtending axes do not taper significantly, and sporangial-axial junctions are not flat. These sporangia are circular (JM235a, Plate 3.5*a*; JM372c, Plate 3.5*b*) to transversely elliptical (RH045, Plate 3.5*c*; JMRH0188_1, Plate 3.5*d*), with sporangial height to width ratios ranging from 0.74 to 1.00 (average 0.9). Sporangial size range is

Figure 3.4: Outlines of *Cooksonia* cf. *cambrensis* specimens from Tredomen Quarry. Scale bar = 1mm

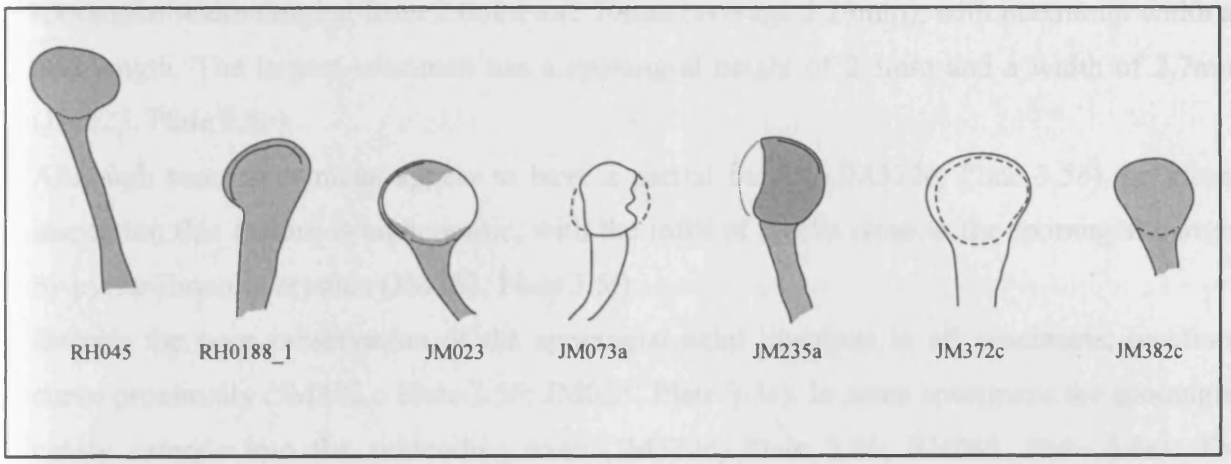

narrow, with sporangial height ranging from 1.68 to 2.40mm (average 2.04mm) and sporangial width ranging from 2.0mm to 2.70mm (average 2.29mm), with maximum width at mid-length. The largest specimen has a sporangial height of 2.3mm and a width of 2.7mm (JM023, Plate 3.5*e*).

Although some specimens appear to have a partial border (JM372c, Plate 3.5*b*), on closer inspection this feature is taphonomic, with the infill of cracks close to the sporangial margin by pyrite-limonite crystals (JM382, Plate 3.5*f*).

Despite the poor preservation of the sporangial-axial junctions in all specimens, junctions curve proximally (JM372,c Plate 3.5*b*; JM023, Plate 3.5*e*). In some specimens the sporangial cavity extends into the subtending axes (JM372c, Plate 3.5*b*; RH045, Plate 3.5*c*). The subtending axes range in width from 0.60 to 1.40mm (average of 1.00mm), and either taper slightly (maximum taper length of 0.8mm) to become parallel-sided, ranging in width from 0.55 to 1.00mm (average 0.70mm) (RH045, Plate 3.5*c*).

Discussion

Cooksonia cambrensis was erected by Edwards (1979), for isotomously branched axes with circular (forma α) to transversely ellipsoidal (forma β) terminal sporangia, with parallel-sided to slightly tapering subtending axes. The Tredomen Quarry specimens may be considered to be *Cooksonia cambrensis* based on sporangia gross morphology, particularly the lack of extensive sporangial-axial junctions, with little or no tapering of the subtending axes. However, all Tredomen Quarry sporangia specimens are larger (average of 2.05mm in height and 2.29mm in width) than the type specimens of *Cooksonia cambrensis* (that do not exceed more than 1.3mm in height and 1.7mm in width), and subsequent examples from other localities (Fanning 1987, Fanning et al. 1992).

The extension of the sporangial cavity into the subtending axis has not previously been observed from *Cooksonia cambrensis*, but is one of the diagnostic features of *Cooksonia banksii* (Habgood et al. 2002). The sporangia of *Cooksonia banksii* however are more discoidal in shape than typical for *Cooksonia cambrensis*, and are not often found in compression. Another species with a sunken sporangium is *Cooksonia paranensis* (Gerrienne et al. 2001), from lower Lochkovian strata of the Paraná Basin, Brazil. However, *C. paranensis* possess distinctive plate or bowl-shaped sporangia, with a gradually tapering subtending axis, and no clear sporangial-axial junction. The Tredomen Quarry specimens possess sporangia that are more globular in shape, with rounded tops. Due to poor preservation no information regarding anatomy or branching habit of these megafossils could

be obtained, and limits the assignment of these circular sporangia to *Cooksonia* cf. *cambrensis*.

Terminal sporangia incertae sedis

cf. *Uskiella reticulata / Tarrantia salopensis* Fanning et al. 1992

Morphology

Thirty-one specimens of unbranched and branched axes with vertically ovate to circular terminal sporangia that are consistently greater in height than width were discovered in green fine-grained sandstones and siltstones (outlines shown in Figure 3.5). Specimens are sporangia with subtending axes, with three specimens exhibiting branching (JM279a, Plate 3.6*a*; JM013d, Plate 3.6*b*; RHSp110, Plate 3.6*g*). Despite some sporangia being isodiametric (JM013b, Plate 3.6*c*), in most cases sporangial height exceeds width (average height to width ratio 1.37) (JM006a, Plate 3.6*d*; JM111a, Plate 3.6*e*). Only one specimen exhibits a height that exceeds twice the width (JM390a, Plate 3.6*f*). Sporangial height ranges from 1.13 to 3.6mm (average 2.31mm), and the width ranges from 1.0 to 2.7mm (average 1.73mm). The largest sporangium measures 3.6mm in height and 2.7mm in width (RHSp110, Plate 3.6*g*). Sporangia shape ranges from vertically elliptical with parallel sides (JM279a, Plate 3.6*h*) or slightly tapering apices (JM092, Plate 3.6*i*) to circular (JM013b, Plate 3.6*c*). Maximum width always occurs at mid-height.

In light microscopy, most specimens appear to show smooth, peripheral zones or borders around the margin of the sporangia, that remain a constant width (~50μm) (RH008_2, Plate 3.6*j*), and ends at the junction with the subtending axes and are often more compressed compared with the central sporangial wall. In some specimens, these central areas appear to have a granular or reticulate appearance (JM328a, Plate 3.6*k*).

Although the sporangial-axial junctions are unclear, the bases of the sporangia are clearly marked by a sudden decrease in width into the subtending axes. The subtending axes widen towards sporangia bases (JM013d, Plate 3.6*l*), or are parallel-sided. Axes width ranges from 0.2 to 1.30mm (average 0.54mm) and, where dichotomous branching occurs, axes width increases before branching and decreases equally after branching, between an angle of 45 to 80°. Branching in specimen JM279a indicates at least two anisotomous dichotomies (Plate 3.6*a*). The largest specimen, at 11.4mm in height (RHSp110, Plate 3.6*g*) exhibits pseudomonopodial branching with at least four dichotomies.

Figure 3.5: Outlines of cf. *Uskiella reticulata / Tarrantia salopensis* specimens from Tredomen Quarry. Scale bar = 1mm

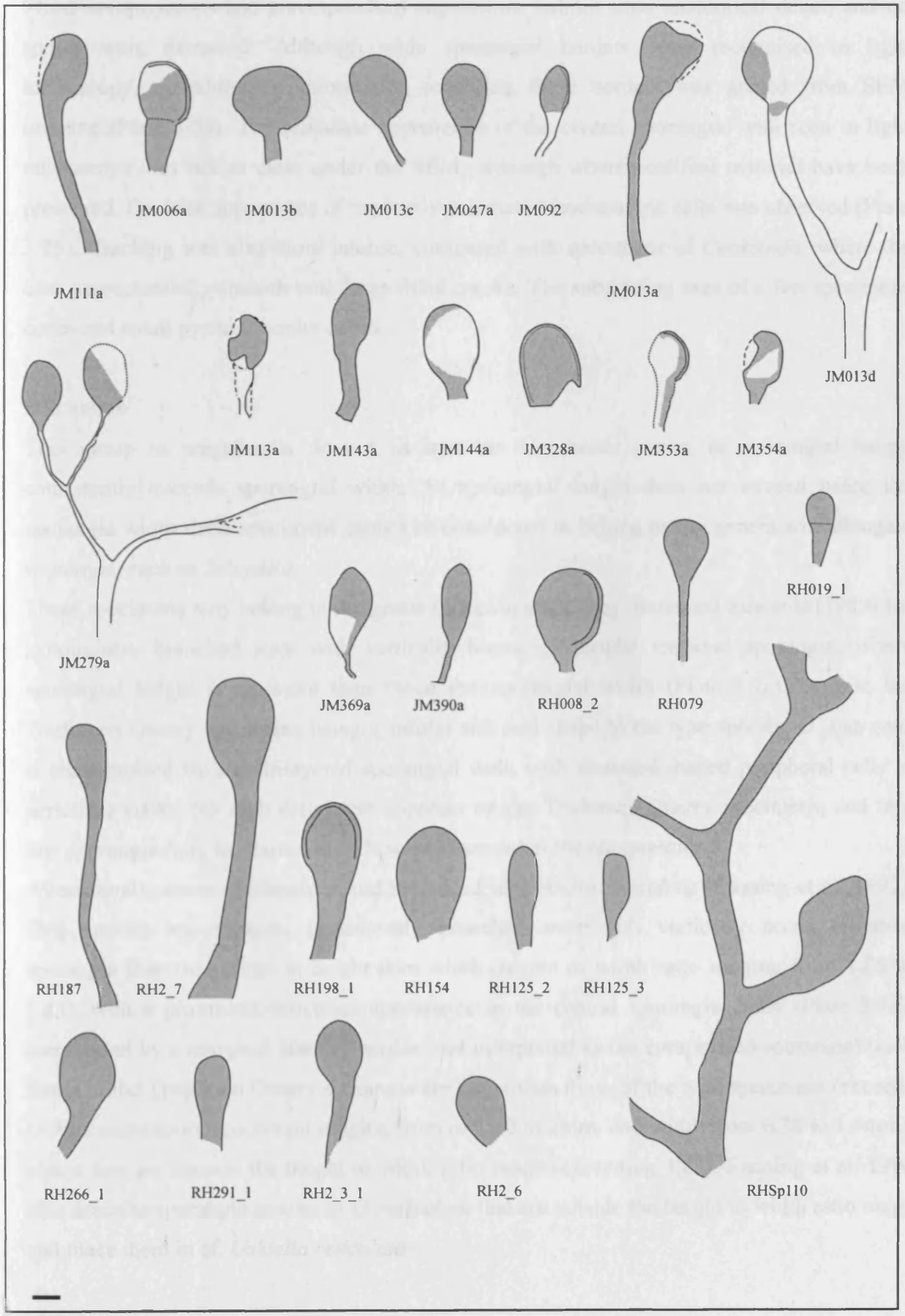

Anatomy

These compressions and corresponding impressions exhibit little anatomical detail, and no spores were extracted. Although wide sporangial borders were recognised in light microscopy, no additional information regarding these borders was gained from SEM imaging (Plate 3.7*a*). The reticulate appearance of the central sporangial wall seen in light microscopy was not as clear under the SEM, although where coalified material have been preserved, the faint appearance of randomly-orientated isodiametric cells was observed (Plate 3.7*b*). Cracking was also more intense, compared with specimens of *Cooksonia,* where the coal was essentially smooth with large filled cracks. The subtending axes of a few specimens contained small pyrite-limonite cubes.

Discussion

This group of megafossils do not fit into the *Cooksonia* genus, as sporangial height consistently exceeds sporangial width. As sporangial height does not exceed twice the sporangia width these specimens cannot be considered to belong to any genera with elongate sporangia, such as *Salopella.*

These specimens may belong to the genus *Uskiella*, erected by Shute and Edwards (1989) for isotomously branched axes with vertically borne, ellipsoidal terminal sporangia, where sporangial height is no more than twice the sporangial width (Plate 3.7*c*). Despite the Tredomen Quarry specimens being a similar size and shape to the type species, *U. spargens* is characterised by a multilayered sporangial wall, with diamond-shaped peripheral cells in periclinal view. No such cells were apparent on the Tredomen Quarry specimens, and in a few sporangia faint isodiametric cells were observed in the compression.

Alternatively, some specimens could be placed in *Uskiella reticulata* (Fanning et al. 1992). This species encompasses isotomously branched axes with vertically borne elliptical sporangia that are greater in height than width (height to width ratio ranging from 1.25 to 1.83), with a prominent reticulate appearance in the central sporangial body (Plate 3.7*d*), surrounded by a marginal zone or border, and interpreted as the compressed sporangial wall. Some of the Tredomen Quarry sporangia are larger than those of the type specimens (exceeds *U. reticulata* sporangia height ranging from of 1.50 to 2mm, and width from 0.38 to 1.5mm), plus a few are outside the height to width ratio range (exceeding 1.83). Fanning et al. 1992 also describe sporangia similar to *U. reticulata* that are outside the height to width ratio range and place them in cf. *Uskiella reticulata.*

Fanning et al. 1992 describe specimens similar to *Uskiella reticulata* from Targrove Quarry, as vertically borne, elliptical to ovate sporangia with parallel-sided subtending axes, and a sporangial height to width ratio from 1.3 to 2, with sporangial height ranging from 0.38 to 2.63mm (Plate 3.7*e*). Although the central areas of the sporangia walls have been described as differentiated from a marginal peripheral zone, the lack of a reticulate or granular texture to the sporangial walls as observed in *Uskiella*, resulted in the formation of a new genus, *Tarrantia* Fanning et al. (1992). The sporangia of the type species *Tarrantia salopensis* Fanning et al. (1992), essentially have a very similar basic morphology to those of *Uskiella reticulata*, and therefore some of the Tredomen Quarry specimens may be better placed in *Tarrantia salopensis*.

As these Tredomen Quarry specimens do not have sporangial walls with reticulate textures, and show a range of sizes and shapes, some with greater height: width ratios, these specimens shall only be considered as cf. *Uskiella reticulata/ Tarrantia salopensis*, mainly as a result of poor preservation. It must also be noted that the branching habits of the Tredomen Quarry specimens are more complex that *Uskiella reticulata* and *Tarrantia salopensis*, with pseudomonopodially and anisotomously branched terminal axes.

Genus *Salopella* Edwards and Richardson 1974

Salopella allenii Edwards and Richardson 1974

Morphology

Eighteen coalified compressions of large elongate sporangia either attached to, or in association with fragmentary wide unbranched and branched axes (outlines shown in Figure 3.6) were recovered from green trough-cross-bedded sandstones. Terminal sporangia are elongate and fusiform in shape, with tapering apices (JM005b, Plate 3.8*a*), and a range of tip morphologies from pointed, blunt, rounded or extended to globular tips (JM006a, Plate 3.8*b*; JM007a, Plate 3.8*c*; JM005b, Plate 3.8*d*). Sporangial height ranges from 4.0mm to 11.9mm (average 9.24mm), while width ranges from 1.0mm to 3.14mm (average 2.45mm). The largest sporangium is 11.19mm in height and 3.14mm in width (RHSp151_1, Plate 3.8*e*), while the smallest measures 4.0mm in height and 1.0mm in width (JM060c). Sporangial width is at least a third of height, with height to width ratio ranging from 3.14 to 4.5 (average 3.82). Maximum width occurs approximately at mid-length.

Figure 3.6: Outlines of *Salopella allenii* specimens from Tredomen Quarry. Scale bar = 1mm

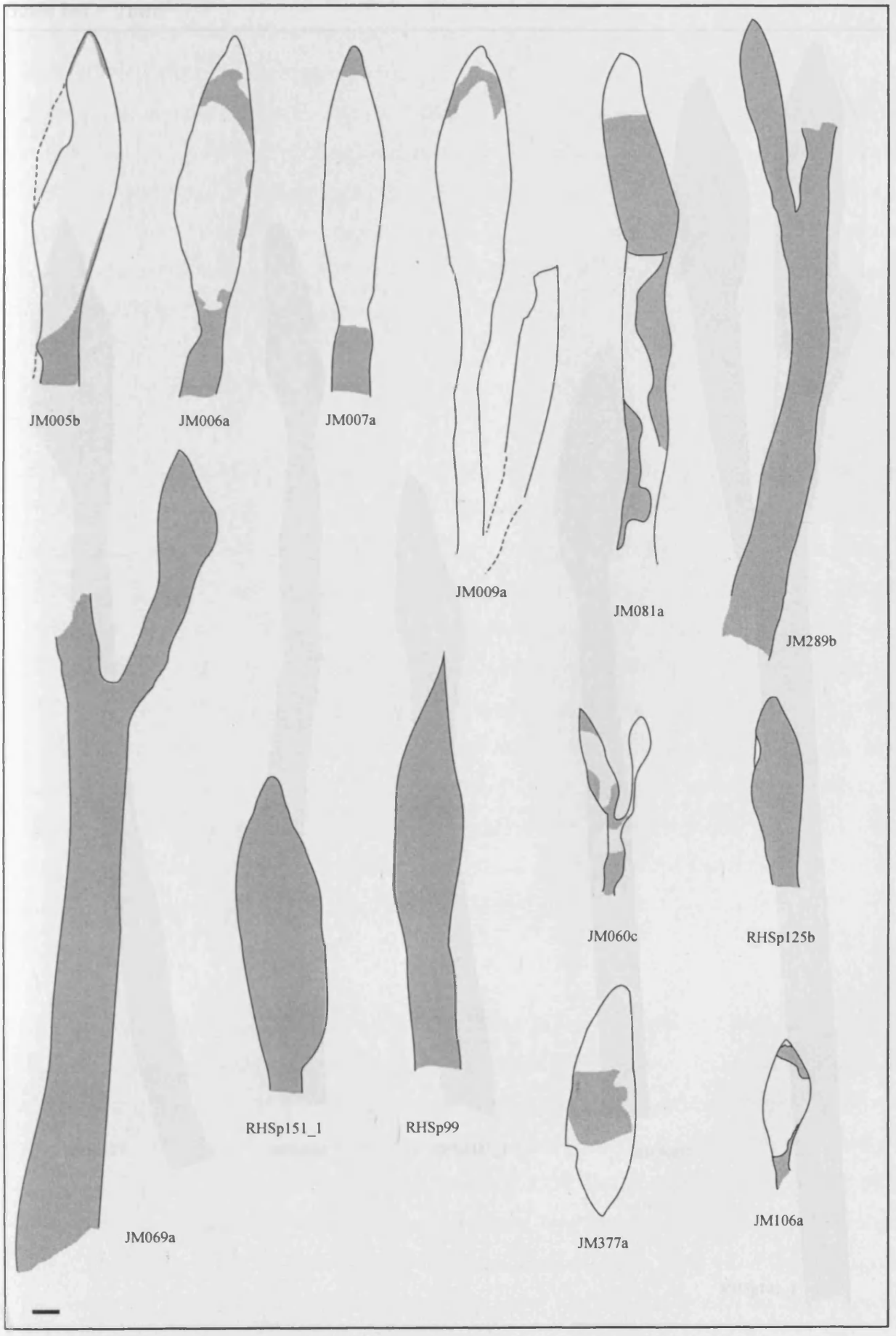

Figure 3.6: Outlines of *Salopella allenii* specimens from Tredomen Quarry (continued). Scale bar = 1mm

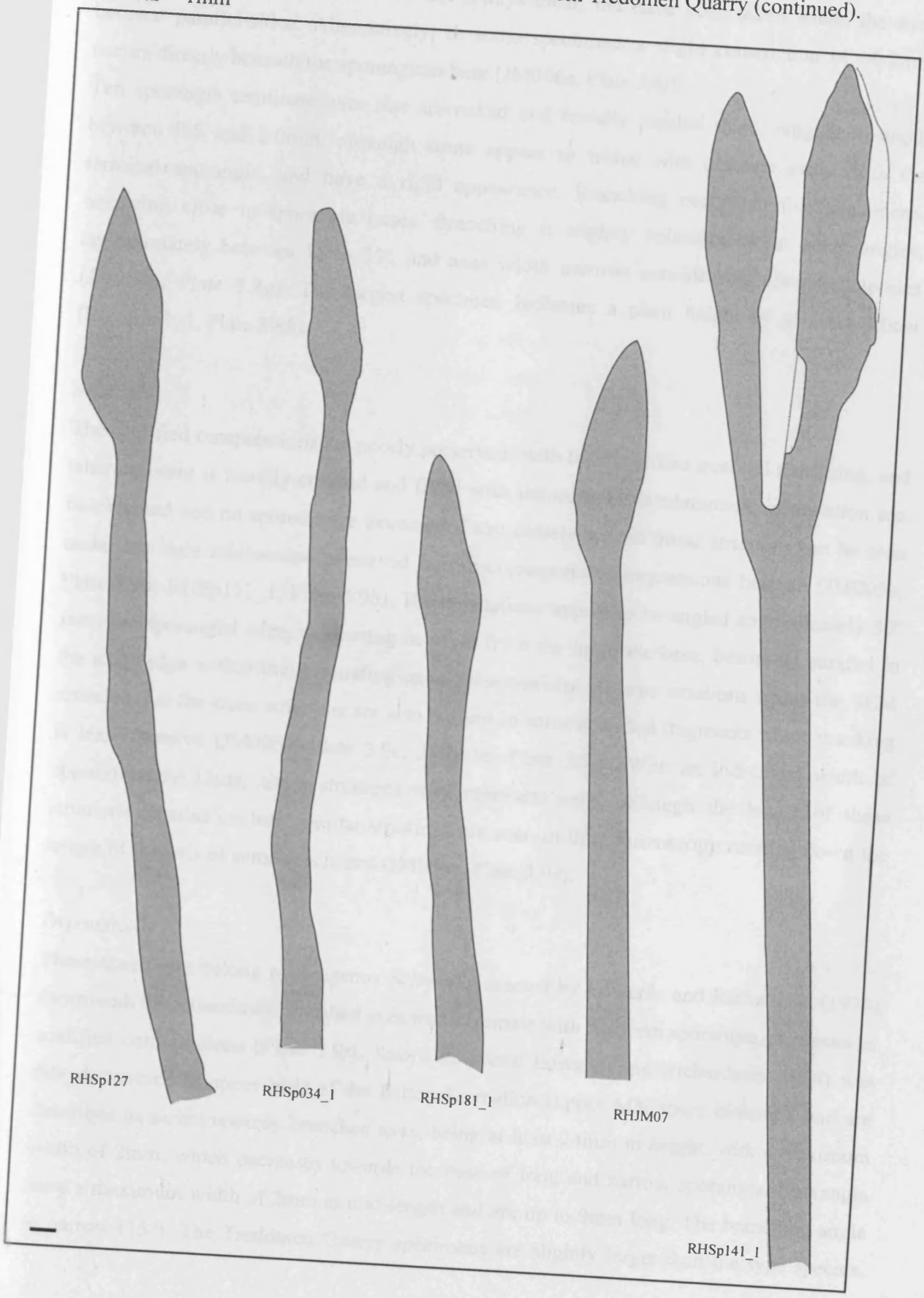

The sporangial-axial junctions are not always clear, but have been taken where the axes become parallel-sided. Alternatively, in some specimens a slight constriction of ~0.2mm occurs directly beneath the sporangium base (JM006a, Plate 3.8*f*).

Ten sporangia terminate axes that are naked and broadly parallel-sided, ranging in width between 0.5 and 2.0mm, although some appear to widen with distance away from the terminal sporangia, and have a rigid appearance. Branching occurs in five specimens, occurring close to sporangia bases. Branching is slightly anisotomous, at acute angles, approximately between 15 to 35°, and axes width narrows considerably after dichotomies (JM289b, Plate 3.8*g*). The largest specimen indicates a plant height of at least 6.0cm (RHSp141_1, Plate 3.8*h*).

Anatomy

The coalified compressions are poorly preserved, with little coalified material remaining, and where present is heavily cracked and filled with limonite. Little anatomical information can be obtained and no spores were extracted. Faint closely spaced linear striations can be seen under the light microscope preserved on the corresponding impressions beneath (JM005b, Plate 3.9*a*; RHSp151_1, Plate 3.9*b*). These striations appear to be angled approximately 30° from the sporangial edge, decreasing in angle from the tip to the base, becoming parallel to the axial edge within the subtending axes. Observations of these striations under the SEM revealed that the same striations are also present in some coalified fragments where cracking is less intensive (JM006a, Plate 3.9c; JM005b, Plate 3.9*d*). With an individual width of approximately 15μm, these striations may represent cells, although the length of these striations remains unclear. Similar striations are seen in light microscopy running down the length of the axis of some specimens (JM006a, Plate 3.9*e*).

Discussion

These specimens belong to the genus *Salopella*, erected by Edwards and Richardson (1974) for smooth dichotomously branched axes that terminate with fusiform sporangia, preserved as coalified compressions (Plate 3.9*f*). *Salopella allenii* Edwards and Richardson (1974) was first discovered in upper beds of the Ditton Formation (upper MN spore biozone), and are described as dichotomously branched axes, being at least 24mm in height, with a maximum width of 2mm, which decreases towards the base of long and narrow sporangia. Sporangia have a maximum width of 2mm at mid-length and are up to 9mm long. The branching angle is narrow (15°). The Tredomen Quarry specimens are slightly larger than the type species,

with the largest sporangium 11.9mm in height and 3.14mm in width. Fifteen specimens of seventeen retain a similar height to width ratio to the type specimen (3.14 to 4.5 compared to 4.5). The remaining two specimens (specimens 5 and 10) are slightly shorter in length, but have similar widths to the longer specimens, making them appear squatter, with height to width ratios of 2.6-2.7. This may be due to distortion during compression or are only partial sporangia.

Despite the broad similarities in sporangia shape of *Salopella allenii* to *Aglaophyton major* (Edwards 1986), due to the lack of detailed anatomical data from the coalified compressions and the fragmentary nature of the Tredomen Quarry specimens, any comparisons to the Rhynie chert *Aglaophyton major* anatomy or branching habit was not possible and was the basis of erecting the *Salopella* genus (Edwards and Richardson 1974).

Subsequently other species of *Salopella* have been described, notably *Salopella marcensis* discovered in rocks from Targrove Quarry, Shropshire of lower Dittonian (Lochkovian) age (Fanning et al. 1992). There were smaller plants (6.38mm in height), with smaller fusiform sporangia (0.75-3.38mm in height and 0.25-0.88mm in width), terminating isotomously branched axes, with wider branching angles (30 to 60°) than seen in these specimens and *Salopella allenii*. A recent revisit to Targrove Quarry revealed one specimen of *Salopella allenii* (Plate 3.9*g*), previously not recorded at this locality. Sporangial dimensions are slightly larger than the specimens from Tredomen Quarry, with a sporangial height of 16.7mm and a width of 5.0mm.

The oldest specimens belonging to *Salopella* were collected from Perton Lane, Hereford of lower Downtonian (Přídolí) age by Fanning (1987). These specimens however are more similar to *Salopella marcensis* in size, with sporangial height between 2.6mm and 2.99mm, and sporangial width between 0.55 and 0.78mm (Fanning 1987).

Salopella australis and *Salopella caespitosa* have been described from Late Silurian to Early Devonian flora of Victoria, Australia (Tims and Chambers 1984). Despite the Tredomen Quarry specimens being close in size to *Salopella australis*, sporangia described from this species are not fusiform in shape, but are parallel-sided in the basal half, with unclear sporangial-axial junctions. Although sporangia of *Salopella caespitosa* are more similar in shape to these specimens, with a more definite base, sporangia are smaller (4.5mm in height, 1.7mm in width), and are attached to axes with at least three orders of dichotomy, not seen in Tredomen Quarry specimens.

Similarities in morphology can be made between these specimens and *Anthoceros*, an extant hornwort (bryophyte) with elongate monosporangiate sporophytes (Shaw and Renzaglia

2004). In particular, the sporangia possess a similar variation in tip morphology to those seen in these specimens. *Anthoceros* axes however do not branch, and are much smaller, with sporangial width no more than 1mm in diameter.

It is therefore most appropriate to place these specimens in *Salopella allenii*, based on size, shape of sporangia, and branching angles, despite the lack of *in situ* spores.

Salopella* cf. *marcensis Fanning, Edwards and Richardson 1992

Morphology

A further eight specimens with fusiform sporangia (outlines shown in Figure 3.7) were recovered from green trough-cross-bedded sandstones. Small fusiform sporangia with tapering apices terminate narrow, naked unbranching or isotomously branching axes (RHSp302, Plate 3.10*a*). Sporangial tip morphology varies from rounded to pointed, with one specimen having an extended tip (JM346a, Plate 3.10*b*; JM394b, Plate 3.10*c*). Sporangial height ranges from 1.60 to 3.38 mm (average 2.47 mm), with width ranging from 0.50 to 1.5mm (average 0.83mm). The largest sporangium measures 3.38mm in height and 1.50mm in width (JM021, Plate 3.10*d*), whilst the smallest measures 1.60mm in height and 0.50mm in width (JM266a, Plate 3.10*e*). The maximum width of sporangia occurs at mid-length. Height to width ratio ranges between 2.25 to 4.0 (average 3.10).

Where axes are attached, the subtending axes are narrow, naked and parallel-sided, with a clear junction between the sporangia and axes in most cases. One specimen shows a narrowing of the axis or constriction directly beneath the sporangium base. Axes width ranges from 0.15-0.63mm (average 0.39mm). Four specimens have dichotomously branched axes, with branching angles between 35 and 90°. At least three isotomous dichotomies have been observed in one specimen, giving a minimum plant height of 22.8mm (specimen JM394b, Plate 3.10*f*; Figure 3.7). Although axis width generally remains constant, axis width increases slightly proximal to branch points, and decreases distally to branch points, and therefore axes are wider at the base of the plant.

Anatomy

Due to the poor preservation of the coalified compressions, little anatomical information was obtained, and no spores were extracted. In light microscopy, one sporangium exhibits faint linear striations running parallel to the long axis of the sporangium, tapering to the apex

Figure 3.7: Outlines of *Salopella* cf. *marcensis* specimens from Tredomen Quarry. Scale bar = 1mm

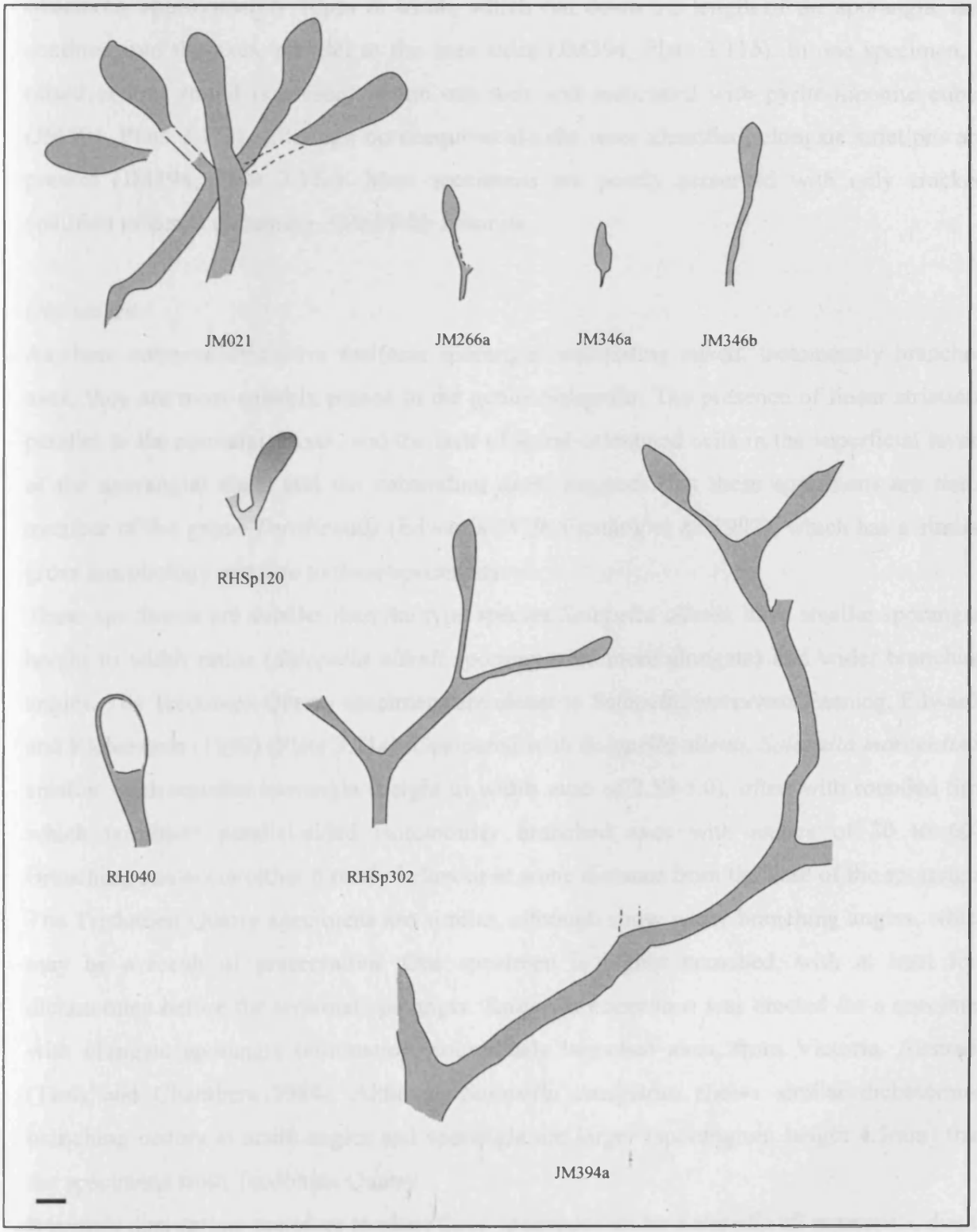

(JM394, Plate 3.11*a*). Under the SEM, a few specimens show elongate cellular-like structures, approximately 10μm in width, which run down the length of the sporangia, and continue into the axes, parallel to the axes sides (JM394, Plate 3.11*b*). In one specimen, a raised central strand is present within one axis and associated with pyrite-limonite cubes (JM394, Plate 3.11*c*). Although no unequivocal cells were identified, elongate striations are present (JM394, Plate 3.11*d*). Most specimens are poorly preserved with only cracked coalified material remaining, filled with limonite.

Discussion

As these compressions have fusiform sporangia terminating naked, isotomously branched axes, they are most suitably placed in the genus *Salopella*. The presence of linear striations parallel to the sporangial axes, and the lack of spiral-orientated cells in the superficial layers of the sporangial walls and the subtending axes, suggests that these specimens are not a member of the genus *Tortilicaulis* (Edwards 1979, Fanning et al. 1992), which has a similar gross morphology and size to these specimens.

These specimens are smaller than the type species *Salopella allenii*, have smaller sporangial height to width ratios (*Salopella allenii* sporangia are more elongate) and wider branching angles. The Tredomen Quarry specimens are closer to *Salopella marcensis* Fanning, Edwards and Richardson (1992) (Plate 3.11*e*). Compared with *Salopella allenii*, *Salopella marcensis* is smaller, with squatter sporangia (height to width ratio of 2.59-5.0), often with rounded tips, which terminate parallel-sided isotomously branched axes with angles of 30 to 60°. Branching can occur either directly below or at some distance from the base of the sporangia. The Tredomen Quarry specimens are similar, although show wider branching angles, which may be a result of preservation. One specimen is highly branched, with at least four dichotomies before the terminal sporangia. *Salopella caespitosa* was erected for a specimen with elongate sporangia terminating isotomously branched axes, from Victoria, Australia (Tims and Chambers 1984). Although *Salopella caespitosa* shows similar dichotomies, branching occurs at acute angles and sporangia are larger (sporangium height 4.5mm) than the specimens from Tredomen Quarry.

It is most appropriate therefore to place these specimens under *Salopella* cf. *marcensis*, due to their similarities in gross morphology and size to *Salopella marcensis*, but differ with wider branching angles.

Elongate club-shaped sporangia

Morphology

Eleven specimens of elongate, club-shaped sporangia were collected from green trough-cross-bedded sandstones, with 3 specimens terminating dichotomously branched, naked axes (outlines shown in Figure 3.8). Terminal sporangia are elongate with broad rounded tips (RHPB, Plate 3.12*a*). The sporangial-axial junctions are indistinctive, and two possible positions have been postulated (arrows a and b JM016c, Plate 3.12*b*). Junctions in position (a) are based on the curvature of the sporangial tip, the sporangia base located where the sides begin to taper. Junctions in position (b) occur where axial sides become parallel-sided. As a result, two sporangia shapes are possible; a vertically orientated hemispherical shape with a flat junction or an elongate club-shape, with no clearly defined junction with the subtending axes. Sporangial height ranges from 1.00 to 2.20mm (average 1.43mm) with a junction in position (a), while sporangial width ranges from 1.20 to 2.50mm (average 1.62mm). Sporangial height to width ratio ranges up to 1.29, and therefore height does not exceed twice the width. Alternatively, for a junction in position (b), sporangial height ranges from 2.06 to 5.60mm (average 3.72mm), and with a width range of 1.2 to 2.5mm (average 1.66mm). Sporangia are elongate with height to width ratios of 1.19 to 4.10 (average 2.31). The maximum width occurs in the top third of sporangia height. Sporangia tips are broad and are bluntly rounded (RHSp20_1, Plate 3.12*c*).

A pronounced marginal band up to approximately 150μm wide, is seen in all specimens, running around the periphery of the whole sporangium and possible subtending axis (e.g. RH117_4, Plate 3.12*d*; Sp034_2, Plate 3.12*e*). The sporangia gradually taper into parallel-sided, isotomously branched axes (JM262a, Plate 3.12*f*). Axes width ranges from 0.4 to 0.8mm (average 0.58mm), and branching occurs at an angle of 50 to 90°. Sporangial to axial junctions are unclear, and although daughter axes narrow after dichotomies, axes with non-parallel sides gradually widen above a dichotomy. The largest specimen is 10.8mm in height, with two dichotomies (JM371, Plate 3.12*g*).

Anatomy

These coalified compressions are poorly preserved in terms of anatomical detail and no spores were recorded. The coalified compressions are partial, with the corresponding impressions beneath, and are sometimes associated with pyrite-limonite cubes, particularly the axes. Some features are more apparent under the SEM, particularly the thick borders

Figure 3.8: Outlines of elongate club-shaped specimens from Tredomen Quarry.
Scale bar = 1mm

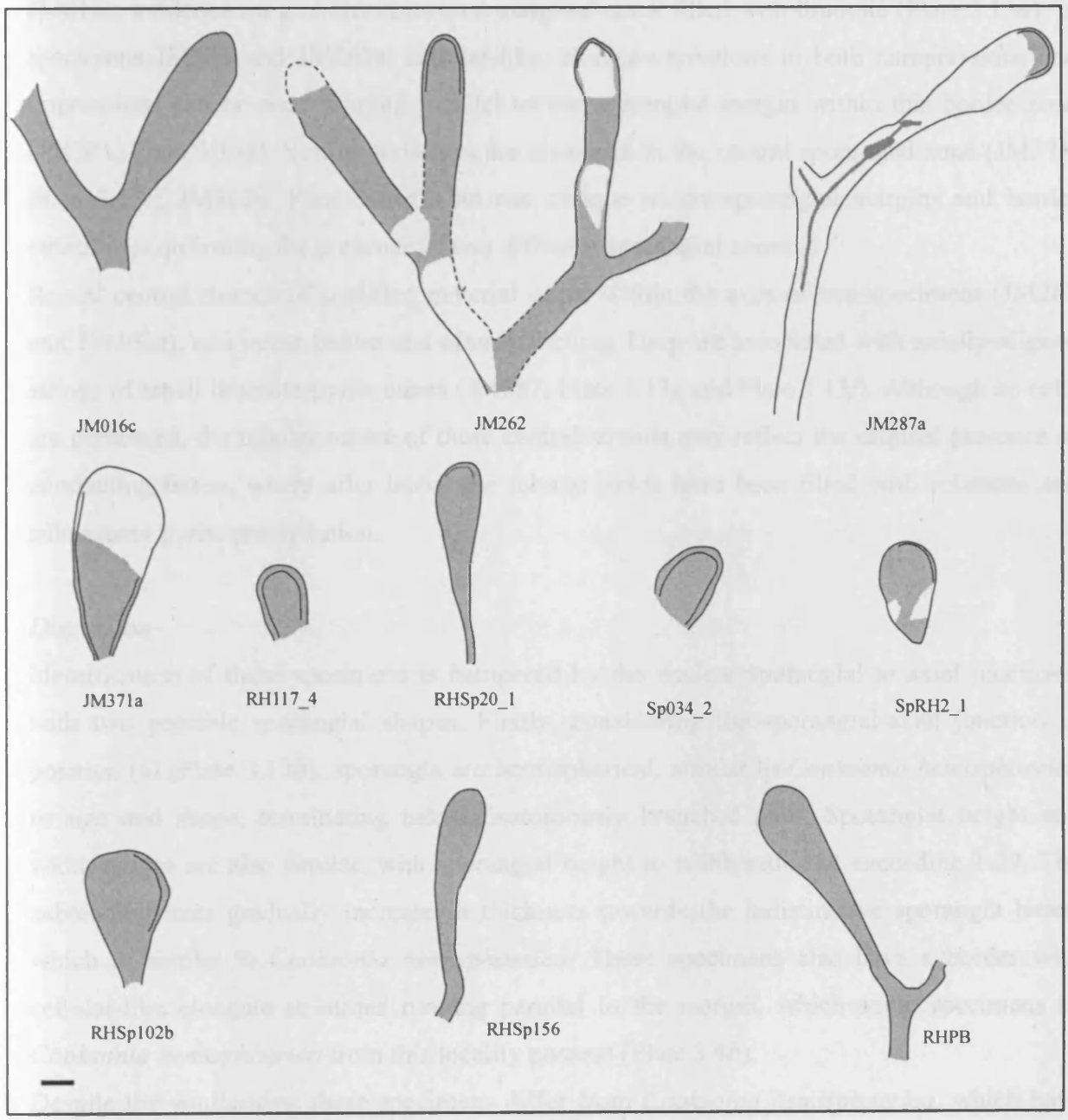

around the margins of the sporangia, ranging from 60 to 150μm in thickness. In specimen JM016c, evidence for a border rests on a marginal crack filled with limonite (Plate 3.13*a*). In specimens JM371 and JM261a, cellular-like, elongate striations in both compressions and impressions can be seen running parallel to the sporangial margin within this border zone (JM371, Plate 3.13*b*). Similar striations are also seen in the central sporangial zone (JM371, Plate 3.13c; JM262a, Plate 3.13*d*), but run oblique to the sporangial margins and border striations, confirming the presence of two different sporangial zones.

Raised central strands of coalified material occur within the axes of two specimens (JM287 and JM262a), and occur before and after branching They are associated with axially-aligned strings of small limonite-pyrite cubes (JM287, Plate 3.13*e* and Plate 3.13*f*). Although no cells are preserved, the tubular nature of these central strands may reflect the original presence of conducting tissue, where after burial the tubular voids have been filled with solutions and subsequent pyrite precipitation.

Discussion

Identification of these specimens is hampered by the unclear sporangial to axial junctions, with two possible sporangial shapes. Firstly, considering the sporangial-axial junction in position (a) (Plate 3.12*b*), sporangia are hemispherical, similar to *Cooksonia hemisphaerica* in size and shape, terminating naked, isotomously branched axes. Sporangial height and width ranges are also similar, with sporangial height to width ratio not exceeding 1.29. The subtending axes gradually increase in thickness towards the indistinctive sporangia bases, which is similar to *Cooksonia hemisphaerica*. These specimens also have a border with cellular-like elongate striations running parallel to the margin, which some specimens of *Cooksonia hemisphaerica* from this locality possess (Plate 3.4*b*).

Despite the similarities, these specimens differ from *Cooksonia hemisphaerica*, which have clearly defined sporangial bases, slightly more circular sporangia, and subtending axes that taper from the base of the sporangia to a greater degree, to become parallel-sided before a dichotomy. In the new specimens, the subtending axes width continues to decrease gradually until the dichotomy below. As shown in specimen JM371a (Plate 3.12*g*), the border runs around not only the tip, but also down the whole length of the sporangial body and therefore a sporangial-axial junction in position (b) may be more appropriate.

Recognition of junctions in position (b) transform sporangia into a more elongate club-shape, with a sporangial height to width ratios from 1.19 to 4.10 (average 2.31). This range is similar

to that of *Salopella*, but the new specimens are not fusiform in shape with tapering apices or pointed tips, and therefore do not belong to this genus.

Steganotheca striata Edwards (1970a) also possess sporangia that are longer than wide. This genus is characterised by isotomously branched axes terminated by vertically elongate sporangia, with truncated to rounded apices. Although the Tredomen Quarry specimens are similar, sporangia of *Steganotheca striata* are more parallel-sided and cup-shaped, and have a clearer junction at the sporangia base. Additionally, the tip may be sharply truncated, unlike the Tredomen Quarry specimens that are broadly rounded. *Steganotheca striata* is also characterised by the presence of fine striations running obliquely to the sporangial wall, which are not present in the Tredomen Quarry specimens.

The sporangia of these specimens are more similar to the genus *Dutoitea* Høeg 1930, an early rhyniophytoid endemic to South Africa from the Lower Devonian (Rayner 1988). In particular, *Dutoitea alfreda* Plumstead 1967 has been described as club-shaped sporangia terminating isotomously to anisotomously branched axes. Sporangia are of a similar size, with sporangial height of *Dutoitea alfreda* ranges from 2.0 to 4.0mm (Rayner 1988). As *Dutoitea* is only known from the southern hemisphere, and is potentially younger in age, for now these specimens will not be placed in this genus.

Fanning (unpublished thesis 1987) discovered similar elongate terminal features attached to fragments of wide isotomously branched axes from Targrove Quarry that were assigned to *Hostinella* Barrande. However, *Hostinella* is usually retained for sterile dichotomously branched axes and no fertile portions have been formally described. Although most similar to *Cooksonia*, these specimens will remained unassigned to any genus at present, as a result of great variability amongst the few specimens collected and poor preservation of anatomical detail.

3.2.2: *Early embryophyte mesofossils*

A second major group of plant fossils was discovered within green wavy to planar-laminated siltstones, where lamination surfaces are packed with vegetative debris, consisting of highly fragmented, minute, naked, fertile branching axes (mesofossils up to 5.5mm in total specimen length), plus non-embryophyte fragments, minute coalified threads, and non-vegetative fragments (possibly eurypterid or cephalaspid). The minute branching axes are coalified and extremely friable. Preservation of gross morphology is good, with a lot of diversity, but unfortunately anatomical detail is poor and features such as sporangial-axial junctions are

often unclear. This group of minute fossils are briefly described in Appendix I*a*, whilst measurements and calculations are presented in Appendix III.

This second group has been separated from the megafossils described above primarily based on size, the largest sporangium being half the size of the smallest megafossil sporangium (Figure 3.9*a*). The maximum sporangium height recorded was 1.10mm (Appendix III), but the majority of sporangia are well below 1mm in height (Figure 3.9*a*, Appendix III), leading to these specimens being referred to as mesofossils.

Similar mesofossils were discovered from a middle Lochkovian locality on the Welsh Border, approximately 80km northeast of Tredomen Quarry (Edwards 1996, Edwards 2000 and Edwards and Axe 2004). These three-dimensional, exceptionally well-preserved, minute sporangia share a similar size range and diversity to the Tredomen Quarry mesofossils. Anatomical details have been very well-preserved via charcoalification, including *in situ* trilete and cryptospores and provide some clues to the affinity of these minute plants. As the Tredomen Quarry specimens have been preserved as coalified compressions, anatomical information has been lost, hence determining the affinity of these specimens is challenging. However, the well-preserved sporangia from the middle Lochkovian locality could be considered as broadly synonymous with the Tredomen Quarry specimens.

Unfortunately, with very few exceptions, the well-preserved charcoalified sporangia do not possess sufficiently long axes to determine the branching patterns of the plants that bore these sporangia (Edwards 1996, Edwards 2000). Without this information, it may be argued that these sporangia represent just the fertile, possibly immature, tips of larger plants, and therefore should be placed in the appropriate genera. The mesofossils from Tredomen Quarry provide the first evidence that these minute sporangia were attached to isotomously and anisotomously branched axes (Figure 3.9*a*). For this reason, these minute plants have not been placed in existing genera, but separated into a different, minute component of Lower Devonian vegetation.

Six broad types of mesofossil have been recognised from the Tredomen Quarry collection, based on sporangial morphology, sporangia arrangement and to a lesser degree, branching habit. Typical examples of each mesofossil type are shown in Figure 3.9*b*, along with sporangial dimensions. Type A mesofossils are anisotomously branched axes, terminated by pairs of circular to slightly elliptical sporangia (Figure 3.9*b*). Type B mesofossils are mostly isotomously branched axes, with some evidence of anisotomous branching in the terminal axes, terminated by vertically elongate, elliptical sporangia (Figure 3.9*b*). These two types are

Figure 3.9: a: Comparisons between the size and branching patterns of mesofossils and megafossils, b: Typical examples of the six main types of mesofossil

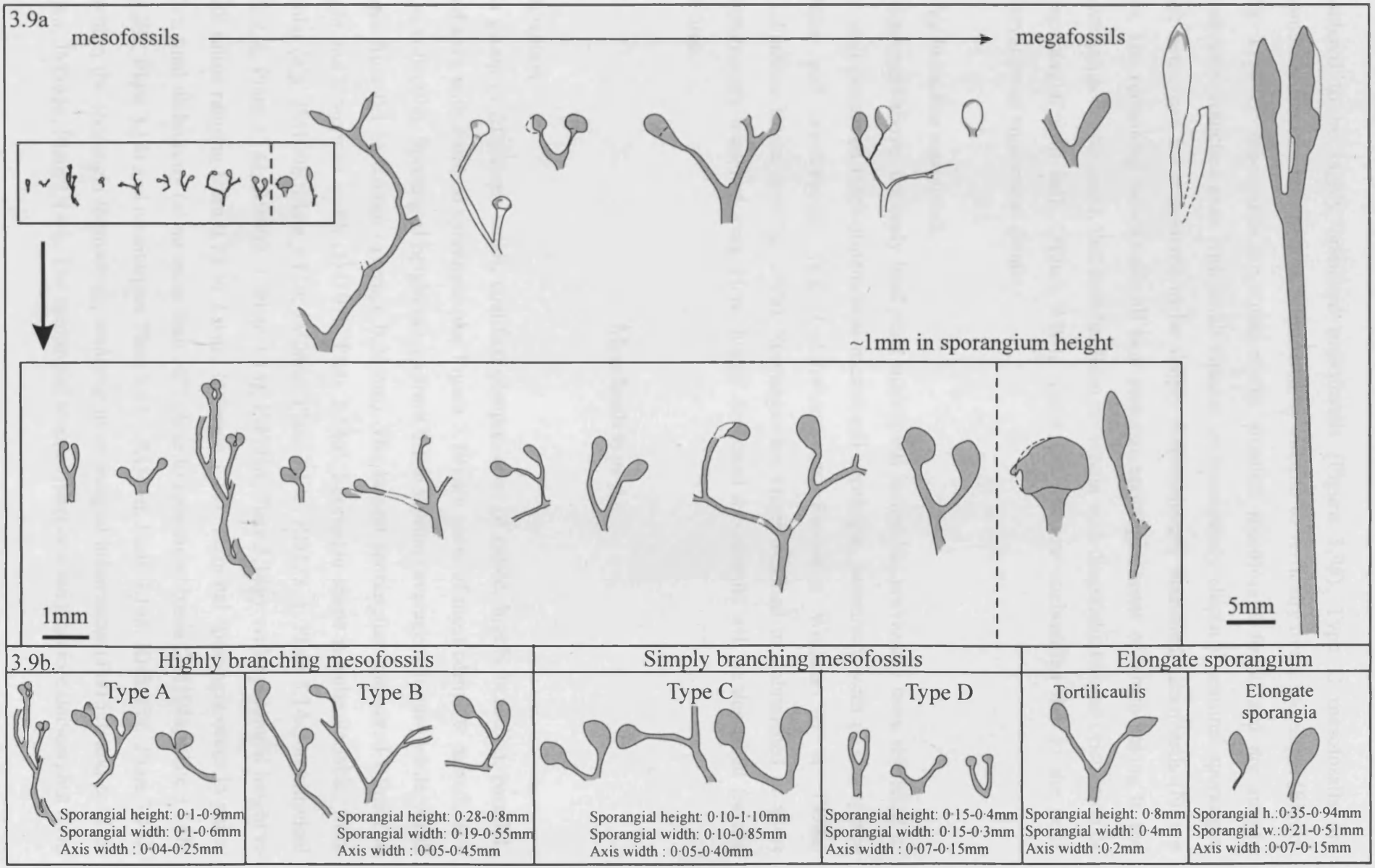

considered to be highly branched mesofossils (Figure 3.9*b*). Type C mesofossils are isotomously branched short axes, terminated by circular to vertically ovate sporangia (Figure 3.9*b*). Type D mesofossils are some of the smallest mesofossils found and are simply isotomously branched axes with small circular or transversely elliptical terminal sporangia. These two types are considered to be simply dichotomously branched mesofossils (Figure 3.9*b*). The remaining mesofossils all bear elongate sporangia, some of which belong to the known genus *Tortilicaulis*, that bear fusiform sporangia with diagnostic twisted orientation of the sporangial wall cells (Figure 3.9*b*), whilst the rest are unclassified due to the poor preservation of anatomical details.

Highly branched mesofossils

As discussed above, the early land plant mesofossil record has previously been restricted to very well-preserved three-dimensional mesofossil sporangia, sometimes with *in situ* spores (triletes and cryptospores) (e.g. *Culilletheca* and *Fusitheca* Wellman et al. 1998a, *Grisellatheca* Edwards et al. 1999). Sporangia are either attached to unbranched or short dichotomously branched axes. Here, highly branched mesofossils will be described for the first time.

Mesofossil type A

Description

This group of fifty-three small, coalified compressions of naked, highly branched, parallel-sided axes with terminal sporangia (see Figure 3.10) are some of most complete mesofossils in the collection. Sporangial height ranges from 0.1 to 0.9mm (average 0.36mm) while width ranges from 0.1 to 0.6mm (average 0.28mm). The largest sporangium measured 0.9mm in height and 0.5mm in width (JM197b, Plate 3.14*a*). Sporangia shape is quite variable, from circular (e.g. JM190b, Plate 3.14*b*; JM086c, Plate 3.14*c*; RH128_1, Plate 3.14*d*) to elliptical (JM323c, Plate 3.14*e*; RH002_1, Plate 3.14*f*; JM095d, Plate 3.14*g*), with sporangial height to width ratios ranging from 0.72 to 2.0mm (average 1.30). Terminal sporangia occur in pairs, with a final dichotomy (at no more than 30°) close to sporangial bases (JM194a, Plate 3.14*h*; JM123a, Plate 3.14*i* and counterpart Plate 3.14*j*; JM365d, Plate 3.14*k*; RHSp006, Plate 3.14*l*) or within the sporangia themselves, resulting in sporangial bifurcation (JM153b and c, Plate 3.14*m*; JM365c, Plate 3.14*n*). The sporangial to axial junctions are therefore unclear, but have

Figure 3.10: Outlines of mesofossil type A specimens from Tredomen Quarry. Scale bar = 1mm

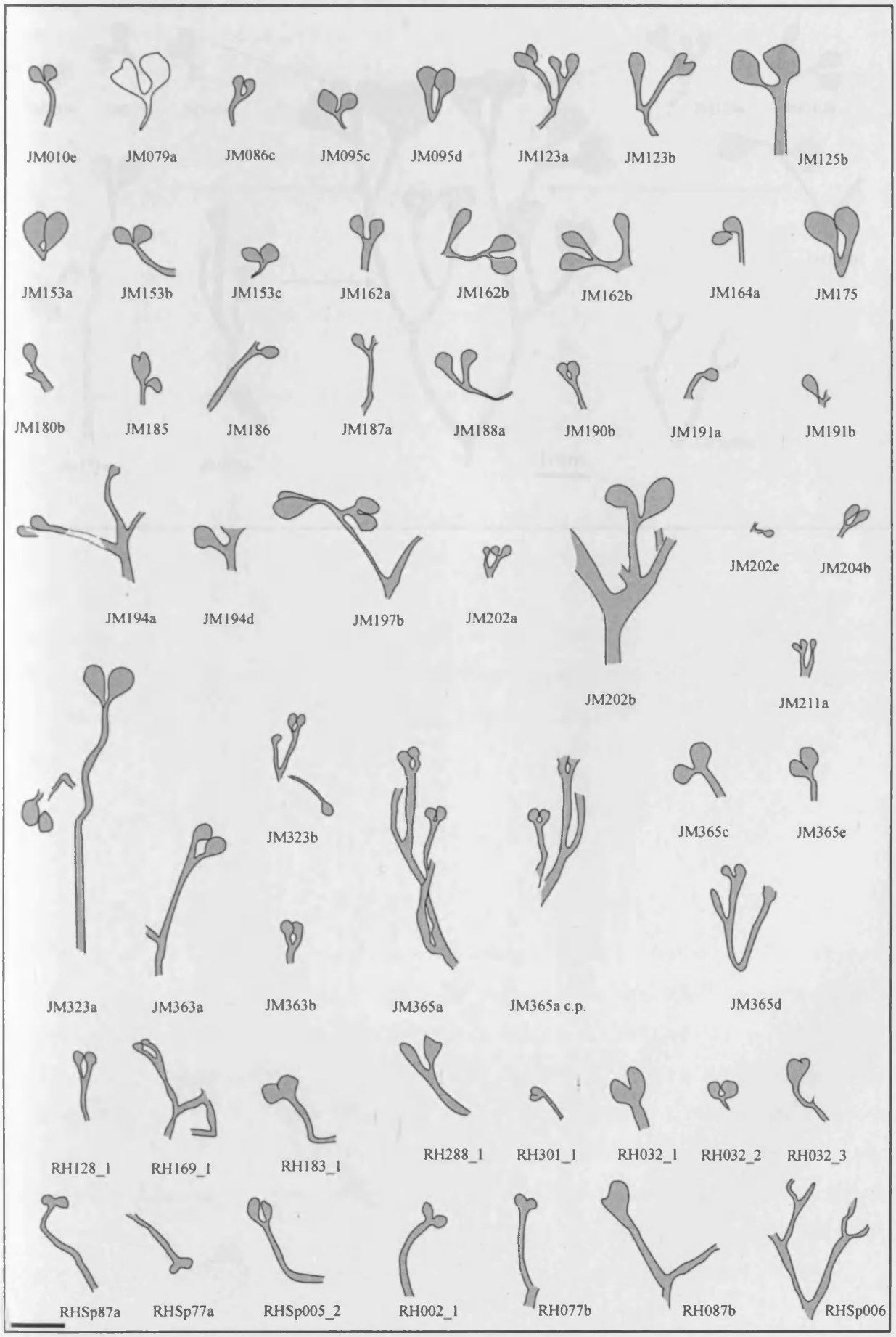

Figure 3.11: Reconstruction of mesofossil type A.

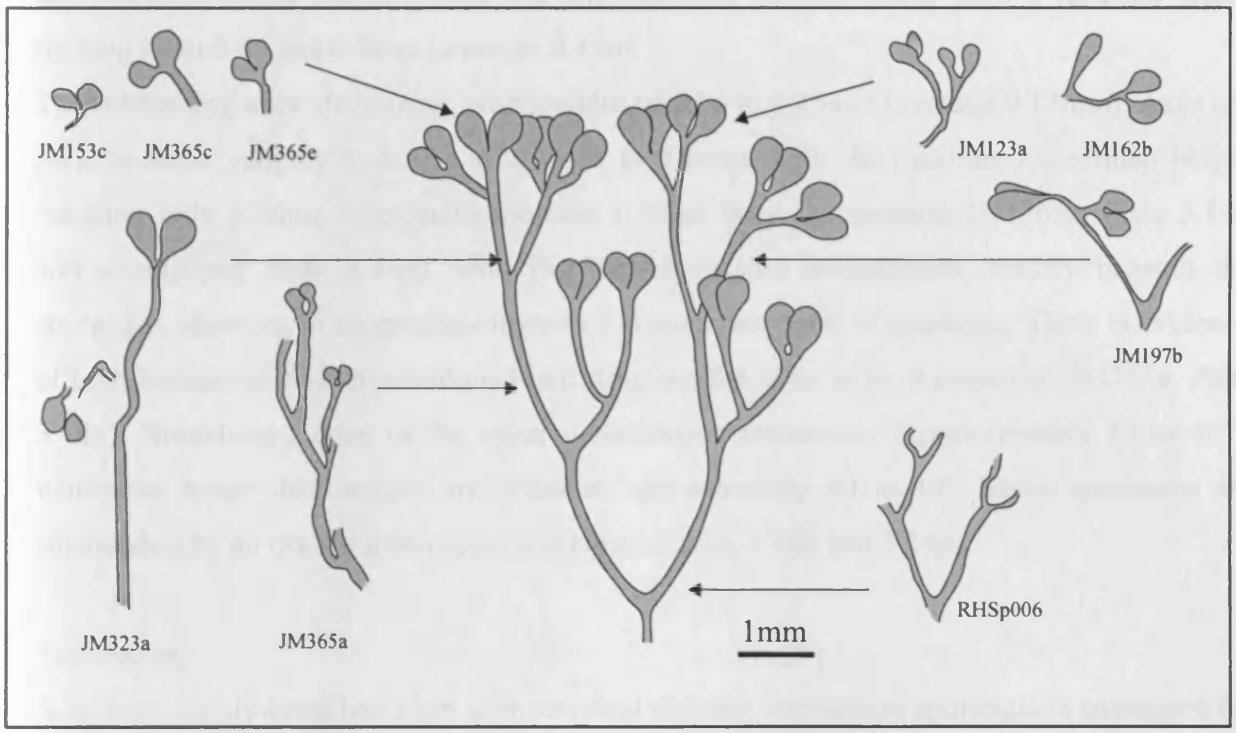

approximately been placed where the axes become parallel-sided, with a junction width ranging from 0.04 and 0.2mm (average 0.1mm).

The subtending axes are narrow, with a width of 0.04 to 0.25mm (average 0.12mm). Axes are parallel-sided, ranging in length from 0.15 to 4.8mm, with the maximum specimen height reaching only 5.5mm. Specimens indicate at least three dichotomies (JM365a, Plate 3.14*o* and counterpart Plate 3.14*p*), with two closely-spaced dichotomies directly beneath the sporangia, resulting in sporangial clusters of at least two pairs of sporangia. There is evidence of both isotomous and anisotomous branching, but the latter is most common (JM365a, Plate 3.14*o*). Branching angles in the upper dichotomies are narrow (approximately 30 to 40°), whilst the lower dichotomies are wider at approximately 60 to 80°. Some specimens are surrounded by an orange iron-oxide halo (Plate 3.14*n*, 3.14*o* and 3.14*p*).

Discussion

A minute, highly-branched plant with terminal circular to elliptical sporangia is envisaged for this group, shown in Figure 3.11. This plant is envisaged to be at least 1cm in height, with narrow, parallel-sided axes up to 500μm in width. Pairs of circular to slightly elliptical sporangia often occur directly above the final dichotomies, or sporangia are forked themselves. As branching is predominately anisotomous and branching angles in the final dichotomies are narrow (around 30 to 40° compared with the lower dichotomies at 60°), sporangia pairs occur in clusters.

Mesofossil type B

Description

This group contains forty-six specimens of minute, naked, highly branched axes with longitudinally elliptical sporangia (outlines shown in Figure 3.12). Compared to the sporangia of mesofossil type A, sporangia are more elongate, with sporangial height to width ratios ranging from 0.9 to 2.73 (average 1.59). Maximum sporangial width occurs at or slightly above mid-height (JM214a, Plate 3.15*a*; JM206a, Plate 3.15*b* and RH077a, Plate 3.15*c*). Sporangial height ranges from 0.28mm to 0.80mm (average 0.49mm), whilst sporangial width ranges from 0.19mm to 0.55mm (average 0.32mm). The largest sporangium measures 0.7mm in height and 0.55mm in width (JM164d, Plate 3.15*d*), whilst the smallest sporangium measures 0.3mm in height and 0.2mm in width (JM164c, Plate 3.15*e*).

Figure 3.12: Outlines of mesofossil type B specimens from Tredomen Quarry. Scale bar = 1mm

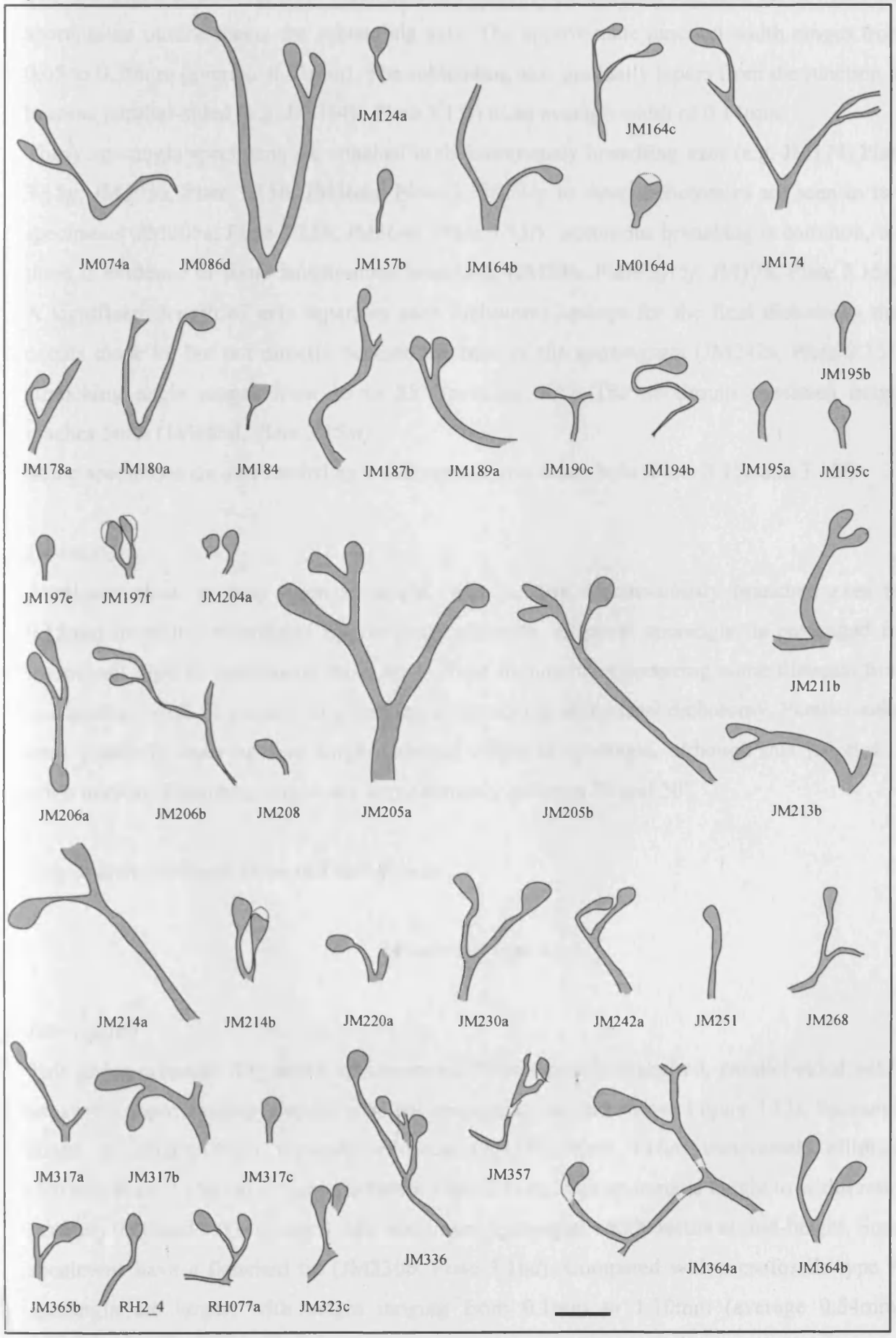

The sporangial to axial junction is not clear on most specimens, and has been taken where the sporangium outline meets the subtending axis. The approximate junction width ranges from 0.05 to 0.30mm (average 0.13mm). The subtending axis gradually tapers from the junction to become parallel-sided (e.g. JM364b, Plate 3.15*f*) to an average width of 0.14mm.

Thirty sporangia specimens are attached to dichotomously branching axes (e.g. JM174, Plate 3.15*g*; JM205a, Plate 3.15*h*; JM364a, Plate 3.15*i*). Up to three dichotomies are seen in two specimens (JM205a, Plate 3.15*h*; JM364a, Plate 3.15*i*). Isotomous branching is common, but there is evidence of some anisotomous branching (JM336, Plate 3.15*j*; JM178, Plate 3.15*k*). A significant length of axis separates each dichotomy, except for the final dichotomy that occurs close to, but not directly beneath the base of the sporangium (JM242a, Plate 3.15*l*). Branching angle ranges from 15 to 85° (average 50°). The maximum specimen height reaches 5mm (JM086d, Plate 3.15*m*).

Some specimens are surrounded by a dull orange iron-oxide halo (Plate 3.15*e* and 3.15*l*).

Discussion

A minute plant, at least 5mm in height, with acutely dichotomously branched axes (c. 0.15mm in width) terminated by vertically elongate, elliptical sporangia, is envisaged for mesofossil type B. Specimens show up to three dichotomies occurring some distance from one another, with an element of anisotomous branching in the final dichotomy. Parallel-sided axes gradually taper up into single terminal elliptical sporangia, although this junction is often unclear. Branching angles are approximately between 30 and 50°.

Simple dichotomously branched mesofossils

Mesofossil type C

Description

This group contains fifty-seven specimens of dichotomously branched, parallel-sided naked axes with approximately circular terminal sporangia (outlines shown Figure 3.13). Sporangia shape is variable from vertically elliptical (JM188, Plate 3.16*a*) transversely elliptical (JM154, Plate 3.16*b*) to circular (JM100b, Plate 3.16*c*), with sporangial height to width ratios between 0.80 and 2.0 (average 1.23). Maximum sporangial width occurs at mid-height. Some specimens have a flattened tip (JM230b, Plate 3.16*d*). Compared with mesofossils type A, sporangia are larger, with height ranging from 0.1mm to 1.10mm (average 0.54mm),

Figure 3.13: Outlines of mesofossil type C specimens from Tredomen Quarry. Scale bar = 1mm

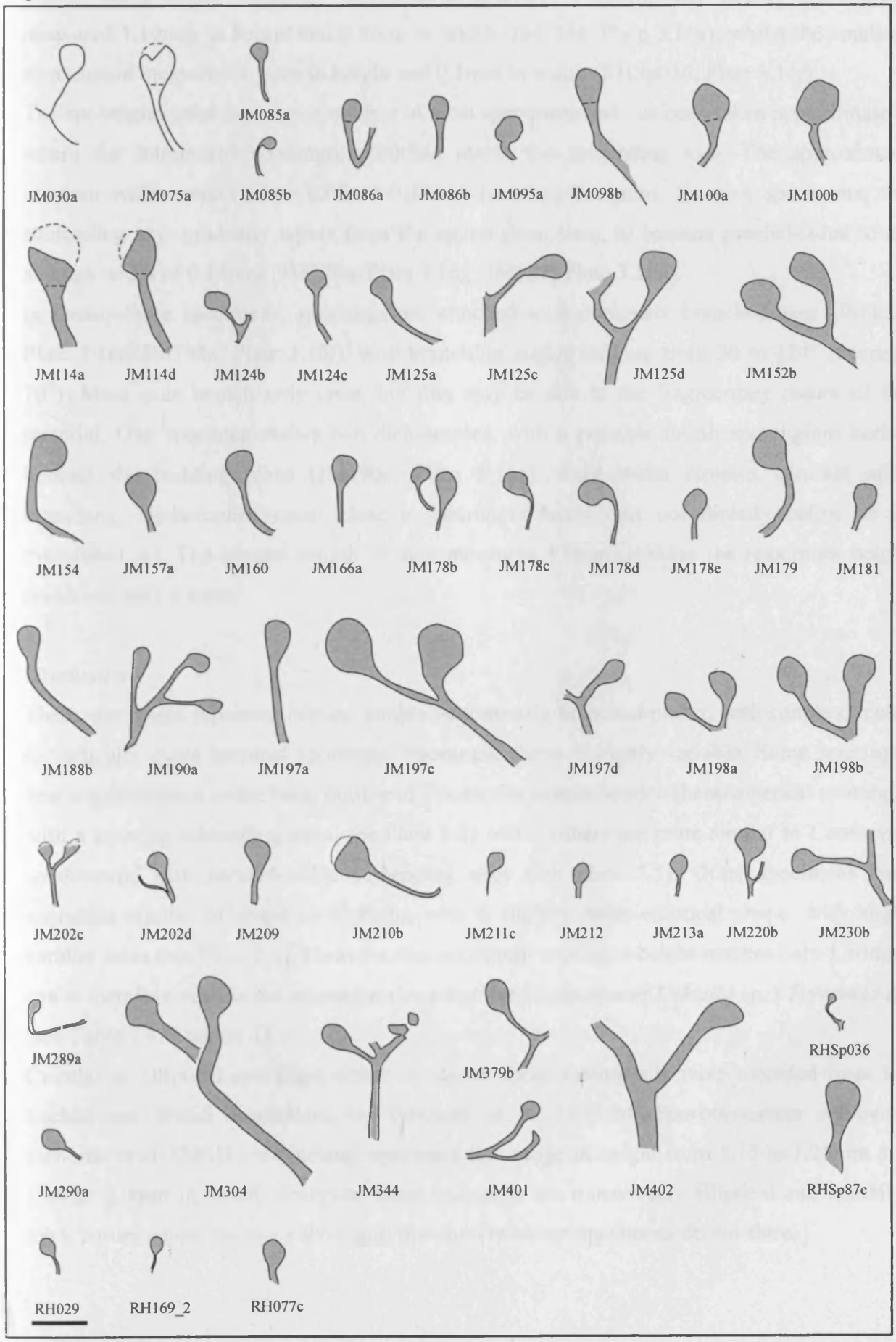

whilst width ranges from 0.1 to 0.85mm (average 0.45mm). The largest sporangium measured 1.10mm in height and 0.8mm in width (JM114a, Plate 3.16*e*), whilst the smallest sporangium measured 0.1mm in height and 0.1mm in width (RHSp036, Plate 3.16*f*).

The sporangial-axial junction is unclear in most specimens and has been taken approximately where the interpreted sporangium outline meets the subtending axis. The approximate junction width ranges from 0.05 to 0.45mm (average 0.14mm). In most specimens, the subtending axis gradually tapers from the sporangium base, to become parallel-sided to an average width of 0.14mm (JM179a, Plate 3.16*g*; JM181, Plate 3.16*h*).

In twenty-three specimens, sporangia are attached to isotomously branched axes (JM402, Plate 3.16*i*; JM198a, Plate 3.16*j*), with branching angles ranging from 30 to 124° (average 70°). Most axes branch only once, but this may be due to the fragmentary nature of the material. One specimen shows two dichotomies, with a possible fourth sporangium buried beneath the bedding plane (JM190a, Plate 3.16*k*). Axes width remains constant after branching. Dichotomies occur close to sporangia bases (but not directly below as in mesofossil A). The longest length of axis measures 4.0mm, making the maximum height preserved only 4.6mm.

Discussion

These specimens represent minute, simple isotomously branched plants, with simple circular to vertically ovate terminal sporangia. Sporangia shape is highly variable. Some sporangia bear a resemblance to the basic outline of *Cooksonia hemisphaerica* (hemispherical sporangia with a tapering subtending axes, see Plate 3.3) whilst others are more similar to *Cooksonia cambrensis*, with parallel–sided subtending axes (see Plate 3.5). Other specimens bear sporangia similar in shape to *Uskiella*, with a slightly more elliptical shape, with slight parallel sides (see Plate 3.6). However, the maximum sporangia height reaches only 1.10mm, and is therefore outside the sporangia size range for *Cooksonia* or *Uskiella* sp. / *Tarrantia* sp. (see Table 1.4, Chapter 1).

Circular to elliptical sporangia closer in size to these mesofossils were recorded from the Lochkovian Welsh Borderland by Edwards et al. (2001b). *Sporathylacium salopense* Edwards et al. (2001b) are isolated sporangia that range in height from 1.15 to 1.25mm and 1.14 to 2.0mm in width. However, these sporangia are transversely elliptical and exhibit a thick border where the two valves split that the Tredomen specimens do not show.

Mesofossil type D

Description

This group encompasses fourteen specimens of minute, dichotomously branched axes with small, circular or transversely elliptical terminal sporangia (Figure 3.14). These specimens are particularly small, with maximum sporangial height being only 1.7mm. Sporangia shape ranges from circular (JM157c, Plate 3.17*a*; JM187c, Plate 3.17*b*; JM194c, Plate 3.17*c*) to transversely elliptical (JM010f, Plate 3.17*d*; RH128_2, Plate 3.17*e*; RH050_2, Plate 3.17*f*), with sporangial height ranging from 0.15mm to 0.40mm (average 0.23mm) and sporangial width ranging from 0.15mm to 0.30mm (average 0.22mm). The largest sporangium measures 0.4mm in height and 0.3mm in width (JM290b, Plate 3.17*g*). Height to width ratios ranges from 0.6 to 1.50 (average 1.06).

The sporangial to axial junction is unclear in all specimens, and taken where the interpreted sporangia outlines met the subtending axes. The approximate junction width ranges from 0.07mm to 0.15mm (average 0.1mm). Unlike mesofossils A to C, the subtending axes do not taper gradually but sporangia are attached to parallel-sided axes, with an average width of 0.12mm (JM114c, Plate 3.17*h*). In some specimens the subtending axes curve towards each other (JM187c, Plate 3.17*b*; JM010f, Plate 3.17*d*; JM110a, Plate 3.17*i*). Branching is isotomous, specimens branching only once at some distance from the bases of the sporangia (JM110a, Plate 3.17*i*). Branching angle ranges from 10 to 90° (average 51°).

Some specimens are surrounded by a dull orange iron-oxide halo (Plate 3.17*i*).

Discussion

These mesofossils represent minute, simply isotomously branched plants with terminal circular to transversely elliptical sporangia. Only unbranched and axes with one dichotomy have been preserved. Although one specimen (RH050_2) resembles *Cooksonia pertoni* Lang 1937 in gross morphology (transversely elliptical or discoidal sporangia), sporangial height to width ratio often exceeds 1.0, which is not considered cooksonoid (Edwards 1996). The subtending axes of these mesofossils are parallel-sided, unlike the broad sporangial-axial junction and sharply tapering subtending axes of *C. pertoni*.

Figure 3.14: Outlines of mesofossil type D specimens from Tredomen Quarry. Scale bar = 1mm

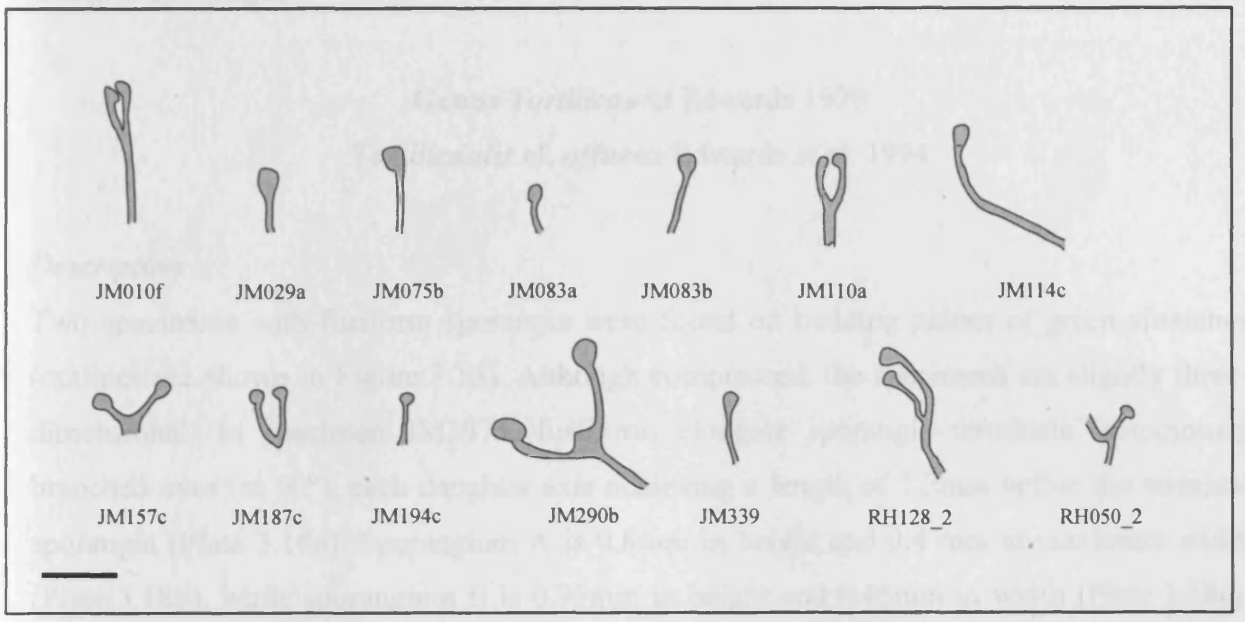

Elongate sporangia

Genus *Tortilicaulis* Edwards 1979

Tortilicaulis* cf. *offaeus Edwards et al. 1994

Description

Two specimens with fusiform sporangia were found on bedding planes of green siltstones (outlines are shown in Figure 3.15). Although compressed, the specimens are slightly three-dimensional. In specimen JM397a, fusiform, elongate sporangia terminate isotomously branched axes (at 60°), each daughter axis achieving a length of 1.2mm before the terminal sporangia (Plate 3.18*a*). Sporangium A is 0.8mm in height and 0.4 mm at maximum width (Plate 3.18*b*), while sporangium B is 0.95mm in height and 0.45mm in width (Plate 3.18*c*). Maximum width occurs just below mid-height. Sporangium A tapers to the apex, and has a rounded tip (JM397a, Plate 3.18*b*). Sporangium B also tapers to the apex but has a pointed tip (JM397a, Plate 3.18*c*). The sporangial to axial junctions are not clearly marked, but taken where the axes become parallel-sided. Axis width is an average of 0.2mm, widening slightly below the dichotomy (0.3mm), and narrowing to 0.15 to 0.2mm after branching and to 0.1mm directly beneath the sporangia.

Specimen RHSp012_1 is very similar; small isotomously branched axes with fusiform terminal sporangia (Plate 3.18*d*). The one complete sporangium is 0.83mm in height and 0.37mm in width. The sporangium tapers into the parallel-sided subtending axis, with a dichotomy close to the base of the sporangium, with a total specimen length of 1.54mm and an axis width of 0.19mm. The second sporangium is not as clearly defined and is partially buried.

Under the light microscope, elongate striations can be seen in the coalified compression and impression beneath, running the length of the axis and sporangium at an oblique angle (approximately 40°) to the respective margins, giving a twisted appearance (JM397a, Plate 3.18*c*). Under the SEM, these cell-like striations can be seen to have a fusiform shape, in filled with limonite-pyrite cubes (JM397a, Plate 3.18*e*). Cell width is approximately 15 to 20μm, with an unknown length. Cell length is oblique to the sporangium margin and cells appear twisted in the subtending axis (JM397a, Plate 3.18*f*), although are parallel to the axis margin at the dichotomy. Questionable stomata were seen along the axis (JM397a, Plate 3.18*g*), but may an artefact of preservation, particularly as the specimen is covered with

Figure 3.15: Outlines of *Tortilicaulis* cf. *offaeus* specimens from Tredomen Quarry. Scale bar =1mm.

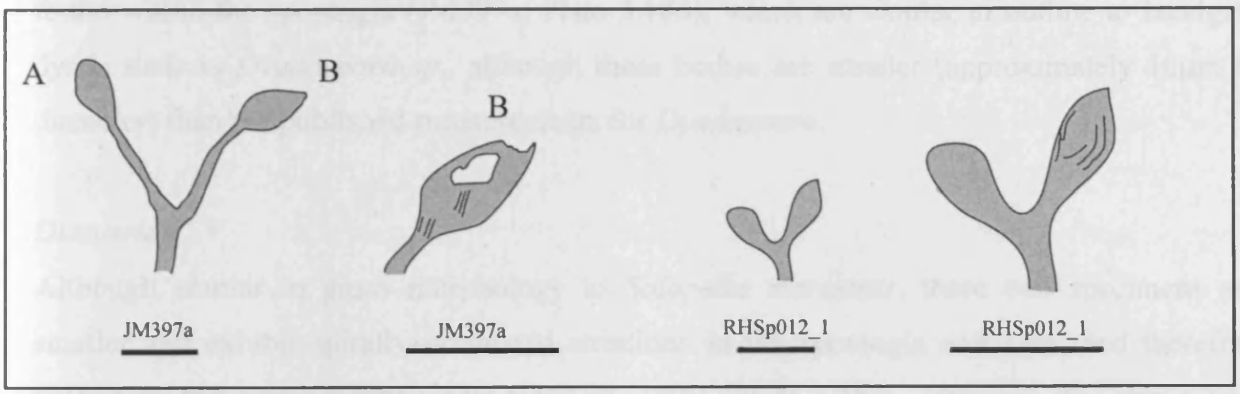

irregular minerals and microbial residue. Additionally, smooth, sub-circular features were found within the sporangia (JM397a, Plate 3.18*h*), which are similar in outline to laevigate dyads such as *Dyadospora sp.*, although these bodies are smaller (approximately 10μm in diameter) than the published measurements for *Dyadospora*.

Discussion

Although similar in gross morphology to *Salopella marcensis*, these two specimens are smaller and exhibit spirally–orientated striations in the sporangia and axes, and therefore belong to the genus *Tortilicaulis* Edwards 1979 (Plate 3.18*i*). Although this genus was erected for unbranched, twisted axes with terminal fusiform to oval sporangia from the Freshwater East Formation (lower Přídolí), dichotomously branched specimens of the type species, *Tortilicaulis transwalliensis,* were found in younger Dittonian rocks at Targrove Quarry (Fanning et al. 1992). In both cases, elongate sporangia taper to a tip, which varies in morphology from pointed to rounded. Superficial cells in the sporangial wall are oblique or spirally orientated. The overall sporangial dimensions from the Freshwater East specimens were 2.07mm in height and 0.8mm in width, with a height to width ratio of 2.59. Of the Targrove specimens, sporangia height ranges from 1.63 to 7.17mm, and 0.63 to 1.81mm in width, with a height-width ratio averaged at 4.35.

The Tredomen Quarry specimens differ from *T. transwalliensis* with a sporangial height below the *T. transwalliensis* range, and the sporangia are slightly squatter in shape, with the height to width ratio lower at 2.1. Additionally, specimens of *T. transwalliensis* from Targrove had apices that were more pointed.

A second, smaller species of *Tortilicaulis* was erected by Edwards et al. (1994), from exceptionally well-preserved specimens from the middle Dittonian of the Welsh Borderland. *Tortilicaulis offaeus* is a plant with smooth dichotomously branched axes (0.06 to 1.4mm wide) that terminate with ellipsoidal elongate sporangia that possess rounded apices (Plate 3.18*j*). Although the sporangia are known to bifurcate, individual sporangia range in height from 0.31 to 0.89mm and 0.19 to 0.54mm in width, with a height-width ratio of 1.5 to 2.9. Unlike the Tredomen Quarry specimens, *in situ* trilete spores were recovered, with narrow equatorial crassitude, and fine grana ornamentation (Edwards et al. 1994).

The Tredomen Quarry specimens are closest in size and gross morphology to *Tortilicaulis offaeus*, but because they lack any anatomical details or *in situ* spores, they should remain as *Tortilicaulis* cf. *offaeus*.

Other elongate mesofossil sporangia

Description

A further eight specimens of elongate sporangia attached to naked, unbranched subtending axes were discovered (Figure 3.16). Sporangial height to width ratio ranges from 1.35 to 2.25 (average 1.85), with maximum width occurring at mid-height. Sporangia shape is quite variable, from fusiform (JM095b, Plate 3.19*a*) to bulbous (RH2_8, Plate 3.19*b*). Sporangia taper to a tip, which ranges in morphology from pointed (RH248_1, Plate 3.19*c*; RH005_1 Plate 3.19*d*), to rounded (JM280a, Plate 3.19*e*; RHSp52b, Plate 3.19*f*) to blunt (JM074b, Plate 3.19*g*). Sporangial height ranges from 0.35mm to 0.94mm (average 0.72mm), whilst sporangial width ranges from 0.21mm to 0.51mm (average 0.38mm). The largest sporangium measured 0.94mm in height, and 0.51mm in width (JM037a, Plate 3.19*h*).

The sporangial to axial junctions are unclear on all specimens, but ranges approximately from 0.07 to 0.18mm in width (average 0.12mm). The subtending axes gradually taper away to become parallel-sided, ranging in width between 0.07 and 0.15mm (average 0.10mm). These axes are too fragmentary to ascertain branching type, with the longest of subtending axes only 1.36mm in length.

Some specimens are associated with orange iron-oxide haloes (Plate 3.19*b* and 3.19*c*).

Discussion

Although these specimens are most similar in gross morphology and size to *Tortilicaulis offaeus* Edwards et al. (1994), there is no anatomical evidence to suggest that peripheral sporangial wall cells have a spiral orientation, and therefore they cannot be included in the genus *Tortilicaulis*. The larger specimens with tapering apices and rounded to blunt tips, such as specimens JM095b and RH005_1 are similar to *Salopella marcensis*. Edwards et al. (1994) also described *Salopella*-like elongate sporangia similar to the Tredomen Quarry specimens, with a size range from 0.35mm to 0.86mm. Therefore the majority of these specimens will be assigned to cf. *Salopella marcensis*.

3.2.3: *Non-embryophytes and non-vegetative fossils*

A third major group of fossils, the non-embryophytes, was found within horizons at the base of Tredomen Quarry (PB2 in Figure 2.2, Chapter 2), within green intraformational

Figure 3.16: Outlines of other mesofossils with elongate sporangia from Tredomen Quarry. Scale bar = 1mm

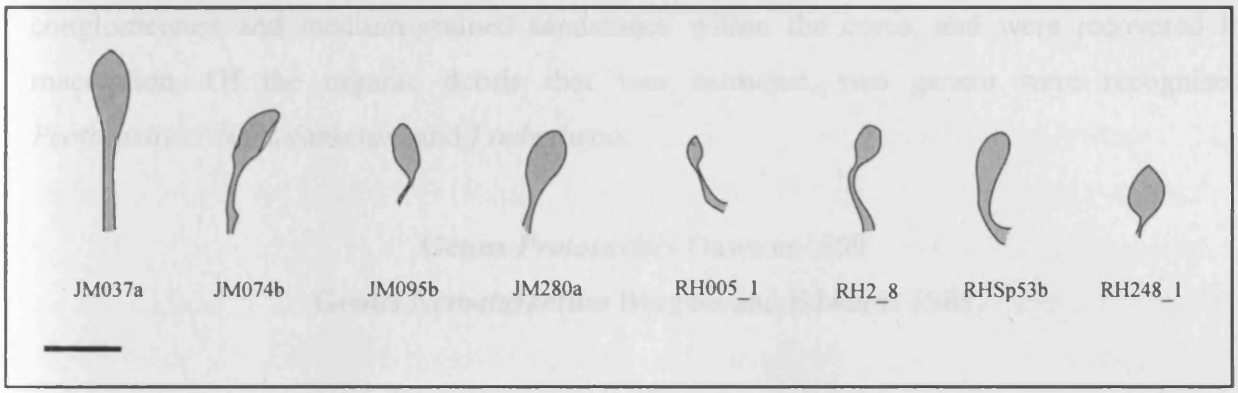

conglomerates and planar-bedded, medium-grained green sandstones, in association with cephalapid specimens (Plate 3.20*a*). Fragments of non-embryophytes were also found in conglomerates and medium-grained sandstones within the cores, and were recovered by maceration. Of the organic debris that was extracted, two genera were recognised; *Prototaxites* / *Nematasketum* and *Pachytheca*.

Genus *Prototaxites* Dawson 1859

Genus *Nematasketum* Burgess and Edwards 1988

Description

The largest and most common fossils found within Tredomen Quarry and cores are wood-like fragments with longitudinal striations, which can be found preserved in two ways. Firstly, charcoalified three-dimensionally preserved, wood-like fragments up to 2cm in diameter are found in intraformational conglomerates (Plate 3.20*b*). Preservation is excellent, with clear anatomical structures preserved. Secondly, larger coalified compressions can be found just above the conglomerates within medium-grained green sandstones (largest being an axial-like fossil 5cm in width and 30cm in length, Plate 3.20*c*). These compression fossils are often poorly preserved, with no anatomy present, and appear as black irregular-shaped patches along bedding planes of the sandstones (Plate 3.20*d*). However, where partial three-dimensional preservation has occurred, anatomical detail is visible (Plate 3.20*e*). Although some fragments are eroded and misshapen, some specimens do still retain their overall morphology. A number of specimens are greater in length than width, and taper to a broad point (Plate 3.20*f* and Plate 3.20*g*). Other specimens are parallel-sided (Plate 3.20*h*). Oval shaped protuberances, aligned parallel to the fragment length, occur on two specimens (Plate 3.20*i* and Plate 3.20*j*). All fragments are associated with iron-oxide weathering.

Anatomy

In both charcoalified, and the partially three-dimensional coalified compressions, fragments are made up of parallel-aligned tubes of different sizes and widths (Plate 3.21*a* and Plate 3.21*b*). The structure essentially has three types of tube. Firstly the most obvious component consists of relatively wide (approximately 10 to 20μm in diameter), uniformly thick-walled tubes (5μm). These tubes are parallel aligned, straight and unbranching, with smooth external and internal surfaces (Plate 3.21*c*). In cross section, these tubes are generally circular in

shape, but oval shaped tubes have also been observed. The length of these relatively large tubes is undetermined, but can reach a length of at least 300μm.

The second type of tube is similar in dimensions to the wide, smooth-walled tube, although they are more sinuous, and have anastomosing or incomplete thickenings, 1 to 2μm thick and approximately 2μm apart, on the inner surface of the tube (Plate 3.21*d* and Plate 3.21*e*). However, it has been noted that these interior thickenings can disappear along the length of the tube (Plate 3.21*f*). In most cases these large tubes are unbranched, but cross-sections reveal evidence that some may branch, although this is unclear (Plate 3.21*g* and Plate 3.21*h*). These tubes are much less common than the smooth-walled types, with only three or four occurring per fragment, usually in the same region.

The third tube type joins the larger tubes together, forming a network of smaller tubes (approximately 5μm in diameter) (Plate 3.21*i*). These smaller tubes are either unbranched or branched, and can either be parallel-aligned with the larger tubes (Plate 3.21*j*), or randomly orientated (Plate 3.21*i*). The proportion of large tubes to small filaments varies from large tube walls touching (Plate 3.21*k*), to large tubes sparsely distributed amongst masses of smaller ones (Plate 3.21*l*). This density change occurs between different fragments, but also within one fragment.

Discussion

These specimens are similar to the striated, charcoalified fragments described by Burgess and Edwards (1988), which were initially described as *Prototaxites* sp., but were assigned to a new genus, *Nematasketum* Burgess and Edwards (1988) after anatomical analysis. The type species, *Nematasketum diversiforme* was described as consisting of: wide, thick-walled, unbranched tubes with smooth, inner surfaces; wide, branched tubes with thickenings on the inner surfaces of tube walls (annular, anastomosing or incomplete); a network of narrow, branched filaments with smooth walls and septa; and infrequent wider, smooth-walled, branched, thin-walled filaments. The Tredomen Quarry specimens are very similar, although the wide, branched tubes with internal thickenings are less abundant, and the evidence for branching is equivocal. Burgess and Edwards (1988) also described medullary spots; sub-spherical to spherical clusters of very narrow, randomly orientated branching smooth-walled tubes, which have not been seen in the Tredomen Quarry specimens, and are being studied at depth in another study.

These fragments are also broadly similar to silicified axial fragments described from the Emsian Gaspé Bay, which were described by Dawson (1859), as having parallel-aligned

striations, consisting of tubes of different sizes, for which Dawson erected a new genus, *Prototaxites*. Hueber (2001) published a review of *Prototaxites*, and provided a systematic description for the genus based on an original specimen Dawson collected, *Prototaxites loganii*. Three types of 'tubes' or hyphae were recognised: 'skeletal' hyphae are thick-walled, relatively large, straight or sinuous, long, aseptate and unbranched; 'generative' hyphae are thin-walled, large, septate, and profusely branched; and 'binding' hyphae are smaller, septate, profusely branched, forming an irregular mesh surrounding the larger hyphae. Hueber then compared Dawson's specimen with other specimens of *Prototaxites loganii*, *Prototaxites southworthii* (Arnold 1952) and *Prototaxites* sp. from Australia, and concluded that the anatomy described was consistent.

The anatomy of the Tredomen Quarry specimens described here are broadly similar to those described by Hueber (2001), with large thick-walled, aseptate, unbranching hyphae, surrounded by a network of smaller, branching hyphae. However, the thin-walled, septate, branching 'generative' hyphae described by Hueber have not been observed in the Tredomen Quarry specimens. Additionally, all hyphae in *Prototaxites* are smooth-walled, with no evidence for thickenings on the interior surface of the hyphae as seen in the Tredomen Quarry specimens. Therefore, these specimens are different from *Prototaxites loganii*.

Therefore the Tredomen Quarry specimens with well-preserved anatomy, showing wide, branching hyphae with internal thickenings, will be named *Nematasketum* sp. However, most specimens collected are too poorly preserved to observed anatomy, and will remain as *Prototaxites* sp., based on the longitudinal striations on the surface of the fossil.

When Dawson (1859) erected the genus *Prototaxites*, the name suggests that his intention was to classify the genus with conifers (*Taxus*). In 1872, Carruthers restudied Dawson's samples and illegitimately renamed *Prototaxites* as *Nematophycus*, and classified the genus under the green algae, Codiaceae. Since then the affinity of *Prototaxites* has been subject of much controversy. In 1889, Penhallow illegitimately renamed *Prototaxites* to *Nematophyton* and classified the genus under the brown algae, Laminariaceae, despite growing evidence of a terrestrial habitat for these organisms. It was not until Church in 1919 that the first suggestion that *Prototaxites* might be a fungus was proposed. Since then, numerous specimens of *Prototaxites* have been collected from Upper Silurian to Upper Devonian terrestrial strata from the Anglo-Welsh Basin (Edwards and Richardson 1974, Edwards and Rogerson 1979), central Europe (Schmidt and Teichmuller 1954), Canada (Arnold 1952), Australia (Hueber 2001), as well as the largest specimen in Saudi Arabia, 1.37m in diameter at the base, and

5.3m long (Hueber 2001). Hueber (2001) placed the genus in the class Basidiomycetes, as a sporophore of higher fungi comprised of filamentous hyphae.

Boyce et al. (2007) provided further evidence supporting the hypothesis that *Prototaxites* was a fungal-like organism, by comparing the stable carbon isotope range of organic matter from *Prototaxites* and vascular plants from the Lower and Upper Devonian. Boyce et al. determined that in the Lower Devonian $\delta^{13}C$ values for *Prototaxites* and vascular plants were similar, whilst in the Upper Devonian *Prototaxites* values were either similar or significantly heavier, suggesting *Prototaxites* was a heterotroph, living on an isotopic heterogeneous landscape (Boyce et al. 2007) (see Chapters 7 and 8 for further discussion).

Hyphae

Within the green, wavy-laminated siltstone horizons of plant bed 1(PB1, Figure 2.2, Chapter 2), minute coalified strands occur in association with the mesofossils and megafossils. When observed closely, these strands are banded tubes, are no more than 50μm in width, and intertwine or bifurcate (Plate 3.22*a*). They appear to weave in and out of the top surface of the rock (Plate 3.22*b*). In places they are densely packed, parallel-aligned, and form an axial-like structure which branches (Plate 3.22*c*), or appear mat-like, with tubes running at a variety of angles to each other (Plate 3.22*d*). Under the SEM it has been observed that some of these tubes are infilled with limonite, which has preserved the annular thickenings of the internal walls as impressions (Plate 3.22*e*, taken by Rhian Hicks). Fragments are also commonly associated with orange iron-oxide.

The presence of banded tubes in Lower Silurian to Lower Devonian strata have been known for some time (Lang 1937, Edwards 1982, Burgess and Edwards 1991, Edwards and Wellman 1996). Although their affinity and ecology is controversial, there is a consensus that these banded tubes derived from nematophytes, a group of enigmatic terrestrial organisms from the Silurian and Early Devonian, including *Prototaxites*, *Nematasketum* and *Nematothallus* (Gray et al. 1985, Burgess and Edwards 1991, Wellman 1995, Edwards and Wellman 1996, Taylor and Wellman 2009). Pratt et al. (1978) first suggested that these banded tubes might be water-conducting cells. Taylor and Wellman (2009) compared dispersed banded tubes with vascular plant tracheids, bryophyte rhizoids and conducting cells, as well as fungal hyphae, and hypothesised that the function of these banded tubes may be either: internal transport in early vascular plants or mosses; anchorage similar to rhizoids; or acquisition and transportation of water and nutrients, similar to fungal hyphae. The latter

function fits with the hypothesis that some nematophytes, namely *Prototaxites*, was a fungal-like organism (Boyce et al. 2007).

Pachytheca (Hooker 1853)

Found in association with *Prototaxites*, within intraformational conglomerates of plant bed 2 (PB2, Figure 2.2, Chapter 2), are small coalified spheres (no more than 1.5mm in diameter) with a smooth, vitreous outer surface (Plate 3.23*a* and Plate 3.23*b*). Where these spheres are fractured, a multi-layered internal structure can be seen under SEM, with three main layers (Plate 3.23*c*).

The central core is poorly preserved and missing from these specimens. Small portions however do remain, and consist of narrow tubes (0.5 to 1μm thick), which are randomly orientated, bifurcating and anastomosing (Plate 3.23*d*). This central core is surrounding by radially arranged tubes, making up the bulk of the sphere (Plate 3.23*e*). These tubes are approximately 10μm in diameter and 2 to 3μm apart. Where the interior of these tubes is visible, it is revealed that many tubes possess annular thickenings (Plate 3.23*f*). Some tubes also possess a thin, flattened septal-like body that runs down the centre, appearing to split the tube in half (Plate 3.23*g* and Plate 3.23*h*). Where these tubes met the central core, they often possess bulbous ends (Plate 3.23*i*), whilst the outer ends appear open, although narrower (Plate 3.23*j*), and covered with a smooth amorphous layer (1-2μm thick) (Plate 3.23*j* and Plate 3.23*k*). In one specimen, this layer is surrounded by a thicker layer (approximately 50μm thick) and has a sponge like texture with small voids (Plate 3.23*l*). These spheres can be placed in the genus *Pachytheca* Hooker 1853 (Hooker 1889), and are thought to be of algal affinity (Niklas 1976).

Detailed descriptions and analysis of *Pachytheca* was beyond the scope of this thesis, however the structures described here are very similar to those in a comprehensive investigation of the genus by Elena Méndez (unpublished thesis, 1997), based on material from a middle Lochkovian locality, approximately 80km northeast of Tredomen Quarry, as well as .

3.3: Chapter discussion and summary

The Tredomen Quarry palaeobotanical collection indicates that during the Early Devonian (early Lochkovian) the landscape around central-South Wales was inhabited by at least the

following components; a diverse assemblage of simple axial plants with smooth naked axes, terminating in sporangia (the megafossils); minute, complexly branched axial plants with a range of sporangial morphologies (the mesofossils); and the non-embryophytes, including a fungal-like organism, *Prototaxites*/ *Nematasketum*, and the enigmatic *Pachytheca*.

Changes in early embryophyte characters between lower Přídolí and lower Lochkovian strata from the Anglo-Welsh Basin.

The most recognisable group of plant fossils from Tredomen Quarry were the megafossils: predominately dichotomously branched naked axes, terminated by sporangia with a range of morphologies, from squat and reniform, to elongate and fusiform. These megafossils have been identified as stem-group early land plants that resemble the later vascular plants (tracheophytes), but with the exception of *Cooksonia* (Edwards et al. 1992), lack any evidence for tracheids, and therefore should be referred to as rhyniophytoids. This group is commonly known from the Lower Devonian, represented at Tredomen Quarry by *Cooksonia*, cf. *Uskiella / Tarrantia*, *Salopella* and a new genus of dichotomously branched axes with club-shaped sporangia.

Differences in sporangial and branching characters have been observed between Late Silurian (Přídolí) and Early Devonian (lower Lochkovian) rhyniophytoid specimens from Anglo-Welsh Basin and global localities. Sporangia from Early Devonian rhyniophytoids from the Anglo-Welsh Basin are overall slightly larger than those from the Late Silurian (Přídolí). Specimens of cf. *Cooksonia caledonica* from lower Přídolí strata from Freshwater East Bay, Pembrokeshire (Edwards 1979) have smaller sporangial height and width ranges compared to the lower Lochkovian Tredomen Quarry specimens, which are closer in size to *Renalia heuberi* from the Emsian Gaspé Bay, Canada (Gensel 1976) (see Table 3.1). Přídolí specimens of *Cooksonia hemisphaerica* and *Cooksonia cambrensis* from Freshwater East Bay also have smaller sporangial dimensions compared to specimens from Tredomen and Targrove Quarries (Table 3.1).

In terms of sporangial morphology, the rhyniophytoid taxa of the Late Silurian Anglo-Welsh Basin predominately bore sporangia with height to width ratios below or equal to 1, resulting in discoidal, reniform or hemispherical sporangia (e.g. *Cooksonia pertoni*, cf. *Cooksonia caledonica*, *Hollandophyton colliculum*, *Cooksonia cambrensis*, *Cooksonia hemisphaerica*). Only a few taxa bore small, slightly elongate sporangia (e.g. *Steganotheca*, *Caia* and *Tortilicaulis*) (see Table 1.4, Chapter 1). In contrast a number of rhyniophytoid taxa with

Table 3.1: Comparisons of rhyniophytoid dimensions between Tredomen Quarry, other Anglo-Welsh Basin and global localities.
AWB = Anglo-Welsh Basin. BBQ = Brecon Beacons Quarry.

Species		Sporangia Height mm	Sporangia Width mm	Height : width ratio	Junction width mm	Axis width mm	Age	Reference
cf. *Cooksonia caledonica*, Tredomen Quarry, AWB		**0.8- 2.40 (1.55)**	**1.22-2.90 (2.18)**	**0.53- 0.98 (0.71)**	**0.5-1.54 (0.96)**	**0.2-1.0 (0.6)**	**Lower Lochkovian**	this thesis
Cooksonia caledonica, Scotland	globular	1.2-2.0 (1.7)	1.3-2.2 (1.8)	c.0.7	/	0.4-1.8 (0.65)	Lochkovian	Edwards 1970a
	oval	1.1-1.8 (1.6)	1.8-3.0 (2.4)				Lochkovian	
cf. *Cooksonia caledonica*, Freshwater East Bay, AWB.		0.8-1.7 (0.47)	0.4-1.7 (0.8)	0.63	0.15-0.9 (0.33)	0.1-0.45 (0.15)	Lower Přídolí	Edwards 1979
Renalia hueberi, Gaspé Bay, Canada		0.75-2.5	0.75-3.5	/	/	0.5-1.5	Emsian	Gensel 1976
Cooksonia cf. *caledonica*, Bolivia		0.92-1.5	1.4-1.79	c. 0.85	/	0.3-0.5	Ludlow-Lower Přídolí	Morel et al. 1995
Resilitheca salopensis, Clee Hills, AWB		1.07-2.07 (1.36)	1.17-4.21 (2.13)	/	/	0.18-0.91	Mid Lochkovian	Edwards et al. 1995
***Cooksonia hemisphaerica*, Tredomen Quarry, AWB**		**0.89-2.8 (1.86)**	**0.7-3.1 (1.79)**	**0.75-1.5 (1.05)**	**0.4-2.5 (1.06)**	**0.13-1.4 (0.58)**	**Lower Lochkovian**	this thesis
Cooksonia hemisphaerica, Targrove Quarry, AWB		0.68-2.08	0.83-3.25	c. 1.06 up to 1.5	/	0.27-1.07 (0.60)	Lower Lochkovian	Lang 1937, Fanning et al. 1992
Cooksonia hemisphaerica, Freshwater East Bay, AWB		0.2-2.0	0.3-2.0	0.98	0.15-0.7	0.25-1.6	Lower Přídolí	Edwards 1979
***Cooksonia* cf. *cambrensis*, Tredomen Quarry, AWB**		**1.68-2.40 (2.04)**	**2.0-2.70 (2.29)**	**0.74-1.0 (0.9)**	**0.6-1.4 (1.0)**	**0.55-1.0 (0.7)**	**Lower Lochkovian**	this thesis
Cooksonia cambrensis Freshwater East Bay, AWB	forma α	0.5-0.95	0.4-0.9	c. 0.99	0.1-0.38	0.06-0.5	Lower Přídolí	Edwards 1979
	forma β	0.3-1.3	0.35-1.77	c. 0.73	0.06-0.5			
cf. *Uskiella/ Tarrantia sp.*, Tredomen Quarry, AWB		**1.13-3.6 (2.32)**	**1.0- 2.7 (1.73)**	**0.88- 2.80 (1.40)**	**0.2-1.5 (0.77)**	**0.2- 1.30 (0.54)**	**Lower Lochkovian**	this thesis
Uskiella spargens, AWB	Llanover Quarry	3.0-5.3 (3.94)	2.0-4.0 (2.89)	c. 1.3	1.4-1.2	c.0.93	Upper Lochkovian-Lower Pragian	Shute and Edwards 1989
	BBQ	1.4-4.4 (2.6)	1.0-3.5 (2.26)	c. 1.15	0.3-1.2	c.0.7		

Table 3.1: Comparison of rhyniophytoid dimensions between Tredomen Quarry, other Anglo-Welsh Basin and global localities (continued).

Species		Sporangia Height mm	Sporangia Width mm	Height : width ratio	Junction width mm	Axis width mm	Age	Reference
Uskiella reticulata, Targrove Quarry, AWB		0.53-2.0	0.38-1.50	1.25-1.83	0.05-0.50	0.05-0.5	Lower Lochkovian	Fanning et al. 1992
Tarrantia salopensis, Targrove Quarry, AWB		0.38-2.63	0.25-2.0mm	1.3-2.0	/	0.13-0.88	Lower Lochkovian	Fanning et al. 1992
***Salopella allenii*, Tredomen Quarry, AWB**		**4.0- 11.9 (9.24)**	**1.0- 3.14 (2.45)**	**3.14-4.5 (3.82)**	**0.3- 2.0 (1.16)**	**0.5-2.0 (1.49)**	**Lower Lochkovian**	this thesis
Salopella allenii, Clee Hills, AWB		2	9	4.5	1.1	1.1-2.0	Mid -Up. Lochkovian	Edwards and Richardson 1974
Salopella australis, Australia		6.5-14	1.3-2.9	c. 5.6	/	0.9-2.4	Late Sil.- Early Dev.	Tims and Chambers 1984
Salopella caespitosa, Australia		4.5	1.7	2.64	1.7	1.1-1.9	Late Sil.- Early Dev.	Tims and Chambers 1984
***Salopella* cf. *marcensis* Tredomen Quarry, AWB**		**1.6-3.38 (2.47)**	**0.5-1.5 (0.85)**	**2.25-4.0 (3.07)**	**0.15-0.63 (0.28)**	**0.15-0.63 (0.39)**	**Lower Lochkovian**	this thesis
Salopella marcensis, Targrove Quarry, AWB		0.75-3.38 (1.6)	0.25-0.88 (0.54)	2.59-5.0	/	0.05-0.5	Lower Lochkovian	Fanning et al. 1992
Elongate club-shaped sporangia, Tredomen Quarry, AWB	**a**	**1.0-2.2 (1.43)**	**1.2-2.5 (1.62)**	**0.59-1.29 (0.92)**	**0.5-1.36 (0.98)**	**0.4-0.8 (0.58)**	**Lower Lochkovian**	this thesis
	b	**2.06-5.6 (3.72)**	**1.2-2.5 (1.66)**	**1.19-4.10 (2.31)**				
Steganotheca striata, Chapel Horeb, AWB		1.8-2.7	1.0-1.5	c. 1.8	/	0.4-0.8	Lochkovian	Edwards 1970

relatively large vertically-borne elliptical to elongate sporangia appeared in the Early Devonian: *Uskiella reticulata, Tarrantia salopensis*, *Salopella allenii, Salopella marcensis* and the new genus discovered from Tredomen Quarry with elongate, club-shaped sporangia. Although no clear dehiscence lines were recognised from the Tredomen Quarry specimens due to poor preservation, it must be noted that this sporangial character also changed between the Přídolí and the Early Devonian. The earliest rhyniophytoid sporangia show no modifications of sporangial wall cells to suggest the presence of controlled, predetermined dehiscence mechanisms (e.g. *Cooksonia cambrensis*, *Cooksonia hemisphaerica*, *Cooksonia pertoni*) (Edwards and Fanning 1985, Fanning et al. 1992, Edwards 1996). Instead spore dispersal likely occurred by the disintegration of the distal part of the sporangium (Edwards 1996). By the Late Silurian however, spore dispersal in some rhyniophytoid taxa occurred via the splitting of valves, either by the removal of a lid-like valve (e.g. circular sporangia described by Edwards 1996), or splitting into two equal valves (e.g. *Hollandophyton colliculum* Rogerson et al. 2002).

These two forms of dehiscence continued into the Lochkovian (e.g. *Cooksonia banksii* Habgood et al. 2002; cf. *Cooksonia caledonica* Fanning et al. 1992, *Resilitheca salopensis* Edwards et al. 1995b, and *Sporathylacium salopense* Edwards et al. 2001). By the Early Devonian, elongate sporangia had appeared with evidence of predetermined dehiscence mechanisms, by splitting of the sporangium into two equal halves, down the longest sporangial axis e.g. *Uskiella spargens* (Shute and Edwards 1989), *Salopella* cf. *marcensis* (Edwards and Richardson 1994), *Tortilicaulis transwalliensis* (Edwards 1979). Twisting of the cell walls in *Tortilicaulis* may be part of the dehiscence mechanism, a character observed in certain extant mosses and liverworts (Edwards 1979), as well as *Psilophyton* (Banks et al. 1975, Edwards et al. 1994).

Differences in sporangia characters were not the only differences observed between Late Silurian and Early Devonian rhyniophytoids. The Tredomen Quarry specimens show more complex branching patterns (anisotomously and pseudomonopodially branched axes) compared with the simple, isotomously branched axes of the Přídolí specimens. Specimens of *Cooksonia hemisphaerica*, *Uskiella reticulata/ Tarrantia salopensis* and *Salopella allenii* from Tredomen Quarry have been described as having an element of anisotomous branching, while pseudomonopodial branching has been observed in specimens of cf. *Cooksonia caledonica* / *Renalia* sp.

The changes in sporangia and branching characters of rhyniophytoids observed from the lower Přídolí to lower Lochkovian are all related to increasing the quantity and effectiveness

of spore dispersal. An overall increase in sporangial size and a trend towards elongation of sporangial shape allow increased spore production within individual sporangia. Anisotomous and pseudomonopodial branching increased the number of axes and hence spore production of the whole plant. Development of predetermined dehiscence mechanisms, particularly within elongate sporangia improved spore dispersal effectiveness. The inferred improved spore dispersal between the Late Silurian and Early Devonian may have been driven by increased competition. This supports the competitive replacement of lineages hypothesis suggested by Edwards and Davies (1990), with innovations in sporangial and branching characters resulting in the diversification of the zosterophylls potentially at the expense of the rhyniophytes.

Mesofossil affinity

The second group of Lower Devonian vegetation recognised from Tredomen Quarry are minute, simple to complexly branched naked axes, terminated by sporangia with a range of morphologies. This diverse group have been separated from the rhyniophytoids based on two criteria: size, with the largest sporangium being half the size of the smallest rhyniophytoid sporangium; and complexity of branching, these fossils being the first examples of minute sporangia attached to branching axes.

Similar minute sporangia have been discovered from Přídolí and middle Lochkovian localities (Edwards 1996, Edwards 2000), which can be considered to be broadly synonymous to the Tredomen Quarry specimens. However, although the Přídolí and middle Lochkovian sporangia are exceptionally well-preserved via charcoalification, revealing anatomical details and *in situ* spores, they are at best attached to short lengths of branching axes, and branching patterns could not be determined. It had not been possible to distinguish these minute sporangia from the fertile, possibly immature tips of larger rhyniophytoids. The fossils from Tredomen Quarry however provide for the first time evidence of a separate component of turf-sized vegetation living alongside the larger rhyniophytoids.

The affinity of these minute plants is highly contentious. It is without doubt that some of the specimens from the Přídolí and middle Lochkovian localities are early tracheophytes, with evidence of tracheids (*Cooksonia pertoni,* Edwards et al. 1992) and *in situ* triletes (*C. pertoni*, Fanning et al. 1998; *Tortilicaulis offaeus*, Edwards et al.1994; cf. *Horneophyton* sp., Edwards and Richardson 2000). Other specimens were found to contain cryptospores, both as dyads (within *Fusitheca fanningiae* and *Culullitheca richardsonii*, Wellman et al. 1998) and permanent tetrads (within *Grisellatheca salopensis*, Edwards et al. 1999). It has been

suggested that the permanent tetrads, that are found in abundance in the dispersed spore record as far back as the Llanvirn (Strother et al. 1996), were produced by plants of bryophytic grade (Gray et al. 1985, Edwards et al. 1998). Despite similarities in sporangial size and the presence of *in situ* cryptospores in some sporangia, the new evidence indicates that these minute Early Devonian plants were complexly branched, and therefore unlikely that they were true bryophytes, as the sporophyte of extant bryophytes are simple unbranching axes, each terminated by a single capsule (Shaw and Renzaglia 2004).

Unfortunately the coalified axes of the mesofossils from Tredomen Quarry were too poorly preserved to ascertain if these minute plants contained water-conducting tissues. However, vascular tissues have been recorded from some minute specimens (Edwards 2000, Edwards 2003), including simple tracheids found in a *Cooksonia pertoni* axis, Edwards et al. (1992). Rare stomata have also been reported (Edwards 2000). These characters suggest affinity with the early tracheophytes.

Little is known regarding growth habit or life cycle of these mesofossils or indeed the larger rhyniophytes, mainly due to the allochthonous nature of the fossil assemblages from the Anglo-Welsh Basin strata, preserving only fragments of the sporophytes. There is no fossil evidence from Anglo-Welsh Basin specimens to determine if these early land plant sporophytes were dependent on a gametophyte generation or were in fact independent, photosynthetic aerial axes, rooted to the substrate by rhizomes (Boyce 2008). However, exceptionally well-preserved early land plant specimens from the Pragian Rhynie chert (including *Aglaophyton major* (Kidston and Lang 1917) Edwards 1986; *Nothia aphylla* (Kidston and Lang 1920) El-Saadawy and Lacey 1979; and *Rhynia gwynne-vaughanii* Kidston and Lang 1917) have been found with basal rhizomes (Edwards 1980, Edwards 1986, Kerp et al. 2001) and in association with independent gametophytes (Remy and Remy 1980, Remy and Hass 1996, Kerp et al. 2004, Taylor et al. 2005). It can therefore be inferred that the Late Silurian to Early Devonian early land plant sporophytes, represented by the megafossils, were not gametophyte dependant, unlike modern bryophytes.

Raven (1984, 1993) quantitatively analysed the homoiohydric apparatus (e.g. water-conducting cells, stomata) of early land plant sporophytes and confirmed that they would have been capable of independent photosynthesis. Boyce (2008) questioned if the smaller mesofossils axes were capable of photosynthesis, relying on the gametophyte for this function. Due to the simplicity of early land plants, Boyce (2008) suggested that all functions required for independence (photosynthesis, structural support, hydraulic and solute transport and desiccation resistance) had to have occurred in the sub-aerial axes. For all these

requirements to be fully functional, Boyce (2008) modelled that the axes must have been at least 1mm in diameter, and that in plants with smaller axes some functions, in particularly photosynthesis, must have been differentiated into a different tissue, most likely the gametophyte. He therefore questioned the independence of *Cooksonia*, a genus which contains a number of species with large size ranges (e.g. *Cooksonia pertoni*), with some specimens with axes that are below 1mm in diameter.

Cooksonia is diagnosed as naked dichotomously branched axes with sporangia that are 'short and wide', with a central strand composed of annular tracheids (Lang 1937, Edwards 1979). As most specimens are poorly preserved with no anatomical details, sporangial morphology has been the main diagnostic feature of these simple plants, with sporangia that have height to width ratios of less than 1. Specimen size has therefore not been a diagnostic feature when identifying specimens at genus level and perhaps the smallest specimens (with axes less than 1mm), including *Cooksonia pertoni* and *Cooksonia banksii*, should not strictly be in the same genus as the larger *Cooksonia hemisphaerica* and *Cooksonia caledonica*. The larger specimens of *Cooksonia* were certainly large enough to be capable of independent photosynthesis, while the smaller specimens, together with the other mesofossils may have been gametophyte dependant. Therefore these mesofossils are best described as stem-group embryophytes with bryophytic characters, including the presence of permanent *in situ* cryptospores and possible gametophyte dependence (although there is no fossil evidence as yet to support this), and were ancestral to the larger rhyniophytes and rhyniophytoids. This group may have evolved prior to the Late Silurian from gametophyte-dependant unbranching bryophytes, the presence of which has been inferred from the permanent cryptospore record that goes back to the Llanvirn (Strother et al. 1996).

Importance of the non-embryophytes in Lower Devonian palaeo-ecosystems

A third group of Lower Devonian vegetation from Tredomen Quarry comprises the non-embryophytes and although rather enigmatic, have the largest biomass preserved of all the fossils in the collection. As colonisation of the land by vascular plants was a key event in Earth history, studies of Silurian and Early Devonian palaeobotany have focussed on the early vascular plants, but perhaps negating the importance of the non-embryophytes in Silurian and Early Devonian landscapes, palaeoecology and the carbon cycle. The most common fossils preserved are charcoalified and coalified fragments of *Nematasketum*/ *Prototaxites*, thought to be a perennial, fungal-like, heterotrophic organism (Hueber 2001, Boyce et al. 2007), supported by large rhizomorphs, from which mycelium emanated into the

substrate (Hillier et al. 2008). Hyphal networks would have absorbed nutrients from the substrate, including deposits rich in rhyniophytoid and rhyniophyte vegetative debris.

The importance of fungal activity during the Early Devonian has also been highlighted from exceptionally well-preserved Rhynie chert specimens, showing fungal interactions with early land plants, algae (to form lichens), other fungi, and even animals (Taylor et al. 2004), either as saprophytes (Taylor et al. 1994), parasites (Taylor et al. 1999) or mutualists (Taylor et al. 1995, Kriggs et al. 2007).

As well as evidence of fungi, *Pachytheca* could represent the algal component at Tredomen Quarry. Niklas (1976) considered *Pachytheca* to be of algal affinity, although other authors have suggested, due to their apparent association within the same fossil assemblages, that these spheres may be the reproductive structures of *Prototaxites* (Dawson 1882, Jonker 1979). However there is no fossil evidence to link *Pachytheca* and *Prototaxites* directly.

Diversity of lower Lochkovian Anglo-Welsh Basin embryophytes in a global context

On the whole, the plant assemblages from Tredomen Quarry are very similar to those collected from the contemporaneous (lower Lochkovian) localities at Targrove Quarry (Fanning et al. 1992) and North Brown Clee Hills (Fanning et al. 1988, Edwards et al. 1994). *Cooksonia hemisphaerica,* cf. *Cooksonia caledonica/ Renalia* sp. and *Uskiella reticulata/ Tarrantia* sp. are abundant in both Tredomen and Targrove Quarries (Figure 3.17), with smaller quantities of *Salopella marcensis, Tortilicaulis* and *Cooksonia cambrensis*. However, the abundance of *Cooksonia pertoni* at Targrove Quarry is not seen at Tredomen Quarry. Whilst *Salopella allenii* is common in Tredomen Quarry, Fanning et al. (1992) did not record its presence at Targrove Quarry, although a recent visit to this locality did reveal one specimen. The dichotomously branched axes terminated by large elongate club-shaped sporangia are also known only from Tredomen Quarry. These local variations in disparity may be due to the effects of taphonomic or lithofacies biases (Edwards 1990). In general however, all specimens from both localities are similar, being only simple, dichotomously branched, naked vascular plants with terminal sporangia.

The megafossil assemblage from Tredomen Quarry therefore supports the theory that during the lower Lochkovian the highest grade of organisation of vegetation across the Anglo-Welsh Basin were the rhyniophytes and rhyniophytoids, and that true zosterophylls (with laterally positioned sporangia) had not yet appeared (at least in the local rock record). Unequivocal

Figure 3.17: Comparison between a) Tredomen Quarry and b) Targrove Quarry palaeobotanical collections.

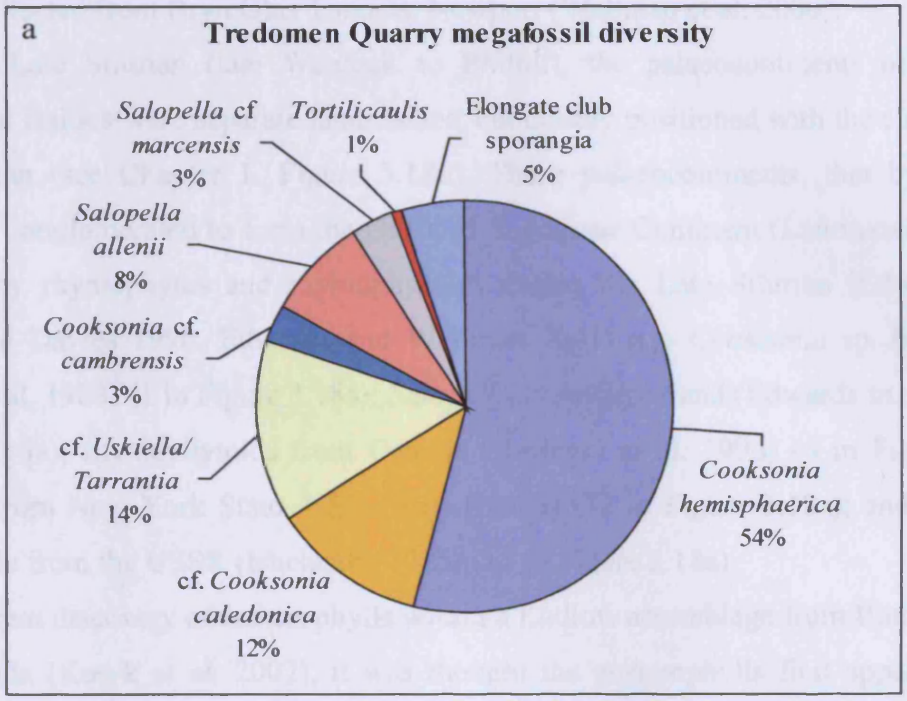

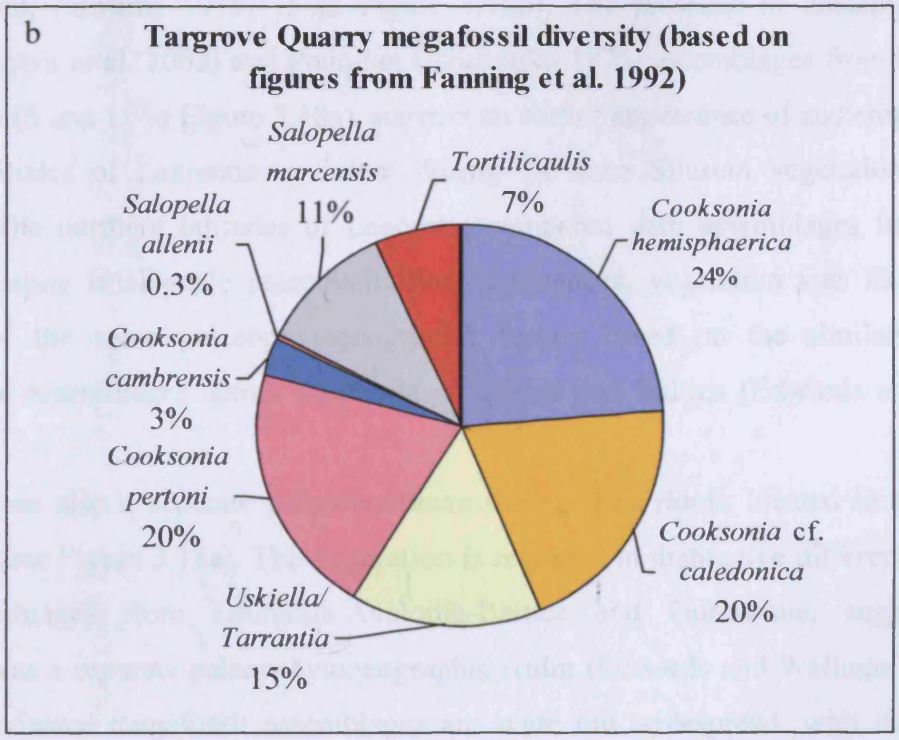

specimens belonging to the zosterophylls did not appear in the Anglo-Welsh Basin until the middle *micrornatus-newportensis* sub-biozone (middle Lochkovian), the oldest recognisable specimen collected from Bryn Glas Tunnels, Newport (Wellman et al. 2000).

During the Late Silurian (late Wenlock to Přídolí), the palaeocontinents of Laurentia, Avalonia and Baltica were separate landmasses, but closely positioned with the closure of the Iapetus Ocean (see Chapter 1, Figure 3.18a). These palaeocontinents, that by the early Lochkovian conglomerated to form the Old Red Sandstone Continent (Laurussia), were also dominated by rhyniophytes and rhyniophytoids during the Late Silurian (Edwards 1990, Edwards and Davies 1990, Edwards and Wellman 2001) e.g. *Cooksonia* sp. from Ireland (Edwards et al. 1983) (1 in Figure 3.18a); *Salopella* from Greenland (Edwards *in progress*) (5 in Figure 3.18a); rhyniophytoids from Canada (Basinger et al. 1996) (6 in Figure 3.18a); *Cooksonia* from New York State, USA (Banks 1973) (12 in Figure 3.18a); and *Cooksonia* and *Salopella* from the USSR (Ishchenko 1975) (11 in Figure 3.18a).

Until the recent discovery of zosterophylls within a Ludlow assemblage from Bathurst Island, Arctic Canada (Kotyk et al. 2002), it was thought the zosterophylls first appeared on the southern margins of Laurussia during the lower Lochkovian (*Zosterophyllum myretonianum* from Scotland, Edwards 1975, 15 in Figure 3.18b). The presence of zosterophylls from Canadian (Kotyk et al. 2002) and Podolian (Ishchenko 1975) assemblages from Ludlow and Přídolí strata (6 and 11 in Figure 3.18a), suggest an earlier appearance of zosterophylls in the northern latitudes of Laurentia, and that during the Late Silurian vegetation was more complex in the northern latitudes of Laurentia compared with assemblages further south. However, despite small-scale palaeolatitudinal differences, vegetation was likely to have been part of the same palaeophytogeographic realm, based on the similarities of the palynological assemblages across Laurentia, Avalonia and Baltica (Edwards and Wellman 2001).

Gondwana was also a separate palaeocontinent during the Přídolí, located in the southern hemisphere (see Figure 3.18a). This separation is reflected in distinctive differences between spore assemblages from Laurentia-Avalonia-Baltica and Gondwana, suggesting that Gondwana was a separate palaeophytogeographic realm (Edwards and Wellman 2001). Late Silurian Gondwana megafossil assemblages are scare but widespread, with rhyniophytoid assemblages from: Bohemia (Obrhel 1962, Schweitzer 1983) (8 in Figure 3.18a); Bolivia (Morel et al. 1995 and Toro et al. 1997) (2 and 7 in Figure 3.18a); Australia (Tims and Chambers 1984) (4 in Figure 3.18a); and Libya (Daber 1971) (13 in Figure 3.18a). These

Figures 3.18: Distribution of megafossil assemblages during a: the Ludlow-Přídolí and b: the :Lochkovian. Modified after Edwards and Wellman 2001.

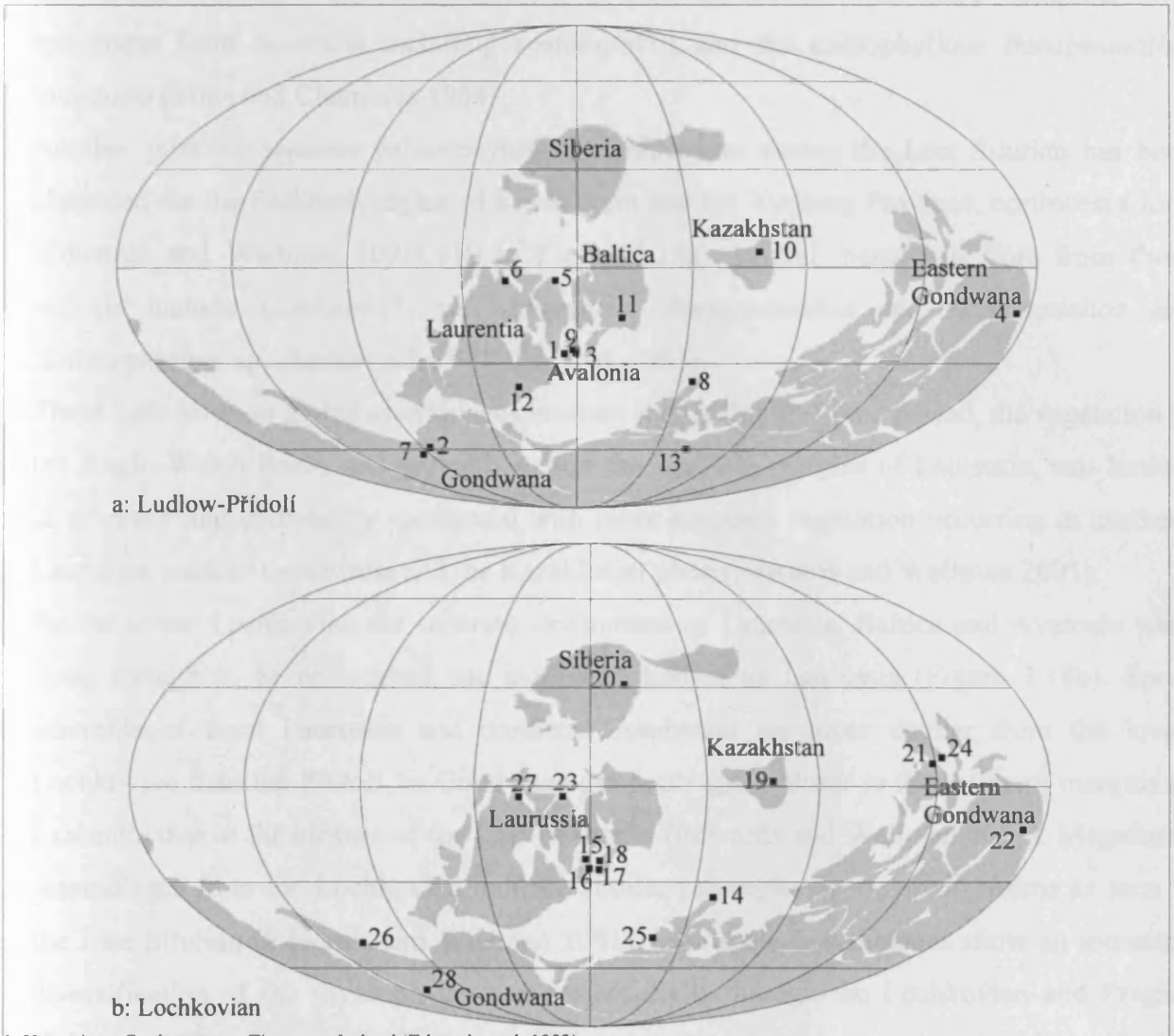

1. Homerian : *Cooksonia* sp., Tipperary, Ireland (Edwards et al. 1983)
2. Late Wenlock/ Ludlow: sterile rhyniophytes, South Bolivia (Toro et al. 1997)
3. Ludfordian-Gorstian: *C. pertoni*, *Cooksonia* sp., *Steganotheca striata*, Powys, Wales (Edwards 1979, Edwards and Rogerson 1979).
4. Late Ludlow: *Baragwanathia longifolia*, *Salopella australis*, *Hedeia* sp., zosterophylls, Victoria, Australia (Tims and Chambers 1984).
5. Ludlow/? Ludfordian: *Salopella* sp., North Greenland (Edwards *in progress*).
6. Ludlow: Cooksonioid types, Bathurst Island, Arctic Canada (Basinger et al. 1996). Zosterphylls (Kotyk et al. 2002).
7. ?Ludlow/ Přídolí: *Cooksonia* cf. *caledonica*, Bolivia (Morel et al. 1995).
8. Přídolí: *Cooksonia*, *Cooksonia bohemica* Bohemia (Obrhel 1962, Schweitzer (1983).
9. Přídolí: *C. pertoni*, *C. caledonica*, *C.cambrensis*, *C. hemisphaerica*, *Tortilicaulis transwalliensis*, *Psilophytites* sp., Dyfed, Wales (Lang 1937, Fanning et al. 1990, 1991a and b, Edwards 1979), *Steganotheca striata* (Edwards and Rogerson 1979).
10. Přídolí: *Cooksonella* sp., ?*Baragwanathia* sp. ?*Taeniocrada* sp. *Jugumella burubaensis*, Balkhash area, Kazakhstan (Senkevitch 1975)
10. Přídolí: *Cooksonella*, *Junggaria spinosa*, ?*Lycopodolica*, *Salopella xinjiangensis*, *Zosterophyllum* sp., Xinjiang, China (Cai et al. 1993).
11. Přídolí: *C. pertoni*, *C.hemisphaerica*, *Eorhynia* (*Salopella*), ?*Zosterophyllum* sp., *Lycopodolica*, Podolia, USSR (Ishchenko 1975).
12. Late Přídolí: *Cooksonia* sp. New York State, USA (Banks 1973).
13. Přídolí: *Cooksonia* sp. Libya (Daber 1971).
14: Lowermost Lochkovian: *Cooksonia downtonensis*, Bohemia (Obrhel 1968).
15: Lower Lochkovian: *Zosterophyllum myretonianum*, *C. caledonica* Scotland (Lang 1927, Edwards 1975), *Z. fertile* (Edwards 1972).
16: Lower-mid Lochkovian: *Tortilicaulis transwalliensis*, *Resilitheca*, *Uskiella reticulata*, *Tarrantia salopensis*, *C. hemisphaerica*, *C. pertoni*, *C. cambrensis*, *C. caledonica*, *S. marcensis*, Targrove Quarry, Shropshire, UK (Edwards and Fanning 1985). *Salopella* cf. *marcensis*, *Tortilicaulis offaeus*, *Resilitheca salopensis*, *C. pertoni*, *Grisellatheca salopensis*, *C. hemisphaerica*, cf. *Sporogonites*, *Pertonella* sp. *Fusitheca fanningiae*, *Cululitheca richardsonii*, *Tarrantia salopensis* Brown Clee Hill, Shropshire, UK (Edwards et al. 1994).
17: Upper Lochkovian: *Z. fertile*, Belgium (Leclercq 1942).
18: Upper Lochkovian: *Drepanophycus spinaeformis*, *Taeniocrada* sp.?, *Zosterophyllum rhenanum*, Rhineland, Germany (Schweitzer 1983).
19: ?Basal Gedinnian: *Cooksonella sphaerica*, *Taeniocrada pilosa*, *Jugumella burubaensis*, Balkhash, Kazakhstan (Senkevitch 1975).
20: Gedinnian: *Zosterophyllum*, *C. pertoni*, *Stolophyton acyclicus*, *Juliphyton glazkini*, *Uksunaiphyton ananievi*, *Pseudosajania pimula*, *Salairia bicostata*, Siberia (Stepanov 1975).
21: Gedinnian: *Zosterophyllum* sp. south-west China (Li and Cai 1978)
22: ?Lochkovian: *Baragwanathia longifolia*, *Zosterophyllum* n. sp., *Baragwanathia* n. sp., Victoria, Australia (Tims)
23: Gedinnian: *Hostinella*, *Taeniocrada*, *Zosterophyllum*, Spitsbergen (Høeg 1942).
24: ?Gedinnian: Undetermined terminal sporangia, *Viet Nam* (Janvier et al. 1987).
25: Gedinnian: *Sciadophyton steinmanni*, Spain (Alvarez-Ramis 1988, unpublished abstract)
26: ?Lochkovian: 2 new rhyniophytoids, 1 plant with enations, Argentina (Edwards et al. 2001c).
27: Lochkovian: not specified, Bathurst Island, Arctic Canada (Basinger et al. 1996).
28:?Lochkovian: *C.* cf. *pertoni*, *Sporogonites* sp., cf. *C. cambrensis*, *Pertonella* sp., *Salopella* sp., Brazil (Mussa et al. 1996, Gerrienne 1999)

assemblages indicate that vegetation in eastern Gondwana was more complex, with specimens from Australia including zosterophylls and the microphyllous *Baragwanathia longifolia* (Tims and Chambers 1984).

Another possible separate palaeophytogeographic realm during the Late Silurian has been identified for the Balkhash region of Kazakhstan and the Xinjiang Province, northwest China (Edwards and Wellman 2001) (10 in Figure 3.18a). Přídolí megafossil flora from these regions include *Cooksonella* sp., *Junggaria*, *Baragwanathia* sp., ?*Lycopodolica* and *Zosterophyllum* sp. (Senkevitch 1975, Cai et al. 1993).

These Late Silurian global assemblages indicate that during this time period, the vegetation in the Anglo-Welsh Basin, and probably across the southern margins of Laurentia, was limited in diversity and complexity, compared with more complex vegetation occurring in northern Laurentia, eastern Gondwana and the Kazakhstan plate (Edwards and Wellman 2001).

By the lower Lochkovian the separate landmasses of Laurentia, Baltica and Avalonia were close enough to be considered one continent, known as Laurussia (Figure 3.18b). Spore assemblages from Laurussia and northern Gondwana are more similar from the lower Lochkovian than the Přídolí, as Gondwana gradually grew closer to the southern margins of Laurentia due to the closure of the Iapetus Ocean (Edwards and Wellman 2001). Megafossil assemblages from the Lochkovian indicate similar palaeophytogeographic realms as seen in the Late Silurian (Edwards and Wellman 2001). Laurussian assemblages show an increased diversification of the rhyniophytes and zosterophylls through the Lochkovian and Pragian (Edwards 1990). Eastern Gondwana and Kazakhstan assemblages continued to diversify, but remained as separate phytoprovinces into the Lochkovian. The main difference between the Přídolí and Lochkovian global megafossil assemblages, was the appearance of another phytoprovince from Siberia, including *Zosterophyllum*, and a number of genera unique to Siberia (Stepanov 1975) (20 in Figure 3.18b), that indicate a possible differentiation of the northern Laurussia palaeophytogeographic realm.

CHAPTER 4 : GEOMETRIC MORPHOMETRICS OF EARLY EMBRYOPHYTES

4.1: INTRODUCTION

The strict biological definition of a species is a fundamental category of taxonomic classification which encompasses a group of organisms that have the ability to interbreed, and are reproductively isolated from other species (Mayr 1942). However, this is often not possible to observe in nature, and is certainly not possible in palaeontology. Therefore, palaeotological taxonomists rely on morphological characteristics to distinguish between groups of organisms.

Unfortunately, early land plants have few diagnostic characters, with most Upper Silurian to Lower Devonian plant fossils being naked, axial plants traditionally defined by sporangial shape and to a lesser extent, size. Therefore, definition of early land plant species is heavily reliant on sporangial morphology. This is particularly the case when studying sporangia from coalified compression fossils, as a thin coaly film with little information regarding original anatomy or *in situ* spores is often the only remaining part.

Variance in shape and size within a group of fossils is not only the result of original biological variance (e.g. phenotypic or ontogenetic), but also preservational or taphonomic (all the processes the organism is subjected to as it becomes fossilised, such as orientation of compression, diagenesis and tectonic deformation). Therefore, precautions must be taken when considering the causes of shape variation.

Morphometrics (the study of shape and size by measurement) allows a quantitative approach to studying shape variance, the notion of which has long been known (Thompson 1917). Morphometrics have contributed vastly to palaeontology, not only by quantifying morphospecies for taxonomy, but also in studies of intra-species shape variation (microevolution), ontogeny, ecophenotypes, polymorphism and sexual dimorphism (Hammer and Harper 2006).

There are several methods of measurement in morphometrics, which are developing rapidly with more advanced techniques becoming readily available (Hammer and Harper 2006). 'Traditional' morphometrics took off in the 1960s and 70s and include univariate (comparisons using a single measurement such as length or width), bivariate (using two measurements) or multivariate analysis (using multiple measurements). Several statistical models were developed for multivariate analysis, including Principal Component Analysis

(PCA). However, difficulties with multivariate morphometrics have been encountered. In particular, a set of linear measurements does not necessary represent shape efficiently (i.e. measurements such as maximum height and maximum width for one shape could be the same for a completely different shape) (Adams et al. 2004). Additionally, traditional analysis is often difficult to visualise or awkward to compare between groups, with many graphical plots.

In the late 80s and early 90s, more advanced morphometric techniques based on shape geometry were developed, known as geometric morphometrics (Kendall 1984, Rohlf and Bookstein 1990, Bookstein 1991), particularly with the use of more complex numerical modelling via dedicated computer programs. One such method is the use of landmarks, where a number of homologous points are defined around a two-dimensional shape, such as a leaf (Wolfe 1993), and then these landmarks can be compared between shapes.

One of the benefits of using geometric morphometrics is that multivariate datasets based on shape geometry can be visualised much more easily than using traditional morphometrics. Each shape measured can be represented as a point in multidimensional space, and a number of shapes can form 'point clouds'. The number of dimensions depends on the number of landmarks per shape (two dimensions are given to each landmark, so a shape with 40 landmarks could be plotted on 80 dimensions) (Bensmihen et al. 2008). In practice, the visualisation of a multivariate dataset needs to be restricted to 2 or 3 dimensions. Principal Component Analysis is a data reduction method by which a large number of interrelated variables are reduced to a few uncorrelated principal components that make up the majority of the shape variance observed (Jolliffe 2002, Hammer and Harper 2006). These components are represented in a coordinate system in which axes correspond to the most important aspects to shape variance (and hence are known as principal components) and can be interpreted (Hammer and Harper 2006).

Principal components can be plotted in 1D, 2D or 3D plots, either using raw data or standard deviations. Point clouds or ellipsoids can be defined, which approximates a morphospace for that group, and encompasses all possible shapes that could arise when varying the principal components plotted to plus or minus 2 standard deviations.

In this chapter an attempt to quantify the variance in shape and size of the Tredomen Quarry sporangia collection, described in Chapter 3, is made. Both allometric and non-allometric (includes scaling) models have been generated, and using Principal Component Analysis, sporangial shape and size changes as a result of varying degrees and combinations of principal components can be visualised. Models comparing species and genera 'groups' have

been generated, as well as models for individual species, such that analysis of intra-species variation can be made. The model also has the capacity to classify new specimens according to the shape's principal components.

4.2: METHODS

The geometric morphometric statistical model and subsequent Principal Component Analysis were generated using the AAMToolbox (Active Appearance Model) (version 6.6) created by Dr. A. I. Hanna, (UEA, Norwich) for MATLAB, a language for technical numerical computing (version R2007a) (Hanna 2007). The following procedure was conducted:

1. Outlines of 224 sporangia were traced from the original photographs (Appendix IV) and scaled to 1mm = 5mm (Figure 4.1*a*). An additional 15 outlines of sporangia were traced and scaled from images of species holotypes and other species of interest for shape comparison. The outlines were also rotated so all specimens were in the same orientation (aligned so that the sporangial–axial junction was horizontal). These outlines were then saved as jpeg files, with the same pixel dimensions (296 x 886). These files were then copied into the 'cropped' sub folder of a new 'project' within the AAMToolbox.

2. A single sporangium with distinctive features was then chosen as the 'Point Model Template'. A specimen of *Cooksonia* cf. *caledonica* was chosen and using the 'Template Editor' tool (Figure 4.1*b*), primary landmark points were selected. These landmarks are placed in the most fundamental points of the shape, and should be recognisable in all sporangia. 12 primary points were selected (red points in Figure 3.16*b*); 2 points where the subtending axis joins the base of the sporangium, 1 point in the centre of the sporangial–axial junction (and where the junction the curved, this point also marks the maximum deviation from the horizontal), 1 point at the sporangium maximum height, 4 points at maximum width which also mark the length of straight parallel sides and 4 points in the corners of the sporangium, which mark significant breaks in outline curvature. Secondary points (in black in Figure 4.1*b*) were then placed along the sporangium outline between primary points, and evenly spaced

Figure 4.1: AAMToolbox methods: a: Template Creator, b: Template Editor Tool, and c: Point Model Editor

a

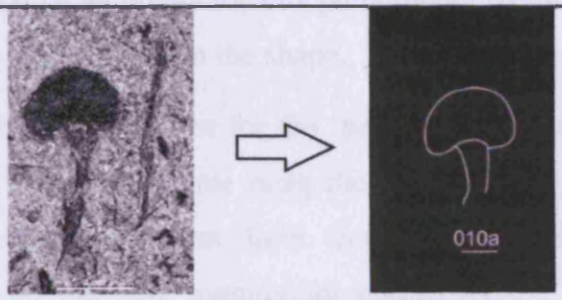

Creation of sporangial outlines from original photographs

b

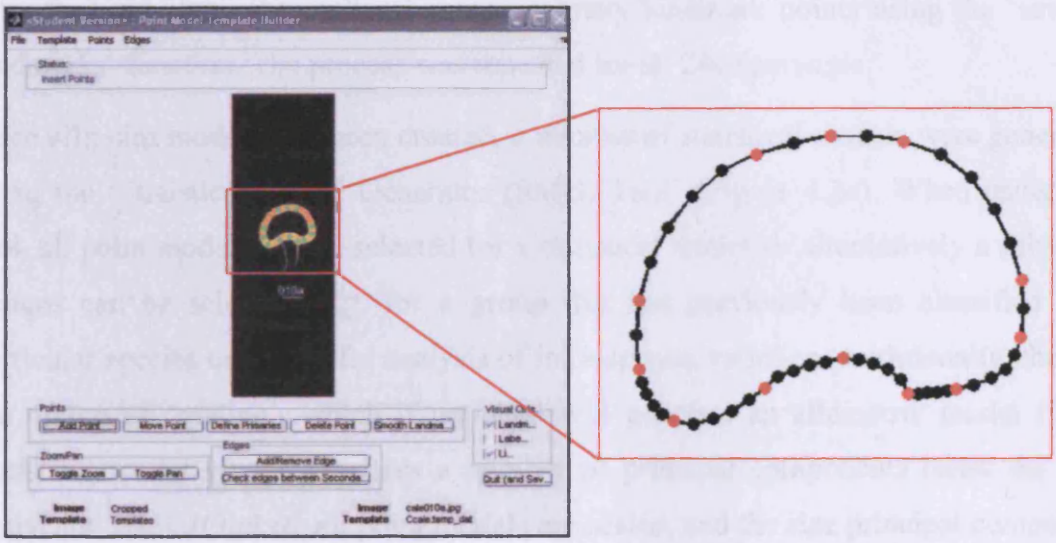

Template Editor Tool (left). Landmarks placed on template sporangium. Red points are primary landmarks, whilst black points are secondary landmarks (right).

c

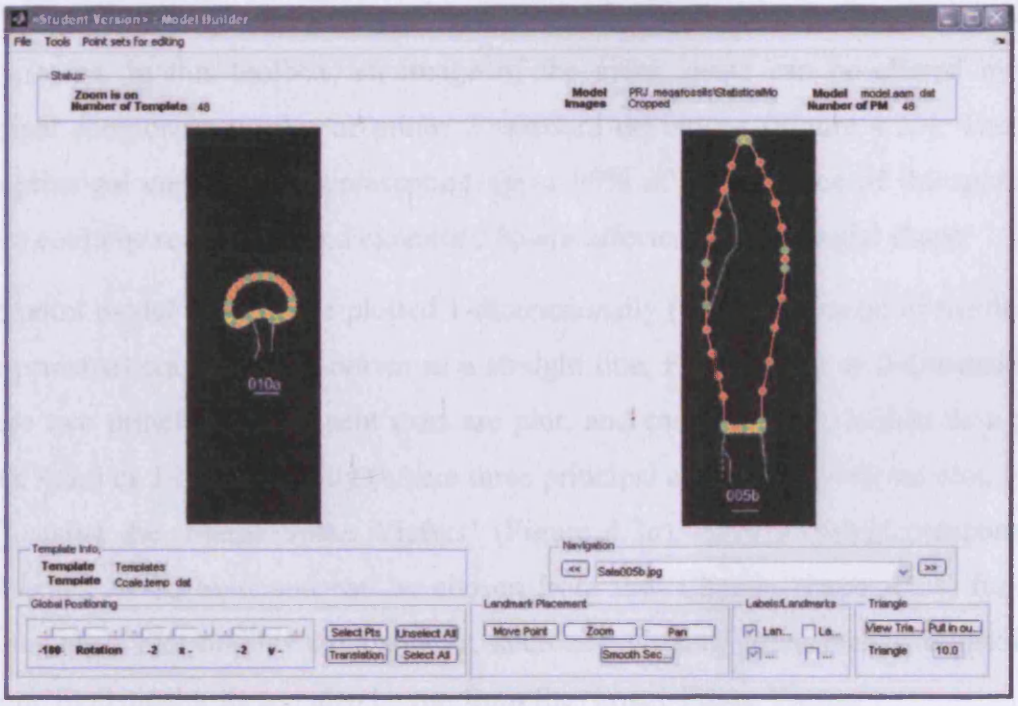

Point Model Editor. Template appears in the left hand box, whilst the landmarks are repositioned around the specimen outline in the right hand box.

out automatically using the 'smooth landmarks' function in the 'Template Editor' toolbox, giving a total of 48 points for this point model template. Finally, points were joined together with 'edges' to form the shape.

3. Once the template had been chosen for the 'project', the outline of each sporangium was then compared with the template using the 'Point Model Editor' (Figure 4.1*c*). In this toolbox, each landmark point from the template was repositioned into the appropriate feature on the new sporangium outline. Again, secondary points were smoothed out along the outline between primary landmark points using the 'smooth landmarks' function. The process was repeated for all 240 sporangia.

4. Once all point models had been created, a number of statistical models were generated using the 'Statistical Model Generator (SMG) Tool' (Figure 4.2*a*). When using this tool, all point models can be selected for a statistical model, or alternatively a subset of images can be selected (e.g. for a group that has previously been classified to a particular species or genus) for analysis of intra-species variation. Additionally, there is the option of 'scaling', which if unticked will generate an allometric model (i.e. a statistical model which generates a number of principal components based on both shape and size). If ticked, all point models are scaled, and the size principal component is removed, with only components affecting the shape remaining.

5. For each statistical model generated, a 'PCA walk' (Principal Component Analysis) was created. In this toolbox, an image of the mean shape can be altered by each principal component to plus or minus 2 standard deviations (Figure 4.2*b*). Therefore each principal component (representing up to 99% of the variance of the sporangial shape) could be recognised and examined how it affected the sporangial shape.

6. Each point model can then be plotted 1-dimensionally (where the range of the data for each principal component is drawn as a straight line, Figure 4.3*b*) or 2-dimensionally (where two principal component axes are plot, and each specimen occurs as a point, Figure 4.3*c*) or 3-dimensionally (where three principal component axes are plot, Figure 4.3*d*), using the 'Shape Space Viewer' (Figure 4.3*a*). Each principal component is represented by an axis, and can be chosen from the 'Choose Shape Axes' function. Various other plot options are available, such as including group means, ellipsoids or vectors. Statistical tests can also be run from the 'Shape Space Viewer'.

Figure 4.2: AAMToolbox methods: a: Statistical Model Generator Tool, b: PCA walks

a

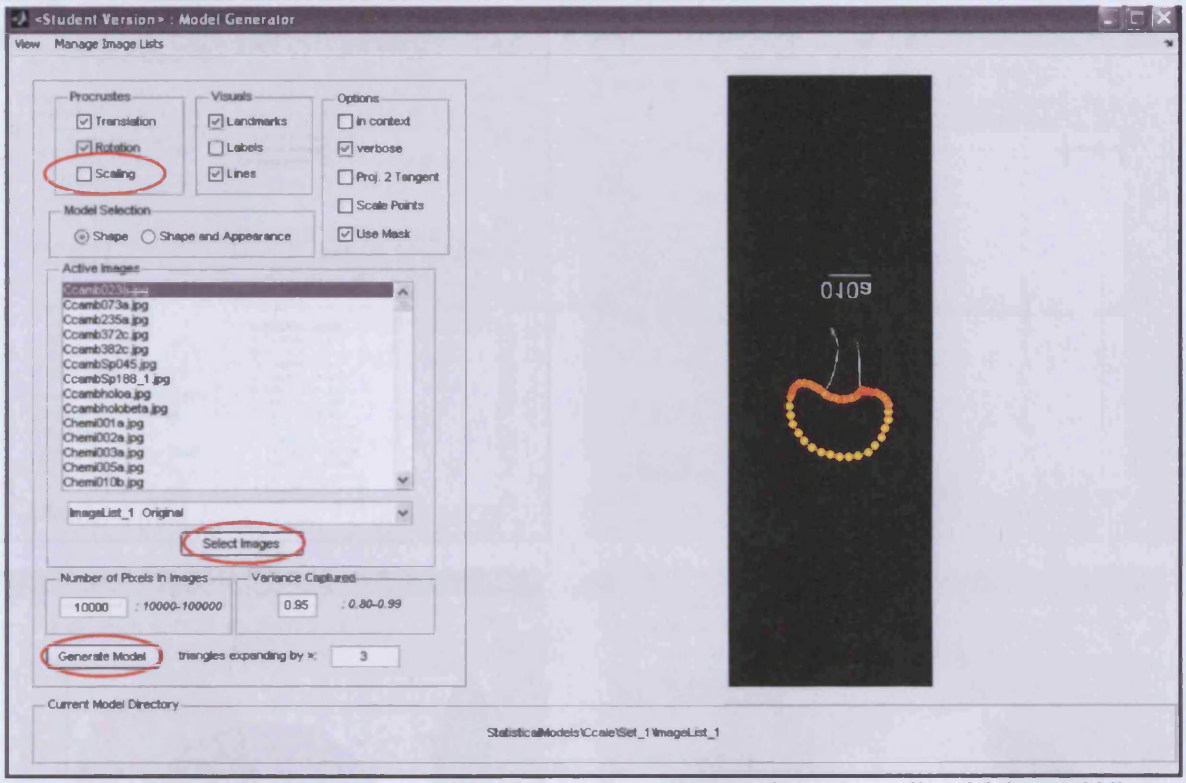

Figure 4.2a: Statistical Model Generator (SMG) Tool. The top ellipse shows the scaling tick box, middle ellipse show the function to select images for the model, and the bottom ellipse to generate the model.

b

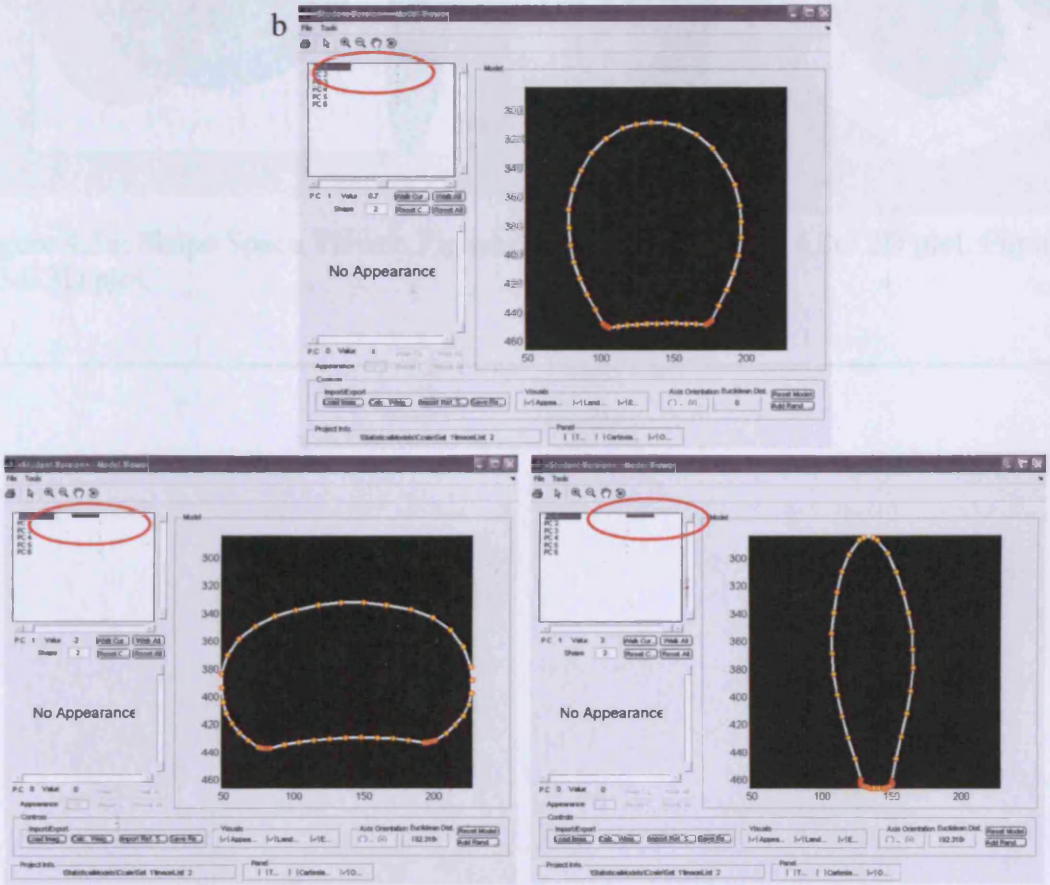

Figure 4.2b: Top: PCA 'walk' showing mean shape in right hand box. Note principal component 1 is set to the mean. Bottom left: principal component 1 is set to - 2 standard deviations, and resulting shape is shown. Bottom right: The resulting shape when the principal component 1 is set to + 2 standard deviations.

Figure 4.3: AAMToolbox methods: Point Model Plots in Shape Space Viewer

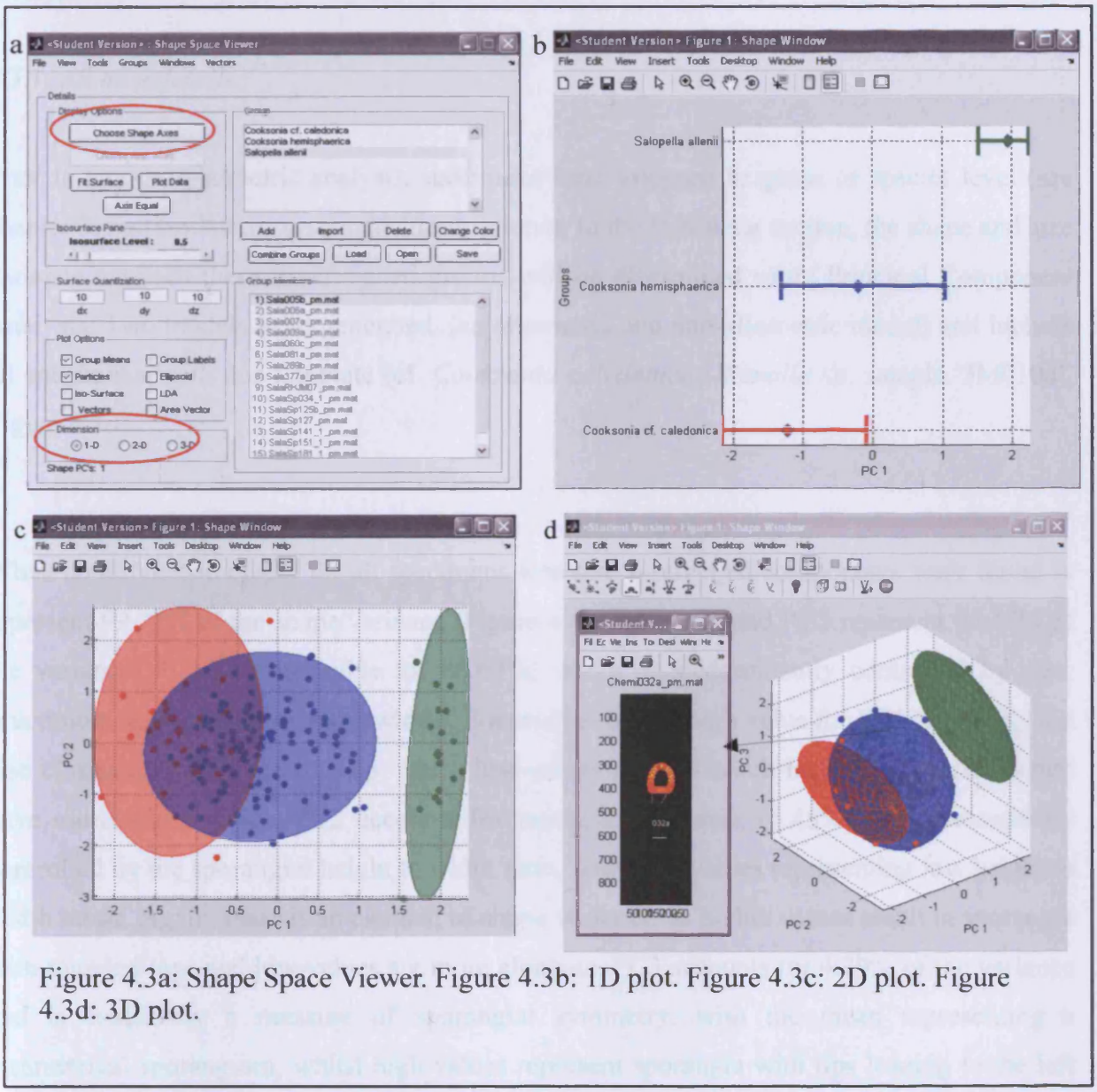

Figure 4.3a: Shape Space Viewer. Figure 4.3b: 1D plot. Figure 4.3c: 2D plot. Figure 4.3d: 3D plot.

4.3: RESULTS

4.3.1: *All megafossils*

Prior to any morphometric analysis, specimens were assigned to genus or species level (see chapter 3, section 3.2 for systematic descriptions). In the following section, the shape and size variance between these pre-assigned groups will be determined using Principal Component Analysis. Two models were generated, (an allometric and non-allometric model) and include all specimens, with one template (cf. *Cooksonia caledonica* / *Renalia* sp. sample 'JM010a', Figure 4.1*a*).

Allometric model

When an allometric model for all specimens was run, 6 principal components were found to represent 99.12% of the shape variance (Figure 4.4). PC1, PC2 and PC3 represent 96.42% of the variance. PC1 is responsible for 86.69%, which is predominantly controlled by size, (maximum height and maximum width). Shapes that have a high value for PC1 are larger, but also elongated with a tapering tip, whilst low values for PC1 result in smaller sporangia that have more rounded tips. PC2 accounts for much less variance (5.45%) and is essentially controlled by the sporangial height to width ratio, with high values representing low height to width ratios. Again, there is an element of shape variance, as higher values result in sporangia with rounded tops and low values are more elongate. PC3 accounts for 4.29% of the variance and is essentially a measure of sporangial symmetry, with the mean representing a symmetrical sporangium, whilst high values represent sporangia with tips leaning to the left and low values tips leaning to the right.

The remaining principal components represent less than 3% variance, and so are much less significant in this allometric model. However, they do represent changes in shape. PC4 is controlled by the position of maximum width, which has an effect on the upper half of the sporangia. PC5 is controlled by the length of straight edges at the maximum width, and therefore the 'squareness' of the shape. Finally, PC6 is controlled by the length of the sporangial-axial junction, and the curvature of the lower part of the sporangia.

Figure 4.4: Sporangial shape variation for all specimens from an allometric model.

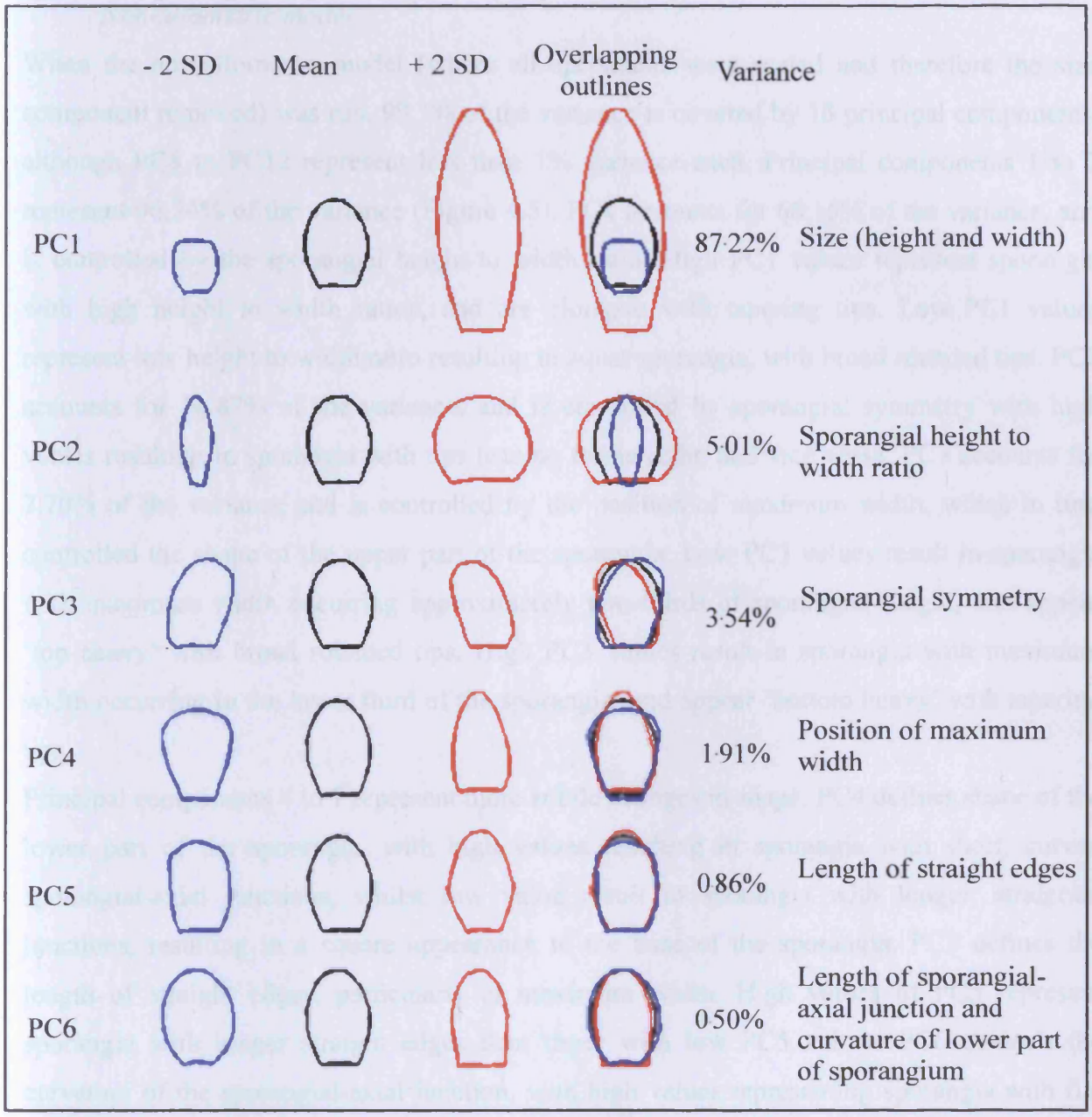

Figure 4.4: Sporangial shape variation for all specimens represented by 6 principal components from an allometric model. Each principal component (PC) shows the mean shape outline, with outlines to the left minus two standard deviations, and outlines to right plus two standard deviations. For comparison, the outlines are also overlain. The % of variance represented by each principal component is also shown. An explanation of the control on each principal component is given on the right.

Non-allometric model

When the non-allometric model (where all specimens were scaled and therefore the size component removed) was run, 99.1% of the variance is covered by 13 principal components, although PC8 to PC12 represent less than 1% variance each. Principal components 1 to 7 represent 96.34% of the variance (Figure 4.5). PC1 accounts for 66.15% of the variance, and is controlled by the sporangial height to width ratio. High PC1 values represent sporangia with high height to width ratios, and are elongate with tapering tips. Low PC1 values represent low height to width ratio resulting in squat sporangia, with broad rounded tips. PC2 accounts for 14.87% of the variance, and is controlled by sporangial symmetry with high values resulting in sporangia with tips leaning to the right, and vice versa. PC3 accounts for 7.70% of the variance and is controlled by the position of maximum width, which in turn controlled the shape of the upper part of the sporangia. Low PC3 values result in sporangia with maximum width occurring approximately two-thirds of sporangial height, and appear 'top heavy' with broad rounded tips. High PC3 values result in sporangia with maximum width occurring in the lower third of the sporangia, and appear 'bottom heavy' with tapering tips.

Principal components 4 to 7 represent more subtle changes in shape. PC4 defines shape of the lower part of the sporangia, with high values resulting in sporangia with short, curved sporangial-axial junctions, whilst low value result in sporangia with longer, straighter junctions, resulting in a square appearance to the base of the sporangia. PC5 defines the length of straight edges, particularly at maximum width. High values of PC5 represent sporangia with longer straight edges than those with low PC5 values. PC6 controls the curvature of the sporangial-axial junction, with high values representing sporangia with flat junctions and low values representing curved junctions. PC7 is controlled by the symmetry of the sporangial-axial junction in relation to the rest of the sporangia.

Summary

The allometric model indicated that sporangial size and sporangial height to width ratios are the most significant causes of variation amongst all megafossils. In the non-allometric model, sporangial height to width ratios, sporangial symmetry and sporangial maximum width are the most significant causes of variation. Sporangial asymmetry is most likely the result of taphonomy, as sporangia are likely to be symmetrical in life, which may be altered during compression.

Figure 4.5: Sporangial shape variation for all specimens from a non-allometric model.

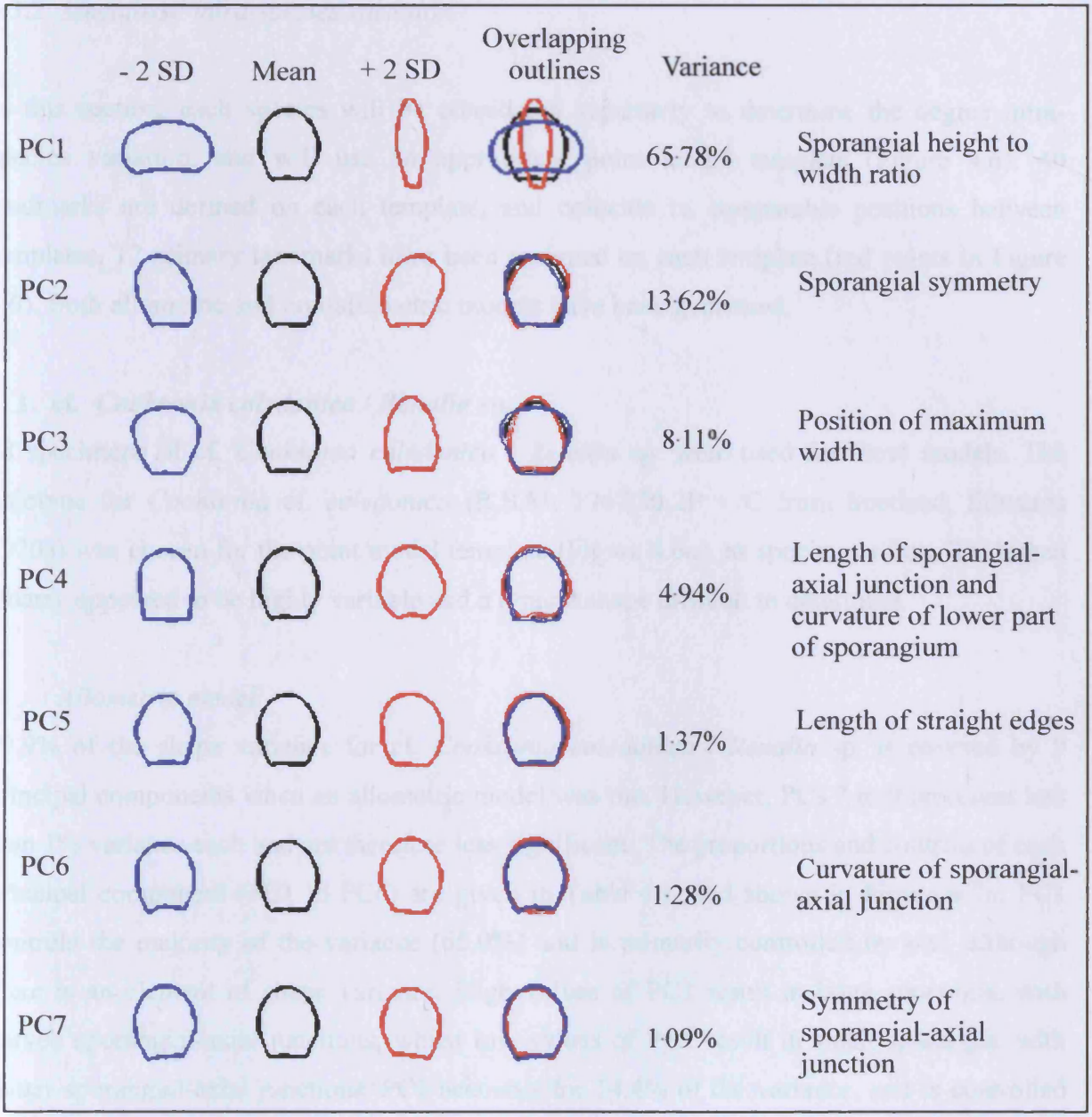

Figure 4.5: Sporangial shape variation for all specimens represented by 7 principal components from a non-allometric model.

4.3.2: *Megafossil intra-species variation*

In this section, each species will be considered separately to determine the degree intra-species variation, and will use an appropriate point model template (Figure 4.6). 40 landmarks are defined on each template, and coincide to comparable positions between templates. 12 primary landmarks have been assigned on each template (red points in Figure 4.6). Both allometric and non-allometric models have been generated.

1. cf. *Cooksonia caledonica* / *Renalia* sp.

28 specimens of cf. *Cooksonia caledonica* / *Renalia* sp. were used for these models. The holotype for *Cooksonia* cf. *caledonica* (R.S.M. 1967.30.2P + C from Scotland, Edwards 1970a) was chosen for the point model template (Figure 4.6*a*), as specimens from Tredomen Quarry appeared to be highly variable and a typical shape difficult to determine.

Allometric model

99.9% of the shape variance for cf. *Cooksonia caledonica* / *Renalia* sp. is covered by 9 principal components when an allometric model was run. However, PCs 7 to 9 represent less than 1% variance each and are therefore less significant. The proportions and controls of each principal component (PC1 to PC6) are given in Table 4.1, and shown in Figure 4.7*a*. PC1 controls the majority of the variance (65.0%) and is primarily controlled by size, although there is an element of shape variance. High values of PC1 result in large sporangia, with curved sporangial-axial junctions, whilst low values of PC1 result in small sporangia, with flatter sporangial-axial junctions. PC2 accounts for 14.4% of the variance, and is controlled by sporangial symmetry, with the mean shape symmetrical, low values resulting in sporangial tips leaning to the left and high values resulting in sporangial tips leaning to the right. PC3 accounts for 10.77% of the variance and is primarily controlled by sporangial height to width ratios, where high PC3 values result in sporangia that are wider than high, and vice versa. The remaining three components represent subtler changes to sporangial shape, such as the length, curvature and symmetry of the sporangial–axial junctions (see Table 4.1, Figure 4.7*a*).

Figure 4.6: Point model templates used for each species model

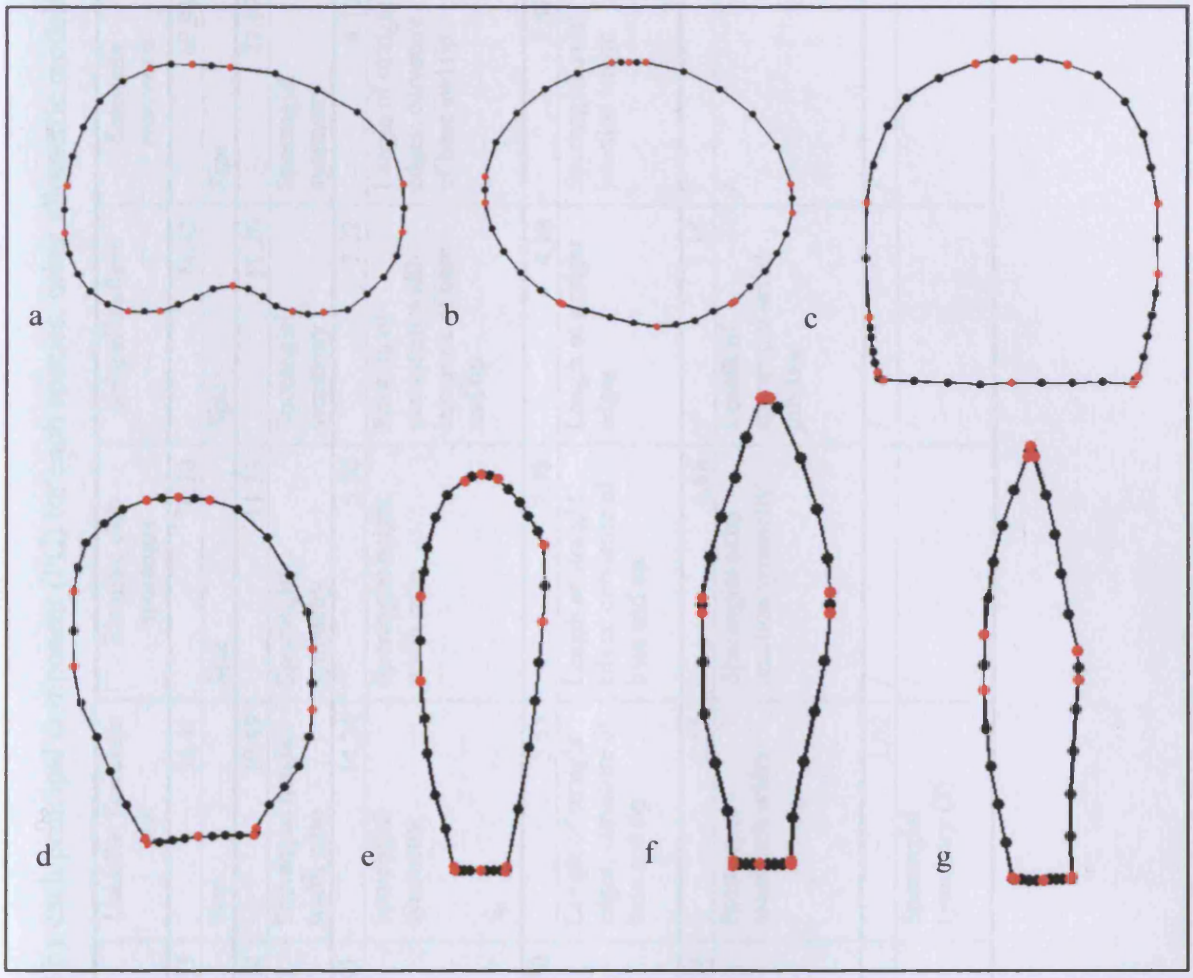

Figure 4.6: Templates used for each species model. a: template for cf. *Cooksonia caledonica* (from *Cooksonia caledonica* holotype R.S.M. 1967.30.2P + C from Scotland, Edwards 1970a). b: template for *Cooksonia* cf. *cambrensis* (from specimen JM023a). c: template for *Cooksonia hemisphaerica* (from specimen JM005a). d: template for cf. *Uskiella/ Tarrantia* sp. (from holotype *Uskiella reticulata* Fanning et al. 1992, NMW 91. 42G, 25). e: template for elongate club-shaped sporangia (from specimen JM016c). f: template for *Salopella allenii* (from specimen JM005b). g: Template for *Salopella* cf. *marcensis* (from holotype of *Salopella marcensis*, Fanning, Edwards and Richardson 1992, NMW 91. 42G. 19 (Fig. 28)).

Table 4.1: Proportions and controls on shape variance represented by each principal component (PC) for each species, using allometric models.

Species		cf. *Cooksonia caledonica*	*Cooksonia* cf. *cambrensis*	*Cooksonia hemisphaerica*	*Uskiella/ Tarrantia* sp.	Elongate club sporangia	*Salopella allenii*	*Salopella marcensis*
PC1	%	65.00	47.75	73.33	54.41	78.10	74.42	60.91
	control	Size	Size	Size	Size	Size	Size	Size
PC2	%	14.40	28.55	11.12	19.89	11.33	11.26	27.17
	control	Sporangial symmetry	Sporangial symmetry	Sporangial height: width ratio	Sporangial height: width ratio	Sporangial symmetry	Sporangial symmetry	Sporangial symmetry
PC3	%	10.77	14.63	6.91	14.24	5.80	7.22	8.10
	control	Sporangial height: width ratio	Sporangial height: width ratio	Sporangial symmetry	Sporangial symmetry	Sporangial height: width ratio	Position of maximum width; curvature of base and tip	Length of straight edges; curvature of base and tip
PC4	%	3.15	5.07	3.60	5.53	2.98	4.18	2.81
	control	Sporangial-axial junction length; curvature of base.	Maximum width	Position of maximum width	Length of straight edges; curvature of base and tip	Length of straight edges; curvature of base and tip	Length of straight edges	Sporangial-axial junction length
PC5	%	2.58	2.95	1.24	2.55	0.88	1.14	/
	control	Length of straight edges; curvature of sporangial-axial junction.	Sporangial symmetry (2)	Sporangial-axial junction length; curvature of base.	Position of maximum width	Sporangial-axial junction symmetry	Length of sporangial -axial junction	/
PC6	%	1.42	/	/	1.02	/	/	/
	control	Sporangial-axial junction symmetry	/	/	Sporangial symmetry (2)	/	/	

Figure 4.7: Sporangial shape variation for cf. *Cooksonia caledonica / Renalia* sp. from a: an allometric model, b: a non-allometric model

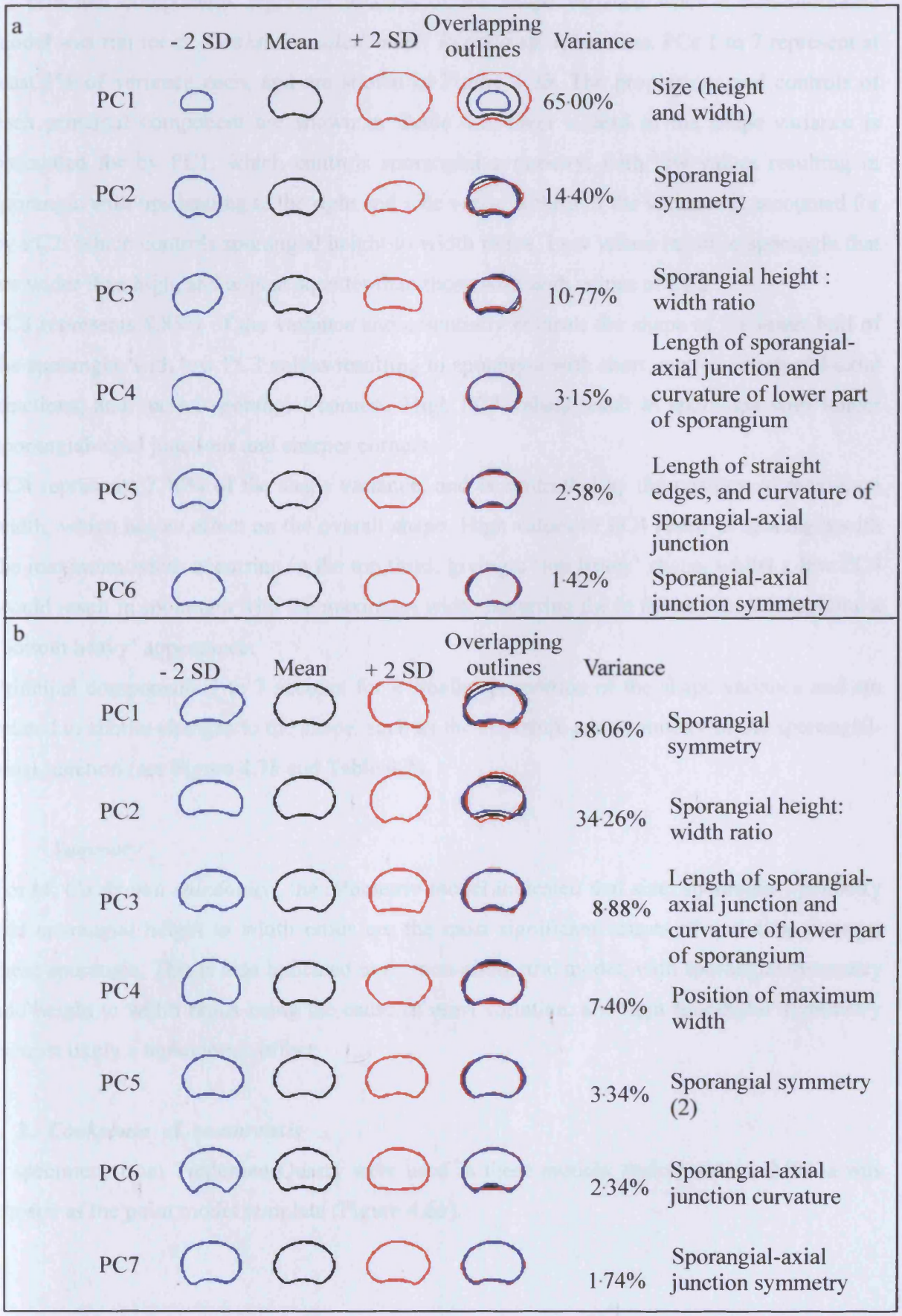

Non-allometric model

12 principal components represent 99.05% of the shape variance when a non-allometric model was run for cf. *Cooksonia caledonica* / *Renalia* sp. specimens. PCs 1 to 7 represent at least 1% of variance each, and are shown in Figure 4.7*b*. The proportions and controls of each principal component are shown in Table 4.2. Over a third of the shape variance is accounted for by PC1, which controls sporangial symmetry, with low values resulting in sporangia with tips leaning to the right and vice versa. A third of the variance is accounted for by PC2, which controls sporangial height to width ratios. Low values result in sporangia that are wider than high, and appear squatter than those with high values of PC2.

PC3 represents 8.88% of the variance and essentially controls the shape of the lower half of the sporangia, with low PC3 values resulting in sporangia with short, curved sporangial-axial junctions, and curved sporangial corners. High PC3 values result in sporangia with longer sporangial-axial junctions and sharper corners.

PC4 represents 7.40% of the shape variance, and is controlled by the position of maximum width, which has an effect on the overall shape. High values of PC4 result in sporangia with the maximum width occurring in the top third, giving a 'top heavy' shape, whilst a low PC4 would result in sporangia with the maximum width occurring the in the bottom third, giving a 'bottom heavy' appearance.

Principal components 5 to 7 account for a smaller proportion of the shape variance and are related to subtler changes to the shape, such as the curvature and symmetry of the sporangial-axial junction (see Figure 4.7*b* and Table 4.2).

Summary

For cf. *Cooksonia caledonica*, the allometric model indicated that size, sporangial symmetry and sporangial height to width ratios are the most significant causes of variation amongst these sporangia. This is also indicated in the non-allometric model, with sporangial symmetry and height to width ratios being the cause of most variation, although sporangial asymmetry is most likely a taphonomic effect.

2. *Cooksonia* cf. *cambrensis*

7 specimens from Tredomen Quarry were used in these models, and specimen JM023a was chosen as the point model template (Figure 4.6*b*).

Table 4.2: Proportions and controls on shape variance represented by each principal component (PC) for each species, using non-allometric models.

Species		cf. *Cooksonia caledonica*	*Cooksonia* cf. *cambrensis*	*Cooksonia hemisphaerica*	*Uskiella/ Tarrantia* sp.	Elongate club sporangia	*Salopella allenii*	*Salopella marcensis*
PC1	%	38.06	55.90	37.78	44.90	56.84	46.02	58.20
	control	Sporangial symmetry	Sporangial symmetry	Sporangial H:W ratio	Sporangial H:W ratio	Sporangial H:W ratio	Sporangial symmetry	Sporangial symmetry
PC2	%	34.26	26.88	27.90	30.47	25.20	30.50	20.56
	control	Sporangial height: width ratio	Sporangial height: width ratio	Sporangial symmetry	Sporangial symmetry	Sporangial symmetry	Position of maximum width	Length of straight edges
PC3	%	8.88	10.17	15.30	10.93	10.30	11.48	14.99
	control	Sporangial-axial junction length; curvature of sporangium base.	Maximum width	Position of maximum width	Sporangial-axial junction length; curvature of base and tip.	Length of straight edges; curvature of base and tip	Length of straight edges	Position of maximum width
PC4	%	7.40	4.79	4.59	5.21	3.64	5.29	4.08
	control	Position of maximum width.	Length of straight edges	Sporangial-axial junction width; curvature of base	Position of maximum width	Sporangial-axial junction symmetry	Sporangial –axial junction length	Sporangial-axial junction length
PC5	%	3.34	1.55	3.27	2.82	1.88	2.12	1.25
	control	Sporangial symmetry (2)	Sporangial symmetry (2)	Length of straight edges	Length of straight edges	Sporangial-axial junction length	Maximum width	Sporangial symmetry (2)
PC6	%	2.34	/	/	1.47	/	1.21	/
	control	Sporangial-axial junction curvature	/	/	Sporangial symmetry (2)	/	Sporangial-axial junction symmetry	/
PC7	%	1.74	/	/	/	/	/	/
	control	Sporangial-axial junction symmetry	/	/	/	/	/	/

Allometric model

99.25% of the variance for the allometric model ran for *Cooksonia* cf. *cambrensis* is accounted for by 5 principal components, and are shown in Figure 4.8*a*. The proportions and controls of the principal components are compared in Table 4.1. Just under half of the variance is accounted for by PC1, and is controlled by size, with high PC1 values resulting in larger sporangia. PC2 accounts for just under a third of the variance and is controlled by sporangial symmetry, with high values resulting in sporangial tips leaning to the left and vice versa. Sporangial height to width ratios control PC3, which represents 14.63% of the variance. Low values of PC3 result in higher sporangial height: width ratios, with broader, squatter sporangia. PC4 and PC5 represent smaller proportions of the variance (Table 4.1) and are controlled by maximum width and sporangial symmetry with relation to the sporangial-axial junction (see Figure 4.8*a*).

Non-allometric model

When a non-allometric model for *Cooksonia cambrensis* was run, 99.29% of the variance was represented by 5 principal components (shown in Figure 4.8*b* and Table 4.2). Just over half of the shape variance was resolved by PC1, controlled by sporangial symmetry. 26.88% of the variance is accounted for by PC2, which is controlled by sporangial height to width ratios, with low values resulting in broader, squatter sporangia. PC4 and PC5 represent subtler changes to the shape (see Figure 4.8*b* and Table 4.2) such as the length of straight edges, which controls the 'square-ness' of the sporangia.

Summary

For *Cooksonia* cf. *cambrensis*, the allometric models indicate that most of the shape variance is controlled by size, sporangial symmetry and sporangial height to width ratios. This is also indicated in the non-allometric models, where sporangial symmetry and sporangial height to width ratios control the majority of shape variance.

3. *Cooksonia hemisphaerica*

123 specimens of *Cooksonia hemisphaerica* were outlined, and point models were generated from a new template created from specimen JM005a (Figure 4.6*c*), using 40 landmark points.

Figure 4.8: Sporangial shape variation for *Cooksonia* cf. *cambrensis* from a: an allometric model, and b: a non-allometric model.

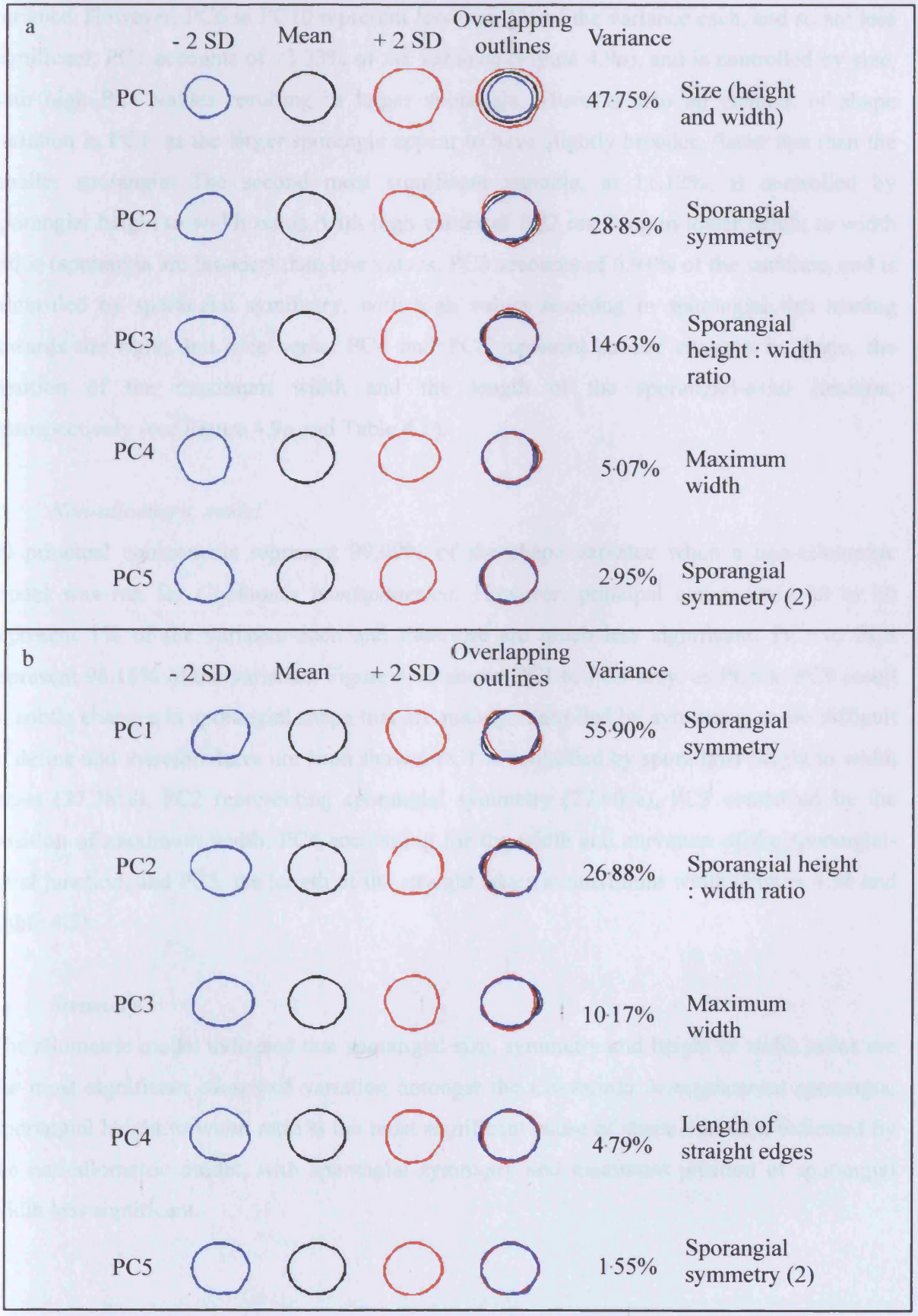

Allometric model

When an allometric model was run, 10 principal components represent 99.04% of the shape variance. However, PC6 to PC10 represent less than 1% of the variance each, and so are less significant. PC1 accounts of 73.33% of the variance (Figure 4.9*a*), and is controlled by size, with high PC1 values resulting in larger sporangia. There is also an element of shape variation in PC1, as the larger sporangia appear to have slightly broader, flatter tips than the smaller sporangia. The second most significant variable, at 11.12%, is controlled by sporangial height to width ratios, with high values of PC2 resulting in lower height to width ratios (sporangia are broader) than low values. PC3 accounts of 6.91% of the variance, and is controlled by sporangial symmetry, with high values resulting in sporangial tips leaning towards the right, and vice versa. PC4 and PC5 represent subtler changes in shape, the position of the maximum width and the length of the sporangial-axial junction, retrospectively (see Figure 4.9*a* and Table 4.1).

Non-allometric model

20 principal components represent 99.09% of the shape variance when a non-allometric model was run for *Cooksonia hemisphaerica*. However, principal components 10 to 20 represent 1% of the variance each and therefore are much less significant. PC1 to PC9 represent 96.16% of the variance. Figure 4.9*b* shows PC1 to PC5 only, as PC6 to PC9 result in subtle changes in sporangial shape that are mainly controlled by symmetry or are difficult to define and therefore have not been shown. PC1 is controlled by sporangial height to width ratios (37.78%), PC2 representing sporangial symmetry (27.90%), PC3 controlled by the position of maximum width, PC4 accounting for the width and curvature of the sporangial-axial junction, and PC5, the length of the straight edges at maximum width (Figure 4.9*b* and Table 4.2).

Summary

The allometric model indicated that sporangial size, symmetry and height to width ratios are the most significant causes of variation amongst the *Cooksonia hemisphaerica* sporangia. Sporangial height to width ratio is the most significant cause of shape variation indicated by the non-allometric model, with sporangial symmetry and maximum position of sporangial width less significant.

Figure 4.9: Sporangial shape variation for *Cooksonia hemisphaerica* from a: an allometric model, b: a non-allometric model.

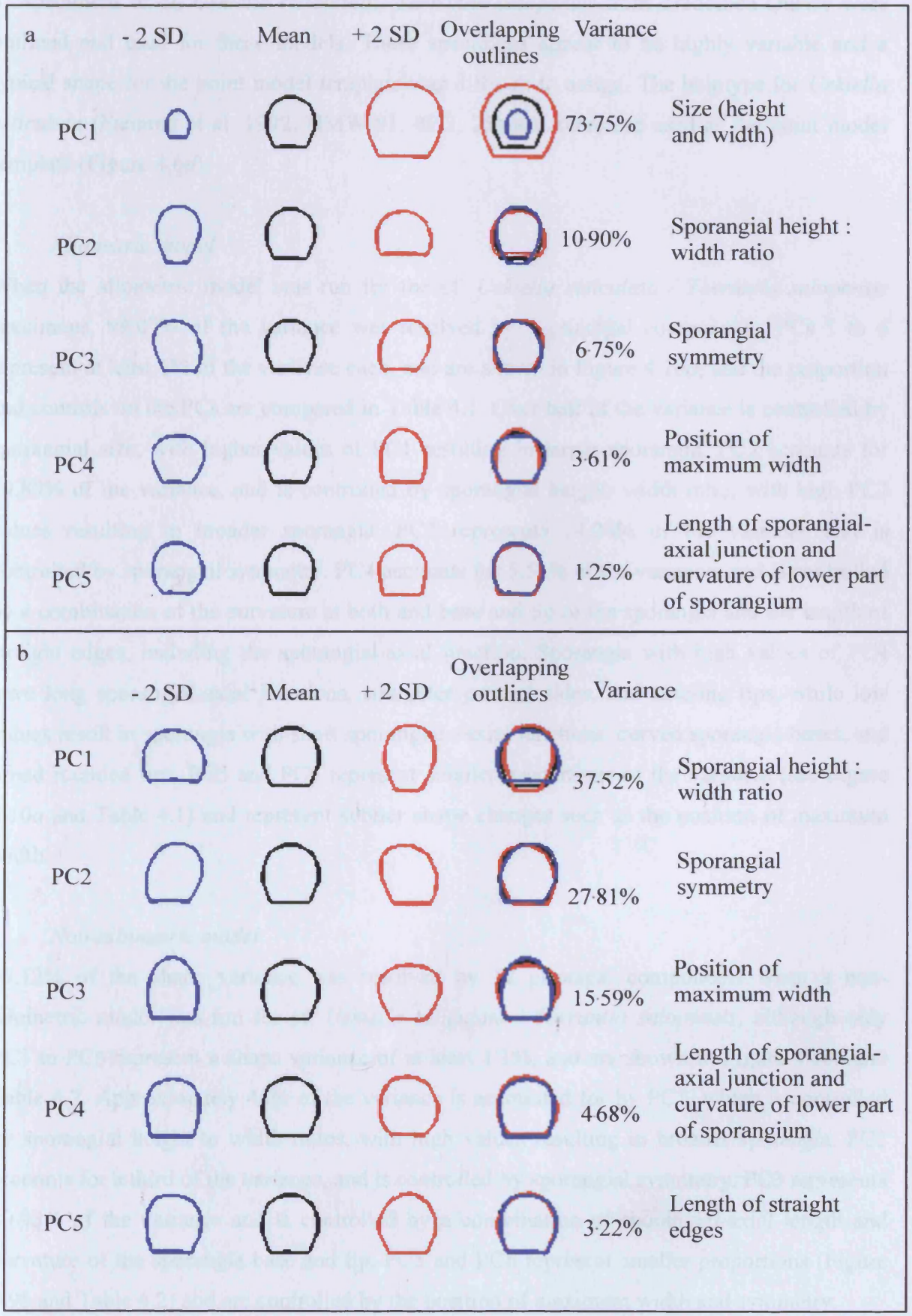

4. cf. *Uskiella reticulata / Tarrantia salopensis*

31 specimens of cf. *Uskiella reticulata / Tarrantia salopensis* from Tredomen Quarry were outlined and used for these models. These specimens appear to be highly variable and a typical shape for the point model template was difficult to assign. The holotype for *Uskiella reticulata* (Fanning et al. 1992, NMW 91. 42G, 25) was therefore used as the point model template (Figure 4.6*d*).

Allometric model

When the allometric model was run for the cf. *Uskiella reticulata / Tarrantia salopensis* specimens, 99.07% of the variance was resolved by 9 principal components. PCs 1 to 6 represent at least 1% of the variance each, and are shown in Figure 4.10*a*, and the proportion and controls on the PCs are compared in Table 4.1. Over half of the variance is controlled by sporangial size, with higher values of PC1 resulting in larger sporangia. PC2 accounts for 19.89% of the variance, and is controlled by sporangial height: width ratio, with high PC2 values resulting in broader sporangia. PC3 represents 14.24% of the variance and is controlled by sporangial symmetry. PC4 accounts for 5.53% of the variance, and is controlled by a combination of the curvature at both and base and tip of the sporangia and the length of straight edges, including the sporangial-axial junction. Sporangia with high values of PC4 have long sporangial-axial junctions, straighter parallel sides, and tapering tips, while low values result in sporangia with short sporangial –axial junctions, curved sporangia bases, and broad rounded tips. PC5 and PC6 represent smaller proportions of the variance (see Figure 4.10*a* and Table 4.1) and represent subtler shape changes such as the position of maximum width.

Non-allometric model

99.12% of the shape variance was resolved by 12 principal components when a non-allometric model was run for cf. *Uskiella reticulata / Tarrantia salopensis*, although only PC1 to PC6 represent a shape variance of at least 1.1%, and are shown in Figure 4.10*b* and Table 4.2. Approximately 45% of the variance is accounted for by PC1, which is controlled by sporangial height to width ratios, with high values resulting in broader sporangia. PC2 accounts for a third of the variance, and is controlled by sporangial symmetry. PC3 represents 10.93% of the variance and is controlled by a combination of sporangial-axial length and curvature of the sporangia base and tip. PC5 and PC6 represent smaller proportions (Figure 4.9*b* and Table 4.2) and are controlled by the position of maximum width and symmetry.

Figure 4.10: Sporangial shape variation for cf. *Uskiella reticulata / Tarrantia salopensis* from a: an allometric model, b: a non-allometric model.

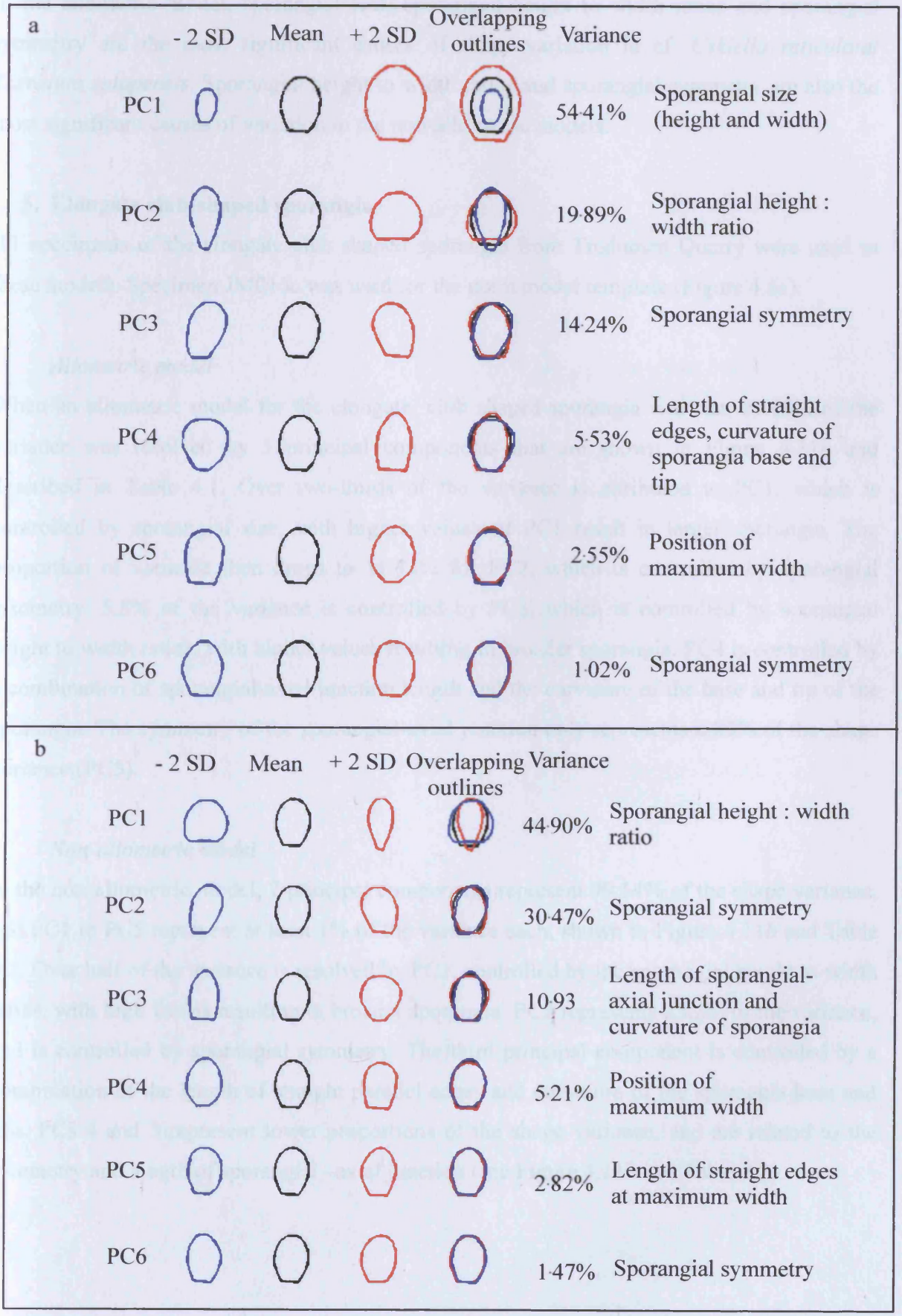

Summary

In the allometric model, sporangial size, sporangial height to width ratios and sporangial symmetry are the most significant causes of shape variation in cf. *Uskiella reticulata/ Tarrantia salopensis*. Sporangial height to width ratios and sporangial symmetry are also the most significant causes of variation in the non-allometric models.

5. Elongate club-shaped sporangia

11 specimens of the elongate club shaped sporangia from Tredomen Quarry were used in these models. Specimen JM016c was used for the point model template (Figure 4.6*e*).

Allometric model

When an allometric model for the elongate, club shaped sporangia was run, 99.08% of the variance was resolved by 5 principal components that are shown in Figure 4.11*a* and described in Table 4.1. Over two-thirds of the variance is attributed to PC1, which is controlled by sporangial size, with higher values of PC1 result in larger sporangia. The proportion of variance then drops to 11.33% for PC2, which is controlled by sporangial symmetry. 5.8% of the variance is controlled by PC3, which is controlled by sporangial height to width ratios, with higher values resulting in broader sporangia. PC4 is controlled by a combination of sporangial-axial junction length and the curvature of the base and tip of the sporangia. The symmetry of the sporangial-axial junction only represents 0.88% of the shape variance (PC5).

Non-allometric model

In the non-allometric model, 7 principal components represent 99.14% of the shape variance, and PC1 to PC5 represent at least 1% of the variance each, shown in Figure 4.11*b* and Table 4.2. Over half of the variance is resolved by PC1, controlled by the sporangial height to width ratios, with high values resulting in broader sporangia. PC2 represents 25.2% of the variance, and is controlled by sporangial symmetry. The third principal component is controlled by a combination of the length of straight parallel edges and curvature of the sporangia base and tips. PCs 4 and 5 represent lower proportions of the shape variance, and are related to the symmetry and length of sporangial –axial junction (see Figure 4.11*b* and Table 4.2).

Figure 4.11: Sporangial shape variation for elongate club-shaped sporangia from a: an allometric model, b: a non-allometric model.

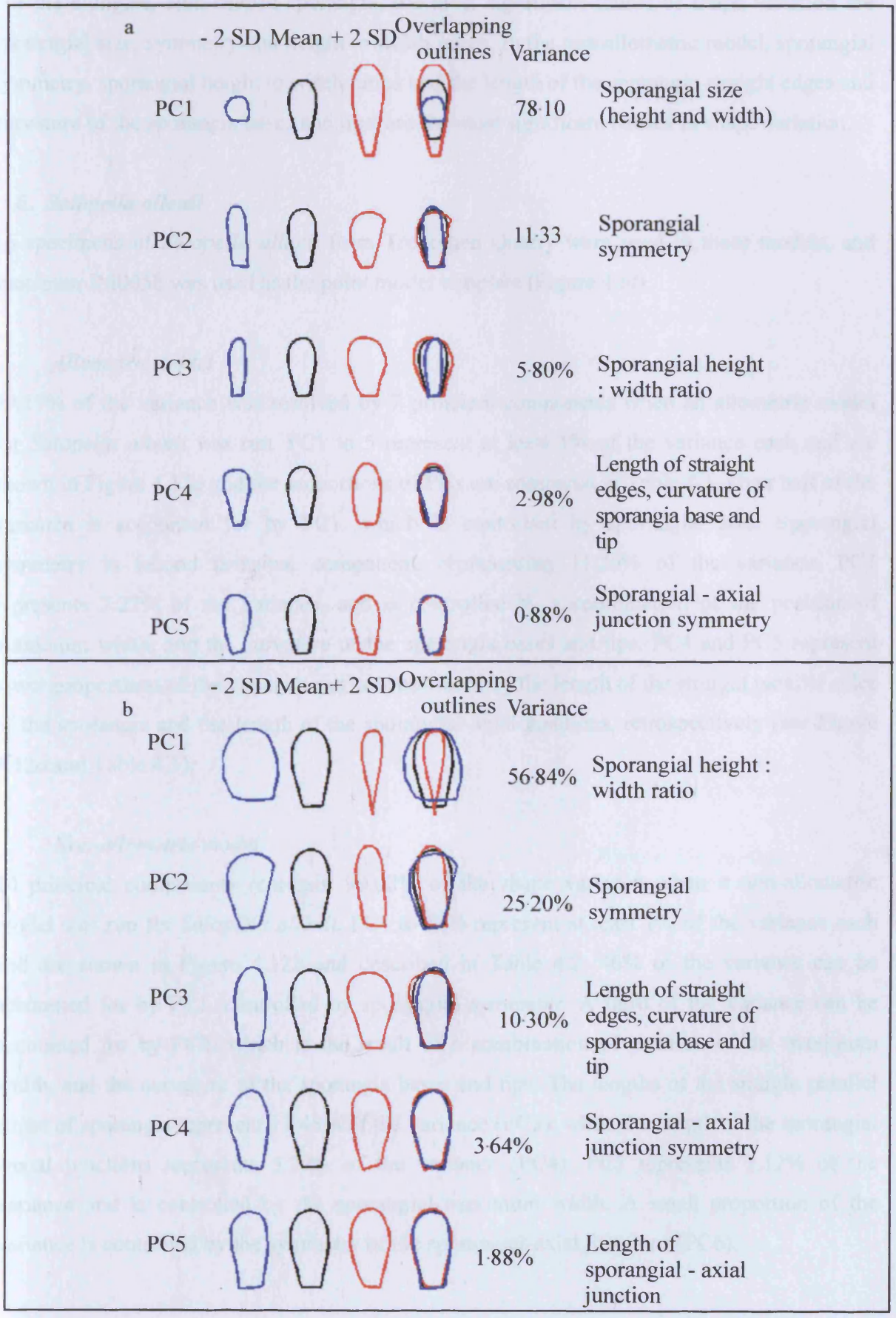

Summary

For the elongate, club-shaped sporangia, the most significant causes of shape variation are sporangial size, symmetry and height to width ratios. In the non allometric model, sporangial symmetry, sporangial height to width ratios and the length of the sporangia straight edges and curvature of the sporangia bases and tips, are the most significant causes of shape variation.

6. *Salopella allenii*

16 specimens of *Salopella allenii* from Tredomen Quarry were used in these models, and specimen JM005b was used as the point model template (Figure 4.6*f*).

Allometric model

99.17% of the variance was resolved by 7 principal components when an allometric model for *Salopella allenii* was run. PC1 to 5 represent at least 1% of the variance each and are shown in Figure 4.12*a* and the proportions of PCs are compared in Table 4.1. Over half of the variance is accounted for by PC1, which is controlled by sporangial size. Sporangial symmetry is second principal component, representing 11.26% of the variance. PC3 represents 7.22% of the variance, and is controlled by a combination of the position of maximum width, and the curvature of the sporangia bases and tips. PC4 and PC5 represent lower proportions of the variance and are controlled by the length of the straight parallel sides of the sporangia and the length of the sporangial-axial junctions, retrospectively (see Figure 4.12*a* and Table 4.1).

Non-allometric model

10 principal components represent 99.08% of the shape variance when a non-allometric model was run for *Salopella allenii*. PC1 to PC6 represent at least 1% of the variance each and are shown in Figure 4.12*b* and described in Table 4.2. 46% of the variance can be accounted for by PC1, controlled by sporangial symmetry. A third of the variance can be accounted for by PC2, which is the result of a combination of position of the maximum width, and the curvature of the sporangia bases and tips. The lengths of the straight parallel edges of sporangia represent 11.48% of the variance (PC3), while the length of the sporangial –axial junctions represents 5.29% of the variance (PC4). PC5 represents 2.12% of the variance and is controlled by the sporangial maximum width. A small proportion of the variance is controlled by the symmetry of the sporangial-axial junctions (PC6).

Figure 4.12: Sporangial shape variation for *Salopella allenii* from a: an allometric model, b: a non-allometric model.

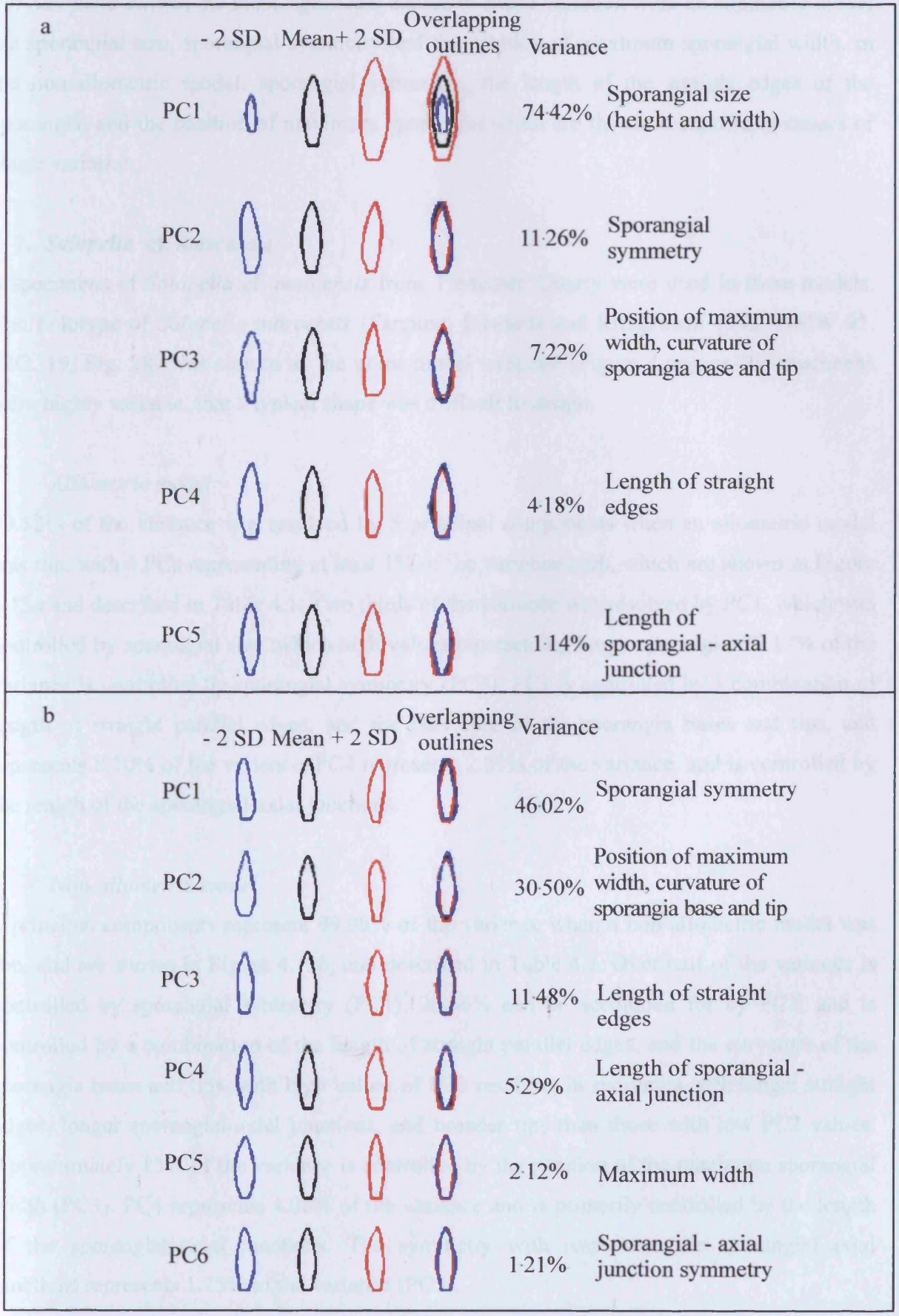

Summary

For *Salopella allenii*, the most significant causes of shape variation from an allometric model are sporangial size, sporangial symmetry and the position of maximum sporangial width. In the non-allometric model, sporangial symmetry, the length of the straight edges of the sporangia, and the position of maximum sporangial width are the most significant causes of shape variation.

7. *Salopella* cf. *marcensis*

8 specimens of *Salopella* cf. *marcensis* from Tredomen Quarry were used in these models. The holotype of *Salopella marcensis* (Fanning, Edwards and Richardson 1992, NMW 91. 42G. 19, Fig. 28) was chosen as the point model template (Figure 4.6*g*), as the specimens were highly variable, that a typical shape was difficult to assign.

Allometric model

99.52% of the variance was resolved by 5 principal components when an allometric model was run, with 4 PCs representing at least 1% of the variance each, which are shown in Figure 4.13*a* and described in Table 4.1. Two thirds of the variance was resolved by PC1, which was controlled by sporangial size, which high values representing larger sporangia. 27.17% of the variance is controlled by sporangial symmetry (PC2). PC3 is controlled by a combination of length of straight parallel edges, and the curvature of the sporangia bases and tips, and represents 8.10% of the variance. PC4 represents 2.81% of the variance, and is controlled by the length of the sporangial-axial junctions.

Non-allometric model

5 principal components represent 99.09% of the variance when a non-allometric model was run, and are shown in Figure 4.13*b*, and described in Table 4.2. Over half of the variance is controlled by sporangial symmetry (PC1). 20.56% can be accounted for by PC2, and is controlled by a combination of the length of straight parallel edges, and the curvature of the sporangia bases and tips, with high values of PC2 resulting in sporangia with longer straight edges, longer sporangial-axial junctions, and broader tips than those with low PC2 values. Approximately 15% of the variance is controlled by the position of the maximum sporangial width (PC3). PC4 represents 4.08% of the variance and is primarily controlled by the length of the sporangial–axial junctions. The symmetry with respect to the sporangial–axial junctions represents 1.25% of the variance (PC5).

Figure 4.13: Sporangial shape variation for *Salopella* cf. *marcensis* from a: an allometric model b: a non-allometric model.

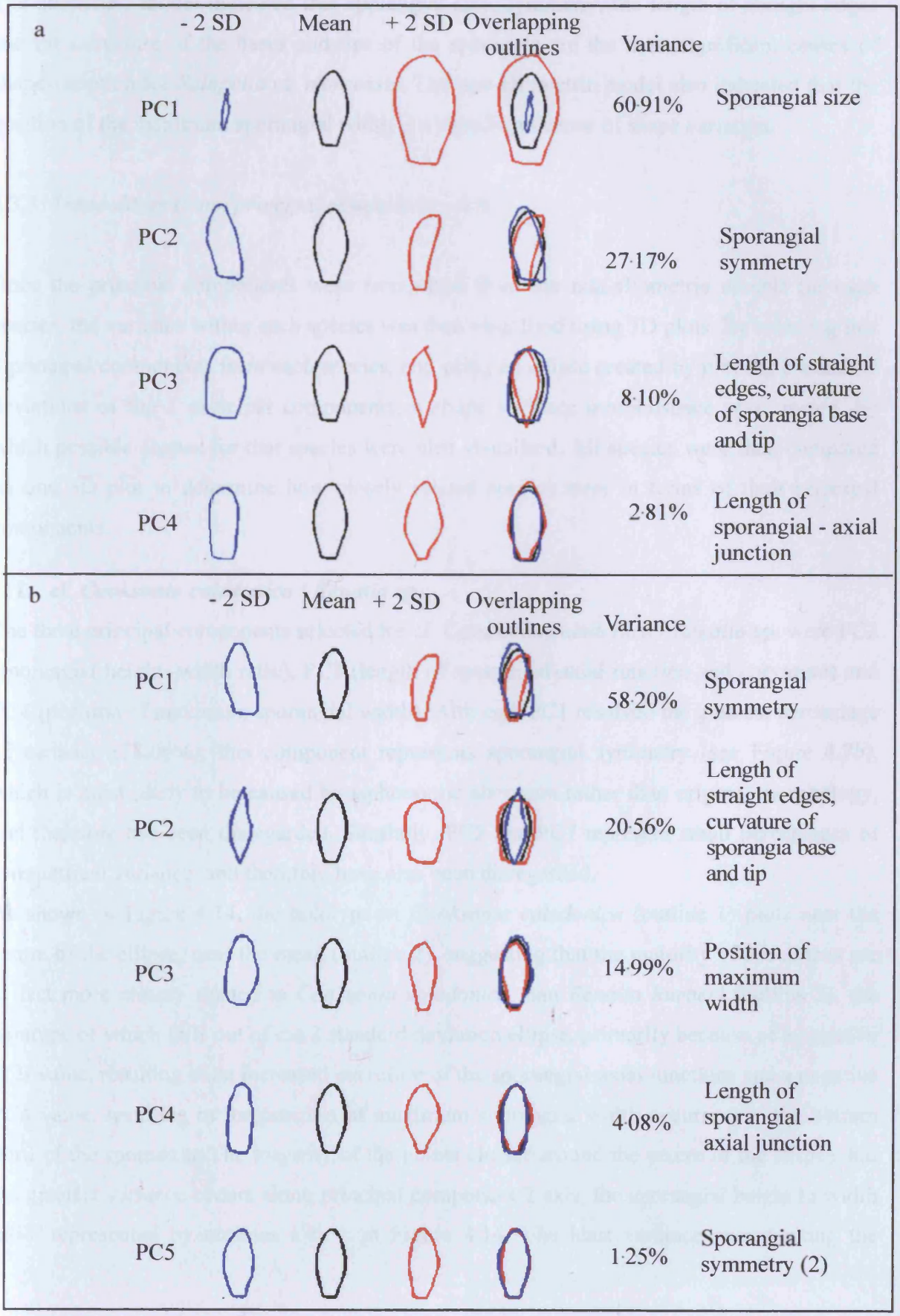

Summary

The allometric model indicated that sporangial size, symmetry, the length of straight edges and the curvature of the bases and tips of the sporangia are the most significant causes of shape variation for *Salopella* cf. *marcensis*. The non-allometric model also indicated that the position of the maximum sporangial width is a significant cause of shape variation.

4.3.3: *Three-dimensional principal components plots*

Once the principal components were recognised from the non-allometric models for each species, the variance within each species was then visualised using 3D plots. By selecting just 3 principal components from each species, and using an ellipse created by plotting 2 standard deviations of the 3 principal components, a shape variance morphospace was created, by which possible shapes for that species were also visualised. All species were then compared on one 3D plot to determine how closely related species were in terms of their principal components.

1. cf. *Cooksonia caledonica* / *Renalia* sp.

The three principal components selected for cf. *Cooksonia caledonica* / *Renalia* sp. were PC2 (sporangial height: width ratio), PC3 (length of sporangial-axial junction and curvature) and PC4 (position of maximum sporangial width). Although PC1 resolved the greatest percentage of variance (38.06%), this component represents sporangial symmetry (see Figure 4.7*b*), which is most likely to be caused by taphonomic alteration rather than original morphology, and therefore has been disregarded. Similarly, PC5 and PC7 represent small percentages of symmetrical variance, and therefore have also been disregarded.

As shown in Figure 4.14, the holotype of *Cooksonia caledonica* (outline 1) plots near the centre of the ellipse, near the mean (outline 2), suggesting that the majority of specimens are in fact more closely related to *Cooksonia caledonica* than *Renalia hueberi* (outline 3), the paratype of which falls out of the 2 standard deviation ellipse, primarily because of a negative PC3 value, resulting in an increased curvature of the sporangial-axial junctions and a negative PC4 value, resulting in the position of maximum sporangial width occurring in the bottom third of the sporangia. The majority of the points cluster around the centre of the ellipse, but the greatest variance occurs along principal component 2 axis, the sporangial height to width ratio, represented by outlines a to c in Figure 4.14. The least variance occurs along the

Figure 4.14:Three-dimensional plot showing morphospace of cf. *Cooksonia caledonica* / *Renalia* sp. using PC2, PC3 and PC4.

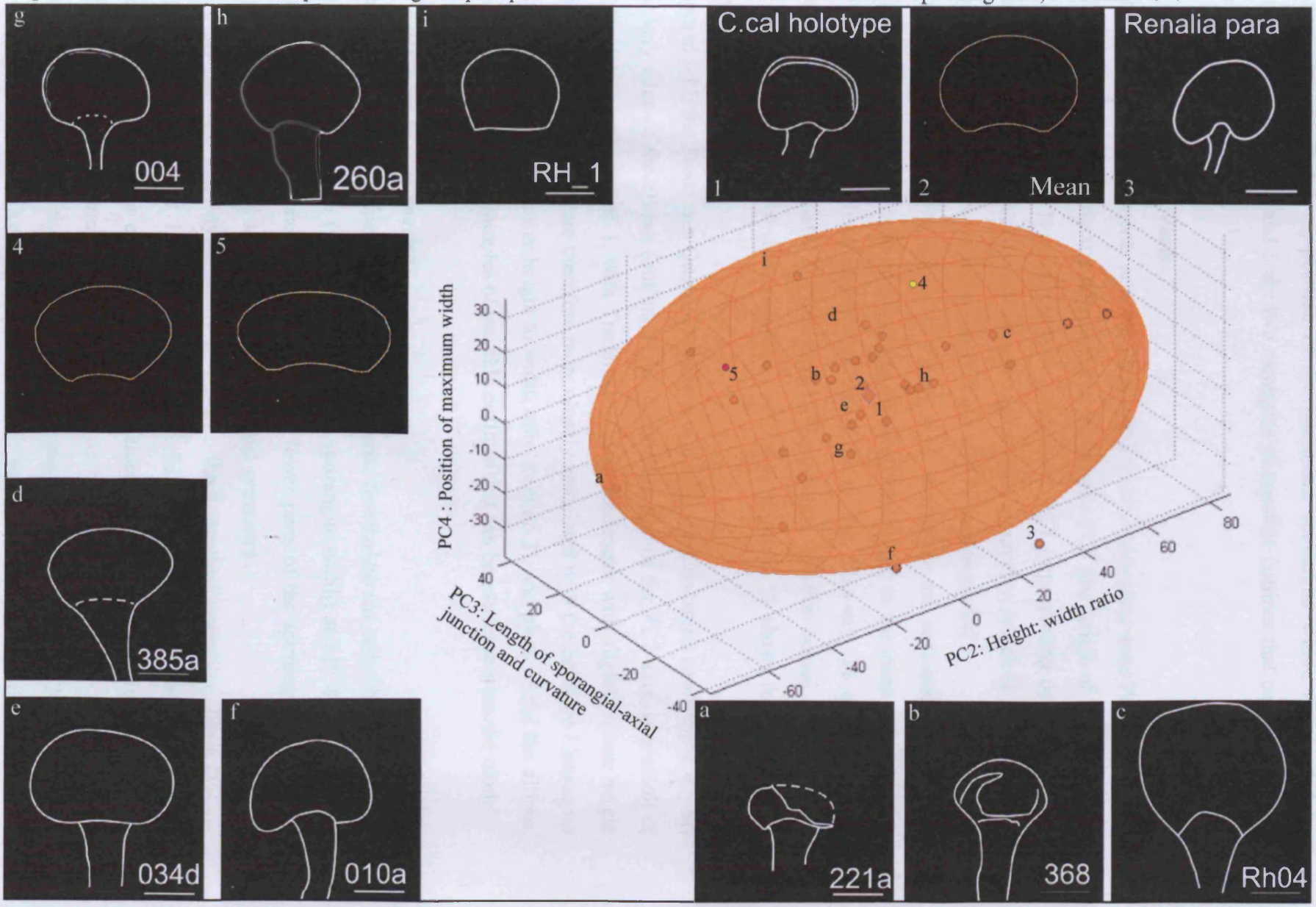

Principal component 4 axis, position of the maximum sporangial width, represented by outlines g to i. Outlines 4 and 5 are two examples of possible outlines that can be extracted from the model.

2. *Cooksonia* cf. *cambrensis*

The three principal components selected for *Cooksonia* cf. *cambrensis* were PC2 (sporangial height: width ratio), PC3 (maximum sporangial width) and PC4 (the length of straight edges) (see Figure 4.8*b*). Similar to cf. *Cooksonia caledonica*, PC1 (representing over 50% of the variance) has been disregarded as it represent sporangial symmetry, which is likely to be an effect of taphonomy. For the same reason PC5 has also been disregarded.

When plotted as a 3D plot, shown in Figure 4.15, the points are scattered across the 2 standard deviation ellipse, with no clustering and few points close to the mean value (outline 1). Three of the nine outlines plotted fell out of the ellipse. This may be due to the low number of specimens available for this model. The greatest variation occurs along the PC2 axis (height to width ratio), but as outlines a to c in Figure 4.15 show, this variation is actually quite slight.

Compared with the Tredomen Quarry specimens, the holotype *Cooksonia cambrensis* **α** plots at the very edge of the ellipse (outline 2), at the positive end of the PC2 axis, as a result of height to width ratio around 1, with Tredomen Quarry specimens with slightly lower height to width ratios. Specimens are therefore more closely associated with the holotype *Cooksonia cambrensis* **β**, also has a lower height to width ratio (outline 3), and plots within the ellipse. Outlines 4 and 5 are two examples of possible outlines that can be extracted from the model.

3. *Cooksonia he misphaerica*

The three principal components chosen for *Cooksonia hemisphaerica* were PC1 (sporangial height to width ratio), PC3 (position of maximum sporangial width) and PC4 (length of the sporangial-axial junction and the curvature of the lower parts of the sporangia) (see Figure 4.9*b*). PC2 was disregarded as it represents sporangial symmetry.

On the 3D plot, the majority of points do fall into the 2 standard deviation ellipse (Figure 4.16), with only 6 out of 123 specimens plotted falling outside the ellipse. Most points broadly cluster around the centre of the ellipse, close to the mean value (outline 1). The greatest variation occurs along the PC1 axis, as shown by outlines a to c.

Cooksonia hemisphaerica was first described by Lang (1937), and outlines 2 and 3 are two examples from his Targrove Quarry collection, which he used to define *Cooksonia*

Figure 4.15: Three-dimensional plot showing morphospace of *Cooksonia* cf. *cambrensis* using PC2, PC3 and PC4

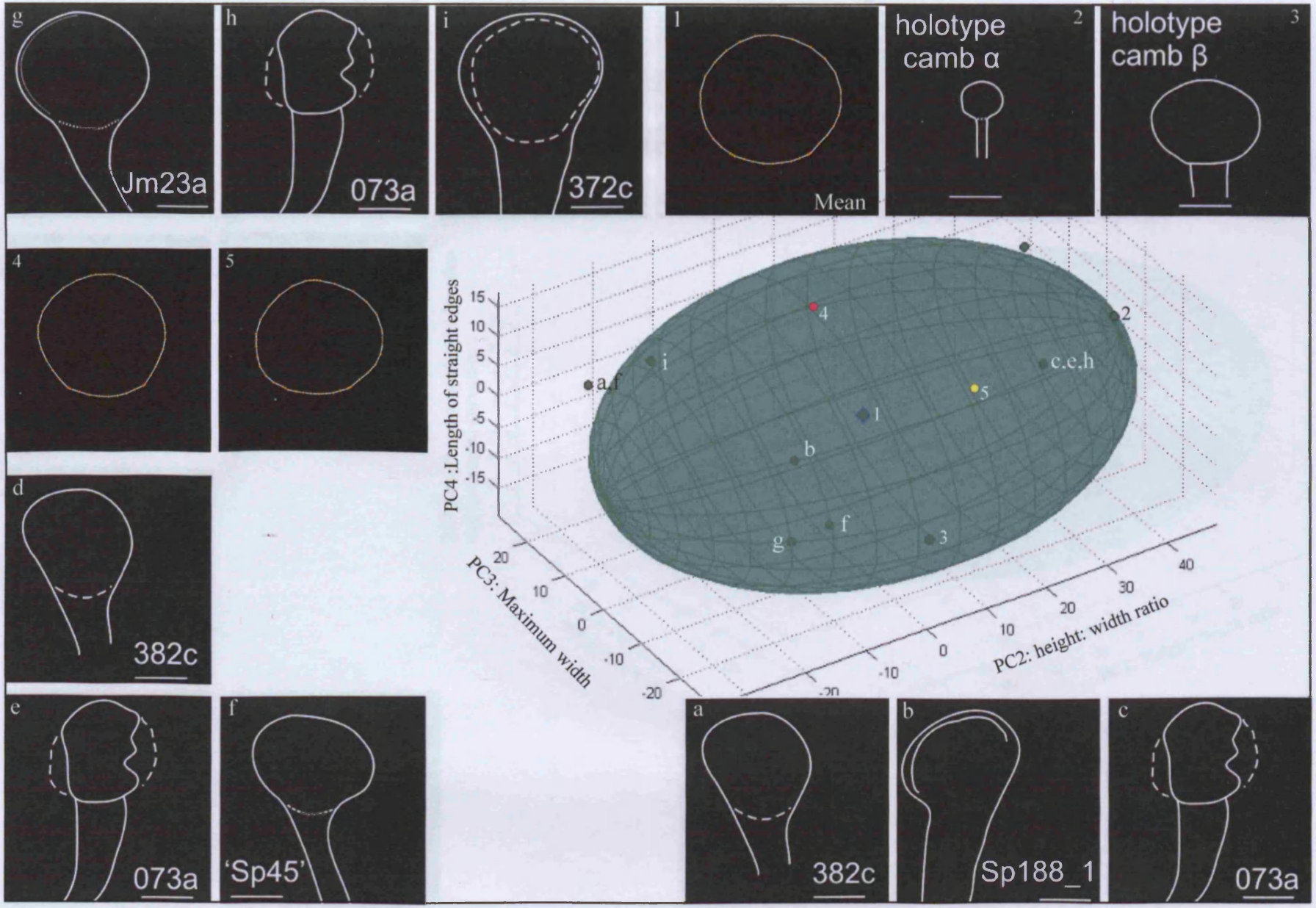

Figure 4.16: Three-dimensional plot showing morphospace of *Cooksonia hemisphaerica* using PC1, PC3 and PC4

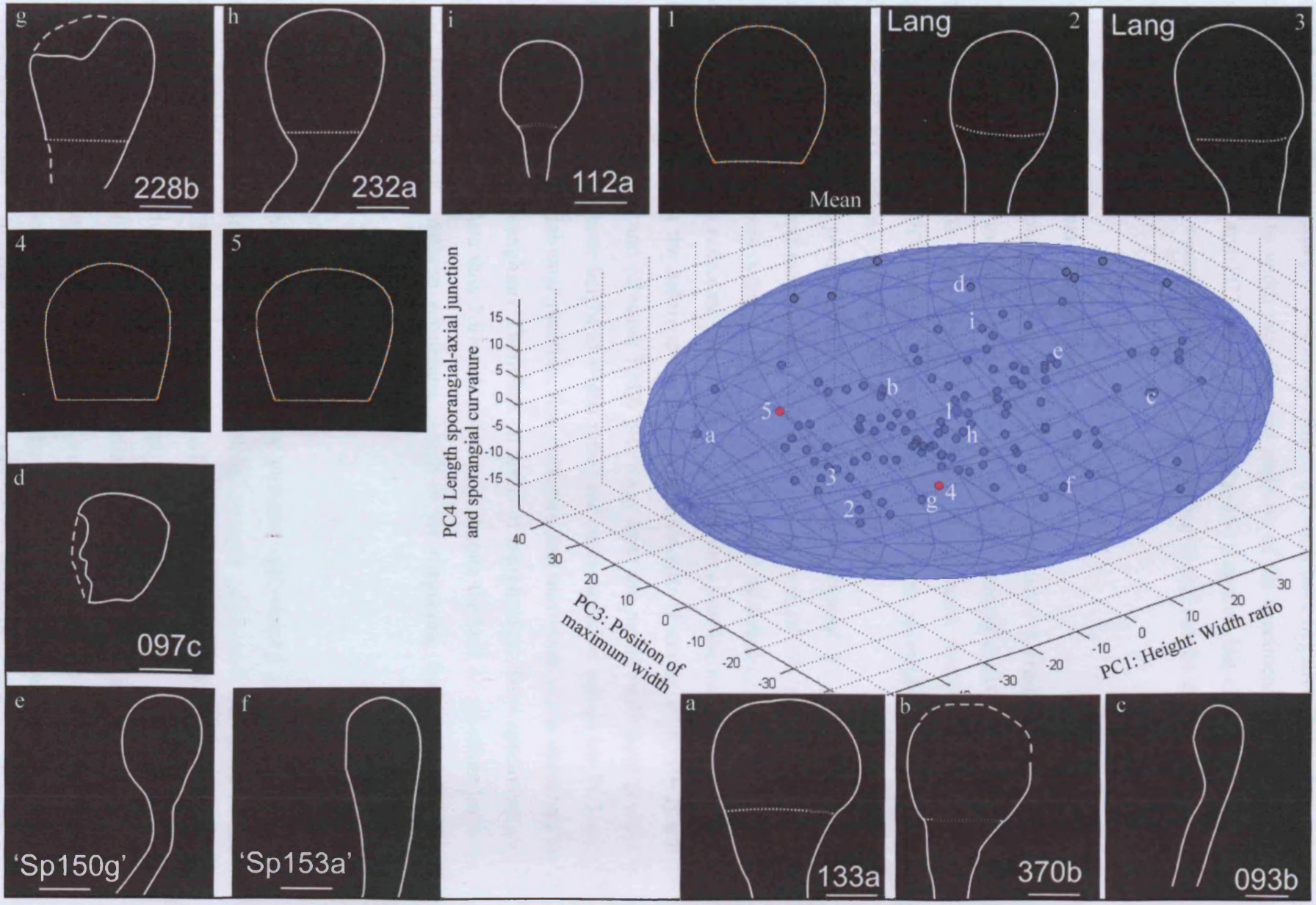

hemisphaerica. Both outlines plot within the ellipse, although have negative PC1 values, i.e. they have a lower height to width ratio than the majority of the specimens from Tredomen Quarry. In terms of PC2 and PC3 the outlines are slightly negative, but close to the mean. Outlines 4 and 5 are two examples of possible morphologies that can be extracted from the model.

4. cf. *Uskiella reticulata / Tarrantia salopensis*

The three principal components selected for cf. *Uskiella reticulata / Tarrantia salopensis* are PC1 (sporangial height to width ratio), PC3 (length of sporangial-axial junctions and curvature of the sporangia bases) and PC4 (position of maximum sporangial width) (see Figure 4.10*b*). PC2 and PC6 were disregarded as they represent sporangial symmetry and PC4 represents less variance than PC5 so was selected over PC5.

When plotted in the 3D plot, the outlines are scattered throughout the ellipse, with few clustering around the mean (see Figure 4.17). Five outlines out of 34 fall outside of the ellipse. The greatest variance occurs along axis PC1, illustrated by outlines a to c.

The holotype for *Uskiella reticulata* (Fanning et al. 1992) plots near the mean shape for this ellipse (outline 2), whilst the holotype for *Tarrantia salopensis* (Fanning et al. 1992) and *Uskiella spargens* (Shute and Edwards 1989) plot away from the mean, with more positive values for PC1 (i.e. a greater height to width ratio) and more negative values for PC3 and PC4 (i.e. shorter sporangial-axial junction, less curvature and maximum width occurring at half the length of the sporangium). Therefore, in terms of morphology, these specimens are most like *Uskiella reticulata* than *Tarrantia salopensis*, despite the lack of reticulate texture of the sporangial wall in these specimens, which is the diagnostic feature for *Uskiella reticulata*.

5. Elongate club-shaped sporangia

The three principal components selected for the elongate club-shaped sporangia are PC1 (sporangial height to width ratio), PC3 (length of straight edges and curvature of the sporangium base), and PC5 (length of the sporangial-axial junction) (see Figure 4.11*b*). PC2 and PC4 were disregarded as they represent sporangial symmetry.

When plotted on a 3D plot (Figure 4.18), 2 outlines out of 11 fall outside the ellipse, and points are scattered throughout the ellipse, with no clustering around the mean (outline 1). The greatest variance occurs along PC1 (the height to width ratio), illustrated by outlines a to c. Variance along PC3 is illustrated by outlines d to f, whilst the smallest variance along PC5

Figure 4.17: Three-dimensional plot showing morphospace of cf. *Uskiella reticulata / Tarrantia salopensis* using PC1, PC3 and PC4

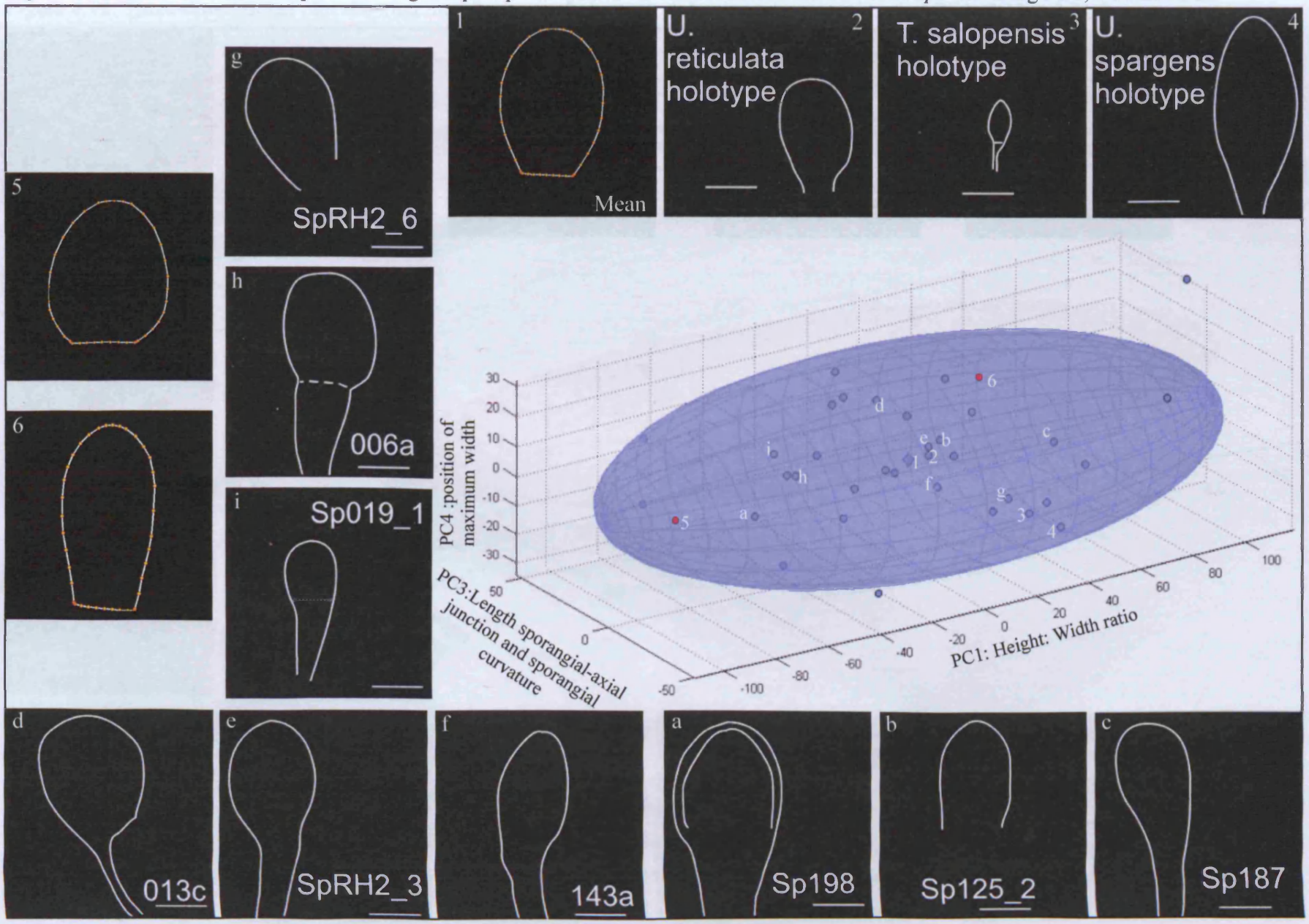

Figure 4.18: Three-dimensional plot showing morphospace of elongate club- shaped sporangia using PC1, PC3 and PC5.

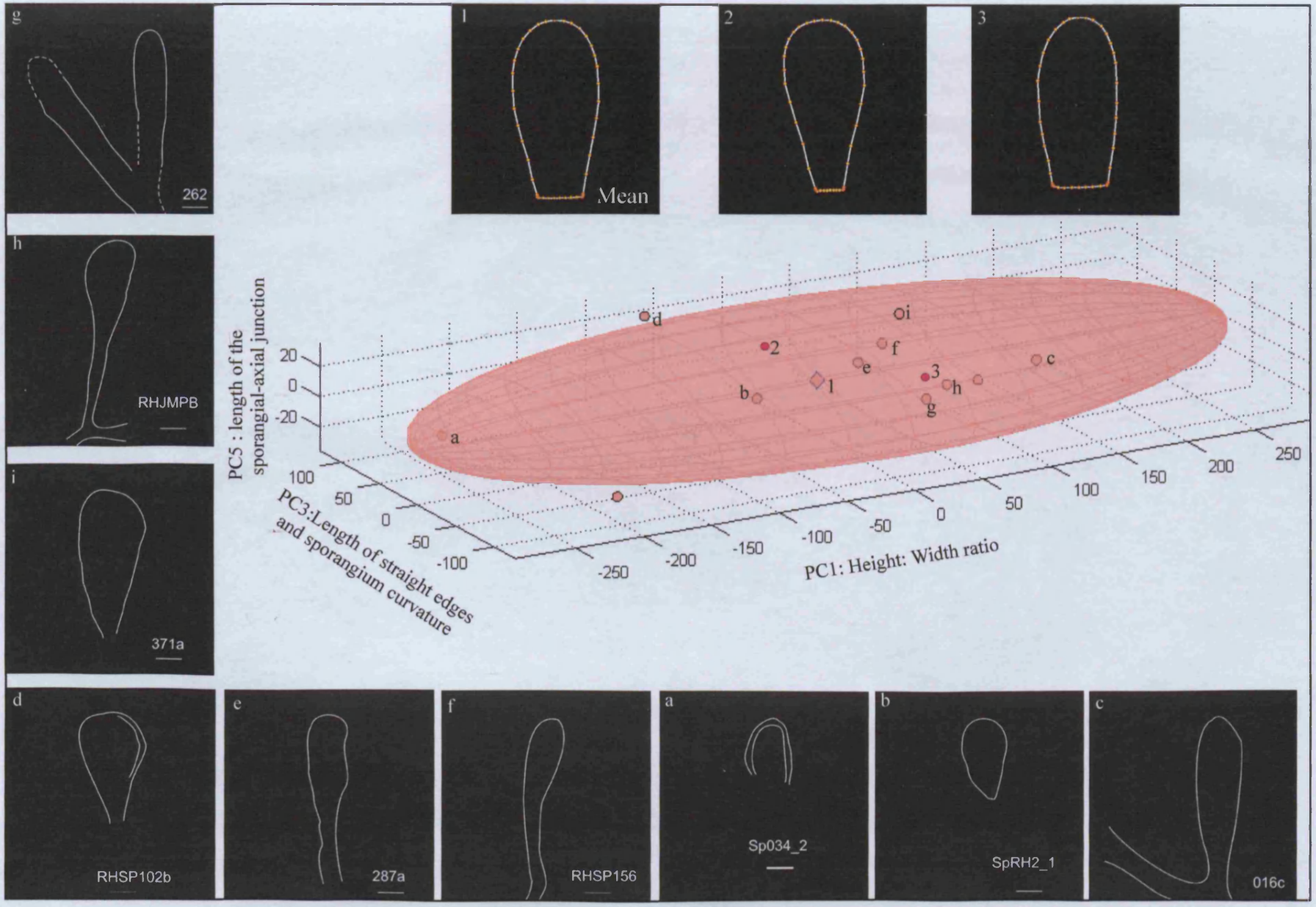

is illustrated by outlines g to i. As these specimens are considered a new genus, there are no holotypes to compare these specimens with. Outlines 2 and 3 represent possible morphologies extracted from this model.

6. *Salopella allenii*

The three principal components chosen for *Salopella allenii* are PC2 (position of maximum sporangial width and curvature of the sporangia), PC3 (length of straight edges) and PC4 (length of the sporangial-axial junction) (see Figure 4.12*b*). PC1 and PC6 were disregarded as they represent sporangial symmetry, and PC5 represents a small percentage of variance.

When plotted on a 3D plot (see Figure 4.19), the outlines are scattered throughout the ellipse, with no clustering around the mean (outline 1). However, there are low numbers of outlines in this model, and therefore not representative of a whole population. Two out of nineteen outlines plotted outside of the ellipse, one of which is the holotype for *Salopella caespitosa* Tims and Chambers (1984) (outline 2), and therefore the specimens from Tredomen Quarry are not closely related to this species. However, the holotype for *Salopella australis* Tims and Chambers (1984) (outline 3) and *Salopella allenii* Edwards and Richardson (1974) (outline 4) plots close to the mean value, suggesting that the Tredomen Quarry specimens are closely related to *Salopella allenii*, but also that *Salopella australis* is also very similar at least in morphology.

The greatest variance occurs along PC2, the position of the maximum width and the curvature of the sporangium base, illustrated by outlines a to c. Variance along PC3 is illustrated by outlines d to f and variance along PC4 is illustrated by outlines g to i. Two examples of possible morphologies that can be extracted from this model are shown in outlines 5 and 6.

7. *Salopella* cf. *marcensis*

The three principal components chosen for *Salopella marcensis* are PC2 (length of the straight edges, and curvature of the sporangium), PC3 (position of maximum sporangial width) and PC4 (length of the sporangial-axial junction) (see Figure 4.13*b*). PC1 and PC5 were disregarded as they represent sporangial symmetry.

When the outlines were plotted in a 3D plot, the points were scattered throughout the ellipse (Figure 4.20). As with *Salopella allenii*, the lack of specimens means that this is not likely to be representative of the whole species. Three out of the nine specimens plot outside of the ellipse. There is slight clustering around the mean (outline 1). The holotype of *Salopella*

Figure 4.19: Three-dimensional plot showing morphospace of *Salopella allenii* using PC1, PC3 and PC5

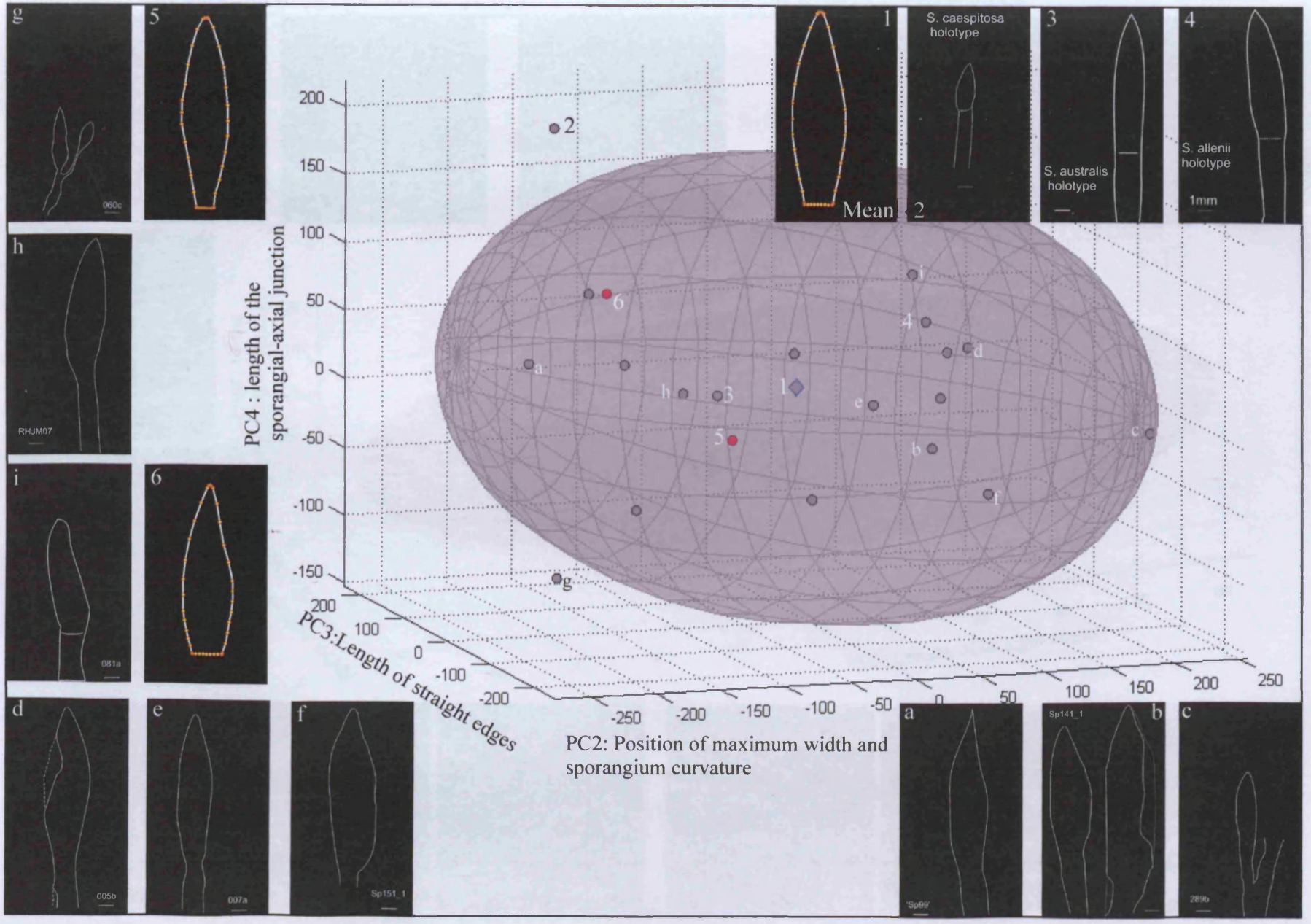

Figure 4.20: Three-dimensional plot showing morphospace of *Salopella* cf. *marcensis* using PC2, PC3 and PC4.

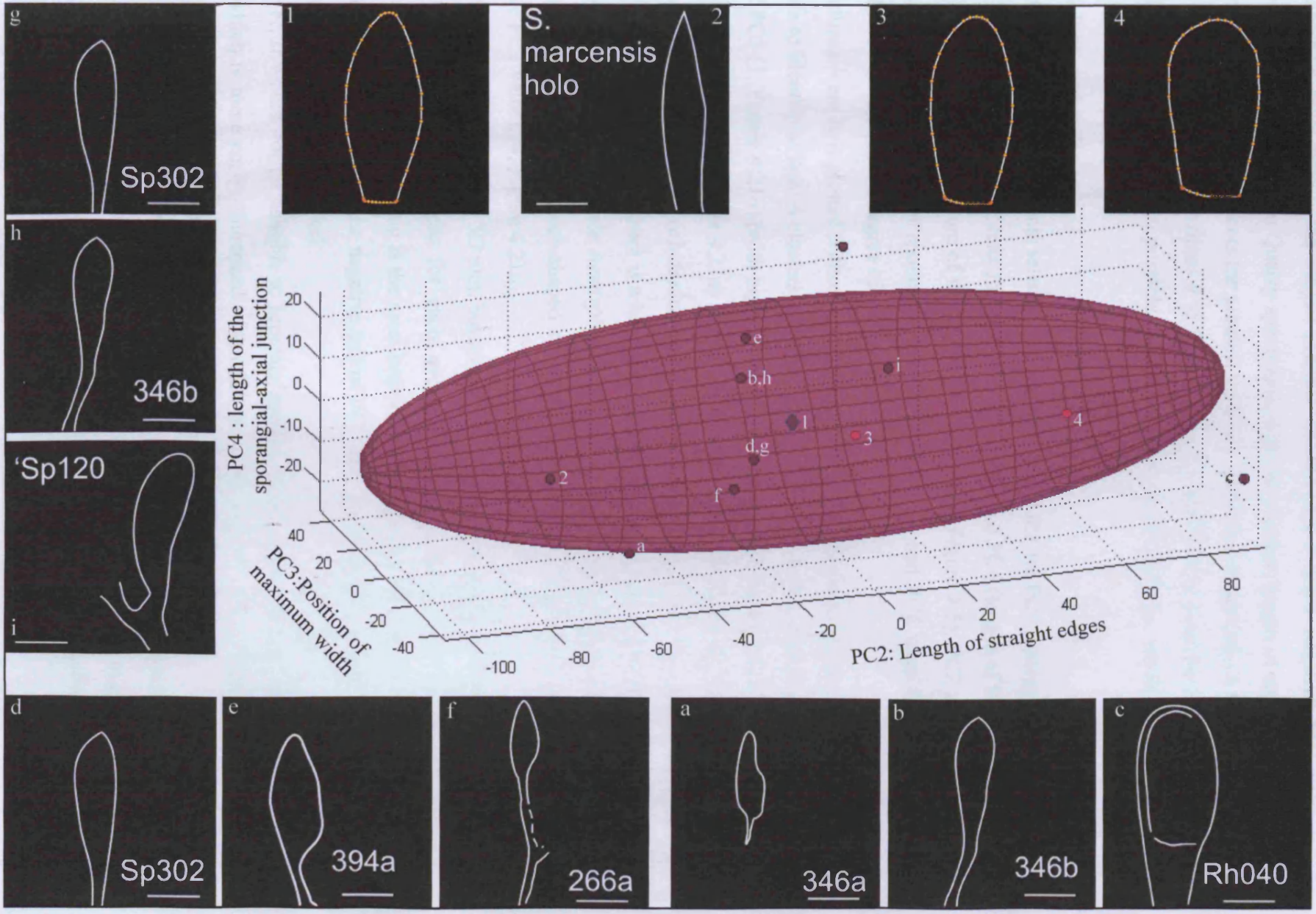

cf. *marcensis* plots within the ellipse (outline 2), but has a more negative PC2 value compared with the Tredomen Quarry specimens, with the shortest length of straight vertical sporangial edges. PC2 represents the greatest variance, illustrated by outlines a to c. Variance along PC3 is illustrated by outlines d to f, and variance along PC4 is illustrated by outlines g to i. Outlines 3 and 4 represent possible morphologies extracted from this model.

8. All m egafossils

The three principal components selected for all the megafossils are PC1 (sporangial height to width ratio), PC3 (position of maximum sporangial width) and PC4 (length of the sporangial-axial junction and the curvature of the sporangia bases) (see Figure 4.5). PC2 and PC7 were disregarded as they represent sporangial symmetry, and PC5 and PC6 were disregarded as they represent only a small degree of variance.

The outlines were first plotted without indicating species identification (Figure 4.21*a*). It was possible to identify at least 4 clusters, mainly separated by PC1, with a cluster at the positive end of PC1 (1, Figure 4.21*a*) (with high sporangial height to width ratios) and a cluster at the negative end of PC1 (2, Figure 4.21*a*) (low sporangial height to width ratios). These represent *Salopella* and cf. *Cooksonia caledonica*, respectively. On the whole, most points plot with a negative value, in particular there is a large cluster with slight negative PC1 values (3, Figure 4.21*a*), likely to be *Cooksonia hemisphaerica* or cf. *Cooksonia cambrensis*. cf. *Uskiella / Tarrantia* and the elongate club-shaped sporangia are represented by the cluster with slight positive PC1 values (4, Figure 4.21*a*).

Figure 4.21*b* shows the same 3D plot, but identifies which species each plot belongs to, and a two standard deviation ellipse for each species/ group. As discussed above, PC1, the sporangial height to width ratio is the most important factor in the separation of species, with cf. *Cooksonia caledonica* at the negative end of PC1 axis, and *Salopella allenii* and *Salopella* cf. *marcensis* at the positive end.

However, it would not be possible to separate species based on the variance along PC3 and PC4, which is more easily illustrated in the 2D plots, Figures 4.21*c* to *e*. Points are widely scattered and do not show any clustering.

There is also overlap between species ellipses, noticeably between all *Cooksonia* species and cf. *Uskiella reticulata / Tarrantia salopensis*. Both *Salopella* species overlap, and with some degree overlap with the elongate club-shaped sporangia and cf. *Uskiella reticulata / Tarrantia salopensis*.

Figure 4.21: Plots showing morphospaces of all megafossils *a* and *b*: 3D plots. *c*, *d* and *e*:2D plots.

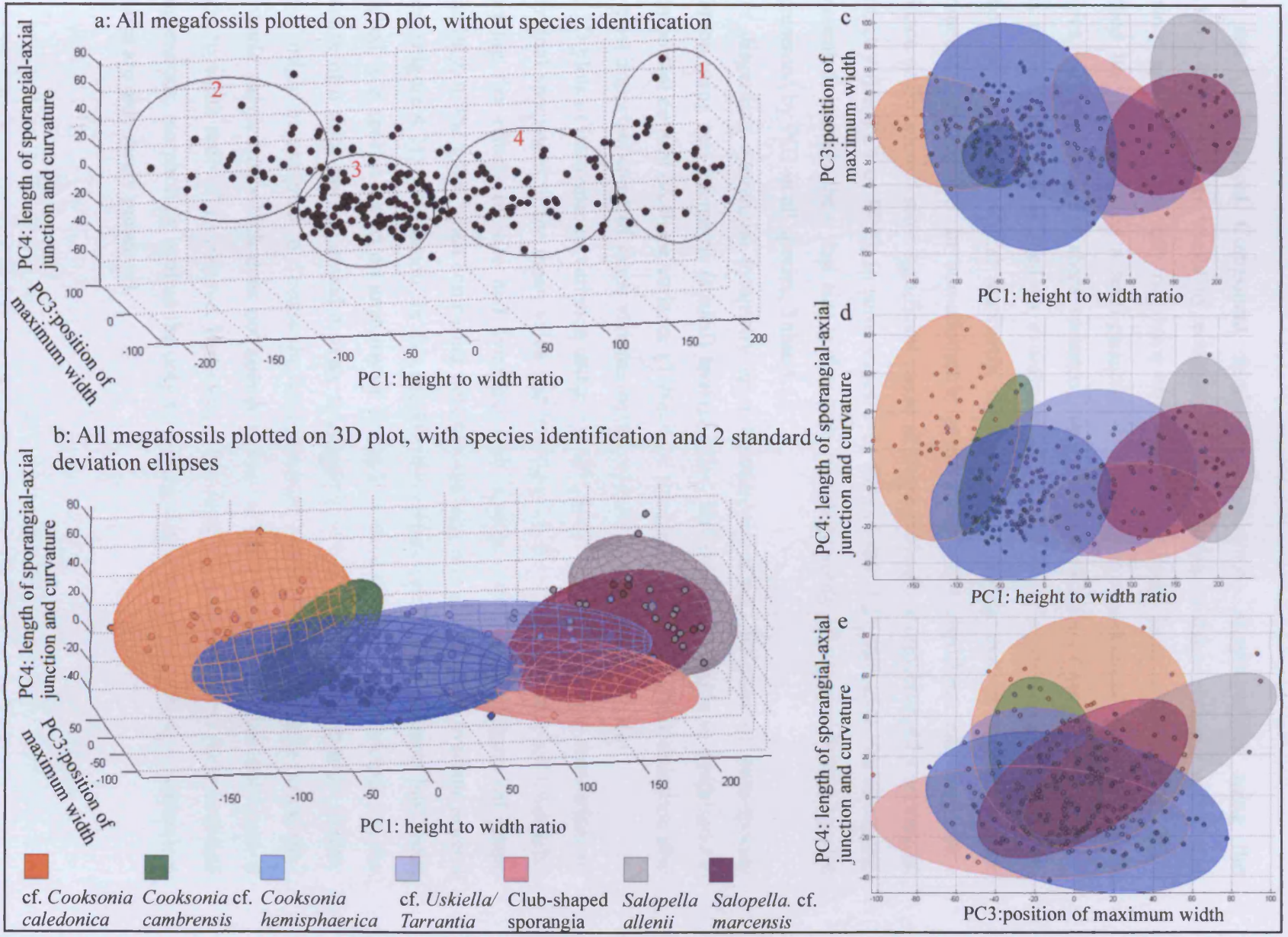

4.4: CHAPTER SUMMARY AND ASSESSMENT

The use of Principal Component Analysis in geometric morphometrics using the AAMToolbox, has been useful to recognise the main causes of shape variance within and between species, which may not have been recognised using basic measurements. This method has also provided a semi-quantitative approach to determining early land plant species, with percentages of shape variance being calculated (Tables 4.1 and 4.2).

This method has also allowed an evaluation of the degree of shape variance caused by taphonomy, using sporangial symmetry as a proxy, assuming that all sporangia were symmetrical during life. In non-allometric models, the most significant cause of shape variance or the second most significant cause of shape variance is represented by sporangial symmetry (i.e. PC1 or PC2), in some cases over 50% (Table 4.2). However, the allometric (non-scaled) models show that size is the most important cause of variance within species (represented by PC1 in all species, Table 4.1).

After disgarding sporangial symmetry as a taphonomic effect, 3D-plots of intra-species variation using non-allometric (scaled) models, show that sporangial height to width ratio is an important control on shape variance (Table 4.2). Sporangial height to width ratios are also the most important cause of shape variance between species (Figure 4.21*a* to *d*).

The 3D plots of intra-species variation using non-allometric models also allow comparison of individual specimens to the mean value and holotype for that particular species. Even after removing the effects of size and symmetry, all species show a high degree of shape variability, to the point when comparing between species, one ellipse often overlaps several others (Figure 4.21). The reason for this maybe that certain individual specimens have been assigned to a species based on anatomy or features, with less emphasis on shape, e.g. the presence of a thick border around a ovate sporangium with a height to width ratio slightly over 1 might be assigned to *Cooksonia hemisphaerica* rather than cf. *Uskiella reticulata* / *Tarrantia salopensis*, which does not appear to have a significant border, but does have a height to width ratio of 1 or above. However, when working with early land plant coalified compressions, morphology is often the only remaining data that can be gained, as anatomical features are only rarely preserved.

CHAPTER 5 : THE DISPERSED SPORE RECORD

5.1: INTRODUCTION

In Chapter 3, the diversity of early land plants inhabiting the Lower Devonian landscape, now located in central South-Wales, has been described in terms of the plant megafossil collection from Tredomen Quarry. A number of established naked, dichotomously branched early land plant species have been described, as well as known taxa of non-embryophytes. Previously undescribed minute branching axes with terminal sporangia (mesofossils) are a third component to Lower Devonian palaeoecology.

Despite early land plant megafossils revealing key information regarding gross morphology, physiology and to some extent affinity, the dispersed spore record provides a much larger database to study diversity, evolution and plant distribution patterns. In extant spores, the tough biopolymer sporopollenin is the main constituent of spore wall composition, which is chemically and physically stable (Guildford et al. 1988). Fossil and extant spore wall compositions have been compared using ^{13}C Solid State NMR, and have been found to have significantly different compositions (Hemsley et al. 1996). However, after considering the effects of diagenesis and experimental reconstruction of these effects on extant spore walls, the composition of fossil spore walls can be assumed to be similar to sporopollenin (Hemsley et al. 1996). This means that sporomorphs had a much higher preservation potential than the parent vegetation, with sporomorphs retaining their original morphology and structure. The dispersed spore record therefore can be considered to be more representative of the diversity of early land vegetation. One plant would have produced numerous spores that were widely distributed, and so potential for preservation was much increased.

Sporomorph species are variable, with clear distinctive features, and are therefore particularly useful in biostratigraphy. The Anglo-Welsh Basin is predominately dated via fish and spore biozones (see Chapter 1, section 1.2.3). However, the rarity of green fine-grained sandstone and siltstone horizons in which the most well-preserved spore assemblages are found (see Chapters 6 and 7) means that only a few, scattered assemblages exist at the base of the St. Maughans Formation and fewer in the Raglan Mudstone Formation.

The utilisation of the dispersed spore record as a measurement for diversity and use in biostratigraphy does not come without problems. Firstly, their minute size and tough polymer wall that allows such good preservation also means that sporomorphs are easily reworked,

often without altering the morphology or structure. Secondly, few spore taxa from the dispersed spore record can be related to *in situ* spores, due to lack of, and relative poor preservation of parent vegetation, hampering diversity studies.

Thirdly, it is also possible that more than one sporomorph taxon can be found within one plant species e.g. it has been discovered at least four trilete taxa are found within the sporangia of similar morphology to *Cooksonia pertoni*, each with a different exospore ornamentation: crassitate, distally laevigate *Ambitisporites*; crassitate, distally verrucate and reticulate *Synorisporites*; crassitate *Streelispora-Aneurospora*, both distally sculptured with coni, but only *Streelispora* possessing proximal tripapillae (Fanning et al. 1988, Habgood et al. 2002). As the sporangia were similar in gross morphology, Fanning et al. (1988) erected three sub-species of *Cooksonia pertoni* to accommodate the variation in the *in situ* triletes, although it would not be possible to distinguish between these sub-species based on gross morphology alone. The adaptive significance of a sculptured exine is not fully understood, but hypotheses include adaptation for better wind dispersal, defence against fauna, or aiding spore germination (Fanning et al. 1988, Edwards and Richardson 1996, Burgess and Richardson 1999). If this is a common feature of early land plants, then the integration of the *in situ* spore record with the dispersed spore record becomes more challenging.

Finally, well-preserved sporomorph assemblages are restricted to certain lithofacies (fine-grained green sandstones and siltstones), and difficulties in obtaining enough material to count a significant number of sporomorphs (c.200 spores) have been experienced.

In this chapter, early land plant diversity during the Lower Devonian has been measured using five dispersed spore assemblages, from a range of green lithofacies, occurring at different depths within the Tredomen Quarry correlated core sequence (see Figure 6.1, Chapter 6). All sampled horizons occur above carbonate-nodule-rich horizons interpreted as the Bishop's Frome Limestone, and therefore all assemblages occur within the St. Maughans Formation (Table 1.1, Chapter 1). Sporomorphs have been fully described, as many specimens represent new taxa, or provide additional information on published taxa. Each assemblage has then been compared with published assemblages and assigned to a suitable sub-biozone and equivalent age. Where possible, dispersed spore specimens have been compared with published *in situ* spore data, providing further insight into the type of vegetation within the area. Additionally, changes in sporomorph nature (e.g. sculpture type) through the Tredomen Quarry sequence are noted, with implications regarding evolution and palaeoenvironment.

5.2: TREDOMEN QUARRY SPORE ASSEMBLAGES

Samples for maceration were taken from a range of green lithofacies; intraformational conglomerates, fine to medium-grained sandstones, siltstones and mudstones. Of the eighteen macerations performed using the HF techniques described in section 2.1.1 of Chapter 2, only five assemblages contained sufficient numbers of well-preserved sporomorphs for analyses (see Appendix V*a*). The five well-preserved sporomorph assemblages were sampled from the following green horizons, and are labelled on Figure 6.1 of Chapter 6 (BH1 = Borehole 1, BH2 = Borehole 2 and PB = Plant Bed);

1. Assemblage 1 (BH1-6): 0m (quarry surface): fine-grained trough-cross-bedded sandstones (lithofacies 2b, Chapter 6) and wavy to planar-laminated siltstones (lithofacies 3a, Chapter 5).
2. Assemblage 2 (BH1-1): 11.28m depth within borehole 1 / 11.28m beneath the quarry surface: fine-grained trough-cross-bedded sandstones (lithofacies 2b, Chapter 6).
3. Assemblage 3 (PB1): 11.80m depth within borehole 1 / 11.80m beneath the quarry surface: medium-grained planar-bedded sandstones (lithofacies 2a, Chapter 6).
4. Assemblage 4 (BH2-1): 7.60m depth in Borehole 2 / 21.60m beneath quarry surface: planar-laminated siltstones (lithofacies 3a, Chapter 6).
5. Assemblage 5 (BH1-3): 28.20m depth within borehole 1 / 28.20m beneath quarry surface: planar-laminated siltstones.

Sporomorph assemblages were then counted using light microscopy or SEM imaging. At least 200 spores were counted in each assemblage, more if spores were easily found (species counts in Appendix V*b*). Cumulative plots of each assemblage show that the graph flattens out approximately around 200 counts, and therefore the species counted represent most of the species within that assemblage (Figure 5.1). Ninety sporomorph taxa (cryptospores and triletes) have been described, 61 of which are recognised published spore taxa (Table 5.1*a* and *b*).

Sporomorph taxa have been described using terminology from the relevant holotype description, or by using Grebe (1971) and Punt et al. (2007). Figure 5.2 illustrates the main terminology and measurements used. Triletes are classified according to Potonié and Kremp (1954), whilst all cryptospore taxa are classified according to the classification scheme devised by Richardson (1996a) (Table 5.2). Sporomorphs were recorded in a database (Appendix I*b*). Original spore counts and measurement data can be found in Appendix V*b* to *d*.

Figure 5.1: Cumulative graphs for each palynological assemblage.

Figure 5.1a: Assemblage 1.

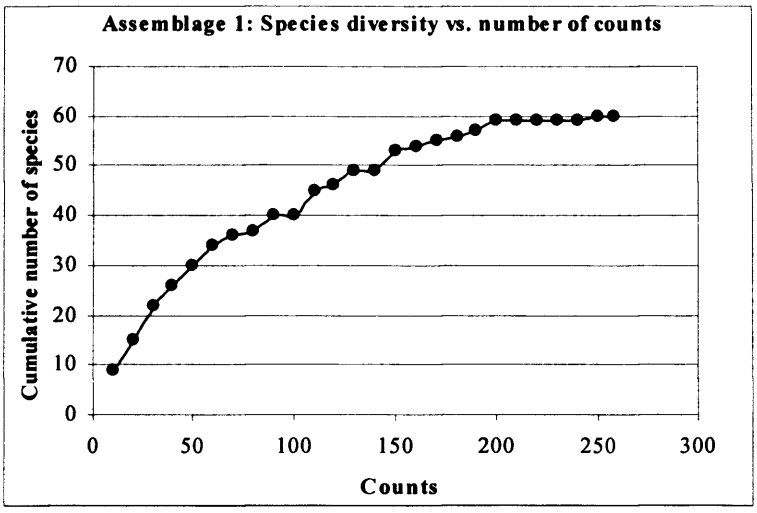

Figure 5.1b: Assemblage 2.

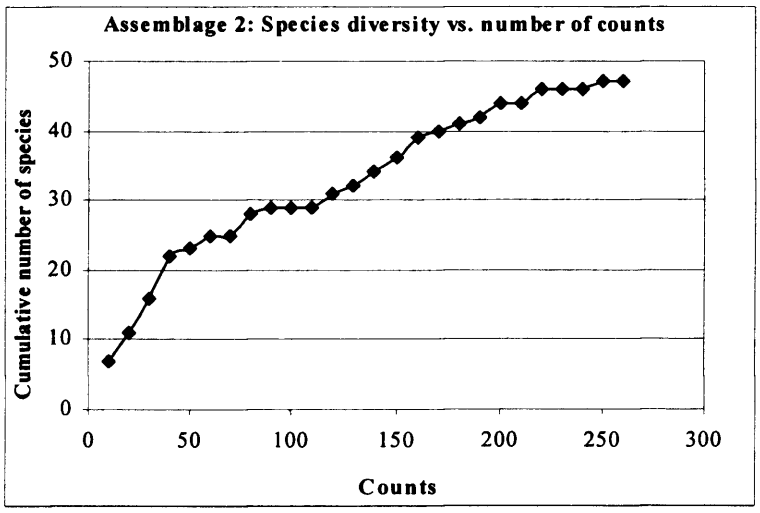

Figure 5.1c: Assemblage 3.

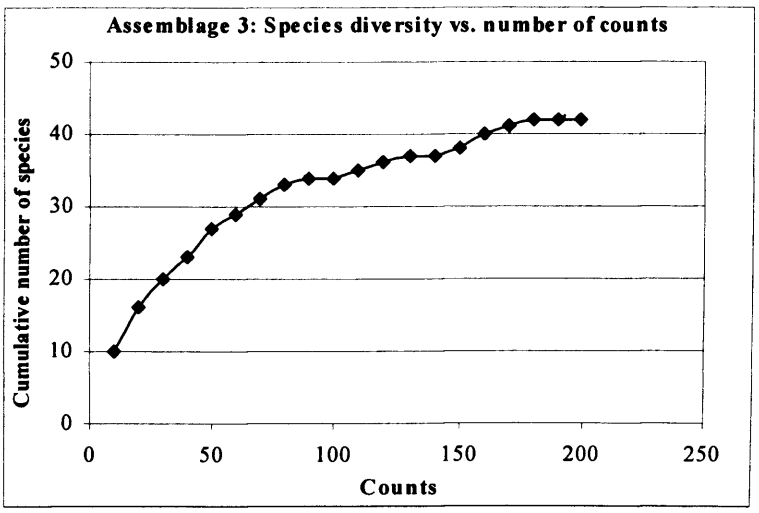

Figure 5.1: Cumulative graphs for each palynological assemblage (continued).

Figure 5.1d: Assemblage 4.

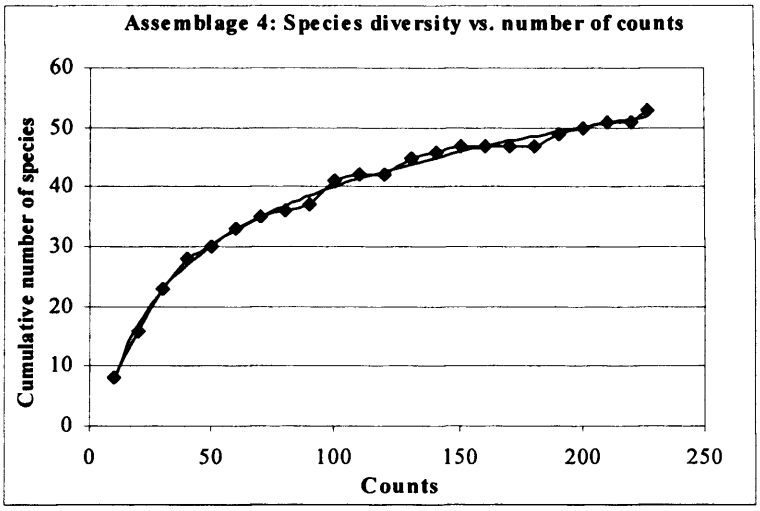

Figure 5.1e: Assemblage 5.

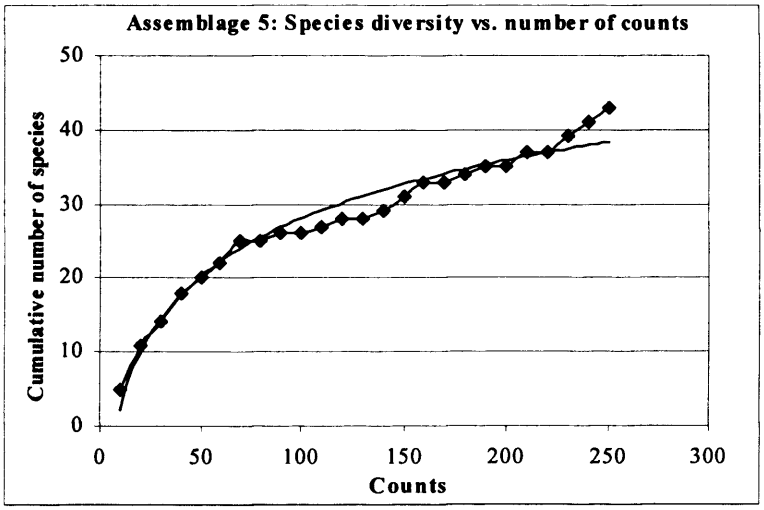

Table 5.1a: Sporomorph taxa from Tredomen Quarry and their distribution, arranged taxonomically.

CRYPTOSPORES			5	4	3	2	1
Permanent fused tetrads - laevigate	1	*Cheilotetras caledonica*		●	●	●	●
	2	*Cheilotetras* sp.		●			●
Permanent fused tetrads - sculptured	3	Fused apiculate tetrad (?gen. nov.)	●				
	4	Fused verrucate tetrad (?gen. nov.)		●	●	●	●
	5	Fused murornate tetrad (?gen. nov.)			●		●
Permanent unfused tetrads- laevigate	6	*Tetrahedraletes medinensis* var. *medinensis*	●	●	●	●	●
	7	*Tetrahedraletes medinensis* var. *parvus*	●	●	●	●	●
	8	*Rimosotetras problematica*	●				●
Perm. unf. tet. sculpt	9	*Acontotetras inconspicus*	●	●	●		
Triads- sculptured	10	Apiculate triad					●
	11	Verrucate triad	●	●			●
	12	Murornate triad	●				●
Pseudodyads - laevigate	13	*Pseudodyadospora* cf. *laevigata*		●	●	●	●
	14	*Pseudodyadospora petasus*	●	●	●	●	●
True dyads - laevigate	15	*Dyadospora murusattenuata*	●	●	●	●	●
	16	*Dyadospora murusdensa*	●	●	●	●	●
Hilates - laevigate	17	*Artemopyra* sp. A (?sp. nov.)	●	●			
	18	*Artemopyra* cf. *robusta*		●			
	19	*Laevolancis divellomedia*	●	●	●	●	●
	20	*Laevolancis plicata*	●	●	●	●	●
Hilates - apiculate	21	*Cymbohilates allenii* var. *allenii*		●	●	●	●
	22	*Cymbohilates allenii* var. *magnus*	●	●	●	●	●
	23	*Cymbohilates* cf. *amplus*		●		●	●
	24	*Cymbohilates cymosus*					●
	25	*Cymbohilates disponerus*	●	●	●		●
	26	*Cymbohilates horridus*				●	●
	27	*Cymbohilates horridus* var. A (?sp. nov.)		●	●	●	●
	28	*Cymbohilates* cf. *horridus* (?sp. nov.)	●				
	29	*Cymbohilates* cf. *microgranulatus*		●	●	●	
	30	*Cymbohilates variabilis* var. *parvidecus*		●	●	●	●
	31	*Cymbohilates variabilis* var. *variabilis*	●	●	●	●	●
	32	*Cymbohilates variabilis* var. B (?sp. nov.)			●		●
	33	*Cymbohilates* spp.	●		●		
Hilates - murornate	34	*Chelinohilates erraticus*	●	●	●	●	●
	35	*Chelinohilates* cf. *lornensis*	●			●	
	36	*Chelinohilates sinuosus* var. *angustus*		●			
	37	*Chelinohilates sinuosus* var. *sinuosus*		●			●
	38	*Chelinohilates* sp A. (?sp. nov.)		●			●
	39	*Chelinohilates* spp.	●	●		●	●
Hilate - verrucate	40	*Hispanaediscus major*				●	
	41	*Hispanaediscus* cf. *major*				●	
	42	*Hispanaediscus verrucatus*	●	●	●	●	●
	43	*Hispanaediscus* cf. *verrucatus*		●			
	44	*Hispanaediscus wenlockensis*			●		●
Non-hilates laevigate	45	Laevigate alete monads	●	●	●	●	●
Enveloped tetrads	46	*Velatitetras* cf. *cristata*	●			●	
	47	*Velatitetras* cf. *reticulata*		●	●		●
	48	*Velatitetras rugulata*		●		●	
	49	*Velatitetras* sp B. (?sp. nov.)		●		●	
	50	*Velatitetras* sp. C (?sp. nov.)					●

Table 5.1a (continued): Sporomorph taxa from Tredomen Quarry and their distribution, arranged taxonomically.

Enveloped unfused dyad	51	*Abditusdyadus histosus*				●	●
Enveloped fused dyads	52	*Segestrespora* cf. *membranifera*					●
Enveloped non-hilates	53	*Qualisaspora sinuata*					●
Incertae sedis ?Enveloped	54	Clustered spinose sculpture				●	●
	55	Apiculate sculpture					●
	56	Slender to spatulate spinose sculpture					●
	57	Spatulate sculpture		●			●
	58	Broad murornate sculpture	●	●	●		
	59	Sinuous murornate sculpture		●			
	60	Verrucate sculpture		●			
Laevigate triletes	61	*Retusotriletes dittonensis*	●	●	●	●	
	62	*Retusotriletes* cf. *dittonensis*	●		●	●	●
	63	*Retusotriletes* cf. *triangulatus*				●	
	64	*Retusotriletes* cf. *triangulatus* var. *minor*	●			●	
	65	*Retusotriletes* spp.	●	●	●	●	●
	66	*Ambitisporites avitus*	●		●	●	●
	67	*Ambitisporites avitus* var. *minor* (?var. nov)	●	●	●	●	●
	68	*Ambitisporites dilutus*	●	●	●	●	●
	69	*Ambitisporites warringtonii*	●	●	●	●	●
	70	*Ambitisporites* sp. A (?sp. nov)				●	
	71	*Ambitisporites* spp.	●	●	●	●	●
	72	*Archaeozonotriletes chulus* var. *inframurinatus*					●
	73	*Archaeozonotriletes chulus* var. *chulus*		●			
	74	*Archaeozonotriletes chulus* var. *nanus*					●
	75	*Archaeozonotriletes* spp.					●
Apiculate triletes	76	*Apiculiretusispora* spp.			●	●	●
	77	*Emphanisporites protophanus*				●	
	78	*Emphanisporites* sp. B	●		●		
	79	*Emphanisporites* spp.	●			●	
Murornate triletes	80	*Streelispora* spp./ *Aneurospora* spp.		●	●		●
	81	*Aneurospora* sp.			●		●
	82	*Streelispora newportensis*		●			●
	83	*Scylaspora* sp.	●	●			
	84	*Scylaspora* cf. *scripta*	●				
	85	*Scylaspora downiei*			●	●	
	86	*Scylaspora* cf. *kozlica*	●				
	87	*Synorisporites* sp.	●	●	●		
	88	*Synorisporites tripapillatus*		●			●
Patinate triletes	89	*Chelinospora* spp.	●	●			●
Perispore triletes	90	*?Perotrilites microbaculatus*	●			●	●
Acritarchs	91	*Acritarchs*	●	●	●	●	●

Table 5.1b: Sporomorph taxa from Tredomen Quarry and their distribution, arranged in order of first appearance.

		5	4	3	2	1
1	*Acritarchs*	●	●	●	●	●
2	*Tetrahedraletes medinensis* var. *medinensis*	●	●	●	●	●
3	*Tetrahedraletes medinensis* var. *parvus*	●	●	●	●	●
4	*Rimosotetras problematica*	●				●
5	Verrucate triad	●	●			●
6	Murornate triad	●				●
7	*Pseudodyadospora petasus*	●	●	●	●	●
8	*Dyadospora murusattenuata*	●	●	●	●	●
9	*Dyadospora murusdensa*	●	●	●	●	●
10	*Laevolancis divellomedia*	●	●	●	●	●
11	*Laevolancis plicata*	●	●	●	●	●
12	*Cymbohilates allenii* var. *magnus*	●	●	●	●	●
13	*Cymbohilates disponerus*	●	●	●		●
14	*Cymbohilates variabilis* var. *variabilis*	●	●	●	●	●
15	*Chelinohilates erraticus*	●	●	●	●	●
16	*Chelinohilates* spp.	●	●		●	●
17	*Hispanaediscus verrucatus*	●	●	●	●	●
18	Laevigate alete monads	●	●	●	●	●
19	*Retusotriletes* cf. *dittonensis*	●		●	●	●
20	*Retusotriletes* spp.	●	●	●	●	●
21	*Ambitisporites avitus*	●		●	●	●
22	*Ambitisporites avitus* var. *minor* (?var. nov)	●	●	●	●	●
23	*Ambitisporites dilutus*	●	●	●	●	●
24	*Ambitisporites warringtonii*	●	●	●	●	●
25	*Ambitisporites* spp.	●	●	●	●	●
26	*Chelinospora* spp.	●	●			●
27	*?Perotrilites microbaculatus*	●			●	●
28	Fused apiculate tetrad (?gen. nov.)	●				
29	*Cymbohilates* cf. *horridus* (?sp. nov.)	●				
30	*Scylaspora* cf. *scripta*	●				
31	*Scylaspora* cf. *kozlica*	●				
32	*Artemopyra* sp. A (?sp. nov.)	●	●			
33	*Scylaspora* sp.	●	●			
34	*Acontotetras inconspicus*	●	●	●		
35	*Cymbohilates* spp.	●		●		
36	Enveloped; broad murornate sculpture	●	●	●		
37	*Emphanisporites* sp. B	●		●		
38	*Synorisporites* sp.	●	●	●		
39	*Chelinohilates* cf. *lornensis*	●			●	
40	*Velatitetras* cf. *cristata*	●			●	
41	*Retusotriletes dittonensis*	●	●	●	●	
42	*Retusotriletes* cf. *triangulatus* var. *minor*	●			●	
43	*Emphanisporites* spp.	●			●	
44	*Artemopyra* cf. *robusta*		●			
45	*Chelinohilates sinuosus* var. *angustus*		●			
46	*Hispanaediscus* cf. *verrucatus*		●			
47	Enveloped; sinuous murornate sculpture		●			
48	Enveloped; verrucate sculpture		●			
49	*Archaeozonotriletes chulus* var. *chulus*		●			
50	*Cymbohilates* cf. *microgranulatus*		●	●	●	

Table 5.1b: (continued) Sporomorph taxa from Tredomen Quarry and their distribution, arranged in order of first appearance.

51	*Velatitetras rugulata*		•		•	
52	*Velatitetras* sp B. (?sp. nov.)		•		•	
53	*Cheilotetras caledonica*		•	•	•	•
54	*Cheilotetras* sp.		•			•
55	Fused verrucate tetrad (?gen. nov.)		•	•	•	•
56	*Pseudodyadospora* cf. *laevigata*		•	•	•	•
57	*Cymbohilates allenii* var. *allenii*		•	•	•	•
58	*Cymbohilates* cf. *amplus*		•		•	•
59	*Cymbohilates horridus* var. A (?sp. nov.)		•	•	•	•
60	*Cymbohilates variabils* var. *parvidecus*		•	•	•	•
61	*Chelinohilates sinuosus* var. *sinuosus*		•			•
62	*Chelinohilates* sp A. (?sp. nov.)		•			•
63	Enveloped; spatulate sculpture		•			•
64	*Velatitetras* cf. *reticulata*		•	•		•
65	*Streelispora* spp./ *Aneurospora* spp.		•	•		•
66	*Streelispora newportensis*		•			•
67	*Synorisporites tripapillatus*		•			•
68	*Scylaspora downiei*			•	•	
69	Fused muromate tetrad (?gen. nov.)			•		•
70	*Cymbohilates variabilis* var. B (?sp. nov.)			•		•
71	*Hispanaediscus wenlockensis*			•		•
72	*Apiculiretusispora* spp.			•	•	•
73	*Aneurospora* sp.			•		•
74	*Hispanaediscus major*				•	
75	*Hispanaediscus* cf. *major*				•	
76	*Retusotriletes* cf. *triangulatus*				•	
77	*Ambitisporites* sp. A (?sp. nov)				•	
78	*Emphanisporites protophanus*				•	
79	*Cymbohilates horridus*				•	•
80	*Abditusdyadus histosus*				•	•
81	Enveloped; clustered spinose sculpture				•	•
82	Apiculate triad					•
83	*Cymbohilates cymosus*					•
84	*Velatitetras* sp. C (?sp. nov.)					•
85	*Segestrespora* cf. *membranifera*					•
86	*Qualisaspora sinuate*					•
87	Enveloped; apiculate sculpture					•
88	Enveloped; slender spinose sculpture					•
89	*Archaeozonotriletes chulus* var. *inframurinatus*					•
90	*Archaeozonotriletes chulus* var. *nanus*					•
91	*Archaeozonotriletes* spp.					•

Figure 5.2: Sporomorph terminology and measurements

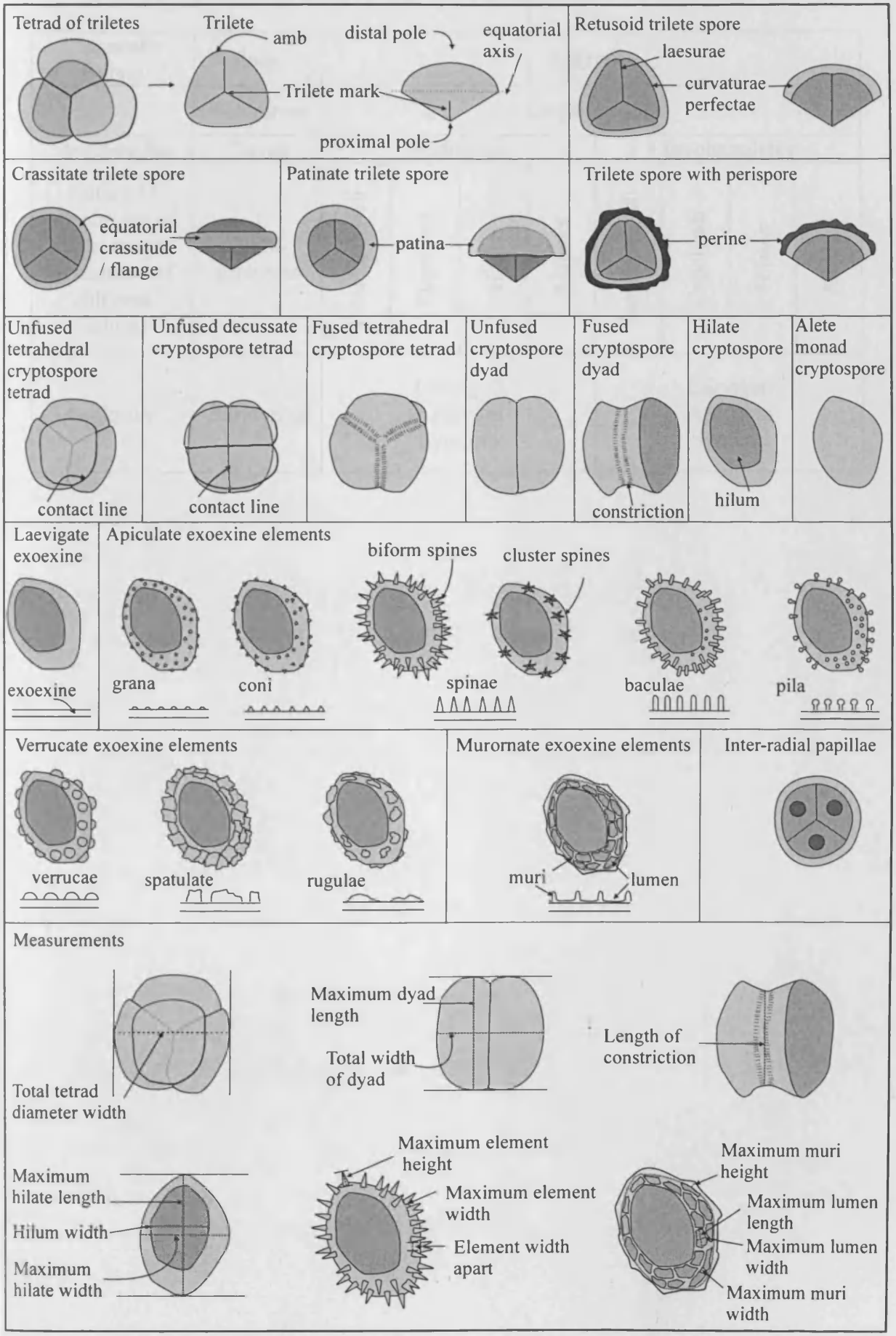

Table 5.2: Cryptospore classification scheme (after Richardson 1996a).

Diagnostic feature	Rank	Category							
	Anteturma	Cryptosporites							
Stratification	Turma	Nudialetes				Involucraletes			
Nature of attachment of units/ nature or absence of unit area (hilum)	Supra-subturma	Pseudopolyadi	Eupolyadi	Hilates	Ahilates	Pseudopolyadi	Eupolyadi	Hilates	Ahilates
Sculpture	Infraturma	Laevigati Apiculati Synorati				Laevigati Apiculati Synorati			

5.3: SYSTEMATIC DESCRIPTIONS

Where possible spores have been assigned to at least genus level, if not species. New species are marked with (sp. nov.) after the spore name, while new variations are marked with (var. nov.) although these new classifications are not official.

5.3.1: *Cryptospores*

Anteturma **CRYPTOSPORITES** Richardson, Ford and Parker 1984

Turma **NUDIALETES** Richardson 1996a

Multiple or single cryptospore units without an external envelope.

Suprasubturma **PSEUDOPOLYADI** Richardson 1996a

Multiple cryptospore units that are fused.

Infraturma **LAEVIGATI** Richardson 1996a

Eucryptospores with a smooth exine.

Genus **CHEILOTETRAS** Wellman and Richardson 1993

Cheilotetras caledonica Wellman and Richardson 1993

Plate 5.1*a* - *g*

Description: Naked, permanently fused, tetrahedral tetrad with a laevigate exine. No visible contact line between sub-circular spore units. Each spore possesses an equatorial flange extending beyond the fused junction, and walls are invaginated.

Dimensions: Tetrad diameter 21.6 (35.8) 54.0μm. 19 specimens measured.

Comments: Some specimens are smaller than the published size range (29 to 65μm). Some specimens are similar to those found in *Grisellatheca salopensis* Edwards et al. 1999, a bifurcating mesofossil from the mid-Lochkovian.

Occurrences: Assemblages 1 to 4.

Age range: Late Wenlock (Homerian) to Přídolí (Wellman 1993a, Wellman and Richardson 1993, Burgess and Richardson 1995). ?*In situ* middle Lochkovian (Edwards et al. 1999).

Cheilotetras sp.

Plate 5.1*h – l*

Description: Naked, permanently fused, tetrahedral or decussate tetrad with a laevigate exine. No visible contact lines between sub-circular spore units. Unlike *Cheilotetras caledonica,* spore units of *Cheilotetras* sp. do not possess equatorial flanges, and walls may or may not be invaginated.

Dimensions: Tetrad diameter 33.8 (39.7) 50.8μm. 6 specimens measured.

Comments: Similar to those described in Wellman 1996 as *Cheilotetras* sp., but larger (specimens described by Wellman have diameters between 21.0 (28.0) 39.0μm). Similar sized fused laevigate tetrads from Xiajiang, China are assigned to *Cheilotetras* sp. (Wang et al. 1997).

Occurrences: Assemblages 1 and 4.

Age range: Caradoc (Sandbian-early Katian) to early Přídolí (Wellman 1996, Wang et al. 1997).

Genus **PSEUDODYADSPORA** Johnson 1985

Pseudodyadospora petasus Wellman and Richardson 1993

Plate 5.2*a – f*

Description: Naked, permanently fused, laevigate dyad of equally-sized sporal bodies. The outline of an individual sporal body is elongate to sub-circular. The bodies are arranged as two 'dishes' attached at the base. There is no visible line of contact; the junction marked by a constriction. Exine is thin and sometimes folded. Distal walls are invaginated.

Dimensions: Maximum spore length 21.5 (31.1) 54.2μm, at constriction 18.1 (25.2) 37.7μm; Total diameter 12.3 (25.0) 45.2μm. 46 specimens measured.

Comments: This assemblage contains smaller specimens than previous investigations, with the smallest published diameter for *Pseudodyadospora petasus* at 26.0μm (Wellman and Richardson 1993). Similar *in situ* dyads are found within *Fusitheca fanningiae* Wellman et al. (1998a), a mesofossil with an elongate sporangium attached to a bifurcating axis, from the mid Lochkovian.

Occurrences: Assemblages 1 to 5.

Age range: ?Late Ordovician to Lochkovian (Wellman and Richardson 1993, Wang et al. 1997).

Pseudodyadospora cf. *laevigata*

Plate 5.2*g* – *l*

Description: Naked, permanently fused, laevigate dyad of equally-sized sporal bodies. Outline of individual sporal body is elongate to sub-circular. No visible line of contact; junction is marked by a slight thickening of the exine. Walls are either invaginated or inflated.

Dimensions: Maximum length 23.6 (33.0) 47.7μm; maximum width 17.4 (26.9) 34.3μm. 8 specimens measured.

Comments: Poor preservation of these spores inhibits identification. Spores are similar to *Pseudodyadospora laevigata* Johnson 1985, but are smaller (*P. laevigata* ranges from 41.0 to 60.0μm). Spores of a similar size range (length 22.0 to 42.0μm, width 16.0 to 28.0μm) are described as *Pseudodyadospora* cf. *laevigata* from the Llandovery, Wales by Burgess 1991.

Occurrences: Assemblages 1 to 4.

Age range: Caradoc (Sandbian-early Katian) to late Aeronian (Richardson 1988, Wellman 1996, Wang et al. 1997). Fused dyads similar to *Pseudodyadospora laevigata* are known from the Llanvirn (Strother et al. 1996).

Infraturma **APICULATI** Richardson 1996a

Eucryptospores with exine ornamented with apiculate sculpture (grana, coni, spinae).

APICULATE FUSED TETRAD

Plate 5.3*a*

Description: Naked, permanently fused sub-circular tetrad, with an apiculate to verrucate sculptured distal exine. Distal walls are invaginated, and the contact area is indistinctive. Individual spores are circular, with thick equatorial regions. Sculpture consists of large grana to verrucae elements.

Dimensions: Tetrad diameter 34.6μm. Sculpture height 0.9μm, width at base 1.2μm and approximately 1.3μm apart. 1 specimen measured.

Comments: This apiculate sculptured fused tetrad does not belong to any known genera. *Cheilotetras* sp. is restricted to fused tetrads with laevigate distal exines, whilst *Acontotetras* sp. has a similar sculpture, but consists of unfused units. If a tightly adherent envelope is present, this specimen would belong to *Velatitetras*, a genus encompassing fused or unfused

enveloped tetrads, with or without sculpture (Burgess 1991). However, no envelope is present.

Occurrence: Assemblage 5.

Infraturma **SYNORATI** Richardson 1996a

Eucryptospores with exine ornamented with murornate or verrucate sculpture.

VERRUCATE FUSED TETRADS

Plate 5.3*b* - *j*

Description: Permanently fused, naked tetrads with verrucate to rugulate sculptured distal exine. Specimens are quite variable, and are unlikely to belong to the same genus. At least two groups can be recognised; those with small, uniformly-sized and evenly spaced verrucae on the distal surfaces (*b* to *e*, Plate 5.3), and those with irregularly-sized and closely spaced verrucae, where 2 or 3 verrucae may fuse together to form small rugulae (*f* to *j*, Plate 5.3). Contact areas are indistinctive, although sculptural elements become misshapen towards the individual spore equators (elongate perpendicular to the contact area). Distal walls are mostly inflated, but can also be invaginated.

Dimensions: Tetrad diameter 26.6 (31.5) 57.8μm. Sculpture height 0.3 (1.0) 2.1; width 0.8 (1.8) 3.2; 0.2 (1.4) 5.0 apart. 14 specimens measured.

Comments: This group does not belong to any known genera. Some specimens are similar to *Velatitetras rugosa* (Strother and Traverse 1979 emend. Steemans et al. 1996) or *Velatitetras rugulata* (Burgess 1991). However these are enveloped species, and rugulae are more prominent. If unfused, this group would either belong to *Cymbohilates* or *Hispanaediscus*. Alternatively, these maybe tetrads of verrucae sculptured triletes such as *Synorisporites*. However, there is no evidence of clear contact lines between spore units. Similar specimens are described as 'murornate fused tetrads' from Wenlock assemblages by Burgess and Richardson (1991), and placed in *incertae sedis*. As a separate group of fused tetrads with distinctive murornate sculptures have been discovered in this assemblage, it would be preferable to call these verrucate fused tetrads.

Occurrences: Assemblages 1 to 4.

MURORNATE FUSED TETRADS

Plate 5.3*k* - *l*

Description: Naked, permanently fused tetrads with murornate sculptured distal exine. Individual spores have a circular amb. The distal surfaces are sculptured with irregularly spaced and convolute narrow muri. Muri become more regularly spaced and perpendicularly aligned towards the contact area. Walls are invaginated or partially inflated. One specimen shows equatorial thickening of individual spore units.

Dimensions: Tetrad diameter 25.4 (32.1) 38.3μm; muri height 0.3 (0.8) 3.0μm; muri width 0.3 (0.7) 3.0μm; lumen diameter 2.3 (3.2) 4.7μm. 4 specimens measured.

Comments: This group does not belong to any known genera. If enveloped, this group would most closely resemble *Velatitetras cristata* (Burgess and Richardson 1995), with irregularly arranged convoluting muri. If unfused, these tetrads would belong to *Chelinohilates*. Alternatively, these may be tetrads of trilete spores with murornate sculpture, such as *Chelinospora*.

Occurrences: Assemblages 1 and 3.

Suprasubturma **EUPOLYADI** Richardson 1996a

Cryptospore with multiple units that closely adhere, but not fused.

Infraturma **LAEVIGATI**

Genus **TETRAHEDRALETES** Strother and Traverse 1979 emend. Burgess 1991

Tetrahedraletes medinensis Burgess 1991

Plate 5.4*a* - *l*

Description: Unfused 'permanent' laevigate tetrads, with clear contact lines between sub-triangular to sub-circular spore units. Tetrads can either be tetrahedral or decussate. In general, tetrads with sub-triangular spore units often have inflated walls, whilst tetrads with sub-circular spore units tend to have invaginated walls, and may have an equatorial crassitude. However, single tetrads with both invaginated and inflated walls do occur. The spore units either tightly adhere, or are partially loose. Each spore unit has a pronounced equatorial crassitude or flange. Two varieties have been assigned according to size.

Tetrahedraletes medinensis var. *medinensis* Burgess 1991

Plate 5.4*a* – *f*

Dimensions: Large tetrads (over 35.0μm in total diameter); 35.2 to 80.0μm (44.2μm). 54 specimens measured.

Occurrences: Assemblages 1 to 5.

Tetrahedraletes medinensis var. *parvus* Burgess 1991

Plate 5.4*g* – *l*

Dimensions: Small tetrads (below 35.0μm in total diameter); 19.0 to 34.7μm (27.7μm). 62 specimens measured.

Occurrences: Assemblages 1 to 5.

Comments: A study by Gray (1988) recognised that tetrad size increases through time, with the smaller variety occurring predominately in the Late Ordovician, whilst the larger variety appears in the Silurian. *In situ* spores resembling *Tetrahedraletes medinensis* were found in lower Přídolí and middle Lochkovian mesofossils (Edwards et al. 1999).

Age range: ?Llanvirn (Strother et al. 1996). Caradoc (Sandbian-Katian) (Richardson 1988, Wellman 1996), Llandovery (Burgess 1991) Přídolí (Burgess and Richardson 1995), ?*in situ* middle Lochkovian (Edwards et al. 1999).

Genus **RIMOSOTETRAS** Burgess 1991

Rimosotetras problematica Burgess 1991

Plate 5.5*a* and *b*

Description: Adherent to partially loose laevigate tetrahedral tetrads. Single spore units are sub-circular in outline, and possess a narrow equatorial crassitude or flange. Clear contact lines and constrictions mark the junctions between spore units. Walls are invaginated and slightly folded.

Dimensions: Total diameter range from 28.4 to 34.1μm (29.9μm). 2 specimens measured.

Occurrences: Assemblages 1 and 5.

Age range: latest Ordovician to late Rhuddanian (Burgess 1991).

Genus **DYADOSPORA** Strother and Traverse 1979 emend. Burgess and Richardson 1991

Plate 5.5*c* - *l*

Description: Unfused, non-permanent, naked dyads with laevigate distal exine. Clear contact lines occur between spore units of equal size. Dyads either tightly adhere or are partially separated to two laevigate hilates. Individual spores sub-circular to elliptical. Two species have been erected on the basis of different spore wall characteristics.

Dyadospora murusdensa Strother and Traverse 1979 emend. Burgess and Richardson 1991

Plate 5.5*c* - *g*

Description: Distally inflated, robust walled *Dyadospora*, without folds. Where dyads are seen to be separating, the hila observed in the proximal surfaces of both hilates are sometimes roughly sculptured with micrograna.

Dimensions: Dyad maximum length 15.7 (30.4) 45.7μm; single hilate width 11.1 (22.6) 38.9μm; total width 15.7 (33.3) 63.3μm. 70 specimens measured.

Comments: Size range of *Dyadospora murusdensa* from this assemblage is larger than the published range (23.0 to 47.0μm in length, 21.0 to 46.0μm in total width) (Burgess and Richardson 1991). The separation of *Dyadospora murusdensa* may produce the species *Laevolancis divellomedia* (see page 5-19). Similar smooth walled dyads have been found *in situ* within spore masses and the mesofossil *Culullitheca richardsonii* from the mid-Lochkovian (Fanning et al. 1991a, Wellman et al. 1998a).

Occurrences: Assemblages 1 to 5.

Age range: ?Llanvirn (Strother et al. 1996), Caradoc (Wellman 1996) to Lochkovian (Wellman and Richardson 1996).

Dyadospora murusattenuata Strother and Traverse 1979 emend. Burgess and Richardson 1991.

Plate 5.5*h* - *l*

Description: A thin walled *Dyadospora* species, where the walls are broadly folded. Often poorly preserved in this assemblage due to thin nature of walls. Walls often invaginated.

Dimensions: Dyad maximum length 24.6 (31.3) 43.4μm, single width 17.5 (24.7) 37.6μm, total width 21.6 (34.1) 69.4μm. 22 specimens measured.

Comments: Size range of *Dyadospora murusattenuata* from this assemblage is larger than published range (22.0 to 39.0μm in length, 20.0 to 37.0μm in total width) (Burgess and Richardson 1991). The separation of *Dyadospora murusattenuata* may produce the species *Laevolancis plicata* (see page 5-20).

Occurrences: Assemblages 1 to 5.

Age range: early Rhuddanian (Richardson 1988) to Lochkovian (Wellman and Richardson 1996).

Infraturma **APICULATI**

Genus **ACONTOTETRAS** Richardson 1996a

Acontotetras inconspicus Richardson 1996a

Plate 5.6*a* to *f*

Description: Unfused, permanent, naked tetrads with apiculate sculptured distal exine. Contact lines are clear between sub-circular to sub-triangular spore units. Distal walls are invaginated, and each spore unit has an equatorial crassitude. The distal surface is sculptured with evenly spaced apiculate elements, either grana or microconi.

Dimensions: Total tetrad diameter 17.7 (25.1) 37.7μm; sculpture height 0.3 (0.6) 0.9μm; sculpture width 0.5 (0.8) 1.2μm, sculpture spacing 0.6 (1.0) 1.8μm. 7 specimens measured.

Comments: Sculpture height and sculpture spacing is slightly larger than *Acontotetras inconspicus* (grana are less than 0.5μm in height, and are 0.5 to 1.0μm apart) (Richardson 1996a).

Occurrences: Assemblages 3 to 5.

Age range: ?upper Přídolí to lowermost Lochkovian (*Apiculiretusispora* sp. E. zone), to middle Lochkovian (lower to middle *microrornatus-newportensis* palynosubzones) (Richardson 1996a).

Suprasubturma **HILATES** Richardson 1996a

Infraturma **LAEVIGATI**

Genus **LAEVOLANCIS** Burgess and Richardson 1991

Laevolancis divellomedia Burgess and Richardson 1991

Plate 5.7*a* to *f*

Description: Naked, proximally hilate, alete monads with laevigate exine. Spores are sub-circular to elliptical, with slight equatorial crassitudes. Hila are often sub-central, and can be folded. The hilum area can be smooth, but can also have a rough microgranular sculpture. Walls are rigid, and are either inflated or compressed.

Dimensions: Spore length 13.8 (33.4) 63.1μm, width 8.2 (26.9) 52.5μm. 248 specimens measured.

Comments: This assemblage has a larger size range than published for *Laevolancis divellomedia* (maximum diameter 30.0 (38.0) 49.0μm, minimum diameter 18.0 (30.0) 38.0μm) (Burgess and Richardson 1991). These hilate monads are most likely the product of the separation of rigid walled laevigate dyad species *Dyadospora murusdensa*. *Laevolancis divellomedia* has been found in spore masses and *in situ* within mesofossil sporangia from Přídolí to the mid-Lochkovian, closely associated with partially separating *Dyadospora murusdensa* (Wellman et al. 1998a).

Occurrences: Assemblages 1 to 5.

Age range: ?Caradoc (torn from permanently fused dyads?) (Wellman 1996); early Wenlock (Burgess and Richardson 1991) to Frasnian (Balme 1988).

Laevolancis plicata Burgess and Richardson 1991

Plate 5.7*g* - *l*

Description: Naked, proximally hilate, alete monads with laevigate exine. Spore walls are thin, broadly folded and invaginated. Ambs are sub-circular to elliptical, with slight equatorial crassitudes present. Preservation is often poor.

Dimensions: Spore length 20.5 (33.2) 48.0μm, width 15.7 (26.4) 40.2μm. 40 specimens measured.

Comments: *Laevolancis plicata* is generally smaller than *Laevolancis divellomedia*. These hilate monads are most likely the product of the separation of thin-walled, laevigate dyad species *Dyadospora murusattenuata*.

Occurrences: Assemblages 1 to 5.

Age range: early Wenlock (Burgess and Richardson 1991), to ?upper Přídolí to lowermost Lochkovian (*Apiculiretusispora* sp. E. palynosubzone) (Wellman and Richardson 1996).

Genus **ARTEMOPYRA** Burgess and Richardson 1991 emend. Richardson 1996a

Artemopyra cf. *robusta* Wellman and Richardson 1996

Plate 5.8*a* - *b*

Description: Naked, alete monad with laevigate distal exine and proximal hilum sculptured with prominent radial muri (approximately 32). The amb is elliptical in outline. Muri are straight to slightly sinuous, and taper towards the centre of the hilum, and disappear approximately a third from the centre. Exine thickness on distal surface is variable, giving a blotchy appearance, which continues into the proximal hilum in the form of verrucae superimposed onto the radial muri.

Dimensions: Monad length 20.1μm, width 19.1μm; muri height 0.8μm, width 1.0μm, and 0.6μm apart. 1 specimen measured.

Comments: This specimen is most similar to *Artemopyra robusta* Wellman and Richardson 1996, a species erected for hilate monads with a differentially thickened distal exine, and prominent radial muri of a similar size and spacing in the proximal surface. However, the muri in *A. robusta* continues from the equator to the pole, whilst in this specimen muri are fused close to the hilum centre. This specimen is also smaller than the published size ranges for *A. robusta* (diameter 44.0 to 62.0μm). Therefore this specimen should remain *Artemopyra* cf. *robusta*.

Occurrence: Assemblage 4.

Age range: ?upper Přídolí to lowermost Lochkovian (*Apiculiretusispora* sp. E. palynosubzone) (Wellman and Richardson 1996).

Artemopyra sp. A (sp. nov.)

Plate 5.8*c* - *e*

Description: Naked alete monads, with laevigate distal exine and proximal hila sculptured with radial muri. Muri run from the equator, to half way or two-thirds to the hilum centre. Muri are straight to slightly sinuous, low and not prominent. Exine is of uniform thickness.

Dimensions: Monad length ranges from 24.7 (30.1) 35.1μm, width 17.9 (24.4) 29.1μm; muri height 0.2 (0.3) 0.5μm, width 0.9 (1.0) 1.3μm, and 0.3 (0.5) 0.7μm apart. 3 specimens measured.

Comments: Unlike *A. robusta*, this group do not have prominent muri. *A. brevicosta* Burgess and Richardson 1991 is similar, but muri on this species only run from the equator to less

than half way to the hilum centre, whilst in *A. laevigata* (Wellman and Richardson 1996) muri can run to the proximal pole, and show much more variability in muri shape.
Occurrences: Assemblages 4 and 5.

Infraturma **APICULATI**

Genus **CYMBOHILATES** Richardson 1996a emend. Breuer et al. 2007

GRANA OR CONI SCULPTURED CYMBOHILATES

Cymbohilates sculptured with elements that are isodiametric or slightly broader at base than high.

Cymbohilates allenii Richardson 1996a
Plate 5.8*f* – *l*, Plate 5.9*a* - *g*

Description: Naked, proximally hilate monads and dyads with a double-walled exine. The distal and sub-equatorial surfaces are sculptured with closely and irregularly spaced isodiameteric micrograna, grana or microconi. In some specimens the elements are fused at their bases to form clusters or ridges. The proximal hilum is smooth or sculptured with irregularly spaced or concentric folds or muri. In one specimen, folds join to the hilum margin, and form three oval shaped areas. There are two varieties, assigned according to size.

Cymbohilates allenii var. *allenii* Richardson 1996a
Plate 5.8*f* - *l*

Dimensions: Smaller variety of *Cymbohilates allenii* (below 30.0μm in diameter). Total diameter 21.5 (25.0) 29.5μm; sculpture height 0.2 (0.4) 0.5μm, width 0.3 (0.6) 0.9μm, spacing 0.3 (0.6) 1.0μm. 11 specimens measured.
Occurrences: Assemblages 1 to 4.
Age range: ?upper Přídolí to lowermost Lochkovian (*Apiculiretusispora* sp. E palynosubzone) to middle Lochkovian (middle *microrнatus-newportensis* palynosubzone) (Richardson 1996a).

Cymbohilates allenii var. *magnus* Richardson 1996a

Plate 5.9*a* - *g*

Description: Larger variety of *Cymbohilates allenii* (greater than 30.0μm in diameter). Folds in the hilum are more pronounced.

Dimensions: Total diameter 30.0 (38.2) 52.6μm; sculpture height 0.2 (0.4) 1.0μm, width 0.3 (0.6) 1.2μm, spacing 0.2 (0.5) 1.2μm. 22 specimens measured. A dyad of *Cymbohilates allenii var. magnus* is also present in this assemblage. Total length 43.2μm, single spore width 23.2μm, total width 48.9μm; sculpture height 0.8μm, width 0.8μm, spacing 1.0μm.

Occurrences: Assemblages 1 to 5.

Age range: ?upper Přídolí to lowermost Lochkovian (*Apiculiretusispora* sp. E palynosubzone) to middle Lochkovian (middle *micrornatus-newportensis* palynosubzone) (Richardson 1996a).

Cymbohilates cf. *amplus* Wellman and Richardson 1996

Plate 5.9*h* - *i*

Description: Large, naked, proximally hilate monads with circular amb and slight equatorial crassitudes. Distal and sub-equatorial exine sculptured with evenly to irregularly distributed, closely spaced grana, micrograna to microconi. Broad folds also occur in the distal surface. Proximal hila where visible are laevigate with irregular folds.

Dimensions: Total diameter 60.0 (74.6) 86.6μm; sculpture height 0.4 (0.7) 1.0μm, width 0.4 (0.9) 1.3μm, spacing 0.5 (1.1) 1.7μm. 5 specimens measured.

Comments: These specimens have a similar size range to *Cymbohilates amplus* (total diameter 73.0 (87.0) 104.0μm), but the apiculate sculpture is much more irregularly and closely spaced than seen on *C. amplus*. In terms of sculpture type, the apiculate elements are much more similar to those of *Cymbohilates allenii* var. *magnus* or *Cymbohilates microgranulatus* (Wellman and Richardson 1996), with a range of micrograna, grana and microconi, than seen on *Cymbohilates amplus*, where microconi and spinose elements sculpture the distal surfaces. However, due to their large size these specimens do not fit into the *C. allenii* var. *magnus* size range (maximum diameter 56.0μm), and the sculpture is too evenly spaced on *C. microgranulatus*.

Occurrences: Assemblages 1, 2 and 4.

Age range: *Cymbohilates amplus senso stricto* is known from the ?upper Přídolí to lowermost Lochkovian (*Apiculiretusispora* sp. E palynosubzone) (Wellman and Richardson 1996).

Cymbohilates disponerus Richardson 1996a

Plate 5.10*a* - *l*

Description: Naked, proximally hilate cryptospores with sub-circular ambs. Distal and sub-equatorial exine sculptured with regular and evenly spaced coni to microconi. Elements are either isodiametric or broader than high. Proximal surfaces are laevigate, with faint concentric folds close to the hila.

Dimensions: Total diameter 17.9 (23.5) 36.1μm; sculpture height 0.2 (0.4) 0.7μm, width 0.3 (0.6) 1.2μm, spacing 0.5 (1.1) 2.0μm. 20 specimens measured. Non – permanent dyads with similar distal ornamentation are also known from this assemblage. Total length 16.8 (22.5) 28.3μm, single spore width 13.3 (19.9) 28.3μm, total width 14.7 (27.6) 44.0μm; sculpture height 0.3 (0.5) 0.9μm, width 0.5 (0.6) 0.7μm, and 0.5 (1.1) 1.5μm apart. 6 specimens measured. Loose tetrads with a similar distal ornamentation are also present in these assemblages. Total tetrad diameter 43.5 (47.0) 50.4μm, single spore width 26.8 (29.2) 31.5μm; sculpture height 0.6 (0.8) 1.0μm, width 0.6 (0.65) 0.7μm, and 0.7 (0.9) 1.0μm apart. 2 specimens measured.

Comments: These specimens have a larger size range than that published for *Cymbohilates disponerus* (diameter 16.0 to 30.0μm) (Richardson 1996a). Similar *in situ* monads occur within *Salopella* cf. *marcensis* sporangia attached to bifurcating axes, from lower to mid Lochkovian strata (middle *micrornatus-newportensis* palynosubzone) from Shropshire (Edwards et al. 1994, Richardson 1996a). Tetrads may belong to trilete genus *Aneurospora.*

Occurrences: Assemblages 1 and 3 to 5.

Age range: lower and middle Lochkovian (lower and middle *micrornatus-newportensis* palynosubzones) (Richardson 1996a).

Cymbohilates cf. *microgranulatus* Wellman and Richardson 1996

Plate 5.11*a* - *c*

Description: Naked, proximally hilate monads with sub-circular to circular ambs with thin exine. Distal and sub-equatorial surfaces sculptured with evenly-spaced micrograna. Where

sculpture is closely spaced, elements fuse at the base to form small rugulae. Proximal surface is laevigate or with irregular broad folds.

Dimensions: Total diameter 30.7 (35.1) 43.8μm; sculpture height 0.2 (0.3) 0.4μm, width 0.2 (0.5) 0.6μm, and 0.3 (0.6) 1.2μm apart. 8 specimens measured. A non-permanent dyad with similar ornamentation is also known from this assemblage. Total length 28.9μm, single spore 26.3μm, total width 48.3μm; sculpture height 0.4μm, width 0.2μm, 0.4μm apart.

Comments: Often poorly preserved due to the thin nature of the exine. The specimens are most similar to *Cymbohilates microgranulatus* (Wellman and Richardson 1996), with similar distal and proximal surface ornamentation. However, the specimens are too small to belong to *Cymbohilates microgranulatus* (the diameter of *C. microgranulatus* ranges from 44.0 to 74.0μm). The specimens are closer in size to *Cymbohilates allenii* var. *magnus*, but the sculpture on the distal surfaces of this species is slightly larger (grana rather than micrograna), and more irregularly spaced. Therefore these specimens shall be known as *Cymbohilates* cf. *microgranulatus*.

Occurrences: Assemblages 2 to 4.

Age range: *Cymbohilates microgranulatus senso stricto* is known from the ?upper Přídolí to lowermost Lochkovian (*Apiculiretusispora* sp. E palynosubzone) (Wellman and Richardson 1996).

Cymbohilates variabilis Richardson 1996a

Plate 5.11*d* – *l*, Plate 5.12*a* - *h*

Description: Naked, proximally hilate cryptospores with sub-circular to circular ambs. Distal and sub-equatorial areas are sculptured with closely spaced apiculate to verrucate elements of variable shapes and sizes, from grana, coni, verrucae to baculae. Proximal hilum is sculptured with radial muri that may fuse towards the central proximal pole.

Cymbohilates variabilis var. *variabilis* Richardson 1996a

Plate 5.11*d* - *i*

Description: This variety of *Cymbohilates variabilis* is sculptured with large, closely spaced elements on the distal surface. Elements are either low grana or verrucae, with basal width exceeding twice the height in some cases. Where sculpture densely packed, elements fuse together at the base to form wide rugulae. Some rugulae bear coni or grana shaped tips. The

proximal surface is ornamented with thick, straight to sinuous radial muri, that fuse together and thin out towards the proximal pole.

Dimensions: Monad total diameter 27.1 (33.8) 49.0μm; sculpture height 0.5 (1.0) 2.0μm, width 1.2 (1.8) 3.2μm, and 0.2 (1.8) 3.5μm apart. 8 specimens measured. Non-permanent dyads with similar ornamentation are also known from this assemblage. Total length 26.9 (29.2) 31.5μm, single width 23.0 (27.3) 31.5μm, total width 33.0 (35.0) 36.9μm; sculpture height 0.7μm, width 1.4 (1.45) 1.5μm, and 1.5μm apart. 2 specimens measured.

Occurrences: Assemblages 1 to 5.

Age range: lower and middle Lochkovian (lower and middle *micrornatus-newportensis* palynosubzones) (Richardson 1996a).

Cymbohilates variabilis var. *parvidecus* Richardson 1996a

Plate 5.11*j* – *l*

Description: A variety of *Cymbohilates variabilis* with smaller and more sparsely, evenly spaced apiculate elements than *var. variabilis*. Elements range from grana to verrucae. Fusion of elements is less common than is seen on *var. variabilis*. Two examples of proximal surfaces are visible; one where closely-spaced radial muri are thick and prominent, and fuse together at the proximal pole to form a thickened central area; whilst the other is sculptured with six to seven sparsely spaced radial muri, joined together by a concentric muri running close to the hilum edge.

Dimensions: Monad total diameter 12.6 (27.2) 42.5μm; sculpture height 0.3 (0.6) 1.3μm, width 0.5 (1.1) 2.0μm, and 0.4 (1.2) 1.8μm apart. 13 specimens measured.

Comments: Some specimens are smaller than the size range published for *C. variabilis* var. *parvidecus* (diameter 22.0 to 47.0μm). Although the sculpture for *C. variabilis* var. *parvidecus senso stricto* is restricted to less than 2.0μm in height, these specimens have been grouped together due to the arrangement of elements is more similar to var. *parvidecus* than var. *variabilis* (i.e. more evenly spaced).

Occurrences: Assemblages 1 to 4.

Age range: lower and middle Lochkovian (lower and middle *micrornatus-newportensis* palynosubzones) (Richardson 1996a).

Cymbohilates variabilis var. B (var. nov.)

Plate 5.12*a* - *h*

Description: A *Cymbohilates variabilis* variety sculptured with apiculate elements that range in shape and size, that are irregularly and sparsely spaced. Apiculate elements range from grana, micrograna to spatulate elements. Elements often occur in clusters and two to three elements may fuse at their bases to form rugulae or muri. This occurs particularly near the equator, and where dyads have been preserved, they occur perpendicular to the contact area. The proximal surface was not visible on any of the specimens.

Dimensions: Monad total diameter 30.0 (35.4) 40.7μm; sculpture height 0.7 (0.75) 0.8μm, width 0.9μm, and 0.8 (0.9) to 1.0 apart. 2 specimens measured. Non-permanent dyads with a similar ornamentation are also known from these assemblages. Total length 21.5 (22.4) 23.2μm, single width 15.8 (17.0) 18.1μm, total width 25.7 (28.9) 32.1μm; sculpture height 0.3 (0.35) 0.4μm, width 0.5 (0.8) 1.0μm, and 0.5 (1.0) to 1.5 apart. 2 specimens measured.

Comments: This variety is similar to *Cymbohilates variabilis* var. *variabilis*, but sculpture in these specimens occurs only as clusters and elements are more irregularly spaced, and more irregular in shape and size on individual spores.

Occurrences: Assemblages 1 and 3.

SPINOSE SCULPTURED CYMBOHILATES

Cymbohilates sculptured with elements that are at least twice as high as they are wide.

Cymbohilates cymosus Richardson 1996a

Plate 5.13*a* - *f*

Description: Naked hilate, sub-circular to circular cryptospores, sculptured with distinctive spinose elements on the distal surface. Short spines occur in irregularly spaced clusters of 5. These are radially arranged into a star shape, with spine long axes running parallel with the exine surface, and fused at the spine bases. Short biform spines also occur, but are not the diagnostic sculpture. The proximal surface is not visible on any of the specimens.

Dimensions: Monad total diameter 29.4μm, sculpture height 1.5μm, width 0.8μm, and 1.0μm apart. 1 specimen measured. Non-permanent dyads with a similar ornamentation are also known from these assemblages. Total length 36.1 (38.1) 40.0μm, single width 25.3 (30.4) 35.5μm, total width 27.3 (28.7) 30.0μm; sculpture height 1.5μm, width 0.6 (0.8) 0.9μm, 1.0

(1.3) 1.5μm apart. 2 specimens measured. A loose tetrad with similar ornamentation is also known from this assemblage. Total diameter 47.0μm, single spore diameter 30.7μm; sculpture height 1.4μm, width 0.8μm, and 1.7μm apart.

Comments: Dyads of *Cymbohilates cymosus* have not previously been recorded. Spine size is small compared with published measurements (sculpture height 1.0 to 4.0μm, width 1.0 to 3.0μm Richardson 1996a).

Occurrence: Assemblage 1.

Age range: ?upper Přídolí to lowermost Lochkovian (*Apiculiretusispora* sp. E palynosubzone) to the middle Lochkovian (middle *micrornatus-newportensis* palynosubzone) (Richardson 1996a).

Cymbohilates horridus Richardson 1996a

Plate 5.13*g* - *i*

Description: Naked, unfused, non-permanent dyads with spore units of equal size. The distal surfaces are sculptured with prominent spinose elements. Spines either occur as single elements or are biform. Spines are often connected at the base and form sinuous ridges or muri. Spines are slender, with either pointed or slightly rounded tips. Proximal surfaces have not been observed.

Dimensions: Total length 30.5 (36.6) 42.7μm, single width 21.0 (25.2) 29.3μm, total width 40.4 (50.2) 60.0μm; sculpture height 6.0μm, width 2.0 (2.5) 3.0μm, and 4.5 (4.8) to 5.0μm apart. 2 specimens measured.

Comments: Usually found in the hilate monad form. These specimens are smaller than the published size range for monads (50.0 to 90.0μm), although sculpture dimensions are similar (spine length 5.0 to 16.0μm, width 2.0 to 8.0μm) (Richardson 1996a). Similar dyads have been discovered *in situ* from a mid-Lochkovian rhyniophytoid sporangium, attached to a bifurcating axis (Habgood 2000). However, the ultrastructure of these spores suggest that these dyads were permanent, with a spinose sculptured, tightly adherent envelope. Therefore these *in situ* spores are known as *Cymbohilates* cf. *horridus* (Habgood 2000).

Occurrences: Assemblages 1 and 2.

Age range: lower and middle Lochkovian (lower and middle *micrornatus-newportensis* palynosubzones) (Richardson 1996a).

Cymbohilates horridus var. A (var. nov.)

Plate 5.14*a* - *j*

Description: A variety of *Cymbohilates horridus* with a spinose sculpture on the distal and sub-equatorial surface. Elements are small, evenly distributed spines or large coni. Spine tips are pointed, rounded or blunt, and in some cases are more similar to baculae. Elements are either sparsely or closely arranged in the majority of individuals, with only one example where elements fuse to form ridges. The proximal surface is laevigate.

Dimensions: Monad total diameter 13.1 (33.9) 57.6μm; sculpture height 0.5 (1.6) 4.0μm, width 0.5 (0·9) 2.5μm, and 0.5 (1.7) 4.0μm apart. 9 specimens measured. Similar non-permanent dyads with clear contact lines are also known from this assemblage. Total length 32.3 (44.2) 56.0μm, single width 23.0 (28.1) 33.1μm, total width 42.5 (53.3) 64.1μm; sculpture height 1.5 (2.3) 3.0μm, width 1.2 (1.4) 1.5μm, and 0.5 (1.0) 1.5μm apart. 2 specimens measured.

Comments: *Cymbohilates horridus* has a total diameter of at least 50.0μm, whilst these specimens are smaller in size (maximum diameter 57.6μm). The spinose elements on *Cymbohilates horridus* are at least 5.0μm in length and 2.0μm in width, but these specimens exhibit smaller spines (only up to 4.0μm in height and 2.5μm in width). Spine shape also differs, with a greater variety of spine tip morphology. Biform spines and fused ridges are much less common than seen on *C. horridus*. Similar spores have been described by Wellman et al. (2000), as *Cymbohilates* sp. A, which has similar sized elements and sculpture arrangement on the distal surface. However, these spores have a microgranulate sculpture on the proximal surface. Therefore this group has been assigned to *Cymbohilates horridus* var. A.

Occurrences: Assemblages 1 to 4.

Cymbohilates cf. *horridus* (sp. nov.)

Plate 5.14*k* - *l*

Description: A naked ?hilate monad with an evenly and sparsely distributed sculpture on the ?distal surface. Elements are slender spines to bacula or pila. Grana is also present. The distal spore wall is thin and invaginated, with broad folding. The proximal surface is not visible.

Dimensions: Total diameter 32.1μm; sculpture height 1.4μm, width 0.3μm, and 1.8μm apart. 1 specimen measured.

Comments: This specimen is smaller than the minimum size for *C. horridus* (50.0μm). Sculpture is much less rigid and less prominent than in *C. horridus* or *C. horridus* var. A. This may be due to poor preservation. Grana may represent the remaining bases of broken elements. Elements are more slender and more cylindrical in shape than the spinose sculpture of *C. horridus*. However, no other species of *Cymbohilates* are sculptured with individual elements that are at least twice as high as they are wide. Therefore, this specimen is assigned to *Cymbohilates* cf. *horridus*.

Occurrence: Assemblage 5.

Infraturma **SYNORATI**

MURORNATE SCULPTURED CRYPTOSPORES

Cryptospores that are sculptured with muri, that are connected to form a reticulum.

Genus **CHELINOHILATES** Richardson 1996a

Chelinohilates erraticus Richardson 1996a

Plate 5.15*a* to *l*, Plate 5.16*a* - *f*

Description: Naked, proximally hilate monads, circular to sub-circular in amb outline, with double walled exines. A thin, translucent outer wall is either loosely or tightly adherent to the thicker inner wall. The outer wall is sculptured with distinctive reticulum occurring on the distal and sub-equatorial surfaces. Muri are straight to flexuous, becoming more sinuous the more loosely attached the outer exine is from the inner exine. Muri connect together to form a reticulate pattern, forming either rectangular or triangular lumina. In cross section, muri have an undulating outline and generally thickening at reticulum junctions. Muri thickness and lumina size are quite variable, irrespective of total spore diameter, and specimens can be grouped into two main catagories; those with thick muri (and small lumina) and those with thin muri (and large lumina). Muri in the sub-equatorial area are aligned perpendicular to the spore equator. The outer exine is not present over the proximal surface. The proximal hilum is circular and laevigate, with a thickened concentric collar at the hilum edge. Hilum is often poorly preserved and often not visible.

Dimensions: Monad total diameter 27.7 (40.0) 72.0μm; muri height 0.6 (2.3) 4.2μm, width 0.5 (1.7) 3.2μm, lumen longest axis 3.7 (10.2) 21.0μm, smaller axis 1.2 (7.4) 13.8μm. 43 specimens measured.

Non-permanent dyads are also known from these assemblages. Muri close to the contact area are typically aligned perpendicular to the contact line. Total length 26.0 (38.7) 50.6μm; single

width 9.5 (25.4) 35.5μm, total width 20.5 (43.1) 57.4μm; muri height 1.0 (1.9) 5.3μm, width 0.8 (1.6) 4.0μm, lumen longest axis 4.0 (8.3) 13.5μm, shortest axis 2.4 (5.5) 9.0μm. 14 specimens measured.

Loose tetrads with a similar ornamentation are also known from this assemblage. Muri dimensions and reticulate patterns can alter from one spore unit to another in the same tetrad. As seen in the dyads, muri close to the contact lines are aligned perpendicular. Total diameter 42.3 (52.0) 65.0μm, single spore diameter 32.3 (36.3) 41.3μm, muri height 1.0 (1.7) 3.2μm, width 0.5 (1.8) 4.2μm, lumen longest axis 4.8 (9.8) 17.3μm, shorter axis 2.0 (6.1) 16.0μm. 8 specimens measured. A murornate triad similar to *Chelinohilates erraticus* has also been noted.

Comments: Similar to the distal sculpture of trilete species *Chelinospora*. Murornate triads, as well as a few tetrad specimens with a smaller, or absent fourth spore unit, may represent abortion of the fourth spore unit or the breaking up of a non-permanent tetrad unit. In some specimens, muri are thicker than previously reported *Chelinohilates erraticus* (a maximum in muri thickness of 2.0μm, compared with the observed maximum here of 4.2μm (Richardson 1996a)). Although two broad varieties have been recognised on the basis of muri thickness (and subsequent lumina size), sculpture is highly variable and random, with a gradient of muri thickness, and difficult to assign to two varieties, so therefore with remain in one group.

Occurrences: Assemblages 1 to 5.

Age range: ?upper Přídolí to lowermost Lochkovian (*Apiculiretusispora* sp. E palynosubzone) to the middle Lochkovian (middle *micrornatus-newportensis* palynosubzone) (Richardson 1996a).

Chelinohilates cf. *lornensis*

Plate 5.16*g* - *j*

Description: Naked, proximally hilate monads, circular in outline, and sculptured with a distinctive reticulum on the distal surface. Muri are broader than high, and regularly arranged to form a polygonal reticulum pattern, with isodiametric, six-sided lumina. Exine on the muri has an irregular thickness, giving a blotchy appearance. No proximal surface has been observed.

Dimensions: Monad total diameter 17.7 (24.3) 29.0μm; muri height 0.4 (0.7) 1.2μm, muri width 0.7 (0.8) 0.9μm, lumen longest axes 0.7 (1.8) 3.7μm, shortest axis 0.7 (1.7) 3.4μm. 3 specimens measured.

Comments: Muri are too regularly arranged for these specimens to belong to *Chelinohilates eraticus* or *Chelinohilates sinuous*. Although these specimens are similar to *Chelinohilates ornensis* Wellman and Richardson (1996), they are smaller in total diameter (largest specimen is 29.0μm, compared to the size range for *C. lornensis*, 27.0 (36.0) 42.0μm. Muri height is also lower than observed on *C. lornensis* (muri from these specimens are below 1.0μm in height). Therefore these specimens are assigned to *Chelinohilates* cf. *lornensis*.

Occurrences: Assemblages 2 and 5.

Age range: *Chelinohilates lornensis senso stricto* is known from the ?upper Přídolí to lowermost Lochkovian (*Apiculiretusispora* sp. E palynosubzone) (Wellman and Richardson 1996).

Chelinohilates sinuosus Wellman and Richardson 1996

Plate 5.16*k* – *l*, Plate 5.17*a* - *l*

Description: Naked, proximally hilate monads, with a murornate sculpture on the distal surfaces. Muri are sinuous, meandering and bifurcating, irregularly arranged and closely spaced. Muri are thick, particularly where they bifurcate, whilst lumina are small and irregularly shaped. The proximal surface is hidden in all of these specimens. Two varieties have been identified on the basis of muri dimensions.

Chelinohilates sinuosus var. *sinuosus* Wellman and Richardson 1996

Plate 5.16*k* – *l*, Plate 5.17*a* - *d*

Description: *Chelinohilates sinuosus* with thick, bifurcating muri on the distal surface.

Dimensions: Monad total diameter 37.7 (38.9) 40.0μm, muri height 0.6 (1.0) 1.4μm, muri width 1.5μm, lumen longest axis 1.5 (1.6) 1.7μm, shortest axis 1.2μm. 2 specimens measured. A non-permanent dyad with similar ornamentation is also known from this assemblage. Total length 32.6μm, single width 24.6μm, total width 61.5μm; muri height 1.0μm, muri width 1.4μm, lumen longest axis 1.4μm, shortest axis 0.7μm.

Comments: Muri are slightly higher in one specimen compared with those described by Wellman and Richardson 1996 (muri height up to 0.75μm).

Occurrences: Assemblages 1 and 4.

Age range: ?upper Přídolí to lowermost Lochkovian (*Apiculiretusispora* sp. E palynosubzone)) (Wellman and Richardson 1996).

Chelinohilates sinuosus var. *angustus* Wellman and Richardson 1996

Plate 5.17*e* - *f*

Description: *Chelinohilates sinuosus* with narrow, closely spaced muri, and small irregular lumen.

Dimensions: Monad total diameter 22.9μm; muri height 0.2μm, muri width 0.3μm, lumen longest axis 0.6μm, shortest axis 0.5μm. 1 specimen measured.

Comments: Muri are highly irregular, appear to become fused in areas and are particularly close together on this specimen compared with those of Wellman and Richardson 1996.

Occurrence: Assemblage 4.

Age range: ?upper Přídolí to lowermost Lochkovian (*Apiculiretusispora* sp. E palynosubzone)) (Wellman and Richardson 1996).

?*Chelinohilates* sp. A (sp. nov.)

Plate 5.17*g* - *l*

Description: ?Naked hilate monads, with an elliptical amb outline, and a distinctive micromate-apiculate sculpture. ?Distal surface is sculptured with a dense, web-like network of narrow, convoluted muri, resulting in a tight reticulum pattern. The muri are acinoform i.e. they are superimposed with apiculate elements ranging from spines, bacula and pila, where the bases are fused to the muri beneath. The proximal surface is hidden in all of these specimens.

Dimensions: Monad total diameter 29.5 (42.9) 57.7μm; muri height 0.5 (1.1) 1.7μm, width 0.5 (1.0) 1.7μm, element height 0.5 (0.8) 1.2μm, element width 0.5 (0.8) 1.1μm. 3 specimens measured.

Comments: These specimens do not resemble any known genera. As the apiculate elements are superimposed on top of a muri reticulum, these specimens are best placed in *Chelinohilates* genus, rather than *Cymbohilates*. Muri are close in size to those on *Chelinohilates sinuosus* var. *sinuous*, and are closely arranged such as the sculpture of *Chelinohilates sinuous* var. *angustus*. The proximal surface is not visible on these specimens, and it is possible that specimens are enclosed with a sculptured envelope.

Occurrences: Assemblages 1 and 4.

VERRUCATE SCULPTURED CRYPTOSPORES

Cryptospores sculptured with verrucae, elements that are at least 1μm wide, and broader than high.

Genus **HISPANAEDISCUS** Cramer 1966 emend. Burgess and Richardson 1991

Hispanaediscus major Burgess and Richardson 1995

Plate 5.18*a* - *b*

Description: Naked, proximally hilate monad with a verrucate sculptured distal surface. Verrucae are low, broad and relatively widely spaced compared with other *Hispanaediscus* species. Some verrucae fuse together to form rugulae or small muri, but generally verrucae occur as separate elements. No proximal hilum visible on this specimen. *Dimensions*: Monad total diameter 30.0μm, verrucae height 0.9μm, verrucae width 1.5μm, and 1.5μm apart. 1 specimen measured.

Comments: This specimen is slightly smaller than the size range recorded by Burgess and Richardson (1995) for *Hispanaediscus major* (with a minimum total diameter of 37.0μm). However, this specimen is too large and has too regular, widely spaced verrucae to be *Hispanaediscus verrucatus* or *Hispanaediscus irregularis*.

Occurrence: Assemblage 2.

Age range: Ludfordian (upper Ludlow) (Burgess and Richardson 1995).

Hispanaediscus cf. *major*

Plate 5.18*c* - *d*

Description: Naked, ?proximally hilate monad with a verrucate to murornate distal sculpture. Verrucae are small, but are variable in size, low and rounded, and in places fuse to form rugulae or small muri. No proximal surface was seen on this specimen.

Dimensions: Monad total diameter 37.3μm, verrucae height 0.8μm, verrucae width 1.5μm, and 0.8μm apart. 1 specimen measured.

Comments: This specimen is too large to belong to *Hispanaediscus verrucatus*. The distal sculpture is similar to that of *Hispanaediscus major*, with small, low verrucae that fuse together to form rugulae. However, elements are more closely arranged in this specimen, and therefore will be assigned to *Hispanaediscus* cf. *major*.

Occurrence: Assemblage 2.

Hispanaediscus verrucatus Cramer 1966 emend. Burgess and Richardson 1991

Plate 5.18*e* - *l*

Description: Naked, proximally hilate monads, with a verrucate to murornate sculpture on the distal surface. Verrucae are low and broad with either rounded or pointed tips, are closely spaced and in places fused at the base to form larger verrucae, rugulae or short muri. Muri are particularly well-developed in the sub-equatorial region, where muri are perpendicular to the equator. This is particularly evident in the contact areas between the spore units of dyads and tetrads. The proximal hilum is laevigate.

Dimensions: Monad total diameter 20.7 (26.7) 34.1μm; verrucae height 0.4 (0.7) 1.1μm, verrucae width 0.8 (1.5) 2.3μm and 0.5 (0.9) 1.6μm apart. 7 specimens measured. Non-permanent dyads and 'loose' tetrads with a similar ornamentation are also known from these assemblages. Dyad total length 16.8 (21.4) 24.6μm, single width 15.3 (22.6) 25.4μm, total width 27.9 (37.5) 47.7μm; verrucae height 0.3 (1.2) 1.7μm, verrucae width 0.3 (1.6) 2.5μm and 0.5 (0.9) 1.2μm apart. 4 specimens measured. Tetrad total diameter 27.9 (33.7) 40.7μm, single width 18.9 (23.3) 30.0μm; verrucae height 0.5 (1.2) 4.5μm, 0.6 (0.9) 2.0μm, and 0.6 (0.9) 1.5μm apart. 9 specimens measured. Triads with a similar ornamentation are also known from this assemblage.

Comments: The distal sculpture is similar to the distal sculpture of the trilete *Synorisporites verrucatus*. However, there is no evidence of any trilete marks on any of these specimens. Some tetrads are similar to the fused verrucate tetrads also found in these assemblages (see page 5-15), but possess clear contact lines between spore units.

Occurrences: Assemblages 1 to 5.

Age range: Homerian (late Wenlock) to Gorstian (Ludlow) (Burgess and Richardson 1991).

Hispanaediscus cf. *verrucatus*

Plate 5.19*a* - *b*

Description: Naked, proximally hilate monad, sculptured with a verrucae to murornate ornamentation on the distal surface. Verrucae are low and broad, closely spaced, and are often fused to form larger verrucae or broad muri. The proximal hilum is not visible in this specimen.

Dimensions: Monad total diameter 32.3μm, verrucae height 0.8μm, verrucae width 3.0μm, and 0.4μm apart. 1 specimen measured.

Comments: This specimen possesses ornamentation similar to *Hispanaediscus verrucatus*, but verrucae are arranged closer together (less than 0.5μm apart), and fusion is more common, forming muri. The specimen is also larger than the size range for *H. verrucatus* (over 32.0μm). Similar specimens have been reported by Wellman and Richardson (1996) and described as *Hispanaediscus* cf. *verrucatus*.

Occurrence: Assemblage 4.

Age range: ?upper Přídolí to lowermost Lochkovian (*Apiculiretusispora* sp. E palynosubzone)) (Wellman and Richardson 1996).

Hispanaediscus wenlockensis Burgess and Richardson 1991

Plate 4.19*c* - *f*

Description: Naked, proximally hilate monads that sculptured with a verrucate ornamentation on the distal surface. Verrucae are closely spaced if not touching, although fusion between elements is rare. The proximal surfaces are not visible on these specimens.

Dimensions: Monad total diameter 23.2 (25.9) 28.6μm, verrucae height 0.8 (0.95) 0.9μm, verrucae width 1.5 (1.65) 1.8μm, and 0.4 (0.45) 0.5μm apart. 2 specimens measured. A 'loose' tetrad (with a visible contact line) has a similar distal sculpture. Total tetrad diameter 30.0μm, single spore diameter 21.6μm, with verrucae that are 1.2μm in height, 2.1μm in width and 0.8μm apart.

Comments: Sculptural elements on these specimens are too closely arranged and lack of common fusion between elements suggests that they do not belong to *Hispanaediscus verrucatus* or *Hispanaediscus major*. Verrucae are too regular to belong to *Hispanaediscus*? *irregularis*. Distal sculpture is most similar to *Hispanaediscus wenlockensis* Burgess and Richardson (1991), although verrucae are slightly lower (less than 1μm in height).

Occurrences: Assemblages 1 and 3.

Age range: Homerian (Wenlock) (Burgess and Richardson 1991).

Suprasubturma **AHILATES** Richardson 1996a

Naked, alete cryptospore monads

LAEVIGATE ALETE MONADS

Plate 5.20*a* - *l*

Description: Naked, alete (non-hilate) sub-circular to circular monads. Exine is entirely laevigate, and featureless. Exine is often thin and poorly preserved.

Dimensions: Monad total diameter 15.4 (30.9) 64.0μm. 64 specimens measured.

Comments: Maybe undeveloped forms of the enveloped laevigate monads from the genus such as *Strophomorpha* (Miller and Eames 1982). Difficult to distinguish from laevigate sphaeromorph acritarchs or other poorly preserved cryptospores or triletes.

Occurrences: Assemblages 1 to 5.

Age range: Caradoc (Wellman 1996) to early Lochkovian (Wellman 1993b).

Turma **INVOLUCRALETES** Richardson 1996a

Suprasubturma **EUPOLYADI** Richardson 1996a

Genus **VELATITETRAS** Burgess 1991

Velatitetras cf. *reticulata* Burgess 1991

Plate 5.21*a* - *d*

Description: Envelope enclosed, sub-circular, permanent tetrahedral tetrads. Envelope is sculptured with low, narrow sinuous muri that form irregular shaped reticulum.

Dimensions: Total tetrad diameter 35.0 (46.7) 64.0μm, single spore diameter 23.7 (30.6) 40.0μm; muri height 0.6 (1.0) 1.5μm, muri width 0.7 (1.0) 1.3μm, lumen longest axis 1.0 (3.5) 6.4μm, shortest axis 1.0 (2.2) 3.2μm. 6 specimens measured.

Comments: Sculpture is seen to cover spore contact lines, and therefore thin envelopes encompass these tetrads, with a low, irregularly arranged, sinuous reticulate sculpture on the distal surface. Most similar to *Velatitetras reticulata*, which was erected for 'enveloped tetrads ornamented with muri forming a reticulum with small lumen' by Burgess (1991). However, those described are smaller in total diameter 22.0 (27.0) 35.0μm than observed here, although sculpture dimensions are similar. Also similar to *Velatitetras* (*Nodospora*) *retimembrana* Miller and Eames (1982), emend. Wellman and Richardson (1996), although these tetrads are enveloped with a reticulum that is more regular, and muri are no more than 0.75μm in height or width.

Occurrences: Assemblages 1, 3 and 4.

Age range: latest Ordovician to late Aeronian (Llandovery) (Burgess 1991).

Velatitetras rugulata Burgess 1991

Plate 5.21*e* - *h*

Description: Envelope enclosed sub-circular, permanent tetrahedral tetrads. Envelope sculptured with irregularly arranged, low verrucae to rugulae.

Dimensions: Tetrad total diameter 29.2 (36.5) 43.0μm, single spore diameter 20.0 (24.0) 26.3μm; rugulae height 0.5 (0.7) 1.0μm, rugulae width 0.7 (1.1) 1.6μm, and 0.6 (0.9) 1.2μm apart. 6 specimens measured.

Comments: Slightly smaller than the size range recorded by Burgess (1991) for *Velatitetras rugulata* from the Llandovery area (24.0 to 33.0μm). Similar to enveloped tetrads assigned to *Velatitetras* sp. described within a bifurcating mesofossil from the mid-Lochkovian (NMW96.11G.3, Edwards et al. 1999), although these *in situ* tetrads show more of a granular sculpture than rugulae.

Occurrences: Assemblages 2 and 4.

Age range: Caradoc (Wellman 1996) to early Rhuddanian (Llandovery) (Burgess 1991).

Velatitetras cf. *cristata* Burgess and Richardson 1995

Plate 5.21*i* - *l*

Description: Envelope enclosed, sub-circular ?permanent tetrahedral tetrads. The envelope is sculptured with ill-defined anastomosing muri, forming an irregular shaped and projecting reticulum. The envelope is either closely adherent or partially loose.

Dimensions: Tetrad total diameter 29.4 (34.0) 38.5μm, single spore diameter 24.2 (24.8) 25.3μm, muri height 1.5 (1.55) 1.6μm, width 0.3 (0.8) 1.3μm, lumen longest axis 2.6 (3.4) 4.1μm and shortest axis 1.5 (2.5) 3.4μm. 2 specimens measured.

Comments: Smaller than the published size range for *Velatitetras cristata* (42.0μm to 53.0μm in total tetrad diameter) from the Rumney Borehole, Burgess and Richardson (1995). Similar to *Velatitetras reticulata* and *Velatitetras* (*Nodospora*) *retimembrana* Burgess (1991), but muri are more irregularly arranged, with a projecting reticulum.

Occurrences: Assemblage 2 and 5.

Age range: *Velatitetras cristata senso stricto* is known from the Homerian and Gorstian (late Wenlock to early Ludlow) (Burgess and Richardson 1995).

Velatitetras sp. B (sp. nov.)

Plate 5.22*a* - *f*

Description: Envelope enclosed, sub-circular, permanent tetrahedral or decussate tetrads. Envelope sculptured with apiculate elements that cover spore unit contact lines. Specimens are variable and poorly preserved, and are unlikely to belong to the same species. Apiculate elements range from grana to microconi and are either closely-spaced and irregularly arranged, or evenly and regularly arranged. Apiculate elements can also be fused at the base, and where compressed appear spatulate.

Dimensions: Total tetrad diameter 25.8 (40.3) 64.0μm, single spore diameter 18.4 (28.8) 42.6μm, element height 0.6 (1.0) 1.8μm, width 0.7 (1.0) 1.3μm and 0.9 (1.2) 2.0μm apart. 5 specimens measured.

Comments: Similar to the description of *Velatitetras* sp. A Burgess (1991) (*Nodospora* sp. E Richardson 1988), an enveloped tetrad with a granulate ornament, but ornament smaller than observed from these specimens. There are also similarities to *Velatitetras* sp. found within a bifurcating mesofossil from the middle Lochkovian (NMW96.11G.3, Edwards et al. 1999).

Occurrences: Assemblages 2 and 4.

Velatitetras sp. C (sp. nov.)

Plate 5.22*g* - *j*

Description: Envelope enclosed, sub-circular, permanent tetrahedral or decussate tetrad. Envelope sculpture with verrucate elements that cover spore unit contact lines. Verrucae are closely spaced and regularly arranged.

Dimensions: Total tetrad diameter 36.4 (37.5) 38.5μm, single spore diameter 20.7 (22.6) 24.5μm, verrucae height 0.8μm, verrucae width 1.2 (1.6) 2.0μm, and 0.7 (0.9) 1.0μm apart. 2 specimens measured.

Comments: Similar to enveloped tetrads with apiculate elements (*Velatitetras* sp. B). However, the apiculate elements are close to being isodiametric, whilst these specimens are ornamented with elements that are nearly twice as wide as they are high (verrucae). They are also more closely and regularly arranged. These specimens are larger than the recorded diameter of the similar granulate ornamented specimens of *Velatitetras* sp. A Burgess (1991).

Occurrence: Assemblage 1.

Genus **ABDITUSDYADUS** Wellman and Richardson 1996

Abditusdyadus histosus Wellman and Richardson 1996

Plate 5.23*a* - *d*

Description: Envelope enclosed, unfused elliptical dyads. Spore wall thick, but slightly folded. Envelope is sculptured with muri forming a regular reticulum pattern. Muri are low and narrow, and have a point tip in profile. Muri join to form web-like reticulum with small, polygonal-shaped lumina.

Dimensions: Total dyad length 32.0 (35.4) 38.4μm, single spore width 16.8 (19.9) 23.8μm, total width 25.2 (27.8) 32.3μm; muri height 0.2 (0.4) 0.8μm, muri width 0.2 (0.4) 0.8μm, lumen longest axis 1.0 (1.6) 2.4μm and shortest axis 0.7 (1.0) 1.3μm. 3 specimens measured.

Comments: *Abditusdyadus histosus* described by Wellman and Richardson (1996) from Lower Old Red Sandstone from the Lorne area are larger in total length 62.0 (73.0) 83.0μm, although sculpture dimensions are similar. These dyads possess an identical sculpture to the enveloped tetrad *Velatitetras* (*Nodospora*) *retimembrana* (Wellman and Richardson 1996), and is similar to the sculpture of *Velatitetras reticulata*, but muri of *Abditusdyadus histosus* form a more regular reticulum.

Occurrences: Assemblages 1 and 2.

Age range: ?upper Přídolí to lowermost Lochkovian (*Apiculiretusispora* sp. E palynosubzone) (Wellman and Richardson 1996).

Genus **SEGESTRESPORA** Burgess 1991

Segestrespora cf. *membranifera*

Plate 5.23*e* - *f*

Description: Envelope enclosed sub-circular fused dyad. Exine laevigate, with enclosing envelope sculptured with narrow, projecting, sinuous muri, forming an irregular reticulate pattern. Muri are often flattened and appear spatulate.

Dimensions: Dyad length 47.3μm, single spore width 32.6μm, total spore width 45.3μm; muri height 1.3μm, muri width 0.8μm, lumen longest axis 3.1μm, and shortest axis 1.9μm. 1 specimen measured.

Comments: Similar to *Segestrespora* (*Dyadospora*) *membranifera* Johnson (1985) emend. Burgess (1991). However, this specimen is larger than the published dyad total length range from 25.0 to 31.0μm. The envelope reticulum sculpture of this specimen is more irregular, with muri height exceeding 1μm. Therefore this specimen will be assigned to *Segestrespora*

cf. *membranifera*. The sculpture is similar to the enveloped tetrad *Velatitetras* cf. *reticulata* (see page 5-37).

Occurrence: Assemblage 1.

Age range: latest Ordovician to early Rhuddanian (Burgess 1991).

Genus **QUALISASPORA** Richardson, Ford and Parker 1984

Qualisaspora sinuata Higgs 2004

Plate 5.23*g* – *h*

Description: Small ?enveloped sub-circular, non-hilate monads. Sculptured with regularly-spaced, radially-arranged muri from the equator to the central pole on the distal surfaces. Muri are coni-shaped in profile, and are either straight or slightly sinuous, with variable continuity.

Dimensions: Total diameter 20.0 (20.8) 21.5µm; muri height 0.4 (0.5) 0.6µm, muri width 0.4 (0.6) 0.7µm and 0.6 (0.7) 0.8µm apart. 2 specimens measured.

Comments: Enveloped, monad cryptospores that are sculptured with radial muri, which converge on opposite surfaces, belong to the genus *Qualisaspora* Richardson, Ford and Parker (1984). The type species, *Qualisaspora fragilis*, possesses radially arranged muri that spiral from pole to pole. However, this specimen is most similar to *Qualisaspora sinuata* Higgs (2004), which possess non-spiral, radially-arranged sinuous muri.

Occurrence: Assemblage 1.

Age range: *Qualisaspora sinuata* is known from the Freshwater West Formation (Conigar Pit Sandstone Member) dated to the middle Lochkovian (mid *micrornatus-newportensis* palynosubzone) (Higgs 2004).

INCERTAE SEDIS

ENVELOPED (?) MURORNATE SCULPTURED CRYPTOSPORES

BROAD MURORNATE SCULPTURE

Plate 5.24*a* - *c*

Description: Possible enveloped enclosed, sub-circular monads and permanent tetrad, sculptured with broad muri, forming a broad reticulate pattern with large sub-rectangular or sub-triangular lumina, which bear evenly distributed grana elements. Proximal surfaces were not visible.

Dimensions: Monad diameter ranges from 20.7 (26.3) 31.8μm, muri height 1.0 (1.4) 1.7μm, muri width 1.1 (1.6) 2.0μm, grana height 0.4 (0.6) 0.7μm and grana width 0.4 (0.8) 1.1μm. 2 specimens measured. Tetrad total diameter 23.7, muri height 0.7, muri width 1.2, grana height 0.3, and grana width 0.5. 1 specimen measured.

Comments: Similar in general morphology to *Chelinohilates erraticus*, with broad, sinuous muri joining together to form a broad reticulate pattern. However, unlike *Chelinohilates*, lumina are ornamented with grana, which is not included in the *Chelinohilates* genus diagnosis. The *Cymbohilates* genus includes proximally hilate cryptospores that are ornamented with apiculate elements, but does not include a murornate sculpture. Therefore this specimen belongs to a new genus.

Occurrences: Assemblages 3 to 5.

SINUOUS MURORNATE SCULPTURE

Plate 5.24*d* – *e*

Description: Enveloped (?) hilate circular monad, with murornate sculpture on the distal and ?proximal surfaces. Muri on both the ?proximal and distal surfaces are highly irregular, closely spaced, sinuous and bifurcating, are often fused together, and separated by small, irregular lumina.

Dimensions: Total diameter 39.2μm; muri height 0.5μm, muri width 0.9μm, lumen longest axis 2.1μm, shortest axis 2.0μm. 1 specimen measured.

Comments: Although this specimen has a sculpture similar to *Chelinohilates sinuous* var. *sinuous*, it is not clear if the proximal surface has a hilum, and whether in fact this specimen is enclosed with an envelope. Therefore this specimen belongs to a new genus.

Occurrence: Assemblage 4.

ENVELOPED (?) VERRUCATE SCULPTURED CRYPTOSPORES

Plate 5.24*f* - *i*

Description: Enveloped (?) sub-circular monad cryptospores, with a verrucate to murornate sculpture on the distal surfaces. Small, irregularly shaped verrucae are densely packed, and in some areas are fused together at the element bases to form small rugulae or muri. The proximal hilum is not visible on any of these specimens.

Dimensions: Total diameter 28.4 (29.7) 32.3μm, sculpture height 0.4 (0.6) 0.8μm, sculpture width 0.6 (1.5) 3.0μm, sculpture spacing 0.2 (0.3) 0.4μm. 3 specimens measured.

Comments: Sculpture is similar to *Hispanaediscus ?irregularis* (Wellman and Richardson 1996), a possible hilate cryptospore with elements are irregularly shaped and closely packed together (less than 0.5μm). However, elements in these specimens are much smaller (*Hispanaediscus ?irregularis* possesses elements with a minimum height of 1.5μm, and minimum width of 2.0μm), and are seen to fuse together, which does not occur on *H.? irregularis*. *H.? irregularis* is also larger in total diameter (over 36.0μm). These specimens are similar to cf. *Cymbohilates variabilis* described from these Tredomen Quarry assemblages (see page 5-44), but the basic element is more apiculate in nature than verrucate. Therefore these specimens belong to a new genus.

Occurrence: Assemblage 4.

Age range: (*Hispanaediscus irregularis sense stricto* is known from the ?upper Přídolí to lowermost Lochkovian (*Apiculiretusispora* sp. E palynosubzone) (Wellman and Richardson 1996)).

ENVELOPED (?) APICULATE SCULPTURED CRYPTOSPORES

Plate 5.24*j* - *k*

Description: Possibly enveloped enclosed, sub-circular monad with an apiculate sculpture on both the distal and ?proximal surface. Apiculate elements on the distal surface are evenly spaced microconi. These microconi also occur on the proximal surface, but some are fused at the base to form rugulae or are compressed.

Dimensions: Total diameter 24.6μm; sculpture height 0.5μm, width 0.8μm and 1.7μm apart. 1 specimen measured.

Comments: This specimen is similar to *Cymbohilates disponerus* in size and sculpture elements. However, the *Cymbohilates* genus is restricted to hilates with apiculate sculpture on distal and sub-equatorial surfaces only, and therefore this specimen belongs to a new genus.

Occurrence: Assemblage 1.

ENVELOPED (?) SPATULATE SCULPTURED CRYPTOSPORES

Plate 5.25*a* - *h*

Description: This group sub-circular monads and dyads have been grouped together due to their unusual blunt spatulate sculptured envelope, but are unlikely to belong to the same genus. Sculpture is highly variable, consisting of verrucae to spatulate ornament. Element outline can vary from rounded to pointed, and in some cases are biform. Elements are closely spaced and are often fused at the base to form clusters or ridges that project away from the spore wall.

Dimensions: Total diameter 22.6 (32.1) 36.6μm; sculpture height 0.4 (0.9) 1.2μm, width 0.8 (1.3) 2.0μm, and 0.2 (1.1) 2.3μm apart. 4 specimens measured. Dyads are also known from these assemblages. Total length 40.0 (46.0) 52.0μm, single width 28.0 (31.3) 34.6μm, total width 48.6 (58.3) 68.0μm; sculpture height 1.8μm, width 1.8 (2.1) 2.4μm, and 0.8 (0.85) 0.9μm. 2 specimens measured.

Occurrences: Assemblages 1 and 4.

?ENVELOPED SPINOSE SCULPTURED CRYPTOSPORES

SCULPTURED WITH SPINE CLUSTERS

Plate 5.25*i* - *l*, Plate 5.26*a* - *d*

Description: Possibly envelope enclosed, sub-circular monads with closely spaced, highly irregular sculpture on the distal surface of short spines that occur in radial clusters of 3 to 5 into a star shape, that are fused together at the base. In some areas of the distal surface these clusters have fused together to form irregularly shaped rugulae to muri or ridges, or in some specimens completely fused to form reticulum. Other elements are also present (biform short spines and grana). Proximal surface is not visible in any of these specimens.

Dimensions: Monad total diameter 14.7 (21.8) 40.0μm, sculpture height 1.0 (1.5) 2.7μm, width 0.6 (0.8) 1.4μm, and 0.5 (0.8) 1.2μm. 4 specimens measured. Dyad total length 29.6μm, single width 30.0μm, total width 40.0μm, sculpture height 1.4μm, sculpture width 0.6μm, sculpture spacing 0.5μm. 1 specimen measured. Tetrad total diameter 42.5μm, single spore unit diameter 23.1μm, sculpture height 2.5μm, sculpture width 1.5μm, sculpture spacing 1.0μm. 1 specimen measured.

Comments: As the proximal surface is not visible, and these specimens have been found in a cluster, it is not possible to determine if these are hilate monad or tetrad cryptospores. Their small size may suggest that they are monads rather than tetrads. The sculpture may also be attributed to a tightly adherent envelope, and therefore these specimens may belong to genera such as *Velatitetras* or *Rugosphaera*. However, there is no evidence for an envelope. These

specimens bear sculpture most similar to *Cymbohilates cymosus*, but the star-shaped clusters are more irregular, closely spaced and fused together to form ridges, and therefore belong to a new genus. Similar cryptospores are found i*n situ* from elongate mesofossils from Hudwick Dingle (pers. comm. Dianne Edwards).

Occurrences: Assemblages 1 and 2.

SCULPTURED WITH SLENDER TO SPATULATE SPINES

Plate 5.26*e* - *h*

Description: Possible envelope enclosed sub-circular tetrads. Envelope covers spore unit contact lines and sculptured with small, evenly spaced spines. Elements are slender with pointed tips, some of which are biform or fused at the base to form spatulate elements.

Dimensions: Tetrad total diameter 42.8 (45.7) 48.5µm, single spore unit diameter 27.2 (31.8) 36.3µm, sculpture height 3.0µm, width 1.0µm, and 1.3 (1.7) 2.0µm apart. 2 specimens measured.

Comments: Sculpture resembles that of *Cymbohilates horridus* var. A. (sp. nov) (see page 5-28), but these specimens are covered by an envelope.

Occurrence: Assemblage 1.

5.3.2: *Triletes*

Anteturma **SPORITES** Potonié 1893

Turma **TRILETES** Reinsch 1891

Subturma **AZONOTRILETES** Luber 1935 in Luber and Waltz 1938

Infraturma **LAEVIGATI** (Bennie and Kidston) Potonié and Kremp 1954

Genus **RETUSOTRILETES** Naumova emend. Richardson 1965 (non. Streel 1964)

Retusotriletes dittonensis Richardson and Lister 1969

Plate 5.27*a* - *d*

Description: Retusoid sub-circular to sub-triangular trilete spores with laevigate exines on the distal and proximal surfaces. Curvaturae perfectae are distinctive, indicating a contact area smaller than the spore equator (two-thirds to a quarter of the total diameter), with

indentations where each of the laesura meet the curvatura. Laesurae are occasionally thickened into lips, particularly at the junction with the curvaturae. Contact faces are occasionally ornamented with micrograna.

Dimensions: Total diameter 26.3 (30.2) 34.4μm, trilete laesurae thickness 0.5 (0.8) 1.0μm. 8 specimens measured.

Comments: These specimens are smaller than the published size ranges for *Retusotriletes dittonensis* from the Ditton Group (35.0 to 57.0μm) (Richardson and Lister 1969).

Occurrences: Assemblages 2 to 5.

Age range: Lower Lochkovian (Richardson and Lister 1969).

Retusotriletes cf. *dittonensis*

Plate 5.27*e* - *j*

Description: Retusoid, sub-circular trilete spores with a laevigate distal surface, and minute apiculate ornament on the proximal surface. Elements are either micro-coni or micro-grana, no more than approximately 0.5μm in diameter. Curvaturae perfectae are well-developed, occasionally with a slight lip. Trilete laesurae are thin, although they thicken towards the curvature perfectae.

Dimensions: Total diameter 25.2 (30.9) 44.2μm, trilete laesurae thickness 0.5 (0.8) 1.5μm. 7 specimens measured.

Comments: Similar to *Retusotriletes dittonensis*, but with an apiculate sculpture on the proximal surface. However, it must be noted that the features interpreted as elements could be bacteria or a residue.

Occurrences: Assemblages 1 to 3 and 5.

Retusotriletes cf. *triangulatus* Streel 1967, *sensu* Richardson and Lister 1969

Plate 5.28*a* - *b*

Description: Retusoid, sub-circular trilete spores with laevigate distal and proximal surfaces. The curvaturae perfectae are coincidental with the equatorial margin, except where the trilete laesurae meet the margin. The triradiate mark is surrounded by a distinctive thick, darkened area at the apical area. This triangular-shaped area either exhibits convex or straight sides. The laesurae are often sutured, resulting in lighter, thinner exine at the apical pole.

Dimensions: Total diameter 40.3 (42.4) 47.3μm, trilete laesurae thickness 1.0 (1.1) 1.5μm. 4 specimens measured.

Comments: These specimens are small compared with the published size range for *Retusotriletes* cf. *triangulatus* (41 to 68μm) Richardson and Lister 1969, but are over 40μm in diameter.

Occurrence: Assemblage 2.

Age range: Lochkovian (Richardson and Lister 1969). However, similar specimens have been described from the Emsian Battery Point Formation, Quebec (McGregor and Owens 1966).

Retusotriletes cf. *triangulatus var. minor* (var. nov.)

Plate 5.28*c* - *j*

Description: Small retusoid trilete spores with laevigate proximal and distal exine. Similar to *Retusotriletes* cf. *triangulatus*, with curvaturae perfectae and a distinctive darkened, triangular apical area. Trilete laesurae are sutured, with thinning of the exine at the apical pole.

Dimensions: Total diameter 25.5 (33.8) 39.5μm, laesurae thickness 0.4 (0.9) 1.5μm. 17 specimens measured.

Comments: These specimens are identical to *Retusotriletes* cf. *triangulatus*, but are under 40μm in diameter.

Occurrences: Assemblages 2 and 5.

TETRADS OF LAEVIGATE TRILETES

Plate 5.28*k* - *l*

Description: Tetrads consisting of sub-triangular spore units, with clear contact lines, and slight equatorial crassitude on each spore unit. The distal exine of each spore unit is laevigate and spore walls are inflated.

Dimensions: Total tetrad diameter 45.4 (46.4) 47.3μm, single diameter 31.0 (31.3) 31.5μm. 2 specimens measured.

Comments: Similar to unfused cryptospore tetrad species *Tetrahedraletes medinensis*, but spore units are triangular, and not sub-circular, suggesting that these are tetrads of trilete spores, and not cryptospores. Additionally, the spore units of *Tetrahedraletes medinensis* have much more pronounced equatorial thickenings, or flanges (see page 5-16).

Occurrence: Assemblage 1.

Infraturma **APICULATI** (Bennie and Kidston) Potonié 1956

Genus **APICULIRETUSISPORA** Streel 1964

Apiculiretusispora spp.

Plate 5.29*a* to *l*

Description: Retusoid, sub-circular to sub-triangular trilete spores, with apiculate ornament on the distal and proximal surfaces. Apiculate elements range from micro-grana to grana. Elements are closely spaced, either evenly or slightly irregularly. In some specimens, elements are focussed around the trilete laesurae. The curvature perfectae are coincidental to the equatorial margin, and is at least 2µm thick. Laesurae are thick, some associated with folded lips.

Dimensions: Total spore diameter 18.4 (31.3) 42.1µm, laesurae width 0.3 (1.3) 2.3µm, grana height 0.3 (0.4) 0.6µm, grana width 0.3 (0.7) 1.4µm, grana spacing 0.6 (1.2) 3.1µm. 8 specimens measured.

Comments: This group of apiculate sculptured retusoid trilete spores has not been identified beyond genus level, and members are unlikely to belong to one species. Therefore they have been assigned to *Apiculiretusispora* spp. Similar spores are found *in situ* within sporangia of *Cooksonia hemisphaerica* and *Cooksonia* cf. *caledonica* (Fanning et al. 1991).

Occurrences: Assemblages 1 to 3.

Infraturma **MURORNATI** Potonié and Kremp 1954

Genus **EMPHANISPORITES** McGregor 1961

Emphanisporites protophanus Richardson and Ioannides 1973

Plate 5.30*a* - *c*

Description: Sub-circular, retusoid trilete spores, with a distinctive radial, murornate ornamentation on the proximal surface, and ?laevigate distal surface. Muri begin at the curvaturae perfectae margin, and are inconspicuous, occurring in the sub-equatorial region up to half the spore radius. Muri are closely spaced, either straight or slightly sinuous, and are thick in width, but are of low relief. Laesurae are thin, but more pronounced than muri.

Dimensions: Total spore diameter 30.7 (31.4) 32.0μm, laesurae width 0.7 (0.8) 0.9μm, muri height 0.2μm, muri width 0.5 (0.7) 0.9μm, muri spacing 0.3 (0.5) 0.6μm. 2 specimens measured.

Comments: These specimens are slightly smaller than the size range published for *Emphanisporites protophanus* Richardson and Ioannides 1973 (32.0 to 48.0μm in diameter). However, Richardson and Ioannides assign identical spores under 30.0μm in diameter as *Emphanisporites* cf. *protophanus*. Therefore, as these specimens are over 30μm in diameter, they shall be assigned to *Emphanisporites protophanus*.

Occurrence: Assemblage 2.

Age range: Wenlock to Downtonian (Přídolí) (Richardson and Ioannides 1976).

Emphanisporites sp B. Richardson and Lister 1969

Plate 5.30*d* – *f*

Description: Sub-circular to sub-triangular retusoid trilete spores, with distinctive murornate ornamentation on the proximal surface, and verrucate ornamentation on the distal surface. Muri are radial, and can be straight, sinuous or bifurcating. Muri begin at the curvature perfectae, which are coincident with the equatorial margin, and taper gradually to the apical pole. The triradiate mark is inconspicuous as laesurae are similar to muri in shape and dimensions. The distal surface is ornamented with closely and evenly spaced large verrucae or rugulae elements, at least 1μm in width and height.

Dimensions: Total spore diameter 25.2 (26.9) 28.5μm, laesurae width 0.3 (0.9) 1.5μm, muri height 0.6 (1.1) 1.5μm, muri width 0.3 (0.5) 0.6μm, muri spacing 0.3 (0.5) 0.6μm. 2 specimens measured.

Comments: These specimens are most similar to *Emphanisporites* sp. B, described by Richardson and Lister (1969), although they are significantly smaller (compared to 36.0μm to 54.0μm). They are similar in size to *Emphanisporites micrornatus* Richardson and Lister (1969), but are sculptured with larger elements than *E. micrornatus*.

Occurrences: Assemblage 3 and 5.

Age range: Lochkovian (Richardson and Lister 1969).

Emphanisporites spp.

Plate 5.30*g* – *l*

Description: Sub-circular retusoid trilete spores with pronounced curvature perfectae, occurring approximately 3µm from the equatorial margin. Laesurae are thin, but thicken towards the curvature perfectae. The proximal surface bound by the curvaturae is ornamented with low-lying, inconspicuous radial muri that taper and disappear towards the apical pole. Minute grana are sparsely and irregularly distributed on the proximal surface and sub-equatorial region. The distal surface is laevigate, with the occasional minute grana.

Dimensions: Total spore diameter 23.7 (30.8) 35.0µm, laesurae width 0.6 (0.9) 1.5µm, muri height 0.2 (0.2) 0.3µm, muri width 0.5 (0.7) 1.2µm, muri spacing 0.2 (0.7) 1.5µm. 3 specimens measured.

Comments: These specimens have not been assigned beyond *Emphanisporites* due to their poor preservation. However, they are similar to *Emphanisporites epicautus* Richardson and Lister (1969), with a contact area of approximately 4/5th of the spore radius. However, *Emphanisporites epicautus* does not exhibit any minute grana sculpture.

Occurrences: Assemblages 2 and 5.

Subturma **ZONOTRILETES** Waltz 1935 in Luber and Waltz 1938

Infraturma **CRASSITATI** Bharadwaj and Venkatachala 1961

Genus **AMBITISPORITES** Hoffmeister 1959

Ambitisporites avitus Hoffmeister 1959 emend. Richardson and Lister 1969

Plate 5.31*a* - *d*

Description: Sub-circular to sub-triangular, laevigate crassitate trilete spores. The trilete mark is simple, with laesurae that extend to the inside of the equatorial crassitude. Laesurae are slightly raised or sutured, and can be thick or thin. Both the distal and proximal surfaces are laevigate, with one specimen exhibiting a micro-granular ornamentation on the proximal surface.

Dimensions: Total diameter 37.1 (39.9) 53.3µm, crassitude width 2.6 (3.3) 4.2µm, trilete laesurae width 1.0 (1.8) 3.0µm. 9 specimens measured.

Comments: Similar spores found within *Cooksonia pertoni* sporangia are assigned to *Ambitisporites* sp.

Occurrences: Assemblages 1 to 3.

Age range: Aeronian to Přídolí (Richardson and McGregor 1986), ?early Lochkovian (Wellman et al. 2000, Higgs 2004), ? *in situ* within *Cooksonia banskii* from the Lower Lochkovian (Habgood et al. 2002).

Ambitisporites avitus var. *minor* (var. nov.)

Plate 5.31*e* - *l*

Description: Sub-circular to sub-triangular crassitate trilete spores. Laevigate proximal and distal exine, with simple trilete marks. Identical to *Ambitisporites avitus*, but smaller in diameter.

Dimensions: Total diameter 11.3 (29.7) 34.9µm, crassitude width 1.1 (3.0) 3.8µm, trilete laesurae width 0.2 (1.5) 2.5µm. 21 specimens measured.

Comments: All specimens are below 35µm in total diameter, and therefore do not fit into the published size range for *Ambitisporites avitus*. Therefore these specimens have been assigned to a new variety, *Ambitisporites avitus* var. *minor*.

Occurrences: Assemblages 1 to 5.

Ambitisporites dilutus Hoffmeister 1959 emend. Richardson and Lister 1969

Plate 5.32*a* - *f*

Description: Sub-triangular to sub-circular crassitate trilete spores. These spores exhibit thin equatorial crassitudes, with simple trilete marks of thick laesurae that extend to the equatorial margin. Some laesurae are possibly associated with lips, although poor preservation makes interpretation difficult. Both the distal and proximal surfaces are laevigate.

Dimensions: Total diameter 17.8 (30.0) 44.2µm, crassitude width 1.0 (2.1) 3.8µm, trilete laesurae width 0.4 (1.4) 3.0µm. 21 specimens measured.

Comments: The original description of *Ambitisporites dilutus* by Hoffmeister 1959, included laevigate, crassitate trilete spores that exhibited simple trilete marks without lips. These specimens ranged in total diameter from 30.0 to 60.0µm. In 1969, Richardson and Lister recorded similar spores that were slightly smaller (28.0 to 40.0µm and did include lips around the laesurae, and assigned them to *Ambitisporites* cf. *dilutus*. The group described here is likely to contain both species, but due to poor preservation, they will remain as *Ambitisporites dilutus*.

Occurrences: Assemblages 1 to 5.

Age range: Aeronian to Přídolí (Richardson and McGregor 1986). ?Lochkovian (Wellman et al. 2000).

Ambitisporites warringtonii Richardson and Lister 1969 emend. Richardson et al. 2001

Plate 5.32*g* - *k*

Description: Sub-triangular to sub-circular crassitate trilete spores. Distal and proximal surfaces are laevigate. Specimens exhibit a thick equatorial crassitude which thins out in the inter-radial area and is thickest where the trilete laesurae meet the equator. Laesurae then taper toward the apical pole and are often thin or sutured.

Dimensions: Total diameter 20.5 (31.7) 40.9μm, crassitude width 0.8 (2.5) 4.5μm, trilete laesurae 0.2 (0.9) 2.0μm. 17 specimens measured.

Comments: Similar spores to these specimens were described by Richardson and Lister (1969) as *Retusotriletes warringtonii*, and were thought to be retusoid spores with curvaturae perfectae that were coincidental with the spore equator, producing an equatorial thickening. However, more recently they have been re-assigned to the genus *Ambitisporites*, as they are crassitate trilete spores (Richardson et al. 2001). They are similar in size to the originally described *Retusotriletes warringtonii* specimens from the Lower Downtonian and Dittonian strata of the Welsh Borderland (18.0 to 36.0μm).

Occurrences: Assemblages 1 to 5.

Age range: Aeronian to Dittonian (Lochkovian) (Richardson and Lister 1969, Richardson and McGregor 1986).

Ambitisporites sp. A (sp. nov.)

Plate 5.32*l*

Description: Sub-circular crassitate trilete spore, with a thin laevigate proximal and distal exine. Thin laesurae taper towards a dark apex at the apical pole.

Dimensions: Total diameter 37.7μm, crassitude width 3.5μm, trilete laesurae width 1.0μm. 1 specimen measured.

Occurrence: Assemblage 2.

Genus **STREELISPORA** Chaloner and Streel emend. Richardson et al. 1982

Streelispora newportensis Richardson and Lister 1969

Plate 5.33*a* - *d*

Description: Sub-circular to sub-triangular crassitate trilete spores, with three distinctive inter-radial papillae on the proximal surface. Papillae are circular in plan and rounded in profile, and are attached to the equator or laesurae by three or five folds, which are radially arranged. The exine between folds is laevigate. These specimens have a narrow crassitude, and thick laesurae that reach to the spore equator. The distal surface is sculptured with apiculate ornamentation. The elements are broad coni with rounded apices, and are evenly spaced.

Dimensions: Total spore diameter 24.8 (24.9) 25.0μm, crassitude width 1.3 (2.0) 2.6μm, laesurae width 1.7 (1.75) 1.8μm, distal sculpture height 0.5 (0.55) 0.6μm, sculpture width 0.6 (0.7) 0.8μm, sculpture spacing 1.5 (2.1) 2.7μm. 2 specimens measured.

Comments: Very distinctive spore species, which is one of the key index species for the *micrornatus-newportensis* biozone. Similarities with *Aneurospora* sp. (Chaloner and Streel) Richardson and Lister (1969), and where the proximal surface is not visible a distinction between the two species is not possible (see the next section).

Occurrences: Assemblages 1 and 4.

Age range: Lochkovian (Richardson and Lister 1969).

Genus **ANEUROSPORA** Streel emend. Richardson et al. 1982

Plate 5.33*e* - *l*

Description: Sub-circular to sub-triangular crassitate trilete spores. Equatorial crassitude is thick, especially where trilete laesurae meet the equator. The trilete mark is simple, and the proximal surface is laevigate, with no inter-radial papillae. The distal surface is sculptured with evenly spaced apiculate elements. Elements range from grana, coni with rounded or pointed apices, or slender cones with rounded apices.

Dimensions: Total spore diameter 17.0 (29.8) 81.6μm, crassitude width 0.9 (2.9) 7.6μm, laesurae width 0.5 (1.6) 4.3μm, distal surface sculpture height 0.3 (0.7) 2.6μm, sculpture width 0.3 (0.8) 3.4μm, sculpture spacing 0.4 (1.2) 4.3μm. 12 specimens measured.

Comments: A further 11 specimens of crassitate trilete spores with apiculate ornamentation on the distal surface cannot be distinguished between *Streelispora newportensis* or

Aneurospora sp, as the proximal surface is not visible. Therefore these specimens have been assigned to *Streelispora – Aneurospora*. Total spore diameter 19.2 (27.3) 35.5μm, crassitude width 1.6 (3.2) 3.9μm, laesurae width 0.3 (0.6) 1.3μm, sculpture height 0.5 (0.6) 0.8μm and sculpture width 1.0 (1.5) 2.5μm.

Tetrads with similar distal sculpture are also grouped as *Streelispora - Aneurospora*. Total tetrad diameter 26.4 (32.0) 37.6μm, single diameter 16.3 (22.2) 30.7μm, crassitude width 0.4 (1.2) 1.6μm, sculpture height 0.3 (0.45) 0.8μm, sculpture width 0.2 (1.1) 3.1μm, and sculpture spacing 0.5 (0.8) 1.5μm. 4 specimens measured.

Occurrences: Assemblages 1 and 3 (*Streelispora-Aneurospora* from assemblages 1 to 4).

Genus **SCYLASPORA** Burgess and Richardson 1995

Scylaspora cf. *scripta* Burgess and Richardson 1995

Plate 5.34*a* - *b*

Description: Sub-circular, equatorially crassitate trilete spore. Distinctive proximal surface sculptured with irregularly arranged, low-lying convoluted muri or rugulae elements within the inter-radial areas. The trilete mark is sutured and laevigate lips surround laesurae. The equatorial crassitude is thick and laevigate. The distal surface is not visible.

Dimensions: Total spore diameter 32.4μm, crassitude width 2.5μm, laesurae width 2.0μm, sculpture height 1.0μm, sculpture width 1.5μm, sculpture spacing 2.1μm 1 specimen measured.

Comments: This specimen is most similar to *Scylaspora scripta* Burgess and Richardson (1995), but here the proximal elements are larger and more sparsely arranged. As the distal surface is also not visible, this specimen has been assigned to *Scylaspora* cf. *scripta*.

Occurrence: Assemblage 5.

Age range: (*Scylaspora scripta* is known from strata of Homerian age, from the Rumney Borehole, Burgess and Richardson 1995).

Scylaspora downiei Burgess and Richardson 1995

Plate 5.34*c* - *h*

Description: Sub-circular crassitate trilete spores, with equatorial crassitude of variable thickness. The trilete mark is simple, with thin laesurae that are slightly folded or sinuous. Laesurae sometimes extend to the equator or just to the inside of the equatorial crassitude.

The proximal surface is ornamented with closely spaced, irregularly-arranged, large verrucae to rugulae. This ornamentation can also occur on the sub-equatorial and equatorial area. In one specimen, the distal surface is ornamented with micro-granular elements that are closely spaced and in some places coalesce.

Dimensions: Total spore diameter 17.4 (26.5) 36.0μm, crassitude width 2.6 (3.7) 5.3μm, laesurae width 1.0 (1.4) 2.1μm, sculpture height 0.2 (0.8) 1.5μm, sculpture width 0.2 (1.4) 3.4μm, sculpture spacing 0.3 (0.8) 1.3μm. 5 specimens measured.

Comments: These specimens have a larger size range than the published size range for *Scylaspora downiei* (25.0 to 31.0μm).

Occurrences: Assemblages 2 and 3.

Age range: Known from Homerian and Gorstian strata (late Wenlock to early Ludlow) from the Rumney Borehole (Burgess and Richardson 1995).

Scylaspora cf. *kozlica* Dufka Richardson et al. 2001

Plate 5.34*i*

Description: Sub-circular to sub-triangular trilete spore with narrow equatorial crassitude. The trilete mark is simple, with laesurae extending to $4/5^{th}$ of the total spore diameter. It appears that a slight thickening occurs at the equator, and may be due to a membranous extension at the equator. The proximal surface is ornamented with small irregular rugulae or micrograna. The distal surface is not visible.

Dimensions: Total spore diameter 36.9μm, crassitude width 1.8μm, laesurae width 1.3μm, sculpture height 0.6μm, sculpture width 0.5μm, sculpture spacing 1.0μm. 1 specimen measured.

Comments: This specimen is poorly preserved, but is most similar to *Scylaspora* cf. *kozlica* Dufka comb. Richardson et al. (2001), although it is poorly preserved and the distal surface is not visible.

Occurrence: Assemblage 5.

Age range: Known from the Late Ludlow to the Přídolí (Richardson et al. 2001).

Scylaspora sp.

Plate 5.34*j* - *l*

Description: A group of unassigned crassitate trilete spores with verrucate to rugulate sculpture on the proximal surface have been grouped in *Scylaspora* spp. Specimens are variable, ranging from one specimen that is sub-circular with a narrow crassitude and sculptured with a closely-spaced network of rugulae. This ornamentation also occurs on the sub-equatorial region, where rugulae are arranged perpendicular to the equator. The trilete mark is indistinctive. A second specimen is quite different, with a sub-triangular amb outline, a thick crassitude with possible evidence of a multilayered exine. The proximal surface is sculptured with closely spaced convoluted rugulae around the apical pole. The remaining contact area and the distal surface is laevigate.

Comments: These specimens have only been assigned to the genus level due to the lack of specimens.

Occurrences: Assemblages 4 and 5.

Genus **SYNORISPORITES** Richardson and Lister 1969

Synorisporites tripapillatus Richardson and Lister 1969

Plate 5.35*a* - *d*

Description: Sub-circular to sub-triangular trilete spores with equatorial crassitudes. Proximal surface distinctive with three inter-radial papillae, and a narrow trilete mark associated with thick folds parallel to the trilete laesurae, and reach the spore equator. Each papillae is circular in plan, and rounded in profile. The remaining contact area is laevigate or associated with small verrucate. The distal surfaces are not completely visible, but are sculptured with elements that are rounded, or slightly pointed in profile and are likely to be broad verrucate.

Dimensions: Total spore diameter 24.7 (30.1) 35.4μm, crassitude width 2.3 (2.7) 3.0μm, laesurae width 1.5 (1.8) 2.0μm, sculpture height 0.7 (0.8) 0.9μm, sculpture width 1.0 (1.6) 2.1μm, sculpture spacing 0.5μm. 2 specimens measured.

Comments: Due to the lack of information regarding the ornamentation on the distal surface, these specimens are difficult to classify. These specimens are similar to *Synorisporites tripapillatus*, which have three inter-radial papillae. However, *S. tripapillatus* is sculptured with muri on the distal surface. These specimens are also similar to *Synorisporites verrucatus*, but this species does not have inter-radial papillae on the proximal surface. These

specimens are most similar to *Synorisporites* sp. A (Richardson and Lister 1969), although one specimen is smaller than the published size range (30.0 to 45.0μm) (Richardson and Lister 1969).

Occurrences: Assemblages 1 and 4.

Age range: Lochkovian (Richardson and Lister 1969).

Synorisporites sp.

Plate 5.35*e - j*

Description: The following specimens have been assigned to genus level only. These specimens are sub-triangular crassitate trilete spores, with a distal surface sculptured with irregular, broad verrucae or rugulae, sometimes with pointed apices. The proximal surfaces are sculptured with large rugulae and convoluted muri. Equatorial crassitudes are thick, with thin trilete laesurae reaching the inside of the crassitude. In one specimen, the trilete mark is associated with lips that reach the crassitude.

Dimensions: Total spore diameter 19.3 (26.3) 33.8μm, crassitude width 2.0 (2.9) 3.3μm, laesurae width 0.5 (1.1) 1.5μm, sculpture height 0.5 (0.8) 1.3μm, sculpture width 0.5 (1.4) 2.8μm, sculpture spacing 0.5 (0.8) 1.6μm. 8 specimens measured.

Occurrences: Assemblages 3 to 5.

Infraturma **PATINATI** Butterworth and Williams emend. Smith and Butterworth 1967

Trilete spores with a thickening of the distal and equatorial exine.

Genus **ARCHAEOZONOTRILETES** Naumova emend. Allen 1965

Archaeozonotriletes chulus Richardson and Lister 1969

Description: Sub-circular to sub-triangular trilete spores with patina. Exine in the equatorial region is thickened, with a simple trilete mark extending to the inside of the equatorial crassitude. Proximal and distal surfaces are generally laevigate, although the distal surface does sometimes exhibit a micro-ornament (micro-granular sculpture). Three variations of *Archaeozonotriletes chulus* have been found in these assemblages.

Archaeozonotriletes chulus var. *nanus* Richardson and Lister 1969

Plate 5.36*a*

Description: A variety of *Archaeozonotriletes chulus* that is less than 36.0μm in diameter.

Dimensions: Total diameter 30.2μm, crassitude width 3.5 (4.0) 4.5μm, laesurae width 1.2 (1.25) 1.3μm. 2 specimens measured.

Occurrence: Assemblage 1.

Age range: late Llandovery to lower Lochkovian (Richardson and Lister 1969, Richardson and McGregor 1986).

Archaeozonotriletes chulus var. *chulus* Richardson and Lister 1969

Plate 5.36*b* - *e*

Description: A variety of *Archaeozonotriletes chulus* over 36.0μm in diameter.

Dimensions: Total diameter 37.1 (37.2) 37.3μm, crassitude width 5.2 (6.35) 7.5μm, laesurae width 1.6 (1.95) 2.3μm. 2 specimens measured.

Occurrence: Assemblage 4.

Age range: Llandovery to early Eifelian (Richardson and Lister 1969, Richardson and McGregor 1986).

Archaeozonotriletes chulus var. inframurinatus Richardson and Lister 1969

Plate 5.36*f* - *g*

Description: Sub-triangular patinate trilete spore with a radial murornate infrastructure on the proximal surface. The trilete mark is inconspicuous and the central apical zone is thickened. The sub-equatorial and distal surfaces are laevigate.

Dimensions: Total diameter 26.8μm, crassitude width 4.7μm, laesurae width 0.8μm. 1 specimen measured.

Comments: Although this specimen is slightly smaller than the published size range, it has been assigned to *Archaeozonotriletes chulus* var. *infraturminatus*. However, it must be noted that preservation of this specimen is poor.

Occurrence: Assemblage 1.

Age range: ?Wenlock to the early Přídolí (lower Downtonian) (Richardson and Lister 1969).

Genus **CHELINOSPORA** Allen 1965 emend. McGregor and Camfield 1976

Chelinospora spp.

Plate 5.37*a* - *g*

Description: The following specimens have been assigned to genus level only, due to their fragmentary nature and irregularity. These sub-circular to sub-triangular trilete spores are patinate, with thickened distal exine, and at the equator, resulting in an equatorial crassitude. Distal and proximal surfaces are sculptured with an irregular reticulate (murornate) sculpture. The trilete marks are slightly raised, are either straight or sinuous and extend to the equator. Murornate sculpture on the proximal surface is sinuous or convoluted, and closely spaced. The murornate sculpture extends on to the equatorial region and distal surface.

Dimensions: Total spore diameter 25.2 (37.2) 53.8μm, patina width 2.9 (3.9) 5.3μm, laesurae width 1.0 (2.1) 3.2μm, sculpture height 0.5 (1.6) 4.0μm, sculpture width 1.0 (1.8) 2.9μm, sculpture spacing 0.5 (3.3) 12.0μm. 6 specimens measured.

Comments: These spores are not likely to belong to the same species, and have been assigned to genus level only. The murornate sculpture is similar to the cryptospore *Chelinohilates erraticus*, and where the proximal surface is not visible, *Chelinospora* sp. may be mistake for *C. erraticus*.

Occurrences: Assemblages 1, 4 and 5.

Subturma **PERINOTRILITES** Erdtman 1947

Spores with a perine.

Genus **PEROTRILITES** (Erdtman) Couper 1953

(?)*Perotrilites microbaculatus* Richardson and Lister 1969

Plate 5.37*h* - *l*

Description: The following specimens have been assigned to genus level only, due to their fragmentary nature and irregularity. These sub-triangular to sub-circular laevigate trilete spores, with outer, thin perine. Perine closely attached to exine over the proximal surface. Perine sculptured with irregular, closely spaced small elements, including micrograna.

Dimensions: Total spore diameter 17.5 (25.8) 31.5μm, perine width 4.2 (4.5) 5.0μm, laesurae width 1.0 (1.5) 2.6μm. 5 specimens measured.

Occurrences: Assemblages 1, 2 and 5.

Age range: early Lochkovian (Richardson and Lister 1969) to late Lochkovian (Richardson and McGregor 1986).

5.4: ASSEMBLAGE CHARACTERISTICS AND AGE OF TREDOMEN QUARRY STRATA

The taxa shown in Table 5.1*a* and *b* (p5-6 and p5-8), show that the composition of each palynological assemblage is different, and the nature of each assemblage changes through time from the oldest assemblage (Assemblage 5) to the youngest (Assemblage 1). This may be due to diversification, or could be environmental or taphonomic. In the following section, each assemblage is described in terms of the main species present and the proportions of morphotypes, and then compared through time. This data will then be used to determine an age for the sequence, particularly assemblage 1, which will provide an age for the palaeobotanical collection described in Chapter 3.

5.4.1: *Assemblage characteristics*

Assemblage 5

Assemblage five is the oldest of the all assemblages, and was macerated from green planar-laminated siltstones (lithofacies 3a in Chapter 6), 28.20m beneath the quarry surface, from core 1 (see BH1-3 in Figure 6.1). This occurs approximately 41.3m above the calcareous-nodule-rich horizon interpreted as the Bishop's Frome Limestone. The majority of sporomorphs are cryptospores, with a cryptospore to trilete ratio of 5.6 to 1. Twenty-three genera and 42 species are present.

Of the total assemblage, 84.46% of sporomorphs are laevigate, with 75.30% of the total assemblage being laevigate cryptospores (Figure 5.3*a*). Laevigate cryptospore taxa range from both varieties of the unfused tetrad species *Tetrahedraletes medinensis*, to fused dyad taxa *Pseudodyadospora petasus* and true dyad species *Dyadospora murusdensa* and *Dyadospora murusattenuata*. The single most common species in this assemblage is *Laevolancis divellomedia*, a laevigate, hilate monad species detached from *Dyadospora murusdensa*. Two specimens of *Artemopyra* are present, with inconspicuous radial muri on the proximal surface (*Artemopyra* sp. A). Laevigate alete monads are common (8.76%).

In contrast, sculptured cryptospores represent only 9.16% of the total assemblage (Figure 5.3*a*). Apiculate hilate monads are mainly sculptured with evenly spaced micrograna or grana (*Cymbohilates allenii* var. *magnus*, (the larger variety)), or coni, (*Cymbohilates disponerus*). Apiculate hilate monads with irregular, closely-spaced low grana are also present (*Cymbohilates variabilis* var. *variabilis*). Spinose sculptured hilate monads are not common,

Figure 5.3a: Proportions of spore morphotypes from assemblage 5.

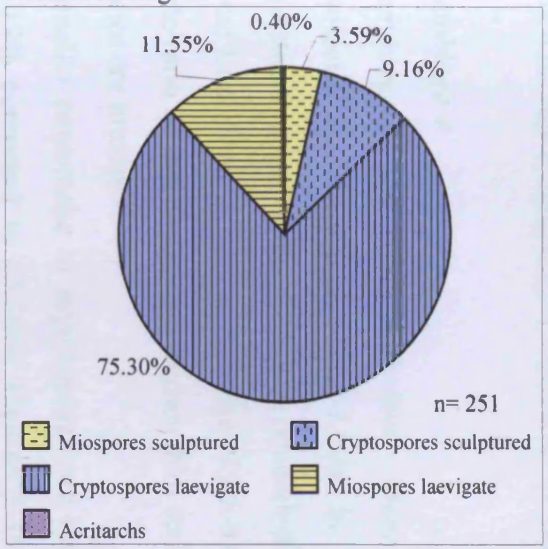

Figure 5.3b: The proportion of spore morphotypes from assemblage 4.

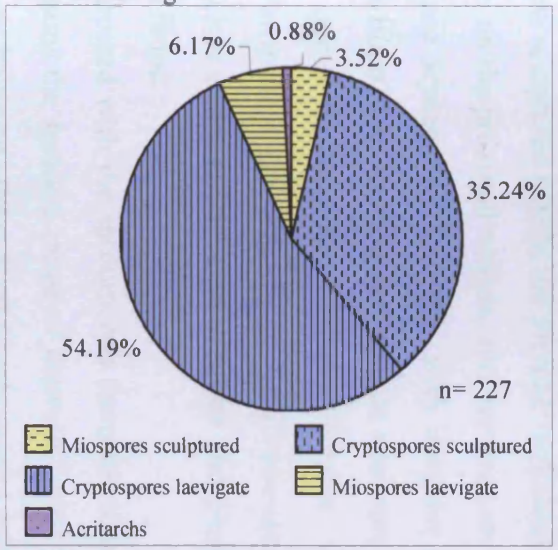

Figure 5.3c: The proportion of spore morphotypes from assemblage 3.

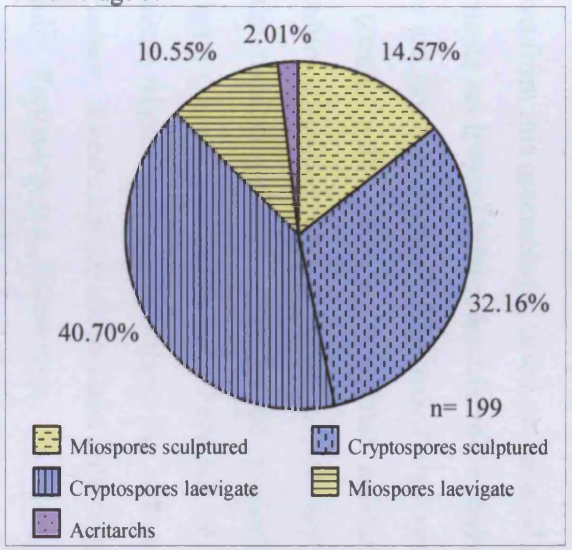

Figure 5.3d: Proportions of spore morphotypes from assemblage 2.

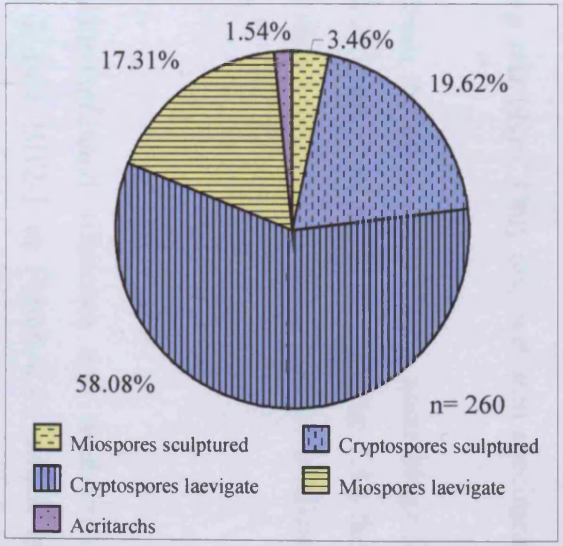

Figure 5.3e: Proportions of spore morphotypes from assemblage 1.

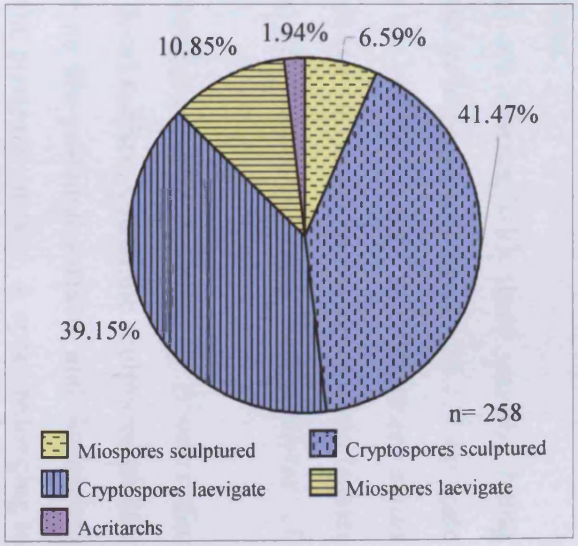

and elements are thin spines or pila (*Cymbohilates* cf. *horridus*). Apiculate tetrads are also known from this assemblage, fused or unfused (*Acontotetras*).

Verrucate sculptured hilate monads and tetrads are present, with low and broad verrucae and some are fused to rugulae (*Hispanaediscus verrucatus*). Murornate sculptured hilate monads and tetrads with either an irregular reticulum (*Chelinohilates erraticus*) or polygonal reticulum (*Chelinohilates* cf. *lornensis*) are also present.

Of the total assemblage, 15.14% of sporomorphs are triletes, with three quarters being laevigate (Figure 5.3*a*). The ratio between crassitate to retusoid triletes is 1.25:1. Laevigate crassitate triletes include *Ambitisporites avitus* and the smaller variety, *Ambitisporites avitus* var. *minor*, *Ambitisporites dilutus* and *Ambitisporites warringtonii*. Laevigate retusoid triletes include *Retusotriletes dittonensis*, *Retusotriletes* cf. *dittonensis* and *Retusotriletes* cf. *triangulatus* var. *minor*.

A few sculptured triletes are present, including the retusoid *Emphanisporites* sp. B with radial muri on the proximal surface, and verrucae on the distal surface. Crassitate sculptured triletes include *Scylaspora* cf. *scripta*, with irregular muri on the proximal surface, and *Scylaspora* cf. *kozlica*, with an irregular rugulate sculpture on the proximal surface. A spore belonging to the genus *Synorisporites* is also present, along with one *Chelinospora* sp., and one (?)*Perotrilites microbaculatus*. One enveloped tetrad is present, *Velatitetras* cf. *cristata*, which is sculptured with an irregular and projecting reticulum. Only one acritarch specimen was found.

Compared with the sporomorph diameter ranges from the other assemblages, assemblage 5 contains the smallest range of diameter, with 90% of spores under 40.0μm (Figure 5.4), the largest being an unclassified *Cymbohilates* spore with a diameter of 65.3μm, and the smallest being a laevigate monad with a diameter of 17.5μm

Assemblage 4

Assemblage 4 was macerated from green planar-laminated siltstones and mudstones (lithofacies 3a in Chapter 6), at 7.60m in core 2 (see BH2-1 in Figure 6.1), which is correlated to approximately 21.60m beneath the quarry surface and 42.9m above the Bishop's Frome Limestone. A high percentage of sporomorphs are cryptospores, with a cryptospore to trilete ratio of 8.4:1, which is higher than seen in assemblage 5. Twenty-five genera and 53 species are present.

A smaller percentage of cryptospores are laevigate in assemblage 4 than in assemblage 5 (54.19% compared to 75.30%, Figures 5.3*a* and *b*). As found in assemblage 5, unfused

Figure 5.4: Distribution of sporomorph diameter ranges through time (Assemblage 5 = oldest assemblage).

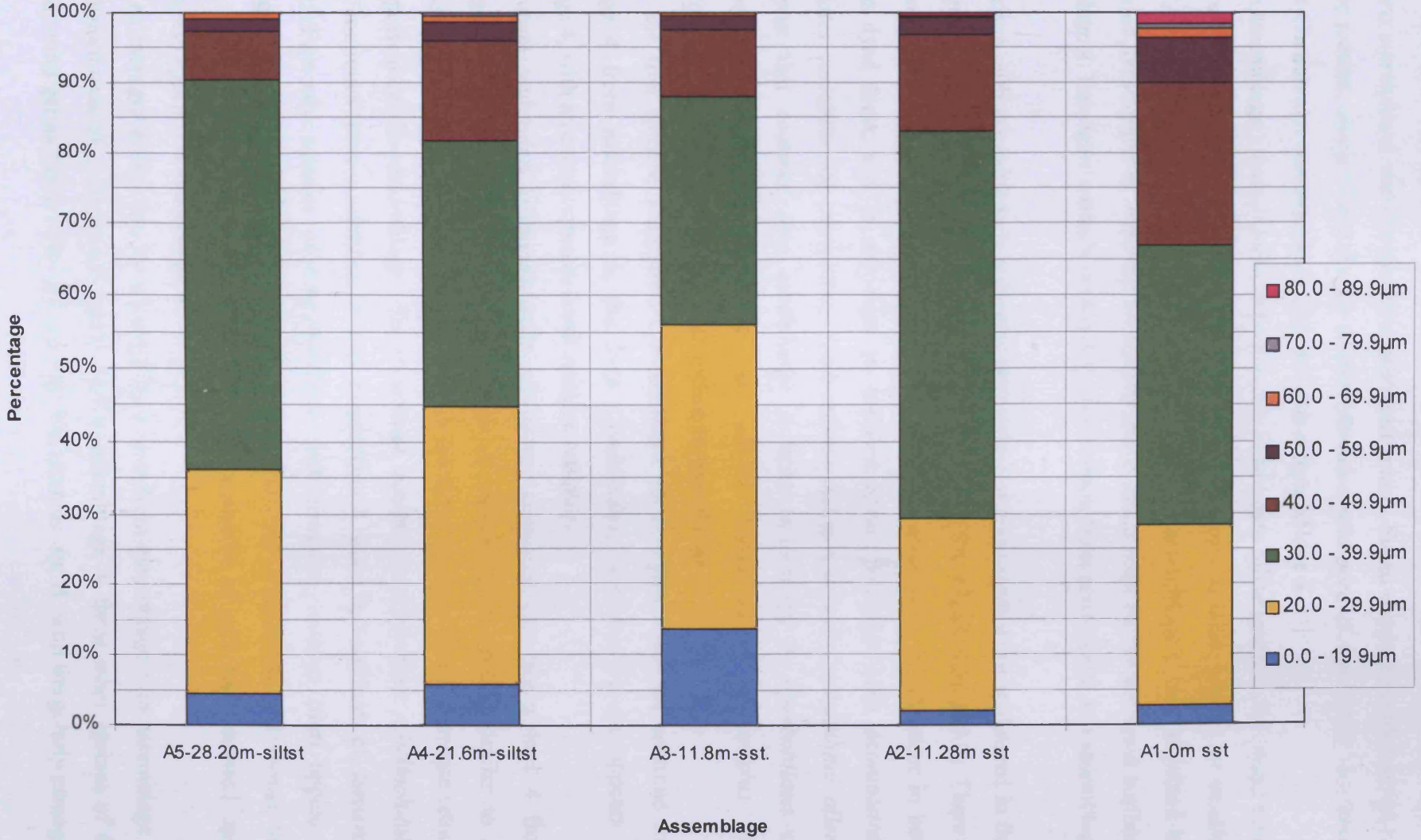

laevigate tetrads *Tetrahedraletes medinensis* are common, as well as unfused dyads *Dyadospora murusdensa* and *Dyadospora murusattenuata*. Fused dyads *Pseudodyadospora petasus* are present, along with a second species *Pseudodyadospora* cf. *laevigata*. The fused tetrad taxa *Cheilotetras caledonica* are also present in assemblage 4.

As seen in assemblage 5 *Laevolancis divellomedia*, a laevigate hilate taxon, is the single most common species found in assemblage 4. *Laevolancis plicata* is also present in smaller numbers. *Artemopyra* sp. A continues to be present from assemblage 5, and is joined by specimens of *Artemopyra* cf. *robusta*, (with distinctive radial muri on the proximal surface) in assemblage 4. Laevigate monads continue to be common from assemblage 5 to assemblage 4.

In comparison with assemblage 5, a greater percentage of cryptospores are sculptured in this assemblage (35.24% of the total assemblage compared to 9.16%, Figure 5.3*a* and *b*). There is an increase in the number of apiculate ornamented cryptospore taxa, which occur in both hilate and dyad form, and in one case an unfused tetrad. Together with *Acontotetras*, *Cymbohilates variabilis* var. *variabilis*, *Cymbohilates disponerus* and *Cymbohilates allenii* var. *magnus* that continue into assemblage 4 from assemblage 5, *Cymbohilates* cf. *microgranulatus*, *Cymbohilates allenii* var. *allenii*, *Cymbohilates* cf. *amplus* and *Cymbohilates variabilis* var. *parvidecus* all appear in assemblage 4.

Although the thin spinose sculptured *Cymbohilates* cf. *horridus* does not continue into assemblage 4 from assemblage 5, the taxa *Cymbohilates horridus* var. A appears in assemblage 4, with an evenly spaced, small spinose sculpture.

The verrucate sculptured *Hispanaediscus verrucatus* continues into assemblage 4 from assemblage 5, and is joined by *Hispanaediscus* cf. *verrucatus*, a species similar to *H. verrucatus*, but is larger, with verrucae to muri on the distal surface. Fused verrucate tetrads are also present in this assemblage. The murornate sculptured cryptospore *Chelinohilates erraticus* continues from assemblage 5 into assemblage 4, but *Chelinohilates* cf. *lornensis* does not. Two new species of *Chelinohilates* with irregular, sinuous muri appear in assemblage 4; *Chelinohilates sinuosus* var. *angustus* and *Chelinohilats sinuosus* var. *sinuosus*. *Chelinohilates* sp. A with the distinctive sculpture of pila superimposed upon reticulum also appears in assemblage 4.

There is an increase in the number of enveloped taxa from assemblage 5 to assemblage 4. Despite *Velatitetras* cf. *cristata* not appearing in assemblage 4, three other species of the enveloped tetrad genus *Velatitetras* are present; *Velatitetras* sp. B, with irregularly arranged

apiculate elements, *Velatitetras* cf. *reticulata*, with an irregular murornate sculpture and *Velatitetras rugulata*, with irregularly arranged low verrucae to rugulae elements.

Of the total assemblage, 9.7% are trilete spores (Figure 5.3*b*), with 6.17% being laevigate. The ratio between crassitate and retusoid triletes is 9.5:1. These include the continuation of retusoid triletes *Retusotriletes dittonensis* from assemblage 5, although *Retusotriletes* cf. *dittonensis* and *Retusotriletes* cf. *triangulatus* var. *minor* are not present. Laevigate crassitate triletes *Ambitisporites avitus* var. *minor*, *Ambitisporites dilutus* and *Ambitisporites warringtonii* continue from assemblage 5, although *Ambitisporites avitus* does not. The laevigate patinate species *Archaeozonotriletes chulus* var. *chulus* first appears in assemblage 4.

Of the sculptured triletes, no retusoid species were recorded. The crassitate, apiculate sculptured *Aneurospora* and index species *Streelispora newportensis* appear in assemblage 4, in monad and tetrad form. Only poorly preserved *Scylaspora* specimens were found and were not assigned to species level. Verrucate sculptured crassitate trilete taxa *Synorisporites tripapillatus* is recorded from assemblage 4. The patinate *Chelinospora* sp. continues from assemblage 5, but (?)*Perotrilites* does not. Two acritarchs are also recorded from assemblage 4.

Compared with the assemblage 5, the total spore diameter range is slightly larger, with 82% of spores with diameters under 40.0μm (Figure 5.4), with the largest spore being *Cymbohilates* cf. *amplus*, at 75.0μm, and the smallest being *Cymbohilates horridus* var. A, at 13.1μm.

Assemblage 3

Assemblage 3 was macerated from green planar-bedded medium-grained sandstones (lithofacies 2a from Chapter 6), at 11.80m beneath the quarry surface in core 1 (PB1 in Figure 6.1), approximately 52.7m above the Bishop's Frome Limestone. This assemblage has a cryptospore to trilete ratio of 2.9:1, which is lower than in assemblages 5 and 4 (Figure 5.3*c*). Twenty-two genera and 42 species are present.

Of the total assemblage, 40.70% are laevigate cryptospores, which is less than assemblages 4 or 5. The fused tetrads *Cheilotetras*, unfused tetrads *Tetrahedraletes medinensis*, fused dyads *Pseudodyadospora petasus* and *Pseudodyadospora* cf. *laevigata* and the unfused dyads *Dyadospora murusdensa* and *Dyadospora murusattenuata* continue from assemblage 4 into assemblage 3, but are reduced in numbers. As seen in assemblage 4 and 5, the single most common taxa in assemblage 3 is *Laevolancis divellomedia*, with only 2 specimens of

Laevolancis plicata. Laevigate monads are reduced in numbers from assemblage 5 to assemblage 3 (from 8.76% to 1.01% respectively). *Artemopyra* sp. A and *Artemopyra* cf. *robusta* do not continue from assemblage 4 into assemblage 3.

Of the total assemblage, 32.16% are sculptured cryptospores. Apiculate sculptured cryptospores are common; apiculate unfused tetrad *Acontotetras inconspicus* and hilate monads and dyads of *Cymbohilates allenii* var. *magnus*, *Cymbohilates allenii* var. *allenii*, *Cymbohilates disponerus*, *Cymbohilates* cf. *microgranulatus* and *Cymbohilates variabilis* var. *parvidecus* all continue from assemblage 4 into assemblage 3, although *Cymbohilates* cf. *amplus* does not. *Cymbohilates variabilis* var. *variabilis* is present, which was also seen in assemblage 5. The first occurrence of *Cymbohilates variabilis* var. B, with a highly irregular apiculate sculpture, is found in this assemblage. A specimen of the spinose sculptured *Cymbohilates horridus* var. A is also present in this assemblage.

Continuing from assemblage 4 and 5, this assemblage contains verrucate hilate monads *Hispanaediscus verrucatus*, but specimens of *Hispanaediscus* cf. *verrucatus* were not found. Fused verrucate sculptured tetrads are also present. The first appearance of the verrucate sculptured cryptospore taxa *Hispanaediscus wenlockensis* occurs in assemblage 3, with a sculpture of verrucae elements that are closely arranged, but do not fuse together.

The murornate sculptured *Chelinohilates erraticus* continues from assemblages 5 and 4, but specimens of *Chelinohilates sinuosus* var. *sinuosus*, *Chelinohilates sinuosus* var. *angustus* and *Chelinohilates* sp. A do not. The first occurrence in the sequence of fused murornate tetrads are found in this assemblage. Enveloped taxa are reduced in numbers from assemblage 4, and only *Velatitetras* cf. *reticulata* continuing into assemblage 3.

Of the total assemblage, 25.12% are trilete spores (Figure 5.3*c*). Unlike assemblages 5 and 4, there are more sculptured triletes than laevigate. The ratio between crassitate and,retusoid trilete spores is 1.9:1 i.e. there is an increase in the proportion of retusoid trilete spores from assemblages 5 and 4 to assemblage 3. Of the laevigate triletes, the retusoid taxa *Retusotriletes dittonensis* continues from assemblages 4 and 5, plus *Retusotriletes* cf. *dittonensis* is present, which was also found in assemblage 5. The laevigate crassitate triletes *Ambitisporites* cf. *avitus* var. *minor*, *Ambitisporites dilutus* and *Ambitisporites warringtonii* continue from assemblage 4, plus *Ambitisporites avitus* is present, which also occurs in assemblage 5.

Of the sculptured triletes, the first occurrence of apiculate sculptured retusoid trilete *Apiculiretusispora* sp. is found in this assemblage. The radially murornate sculptured *Emphanisporites* sp. B, last occurring in assemblage 5, is also present. Of the sculptured crassitate triletes, *Streelispora* *Aneurospora* is common, although there is no definitive

evidence for the index species *Streelispora newportensis*. Three specimens of *Scylaspora* are present, and are the first occurrences of *Scylaspora downiei* in the sequence. There is no evidence of *Synorisporites tripapillatus*, but poorly preserved *Synorisporites* sp. specimens are present. There are no patinate trilete spores present in this assemblage. Four acritarch specimens are also present.

Assemblage 3 has a slightly smaller spore diameter range than assemblage 4, with a larger proportion of smaller spores, and 88% of spores under 40.0μm in diameter (Figure 5.4), the largest spore being *Velatitetras* cf. *reticulata* with a diameter of 64.0μm, and the smallest being *Ambitisporites* cf. *avitus* var. *minor*, with a diameter of 11.3μm.

Assemblage 2

Assemblage 2 was macerated from green, fine-grained, trough-cross-bedded sandstones (lithofacies 2b in Chapter 6), at 11.28m beneath the quarry surface, from core 1 (see BH1-1 in Figure 6.1), which is approximately 53.22m above the Bishop's Frome Limestone. This assemblage has a cryptospore to trilete ratio of 3.74:1, which is lower than assemblages 5 and 4, but higher than assemblage 3. Nineteen genera and 47 species are present.

Of the total assemblage, 58.08% are laevigate cryptospores (Figure 5.3*d*). The fused tetrads *Cheilotetras*, unfused tetrads *Tetrahedraletes medinensis*, fused dyads *Pseudodyadospora petasus* and *Pseudodyadospora* cf. *laevigata*, and the unfused dyads *Dyadospora murusdensa* and *Dyadospora murusattenuata* continue from assemblages 5, 4 and 3. As seen in assemblages 5, 4 and 3 *Laevolancis divellomedia* is the single most common species. *Laevolancis plicata* specimens are also present. Apiculate sculptured cryptospores *Cymbohilates allenii var. allenii*, *Cymbohilates allenii var. magnus*, *Cymbohilates* cf. *microgranulatus*, *Cymbohilates variabilis* var. *variabilis* and *Cymbohilates variabilis* var. *parvidecus* all continue from assemblage 3 into assemblage 2, although *Cymbohilates disponerus*, *Cymbohilates variabilis* var. B and the apiculate tetrad *Acontotetras* do not. *Cymbohilates* cf. *amplus* is present, which also occurs in from assemblage 4. Of the spinose sculptured cryptospores, *Cymbohilates horridus* var. A continues from assemblage 3 to assemblage 2. The first appearance of *Cymbohilates horridus* occurs in this assemblage, in dyad form, with spines at least 5.0μm in length.

Of the verrucate sculptured cryptospores, fused verrucate tetrads and *Hispanaediscus verrucatus* continue from assemblage 3, although *Hispanaediscus wenlockensis* does not. However, two other species of *Hispanaediscus* first appear in this assemblage, *Hispanaediscus major*, sculptured with widely spaced, low verrucae that fuse together to

form rugulae, and *Hispanaediscus* cf. *major*, similar to *H. major*, but with more closely spaced elements.

Chelinohilates erraticus is still present in assemblage 2, along with *Chelinohilates* cf. *lornensis*, which also occurs in assemblage 5. However, no murornate sculptured fused tetrads are present as seen in assemblage 3.

The enveloped tetrad taxa *Velatitetras* cf. *reticulata* is not present in assemblage 2, but *Velatitetras* cf. *cristata*, *Velatitetras* sp. B and *Velatitetras rugulata* reappear in this assemblage. The first appearance of enveloped unfused dyads, *Abditusdyadus histosus*, with a low, regular polygonal reticulum, occurs in this assemblage.

Of the total assemblage, 20.77% of sporomorphs are triletes (Figure 5.3*d*) and 17.31% are laevigate triletes. The ratio between crassitate and retusoid triletes is 1.08:1, i.e. there is an increase in the proportion of retusoid spores from assemblage 3 to assemblage 2. Laevigate retusoid triletes *Retusotriletes dittonensis* and *Retusotriletes* cf. *dittonensis* continue from assemblage 3, and specimens of *Retusotriletes* cf. *triangulatus* var. *minor* reappear, together with the first occurrence of the larger *Retusotriletes* cf. *triangulatus*. The laevigate crassitate triletes *Ambitisporites avitus*, *Ambitisporites avitus var. minor*, *Ambitisporites dilutus*, and *Ambitisporites warringtonii* continue from assemblage 3. The first appearance of *Ambitisporites* sp. A occurs in this assemblage, a laevigate crassitate trilete with a dark apex. There are no laevigate patinate triletes present in this assemblage.

There are fewer sculptured triletes in assemblage 2 than assemblage 3 (3.46% compared to 14.57%, Figure 5.3*c* and *d*). The apiculate retusoid *Apiculiretusispora* sp. continues from assemblage 3. The first appearance of *Emphanisporites protophanus*, a retusoid trilete with radial muri on the sub-equatorial region of the proximal surface, occurs in this assemblage. However, no specimens of *Emphanisporites* sp. B were found. Of the sculptured crassitate trilete spores, only *Scylaspora downiei* is present, with no *Streelispora – Aneurospora* or *Synorisporites* specimens recorded. Two specimens of *?Perotrilites microbaculatus* are also present, which also occur in assemblage 5. Four acritarch specimens were also found in this assemblage.

The spore diameter range for assemblage 3 is similar to assemblage 4 (Figure 5.4), with 83% of spores under 40.0μm in diameter, the largest spore being *Cymbohilates* cf. *amplus* with a diameter of 80.0μm, and the smallest being an unclassified (?) enveloped spore with a clustered spinose sculpture, at a diameter of 14.7μm.

Assemblage 1

Assemblage 1, the youngest of the five assemblages, was macerated from green planar and cross-bedded fine-grained sandstones and siltstones (lithofacies 2b and 3a in Chapter 6), at the quarry surface (BH1-6 in Figure 6.1), which is approximately 62.5m above the Bishop's Frome Limestone. This assemblage has a cryptospore to trilete ratio of 4.38:1. Thirty-one genera and 61 species are present, and therefore is the most diverse of the five assemblages.

Of the total assemblage, 39.15% of sporomorphs are laevigate cryptospores, which is the smallest proportion compared with the four previous, older assemblages (Figure 5.3*a* to *e*). Fused tetrads *Cheilotetras*, unfused tetrads *Tetrahedraletes medinensis*, fused dyads *Pseudodyadospora* cf. *laevigata* and *Pseudodyadospora petasus*, and unfused dyads *Dyadospora murusdensa* and *Dyadospora murusattenuata* continue from assemblage 2 and are still common in assemblage 1. *Laevolancis divellomedia* is common, although is not the most single common cryptospore in the assemblage as seen in the previous four assemblage. *Laevolancis plicata* is also present in small numbers. Laevigate monads are reduced in numbers from assemblage 2.

Of the total assemblage, 41.47% of cryptospore are sculptured, which is higher than the previous four assemblages. Apiculate sculptured cryptospores are common, with *Cymbohilates allenii* var. *allenii*, *Cymbohilates allenii* var. *magnus*, *Cymbohilates* cf. *amplus*, *Cymbohilates variabilis* var. *variabilis* and *Cymbohilates variabilis* var. *parvidecus* continuing from assemblage 2 into assemblage 1, but *Cymbohilates* cf. *microgranulatus* does not. Specimens of *Cymbohilates disponerus* and *Cymbohilates variabilis* var. B return, which were found in assemblage 3.

Of the spinose sculptured cryptospores *Cymbohilates horridus* and *Cymbohilates horridus* var. A continue from assemblage 2 into assemblage 1. The first appearance of *Cymbohilates cymosus*, a spinose sculptured cryptospore in tetrad, dyad, or monad form, with radially arranged, star-shaped spines, is found in this assemblage.

Of the verrucate sculptured cryptospores, the fused verrucate tetrads and *Hispanaediscus verrucatus* continue from assemblage 2, although *Hispanaedisicus major* and *Hispanaediscus* cf. *major* do not. A tetrad of *Hispanaediscus wenlockensis* is present, which is also present in assemblage 3.

Of the murornate sculptured cryptospores, *Chelinohilates erraticus* continues from assemblage 2, and is the single most common species in this assemblage. However *Chelinohilates* cf. *lornensis* does not continue from assemblage 2 into assemblage 1.

Chelinohilates sinuosus var. *sinuosus* and *Chelinohilates* sp. A are present, which were also found in assemblage 4.

More enveloped taxa occur in assemblage 1 than any of the previous four assemblage. *Velatitetras* cf. *reticulata* specimens return, which were also found in assemblage 3. However *Velatitetras* sp. B, *Velatitetras* cf. *cristata* and *Velatitetras rugulata* did not continue from assemblage 2. The first appearance of the enveloped tetrad *Velatitetras* sp. C occurs in this assemblage, sculptured with closely and regularly spaced verrucate elements. The enveloped unfused dyad *Abditusdyadus histosus* continues from assemblage 2. A specimen of *Segestrespora* cf. *membranifera*, a fused dyad with a sculptured envelope of narrow, irregular muri, first appears in assemblage 1. Specimens of *Qualisaspora sinuata*, enveloped alete monads sculptured with radial muri from the equator to the pole, also appear in assemblage 1. Of the total assemblage, 17.44% are trilete spores (Figure 5.3*e*), and 10.85% are laevigate triletes. The ratio between crassitate and retusoid triletes is 5.6:1. The laevigate retusoid triletes are reduced in numbers from assemblage 2, with *Retusotriletes* cf. *dittonensis* continuing into assemblage 1, but not *Retusotriletes dittonensis*, *Retusotriletes* cf. *triangulatus* and *Retusotriletes* cf. *triangulatus* var. *minor*. Of the laevigate crassitate triletes, *Ambitisporites avitus*, *Ambitisporites avitus* var. *minor*, *Ambitisporites dilutus* and *Ambitisporites warringtonii* continue into this assemblage from assemblage 2, but not *Ambitisporites* sp. A. Laevigate patinate triletes reappear, with the first appearance of two varieties of *Archaeozonotriletes chulus*: *Archaeozonotriletes chulus* var. *nanus*, a smaller variety, and *Archaeozonotriletes chulus* var. *inframurinatus*, with faint radial muri on the proximal surface.

Of the sculptured cryptospores, no specimens of *Emphanisporites* or *Scylaspora* continue into assemblage 1. Apiculate retusoid trilete *Apiculiretusispora* sp. continues from assemblage 2. The apiculate crassitate triletes *Streelispora* – *Aneurospora* reappear, in particular the index species *Streelispora newportensis*, which was also found in assemblage 4. A specimen of *Synorisporites triapapillatus* was also found in this assemblage, which was also found in assemblage 4. Specimens of the sculptured patinate trilete *Chelinospora* also reappears, and are also found in assemblage 4. The sculptured triletes with a perispore, (?)*Perotrilites microbaculatus* continue from assemblage 2. 5 acritarch specimens are also found in this assemblage.

The spore diameter range is the largest of the five assemblages, with 68% of spores under 40.0μm in diameter (see Figure 5.4). The largest spore is *Cymbohilates* cf. *amplus*, with a

diameter of 86.6μm, and the smallest spore is *Cymbohilates disponerus*, with a diameter of 16.8μm.

5.4.2: *Age of Tredomen Quarry strata*

It is the presence of certain trilete and cryptospore species that allow an age for the sequence to be determined. The presence of key index species *Streelispora newportensis* in assemblage 1 and assemblage 4 is characteristic of the *micrornatus-newportensis* (MN) spore assemblage biozone, of the early Lochkovian (Richardson and McGregor 1986). This assemblage is only known in the Anglo-Welsh Basin to occur only above the Bishop's Frome Limestone horizon, which is thought to be lowermost Lochkovian in age (see Table 1.1, Chapter 1). The absence of *Emphanisporites micrornatus* Richardson and Lister 1969 suggests that this assemblage is characteristic of the lower MN sub-biozone, as *Emphanisporites micrornatus sensu stricto* is not present until the middle MN sub-biozone (Richardson and McGregor 1986).

The abundance of sculptured hilate cryptospores also supports an early Lochkovian age. Prior to the latest Přídolí, cryptospore assemblages from the Wenlock of Shropshire were predominantly composed of laevigate genera, such as *Laevolancis*, *Dyadospora* and *Tetrahedraletes medinensis*, with only two genera of sculptured hilate cryptospores, *Hispanaediscus* and *Artemopyra* (Burgess and Richardson 1991). However, the appearance of a number of murornate and apiculate sculptured hilates, including *Chelinohilates erraticus* and *Cymbohilates allenii* occurs in the uppermost Přídolí strata from Shropshire (Richardson 1996a). In particular, *Cymbohilates horridus*, *Cymbohilates variabilis*, *Cymbohilates allenii* var. *magnus* and *Cymbohilates disponerus* are known from the Lochkovian St. Maughans Formation strata only.

Considering both trilete and cryptospore components, the Tredomen Quarry strata are placed in the lower (possibly lowermost) *micrornatus-newportensis* spore assemblage sub-biozone of early Lochkovian (Dittonian) age.

5.4.3: *Comparisons with other Late Silurian - Early Devonian assemblages*

Anglo-Welsh Basin

When defining the Silurian and Devonian spore biozones, Richardson and McGregor (1986) used the Ross-Tewkesbury Spur Motorway section (M50) as the reference section of the base

of the *micrornatus-newportensis* biozone, which is coincident with the top Bishop's Frome Limestone, and is close to, but slightly above the Silurian-Devonian boundary (Richardson et al. 2000). Assemblages from Brown Clee Hill strata represent the lower to the upper MN biozone (Richardson and Lister 1969, Richardson 1996a).

Beneath the Bishop's Frome Limestone, uppermost Raglan Mudstone Formation assemblages from Hereford and Worcester have been described by Holland and Richardson (1977) as distinctively different from the lower MN biozone, which does not contain *Streelispora newportensis*, but an unpublished species of *Apiculiretusispora* sp. This zone was later to be defined as the *Apiculiretusispora* sp. E zone (Richardson et al. 2000), and is thought to be lowermost Lochkovian in age. In the Ross-Tewkesbury Spur Motorway section (M50), assemblages directly below the Bishop's Frome Limestone, at the top of the *Apiculiretusispora* sp. E zone, specimens of non-papillate *Aneurospora* appear, and Richardson named this sub-biozone the *Aneurospora* Zone (Richardson et al. 2001) in correlation with Cantabrian sequences.

Barclay et al. (1994) describe assemblages from Ammons Hill near Worcester and, like the upper Tredomen Quarry sequences, *Streelispora newportensis* is present, but *Emphanisporites micrornatus* is not, placing the assemblage in the lower MN sub-biozone. Unlike Tredomen Quarry however, the Ammons Hill assemblages contain more acritarch species, which are thought to be *in situ*, and along with evidence from brackish bivalves and vertebrate remains, it has been hypothesised that Ammons Hill was coastal or was subjected to marine incursions (Barclay et al. 1994). The acritarchs from the Tredomen Quarry assemblage are mainly known from the Ludlow, and are likely to have been reworked.

Chaloner and Streel (1968) describe an assemblage from 'Ditton Group' strata just above the Bishop's Frome Limestone, near Newport. As observed in the Tredomen Quarry sequences, *Streelispora newportensis* was present, but *Emphanisporites micrornatus* was not, placing this assemblage in the lower MN zone.

In 2000, Wellman et al. described an assemblage from Bryn-Glas Tunnels, near Newport, South Wales, which is part of the St. Maughans Formation. This assemblage is similar to Tredomen Quarry, containing *Streelispora newportensis*, an abundance of *Chelinohilates erraticus*, and granulate to verrucate sculptured cryptospores such as *Cymbohilates variabilis* var. *variabilis*. However, the Bryn Glas assemblage also was found to contain *Emphanisporites micrornatus*, placing this assemblage in slightly younger middle MN biozone.

In 2004, Higgs described an assemblage from the Freshwater West Formation, Pembrokeshire, South-West Wales, and was found to contain both *Streelispora newportensis* and two varieties of *Emphanisporites micrornatus*, and therefore was assigned to the mid-MN biozone.

Scotland

Wellman and Richardson (1996) described an assemblage from the Lower Old Sandstone from Lorne, Scotland. The presence of *Aneurospora geikiei* Wellman and Richardson (1996) indicated that the assemblage was at least Early Devonian in age, as no crassitate trilete spores with distinct spinose sculpture are known from the Silurian. Due to absence of *Streelispora newportensis* and *Emphanisporites micrornatus*, Wellman and Richardson (1996) suggested the assemblage belongs to the *Apiculiretisispora* sp. E biozone, the pre-MN biozone which is earliest Devonian in age, but pre-Gedinnian (Table 1.1, Chapter 1).

Richardson et al. (1984) described assemblages from Lower Old Red Sandstone strata from the Strathmore region (Arbuthnott Group), as typical of the lower to middle *micrornatus-newportensis* biozone as defined by the assemblages from the Anglo-Welsh Basin and included: *Chelinospora cassicula* Richardson and Lister (1969); *Emphanisporites epicautus* Richardson and Lister (1969); *Qualisaspora fragilis* Richardson et al. (1984); *Retusotriletes* cf. *trianguluatus* Richardson and Lister (1969); and *Aneurospora* sp. A. However, other species (e.g. ?*Dibolisporites* sp. A and ?*Samarisporites* sp. A) which have not be described from the Anglo-Welsh Basin, exhibit features that are not found in other areas until the Pragian.

Europe

During the Early Devonian, the Ardennes-Rhenish region was in a nearshore shallow marine environment, south of the Old Red Sandstone Continent (see Figure 1.2). The oldest known Devonian assemblages were described by Steemans (1989), and have similarities with the lower *micrornatus-newportensis* biozone of the Anglo-Welsh Basin, and therefore were assigned to the early Gedinnian.

The Cantabrian Mountains of northwest Spain were also covered by a shallow sea during the Late Silurian to Early Devonian, and strata contain terrestrially derived sporomorphs. Richardson et al. (2000) and Richardson et al. (2001), described assemblages in which the Silurian-Devonian boundary was identified using chitinozoans and spores, and new biozones were erected for Přídolí strata, including the pre-MN biozone *Scylaspora elegans-*

Iberoespora cantabrica. The upper part of this assemblage, the *Aneurospora* sub-biozone has also been recognised in the Anglo-Welsh Basin within the Raglan Mudstone Formation.

Through the comparisons with contemporaneous assemblages from Scotland and Europe, the Tredomen Quarry dispersed spore assemblages can be considered as typical of assemblages from across Laurussia during the uppermost Přídolí and lower Lochkovian.

5.5: PALAEOECOLOGICAL TOOL: COMPARISONS WITH PUBLISHED *IN SITU* SPORES

Palynomorphs have a higher preservation potential than their parent plants, due to their composition (see section 5.1). Therefore, palynomorphs could be considered to be a better representation of plant diversity than the parent plant fossils. To determine the possible parent plant diversity in the river catchment area, the palynomorph species present in the Tredomen Quarry sequence that have also been found *in situ*, are listed in Table 5.3. The parent plants indicated by the palynomorphs are indicative of the Late Silurian to Early Devonian, including the plant species described in section 3.2, Chapter 3. Of the megafossils, additional species include; *Caia langii* (Fanning et al. 1990), cf. *Horneophyton* sp. (Edwards and Richardson 2000), *Cooksonia banksii* (Fanning et al. 1988) and *Cooksonia pertoni* ssp. *pertoni* (Lang 1937 emend. Fanning et al. 1988, Habgood et al. 2002). Of the mesofossils, additional species include: *Grisellatheca salopensis* (Edwards et al. 1999), *Fusitheca fanningiae* (Wellman et al. 1998a), *Culullitheca richardsonii* (Wellman et al. 1998a) and *Resilitheca salopensis* (Edwards et al. 1995b).

Table 5.3 indicates that during the Late Silurian and Devonian around the Brecon Beacons area, the embryophytes were more diverse than indicated by the megafossils alone. However, this approach to determining diversity does have set backs. It is often the case that the same spore taxa can be found in different parent plants e.g. *Retusotriletes* sp. can be found in *Caia langii* (Fanning et al. 1990), *Salopella* sp. (Fanning et al. 1991), *Resilitheca salopensis* (Edwards et al. 1995b), *Tarrantia salopensis* (Edwards 1996) and even *Zosterophyllum* sp. (Edwards 1969a). Alternatively, different spore taxa can be found in the same parent plant species, e.g. *Cooksonia pertoni* has been separated into four subspecies purely on the *in situ* spore taxa, despite the overall morphology of the parent plant being the same (Fanning et al.1988, Habgood et al. 2002). *In situ* spores are often classified to genus level only, due to the poor preservation of specimens. For these reasons, diversity studies using palynomorphs cannot be used in isolation, and evidence from megafossils is also required.

Table 5.3: Comparisons between Tredomen Quarry assemblages and published *in situ* spores.

		Spore species	Parent plant	Formation; Age	Reference
Cryptospores	*Fused laevigate*	*Cheilotetras caledonica*	*Grisellatheca salopensis* (bifurcating mesofossils).	St Maughans Formation; middle Lochkovian.	Edwards et al. 1999
		Pseudodyadospora petasus	*Fusitheca fanningiae* (mesofossil with elongate sporangium	St Maughans Formation; middle Lochkovian.	Wellman et al. 1998a
	Unfused laevigate	*Tetrahedraletes medinnensis*	Bifurcating mesofossil (NMW98.23G.2)	St Maughans Formation; middle Lochkovian.	Wellman et al. 1999
		Dyadospora murusdensa	*Culullitheca richardsonii* (mesofossils beaker-shaped sporangium)	St Maughans Formation; middle Lochkovian.	Wellman et al. 1998a
	Hilate laevigate	*Laevolancis divellomedia*	Spore masses and discoidal and elongate sporangia.	Downton Castle Formation/ St Maughans Formation; lower Přídolí to middle Lochkovian.	Wellman et al. 1998b
	Hilate sculptured	?*Cymbohilates* cf. *horridus* (dyads)	Saucer-shaped sporangium attached to bifurcating axis-mesofossil.	St Maughans Formation; middle Lochkovian.	Habgood 2000
		?*Cymbohilates disponerus*	*Salopella* cf. *marcensis*	St Maughans Formation; middle Lochkovian.	Edwards et al. 1994, Richardson 1996a
	Enveloped	*Velatitetras* (similar to *Velatitetras* sp. B)	Discoidal spore mass (NMW98.23G.1)	Downton Castle Formation; lower Přídolí	Edwards et al. 1999
		Velatitetras (similar to *Velatitetras* sp. B)	Bifurcating mesofossil axis with basal sporangium remaining (NMW96.11G.3).	St Maughans Formation; middle Lochkovian	Edwards et al. 1999
		Velatitetras sp.	Elongate, fusiform sporangium (NMW99.19G.2)	St Maughans Formation; middle Lochkovian	Habgood 2000

Table 5.3: Comparisons between Tredomen Quarry assemblages and published *in situ* spores (continued).

Triletes	*Retusoid laevigate*	*Retusotriletes* sp.	*Caia langii*	Downton Group; lower Přídolí	Fanning et al. 1990
		Retusotriletes sp.	*Salopella* sp.	Downton Group; lower Přídolí	Fanning et al. 1991b
		Retusotriletes sp.	*Resilitheca salopensis*	St Maughans Formation; middle Lochkovian	Edwards et al. 1995b
		?*Retusotriletes*.	*Tarrantia salopensis*	St Maughans Formation; middle Lochkovian	Edwards 1996
		Retusotriletes sp.	*Zosterophyllum* sp. cf. *Zosterophyllum fertile*	Senni Formation, Pragian	Edwards 1969a
	Retusoid sculptured	*Apiculiretusispora* sp.	cf. *Cooksonia caledonica*	St Maughans Formation; lower Lochkovian	Fanning et al. 1992
		Apiculiretusispora sp.	*Cooksonia hemisphaerica*	St Maughans Formation; lower Lochkovian	Fanning et al. 1992
		Apiculiretusispora sp.	*Tortilicaulis transwalliensis*	St Maughans Formation; lower Lochkovian	Fanning et al. 1992
		?*Apiculiretusispora* sp.	*Resilitheca salopensis*	St Maughans Formation; middle Lochkovian	Edwards et al. 1995b
		Emphanisporites (cf. *micrornatus*)	cf. *Horneophyton* sp.	St Maughans Formation; middle Lochkovian	Edwards and Richardson 2000
	Crassitate laevigate	*Ambitisporites avitus*	*Cooksonia banksii*	St Maughans Formation; middle Lochkovian	Fanning et al. 1988
		Ambitisporites sp.	*Cooksonia pertoni* ssp. *pertoni*	Downton Group; lower Přídolí	Lang 1937 emend. Fanning et al. 1988, Habgood et al. 2002
		?*Ambitisporites* sp.	*Cooksonia cambrensis*	Downton Group; lower Přídolí	Fanning et al. 1991b

Table 5.3: Comparisons between Tredomen Quarry assemblages and published *in situ* spores (continued).

Triletes	*Crassitate sculptured*	*Streelispora newportensis / Aneurospora*	*Cooksonia pertoni* ssp. *apiculispora*	St Maughans Formation; middle Lochkovian	Fanning et al. 1988
		?*Aneurospora* sp.	*Salopella* cf. *marcensis*	St Maughans Formation; middle Lochkovian	Edwards et al. 1994
		Scylaspora sp.	Elongate sporangia/ spore masses	St Maughans Formation; lower Lochkovian	Wellman 1999
		Synorisporites (*verrucatus*)	*Cooksonia pertoni* spp. *synorispora*	Downton Group; lower Přídolí	Fanning et al. 1988
		Synorisporites tripapillatus	Discoidal spore mass	Downton Group; lower Přídolí	Fanning et al. 1991b
		?*Synorisporites/ Chelinospora*	*Cooksonia pertoni* ssp. *reticulispora*	St Maughans Formation; middle Lochkovian	Habgood et al. 2002
	Patinate	?*Perotriletes microbaculatus*	*Salopella allenii*	St Maughans Formation; middle Lochkovian	Edwards and Richardson 1974

However, the dispersed spore record from Tredomen Quarry does supports the megafossil record in the theory that during the lower Lochkovian embryophyte diversity within the Anglo-Welsh Basin was limited to the rhyniophytoids, rhyniophytes and the cryptospore-producers (which included the stem-group embryophytes with bryophytic characters) (see Chapter 3 discussion).

5.6: PALYNOFACIES

Palynomorphs are not only useful for biostratigraphy and diversity studies, but also for determining the broad habitat of their parent plants, and the possibility of recognising major shifts of these environments (Richardson 1984, Richardson and Rasul 1990). The assemblages that have been described from Tredomen Quarry sequence in section 5.2, are allochthonous in nature. The spores were dispersed from the original parent plants, transported by water or wind into the river systems, to be deposited along with the host sediment some distance downstream. The assemblages therefore represent the general overall diversity of the river catchment area, both from the riverbanks and the distal floodplain, and so distribution patterns cannot be used to distinguish between these two possible habitats. However, distribution patterns and relative abundances of palynomorphs integrated with sedimentological information (the creation of palynofacies) may give clues to the broad distribution patterns of their parent plants between contemporaneous localities or regions within the basin.

Recently Richardson (2002, 2007) tested this hypothesis by comparing the relative abundance and distribution of palynomorphs and determining palynofacies from three Anglo-Welsh Basin contemporaneous localities: Ammons Hill section, Ross to Tewkesbury Spar M50 motorway section and Brown Clee Hill section (see Figure 1.2, Chapter 1) (Richardson 2007). According to their palynological assemblages, these sequences span the uppermost Raglan Mudstone Formation (latest Přídolí to earliest Lochkovian) into the St. Maughans Formation (MN sub-biozones, early Lochkovian), and are therefore contemporaneous with the Tredomen Quarry assemblage.

Richardson (2007) determined that the relative abundance of spore morphotypes reflect the broad environmental setting (Figure 5.5*a-c*). At Ammons Hill, sequences of uppermost Raglan Formation and lower St. Maughans Formation are typical of the Old Red Sandstone (Barclay et al. 1994). However, it is the only known sequence in the Anglo-Welsh Basin with evidence of a marine influence above the Bishop's Frome Limestone (Barclay et al. 1994),

Figure 5.5: Relative abundance of palynomorph morphotypes from the latest Přídolí to the early Lochkovian across the Anglo-Welsh Basin. Modified after Richardson 2007.

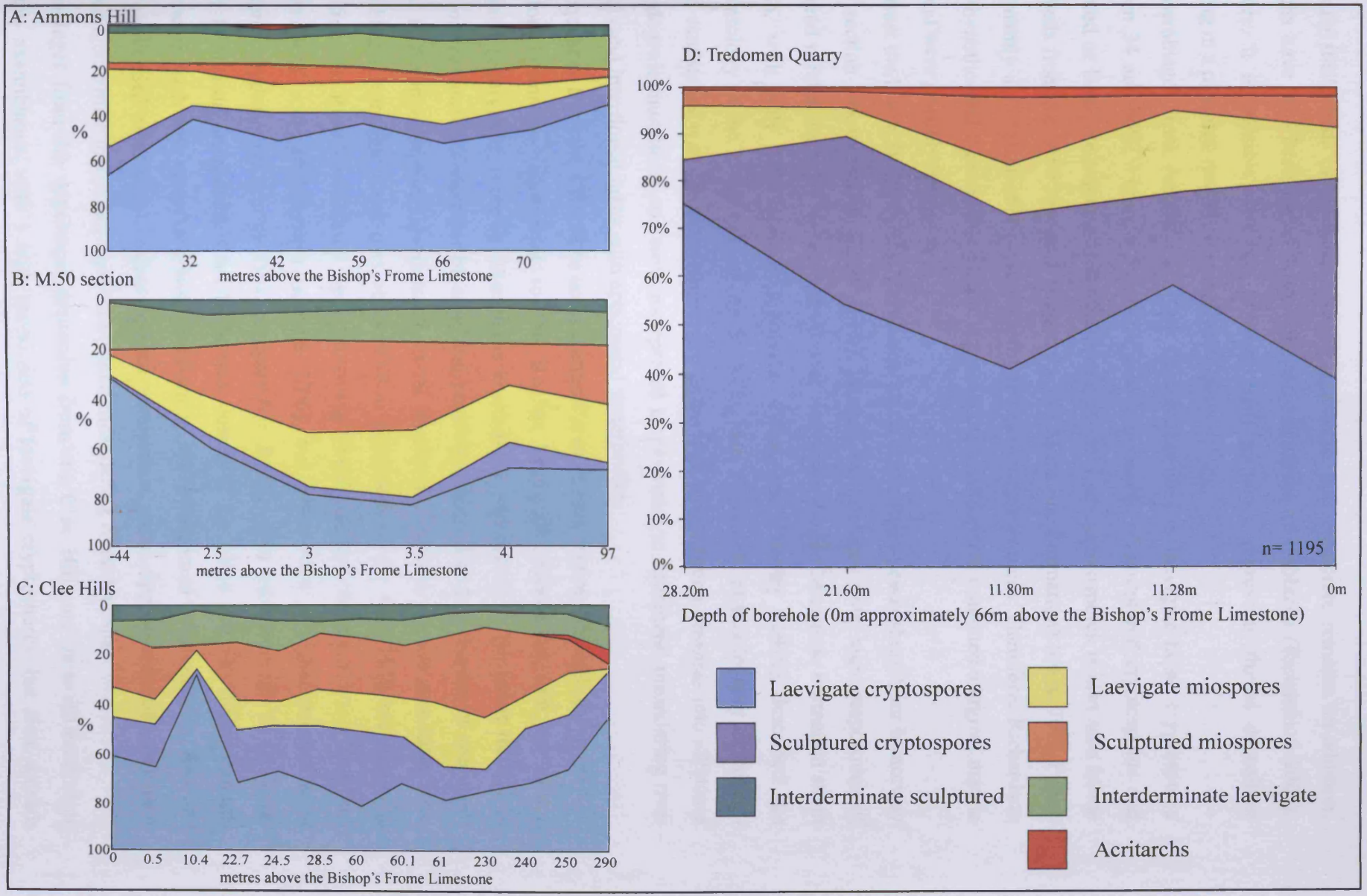

containing shelly beds of brackish bivalves, ostracods and vertebrate remains. In addition, acritarchs have also been found within the palynological assemblages (Richardson 2007). Therefore, it is possible that the Ammons Hill sequence represents fluvial deposition occurring in a marginal marine, distal alluvial plain setting.

The assemblages from Ammons Hill are highly abundant in laevigate hilate cryptospores (between 34 and 66%, Figure 5.5*a*), with low abundances of sculptured cryptospores and sculptured or laevigate triletes. This abundance of laevigate cryptospores is also seen in the lower beds from the M50 sequence (upper Raglan Mudstone Formation) (up to 70%, Figure 5.5*b*), mainly as a result of the presence of the genus *Laevolancis*. Therefore, Richardson (2007) hypothesised those plants producing laevigate cryptospores inhabited marginal marine areas and were possibly halophytic.

In contrast the lower St. Maughans Formation strata at the Ross-Tewkesbury Spur Motorway (M50) section (above 0m in Figure 5.5*b*), contain assemblages with high proportions of sculptured triletes (up to 37%), compared with the upper Raglan Mudstone Formation strata beneath, with only 1% sculptured triletes. Allen and Dineley (1976) described the sedimentology of the lower part of the St. Maughans Formation at this locality as thickly-bedded sandstones with intraformational conglomeratic bases, fining upwards into siltstones and pedogenic mudstones and were interpreted as perennial to ephemeral meandering river channels and interfluvial areas with ephemeral waterbodies.

The sequences from the Clee Hills are a composite of stream sections through the upper Red Downton Formation (equivalent to the Raglan Mudstone Formation) into the Ditton Formation (equivalent to the St. Maughans Formation), and belong to the lower through to upper *micrornatus-newportensis* biozone and possibly above, with the presence of specimens similar to *Emphanisporites zavallatus*, a zonal species for the *breconensis-zavallatus* zone. Assemblages from the lower part of the Ditton Formation of the Clee Hills are similar to those from the Ross-Tewkesbury Spur Motorway (M50) section (Figure 5.5*c*), with a high proportion of sculptured triletes (around 20%), but differ with a higher proportion of sculptured cryptospores (up to 25%, compared to 2-3%). The sedimentology of the lower Ditton Formation around the Clee Hills was described by Allen (1974b) fining upwards cyclothems, each with an erosive base, overlain by intraformational conglomerates, followed by cross-bedded sandstones, planar-bedded sandstones, cross-ripple-laminated sandstones and pedogenic mudstones, and were interpreted meandering river deposits.

Assemblages from the uppermost sequences from the Clee Hills are quite different from previous assemblages, with a high proportion of laevigate cryptospores, but alete monads

rather than hilates. The proportion of sculptured cryptospores remains similar to the lower sequence from the Clee Hills (around 20%), but there is a dramatic drop in the proportion of laevigate and sculptured triletes. Compared with all other assemblages, there is a high proportion of acritarchs, although unlike those from Ammons Hill assemblages, these acritarchs are older and are thought to be reworked from older strata.

Allen (1974b) describes a decrease in the proportion of cross-laminated sandstones and pedogenic mudstones up through the Clee Hills sequences (into the middle to upper MN biozones), with coarser-grained planar-bedded and cross-bedded sandstones and intraformational conglomerates being more prominent, which suggests a more proximal alluvial plain setting compared to the lower Clee Hills sequences and the M50 sequences. Richardson (2007) suggests that plants producing alete monads and sculptured cryptospores such as *Emphanisporites* inhabited these more upland areas of the basin. The presence of reworked acritarchs suggests uplift and erosion of older strata in the region, which supports the proximal alluvial plain setting.

In comparison, the assemblages from lower Tredomen Quarry sequence (lowermost Dittonian) have a high proportion of laevigate cryptospores, ranging from laevigate hilates, unfused dyads and unfused tetrads and alete monads. *Laevolancis* is particularly prominent in the oldest assemblage (28.20m), similar to those assemblages from Ammons Hill. However, in the upper Tredomen Quarry sequence the proportion of sculptured cryptospores becomes increasingly prominent (41.5% at the surface). The proportion of sculptured triletes is low compared with Clee Hills and the M50 sections, but higher than at Ammons Hill. The acritarchs are likely to have been reworked from older strata.

As described in Chapter 6, the sedimentology of the Tredomen Quarry sequence comprise fining upwards packages of intraformational conglomerates, cross-bedded sandstones, cross-laminated siltstones, wavy-laminated siltstones and pedogenic mudstones. An increase in sandstone packages is seen up through the sequence (Figure 6.1). A two-stage possibly perennial sandy meandering river system has been envisaged for the lower Dittonian. The palynomorphs indicate that during the uppermost Downtonian to lowermost Dittonian, Tredomen Quarry was located in a medial alluvial plain setting, followed by a shift closer to a proximal plain setting, with an influx of sculptured cryptospores.

Figures 5.6 to 5.8 are broad palaeogeographic reconstructions for the uppermost Downtonian, lowermost Dittonian and lower Dittonian, modified after Barclay et al. (1994, figures 1.4*b* and *c*), showing the modern day outline of Wales, and incorporating palynological data and

Figure 5.6: Palaeogeography for the upper Downtonian (directly below the Bishop's Frome Limestone, uppermost Přídolí to lowermost Lochkovian) based on palynofacies.

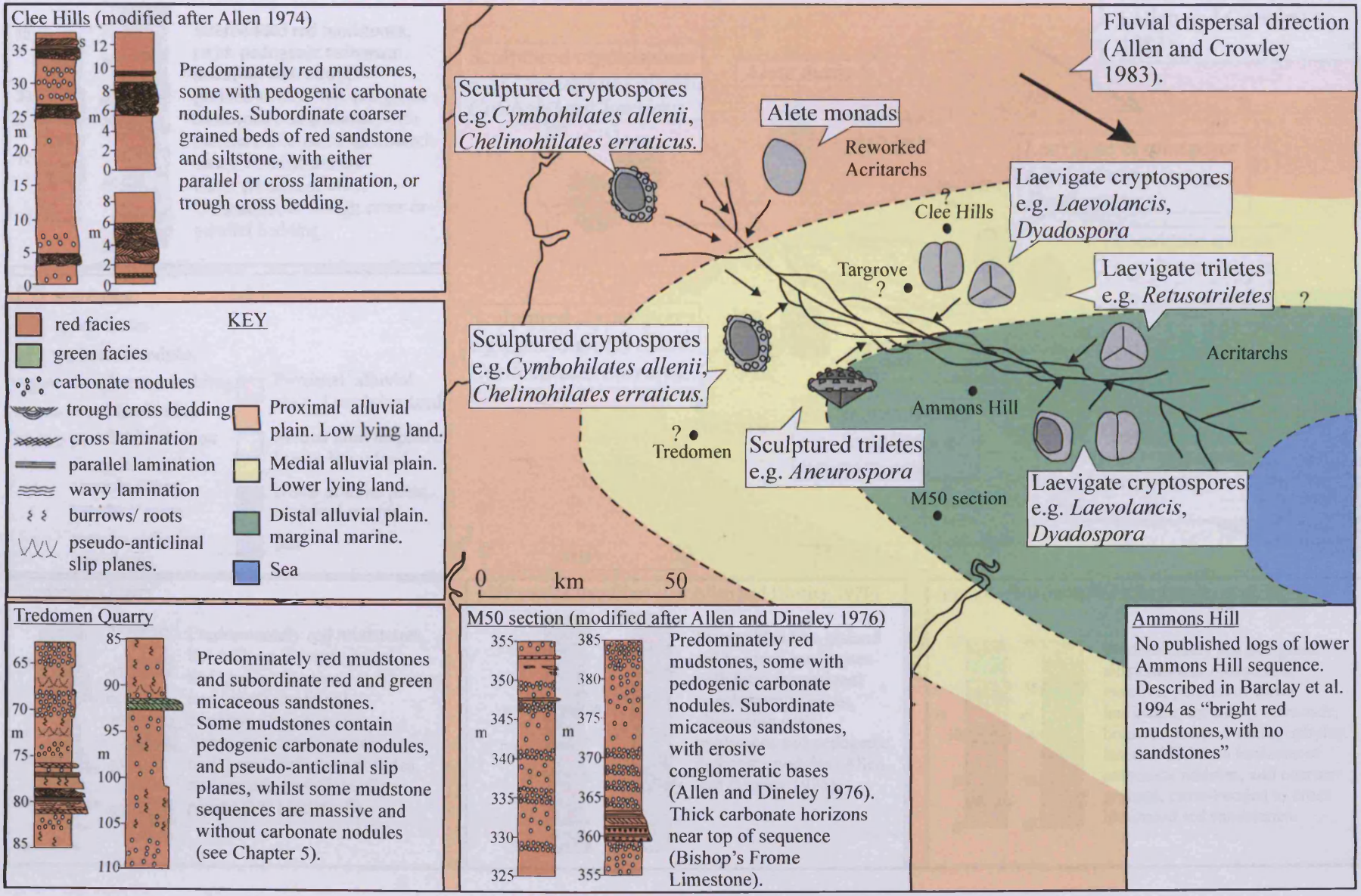

Figure 5.7: Palaeogeography for the lowermost Dittonian (Lochkovian) based on palynofacies.

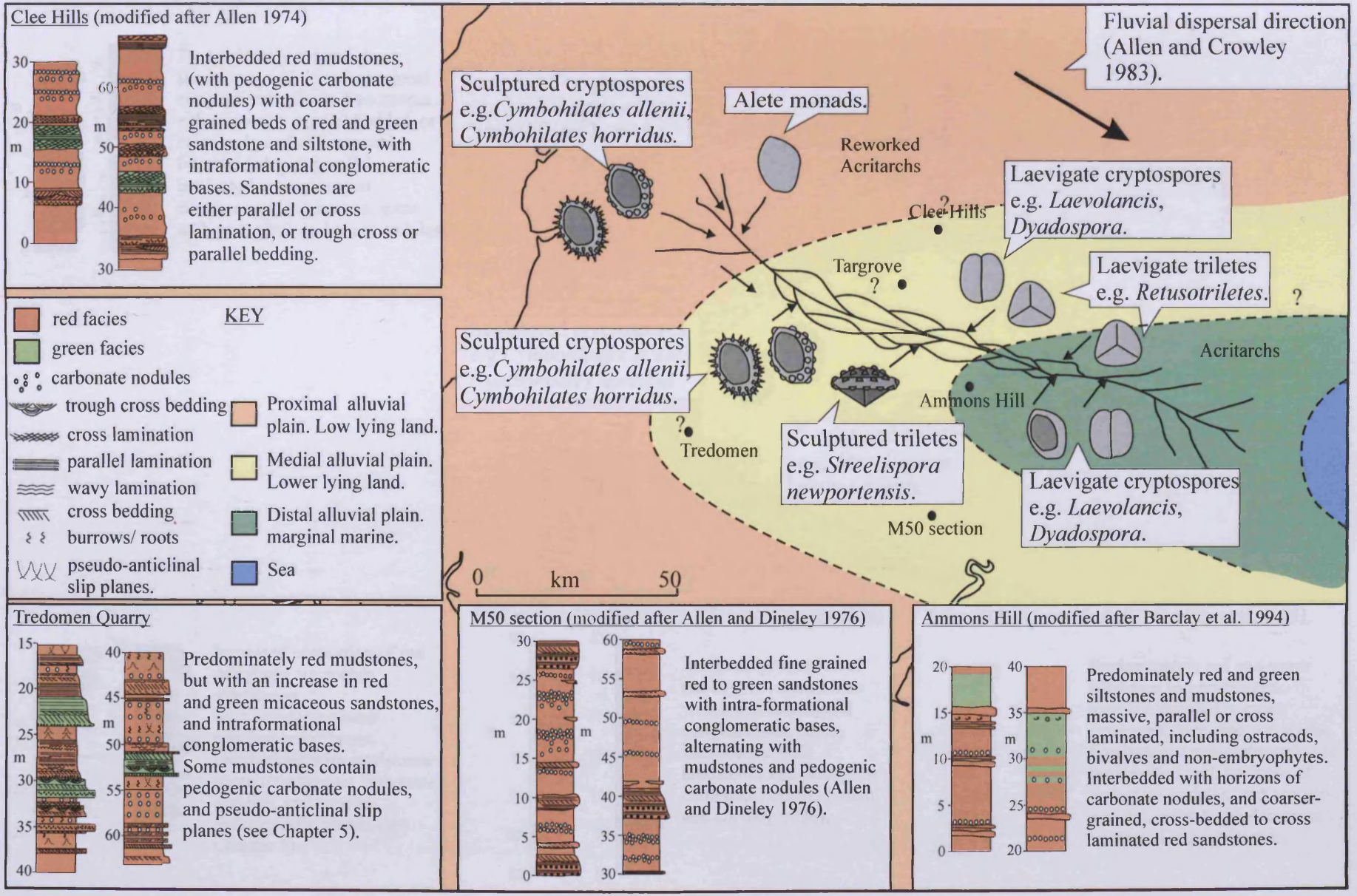

Figure 5.8: Palaeogeography for the lower Dittonian (Lochkovian) based on palynofacies.

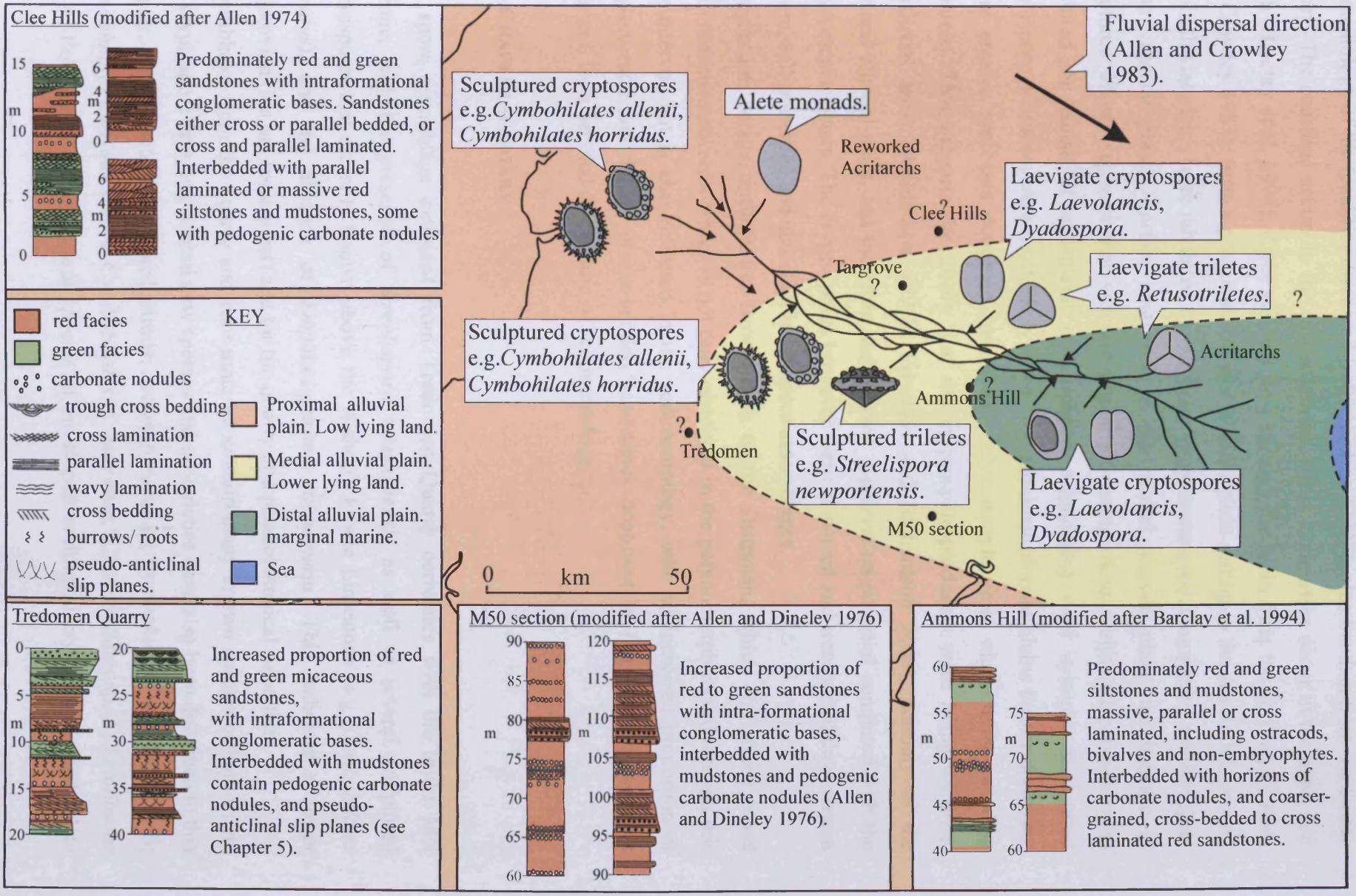

sedimentology of the localities discussed in Richardson (2007), plus the data from Tredomen Quarry. The coastline occurs to the east-southeast, while landmasses occur in the north and south (Barclay et al. 1994). River systems flow through the basin from the northwest (Allen and Crowley 1983), from a proximal to distal alluvial plain setting to the sea. In this model, distal alluvial plains were inhabited by laevigate cryptospore-producing plants, and laevigate trilete vascular plants. Further upstream, in the medial alluvial plain, the increase in sculptured triletes suggests that vascular plants producing these sculptured palynomorphs inhabited the banks of ephemeral or perennial meandering river systems. Sculptured cryptospore producers were most likely inhabiting proximal alluvial plains further upstream, where erosive processes dominant, reworking palynomorphs from older strata including acritarchs. This supports the theory that the cryptospore-producers were living on drier, interfluvial areas (Richardson 1996b, Edwards and Richardson 2000), possibly of the proximal alluvial plain, and therefore had a lower preservation potential compared with the early vascular plants. The cryptospores however were dispersed and transported downstream and are well-preserved and abundant in all spore assemblages.

A regression occurs through the Downtonian to the Dittonian, which shift these broad environments eastwards, which is not only observed in the palynomorph record through this time interval, but is also reflected in the sedimentology, with an increased proportion of conglomeratic and thickly planar-bedded sandstones deposited in fast flow regimes (see Chapter 6 for a detailed description of sedimentology).

5.7: CHAPTER SUMMARY

The spore assemblage extracted from Tredomen Quarry correlates with the lower MN biozone, with the presence of *Streelispora newportensis* as well as several sculptured cryptospores that are only known above the Bishop's Frome Limestone (e.g. *Cymbohilates horridus*), and the absence of *Emphanisporites micrornatus*. This indicates a lower Lochkovian (but not lowermost) age for the quarry and palaeobotanical collection.

Assemblages from the quarry and core material contain many known species of both trilete and cryptospore taxa, but several new species and or varieties have also been described in this chapter, namely: sculptured fused tetrads; *Artemopyra* sp. A; *Cymbohilates variabilis* var. B; *Cymbohilates horridus* var. A; *Cymbohilates* cf. *horridus*; ?*Chelinohilates* sp. A; *Velatitetras* sp. B; *Velatitetras* sp. C; several species of enveloped sculptured cryptospores; and trilete

species *Retusotriletes* cf. *triangularis* var. *minor*, *Ambitisporites avitus* var. *minor* and *Ambitisporites* sp. A.

Broad changes in palynomorph exoexine are observed through the five assemblages from Tredomen Quarry. Sculptured cryptospores not only become more prominent within the assemblages, but become more diverse, especially in terms of the sculptural elements. In assemblage 5, sculptured cryptospores are mostly apiculate with grana or verrucae elements, or are murornate. The new species, *Cymbohilates* cf. *horridus* with thin bacula or pila is the only suggestion of a spinose sculpture. However in assemblage 4, *Cymbohilates horridus* var. A appears, a variety with small spines, which appears to pre-date *Cymbohilates horridus senso stricto*, which is not found until assemblage 2, where it occurs in dyad form.

The adaptive significance of a sculptured exoexine is not fully understood, but it has been hypothesised that these elements may have been adaptations for improvements in wind dispersal, defence against fauna or germination (Fanning et al. 1988, Edwards and Richardson 1996, Burgess and Richardson 1999). Therefore, the increased diversity of sculptured cryptospores during the lower Lochkovian may be related to improving spore survival, which fits into the theory that changes to sporangia and branching characteristics observed in rhyniophytoid and rhyniophyte megafossils between the lower Přídolí and lower Lochkovian were adaptations for improving the quantity and effectiveness of spore dispersal, as a result of competition (see Chapter 3 discussion).

When compared to the *in situ* spore record, the assemblages described here have also given clues to the possible plants inhabiting this river catchment during the Lower Lochkovian. The possible parent plants indicated by the dispersed record are typical of this time interval, and although the dispersed spore record indicates more diversity of the embryophytes (including *Caia langii*, cf. *Horneophyton* sp., *Cooksonia banksii* and *Cooksonia pertoni* ssp. *pertoni*), the highest grade of organisation still remains the rhyniophytes and the rhyniophytoids (see Chapter 3).

Comparative studies with the work of Richardson (2007) on palynofacies and the possible habitats of the parent plants from contemporaneous localities has suggested that Tredomen Quarry was most likely to have been located in a medial alluvial plain setting through the Downtonian to Dittonian, due to high proportion of sculptured cryptospores, but also the presence of lavigate cryptospores and laevigate and sculptured triletes. An increase in sculptured cryptospores into the Dittonian suggests a shift closer to a proximal alluvial plain setting, as a result of regression. The presence of reworked acritarchs suggests uplift and erosion of older strata, possibly Ludlow in age, further upstream during this time interval.

CHAPTER 6 : LOWER DEVONIAN OLD RED SANDSTONE DEPOSITIONAL ENVIRONMENTS

6.1: INTRODUCTION

Chapters 3, 4 and 5 have focussed on the fossil evidence for the nature and diversity of vegetation that inhabited Old Red Sandstone Continent landscapes. However, to gain any understanding of Early Devonian palaeoecology, the sedimentary depositional environments and plant taphonomy must be considered. In this chapter a number of Lower Old Red Sandstone lithofacies from two contemporaneous localities are described and interpreted, and an attempt to recognised cyclicity using Markov Chain Analysis has been made on one of the sequences. With this data, geomorphic models for Late Silurian to the Early Devonian landscape have been proposed for the central Wales and Welsh Borderland area of the Welsh Basin.

6.2: LITHOFACIES DESCRIPTIONS OF TREDOMEN QUARRY STRATA AND CORE

Both cores and outcrops from Tredomen Quarry were logged and correlated (Figures 6.1 to 6.5) (Appendix VI) (see section 2.2.1 and Figures 2.2*a* and 2.2*b* for description of Tredomen Quarry location, borehole positions and location of logged sections). Five main lithofacies were recognised primarily on grain size: intraformational conglomerates, green sandstones, siltstones, heterolithics and red mudstones (assigned 1 to 5). A number of sub-lithofacies were also recognised (which are assigned 1a, 1b, 2a etc.), based on colour, bedforms, composition and lithofacies association. The lithofacies are fully described in Table 6.1. The correlated core was split into lower and upper parts at bed 136 in core 2, at 62.8m depth, where the youngest appearance of the well-developed carbonate nodule-rich horizons occurs (Figure 6.5). The proportions of each sub-lithofacies to the total number of beds are shown in Figure 6.6*a*, and the proportions of each sub-lithofacies to the total sequence thickness are shown in Figure 6.6*b*. Calculations for these proportions; plus the lithofacies association calculations can be found in Appendix VII.

Figure 6.1 : Tredomen Quarry log A

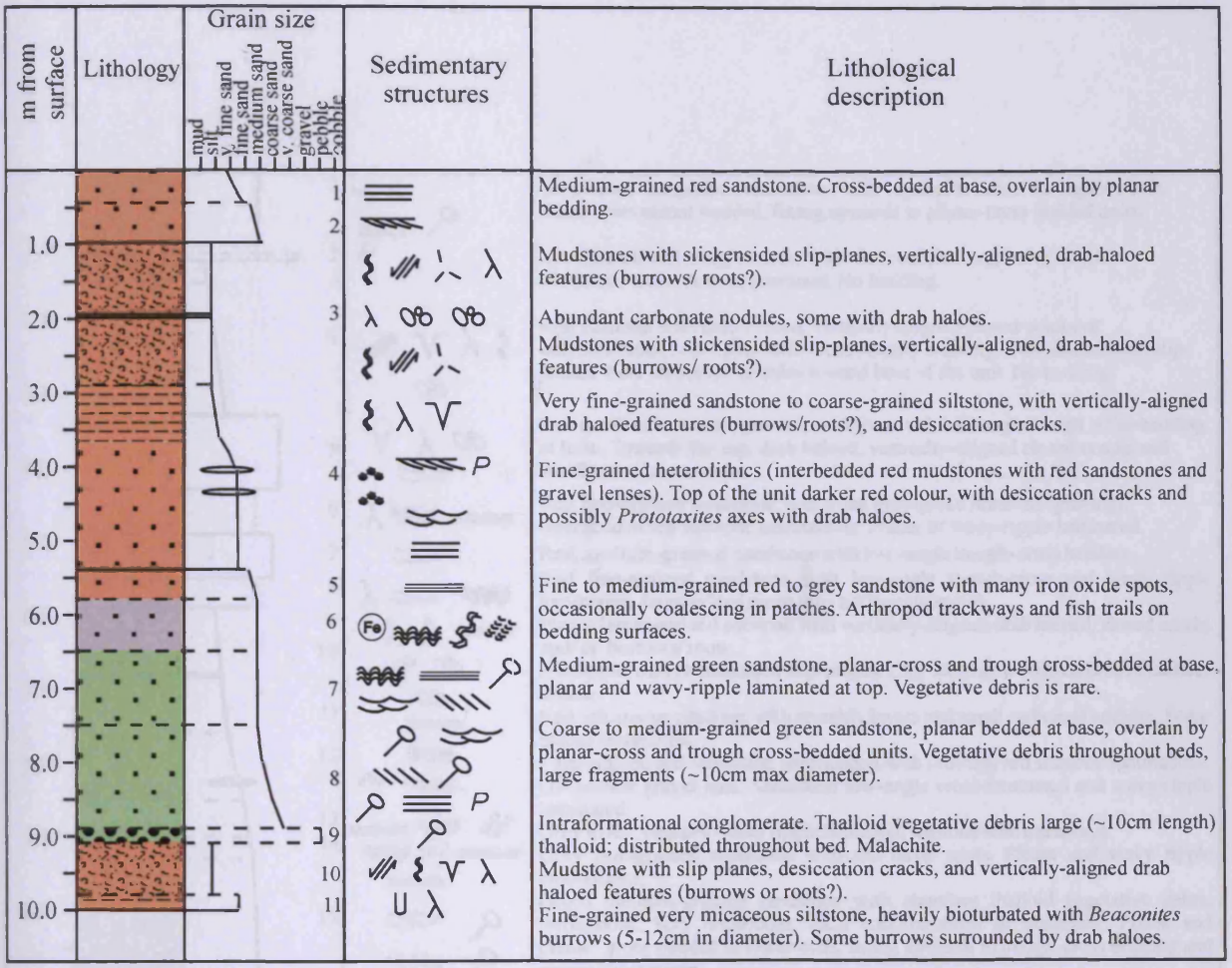

KEY FOR FIGURES 6.1-6.4

- Crumbly mudstone
- Siltstone
- Sandstone
- Red beds
- Green beds
- Convoluted lamination
- Wavy lamination
- Cross-ripple lamination
- Planar lamination
- Trough-cross bedding
- Planar-cross bedding
- Planar bedding
- Mudstone
- Calcrete horizon
- Conglomerate
- Grey beds
- Dark green beds
- Reduction spot
- Patches of iron oxide
- *Prototaxites* preservation
- Plant material
- *Diplichnites* trackways
- *Undichna* (fish trails)
- Vertically- aligned closed cracks or burrows/ roots
- Slickensided pseudo-anticlinal slip planes
- Drab halo
- Blocky fracturing
- Calcrete nodules
- Desiccation cracks
- Gravel lens/ Rip-up clasts
- *Beaconites* burrows

Figure 6.2 : Tredomen Quarry log B

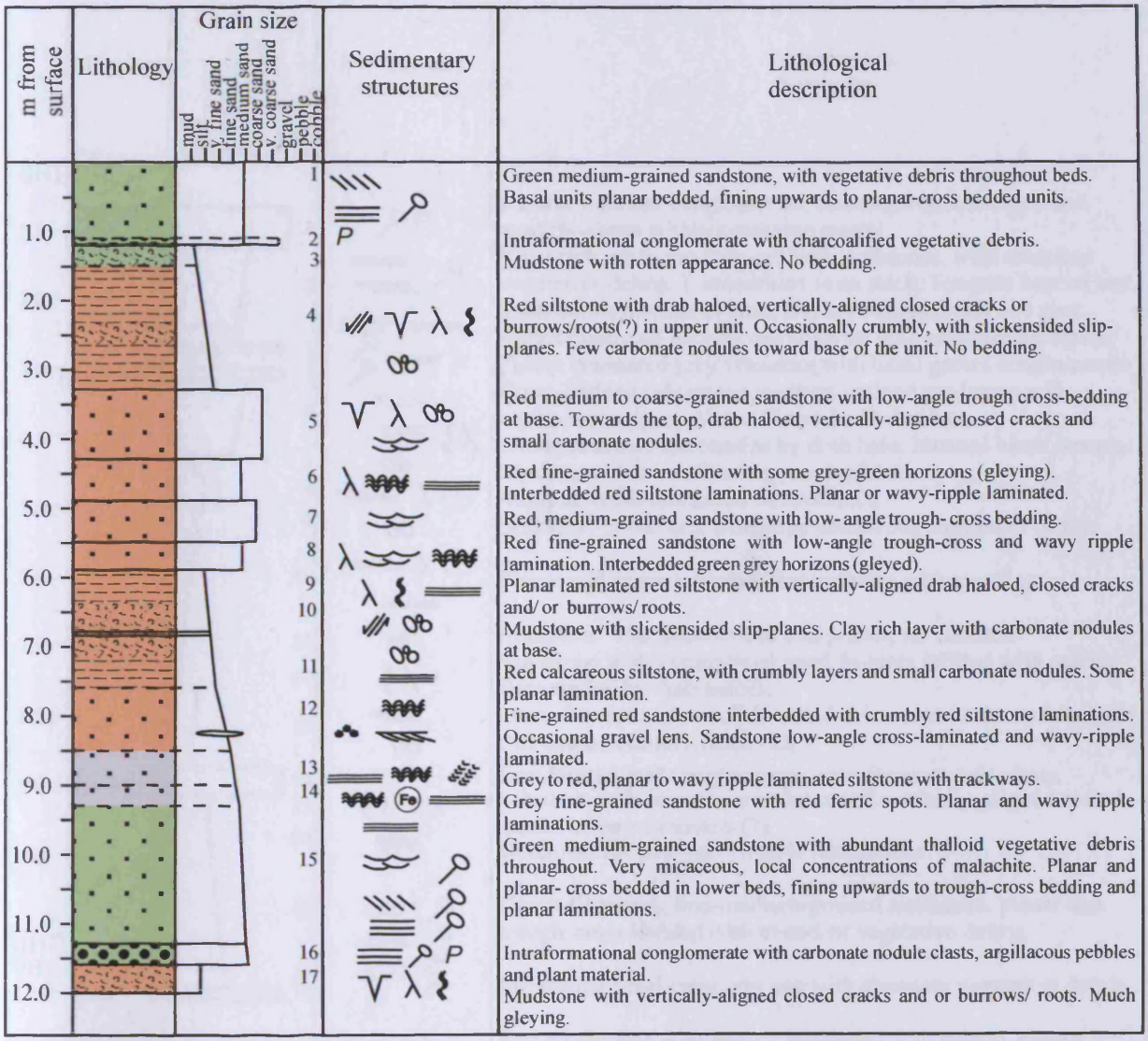

Figure 6.3*a* : Tredomen Quarry Borehole 1, beds 1 to 25

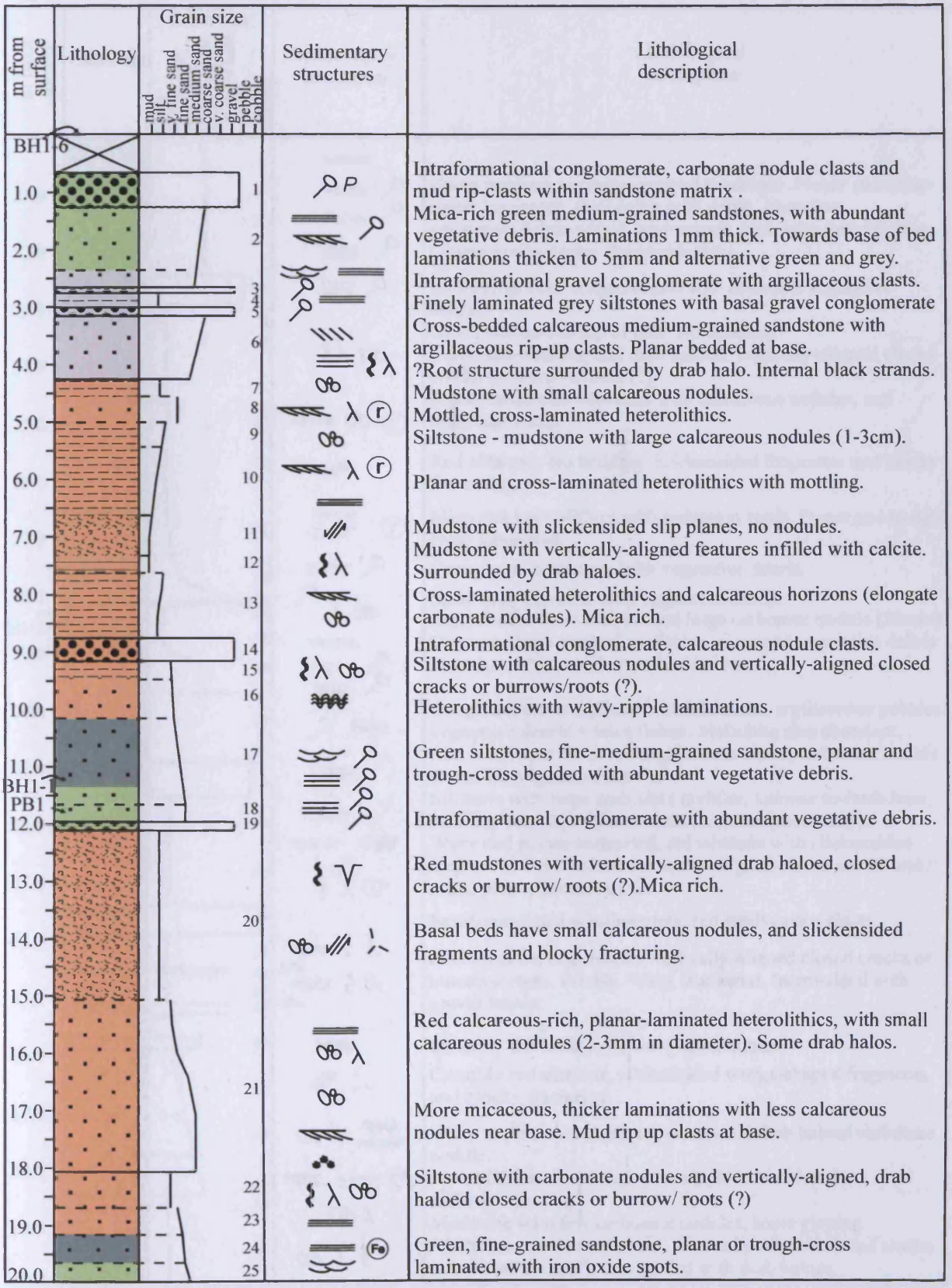

Figure 6.3*b* : Tredomen Quarry Borehole 1, beds 25 to 51

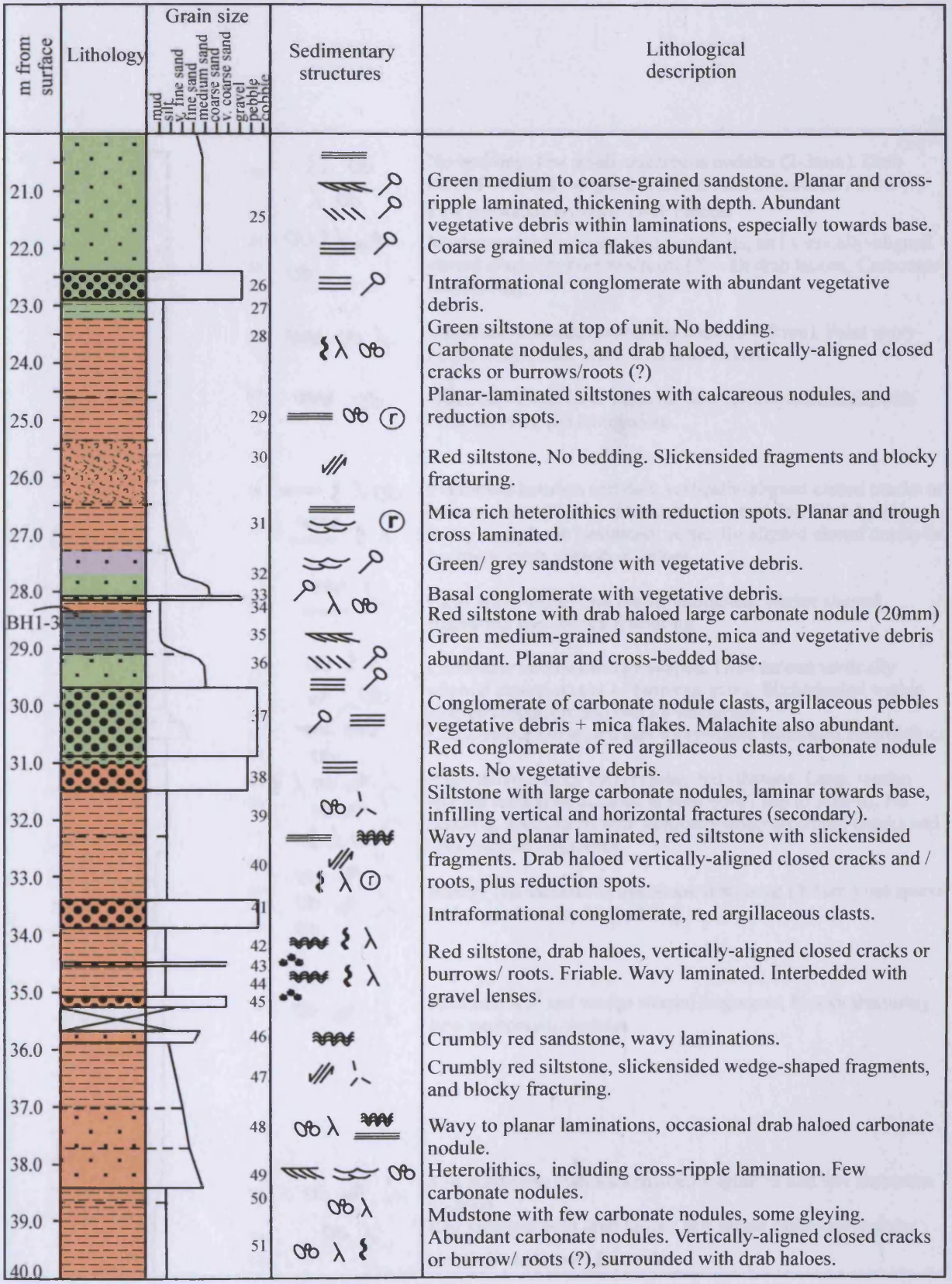

Figure 6.3*c* : Tredomen Quarry Borehole 1, beds 52 to 74

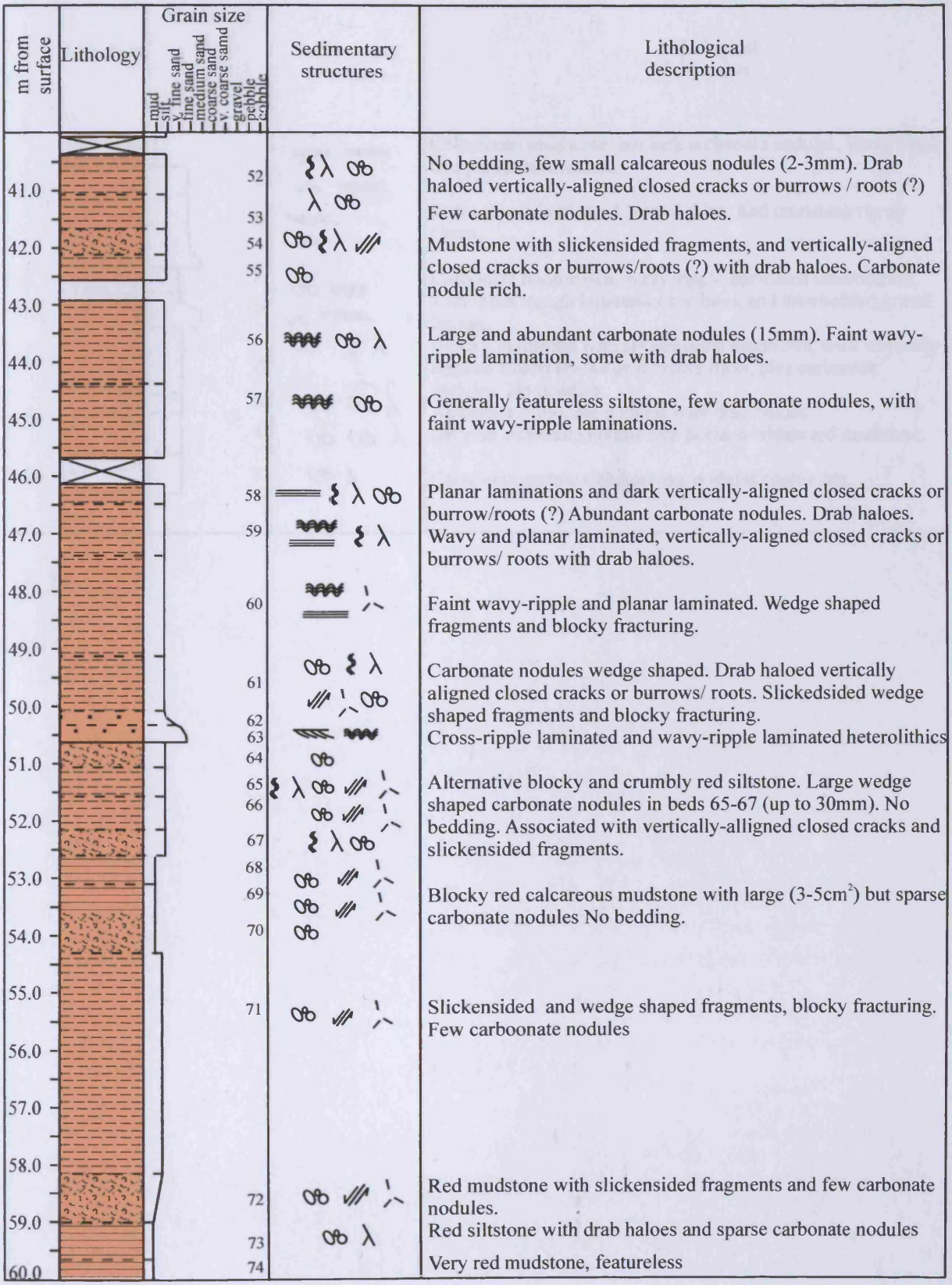

Figure 6.3*d* : Tredomen Quarry Borehole 1, beds 74 to 82

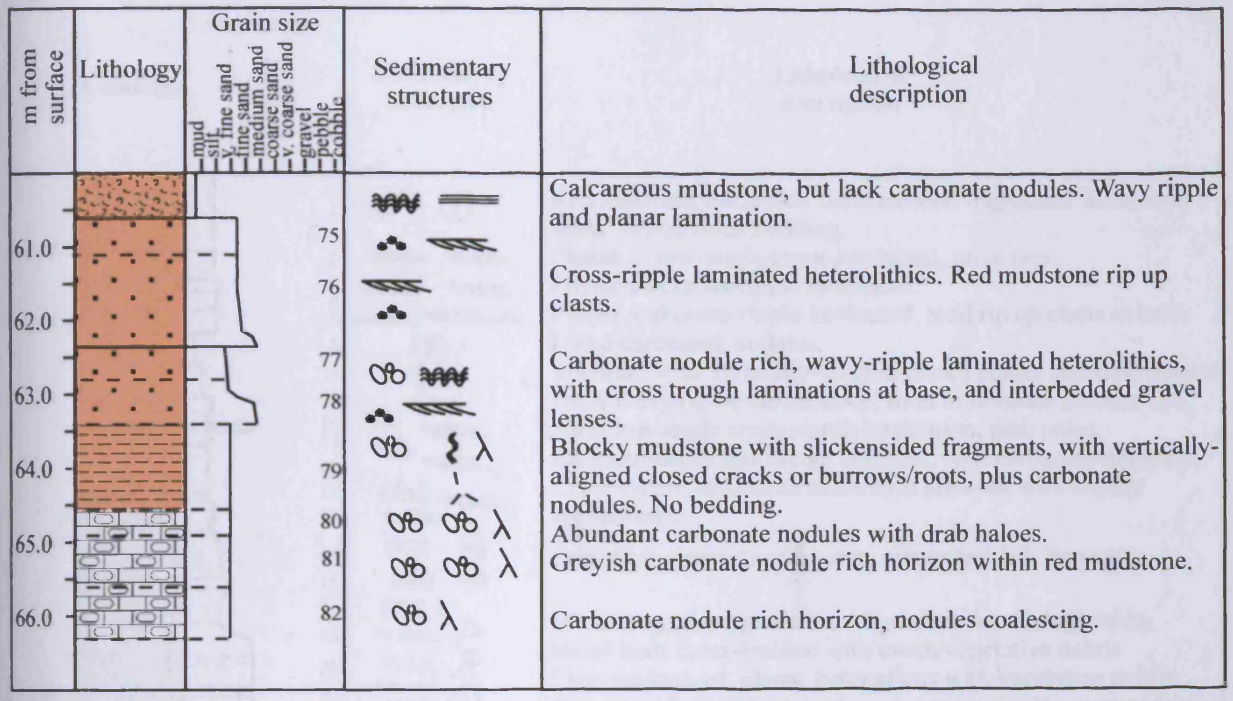

Figure 6.4*a* : Tredomen Quarry Borehole 2, beds 1 to 62

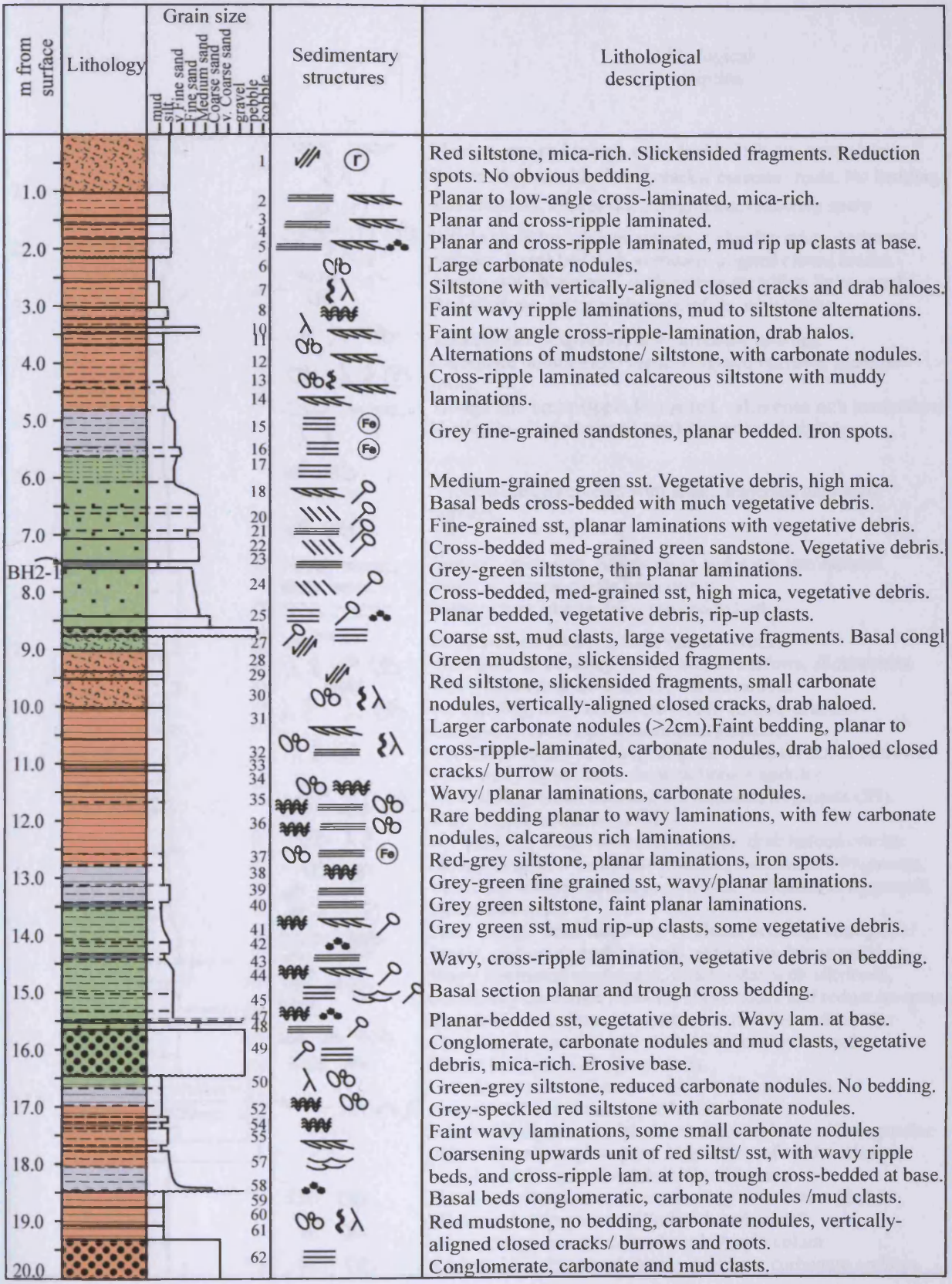

Figure 6.4*b* : Tredomen Quarry Borehole 2, beds 63 to 118

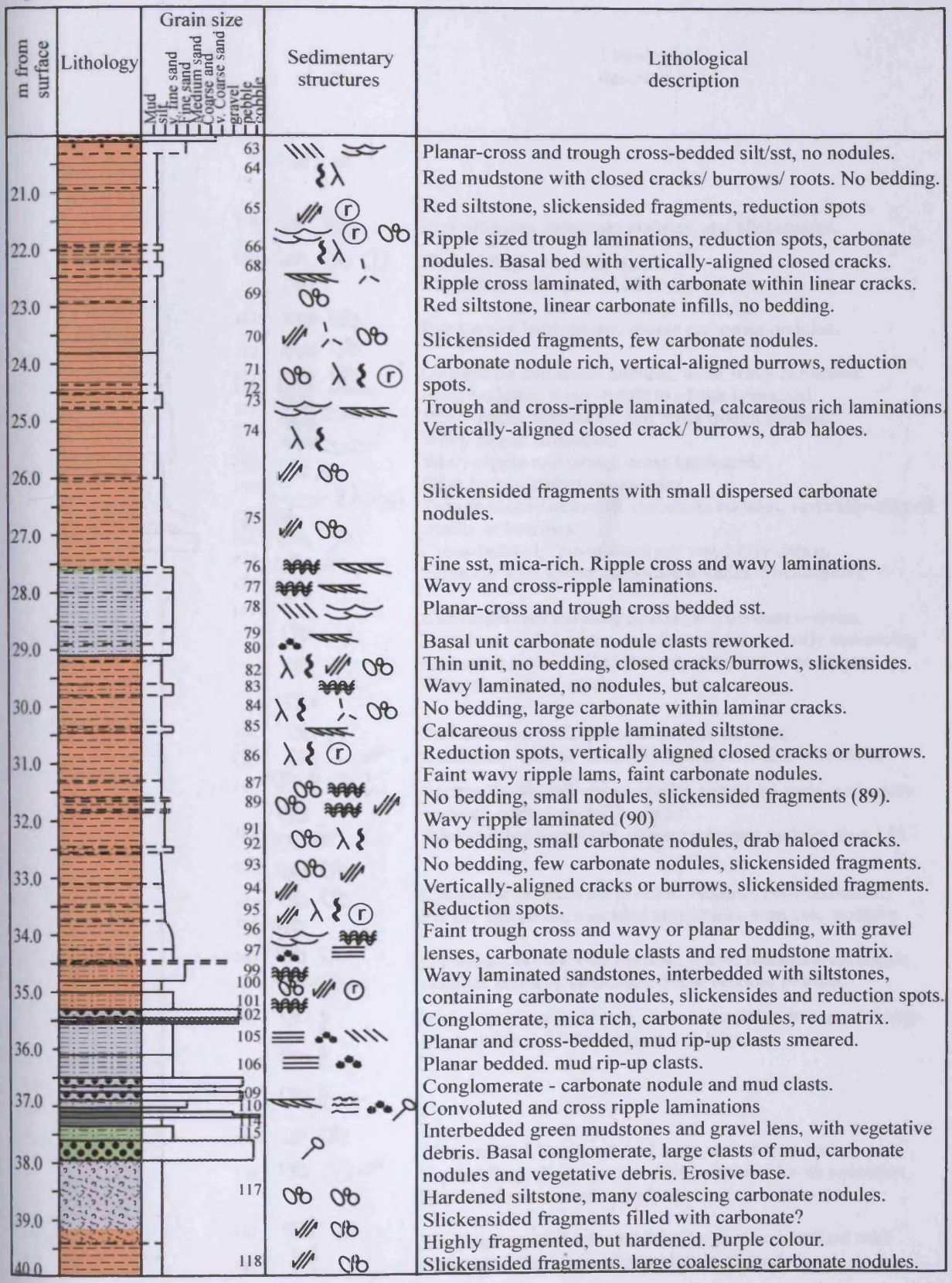

Figure 6.4*c* : Tredomen Quarry Borehole 2, beds 119 to 152

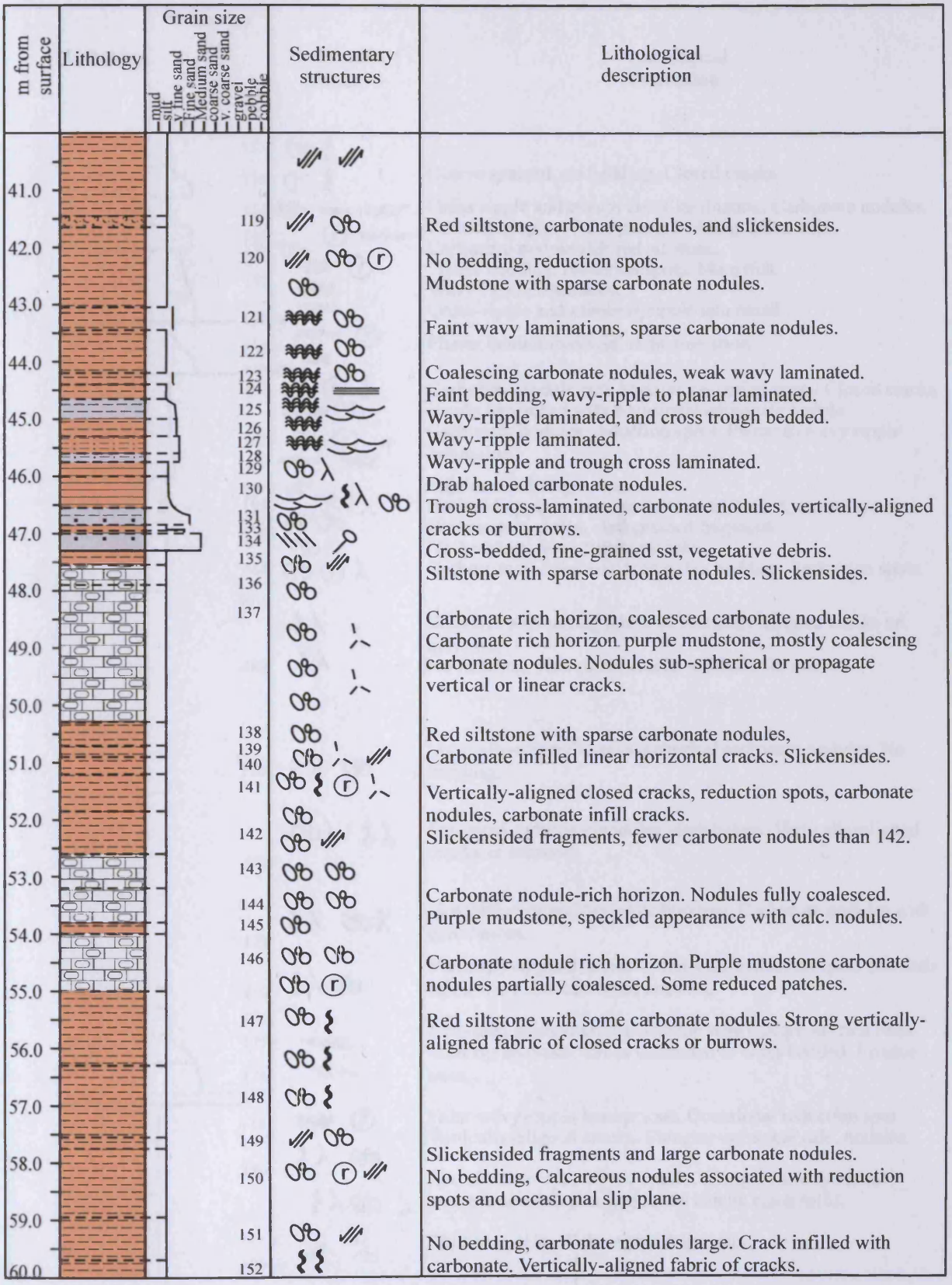

Figure 6.4*d* : Tredomen Quarry Borehole 2, beds 153 to 180

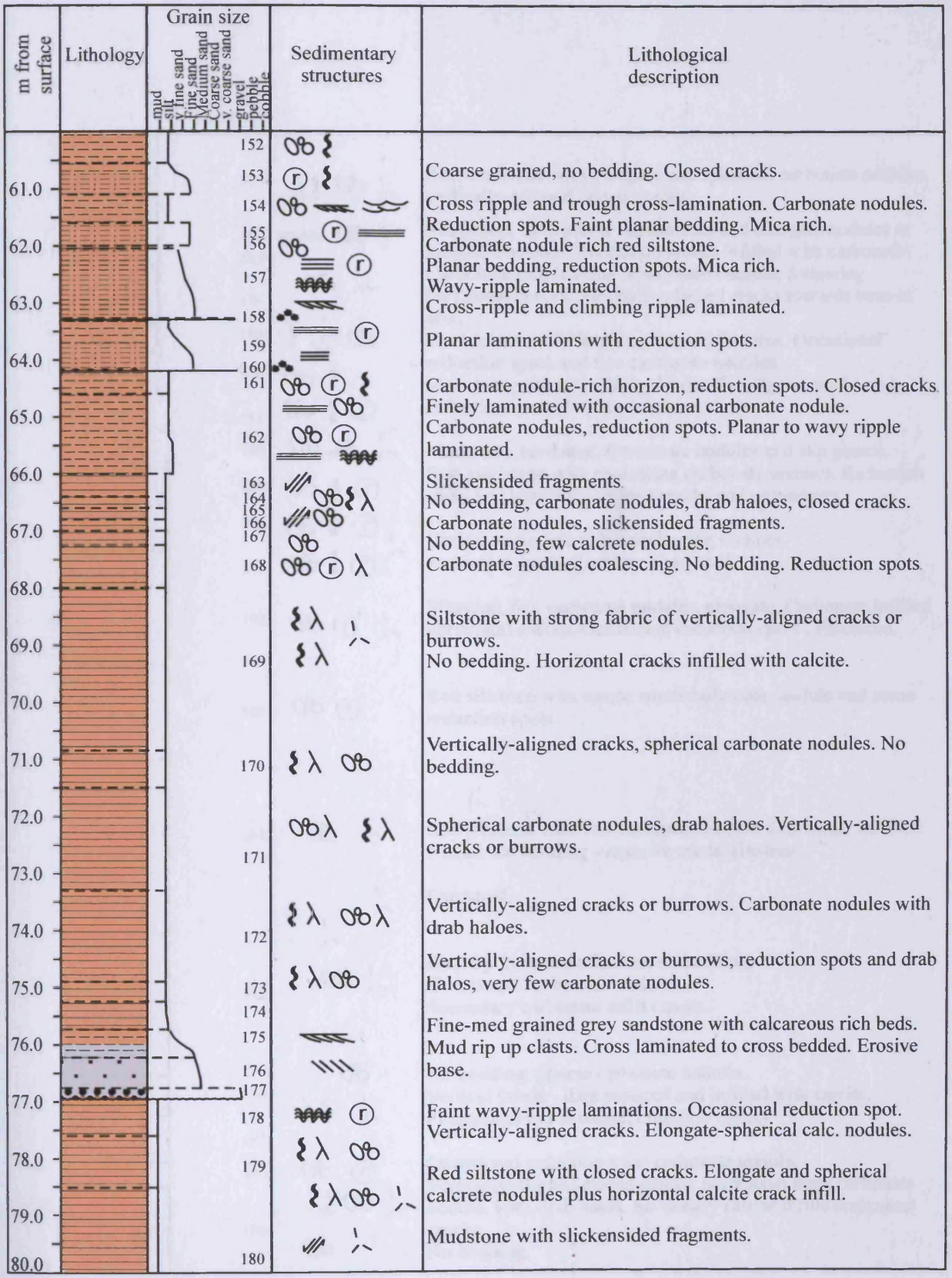

Figure 6.4*e* : Tredomen Quarry Borehole 2, beds 181 to 199

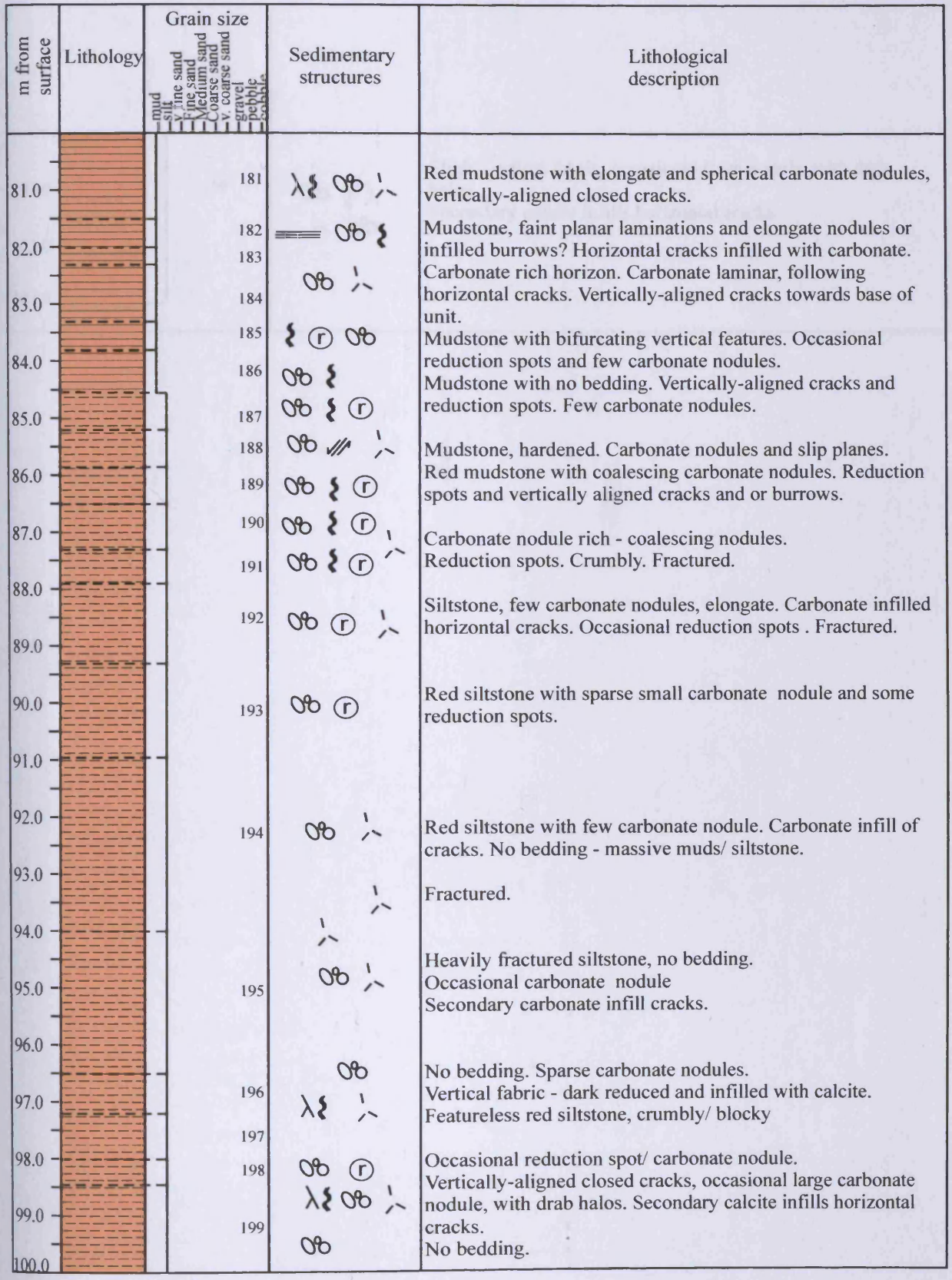

Figure 6.4*f*: Tredomen Quarry Borehole 2, bed 199

m from surface	Lithology	Grain size (mud, silt, v. fine sand, Fine sand, Medium sand, Coarse sand, v. coarse sand, gravel, pebble, cobble)	Sedimentary structures	Lithological description
101.0 102.0 103.0		199		Slight vertical fabric, occasional large nodule, with drab halos. Secondary calcite infills horizontal cracks.

Figure 6.5 : Tredomen Quarry correlated logs

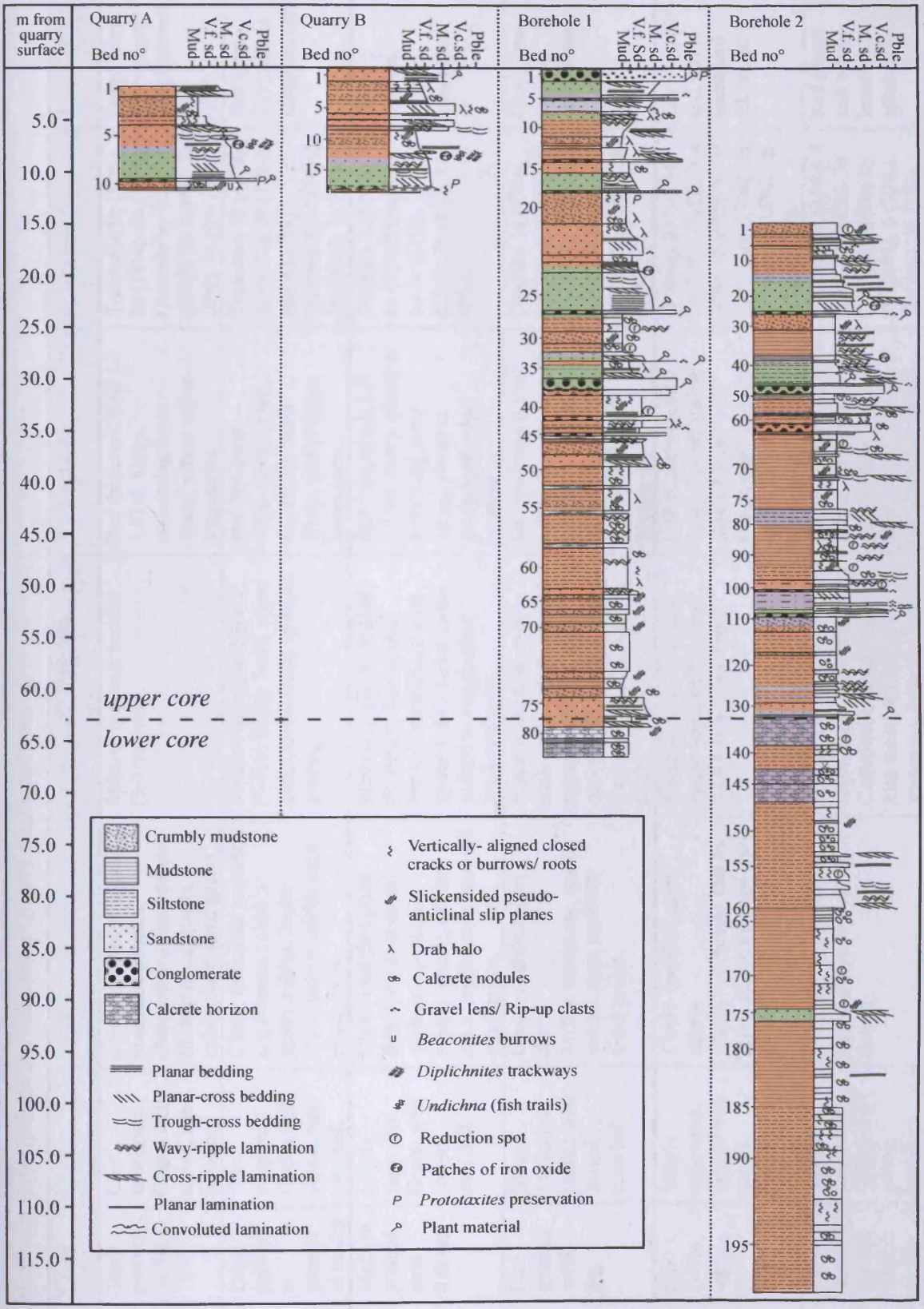

Table 6.1: Lithofacies descriptions for Tredomen Quarry strata and core

	Colour	*Grain size*	*Texture*	*Composition*	*Sedimentary structures*	*Architecture*	*Associations*	*Rock Type*
1a	Green grey	Small pebbles -3.5φ.	Clast supported. Grains well sorted, sub-rounded.	Clasts: carbonate nodules, mudstone pebbles, charcoalified plant debris. Matrix: mica, quartz, calcite sand-sized grains.	Massive to planar bedded (3-4cm thick).	Bed thickness: 0.05 to 1.01m. Sharp, undulating bases. Sharp, planar upper boundaries.	Truncates 5b (52%), 3a (18%), 2b (12%). Overlain by 2a (69%), 2b (19%), 3a (6%), 3b (6%).	Green intra-formational conglomerate
1b	Red	Large pebbles to granule -4 to -2φ	Clast supported. Grains well sorted, sub-rounded.	Clasts: carbonate nodules, argillaceous pebbles, sparry calcite. Matrix: mica, quartz, calcite sand sized grains.	Massive to planar bedded (3-4cm thick). Some upper beds exhibit fining upwards grading.	Bed thickness 0.3 to 0.8m. Sharp, undulating bases. Sharp, planar upper boundaries.	Truncates 5b (49%), 5a (17%), 3b (17%) and 4 (17%). Overlain by 4 (50%), 3b (33%), 1a (17%)	Red intra-formational conglomerate
2a	Green grey	Medium grained sand 0 to 4φ	Matrix supported. Grains well sorted, rounded.	Clasts: coalified plant debris, occasional red mudstone pebbles. Matrix: quartz, calcite, mica, argillaceous sand-silt sized grains.	Massive to planar bedded (0.5mm to 2cm thick). Parting lineations. Fining upwards into planar cross-bedded to trough-cross laminated units	Bed thickness 0.5 to 2.15m. Sharp, planar or undulating bases. Sharp, planar or gradational upper boundaries.	Overlies 1a (79%), 3a (21%). Overlain by 3a (61%), 2b (23%), 3b (8%), 1a (8%).	Green medium - grained sandstones
2b	Green grey	Fine grained sand 3φ.	Matrix supported. Grains well sorted, rounded	Clasts: coalified plant debris. Matrix: mudstone, quartz, calcite, mica sand-silt sized grains.	Planar bedded, or small scale cross-trough or cross-ripple-laminated, and occasional climbing ripple laminated. (0.5 to 2cm thick).	Bed thickness 0.1 to 1.45m. Sharp planar to concave bases. Planar, undulating or gradational upper boundaries.	Overlies 1a (37%), 2a (37%), 3a (13%), 5b (13%). Overlain by 3a (37%), 1a (25%), 5b (25%), 3b (13%).	Green fine-grained sandstones
3a	Green grey	Silt 3.5 to 6φ	Matrix supported. Grains well sorted, rounded	Clasts: coalified plant debris. Matrix: mudstone, calcite, mica, quartz silt-mud sized grains.	Planar to wavy or cross-ripple-laminated (1-2mm thick). Iron oxide spots.	Bed thickness 0.05 to 0.5m. Gradational or planar bases. Gradational or sharp undulating to planar upper boundaries.	Overlies 2a (61%), 2b (23%), 1a (8%), 4 (8%). Overlain by 1a (23%), 2a (23%), 3b (23%), 5b (15%), 2b (8%), 4 (8%).	Green planar and wavy laminated siltstones
3b	Red	Fine grained sand to silt 2.5 to 6φ	Matrix supported. Grains well sorted, rounded.	Mica, mudstone, calcite, quartz silt-mud sized grains.	Planar, wavy-ripple or cross-ripple laminated. Convoluted laminations. Fish trails, arthropod trackways, burrows. Iron	Bed thickness 0.05 to 1.90m. Gradational or planar bases. Gradational or sharp undulating to planar	Overlies 5b (34%), 4 (30%), 1b (8%), 3a (12%). Overlain by 5b (59%), 4 (30%), 1b (4%), 5a (7%).	Red planar and wavy-laminated siltstones

Table 6.1: Lithofacies descriptions for Tredomen Quarry strata and core (continued)

					oxide spots. Few carbonate nodules and vertical prismatic features, drab halos.	upper boundaries.		
4	Red	Coarse grained sand to clay 0.5 to 6φ	Clast or matrix supported. Grains well sorted, sub-rounded	Clasts: carbonate nodules, mudstone clasts. Matrix: mica, argillaceous silt-mud sized grains.	Planar bedded or low-angle inclined heterolithic stratification (IHS). Trough-cross bedding. Wavy-ripple and cross-ripple laminated. Polygonal cracking, prismatic features, drab haloes, mottling. Few carbonate nodules.	Bed thickness 0.05 to 2.95m. Sharp, planar to concave bases. Sharp planar upper boundaries.	Overlies 1b (50%), 5b (31%), 3b (14%), 3a (2%). Overlain by 5b (49%), 3b (26%), 5a (16%), 1a (3%), 1b (3%), 3a (3%).	Heterolithics (planar-bedded and IHS)
5a	Red	Silt to clay 4.5 to 8φ	Matrix supported. Grains well sorted, rounded.	Clasts: sand-sized mud aggregates. Matrix: mica, mudstone, silt-mud sized grains.	Massive appearance. Few bedding features - faint planar or wavy- ripple laminations. Occasional carbonate nodule, drab halo, mottling.	Bed thickness 0.1 to 1.5m. Sharp, planar, undulating or gradational bases. Gradational or sharp, undulating upper boundaries.	Overlies 4 (41%), 5b (42%), 3b (17%), Overlain by 5b (67%), 1b (8%), 3b (8%), 4 (17%).	Massive mudstone
5b i	Purple brown red	Clay <8φ	Massive	Mudstone, calcite clay sized grains.	A to C horizons. Horizon A: prismatic structures, drab haloes, burrows, desiccation cracks. Horizon B: pseudo-anticlinal, slickensided, slip plane surfaces. Horizon C: carbonate nodules.	Bed thickness 0.05 to 2.5m. Gradational bases. Sharp, undulating or planar upper boundaries.	Overlies 4 (35%), 3b (36%), 5a (19%), 2b (5%), 3a (5%). Overlain by 4 (40%), 1a (20%), 3b (20%), 1b (7%), 5a (11%), 2b (2%).	Pedified mudstone
ii	Purple brown red	Clay <8φ	Massive	Mudstone, calcite clay sized grains	No horizons. Carbonate nodules, drab haloes, prismatic structures, burrows, polygonal cracking.	Bed thickness up to 25m. Gradational bases. Sharp, undulating or planar upper boundaries.		

Figure 6.6a: Proportions Tredomen Quarry lithofacies by number of beds

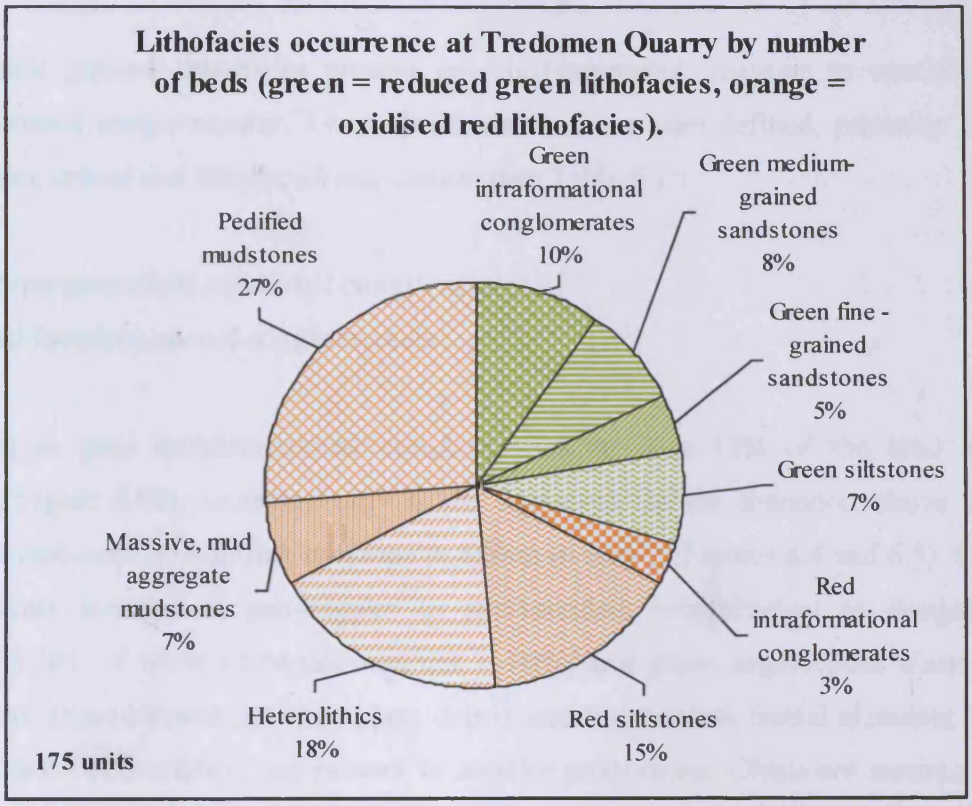

Figure 6.6b: Proportions of Tredomen Quarry lithofacies by lithofacies thickness

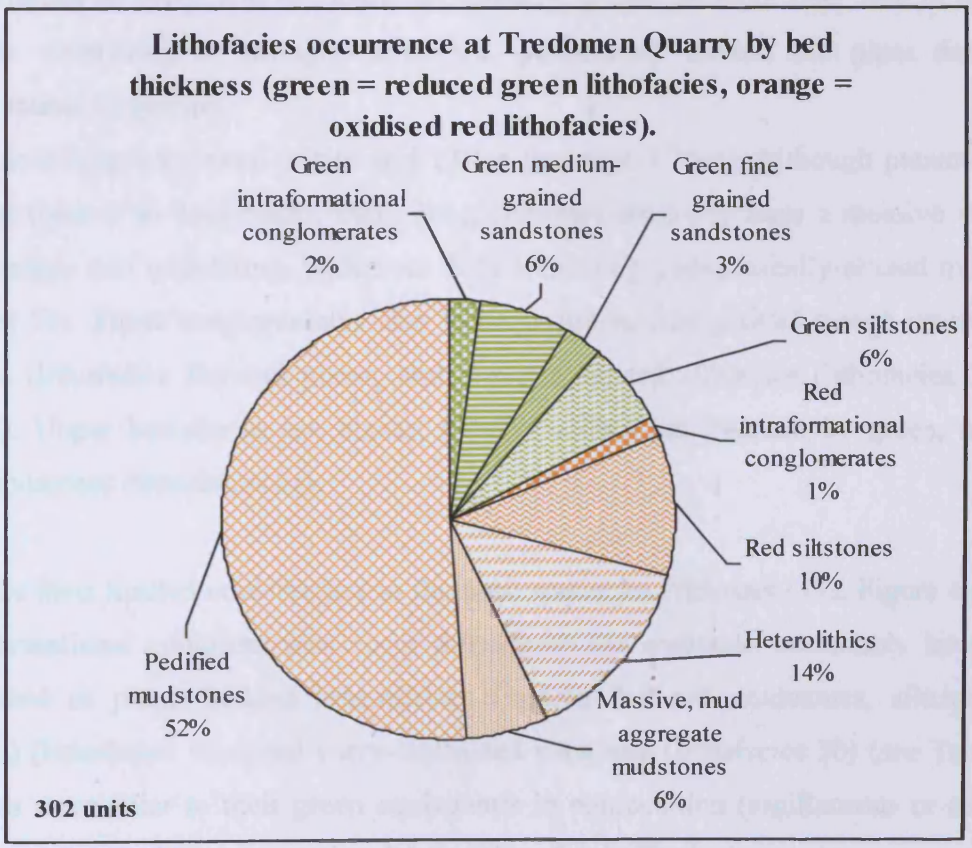

6.2.1: *Intraformational conglomerates* (Plate 6.1)

The coarsest grained lithofacies present are clast-supported, massive to coarsely-bedded intraformational conglomerates. Two sub-lithofacies have been defined, primarily based on composition, colour and lithofacies association (see Table 6.1):

1a: Green-grey intraformational conglomerates
1b: Red intraformational conglomerates

1a: Green to grey intraformational conglomerates are rare (2% of the total sequence thickness, Figure 6.6*b*), occurring only in the upper part of the sequence, above the well-developed carbonate nodule-rich horizons at 62.8m in core 2 (Figures 6.4 and 6.5). Clasts are predominately rounded to sub-angular to sub-rounded, sub-spherical to elongate small pebbles (-3.5φ), of white carbonate nodules (~40%) and green argillaceous clasts (~40%) (Plate 6.1*a*). Disseminated coalified plant debris and fragmentary faunal elements (possibly of fish or arthropod affinity) are present in smaller proportions. Clasts are surrounded by a grey, mica-rich, medium-grained sandstone (2φ) matrix or sparry calcite cement (Plate 6.1*b*). Small quantities of pyrite and malachite are present, grains no more than 1cm in diameter. Iron oxide weathering is strongly-developed, particularly around the plant debris and equivocal faunal fragments.
Bed thickness ranges between 0.05m and 1.01m (average 0.26m). Although planar-bedding does occur (beds 3 to 4cm thick), these conglomerates generally have a massive structure. Bases are sharp and undulating, with over 50% truncating pedogenically-altered mudstones (lithofacies 5b). These conglomerates also truncate green, fine-grained trough-cross-bedded sandstones (lithofacies 2b) and planar and wavy-laminated siltstones (lithofacies 3a) (see Table 6.1). Upper boundaries are planar, 69% of which are overlain by green, medium-grained sandstones (lithofacies 2a).

1b: Despite their limited contribution to the total sequence thickness (1%, Figure 6.6*b*), the red intraformational conglomerates occur throughout the sequence, commonly interbedded with inclined or planar-bedded heterolithics (interbedded red sandstones, siltstones and mudstones) (lithofacies 4) or red wavy-laminated siltstones (lithofacies 3b) (see Table 6.1). These units are similar to their green equivalents in composition (argillaceous or carbonate nodule clasts), but lack any vegetative debris (Plate 6.1*c*). The beds are clast-supported, with

grain sizes ranging from large pebbles (-4φ), to small granules (-2φ). Clasts range from sub-angular to sub-rounded, and sub-spherical to slightly elongate. The matrix consists of fine-grained, mica-rich sandstone (2φ), although occasionally is argillaceous (Plate 6.1*d*).

Units range in thickness from 0.3 to 0.8m, with massive or thick planar-bedding. Bases are undulating and erosional, with 49% truncating pedogenically-altered mudstones (lithofacies 5b), 17% truncating massive mudstones (lithofacies 5a), 17% red wavy-laminated siltstones (lithofacies 3b) and 17% heterolithics (lithofacies 4) (Table 6.1). Some beds exhibit normal grading and fine into muddier fractions (Plate 6.1*e*). Upper boundaries are planar and sharp, with 50% overlain by heterolithics (lithofacies 4), 33% by red wavy-laminated siltstones (lithofacies 3b), and 17% by green intraformational conglomerates (lithofacies 1a) (see Table 6.1).

6.2.2: *Sandstones* (Plate 6.2)

The green sandstone terraces are a striking feature at Tredomen Quarry, despite representing only 9% of the total sequence thickness (Figure 6.6*b*). Green sandstone bodies solely occur in the upper part of the sequence, above the carbonate nodule-rich horizon at bed 136 in core 2 (Figures 6.4 and 6.5). Two sub-lithofacies have been defined, based on grain size, bedforms and lithofacies associations (see Table 6.1):

2a: Medium-grained green-grey sandstones
2b: Fine-grained green-grey sandstones

2a: Green to grey medium-grained sandstones represent 6% of the total sequence thickness (Figure 6.6*b*), and commonly occur overlying green intraformational conglomerates (lithofacies 1a), separated by a sharp planar boundary. These sandstones are also found interbedded with fine-grained green siltstones (lithofacies 3a), or are stacked (Table 6.1). Bed thickness ranges from 0.5 to 2.15m, and up to 100m in lateral extent in outcrop. Grain size ranges from fine to coarse sand (0 to 4φ), but the majority are well-sorted, rounded, sub-spherical, medium sand grains (2φ). These sandstones are predominately composed of quartz grains, but with a large proportion of mica flakes, with a carbonate clay-rich matrix, and therefore described as litharenites. Rare horizons of angular and red, gravel-sized mudstone clasts occur (Plate 6.2*a*). Disseminated plant debris (of non-embryophytes and

rhyniophytoids) is commonly found throughout these units (see Chapters 3 and 7), as well as fragments of cephalaspids.

Lying directly above green conglomerates (lithofacies 1a), these sandstones are massive or planar-bedded (Plate 6.2*b*, 1 in Plate 6.2*c*), with parting lineations (Plate 6.2*d*). Beds fine upwards into larger scale, individual planar-cross-beds (with a dip of 20°) or multistorey units of smaller-scaled, planar (2 in Plate 6.2*c*, Plate 6.2*e*) and trough-cross-laminations (Plate 6.2*f*). Directly beneath the upper boundary, the uppermost beds are speckled with small iron oxide spots, giving a mottled appearance. The upper boundary can be planar or gradational, and overlain by green siltstones (lithofacies 3a), trough and cross-ripple-laminated fine-grained sandstones (lithofacies 2b), red wavy-laminated siltstones (lithofacies 3b) or green intraformational conglomerates (lithofacies 1a) (see Table 6.1).

2b: Fine-grained green sandstones are less common than the medium-grained equivalents (3% of the total sequence thickness, Figure 6.6*b*). These units are less laterally extensive compared to the medium-grained sandstones described above, pinching out to form lenses (Plate 6.2*g*). Bed thickness ranges from 0.1 to 1.45m, with planar or shallow concave bases. These sandstones commonly overlie green conglomerates (lithofacies 1a) or medium-grained sandstones (lithofacies 2a) (see Table 6.1). Additionally, outcrops of individual scour-based, trough-cross-bedded and cross-ripple-laminated fine-grained sandstone units incise into, or are interbedded with green siltstones (lithofacies 3a) or pedogenically-altered red mudstones (lithofacies 5b). These fine-grained sandstones are overlain by green or red siltstones (lithofacies 3a and 3b), or pedogenically-altered mudstones (lithofacies 5b), separated by a planar or undulating erosional boundary.

These units are similar in composition to the green medium-grained sandstones (lithofacies 2a), but have a higher argillaceous content. Laminations alternate between micrite-rich and organic-rich, and are either planar-bedded or small-scale trough-cross or cross-ripple-laminated (Plates 6.2*h* and 6.2*i*), with occasional climbing-ripple-lamination. Well-preserved, partially fragmented coalified compressions of rhyniophytoid fossils are found within these fine-grained sandstone horizons (see Chapter 3 for plant descriptions and Chapter 7 for description of plant taphofacies).

6.2.3: *Siltstones* (Plates 6.3 and 6.4)

Planar and wavy-laminated siltstones represent 16% of the total sequence thickness (Figure 6.6*b*) and are highly variable, in terms of colour, sedimentary features and lithofacies associations. Two sub-lithofacies have been defined (see Table 6.1):

3a: Green to grey, planar and wavy-laminated siltstones

3b: Red, planar and wavy-laminated siltstones

3a: Finely laminated, green to grey siltstones represent 6% of the total sequence thickness (Figure 6.6*b*), and occur only above the well-developed carbonate nodule-rich horizon at bed 136 in core 2. These siltstones commonly occur gradationally above medium or fine-grained sandstones units (lithofacies 2a and 2b), but also above green intraformational conglomerates (lithofacies 1a), or heterolithics (lithofacies 4) (see Table 6.1). Upper boundaries are gradational where red siltstones (Plate 6.3*a*) (lithofacies 3b) or pedogenically-altered mudstones (lithofacies 5b) occur above (Table 6.1). Where these siltstones are overlain by green conglomerates (lithofacies 1a), green cross-bedded sandstones (lithofacies 2a) and heterolithics (lithofacies 4), upper boundaries are sharp and planar or undulating (Table 6.1). Grain size ranges from very fine sand to silt (3.5 to 6 φ), and are mica-rich, but also calcareous or argillaceous in some laminations. Laminations alternate between micritic mica-rich and argillaceous, organic-rich fractions, occurring either as fine planar-laminated or current to wavy-laminated (Plate 6.3*b*), with occasional cross-ripple-lamination (1-2cm thick) (Plate 6.3*c*). Plant debris is commonly preserved along these laminations, including the mesofossils described in Chapter 3 (for description of the plant taphofacies see Chapter 7). Prominent red to purple iron-oxide spots (a few millimetres in diameter) occur in some horizons (Plate 6.3*d* and Plate 6.3*e*).
Faunal specimens are also known from this lithofacies, including myriapod, eurypterid and scorpion fragments, and a complete specimen of a new genus of trigonotarbid (*Arianrhoda bennetti*) (Dunlop and Selden 2004).

3b: Red siltstones represent 10% of the total sequence thickness (Figure 6.6*b*), and gradationally overlie green siltstones (Plate 6.3*a* and 6.3*e*) (lithofacies 3a) or pedogenically-altered mudstones (lithofacies 5b), or are sharply interbedded with heterolithics (lithofacies 4)

or red intraformational conglomerates (lithofacies 1b) (Table 6.1). Bed thickness ranges from 0.05 to 1.90m.

These siltstones have a similar grain size to the green siltstones, ranging from fine sand to muddy silt (2.5 to 6φ), and are well-sorted and rounded where visible. These siltstones are also similar in composition, with a high mica content and argillaceous fraction. However, no organic material is preserved. Stratification occurs as planar or wavy laminations (Plate 6.3*f*), with occasional cross-ripple-laminations (Plate 6.3*g*) or convoluted bedding. Laminations alternate between micrite-rich and argillaceous fractions, similar to the green siltstones.

In the quarry exposures, at the base of these units, bedding planes are covered with fish trails produced by cephalaspids (*Undichna,* Plate 6.4*a*) and arthropod trackways (*Diplithnites gouldi* (Plate 6.4*b*), cf. *Cruziana*) alongside asymmetric current ripples marks, previously described by Morrissey et al. (2004). Some bedding planes have a slightly irregular undulating surface (Plate 6.4*c*) The bases of these units often have a speckled appearance, with the gradual coalescence of iron-oxide spots (Plate 6.4*d*), 0.5-1cm in diameter.

Towards the top of these units, dark-grey vertically-aligned, linear features and carbonate nodules are often surrounded by discoloured, blueish to green zones (known as drab haloes, a term of Retallack 1988). The vertically-aligned features are generally singular and linear, although some appear to bifurcate. They reach up to 10cm in length and are either infilled with sparry calcite, or fine-grained grey siltstone, with surrounding drab haloes 0.5cm in width (Plate 6.4*e*). Drab haloes also mark out polygonal cracking observed on the uppermost bedding plane surfaces (Plate 6.4*f*).

These units also have a speckled appearance, due to the presence of small, fine-grained, calcareous nodules, together with calcite infills of horizontal cracks and sub-vertical fractures. Some horizons are heavily bioturbated with vertically-aligned, elongate, cylindrical burrows that are 5-12cm in diameter and are identified as *Beaconites barretti* burrows (Plate 6.4*g*).

6.2.4: *Heterolithics* (Plate 6.5)

4: Heterolithics are essentially alternating laminations of red sandstones, siltstones and mudstones (Plate 6.5*a*), and are commonly interbedded with red intraformational conglomerates (lithofacies 1b) (Table 6.1). Red heterolithics occur throughout the sequence, representing 4% of the total number sequence thickness (Figure 6.6*b*). Beds range in thickness from 0.05m and 2.95m, with sharp, planar to slightly concave bases and planar

tops. Sharp changes in grain size occur between beds. Red intraformational conglomerates occur beneath heterolithics or as discrete internal gravel lenses (Plate 6.5*a*, 6.5b). Heterolithics incise into red intraformational conglomerates (lithofacies 1a), pedogenically altered mudstones (lithofacies 5b), or red wavy-laminated siltstones (lithofacies 3b) (see Table 6.1). Upper boundaries are planar, overlain by pedogenic and non-pedogenic mudstones (Plate 6.5*c*) (lithofacies 5a and 5b), red wavy-laminated siltstones (lithofacies 3b) or conglomerates (lithofacies 1a and 1b).

Basal beds are dominated by clast-supported, well-sorted and sub-rounded, coarse-grained sandstone (sand grains 0.5φ), composed mainly of carbonate nodule clasts and mud clasts, surrounded by a mica-rich, clay-silt matrix (6φ). In comparison, upper beds are finer with a larger proportion of argillaceous matrix, and in some cases appear matrix-supported. However, units generally do not fine upwards. There is no evidence that organic material has been preserved.

Basal beds either exhibit inclined bedding, (also known as inclined heterolithic stratification or IHS, Thomas et al. 1987), or planar bedding. Inclined units are generally individual beds, with low-angle (<10°) planar-cross or trough-cross-bedding (Plate 6.5*d*). Concave or planar boundaries separate units where they are stacked. Although rare, inclined heterolithics most commonly occur below the well-developed carbonate nodule-rich horizons in the lower part of the sequence. Other heterolithic units are sheet-like and planar-bedded (Plate 6.5*e*), planar bounded, and tabular in nature.

The upper beds of these heterolithic units are finer grained, with trough-cross-bedding, and concave lower boundaries. Wavy-lamination (Plate 6.5*f*) and climbing-ripple-laminations are also present. These beds exhibit polygonal cracking on bedding surfaces, with dark grey vertically-aligned linear features, with purplish drab haloes, plus small green-grey mottles (few millimetres in diameter) (Plate 6.5*g*). Small carbonate nodules, no more than 1cm in diameter, are also present, sparsely dispersed throughout the basal and upper beds, (Plate 6.5*d*).

6.2.5: *Mudstones* (Plates 6.6 and 6.7)

Mudstones are the most common lithofacies in the Tredomen Quarry sequence (58% of the total sequence thickness, Figure 6.6*b*) with the majority occurring below the well-developed carbonate nodule-rich horizons at bed 136 in core 2 (Figures 6.4 and 6.5). There are two sub-lithofacies (see Table 6.1):

5a: Massive, mud aggregate mudstones

5b: Pedified mudstones

5a: Massive mudstones, with no pedogenic features, are not common in the sequence (only 6% of the total sequence thickness, Figure 6.6*b*) and solely occur below the carbonate nodule-rich horizons at bed 136 in core 2. Bed thickness ranges from 0.1 to 1.5m, with a sharp or gradational lower boundary, overlying heterolithics (lithofacies 4), pedogenically-altered mudstones (lithofacies 5b) or red siltstones (lithofacies 3b) (Table 6.1). Upper boundaries are gradational into pedogenically-altered mudstones (lithofacies 5b), or sharply truncated by red intraformational conglomerates (lithofacies 1b), heterolithics (lithofacies 4) or red planar-laminated siltstones (lithofacies 3b) (Table 6.1).

Grains mainly composed of calcareous mudstone, range in size from silt to clay (4.5 to 8φ). No organic material is preserved. There are no obvious bedding features, except for occasional faint planar to wavy-lamination. This gives a massive appearance to the mudstones, which often have a crumbly texture (Plate 6.6*a*). Although the majority of these mudstones are featureless, occasional horizons contain one or two small sparse carbonate nodules (no more than 0.5cm in diameter), which are surrounded by thin blueish-green drab haloes (Plate 6.6*b*). Some areas are locally mottled, with small patches of green-grey discolouration. Weak, dark-grey vertically-aligned linear features are present in some beds, with diffuse discolouration with the surrounding red mudstone. These features are singular and linear, less than 0.5cm in width and 5-10cm in length, with no internal detail preserved (Plate 6.6*c* and 6.6*d*). Occasional sub-horizontal and sub-vertical cracks are infilled with sparry calcite.

Although these beds are not laminated, and have a structureless appearance, on closer inspection the rock fabric consists of small, sub-spherical aggregations of mud, which are sometimes seen to be darker red in colour than the surrounding lighter red mudstone matrix (Plate 6.6*c* and 6.6*d*). These mud aggregates are no more than 1.5mm in diameter and are association with green-grey mottling. In some non-pedogenic, non-laminated mudstone beds, especially those associated with heterolithics (lithofacies 4), gravel-sized carbonate clasts float in a mudstone matrix, with no original texture preserved in the mudstones (Plate 6.6*e*).

5b: Pedogenically-altered mudstones are the most common sub-lithofacies (52% of the total sequence thickness, Figure 6.6*b*), and occur throughout the sequence, although a higher proportion occur below the well-developed carbonate nodule-rich horizon at bed 136 in core

2. Bed thickness ranges from 0.05 to 2.5m. Lower boundaries are gradational, occurring above red laminated siltstones (lithofacies 3b), heterolithics (lithofacies 4) or non-pedogenic mudstones (lithofacies 5a) (Table 6.1). Upper boundaries are sharply undulating, truncated by heterolithics (lithofacies 4), intraformational conglomerates (lithofacies 1a), red planar laminated siltstones (lithofacies 3b) or non-pedogenic mudstones (lithofacies 5a) (Table 6.1). Two main pedified unit types can be recognised:

- Pedified profile type 1 (with three distinct horizons)
- Pedified profile type 2 (with poorly defined horizons)

Pedified profile type 1 (Plate 6.7)

These profiles exhibit carbonate nodule-rich mudstones that are purple to brownish red, generally lack primary sedimentary structures and show three distinct horizons: upper, middle and lower. The upper horizon is recognised by a strong fabric of dark-grey, vertically-aligned linear features, each surrounded by blueish-green drab haloes (Plate 6.7*a*). These features are no more than 10cm in length and 1cm in width, and are either infilled with dark red to grey mudstone or sparry calcite, and in some cases bifurcate. However, in most cases these features are only 3-5cm in length, due to the sharp truncation by the beds above (commonly by heterolithics (lithofacies 4), green intraformational conglomerates (lithofacies 1a), with this uppermost horizon often only 10-20cm thick, or completely absent.

The middle horizon exhibits a series of curved, concave slickensided slip-planes, approximately 30cm in length, intersect to form local pseudo-anticlinal features (Plate 6.7*b*). In some profiles, vertically-aligned linear features from the horizon above are crosscut by pseudo-anticlinal slip planes, where the upper horizon is overprinted by the middle horizon. The pseudo-anticlinal slip-planes often fracture the mudstones into blocks with slickensided surfaces, or where mudstones are more intact and clayey, a crumbly texture is more common.

The lower horizon is recognised by varying intensities of carbonate nodules. Carbonate nodule intensity within the lower horizon varies from sparsely distributed and individual, white micritic, sub-spherical nodules, ranging in size from 2-5mm in diameter, that are often surrounded by dark-grey to blueish drab haloes (Plate 6.7*c*). Elongate nodules also occur, but are less than 5mm in diameter and over 10cm in length (Plate 6.7*d*). In other horizons, carbonate nodules are larger (>5mm in diameter) white to pinkish nodules with some coalesced either into larger spherical nodules or elongate vertical rods over 10cm in length (Plate 6.7*e*). However, the parent mudstones are still visible between the nodules, where

replacement has not occurred. In a few horizons, the parent mudstones have a brecciated appearance, but this texture is produced by the near total coalescence of carbonate nodules, and the infill of sub-horizontal and sub-vertical fractures with sparry calcite (Plate 6.7*f*).
Although profile type 1 is seen throughout the Tredomen Quarry sequences, the majority occur above the two closely-spaced, well-developed carbonate nodule-rich horizons at bed 136 in core 2. Here, the thickest lower horizons in the sequence are also the most carbonate nodule-rich, occurring at beds 136-137 (top at 62.8m) and beds 143-146 (top at 65.5m) of borehole 2, both 2.5m thick and 2m apart (Figures 6.4 and 6.5).

Pedified profile type 2 (Plate 6.7)

Profile type 2 mudstones are red to brownish-red and like profile type 1, lack primary sedimentary structures, and are carbonate nodule-rich. However, unlike profile type 1 mudstones, horizons within profile type 2 are poorly defined. Additionally, profile type 2 mudstones fundamentally lack the curved, pseudo-anticlinal slip-plane surfaces seen in the middle horizons of profile type 1. Instead, a continuous, weak fabric of dark-grey, vertically-aligned linear features (up to 10cm in length and 1cm in width) which are lined with drab haloes, alongside small, sparsely and randomly-orientated elongate carbonate rods, as well as small sub-spherical carbonate nodules (no more than 1cm in diameter) occur throughout the unit (Plate 6.7*g*). Occasionally carbonate nodule-rich C horizons develop, approximately 1m thick (Plate 6.7*h*). These mudstones reach a maximum thickness of 25m, are found in association with heterolithics (lithofacies 4) and massive mudstones (lithofacies 5a), and solely occur in the lower part of the sequence.

6.3: Lithofacies descriptions of Targrove Quarry strata

The Lower Old Red Sandstone strata at Targrove Quarry, Shropshire (see section 2.2.2) dip at 22° to the north-west, and so a composite log was recorded, up to 15m in stratigraphic height (Figure 6.7) (Appendix VI). 4 main lithofacies have been defined, primarily on grain size; intraformational conglomerates, medium-grained sandstones, siltstones and mudstones, and have been assigned into the same main lithofacies established for Tredomen Quarry in section 6.2 (i.e. lithofacies 1, 2, 3 and 5). Five sub-lithofacies have been defined, mainly on bedforms, composition and colour, but also lithofacies associations. Two sub-lithofacies are common to those from Tredomen Quarry and have been assigned the same number

Figure 6.7: Targrove Quarry log

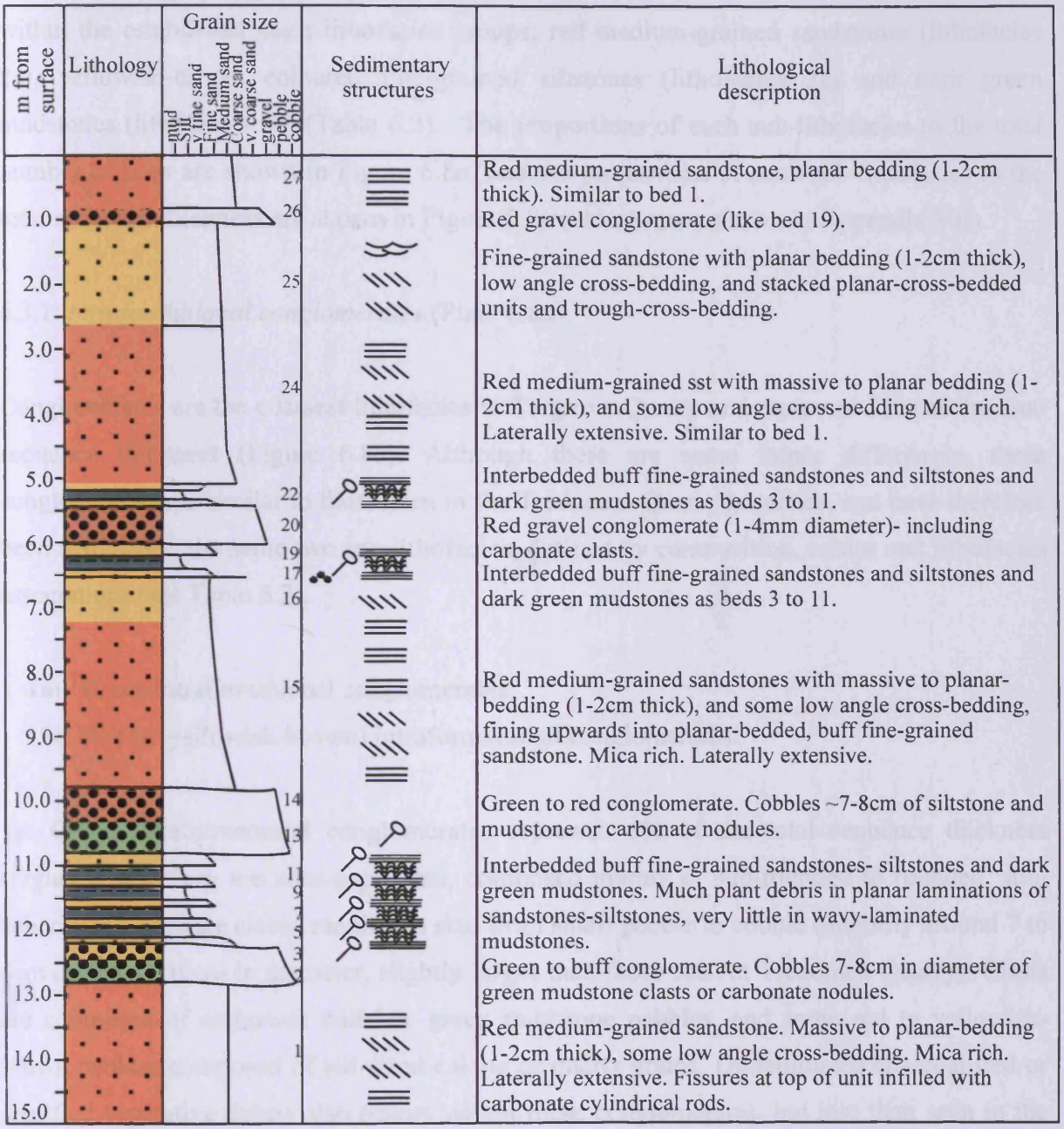

KEY FOR FIGURE 6.7

- Crumbly mudstone
- Siltstone
- Sandstone
- Red beds
- Green beds
- Mudstone
- Calcrete horizon
- Conglomerate
- Dark green beds
- Yellowish-brown beds
- Convoluted lamination
- Cross-ripple lamination
- Planar lamination
- Trough-cross bedding
- Planar-cross bedding
- Planar bedding
- Wavy lamination
- (r) Reduction spot
- Vertically- aligned closed cracks or burrows/ roots
- Slickensided pseudo-anticlinal slip planes
- Drab halo
- Blocky fracturing
- Calcrete nodules
- Desiccation cracks
- Gravel lens/ Rip-up clasts
- *Beaconites* burrows
- *Diplichnites* trackways
- *Undichna* (fish trails)
- Plant material
- P *Prototaxites* preservation
- (Fe) Patches of iron oxide

(lithofacies 1a and 1b). The three remaining sub-lithofacies are assigned new sub-lithofacies within the established main lithofacies groups; red medium-grained sandstones (lithofacies 2c), yellowish-brown coloured fine-grained siltstones (lithofacies 3c) and dark green mudstones (lithofacies 5c) (Table 6.2). The proportions of each sub-lithofacies to the total number of beds are shown in Figure 6.8*a*, and the proportions of each sub-lithofacies to the total sequence thickness are shown in Figure 6.8*b* (calculations shown in Appendix VII).

6.3.1: *Intraformational conglomerates* (Plate 6.8*a*)

Conglomerates are the coarsest lithofacies at Targrove Quarry and represent 22% of the total sequence thickness (Figure 6.8*b*). Although there are some minor differences, these conglomerates are similar to those seen in the Tredomen Quarry sequence, and have therefore been assigned to the same two sub-lithofacies, defined by composition, colour and lithofacies associations (see Table 6.2).

1a: Green intraformational conglomerates
1b: Red (to yellowish-brown) intraformational conglomerates

1a: Green intraformational conglomerates represent 8% of the total sequence thickness (Figure 6.8*b*). They are clast-supported, composed mainly of sub-rounded to rounded, sub-spherical to elongate clasts, ranging in size from small pebble to cobble (majority around 7 to 8cm and up to 10cm in diameter, slightly larger than those seen at Tredomen Quarry). Clasts are composed of carbonate nodules, green mudstone pebbles, and some red to yellowish-brown pebbles composed of silt-sized calcite or quartz grains. Disseminated charcoalified or coalified vegetative debris also occurs within these conglomerates, but less than seen in the green conglomerates at Tredomen Quarry. The matrix is composed of quartz and calcite sand-sized grains, and some mica, although much less than the equivalent conglomerates at Tredomen Quarry.

These conglomerates have a massive structure, with no bedding recognised. Bed thickness ranges from 0.4 to 0.5m. Bed bases are sharp and undulating, and truncate into either red to yellowish-brown medium-grained sandstone (lithofacies 2c) or yellowish-brown very-fine-grained sandstone to siltstone (lithofacies 3c) (Table 6.2). Upper boundaries are sharp and planar or undulating, and are overlain by red to yellowish-brown intraformational conglomerate (lithofacies 1b).

Table 6.2: Lithofacies descriptions for Targrove Quarry strata

	Colour	*Grain size*	*Texture*	*Composition*	*Sedimentary structures*	*Architecture*	*Associations*	*Rock Type*
1a	Green	Small pebbles to cobbles -6 to -4φ	Clast supported. Grains well sorted, sub-rounded.	Clasts: carbonate nodules, green mudstone pebbles, red to buff pebbles with silt-sized grains. Charcoalified vegetative debris. Matrix: quartz, calcite sand sized grains.	Massive. No bedding.	Bed thickness: 0.40 to 0.50m. Sharp, undulating bases. Sharp, planar upper boundaries.	Truncates 2c (50%) and 3c (50%). Overlain by 1b (100%).	Green intra-formational conglomerate
1b	Red to buff coloured	Large pebbles to gravel -5 to -1φ	Clast supported. Grains well sorted, sub-rounded.	Clasts: carbonate nodules, red to buff pebbles with silt-sized grains. Matrix: quartz, calcite sand sized grains and red mud.	Massive. No bedding. Slight normal grading upwards.	Bed thickness: 0.20 to 0.60m. Sharp, undulating bases. Sharp, planar upper boundaries.	Truncates 1a (50%), 3c (25%), 2c (25%). Overlain by 3c (50%), 2c (50%).	Red to yellowish-brown intra-formational conglomerate
2c	Red to buff coloured	Medium grained sand 1 to 2φ (0-1φ at base)	Matrix supported. Grains well sorted, rounded.	Quartz ,mica, calcite sand sized grains.	Massive to planar bedded (1cm to 2cm thick). Slight normal grading upwards. Upper stacked units with low-angle planar-cross or trough-cross-bedded to laminated. Vertical fissures infilled with carbonate nodules, cut by lithofacies above.	Bed thickness 0.16 to 2.5m. Sharp, planar or undulating bases. Sharp, planar or undulating upper boundaries.	Overlies 1b (40%), 2c (40%) and 3c (20%). Overlain by 2c (40%), 1b (20%), 3c (20%), 1a (20%).	Red to yellowish-brown medium - grained sandstones
3c	Buff coloured	Very fine grained sand to silt 3 to 6φ.	Matrix supported. Grains well sorted, rounded.	Clasts: coalified compressed and charcoalified plant debris. Matrix: mudstone, mica, quartz, calcite, silt sized grains.	Planar laminations (0.5mm thick). Slight normal grading upwards. Basal planar laminations blacker every 3-5mm, contain increased amounts of plant debris compared to previous lamination.	Bed thickness 0.1 to 0.2m. Sharp planar bases. Sharp, planar upper boundaries.	Overlies 5c (67%), 1b (22%), 2c (11%). Overlain by 5c (67%), 1a (11%), 1b (11%), 2c (11%).	Yellowish-brown wavy to planar laminated siltstones.

Table 6.2: Lithofacies descriptions for Targrove Quarry strata (continued).

5c	Dark green to dark grey.	Silt to clay 8φ	Matrix supported.	Clasts: some coalified compressed plant debris. Matrix: mudstone, silt-clay sized grains.	Massive to finely planar and wavy-laminations (0.5 mm thick). Coalified material only found in the uppermost laminations below a lithofacies transition above. Remaining laminations barren.	Bed thickness 0.15 to 0.2m. Sharp, planar to gradational bases. Sharp planar upper boundaries.	Overlies 3c (100%). And Overlain by 3c (100%).	Dark green planar and wavy-laminated mudstones.

Figure 6.8a: Proportions of Targrove Quarry lithofacies by the number of beds

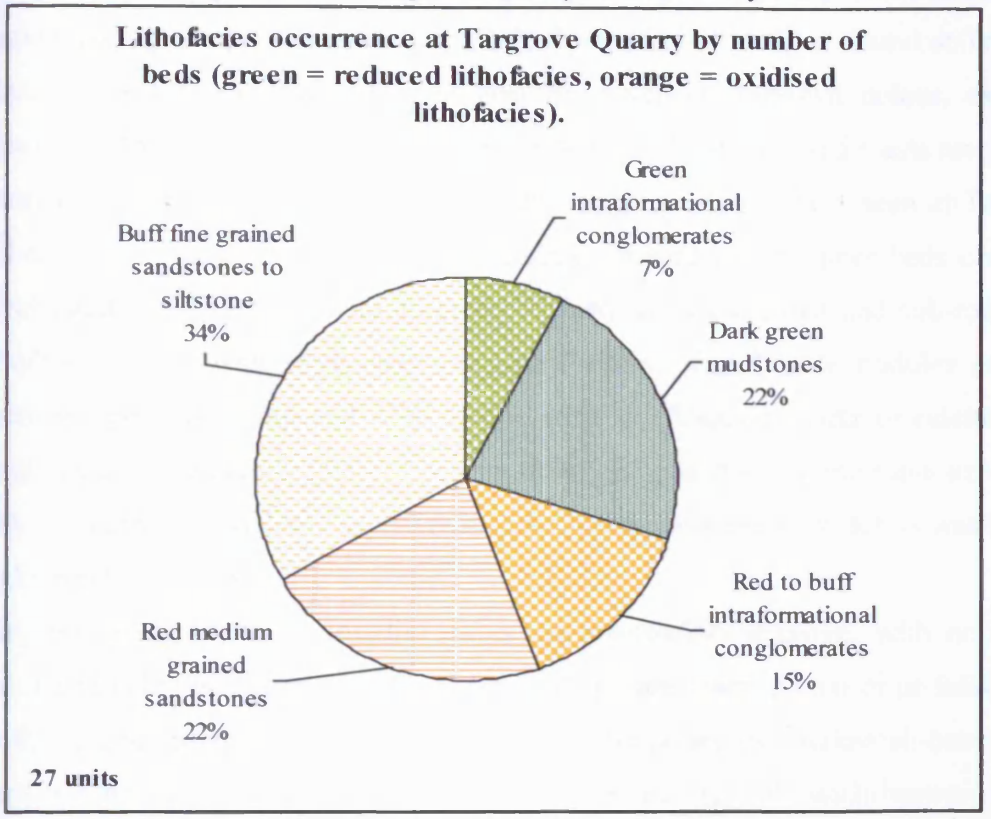

Figure 6.8b: Proportions of Targrove Quarry lithofacies by lithofacies thickness

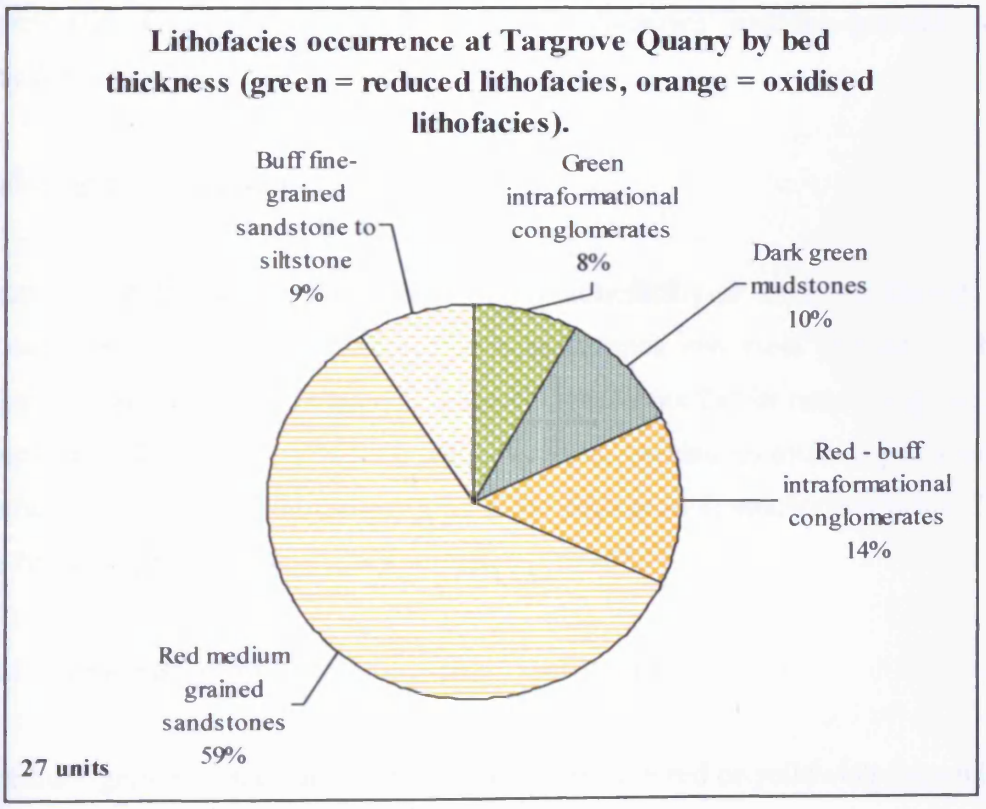

1b: Fourteen percent of the total sequence thickness at Targrove Quarry is composed of red intraformational conglomerates (Figure 6.8*b*), which are similar to those found at Tredomen Quarry, but here these conglomerates can also be a yellowish-brown colour, especially towards the top of the conglomeratic units. Large pebble and cobble-sized clasts are found in the basal beds, with diameters between 4 and 7cm, slightly smaller than seen at Tredomen Quarry. These conglomerates exhibit normal grading upwards, with upper beds containing small gravel-sized clasts (1 to 4cm in diameter). Clasts are well-sorted and sub-rounded to rounded, sub-spherical to elongate, and composed either of carbonate nodules or red to yellowish-brown pebbles, composed of very-fine-sand to silt-sized quartz or calcite grains. These conglomerates are clast-supported, with a matrix of quartz or calcite sand-sized grains or red mud. Similar to the equivalents at Tredomen Quarry, no vegetative debris was found in these conglomerates.

As seen in lithofacies 1a, these conglomerates are structurally massive, with no bedding recognised. Bed thickness ranges from 0.2 to 0.6m. Bases are sharp, planar or undulating, and truncate either green intraformational conglomerates (lithofacies 1a), yellowish-brown, very-fine-grained sandstone to siltstone (lithofacies 3c), or red to yellowish-brown medium-grained sandstone (lithofacies 2c) (Plate 6.8*a*). Upper boundaries are sharp and planar and these red conglomerates are overlain by either yellowish-brown very-fine-grained sandstones to siltstones (lithofacies 3c), or red to yellowish-brown medium-grained sandstone (lithofacies 2c).

6.3.2: *Medium-grained sandstones* (Plate 6.8)

Medium-grained sandstones are the most common lithofacies at Targrove Quarry (59% of total sequence thickness, Figure 6.8*b*). These sandstones are most similar to the green medium-grained sandstones at Tredomen Quarry (lithofacies 2a) in terms of grain size and bed thickness, but also have similarities with the thinly-bedded medium-grained sandstones within the heterolithic units (lithofacies 4), as some beds exhibit similar bedforms. Therefore these have been assigned to a new sub-lithofacies (Table 6.2):

2c: Red to yellowish-brown medium-grained sandstones

2c: The medium-grained sandstones at Targrove Quarry are red or yellowish-brown in colour in the upper beds. Grain size ranges from coarse-grained sand at the base of these units, and

exhibit slight normal grading to medium-grained sand in the majority of the beds. These sandstones are composed primarily of sand-sized, sub-spherical quartz grains, but there is a significant amount of mica and therefore can be described as litharenites, although less than the sandstones from Tredomen Quarry. The matrix is composed of carbonate-rich clay.

Basal units are massive to planar bedded (beds 1 to 2cm thick), (Plate 6.8*b*) and fine upwards into low-angle (3°), planar or trough-cross-bedded or laminated stacked units. Some of these upper units have concave bases (Plate 6.8*b*). In one medium-grained sandstone unit, the upper beds contained sub-vertically-aligned fissures, approximately 0.5m in the length and 3cm in diameter at the widest point (Plate 6.7*c*). These fissures are infilled with carbonate. These fissures do not continue into the next lithofacies above.

Bed thickness ranges from 0.16 to 2.5m. Unit bases are sharp, planar or undulating and overlie red to yellowish-brown intraformational conglomerates (lithofacies 1b), or yellowish-brown very-fine-grained sandstones to siltstones (lithofacies 3c) (Plate 6.8*d*), whilst the remaining are stacked (Table 6.2).

6.3.3: *Very-fine-grained sandstones and siltstones* (Plate 6.9)

Siltstones (and very-fine-grained sandstones) represent 9% of the total sequence thickness at Targrove Quarry (Figure 6.8*b*). They are most similar to the green, wavy to planar-laminated siltstones at Tredomen Quarry (lithofacies 3a). However, unlike the siltstones are Tredomen Quarry, they are tabular, approximately a minimum of 22m in lateral extent, with sharp planar lower and upper boundaries, and are interbedded with dark green mudstones (see section 6.3.4.). Due to these differences in composition, colour and lithofacies association, these siltstones have been assigned to a new sub-lithofacies:

3c: Yellowish-brown, very-fine-grained sandstone to siltstones

3c: The very-fine-grained sandstones to siltstones at Targrove Quarry are yellowish-brown in colour, with grain sizes ranging from very-fine-grained sand at the base of the units, fining upwards to silt-sized grains in the upper beds. Grains are well-sorted and rounded and composed of quartz, calcite and argillaceous grains. Some mica grains are present, but are not as common as seen in the siltstones at Tredomen Quarry. These siltstones also contain a prolific amount of vegetative debris, occurring along the bedding planes of planar-laminations (each 0.5mm thick), some of which are only partially fragmented coalified

compressions and recognisable as rhyniophytoids. Towards the bases of the units, approximately every 3 to 5mm, a black band of laminations are packed with thalloid vegetative debris (possibly *Prototaxites)*, plus possible faunal fragments, whilst upper beds contain less, but more intact fragments (see Chapter 7 for a description of the plant taphofacies).

Bed thickness ranges from 0.1 to 0.2m. Both lower and upper boundaries of these siltstones are sharp and planar (Plate 6.9*a*), and overlie red intraformational conglomerates (lithofacies 1b), or red medium-grained sandstones (lithofacies 2c) (Plate 6.8*d*), but are more commonly interbedded with dark green mudstones (lithofacies 5c) (Plates 6.9*a*, 6.9*b* and 6.9*c*) (Table 6.2). These siltstones are either overlain by dark green mudstones (lithofacies 5c), green intraformational conglomerates (lithofacies 1a), red intraformational conglomerates (lithofacies 1b) or red medium-grained sandstones (lithofacies 2c) (Table 6.2).

6.3.4: *Mudstones* (Plate 6.9)

Mudstones represent 10% of the total sequence thickness at Targrove Quarry (Figure 6.8*b*). These mudstones are unlike those seen at Tredomen Quarry, in terms of colour, bedforms and composition, and therefore have been assigned a new sub-lithofacies:

5c: Dark green to dark grey mudstones

5c: Unlike the mudstones seen in the Tredomen Quarry sequence, these mudstones are dark green to dark grey in colour, and are either massive in structure or finely, wavy or planar-laminated (maximum of 0.5mm thick). These mudstones are mainly composed of argillaceous silt-sized grains to clay. The majority of the mudstone units are barren of any vegetative debris, although some coalified, non-embryophyte debris is present in the uppermost laminations, just below the base of the interbedded yellowish-brown siltstones above (lithofacies 3c).

Bed thickness ranges between 0.15 and 0.2m, and are laterally extensive. Lower boundaries are either sharp and planar, or gradational, and always occur interbedded with yellowish-brown siltstones (lithofacies 3c) (Plates 6.9*a* and 6.9*b*) and in some cases appear to gradually wedge or pinch out (Plate 6.9*c*). Upper boundaries are sharp and planar, where yellowish-brown siltstones occur above.

6.4: LITHOFACIES INTERPRETATIONS

Table 6.3 summarises the five main lithofacies from both Tredomen Quarry and Targrove Quarry sequences, together with interpretations for sedimentary processes and the resulting sedimentary elements, and finally interpretations of the overall geomorphic models.

6.4.1: *Intraformational conglomerates*

The conglomeratic beds at both Tredomen Quarry and Targrove Quarry overlie sharp, planar erosive bases and were deposited as clast-supported, coarsely planar to massive beds, suggesting transportation as traction or saltation along fluvial channel bases, under supercritical flow (>1m/s) (Miall 1996, Bridge 2006, Church 2006). Similar beds are described from time-equivalent sequences in Shropshire and Pembrokeshire by Allen (1964), Allen and Dineley (1976), Allen and Williams (1978), and recently by Hillier et al. (2007) as basal lag for multi-storey sandstone complexes.

At Tredomen Quarry, where conglomeratic beds (mostly reduced green, as lithofacies 1a) overlie major erosional boundaries, with cross-bedded, multi-storey sandstone beds occurring above (lithofacies 2a), they represent major channel lag deposits, with conglomeratic erosive bases likely representing long-term channel migration and avulsion (Miall 1996, Bridge 2003).

Where thinner conglomeratic units (often oxidised red as lithofacies 1b) are interbedded between heterolithics (lithofacies 4) massive mudstones (lithofacies 5a), they may represent basal crevasse splay beds, where during flood conditions, unconfined flow carries coarser material to the distal portions of the fluvial system, followed by deposition of overbank fines in a lower flow regime. Gravel beds interbedded between overbank fines may represent a brief return to supercritical flow. The undulating bases of the oxidised red conglomerates (lithofacies 1b) represent erosional boundaries associated with minor channel scouring or crevasse splaying.

The same can be seen in Targrove Quarry, where red to yellowish-brown conglomerates (lithofacies 1b) with erosive bases either occur as the basal lag of red-medium-grained sandstone bodies (lithofacies 2c), or are interbedded with much finer-grained, laterally extensive siltstone and mudstone interbedded sequences (lithofacies 3c and 5c), where they may represent basal crevasse splay beds deposited under supercritical flow.

Table 6.3: Lithofacies interpretations for Tredomen Quarry and Targrove Quarry

	Lithofacies	*Processes*	*Sedimentary element(s)*	*Geomorphic model*
1a	Green to grey, clast-supported, massive to planar-bedded, intraformational conglomerates. Thinly-bedded, undulating base. Laterally extensive.	Erosion, reworking. Upper flow regime bedload transport. Vertical accretion. Rapid burial and iron reduction.	Gravel bar / basal channel lag. Base of perennial channels or crevasse splays.	Sand-dominated, possibly perennial river channel lag/ basal crevasse splay lag.
1b	Red, clast-supported, massive to planar-bedded, intraformational conglomerate. Thinly-bedded, undulating base.	Erosion, reworking. Upper flow regime bedload transport. Vertical accretion. Exposure and iron oxidation.	Gravel bar/ basal heterolithic channel lag. Base of ephemeral channel bar, or crevasse splay.	Ephemeral (dryland), mud-dominated river channel lag/ basal crevasse splay lag.
2a	Planar and planar-cross-bedded, medium-grained micaceous green to grey sandstones. Thickly bedded, normal grading upwards, planar boundaries. Parting lineations and rip up clasts in basal units.	Erosion. Upper flow regime – bedload/ saltation. Vertical accretion and lateral accretion of 2D dunes. Rapid burial and iron reduction.	2D dune migration, accretion on point or transverse bar of major river channel.	Sand-dominated, possibly perennial river channel.
2b	Green to grey, small-scale trough-cross-bedded and cross-ripple-laminated fine-grained micaceous sandstones. Alternating calcareous and organic-rich laminations.	Lateral accretion in lower flow regime of 3D dunes. Iron reduction. Small scale erosive scours.	3D dune migration, lateral accretion on upper point bar, transverse bar or bar top channels. Minor channel sandstones.	Sand-dominated, possibly perennial minor river channel/ crevasse splay channel.
2c	Massive to planar bedded, red to yellowish-brown medium-grained sandstone. Stacked units of low-angle, planar-cross or trough-cross-bedded or laminated siltstone in the upper beds, some with concave bases.	Erosion. Upper flow regime Transportation by bedload and saltation Vertical and lateral accretion. Lateral accretion of 2D and 3D dunes.	2D dune migration and some 3D dune migration, and lateral accretion on point or transverse bar of possible ephemeral low- angle river channel or crevasse splay.	Minor crevasse splay channels of sand-dominated, possibly perennial or ephemeral river system.
3a	Green to grey planar and wavy-laminated siltstones. Thinly-bedded, alternating calcareous silt and organic rich mud, plus mottling (iron oxide spots).	Vertical accretion. Slight hydraulic reworking. Wavy and current ripple laminations. Iron reduction and rapid burial.	Floodplain deposition, proximal to channels. Abandoned meanders, backswamps or waterholes (lacustrine).	Floodplain proximal to sand-dominated, possibly perennial river.

Table 6.3: Lithofacies interpretations for Tredomen Quarry and Targrove Quarry (continued)

3b	Red planar and wavy-laminated siltstones. Thinly-bedded, alternating calcareous silt and mud. Climbing-ripple-laminations, convoluted bedding. Mottling. Sparse distribution of carbonate nodules, grey vertical fabric.	Vertical accretion. Slight hydraulic reworking– wavy and current ripple laminations. Exposure, pedogenesis.	Floodplain deposition, distal to channels. Exposed, ephemeral abandoned meanders, backswamps or waterholes (lacustrine).	Floodplain of sand-dominated possibly perennial river or ephemeral (dryland), mud-dominated river.
3c	Yellowish-brown very fine-grained sandstone to siltstone, finely planar-laminated, with prolific vegetative debris occurring as black bands. Sharp, planar upper and lower boundaries, interbedded with 5c.	Erosion, vertical accretion of bedload in upper or lower flow regime?	Unconfined vertical accretion by crevasse splays/ overbank floodplain fines.	Floodplain or crevasse splay of possibly perennial or ephemeral, sand dominated river.
4	Red inclined or planar interbedded gravel, sand, silt and mud. Low-angle cross-bedded units with concave erosional bases. Small scale trough-cross-bedding and cross-ripple-lamination. Upper units with vertical fabric, carbonate nodules, drab halos.	Erosion, upper flow regime. Vertical accretion and lateral migration of 2D and 3D dunes. High discharge, sporadic events. Weak pedogenesis.	Lateral accretion of ephemeral channels bars. Unconfined vertical accretion by crevasse splays / flooding. Ephemeral braided channels and ephemeral crevasse splays.	Ephemeral (dryland), mud-dominated river channels.
5a	Featureless massive mudstones. Occasional planar laminations. Drab haloed vertical fabric and sparse carbonate nodules.	Vertical accretion of overbank suspended fines or mud aggregates. Confined lower flow regime. Weak pedogenesis.	Overbank floodplain fines or accretion of mud aggregates in ephemeral muddy channels.	Ephemeral (dryland), mud-dominated river channels.
5b	Pedified mudstones. No primary stratification, dark grey vertically-aligned fabric, curved pseudo anticlinal slip-plane surfaces, and varying intensity of carbonate nodules.	Vertical accretion of suspended fines, or mud aggregates. Pedogenesis.	Overbank floodplain fines as bedload.0 Prolonged exposure and pedification.	Pedified floodplain of sand-dominated, possibly perennial river or ephemeral (dryland), mud- dominated braided river.
5c	Dark green, massive to wavy or planar-laminated mudstone. Planar or gradational lower boundary. Laterally extensive. Interbedded with 3c.	Vertical accretion in lower flow regime of suspended load. Slight hydraulic reworking to wavy ripple laminations.	Unconfined vertical accretion by crevasse splays/ overbank floodplain fines.	Floodplain or crevasse splay of possibly perennial or ephemeral river system.

6.4.2: *Sandstones*

Thick, multi-storey sheet-like sandstones (lithofacies 2a and 2c) that overlie basal conglomeratic lags were deposited rapidly during high-energy events as bed load (Collinson 1996).

At Tredomen Quarry, green medium-grained sandstones (lithofacies 2a) exhibit planar-bedding with parting lineations that indicate vertical accretion in an upper flow regime (around 1 m/s, with a water depth of 0.25 to 0.5m for medium sand grains) (Miall 1996). This is supported by the presence of eroded, fragmentary and randomly-orientated vegetative material, occurring parallel or oblique to bedding planes, as well as mud-rip up clast horizons, which may represent traction beds on channel floors or basal lags of crevasse splay deposits.

The planar-cross-bedded units observed from the upper beds of lithofacies 2a could represent lateral accretion on the inside of a migrating, channel meander (accretion on a point bar) (Allen 1964, Bridge 2003, 2006). Overlying gradationally, smaller-scaled, planar-bound and multistorey cross-bedded units occurs, created by the migration of straight-crested 2D dunes in the lower dune field flow regime (0.5m/s for grains approximately 0.5mm in diameter), depositing sand on the upper point bar (Miall 1996, Bridge 2003, 2006).

Alternatively, as it is difficult to determine from core if accretion occurred laterally or downstream, these sets of planar cross-bedded sandstones may have been deposited via downstream accretion and represent transverse bars instead of point bars. If this is the case, the absence of point bars would suggest that the rivers were not meandering.

Occurring mainly above lithofacies 2a, green fine-grained sandstones (lithofacies 2b) have concave, scour-shaped bases and are stacked, small-scale trough-cross, cross-ripple and climbing-ripple-laminated. The ripples were generated in a lower flow regime (less than 0.6 m/s for grain between 0.125-0.25mm in diameter) from a unidirectional smooth flow (Miall 1996, Bridge 2003). Cross-ripple laminations represent migration of straight crested ripples, with equal sedimentation and erosion rates. The occurrences of climbing-ripple-laminations represent an increase in sedimentation rates above erosion rates, preserving the stoss sides of the ripples (Allen 1971). The migration of curved-crested 3D dunes, generated from turbulent flow, created the trough-cross-bedded units, with erosional, small-scale scour bases (Miall 1996). These channelised units may represent minor bar-top channels, which incised into finer grained, reduced siltstones, or where these units occur gradationally above reduced medium-grained sandstones, reworking or accretion of upper bar sediments.

Similar Old Red Sandstone sequences from the St. Maughans Formation and the equivalents are described by Allen and co-authors (Allen and Tarlo 1963, Allen 1964, Allen and Williams 1978), as classic perennial, meandering channel fining-upwards sequences, with conglomeratic basal lags.

At Targrove Quarry, red to yellowish-brown medium-grained sandstones (lithofacies 2c) exhibit horizontal bedding, planar or trough cross-bedding, indicating a similar upper flow regime, vertical accretion and lateral accretion of 2D and 3D dunes, as interpreted for lithofacies 2a and 2b. However, cross-beds dip at a much lower angle than observed in lithofacies 2a and 2b (3° compared to 20°), suggesting that lateral accretion occurred on lower-angle channels or bars. Slight normal grading is observed within these sandstones, but the classic fining upwards sequence of a perennial, meandering channel is not present. Instead, these sandstones are interbedded sharply with either conglomerates (lithofacies 1a and 1b) or much finer grained siltstone-mudstone interbedded sequences (lithofacies 3c and 5c), and therefore may represent minor crevasse splay channels. These sandstones also resemble the much thinner bedded, red medium-grained sandstones that are interbedded within red siltstones and mudstones of the heterolithics units observed at Tredomen Quarry (see section 6.2.4), and may either represent minor crevasse splay channels, or lateral accretion of ephemeral channels (see section 6.4.4 for heterolithics interpretations). The presence of large fissures within the upper units of lithofacies 2c, infilled with carbonate cylindrical rods that are cut by the conglomeratic beds above, may indicate that the top of these sandstones were exposed, with fissures either representing polygonal cracking or the anchoring system of large fungal-like organism, *Prototaxites* (similar to structures described by Hillier et al. 2008) (see Chapters 3 and 7), and could represent ephemeral channels.

6.4.3: *Siltstones*

Siltstones are found at both Tredomen Quarry and Targrove Quarry and were deposited when silt-sized grains were transported by suspension in either an upper or lower flow regime. Silt either settled out from floodwaters or upper crevasse splay deposits on the floodplain, which resulted in either laterally extensive vertical accretion, or confined bar-top deposits, proximal to the channel deposits (Miall 1996).

Rare green siltstones at Tredomen Quarry (lithofacies 3a) are not laterally extensive and occur in close proximity to, or are interbedded with fine-grained green sandstones (lithofacies 2b), and therefore were closely associated with the minor channel deposits described in

section 6.4.2. Alternating argillaceous, organic-rich laminations with micrite-rich laminations may be the result of fluctuating flow, possibly associated with seasonality. Wavy and cross-ripple-laminations resulted from the reworking of this material by wind-generated wave or current flow.

Conversely, yellowish-brown horizontally laminated siltstones (lithofacies 3c) at Targrove Quarry are laterally extensive, and interbedded sharply with lithofacies 1b and 2c, (red conglomerates and red medium-grained sandstones), which have been interpreted as basal crevasse splay lag and channel deposits (sections 6.4.2 and 6.4.3). These siltstones may have been deposited as upper crevasse splay beds, in an upper flow regime, resulting in laterally extensive vertical accretion.

Overlying the reduced siltstones at Tredomen Quarry, red oxidised siltstones (lithofacies 3b) show signs of exposure and weak pedogenesis. Basal units are horizontally laminated, which were deposited from suspension and were locally reduced. Wavy and current-ripple laminations resulted from the reworking of material by shallow floodwaters in lower flow conditions. The vertically-aligned linear features that occur in the upper beds may represent closed desiccation cracks, burrows or rhizoliths (roots). Polygonal cracking on some bedding surfaces, indicate periods of wetting, exposure and subsequent drying. Iron reduction spots and blue-purple drab haloes surround these vertically-aligned linear features, along with sparse carbonate nodules. Drab haloes (also known as pseudo-gleying) formed as a result of a fluctuating water table near the surface, or water logging (Duchaufour 1982, Wright 1992). Periodic water logging of soils at the surface resulted in reduced waters penetrating previously formed desiccation cracks and burrows, resulting in localised iron reduction (drab haloes) around the remaining oxidised siltstone.

Towards the base of the red siltstones, the *Undichna* fish trails found in association with *Diplichnites* arthropod trackways (Morrissey et al. 2004), have been interpreted as 'cruising' or resting traces of cephalaspid fish, in a "fluvial backwater or floodplain pool" environment (Morrissey et al. 2004). Possible makers of the *Diplichnites* trackways include the kampecariid myriapods or euthycarcinoids (Morrissey et al. 2004).

The oxidised siltstones could be distal floodplain deposits, or ephemeral deposition and reworking of material within abandoned or isolated portions of the fluvial system, such as abandoned meanders, or larger scale waterholes or billabongs, created by the channel expansion and scouring, which may have been subsequently abandoned (Knighton and Nanson 2000). Seasonal drying of these waterbodies resulted in weak pedogenesis.

6.4.4: *Heterolithics*

The oxidised heterolithics at Tredomen Quarry exhibit similar features to the reduced channel sandstones and siltstones (lithofacies 2a, 2b and 3a), (cross and planar-bedded units with erosional, channelised bases) and were deposited from bedload and suspension within fluvial channels, with oxidised intraformational conglomerates (lithofacies 1b) at the base as channel lag.

However, the oxidised heterolithics differ from the reduced sandstones and siltstones with the lack of ordered, gradationally fining-upwards, multi-storey sequences. Instead, these deposits consist of thinly-bedded, unordered sequences of laminations with sharp changes in grain size, indicating a sharp fluctuation in flow regime (ranging from >1m/s for pebble-sized grains transported as bedload and deposited as channel lag or gravel lenses, to less than 0.6m/s for silt grains to form cross-ripple-lamination).

Similarly to the cross-bedded green sandstones (lithofacies 2a), inclined heterolithics represent lateral accretion of migrating channel point bars, or downstream accretion of transverse bars. However, the inclined heterolithics exhibit trough cross-bedding at shallower dip angles (<10°) than seen in the green sandstone units and are much thinner, indicating that these units may represent the migration of shallow bars in minor channels. These channels were muddier than the green sandstone channels (lithofacies 2a and 2b), and deposition occurred under an ephemeral flow regime, with sharp fluctuations in flow with periods of exposure resulting in slight pedogenesis. Similar heterolithic sequences are described by Marriott and Wright (2004) for the Moor Cliffs Formation, the lateral equivalent of the Raglan Mudstone Formation in Pembrokeshire. Shallow, channel related muddy accretionary benches from the Channel County modern dryland rivers systems described by Gibling et al. (1998), show analogous mud-dominated inclined heterolithic units.

Planar-bedded heterolithics are thin and tabular in nature and represent unconfined deposition, either in an upper flow regime, such as crevasse splay deposits, or where localised channel scouring occurred to form waterholes or billabongs (Knighton and Nanson 2000). Alternatively, deposition may have occurred in distal floodouts, where river competence was lost and sediment was deposited under low flow regime. Both waterholes and floodouts are common in the Channel Country, Australia, and are components of river systems on low gradient landscapes (Knighton and Nanson 2000, Tooth 2000). Rivers of the Channel Country are wide, active multi-channel belts that comprise numerous anastomosing to braided channels (Gibling et al. 1998), and maybe a modern analogue for the ephemeral,

muddy channels envisaged for the deposition of Old Red Sandstone oxidised heterolithics (see Appendix IX).

5.4.5: *Mudstones*

The red massive mudstones at Tredomen Quarry (lithofacies 5a), may be interpreted as structureless, bioturbated floodplain fines, deposited from suspension, where no to weak pedogenesis had occurred due to a rapid sedimentation rate. However, on closer inspection the mudstones are composed of mud aggregates. This type of texture is known as pseudo-pedodestratification, a term coined by Müller et al. (2004) for channel sediments that have lost their original texture of reworked mud aggregates. This texture is often lost due to compaction (Müller et al. 2004), and is only visible here due to an apparent difference in composition between the mud aggregates and the matrix, or where calcite or quartz clasts occur along side the mud aggregates.

Similar aggregates, formed pedogenically, are known to be reworked from modern and ancient floodplains, and deposited as bedload aggregates (Ékes 1993, Maroulis and Nanson 1996, Müller et al. 2004, Wright and Marriott 2007). These mud aggregates occur interbedded with coarser grained heterolithic units. Potentially, these reworked mud aggregates were re-deposited on floodplains, and became re-pedified or deposited as abandoned channel fills, making interpretation difficult.

Pedified profiles type 1 are distinctive from type 2 profiles, with three clear horizons that resemble calcic palaeo-Vertisols. Modern Vertisols form in swelling-clay-rich soils (e.g. smectite), that have experienced a strong wet-dry seasonal or flood related contrast in soil moisture (NRCS 1999).

In these palaeosols, the upper horizon is the equivalent of the A-horizon of modern and palaeo-Vertisols. From the Tredomen Quarry sequences, this horizon is poorly preserved, primarily due to incision of major channel migration above, resulting in the removal of horizon A. However, A-B horizons are present, where the fabric of dark-grey, vertically-aligned linear features might represent the closed bases of the long desiccation cracks. These are seen above and locally overprinting the middle, structural B-horizon. Other, bifurcating linear features are present, created by the pseudo-gleying of burrows or roots. Fossil evidence from Tredomen Quarry indicate that plants only grew up to a minimum of 6cm in height (*Salopella allenii* specimen), with axes no more than 2mm in width (see Chapter 3), and therefore may not have had sufficiently sized rooting systems to form vertically-aligned

linear features up to 10cm in length. Exceptional preservation of rhizomal axes of basal embryophytes in the Rhynie Chert, Scotland, indicates shallow to creeping rooting systems (e.g. *Aglaophyton*, Edwards 1986) rather than tap rooting systems. Alternatively, similar bifurcating features have recently been interpreted as possible anchorage and nutrient seeking hyphal aggregations for a fungal-like organism such as *Prototaxites* (Hillier et al. 2008).

The middle horizons of these palaeosols are distinctive with slickensided, anticlinal slip-plane surfaces that are comparable to the structural B-horizon of modern Vertisols. It was the shrinking and swelling of the clays, as a result of changing hydration states that produced the distinctive middle structural B-horizon as seen in modern Vertisols (Wilding and Tessier 1988). Shear stresses were created as the soils unevenly expanded and contracted, forming the slip-plane surfaces where the soil lost strength.

Beneath the structural B-horizon, the C-horizon contains varying intensities of carbonate nodules. These are analogous to the nodules interpretated as pedogenic calcretes by Allen (1986), which are widespread in the Old Red Sandstone of South Wales. At Tredomen Quarry, these near surface accumulations of calcium carbonate range in developmental stages I to III, as defined by Machette (1985): stage I consists of isolated, sparse calcrete glaebules 5-10mm in diameter, stage II exhibits large, vertical calcrete rods, 10-40mm in diameter and 200mm long, while stage III forms a matrix of coalescing calcrete nodules, with up to 60% carbonate content. Calcrete developmental stages are related to soil residence time, i.e. the amount of time spent in the pedogenic zone, which is related to deposition rates of the host sediment (Wright and Marriott 1996). For a stage II to III calcrete horizon to develop, a residence time of 10^4 to 0.5 x 10^6 years is required, meaning that sedimentary rates were as slow as 2 to 0.02mm 10^3 a^{-1} (Wright and Marriott 1996). Therefore, the two well-developed calcrete bands (interpreted as the Bishop's Frome Limestone), represent a significant period of pedogenesis (potentially the two calcrete bands represent up to one million years) and hence a prolonged period of very little or no deposition.

The palaeo-Vertisols are rarely found as complete individual profiles, and are often stacked, generated by a series of depositional and erosional events, representing a dynamic floodplain (Marriott and Wright 2006). Tredomen Quarry palaeo-Vertisol profiles represent cumulate or composite sequences. In cumulate profiles, aggraded sequences form as a result of slow, continuous sedimentation, as the whole profile aggrades upwards, and gradual overprinting occurred (Marriott and Wright 1993, 2006). In composite profiles episodic, higher rates of sedimentation partially buried the profile, and a new profile develops, partially overprinting the profile beneath.

Calcretes typically (but not always) develop in semi-arid climates, with a net moisture deficiency (Wright 2007). Estimates of annual precipitation range from 100-500mm (Goudie 1983), 500-700mm (Khadkikar et al. 2000), to estimates from modern US calcic soils with a mean annual precipitation of <760mm (Royer 1999). 65% of modern Vertisol associated calcrete horizons occur in an ustic soil moisture regime (limited moisture, with a rainy season) (NRCS 1999). Mean annual temperature has been estimated at 16-20°C, based on the localities of modern day calcretes (Goudie 1983).

Below the Bishop's Frome Limestone, pedified type 2 profiles are more common. In these palaeosols the A and the middle structural B-horizon usually associated with palaeo-Vertisols are absent. Instead these palaeosol bearing sequences are thick cumulate profiles resulting in stacked C-horizons with little evidence of erosional surfaces. These carbonate nodule horizons are less well-developed, with stage I to II calcrete horizon development, indicating a shorter residence time of $0.5x10^3$ to $0.2x10^6$ years (Wright and Marriott 1996), and a more gradual accumulation of sediment compared to the rapid burial, followed by low sedimentation rates required for well-developed calcrete C-horizons in the composite profiles of the observed palaeo-Vertisols. This may explain why horizons A and B were never preserved as the soil was gradually buried and abandoned, leaving only a stacked record of C-horizons.

Alternatively, the lack of a structural B-horizon in pedified profile type 2 mudstones may be due to the absence of frequent wetting and drying and therefore no process to form the pseudo-anticlinal slip-plane surfaces, as might have been the case on the distal portions of the floodplain, or the isolated terraces above the main channels. In this case, profiles would be more comparable to an Aridisol in modern soil classification (Retallack 2001).

The dark green to grey mudstones at Targrove Quarry (lithofacies 5c), were deposited by vertical accretion from suspension in a lower flow regime, resulting in the massive to finely laminated structure. Slight hydraulic reworking occurred, and resulted in wavy-lamination. These beds are essentially finer-grained equivalents of the green wavy or planar-laminated siltstones at Tredomen Quarry (lithofacies 3a), and represent either overbank floodplain deposits or upper crevasse splay deposits. As these mudstones are laterally extensive, and exhibit sharp, planar upper and lower boundaries, interbedded with laterally extensive siltstones (lithofacies 3c), they are most likely to be the upper beds of crevasse splay deposits.

6.5: MARKOV CHAIN ANALYSIS OF TREDOMEN QUARRY STRATA

Through observations of the Tredomen Quarry sequence (Figures 6.1 to 6.5), it appears that in certain sections, the arrangement of lithofacies defined in section 6.2 could be described as ordered or cyclic. This can also be described as possessing a Markovian property, where in a sequence of mutually exclusive states (in this case lithofacies), one state exhibits a dependence on the previous state (Powers and Easterling 1982). A test for the Markovian property, and the recognition of the most common state changes, may give clues to the stability or regularity to the sedimentation of the system.

To test if a sequence exhibits a Markovian property, a matrix of the state transitions from that sequence can be tested against statistical independence, using the following statistic:

$$\chi^2 = \sum \frac{(O-E)^2}{E}$$

Where O is the observed number of transitions from one lithofacies to the next, E is the number of expected lithofacies transitions if the sequence states were independent (Davis 2002). The value of χ^2 (with a specific number of degrees of freedom (v), calculated from the number of defined states in the sequence (m); ($v = (m-1)^2$), can then be compared to critical values from chi-squared distribution tables to determine the degree of statistical independence. The more the χ^2 value exceeds the critical value, the less likely the sequence is independent. That is, using the χ^2 test can determine if lithofacies states are independent or dependant on the previous state.

To test the hypothesis, two types of analysis can be performed, which depends on sampling technique. In Markov Chain Analysis, an *observed transitions* matrix is constructed from a sequence of lithologies sampled at a regular interval (10cm in this case) (Appendix VIII). This matrix is then used to create an *expected transitions* matrix, by dividing the fraction of each observed transition by the total number of transitions, to create a *fixed probability vector* for each matrix row, which is then converted into the *expected transitions probabilities* matrix (Davis 2002). Before these can be compared with the *observed transitions* matrix, probabilities are converted to total numbers, by multiplying each probability by the corresponding total number of observed transitions for that row. The resulting *expected transitions* matrix is then compared to the *observed transitions* matrix using the χ^2 statistic.

The total sequence was first tested using this method. States were defined as the lithofacies described in section 6.2: green conglomerates, red conglomerates, green cross-bedded medium-grained sandstones, green trough-cross-bedded, fine-grained sandstones, green

siltstones, red siltstones, heterolithics, non-pedogenic mudstones and pedogenic mudstones, and an *observed transitions* matrix was created (Table 6.4*a*). When the total sequence was tested, a strong Markovian property was recognised, with a χ^2 of 6117.35 exceeding the critical chi-squared value of 93.22 (with 64 degrees of freedom and 99% confidence level) (Table 6.4*c*). This indicates that at least a portion of the sequence exhibits a Markovian property. However, from observations of the lower portion of the sequence, it appears to be significantly different to the upper portion, and therefore two further tests were conducted on the two separate sequences. The base of the upper portion is defined as the first bed after the shallowest occurrence of a well-developed palaeo-Vertisol C-horizon (calcrete) at bed 136 of borehole 2, 62.8m below the quarry surface (Figures 6.4 and 6.5).

When tested with the χ^2 test, both portions of the sequence resulted in χ^2 values that exceeded the critical chi-squared values of 93.22, for a 99% confidence level and 64 degrees of freedom (Table 6.4*c*). However, a much stronger Markovian property was recognised in the upper sequence (with a χ^2 of 2375.05), compared with a weaker Markovian property for the lower sequence (with a χ^2 of 152.34). This suggests that lithofacies transitions in the upper sequence are more dependent on the previous transition (i.e. more ordered) than in the lower sequence.

However, using this method of Markov Chain Analysis can distort the χ^2 test. If transitions are recorded using a fixed sampling interval, transitions frequencies in the matrix reflect bed thickness (Table 6.4*a*). If the sampling interval used is small, values for same-state transitions can occur in the matrix, returning exaggerated χ^2 values. However, if the sampling interval is too large, transitions may be lost.

An alternative method, Embedded Markov Chain Analysis, can be used to avoid recording same-state transitions and records transitions as they occur, regardless of bed thickness (Powers and Easterling 1982). However, zero values for the same-state transitions would occur within the *observed transitions* matrix (Table 6.4*b*), voiding the use of a *fixed probability vector* in the calculation of the *expected transition probabilities* matrix, as unwanted probabilities for same-state transitions would be created.

To avoid this problem, values for same-state *observed transitions* are estimated using trial-and-error (Davis 2002). *Fixed probability vectors* are calculated using estimates for the diagonals within the *observed transitions* matrix, and subsequently calculated vector values are used as transitions probabilities for the same-state transitions. These probabilities are then powered, multiplied by the grand total and then used as new estimates for the diagonals in a second *observed transitions* matrix. This process is repeated until the estimated transitions

Table 6.4a: Observed transition matrix for Markov Chain Analysis of the Tredomen Quarry sequence.

		TO									Row totals
		1a	*1b*	*2a*	*2b*	*3a*	*3b*	*4*	*5a*	*5b*	
FROM	*1a*	35	0	11	3	1	0	1	0	0	51
	1b	1	20	0	0	0	4	3	1	0	29
	2a	1	0	107	3	8	1	0	0	0	120
	2b	2	0	0	46	3	1	0	0	2	54
	3a	3	0	3	1	52	3	1	0	2	65
	3b	0	2	0	0	0	154	5	2	15	178
	4	1	1	0	0	1	6	225	4	15	253
	5a	0	2	0	0	0	1	1	90	6	100
	5b	9	3	0	1	0	8	18	3	994	1036
Column totals		52	28	121	54	65	178	254	100	1034	**1886**
										Grand total	1886
										Number of transitions	1885

Table 6.4b: Observed transition matrix for Embedded Markov Chain Analysis of the Tredomen Quarry sequence.

		TO									Row totals
		1a	*1b*	*2a*	*2b*	*3a*	*3b*	*4*	*5a*	*5b*	
FROM	*1a*		0	11	3	1	0	1	0	0	16
	1b	1		0	0	0	4	3	1	0	9
	2a	1	0		3	8	1	0	0	0	13
	2b	2	0	0		3	1	0	0	2	8
	3a	3	0	3	1		3	1	0	2	13
	3b	0	2	0	0	0		5	2	15	24
	4	1	1	0	0	1	6		4	15	28
	5a	0	2	0	0	0	1	1		6	10
	5b	9	3	0	1	0	8	18	3		42
Column totals		17	8	14	8	13	24	29	10	40	**163**
										Grand total	163
										Number of transitions	163

Table 6.4c: Summary of Markov Chain Analysis and Embedded Markov Chain Analysis of Tredomen Quarry sequence.

	Series	t	m	v	$\chi 2$	critical value $\alpha 0.05$	critical value $\alpha 0.01$
Markov Chain Analysis	Total	1885	9	64	6117.35	83.68	93.22
	Upper sequence	1296	9	64	2375.05	83.68	93.22
	Lower sequence	588	5	16	152.34	26.29	32.00
Embedded Markov Chain Analysis	Total	163	9	55	78.19	73.31	82.29
	Upper sequence	154	9	55	97.55	73.31	82.29
	Lower sequence	21	5	11	0.189	19.68	24.73

frequencies for the diagonals remain the same after the matrix is powered. The *fixed probability vectors* calculated from this final matrix are used to create an *expected probabilities* matrix, assuming that the probability of a state transition equals the sum of the probability vectors of those two states. The resulting *expected probabilities* matrix is converted to expected frequencies by multiplying each element by the grand total of the final estimated transitions frequencies matrix. Before the *expected frequencies* matrix can be used against the observed frequencies matrix in the χ^2 test, the estimated diagonals are taken out of the matrix.

When the total sequence was tested against the χ^2 test using the embedded Markov Chain technique, χ^2 of 78.19 did not exceed the critical chi-squared value of 82.29 for a 99% confidence level, but did exceed the critical value of 73.31 for a 95% confidence level (with 55 degrees of freedom, calculated from $v = (m-1)^2 - m$) (Table 6.4*c*). When the upper sequence was tested separately, a conservative χ^2 value of 97.55 exceeded a critical value of 82.29 (Table 6.4*c*), whilst the lower sequence χ^2 value failed to exceed the critical value. Therefore, Embedded Markov Chain Analysis has shown that the upper sequence exhibits a Markovian property to a 99% confidence level, whilst the lower sequence does not.

The most common transitions (at least 3 occurrences) for the total sequence are shown in Figure 6.9*a*. Large arrows indicate transitions that have at least 5 occurrences. The dark-grey shaded area envelopes those transitions that occur in the lower sequence only. The dark grey shaded area also envelopes all the lithofacies that are oxidised red, whilst the remaining are lithofacies are all green. There is no clear sequence to the most common transitions in the dark grey shaded area, and interbedding between lithofacies is common, particularly between the heterolithics (lithofacies 4), pedogenic mudstones (lithofacies 5b) and the red wavy-laminated siltstones (lithofacies 3b). However, between the remaining lithofacies, a clear sequence is recognised; pedogenic mudstones (lithofacies 5b), to green intraformational conglomerates (lithofacies 1a), to planar and cross-bedded medium-grained sandstones (lithofacies 2a) to either green fine-grained sandstones (lithofacies 2b) or green wavy-laminated siltstones (lithofacies 3a), followed by red wavy-laminated siltstones (lithofacies 3b), and pedogenic mudstones (lithofacies 5b). Red intraformational conglomerates (lithofacies 1b), followed by heterolithics (lithofacies 4) also occur in the upper sequences, interbedded with red wavy-laminated siltstones (lithofacies 3b). A schematic log of these transitions for the upper sequence is shown in Figure 6.9*b*.

Although the Markov Chain Analysis was statistically inconclusive, by comparing the upper and lower sequences, it appears that the strata in the upper sequence were deposited in a

Figure 6.9a: Most common lithofacies transitions in Tredomen Quarry sequence

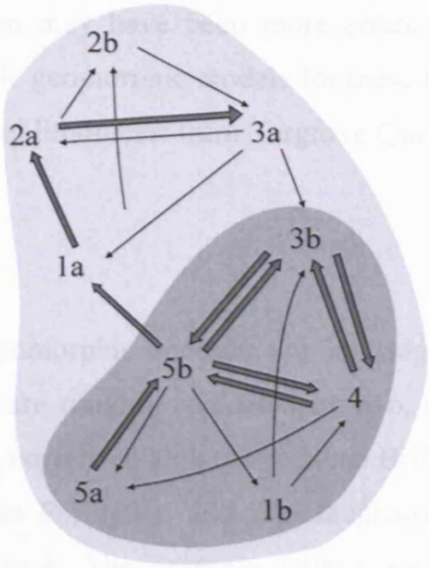

Figure 6.9b: Schematic log based on most common lithofacies transitions from the upper sequence of Tredomen Quarry core.

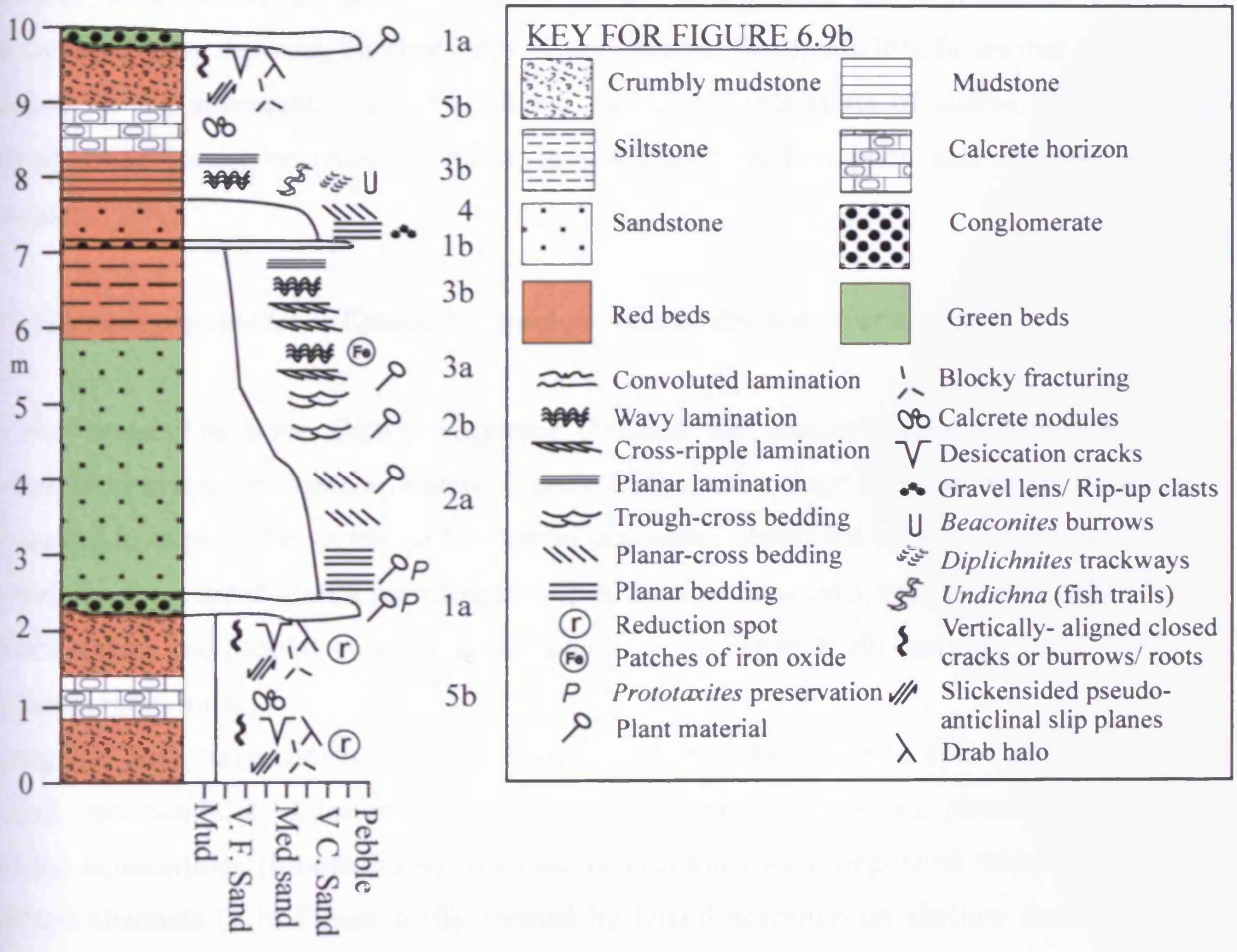

system that produced a more regular sedimentary response, unlike the strata in the lower sequence, where sedimentation may have been more erratic and episodic. The following section will discuss the possible geomorphic models for these two sequences from Tredomen Quarry, incorporating additional lithofacies from Targrove Quarry.

6.6: GEOMORPHIC MODELS

Separate depositional and geomorphic models are envisaged for the lower and upper Tredomen Quarry sequences, are roughly separated by two, closely-spaced palaeo-Vertisol stage III calcrete (C) horizons, correlated with the regional Bishop's Frome Limestone, which separates the Raglan Mudstone Formation and St. Maughans Formation (the Downtonian-Dittonian boundary) in the region. The Targrove Quarry sequence will be included in the geomorphic model for the upper sequence, as evidence suggests that strata are of lower Dittonian age (see section 2.2.2).

A major change in lithofacies associations and sedimentation style occurs across this boundary, from unordered, predominately oxidised, fine-grained and argillaceous channel and crevasse splay deposits, interbedded with argillaceous floodplain lithofacies that are often pedified, to the appearance of more ordered, fining-upwards strata of coarse to medium-grained green sandstone channel bodies, interbedded with floodplain and crevasse splay deposits.

6.6.1: *Geomorphic model 1: Ephemeral, mud-dominated dryland river system*

For the lower Tredomen Quarry sequence (beneath the Bishop's Frome Limestone), a dryland river system has been envisaged (Figure 6.10). A two-stage depositional environment is required to explain the variety of lithofacies deposited, controlled by wet and dry seasons. Essentially, there are at least 6 sedimentary depositional components, represented by different sub-lithofacies and lithofacies associations (numbered in Figure 6.10) that together comprise the geomorphic model.

During the first stage, under periods of high discharge, fast-flowing ephemeral channels formed, represented by intraformational conglomerates (lithofacies 1b), planar-bedded and inclined heterolithics (lithofacies 4). Inclined heterolithics were deposited within the main drainage channels (1 in Figure 6.10), formed by lateral accretion on shallow muddy point

Figure 6.10: Geomorphic model 1: Two-stage, ephemeral, mud-dominated dryland river system

2. Massive oxidised mudstones (lithofacies 5a). Rare wavy to planar-lamination. Desiccation cracks. Mudstone composed of mud aggregates with occasional 'rip-up' clasts in a matrix of mudstone: Lateral accretion of **mud aggregates,** transported as bedload in **ephemeral channels.**

4. Wavy to planar and cross-ripple-laminated oxidised siltstones (lithofacies 3b). Weakly pedified; desiccation cracks, pseudo-gleying and bioturbation: **Wave reworking of sediment in ephemeral, abandoned channels or waterholes, with periodic, weak pedogenesis.**

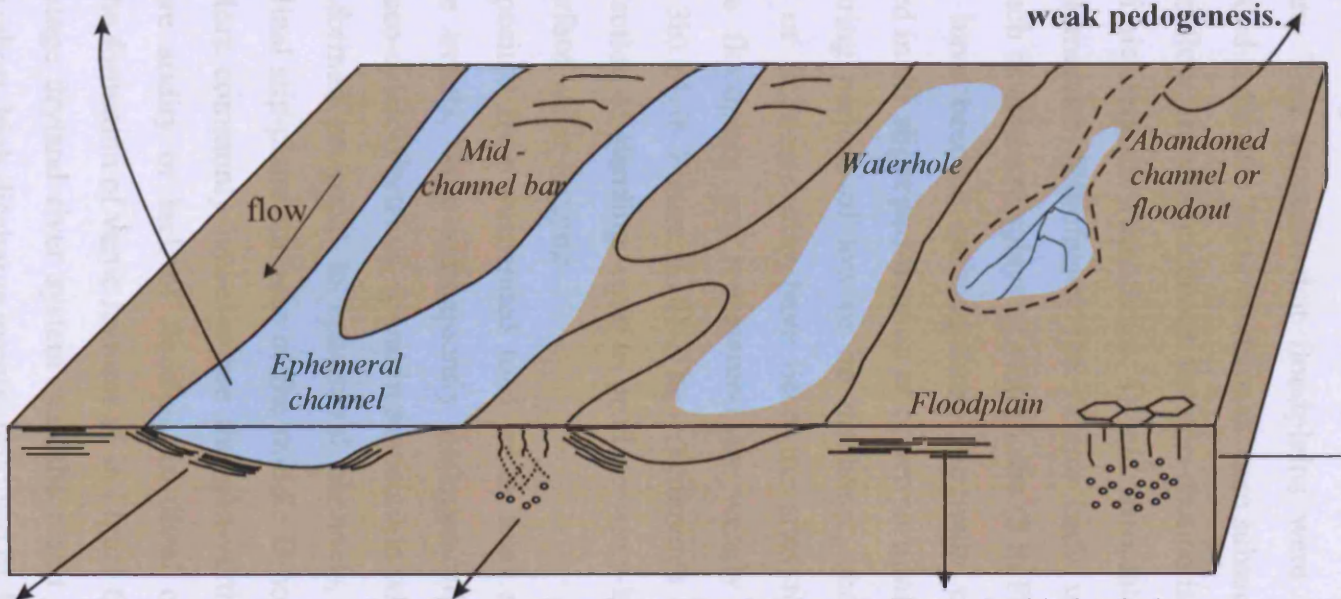

6. Pedified mudstones lacking pseudo-anticlinal slip-plane surfaces. Horizons weakly-developed, cumulate, with elongate carbonate nodules. These **non-Vertic (or Aridisol) palaeosols** (lithofacies 5b) may not have experienced a strong seasonal moisture contrast, due a **distal or isolated position on the floodplain.**

1. Low angle, planar-cross-bedded oxidised heterolithics (IHS) (lithofacies 4), with occasional conglomeratic base and gravel lenses (lithofacies 1b). Upper beds wavy to cross-ripple-laminated and weak pedified: **Lateral accretion of ephemeral channels.**

5. Pedogenically-altered floodplain mudstones: **palaeo-calcic-Vertisols** (lithofacies 5b). Cumulate profiles. Slip-plane surfaces indicate a **strong seasonal moisture contrast**. Association with oxidised heterolithics and massive featureless mudstones. Developed **proximal to ephemeral channels**.

3. Planar-bedded, tabular heterolithics (lithofacies 4) and thinly-bedded conglomerates (lithofacies 1b). Weak pedogenesis (desiccation cracks, reduction spots and sparse carbonate nodules) in upper beds. **Unconfined flow and vertical accretion (crevasse splays, floodouts or waterholes).**

KEY
- polygonal desiccation cracks
- planar lamination / bedding
- low-angle cross-lamination / bedding
- vertically-aligned features (burrows/ roots/cracks?)
- slickensided pseudo-anticlinal slip-planes
- carbonate nodules

bars, interbedded with intraformational conglomerates or gravel lenses (lithofacies 1b), which represent a periodic higher flow regime. The ephemeral nature of these channels is represented by sharp changes in grain size, resulting from sharp fluctuations in flow regime, and the weak pedogenesis of some of the upper heterolithic beds.

Mud aggregate mudstones (lithofacies 5a) also represent channel deposition during high discharge (2 in Figure 6.10). Muddy floodplains were continually being eroded and reworked by ephemeral channels, and pedogenically-produced mud aggregates were transported as bedload during high discharge events, and re-deposited as lateral accretion on muddy channels or point bars. This suggests that floodplains were not stable surfaces solely deposited from suspended sediment. These mudstones were subsequently re-pedified.

As well as channelised flow, there is evidence for non-channelised, unconfined flow in the planar-bedded heterolithic deposits (lithofacies 4) and associated basal beds of oxidised intraformational conglomerates (lithofacies 1b). These beds were deposited by vertical accretion in settings such as crevasse splays or waterholes (3 in Figure 6.10). These scoured-out depressions may have become isolated from the main channels and subsequently exposed, which resulted in the slight pedification of upper portions of heterolithic deposits.

The second stage, during periods of low or no discharge, abandoned channel meanders (oxbows), waterholes or floodouts may have been the sites for ephemeral lakes. These isolated areas on the floodplain are represented by weakly pedified planar-laminated siltstones (lithofacies 3b) (4 in Figure 6.10). These sediments were slightly reworked by wind-generated wave action of standing water to produce wavy-laminations. Pseudo-gleying indicates periods of surface water-logging.

Mudstones, either deposited from suspended load or as mud aggregates within channels during high discharge events, were subsequently pedogenically-altered during dry, low discharge periods. Palaeo-calcic-Vertisols, found in association with the inclined heterolithics (lithofacies 4), were formed proximal to ephemeral channels, where due to a moisture contrast, pseudo-anticlinal slip-plane surfaces of the middle B-horizon were able to develop (5 in Figure 6.10). More commonly however are the non-vertic, cumulate C-horizons or palaeo-Aridisols, where aridity or lack of flooding in distal or isolated portions of the floodplain prevented the formation of vertic features (6 in Figure 6.10).

Essentially, this two-stage dryland river system was the result of a sporadic, flashy flow regime (low frequency, short, high discharge events, followed by longer, but irregular periods of low or no discharge) on a low gradient landscape in a seasonal, semi-arid climate. During high discharge events, the system responded by extending the channel system laterally, via

more channels or splaying, scouring to produce waterholes, and channel expansion. During periods of low discharge, the system responded by abandonment and loss of river competence to form floodouts. Exposure of floodplain and abandoned channels resulted in pedogenesis.
Similar geomorphic models have been described by Love and Williams (2000) and Marriott and Wright (1993, 2004) for the Moor Cliffs Formation, south of the Ritec Fault in southwest Wales, which is contemporaneous to the Raglan Mudstone Formation. Both models show similarities to the dryland river systems of the Channel Country, Australia (Gibling et al. 1998, Nanson et al. 1986) with the deposition of low-angle inclined, muddy heterolithics on point bars. These rivers are ephemeral, anastomosing to braided, multi-channel systems in semi-arid climates, and may be analogous to the Late Silurian Old Red Sandstone river systems (discussed in Appendix IX).

6.6.2: *Geomorphic model 2*: *Two-stage, sand-dominated meandering river system*

A separate geomorphic model can be envisaged for the deposits in the upper Tredomen Quarry and Targrove Quarry sequences. 5 sedimentary depositional components have been interpreted from 6 sub-lithofacies and associations (Figure 6.11).
The fundamental difference between this geomorphic system and the dryland river system model for the lower sequence is the regular appearance of thick units of fining-upwards and multistorey reduced sandstone bodies. The bases of these sandstone complexes indicate channel erosion (basal channel lag (lithofacies 1a), followed by repeated, planar-bedded sandstones with parting lineations (lithofacies 2a)) (1 in Figure 6.11), and represent the high discharge stages of this system. The overlying planar-cross and trough-cross-bedded sandstones (lithofacies 2a and 2b) indicate a gradual decrease in flow speeds, which may have resulted in the deposition of classic fining-upwards units of perennial meandering rivers, if the assumption that planar cross-bedded units were deposited by lateral accretion of migrating point bars is made. Wavy and planar-laminated siltstones (lithofacies 3a) and fine-grained sandstones (lithofacies 2b) are interbedded with minor channel sandstones, and may represent the upper point bars or proximal floodplains, where material was deposited by vertical accretion and reworked (2 on Figure 6.11).
High discharge, unconfined flow transported bedload to the floodplains via crevasse splays, depositing intraformational conglomeratic lags (lithofacies 1a and 1b) and tabular sheets of medium-grained sandstones (lithofacies 2c) (3 on Figure 6.11). Upper units of crevasse splay deposits are represented by interbedded planar-bound siltstone and mudstone sequences

Figure 6.11: Geomorphic model 2: Two-stage, sand-dominated meandering river system

3.Conglomeratic units (lithofacies 1a and 1b), interbedded with tabular sheets of low-angle planar and trough-cross-bedded, medium-grained sandstone (lithofacies 2c) and laterally extensive sequences of interbedded siltstones and mudstones (lithofacies 3c and 5c). **Crevasse splay deposition.**

4. Weakly pedified (desiccation cracks, reduction mottling), wavy to cross-ripple-laminated oxidised siltstones (lithofacies 3b), with arthropod trackways, fish trails and *Beaconites* burrows. **Ephemeral, abandoned meanders (oxbows) or waterholes, with channel fill periodically pedified or reworked by standing water.**

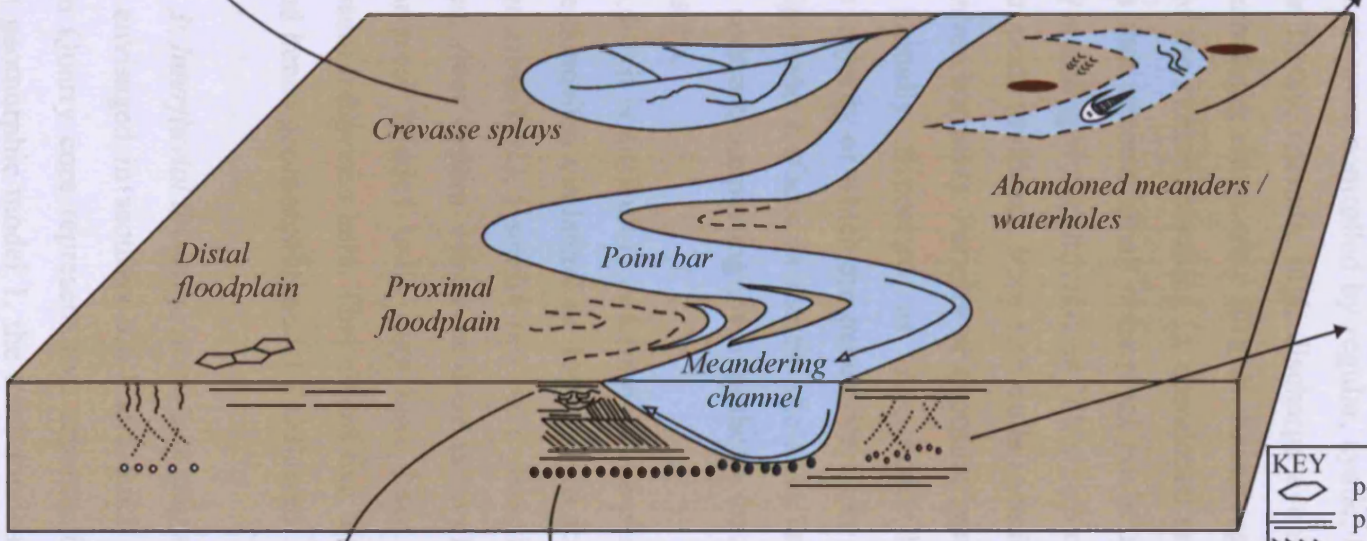

5. Pedogenically-altered, floodplain mudstones (lithofacies 5b): oxidised **palaeo-calcic- Vertisols** produced in an overall **moisture deficient climate**, but with a strong seasonal moisture contrast.

2. Wavy and planar-laminated siltstones (lithofacies 3a), interbedded with trough-cross-bedded, fine-grained sandstones (lithofacies 2b): **upper point bar and proximal floodplain, with minor channels.**

1. Fining-upwards sequence from basal conglomerate (lithofacies 1a) and planar-bedded medium-grained sandstones (lithofacies 2a), followed by planar-cross-bedded medium to fine-grained sandstones (lithofacies 2b): **lateral migration of meandering, possibly perennial channel.**

KEY
- polygonal desiccation cracks
- planar lamination / bedding
- cross-lamination / bedding
- trough-cross-lamination / bedding
- wavy-lamination
- conglomerate
- vertically-aligned features (burrows/ roots/cracks?)
- slickensided pseudo-anticlinal slip-planes
- carbonate nodules
- *Beaconites* burrows
- *Diplichnites* trackways
- Cephalaspid
- *Undichna* trails

(lithofacies 3c and 5c) that are interbedded with conglomeratic lithofacies. Here finer-grained material is washed out onto the floodplains.

These deposits, traditionally interpreted as classic perennial meandering channel and crevasse splay deposits (Allen 1964), are interbedded with lithofacies that are similar to the low or no discharge stages of the ephemeral, mud-dominated dryland river system, interpreted for the lower sequences. Therefore, this model has been envisaged as two-stage (high to little or no discharge), with fluvial style and deposition controlled by wet and dry seasons. It can be hypothesised these sequences were controlled by regular, cyclic, less variable high discharge events compared with the flashy, sporadic high discharge events of the Raglan Mudstone Formation sequences. Meandering rivers were formed during regular wet seasons, followed by a gradual drying out of the system, resulting in abandoned or isolated meanders (oxbow lakes) or scour structures that became small ephemeral pools or lakes (4 in Figure 6.11). Material was reworked by standing water (lithofacies 3b), which may have provided a habitat for cephalaspids and arthropods (evidence from fish trails (*Undichna*), arthropod trackways (*Diplichnites*) and *Beaconites* burrows). Periods of exposure resulted in slight pedogenesis. Floodplain mudstones, initially deposited as suspended load, were exposed and pedogenically-altered, the majority of which are palaeo-Vertisols (lithofacies 5b) (5 in Figure 6.11), with distinctive slip-plane surfaces in the middle structural B-horizon as a result of periodic, strong moisture contrast, supporting the hypothesis that this system was controlled by strong wet and dry seasons.

As explained in section 6.4.2, it is difficult to determine if the planar-cross bedded sandstone units (lithofacies 2a) were deposited via lateral or downstream accretion. Geomorphic model 2 assumes that the planar cross-bedded sandstones were deposited by lateral accretion on point bars of a meandering river system. However there is no clear evidence for point bars *senso stricto*, and planar-cross bedded units may have been deposited by downstream accretion and hence represent transverse bars. This means that the rivers may not necessarily have been meandering, and hence geomorphic model 2 is flawed.

6.6.3: *Geomorphic model 3*: *Interfluvial drainage and trunk channel model*

The geomorphic models envisaged in sections 6.6.1 and 6.6.2 suggest that the lower and upper strata of Tredomen Quarry core represent two separate fluvial systems that are not coeval. It is assumed that geomorphic model 1, the mud-dominated dryland river system of the Raglan Mudstone Formation, was replaced by geomorphic model 2, the sand-dominated meandering river system around the Silurian-Devonian boundary, and deposited the St.

Maughans Formation. However, a third model can be envisaged, combining geomorphic models 1 and 2, based on the work of Allen and Williams (1979).

Allen and Williams (1979) envisaged two types of drainage that occurred across the low-lying landscapes of the Anglo-Welsh Basin, based on two distinct types of conglomerate. They described type A conglomerates as 0.1 to 2m in thickness, massive or planar-bedded and composed of pebble to cobble-sized reworked carbonate nodules and mudstone clasts, with some minor exotic clasts and coalified plant material. They emphasised that the key feature of these conglomerates was their association with sandstone, with a matrix composed predominately of quartoze sandstone, as well as the conglomerates as a whole being associated with large sandstone complexes. Type A conglomerates described by Allen and Williams (1979) are similar to those of lithofacies 1a from Tredomen Quarry, and have been interpreted as basal channel lag of meandering channels (geomorphic model 2).

Allen and Williams (1979) described conglomerate type B as being much thinner (0.1m thickness), planar-bedded, and composed of granule to pebble-sized reworked carbonate nodules and mudstone clasts, in a matrix of either mudstone or sparry calcite cement, with no evidence of any coalified plant material. These conglomerates are generally lacking in sandstone, and are associated with siltstone and mudstone packages. Type B conglomerates described by Allen and Williams (1979) are similar to those of lithofacies 1b from Tredomen Quarry, and have been interpreted as ephemeral interfluvial channels or basal crevasse splay deposits.

Allen and Williams (1979) proposed from these two types of conglomerates, two types of drainage that were coeval: large trunk channels which were basin-wide, and transported material from one part of the basin to another, including exotic pebbles and sand-sized clasts (conglomerate type A); and interfluvial floodplain drainage channels, which transported local material from the floodplain, such as reworked carbonate nodules or pedogenically-formed mud aggregates (conglomerate type B).

From this interfluvial-trunk channel model of Allen and Williams (1979), it can be envisaged that geomorphic model 1 and geomorphic model 2 are of different magnitudes of scale, and that geomorphic model 1 may be superimposed onto geomorphic model 2 (Figure 6.12). This model envisages that the ephemeral channels of geomorphic model 1 were incipient, interfluvial floodplain drainage systems that responded to local rainfall events during the dry seasons as well as the larger scaled wet seasons (1 in Figure 6.12). During dry seasons, the main trunk channels were either completely dry or contained stagnant waterholes (2 in Figure 6.12). On the floodplain, abandoned meanders or floodouts also may have contained stagnant

Figure 6.12: Geomorphic model 3: Interfluvial drainage and trunk channel model

1. Incipient, ephemeral interfluvial drainage: low angle planar-cross-bedded heterolithics (lithofacies 4) and thinly-bedded conglomerates with mudstone matrix (lithofacies 1b), interbedded with massive mud-aggreate mudstones (lithofacies 5a).

2. Waterholes or abandoned meanders: Planar, wavy to cross-ripple-laminated oxidised siltstones (lithofacies 3b) and weak pedogenesis (lithofacies 5b). Wind-generated reworking of sediment in ephemeral, possibly stagnant waters.

3. Floodout or crevasse splay: Planar-bedded tabular heterolithics (lithofacies 4) and weak pedogenesis (lithofacies 5b). Unconfined flow and vertical accretion.

4. Pedogenically-altered floodplain mudstones: development of non-vertic palaeosols (palaeo-Aridisols?) on the distal, isolated floodplain (lithofacies 5b).

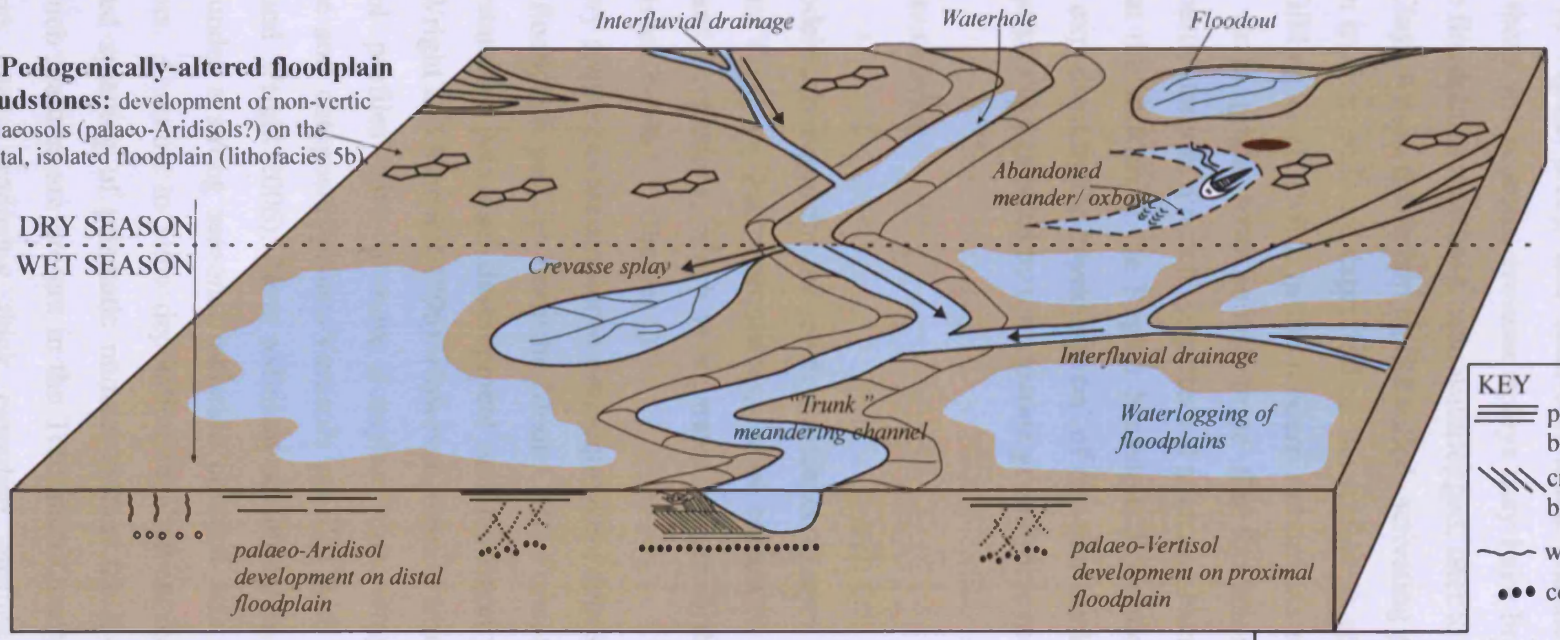

KEY
- planar lamination/ bedding
- cross-lamination/ bedding
- wavy-lamination
- conglomerate
- trough-cross-lamination / bedding
- polygonal desiccation cracks
- vertically-aligned features (burrows/ roots/cracks?)
- slickensided pseudo-anticlinal slip-planes
- carbonate nodules
- *Beaconites* burrows
- *Diplichnites* trackways
- Cephalaspid
- *Undichna* trails

7. Crevasse splays and floodplain waterlogging: Tabular sheets of conglomerates (lithofacies 1a, 1b) and low-angle-planar and trough-cross-bedded sandstones (lithofacies 2c) interbedded with planar-laminated siltstones and mudstones (lithofacies 3c, 5c). Waterlogging of floodplain.

6. "Trunk" channel: Basal channel lag conglomerate (lithofacies 1a), fining upwards to planar and planar-cross-bedded medium-grained sandstone (lithofacies 2a), cross-ripple-laminated fine-grained sandstones (lithofacies 2b) and wavy to planar-laminated siltstones (lithofacies 3a). Sand-dominated trunk channel.

5. Pedogenically-altered floodplain mudstones: palaeo-calcic Vertisol development on the proximal floodplain (lithofacies 5b), with an overall moisture defincient climate, but strong seasonal moisture constrast. Pseudo-gleying as a result of waterlogging by stagnant waters on the floodplains.

waters (2 and 3 in Figure 6.12). The floodplain mudstones were pedogenically-altered, either as non-Vertic palaeosols on the distal or isolated floodplains or as palaeo-calcic Vertisols on the proximal floodplains (4 and 5 in Figure 6.12). During wet seasons, the trunk channels were activated (6 in Figure 6.12), and sand-dominated channels deposited sandstone complexes. During these wet seasons, crevasse splays may have breached the river levees, and vast areas of the floodplains may have been waterlogged, later to become stagnant waters (7 in figure 6.12). Clays within floodplain soils swelled, activating pseudo-anticlinal curved slip-planes, which in modern soils are expressed on the surface as gilgai structures (Wilding and Tessier 1988, Gibling et al. 1998). In the modern floodplains of the Channel Country, Australia, in some areas gilgai have contribute to the formation of floodplain-surface incipient channels, particularly in a reticulate pattern (Fagan and Nanson 2004). Geomorphic model 3 implies that the shift from the Raglan Mudstone Formation to the St. Maughans Formation could be explained by the 'switching on' of remnant trunk channels, rather than a shift in fluvial geomorphology implied by the separate geomorphic model 1 and 2.

6.7: REGIONAL COMPARISONS

The geomorphic models envisaged for the lower Tredomen Quarry sequence and the upper Tredomen Quarry and Targrove Quarry sequences, can be correlated to the Raglan Mudstone and the St. Maughans Formations, which is separated by the Bishop's Frome Limestone regional marker horizon (Table 1.1, Chapter 1).

The Tredomen Quarry sequences are similar to time-equivalent deposits in Pembrokeshire. In particular, pedified floodplain profiles from the Moor Cliffs Formation have been working examples for understanding palaeosol development and taphonomy (Marriott and Wright 1993, 2004, 2006, Wright and Marriott 1996). However, despite similarities the Moor Cliffs Formation palaeosol profiles have a more complex taphonomy, with truncated and reactivated cumulate and composite palaeo-Vertisols profiles with stage II to III calcrete horizons (Marriott and Wright 2006). Slow sediment accumulation (0.02 - 0.2mm/yr) and Vertisol formation under a strong seasonal moisture contrast was periodically punctuated with erosional events. A return to slow deposition resulted in reactivation of slip-plane surfaces, with fanned splaying of prismatic nodules within the B-horizons (Marriott and Wright 2006). No such features are present in the Tredomen Quarry sequences, suggesting higher sedimentation rates, producing thick cumulate profiles of weakly-developed palaeosols.

A higher sedimentation rate in the Welsh Borderlands during the uppermost Přídolí can also explain the inconsistencies between the Bishop's Frome Limestone and the Pembrokeshire equivalent, the Chapel Point Calcrete. The most prominent outcrops of the stage III- IV calcrete horizon occur at Llansteffan, near Carmarthen (Plate 6.9d), where it reaches approximately 16m in thickness, with subordinate interbedded mudstones and siltstones that are either heterolithics or vertic palaeosols (Plate 6.9e) (Marriott and Wright 1993, 1996). These sections are condensed profiles of stacked, well-developed calcrete horizons, each representing up to 0.5 x 10^6 years residence time at slow sedimentation rates (0.002mm/yr). Similar outcrops are found at Freshwater West, Manorbier Bay and Lydney (Jenkins 1998, Barclay et al. 2005). Poor exposures of the Bishop's Frome Limestone in the Shropshire and Welsh Borderlands are thinner (around 2m), less well-developed (stage II-III) and often occur- as two closely-spaced calcrete bands (Barclay et al. 2005). A higher rate of sedimentation in this area would have decreased the residence time, resulting in less-developed horizons, plus a gradual aggredation of sediments.

The temporal change in geomorphic setting from the Raglan Mudstone Formation to the St. Maughans Formation (and equivalents) could be attributed to an increase in annual precipitation across the region, resulting in the initiation of meandering sand-dominated fluvial systems. This shift in river style and floodplain characteristics from the Downtonian to Dittonian could be due to climate change from a semi-arid environment with occasional short-lived high discharge events, to a wetter climate, with greater seasonal moisture variability, producing stronger, prolonged high discharge events.

An alternatively explanation, rather than an overall increase in precipitation across the Anglo-Welsh Basin, is a change in storm style across the Downtonian-Dittonian boundary. Based on sedimentological analysis of the Moor Cliff Formation and the Rat Island Mudstone Member of the Freshwater West Formation, Marriott and Wright (1993) recognise a change from a flashy, highly-variable regime to a more ordered, less variable regime, and hypothesised this as a result of a shift in the type, size and frequency of storms during the wet season. This shift has also been recognised between the lower and upper sequences of the Tredomen Quarry core.

A comparison between Pembrokeshire and southeast Wales show that lateral changes in contemporaneous depositional environments also occurred, and may represent subtler changes in distribution and intensity of precipitation across the Anglo-Welsh Basin. Regional variabilities may be tectonically controlled, altering topography and hence orographic effects and catchment areas, as well as changes in sedimentary rates and reactivation of floodplains.

For example, the floodplain facies of Moor Cliffs Formation show evidence of sporadic erosional events and reactivation (Marriott and Wright 2006), possibly due to base level changes related to the proximity of the Benton Fault (Williams and Hillier 2004). Comparatively, the Tredomen Quarry sequences show no reactivation features, and sediment accretion occurred gradually.

6.8: CHAPTER SUMMARY

Sedimentological analysis of Upper (uppermost) Silurian to Lower Devonian strata from Tredomen Quarry and Targrove Quarry has resulted in the recognition of 5 main lithofacies of the Old Red Sandstone: intraformational conglomerates; sandstones; siltstones; heterolithics and mudstones. However, several sub-lithofacies were also recognised (see Tables 6.1 and 6.2) and the following sedimentary elements were recognised from quarry outcrops and lithofacies associations.

Firstly, channels are represented by the association of reduced intraformational conglomerates (lithofacies 1a), representing basal channel lag, overlain by planar-bedded, medium-grained sandstones (lithofacies 2a) deposited by vertical accretion on channel floors under fast flow regimes. Bars (point or transverse) are represented by planar-cross-bedded, medium-grained sandstones (lithofacies 2a), deposited by lateral accretion of 2D dunes on lower bars, and by trough-cross-bedded, cross-ripple and climbing-ripple-laminated, fine-grained sandstones (lithofacies 2b) deposited by lateral accretion of 3D dunes on upper bars.

Secondly the presence of ephemeral, possibly anastomosing channels has been interpreted from the association of oxidised intraformational conglomerates (lithofacies 1b), deposited as basal channel lag, overlain by low-angle planar-cross-bedded and trough-cross-bedded medium-grained sandstones (lithofacies 2c), and low-angle planar-cross-bedded heterolithics (lithofacies 4), deposited by accretion on the banks of shallow, muddy ephemeral channels. Massive oxidised mudstones, originally formed from mud aggregates (lithofacies 5a), have been interpreted as vertical or lateral accretion within muddy ephemeral channels.

Thirdly, several lithofacies have been interpreted as occurring under high velocity, unconfined flow regimes, and represent crevasse splays deposits. Both reduced and oxidised conglomerates (lithofacies 1a and 1b) occur at the base of, or occur as gravel horizons or lenses within, tabular planar-bedded sheets of medium-grained sandstone (lithofacies 2c) or heterolithics (lithofacies 4), representing vertical accretion by unconfined high velocity flow at the base of crevasse splay deposits. Finely planar-laminated fine-grained sandstones and

siltstones (lithofacies 3c and 5c) that occur above, or are interbedded with, these tabular sandstone sheets, represent upper crevasse splay deposits.

Fourthly, reduced or oxidised planar-laminated or wavy-laminated siltstones (lithofacies 3a and 3b), interpreted as vertical accretion on the upper point bar or proximal floodplain, or within abandoned meanders or waterholes, with slight hydraulic reworking via wind or current. This interpretation is supported by presence of arthropod trackways, burrows and fish trails, though to have been formed in shallow, low-velocity or stagnant waters (Morrissey et al. 2004). Slight pedogensis of these siltstones, including the precipitation of small carbonate nodules, suggest periods of exposure.

Finally floodplains are represented by pedified mudstones (lithofacies 5b), originally deposited from suspension by vertical accretion under a low-velocity flow regime, as overbank fines. Subsequent exposure of these mudstones resulted in pedogensis. Two palaeosol types have been recognised: palaeo-Vertisols, with distinctive curved, pseudo-anticlinal, slickensided slip-plane surfaces, (formed by the shrinking and swelling of clays as a result of wetting and drying phases), and the presence of varying intensities of carbonate nodule precipitation; and palaeosols lacking pseudo-anticlinal slip planes, with less well-developed carbonate nodule horizons, interpreted as palaeosols similar to the modern Aridisols.

There is a clear shift in lithofacies association around the Bishop's Frome Limestone (approximately 33m above the Silurian- Devonian boundary), from the Raglan Mudstone Formation (lower core) into the St. Maughans Formation (upper core) (see Table 1.1, Figure 6.4 and 6.5). Essentially the sedimentology changes from unordered, predominately oxidised argillaceous pedified floodplain deposits, interbedded with fine-grained and argillaceous channel, crevasse splay and waterhole deposits, to more ordered, fining upwards sandstone-siltstone channel packages, interbedded with crevasse splay, abandoned meander/ waterhole and floodplain deposits.

Geomorphic models have been envisaged for the Raglan Mudstone Formation (uppermost Silurian to the lowermost Devonian) a two-stage, ephemeral, mud-dominated, possibly anastomosing channel river system (see Figure 6.10), and for the St. Maughans Formation (Lower Devonian) a two-stage, sand-dominated meandering river system (see Figure 6.11). Alternatively, geomorphic model 3 implies that the systems represented by the Raglan Mudstone Formation and the St. Maughans Formation respectively, were actually coeval but operated at different magnitudes of scale. This model envisages that the smaller, incipient ephemeral channels on the floodplain, that operated during local rainfall events are

'superimposed' on a larger trunk stream river system that only operated during periods of extensive, basin-wide flood events. Therefore this model suggests, rather than a shift in fluvial style, the switching on of remnant trunk channels.

Possible causes for the shift in geomorphic setting or the switching on of trunk channels include climate change, either due to: an overall increase in long-term precipitation during the Early Devonian, or; a change of storm type, size and frequency during the wet season, which caused increased seasonal variability, and the initiation of regular high discharge events, and formation of meandering fluvial systems. Alternatively, local tectonics may have altered topography, causing a local orographic effect and changes to the catchment area, which may have increased sedimentation rates or altered the amount of accommodation space available in the basin. A regression of the coastline to the east through the uppermost Silurian to Lower Devonian, suggested by the palaeogeographic reconstructions of Barclay et al. (1994) and supported by analysis of regional palynological assemblages (Chapter 5), would potentially alter base level, and Tredomen Quarry gradually shifted from an medial alluvial plain setting, further upstream to a proximal alluvial plain setting (see Figures 5.6 to 5.8).

CHAPTER 7 : TAPHOFACIES AND TAPHONOMIC CONSTRAINTS ON PALAEOECOLOGICAL INTERPRETATIONS

7.1: INTRODUCTION

In the past, palaeobotanical studies of the Lower Old Red Sandstone from the Anglo-Welsh Basin have focussed on the physiology, taxonomy and evolution of Late Silurian to Early Devonian plants, including the discovery of the earliest examples of vascular tissue from Late Silurian rhyniophytes, a key adaptation for terrestrialisation (Edwards and Richardson 2004). Preservational processes have been investigated, including pyritisation (Edwards 1981), and charcoalification as a result of wildfires (Edwards and Axe 2004, Glasspool et al. 2004). Palaeoecological studies however have been hampered by the lack of well-preserved plant body fossils, especially those found in their original growth position. The dispersed spore record indicates a significant bias in the body fossil record, with only a small proportion of dispersed spore taxa recognised in the *in situ* record (Edwards and Richardson 1996, Edwards and Wellman 2001).

Palaeoecological studies are restricted by taphonomy; all the processes involved in the transition from original plant material in the living, *in situ* growth position to the final fossil specimen. Before any palaeoecological models can be proposed, a better understanding of the role of taphonomy in plant fossil preservation and distribution is required. This can be achieved using an integrated approach between sedimentology and palaeobotany. Few attempts have been made to integrate both sedimentological facies and palaeobotanical assemblages from the Silurian to Devonian strata (Griffing et al. 2000, Hotton et al. 2001, Allen and Gastaldo 2006) and none in classic UK fossiliferous localities.

As described in Chapter 6, a number of lithofacies from lowermost to lower Lochkovian Old Red Sandstone strata have been recognised and three geomorphic models have been proposed: a two-stage ephemeral mud-dominated dryland river system; a two-stage sand-dominated meandering river system; and a combination of both models in a interfluvial drainage and trunk channel model. It was also recognised that some lithofacies are associated with fossil plant assemblages, which differ in assemblage composition and preservation type between lithofacies. These associations were termed taphofacies.

In this chapter, each taphofacies will be defined and interpreted, and an assessment on the main taphonomic controls made. The taphofacies are then superimposed onto the geomorphic

models for the St. Maughans Formation, and a taphofacies and palaeoecological model proposed.

7.2: TAPHOFACIES

Fossilised vegetative material is rare within Old Red Sandstone strata, and at Tredomen Quarry and Targrove Quarry it is only found within reduced lithofacies. This restricts palaeobotanical and palaeoecological studies to strata above the Bishop's Frome Limestone at least in the central South Wales and Welsh Borderland area (Table 1.1, Chapter 1). Well-preserved, partially intact, recognisable plant fossils are rare, with the majority of fossils disseminated or highly fragmented, and distributed throughout the lithofacies units, and therefore allochthonous in nature (transported away from the growth habitat).
The following taphofacies have been recognised, from both Tredomen Quarry and Targrove Quarry, based on the combination of lithofacies description and associations, fossil identification and preservation, and fossil orientation. Each taphofacies has been summarised with interpretations in Table 7.1.

7.2.1: *Taphofacies descriptions*

Taphofacies 1: Charcoalified fragments within green-grey intraformational conglomerates (lithofacies 1a)

Fossilised vegetative debris has been found sparsely distributed throughout the green, intraformational conglomeratic beds within the Tredomen Quarry sequence (lithofacies 1a, Chapter 6), as small, three-dimensional, randomly-orientated fragments (largest 1cm by 0.5cm) (Plate 7.1*a*) (Table 7.1). SEM analysis of these fragments revealed at least two recognisable genera. Firstly, large axial-like, striated fragments (Plate 7.1*b*), are composed of parallel-aligned tubes, approximately 0.05mm in width, some with internal thickenings (Plate 7.1*c*). These fragments are most similar to *Nemataskетum* Burgess and Edwards (1988) or *Prototaxites* (see Chapter 3 for full description). However, no information regarding the overall morphology of these specimens can be determined, as material is too fragmentary. The texture of some of the tube walls within the *Prototaxites* / *Nemataskетum* fragments suggest blistering and cell homogenisation as a result of charcoalification (Plate

Table 7.1: Taphofacies and their interpretations

	Fossil debris composition and distribution	*Lithofacies*	*Taphofacies interpretations*
1	Three-dimensionally preserved, charcoalified fragments of *Prototaxites/ Nematasketum* and *Pachytheca* distributed through conglomeratic units. Associated with iron-oxide. Possible cephalaspid fragments associated with iron-oxide weathering, occur along basal planar bedding plane surfaces.	Lithofacies 1a (Tredomen Quarry and Targrove Quarry): Green to grey, clast-supported, massive to planar-bedded, intraformational conglomerates. Thinly-bedded, undulating base. Laterally extensive. Lithofacies 2a most commonly occurs above.	Charcoalification of vegetation by wildfires. Charcoal fragments entrained and eroded by upper flow regime, transported as bedload, deposited as basal lag of major channels or basal crevasse splays. Allochthonous assemblage.
2	Large thalloid vegetative fragments of coalified and charcoalified *Prototaxites/ Nematasketum*, occasional poorly preserved axial early land plant, often associated with iron-oxide. Slightly oblique or along bedding plane surfaces. Worked into foresets of planar beds within upper sandstone units. Randomly orientated. Whole cephalapid specimens preserved.	Lithofacies 2a (Tredomen Quarry): Planar and planar-cross-bedded, medium-grained green to grey micaceous sandstones. Thickly-bedded, normal grading upwards, planar boundaries. Parting lineations and rip up clasts at base.	Charcoalified and non-charcoalified fragments entrained and eroded by upper flow regime. Bedload transport. Deposited within basal channel and lower bar deposits. Rapid burial resulted in moderately well – preserved coalified compressions and whole fish specimens. Allochthonous assemblage.
3	Large, well-preserved, partially intact sterile or fertile branching axes of early land plants. Coalified compressions with limonite coatings occur along or oblique to planar-bedding surfaces or foresets of trough-cross-laminated units. Randomly orientated. Rare pyrite-limonite crystals found within axial cells.	Lithofacies 2b (Tredomen Quarry): Green to grey, small-scale trough-cross-bedded and cross-ripple-laminated fine-grained micaceous sandstones. Confined units, with concave bases, either stacked, or interbedded with wavy to planar -laminated siltstones. Alternating calcareous and organic-rich laminations.	Non-charcoalified fragments transported as suspension. Lower flow regime compared to taphofacies 1 and 2. Microbial film development. Deposition by lateral accretion on upper bar deposits, or minor bar top channels. Allochthonous assemblage. Mineral encrustation develops over organic material. Pyrite precipitation within cellular structure, converted to limonite (hydrated-iron-oxide).
4	Minute branching, sterile and fertile mesofossils, and vegetative debris including *Prototaxites/ Nematasketum* fragments. Coalified compressions, packed along planar-laminated surfaces, or within discrete lenses. Some specimens associated with orange iron-oxide.	Lithofacies 3a (Tredomen Quarry): Green to grey planar and wavy-laminated siltstones. Thinly-laminated, alternating calcareous silt and organic rich mud, plus mottling (iron-oxide spots).	Non- charcoalified minute fragments hydraulically sorted in a low flow regime, transported via suspension, and deposited as vertical accretion, resulting in planar-laminations. Reworking of sediment by wind-generated wave ripples resulted organic material occurring within discrete lenses at the base of ripple crests. Some pyrite precipitation within cellular structure, converted to iron-oxide.
5	Minute banded tubes, no more than 0.05mm in width, occur along the top of planar lamination surfaces of lithofacies 3a, and above taphofacies 4. Tubes occur within networks, and usually parallel-aligned, with internal thickenings. Fragments associated with limonite and orange iron-oxide.	Lithofacies 3a (Tredomen Quarry): Green to grey planar and wavy-laminated siltstones. Thinly-laminated, alternating calcareous silt and organic rich mud, plus mottling (iron-oxide spots).	*In situ* (?) growth of organism of putative fungal affinity, with hyphal tubes propagating organic, nutrient-rich siltstone horizons (of taphofacies 4) of the upper bar tops / levees or proximal floodplains. ?Autochthonous assemblage.

Table 7.1: Taphofacies and their interpretations (continued)

6	Coalified compressions of thalloid *Prototaxites/ Nematasketum* and ?*Nematothallus* cuticle. Occasional small sterile axial fragment. Fragment packed along planar-lamination surfaces, randomly orientated. Blacker bands of laminations containing increased amounts of organic material occur every 3 to 5mm.	Basal beds of Lithofacies 3c (Targrove Quarry): Yellowish-brown very-fine-grained sandstones, finely planar-laminated. Sharp, planar upper and lower boundaries, interbedded with lithofacies 5c. Laterally extensive.	Non-charcoalified fragments transported via bedload under an unconfined upper flow regime, removing material from the main channels, out into crevasse splay deposits. Deposition by vertical accretion along planar bound sandstone laminations. Allochthonous assemblage.
7	Large, well-preserved coalified compressions, partially intact, sterile and fertile branching axes of early land plants, e.g. *Salopella allenii*. Occasional thalloid fragment of ?*Nematothallus* cuticle. Occur along the bedding surfaces of planar-laminations, randomly orientated. Axial plants associated with limonite.	Upper beds of Lithofacies 3c (Targrove Quarry): Yellowish- brown siltstone, planar laminated. Sharp, planar upper and lower boundaries, interbedded with lithofacies 5c. Laterally extensive.	Non-charcoalified fragments transported via saltation or suspension under an unconfined upper flow regime (although slightly lower than interpreted for taphofacies 6). Microbial biofilm development. Deposited as upper crevasse splay deposits by vertical accretion, along or oblique to planar bound siltstone laminations. Mineral encrustation develops over organic material. Allochthonous assemblage.
8	Mostly barren, occasional rounded thalloid, coalified compression of ?*Nematothallus* cuticle in uppermost beds, beneath planar boundary with lithofacies 3c. Occurring along or oblique to planar-laminations, or with massive structure.	Lithofacies 5c (Targrove Quarry): Dark green, massive to wavy or planar-laminated mudstone. Planar or gradational lower boundary. Laterally extensive. Interbedded with 3c.	Non-charcoalified fragments hydraulically sorted into the finest fractions, transported by suspension in unconfined lower flow regime. Deposited as uppermost crevasse splay deposits by vertical accretion, along or oblique to planar laminations. Reworking by wind-generated wave ripples. Preservation of megafossils only in uppermost beds due to rapid burial. Allochthonous assemblage.
9	Large, three dimensional, striated axial-like vegetative fragments bifurcating along the top surface of red siltstones. Poorly preserved cast?	Lithofacies 3b (Tredomen Quarry): Red planar and wavy-laminated siltstones. Thinly-bedded, alternating calcareous silt and mud. Climbing-ripple-laminations, convoluted bedding. Mottling. Sparse distribution of carbonate nodules, polygonal cracking.	? *In situ* growth of ?organism of putative fungal affinity. Thick axial-like vegetative fragments along the top surfaces of siltstone horizons of abandoned ephemeral lakes or floodplain.

7.1*d*), similar to charcoalified fragments described by Edwards and Axe (2004). Secondly, numerous charcoalified, small, multi-layered spheres of *Pachytheca* (Plate 7.1*e*, see Chapter 3) were extracted from the conglomeratic units.

Vegetative fragments are commonly associated with iron oxide weathering. Equivocal, non-plant fragments with strong iron oxide weathering are also worked into the conglomeratic beds, possibly being fragments of cephalaspids (such as the armoured head plates). These fragments are found along the bedding planes of coarse planar-bedding (similar to cephalaspid fossils found in other conglomeratic beds from across the Anglo-Welsh Basin, described by Dineley and Loeffler (figure 34.6, 1999).

Taphofacies 2: Large thalloid fragments within medium-grained green-grey sandstones (lithofacies 2a)

Abundant vegetative debris has been found dispersed throughout green, mica-rich, medium-grained, planar-bedded and planar-cross-bedded sandstones within the Tredomen Quarry sequences (lithofacies 2a, Chapter 6) (Table 7.1). Two fractions are present. Firstly, large partially fragmented, three-dimensional or compressed, charcoalified and coalified thalloid non-embryophyte fragments (approximately between 5-10cm in length, 3-4 cm in width, maximum of 20cm in length and 4cm in width) (Plate 7.1*f*), plus small poorly preserved and heavily fragmented early land plants (*Cooksonia hemisphaerica*) (see Chapter 3), occur within the basal planar-bedded sandstone units (Plate 7.1*g*). The large thalloid fragments are somewhat enigmatic, with some coalified compressions with little or no original structure. Although the fragments are eroded, the general morphology is elongate, thick and axial-like, some tapering slightly towards the end, with an eroded rounded to flattened tip (Plate 7.1*h*). Occasional coalified compressions and charcoalified fragments are well-preserved, with internal structures revealing a tubular structure, and are therefore likely to be *Prototaxites* or *Nemataskétum* (Burgess and Edwards 1988) (Plate 7.1*i*) (see Chapter 3). Most fragments are associated with orange iron oxide weathering. *Pachytheca* spheres have also been found in this assemblage (see Chapter 3). Fish fragments such as head shield pieces may account for some of the enigmatic fragments within this assemblage. A significant cephalaspid bed has been found within these basal beds, preserving whole specimens (Keith Jones, personal communication) (Plate 7.1*j*).

Secondly, poorly preserved, disseminated thalloid and axial vegetative debris (less than 5mm in diameter) occur along the bedding plane surfaces of planar-cross-bedded sandstone units,

which occur above the planar-bedded sandstone units (lithofacies 2a, Chapter 6) (Plate 7.1*k*). In comparison to the lower beds, the proportion of plant material is much reduced and more fragmentary in nature. However, the debris does appear to contain a higher proportion of axial fragments compared to the lower beds. In the upper parts of these sandstone units, where grain size is finer (see Chapter 6), debris has also been worked along the foresets of cross-ripple-laminations, occurring at base of each lamination (Plate 7.1*l*). In places, these organic-rich laminations are associated with brown iron-oxide weathering and are interbedded with micrite-rich, grey laminations.

Unlike the fossilised material in taphofacies 1, where large fragments are dispersed through the conglomeratic units, vegetative material within the medium-grained sandstones are found slightly oblique to, or along the bedding plane surfaces, in a disordered orientation.

Taphofacies 3: Axial fragments within fine-grained green-grey sandstones (lithofacies 2b)

The most well-preserved plant fossils are found in the Tredomen Quarry sequences, within fine-grained, trough-cross-bedded, planar to cross-ripple-laminated mica-rich green sandstones to siltstones, particularly those that are restricted in unit width, and have concave bases (lithofacies 2b, Chapter 6) (Plate 7.2*a*, Table 7.1). Despite having a lower proportion of plant material within these fine-grained sandstones, fossils are more intact, and are recognisable as a number of dichotomously branched early land plants (including *Cooksonia* cf. *caledonica* (Plate 7.2*b*), *Cooksonia hemisphaerica* (Plate 7.2*c*), *Cooksonia* cf. *cambrensis*, *Salopella allenii* and cf. *Uskiella reticulata* / *Tarrantia salopensis*) (see Chapter 3 for plant descriptions). Many specimens are fertile, with sporangia that are at least 2mm in width (Chapter 3, Appendix II), but are also found amongst sterile branching and non-branching axis of *Hostinella* and enigmatic thalloid fragments, most likely to be *Prototaxites* / *Nematasketum* or *Nematothallus*. The majority of plant fossils are preserved as coalified compressions, with corresponding well-preserved impressions within a fine-grained, hydrated-iron-oxide-rich coating (limonite), which occurs between the coalified compressions and the coarser host rock (Plate 7.2*d*). Pyrite is rare, but is occasionally found surrounding cell walls within the central strands of axes, where it has often been altered to limonite or orange iron-oxide weathering. This results in partial three-dimensional preservation (Plate 7.2*e*). Plant material is randomly-orientated along or slightly oblique (Plate 7.2*f*) to planar lamination surfaces, or along the foresets of trough-cross-laminations (Plate 7.2*g*).

Taphofacies 4: Minute axial fragments within green-grey planar to wavy-laminated siltstones (lithofacies 3a)

Within wavy to planar-laminated green siltstones at Tredomen Quarry (lithofacies 3a, Chapter 6), small moderately well-preserved coalified compression fossils are abundant (Plate 7.2*h*) (Table 7.1). Lamination surfaces are packed with randomly-orientated, minute dichotomously branched axes with sporangia that are no more than 1.10mm in height (mesofossils described in Chapter 3) (Plate 7.2*i*, 7.2*j*, 7.2*k*), as well as fragmented, sterile branched and non-branched axes. Minute fossils are associated with orange iron-oxide weathering and occasionally a limonite covering. Small thalloid fragments are also present (average 4.4mm by 2.5mm in width), most likely to be either *Prototaxites / Nemataskетum* or *Nematothallus* (Plate 7.2*l*). Debris is restricted to the bedding planes of planar laminations or occurs within discrete lenses.

A number of faunal specimens have also been discovered from these plant-rich green siltstone beds. In particular, a new genus of trigonotarbid (*Arianrhoda bennetti*), plus myriapod, eurypterid and scorpion fragments have been recovered (Dunlop and Selden 2004).

Taphofacies 5: Minute banded tubes within green-grey, planar to wavy-laminated siltstones (lithofacies 3a)

Taphofacies 5 is associated with taphofacies 4, within green-grey, planar and wavy-laminated siltstones (lithofacies 3a from Tredomen Quarry, Chapter 6). Minute hyphal-like banded tubes either occur individually, or as part of a networked structure, where tubes are often parallel-aligned, intertwining and bifurcating along, or slightly oblique to the top surface of horizontal laminations (Plate 7.3*a*, 7.3*b*). These banded tubes occur on top of the mesofossils and vegetative debris of taphofacies 4, often preserved as internal moulds in limonite (hydrated-iron-oxide) (Plate 7.3*c*). These tubes are also associated with orange iron-oxide weathering.

Taphofacies 6: Thalloid fragments within yellowish-brown, very-fine-grained sandstone (lithofacies 3c)

Within the basal units of laterally extensive, planar-laminated, yellowish brown very-fine-grained sandstones of lithofacies 3c (Chapter 6) from Targrove Quarry, lamination surfaces are packed with coalified compressions of equivocal vegetative debris (Plate 7.3*d*) (Table 7.1). Blacker bands of planar laminations occur every 3 to 5cm, and contain an increased amount of organic material. Fragment size ranges from less than 1mm up to 3 or 4cm in diameter. Most fragments are rounded, thalloid specimens that resemble *Nematothallus* cuticles (Plate 7.3*e*), but are poorly-preserved compressions, with very little anatomical information. Some fragments do appear striated (Plate 7.3*f*) and are likely to be *Prototaxites / Nemataskетum*, similar to those fragments found within taphofacies 2. *Pachytheca* has also been found (Plate 7.3*g*) (see Chapter 3). Highly fragmentary, small sterile and fertile axial fragments are also found within these basal units (Plate 7.3*h*), but are rare and poorly preserved. Equivocal faunal fragments, possibly of fish or arthropod affinity, are associated with iron oxide weathering, are also present.

Taphofacies 7: Axial fragments within yellowish-brown siltstones (lithofacies 3c)

The most well-preserved fossils found at Targrove Quarry are found within the upper beds of the laterally extensive lithofacies 3c; yellowish-brown, planar-laminated siltstones (Plate 7.4*a*) (see Chapter 6) (Table 7.1). Large, partially intact, moderately well-preserved fertile and sterile dichotomously branched axes of early land plants (Plates 7.4*b*) (including a large *Salopella allenii* sporangium (Plate 7.4*c*)) have been found (see Chapter 3), as well as the occasional rounded thalloid fragment, possibly being *Nematothallus* cuticles (Plate 7.4*d*). These fossils are preserved as coalified compressions, and are randomly orientated either parallel or slightly oblique to planar lamination surfaces. Fossils are much less common within these laminations compared to the basal very-fine-grained sandstone beds below (taphofacies 6). Axial plants are associated with a limonite covering.

Taphofacies 8: Thalloid fragments within dark green-grey mudstones (lithofacies 5c).

Although the laterally extensive dark green-grey, wavy to planar-laminated mudstones at Targrove Quarry (lithofacies 5c, Chapter 6) are mostly barren of any vegetative debris, the uppermost beds (just beneath a planar boundary with yellowish-brown very-fine-grained sandstone of lithofacies 3c) do contain the occasional thalloid coalified compression fossil (Plate 7.4*e*). Fragments are rounded and resemble those from taphofacies 4, and are possibly

Nematothallus cuticle fragments. These compressions occur either along or slightly oblique to lamination surfaces, or occur within the massive structure of the mudstone.

Taphofacies 9: Striated axial fragments within red wavy to planar-laminated siltstones (lithofacies 3b)

This final taphofacies occurs within wavy or planar-laminated red siltstones (lithofacies 3b) at Tredomen Quarry (Chapter 6). On the uppermost bedding surfaces of these siltstones, rare axial-like features appear to bifurcate across the surface (Plate 7.4*f* and *g*). These features are three-dimensional preserved, and appear to have a fine, linear striated texture (striations less than 1cm) on the surface, that are similar to the parallel-arranged tubes of *Prototaxites*.

7.2.2: *Taphofacies interpretations*

In this section the taphonomic history of each taphofacies is interpreted based on assemblage composition, preservation type, lithofacies and lithofacies associations, which has been summarised in Table 7.1. The taphofacies have also been assigned to either allochthonous (transported from growth habitat) or autochthonous (within growth habitat) assemblages.

Allochthonous assemblages

The following seven taphofacies are all allochthonous assemblages. Material was transported either by bedload, saltation or suspension by varying flow regimes, within either confined channels or unconfined crevasse splay deposits. Deposition occurred either as vertical or lateral accretion, with each taphofacies containing hydraulically sorted and therefore stratinomically partitioned organic material.

Taphofacies 1: Charcoalified fragments within basal channel lag and crevasse splay deposits.

Charcoalified material within the green intraformational conglomerates (lithofacies 1a, Chapter 6) is highly fragmented and randomly distributed throughout the lithofacies unit, which suggests a highly transported allochthonous assemblage. No embryophytes were extracted from the conglomeratic facies, only small pieces of three-dimensionally preserved, fungal-like organism *Prototaxites* / *Nematasketum*, and *Pachytheca*.

Despite the fragmented nature of this material, anatomy is well-preserved, as a result of pre-burial charcoalification. Charring of organic material by wildfires converted these fragments to fusinite, which may have increased the rigidity of fragments, decreasing the effects of erosion, and allowed the three-dimensional structure after compression of the sediments to be preserved (Edwards and Axe 2004). Through comparisons with experimental charcoalification (Scott 1989, Jones and Chaloner 1991, Edwards and Axe 2004), an estimate of the temperature at which similar charcoalified fossilised fragments from the Clee Hills and Ludford Lane were charred was suggested to be at least 400°C, based on reflectance values, suggesting that these were low-temperature or smouldering wildfires (Glasspool et al. 2004, Glasspool et al. 2006). The possibility of wildfires during the Early Devonian is supported by levels of O_2 predicted around 18% of atmospheric composition (Berner 2006), which was sufficient to support fires (Glasspool et al. 2006). Charcoalification of vegetation such as *Prototaxites* most likely occurred during the dry season of the strongly seasonal semi-climate envisaged for the Lower Devonian St. Maughans Formation (inferred by the presence of palaeo-calcic-Vertisols, lithofacies 5b; see geomorphic model 2, Chapter 6), especially towards the end of the season, with the onset of storms and associated lightning.

During the wet seasons, charcoalified vegetative material was then entrained during high discharge events under an upper flow regime, transported as bedload, and subsequently deposited within basal channel lag and crevasse splay deposits (lithofacies 1a, Chapter 6). The effects of charcoalification on the depositional behaviour of wood fragments were studied by Vaughan and Nichols (1995). They determined that permeability and fragment size were the main properties that altered depositional behaviour, these properties differing with the type of plant material charred, maximum temperature of charring, exposure time at this temperature and the availability of oxygen.

Experimental charcoalified wood fragments were charred at temperatures between 300 and 400°C (Vaughan and Nichols 1995), and showed fluctuations in density between 0.3 and 0.5gm/cc with increasing temperature, due to the loss of water and volatiles and wood shrinkage. These are relatively small changes in density, which still remain very low, suggesting that fragments would have floated on the surface of waterbodies.

However, the degree of fracturing and cell wall homogenisation of charcoal fragments affected permeability and hence the degree of water saturation. Vaughan and Nichols (1995) experimental charcoal revealed that in fragments burnt to 400°C, although cell wall homogenisation was complete, large fractures had developed with the release of volatiles, with further fracture development with increased temperature. They placed their experimental

charcoalified fragments in a wave tank, and found that fragments burnt to over 300°C sank immediately to the bottom of the tank, most likely due to rapid water saturation. The time taken for water saturation also depends on the size of the fragment, with larger fragments taking longer to waterlog, and hence slower to settle.

Sorting and erosion of the charcoalified fragments in the Tredomen Quarry samples left assemblages of pieces between 1-3mm in diameter, similar to the smallest clast sizes within the conglomerates. As most of the charcoalified fragments of vegetation are most commonly found within intraformational conglomerates and therefore were likely to have been waterlogged and sank to the bottom, to be transported as bedload along with pebble-sized clasts.

Taphofacies 2: Large thalloid, non-embryophyte fragments within major channel sandstones

Overlying the conglomeratic deposits, planar-bedded, medium-grained green sandstones (lithofacies 2a, Chapter 6) contain prolific amounts of large thalloid fragments (including *Prototaxites* or *Nemataskетum*). Charcoalified and non-charcoalified organic fragments may have been entrained and eroded by high discharge events, under a high velocity flow regime, where material was transported as bedload and subsequently deposited by vertical accretion, along with medium sand-sized grains in basal channel deposits. Although this is a similar taphonomic history to taphofacies 1, taphofacies 2 may have been deposited with a slightly reduced flow velocity, as material is less fragmentary, suggesting either a reduction in erosion or less transportation. Non-coalified thalloid fragments were moderately well-preserved possibly due to the rapid burial of material. The complete fish specimens that have been found within this taphofacies may also have been buried rapidly during a high discharge event, and likely died through asphyxiation (personal communication Nigel Trewin).

Taphofacies 2 also occurs within planar-cross-bedded, medium-grained sandstone units above the basal planar-bedded sandstones (lithofacies 2a, Chapter 6), which contain an increased amount of axial debris. Material may have been eroded and transported as bedload in a high-velocity flow regime, and deposited as lateral accretion with medium to fine sand-sized grains, within lower channel bar deposits.

Taphofacies 3: Fertile embryophytes within minor channel sandstones

As most well-preserved plant fossils from Tredomen Quarry are found within this taphofacies, with material partially intact and often still retaining sporangia, these plants likely experienced a lesser degree of erosion and transportation compared to material in taphofacies 1 and 2. Taphofacies 3 occurs within fine-grained, trough-cross and cross-ripple-laminated sandstones (lithofacies 2b, Chapter 6), often with concave bases, which occur gradationally above planar-cross-bedded medium-grained sandstones (lithofacies 2a, Chapter 6). The fine-grained sandstones may be interpreted as accretion of upper bars or levees, or as minor channel sandstones that may have incised into the upper bar to bar top siltstones (wavy and planar-laminated siltstones, interpreted as proximal floodplain siltstones, lithofacies 3a, Chapter 6). Therefore, these higher plants may have grown on the top surfaces of upper bars, and experienced minor transportation in suspension within minor bar top channels, to be deposited close by. However, this assemblage is still considered to be allochthonous, with material occurring either parallel or slightly oblique to bedding, with a random orientation and distribution.

Whilst in suspension or subsurface sediments, plant material was subjected to decay and chemical alterations, as well as slight physical alteration via erosion. Experimental studies on modern leaf samples indicate that decay by microbial action via biofilms occurs rapidly once material is submerged in water (Spicer 1977, Dunn et al. 1997, Grimes et al. 2001). A number of the well-preserved higher plant coalified compressions from Tredomen Quarry are associated with impressions within fine-grained, hydrated-iron-oxide (limonite) layers. This is similar to the iron-rich mineral encrustations described by Spicer (1977) and Dunn et al. (1997) in their experiments that developed on modern leaves that were submerged in water and decayed by microbial action. Dunn et al. (1997) proposed that the microbial biofilms allow the otherwise hydrophobic plant material to attract Fe^{3+} ions, providing a protective inorganic encrustation against further decay.

Bacterial decay may also explain the pyrite precipitation that occurred with the axes of a few specimens. Sulphate-reducing bacteria produces hydrogen sulphide, which when reacts with iron minerals within the sediment, produces iron monosulphides (Grimes et al. 2001, Brock et al. 2006). It has been proposed that these iron monosulphides are converted to pyrite by reaction with either polysulphides or aqueous sulphur, which occurs in low concentrations in freshwater environments (Brock et al. 2006). Pyrite formed within and around cell walls,

particularly the microbially degradable components of plant physiology, such as the water-conducting tissues of the axes central strands (Kenrick and Edwards 1988).

This evidence of bacterial interaction with the plant material suggests that the plant material remained in the water column or subsurface sediments for a significant amount of time, possibly during periods of standing water, under stagnant conditions, suggesting that these minor channels were at times cut off from the main flow and abandoned.

Taphofacies 4: Mesofossils and vegetative debris within upper bar or proximal floodplain siltstones.

Taphofacies 4 contains much smaller vegetative debris than seen in taphofacies 2 and 3, but fragments are still recognisable as axial or thalloid. Fragments of minute fertile and sterile mesofossils, together with small, highly fragmented *Prototaxites* or *Nemataskctum* pieces, were transported via suspension under a low velocity flow regime, and hence separated from larger material by hydraulic sorting. These highly-sorted small fragments were subsequently deposited in a random orientation, along with silt-sized grains as vertical accretion on upper bar tops or proximal floodplains, resulting in planar-laminations with organic-rich fractions occurring at the base (lithofacies 3b, Chapter 6). Reworking of these siltstones by wind-generated wave ripples resulted in material winnowing into the lower ripple crests, resulting in discrete lenses of organic material. Where cross-ripple-lamination occurs, debris was also worked into the foresets of the ripples.

The mesofossils are moderately well-preserved as coalified compressions, and still retain their sporangia, suggesting low erosion rates or short transportation time. These mesofossils may have been living on the upper bar tops or proximal floodplains, although the allochthonous nature of this assemblage means that this statement has not been confirmed with fossil evidence. The mesofossils and other debris within taphofacies 4 only rarely exhibit any limonite envelopes, and are not associated with pyrite-limonite cubes, like the larger early land plant fossils for taphofacies 3, although some specimens are associated with orange iron-oxide staining. The lack of any significant limonite encrustations may be because fragments were buried too rapidly and avoided interaction with bacterial biofilms within the channel waters.

Taphofacies 6: Thalloid, non-embryophyte fragments within upper crevasse splay sandstones

Small thalloid fragments, possibly *Prototaxites* / *Nemataskетum* or *Nematothallus*, plus *Pachytheca* specimens, are found at the base of planar-bound, laterally extensive, very-fine-grained sandstones to siltstone units (lithofacies 3c, Chapter 6), which have been interpreted as one of two fractions deposited as the upper beds of crevasse splays deposits (see Chapter 6). The small fragmentary thalloid material are highly eroded, which suggests debris was transported as bedload during high discharge events, where a high velocity flow regime resulted in the breaking of river channel banks or levee, transporting material away from the main channels, and deposited it on the floodplains as crevasse splay deposits. A high velocity flow regime resulted in vertical accretion of very-fine sand-sized and silt-sized grains together with the organic debris, into planar-laminations. The blacker bands of laminations may result from the fluctuation of flow rates, with the deposition of organic material occurring during slightly lower flow rates. The rapid burial of organic material within the crevasse splay deposits resulted in moderately well-preserved coalified compressions.

Taphofacies 7: Fertile embryophytes within uppermost crevasse splay siltstones.

The most well-preserved plant fossils at Targrove Quarry occur within laterally extensive planar-laminated siltstones beds (lithofacies 3c, Chapter 6), occurring above the very-fine-grained sandstones described above for taphofacies 6. These siltstones have been interpreted as the upper parts of fining upwards units, deposited on the upper beds of crevasse splay deposits (Chapter 6). Plant fragments are moderately well-preserved and are partially intact, with some specimens retaining their sporangia, suggesting a lesser degree of erosion and transportation than the material found in taphofacies 6. Transportation of material may have occurred as saltation or suspension, in a high velocity flow regime (although not as fast as taphofacies 6), where unconfined flow removed material from the main channels to the floodplains due to the breaking of river banks or levees, and subsequently deposited by vertical accretion in upper crevasse splay deposits.

As seen in taphofacies 3, plant debris is associated with limonite, which often preserved an impression between the coalified compression and the host sediment. Therefore it is likely that organic material began to decay within the water column, and attracted a microbial biofilm that surrounded the specimens, and resulted in inorganic encrustations to protect the

organic material as explained for similar fossils in taphofacies 3 (see above). The evidence for bacterial interaction with the plant material suggests that the plant material had been in the water column for a significant amount of time, possibly in standing, stagnant waters occurring at the most distal portions of the crevasse splay.

Taphofacies 8: Thalloid fragments within uppermost crevasse splay or floodplain mudstones.

The laterally extensive dark-green wavy to planar-laminated mudstones (lithofacies 5c, Chapter 6) found above the yellowish-brown sandstone to siltstone units at Targrove Quarry have been interpreted as uppermost crevasse splay deposits, where the finest grains were transported via suspension from the main channels to the most distal part of the crevasse splay and floodplains (Chapter 6), by a very low velocity regime compared to flows which transported taphofacies 6 and 7. Any organic material that was hydraulically sorted into this fraction (?*Nematothallus* cuticle) was also transported by suspension, and deposited by vertical accretion as planar laminations. Later reworking by wind-generated wave ripples resulted in wavy-lamination and may have reworked organic material. However, megafossils are rare in these horizons, occurring only in the uppermost laminations, just below the erosive planar lower boundary of sandstone-siltstone units above. This may be because the majority of plant material was not buried due to lack of sediment at the crevasse splay end, and therefore subjected to an increased chance of decay. Preservation occurred only after rapid burial, after high discharge events and the deposition of lower crevasse splay beds above.

Autochthonous assemblages

In general, the majority of taphofacies assemblages in the fluvial environments are allochthonous with rare occurrences autochthonous assemblages, which are usually defined where rooting systems are seen preserved *in situ* through the rock sequence (Hotton et al. 2001). The following taphofacies from Tredomen Quarry have been interpreted as autochthonous assemblages, giving clues to the growth habitat of the preserved vegetation.

Taphofacies 5: ?Fungal hyphae within upper bar siltstones

This taphofacies occurs only in association with taphofacies 4 (the allochthonous vegetative and mesofossil debris assemblage, within the green, wavy-laminated mica-rich siltstones).

Minute hyphal-like tubes, with internal thickenings, appear to weave in and out of the top layer of sediment of green-grey, planar and wavy-laminated siltstones (lithofacies 3a, Chapter 6). These tubes do occur individually, but often form part of an intertwining and bifurcating network of tubes, which may represent hyphal networks of putative fungal affinity, possibly *Prototaxites*. If correct, the presence of these hyphae support the hypothesis that *Prototaxites* and related fungal-like organisms were heterotrophs (Boyce et al. 2007), and took advantage of the nutrient-rich substrates, the highly organic debris-rich horizon deposited as taphofacies 4. It is unlikely these banded tubes represent the re-establishment of vascular plant rhizoids after burial, as all the vascular plants deposited were highly fragmented debris. Therefore, this may represent *in situ* behaviour of a larger fungal-like organism with mycelia.

Taphofacies 9: ?Fungal vegetative remains within ephemeral lake or floodplain siltstones.

The rare, poorly-preserved axial-like features of taphofacies 9, may represent axes or 'roots', possibly occurring *in situ* on the bedding surfaces of red, wavy and planar-laminated siltstones, interpreted as ephemeral lake or exposed floodplain deposits (lithofacies 3b, Chapter 6). Although these siltstone surfaces are also covered with abundant pseudo-gleyed polygonal desiccation cracks that may give the appearance of branching axes, the axial-like features found at Tredomen Quarry are similar to the 'rooting structures' described by Hillier et al. (2008). Morphotype 1 'rooting structures' have been described from Lower Devonian Old Red Sandstone strata from across the Anglo-Welsh Basin, as horizontal axial-like structures with diameters between 0.5 to 11mm, that meander across bedding planes, with localised tapers and swells, and often with a gnarled or ridged appearance (Hiller et al. 2008). They interpret these features, together with larger, vertical, downwards tapering and bifurcating 'rooting structures' (morphotype 2) as possible *in situ* anchoring structures of fungal-like organisms such as *Prototaxites*. Morphotype 1 and 2 were found from a range of depositional environments across the Anglo-Welsh Basin (Hiller et al. 2008), but the association with ephemeral channel and crevasse splay deposits and vertic palaeosols (indictors of a strong seasonal moisture contrast), suggests that these fungal-like organisms were capable of surviving drier, harsher environments than perhaps the higher (early embryophytes).

7.2.3: *Taphofacies model*

A 3D taphofacies model for the Lower Devonian (lower Lochkovian) has been constructed (Figure 7.1), which incorporates the taphofacies descriptions and interpretations from Tredomen and Targrove Quarries, with a geomorphic model for the St. Maughans Formation. It would be inappropriate to use geomorphic model 1 (the ephemeral mud-dominated river system), as this is based on lowermost Lochkovian Raglan Mudstone Formation strata, which is barren of any plant fossil material. As the interpretation of planar-cross-bedded sandstone units is difficult from core, it cannot be assumed that these units represent point bar deposits on meandering channels, and therefore this model may be flawed. The interfluvial-drainage and trunk channel model (geomorphic model 3) has been used, with all lithofacies from both formations represented (see Figure 6.12, Chapter 6). The model has been split into wet and dry seasons to illustrate the two-stage nature (high to low or no discharge) of this system.

Using geomorphic model 3, it has been hypothesised (in Chapter 6) that the change in sedimentology seen at the Silurian-Devonian boundary was due to the switching on of truck channels, rather than a change in fluvial style, possibly as a result of climate change. It has been hypothesised that the climate shifted from a 'dry phase' to a 'wet phase', with increased seasonality (stronger, longer wet seasons) at the start of the Devonian (see Chapter 6). During the lower Lochkovian, sand-dominated trunk river channels were therefore activated, with evidence of major channels with basal lags, minor channels, fining upwards bars and crevasse splay deposits (Figure 7.1) (see geomorphic model 3, Chapter 6).

During the wet season, initial discharge was high enough to burst riverbanks, resulting in the formation of crevasse splays, and extensive areas of the floodplain were covered with shallow surface waters (1 and 2, Figure 7.1). In very large flood events, floodwaters may have swept across the whole floodplain, washing river levees away (3, Figure 7.1).

During these high periods of discharge and vertical erosion, charcoalified and non-charcoalified fragments of non-embryophytes, mud rip-up clasts and reworked carbonate nodules were transported from the floodplains into the trunk channels by floodwaters (3, Figure 7.1) and incipient floodplain drainage channels (4, Figure 7.1). This material was deposited on the channel and crevasse splays floors (TF1, Figure 7.1). Fauna such as cephalaspids, eurypterids and arachnids that may have inhabited waterholes or abandoned sections during the dry season, were washed out by floodwaters, transported into the main channels, and incorporated into the channel bed deposits. After the initial high-discharge and deposition of pebble-sized clasts, non-charcoalified non-embryophyte debris was deposited

Figure 7.1: Taphofacies model for the Lower Devonian St. Maughans Formation

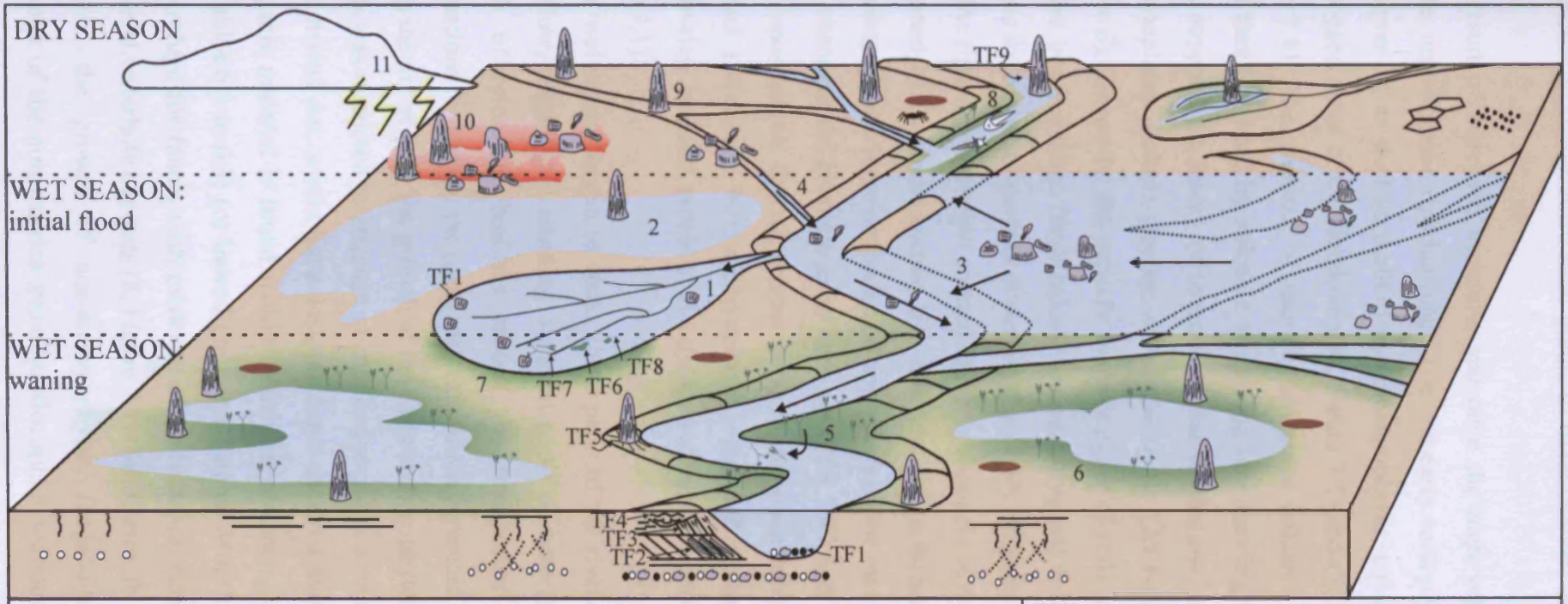

WET SEASON (initial flood event):
1: High velocity floodwaters burst trunk channel levees, formed crevasse splay. Reworked floodplain material (charcoalified non-embryophytes, carbonate nodule clasts and mud rip-up clasts, including pedogenically-formed mud aggregates) was transported from the trunk channel and deposited as basal crevasse splay deposits (TF1).
2: Extensive areas of the floodplain covered by shallow floodwaters.
3: High velocity floodwaters transported reworked floodplain material into the trunk channels, and deposited as basal lag (TF1) and along the foresets of cross-bedded medium-grained sandstone (TF2).
4: Reworked floodplain material transported by interfluvial, incipient drainage channel into the trunk channel.
WET SEASON (waning):
5: Riparian vegetation (including early embryophytes, mesofossils and thalloid non-embryophytes) on banks and levees of the trunk channel. Transported as suspension, and deposited on upper point bars of the main trunk channel (TF3 and TF4). Non-embryophyte, fungal-like organism growth on upper point bars and proximal floodplains, supported by hyphal networks, absorbing nutrients from the vegetative debris within the sediments (TF5).
6: Riparian vegetation around waterlogged areas of the floodplain.
7: Riparian vegetation around distal crevasse splay. Transported by suspension, deposited as upper crevasse splay deposits (TF6, TF7,TF8).
DRY SEASON:
8: Restricted vegetative growth and faunal activity around waterholes and abandoned portions of the system.
9: Growth of non-embryophyte, fungal-like organisms around waterholes and proximal floodplains, on nutrient-rich sediments.
10: Storms and lightning with the onset of the wet season.
11: Charcoalification of non-embryophyte, fungal-like organisms by smouldering wildfires, sparked by lightning.

KEY
- water
- sediment/ rock
- vegetation: rhyniophytes, rhyniophytoids, mesofossils, thalloid non-embryophytes
- planar lamination/bedding
- cross-lamination/bedding
- trough-cross-lamination/ bedding
- wavy-lamination
- intraformational conglomerate
- mud-rip up clast
- pedogenic mud aggregates
- polygonal desiccation cracks
- vertically-aligned features (burrows/roots/cracks?)
- carbonate nodules
- slickensided pseudo-anticlinal slip-planes
- living *Prototaxites*
- dead charcoalified *Prototaxites*
- embryophytes (green=living black=fossil)
- *Beaconites* burrows
- cephalaspid
- eurypterid
- arachnid
- lightning
- wildfire
- direction of flow

along with medium-grained sand grains in basal channel or basal bar deposits (TF2, Figure 7.1).

As a result of increased moisture, and once the high velocity floodwaters had subsided, delicate, opportunistic riparian plants (i.e. the early embryophytes and mesofossils described in Chapter 3), as well as thalloid non-embryophytes, colonised riverbanks (5, Figure 7.1), waterlogged areas of the floodplain (6, Figure 7.1) and distal portions of crevasse splays (7, Figure 7.1). The presence of laterally extensive volcanic ash-fall tuffs across the Anglo-Welsh Basin, formed by volcanic ash falling into standing water (Allen and Williams 1981, 1982), supports the theory of extensive areas of shallow, standing or low velocity water on the floodplains. Pseudo-gleying within the upper (A) horizon of palaeosols (described in Chapter 6), formed by the periodic water-logging of soils by reduced waters and subsequent localised iron reduction (drab haloes) around polygonal desiccation cracks and burrows, also supports the notion of periods of standing, possibly stagnant waters on the floodplains.

Once the riparian vegetation entered the river channels, it was transported by suspension, and partitioned by hydraulic sorting into a number of taphofacies: the megafossils and thalloid non-embryophytes were deposited on upper bars of the main truck channel (TF3, Figure 7.1), minor channels and crevasse splay deposits (TF6, TF7 and TF8, Figure 7.1); the mesofossils were deposited on the uppermost bars of the main trunk channel (TF4, Figure 7.1) or proximal floodplain. Non-embryophytic, fungal-like organisms took advantage of the nutrient-rich bar and proximal-floodplain sediments, supported by hyphal networks (TF5, Figure 7.1).

As the wet season began to wane, these parts of the river may have been cut off from the main flow, resulting in standing, stagnant pools of water, which would have promoted the growth of microbial biofilms around the transported vegetation, attracting iron-rich encrustations to form on the plant surfaces, which protected them from further decay.

During the dry season, the growth of the early embryophytes around riverbanks subsided, and growth was restricted to stagnant abandoned sections or waterholes (8, Figure 7.1), but with further drying out, would have desiccated and decayed away. This is a possible reason why no organic material is found within ephemeral channels, waterholes or floodplain deposits (see Tables 6.1 to 6.3) (or indeed the upper Raglan Mudstone Formation). Waterholes were also a refuge for fauna, with evidence of cephalaspid, eurypterid, and arthropod activity in ephemeral waterhole deposits (8, Figure 7.1) (lithofacies 3b, Chapter 6).

However, the growth of non-embryophytic, fungal-like organisms continued, taking advantage of the nutrient-rich proximal-floodplain sediments (9, Figure 7.1). This supports

the hypothesis that these fungal-like organisms were heterotrophic, obtaining nutrients from various sources from the substrate (Boyce et al. 2007). *Prototaxites* / *Nemataskетum* grew close to waterholes (TF9), suggesting that this organism was perennial and had the ability to survive in harsh, moisture-deficient environments.

Charcoalification of *Prototaxites* (10, Figure 7.1) occurred by smouldering wildfires that were likely to have been ignited by storm-generated lightning (11, Figure 7.1). Studies of the distribution and frequency of thunderstorms across modern day Australia indicate a high frequency of storm-generated lightning and associated wildfires in areas of high moisture and low pressure across northern Australia during the wet season (October to March), controlled by the north Australian monsoon (Kuleshov et al. 2002, 2009). Therefore charcoalification of *Prototaxites* likely took place with the onset of the wet seasons.

7.3: TAPHONOMIC CONSTRAINTS ON UNDERSTANDING PALAEOECOLOGY

Palaeoecological studies of plant assemblages are severely hampered by taphonomic constraints. The original composition of the vegetative tissue is the first control on the final fossil assemblage. As well as possessing a resistant waxy cuticle (Edwards et al. 1982), early land plants contained tracheids (tubes with thickened walls making up the vascular system), which were likely to be originally composed of lignin, a recalcitrant polymer, thus increased preservation potential (Edwards 2003). In contrast, it can be inferred that as very few cryptospore-producing plants have been preserved, as a result of soft tissue composition.

The pre-burial alteration of plant tissue may have increased preservation potential. Charcoalification not only preserves internal anatomy, but also provides resistance to erosion, possibly due to cell homogenisation. Charcoalification has been important for the preservation of minute sporangia at other Lochkovian localities, which are similar to the mesofossils from Tredomen Quarry (see Chapter 3) (Edwards 1996, Edwards 2000, Edwards and Axe 2004). Charcoalification therefore provides potentially a better representation of vegetation inhabiting the floodplains than non-charcoalified assemblages.

Mineralisation may also have increased preservation potential of vegetation. Limonite coatings around megafossil specimens, formed by microbial biofilms (Spicer 1977, Dunn et al. 1997), protected the vegetation from further decay. Pyrite precipitation in anoxic, sulphate-reducing bacteria-rich waters (Grimes et al. 2001, Brock et al. 2006), occurred within and around cell walls, such as water-conducting tissues of axes central strands, and in some cases resulted in partial three-dimensional preservation.

The main control on the distribution of plant material within the system and the most detrimental to palaeoecological reconstructions is the stratinomic partitioning as a result of hydraulic sorting. Fragments were physically degradated by hydraulic erosion. However, the embryophytes (megafossils and mesofossils) were the least degradated, possibly because the growth of these plants around the riverbanks did not begin until floodwaters subsided and erosive power was reduced. Additionally, embryophytic debris potentially was not transported as far the charcoalified fragments, which were transported by floodwaters from the distal floodplains.

7.4: CHAPTER SUMMARY

By integrating sedimentological analysis and palaeobotany, nine taphofacies were recognised from Tredomen Quarry and Targrove Quarry. Seven taphofacies are allochthonous and are associated with a sand-dominated river channels and crevasse splays: charcoalified fragments within channel lag or basal crevasse splay conglomeratic deposits; large thalloid fragments with green, medium-grained major channel sandstones; fertile embryophytes within green fine-grained minor channel and bar sandstones; mesofossil and vegetative debris within upper bar or proximal floodplain siltstones; thalloid fragments within upper crevasse splay sandstones; fertile embryophytes within uppermost crevasse splay siltstones; and thalloid fragments within uppermost crevasse splay or floodplain mudstones. Two autochthonous assemblages have also been interpreted; fungal hyphae within upper bar siltstones; and fungal vegetative remains within ephemeral lake / waterhole or floodplain siltstones.

The taphonomic controls that constrain palaeoecological interpretations were found to be pre-burial composition, physical and chemical taphonomic processes, hydraulic sorting and stratinomic partitioning of plant material, resulting in the distribution of plant material into different lithofacies.

Fossilised material is restricted to the St. Maughans Formation, above the Bishop's Frome Limestone, and so the taphofacies model was based on the interfluvial-drainage and 'trunk' channel model devised for the Lower Devonian in Chapter 6 (Figure 6.12), with evidence of strong seasonality (distinctive wet and dry seasons), with all lithofacies represented. The taphofacies model is based on these prolonged wet seasons, with each taphofacies representing a different hydraulic stage of the river system, from beginning of the wet season, the gradual subsidence of flow, to finally drying out into the dry season.

The response of vegetation to each hydraulic stage is recorded. In the dry season, it is hypothesised that very little embryophytic growth occurred, with no preservation of any plant fossils within ephemeral channel and floodplain deposits. This delicate vegetation would have desiccated and decayed in harsh moisture-deficient environments. There is some evidence however that the fungal-like organisms (*Prototaxites* / *Nemataskетum*) were able to survive through the drier periods, and hence were more perennial in nature than the embryophytes. These organisms, together with cephalaspids and arthropods, may have taken advantage of abandoned waterholes, or may have even been able to survive on the floodplain. During the wet season, once the initial high velocity regimes had subsided, the main flow was confined to the channels, and due to the increased soil moisture, the opportunistic delicate rhyniophytes, rhyniophytoids and mesofossils began to flourish on riverbanks. It was at this point that these early land plants entered the river system, and were transported by suspension and deposited on the upper bar, minor channels and proximal floodplains. These areas may have been cut off from the main 'trunk' channel, creating waterholes or abandoned sections, containing standing stagnant waters, promoting the growth of microbial activity. This may explain why these fossils are well-preserved, as they have only been transported from the riverbanks downstream by a relatively low flow regime, and further protected against decay via iron-encrustations, initiated by microbial biofilm activity. Non-embryophytic growth also returned, with fungal-like organisms taking advantage of the newly deposited nutrient-rich deposits of the upper bar and proximal floodplain. As further drying of the system continued, the embryophytes receded, while fungal-like organisms and other non-embryophytes were able to survive.

CHAPTER 8 : ESTIMATING THE ATMOSPHERIC pCO_2 LEVEL DURING THE EARLY DEVONIAN USING STABLE ISOTOPIC ANALYSIS

8.1: INTRODUCTION

One of the most important challenges facing scientists today is to understand and predict the perturbations in the Earth's climate, particularly as a result of the dramatic increase in anthropogenic emissions in the last few centuries. Atmospheric levels of carbon dioxide have risen from pre-industrial levels around 270ppmV (Wigley 1983, Barnola et al. 1987) to 385ppmV today (Tans NOAA/ESRL 2008). To understand the role of carbon dioxide as a greenhouse gas and to predict its effects on the Earth's future climate, knowledge of past CO_2 levels and associated palaeoclimatic and palaeoecological changes is essential.

Direct measurements of past CO_2 levels are only available from relatively recent sources. Deep ice cores contain entrapped air inclusions, which provide a direct record of palaeoatmospheric compositions, particularly carbon dioxide and methane. In 2005, the European Project for Ice Coring in Antarctica (EPICA) extended the Vostok ice core record (Petit et al. 1999) by an additional 360,000 years (Siegenthaler et al. 2005, Lüthi et al. 2008), and determined that in the last 800,000 years CO_2 levels have not exceeded 300ppmV until the industrial era.

There have been several approaches to modelling past climates and estimating past CO_2 levels using theoretical techniques, including modelling mantle evolution and degassing (Tajika and Matsui 1992, Tajika 1998). Over the past two decades, Berner developed GEOCARB, a geochemical model to estimate pCO_2 levels over the Phanerozoic. GEOCARB is based on the long-term exchange of carbon between the atmosphere, the rock record and the oceans (Berner 1991, 1994, Berner and Kothavala 2001). The most recent update of the model, GEOCARBSULF, incorporates modelling of the sulphur cycle, and estimates of O_2 levels over the Phanerozoic (Berner 2006). Input data include the weathering rates of Ca and Mg silicates, weathering of sedimentary organic matter, rates of uplift, the evolution of plants and burial of carbonates (Berner and Kothavala 2001). Essentially the GEOCARB models estimate very high pCO_2 levels during the Early Palaeozoic, with a dramatic drop during the Devonian and Carboniferous, returning to high levels during the Mesozoic, and a gradual decrease through the Cenozoic (Figure 8.1) (Berner and Kothavala 2001).

Figure 8.1: Estimates of Phanerozoic atmospheric ρCO_2 levels from geochemical models GEOCARB III and GEOCARBSULF (modified from Berner 2006). RCO_2 is the mass of atmospheric Co_2 of the past time divided by the pre-industrial atmospheric CO_2 level (300ppmV).

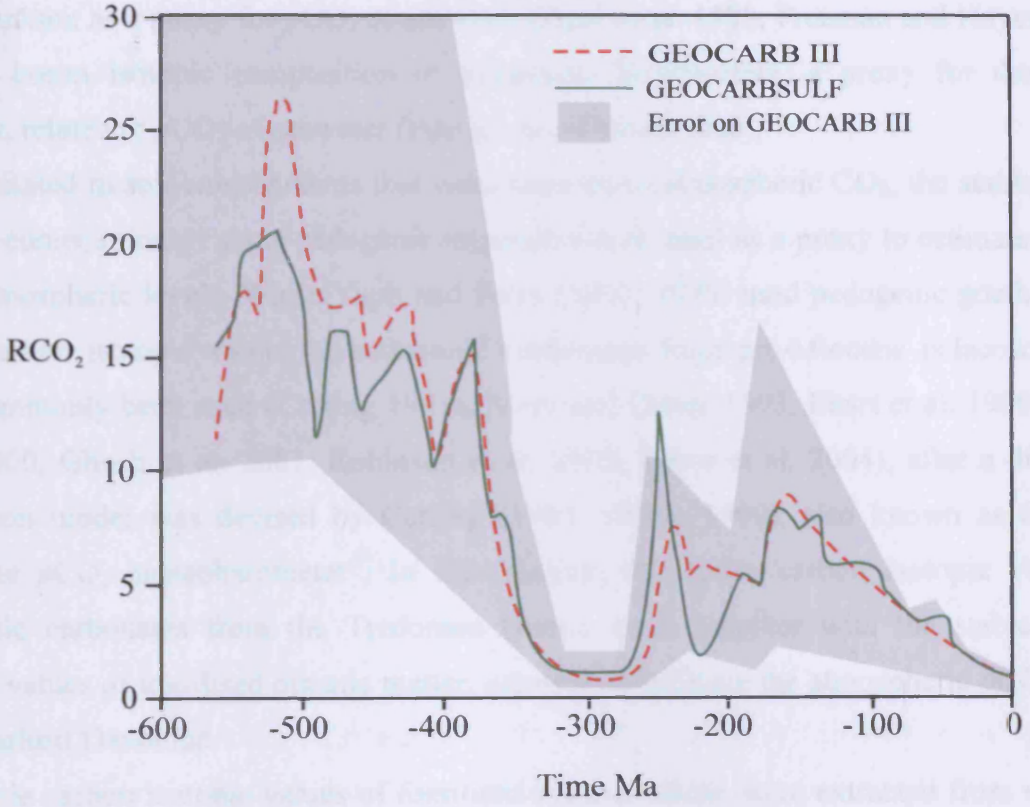

To ground truth these long-term, carbon-cycle geochemical models, proxies that estimate atmospheric CO_2 levels are used to verify the values estimated (Royer et al. 2004). These include: plant stomatal densities due to the inverse relationship to atmospheric ρCO_2 (McElwain and Chaloner 1995, 1996, Royer 2001); the carbon isotopic composition of phytoplankton as a proxy for ρCO_2 of seawater (Popp et al. 1989, Freeman and Hayes 1992); and the boron isotopic composition of planktonic foraminifera, a proxy for the pH of seawater, related to ρCO_2 of seawater (Pearson and Palmer 2000).

If precipitated in soil environments that were exposed to atmospheric CO_2, the stable carbon isotopic composition of some pedogenic minerals can be used as a proxy to estimate palaeo-ρCO_2 atmospheric levels. While Yapp and Poths (1992, 1996) used pedogenic goethites, the stable carbon isotopic values of pedogenic carbonates from pre-Miocene palaeosols have more commonly been used (Cerling 1991a, Mora and Driese 1993, Ekart et al. 1999, Driese et al. 2000, Ghosh et al. 2001, Robinson et al. 2002, Tabor et al. 2004), after a diffusion-production model was devised by Cerling (1984, 1991a, 1999), also known as the "soil carbonate ρCO_2 palaeobarometer". In this chapter, the stable carbon isotopic values of pedogenic carbonates from the Tredomen Quarry core, together with the stable carbon isotopic values of fossilised organic matter, are used to estimate the atmospheric ρCO_2 levels of the earliest Devonian.

The stable carbon isotopic values of fossilised organic matter were extracted from coalified axial plants and *Prototaxites*. Not only are these values needed for the soil carbonate ρCO_2 palaeobarometer (see later), they also give clues to the metabolic pathways used by Silurian-Devonian vegetation and the possibility to identify trophic relationships within the ecosystem. The different metabolic pathways used by modern plants (namely C3, C4 and CAM) fractionate carbon to different degrees, reflected in the isotopic value of the tissue. The stable carbon isotopic value for modern C3 plants ranges from -23‰ to -34‰ (average -27‰), whilst for C4 the values range between -8‰ and -16‰ (average -13‰) (Deines 1980). The first fossil evidence of C4 plants (with Kranz anatomy) is of Late Miocene age (Thomasson et al. 1986, Tidwell and Nambudiri 1989), although molecular genetic studies suggest that the C4 pathway evolved earlier, in the Oligocene (Gaut and Doebley 1997, Kellogg 1999, 2001), which is supported by carbon isotopic values from palaeosol carbonate (Fox and Noch 2003). However, C4 plants did not become a dominated component of terrestrial ecosystems until the Miocene (Osborne and Beerling 2006) and therefore it is likely that C3 type plants dominated pre-Miocene ecosystems.

Recent work on the isotopic values of *Prototaxites* suggests that this fungal-like organism may have been heterotrophic, as fossilised material is isotopically heavier than typical C3 plants (Boyce et al. 2007). In this chapter, the stable carbon isotopic values of fossilised organic matter from Tredomen Quarry are determined and compared with the known values of C3 plants.

Stable oxygen isotopes can also be extracted from pedogenic carbonates. There have been several attempts to correlate the isotopic composition of oxygen from pedogenic carbonates ($\delta^{18}O_{calcite}$) and that of the meteoric waters ($\delta^{18}O_{water}$) in which the carbonates were precipitated (e.g. Salomons et al. 1978, Rabenhorst et al. 1984). Cerling (1984) proved a positive correlation between $\delta^{18}O_{calcite}$ and $\delta^{18}O_{water}$ from modern soil carbonates. Through equations developed by Friedmann and O'Neil (1977) and Fricke and O'Neil (1999), the isotopic composition of stable oxygen from pedogenic carbonates can be used to estimate palaeo-temperatures.

8.2: Using stable carbon isotopes from pedogenic carbonate to estimate palaeo-ρCO_2 levels.

The use of pedogenic carbonate nodules to calculate palaeo-ρCO_2 atmospheric levels relies on the assumption that soil carbonate precipitates in equilibrium with soil air, and that the stable carbon isotopic values extracted from pedogenic carbonates reflect that of soil CO_2 (Cerling 1991a, 1999). Soil CO_2 (ppmV) is a mixture of atmospheric CO_2 (ppmV) and soil-respired CO_2 (a flux measured in mmoles/m^2/hr), the former sourced from root respiration and microbial oxidation of organic matter in the soil (Cerling 1991b). In modern soils, the partial pressure and isotopic composition of soil CO_2 is primarily controlled by the relative contribution of soil-respired CO_2 from C3 and C4 plants (with an average $\delta^{13}C$ value of -27‰ and -13‰, respectively (Deines 1980)), productivity rates and temperature (Cerling 1991a). With relatively low concentration of CO_2 in the atmosphere today (~385ppmV), the contribution from the atmosphere is low and therefore does not significantly alter the isotopic composition of soil CO_2 (Cerling 1991b). This does not hold true however for pre-Miocene soils, as C4 plants did not evolve until the Oligocene, and did not become prominent until the Miocene (Tidwell and Nambudiri 1989, Kellogg 1999, Cerling 1999). Instead, pre-Miocene ecosystems were primarily C3-dominated and with atmospheric CO_2 levels relatively higher than today, the isotopic composition of soil CO_2 was controlled by the relative contributions from atmospheric CO_2 (with relatively positive $\delta^{13}C$ values compared with organic matter)

and C3 soil-respired CO_2. Cerling (1984, 1991a) developed a steady state diffusion-production model to describe the stable carbon isotopic composition of soil CO_2 (Cerling 1999), and concluded that there was a positive correlation between higher ρCO_2 levels in the atmosphere and more positive values of $\delta^{13}C$ in pedogenic carbonates. The diffusion-production model uses ρCO_2 of the atmosphere as a boundary condition, and therefore the model was recast so that soil carbonates from palaeosols could be studied to estimate pre-Miocene palaeo-ρCO_2 atmospheric levels.

The following sections briefly explain the diffusion-production model of Cerling (1984, 1991a, 1999), and the equation, parameters and assumptions used for the "soil carbonate ρCO_2 palaeobarometer".

8.2.1: *Carbon dioxide in soils*

In 1984, Cerling developed a model to describe the steady-state condition of soil CO_2 by a diffusion-reaction equation:

$$\frac{\partial C_s^*}{\partial t} = D_s^* \frac{\partial^2 C_s^*}{\partial z^2} + \phi_s^*(z) \qquad \text{(equation 1)}$$

where C_s^* = concentration of CO_2 in the soil (moles/cm^3), t = time (s), D_s^* = diffusion coefficient for CO_2 in soil (cm^{2}s^{-1}) (by Kirkham and Powers 1972), $\phi_s^*(z)$ = depth dependant production rate of soil CO_2. * refers to bulk CO_2 without isotopic distinction. Assuming that soil is a one-dimensional box with an impermeable, no-flux boundary at depth (L), and the following boundary conditions exist;

$$\text{at } z = 0,\ C_s^* = C_a^*$$

$$\text{at } z = L,\ \frac{\partial C_s^*}{\partial z} = 0$$

(where C_a is atmospheric CO_2), solving equation 1 results in:

$$C_s^*(z) = S(z) + C_a^* \qquad \text{(equation 2)}$$

where S(z) is the contribution of soil-respired CO_2 (Cerling 1991b, 1999, Ekart 1999). Using equation 2, and a pre-industrial atmospheric concentration was 300ppmV, Cerling (1984, 1991b) calculated CO_2 concentration profiles for modern soils (Figure 8.2a, Cerling 1999). Most soils follow the shape of the model profile, but vary in intensity as a result of

Figure 8.2a: Model of the concentration of soil CO_2 with depth, based on modern soils (modified from Cerling 1999).

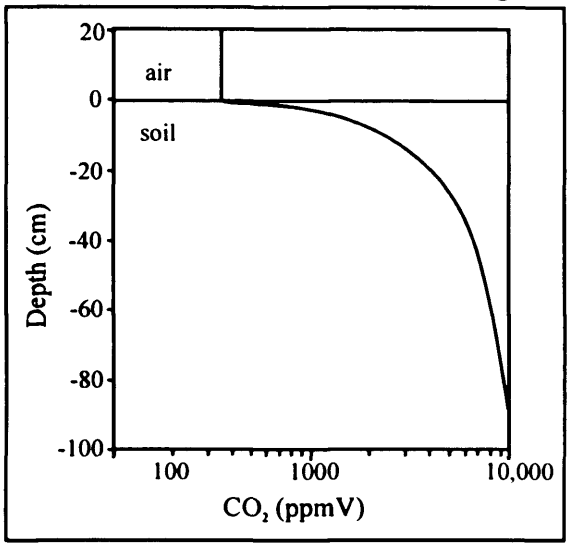

Figure 8.2b: Variation in CO_2 concentration with depth for soils of differing respiration rates (modified from Cerling 1999).

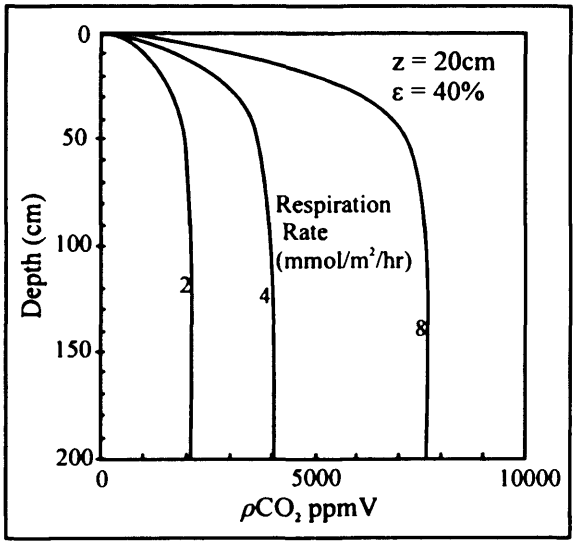

Figure 8.2c: Variation in CO_2 concentration with depth for soils of differing porosities (modified from Cerling 1999).

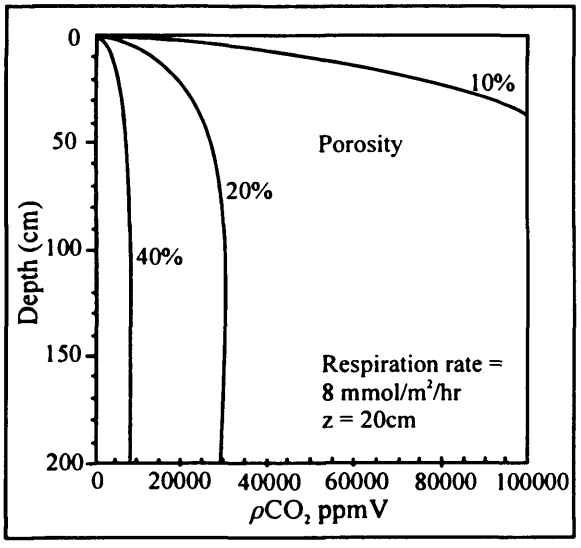

Figure 8.2d: Variation in CO_2 concentration with depth, for soils of differing depths of production (modified from Cerling 1999).

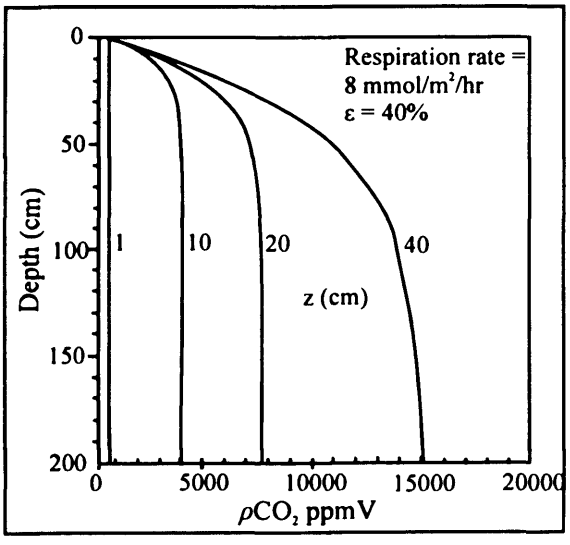

increased respiration rates, porosities and characteristic depth of CO_2 production (Figures 8.2b, 8.2c and 8.2d, respectively). Considering the types of vegetation present during the earliest Devonian, the contribution of CO_2 from small, shallow rooting vascular plants (see Chapter 3) would be low, especially in semi-arid hostile environments (see Chapter 6) and therefore production of soil-respired CO_2 may have been restricted to the top 10cm of soil. However the contribution of CO_2 from non-embryophytes is unknown. Recent evidence suggests that fungal-like organisms (*Prototaxites*) may have possessed rooting systems up to 60cm in depth, but it is not known if these were true roots capable of respiration or purely anchoring systems (Hillier et al. 2008). Pre-vascular biological activity in soils has also been inferred indirectly from geothites (Yapp and Poths 1994).

8.2.2: *Stable carbon isotopes of soil CO_2*

In terms of isotopic composition, soil CO_2 is isotopically heavier than soil-respired CO_2 (i.e. contains a higher relative abundance of C-13 than C-12) due to the mixing of isotopically heavy atmospheric CO_2 and isotopically lighter soil-respired CO_2. Cerling (1991a) modified equation 1 to model the distribution of $\delta^{13}C(CO_2)$ through soil with depth:

$$\frac{\partial C_s^n}{\partial t} = D_s^{\bullet} \frac{\partial^2 C_s^n}{\partial z^2} + \phi_s^n(z) \qquad \text{(equation 3)}$$

where n = the isotopic composition of $^{13}CO_2$ or $^{12}CO_2$. Solving equation 3 results in:

$$\delta_s(z) = \left(\frac{1}{R_{PDB}} \left[\frac{S(z) \dfrac{D_s^{\bullet}}{D_s^{13}} \hat{\delta}_{\phi} + C_a^{\bullet} \hat{\delta}_a}{S(z)\left(1 - \dfrac{D_s^{\bullet}}{D_s^{13}} \hat{\delta}_{\phi}\right) + C_a^{\bullet}(1 - \hat{\delta}_a)} \right] - 1 \right) \times 1000$$

where (equation 4)

$$\hat{\delta}_i = \left[\frac{R_{PDB}\left(\dfrac{\delta_i}{1000} + 1\right)}{1 + R_{PDB}\left(\dfrac{\delta_i}{1000} + 1\right)} \right]$$

where δ_s = permil value for soil CO_2, δ_a = permil value for atmospheric CO_2, and $\delta\phi$ = permil value for soil-respired CO_2, R_{PDB} = ratio of $^{13}C/^{12}C$ in the isotopic reference standard PDB and D_s^{13} = diffusion coefficient for $^{13}CO_2$. Assuming modern temperature and pressure (25°C,

1 bar), 300ppmV CO_2 in the atmosphere with an isotopic composition of -6.5‰, Cerling (1991a) modelled the distribution of $\delta^{13}C$ (CO_2) through a soil profile (Figure 8.3). Two main observations were made; firstly that isotopic value of soil CO_2 is not constant through the soil; $\delta^{13}C$ shifts to more negative values with depth, yet becomes constant from a depth of 30cm. Secondly, as $^{13}CO_2$ and $^{12}CO_2$ have different diffusion coefficients, the isotopic composition of soil CO_2 is at least 4.4% enriched relative to soil-respired CO_2 (Cerling 1984, Cerling 1991a, 1991b). Davidson (1995) suggested that this difference might be less if the isotopic composition of atmospheric CO_2 is similar to the isotopic composition of soil-respired CO_2.

8.2.3: *Soil carbonate pCO_2 barometer equation*

The solution (equation 4) to the diffusion equation for $^{12}CO_2$ and $^{13}CO_2$ (equation 3) developed by Cerling (1991a) proved that the isotopic composition of soil CO_2 is related to the concentration of atmospheric pCO_2 levels. Cerling (1999) recast the solution to calculate pCO_2:

$$C_a = S(z)\frac{\delta^{13}C_s - 1.0044\delta^{13}C_\phi - 4.4}{\delta^{13}C_a - \delta^{13}C_s} \qquad \text{(equation 5)}$$

where S(z) is the concentration of soil-respired CO_2 and $\delta^{13}C_s$, $\delta^{13}C_a$ and $\delta^{13}C_\phi$ is the isotopic composition of soil CO_2, atmospheric CO_2 and soil respired CO_2, respectively. The following section explains each parameter and how each value has been estimated in terms of the earliest Devonian.

1. **Isotopic composition of soil CO_2 ($\delta^{13}C_s$)**

The isotopic composition of soil CO_2 is estimated from the isotopic composition of pedogenic carbonate ($\delta^{13}C_{pc}$), assuming that the soil carbonate precipitated in equilibrium with soil air. This relationship is temperature dependant, and the fractionation factor is calculated by:

$$\varepsilon_{cal\text{-}CO_2} = 11.98 - 0.12 \times T°C \qquad \text{(equation 6)}$$

where $\varepsilon_{cal\text{-}CO_2}$ = calcite-CO_2 enrichment factor and T°C = temperature (Romanek et al. 1992). At a temperature of 25°C a fractionation factor of -8.98‰ is used. Comparing the modern day mean annual temperatures of the same latitude estimated for the Anglo-Welsh Basin is

Figure 8.3: The distribution of $\delta^{13}C$ through the soil profile (modified from Cerling 1991a).

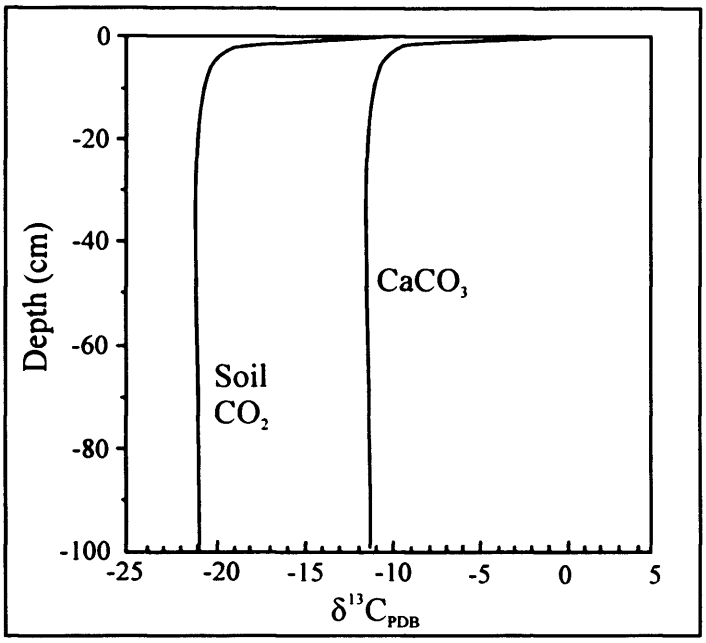

one method of estimating palaeo-temperatures. If preservation of the pedogenic carbonates is pristine, the isotopic composition of oxygen isotopes may also be used to estimate palaeo-temperature, using a simultaneous solution of two equations, where T is temperature in Kelvin:

$$\delta^{18}O_{calcite(SMOW)} - \delta^{18}O_{water(SMOW)} = 2.78\ (10^6\ T^{-2}) - 2.89 \qquad \text{(equation 7)}$$

$$\delta^{18}O_{water(SMOW)} = 0.498\ (T - 273) - 13.20 \qquad \text{(equation 8)}$$

where equation 7 is the fractionation of oxygen isotopes from meteoric waters to carbonate during soil formation (Friedman and O'Neil, 1977) and equation 8 is the correlation between $\delta^{18}O_{water}$ and mean annual temperature (Fricke and O'Neil 1999). Nordt et al. (2003) devised an equation to combine equations 7 and 8, to estimate mean annual temperature directly from the isotopic value of $\delta^{18}O_{calcite}$:

$$-0.498T^3 + (\delta^{18}O_{calcite(SMOW)} + 152.04)T^2 - 2.78 \times 10^6 = 0 \qquad \text{(equation 9)}$$

Once the fractionation factor has been the determined, $\delta^{13}C_s$ can be calculated from $\delta^{13}C_{pc}$ using this equation (Romanek et al. 1992):

$$[(\delta^{13}C_{pc} + 1000)/(\delta^{13}C\,\varepsilon_{(l-CO_2} + 1000) - 1] * 1000 \qquad \text{(equation 10)}$$

assuming that carbonate precipitated at a depth of at least 30m, as it is at this point that S(z) reaches a constant value (Cerling 1999).

It is essential that the palaeosols used for the soil carbonate ρCO_2 barometer are suitable. Firstly, only calcic palaeosols with significant carbonate precipitation are useful, such as palaeo-Vertisols or palaeo-Aridisols (Ekart et al. 1999). These palaeosols can be recognised by the criteria set out by Retallack (1988, 2001).

Secondly, care must be taken to identify pedogenic carbonates *senso stricto*, and not phreatic carbonates, which would record the isotopic composition of groundwater instead of soil air (Wright and Vanstone 1991). Distinguishing between these two types of calcrete is difficult, particularly if pedogenic carbonates have been overprinted with secondary alteration by

groundwater carbonate precipitation during diagenesis (Wright and Tucker 1991, Pimentel et al. 1996, Williams and Krause 1998).

Pimentel et al. (1996) provided some criteria to differentiate between pedogenic and groundwater calcretes. Pedogenic carbonate horizons are thinly bedded, with a sharp top and gradational base, and are associated with distinctive pedogenic horizons. Groundwater carbonates do not exhibit any horizonation, possessing a massive structure and are normally much thicker (at least 10m). The base and top of groundwater carbonates are typically gradational. Pedogenic carbonates are often associated with stable floodplains, where groundwater carbonates are typically associated with drainage channels or playa lake deposits.

In terms of macro-fabrics, pedogenic carbonates can be nodular (from spherical to elongate in shape), massive or laminar, whilst groundwater carbonates normally lack these fabrics. Rhizoconcretions are more common in pedogenic carbonates (although less so in Late Silurian - Early Devonian palaeosols).

In terms of micro-fabrics, pedogenic carbonates are composed of microcrystalline calcite (micrite) with some sparry calcite, whilst groundwater carbonates are often composed of a greater crystal size range of calcite and dolomite grains. Two end member micro-fabrics of pedogenic carbonates have been proposed by Wright and Tucker (1991). In alpha-fabrics, the groundmass is composed of dense finely-grained micrite, with nodules picked out by circum-granular cracks. Other significantly sized cracks are present, often infilled with calcite spar. Floating grains of the host sediment may also be preserved, sometimes with a radially-arranged rim of sparry calcite. Beta-fabrics show evidence of a biological contribution to carbonate precipitation, with such features as microbial coatings, calcified tubules, *Microcodium*, alveolar septal fabrics and needle fibre calcite (Wright 2007). Groundwater carbonates do not usually exhibit beta fabrics. Cement in pedogenic carbonates is typical of precipitation in vadose environments (meniscus or pendant cements), which are not common in groundwater carbonates.

Having isolated pedogenic carbonates, not all are suitable for the ρCO_2 palaeobarometer. Soil formation must have occurred in aerobic, subaerial conditions, and therefore gleyed or anaerobic soils are not appropriate (Cerling 1991a, Ekart et al. 1999). If significant recrystallisation has occurred as a result of burial diagenesis or overprinting, $\delta^{13}C$ and especially $\delta^{18}O$ values may have been altered and therefore unusable for ρCO_2 calculations (Cerling 1991a, Quast et al. 2006, Miller et al. 2007).

2. Isotopic composition of atmospheric CO_2 ($\delta^{13}C_a$)

In Cerling's original calculations of atmospheric ρCO_2 levels from the Mesozoic and Cenozoic palaeosols (1991a), it was assumed that the isotopic composition of atmospheric CO_2 is -6.5‰, and that this value remained constant through time. It has been proved however that $\delta^{13}C_a$ varies through time (Veizer et al. 1999), and this therefore must be taken into account when calculating ρCO_2

There are two methods of estimating the isotopic composition of atmospheric CO_2. The first method uses the isotopic composition of shallow marine carbonates in the rock record as a proxy. Ekart et al. (1999) and Robinson et al. (2002) assume that the difference in isotopic composition between surface oceanic carbonates and atmospheric carbon dioxide is -8‰, based on the comparison of pre-industrial CO_2 trapped in glacial ice (Friedli et al. 1986) and contemporaneous surface ocean carbonates (Veizer et al. 1999). Other authors (Mora et al. 1996) use a fractionation factor of -7‰ suggested by Friedman and O'Neill (1977), whilst Nordt et al. (2003) uses a fractionation factor of -8.5‰, suggested by Lynch-Stieglitz et al. (1995).

According to the curve generated by Veizer et al. (1999) the isotopic composition of surface oceanic carbonates ($\delta^{13}C_{oc}$) during the earliest Devonian is around +2‰, and therefore the isotopic composition of atmospheric CO_2 ($\delta^{13}C_a$) is estimated as -6‰, using the fractionation factor suggested by Ekart et al. (1999). Saltzman (2002) and Buggisch and Mann (2004) however have indicated a positive excursion in $\delta^{13}C_{oc}$ at the Silurian – Devonian boundary (418Ma) from high-resolution data from shallow marine limestones from the Přídolí - Lochkovian of North American and Europe. A maximum excursion of 5.8‰ occurs in limestones from Nevada (Saltzman 2002), possibly as a result of increased terrestrial weathering and/ or burial of organic carbon. From both Saltzman (2002) and Buggisch and Mann (2004) the average value of $\delta^{13}C_{oc}$ for the Silurian –Devonian boundary is +3.6‰, and therefore the isotopic composition of atmospheric CO_2 could be enriched to - 4.4‰.

The second method to estimate the isotopic composition of atmospheric CO_2 uses the isotopic composition of organic matter, if available (Gröcke 2002, Nordt et al 2003). Assuming that fossilised organic matter accurately reflects the isotopic composition of the original vegetative tissue, the following equation devised by Arens et al. (2000) can be used:

$$\delta^{13}C_a = (\delta^{13}C_{org} + 18.67)/1.10 \qquad \text{(equation 11)}$$

As discussed by Gröcke (2002) however, it cannot be assumed that the isotopic composition of organic matter does not alter due to fossilisation processes. Additionally, the type of vegetation fossilised must also be considered. These two problems will be discussed in the following section.

3. Isotopic composition of soil-respired CO_2 ($\delta^{13}C\phi$)

There are several methods by which the isotopic composition of soil-respired CO_2 can be estimated, depending on what information the palaeosols studied can provide. In situations where organic matter has not been preserved, the isotopic composition of soil-respired CO_2 may be assumed to be consistent with the value for modern day C3 plants, -26‰ (Cerling 1991a, Mora et al. 1991, Mora and Driese 1993). This assumes that the isotopic composition of soil-respired CO_2 remains the same through the Phanerozoic. Buchmann et al. (1998) however showed that the isotopic composition of soil-respired CO_2 is directly related to the isotopic composition of the atmosphere. Ekart et al. (1999) therefore use a fractionation factor of -18‰ between the estimated $\delta^{13}C_a$ and $\delta^{13}C\phi$, also used by Robinson et al. (2002). Alternatively the equation of Arens (2000) (equation 11) can be used to estimate $\delta^{13}C\phi$ from $\delta^{13}C_a$ (Prochnow 2006).

Where fossilised organic matter has been preserved, it can be used to estimate soil-respired CO_2 (Cerling 1999, Mora et al. 1996, Ghosh et al. 2001). This assumes that a) the isotopic composition of organic matter ($\delta^{13}C_{org}$) reflects the isotopic composition of soil-respired CO_2 ($\delta^{13}C\phi$) and b) the isotopic composition of organic matter remains the same during fossilisation.

The different chemical components that make up modern plant tissue not only have different isotopic signatures from the bulk $\delta^{13}C_{org}$, but also have different resistances against degradation (Gröcke 2002) (Figure 8.4). Lipids, lignin and cellulose have more negative isotopic compositions compared to bulk $\delta^{13}C_{org}$, and have a higher preservation potential, where as carbohydrates, hemicellulose and pectin have more positive isotopic compositions compared to bulk $\delta^{13}C_{org}$, and have low preservation potential. Fossilised plants therefore should be depleted in $\delta^{13}C$, if ^{13}C-enriched components have degradated, leaving ^{13}C-depleted components remaining (Gröcke 2002). Spiker and Hatcher (1987) show this in the early diagenesis of fossilised wood.

It is also assumed that the chemical components that make up modern plant tissue are the same in Late Silurian - Early Devonian vegetation. This assumption cannot be made, as

Figure 8.4: The variation in $\delta^{13}C$ ratios for the different chemical components of modern plants compared with the average bulk value of -27‰ (modified from Gröcke 2002)

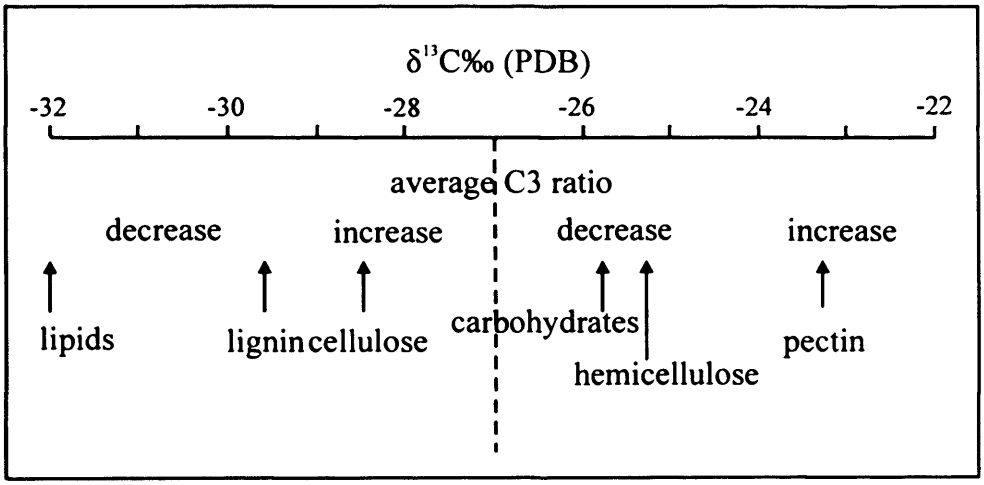

unequivocal evidence for a lignin component in earliest Devonian vascular vegetation has not been found (Ewbank et al. 1996, Edwards et al. 1997). Using pyrolysis, the chemical composition of vascular plant fossils from the Lower Devonian (namely *Psilophyton* and *Renalia*) was found to be predominately *n*-alkanes and *n*-alk-1-enes, together with alkylphenols, alkylbenzenes and alkylnapthalenes (Ewbank et al. 1996, Edwards et al. 1997). The aliphatic compounds found can be attributed to the biomacromolecule cutan, which is a main constituent of cuticle. The aromatic components could represent the thermal degradation of several different biomolecules, including lignin, non-lignin phenolic acids, flavonoids and non-lignin polyphenols (Ewbank et al. 1996, Edwards et al. 1997). It is therefore impossible to assess the possible depletion of $\delta^{13}C$ in fossilised organic matter resulting from the degradation of isotopically heavier components, because the components themselves are too poorly known.

Depletion in ^{13}C does not however occur in most fossilised plants, in fact ^{13}C-enrichment, up to +3‰ compared to the bulk isotopic composition of modern C3 plants, is often observed (Gröcke 2002). This has been explained by the release of ^{13}C-depleted volatiles during coalification (Vyshemirskiy et al. 1975) and charcoalification (Jones and Chaloner 1991). The fossils from Tredomen Quarry have been coalified or charcoalified (see Chapter 3) and therefore the organic matter extracted may be isotopically enriched with respect to the original plant tissue.

There is an additional complication to determining the isotopic composition of Silurian - Devonian vegetation, with the assumption that all vegetation from the pre-Miocene fractionated CO_2 via the C3 metabolic pathway. If non-embryophytes such as *Prototaxites* were in fact able to make a contribution to soil-respired CO_2 (see discussion in "Carbon dioxide in soils" section above), the isotopic composition and chemical composition of its organic matter could be significantly different to C3 vascular plants. Boyce et al. (2007) have indicated that fragments of *Prototaxites* are either similar to C3 vascular plants (-26.6‰) or up to 11‰ enriched in ^{13}C (-15.6‰). Boyce et al. (2007) reconciled this enrichment by suggesting that *Prototaxites* was a heterotroph, consuming not only C3 plants, but also lichens (with an average isotopic composition of around -24‰, Jahren et al. 2003), and cyanobacterial microbial soil crusts (with an average isotopic composition of around -12‰ (Evans and Belnap 1999)). This must be considered when estimating the isotopic composition of organic matter for the soil carbonate ρCO_2 palaeobarometer.

4. Concentration of soil-respired CO_2 (S(z))

S(z) is a function of respiration rate, soil porosity, tortuosity and the characteristic depth of production of soil-respired CO_2 (Cerling 1991a). Based on modern examples, soils with low productivity, often found in arid or semi-arid environments, have a value of S(z) between 3000ppmV and 5000ppmV (Cerling 1991a, Mora et al. 1996, Ghosh et al. 2001). For soils with high production rates, predominately in well-drained temperate to tropical environments, S(z) is between 5000 and 10,000ppmV (Cerling 1991a, Robinson et al. 2002). For gleyed soils the concentration of soil-respired CO_2 can be up to 25,000ppmV (Cerling 1991a).

The Devonian palaeosols from Tredomen Quarry have been interpreted as palaeo-Vertisols developing in an overall semi-arid environment (see Chapter 6). Palaeobotanical evidence suggests very shallow rooting systems and low productivity of vascular plants at least. A minimum value of 3000ppmV will therefore be used in the soil carbonate ρCO_2 palaeobarometer equation for these palaeosols. As there is evidence of wetter periods (see Chapter 6), 7000ppmV will be used as a maximum value, which is also applied by Mora et al. (1996) for similar palaeosols from the Silurian and Devonian of North America.

8.3: Results

8.3.1: *Selection of carbonate nodules*

Twelve carbonate nodules were selected from Tredomen Quarry core borehole 2, (BH2, Figures 6.4 and 6.5). Initially the search for appropriate carbonate nodules started with the recognition of palaeosols, by their distinctive development of horizons; carbonate horizons in association with evidence for bioturbation (burrows and roots) and evidence for the shrinking and swelling of clays (slicken-sided slip planes). Palaeosols with any reduced horizons or gleying were avoided, as reduction may represent soil formation under waterlogged or anaerobic conditions, and therefore unsuitable for the ρCO_2 palaeobarometer. The remaining carbonate horizons were then checked for any obvious evidence of recrystallisation or any significant secondary fracture fill, which would alter the $\delta^{13}C$ value and hence avoided.

Once suitable pedogenic carbonate horizons were chosen, carbonate nodules were extracted from different core depths, with a range of sizes, morphologies (spherical or elongate), and estimated developmental stage of the host palaeosol (from stage I to stage III). Each nodule was thin-sectioned and stained with Alizarin Red S and potassium ferricyanide, to identify primary and diagenetic phases and to analyse the micro-fabrics present. Only five nodules were deemed suitable for isotopic analysis, as they were composed of primary micrite with

little evidence of recrystallisation, whilst the remaining selected nodules all exhibited evidence of recrystallisation, which may reset isotopic values.

Nodule 1

Nodule 1 was extracted from a stage I to II palaeo-Vertisol at a depth of 2.4m from the top of borehole 2 (approximately 17.4m from the quarry surface). The nodule is medium-sized (approximately $2cm^3$), semi-spherical to slightly elongate in shape, and surrounded by massive mudstones (Plate 8.1a). The nodule has a sharp boundary and surrounded by radial cracks. Two obvious horizontal cracks cut through the micrite and are filled with sparry calcite, but these cracks do not extend into the host mudstones. In thin section, the groundmass is composed of microcrystalline calcite, being a light pink colour where stained (Plate 8.1b). The largest crystals found were less than 50μm in diameter. Internal cracks are filled with sparry calcite up to 0.5mm in diameter (Plate 8.1c). Small patches of segregated iron are distributed throughout the nodule (Plate 8.1b), or occur lining the sparry calcite infilled cracks (Plate 8.1d). Floating host sediment grains are rare, but a few corroded grains could be found. There is no evidence of any beta-fabric features.

Nodule 4

Nodule 4 was taken from a stage I to II palaeo-Vertisol, at a depth of 18.95m from the top of borehole 2 (approximately 33.05m from the quarry surface). The nodule is elongate or cylindrical in shape, medium-sized (1cm in circumference, 6cm in length) with a sharp boundary, separated from the massive mudstone host by radial cracks (Plate 8.1e). It is clear that this nodule is actually composed of several coalesced nodules in a matrix of larger-sized calcite crystals. The thin section shows a groundmass of microcrystalline calcite, stained light pink to slightly purple, suggesting that the presence of some ferroan calcite (Plate 8.1f). A greater degree of iron segregation is present compared to nodule 1. Rare floating grains of the original material can be seen with corroded edges. Sparry calcite up to 0.5mm in diameter occurs between micritic nodules. No beta fabrics features were found.

Nodule 8

A stage II palaeo-Vertisol occurs at a depth of 40.10m from the top of borehole 2, approximately 55.1m from the quarry surface. A large-sized spherical nodule was extracted (approximately $5cm^3$), with the appearance of several smaller coalesced nodules, separated by larger calcite grains (Plate 8.1g). The definition of the nodule edge is more diffuse than

seen in nodules 1 and 4. Despite this, radial fractures have developed around the coalesced nodule. The groundmass is composed of microcrystalline calcite, staining light pink in colour (Plate 8.1h). Much iron segregation has occurred, either in the centre (Plate 8.2a) or distributed throughout the nodule (Plate 8.1h). Cracks and inter-nodular material is composed of calcite spar crystals between 0.5 and 1mm in diameter. No beta fabrics were recognised.

Nodule 9

Nodule 9 was extracted from a stage II to III palaeo-Vertisol, at a depth of 48.40m from the top of borehole 2, approximately 63.4m from the quarry surface. This carbonate nodule horizon is thought to be the regional marker horizon, the Bishop's Frome Limestone. This C-horizon consists almost completely of coalesced spherical carbonate nodules, with some displaced angular-edged mudstone fragments (Plate 8.2b). Inter-nodular material appears to be composed of large calcite grains. Thin sections reveal that each nodule is composed of microcrystalline calcite, stained a light pink colour (Plate 8.2c). Unlike nodules 1 to 8 however, the calcite grains increase in size slightly from the centre of the nodule, up to a maximum of 0.05mm in diameter towards the edge of the nodule (Plate 8.2c). Iron segregation is also present, particularly in the nodule centre. The angular-edged displaced mudstones are surrounded by radially arranged sparry calcite, which also occurs between coalesced nodules (Plate 8.2d). No beta fabrics were found.

Nodule 12

Taken from a depth of 58.70m from the top of borehole 2 (approximately 73.7m from the quarry surface), nodule 12 was extracted from a stage I to II non-Vertic palaeosol. This spherical nodule is large ($4cm^3$), composed of smaller coalesced spherical nodules, with a sharp boundary, surrounded by radial cracks (Plate 8.2e). The thin section shows that individual nodules are composed of microcrystalline calcite, stained light pink, with some degree of iron segregation (Plate 8.2f, 8.2g). Secondary sparry calcite can be found between some coalesced nodules (Plate 8.2f, 8.2h). No beta fabrics were recognised.

Using a microdrill, carbonate powder was then extracted from each of the five nodules, focussing particularly where primary micrite was located, avoiding fracture fills and displaced host sediment. The carbonate was then analysed as described in section 2.1.3.

8:3:2: *Organic matter used for stable isotope analysis.*

For the best ρCO_2 palaeobarometer estimate, ideally the organic matter chosen for isotopic analysis should be sourced from the same palaeosols as the pedogenic carbonates. In the earliest Devonian however, as the taphofacies model in Chapter 7 shows, fossilised vegetation is restricted to reduced conglomerates, sandstones and siltstones, interpreted as channel deposits rather than floodplain deposits. It was therefore not possible to sample organic matter that would have been directly contributing soil- respired CO_2 at the time of carbonate precipitation of the chosen nodules. It must be assumed that the organic matter preserved in the channel deposits represent the vegetation growing on the floodplains during soil formation.

Two types of vegetation were sampled from the quarry surface for isotopic analysis: the embryophytes, namely the axes of coalified rhyniophytoids; and the non-embryophytes, namely coalified and charcoalified samples of *Prototaxites*. The material was isolated and treated as described in section 2.1.2 and 2.1.3 of Chapter 2.

8.3.3: *Stable carbon and oxygen isotopic composition of pedogenic carbonate and organic matter.*

The stable carbon and oxygen isotopic composition of the pedogenic carbonate extracted from the nodules described above can be found in Table 8.1. The $\delta^{13}C_{pc}$ values range from -8.07‰ to -11.79‰ (average -9.99‰). Standard deviations of between 0.01 and 0.07 indicate that these values would be replicable. Compared with the $\delta^{13}C_{pc}$ values extracted from carbonates through the Palaeozoic (Ekart et al. 1999), this is a typical range for $\delta^{13}C_{pc}$.

Using equation 10 and assuming carbonate precipitation occurred at 25°C, the average isotopic composition of soil CO_2 is estimated to be -18.8‰. This value is significantly more negative than the estimated value of atmospheric $\delta^{13}C$ for the earliest Devonian, -6‰. This proves that there must have been significant root respiration in the soils during the earliest Devonian, contributing isotopically lighter soil-respired CO_2 into the soils. There is no evidence however of any beta microfabrics present in the carbonate nodules, suggesting that the vegetation did not have a role in carbonate production, unlike in later calcic-palaeosols (Wright et al. 1995, Verrecchia et al. 1995).

The $\delta^{18}O_{pc}$ values range from -8.42‰ to -11.39‰ (average -9.93‰). A cross plot of $\delta^{13}C_{pc}$ and $\delta^{18}O_{pc}$ places these carbonates close to data from modern coastal soil carbonates (Cerling 1984) (Figure 8.5), despite no evidence of a marine influence on these palaeosols. This may be because $\delta^{18}O_{pc}$ values have been altered due to burial diagenesis (Cerling 1984). Oxygen

Table 8.1: Stable carbon and oxygen isotopic values extracted from pedogenic carbonate nodules from Tredomen Quarry core.

Sample	Depth m	$\delta^{13}C_{pc}$ (vs. PDB) ‰	St. dev.	$\delta^{18}O_{pc}$ (vs. PDB) ‰	St. dev.
1	2.40	-8.0736762	0.01	-11.3884638	0.02
4	18.95	-11.7940947	0.02	-8.4161020	0.04
8	40.10	-10.9306272	0.02	-10.7774540	0.04
9	48.40	-9.8438433	0.02	-9.5611139	0.07
12	58.70	-9.3131803	0.02	-9.4943827	0.04
	Average	**-9.99**	**0.02**	**-9.93**	**0.04**

Table 8.2: Stable carbon isotopic values extracted from fossilised organic matter from Tredomen Quarry

Sample	Run 1: $\delta^{13}C_{org}$ (vs. PDB) ‰	Run 2:$\delta^{13}C_{org}$ (vs. PDB) ‰	Mean: $\delta^{13}C_{org}$ (vs. PDB) ‰
Rhyniophytoid 1	-24.24	-24.12	-24.18
Rhyniophytoid 2		-24.98	-24.98
Average			**-24.58**
Charcoalified *Prototaxites* 1	-24.50	-24.60	-24.55
Charcoalified *Prototaxites* 2	-25.40	-25.60	-25.50
Average			**-25.03**
Non-charcoalified *Prototaxites*	-26.90	-26.80	-26.85
Average *Prototaxites*			**-25.63**
		Total average	**-25.21**

Figure 8.5

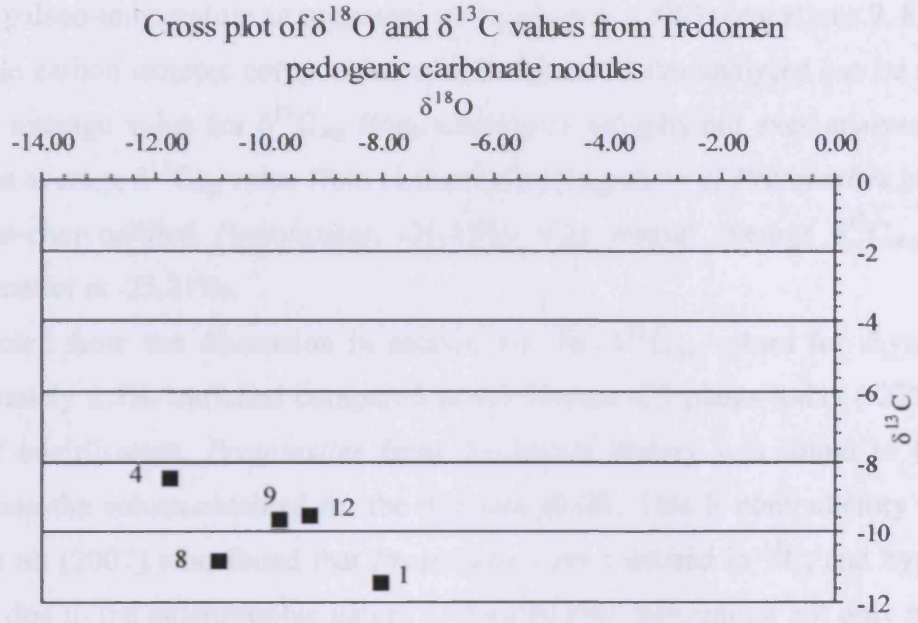

Figure 8.6

Cross plots of $\delta^{13}C$ and $\delta^{13}O$ values extracted from pedogenic carbonate nodules from across the Anglo-Welsh Basin, additional data from Eden (2007) and Jenkins (1998)

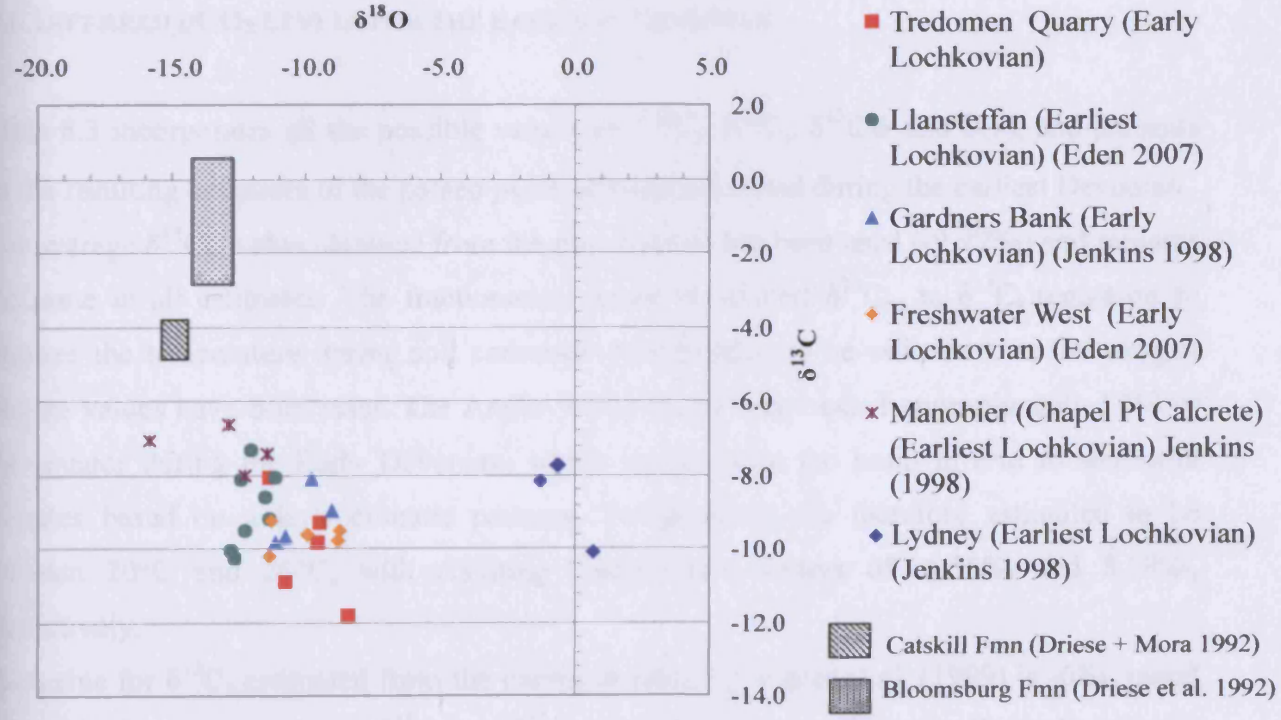

isotopes may become depleted by up to 10‰, especially from palaeosols of this age (Cerling 1991a, Driese et al. 2000, Quast et al. 2006). The $\delta^{18}O_{pc}$ values therefore cannot be used to estimate palaeo-temperature as suggested by Nordt et al. (2003) (equations 7, 8 and 9).

The stable carbon isotopic composition of the organic matter analysed can be found in Table 8.2. The average value for $\delta^{13}C_{org}$ from coalified rhyniophytoid axes analysed is -24.58‰, whilst the average $\delta^{13}C_{org}$ value from charcoalified fragments of *Prototaxites* is -25.03‰, and from non-charcoalified *Prototaxites*, -26.85‰. The overall average $\delta^{13}C_{org}$ value for all organic matter is -25.21‰.

As expected from the discussion in section 8.2, the $\delta^{13}C_{org}$ values for rhyniophytoids are approximately 2.5‰ enriched compared to the average C3 plants today (-27‰), likely as a result of coalification. *Prototaxites* from Tredomen Quarry was found to be isotopically lighter than the values obtained for the rhyniophytoids. This is contradictory to the work of Boyce et al. (2007) who found that *Prototaxites* was enriched in ^{13}C, and hypothesised that this was due to the heterotrophic nature of *Prototaxites*, consuming not only rhyniophytoids, but also microbial soil crusts and lichens, which are relatively isotopically heavy. The isotopically lighter values for *Prototaxites* could be explained by consuming rhyniophytoids and bryophytes, which have an isotopic value of around -29‰ (Jahren et al. 2003).

8.4: Inferred ρCO_2 levels for the earliest Devonian

Table 8.3 incorporates all the possible values for $\delta^{13}C_s$, $\delta^{13}C_a$, $\delta^{13}C\phi$ and S(z), and presents all the resulting estimates of the palaeo-ρCO_2 atmospheric level during the earliest Devonian. The average $\delta^{13}C_{pc}$ value obtained from the five nodules has been used (-9.99‰) and remains the same in all estimates. The fractionation factor to convert $\delta^{13}C_{pc}$ to $\delta^{13}C_s$ (equation 6) requires the temperature during soil carbonate precipitation to be estimated, as the oxygen isotope values have been reset. The Anglo-Welsh Basin was located approximately 17°S of the equator during the Early Devonian, which would place the basin in arid to semi-arid climates based on today's climatic patterns. Temperatures are therefore estimated to be between 20°C and 25°C, with resulting fractionation factors of -9.58‰ and 8.98‰, respectively.

The value for $\delta^{13}C_a$ estimated from the curves devised by Viezer et al. (1999) is -6‰, based on an 8‰ difference between $\delta^{13}C_a$ and $\delta^{13}C$ of shallow ocean carbonates. From the average

Table 8.3: All estimates of atmospheric ρCO_2 levels for the Late Silurian to Early Devonian.

	$\delta^{13}C_{cc}$ ‰	$\delta^{13}C_s$ ‰	$\delta^{13}C_\phi$ ‰	$\delta^{13}C_a$ ‰	S(z) (ppmV)	Ca (ρCO_2) (ppmV)	ρCO_2 / PAL
A	-9.99	-18.80	-25.21	-5.95	3000.00	495	1.65
	-9.99	-18.80	-25.21	-5.95	7000.00	1154	3.85
B	-9.99	-18.80	-25.21	-4.40	3000.00	442	1.47
	-9.99	-18.80	-25.21	-4.40	7000.00	1030	3.43
C	-9.99	-18.80	-24.58	-5.37	3000.00	332	1.11
	-9.99	-18.80	-24.58	-5.37	7000.00	775	2.58
D	-9.99	-18.80	-24.58	-4.40	3000.00	310	1.03
	-9.99	-18.80	-24.58	-4.40	7000.00	723	2.41
E	-9.99	-19.38	-25.21	-5.95	3000.00	343	1.14
	-9.99	-19.38	-25.21	-5.95	7000.00	800	2.67
F	-9.99	-19.38	-25.21	-4.40	3000.00	308	1.03
	-9.99	-19.38	-25.21	-4.40	7000.00	718	2.39
G	-9.99	-19.38	-24.58	-5.37	3000.00	194	0.65
	-9.99	-19.38	-24.58	-5.37	7000.00	452	1.51
H	-9.99	-19.38	-24.58	-4.40	3000.00	181	0.60
	-9.99	-19.38	-24.58	-4.40	7000.00	422	1.41

A: Temperature = 25°C. $\delta^{13}C\phi$ = average $\delta^{13}C_{org}$ value of all fossilised organic matter. $\delta^{13}C_a$ estimated from fossilised organic matter.

B: Temperature = 25°C. $\delta^{13}C\phi$ = average $\delta^{13}C_{org}$ value of all fossilised organic matter. $\delta^{13}C_a$ estimated from shallow ocean carbonates.

C: Temperature = 25°C. $\delta^{13}C\phi$ = average $\delta^{13}C_{org}$ value of fossilised rhyniophytoid organic matter. $\delta^{13}C_a$ estimated from fossilised organic matter.

D: Temperature = 25°C. $\delta^{13}C\phi$ = average $\delta^{13}C_{org}$ value of fossilised rhyniophytoid organic matter. $\delta^{13}C_a$ estimated from shallow ocean carbonates.

E: Temperature = 20°C. $\delta^{13}C\phi$ = average $\delta^{13}C_{org}$ value of all fossilised organic matter. $\delta^{13}C_a$ estimated from fossilised organic matter.

F: Temperature = 20°C. $\delta^{13}C\phi$ = average $\delta^{13}C_{org}$ value of all fossilised organic matter. $\delta^{13}C_a$ estimated from shallow ocean carbonates.

G: Temperature = 20°C. $\delta^{13}C\phi$ = average $\delta^{13}C_{org}$ value of fossilised rhyniophytoid organic matter. $\delta^{13}C_a$ estimated from fossilised organic matter.

H: Temperature of = 20°C. $\delta^{13}C\phi$ = average $\delta^{13}C_{org}$ value of fossilised rhyniophytoid organic matter. $\delta^{13}C_a$ estimated from shallow ocean carbonates.

PAL = 300ppmV (pre-industrial atmospheric levels).

$\delta^{13}C$ value of all fossilised organic matter (-25.21‰), $\delta^{13}C_a$ was also estimated to around -6‰, using the equation of Arens et al. 2000 (equation 11). Ekart et al. (1999) uses an estimated value of -6.3‰ for the Early Devonian. High-resolution studies of marine carbonates however have shown a positive excursion in $\delta^{13}C$ at the Silurian - Devonian boundary (Saltzman 2002 and Buggisch and Mann 2004), which would potentially mean an enriched $\delta^{13}C_a$ value of -4.4‰.

The value for $\delta^{13}C\phi$ can be estimated to be around -26‰ based on modern C3 plant values. Using the Arens et al. (2000) method (equation 11), $\delta^{13}C\phi$ is estimated as -25.27‰ based an atmospheric value of -6‰, and -23.51‰ based on an atmospheric value of -4.4‰. Excluding the latter, these estimates are supported by the values from fossilised organic matter that been found associated with these palaeosols, with an overall average of -25.21‰. The degree of enrichment of the organic matter by coalification is unknown, and therefore it must be assumed that fossilised organic matter represents that of the original.

A minimum value of 3000ppmV is used for S(z), estimated from modern soil profiles from semi-arid environments and those of low productivity. A maximum value of 7000ppmV for S(z) was chosen, to represent the periodic increases in rainfall and subsequent envisaged increases in productivity, as hypothesised from the sedimentological analysis and taphofacies model (see Chapters 6 and 7).

Including all estimates a large range of values for the ρCO_2 level during the earliest Devonian have been calculated, between **181 to 1154ppmV** (Table 8.3). Several estimates however, are less valid that others. The estimates that use a value of -4.4‰ for $\delta^{13}C_a$ may not be valid (estimates B, D, F and H), as the value for $\delta^{13}C_a$ calculated from organic matter are similar to those calculated indirectly from shallow marine carbonates (-5.95‰ and -5.37‰ compared to -6‰, respectively).

The use of $\delta^{13}C_{org}$ from fossilised rhyniophytoids alone may not be appropriate (estimates C and G), as there is evidence that Late Silurian to Early Devonian ecosystems were diverse, including fungal-like organisms, lichens, bryophytes and microbial soil crusts, each with different $\delta^{13}C_{org}$ values. The bulk $\delta^{13}C$ value of soil-respired CO_2 may therefore be significantly different than if soil-respired CO_2 was sourced from C3 plants alone. As *Prototaxites* more accurately reflects this diversity, it may be more appropriate to use the overall $\delta^{13}C_{org}$ values.

The variable between the remaining estimates A and E is the temperature used for the fractionation factor between $\delta^{13}C_{pc}$ to $\delta^{13}C_s$. Using 20°C, the ρCO_2 level is estimated to be

between 343 and 800ppmV, while using 25°C estimates 495 to 1154ppmV (Table 8.3). The lowest estimates using 20°C are similar to present atmospheric levels (assumed to be 365ppmV as used by Ekart et al. 1999). Present atmospheric levels are associated with icehouse conditions, similar to the late Visean to Permian (see Figure 8.1). As there is no evidence of ice present during the Early Devonian, it is more likely that estimation A provides the closest range for the ρCO_2 level during the Early Devonian (between **495 to 1154ppmV**).

Comparison with other data sets

Eden (MESci thesis, 2007) analysed pedogenic carbonates from the Chapel Point Calcrete, Pembrokeshire, which is the equivalent of the Bishop's Frome Limestone (Table 1.1, Chapter 1). Carbonate nodules were extracted from two localities: Llansteffan and Freshwater West (see Figure 1.3, Chapter 1). The results of the isotopic analysis are presented in Table 8.4. Compared to the values obtained from Tredomen Quarry, the average values of $\delta^{13}C_{pc}$ for both Llansteffan and Freshwater West are slightly enriched (-8.89‰ and -9.68‰. respectively) (Figure 8.6). In terms of $\delta^{18}O_{pc}$, values from Llansteffan and Freshwater West are slightly depleted compared to those from Tredomen Quarry (-12.05‰ and -10.06‰, respectively). Assuming that all the other parameters are the same, substituting the $\delta^{13}C_{pc}$ value of estimation A to those from Llansteffan and Freshwater West result in a range of ρCO_2 levels between **818 to 1910ppmV** and **580 to 1354ppmV**, respectively.

Jenkins (1998) analysed pedogenic carbonates from a number of different localities across the Anglo-Welsh Basin, the results of which are shown in Table 8.5. The values of $\delta^{13}C_{pc}$ taken from pedogenic carbonates of the Chapel Point Calcrete at Manorbier, Pembrokeshire are slightly enriched compared to the results of Eden (2007) and this study, with an average of -7.29‰, while values of $\delta^{18}O_{pc}$ are slightly depleted (average of -13.13‰). The results from Gardners Bank, from lower Lochkovian strata from Shropshire have similar values to the carbonates from Tredomen Quarry (this study) and Freshwater West (Eden 2007), with an average $\delta^{13}C_{pc}$ value of -9.16‰ and an average $\delta^{18}O_{pc}$ value of -10.22‰ (Figure 8.6). The values of taken from Lydney, Gloucestershire, are significantly different compared to those from the other Anglo-Welsh Basin localities, with very enriched $\delta^{18}O_{pc}$ values (average -0.47‰) and slightly enriched $\delta^{13}C_{pc}$ values (average -8.46‰). The significant difference stable oxygen isotopic values may be a result of dolomitisation that was observed within these nodules, which may be evidence of a marine influence (Jenkins 1998).

Table 8.4: Stable carbon and oxygen isotopic values extracted from pedogenic carbonate nodules from Llansteffan and Freshwater West, collated by Eden (2007)

Locality	Sample	$\delta^{13}C_{pc}$ (vs. PDB) ‰	$\delta^{18}O_{pc}$ (vs. PDB) ‰
Llansteffan	1a	-7.33	-12.03
	1b	-8.08	-11.18
	1c	-8.15	-12.42
	2b	-9.18	-11.39
	2c	-8.59	-11.53
	3	-10.06	-12.85
	4a	-9.50	-12.32
	4bLL	-10.26	-12.69
AVERAGE		**-8.89**	**-12.05**
Freshwater West	F3A2	-9.52	-8.73
	F3B	-9.23	-11.33
	F3C1	-9.80	-8.85
	F3C2	-10.22	-11.40
	F3D	-9.63	-9.98
AVERAGE		**-9.68**	**-10.06**

Table 8.5: Stable carbon and oxygen isotopic values extracted from pedogenic carbonate nodules from Lydney, Manobier and Gardners Bank, collated by Jenkins (1998)

Locality	Sample	$\delta^{13}C_{pc}$ (vs. PDB) ‰	$\delta^{18}O_{pc}$ (vs. PDB) ‰
Lydney	P3	-8.20	-1.26
	P3	-7.78	-0.62
	P4	-10.10	0.68
	P4	-7.75	-0.67
AVERAGE		**-8.46**	**-0.47**
Manobier (Chapel Point Calcrete)	MB 8 (1)	-7.04	-15.86
	MB 8 (2)	-6.65	-12.93
	MB 8 (3)	-7.45	-11.45
	MB 8 (4)	-8.01	-12.28
AVERAGE		**-7.29**	**-13.13**
Gardners Bank	GB1	-9.83	-11.17
	GB2	-9.68	-10.79
	GB3	-8.98	-9.08
	GB4	-8.15	-9.83
AVERAGE		**-9.16**	**-10.22**

Quast et al. (2006) studied carbonate nodules from three Anglo-Welsh Basin localities from the latest Přídolí (Ffairfach, Carmarthenshire) and earliest Lochkovian (Lydney, Gloucestershire and Llansteffan, Pembrokeshire), and reported a large variation in stable carbon and oxygen isotopic values of the extracted pedogenic carbonates. They hypothesised that contemporaneous localities across the Anglo-Welsh Basin should have similar isotopic values, and the variation seen was attributed to secondary alteration of the pedogenic carbonate nodules either by groundwater or burial diagenesis, confirmed by recrystallisation in thin sections. Therefore, Quast et al. (2006) deemed the nodules of the Anglo-Welsh Basin as un-usable for soil carbonate ρCO_2 palaeo-barometer calculations. Figure 8.6 does show that there is slightly variation in the values between Anglo-Welsh Basin localities, particularly between Pembrokeshire and those of the Welsh Borderland. Values of $\delta^{18}O_{pc}$ from Manorbier and Llansteffan are slightly depleted compared to those from Tredomen Quarry and Gardners Bank, while $\delta^{13}C_{pc}$ values from Manorbier and Llansteffan are slightly enriched compared to Tredomen Quarry. This may be due to variable burial depth across the Anglo-Welsh Basin, estimated to be around 2km in the east, up to 6km in the west (Parker et al. 1983, Soper and Woodcook 2003). However, as discussed throughout this chapter, soil CO_2 does not only vary with atmospheric CO_2, but also with the contribution of soil-respired CO_2, which is likely to be different between localities. Additionally, the pedogenic carbonates used in this study were carefully selected, with no textural evidence of any recrystallisation. The only significantly different stable values were those taken from Lydney, and can be attributed to dolomitisation.

The ρCO_2 level for the Early Devonian from the GEOCARBSULF curve (Berner 2006) is estimated to be around 3000ppmV, ten times pre-industrial atmospheric level (300ppmV) (Figure 8.7). Estimates from the palaeosol record for the Late Silurian through to the Carboniferous are mostly provided by Driese and Mora (Driese et al. 1992, 2000, Mora et al. 1996, and references within), from pedogenic carbonates from similar deposits to the Old Red Sandstone: the Upper Silurian Bloomsburg Formation and the Upper Devonian Catskill Formation, both outcropping in north-west U.S.A. The estimates of Mora et al. (1996) are in reasonable correlation with GEOCARBSULF curve (Figure 8.7).

The estimates from the Anglo-Welsh Basin pedogenic carbonates are considerably lower than the estimates of the GEOCARBSULF and the palaeosol record from the Bloomsburg and Catskill Formations, the maximum estimation being only ~5 x PAL (Figure 8.7). This may be due to the unsuitability of the pedogenic carbonates from the Anglo-Welsh Basin for isotopic analysis (Quast et al. 2006), including resetting of the isotopic values due to recrystallisation.

Figure 8.7: Predictions of atmospheric ρCO_2 levels of the Palaeozoic, estimated from geochemical model, GEOCARBSULF, and the palaeosol record from this study and Mora et al. (1996).

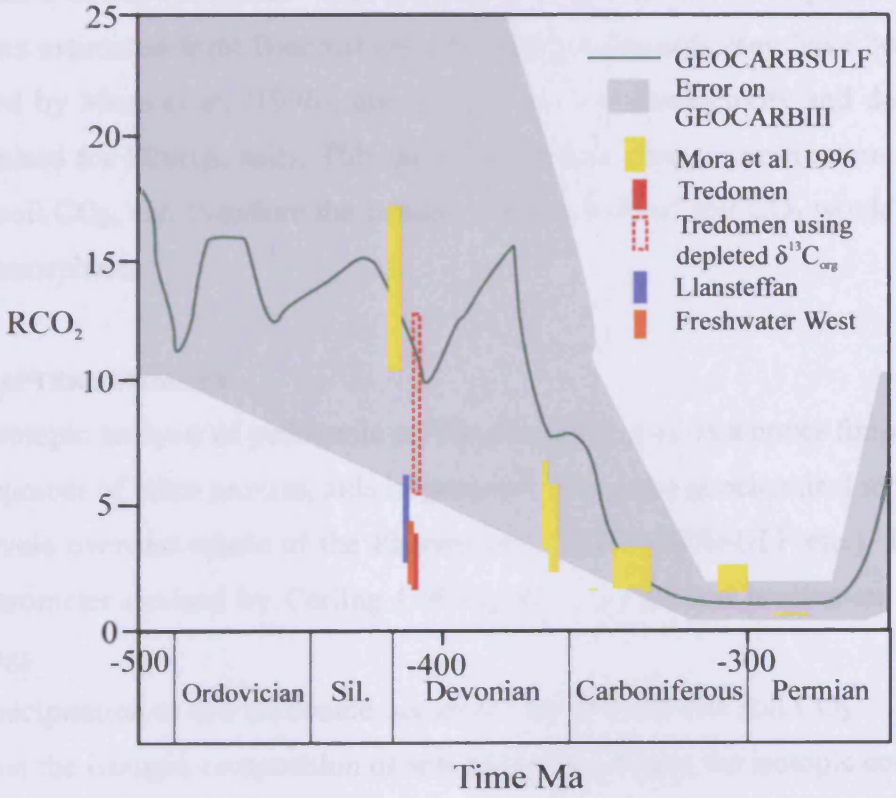

It may also be due to the ~3‰ enrichment of fossilised organic matter during coalification (see page 8-15). If the value of the overall fossilised matter (-25.51‰) is replaced by a depleted value of -28.51‰, estimated values of ρCO_2 levels range from 1654 to 3860ppmV, which has a better correlation with the GEOCARBSULF curve (Figure 8.7). Alternatively, the values estimated from Bloomsburg Formation palaeosols may have been overestimated, suggested by Mora et al. (1996), due to the very low productivity and depth of production hypothesised for Silurian soils. This would result in a greater contribution from atmospheric CO_2 to soil CO_2, and therefore the isotopic composition of soil CO_2 would be similar to that of the atmosphere.

8.5: CHAPTER SUMMARY

Stable isotopic analysis of pedogenic carbonate can be used as a proxy for ρCO_2 levels, which with a number of other proxies, aids in ground-truthing the geochemical models that estimate ρCO_2 levels over the whole of the Phanerozoic (GEOCARBSULF etc.). The soil carbonate ρCO_2 barometer devised by Cerling (1991a) relies on several parameters and assumptions, including;

a) precipitation of soil carbonate occurs in equilibrium with soil CO_2.
b) that the isotopic composition of soil carbonate reflects the isotopic composition of soil CO_2.
c) the pedogenic carbonate sampled was precipitated at a depth of at least 30cm from the soil-air interface, where S(z) remains constant.
d) the pedogenic carbonate sampled was precipitated in subaerial, aerobic conditions, is composed of primary micrite, with no overprinting or recrystallisation.
e) when calculating estimates for the parameter $\delta^{13}C_a$, an assumption of a difference of -8‰ between $\delta^{13}C_{oc}$ and $\delta^{13}C_a$.
f) where fossilised organic matter has not been preserved, an assumption is made that pre-Miocene ecosystems were dominated by C3 plants, with an isotopic value of -26‰, and that this value remains the same through the rest of the Phanerozoic. Alternatively, a difference of -18‰ is assumed from $\delta^{13}C_{oc}$.
g) where fossilised organic matter has been preserved, it is assumed that $\delta^{13}C_{org}$ reflects $\delta^{13}C_s$, and has not been altered by fossilisation.
h) the chemical components that make up modern plant tissue are the same as in the Late Silurian to Early Devonian and that carbon fractionation was via the C3 pathway.

i) the fossilised vegetation preserved with the channel deposits represent the types of vegetation growing on the floodplain at the time of carbonate precipitation

j) soils in semi-arid to arid environments with low productivity have a S(z) value of around 3000ppmV, whilst soils from well-drained temperate climates have S(z) values between 5000 to 10,000ppmV.

The most appropriate estimate for the atmospheric ρCO_2 levels for the earliest Devonian, estimated from Tredomen Quarry palaeosols, range between 495 to 1154ppmV, or 1.65 to 3.85 times pre-industrial atmospheric level. Similar estimation have been made from Llansteffan (818 to 1910ppmV) and Freshwater West (580 to 1354ppmV). These estimates are lower than expected for the earliest Devonian compared with the geochemical model, GEOCARBSULF, which estimates ρCO_2 levels up to 10 times pre-industrial atmospheric level. Mora et al. (1996) estimated ρCO_2 atmospheric levels of 3200 to 5200ppmV (10.6 to 17.3 times pre-industrial atmospheric level), from palaeosols from the latest Silurian Bloomsburg Formation. This difference may be due to the unsuitability of the pedogenic carbonates from the Anglo-Welsh Basin, as a result of alteration during burial diagenesis, although there is no textural evidence from the nodules sampled to support this. Alternatively, as the value of $\delta^{13}C_{org}$ is an important variable for the soil carbonate ρCO_2 barometer, the assumption that the isotopic composition of fossilised organic matter reflects that of the original tissue, may not be suitable. Adjusting fossilised organic matter values by 3‰ does result in ρCO_2 estimates that are closer to the GEOCARBSULF estimates, however, as the true value of enrichment is unknown, this method cannot be considered valid.

Alternatively, the GEOCARBSULF model and estimates of the Late Silurian ρCO_2 may have been overestimated, as Silurian soils have very low, shallow production rates, and the contribution of atmospheric CO_2 to the soil CO_2 would have been much higher than during the Devonian onwards.

There is also an assumption than all vegetation used C3 metabolic pathways, but evidence from the isotopic composition of rhyniophytoids and fungal-like organism *Prototaxites* suggests that Early Devonian ecosystems were in fact diverse, each component potentially fractionating CO_2 to different degrees, possibly as a result of different metabolic pathways to those known from extant plants. The carbon isotopic value from *Prototaxites* was isotopically lighter than values from rhyniophytoids. This suggests that *Prototaxites* from this locality were consuming rhyniophytoids and bryophytes.

CHAPTER 9 : RECONSTRUCTING LOWER DEVONIAN VEGETATION AND HABITATS FROM OLD RED SANDSTONE STRATA FROM THE ANGLO-WELSH BASIN

There were five main objectives for investigation in this thesis, the final being a synthesis of all palaeobotanical, palynological and geochemical data with the envisaged taphonomic and geomorphic models, in an attempt to understand the habitats and possible palaeo-ecosystems of early land plants during the Lower Devonian.

The megafossils and dispersed spore assemblages from Tredomen Quarry have been useful in confirming that during the lower Lochkovian, embryophyte diversity within the Anglo-Welsh Basin (and possibly the southern margins of the Old Red Sandstone Continent, Laurussia), was limited to the rhyniophytes and rhyniophytoids, compared to other global assemblages (see discussions in Chapters 3 and 5). The megafossils from Tredomen Quarry have also been used in a comparison between lower Přídolí and lower Lochkovian rhyniophyte and rhyniophytoid specimens from across the Anglo-Welsh Basin. A general trend towards larger, more vertically-elongate sporangia, predetermined dehiscence mechanisms, and anisomously and pseudomonopodially branched axes, has been recognised, and interpreted as adaptations for increased spore production (per sporangia and per plant) and spore dispersal effectiveness (see Chapter 3 discussion). An increase in the diversity of sporomorphs with sculptured exoexine, in particular cryptospores, has been identified between uppermost Přídolí and lower Lochkovian spore assemblages from Tredomen Quarry (see Chapter 5), first recognised in contemporaneous assemblages across the Anglo-Welsh Basin by Richardson (1996a, 1996b), and has been hypothesised as adaptation for enhancing spore dispersal and germination (see Chapter 5). These adaptations in the early embroyphytes and sporomorphs may indicate an increase in competition during the early Lochkovian.

The highly branched mesofossils from Tredomen Quarry are thought to be synonymous to the well-presented charcoalified minute sporangia and axes from the lower Přídolí to the middle Lochkovian, and have been key to interpretations of affinity. This group has been interpreted as stem-group early embryophytes with complexly branched axes, but with bryophytic characters, including *in situ* cryptospores (see Chapter 3 for discussion). This group may have evolved from gametophyte-dependant unbranching bryophytes (the presence of which has been inferred back to the Llanvirn, based on permanent cryptospores in the

dispersed spore record), and through sequential acquisition of characters, evolved into stem-group embryophytes, ancestral to the rhyniophytoids and rhyniophytes.

Although enigmatic, the non-embryophytes represent the largest biomass at Tredomen Quarry. As phytoterrestisation by the vascular plants was a key event in Earth's history, studies on Lower Devonian palaeobotany have mainly focussed on the embryophytes, but perhaps negating the importance of the non-embryophytes in Silurian and Early Devonian landscapes, palaeoecology and the carbon cycle. Representatives of fungi (*Prototaxites*), algae (*Pachytheca*) and cyanobacterial biofilms (inferred from limonite-coating around megafossil specimens) were found at Tredomen Quarry, indicating that the rhyniophytoids, despite their importance for vascular land plant evolution, were likely to have been a small component of lower Lochkovian palaeo-ecosystems.

Despite the useful applications of the Tredomen Quarry plant fossil and dispersed spore assemblages in understanding the diversity, disparity and affinity of Anglo-Welsh Basin terrestrial vegetation, due to the allochthonous nature of the plant assemblages (see Chapter 7) there is little direct evidence to make any conclusions regarding Lower Devonian palaeoecology. Therefore this synthesis will focus on:

1) evidence for a shift in early land plants habitats (inferred from geomorphic models based on sedimentological analysis) across the Downtonian-Dittonian boundary, and the possible causes for this shift.
2) the use of palynofacies in determining broad, basin-wide habitats.
3) the taphonomic constraints on palaeoecological studies of Lower Devonian vegetation.
4) evidence for seasonal control on vegetative growth, based on sedimentological and taphonomic analysis.
5) indirect evidence for significant phytoterrestrialisation and associated soil productivity from Lower Devonian palaeosols, and the implications on levels of atmospheric ρCO_2 levels.

9.1: Early land plant habitats and possible causes for a change at the Downtonian (Přídolí)-Dittonian (Lochkovian) boundary

The habitats colonised by Lower Devonian vegetation can be inferred from the geomorphic models envisaged for the uppermost Silurian and lower Lochkovian via sedimentological analysis (see Chapter 6). Tredomen Quarry core was split into upper and lower sequences,

based on a shift in sedimentology, roughly marked by two, closely-spaced calcrete (C) horizons of a stage III palaeo-calcic-Vertisols, which have been correlated with the regionally significant Bishop's Frome Limestone. The lower sequence therefore was correlated with the Raglan Mudstone Formation, and a two-stage ephemeral mud-dominated dryland river system was envisaged (see Chapter 6, Figure 6.10). The upper sequences of Tredomen Quarry core, and outcrops from Targrove Quarry, were correlated with the St. Maughans Formation, and a two-stage sand-dominated river system has been envisaged (see Chapter 6, Figure 6.11).

The geomorphic models envisaged for the Raglan Mudstone Formation (Figure 6.10) and the St. Maughans Formation (Figure 6.11) suggest that there was a shift in fluvial style and potential habitats across the Downtonian-Dittonian boundary, separated by very well-developed calcrete horizons that represent a significant period of pedogensis, and little or no deposition. In this scenario, the river system shifted from an ephemeral mud-dominated dryland system, with ephemeral channels, waterholes and crevasse splays, and associated calcic-Aridisols, to a two-stage system with the same ephemeral channels and floodplain elements, but punctuated with regular appearances of sandier, possibly perennial channels and associated calcic-Vertisols. Vegetation that may have previously been surviving only around ephemeral waterholes were able to spread into the new habitats associated with the perennial rivers (e.g. along river banks and crevasse splay channels).

Alternatively, a third geomorphic model has been envisaged, where all channel and floodplain associations from both models are coeval, but operating at different magnitude of scale (see Chapter 6, Figure 6.12). This model envisages that ephemeral channel and floodplain lithofacies described from the lower Tredomen Quarry core represent small, muddy, interfluvial channels on the floodplain that operated both during local rainfall events and high velocity flood events. These interfluvial channels were superimposed on a larger 'trunk' stream river system, represented by the larger, sand-dominated, possibly perennial channels and associated palaeo-calcic-Vertisols seen in the upper Tredomen Quarry core. These channels operated only during periods of extensive, basin-wide flood events. In this scenario, rather than a shift in fluvial style, remnant 'trunk' channels were 'switched on' during the lowermost Dittonian.

The appearance of sand-dominated channels during the lowermost Dittonian, providing potential habitats for early land vegetation, may be explained by two main causes that are applicable to both scenarios: tectonic activity and climate change.

Tectonic activity

Major regional tectonic activity could explain the abrupt basin-wide appearance of coarser-grained lithofacies in the lowermost Dittonian. Using palaeo-current directions and sedimentary petrology, it has been modelled that during the upper Downtonian the Anglo-Welsh Basin rivers were large, south-easterly flowing dispersal systems, sourced from the newly-formed Caledonides, located northwest of the basin (Simon and Bluck 1982, Allen and Crowley 1983). Sedimentary strata from the Downtonian Anglo-Welsh Basin were found to contain metamorphic and heavy minerals, which were linked back to the metamorphic terranes of the Caledonides (Allen 1974b, Allen and Crowley 1983). They found that lower Dittonian strata contained less metamorphic and heavy minerals, and more volcanic-derived and exotic sedimentary clasts. This change in petrology and increase in grain size suggested a change in provenance, and Allen and Crowley (1983) suggested that uplift and erosion of the Irish Sea High around the Downtonian-Dittonian boundary provided a closer source area for the Anglo-Welsh Basin. Crowley et al. (2009) hypothesised that the change in sediment supply was due to a change in regional basin tectonics, shifting from a post-Iapetus foreland basin to the development of transtensional basins on the Avalonian margin.

Major regional tectonic activity that may have caused the uplift of the Irish Sea High could be associated with the numerous Downtonian basin-wide volcanic ash-fall tuff beds, in particular the Townsend Tuff Bed (Allen and Williams 1981). This thick, cumulative bed of volcanic ash-fall deposits occurs approximately 100m below the Bishop's Frome Limestone (Downtonian-Dittonian boundary) and represents a large, but distant Plinian-style eruption (Allen and Williams 1981, 1982). This volcanism may have been associated with major tectonic activity outside the Anglo-Welsh Basin. The Bishop's Frome Limestone that occurs above the Townsend Tuff Bed, at the top of the Downtonian, represents a period tectonic quiescence, with little or no deposition and extensive pedogensis. This may represent a pause in tectonic activity, resulting in basin-wide shut down and sediment starvation, which was reactivated at the beginning of the Dittonian.

The shift in fluvial style or reactivation of 'trunk' channels at the Downtonian-Dittonian boundary may also be explained by local tectonic faulting, resulting in uplift, subsidence, changes to incision rates and accommodation space. Owen and Hawley (2000) studied middle Lochkovian strata from Pantymaes Quarry, near Sennibridge, central South Wales, and hypothesised that the variable architecture of the sandstone associations (interpreted as a high-sinuosity, braided sand-dominated system) could be explained by episodic displacement of the Carreg Cennen Disturbance, approximately 2km north of the Pantymaes Quarry, and

part of the Church Stretton Lineament of the Welsh Borderland Fault System, that was active during the Early Devonian (Weaver 1976, Woodcock 1988) (Figure 1.2, Chapter 1). The mudstone association at Pantymaes Quarry, interpreted as a low-sinuosity meandering system, represents stability and quiescence of the Carreg Cennen / Llandyfaelog Disturbance. Tredomen Quarry lies approximately 3km south of the Swansea Valley Disturbance, also part of the Church Stretton Lineament. Movement of this local fault system may have caused increased incision rates, increased accommodation space, and the uplift and erosion of the hanging wall, causing the activation of the sand-dominated, possibly perennial river systems. Williams and Hillier (2004) also suggested local fault systems as a possible control on sedimentation. They hypothesised that sandstone architecture of the Downtonian Moor Cliff Formation and lower Dittonian Conigar Pit Sandstone Member (of the Freshwater West Formation) from Pembrokeshire, may have been controlled by the local Benton Fault.

Climate change

The presence of palaeo-Vertisols within Anglo-Welsh Basin floodplain lithofacies has long been used as an indicator that the climate of the Lower Old Red Sandstone was semi-arid, overall moisture deficient, but with strong, distinctive seasons (Allen 1974a, Allen and Williams 1979, Marriott and Wright 1993). Together with the appearance of perennial channel sandstone complexes, the shift from predominately palaeo-calcic-Aridisols to predominately palaeo-calcic-Vertisols suggests a shift to an overall wetter climate, with stronger seasonality, at the beginning of the Dittonian. Stronger, longer wet seasons could have produced prolonged high-velocity discharge events, and activated perennial, sand-dominated channels. Floodplain mudstones were subjected to regular and stronger seasonal wetting and drying, causing palaeo-calcic-Vertisol development.

A local climatic effect as a result of local or regional tectonism provides one explanation for the shift to a wetter climate at the beginning of the Dittonian. Uplift of areas such as the Irish Sea High may have altered airflow patterns to produce an overall wetter climate. The uplift of the source area may have caused orographically-induced precipitation in the headwaters, resulting in erosion and high discharge events further downstream, producing sand-dominated perennial channels. However these tectonically-driven local climatic effects cannot explain the increased Vertisol development of the floodplains in the internal parts of the basin. Precipitation may have occurred only in the proximal areas of the basin, close to the uplifted sediment source areas. Uplifted areas may also have caused a rain shadow effect, causing a drier climate in internal parts of the basin. It is more likely that if the shift in fluvial

style or reactivation of 'trunk' channels was caused by climate change, it would have been basin-wide.

The upper sequences of Tredomen Quarry core were found to be cyclic (see Chapter 6), with regular episodes of reduced, sand-dominated perennial channels. This suggests that the climatic control on sedimentation may also have been cyclic. One possible control on discharge might have been a tropical monsoon. A monsoonal semi-arid climate has also been suggests as a source of punctuated perennial flow that deposited the sandstone complexes of the Conigar Pit Sandstone Member (Hillier et al. 2007).

A modern analogue could be the North Australian monsoon, which passes over the Great Dividing Range, and controls discharge to Lake Eyre Basin (Rust 1981, Maroulis et al. 2007) (see Appendix IX). Although there are uncertainties over the controls on the North Australian monsoon, it is thought to be driven by the larger Asian monsoon, itself strengthened by Northern Hemisphere insolation minima, and therefore controlled by Milankovitch cycles (Magee et al. 2004). By combining stratigraphy, sedimentology and chronology, workers of the Lake Eyre Basin recognised distinctive wet and dry phases that were correlated between eolian, alluvial and lacustrine deposits (for details see Gardner et al. 1987, Nanson et al. 1992, Magee et al. 1995, Croke et al. 1999, Magee et al. 2004, Maroulis et al. 2007). These wet and dry phases have been correlated to Late Quaternary glacial and inter-glacial oscillations, with the largest wet phase linked to last interglacial (marine oxygen isotope stages 5, around 110ka) (Nanson et al. 1992, Croke et al. 1999, Magee et al. 2004). However, the intensity of the wet phases was controlled by monsoonal intensity. Peak strength of the North Australian monsoon has been correlated with the wet phase of the last interglacial (Croke et al. 1999, Magee et al. 2004), and the deposition of a significant sand sheet across the Channel Country that lies beneath thin muddy lithofacies of the modern Channel Country. Evidence suggests that from ~110ka onwards the monsoon weakened, with a sub-pluvial event at marine oxygen isotope event 3 (~50-30ka) (Nanson et al. 1992) controlled by a moderately effective monsoon, and the low monsoonal intensities of the Holocene.

A similar scenario could be hypothesised for the Anglo-Welsh Basin. An overall increase in monsoonal strength across the Downtonian-Dittonian boundary could explain stronger seasonality in the lower Dittonian, inferred from the increase in palaeo-calcic-Vertisol development and appearance of sand-dominated channels.

9.2: EVIDENCE OF BROAD, BASIN-WIDE HABITATS USING PALYNOFACIES

Like the megafossil record, the dispersed spore record is allochthonous in nature, with palynomorphs transported by wind or water into river systems, and deposited some distance from their original habitat. The dispersed spore record therefore cannot be used in the recognition of local palaeoecological patterns i.e. differences between plant assemblages from different elements of the river system, such as the river banks and floodplains. However, broad palynofacies, created by the combination of basin-wide distribution patterns and relative abundances of palynomorphs with sedimentological analysis, might give clues to the broad distribution patterns of the parent plants and habitats across the Anglo-Welsh Basin (Richardson 2007, see Chapter 5).

Richardson (2007) hypothesised that the relative abundances of certain spore morphotypes reflect broad environmental settings: sculptured cryptospores and reworked sporomorphs are common within strata interpreted as the proximal alluvial plain (e.g. upper Dittonian of the Clee Hills); sculptured and laevigate triletes are common within strata interpreted as the medial alluvial plain (e.g. upper Downtonian and lower Dittonian of the M.50 section); while laevigate cryptospores and laevigate triletes are common in strata interpreted as the distal, marginal marine, alluvial plain (e.g. lower Dittonian of Ammons Hill) (see Richardson 2007, Chapter 5, particularly Figures 5.6 to 5.8). Therefore, the assemblages from Tredomen Quarry suggest a medial alluvial plain setting during the lower Lochkovian, with a high proportion of sculptured cryptospores transported from further upstream, but also the presence of laevigate and sculptured triletes and laevigate cryptospores.

This hypothesis suggests that the sculptured-cryptospore-producers (possibly including the stem-group embryophytes with bryophytic characters, Chapter 3) predominately inhabited upstream, proximal alluvial plain habitats, and may have been capable of surviving drier interfluvial areas, possibly finding refuge around ephemeral waterholes or waterlogged areas of the floodplain, a hypothesis first suggested by Richardson (1996a) and Edwards and Richardson (2004). The trilete-producers, the vascular plants, were more common downstream, across medial and distal alluvial plain habitats, along the riverbanks of broad channel belts. The laevigate-cryptospore-producers (possibly with bryophytic physiology) were more common across distal, possibly estuarine, alluvial plain habitats.

The increase in sculptured cryptospore abundance and diversity recognised within the Tredomen Quarry assemblages between the lowermost Dittonian and lower Dittonian therefore may not be a record of the diversification of the sculptured-cryptospore-producers

as suggested in Chapter 5, but due to the overall regression that was occurring across the Anglo-Welsh Basin throughout the Late Silurian and Devonian (see Chapter 1). This regression shifted these broad habitats further east, and Tredomen Quarry may have shifted closer to a proximal alluvial plain setting, and hence recorded more sculptured cryptospores.

9.3: Taphonomic constraints on palaeoecological studies of Lower Devonian vegetation.

Fossil shape distortion by taphonomy

Although there are rare exceptions, the early land plant fossils from Tredomen Quarry are typical of the type of preservation from Old Red Sandstone basins; fragmentary coalified compressions with little or no anatomical detail, found within reduced fluvial lithofacies that are allochthonous in nature (see Chapter 7).

The identification of many early land plants is often made from sporangial morphology alone (see Chapters 3 and 4). From the geometric morphometric analysis conducted on the rhyniophytoid sporangia from Tredomen Quarry (see Chapter 4), it was discovered that one of the main controls on shape variance between specimens was asymmetry, in some cases causing over half of the variance (see Tables 4.1 and 4.2, Chapter 4). This is likely to be a result of post-burial taphonomic processes, rather than biological, and therefore could seriously hamper diversity studies. Care therefore must be taken to evaluate the degree of shape distortion as a result of taphonomy when identifying by sporangial morphology alone.

It must also be noted that most of these coalified compression fossils occur slightly oblique to the fractured plane in which they are viewed, and are therefore partially buried beneath thin layers of rock. This can alter the perceived sporangial morphology, and care must be taken during preparation in removing the grains or rock flakes to reveal the whole specimen.

Pre-burial plant tissue composition

One of the main controls on preservation is the pre-burial histological composition of the vegetative material. The original composition of plant tissue determined preservation potential of that group, with a bias towards the preservation of early vascular plants, with axes strengthened by lignin, a recalcitrant biopolymer (Edwards 2003). Despite evidence from the dispersed spore record for wide-spread and abundant cryptospores, body-fossil evidence of cryptospore-producers is limited, suggesting that this group had low preservation potential, possibly due to lack of recalcitrant tissues. The only evidence of *in situ*

cryptospores comes from the mesofossil group, interpreted as stem-group embryophytes with bryophytic characters (see above and Chapter 3). The very-well-preserved spore-containing mesofossils from Přídolí and middle Lochkovian localities have only been preserved due to charcoalifcation by low-temperature smouldering wildfires, possibly ignited by lightning (Edwards 2000, Edwards and Axe 2004, Glasspool et al. 2004, 2006). Charcoalification increased the preservation potential of these plants, either as a result of cell homogenisation, or by the elimination via wildfires of bacteria and fauna responsible for the decay of vegetation. The charcoalification process was therefore able to 'capture' the diversity of vegetation that ordinarily would not have been preserved.

There are a few exceptions where material has been very well preserved due to mineralisation processes. Pyritisation has been important for understanding tracheid construction of early land plants (e.g. *Gosslingia breconsensis*, Kenrick and Edwards 1998, and *Sennicaulis hippocrepiformis,* Edwards 1981, Kenrick et al. 1991). The precipitation of pyrite within plant material is thought to take place within microbial-driven anoxic waters and subsurface sediments (Rickard and Luther 1997, Grimes et al. 2001, 2002, Brock et al. 2006). Precipitation occurred within and around cell walls, particularly within the xylem and other plant components susceptible to microbial degradation (Kenrick and Edwards 1998). Pyritisation prevented the further decay of organic material, and compression during burial, resulting in well-preserved three-dimensional fossils.

Only traces of pyrite precipitation remain in the early embryophyte specimens from Tredomen Quarry, now converted to limonite cubes (see Chapter 3). This suggests that the specific conditions required for pyrite precipitation were not met in this system; in particular stagnant waterbodies may not have been sufficiently anoxic due to their ephemeral nature. However, some evidence of microbial activity is present, in the form of fine-grained limonite coating and iron-oxide haloes around coalified specimens. The limonite coatings are similar to the iron-rich mineral encrustations described by Spicer (1977) and Dunn et al. (1997) under experimental conditions involving modern leaves submerged in water and decayed by microbial action.

Stratinomic partitioning and preservation potential of taphofacies

A major taphonomic control on plant preservation and constraint on Lower Devonian plant palaeo-ecological studies is the stratinomic partitioning of vegetation prior to burial, as a result of fluvial hydrological sorting. As described in Chapter 7, several taphofacies have been identified, including well-preserved rhyniophytoids and the stem-group embryophytes

found within trough-cross-bedded, fine-grained sandstones and wavy to planar-laminated siltstones, interpreted as minor channels, upper bars, and crevasse splay deposits. By comparison, charcoalified fragments of *Prototaxites* / *Nematasketum* were preserved within conglomerate basal lags of major channels or crevasse splay deposits.

To determine if certain lithofacies (and the plant assemblages preserved within) are more commonly preserved than others, the relative proportions of each Old Red Sandstone lithofacies have been calculated from different Lochkovian localities across the Anglo-Welsh Basin (Figure 9.1). Percentages have been calculated for each lithofacies by the proportion of total lithofacies bed thickness against total log thickness. Logs from this thesis have been used for Tredomen and Targrove Quarries, whilst published data have been used for the Ditton Formation from the Clee Hills (Allen 1974b), the St. Maughans Formation from Ammons Hill (Barclay et al. 1994) and the M.50 section, Herefordshire (Allen and Dineley 1976) and the Conigar Pit Sandstone Member of the Freshwater West Formation, from Freshwater West (Hillier et al. 2007). Lithofacies that contain plant material have been highlighted from each plot in Figure 9.1, and are marked with an asterisk (*) in the key, with two asterisks (**) for well-preserved plant material.

It is clear from all localities that lithofacies containing plant material are significantly less common than those without. Plant material is restricted to lithofacies interpreted as perennial deposits: major and minor channels, bars, crevasse splays and proximal floodplain (Figures 9.1*a-f*). Very well-preserved plant fossils are restricted to lithofacies deposited by moderate-velocity perennial flow (upper bars, minor channels, upper crevasse splays and the proximal floodplain) (Figures 9.1*a* and *b*).

In contrast, high-velocity ephemeral and perennial deposits that do not contain plant material are common (basal channel and crevasse splay deposits) (Figures 9.1*a-f*). Floodplain mudstones (including pedified and non-pedified) are also a commonly preserved lithofacies.

This suggests that the preservational potential of channel elements containing well-preserved plant fossils is low. This might be because these elements were deposited during the waning of the wet season and onset of the dry season, including perennial channel bars, minor channels, proximal floodplains, ephemeral waterholes and upper crevasse splay deposits (see Figure 7.1, Chapter 7). Although these elements remained through the dry season, they were likely to have been eroded away with the high-velocity events at the start of the next wet season. Therefore the preservation of plant assemblages not only depends on the preservation of the plant material itself, but also on the preservation of the channels elements in which they have been deposited.

Figure 9.1: Percentages of Old Red Sandstone lithofacies from different Lochkovian localities across the Anglo-Welsh Basin (orange=oxidised, green= reduced)

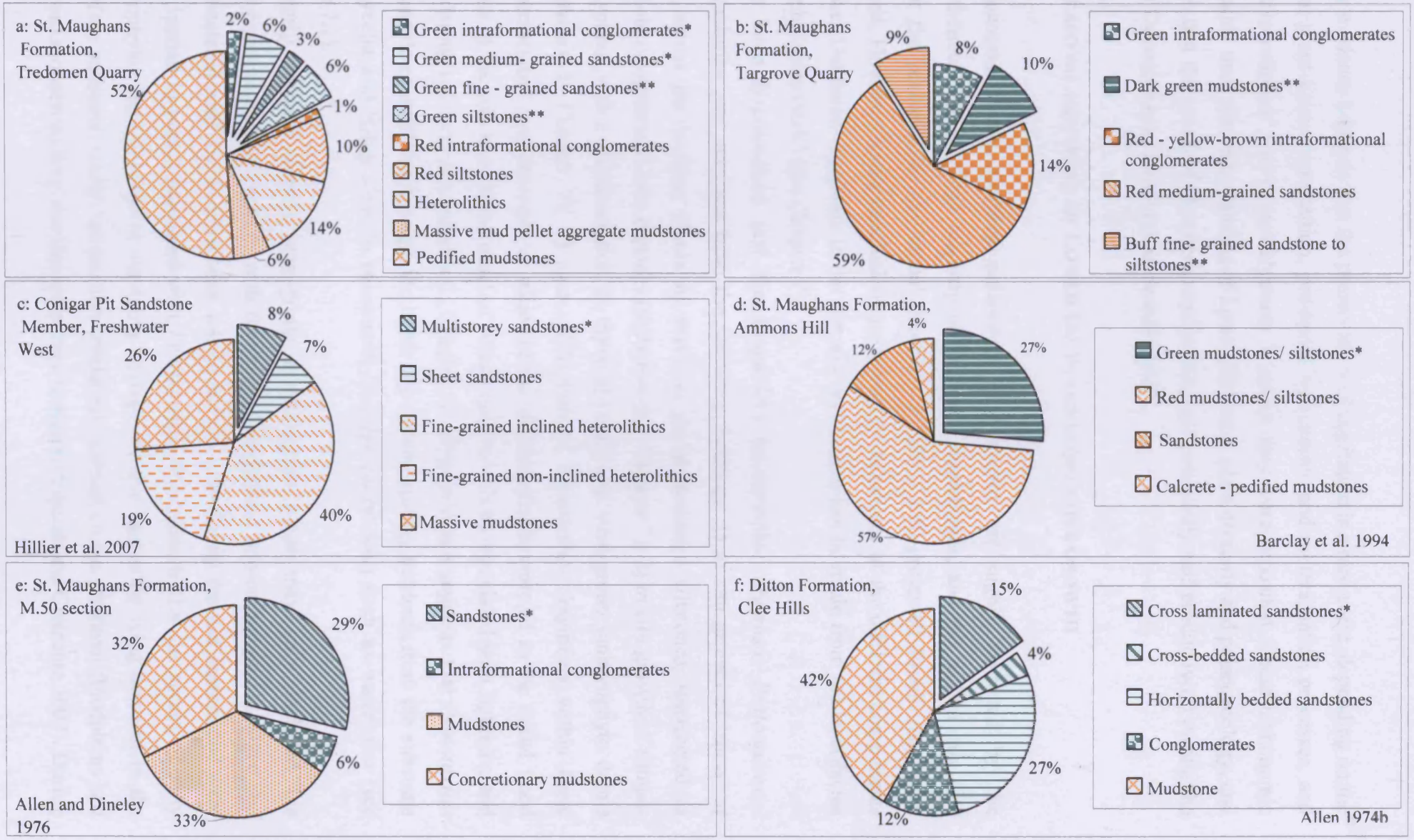

All the evidence suggests that the preservation of vegetation is a rare event, depending on the original plant tissue composition, pre-burial taphonomic and mineralisation processes, and the preservation of the channel elements in which they were deposited. These taphonomic constraints limit the understanding of Lower Devonian plant diversity and palaeoecology, and implies that the extent of phytoterrestrialisation (and potentially soil productivity) during the Lower Devonian may have been underestimated.

9.4: Seasonal controls on Lower Devonian vegetative growth

As discussed above, detailed palaeoecological studies are highly restricted by the allochthonous nature of the majority of the plant assemblages, and the taphonomic bias against the preservation of channel elements in which well-preserved fossils may have occurred. However, broad conclusions regarding the behaviour of the different components of Lower Devonian vegetation to the wet and dry seasons can be made from the taphofacies and taphofacies model (see Chapter 7).

It has been hypothesised that the fungal-like heterotrophic organism *Prototaxites* / *Nematasketum* was perennial from the following evidence: 1) *in situ* growth of 'roots' or 'axes' across the bedding planes of wavy to planar-laminated siltstones, interpreted as waterhole or ephemeral lake deposits (taphofacies 9, Chapter 7); 2) *in situ* growth of fungal-like hyphae, within siltstones rich in rhyniophytoids and stem-group embryophyte debris (taphofacies 5, Chapter 7); 3) charcoalification of *Prototaxites* fragments within basal intraformational conglomerates or major perennial channels, interpreted as the initial flood deposits of the wet season, the onset of which may have been associated with lightning and smouldering wildfires (taphofacies 1, Chapter 7). This evidence suggests that *Prototaxites* was capable of surviving through the harsh dry season, gaining nutrients from the substrate via mycelia and living close to ephemeral, stagnant waterbodies such as waterholes (see Figure 7.1).

The early vascular plants, stem-group embryophytes (that may have included the cryptospore-producers), together with the enigmatic, thalloid non-embryophytes, algae and cyanobacterial mats would have been able to survive only during the wet season, and were more riparian in nature compared with *Prototaxites*. It is possible that the spores of early embryophytes were capable of surviving through the dry season by lying dormant in the subsurface substrate, within desiccation cracks that formed on the proximal floodplains and river banks, observed from modern temporary wetlands (Espinar and Clemente 2007). During

the wet season, these spores then resurfaced as a result of waterlogging, where they germinated (Espinar and Clemente 2007).

The lack of these groups within high-velocity perennial flow deposits suggests that either the floodwaters were too erosive for these plants to be preserved, or that these delicate plants did not colonise the river banks until the initial high-velocity perennial flow subsided (see Figure 7.1). These well-preserved plants are found within upper bar, minor channel, upper crevasse splay deposits and proximal floodplains, deposited during moderate-perennial flow.

9.5: Soil productivity and climate feedback as a result of Lower Devonian phytoterrestrialisation

Using stable carbon isotopes extracted from pedogenic carbonates and fossilised organic matter from Tredomen Quarry, ρCO_2 atmospheric levels during the Lower Devonian have been estimated as between 495 and 1154ppmV (see Chapter 8 for all equation parameters and assumptions made). This estimate, together with other estimates from Old Red Sandstone Anglo-Welsh Basin pedogenic carbonates (Eden 2007, Jenkins 1998), are much lower than expected compared with the geochemical model GEOCARBSULF (Berner 2006). Quast et al. (2006) suggested that this was because the pedogenic carbonates from the Anglo-Welsh Basin were unsuitable for the soil carbonate ρCO_2 barometer, due to recrystallisation and re-setting of the isotopic signatures. However, care was taken to extract primary pedogenic micrite, and normal isotopic values expected of primary pedogenic carbonate were obtained from nodules across the Anglo-Welsh Basin.

The use of fossilised organic matter as a proxy for the original isotopic value of vegetation, may also have caused lower predictions than expected, as plant fossils are typically enriched by ~ 3‰ during coalification (Gröcke 2002) (see Chapter 8). Taking this enrichment into consideration, re-calculated values are closer to the GEOCARBSULF curve (Figure 8.7, Chapter 8).

Alternatively, the ρCO_2 levels estimates from the GEOCARBSULF geochemical model (Berner 2006) of the Lower Devonian have been overestimated. One reason for this could be the underestimation of the extent of phytoterrestisatial and soil productivity during the Lower Devonian. Soil productivity can be estimated using the stable carbon isotopic value of soil CO_2, which is a mixture of soil-respired CO_2 (from plant respiration and microbial activity), that has an average value of -26‰ for C3 plants, and atmospheric CO_2 with a relatively heavier average isotopic value of -6‰. The average stable carbon isotopic value for soil CO_2

was estimated to be -18.8‰, which is significantly lighter than atmospheric CO_2, suggesting a significant input of soil-respired CO_2. This underestimation of soil productivity and associated phytoterrestrialisation during the lowermost Devonian may be due to the poor preservation of plant material as a result of taphonomic constraints (see section 9.4 above). An increase in soil productivity during the lowermost Devonian may have caused increased CO_2 drawdown, through enhanced chemical weathering, a significant parameter used in geochemical models GEOCARB III and GEOCARBSULF (Berner and Kothavala 2001, Berner 2006).

Using experimental microcosms on the nearest living equivalents of Lower Devonian vegetation, Baars et al. (2008) showed that the early vascular plants would have needed significant rooting systems (of similar size as extant *Equisetum*) to enhance soil-respired CO_2 levels sufficiency for the production of carbonic acid and subsequent silica dissolution, and that vegetation with simple rhizomatous systems (early embryophytes), rhizoids (bryophytes) or no rooting systems (algae) were unlikely to have produced significant quantities of soil-respired CO_2. However, organic acids may also have been formed in the soil via the decomposition of organic matter by micro-organisms or bacteria. In particular, the large biomass of fungi-like organisms such as *Prototaxites* may have provided sufficient levels of organic matter in the soil for carbonic acid production via decomposition.

CONCLUSIONS

1. Tredomen Quarry palaeobotanical collection from central-South Wales is typical of lower Lochkovian vegetation from the Anglo-Welsh Basin, with three main components: megafossils of simple, dichotomously branched naked axes; mesofossils of simple to complexly branched minute axes terminated by minute sporangia; and non-embryophytes.
2. The megafossils have been identified as stem group embryophytes to the later tracheophytes: the rhyniophytes and rhyniophytoids, including *Cooksonia hemisphaerica*, cf. *Cooksonia caledonica/ Renalia* sp., *Cooksonia* cf. *cambrensis*, cf. *Uskiella reticulata / Tarrantia salopensis*, *Salopella allenii*, *Salopella* cf. *marcensis* and a new genus of dichotomously branched axes terminated by elongate, club-shaped sporangia.
3. Geometric morphometrics and Principal Component Analysis of the early embryophyte sporangia indicate not only significant intra-species variations, but a strong control on shape variance by asymmetry, interpreted as a taphonomic effect, highlighting the problems of identifying early embryophytes using sporangial morphology alone.
4. Changes in rhyniophyte and rhyniophytoid characteristics, including sporangial size, morphology, dehiscence mechanism and complexly of branching, have been observed between lower Přídolí and lower Lochkovian megafossil specimens from across the Anglo-Welsh Basin. These character changes have been interpreted as adaptations for increased spore production and spore dispersal effectiveness, possibly due to increased competition for height and space in the lower Lochkovian.
5. The mesofossils from Tredomen Quarry have been key to interpreting the minute sporangia and axes recorded in the Anglo-Welsh Basin from the lower Přídolí to middle Lochkovian (Edwards 1996, 2000) as a separate group from the rhyniophytes and rhyniophytoids; turf-sized vegetation thought to be stem-group early embryophytes with bryophytic characters (including *in situ* cryptospores). This group may have evolved from the unbranching, gametophyte-dependant bryophytes, the presence of which has been inferred from permanent cryptospores as far back as the Llanvirn (Strother et al. 1996), and were ancestral to the rhyniophytoids and rhyniophytes.
6. The presence of a relatively large biomass of non-embryophytes at Tredomen Quarry (predominately from *Prototaxites / Nematasketum* specimens) highlights the importance

of non-embryophytes in Lower Devonian palaeoecosystems and the carbon cycle. The presence of *Pachytheca*, and evidence of microbial biofilm activity at Tredomen Quarry also implies that other vegetation types apart from the early embryophytes would have been major components of the palaeoecosystems of the Lower Devonian landscape.

7. Comparisons between the dispersed spore assemblages from Tredomen Quarry and published *in situ* spore record, together with the megafossil evidence, supports the theory that the highest grade of organisation across the Anglo-Welsh Basin during the lower Lochkovian were the rhyniophytes and rhyniophytoids, despite the presence of more complex vegetation in northern Laurussia, eastern Gondwana, the Kazakhstan plate and Siberia during the same time interval (Edwards and Wellman 2001).
8. Several new spore taxa with sculptured exoexine have been described from the dispersed spore record from Tredomen Quarry, including; sculptured fused tetrads, *Cymbohilates variabilis* var. B, *Cymbohilates horridus* var. A, *Cymbohilates* cf. *horridus*, ?*Chelinohilates* var. A; *Velatitetras* sp. B, *Velatitetras* sp. C and several enveloped sculptured cryptospores.
9. These additional palynomorph taxa are part of a general trend of increased abundance and diversity of sculptured cryptospores between the uppermost Přídolí and lower Lochkovian seen in Tredomen Quarry and contemporaneous assemblages from localities across the Anglo-Welsh Basin (Richardson 1996a, b). The diversification of palynomorphs with a sculptured exoexine may be an adaptation for spore survival, by improved wind dispersal or germination. This may be related to the inferred increased competition during the lower Lochkovian that drove the adaptations of the megafossils (see point 4).
10. Using the hypothesis of Richardson (2007) that relative abundances of certain spore morphotypes reflect broad environmental settings, broad habitats have been envisaged across the Anglo-Welsh Basin, with Tredomen Quarry assemblages suggesting a medial alluvial plain setting during the uppermost Přídolí with shift to a more proximal alluvial plain setting as a result of the overall regression that occurred across the Anglo-Welsh Basin between the Late Silurian and Early Devonian. This is an alternative reason for the influx of sculptured cryptospores around the lower Lochkovian.
11. Lower sequences from the Tredomen Quarry core (beneath the Bishop's Frome Limestone) have been correlated with the Raglan Mudstone Formation, and a two-stage, ephemeral mud-dominated dryland river system has been envisaged. In contrast, the upper sequences of the core (above the Bishop's Frome Limestone) have been

correlated to the St. Maughans Formation, and a two-stage sand-dominated possibly perennial meandering river system has been envisaged. In both models, a semi-arid climate with distinctive wet and dry seasons can be inferred from the presence of palaeo-calcic-Vertisols.

12. The regular appearance of sandier, possibly perennial, meandering channels and associated palaeo-calcic-Vertisols in the St. Maughans Formation suggests either a change in fluvial morphology, or the switching-on of remnant trunk channels during the lower Lochkovian. Possible causes for this shift include: reactivation of regional tectonics after a period of quiescence (inferred from the Bishop's Frome Limestone), resulting in a closer, sandier source area (the Irish Sea High); activation of local tectonics fault systems, resulting in changes to incision rates and accommodation space, as well as uplift and erosion of the hanging wall and changes to local rainfall patterns; or local climate change such as increased intensity of tropical monsoons.
13. The shift to a more perennial stable river system in the lower Lochkovian allowed early land plants that previously may have been surviving only around ephemeral waterholes and waterlogged areas of the floodplain to spread into these new habitats (e.g. perennial river banks, crevasse splays).
14. Palaeoecological studies are severely hampered by taphonomic constraints. Preservation depends upon the original or altered composition of plant tissue (with a bias towards the lignified embryophytes and charcoalified organic material) and mineralisation processes, including pyritisation and the formation of iron-encrustations around organic matter (subsequently protecting it against further decay).
15. The most significant taphonomic constraint is the stratinomic partitioning of vegetation prior to burial by fluvial hydraulic sorting. Several taphofacies have been described, and it was recognised that plant material is generally restricted to lithofacies that represent channel elements of a perennial meandering river system, deposited under moderate velocity flow. These channel elements were found to have low preservational potential in comparison with those associated with high-velocity flow and the floodplain lithofacies. These elements may have been deposited during the wanning of the wet season, and remained through the dry season, but were eroded away during the floodwaters of following wet season. Therefore, the extent of phytoterrestrialisation and hence soil productivity may have been underestimated.
16. Despite the lack of information for palaeoecological studies, the taphofacies model has allowed for the recognition of a seasonal control on the growth of different vegetation

types during lower Lochkovian. Fungal-like heterotrophic organisms *Prototaxites* are thought to be perennial, with evidence of mycelia growth and rooting structures around ephemeral waterholes. *Prototaxites* specimens are often charcoalified, which occurred during the end of the dry season and onset of the wet season, when increased occurrences of storm-generated lightning igniting wildfires. *Prototaxites* may have been able to survive by extracting nutrients from previously deposited organic-rich sediments, with evidence of extensive mycelia and a range of stable carbon isotopic signatures (Boyce et al. 2007, Hillier et al. 2008).

17. In contrast, the embryophytes, thalloid non-embryophytes (?nematophytes), cyanobaterial mats and algae were only able to survive during the wet season, colonising river banks and waterlogged areas of the floodplain after the initial floodwaters subsided. During the dry season, although the plants desiccated, spores likely lay dormant within the subsurface substrate, possibly within desiccation cracks. Spores resurfaced during the wet season as a result of waterlogging, and were able to germinate.
18. There is indirect evidence for significant soil productivity on Lower Devonian floodplains, via the stable carbon isotopic signature of carbonate nodules from palaeo-calcic-Vertisols. A significant different between the calculated soil-CO_2 isotopic value (-18.8‰) and the inferred atmospheric CO_2 isotopic value (-6‰) suggests a significant contribution of soil-respired CO_2, via plant respiration and decomposition of organic matter by microbial action. Increased soil productivity may have increased chemical weathering, through the formation of carbonic acid, and subsequent silica dissolution.
19. Levels of atmospheric ρCO_2 in the Lower Devonian have been estimated to have been between 495 and 1154ppmV, using the soil carbonate ρCO_2 barometer. This range is significantly lower than values estimated from the geochemical model GEOCARBSULF (Berner 2006). This discrepancy may be due to the resetting of the isotopic signatures by recrystallisation of pedogenic carbonates, or due to the enrichment of the isotopic signature of organic matter during coalification.
20. An alternative explanation for the discrepancy would be the underestimation of soil productivity and chemical weathering in Lower Devonian soils, an important parameter in these geochemical models for CO_2 drawdown, as a result of the taphonomic constraints on plant preservation.
21. Although interpretations of Lower Devonian palaeoecosystems from Anglo-Welsh Basin Old Red Sandstone strata are highly restricted by taphonomy, this investigation

has provided more information on the primary producers (the rhyniophytes and rhyniophytoids, and the recognition of minute stem-group embryophytes), as well as further evidence of the decomposers, viz. fungi-like organisms such as *Prototaxites*. However, there is an absence of direct evidence of early land plant habitats, due to the allochthonous nature of the assemblages. There is also no direct evidence of the consumers within the ecosystem. Elsewhere coprolites have been used as indicators for the presence of detritivores (Edwards et al. 1995a), but there is no evidence from Tredomen Quarry.

22. Future work could focus on a detailed analysis of the mesofossils, as the middle Lochkovian locality at Brown Clee Hill, Shropshire continues to be productive. Studies could include morphological, anatomical and ultrastructural analysis of sporangia, *in situ* spores and axes using SEM, TEM (transmission electron microscopy) and LM techniques, to understand the biodiversity, affinity, development and functioning of these pioneering land plants, and to understand their relationship with the tracheophytes and bryophytes. These studies might also allow for the recognition of ontogeny, from axes and *in situ* spore wall ultrastructure. Further information on *in situ* spores could also be compared against the dispersed spore record, to explore local and regional variations in vegetation, developing the use of palynofacies, with an emphasis in identifying habitats across the Anglo-Welsh Basin.

    Future work could also focus on the affinity of the non-embryophytes, including the search for more evidence that *Prototaxites* was a fruiting body of a giant basidiomycete (Hueber 2001), with rooting rhizomorphs that produced mycelia for nutrient acquisition (Hillier et al. 2008). Further studies of nematophytalean complexes may allow for the identification of lichens, while a detailed study of *Pachytheca* may elucidate its affinity, and preliminary investigations have identified juvenile specimens and hence ontogeny (Dianne Edwards pers. comm.). Ideally new localities and specimens would provide evidence of interactions between early land plants, fungi, lichen and algae, not only with each other, but also with the soil and the consumers within the ecosystem, particularly the detritivores.

    The geomorphic and taphofacies models could be tested at other Old Red Sandstone localities, from contemporaneous, younger or older strata. Lithofacies (representing geomorphic elements) may contain different taphofacies in different geomorphic settings e.g. the marginal marine Old Red Sandstone strata of the lower Přídolí may produce a completely different set of taphofacies compared to Tredomen Quarry.

Further work is also needed in the comparison between Old Red Sandstone strata from the Anglo-Welsh Basin and modern dryland landscapes, including the Channel Country, central Australia, to gain a better understanding of dryland river processes and resulting geomorphology.

The taphofacies model may be useful in the search for new palaeobotanical localities, with the knowledge of which lithofacies commonly contain well preserved plant fossils. New localities may reveal more information regarding habitat and palaeoecosystems, ideally with the discovery of autochthonous assemblages, providing direct evidence.

Finally, in depth studies of the Anglo-Welsh Basin palaeosols, particularly of regional variability, would enable an assessment on the degree of recrystallisation of pedogenic carbonate and the degree of burial diagenesis that occurred across the basin, which may have altered the extracted stable carbon isotopic signatures that are used in the estimates of atmospheric ρCO_2 levels.

REFERENCES

ADAMS D.C., ROHLF J.F. AND SLICE D.E. 2004. Geometric morphometrics: ten years of progress following the 'revolution'. *Italian Journal of Zoology* **71**: 5-16.

ALGEO T.J., BERNER R.A., MAYNARD J.B. AND SCHECKLER S.E. 1995. Late Devonian oceanic anoxic events and biotic crises: "rooted" in the evolution of vascular land plants? *GSA Today* **5**: 45-66.

ALGEO T.J., SCHECKLER S.E. AND MAYNARD J.B. 2001. Effects of the Middle to Late Devonian spread of vascular land plants on weathering regimes, marine biotas, and global climate. In GENSEL P.G. AND EDWARDS D. (EDS.) *Plants invade the land: evolutionary and environmental perspectives*. Columbia University Press, New York: Chapter **12**: 213-236.

ALLEN J.P. AND GASTALDO R.A. 2006. Sedimentology and taphonomy of the Early to Middle Devonian plant-bearing beds of the Trout Valley Formation, Maine. In GREB S.F. AND DIMICHELE W.A. (EDS). *Wetlands through time*. Geological Society of America Special Paper **399**: 57-78.

ALLEN J.R.L. 1964. Studies in fluviatile sedimentation: six cyclothems from the Lower Old Red Sandstone, Anglo-Welsh Basin. *Sedimentology* **3**: 163-198.

ALLEN J.R.L. 1971. Instantaneous sediment deposition rates deduced from climbing-ripple cross-lamination. *Journal of the Geological Society* **127**: 553-561.

ALLEN J.R.L. 1974a. Studies in fluviatile sedimentation: implications of pedogenic carbonate units, Lower Old Red Sandstone, Anglo-Welsh outcrop. *Geological Journal* **9**: 181-208.

ALLEN J.R.L. 1974b. Sedimentology of Old Red Sandstone (Siluro-Devonian) in Clee Hills Area, Shropshire, England. *Sedimentary Geology* **12(2)**: 73-167.

ALLEN J.R.L. 1977. Wales and the Welsh Borders. *In* HOUSE M.R., RICHARDSON J.B., CHALONER W.G., ALLEN J.R.L., HOLLAND C.H., WESTOLL T.S. (EDS.). A correlation of Devonian Rocks of the British Isles, House Special Report, *Geological Society of London* **8**: 40–54.

ALLEN J.R.L. 1983. Studies in fluviatile sedimentation; bars, bar-complexes and sandstone sheets (low sinuosity braided streams) in the Brownstones (L. Devonian), Welsh Borders. *Sedimentary Geology* **33**: 237-293.

ALLEN J.R.L. 1986. Pedogenic calcretes in the Old Red Sandstone facies (Late Silurian-Early Carboniferous) of the Anglo-Welsh Area, southern Britain. In WRIGHT V.P. (ED). *Paleosols*: *their recognition and interpretation,* Blackwell Scientific, London: 58-86.

ALLEN J.R.L. AND CROWLEY S.J. 1983. Lower Old Red Sandstone fluvial dispersal systems in the British Isles. *Transactions of the Royal Society of Edinburgh* **74**: 61-68.

ALLEN J.R.L. AND DINELEY D.L. 1976. The succession of the Lower Old Red Sandstone (Siluro-Devonian) along the Ross-Tewkesbury Spur Motorway (M.50), Hereford and Worcester. *Geological Journal* **11**: 1-14.

ALLEN J.R.L. AND TARLO L.B. 1963. The Downtonian and Dittonian facies of the Welsh Basin. *Geological Magazine* **100**: 129-155.

ALLEN J.R.L. AND WILLIAMS B.P.J. 1978. The sequence of the earlier Lower Old Red Sandstone (Siluro-Devonian), north of Milford Haven, southwest Dyfed (Wales). *Geological Journal* **13**: 113-136.

ALLEN J.R.L. AND WILLIAMS B.P.J. 1979. Interfluvial drainage on Siluro-Devonian alluvial plains in Wales and the Welsh Borders. *Journal of the Geological Society, London* **136**: 361-366.

ALLEN J.R.L. AND WILLIAMS B.P.J. 1981. Sedimentology and stratigraphy of the Townsend-Tuff-Bed (Lower-Old-Red-Sandstone) in South Wales and the Welsh Borders. *Journal of the Geological Society* **138**: 15-29.

ALLEN J.R.L. AND WILLIAMS B.P.J. 1982. The architecture of an alluvial suite: rocks between the Townsend Tuff and Pickard Bay Tuff Beds (Early Devonian), Southwest Wales. *Philosophical Transactions of the Royal Society London, Series B* **297**: 51-89.

ALLEN J.R.L., THOMAS R.G. AND WILLIAMS B.P.J. 1977. Field Meeting: The facies of the Lower Old Red Sandstone, north of Milford Haven, southwest Dyfed, Wales. *Proceedings of the Geological Association* **92(4)**: 251-267.

ALLEN J.R.L., THOMAS R.G. AND WILLIAMS B.P.J. 1982. The Old Red Sandstone north of Milford Haven. In BASSETT M.G. (ED) Geological Excursions in Dyfed, Southwest Wales. Published for the Geologists' Association, South Wales Group by the National Museum of Wales: 327pp.

ALLEN K.C. 1965. Lower and Middle Devonian spores of North and Central Vestspitzbergen. *Palaeontology* **8**: 687-748.

ARENS N.C., JAHREN H.A. AND AMUNDSON R. 2000. Can C3 plants faithfully record the carbon isotopic composition of atmospheric carbon dioxide? *Paleobiology* **26(1)**: 137-164.

ARNOLD C.A. 1952. A specimen *Prototaxites* from the Kettle Point Black Shale of Ontario. *Palaeontographica B* **93**: 45-56.

BAARS C., JONES T.H. AND EDWARDS D. 2008. Microcosm studies of the role of land plants in elevating soil carbon dioxide and chemical weathering. *Global Biogeochemical Cycles* **22** GB3019.

BALL H.W. AND DINELEY D.L. 1961. The Old Red Sandstone of Brown Clee Hills and the adjacent area. I. Stratigraphy. *Bulletin of the British Museum Natural History (Geology)* **5**:175-242.

BALME B.E. 1988. Miospores from Late Devonian (Early Frasian) strata, Carnarvon Basin, Western Australia. *Palaeontographica B* **209**: 109-166.

BANKS H.P. 1973. Occurrence of *Cooksonia*, the oldest vascular land plant macrofossil, in the Upper Silurian of New York State. *Journal of the Indian Botanical Society* **50A**: 227-235.

BANKS H.P., LECLERCQ S. AND HUEBER F.M. 1975. Anatomy and morphology of *Psilophyton dawsonii* sp. n. from the late Lower Devonian of Quebec (Gaspé), and Ontario, Canada. *Palaeontographica Americana* **8**: 77-127.

BARCLAY W.J. AND WILBY P.R. 2003. Geology of the Talgarth district - a brief explanation of the geological map. Sheet Explanation of the British Geological Survey. 1:50,000 Sheet 214 Talgarth (England and Wales).

BARCLAY W.J., BROWNE M.A.E., MCMILLAN A.A., PICKETT E.A., STONE P. AND WILBY P.R. 2005. *The Old Red Sandstone of Great Britain.* Peterborough, Joint Nature Conservation Committee.

BARCLAY W.J., RATHBONE P.A., WHITE D.E. AND RICHARDSON J.B. 1994. Brackish water faunas from the St Maughans Formation: the Old Red Sandstone section at Ammons Hill, Hereford and Worcester, UK, re-examined. *Geological Journal* **29**: 369-379.

BARNOLA J.-M., RAYNAUD D., KOROTKEVICH Y.S. AND LORIUS C. 1987. Vostok ice core provides 160,000-year record of atmospheric CO_2. *Nature* **329**: 408-414.

BASINGER J.F., KOTYK M.E. AND GENSEL P.G. 1996. Early land plants from the Late Silurian-Early Devonian of Bathurst Island, Canadian Arctic Archipelago. *Geological Survey of Canada, Current Research* **1996B**: 51-60.

BASSETT M.G. 1982 (ED.) Geological Excursions in Dyfed, Southwest Wales. Published for the Geologists' Association, South Wales Group by the National Museum of Wales: 327pp.

BASSETT M.G., LAWSON J.D. AND WHITE D.E. 1982. The Downton Series as the fourth Series of the Silurian System. *Lethaia* **15**: 1-24.

BEERBOWER J.R. 1985. Early development of continental ecosystems. In TIFFNEY B.H. (ED.) *Geological factors and the evolution of plants.* New Haven: Yale University Press: 47-92.

BENSMIHEN S., HANNS A.I., LANGLADE N.B., MICOL J.L., BANGHAM A. AND COEN E.S. 2008. Mutational spaces for leaf shape and size. *HFSP Journal* **2**: 110-120.

BERNER R.A. 1991. A model for atmospheric CO_2 over Phanerozoic time. *American Journal of Science* **291**: 339-376.

BERNER R.A. 1994. GEOCARB II: A revised model of atmospheric CO_2 over Phanerozoic time. *American Journal of Science* **294**: 56-91.

BERNER R.A. 1997. The rise of plants and their effect on weathering and atmospheric CO_2. *Science* **276**: 544-546.

BERNER R.A. 1998. The carbon cycle and CO_2 over Phanerozoic time: the role of land plants. *Philosophical Transactions of the Royal Society of London B* **353**: 75-82.

BERNER R.A. 2006. GEOCARBSULF: A combined model for Phanerozoic atmospheric O_2 and CO_2. *Geochimica et Cosmochimica Acta* **70**: 5653-5664.

BERNER R.A. AND KOTHAVALA Z. 2001. GEOCARB III: A revised model of atmospheric CO_2 over Phanerozoic time. *American Journal of Science* **301**: 182-204.

BHARADWAJ D.A. AND VENKATACHALA B.S. 1961. Spore assemblage out of a Lower Carboniferous shale from Spitsbergen. *Palaeootanist* **10**: 18-47.

BHATTACHARYA D. AND MEDLIN L. 1998. Algal phylogeny and the origin of land plants. *Plant Physiology* **116**: 9-15.

BOOKSTEIN F.L. 1991. Morphometric tools for landmark data: Geometry and Biology. Cambridge Univ. Press, Cambridge: 435pp.

BOYCE K.C. 2008. How green was *Cooksonia*? The importance of size in understanding the early evolution of physiology in the vascular plant lineage. *Paleobiology* **34(2)**: 179-194.

BOYCE K.C., HOTTON C.L., FOGEL M.L., CODY G.D., HAZEN R.M., KNOLL A.H. AND HUEBER F.M. 2007. Devonian landscape heterogeneity recorded by a giant fungus. *Geology* **35**: 399-402.

BREUER P., AL-GHAZI A., AL-RUWAILI M., HIGGS K.T., STEEMANS P. AND WELLMAN C.H. 2007. Early to Middle Devonian miospores from northern Saudi Arabia. *Revue de micropaléontologie* **50**: 27-7.

BRIDGE J.S. 2003. Rivers and floodplains: Forms, Processes, and Sedimentary Record. Blackwell Science Ltd: Oxford: 491pp.

BRIDGE J.S. 2006. Fluvial facies models: recent developments. Facies Models Revisited, *SEPM* Special Publication no. **84**: 81-170.

BROCK F., PARKES J.R. AND BRIGGS D.E.G. 2006. Experimental pyrite formation associated with decay of plant material. *Palaios* **21**: 499-506.

BUCHMANN N., BROOKS R.J., FLANAGAN L.B. AND EHLERINGER J.R. 1998. Carbon isotopic discrimination of terrestrial ecosystems. In GRIFFITHS H. (EDS.) *Stable isotopes: integration of biological, ecological and geochemical processes*: Oxford, UK, BIOS Scientific Publications: 203-221.

BUGGISCH W. AND MANN U. 2004. Carbon isotope stratigraphy of Lochkovian to Eifelian limestones from the Devonian of Central and South Europe. *International Journal of Earth Sciences* (*Geologische Rundschau*) **93**: 521-541.

BURGESS N.D. 1991. Silurian cryptospores and miospores from the type Llandovery area, Southwest Wales. *Palaeontology* **34**: 575-599.

BURGESS N.D. AND EDWARDS D. 1988. A new Palaeozoic plant closely allied to *Prototaxites* Dawson. *Botanical Journal of the Linnean Society* **97**: 189-203.

BURGESS N.D. AND EDWARDS D. 1991. Classification of uppermost Ordovician to Lower Devonian tubular and filamentous macerals from the Anglo-Welsh Basin: *Botanical Journal of the Linnean Society* **106**: 41-66.

BURGESS N.D. AND RICHARDSON J.B. 1991. Silurian cryptospores and miospores from the Wenlock, Shropshire, England. *Palaeontology* **34**: 601-628.

BURGESS N.D. AND RICHARDSON J.B. 1995. Late Wenlock to early Přídolí cryptospores and miospores from south and southwest Wales, Great Britain. *Palaeontographica B* **236**: 1-44.

BURGESS N.D. AND RICHARDSON J.B. 1999. Sporomorph evolution in the Anglo-Welsh Basin: tempo and parallelism. In KURMANN M.H. AND HEMSLEY A.R. (EDS.) *The evolution of plant architecture*. Whitstable Lith Printers Ltd., Linnaean Society London and The Royal Botanic Gardens, Kew: 35–49

BUTTERWORTH M.A. AND WILLIAMS R.W. 1958. The small spore floras of coals in the Limestone Coal Group and Upper Limestone Group of the Lower Carboniferous of Scotland. *Transactions of Royal Society of Edinburgh* **58**: 353-392.

CAI C.-Y., DOU Y.-W. AND EDWARDS D. 1993. New observations on a Přídolí plant assemblage from north Xinjiang, northwest China, with comments on its evolutionary and palaeogeographical significance. *Geol. Mag.* **130**: 155-170.

CAPUTO M.V. 1985. Late Devonian glaciation in South America. *Palaeogeography, palaeoclimatology and palaeoecology* **51**: 291-317.

CARRUTHERS W. 1872. On the history, histological structure, and affinities of *Nematophycus logani* Carr. (*Prototaxites logani* Dawson), an alga of Devonian age. *Monthly Microscopical Journal* **8**: 160-172.

CERLING T.E. 1984. The stable isotopic composition of modern soil carbonate and its relationship to climate. *Earth and Planetary Science Letters* **71**: 229-240.

CERLING T.E. 1991a. Carbon dioxide in the atmosphere; evidence from Cenozoic and Mesozoic paleosols. *American Journal of Science* **291**: 377-400.

CERLING T.E. 1991b. On the isotopic composition of carbon in soil carbon dioxide. *Geochimica et Cosmochimica Acta* **55**: 3403-3405.

CERLING T.E. 1999. Stable carbon isotopes in palaeosol carbonates. In THIRY M. AND SIMON-COINÇON R. (EDS.) *Palaeoweathering, palaeosurfaces, and related continental*

deposits. Special Publications of the International Association of Sedimentologists. Blackwell Publishing.

CHALONER W.G. AND STREEL M. 1968. Lower Devonian spores from South Wales. *Argumenta Palaeobotanica* **1**: 87-101.

CHANNELL J.E.T., MCCABE C. AND WOODCOCK N.H. 1992. Early Devonian (pre-Acadian) magnetisation directions in the Lower Old Red Sandstone of South Wales (UK). *Geophyiscal Journal International* **108**: 883-894.

CHURCH A.H. 1919. Thallasiophyta and the subaerial transmigration. Oxford University Press, Oxford. *Oxford Botanical Memoirs* No. 3.

CHURCH M. 2006. Bed material transport and the morphology of alluvial river channels. *Annual Review of Earth and Planetary Sciences* **34**: 325-354.

COLLINSON J.D. 1996. Chapter 3: Alluvial sediments. In READING H.G. (ED.) *Sedimentary environments: processes, facies and stratigraphy*. Blackwell Publishing Limited: Oxford: 704pp.

COUPER R.A. 1953. Upper Mesozoic and Cainozoic spores and pollen grains from New Zealand. *N.Z. Geol. Surv. Palaeont. Bull.* **22**: 1–73.

CRAMER F.H. 1966. Hoegispheres and other microfossils *incertae sedis* of the San Pedro Formation (Siluro-Devonian Boundary) near Valporquero, Léon, NW Spain. *Notas y Commuicaciones del Instituto Geologico y Minero de España* **86**: 75-94.

CROFT W.N. AND LANG W.H. 1942. The Lower Devonian flora of the Senni Beds of Monmouthshire and Breconshire. *Philosophical Transactions of the Royal Society of London B* **231**: 131-163.

CROKE J.C., MAGEE J.W. AND WALLENSKY E.P. 1999. The role of the Australian Monsoon in the western catchment of Lake Eyre, central Australia, during the Last Interglacial. *Quaternary International* **57/58**: 71-80.

CROWLEY S.F., HIGGS K.T., PIPER J.D.A. AND MORRISSEY L.B. 2009. Age of the Peel Sandstone Group, Isle of Man. *Geological Journal*, **44**: 57-78.

DABER R. 1971. *Cooksonia* – one of the most ancient psilophytes – widely distributed, but rare. *Botanique (Nagpur)* **2**: 35-40.

DAVIDSON G.R. 1995. The stable isotopic composition and measurements of carbon in soil CO_2. *Geochimica et Cosmochimica Acta* **59(12)**: 2485-2489.

DAVIS J.C. 2002. Statistics and data analysis in geology. Third Edition. John Wiley and Sons, New York: 638pp.

DAWSON J.W. 1859. On the fossil plants from the Devonian rocks of Canada, *Quarterly Journal of the Geological Society of London* **15**: 477-488.

DAWSON J.W. 1882. Notes on *Prototaxites* and *Pachytheca* discovered by Dr. Hicks in the Denbighshire Grits of Corwen, North Wales. *Quaternary Journal of the Geological Society of London* **38**: 103-107.

DEINES P. 1980. The isotopic composition of reduced organic carbon. In FRITZ A.P. AND FONTES J.CH. (EDS.) *Handbook of Environmental Isotope Geochemistry 1. The Terrestrial Environment*, Elsevier, Amsterdam: 329-406.

DEWEY J.F. AND STRACHAN R.A. 2003. Changing Silurian-Devonian relative plate motion in the Caledonides: sinistral transpression to sinistral transtension. *Journal of the Geological Society* **160**: 219- 299.

DINELEY D.L. AND LOEFFLER E.J. 1999. Upper Silurian and Lower Devonian vertebrate communities from the Anglo-Welsh Basin. In BOUCOT A.J. AND LAWSON J.D. (EDS.) *Paleocommunities: case study from the Silurian and Lower Devonian,* Cambridge University Press, Cambridge: 425-437.

DRIESE S.G., MORA C.I., COTTER E. AND FORMAN J.L. 1992. Palaeopedology and stable carbon isotope chemistry of Late Silurian vertic palaeosols, Bloomsburg Formation, central Pennsylvania. *Journal of Sedimentary Research* **62**: 825-841.

DRIESE S.G., MORA C.I. AND ELICK J.M. 2000. The Paleosol record of increasing plant diversity and depth of rooting and changes in atmospheric ρCO_2 in the Siluro-Devonian. In GASTALDO R.A. AND DIMICHELE W.A. (EDS.) *Phanerozoic terrestrial ecosystems, a short course*. New Haven CT, The Palaeontological Society Papers **6**: 47-61.

DUCHAUFOUR P. 1982. Pedology. Allen and Unwin: London.

DUNLOP J.A. AND SELDEN P.A. 2004. A trigonotarbid arachnid from the Lower Devonian of Tredomen, Wales. *Palaeontology* **47(6)**: 1469-1476.

DUNN K.A., MCLEAN R.J.C., UPCHURCH G.R. AND FOLK R.L. 1997. Enhancement of leaf fossilization potential by bacterial biofilms. *Geology* **25**: 1119-1122.

EDEN S.E. 2007. Marine incursions, terrestrial plants and atmospheric CO_2 levels in the lower Devonian: evidence from the Chapel Point Calcrete, South Wales. MESci Thesis, Cardiff University.

EDWARDS D. 1968. A new plant from the Lower Old Red Sandstone of South Wales. *Palaeontology* **11**: 683-690.

EDWARDS D. 1969a. *Zosterophyllum* from the Lower Old Red Sandstone of South Wales. *New Phytologist* **68**: 923-931.

EDWARDS D. 1969b. Further observations on *Zosterophyllum llanoveranum* from the Lower Devonian of South Wales. *American Journal of Botany* **56(2)**: 201-210.

EDWARDS D. 1970a. Fertile Rhyniophytina from the Lower Devonian of Britain. *Palaeontology* **13**: 451-461.

EDWARDS D. 1970b. Further observations on the Lower Devonian plant, *Gosslingia breconensis* Heard. *Philosophical Transactions of the Royal Society of London B* **258**: 225-243.

EDWARDS D. 1972. A *Zosterophyllum* fruitification from the Lower Old Red Sandstone of Scotland. *Review of Palaeobotany and Palynology* **14**: 77-83.

EDWARDS D. 1975. Some observations on the fertile parts of *Zosterophyllum myretonianum* Penhallow from the Lower Old Red Sandstone of Scotland. *Transactions of the Royal Society of Edinburgh* **69**: 251.

EDWARDS D. 1979. A Late Silurian flora from the Lower Old Red Sandstone of S-W Dyfed. *Palaeontology* **22**: 23-52.

EDWARDS D. 1981. Studies on Lower Devonian petrifactions from Britain. 2. *Sennicaulis*, a new genus for sterile axes based on pyrite and limonite petrifactions from the Senni Beds. *Review of Palaeobotany and Palynology* **32**: 207-226.

EDWARDS. D. 1982. Fragmentary non-vascular plant microfossils from the Late Silurian of Wales: *Botanical Journal of the Linnean Society* **84**: 223-256.

EDWARDS D. 1990. Constraints on Silurian and Early Devonian phytogeographic analysis based on megafossils. In MCKERROW W.S. AND SCOTESE C.R. (EDS). Palaeozoic Palaeogeography and Biogeography. *Geological Society Memoirs* **12**: 233-242.

EDWARDS D. 1996. New insights into early land ecosystems: A glimpse of a Lilliputian world. *Review of Palaeobotany and Palynology* **90**: 159-174.

EDWARDS D. 2000. The role of Mid-Palaeozoic mesofossils in detection of early bryophytes. *Philosophical Transactions of the Royal Society of London B* **355**: 733-755.

EDWARDS D. 2003. Xylem in early tracheophytes. *Plant Cell and Environment* **26**: 57-72.

EDWARDS D. AND AXE L. 1992. Stomata and mechanics of stomatal functioning in some early land plants. *Cour. Forschungsinst. Senckenberg* **147**: 59-73.

EDWARDS D. AND AXE L. 2004. Anatomical evidence in the detection of the earliest wild fires. *Palaios* **19**: 113-128.

EDWARDS D. AND DAVIES M.S. 1990. Interpretations of early land plant radiations: 'Facile adaptations guesswork' or reasoned speculation? In TAYLOR P.D. AND LARWOOD

G.P. (EDS.) *Major Evolutionary Radiations*. The Systematics Association Special Volume **42**: 351-376.

EDWARDS D. AND FANNING U. 1985. Evolution and environment in the Late Silurian-Early Devonian: The rise of the pteridophytes. *Philosophical Transactions of the Royal Society of London B* **309**: 147-165.

EDWARDS D. AND FEEHAN J. 1980. Records of *Cooksonia*-type sporangia from late Wenlock strata in Ireland. *Nature* **287**: 41-42.

EDWARDS D. AND KENRICK P. 1986. A new zosterophyll from the Lower Devonian of Wales. *Botanical Journal of the Linnean Society* **92**: 269-283.

EDWARDS D. AND RICHARDSON J.B. 1974. Lower Devonian (Dittonian) plants from the Welsh Borderland. *Palaeontology* **17**: 311-324.

EDWARDS D. AND RICHARDSON J.B. 1996. Review of *in situ* spores in early land plants. In JANSONIUS J. AND MCGREGOR D.C. (EDS.), *Palynology: Principles and Applications*, Chapter 14A. American Association of Stratigraphic Palynologists Foundation, Vol. **1**: 391-407.

EDWARDS D. AND RICHARDSON J.B. 2000. Progress in reconstructing vegetation on the Old Red Sandstone Continent: two *Emphanisporites* producers from the Lochkovian sequence of the Welsh Borderland. *In* FRIEND P.D. AND WILLIAMS B.P.J. (EDS.) *New perspectives on the Old Red Sandstone. Geological Society of London, Special Publication* **180**: 355-370.

EDWARDS D. AND RICHARDSON J.B. 2004. Silurian and Lower Devonian plant assemblages from the Anglo-Welsh Basin: a palaeobotanical and palynological synthesis. *Geological Journal* **39(3-4)**: 375-402.

EDWARDS D. AND ROGERSON E.C.W. 1979. New records of fertile Rhyniophytina from the Late Silurian in Wales. *Geological Magazine* **116**: 93-98.

EDWARDS D. AND SELDEN P.A. 1993. The development of early terrestrial ecosystems. *Botanical Journal of Scotland* **46**: 337-366.

EDWARDS D. AND WELLMAN C.H. 1996. Older plant macerals (excluding spores).In JANSONIUS J. AND MCGREGOR D.C. (EDS) *Palynology: Principles and Applications* American Association of Stratigraphic Palynologists Foundation, Publishers Press, Salt Lake City, vol **1**: 383-387.

EDWARDS D. AND WELLMAN C.H. 2001. Embryophytes on land: the Ordovician to Lockhovian (Lower Devonian) record. In GENSEL P.G. AND EDWARDS D. (EDS.) *Plants invade the land: evolutionary and environmental perspectives*. Columbia University Press, New York: Chapter **2**: 3-28.

EDWARDS D., AXE L. AND MÉNDEZ E. 2001b. A new genus for isolated bivalved sporangia with thickened margins from the Lower Devonian of the Welsh Borderland. *Botanical Journal of the Linnean Society* **137**: 297-310.

EDWARDS D., DAVIES K.L. AND AXE L. 1992. A vascular conducting strand in the early land plant *Cooksonia*. *Nature* **357**: 683-685.

EDWARDS D., EDWARDS D.S. AND RAYNER R. 1982. The cuticle of early vascular plants and its evolutionary significance. In CUTLER D.F., ALVIN K.L. AND PRICE C.E. (EDS.) *The Plant Cuticle*. Academic Press for the Linnean Society, London: 341-361.

EDWARDS D., EWBANK G. AND ABBOTT G.D. 1997. Flash pyrolysis of the outer cortical tissues in Lower Devonian *Psilophyton dawsonii*. *Botanical Journal of the Linnean Society* **124(4)**: 335-360.

EDWARDS D., FANNING U., DAVIES K.L., AXE L. AND RICHARDSON J.B. 1995b. Exceptional preservation in Lower Devonian coalified fossils from the Welsh Borderland - a new genus based on reniform sporangia lacking thickened borders. *Botanical Journal of the Linnean Society* **117(3)**: 233-254.

EDWARDS D., FANNING U. AND RICHARDSON J.B. 1986. Stomata and sterome in early land plants. *Nature* **323**: 438-440.

EDWARDS D., FANNING U. AND RICHARDSON J.B. 1994. Lower Devonian coalified sporangia from Shropshire: *Salopella* Edwards and Richardson and *Tortilicaulis* Edwards. *Botanical Journal of the Linnean Society* **116**: 89-110.

EDWARDS D., FEEHAN J. AND SMITH D.G. 1983. A late Wenlock flora from Co. Tipperary, Ireland. *Botanical Journal of the Linnean Society* **86**: 19-36.

EDWARDS D., KENRICK P. AND CARLUCCIO L.M. 1989. A reconsideration of cf. *Psilophyton princeps* (Croft and Lang 1942), a zosterophyll widespread in the Lower Old Red Sandstone of South Wales. *Botanical Journal of Linnean Society* **100(4)**: 293-318.

EDWARDS D., MOREL E.M., PARAEDES F., GANUZA D.G. AND ZUANIAGA A. 2001a. Plant assemblages from the Silurian of southern Bolivia and their palaeogeographic significance. *Botanical Journal of the Linnean Society* **135(3)**: 229-250.

EDWARDS D., MOREL E.M., POIRÉ D.G. AND CINGOLANI C.A. 2001c. Land plants in the Devonian Villavicencio Formation, Mendoza Province, Argentina. *Review of Palaeobotany and Palynology* **116**: 1-18.

EDWARDS D., SELDEN P.A., RICHARDSON J.B. AND AXE L. 1995a. Coprolites as evidence for plant-animal interaction in Siluro-Devonian terrestrial ecosystems. *Nature* **377**: 329-331.

EDWARDS D., WELLMAN C.H. AND AXE L. 1998. The fossil record of early land plants and interrelationships between primitive embryophytes: too little and too late? In BATES J.W., ASTON N.W. AND DUCKETT J.G. (EDS.) *Bryology for the Twenty-first Century.* British Bryology Society. Chapter **2**: 15-43.

EDWARDS D., WELLMAN C.H. AND AXE L. 1999. Tetrads in sporangia and spore masses from the Upper Silurian and Lower Devonian of the Welsh borderland. *Botanical Journal of the Linnean Society* **130**: 111-115.

EDWARDS D. S. 1980. Evidence for the sporophytic status of the Lower Devonian plant *Rhynia gwynne-vaughanii* Kidston and Lang. *Review of Palaeobotany and Palynology* **29**: 177-188.

EDWARDS D.S. 1986. *Aglaophyton major*, a non-vascular land-plant from the Devonian Rhynie chert. *Botanical Journal of the Linnean Society* **93**: 173-204.

EKART D.D., CERLING T.E., MONTAÑEZ P.I. AND TABOR N.J. 1999. A 400 million year carbon isotope record of pedogenic carbonate: implications for paleoatmopheric carbon dioxide. *American Journal of Science* **299**: 805-827.

ÉKES C. 1993. Bedload-transported pedogenic mud aggregates in Lower Old Red Sandstone in Southwest Wales. *Journal of the Geological Society, London* **150**: 469-471.

EL-SAADAWY W. AND LACEY W. S. 1979. Observations on *Nothia aphylla* Lyon ex Høeg. *Review of Palaeobotany and Palynology* **27**: 119-147

ERDTMAN G. 1947. Suggestions for the classification of fossil and recent pollen grains and spores. *Svensk Bot. Tidskr.* **41**: 104-114.

ESPINAR J.L. AND CLEMENTE L. The impact of vertic soil cracks on submerged macrophyte diaspore bank depth distribution in Mediterranean temporary wetlands. *Aquatic Botany* **87**: 325-328.

EVANS R.D. AND BELNAP J. 1999. Long-term consequences of disturbance on Nitrogen dynamics in an arid ecosystem. *Ecology* **80(1)**: 150-160.

EWBANK G., EDWARDS D. AND ABBOTT G.D. 1996. Chemical characterization of Lower Devonian vascular plants. *Organic geochemistry* **25(8)**: 461-473.

FAGAN S. AND NANSON G.C. 2004. The morphology and formation of floodplain-surface channels, Cooper Creek Australia. *Geomorphology* **60**: 107-128.

FANNING U. 1987. Late Silurian-Early Devonian plant assemblages in the Welsh Borderland. PhD Thesis, Cardiff University.

FANNING U., EDWARDS D. AND RICHARDSON J.B. 1990. Further evidence for diversity in the Late Silurian land vegetation. *Journal of the Geological Society* **147**: 725-728.

FANNING U., EDWARDS D. AND RICHARDSON J.B. 1991a. A new rhyniophytoid from the Late Silurian of the Welsh Borderland. *Neues Jahrbuch für Geologie und Paläontologie Abhandlungen* **183**: 37-47.

FANNING U., EDWARDS D. AND RICHARDSON J.B. 1992. A diverse assemblage of early land plants from the Lower Devonian of the Welsh Borderland. *Botanical Journal of the Linnean Society* **109**: 161-188.

FANNING U., RICHARDSON J.B. AND EDWARDS D. 1988. Cryptic evolution in an early land plant. *Evolutionary trends in plants* **2**:13-24.

FANNING U., RICHARDSON J.B. AND EDWARDS D. 1991b. A review of *in situ* spores in Silurian land plants. In BLACKMORE S. AND BARNES S.H. (EDS.) *Pollen and spores: patterns of diversification*, Systematic Association Special Volume **44**, Clarendon Press, Oxford, 25-47.

FLEMING J. 1831. On the occurrence of scales of vertebrated animals in the Old Red Sandstone of Fifeshire. *Edinburgh Journal of Natural and Geological Science* **3**: 81-86.

FOX D. L. AND KOCH P. L. 2003. Tertiary history of C4 biomass in the Great Plains, USA. *Geology* **31**: 809-812.

FREEMAN K.H. AND HAYES J.M. 1992. Fractionation of carbon isotopes by phytoplankton and estimates of ancient CO_2 levels. *Global Biogeochemical Cycles* **6**: 185-198.

FRICKE H. AND O'NEIL J. 1999. The correlation between $^{18}O/^{16}O$ ratios of meteoric water and surface temperature: Its use in investigating terrestrial climate change over geologic time. *Earth and Planetary Science Letters* **170**: 181-196.

FRIEDLI H., LÖTSCHER H., OESCHGER H., SIEGENTHALER U. AND STAUFFER B. 1986. Ice core record of the 13C/12C ratio of atmospheric CO_2 in the past two centuries. *Nature* **324**: 237-238.

FRIEDMAN I. AND O'NEIL J. 1977. Compilation of stable isotope fractionation factors of geochemical interest: Reston, Virginia, U.S. Geological Survey Professional Paper **440-KK**: 1-12.

FRIEND P.F., WILLIAMS B.P.J., FORD M. AND WILLIAMS E.A. 2000. Kinematics and dynamics of Old Red Sandstone basins. In FRIEND P.F. AND WILLIAMS B.P.J. (EDS.) *New Perspectives on the Old Red Sandstone*. London, Geological Society Special Publication **180**: 29-60.

GARNER G.J., MORTLOCK A.J., PRICE D.M., READHEAD M.L. AND WASSON R.J. 1987. Thermoluminescence and radiocarbon dating of Australian desert dunes. *Australian Journal of Earth Science* **34**: 343-357.

GAUT B.S. AND DOEBLEY J.F. 1997. DNA sequence evidence for the segmental allotetraploid origin of maize. *Proceedings of the National Academy of Sciences, USA* **94**: 6809–6814.

GENSEL P.G. 1976. *Renalia hueberi*; a new plant from the Lower Devonian of Gaspé. *Review of Palaeobotany and Palynology* **22(1)**: 19-37.

GERRIENNE P. 1999. Lower Devonian plant mesofossils from the Parana Basin, Brazil: General introduction, descriptions, age significant and correlation with floral succession from Laurussia and Gondwana. In RODRIGUES M.A.C. AND PERIERA E. (EDS.) *Ordovician/ Devonian palynostratigraphy in western Gondwana: Update, problems and perspectives*. Faculdade de Geologia, Rio de Janeiro: 165-178.

GERRIENNE P., BERGAMASCHI S., PEREIRA E., ROGRIGUES M-A.C. AND STEEMANS P. 2001. An Early Devonian flora, including *Cooksonia*, from the Paraná Basin, Brazil. *Review of Palynology and Palaeobotany* **116**: 19-38.

GHOSH P., GHOSH P. AND BHATTACHARYA S.K. 2001. CO_2 levels in the Late Palaeozoic and Mesozoic atmosphere from soil carbonates and organic matter, Satpura Basin, Central India. *Palaeogeography, Palaeoclimatology and Palaeoecology* **170**: 219-236.

GIBLING M.R., NANSON G.C. AND MAROULIS J.C. 1998. Anastomosing river sedimentation in the Channel Country of Central Australia. *Sedimentology* **45**: 595-619.

GLASSPOOL I.J., EDWARDS D. AND AXE L. 2004. Charcoal in the Silurian as evidence for the earliest wildfires. *Geology* **32**: 381-383.

GLASSPOOL I.J., EDWARDS D. AND AXE L. 2006. Charcoal in the Early Devonian: A wildfire-derived Konservat-Lagerstätte. *Review of Palaeobotany and Palynology* **142 (3-4)**: 131-136.

GOUDIE A.S. 1983. Dust storms in space and time. *Progress in Physical Geography* **7**: 502-530.

GRAHAM L.E. AND GRAY J. 2001. The origin, morphology, and ecophysiology of early embryophytes: neonotological and paleontological perspectives. In GENSEL P.G. AND EDWARDS D. (EDS.) *Plants invade the land: evolutionary and environmental perspectives*. Columbia University Press: New York. Chapter **8**: 140-158.

GRAY J. 1988. Land plant spores and the Ordovician/Silurian boundary. *Bulletin of the British Museum (Natural History): Geology* **43**: 351-358.

GRAY J., CHALONER W.G. AND WESTOLL T.S. 1985. The microfossil record of early land plants: advances in understanding of early terrestrialization, 1970-1984: *Philosophical Transactions of the Royal Society of London B* **309**: 167-195.

GREBE H. 1971. A recommended terminology and descriptive method for spores. *Comm. Intern. Microflore Paléoz., 4: Les Spores*. **1**: 7-34.

GRIFFING D.H., BRIDGE J.S. AND HOTTON C.L. 2000. Coastal-fluvial palaeoenvironments and plant palaeoecology of the Lower Devonian (Gaspé Bay), Québec, Canada. In FRIEND P.F. AND WILLIAMS B.P.J (EDS.) *New Perspectives on the Old Red Sandstone*, Geological Society of London Special Publication **180**: 61-84.

GRIMES S.T., BROCK F., RICKARD D., DAVIES K.L., EDWARDS D., BRIGGS D.E.G. AND PARKES R.J. 2001. Understanding fossilization: Experimental pyritization of plants. *Geology* **29**: 123-126.

GRIMES S.T., DAVIES K.L., BUTLER I.B., BROCK F., EDWARDS D., RICKARD D., BRIGGS D.E.G. AND PARKES R.J. 2002. Fossil plants from the Eocene London Clay: the use of pyrite textures to determine the mechanism of pyritization. *Journal of the Geological Society* **159**: 493-501.

GRÖCKE D.R. 2002. The carbon isotope composition of ancient CO_2 based on higher-plant organic matter. *Philosophical Transactions of the Royal Society of London A* **360**: 633-658.

GUILDFORD W.J., SCHNEIDER D.M., LABOVITZ J. AND OPELLA J. 1988. High resolution solid-state '3C NMR Spectroscopy of sporopollenins from different plant taxa. *Plant Physiology* **86**: 134-136.

HABGOOD K.S. 2000. Two cryptospore-bearing land plants from the Lower Devonian (Lockhovian) of the Welsh Borderlands. *Botanical Journal of the Linnean Society* **133**: 203-227.

HABGOOD K.S., EDWARDS D. AND AXE L. 2002. New perspectives on *Cooksonia* from the Lower Devonian of the Welsh Borderland. *Botanical Journal of the Linnean Society* **139**: 339-359.

HAMMER Ø. AND HARPER D. 2006. Chapter 4: Morphometrics. In *Palaeontological data analysis*. Blackwell Publishing, Oxford: 78-156.

HANNA A.I. 2007. AAMToolbox: A shape and appearance modelling toolbox for Matlab: User Guide. Online PDF. UEA, Norwich.

HEMSLEY A.R., SCOTT A.C., BARRIE P.J. AND CHALONER W.G. 1996. Studies of fossil and modern spore wall biomacromolecules using ^{13}C solid-state NMR. *Annals of Botany* **78**: 83-94.

HIGGS K.T. 2004. An Early Devonian (Lochkovian) microflora from the Freshwater West Formation, Lower Old Red Sandstone, southwest Wales. *Geological Journal* **39**: 359-374.

HILLIER R.D. 2000. Silurian marginal marine sedimentation and the anatomy of the marine -Old Red Sandstone transition in Pembrokeshire, SW Wales. In FRIEND P.F. AND WILLIAMS B.P.J. (EDS.) *New Perspectives on the Old Red Sandstone*, Geological Society Special Publications, London, **180**: 343-354.

HILLIER R.D. AND WILLIAMS B.P.J. 2004. Sedimentation and tectonics: the marine Silurian-basal Lower Old Red Sandstone transition in southwest Wales. *Geological Journal* **39**: 237-256.

HILLIER R.D. AND WILLIAMS B.P.J. 2007. The Ridgeway Conglomerate Formation of SW Wales, and its implications. The end of the Lower Old Red Sandstone? *Geological Journal* **42**: 55-87.

HILLIER R.D., EDWARDS D. AND MORRISSEY L.B. 2008. Sedimentological evidence for rooting structures in the Lower Devonian Anglo-Welsh Basin (UK), with speculation in their producers. *Palaeogeography, Palaeoclimatology, Palaeoecology* **270**: 366-380.

HILLIER R.D., MARRIOTT S.B., WILLIAMS B.P.J. AND WRIGHT V.P. 2007. Possible climate variability in the Lower Old Red Sandstone Conigar Pit Sandstone Member (Early Devonian), South Wales, UK. *Sedimentary Geology* **202** (1-2): 35-57.

HØEG O.A. 1942. The Downtonian and Devonian flora of Spitzburgen. *Norges Svalbard- og Ishaus-Unders. Skr.* **83**: 1-228.

HOFFMEISTER W.S. 1959. Lower Silurian plant spores from Libya. *Micropaleontology* **5(3)**: 331-334.

HOLLAND C.H. AND RICHARDSON J.B. 1977. The British Isles; in *The Silurian-Devonian boundary*, MARTINSSON, A. (EDS); International Union of Geological Sciences, Series A, Stuttgart, no.5: 35-44.

HOOKER J.D. 1889. Pachytheca. *Annals of Botany* **3**: 135-140.

HOTTON C.L., HUEBER F.M., GRIFFING D.H. AND BRIDGE J.S. 2001. Early terrestrial plant environments: an example from the Emsian of Gaspé, Canada. In GENSEL P.G. AND EDWARDS D. (EDS.) *Plants invade the land: evolutionary and environmental perspectives*. Columbia University Press: New York: Chapter **11**: 179-212.

HUEBER F.M. 2001. Rotted wood-alga-fungus: the history and life of *Prototaxites* Dawson 1859. *Review of Palaeobotany and Palynology* **116**: 123-158.

ISHCHENKO T.A. 1975. The Late Silurian flora of Podolia. *Institute of Geological Science,* Academy of Science of the Ukrainian SSR, Kiev.

JAHREN H., PORTER S. AND KUGLITSCH J.J. 2003. Lichen metabolism identified in Early Devonian terrestrial organisms *Geology* **31**: 99-102.

JAMES D.M.D. 1987. Tectonics and sedimentation in the Lower Palaeozoic back-arc basin of S. Wales, UK: some quantitative aspects of basin development. *Norsk Geologisk Tidsskrift* **67**: 419-428.

JANVIER P., BLIECK A., GERRIENNE P. AND THANH T.-D. 1987. Faune et flore de la Formation de Sika (Dévonien inférieur) dans la presquîle de Dô Son (Viêt Nam). *Bull. Mus. Nat. Hist. Nat. Paris* **4e**, serie 9, section C: 291-301.

JENKINS G. 1998. An investigation of marine influence during deposition of the Lower Old Red Sandstone, Anglo-Welsh Basin. PhD Thesis, Cardiff University.

JERAM A. J., SELDEN P.A. AND EDWARDS D. 1990. Land animals in the Silurian: Aracheids and Myriapods from Shropshire, England. *Science* **250**: 658-661.

JOHNSON N.G. 1985. Early Silurian palynomorphs from Tuscarora Formation in central Pennsylvnian and their palaeobotanical and geological significant. *Review of Palaeobotany and Palynology* **45**: 307-360.

JOLLIFFE I.T. 2002. Principal Component Analysis. 2nd Edition. Springer Series in Statistics. Springer New York.

JONES T.P. AND CHALONER W.G. 1991. Fossil charcoal, its recognition and palaeoatmospheric significance. *Palaeogeography, Palaeoclimatology, Palaeoecology* **97**: 39-50.

JONKER F.P. 1979. *Prototaxites* in the Lower Devonian. *Palaeontographica B* **171**: 39-56.

KELLOGG E.A. 1999. Phylogenetic aspects of the evolution of C4 photosynthesis. In: SAGE R.F. AND MONSON R.K. (EDS.). *C4 plant biology*. San Diego, CA, USA: Academic Press, 411-444.

KELLOGG E. A. 2001. Evolutionary history of the grasses. *Plant Physiology* **125**: 1198-1205.

KENDALL D.G. 1984. Shape manifolds, procrustean metrics and complex projective shapes. *Bulletin of the London Mathematical Society* **16**: 81-121.

KENRICK P. 1988. Studies on Lower Devonian plants from South Wales. PhD thesis, University of Wales, Cardiff.

KENRICK P. AND CRANE P.R. 1997. The origin and early evolution of plants on land. *Nature* **389**: 33-39.

KENRICK P. AND EDWARDS D. 1988. A new zosterophyll from a recently discovered exposure of the Lower Devonian Senni Beds in Dyfed, Wales. *Botanical Journal of the Linnean Society* **98**: 97-115.

KENRICK P., EDWARDS D. AND DALES R.C. 1991. Novel ultrastructure in water-conducting cells of the Lower Devonian plant *Sennicaulis hippocrepiformis*. *Palaeontology* **34:** 751-766.

KERP H., HASS H. AND MOSBRUGGER V. 2001. New data on *Nothia aphylla* Lyon, 1964 ex El Saadawy et Lacey, 1979: a poorly known plant from the Lower Devonian Rhynie chert. *In* GENSEL P. G. AND EDWARDS D. (EDS) *Plants invade the land: evolutionary and environmental perspectives*. Columbia University Press, New York: Chapter **4**: pp. 52-82.

KERP H., TREWIN N. H. AND HASS H. 2004. New gametophytes from the Early Devonian Rhynie chert. *Transactions of the Royal Society of Edinburgh: Earth Sciences* **94**: 411-428.

KHADKIKAR A.S., CHAMYAL L.S. AND RAMESH R. 2000. The character and genesis of calcrete in Late Quaternary alluvial deposits, Gujarat, western India, and its bearing on the interpretation of ancient climates. *Palaeogeography, Palaeoclimatology, Palaeoecology* **162**: 239-261.

KIDSTON R. AND LANG W. H. 1917. On Old Red Sandstone plants showing structure, from the Rhynie chert bed, Aberdeenshire. Part I. *Rhynia gwynne-vaughani* Kidston & Lang. *Transactions of the Royal Society of Edinburgh* **51(24)**: 761-784.

KIDSTON R. AND LANG W. H. 1920. On Old Red Sandstone plants showing structure, from the Rhynie chert bed, Aberdeenshire. Part III. *Asteroxlon mackiei*, Kidston and Lang. *Transactions of the Royal Society of Edinburgh* **52(26)**: 643-680.

KING L.M. 1994. Subsidence analysis of Eastern Avalonian sequences: implications for Iapetus closure. *Journal of the Geological Society, London* **151**: 647-657. KIRKHAM D. AND POWERS W.L. 1972. *Advanced soil physics*. New York, Wiley-Interscience.

KNIGHTON A.D. AND NANSON G.C. 2000. Waterhole form and process in the anastomosing channel system of Cooper Creek, Australia. *Geomorphology* **35**: 101-117.

KOTYK M.E., BASINGER J.F., GENSEL P.G. AND DE FREITAS T.A. 2002. Morphologically complex plant macrofossils from the Late Silurian of Artic Canada. *American Journal of Botany* **89**: 1004-1013.

KRINGS M., TAYLOR T.N., HASS H., KERP H., DOTZLER N. AND HERMSEN E.J. 2007. Fungal endophytes in a 400-million-yr-old land plant: infection pathways, spatial distribution, and host responses. *New Phytologist* **174**: 648-657.

KULESHOV Y., HOEDT G.-D., WRIGHT W. AND BREWSTER A. 2002. Thunderstorm distribution and frequency in Australia. *Australian Meterological Magazine* **51**: 145-154.

KULESHOV Y., MACKERRAS D. AND DARVENIZA M. 2009. Spatial distribution and frequency of thunderstorms and lightning in Australia. In BETZ H.D., SCHUMANN U. AND LAROCHE P. (EDS.) *Lightning: Principles, Instruments and applications*, Springer. Chapter **8**: 187-208.

LANG W.H. 1927. Contributions to the study of the Old Red Sandstone flora of Scotland. VI. On *Zosterophyllum myretonianum*, Penh., and some other plant-remains from the Carmyllie Beds of the Lower Old Red Sandstone. *Transactions of the Royal Society of Edinburgh* **55**: 443-455.

LANG W.H. 1937. On the plant-remains from the Downtonian of England and Wales. *Philosophical Transactions of the Royal Society of London B* **227**: 245-291.

LECLERCQ S. 1942. Quelques plantes fossils recueillies dans le Dévonien inférieur des environs de Nonceveux (Bordure orientale du basin de Dinant). *Bulletin. Soc. Géol. Belg.* **65**: 193-211.

LI X.-X. AND CAI C.-Y. 1978. A type-section of Lower Devonian strata in southwest China with brief notes on the succession and correlation of its plant assemblages. *Acta Geol. Sin.* **52**: 1-12 (in Chinese with English abstract).

LOVE S.E. AND WILLIAMS B.P.J. 2000. Sedimentology, cyclicity and floodplain architecture in the Lower Old Red Sandstone of SW Wales. In FRIEND P.F. AND WILLIAMS B.P.J (EDS.) *New perspectives on the Old Red Sandstone*. Geological Society, London Special Publication **180**: 371-388.

LUBER A.A. AND WALTZ I.E. 1938. Klassifikatsiya I stratigraphicheskoe znachenie spor nekotorich kamennoughol'nich mestorojdenii SSSR. Trudy TSNIGRI, Moscow **105**: 1-45.

LÜTHI D., LE FLOCH M., BERNHARD B., BLUNIER T., BARNOLA J.-M., SIEGENTHALER U., RAYNAUD D., JOUZEL J., FISCHER H., KAWAMURA K., AND STOCKER T. F. 2008. High-resolution carbon dioxide concentration record 650,000-800,000 years before present. *Nature* **453**: 379-382.

LYNCH-STIEGLITZ J., STOCKER T., BROECKER W. AND FAIRBANKS R. 1995. The influence of air-sea exchange on isotopic composition of oceanic carbon: observations and modelling. *Global Biogeochemical Cycles* **9**: 653-665.

MACHETTE M.N. 1985. Calcic soils of the southwestern United States. In *Soils and Quaternary Geology of the South West United States.* Special Papers of the Geological Society of America **203**: 1-21.

MAGEE J.W., BOWLER J.M., MILLER G.H. AND WILLIAMS D.L.G. 1995. Stratigraphy, sedimentology, chronology and palaeohydrology of Quaternary lacustrine deposits at Madigan Gulf, Lake Eyre, South Australia. *Palaeogeography, Palaeoclimatology, Palaeoecology* **113**: 3-42.

MAGEE J.W., MILLER G.H., SPOONER N.A. AND QUESTIAUX D. 2004. Continuous 150 k.y. monsoon record from Lake Eyre, Australia: insolation-forcing implications and unexpected Holocene failure. *Geology* **32:** 885-888.

MALEK L., LÄTTIG K., HIESEL R., BRENNICKE A. AND KNOOP V. 1996. RNA editing in bryophytes and a molecular phylogeny of land plants. *EMBO Journal* **15**: 1403-1411.

MAROULIS J.C. AND NANSON G.C. 1996. Bedload transport of aggregated muddy alluvium from Cooper Creek, Central Australia: a flume study. *Sedimentology* **43**: 771-790.

MAROULIS J.C., NANSON G.C., PRICE D.M. AND PIETSCH T. 2007. Aeolian–fluvial interaction and climate change: source-bordering dune development over the past ~100 ka on Cooper Creek, central Australia. *Quaternary Science Reviews* **26**: 386 - 404.

MARRIOTT S.B. AND WRIGHT V.P. 1993. Palaeosols as indicators of geomorphic stability in two Old Red Sandstone alluvial suites, South Wales. *Journal of the Geological Society, London* **150**: 1109-1120.

MARRIOTT S.B. AND WRIGHT V.P. 1996. Sediment recycling on Siluro-Devonian floodplains. *Journal of the Geological Society, London* **153**: 661-664.

MARRIOTT S.B. AND WRIGHT V.P. 2004. Mudrock deposition in an ancient dryland system: Moor Cliffs Formation, Lower Old Red Sandstone, southwest Wales, UK. *Geological Journal* **39**: 277-298.

MARRIOTT S.B. AND WRIGHT V.P. 2006. Investigating paleosol completeness and preservation in mid-Paleozoic alluvial paleosols: A case study in paleosol taphonomy from the Lower Old Red Sandstone. In ALONSO-ZARZA A.M. AND TANNER L.H. (EDS.) *Paleoenvironmental Record and Application of Calcretes and Palustrine Carbonates,* Special Paper of the Geological Society of America **416**: 43-52.

MARRIOTT S.B., MORRISSEY L.B AND HILLIER R.D. 2009. Trace fossil assemblages in Upper Silurian tuff beds: Evidence of biodiversity in the Old Red Sandstone of Southwest Wales, UK. *Palaeogeography, Palaeoclimatology, Palaeoecology*, **274**: 160-172.

MAYR E. 1942. Systematics and the origin of species, from the viewpoint of a zoologist. Columbia University Press, New York.

MCELWAIN J.C. AND CHALONER W.G. 1995. Stomatal density and index of fossil plants track atmospheric carbon dioxide in the Palaeozoic. *Annals of Botany* **76**: 389-395.

MCELWAIN J.C. AND CHALONER W.G. 1996. The fossil cuticle as a skeletal record of environmental change. *Palaios* **11**: 376-388.

MCGREGOR D.C. 1961. Spores with proximal radial patterns from the Devonian of Canada. *Bull. Geol. Surv. Canada* **76**: 1-11.

MCGREGOR D.C. AND CAMFIELD M. 1976. Upper Silurian to Middle Devonian spores of the Moose River Basin, Ontario: *Geological Survey of Canada,* Bulletin **263**: 63pp.

MCGREGOR D.C. AND OWENS B. 1966. Illustrations of Canadian fossils. Devonian spores of eastern and northern Canada. *Geol. Surv. Canada papers* **30-66**: 1-66.

MÉNDEZ PADILLA MAQUEO E. 1997. Studies on *Pachytheca* Hooker and its allies from the Lower Devonian of Shropshire. M.Phil. thesis, Cardiff University.

MIALL A.D. 1996. The geology of fluvial deposits: sedimentary facies, basin analysis, and petroleum geology. Springer-Verlag Inc: Berlin: 582pp.

MILLER D.L., MORA C.I. DRIESE S.G. 2007. Isotopic variability in large carbonate nodules in Vertisols: Implications for climate and ecosystem assessments. *Geoderma* **142**: 104-111.

MILLER M.A. AND EAMES L.E. 1982. Palynomorphs from the Silurian Medinna Group (lower Llandovery) of the Niagara Gorge, Lewiston, New York, U.S.A. *Palynology* **6**: 21-254.

MORA C.I. AND DRIESE S.G. 1993. A steep Mid- to Late Paleozoic decline in atmospheric CO_2: evidence from the soil carbonate CO_2 paleobarometer. *Chemical Geology* **107**: 217-219.

MORA C.I., DRIESE S.G. AND COLARUSSO L.A. 1996. Middle to Late Paleozoic atmospheric CO_2 levels from soil carbonate and organic matter. *Science* **271**: 1105-1107.

MORA C.I., DRIESE S.G. AND SEAGER P.G. 1991. Carbon dioxide in the Paleozoic atmosphere: evidence from carbon-isotope compositions of pedogenic carbonate. *Geology* **19**: 1017-1020.

MOREL E., EDWARDS D. AND RODRIGUEZ M.I. 1995. The first record of *Cooksonia* from South America in Silurian rocks of Bolivia. *Geological Magazine* **132**: 449-452.

MORRISSEY L.B. AND BRADDY S.J. 2004. Terrestrial trace fossils from the Lower Old Red Sandstone, Southwest Wales. *Geological Journal* **39(3-4)**: 317-336.

MORRISSEY L.B., BRADDY S.J., BENNETT J.P., MARRIOTT S.J. AND TARRANT P.R. 2004. Fish trails from the Lower Old Red Sandstone of Tredomen Quarry, Powys, Southeast Wales. *Geological Journal* **39(3-4)**: 337-358.

MÜLLER R., NYSTUEN J.P. AND WRIGHT V.P. 2004. Pedogenic mud aggregates and palaeosol development in ancient dryland river systems: criteria for interpreting alluvial mudrock origin and floodplain dynamics. *Journal of Sedimentary Research* **74**: 537-551.

MUSSA D., BORGHI L., BERGAMASCHI S., SCHUBERT G., PEREIRA E. AND RODRIGUEZ M.A.C. 1996. Estudo Preliminar da Tafoflora de Formação Furnas, Bacia do Paraná, Brasil. *Annal Acad. Braz. Ci.* **68**: 65-89.

NANSON G.C., PRICE D.M. AND SHORT S.A. 1992. Wetting and drying of Australia over the past 300 ka. *Geology* **20**: 791-794.

NANSON G.C., RUST B.R. AND TAYLOR G. 1986. Coexistent mud braids and anastomosing channels in an arid-zone river: Cooper Creek, Central Australia. *Geology* **14**: 175-178.

NATIONAL RESOURCES CONSERVATION SERVICE. 1999. A basic system of soil classification for the making and interpreting soil surveys. Second Edition. United States Department of Agriculture.

NAUMOVA S.N. 1953. Spore-pollen assemblages of the Upper Devonian of the Russian Platform and their stratigraphic significance. *Tr. Inst. Geol. Nauk. Akud. S.S.S.R.* **143(60)**: 1-154.

NEWMAN M.J. AND ROOD R.T. 1977. Implications of solar evolution for the Earth's early atmosphere. *Science* **198**: 1035-1037.

NIKLAS K.J. 1976. Morphological and ontogenetic reconstructions of *Parka decipiens* Fleming and *Pachytheca* Hooker from the Lower Old Red Sandstone, Scotland. *Transactions of the Royal Society of Edinburgh* **69**: 483-499.

NORDT L., ATCHLEY S. AND DWORKIN S. 2003. Terrestrial evidence for two greenhouse events in the latest Cretaceous. *GSA Today* **13**: 4-9.

OBRHEL J. 1962. Die flora der Pridoli-Schichten (Budnany-Stufe) des mittelböhmishcen Silurs. *Geologie* **11**: 83-97.

OBRHEL J. 1968. Die Silur- und Devonflora des Barrandiums. *Palaeontol. Abh. Berlin* **2**: 635-793.

OSBORNE C.P. AND BEERLING D. 2006. Nature's green revolution: the remarkable evolutionary rise of C4 plants. *Philosophical Transactions of the Royal Society B* **361**: 173-194.

OWEN G. 1995. Senni Beds of the Devonian Old Red Sandstone, Dyfed, Wales - anatomy of a semiarid floodplain. *Sedimentary Geology* **95 (3-4)**: 221-235.

OWEN G. AND HAWLEY D. 2000. Depositional setting of the Lower Old Red Sandstone at Panytmaes Quarry, central South Wales: new perspectives on the significance and occurrence of 'Senni Beds' facies. In FRIEND P.F. AND WILLIAMS B.P.J. (EDS.) *New perspectives on the Old Red Sandstone. Geological Society of London, Special Publication* **180**: 389-400.

OWEN T., CESS R.D. AND RAMANATHAN V. 1979. Enhanced CO_2 greenhouse to compensate for reduced solar luminosity on early Earth. *Nature* **277**: 640-642.

PARKER A., ALLEN J.R.L. AND WILLIAMS B.P.J. 1983. Clay mineral assemblages of the Townsend Tuff Bed (Lower Old Red Sandstone). South Wales and the Welsh Borders. *Journal of the Geological Society*, **140**: 769-779.

PEARSON P.N. AND PALMER M.R. 2000. Atmospheric carbon dioxide concentrations over the past 60 million years. *Nature* **406**: 695-699.

PENHALLOW D.P. 1889. On *Nematophyton* and allied forms from the Devonian of Gaspé, with introductory notes by Sir William Dawson. *Transactions of the Royal Society of Canada* **6**: 27-47.

PETIT J.R., JOUZEL J., RAYMAUD D., BARNOV N.I., BARNOLA J.-M., BASILE I., BENDER M., CHAPPELLAZ J., DAVISK M., DELAVGUE G., DELMOTTE M., KOTLVAKOV M.V., LEGRAND M., LIPENKOV V.Y., LORIUS C., PÉPIN L., RITZ C., SALTZMANK E. AND STIEVENARD M. 1999. Climate and atmospheric history of the past 420,000 years from the Vostok ice core, Antarctica. *Nature* **399**: 429-436.

PIMENTEL N.L, WRIGHT V.P. AND AZEVEDO T.M. 1996. Distinguishing early groundwater alteration effects from pedogenesis in ancient alluvial basins: examples from the Palaeogene of southern Portugal. *Sedimentary Geology* **105**: 1-10.

PLUMSTEAD E.P. 1967. A general review of the Devonian fossil plants in the Cape System of South Africa. *Palaeontologia Africana* **10**: 1-83.

POPP B.N., TAKIGIKU R., HAYES J.M., LOUDA J.W. AND BAKER E.W. 1989. The post Palaeozoic chronology and mechanism of ^{13}C depletion in primary marine organic matter. *American Journal of Science* **289**: 436-454.

POTONIÉ H. 1893. Die flora des Rotliegenden von Thuringen *Kgl. Preuss Geol.* **9**: 1-29.

POTONIÉ R. 1956. Synopsis der Gattungen der Sporae dispersae. Teil. 1, Sporites. *Beih. Geol. Jb.* **23**: 1-103.

POTONIÉ R. AND KREMP G. 1954. Die Gattungen der paläozoischen Sporae dispersae and ihre Stratigrahie. *Geol. Jb.* **69**: 94-111.

POWERS D.W. AND EASTERLING R.G. 1982. Improved methodology for using embedded Markov chains to describe cyclical sediments. *Journal of Sedimentary Petrology* **52**: 913-923.

PRATT L.M., PHILLIPS T.L. AND DENNISON J.M. 1978. Evidence of non-vascular land plants from the Early Silurian (Llandoverian) of Virginia, U.S.A: *Review of Palaeobotany and Palynology* **25**: 121-149.

PROCHNOW S.J., NORDT L.C., ATCHLEY S.C. AND HUDEC M.R. 2006. Multi-proxy paleosol evidence for Middle and Late Triassic climate trends in eastern Utah. *Palaeogeography, Palaeoclimatology, Palaeoecology* **232**: 53-72.

PUNT W., HOEN P.P., BLACKMORE S., NILSSON S. AND LE THOMAS A. 2007. Glossary of pollen and spore terminology. *Review of Palaeobotany and Palynology* **143**: 1-81.

QIU Y.-L., CHO Y., COX J.C. AND PALMER J.D. 1998. The gain of three mitochondrial introns identifies liverworts as the earliest land plants. *Nature* **394**: 671-674.

QUAST A., HOEFS J. AND PAUL J. 2006. Pedogenic carbonates as a proxy for palaeo-CO_2 in the Palaeozoic atmosphere. *Palaeogeography, Palaeoclimatology and Palaeoecology* **242**: 110-125.

RABENHORST M.C., WILDING L.P. AND WEST L.T. 1984. Identification of pedogenic carbonates using stable isotope and microfabric analyses. *Soil Sci. Soc. Am. J.* **48**: 125-132.

RAVEN J.A. 1984. Physiological correlates of the morphology of early vascular plants. *Botanical Journal of the Linnean Society* **88**: 105-126.

RAVEN J.A. 1993. The evolution of vascular plants in relation to quantitative functioning of dead water-conducting cells and stomata. *Biological Review* **68**: 337-363.

RAVEN J.A. AND EDWARDS D. 2004. Physiological evolution of lower embryophytes: adaptations to the terrestrial environment. In HEMSLEY A. AND POOLE. I. (EDS.) *The evolution of plant physiology: from whole plant to ecosystems*. Linnean Society of London Symposium Series **21**, Elsevier Academic Press.

RAYNER R.J. 1988. Early land plants from South Africa. *Botanical Journal of the Linnean Society* **97**: 229-237.

REINSCH P.F. 1891. Micro-Palaephytologia Formationis Carboniferae, vol. 1, *Continens Trileteas et Stelideas*. Theo Krische, Erlangen, London.

REMY W. AND HASS H. 1996. New information on gametophytes and sporophytes of *Aglaophyton major* and inferences about possible environmental adaptations. *Review of Palaeobotany and Palynology* **90**: 175-193.

REMY W. AND REMY R. 1980. Devonian gametophytes with anatomically preserved gametangia. *Science* **208**: 295-296.

RENZAGLIA K.S., DUFF R.J., NIKRENT D.L, GARBARY D.J. 2000. Vegetative and reproductive innovations of early land plants: implications for a unified phylogeny. *Philosophical Transactions of the Royal Society B* **355**:769-793.

RETALLACK G.J. 1988. Field recognition of paleosols. In REINHARDT J. AND SIGLEO W.R. (EDS.) *Paleosols and weathering through geological time: principles and applications. Special Paper of the Geological Society of America* **216**: 1-20.

RETALLACK G.J. 1997. Early forest soils and their role in Devonian global change. *Science* **276**: 583-585.

RETALLACK G.J. 2001. Soils of the past: an introduction to Paleopedology. Second Edition. Blackwell Science, Oxford: 404pp.

RICHARDSON J.B. 1965. Middle Old Red Sandstone spore assemblages from the Orcadian basin north-east Scotland. *Palaeontology* **7(4)**: 559-605.

RICHARDSON J.B. 1967. Some British Lower spore assemblages and their stratigraphic significance. *Review of palaeobotany and palynology* **1**: 111-129.

RICHARDSON J.B. 1974. The stratigraphic utilization of some Silurian and Devonian miospore species in the northern hemisphere: an attempt at a synthesis. *International Symposium on NAMUR* **9**: 1-13.

RICHARDSON J.B. 1984. Mid–Paleozoic palynology, facies and correlation. *Proceedings of 27th International Geological Congress* **1**: 341-365.

RICHARDSON J.B. 1988. Late Ordovician and Early Silurian cryptospores and miospores from northeast Libya. *In* EL-ARNAUTI A., OWENS B. AND THUSU B. (EDS.) *Subsurface palynostratigraphy of northeast Libya*. Benghazi, Libya: Garyounis University Publications: 89-110.

RICHARDSON J.B. 1996a. Taxonomy and classification of some new Early Devonian cryptospores from England. *Special Papers in Palaeontology* **55**: 7-40.

RICHARDSON J.B. 1996b. Lower and Middle Palaeozoic records of terrestrial palynomorphs. In JANSONIUS J. AND MCGREGOR D.C. (EDS.) *Palynology: principles and applications*, Chapter 18A. American Association of Stratigraphic Palynologists Foundation, Vol. **2**: 555-574.

RICHARDSON J.B. 2002. English Lower Devonian cryptospores and the habit and habitat of their parent plants. *In* BROCK G.A. AND TALENT J.A. (EDS.) *IPC 2002, First International Palaeontological Congress Geological Society of Australia, Abstracts* **68**: 137.

RICHARDSON J.B. 2007. Cryptospores and miospores, their distribution patterns in the Lower Old Red Sandstone of the Anglo-Welsh Basin, and the habitat of their parent plants. *Bulletin of Geosciences* **84**: 355-364.

RICHARDSON J.B. AND IOANNIDES N.S. 1976. Silurian palynomorphs from the Tanezzuft and Acacus formations, Tripolitania, North Africa. *Micropalaeontology* **19**: 257-307.

RICHARDSON J.B. AND LISTER T.R. 1969. Upper Silurian and Lower Devonian spore assemblages from the Welsh Borderland and South Wales. *Palaeontology* **12**: 37-43.

RICHARDSON J.B. AND MCGREGOR D.C. 1986. Silurian and Devonian spore zones of the Old Red Sandstone Continent and adjacent regions. *Geological Survey of Canada*, Bulletin **364**: 1-79.

RICHARDSON J.B. AND RASUL S.M. 1990. Palynofacies in a Late Silurian regressive sequence in the Welsh Borderland and Wales. *Journal of the Geological Society, London* **147**: 675-686.

RICHARDSON J.B., FORD J.H. AND PARKER F. 1984. Miospores, correlation and age of some of Scottish Lower Old Red Sandstone sediments from the Strathmore region (Fife and Angus). *Journal of micropalaeontology* **3(2)**: 109-124.

RICHARDSON J.B., RASUL S.M. AND AL-AMERI T. 1981. Acritarchs, miospores and correlation of the Ludlovian- Downtonian and Silurian- Devonian boundaries. *Review of Palaeobotany and Palynology* **34**: 209-224.

RICHARDSON J.B., RODRINGUEZ R. AND SUTHERLAND S.J.E. 2000. Palynology and recognition of the Silurian/ Devonian boundary in some British terrestrial sediments by correlation with Cantabrian and other European marine sequences - A process report. *In*

BULTYNCK P. (ED.) Subcommission of Devonian Stratigraphy Fossil groups important for boundary definition, *Courier Forschungsinstitut Senkenberg* **220**: 1-7.

RICHARDSON J.B., RODRINGUEZ R. AND SUTHERLAND S.J.E. 2001. Palynological zonation of Mid-Palaeozoic sequences from the Cantabrian Mountains, NW Spain: implications for inter-regional and interfacies correlation of the Ludford/Pridoli and Silurian/Devonian boundaries, and plant dispersal patterns. *Bulletin of the Natural History Museum, London (Geol)* **57(2)**: 115-162.

RICHARDSON J.B., STREEL M., HASSAN A. AND STEEMANS PH. 1982. A new spore assemblage to correlate between the Breconian (British Isles) and the Gedinnian (Belgium). *Annales de la societe Geologique de Belgique* **105**: 135-143.

RICKARD D.T. AND LUTHER G.W. III 1997. Kinetics of pyrite formation by the H_2S oxidation of iron (II) monosulphide in aqueous solutions between 25 and 125°C: the mechanism. *Geochimica et Cosmochimica Acta* **61**: 135–147.

ROBINSON S.A., ANDREWS J.E., HESSELBO S.P., RADLEY J.D., DENNIS P.F., HARDING I.C. AND ALLEN P. 2002. Atmospheric ρCO_2 and depositional environment from stable-isotope geochemistry of calcrete nodules (Barremian, Lower Cretaceous, Wealden Beds, England). *Journal of the Geological Society, London* **159**: 215-224.

ROGERSON C., EDWARDS D., AXE L. AND DAVIES K. L. 2002. A new embryophyte from the Upper Silurian of Shropshire, England. In WYSE JACKSON P.W., PARKES M.A. AND WOOD R. (EDS.) Studies in Palaeozoic palaeontology and biostratigraphy in honour of Charles Hepworth Holland. *Special papers in Palaeontology* **67**: 233-249.

ROHLF F.J. AND BOOKSTEIN F.L. (EDS.) 1990. Proceedings of the Michigan Morphometrics Workshop, Special Publication no. 2. The University of Michigan Museum of Zoology, Ann Arbor, 380 pp.

ROMANEK C.S., GROSSMAN E.L. AND MORSE J.W. 1992. Carbon isotopic fractionation in synthetic aragonite and calcite: effects of temperature and precipitation rate. *Geochimica et Cosmochimica Acta* **56**: 419-430.

ROYER D.L. 1999. Depth to pedogenic carbonate horizon as a paleoprecipitation indicator. *Geology* **27**: 1123-1126.

ROYER D.L. 2001. Stomatal density and stomatal index as indicators of paleoatmospheric CO_2 concentration. *Review of Palaeobotany and Palynology* **114**:1-28.

ROYER D.L., BERNER R.A., MONTAÑEZ I.P., TABOR, N.J. AND BEERLING D.J. 2004. CO_2 as a primary driver of Phanerozoic climate. *GSA Today* **14 (3)**: 4-10.

RUST B.R. 1981. Sedimentation in an arid-zone anastomosing fluvial system: Cooper's Creek, central Australia. *Journal of Sedimentary Petrology* **51 (3)**: 745-755.

SALOMONS W., GOUDIE A. AND MOOK W.G. 1978. Isotopic composition of calcrete deposits from Europe, Africa and India. *Earth Surface Processes*, **3**: 43-57.

SALTZMAN M.R. 2002. Carbon isotope ($\delta^{13}C$) stratigraphy across the Silurian-Devonian transition in North America: evidence for a perturbation of the global carbon cycle. *Palaeogeography, Palaeoclimatology, Palaeoecology* **187**: 83-100.

SCHMIDT W. AND TEICHMÜLLER M. 1954. Pflanzen-Reste aus dem Gedinne des Hohen Venns. *Geol Jb.* **69**: 89-102.

SCHWEITZER H.-J. 1983. Die Unterdevonflora des Rheinlandes 1. Teil. *Palaeontographica B* **189**: 1-138.

SCOTESE C. 2003. Paleomap Project website. http://www.scotese.com.

SCOTT A.C. 1989. Observations on the nature and origin of fusain. *International Journal of Coal Geology* **12**: 443-475.

SENKEVITCH M.A. 1975. New Devonian psilophytes from Kazakhstan. *Esheg. Vses. Palaeotol. Obschestva* **21**: 288-298 (in Russian).

SHAW J. AND RENZAGLIA K. 2004. Phylogeny and diversification of bryophytes. *American Journal of Botany* **91(10)**: 1557-1581.

SHEAR W.A. AND SELDEN P.A. 2001. Rustling in the undergrowth: animals in early terrestrial ecosystems. In GENSEL P. AND EDWARDS D. (EDS.) *Plants invade the land: evolutionary and environmental perspectives*. Columbia University Press, New York. Chapter **3**: 29-51.

SHUTE C.H. AND EDWARDS D. 1989. A new rhyniopsid with novel sporangium organisation from the Lower Devonian of South Wales. *Botanical Journal of the Linnean Society* **100**: 111-137.

SIEGENTHALER U., STOCKER T.F., MONNIN E., LÜTHI D., SCHWANDER J., STAUFFER B., RAYNAUD D., BARNOLA J.-M., FISCHER H., MASSON-DELMOTTE V. AND JOUZEL J. 2005. Stable carbon cycle-climate relationship during the Late Pleistocene. *Science* **310**: 1313-1317.

SIMON J.B. AND BLUCK B.J. 1982. Palaeodrainage of the southern margin of the Caledonian mountain chain in the northern British Isles. *Transactions of the Royal Society of Edinburgh: Earth Sciences* **73**: 11-15.

SMITH A.H.V AND BUTTERWORTH M.A. 1967. Miospores in the coal seams of the carboniferous of Great Britain. *Special Papers in Palaeontology* **1**: 324pp.

SOPER N.J. AND WOODCOCK N.H. 2003. The lost Old Red Sandstone of England and Wales: a record of post-Iapetan flexure or Early Devonian transtension? *Geological Magazine* **140(6)**: 627-647.

SPICER R.A. 1977. The pre-depositional formations of some leaf impressions. *Palaeontology* **20**: 907-912.

SPIKER E.C.AND HATCHER P.G. 1987. The effects of early diagenesis on the chemical and stable carbon isotopic composition of wood. *Geochimica et Cosmochimica Acta* **51**: 1385-1391.

STEEMANS P. 1989. Palynostratigraphie de l'eodévonien dans l'ouest de l'europe. *Prof. Pap. Mém. Explor. Carte Géol. Min. Belg.* **27**: 453 pp.

STEEMANS P., LE HÉRISSE A. AND BOZDOGAN N. 1996. Ordovician and Silurian cryptospores and miospores from southeastern Turkey. *Review of Palaeobotany and Palynology* **93**: 35-76.

STEEMANS P., LE HÉRISSÉ A., MELVIN J., MILLER M.A., PARIS F., VERNIERS J. AND WELLMAN C.H. 2009. Origin and Radiation of the Earliest Vascular Land Plants. *Science* **324**: 353.

STEPANOV S.A. 1975. Phytostratigraphy of the key sections of the Devonian of the marginal regions of the Kuznetsk Basin. *Trans. Siber. Inst. Geol. Geophys. Min. Res.* **211**: 1-150.

STREEL M. 1964. Une association de spores du Givétien inférieur de la Vesdre, a Goé (Belgique). *Ann. Soc. Géol. De Belgique* **87**: 1-30.

STREEL M. 1967. Associations de spores du Dévonien inférieur Belge et leur signification stratigraphique. *Ibid.* **90**: 11-54.

STROTHER P.K. 1998. Non-marine palynomorphs from the Middle Cambrian Bright Angel Shale, Grand Canyon, USA. Abstracts, CIMP Symposium and Workshops, Pisa, September 11–15 1998, Dipartimento di Scienze della Terra, 27.

STROTHER P.K. AND TRAVERSE A. 1979. Plant microfossils from Llandovery and Wenlock rocks of Pennslyvania. *Palynology* **3**: 1-21.

STROTHER P.K., AL-HAJRI S. AND TRAVERSE A. 1996. New evidence for land plants from the lower Middle Ordovician of Saudi Arabia. *Geology* **24(1)**: 55-58.

TABOR N.J., YAPP C.J. AND MONTAÑEZ I.P. 2004. Geothite, calcite and organic matter from Permian and Triassic soils: Carbon isotopes and CO_2 concentrations. *Geochimica et Cosmochimica Acta* **68**: 1503-1517.

TAJIKA E. 1998. Climate change during the last 150 million years: reconstruction from a carbon cycle model. *Earth and Planetary Science Letters* **160**: 695-707.

TAJIKA E. AND MATSUI T. 1992. Evolution of terrestrial proto-CO_2 atmosphere coupled with thermal history of the earth. *Earth and Planetary Science Letters* **113**: 251-266.

TANS P. 2008. NOAA/ESRL (*www.esrl.noaa.gov/gmd/ccgg/trends/*)

TAYLOR T. N., HASS H. AND KERP H. 1999. The oldest fossil ascomycetes. *Nature* **399**: 648.

TAYLOR T.N., HASS H., KRINGS M., KLAVINS S.D. AND KERP H. 2004. Fungi in the Rhynie chert: a view from the dark side. *Transactions of the Royal Society of Edinburgh: Earth Sciences* **94**: 457-473.

TAYLOR T.N., KERP H. AND HASS H. 2005. Life history biology of early land plants: Deciphering the gametophyte phase. *Proceedings of the National Academy of Sciences of the USA* **102**: 5892-5897.

TAYLOR T.N., REMY W. AND HASS H. 1994. *Allomyces* in the Devonian. *Nature* **367**: 601.

TAYLOR T. N., REMY W., HASS H. AND KERP H. 1995. Fossil arbuscular mycorrhizae from the Early Devonian. *Mycologia* **87**: 560-573.

TAYLOR W.A. AND STROTHER P.A. 2008. Ultrastructure of some Cambrian palynomorphs from the Bright Angel Shale, Arizona, USA. *Review of Palynology and Palaeobotany* **151**: 41-50.

TAYLOR W.A. AND WELLMAN C.H. 2009. Ultrastructure of enigmatic phytoclasts (banded tubes) from the Silurian-Lower Devonian: Evidence for affinities and role in early terrestrial ecosystems. *Palaios* **24**: 167-180.

TIDWELL W.D. AND NAMBUDIRI E.M.V. 1989. *Tomlinsonia thomassonii*, gen. et sp. nov., a permineralized grass from the Upper Miocene Ricardo Formation, California. *Review of Palaeobotany and Palynology* **60**: 165-177.

TIMS J.D. AND CHAMBERS T.C. 1984. Rhyniophytina and Trimerophytina from the early land flora of Victoria, Australia. *Palaeontology* **27(2)**: 265-279.

THOMAS R.G., SMITH D.G., WOOD S.M., VISSER J., CALVERLEY-RANGE E.A. AND KOSTER E.H. 1987. Inclined heterolithic stratification - terminology, descriptions, interpretation and significance. *Sedimentary Geology* **53**: 123-179.

THOMAS R.G., WILLIAMS B.P.J., MORRISSEY L.B., BARCLAY W.J. AND ALLEN K.C. 2006. Enigma variations: the stratigraphy, provenance, palaeoseismicity and depositional history of the Lower Old Red Sandstone Cosheston Group, south Pembrokeshire, Wales. *Geological Journal* **41**: 481-536.

THOMASSON J.R., NELSON M.E., AND ZAKREZEWSKI R.J. 1986. A fossil grass (Gramineae: Chloridoideae) from the Miocene with Kranz anatomy. *Science* **233**: 876-878.

THOMPSON D.W. 1917. On growth and form. Cambridge University Press. 793 p.

TOOTH S. 2000. Process, form and change in dryland rivers: a review of recent research. *Earth-Science Reviews* **51**: 67-107.

TORO M., CHAMON O., SALGUERO R. AND VARGAS C. 1997. Las plantas de la formacion Kirusillas (Silurico) en la region de La Angostura departamento de Cochabamba. *Mem. del. XII Congreso Geol. de Bolivia- Tarija, Bolivia*: 523-529.

TORSVIK T.H., SMETHURST M.A., MEERT J.G., VAN DER VOO R., MCKERROW W.S., BRASIER M.D., STURT B.A. AND WALDERHAUG H.J. 1996. Continental break-up and collision in the Neoproterozoic and Palaeozoic - A tale of Baltica and Laurentia. *Earth Science Reviews* **40**: 229-258.

TRENCH A. AND TORSVIK T.H. 1992. The closure of the Iapetus Ocean and Tornquist Sea: new palaeomagnetic constraints. *Journal of the Geological Society, London* **149**: 867-870.

VAUGHAN A. AND NICHOLS G. 1995. Controls on the deposition of charcoal: implications for sedimentary accumulations of fusain. *Journal of Sedimentary Research*, **A65(1)**: 129-135.

VEIZER J., ALA D., AZMY K., BRUCKSCHEN P., BUHL D., BRUHN F., CARDEN G.A.F., DIENER A., EBNETH S., GODDERIS Y., JASPER T., KORTE C., PAWELLEK F., PODLAHA O.G. AND STRAUSS H. 1999. $^{87}Sr/^{86}Sr$, $\delta^{13}C$ and $\delta^{18}O$ evolution of Phanerozoic seawater. *Chemical Geology* **161**: 59-88.

VERRECCHIA E.P., FREYTET P., VERRECCHIA K.E. AND DUMONT J.L.1995. Spherulites in calcrete laminar crusts: biogenic $CaCO_3$ precipitation as a major contributor to crust formation. *Journal of Sedimentary Research* **65**: 690-700.

VYSHEMIRSKIY V.S., DOIL'NITSYN Y.F., PERTSEVA A.P. AND SHORIN V.P. 1975. The behaviour of stable carbon isotopes in coals during coalification. *Dokl. Akad. Nauk* SSSR **218**: 190-192.

WANG Y., LI J. AND WANG R. 1997. Latest Ordovician cryptospores from southern Xinjiang, China. *Review of Palaeobotany and Palynology* **99**: 61-74.

WEAVER J.D. 1975. Seismically-induced load structures in the basal Coal Measures, South Wales. *Geological Magazine* **113**: 535-543.

WELLMAN C.H. 1993a. A land plant microfossil assemblage of Mid Silurian age from the Stonehaven Group, Scotland. *Journal of Micropalaeontology* **12**: 47-66.

WELLMAN C.H. 1993b. A Lower Devonian sporomorph assemblage from the Midland Valley of Scotland. *Transactions of the Royal Society of Edinburgh, Earth Sciences* **84**: 117-136.

WELLMAN C.H. 1995. "Phytodebris" from Scottish Silurian and Lower Devonian continental deposits. *Review of Palaeobotany and Palynology* **84**: 255-279.

WELLMAN C.H. 1996. Cryptospores from the type area of the Caradoc Series in Southern Britain. *Special Papers in Palaeontology* **55**: 103-136.

WELLMAN C.H. 1999. Sporangia containing *Scylaspora* from the Lower Devonian of the Welsh Borderland. *Palaeontology* **42**: 67-81.

WELLMAN C.H. AND RICHARDSON J.B. 1993. Terrestrial plant microfossils from Silurian inliers of the Midland Valley of Scotland. *Palaeontology* **36(1)**: 155-193.

WELLMAN C.H. AND RICHARDSON J.B. 1996. Sporomorph assemblages from the 'Lower Old Red Sandstone' of Lorne, Scotland. *Special Papers in Palaeontology* **55**: 41-101.

WELLMAN C.H., EDWARDS D. AND AXE L. 1998a. Permanent dyads in sporangia and spore masses from the Lower Devonian of the Welsh Borderland. *Botanical Journal of the Linnean Society* **127**: 117-147.

WELLMAN C.H., EDWARDS D. AND AXE L. 1998b. Ultrastructure of laevigate hilate spores in sporangia and spore masses from the Upper Silurian and Lower Devonian of the Welsh Borderland. *Philosophical Transactions of the Royal Society London* **353**: 1983-2004.

WELLMAN C.H., HABGOOD K., JENKINS G. AND RICHARDSON J.B. 2000. A new plant assemblage (mircofossil and megafossil) from the Lower Old Red Sandstone of the Anglo-Welsh Basin: its implications for the palaecology of early terrestrial ecosystems. *Review of Palaeobotany and Palynology* **109**: 16-96.

WELLMAN C.H., OSTERLOFF P.L AND MOHIUDDIN U. 2003. Fragments of the earliest land plants. *Nature* **425**: 282-285.

WHITE E.I. 1950. The vertebrate fauna of the Lower Old Red Sandstone of the Welsh Borders. *Bulletin of the British Museum (Natural History) Geology Series* **1**: 51-67.

WHITE E.I. 1961. The Old Red Sandstone of Brown Clee Hill and the adjacent area. II Palaeontology. *Bulletin of the British Museum (Natural History) Geology Series* **5(7)**: 243-310.

WIGLEY T. M. L. 1983. The pre-industrial carbon dioxide level. *Climatic Change* **5 (4)**: 315-320.

WILDING L. AND TESSIER L. 1988. Genesis of Vertisols: shrink –swell phenomena. In: WILDING L. AND PUENTES R. (EDS.) *Vertisols: Their Distribution, Properties, Classification, and Management,* Texas A&M University Printing Center, College Station: 55-79.

WILLIAMS B.P.J AND HILLIER R.D. 2004. Variable alluvial sandstone architecture within the Lower Old Red Sandstone, southwest Wales. *Geological Journal* **39**: 257-275.

WILLIAMS C. A. AND KRAUSE F. F. 1998. Pedogenic-phreatic carbonates on a Middle Devonian (Givetian) terrigenous alluvial-deltaic plain, Gilwood Member (Watt Mountain Formation), northcentral Alberta, Canada. *Sedimentology* **45**: 1105-1124.

WOLFE J.A. 1993. A method of obtaining climate parameters from leaf assemblages. USGS Bulletin **2040**: 1-71.

WOODCOCK N.H. 1988. Strike-slip faulting along the Church Stretton Lineament, Old Radnor Inlier, Wales. *Journal of the Geological Society* **145**: 925-933.

WOODCOCK N.H. AND BASSETT M.G. 1993. Geological excursions in Powys, Central Wales. Published on behalf of the Geologists' Association, South Wales Group University of Wales Press/National Museum of Wales.

WOODCOCK N.H. AND GIBBONS W. 1988. Is the Welsh Borderland Fault System a terrane boundary? *Journal of the Geological Society* **145**: 915-923.

WRIGHT V.P. 1992. Paleosol recognition: A guide to early diagenesis in terrestrial settings. In WOLF K.H. AND CHILINGARIAN G.V. (EDS). *Diagenesis III*, Developments in Sedimentology **47**: 591-619.

WRIGHT V.P. 2007. Calcretes. In NASH D.J. AND MACLAREN S.J. (EDS.) *Geochemical Sediments and Landscapes*, Blackwell, Oxford.

WRIGHT V.P. AND MARRIOTT S.B. 1996. A quantitative approach to soil occurrence in alluvial deposits and its application to the Old Red Sandstone of Britain. *Journal of the Geological Society* **153**: 907-913.

WRIGHT V.P. AND MARRIOTT S.B. 2007. The dangers of taking mud for granted: lessons from Lower Old Red Sandstone dryland river systems of South Wales. *Sedimentary Geology* **195**: 91-100.

WRIGHT V.P. AND TUCKER M.E. 1991. Calcretes: Introduction. *International Association of Sedimentologists*, reprint series **3**: 1-22.

WRIGHT V.P. AND VANSTONE S.D. 1991. Assessing the carbon dioxide content of ancient atmospheres using palaeo-calcretes: theoretical and empirical constraints. *Journal of the Geological Society, London* **148**: 945-947.

WRIGHT V.P., PLATT N.H., MARRIOTT S.B. AND BECK V.H. 1995. A classification of rhizogenic (root-formed) calcretes, with examples from the Upper Jurassic–Lower Cretaceous of Spain and Upper Cretaceous of southern France: *Sedimentary Geology* **100**: 143-158.

YAPP C.J. AND POTHS H. 1992. Ancient atmospheric CO_2 pressures inferred from natural goethites. *Nature* **355**: 342-344.

YAPP C.J. AND POTHS H. 1994. Productivity of pre-vascular continental biota inferred from natural geothite. *Nature* **368**: 49-51.

YAPP C.J. AND POTHS H. 1996. Carbon isotopes in continental weathering environments and variations in ancient atmospheric CO_2 pressure. *Earth and Planetary Science Letters* **137**: 71-82.

INTEGRATED APPROACHES TO THE RECONSTRUCTION OF EARLY LAND VEGETATION AND ENVIRONMENTS FROM LOWER DEVONIAN STRATA, CENTRAL-SOUTH WALES

VOLUME II OF II

PLATES AND APPENDICES

A THESIS SUBMITTED TO CARDIFF UNIVERSITY FOR THE DEGREE OF DOCTOR OF PHILOSOPHY BY

JENNIFER LOUISE MORRIS MSCI

SCHOOL OF EARTH AND OCEAN SCIENCES
CARDIFF UNIVERSITY

AUGUST 2009

CONTENTS

VOLUME II OF II

PLATES AND APPENDICES

PLATES

Chapter 3: RECONSTRUCTING VEGETATION FROM OLD RED SANDSTONE STRATA

Plate 3.1: cf. *Cooksonia caledonica*/ *Renalia* sp. specimens..... pP-1

Plate 3.2: cf. *Cooksonia caledonica*/ *Renalia* sp. specimens: anatomy..... pP-2

Plate 3.3: *Cooksonia hemisphaerica* specimens..... pP-3

Plate 3.4: *Cooksonia hemisphaerica* specimens: anatomy..... pP-4

Plate 3.5: *Cooksonia* cf. *cambrensis* specimens..... pP-5

Plate 3.6: cf. *Uskiella reticulata* / *Tarrantia salopensis* specimens..... pP-6

Plate 3.7: cf. *Uskiella reticulata* / *Tarrantia salopensis* specimens: anatomy..... pP-7

Plate 3.8: *Salopella allenii* specimens..... pP-8

Plate 3.9: *Salopella allenii* specimens: anatomy..... pP-9

Plate 3.10: *Salopella* cf. *marcensis* specimens..... pP-10

Plate 3.11: *Salopella* cf. *marcensis* specimens: anatomy.....pP-11

Plate 3.12: Elongate club-shaped sporangia specimens.....pP-12

Plate 3.13: Elongate club-shaped sporangia specimens: anatomy.....pP-13

Plate 3.14: Mesofossil type A specimens..... pP-14

Plate 3.15: Mesofossil type B specimens.....pP-15

Plate 3.16: Mesofossil type C specimens.....pP-16

Plate 3.17: Mesofossil type D specimens.....pP-17

Plate 3.18: *Tortilicaulis* cf. *offaeus* specimens..... pP-18

Plate 3.19: Other mesofossils with elongate sporangia..... pP-19

Plate 3.20: Cephalaspid fish specimen and *Prototaxites* sp. /*Nematasketum* sp. specimens.....pP-20

Plate 3.21: *Prototaxites* sp./*Nematasketum* sp. specimens: anatomy.....pP-21

Plate 3.22: Hyphae specimens..... pP-22

Plate 3.23: *Pachytheca* specimens.....pP-23

Chapter 5: THE DISPERSED SPORE RECORD

Plate 5.1: Fused laevigate tetrads..... pP-24

Plate 5.2: Fused laevigate dyads..... pP-25
Plate 5.3: Fused sculptured tetrads..... pP-26
Plate 5.4: Unfused laevigate tetrads..... pP-27
Plate 5.5: Unfused laevigate tetrads and dyads..... pP-28
Plate 5.6: Unfused sculptured tetrads..... pP-29
Plate 5.7: Laevigate hilate cryptospores..... pP-30
Plate 5.8: Laevigate and apiculate sculptured hilates..... pP-31
Plate 5.9: Apiculate sculptured hilates and dyad..... pP-32
Plate 5.10: Apiculate sculptured hilates, dyads and tetrad..... pP-33
Plate 5.11: Apiculate sculptured hilates and dyad (continued)..... pP-34
Plate 5.12: Apiculate sculptured hilates and dyads (continued)..... pP-35
Plate 5.13: Spinose sculptured hilates, dyads and tetrad..... pP-36
Plate 5.14: Spinose sculptured hilates and dyads (continued)..... pP-37
Plate 5.15: Murornate sculptured hilates, dyads and tetrad..... pP-38
Plate 5.16: Murornate sculptured hilates, dyads and tetrad..... pP-39
Plate 5.17: Murornate sculptured hilates and dyad (continued)..... pP-40
Plate 5.18: Verrucate sculptured hilates, dyads and tetrads..... pP-41
Plate 5.19: Verrucate sculptured hilates and tetrad..... pP-42
Plate 5.20: Laevigate alete monads..... pP-43
Plate 5.21: Enveloped tetrads..... pP-44
Plate 5.22: Enveloped tetrads (continued)..... pP-45
Plate 5.23: Enveloped hilates and dyads..... pP-46
Plate 5.24: *Incertae sedis*..... pP-47
Plate 5.25: *Incertae sedis* (continued)..... pP-48
Plate 5.26: *Incertae sedis* (continued)..... pP-49
Plate 5.27: Laevigate retusoid triletes..... pP-50
Plate 5.28: Laevigate retusoid triletes and tetrads of laevigate triletes..... pP-51
Plate 5.29: Apiculate sculptured retusoid triletes..... pP-52
Plate 5.30: Murornate sculptured retusoid triletes..... pP-53
Plate 5.31: Laevigate crassitate triletes..... pP-54
Plate 5.32: Laevigate crassitate triletes (continued)..... pP-55
Plate 5.33: Apiculate sculptured crassitate triletes..... pP-56
Plate 5.34: Murornate sculptured crassitate triletes..... pP-57
Plate 5.35: Verrucate sculptured crassitate triletes..... pP-58

Plate 5.36: Laevigate patinate triletes..... pP-59
Plate 5.37: Muromate sculptured patinate triletes and triletes with perispores..... pP-60

Chapter 6: LOWER DEVONIAN OLD RED SANDSTONE DEPOSITIONAL ENVIRONMENTS
Plate 6.1: Intraformational conglomerates from Tredomen Quarry..... pP-61
Plate 6.2: Green-grey sandstones from Tredomen Quarry pP-62
Plate 6.3: Siltstones from Tredomen Quarry..... pP-63
Plate 6.4: Siltstones from Tredomen Quarry (continued).....pP-64
Plate 6.5: Heterolithics from Tredomen Quarry..... pP-65
Plate 6.6: Mudstones from Tredomen Quarry.....pP-66
Plate 6.7: Pedified mudstones from Tredomen Quarry pP-67
Plate 6.8: Intraformational conglomerates and sandstones from Targrove Quarry...pP-68
Plate 6.9: a to c: Siltstones and mudstones from Targrove Quarry.....pP-68
d and e: Chapel Point Calcrete at Llansteffan.....pP-69

Chapter 7: TAPHOFACIES AND TAPHONOMIC CONSTRAINTS ON PALAEOECOLOGICAL INTERPRETATIONS
Plate 7.1: Taphofacies 1 and 2.....pP-70
Plate 7.2: Taphofacies 3 and 4..... pP-71
Plate 7.3: Taphofacies 5 and 6..... pP-72
Plate 7.4: Taphofacies 7, 8 and 9.....pP-73

Chapter 8: PREDICTING THE ATMOSPHERIC ρCO_2 LEVEL DURING THE EARLY DEVONIAN USING STABLE ISOTOPIC ANALYSIS
Plate 8.1: Carbonate nodules from Tredomen Quarry, selected for isotopic analysis..... pP-74
Plate 8.2: Carbonate nodules from Tredomen Quarry, selected for isotopic analysis (continued)..... pP-75

APPENDICES

I: TREDOMEN PALAEOBOTANY COLLECTION DATABASE

a: *Megafossil and mesofossil collection*.....on DVD

b: *Palynological collection*.....on DVD

II: MEGAFOSSIL MEASUREMENTS pII-1

III: MESOFOSSIL MEASUREMENTS pIII-1

IV: SHAPES USED IN GEOMETRIC MODELS.....pIV-1

V: PALYNOLOGICAL COUNTS AND MEASUREMENTS

a: *Palynological assemblages collected from Tredomen Quarry strata and core*..... pV-2

b: *Palynological counts of each assemblage*..... pV-3

c: *Spore morphotypes*..... pV-27

d: *Spore size ranges*..... on DVD

VI: TREDOMEN QUARRY AND TARGROVE QUARRY SEDIMENTOLOGICAL DATABASE. pVI-1

VII: TREDOMEN QUARRY AND TARGROVE QUARRY SEDIMENTOLOGICAL ANALYSIS.

a: *Sedimentary analysis of Tredomen Quarry*.....pVII-1

b: *Sedimentary analysis of Targrove Quarry*.....pVII-13

VIII: MARKOV CHAIN ANALYSIS

a: *Markov Chain Analysis of total Tredomen Quarry sequence*..... pVIII-2

b: *Markov Chain Analysis of lower Tredomen Quarry sequence*..... pVIII-5

c: *Markov Chain Analysis of upper Tredomen Quarry sequence*..... pVIII-8

d: *Embedded Markov Chain Analysis of total Tredomen Quarry sequence*... pVIII-12

e: *Embedded Markov Chain Analysis of lower Tredomen Quarry sequence*.. pVIII-26

f: *Embedded Markov Chain Analysis of upper Tredomen Quarry sequence*.. pVIII-41

g: *Markov Chain Analysis results summary*..... pVIII-53

IX: IS THE CHANNEL COUNTRY OF CENTRAL AUSTRALIA A SUITABLE ANALOGUE FOR THE OLD RED SANDSTONE?.....pIX-1

Plate 3.1: cf. *Cooksonia caledonica/ Renalia* sp. specimens

a: JM010a. Reniform sporangium with concave sporangial-axial junction and curved subtending axis.

b: JM109b. Reniform sporangium with concave sporangial-axial junction and slightly curved subtending axis. Sporangium surrounded by border (see arrow).

c: JM034d. Transversely-elliptical sporangium with slightly concave sporangial-axial junction (see arrow).

d: JM385a. Transversely-elliptical sporangium with slightly concave sporangial-axial junction (see arrow). Subtending axis is curved.

e: JM012b. Circular sporangium with concave sporangial-axial junction (see arrow).

f: RHJM04. Circular sporangium with very concave sporangial-axial junction (see arrow).

g: JM118. Largest cf. *Cooksonia caledonica/ Renalia* sp. sporangium. Transversely elliptical sporangium with slightly concave sporangial-axial junction.

h: JM053a. Smallest cf. *Cooksonia caledonica/ Renalia* sp. sporangium. Transversely elliptical sporangium with slightly concave sporangial-axial junction.

i: JM011a. Reniform sporangia with slightly concave sporangial-axial junctions. Sporangial borders taper in towards the sporangial-axial junctions (see arrows). Three axes appear to branch close together, suggesting pseudomonopodial branching.

j: JM035a. Isolated reniform sporangium with very concave sporangial base.

k: JM008. Anisotomously branched axes (see arrow) terminating in transversely elliptical sporangia.

l: JM004. Isotomously branched axes (see arrow) terminating in reniform sporangia, with very concave sporangial-axial junctions.

m: JM368. ? Laterally or pseudomonopodially branched axes (see arrows) terminating in reniform sporangia, with sporangial borders.

Plate 3.1: cf. *Cooksonia caledonica / Renalia* sp. specimens

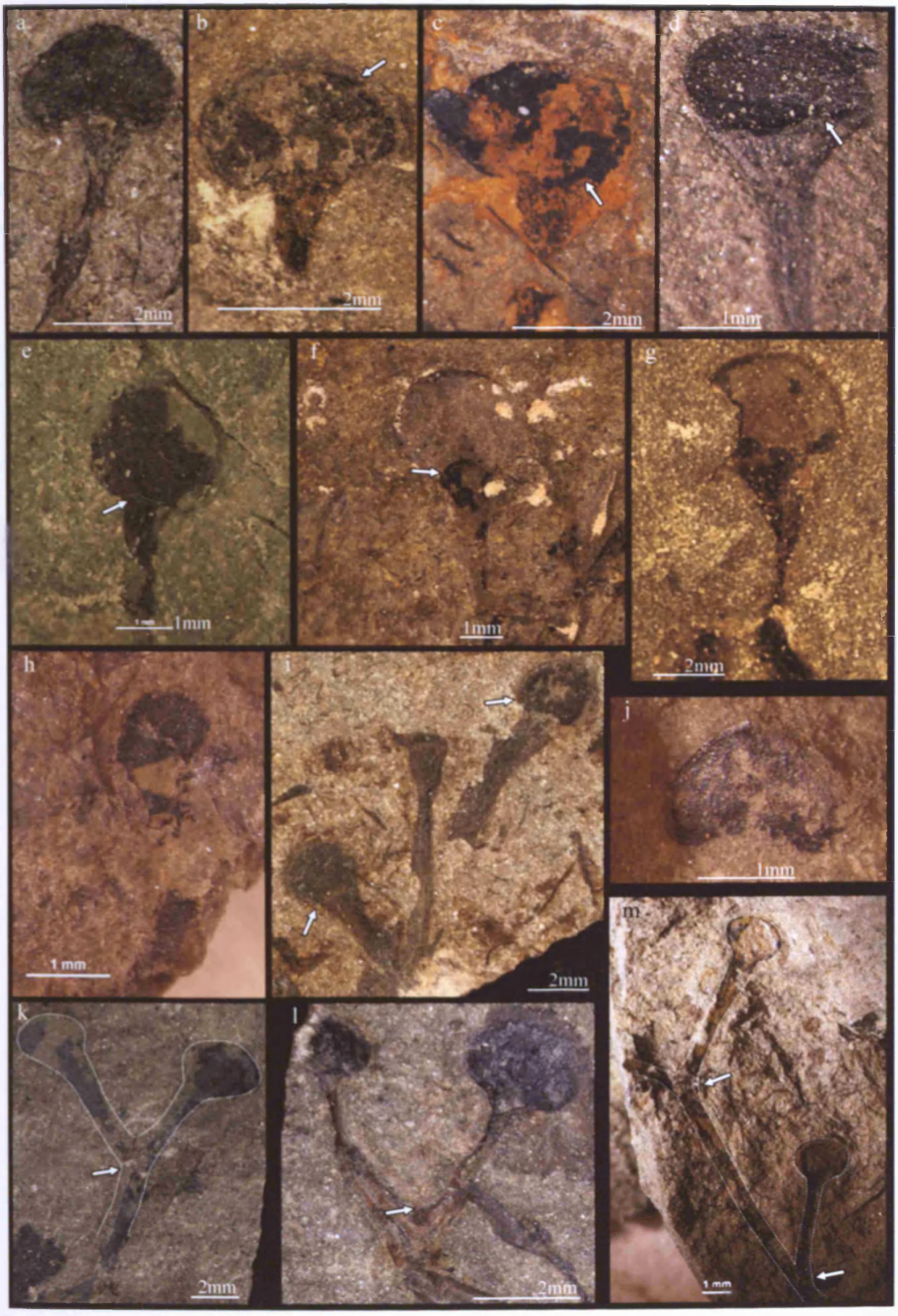

Plate 3.2: cf. *Cooksonia caledonica/ Renalia* sp. specimens: anatomy

a: JM004. SEM image of coalified compression of basal portion of reniform sporangium, and subtending axis, infilled with pyrite-limonite cubes (appear white) aligned parallel to the axis.

b: JM010a. SEM image of coalified compression of reniform sporangium, with pyrite-limonite cubes (appear white) aligned vertically, fanning out from the base of the sporangium (see arrow).

c: JM011. SEM image of central strand of coalified material preserved within subtending axis (see arrow).

d: JM385. SEM image of coalified compression of transversely elliptical sporangium, with peripheral crack around the sporangial margin (see arrow).

e: JM004. SEM image of coalified compression of reniform sporangium with blocky coalified material arranged around the sporangial margin (see arrow).

f: JM368. SEM image of i*n situ* trilete spore with circular amb and equatorial crassitude. Laevigate to granulose proximal ornament.

g: *Cooksonia caledonica* Edwards 1970.

h: *Renalia hueberi* Gensel 1976.

Plate 3.2: cf. *Cooksonia caledonica / Renalia* sp. specimens: anatomy

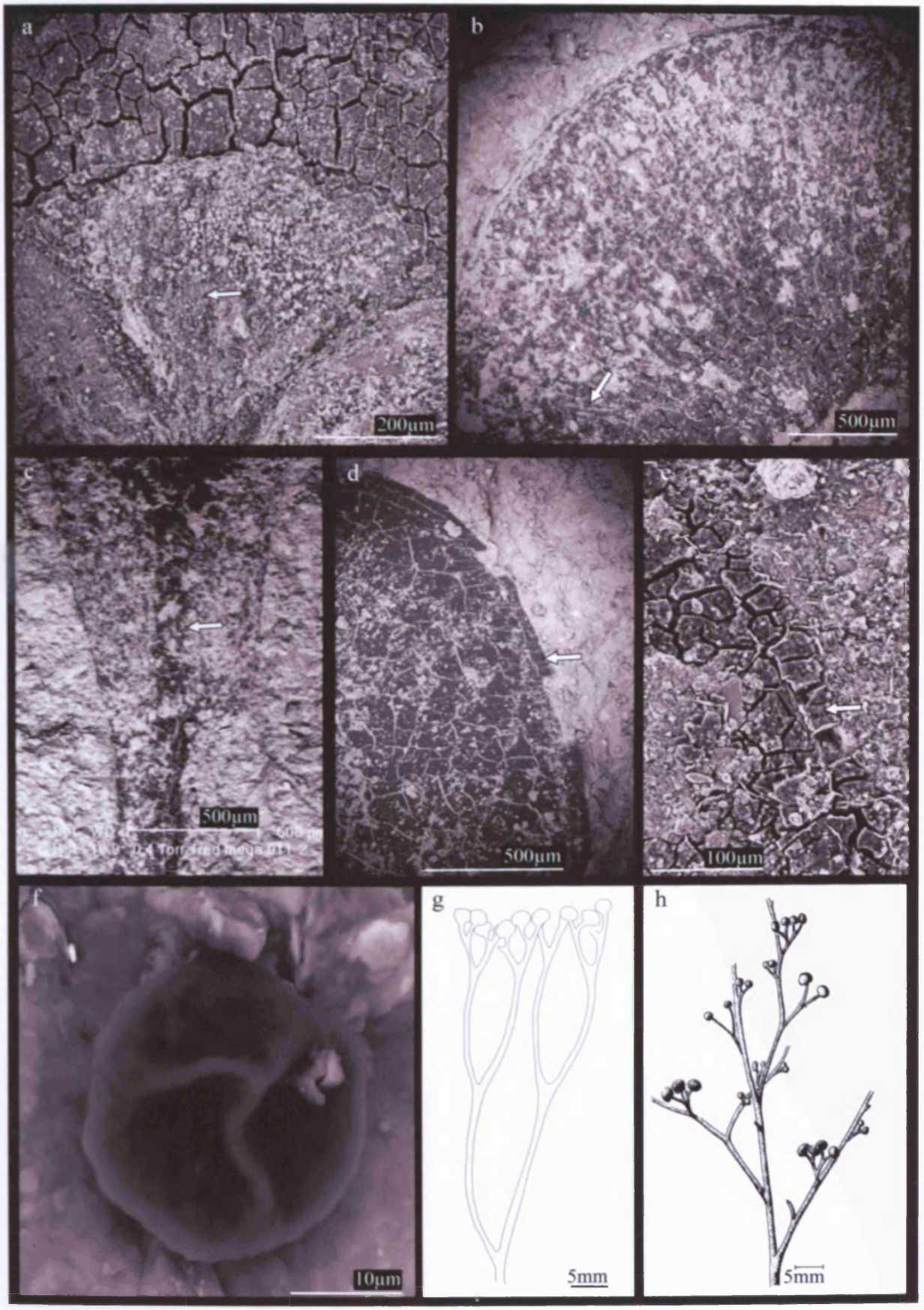

Plate 3.3: *Cooksonia hemisphaerica* specimens

a: JM367. Partial coalified compression and impression of hemispherical sporangium with broad, flatten apex and gradually tapering subtending axis.

b: JM133a. Partial coalified compression and impression of hemispherical sporangium, with flat sporangial-axial junction (see arrow), and gradually tapering subtending axis.

c: RH015. Partial coalified compression and impression of hemispherical sporangium, with flat sporangial-axial junction (see arrow).

d: JM228a. Partial coalified compression and impression of isodiametric sporangium, with flat sporangial-axial junction (see arrow), with gradually tapering subtending axis.

e: JM112a. Coalified compression of isodiametric sporangium with flat sporangial-axial junction (see arrow), with gradually tapering subtending axis.

f: JM374. Partial coalified compression and impression of sporangium, where sporangium height slightly exceeds width. Sporangium surrounded by sporangial border (see arrow).

g: JM121c. Partial coalified compression and impression of hemispherical sporangium with broad, flatten apex, and maximum width occurring in the top third of sporangial height. The sporangial-axial junction is flat (see arrow).

h: JM121b. Isodiametric sporangium with maximum width approximately half sporangial height.

i: JM312b. Largest *Cooksonia hemisphaerica* sporangium, with flat sporangial-axial junction (see arrow).

j: JM012. Isotomously branched axes terminating in hemispherical sporangia, with flat sporangial-axial junctions (see arrows).

k: JM312b. Anisotomously branched axes terminating in hemispherical sporangia, with flat sporangial-axial junctions (see arrows).

Plate 3.3: *Cooksonia hemisphaerica* specimens

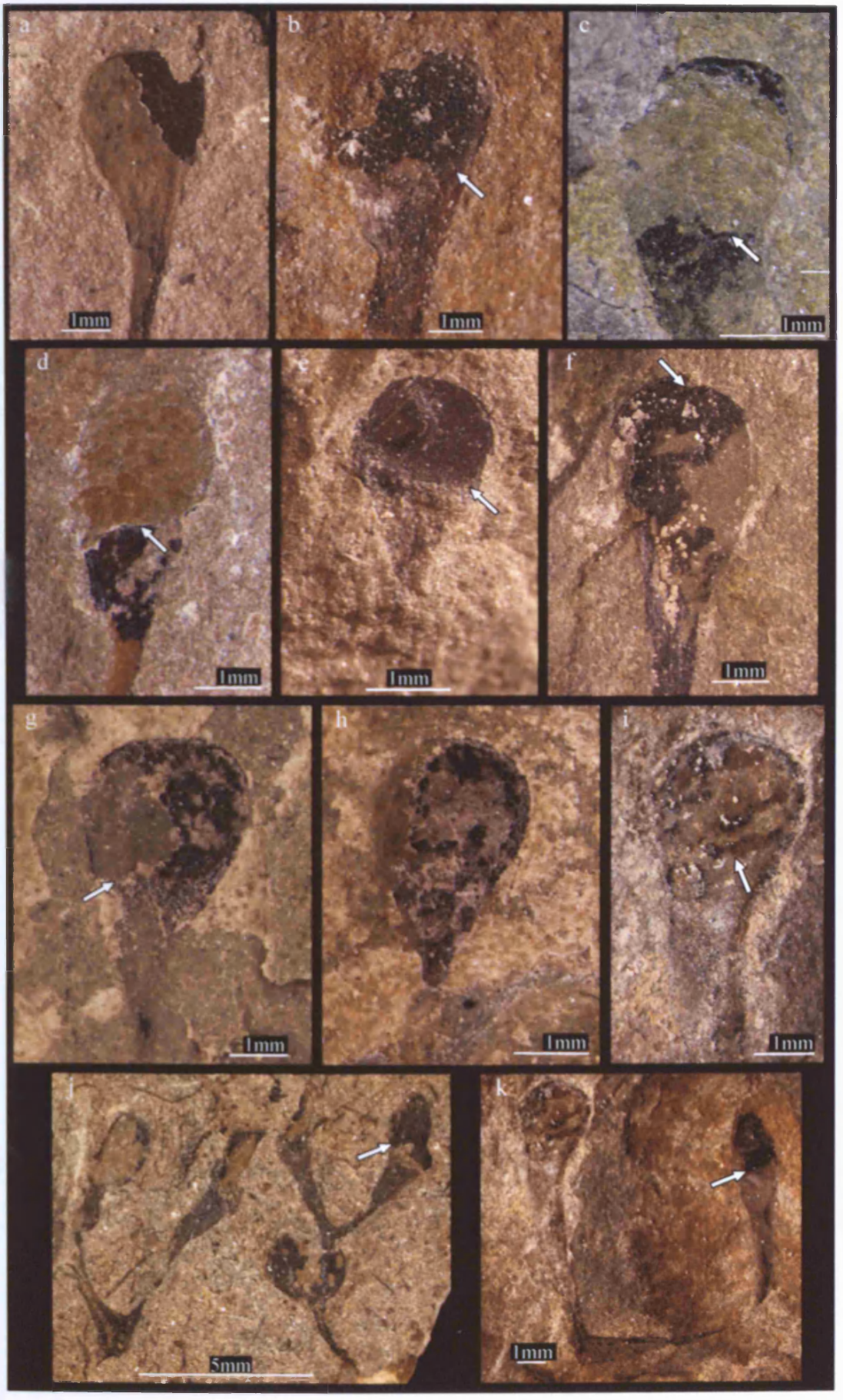

Plate 3.4: *Cooksonia hemisphaerica* specimens: anatomy

a: JM374. SEM image of partial coalified compression of sporangium where sporangial height exceeds width. A peripheral band of coalified material and impression surrounds the sporangium (see arrow), and may represent a compressed sporangial wall.

b: JM003. SEM image of partial coalified compression of the band surrounding a hemispherical sporangium, showing the impression of elongate cells (see arrow) running parallel to the sporangial edge.

c: JM020. SEM image of partial coalified compression of the sporangial wall at the centre of the sporangium, composed of isodiametric, randomly orientated cells (see arrow).

d: JM367. SEM image of partial coalified compression of subtending axis, with elongate, fusiform cracks infilled with pyrite-limonite cubes, aligned parallel to axis length (see arrow). These cracks may represent original cells.

Plate 3.4: *Cooksonia hemisphaerica* specimens: anatomy

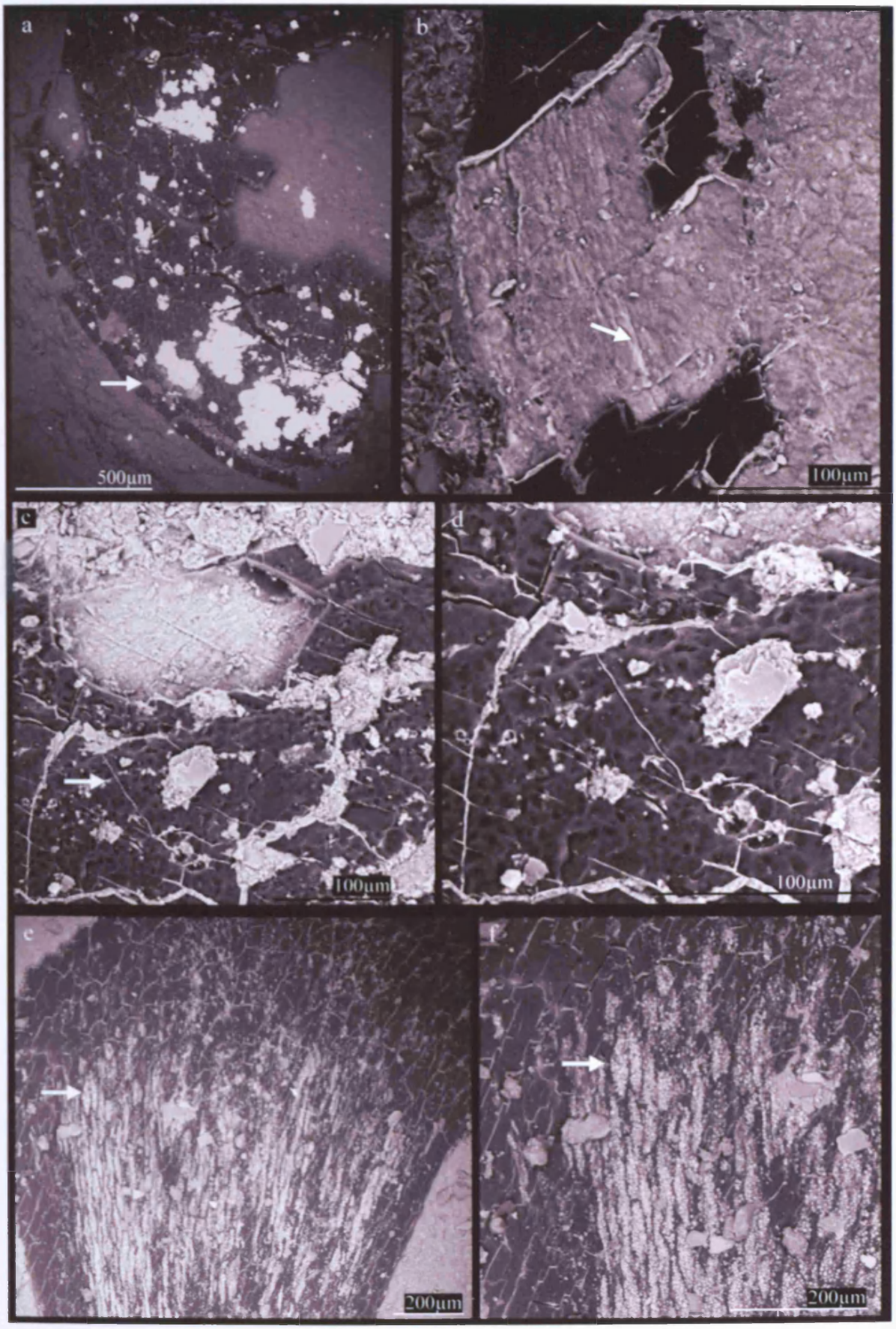

Plate 3.5: *Cooksonia* cf. *cambrensis* specimens

a: JM235a. Circular sporangium with slightly proximally curved sporangial-axial junction (see arrow), and parallel-sided subtending axis.

b: JM372c. Circular sporangium with proximally curved sporangial-axial junction (see arrow), and preferentially preserved sporangial margin. Sporangial cavity extends into the subtending axis.

c: RH045. Transversely elliptical sporangium, with proximally curved sporangial-axial junction (see arrow), and sporangial cavity extends into the parallel-sided subtending axis.

d: RH0188_1. Transversely elliptical sporangium, with proximally curved sporangial-axial junction (see arrow). Preferentially preserved sporangial margin.

e: JM023. Largest *Cooksonia* cf. *cambrensis* specimen. Transversely elliptical sporangium, with proximally curved sporangial-axial junction (see arrow). Preferentially preserved sporangial margin.

f: JM382. SEM image of a circular sporangium, showing a peripheral crack parallel to the outer sporangial margin (see arrow).

Plate 3.5: *Cooksonia* cf. *cambrensis* specimens

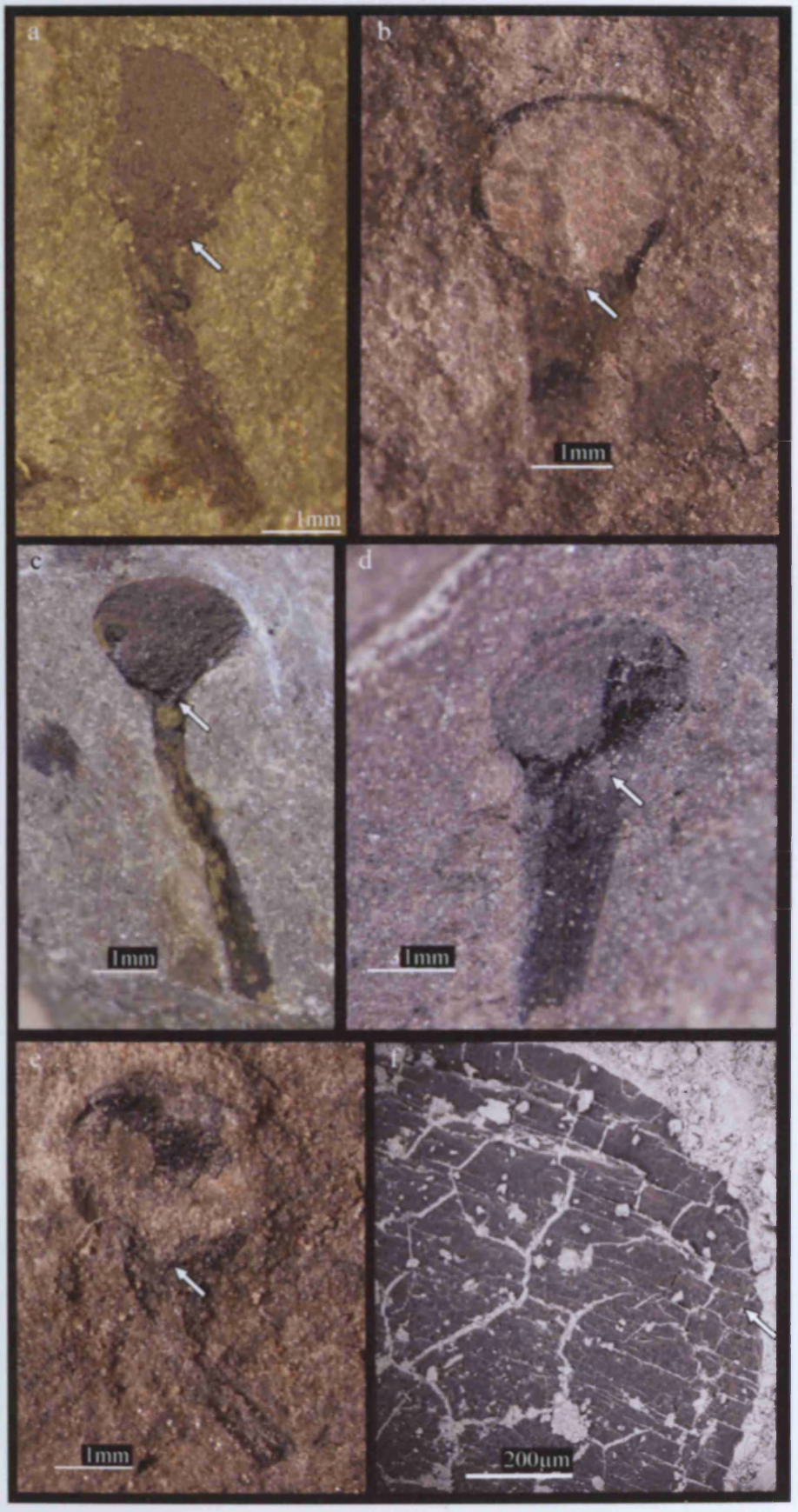

Plate 3.6: cf. *Uskiella reticulata / Tarrantia salopensis* specimens

a: JM279a. Anisotomously branched axes with two branch points (see arrows). Terminal sporangia are vertically ovate and parallel-sided.

b: JM013d. Isotomously branched naked axes, with anisotomous daughter branches. Terminal sporangium is vertically ovate, circular and isodiametric, with preferentially preserved sporangial border (see arrow).

c: JM013b. Isodiametric, circular terminal sporangium, with slightly tapering subtending axis. Preferentially preserved sporangial border (see arrow).

d: JM006a. Vertically ovate sporangium (height exceeds width), attached to a slightly tapering subtending axis. Possible flat sporangial-axial junction (see arrow). Preferentially preserved sporangial border (see arrow).

e: JM111a. Vertically ovate sporangium (height exceeds width), attached to a slightly tapering subtending axis. Preferentially preserved sporangial border (see arrow).

f: JM390a. Vertically ovate sporangium (height exceeds twice width), attached to a slightly tapering subtending axis.

g: RHSp110. Largest cf. *Uskiella reticulata / Tarrantia salopensis* specimen and largest sporangium. Pseudomonopodially branched axes with four branch points (see arrows). One daughter branch terminated with vertically ovate sporangium.

h: JM279a. Parallel-sided ovate sporangium, attached to narrow subtending axis.

i: JM092. Parallel-sided ovate sporangium, with slightly tapering apex and flat sporangial-axial junction (see arrow). Preferentially preserved sporangial border.

j: RH0008_2. Thick sporangial border (see arrow) showing an impression of elongate cells running parallel to the outer sporangial margin.

k: JM328a. Coalified ovate sporangium, with granulate or reticulate texture in the central sporangial wall.

l: JM013d. Circular sporangium attached to narrow parallel-sided subtending axis that widens just below the sporangium base. The sporangial-axial junction is unclear.

Plate 3.6: cf. *Uskiella reticulata / Tarrantia salopensis* specimens.

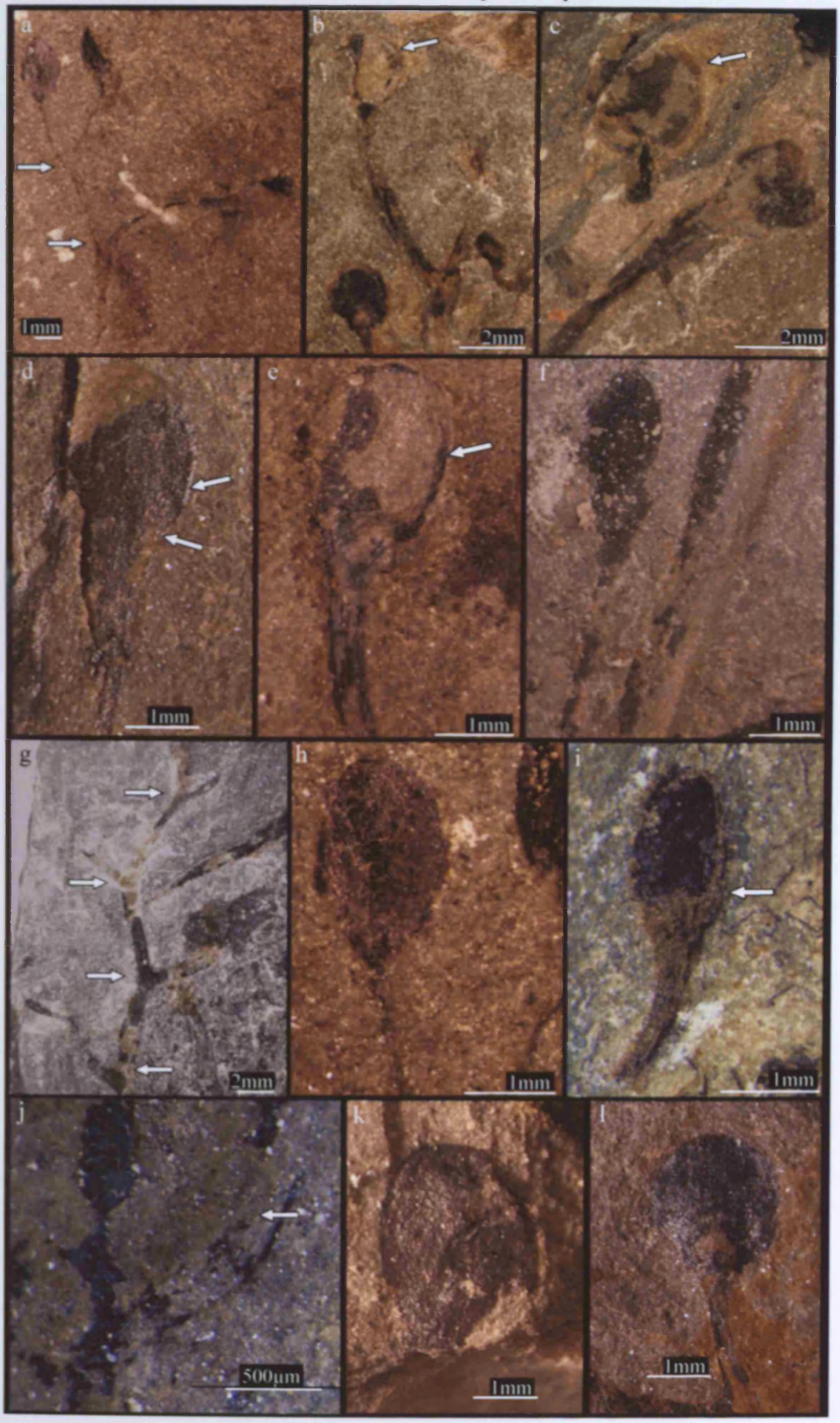

Plate 3.7: cf. *Uskiella reticulata / Tarrantia salopensis* specimens: anatomy

a: JM113. SEM image of outer margin of sporangium, with peripheral crack infilled with pyrite-limonite cubes (see arrow).

b: JM279. SEM image of the central area of the sporangial wall, composed of isodiametric, randomly orientated cells (see arrow).

c: *Uskiella spargens* Shute and Edwards 1989.

d: *Uskiella reticulata* Fanning et al. 1992.

e: *Tarrantia salopensis* Fanning et al.1992.

Plate 3.7: cf. *Uskiella reticulata* / *Tarrantia salopensis* specimens: anatomy

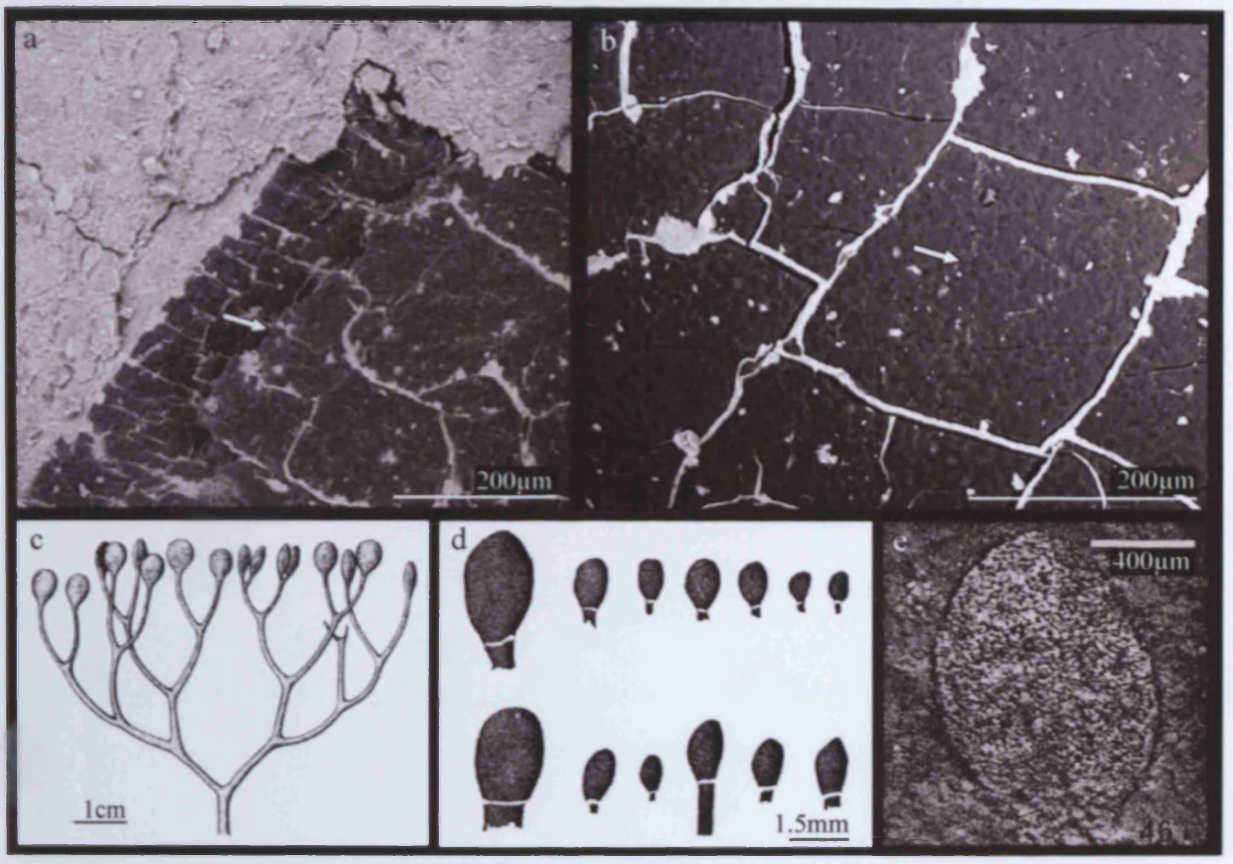

Plate 3.8: *Salopella allenii* specimens

a: JM005b. Partial coalified compression and impression of elongate, fusiform sporangium, with tapering apex.

b: JM006a. Partial coalified compression and impression of elongate fusiform sporangium, with tapering apex, and pointed tip. A layer of limonite is visible between the coalified compression and host rock (see arrow).

c: JM007a. Partial coalified compression and impression of elongate fusiform sporangium, with tapering apex, and flattened tip.

d: JM005b. Partial coalified compression and impression of elongate fusiform sporangium, with tapering apex, and globular tip.

e: RHSp151_1. Partially coalified, elongate fusiform sporangium, with tapering apex, and rounded tip. Largest sporangium of *Salopella allenii*.

f: JM006a. Slight narrowing of axis, or constriction, at sporangial–axial junction (see arrow). Note faint impressions of elongate cells running down the length of the subtending axis (see arrow).

g: JM289b. Anisotomously branched terminal axes, with acute branching angle.

h: RHSp141_1. Largest specimen of *Salopella allenii*. Acutely dichotomously branched axis, with slightly anisotomous branch point (see arrow), terminated by elongate, fusiform sporangia.

Plate 3.8: *Salopella allenii* specimens

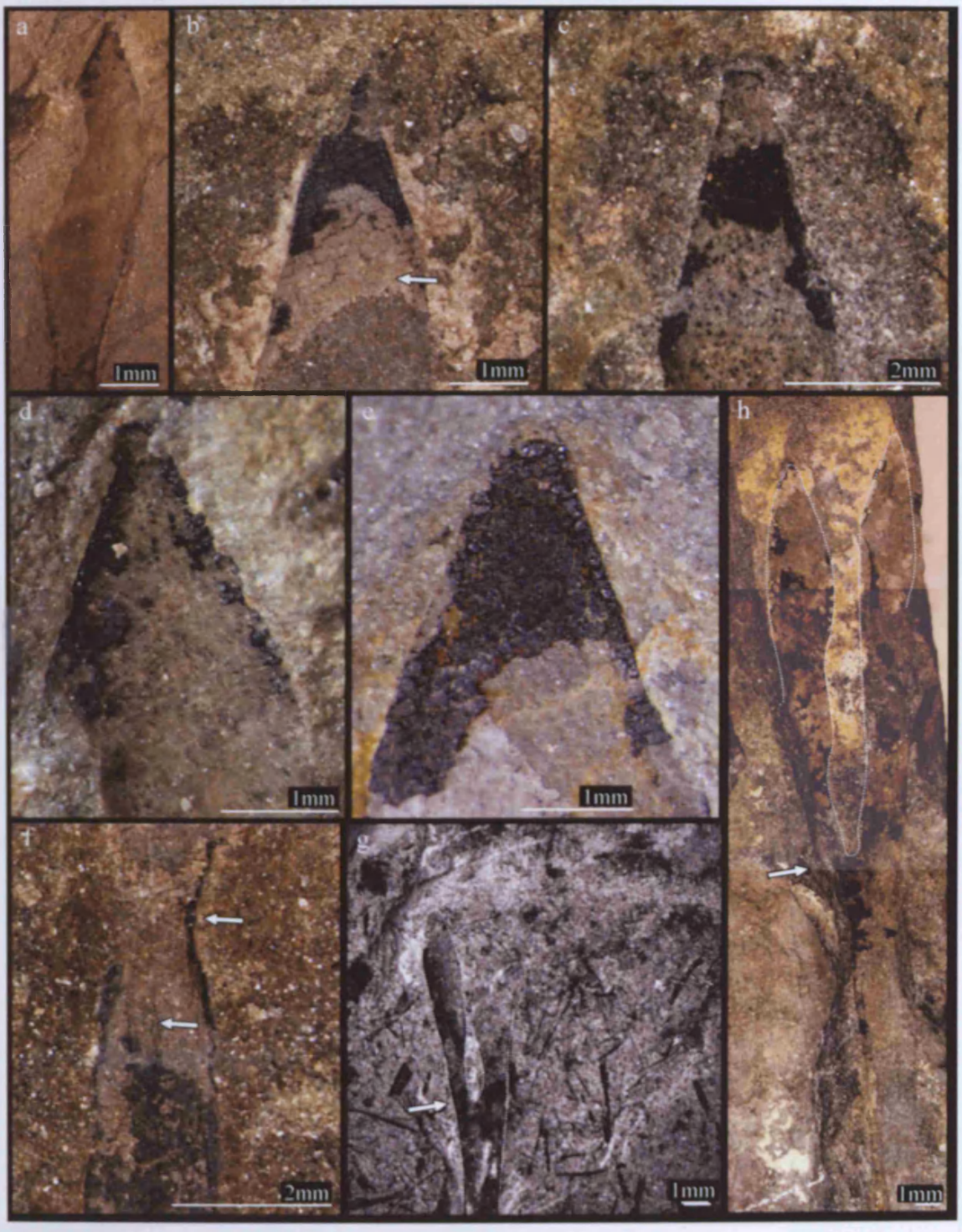

Plate 3.9: *Salopella allenii* specimens: anatomy

a: JM005b. Impression of sporangial wall, showing impressions of elongate cells on the host rock (see arrow) aligned at an angle of approximately 30° to the sporangial edge.

b: RHSp151_1. Impression of sporangial wall, showing impressions of elongate cells on the host rock (see arrow), aligned at an angle to the sporangial edge.

c: JM006a. SEM image of sporangial wall, showing impressions of elongate cells on the host rock (see arrow) and in the coalified compression (see arrow).

d: JM005b. SEM image of sporangial wall, showing impressions of elongate cells on the lost rock (see arrow).

e: JM006a. Elongate striations or cells, running down the length of the subtending axis.

f: *Salopella allenii* Edwards and Richardson 1974.

g: *Salopella allenii* specimen from Targrove Quarry.

Plate 3.9: *Salopella allenii* specimens: anatomy

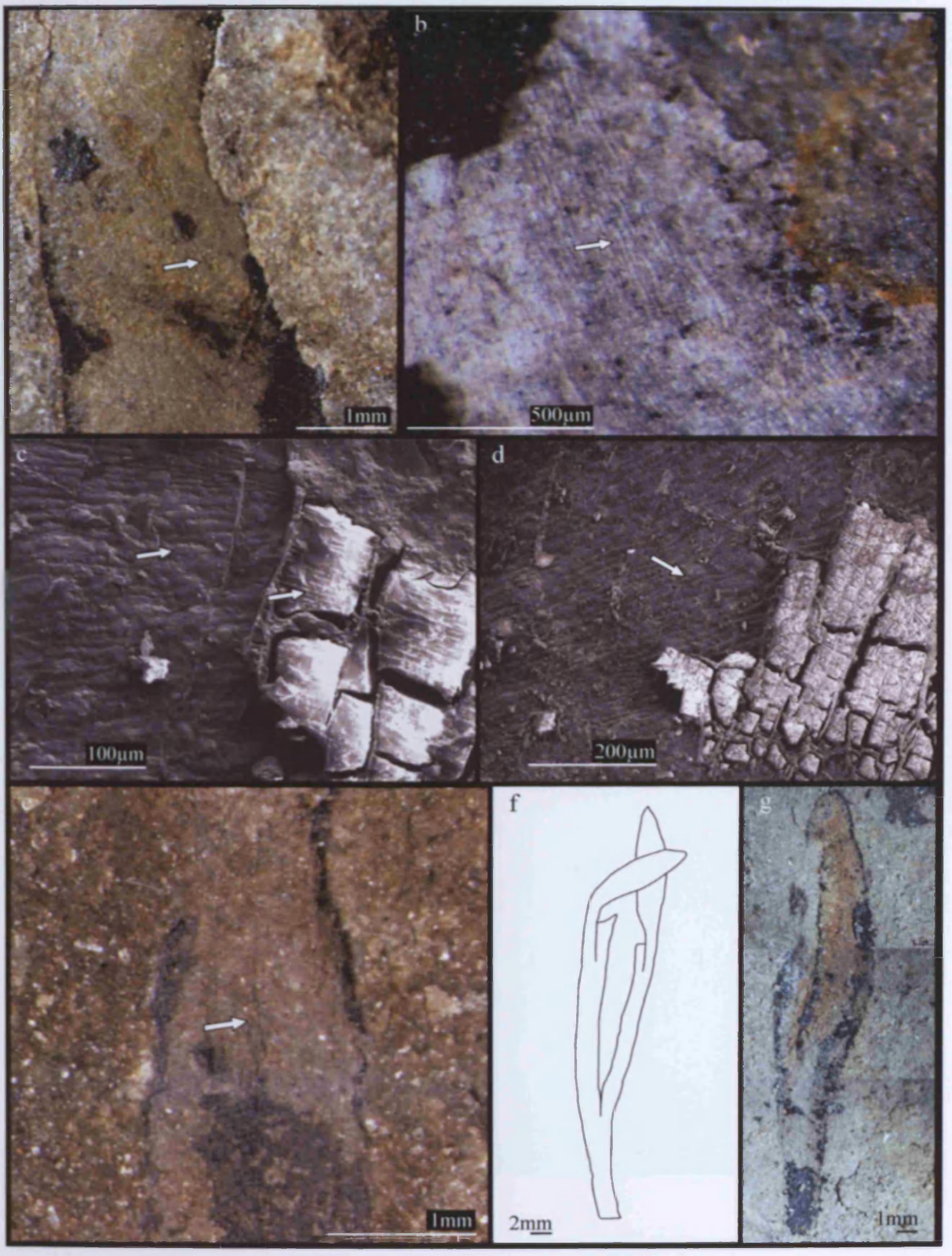

Plate 3.10: *Salopella* cf. *marcensis* specimens

a: RHSp304. Isotomously branched narrow axes with at least two branch points (see arrows), one terminated by a small fusiform sporangium with tapering apex and rounded tip.

b: JM346a. Small elongate fusiform sporangium with tapering apex and rounded tip (see arrow).

c: JM394b. Small elongate fusiform sporangium with tapering apex and pointed, extended tip (see arrow). Slight narrowing of the axis directly beneath the sporangial base.

d: JM021. Largest *Salopella* cf. *marcensis* sporangium. Small elongate fusiform sporangium with tapering apex and pointed tip (see arrow).

e: JM266a. Smallest *Salopella* cf. *marcensis* sporangium. Small elongate fusiform sporangium with tapering apex and rounded tip (see arrow).

f: JM394b. Isotomously branched narrow axes with at least three branch points (see arrows). Terminated by elongate fusiform sporangia with pointed tips (see 3.10*c*).

Plate 3.10: *Salopella* cf. *marcensis* specimens.

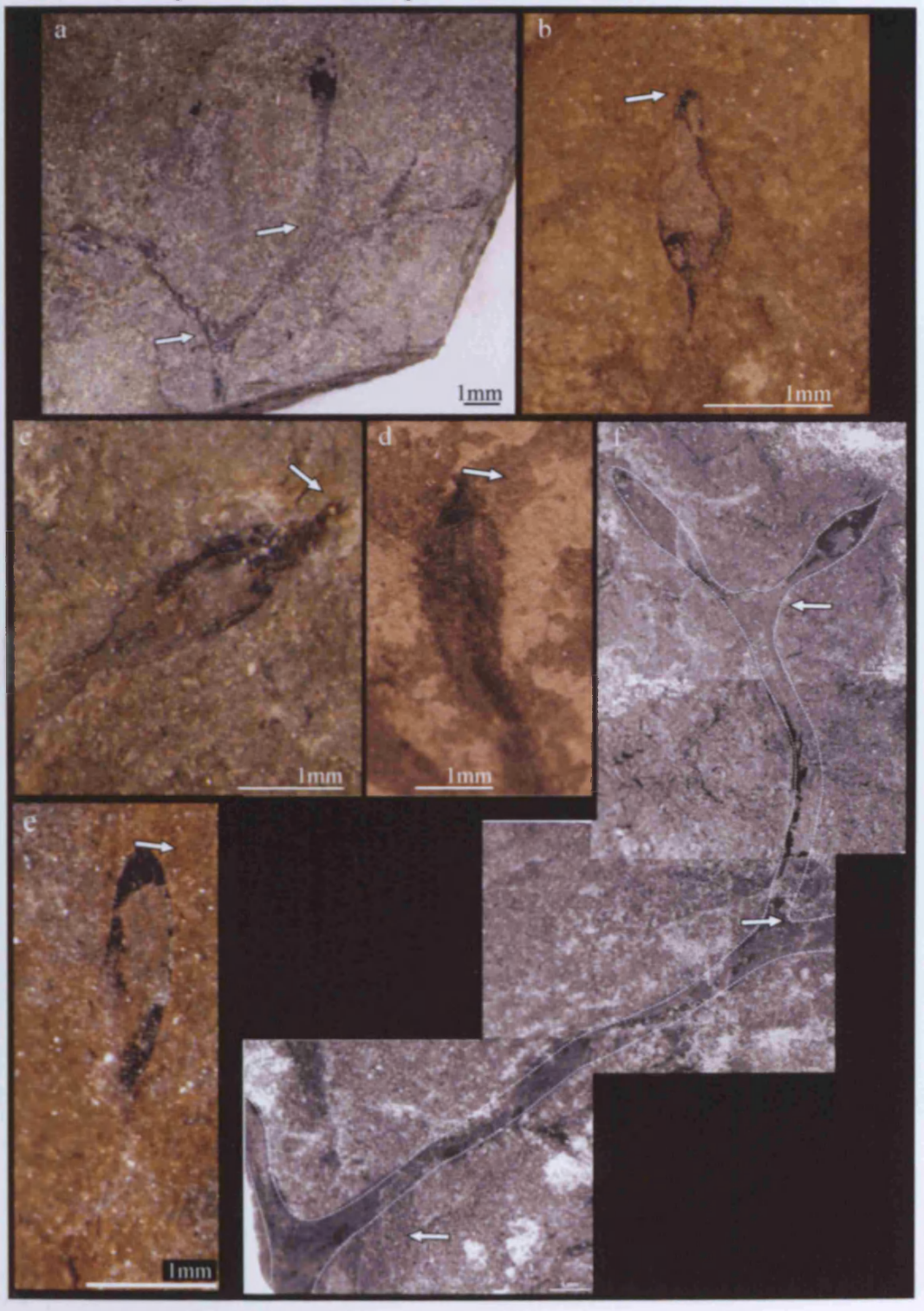

Plate 3.11: *Salopella* cf. *marcensis* specimens: anatomy

a: JM394. Elongate, fusiform sporangium, with elongate striations preserved within the coalified compression (see arrow) and counterpart impression, running parallel to the long axis of the sporangium, and tapering in the apex. Slight narrowing of the axis at the sporangial-axial junction (see arrow).

b: JM394. SEM image of the pointed, extended tip of the elongate, fusiform sporangium shown in 3.11*a*. Elongate cellular-like striations preserved as impressions, running parallel to the sporangium long axis.

c: JM394. SEM image of preferentially preserved coalified central strand within subtending axis (see arrow). Elongate cellular-like striations preserved in the remaining impression, which run parallel down the length of the axis.

d: JM394. SEM image of elongate cellular-like striations preserved in the impression of the subtending axis shown in 3.11*d*.

e: *Salopella marcensis* (Fanning, Edwards and Richardson 1992).

Plate 3.11: *Salopella* cf. *marcensis* specimens: anatomy

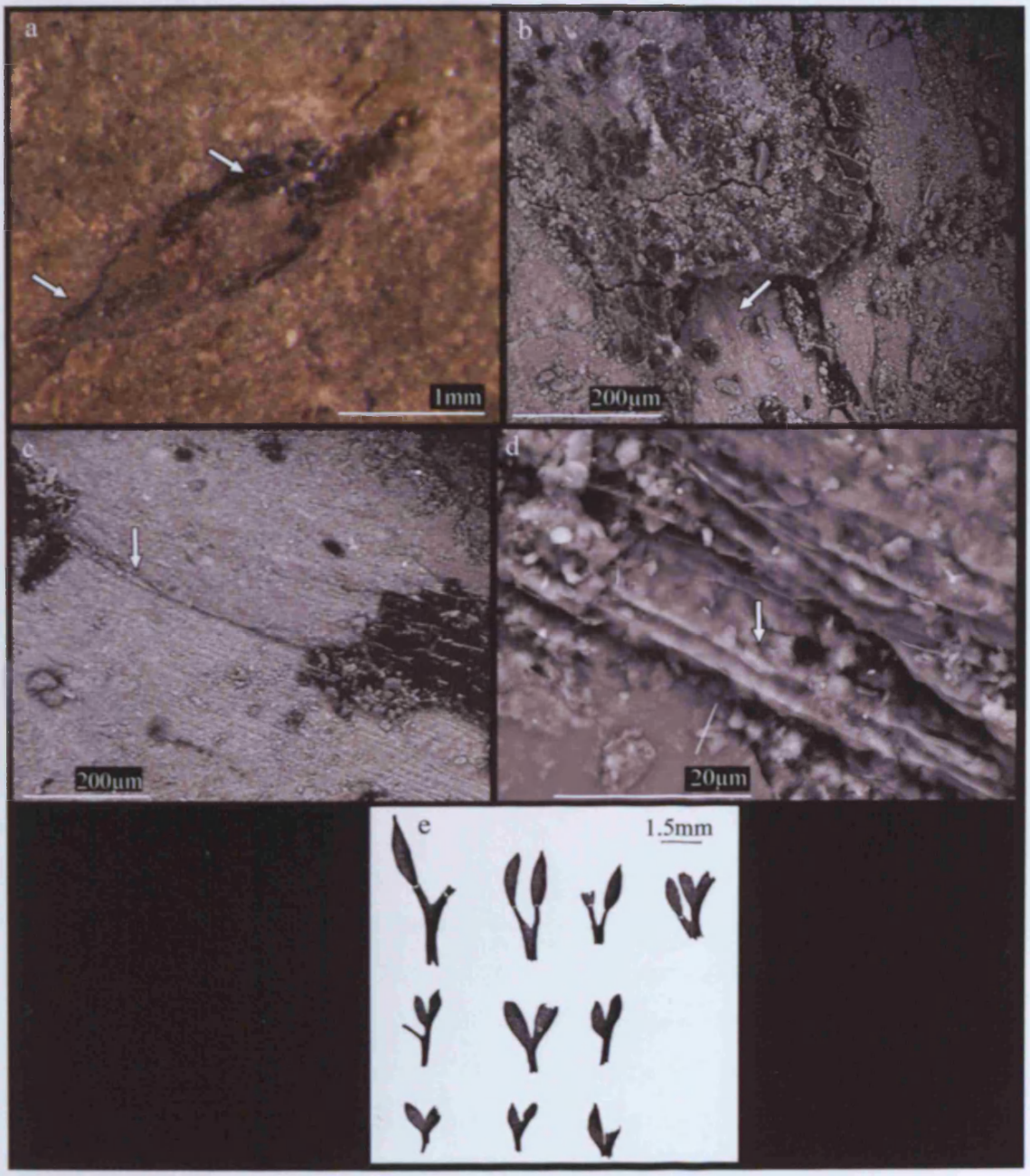

Plate 3.12: Elongate club-shaped sporangia specimens

a: RHPB. Dichotomously branched axes (see arrow), terminated by elongate, club-shaped sporangium, with broad, rounded apex, and maximum sporangial width occurring in the top third of sporangial height. Sporangial-axial junction unclear, but subtending axis gradually tapers down to branch point.

b: Diagram showing possible sporangial-axial junction positions on specimen JM016c.

c: RHSp20_1. Elongate, club-shaped terminal sporangium, with broad rounded apex, where maximum sporangial width is approximately positioned in the top third of sporangial height. Subtending axis gradually tapers away. Preferentially preserved sporangial border visible (see arrow). Sporangial-axial junction unclear, but possible position indicated (see arrow).

d: RH117_4. Elongate, club-shaped terminal sporangium, with broad rounded apex. Preferentially preserved wide sporangial border visible (see arrows). Sporangial-axial junction unclear, but possible position indicated (see arrow).

e: Sp034_2. Elongate club-shaped terminal sporangium, with preferentially preserved wide sporangial border visible (see arrow).

f: JM262a. Isotomously branched axes, with two branch points (see arrows), terminating in elongate, club-shaped sporangia, with preferentially preserved wide sporangial border visible.

g: JM371. The largest sporangium and specimen of all elongate club-shaped sporangia specimens. The sporangial border is visible around the whole sporangium (see arrows). The position of the sporangial-axial junction is unclear.

Plate 3.12: Elongate club-shaped sporangia specimens

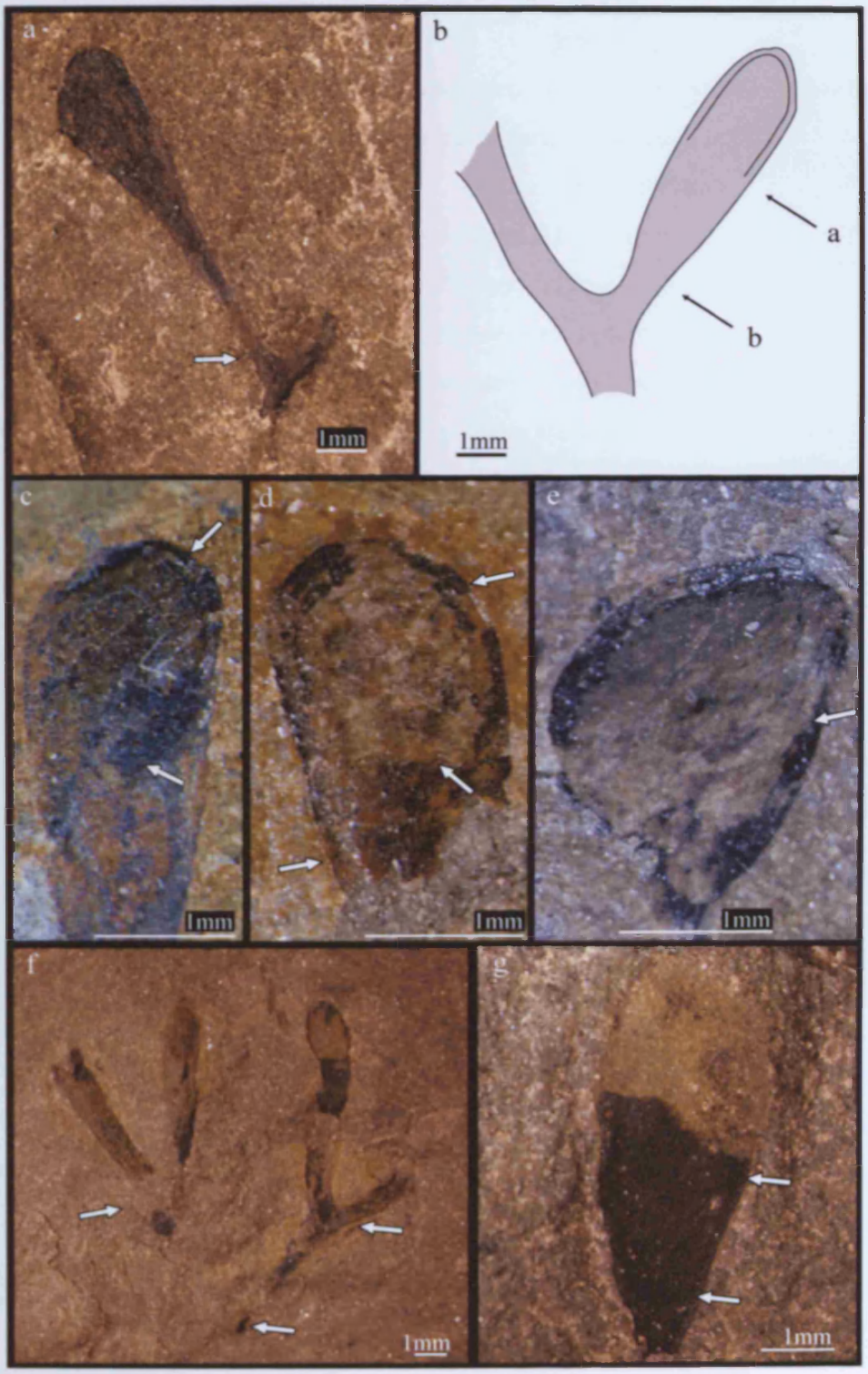

Plate 3.13: Elongate club-shaped sporangia specimens: anatomy

a: JM016c. SEM image of elongate, club-shaped sporangium, showing peripheral crack parallel and close to the outer margin (see arrow), filled with pyrite-limonite cubes.

b: JM371. SEM image of the outer margin of an elongate, club-shaped sporangium. A wide sporangial border has been preserved within the coalified compression, composed of elongate, cell-like striations running parallel to the sporangia outer margin (see arrow).

c: JM371. SEM image of the outer sporangial wall, of an elongate, club-shaped sporangium. Elongate cell-like striations run obliquely to the sporangia outer margin (see arrow).

d: JM262a. SEM image of the outer margin of an elongate, club-shaped sporangium. A wide sporangial border has been preserved within the impression (marked by thick white line). Within this border, elongate cell-like striations are running parallel to the outer sporangial margin (see arrow and thin white line). Within the central area of the outer sporangial wall, impressions of elongate cell-like striations running obliquely to the outer sporangial margin are visible (see arrow and thin white line).

e: JM287. SEM image of a preferentially preserved central strand (see arrow) within the subtending axis terminated by an elongate, club-shaped sporangium. Impressions of cell-like striations run parallel down the length of the subtending axis (see arrow).

f: JM287. SEM image of a preferentially preserved central strand (see arrow) within the subtending axis terminated by an elongate, club-shaped sporangium.

Plate 3.13: Elongate- club shaped sporangia specimens: anatomy

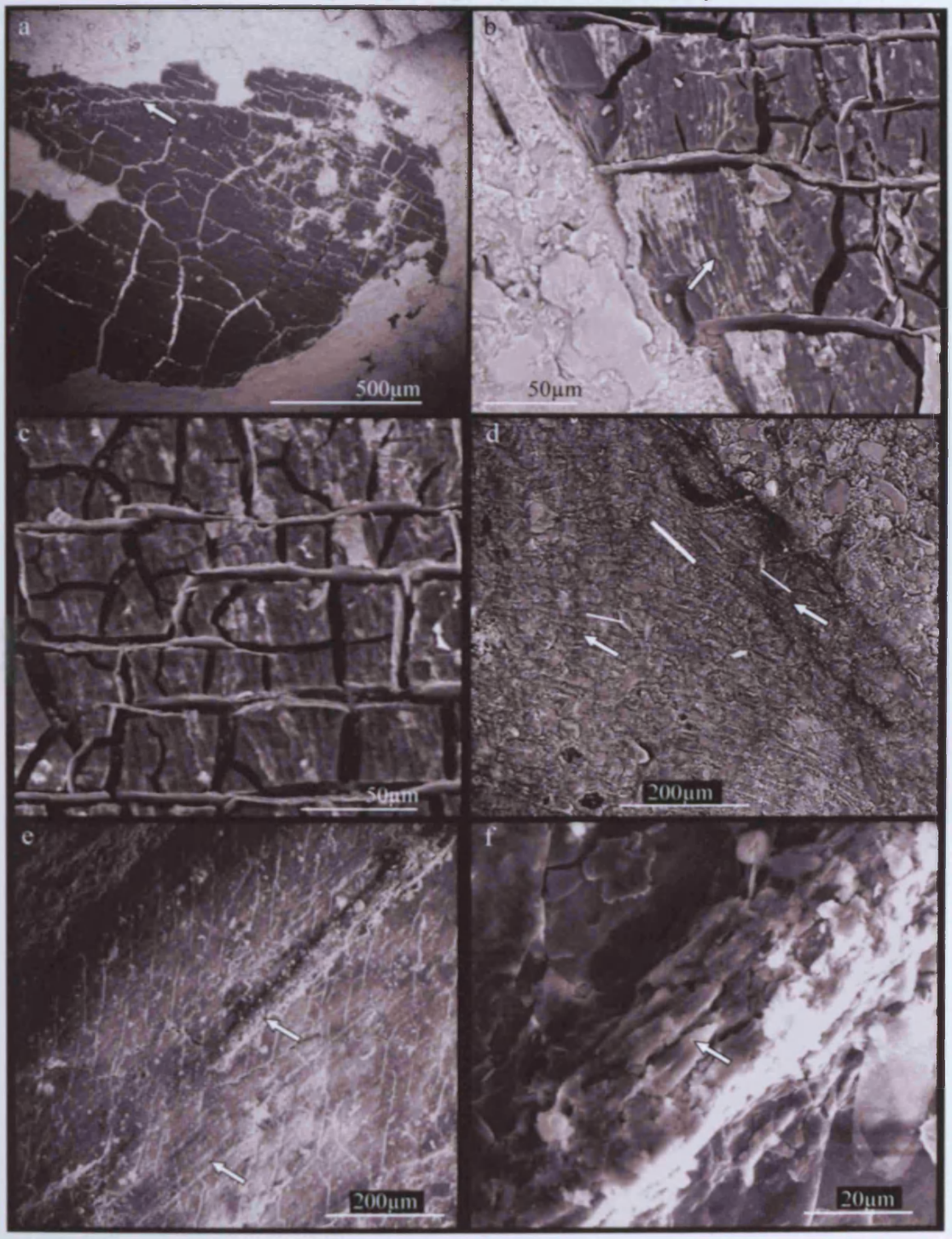

Plate 3.14: Mesofossil type A specimens

a: JM197b. Largest sporangium of type A. Anisotomously branched (see arrows) narrow axis, terminated by two pairs of circular sporangia.

b: JM190b. Terminal dichotomy (see arrow) directly beneath two circular sporangia. Sporangial-axial junction unclear.

c: JM086c. Terminal dichotomy (see arrow) bearing two circular sporangia. Sporangial-axial junction unclear.

d: RH128_1. Terminal dichotomy (see arrow) bearing two circular sporangia. Sporangial-axial junction unclear.

e: JM323c. Terminal dichotomy (see arrow) directly beneath two elliptical sporangia. Sporangial-axial junction unclear.

f: RH002_1. Terminal dichotomy (see arrow) directly beneath two elliptical sporangia. Sporangia may also be interpreted as one bifurcating sporangium.

g: JM095d. Terminal dichotomy (see arrow) bearing two elliptical sporangia. Sporangial-axial junction unclear.

h: JM194a. Dichotomously branched axis (see arrows) with three branch points; one of the final dichotomies occurs close the base of a pair of elliptical sporangia and is slightly anisotomous.

i: JM123a. Anisotomously branched axis (see arrows); final dichotomies close the base of two pairs of elliptical sporangia.

j: JM123a. Counterpart to P3.14*i*.

k: JM365d. Anisotomously branched axis (see arrows); final dichotomies close the base of two pairs of circular sporangia.

l: RHSp006. Isotomously branched axis (see arrows); final dichotomies close the base of a pair of circular sporangia.

m: JM153b +c. Two pairs of terminal elliptical sporangia. Alternatively, interpreted as two bifurcating elliptical sporangia.

n: JM365c. Bifurcating terminal elliptical sporangium.

o: JM365a. Anisotomously branched axis with three branch points (see arrows), terminated by two visible pairs of circular sporangia.

p: JM365a Counterpart to 3.14*o*.

Plate 3.14: Mesofossil type A specimens. Scale bar =1mm.

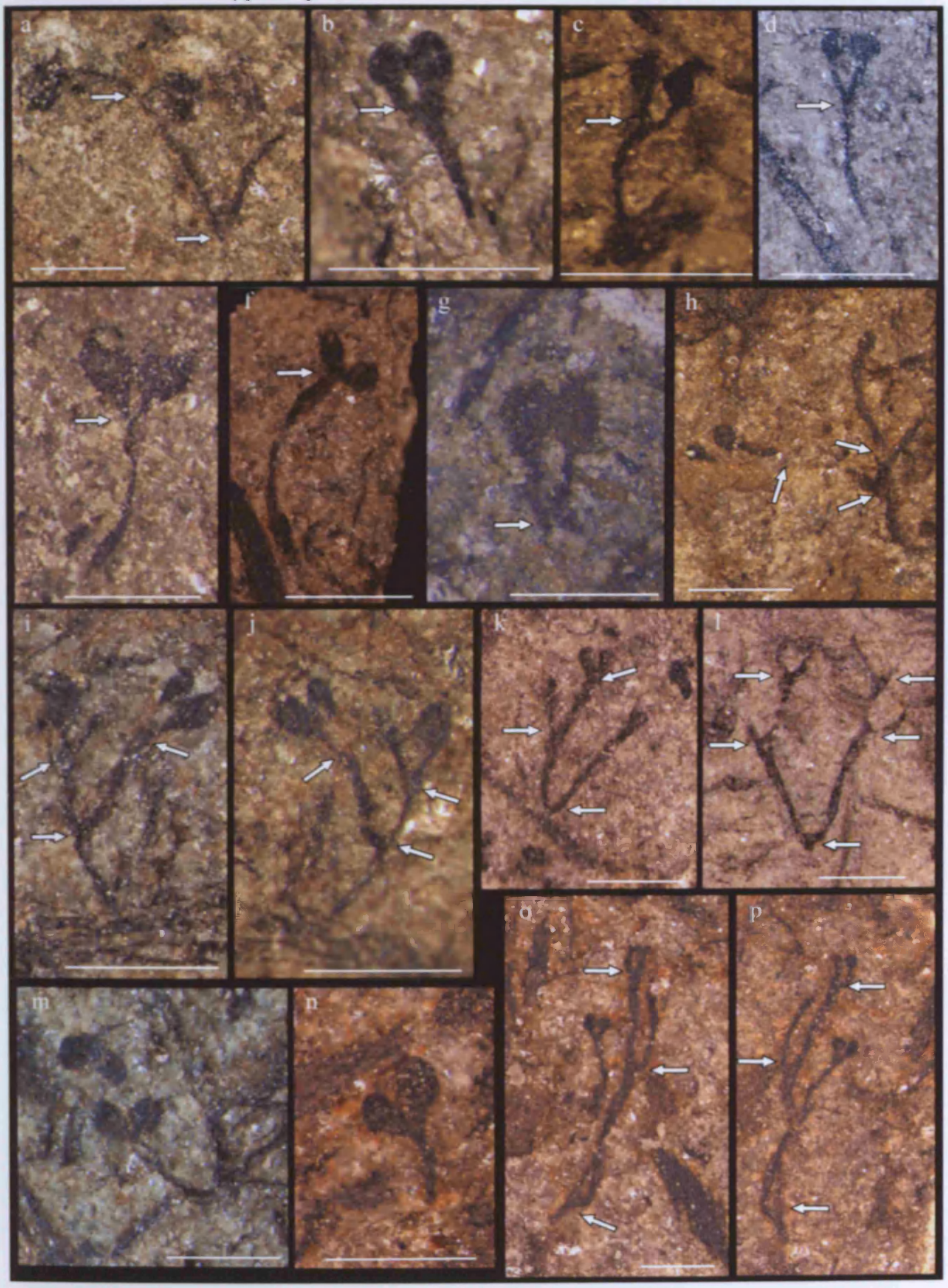

Plate 3.15: Mesofossil type B specimens

a: JM214a. Isotomously branched axis (see arrow), terminated by elongate, elliptical sporangia. Maximum sporangial width occurs approximately at half sporangial height.

b: JM206a. Dichotomously branched axis (see arrow), slightly anisotomous, terminated by elongate, elliptical sporangia. Maximum sporangial width occurs approximately at half sporangial height.

c: RH077a. Slightly anisotomously branched axis (see arrows), with two branch points, terminated by elongate, elliptical sporangia. Maximum sporangial width occurs approximately at half sporangial height.

d: JM164d. Largest sporangium specimens of mesofossil type B. Partially preserved elongate, elliptical sporangium, with short subtending axis.

e: JM164c. Smallest sporangium specimens of mesofossil type B. Isotomously branched axis (see arrow), terminated by elongate, elliptical sporangia.

f: JM364b. Slightly anisotomously branched axes (see arrow), terminated by elongate, elliptical sporangia. Subtending axes gradually tapers away from the sporangia bases and becomes parallel-sided.

g: JM174. Isotomously branched axes (see arrows), with three branch points, one daughter axis terminated by elongate, elliptical sporangium.

h: JM205a. Slightly anisotomously branched axes (see arrows), with three branch points, each terminated by elongate, elliptical sporangia.

i: JM364a. Isotomously branched axes (see arrows), with three branch points, two daughter axes terminated by elongate, elliptical sporangia.

j: JM336. Anisotomously branched axis (see arrow), terminated by elongate, elliptical sporangia.

k: JM178. Anisotomously branched axis (see arrow), with one daughter branch terminated by elongate, elliptical sporangium.

l: JM242a. Isotomously branched axis (see arrow), terminated by elongate, elliptical sporangia. Final dichotomy occurs at some distance from the base of the sporangia.

m: JM086d. Largest specimen of mesofossil type B. Anisotomously branched axis (see arrows), terminated by elongate, elliptical sporangia.

Plate 3.15: Mesofossil type B specimens. Scale bar =1mm.

Plate 3.16: Mesofossil type C specimens

a: JM188. Terminal, vertically ovate sporangium and subtending axis.

b: JM154. Terminal, transversely ovate sporangium and subtending axis.

c: JM100b. Terminal circular sporangium and subtending axis.

d: JM230b. Isotomously branched axis (see arrow), terminated by circular sporangium with flattened tip.

e: JM114a. Largest sporangium of mesofossils type C. Partially preserved vertically ovate sporangium and subtending axis.

f: RHSp036. Smallest sporangium of mesofossils type C. SEM image of dichotomous axis, terminated by a circular sporangium.

g: JM197a. Terminal vertically ovate sporangium and subtending axis. Subtending axis gradually tapers downwards from the sporangial base to become parallel-sided.

h: JM181. Terminal circular sporangium and subtending axis. Subtending axis gradually tapers downwards from the sporangial base to become parallel-sided.

i: JM198a. Isotomously branched axis (see arrow) terminated by circular sporangia.

j: JM402. Isotomously branched axis (see arrow), with one daughter branch terminated by circular sporangium with a flattened tip.

k: JM190a. Isotomously branched axis with two branch points (see arrows), terminated by vertically ovate sporangia.

Plate 3.16: Mesofossil type C specimens.

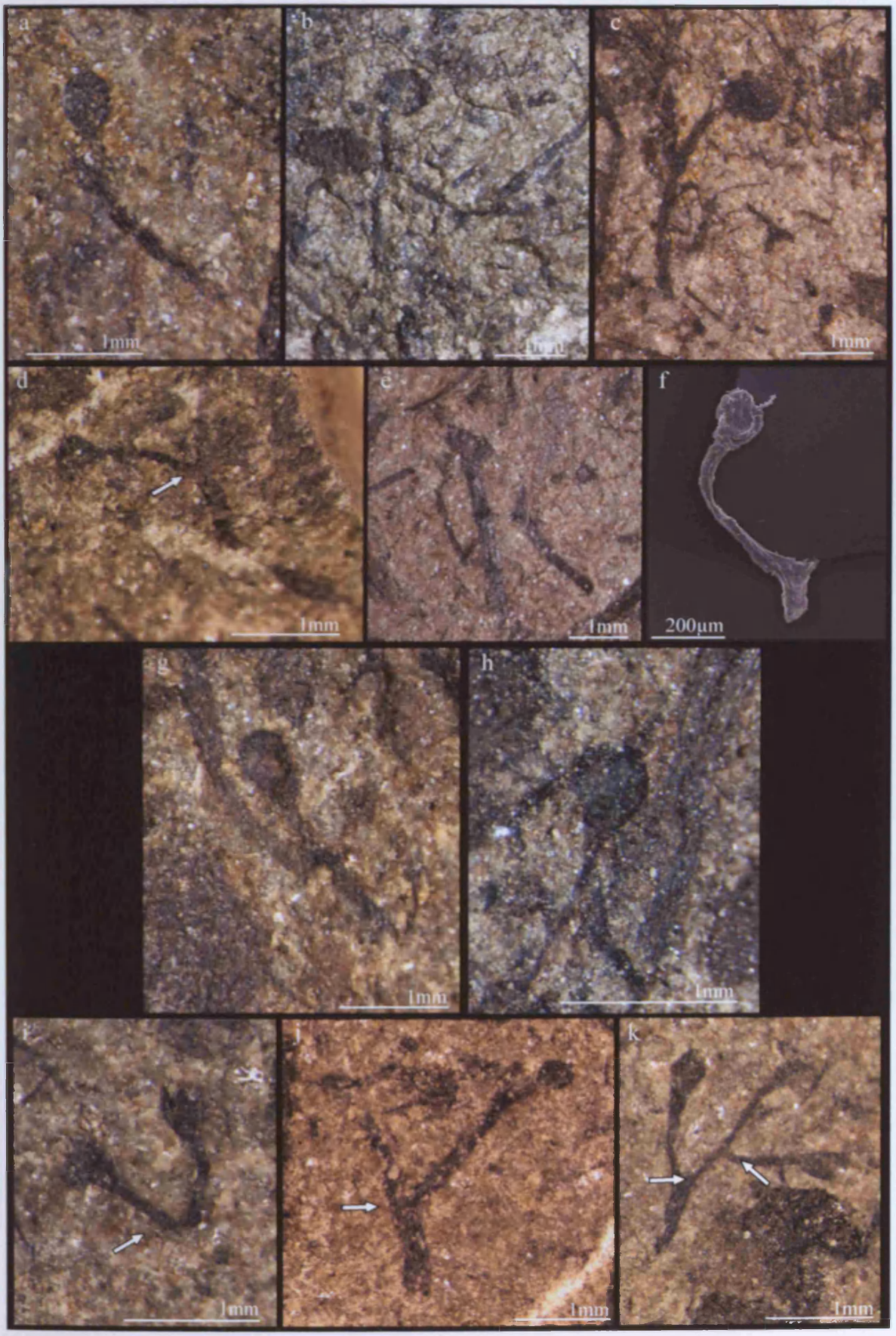

Plate 3.17: Mesofossil type D specimens

a: JM157c. Isotomously branched axis (see arrow), terminated by small circular sporangia.

b: JM187c. Isotomously branched axis (see arrow), terminated by small circular sporangia. Subtending axis curved inwards.

c: JM194c. Small circular terminal sporangium and parallel-sided subtending axis.

d: JM010f. Isotomously branched axis (see arrow), terminated by small transversely elliptical sporangia. Subtending axis curved inwards.

e: RH128_2. Isotomously branched axis (see arrow), terminated by small transversely elliptical sporangia.

f: RH050_2. Isotomously branched axis (see arrow), with one daughter branch terminated by small transversely elliptical sporangium.

g: JM290b. Largest sporangium of mesofossil type D. Isotomously branched axis (see arrow), terminated by small transversely elliptical sporangia. Thickening of the dichotomy centre.

h: JM114c. Terminal circular sporangium, with parallel-sided subtending axis.

i: JM110a. Isotomously branched axis (see arrow), terminated by small circular sporangia. Subtending axis curved inwards.

Plate 3.17: Mesofossil type D specimens.

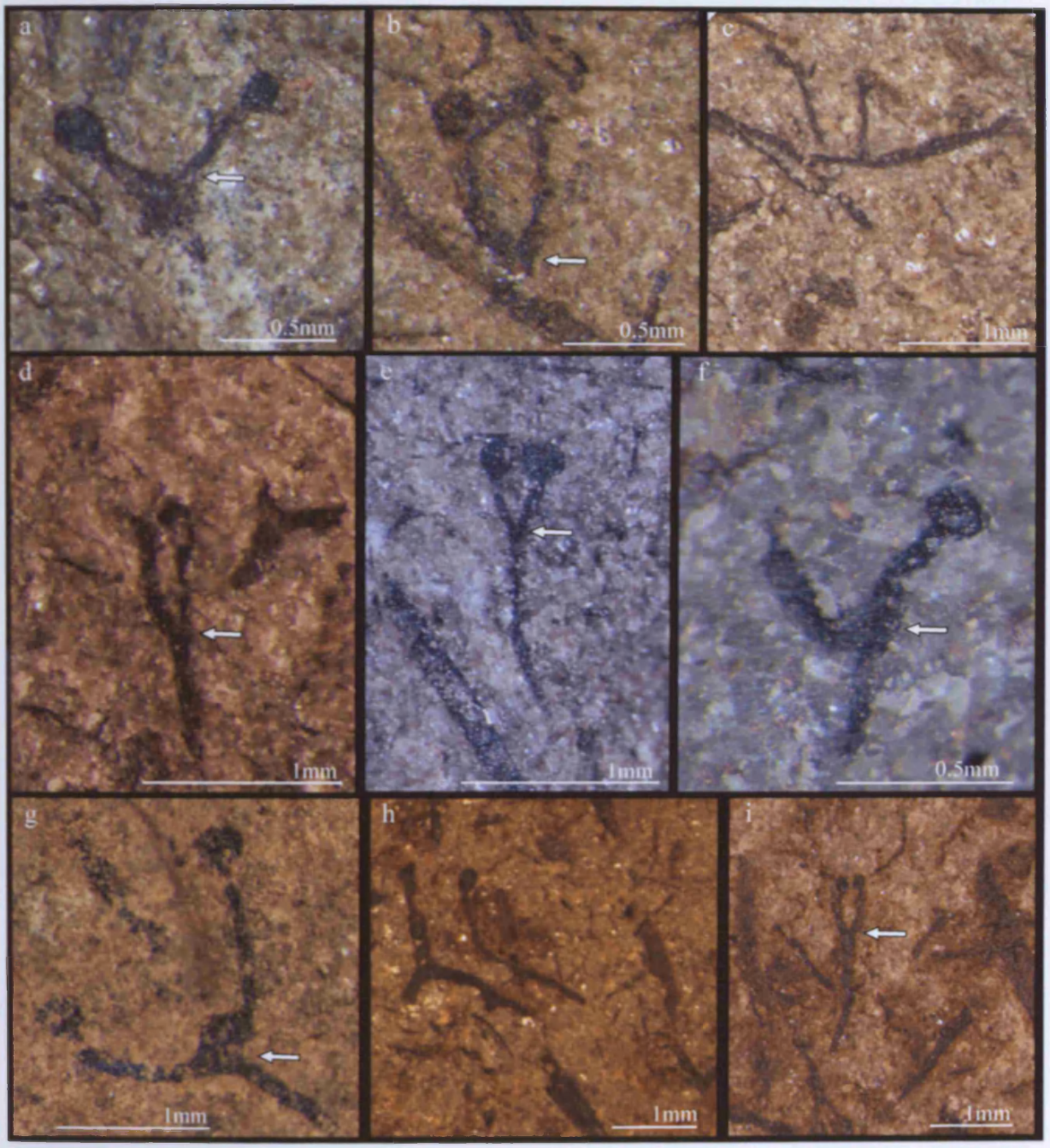

Plate 3.18: *Tortilicaulis* cf. *offaeus* specimens

a: JM397a. Isotomously branched axis (see arrow), terminated by elongate, fusiform sporangia.

b: JM397a. Sporangium A of specimen JM397a. Terminal elongate, fusiform sporangium, with a tapering apex, and rounded tip.

c: JM397a. Sporangium B of specimen JM397a. Terminal elongate, fusiform sporangium, with a tapering apex, and pointed tip. Cell-like, elongate striations can be seen in the sporangium compression and corresponding impression beneath, with a oblique, twisted orientation compared to the sporangium edge.

d: RHSp012_1. Isotomously branched axis (see arrow), terminated by elongate, fusiform sporangia.

e: JM397a. SEM image of sporangium B of specimen JM397a. Elongate cell-like striations run obliquely to the sporangium edge, giving a twisted appearance (see arrow). Cells have a fusiform shape, in filled with pyrite-limonite cubes.

f: JM397a. SEM image of subtending axis of specimen JM397a. Cell-like striations can be seen in coalified compression and impression beneath (see arrow), running oblique to the axis edge, giving a twisted appearance.

g: JM397a. Poorly preserved stomata (?) (see arrow), on the subtending axis of JM397a.

h: JM397a. Poorly preserved dyads similar to the dispersed spore taxa *Dyadospora* sp., in the central area of the sporangial wall of specimen JM397a.

i: *Tortilicaulis* Edwards 1979.

j: *Tortilicaulis offaeus* Edwards et al. 1994.

Plate 3.18: *Tortilicaulis* cf. *offaeus* specimens.

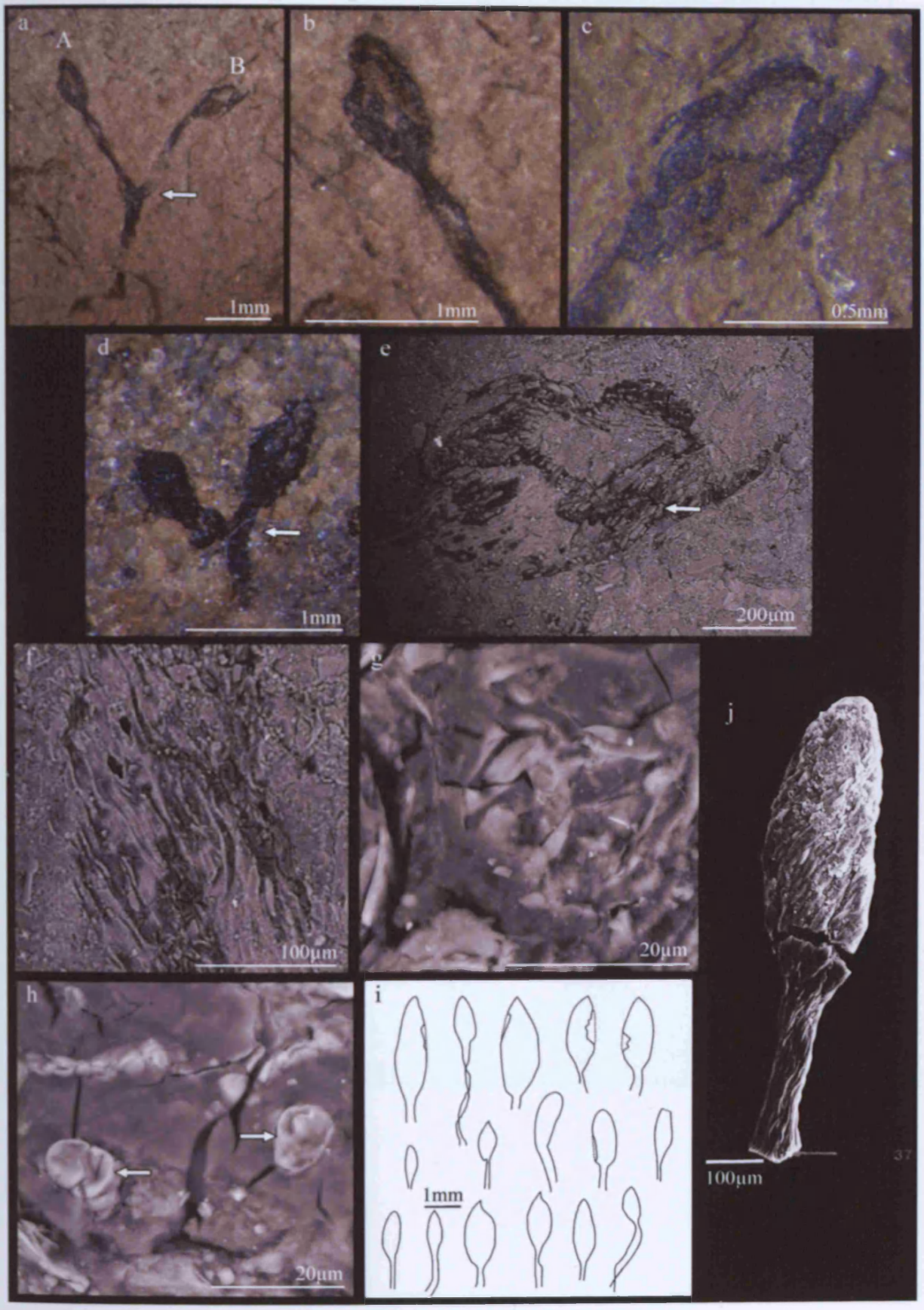

Plate 3.19: Other mesofossils with elongate sporangia

a: JM095b. Elongate, fusiform sporangium with short, narrow subtending axis.

b: RH2_8. Elongate, bulbous sporangium, attached to a narrow subtending axis.

c: RH248_1. Elongate, fusiform sporangium with pointed tip, attached to a narrow subtending axis.

d: RH005_1. Elongate, fusiform sporangium with pointed tip, attached to a subtending axis.

e: JM280a. Elongate, fusiform sporangium with rounded tip, attached to a subtending axis.

f: RHSp52b. Elongate, fusiform sporangium with rounded tip, attached to a subtending axis.

g: JM074b. Elongate sporangium with blunt tip, attached to a subtending axis.

h: JM037a. Elongate sporangium rounded tip, attached to a subtending axis. Largest sporangium of these specimens.

Plate 3.19: Other mesofossils with elongate sporangia.

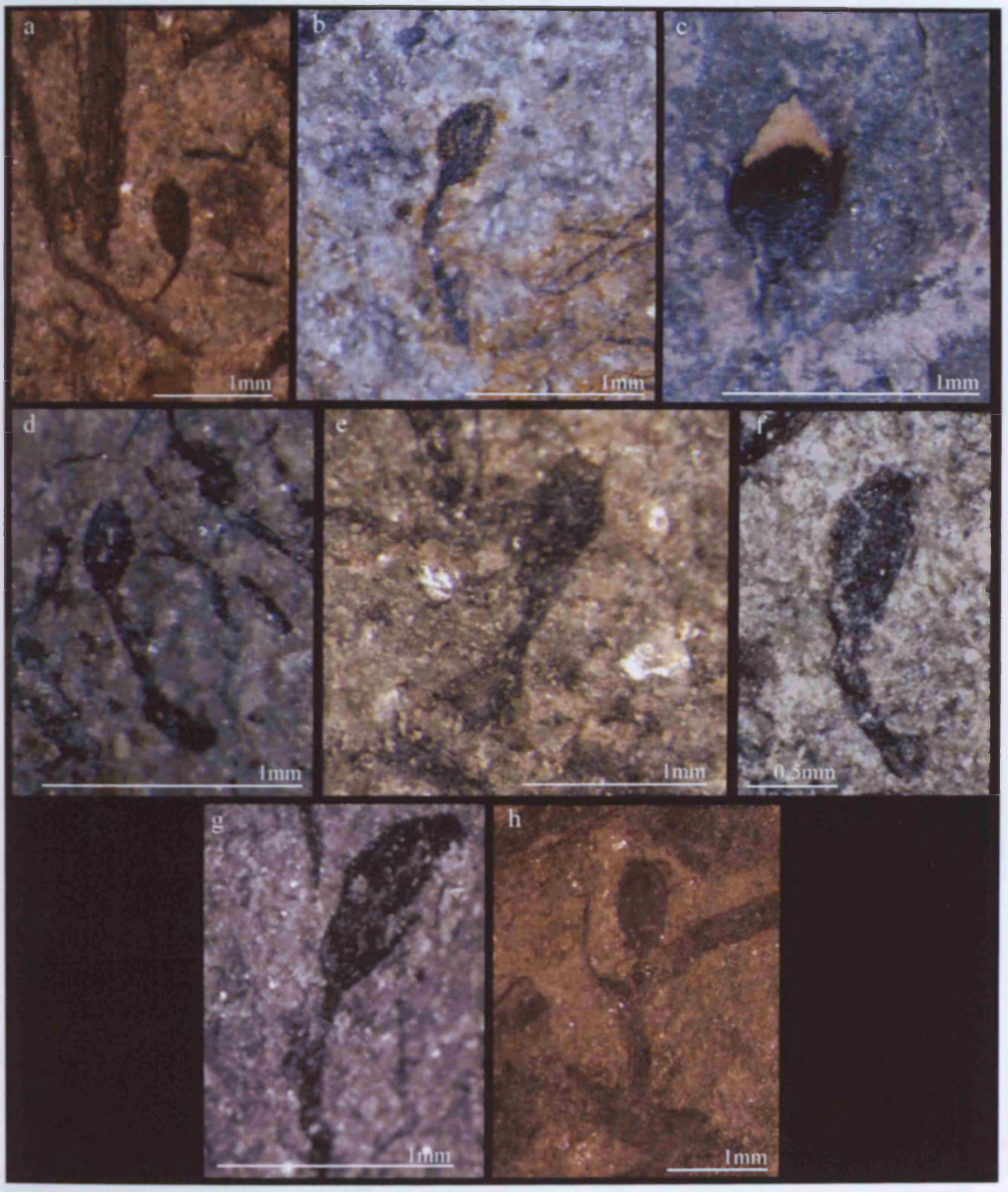

Plate 3.20: Cephalaspid fish specimen and *Prototaxites* sp. / *Nematasketum* sp. specimens

a: Cephalaspid fish found amongst non-embryophytes, and disseminated axial plant fossils.

b: SEM image of three-dimensional, wood-like, charcoalified fragment.

c: Largest coalified compression fossil of *Prototaxites* sp./ *Nematasketum* sp. "axis" from Tredomen Quarry, found in Plant Bed 2.

d: Randomly orientated, partially eroded, coalified compressions of irregularly shaped *Prototaxites* sp./ *Nematasketum* sp., with no anatomical detail.

e: Irregularly-shaped fragment of *Prototaxites* sp./ *Nematasketum* sp., partially preserved three-dimensionally, with longitudinal striations preserved.

f: "Axial" fragment of *Prototaxites* sp./ *Nematasketum* sp., which is elongate, and tapering at one end, with a blunt tip.

g: Elongate, axial-like, parallel-sided fragment of *Prototaxites* sp./ *Nematasketum*, tapering at one end, with a blunt tip.

h: Elongate, axial-like, parallel-sided fragment of *Prototaxites* sp./ *Nematasketum* sp.

i: Elongate, axial-like fragment of *Prototaxites* sp./ *Nematasketum* sp. with elongate striations running parallel to the fragment edge. Oval protuberances (see arrow) with longitudinal axis parallel to the alignment of striations and fragment edge.

j: Elongate, axial-like fragment of *Prototaxites* sp./ *Nematasketum* sp. with three oval shaped protuberances (see arrows), maximum length parallel to the alignment of the axis.

Plate 3.20: Cephalaspid fish specimen and *Prototaxites* sp. / *Nemataskетum* sp. specimens.

Plate 3.21: *Prototaxites* sp./ *Nematasketum* sp. specimens: anatomy

a: Light microscope image of partially three-dimensional coalified fragment of *Prototaxites* sp./ *Nematasketum* sp. Parallel-aligned, longitudinal striations/ tubes visible (see arrows).

b: Axial-like, three-dimensional charcoalified fragment of *Prototaxites* sp./ *Nematasketum* sp. Parallel-aligned tubes visible (see arrows).

c: Cross-section through a three-dimensional charcoalified fragment of *Prototaxites* sp./ *Nematasketum* sp., showing two of the three tube types: the wide, smooth-walled tubes (see arrows), surrounded by branching networks of narrower tubes.

d: Longitudinal view of three-dimensional charcoalified fragment of *Prototaxites* sp./ *Nematasketum* sp., showing densely packed, anastomosing thickenings (see arrows) on the interior wall of wide, thick-walled tube, in a matrix of narrower tubes.

e: Longitudinal view of three-dimensional charcoalified fragment of *Prototaxites* sp./ *Nematasketum* sp., showing anastomosing thickenings (see arrows) on the interior wall of wide, thick- walled tube.

f: Longitudinal view of *Prototaxites* sp./ *Nematasketum* sp. fragment, showing partially complete interior thickenings (see arrow) that are absent further along the tube.

g: Partial longitudinal section the *Prototaxites* sp./ *Nematasketum* sp. fragment, showing possible branching of the thickened wide tubes.

h: Cross-section of *Prototaxites* sp./ *Nematasketum* sp. fragment, showing partially joined wide thick-walled tubes (see arrow), possibly suggesting branching along the length of the tubes.

i: Cross-section of *Prototaxites* sp./ *Nematasketum* sp. fragment, showing large, wide thick-walled tubes surrounded by a network of narrow, randomly-orientated, branching tubes (see arrows).

j: Longitudinal section of *Prototaxites* sp./ *Nematasketum* sp. fragment, showing smaller tubes running parallel to the wider tubes (see arrows).

k: Cross-section view of *Prototaxites* sp./ *Nematasketum* sp. fragment, showing a high density of wide, thick-walled tubes compared with the smaller tubes.

l: Cross-section of *Prototaxites* sp./ *Nematasketum* sp. fragment, showing a low density of wide thick-walled tubes compared with the smaller tubes.

Plate 3.21: *Prototaxites* sp./ *Nematasketum* sp. specimens: anatomy

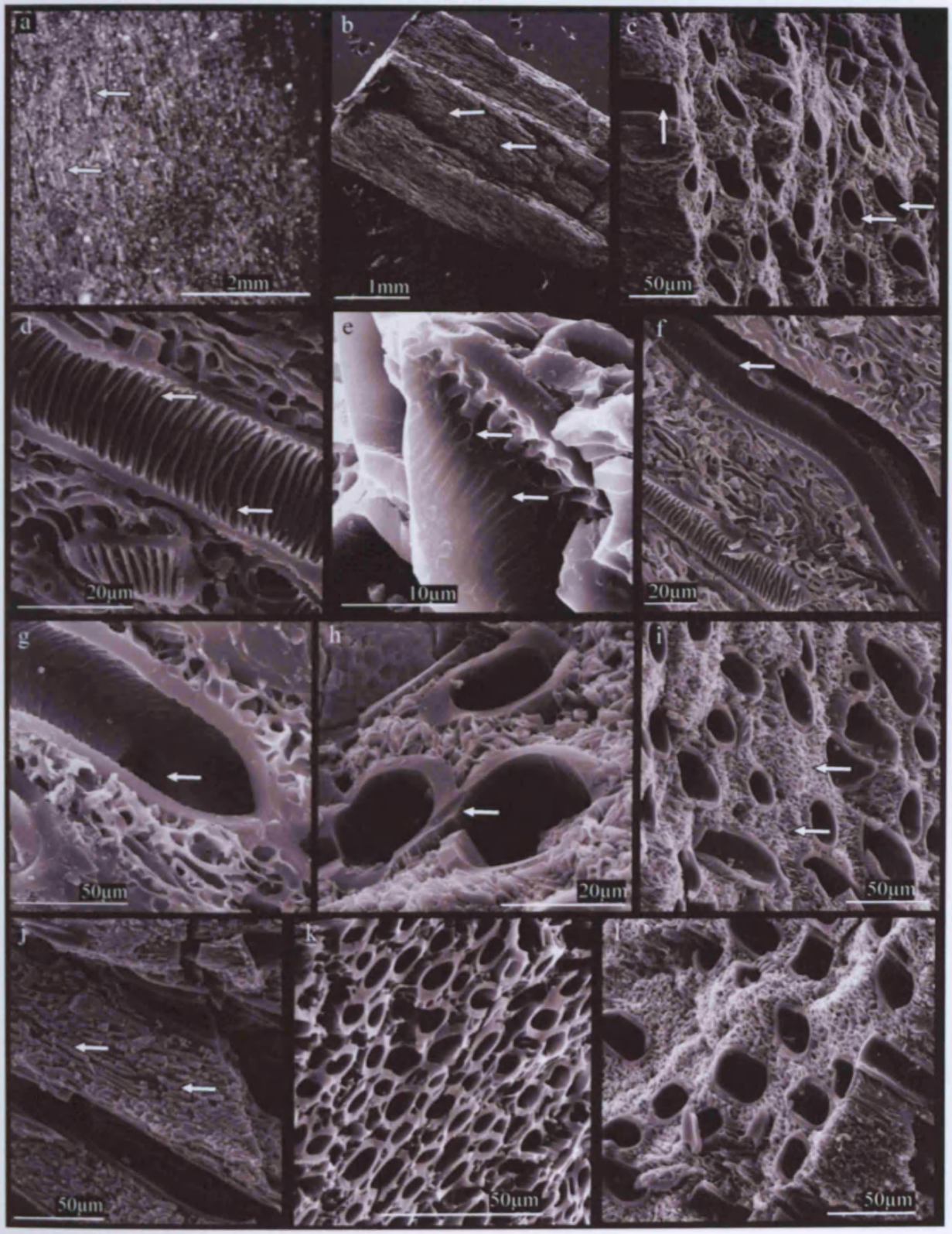

Plate 3.22: Hyphae specimens.

a: Intertwining and bifurcating coalified narrow tubes (see arrows).

b: Tubes that appear to weave in and out of the top surface of rock (see arrows).

c: Densely packed, parallel-aligned tubes, that form an axial-like structure, which branches (see arrow).

d: Densely packed, mat-like narrow tubes, randomly orientated at a variety of angles to each other.

e: Banded tube with annular thickenings on the inner surface. Tube in filled with limonite, with the impression of annular thickenings.

Plate 3.22: Hyphae specimens

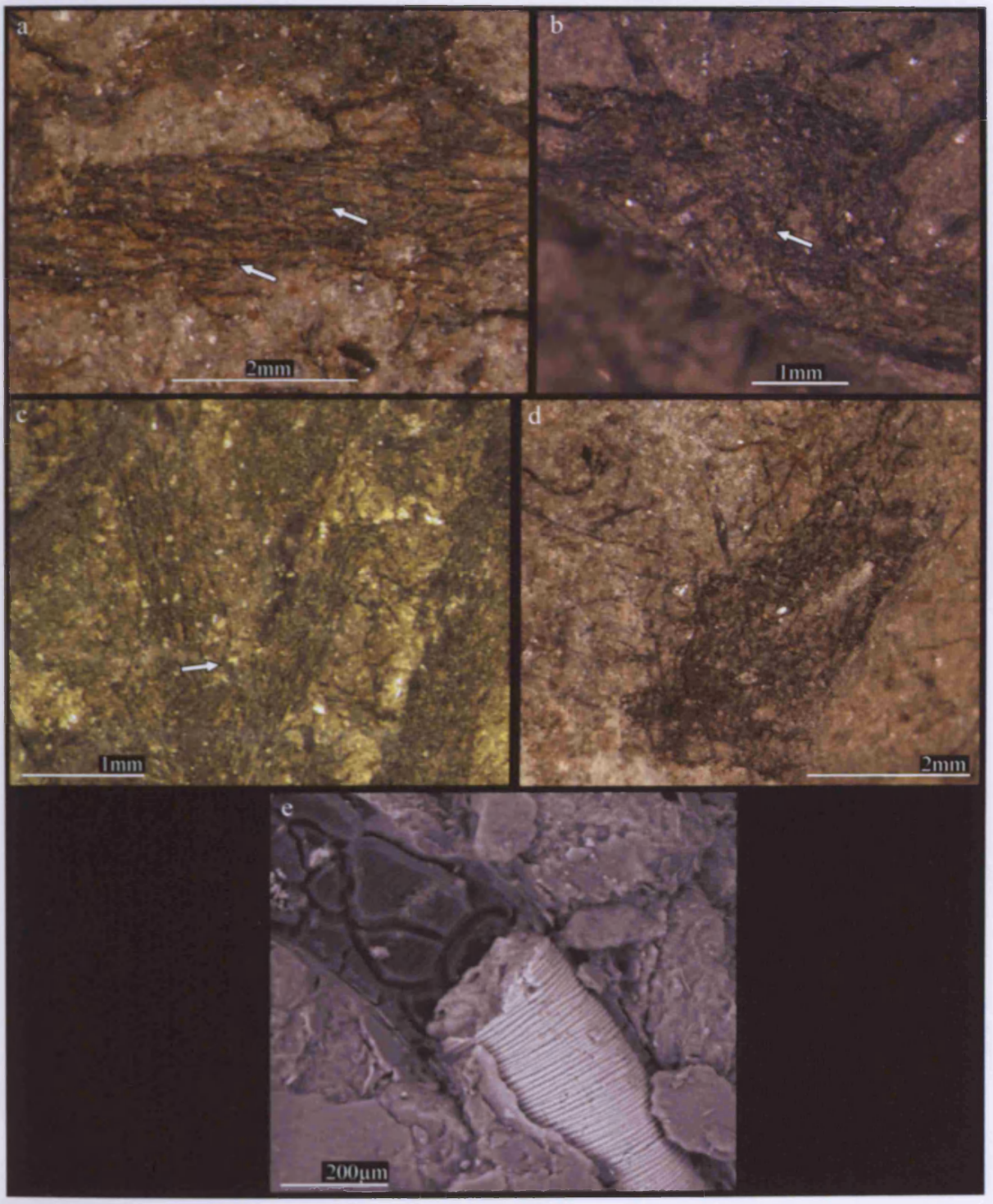

Plate 3.23: *Pachytheca* specimens

a: Small coalified sphere with vitreous outer surface.

b: Partially preserved small coalified sphere. Vitreous outer surface is the only remaining part.

c: Cross-section of a *Pachytheca* specimen, showing three layered structure: inner core (not preserved); radially-arranged tubes around the centre core, that make up the bulk of the sphere; and thin, amorphous outer layer.

d: Preserved portion of the central core, composed of narrow, randomly orientated bifurcating and anastomosing tubes.

e: Cross-section of a *Pachytheca* specimen; radially-arranged tubes around the central core.

f: Cross-section of a *Pachytheca* specimen; close up of radially-arranged tubes shown in 3.23*e*, showing annular thickenings on the inner surfaces (see arrow).

g: Cross-section of radially-arranged tubes shown in 3.23*e* and *f*, showing thin filaments that run down the lengths of some tubes (see arrows).

h: Cross-section of radially-arranged tubes, showing thin filaments that run down the lengths of some tubes (see arrows).

i: Cross-section of radially-arranged tubes, close to the central core, showing that many tubes have bulbous ends (see arrows).

j: Cross-section of radially-arranged tubes, showing the narrowing of the tubes (see arrows) just beneath outer, amorphous layer (see arrow).

k: Specimen showing radially-arranged tubes covered by thin, amorphous layer (see arrow).

l: Specimen showing thickened outer layer of *Pachytheca* (see arrow). Layer has a sponge-like texture with small voids.

Plate 3.23: *Pachytheca* specimens

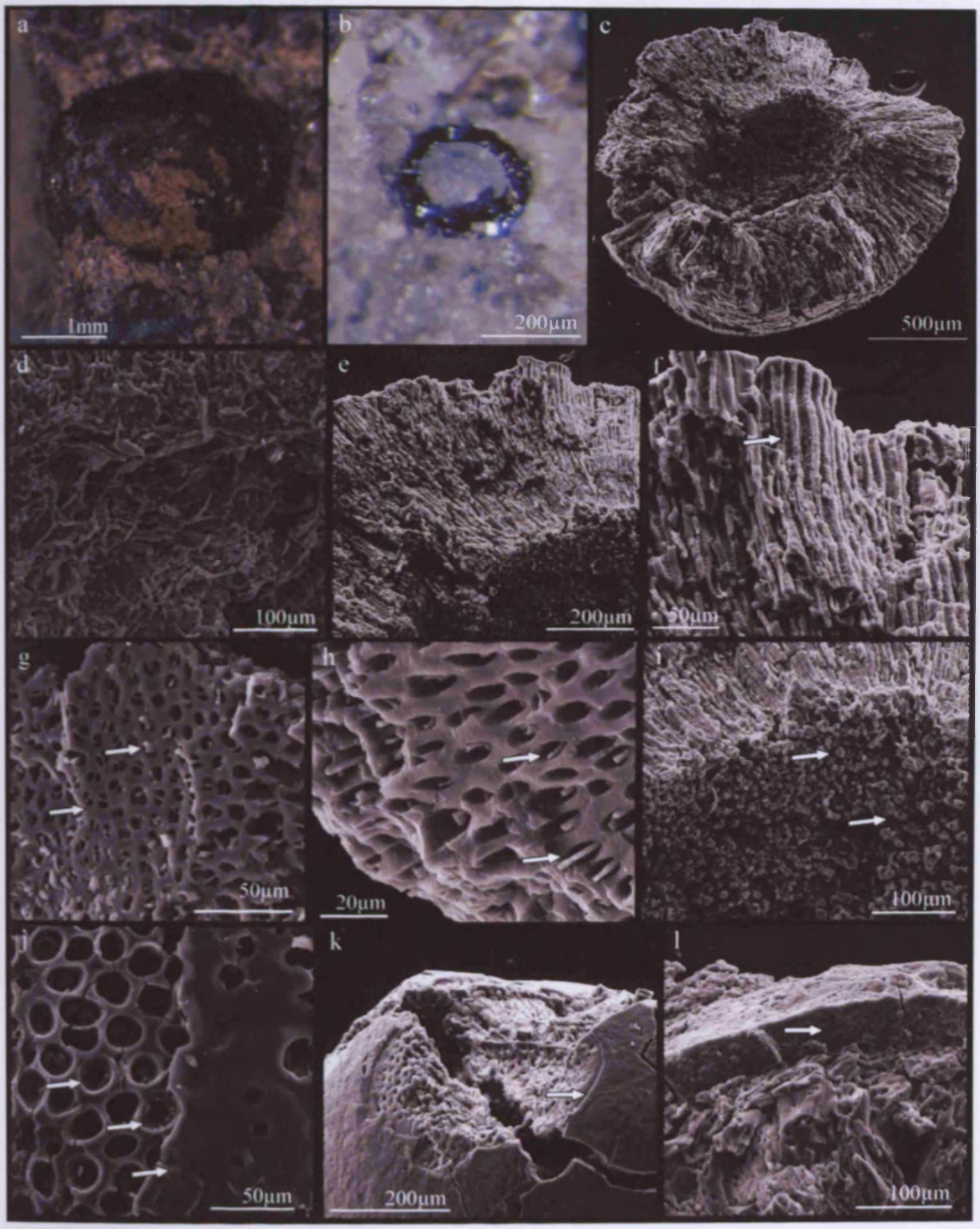

Plate 5.1: Fused laevigate tetrads

a* to *g*: *Cheilotetras caledonica

a: TRE1/153, Assemblage 1. Naked, fused tetrahedral tetrad with invaginated distal walls, and laevigate exine. Junction is marked by thickening of the exine.

b: TRE1/195, Assemblage 1. Naked, fused tetrahedral tetrad with invaginated distal walls, and laevigate exine. Junctions marked by thickening of the exine (see arrows).

c: TRE1/219, Assemblage 1. Naked, fused tetrahedral tetrad with invaginated distal walls, and laevigate exine. Junction is marked by the thickening of exine.

d: TRE1/010, Assemblage 1. Naked, fused tetrahedral tetrad with invaginated distal walls, and laevigate exine. Junctions marked by the thickening of exine (see arrow).

e: TQBH1-1(StubT1-1(2008)-114, Assemblage 2. Naked, fused tetrahedral tetrad with invaginated distal walls, and laevigate exine. Junctions marked by the thickening of exine.

f: TQBH1-1(StubT1-1(2008)-194, Assemblage 2. Naked, fused tetrahedral tetrad with invaginated distal walls, and laevigate exine. Junctions are marked by the thickening of exine.

g: TQBH2-1(StubT2-1(2008)-159, Assemblage 4. Naked, fused decussate (?) tetrad with invaginated distal walls and laevigate exine.

***h to l*: *Cheilotetras* sp.**

h: TRE1/007, Assemblage 1. Naked, fused decussate tetrad, with laevigate exine.

i: TRE1/083, Assemblage 1. Naked, fused tetrahedral tetrad, with laevigate exine.

j: TRE1/084, Assemblage 1. Naked, fused tetrahedral (?) tetrad with laevigate exine.

k: TRE1/143, Assemblage 1. Naked, fused tetrahedral (?) tetrad with laevigate exine.

l: TQBH2-1(StubT2-1(2008)-069, Assemblage 4. Naked, fused tetrahedral (?) tetrad with laevigate exine.

Plate 5.2: Fused laevigate dyads

a* to *f*: *Pseudodyadospora petasus

a: T1-6/PB0 (Stub 1-6)-266, Assemblage 1. Naked, fused dyad, with invaginated distal walls, with laevigate exine. Junction marked by a constriction (see arrow).

b: TQBH1-1(StubT1-2)-062, Assemblage 2. Naked, fused dyad, with invaginated distal walls, with laevigate exine. Junction marked by a constriction.

c: TQBH1-PB1(StubPB1-2008)-099, Assemblage 3. Partial naked, fused dyad, with invaginated walls, with laevigate exine. Junction marked by constriction (see arrow).

d: TQBH2-1(Stub T(2)2-1)-013, Assemblage 4. Naked, fused dyad, with invaginated distal walls, with laevigate exine.

e: TQBH1-3(StubT3-2)-049, Assemblage 5. Naked, fused dyad, with invaginated distal walls, with laevigate exine.

f: TQBH1-3(Stub T1-3(2008)-187, Assemblage 5.Naked, fused dyad, with invaginated distal walls, with laevigate exine. Junction marked by constriction.

g* to *l*: *Pseudodyadospora* cf. *laevigata

g: TRE1/045, Assemblage 1. Naked, fused dyad, with laevigate exine. No visible line of contact between sporal bodies, but exine is slightly thickened.

h: TRE1/047, Assemblage 1. Naked, fused dyad with laevigate exine. No visible line of contact between sporal bodies, but exine is slightly thickened (see arrow).

i: TQBH1-1(StubT1-1)-022, Assemblage 2. Naked, fused dyad (?) with laevigate exine. No visible line of contact between sporal bodies.

j: TQBH1-PB1(StubPB1-2008)-157, Assemblage 3. Naked, fused dyad with laevigate exine. No visible line of contact between sporal bodies, but exine is slightly thickened (see arrow).

k: TQBH2-1(StubT2-1(2008)-059, Assemblage 4. Naked, fused dyad (?) with laevigate exine.

l: TQBH2-1(StubT2-1(2008)-182, Assemblage 4. Naked, fused dyad with laevigate exine. No visible line of contact between sporal bodies, but exine is slightly thickened.

Plate 5.2: Fused laevigate dyads

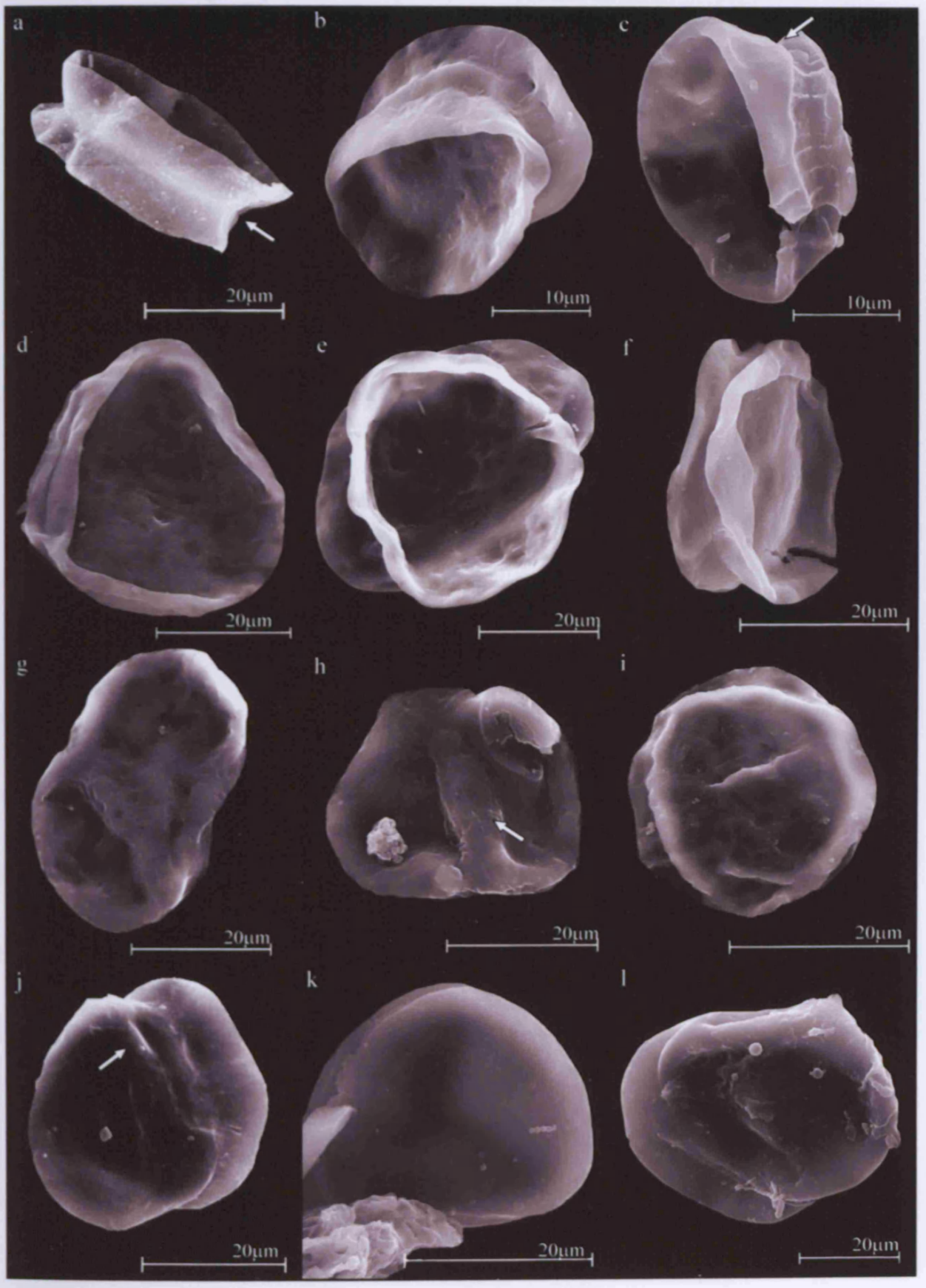

Plate 5.3: Fused, sculptured tetrads

a: ***Apiculate fused tetrad***

a: TQBH1-3(Stub T1-3(2008)-212, Assemblage 5. Naked, fused tetrad with invaginated distal walls, and no visible contact lines. Junctions are marked by exine thickenings (see arrow). Exine sculptured with large grana and verrucae elements.

b* to *j*: *Verrucate fused tetrads

b: T1-6/PB0 (Stub 1-6)-256, Assemblage 1. Naked, fused tetrad with invaginated distal walls. Exine sculptured with irregularly sized, closely spaced verrucae and rugulae (see arrow).

c: TRE1/186, Assemblage 1. Naked, fused tetrad with inflated distal walls. Exine sculptured with irregularly shaped, closely spaced verrucae and rugulae.

d: TRE1/129, Assemblage 1. Naked, fused tetrad with inflated distal walls. Exine sculptured with irregularly shaped, closely spaced verrucae and rugulae.

e: TQBH1-1-037, Assemblage 2. Naked, fused tetrad with inflated distal walls. Exine sculptured with irregularly shaped, closely spaced verrucae and rugulae.

f: TQBH1-PB1-082, Assemblage 3. Naked, fused tetrad with inflated walls. Exine sculptured with irregularly shaped, closely spaced verrucae and rugulae.

g: TQBH1-PB1-109, Assemblage 3. Naked, fused tetrad with inflated walls. Exine sculptured with irregularly shaped, closely spaced verrucae and rugulae.

h: TQBH1-PB1-165, Assemblage 3. Naked, fused tetrad, with inflated walls. Exine sculptured with irregularly shaped, closely spaced verrucae and rugulae.

i: TQBH1-PB1-117, Assemblage 3. Naked, fused tetrad with inflated walls. Exine sculptured with irregularly shaped, closely spaced verrucae and rugulae.

j: TQBH2-1-085, Assemblage 4. Naked, fused tetrad (?) with invaginated walls. Exine sculptured with irregularly shaped, closely spaced verrucae and rugulae.

k* and *l*: *Murornate fused tetrads

k: TRE1/167, Assemblage 1. Naked, fused tetrad, with invaginated walls. Exine has murornate sculpture, which is perpendicular to the contact region (see arrow).

l: TQBH1-PB1-002, Assemblage 3. Naked, fused tetrad with partially inflated walls. Exine sculptured with muri.

Plate 5.3: Fused, sculptured tetrads

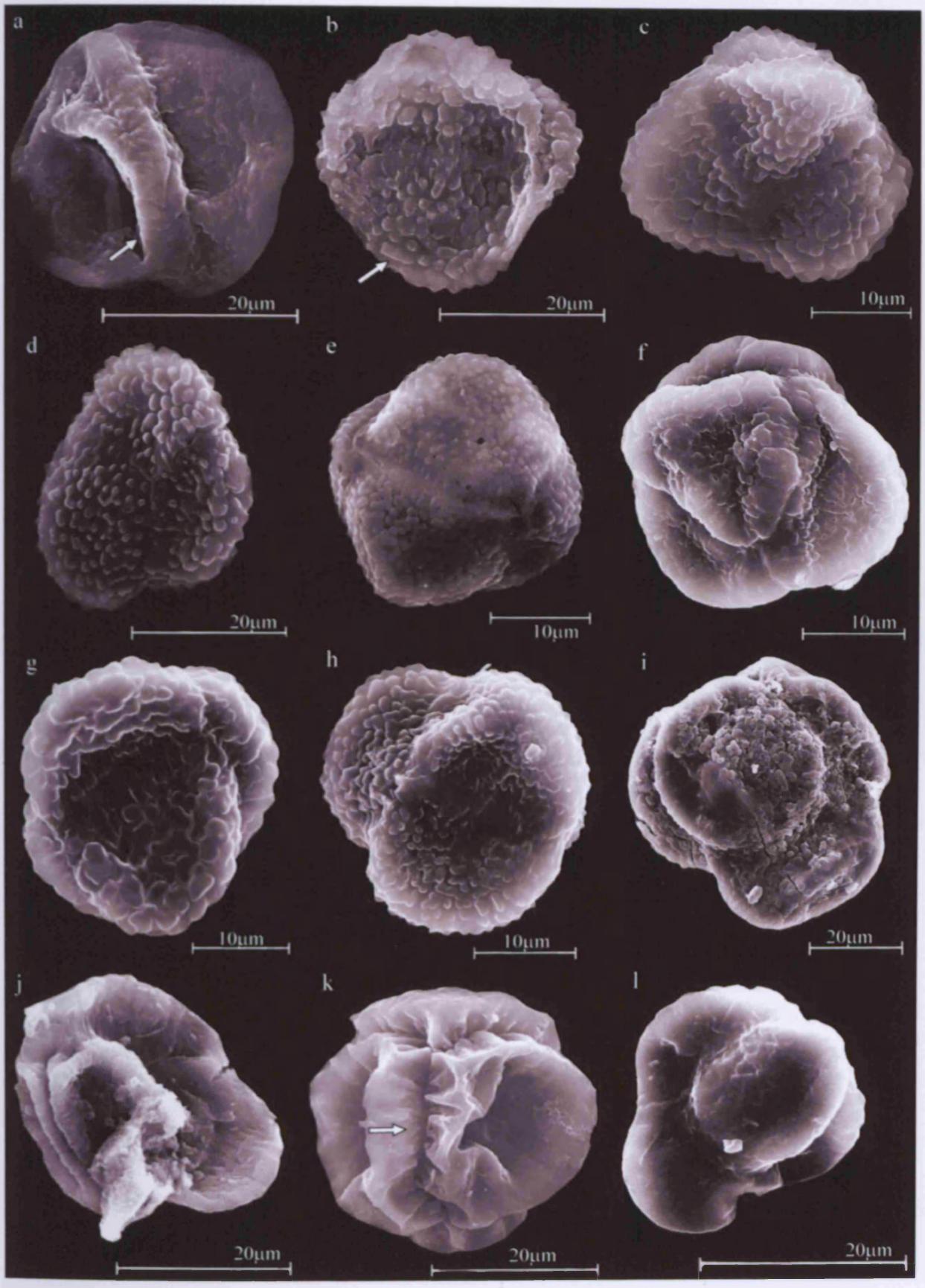

Plate 5.4: Unfused laevigate tetrads

a* to *f*: *Tetrahedraletes medinensis* var. *medinensis

a: T1-6/PB0 (Stub 1-6)-259, Assemblage 1. Naked, unfused decussate tetrad, with laevigate, invaginated distal walls. Clear contact lines are visible (see arrow). Each spore unit has an equatorial crassitude.

b: TQBH1-1-044, Assemblage 2. Naked, unfused tetrahedral tetrad, with partially laevigate invaginated distal walls. Clear contact lines are visible (see arrow).

c: TQBH1-1-093, Assemblage 2. Naked, unfused tetrahedral tetrad, with laevigate, invaginated distal walls. Clear contact lines are visible (see arrow).

d: TQBH2-1-072, Assemblage 4. Naked, unfused tetrahedral tetrad, with laevigate, inflated distal walls. Clear contact lines are visible (see arrow).

e: TQBH1-3-080, Assemblage 5. Naked, unfused tetrahedral tetrad, with some laevigate, invaginated walls, and one inflated wall (see arrow). Clear contact lines are visible.

f: TQBH1-3-228, Assemblage 5. Loose, naked unfused tetrahedral tetrad with partially invaginated distal walls. Clear contact lines are visible.

g* to *l*: *Tetrahedraletes medinensis* var. *parvus

g: TRE1/072, Assemblage 1. Naked, unfused decussate tetrad, with partially invaginated, laevigate distal walls. Clear contact lines are visible.

h: TQBH1-1-145, Assemblage 2. Naked, unfused decussate tetrad, with partially invaginated, laevigate distal walls. Clear contact lines are visible.

i: TQBH1-PB1-035, Assemblage 3. Naked, unfused tetrahedral tetrad, with partially invaginated, laevigate distal walls. Clear contact lines are visible.

j: TQBH2-1-036, Assemblage 4. Naked, unfused tetrahedral tetrad, with invaginated, laevigate distal walls. Clear contact lines are visible.

k: TQBH1-3(Stub T1-3(2008)-196, Assemblage 5. Naked, unfused decussate tetrad with invaginated, laevigate distal walls. Clear contact lines are visible.

l: TQBH1-3(Stub T1-3(2008)-216, Assemblage 5. Naked. Unfused tetrahedral tetrad with partially inflated, laevigate distal walls. Clear contact lines are visible.

Plate 5.4: Unfused laevigate tetrads

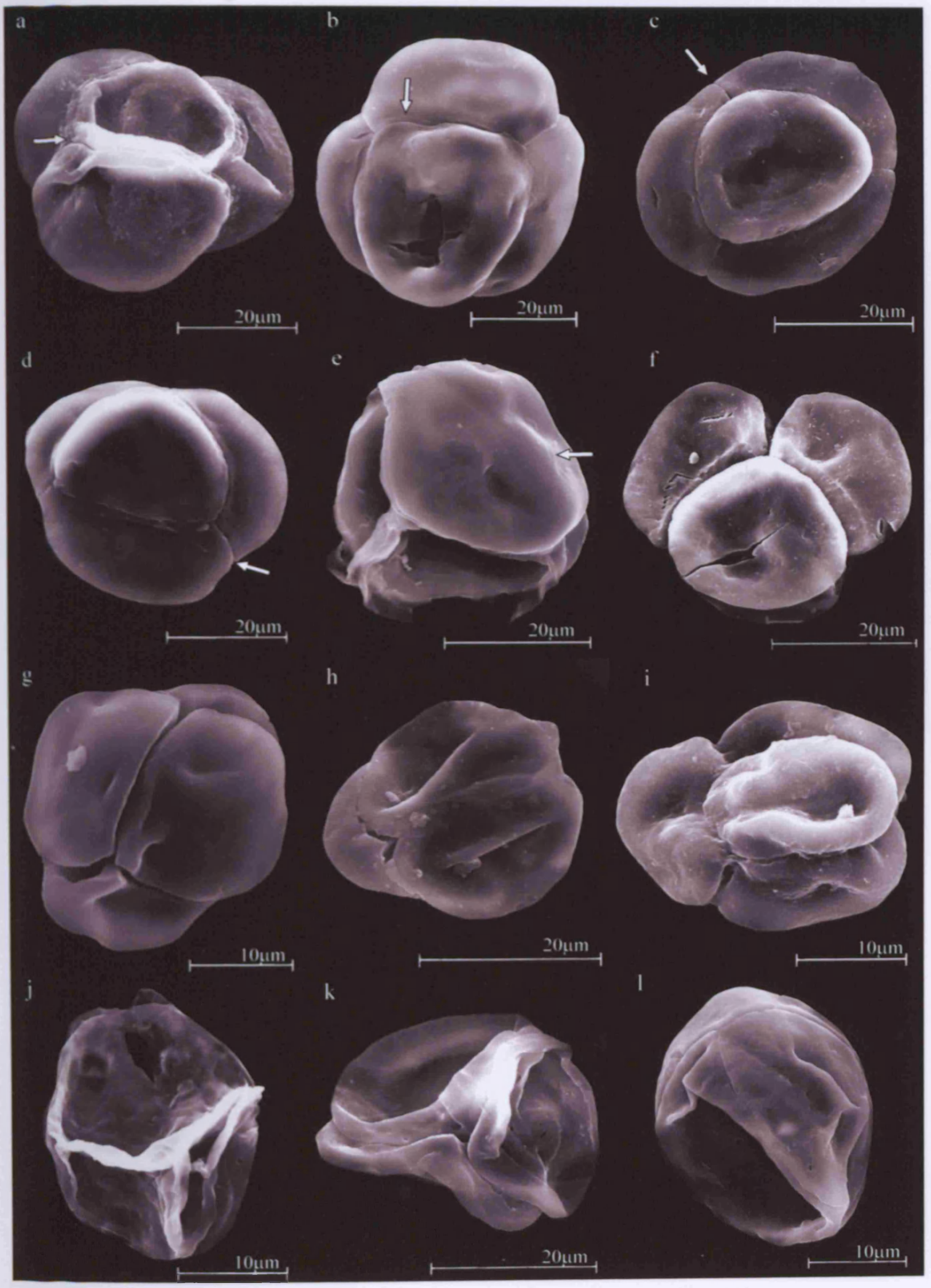

Plate 5.5: Unfused laevigate tetrads and dyads

a* and *b*: *Rimosotetras problematica

a: TRE1/168, Assemblage 1. Partially loose, tetrahedral tetrad, each spore unit with equatorial crassitude and invaginated distal walls. Junction marked by a constriction.

b: TQBH1-3-138, Assemblage 5. Partially loose, tetrahedral tetrad, each spore unit with equatorial crassitude and invaginated distal walls. Junction marked by a constriction.

c* to *g*: *Dyadospora murusdensa

c: TRE1/113, Assemblage 1. Naked, unfused dyad with clear contact lines. Distal walls inflated and laevigate.

d: TQBH2-1-044, Assemblage 4. Partially loose, naked unfused dyad, with clear contact lines. Distal walls inflated and laevigate. Hilum visible in one spore body (see arrow).

e: TQBH2-1-046, Assemblage 4. Naked, unfused dyad with clear contact lines. Distal walls inflated and laevigate.

f: TQBH1-3-004, Assemblage 5. Partially loose, naked, unfused dyad with clear contact lines. Distal walls inflated and laevigate.

g: TQBH1-3-033, Assemblage 5. Naked, unfused dyad, with clear contact lines. Distal walls are invaginated and laevigate.

h* to *l*: *Dyadospora murusattenuata

h: TRE1/205, Assemblage 1. Partially loose unfused dyad, with clear contact lines. Distal walls are thin, invaginated and laevigate.

i: TQBH1-1-123, Assemblage 2. Naked, unfused dyad (?) with invaginated, thin, laevigate distal walls.

j: TQBH1-PB1-054, Assemblage 3. Naked, unfused dyad, with invaginated, thin, laevigate distal walls.

k: TQBH2-1-038, Assemblage 4. Naked, unfused dyad (?) with invaginated, thin, laevigate distal walls.

l: TQBH1-3-090, Assemblage 5. Partially loose unfused dyad, with clear contact lines. Distal walls are thin, invaginated and laevigate.

Plate 5.5: Unfused laevigate tetrads and dyads

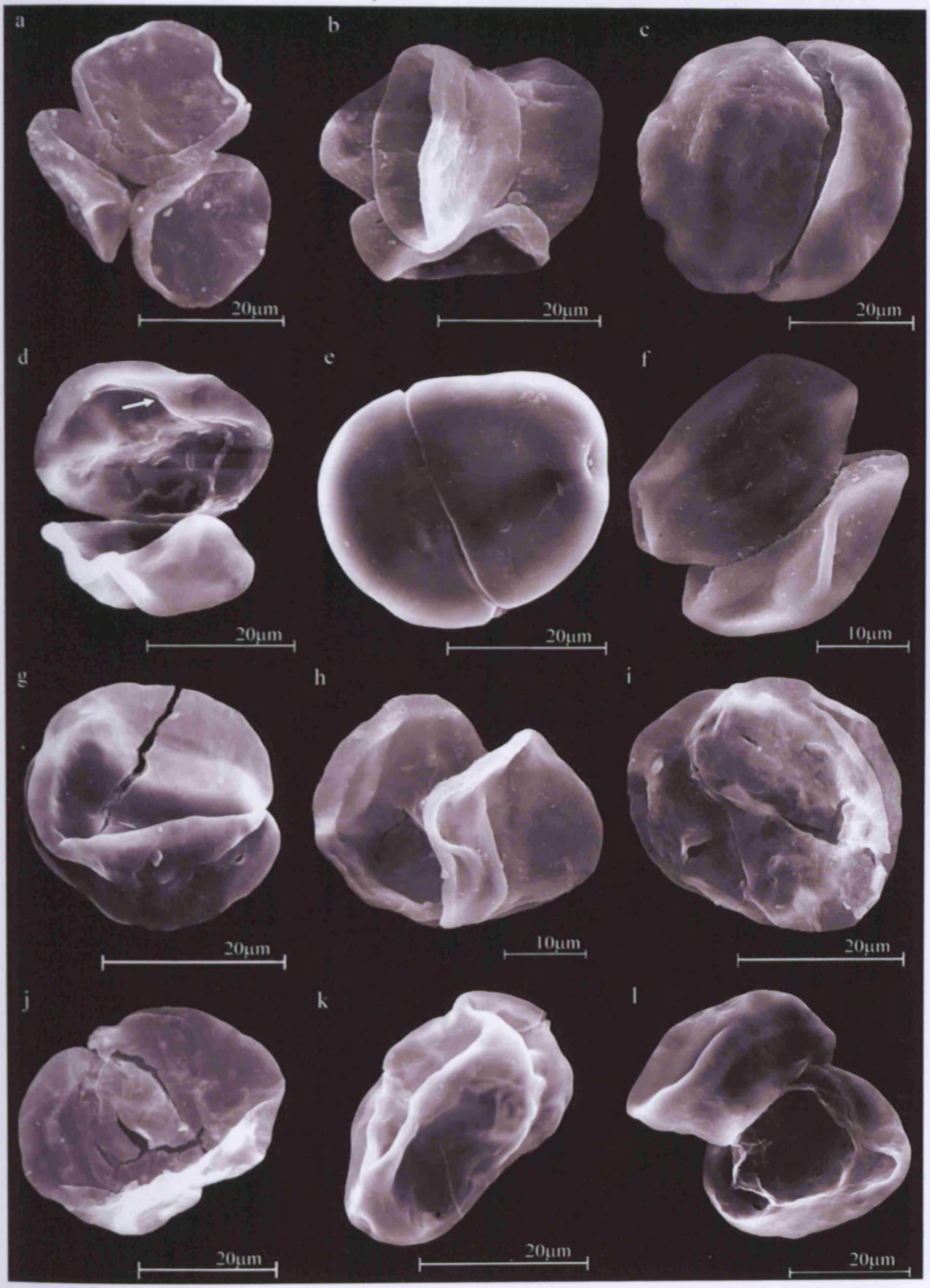

Plate 5.6: Unfused sculptured tetrads

a* to *f*: *Aconotetras inconspicus

a: TQBH1-PB1(StubPB1-2008)-107, Assemblage 3. Naked, unfused tetrad, with clear contact lines between units. Distal walls are invaginated, and sculptured with evenly spaced grana.

b: TQBH2-1(StubT2-1(2008)-082, Assemblage 4. Naked, unfused tetrad with clear contact lines between units. Distal walls are invaginated, and sculptured with evenly spaced grana. Each spore has an equatorial crassitude.

c: TQBH2-1(StubT2-1(2008)-112, Assemblage 4. Naked, unfused tetrad with clear contact lines between units. Distal walls are invaginated, and sculptured with evenly spaced grana. Each spore has an equatorial crassitude.

d: TQBH2-1(StubT2-1(2008)-115, Assemblage 4. Naked, unfused tetrad with clear contact lines between units. Distal walls are invaginated, and sculptured with irregular grana. Each spore has an equatorial crassitude.

e: TQBH2-1(StubT2-1(2008)-205, Assemblage 4. Naked, unfused tetrad with clear contact lines between units. Distal walls are invaginated, and sculptured with grana. Each spore has an equatorial crassitude.

f: TQBH1-3(Stub T1-3(2008)-227, Assemblage 5. Partial, naked unfused tetrad with clear contact lines between units. Distal walls are invaginated, and sculptured with grana. Each spore has an equatorial crassitude.

Plate 5.6: Unfused sculptured tetrads

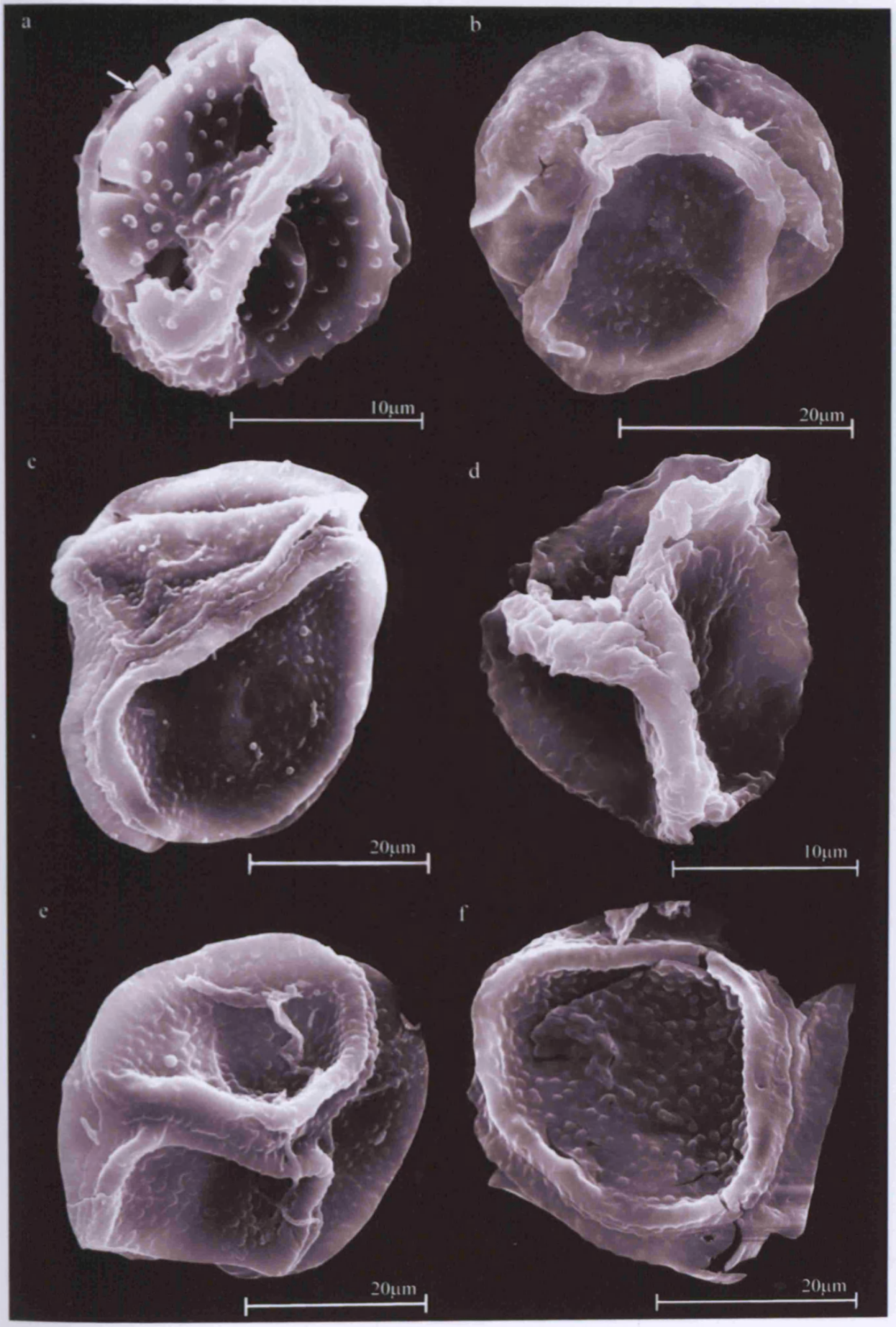

Plate 5.7: Laevigate hilate cryptospores

a* to *f*: *Laevolancis divellomedia

a: TRE1/091, Assemblage 1. Naked, proximally hilate alete monad with laevigate exine. Hilum has an irregular edge (see arrow).

b: TQBH1-1(StubT1-2)-060, Assemblage 2. Naked proximally hilate alete monad with laevigate exine. Hilum has a smooth edge (see arrow).

c: TQBH1-PB1(StubPB1-2008)-073, Assemblage 3. Naked, proximally hilate alete monad with laevigate exine. Hilum has an irregular edge (see arrow).

d: TQBH2-1(StubT(2)2-1)-032, Assemblage 4. Naked, proximally hilate alete monad with laevigate exine. Spore amb is elliptical.

e: TQBH2-1(StubT2-1(2008)-121, Assemblage 4. Naked, proximally hilate alete monad with laevigate exine. Hilum has an irregular edge (see arrow).

f: TQBH1-3(StubT3-2)-077, Assemblage 5. Naked proximally hilate alete monad with laevigate exine. Hilum has a smooth edge (see arrow).

g* to *l*: *Laevolancis plicata

g: TRE1/028, Assemblage 1. Naked, thin walled proximally hilate alete monads, with laevigate exine. Distal walls invaginated and folded.

h: TQBH1-1(StubT1-1)-034, Assemblage 2. Naked, thin walled proximally hilate alete monad with laevigate exine. Distal walls invaginated.

i: TQBH1-PB1(StubPB1-2008)-153, Assemblage 3. Naked, thin walled proximally hilate alete monad with laevigate exine. Distal walls invaginated and folded.

j: TQBH2-1(StubT(2)2-1)-037, Assemblage 4. Naked, thin walled proximally hilate alete monad with laevigate exine. Distal walls invaginated and folded.

k: TQBH1-3(StubT3-1)-014, Assemblage 5. Naked, thin walled proximally hilate alete monad with laevigate exine. Distal walls invaginated.

l: TQBH1-3(StubT3-2)-055, Assemblage 5. Naked thin walled proximally hilate alete monad with laevigate exine. Distal walls invaginated.

Plate 5.7: Laevigate hilate cryptospores

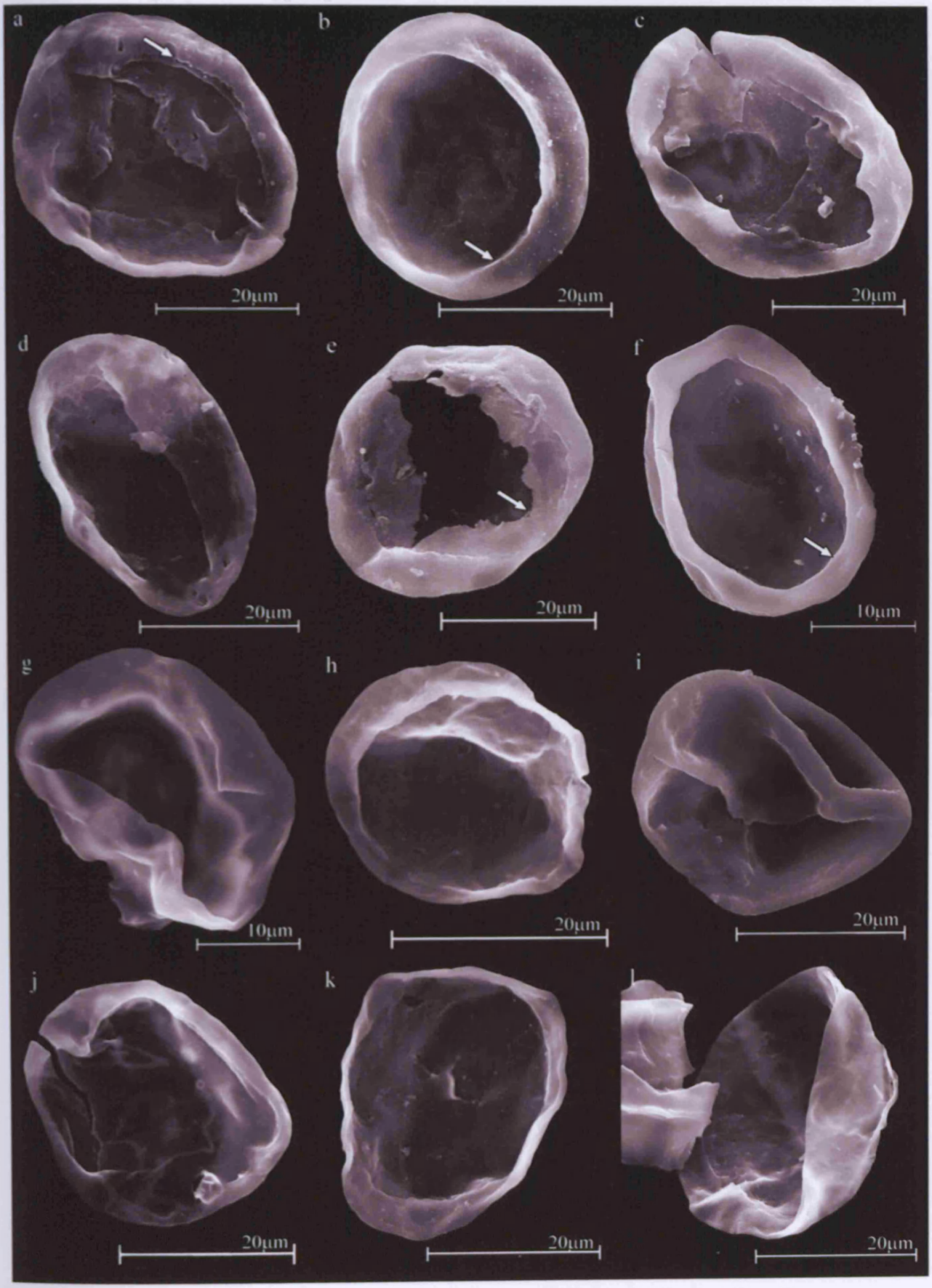

Plate 5.8: Laevigate and apiculate sculptured hilates.

a* and *b*: *Artemopyra* cf. *robusta

a: TQBH2-1-034, Assemblage 4. Naked, alete monad, with laevigate distal exine and proximal irregular hilum (see arrow) sculptured with radial muri.

b: close up of TQBH2-1-034, Assemblage 4. Hilum sculptured with radial muri (see arrow). Muri are straight to slightly sinuous and taper towards the centre.

***c* to *e*: *Artemopyra* sp. A**

c: TQBH1-3-009, Assemblage 5. Naked, alete monad, with laevigate distal exine and proximal hilum sculptured with radial muri (see arrow). Muri run from the equator to half-way into the hilum centre. Muri are straight, low and not prominent.

d: TQBH1-3-129, Assemblage 5. Naked, alete monad, with laevigate distal exine and proximal hilum sculptured with radial muri (see arrow).

e: close up of TQBH1-3-129, Assemblage 5. Hilum sculptured with radial muri, straight to slightly sinuous (see arrow).

f* to *l*: *Cymbohilates allenii* var. *allenii

f: TRE1/138, Assemblage 1. Naked hilate monad with double walled exine. Distal surface sculptured with closely and irregularly spaced micrograna. Proximal surface sculptured with concentric folds or muri.

g: close up of TRE1/138, Assemblage 1. Smooth hilum (see arrow), with micrograna on the distal surface.

h: TQBH1-1-129, Assemblage 2. Naked, hilate monad with irregular hilum (see arrow). Proximal surface smooth, with few muri. Distal surface sculptured with micrograna.

i: close up of TQBH1-1-129, Assemblage 2. Distal surface sculptured with micrograna (see arrow). Proximal surface sculptured with muri.

j: TQBH1-PB1-091, Assemblage 3. Hilate monad with closely- spaced irregular micrograna to microconi (see arrow) on the distal surface.

k: TQBH2-1-023, Assemblage 4. Hilate monad with closely spaced, irregularly micrograna.

l: close up of TQBH2-1-023, Assemblage 4. Smooth hilum (see arrow) with smooth proximal surface.

Plate 5.8: Laevigate and apiculate sculptured hilates

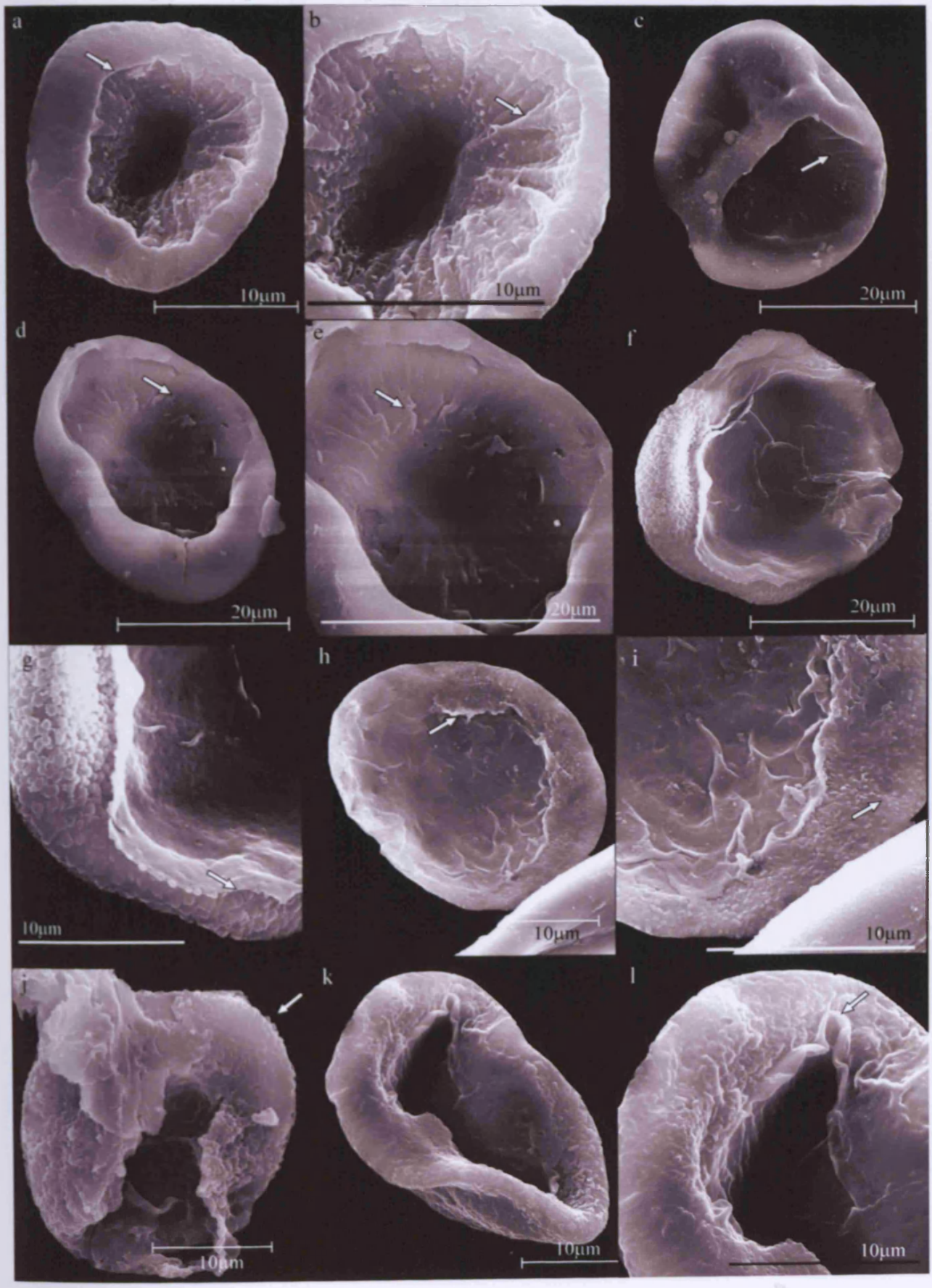

Plate 5.9: Apiculate sculptured hilates and dyad

a* to *h*: *Cymbohilates allenii* var. *magnus

a: TRE1/117, Assemblage 1. Naked hilate monad, with laevigate proximal surface, and distally sculptured with grana and micrograna.

b: TQBH1-1(StubT1-1(2008)-168, Assemblage 2. Naked, hilate monad, with proximally laevigate surface, with concentric folds and muri (see arrow). Distal surface sculptured with micrograna.

c: Close up of TQBH1-1(StubT1-1(2008)-168, Assemblage 2. Distal surface sculptured with micrograna.

d: TQBH1-PB1(StubPB1-2008)-022, Assemblage 3. Naked, hilate monad, with distally sculptured, closely packed micrograna. Proximal surface laevigate.

e: TQBH2-1(StubT2-1(2008)-110, Assemblage 4. Naked, unfused dyad, distal walls sculptured with closely-packed micrograna.

f: Close up of TQBH2-1(StubT2-1(2008)-110, Assemblage 4. Distal surface sculptured with micrograna.

g: TQBH1-3(Stub T1-3(2008)-203, Assemblage 5. Naked, hilate monad, with proximally laevigate hilum. Distal wall sculptured with micrograna and microconi.

h* and *i*: *Cymbohilates* cf. *amplus

h: TRE1/106, Assemblage 1. Large naked, hilate monad, distal walls sculptured with irregularly sized, closely packed micrograna and grana. Proximal surface not visible.

i: Close up of TRE1/106, Assemblage 1. Distal wall sculptured with closely packed, variable sized micrograna and grana.

Plate 5.9: Apiculate sculptured hilates and dyad

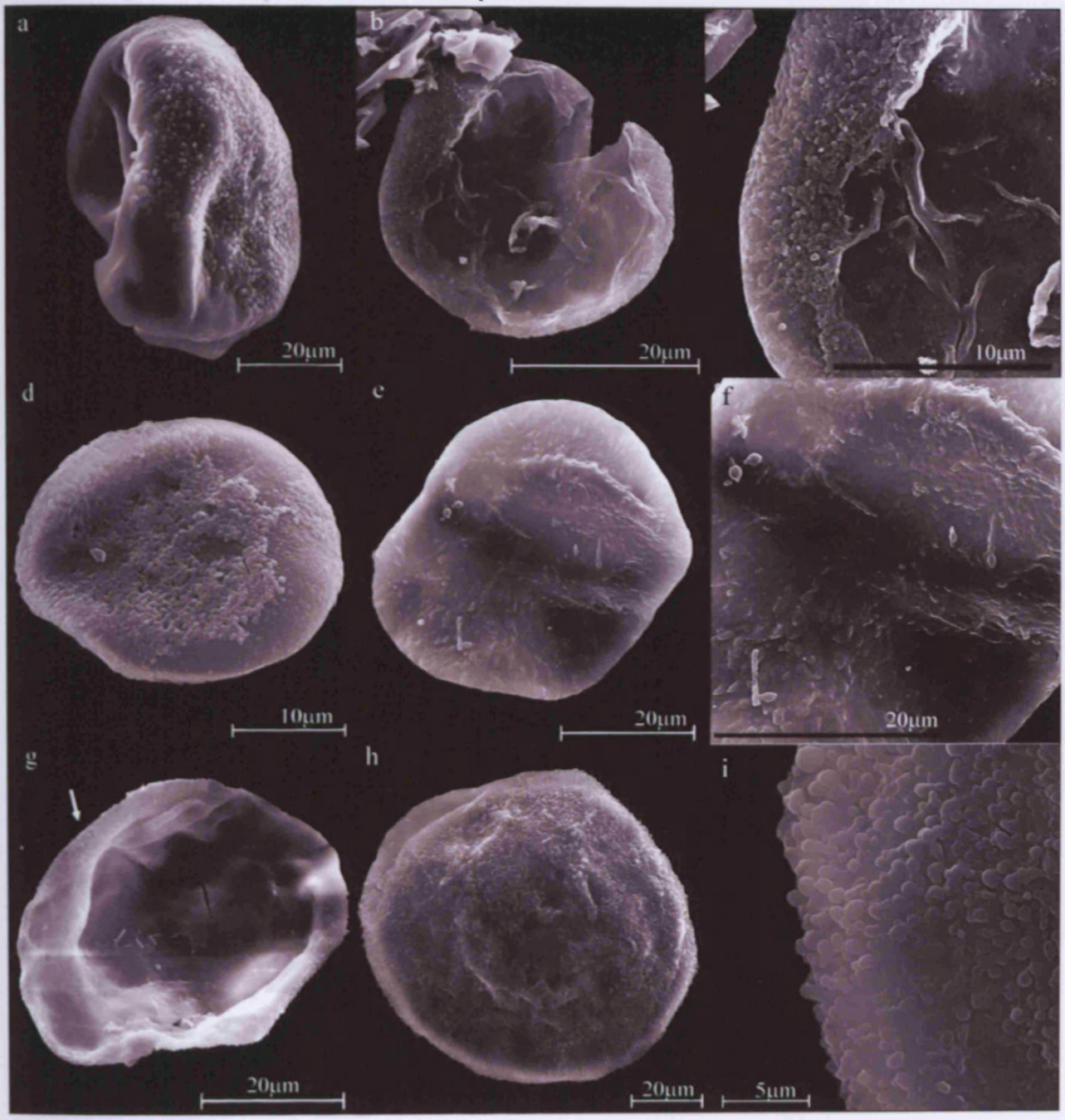

Plate 5.10: Apiculate sculptured hilates and dyads and tetrads (continued)

a* to *l*: *Cymbohilates disponerus

a: TQBH1-PB1(StubPB1-2008)-028, Assemblage 3. Naked, hilate monads, separated from a dyad. Proximal surface laevigate, with thick folds or muri (see arrow). Distal walls sculptured with evenly spaced, isodiametric coni and microconi.

b: Close up of TQBH1-PB1(StubPB1-2008)-028, Assemblage 3. Distal surface sculptured with coni and microconi (see arrow).

c: TQBH1-PB1(StubPB1-2008)-093, Assemblage 3. Naked, hilate monad with laevigate proximal surface, with thick folds and muri. Distal surface sculptured with evenly spaced coni and microconi (see arrow).

d: TQBH2-1(Stub T(2)2-1)-008, Assemblage 4. Naked, hilate monad with laevigate proximal surface, with thick folds and muri. Distal walls sculptured with coni (see arrow).

e: TQBH2-1(StubT2-1(2008)-106, Assemblage 4. Naked, hilate monad, with laevigate proximal surface, with thick folds and muri. Distal surface sculpturd with coni (see arrow).

f: TQBH2-1(StubT2-1(2008)-120, Assemblage 4. Naked, hilate monad, with distal surface sculptured with coni and microconi. Proximal surface not visible.

g: TQBH2-1(StubT2-1(2008)-140, Assemblage 4. Naked, hilate monad, with distal surface sculptured with evenly spaced coni and microconi. Proximal surface laevigate with thick folds and muri.

h: TQBH1-3(StubT3-2)-086, Assemblage 5. Naked hilate monad, with laevigate proximal surface. Distal walls sculptured with closely spaced microconi.

i: Close up of TQBH1-3(StubT3-2)-086, Assemblage 5. Distal wall sculptured with microconi (see arrow).

j: TRE1/141, Assemblage 1. Naked, unfused dyad with distal walls sculptured with evenly spaced microconi.

k: TQBH2-1(StubT(2)2-1)-026, Assemblage 4. Naked, unfused tetrad with distal walls sculptured with evenly spaced coni to grana.

l: Close up of TQBH2-1(StubT(2)2-1)-026, Assemblage 4. Distal surface sculptured with evenly spaced coni to grana

Plate 5.10: Apiculate sculptured hilates, dyads and tetrad

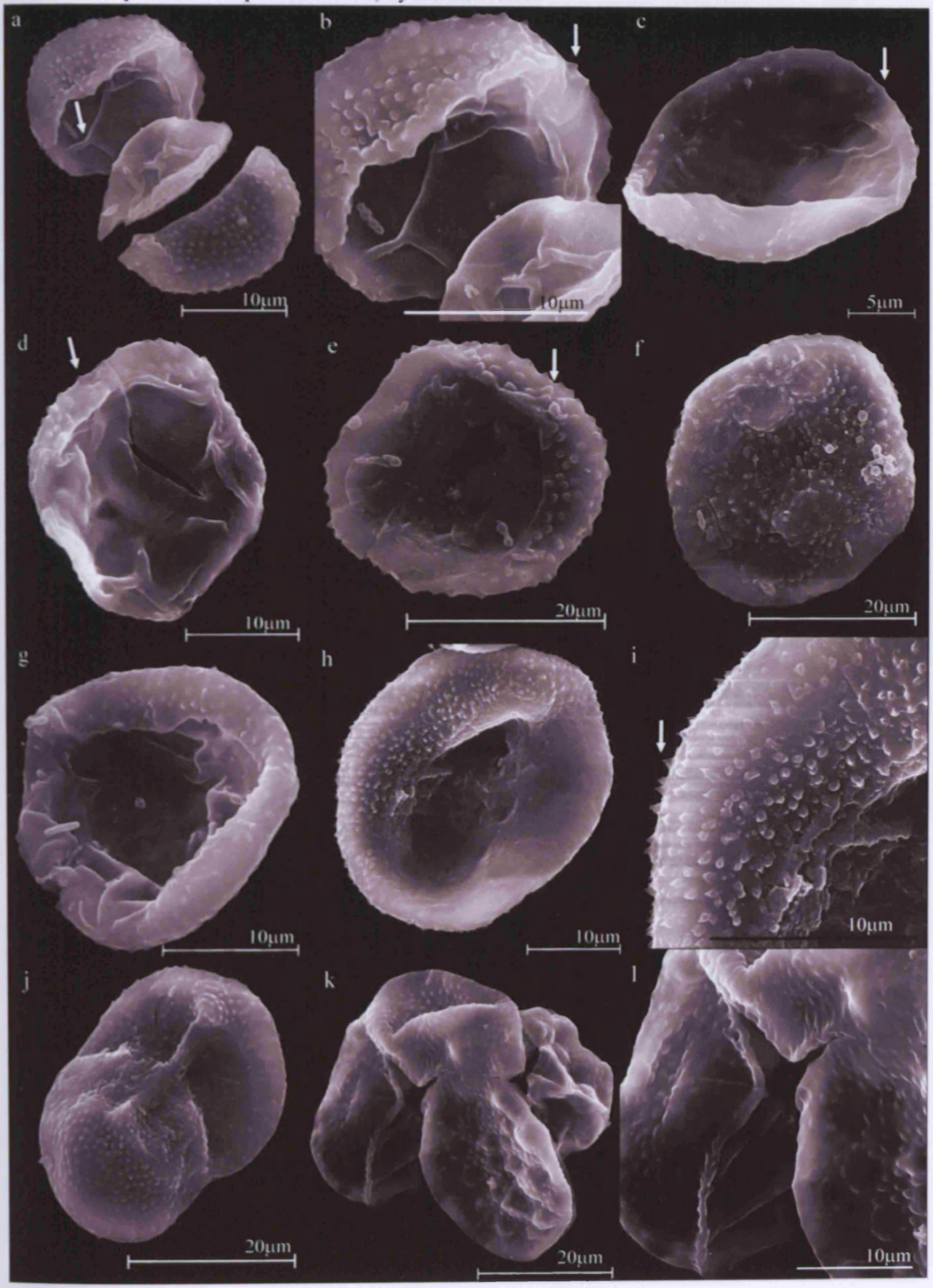

Plate 5.11: Apiculate sculptured hilates and dyads (continued)

a* to *c*: *Cymbohilates* cf. *microgranulatus

a: TQBH2-1-113, Assemblage 4. Naked, alete monad (?), distal surface sculptured with closely spaced micrograna (see arrow). Exine thickly folded.

b: TQBH2-1-218, Assemblage 4. Naked, alete monad, distally sculptured with closely spaced micrograna.

c: Close up of TQBH2-1-218, Assemblage 4. Distal surface sculptured with closely spaced micrograna (see arrow). Proximal surface laevigate, with irregular broad folds.

d* to *i*: *Cymbohilates variabilis* var. *variabilis

d: TRE1/120, Assemblage 1. Naked, hilate monad, distally sculptured with large, closely, irregularly spaced grana and verrucate.

e: Close up of TRE1/120, Assemblage 1. Distal wall sculptured with large grana and verrucate, in some cases fused to form rugulae (see arrow).

f: TQBH1-PB1-196, Assemblage 3. Naked, hilate monad, distally sculptured with large, irregularly spaced grana or verrucae.

g: Close up of TQBH1-PB1-196, Assemblage 3. Distal wall sculptured with large grana and verrucate, in some cases fused to form rugulae (see arrow).

h: TQBH2-1-193, Assemblage 4. Loose, naked, unfused dyad, distally sculptured with large grana to verrucae. Proximal surface laevigate with broad folds.

i: Close up of TQBH2-1-193, Assemblage 4. Loose, unfused dyad, proximal surface laevigate.

j* to *l*: *Cymbohilates variabilis* var. *parvidecus

j: TRE1/232, Assemblage 1. Naked, hilate monad. Distal wall sculptured with evenly, closely spaced large grana to verrucae. Proximally sculptured with closely spaced radial muri, fused at the proximal pole.

k: Close up of TRE1/232, Assemblage 1. Distal wall sculptured with closely spaced large grana and verrucae.

l: TQBH2-1(StubT2-1(2008)-137, Assemblage 4. Naked, hilate monad, distally sculptured with evenly, closely spaced large grana or verrucae. Some elements are fused (see arrow).

Plate 5.11: Apiculate sculptured hilates and dyad

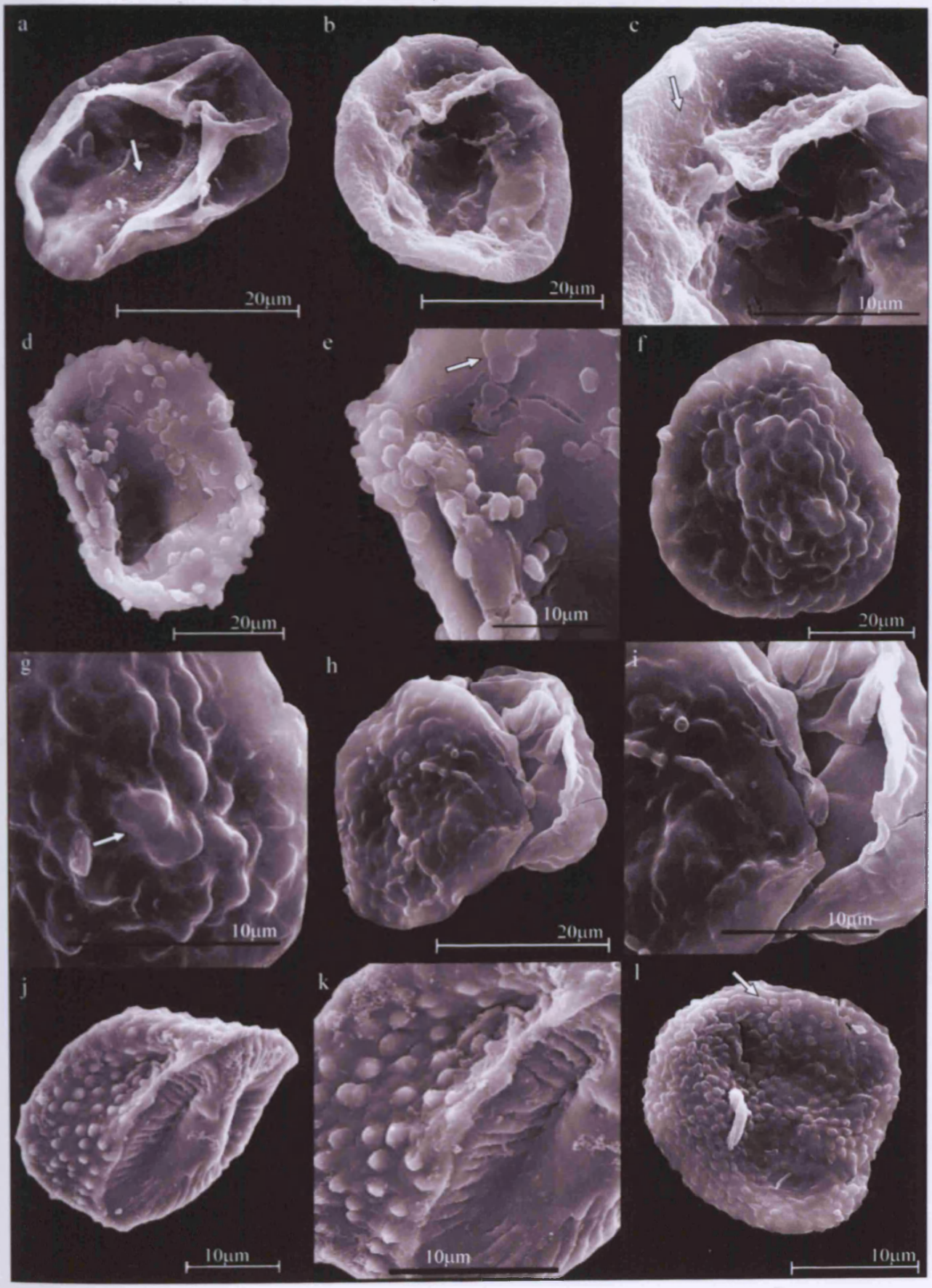

Plate 5.12: Apiculate sculptured hilates and dyads (continued)

***a* to *h*: *Cymbohilates variabilis* var. B (var. nov)**

a: TRE1/098, Assemblage 1. Naked, hilate monad (?). Distal walls sculptured with irregularly spaced, grana and micrograna. Proximal surface not visible.

b: Close up of TRE1/098, Assemblage 1. Distal wall sculptured with grana and micrograna.

c: TQBH1-PB1(StubPB1-2008)-069, Assemblage 3. Naked, hilate monad (?), distal wall sculptured irregularly and sparsely spaced grana, micrograna and spatulate elements. Proximal surface not visible.

d: Close up of TQBH1-PB1(StubPB1-2008)-069, Assemblage 3. Distal wall sculptured with irregularly spaced and irregularly shaped elements, including spatulate and rugulae elements (see arrow).

e: TRE1/069, Assemblage 1. Loose, naked, unfused dyad, with distal wall sculptured with irregularly and sparsely spaced elements, including micrograna.

f: Close up of TRE1/069, Assemblage 1. Loose, naked unfused dyad, with distal wall sculptured with irregular and sparsely spaced elements, including micrograna and rugulae.

g: TRE1/103, Assemblage 1. Naked, unfused dyad, with distal wall sculptured with irregularly and sparsely spaced elements, including spatulate elements (see arrow).

h: Close up of TRE1/103, Assemblage 1. Naked, unfused dyad. Elements close to the contact line are perpendicular (see arrow).

Plate 5.12: Apiculate sculptured hilates and dyads

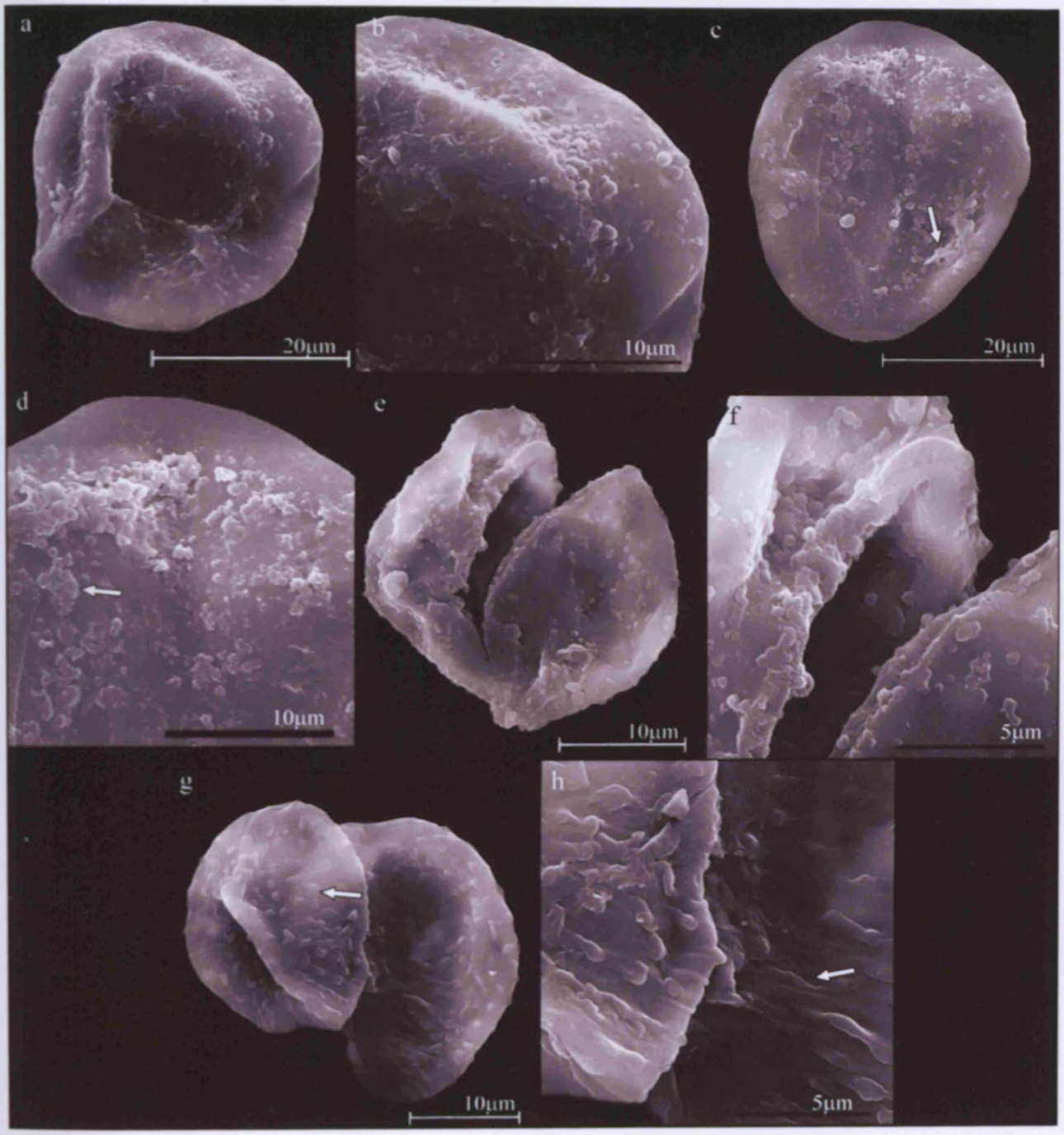

Plate 5.13: Spinose sculptured hilates and dyads

a* to *f*: *Cymbohilates cymosus

a: T1-6/PB0 (Stub 1-6)-277, Assemblage 1. Naked, hilate (?) monad. Distal wall sculptured with closely packed spinose elements, arranged in a star shape, with long axis of spines running parallel with the exine surface. Proximal surface not visible.

b: Close up of T1-6/PB0 (Stub 1-6)-277, Assemblage 1. Naked, hilate monad with distal wall sculptured with spinose elements, arranged in a star shape, with long axis of spines running parallel with exine surface (see arrow). Spines fused at the base.

c: TRE1/115, Assemblage 1. Naked, hilate unfused dyad with distal wall sculptured with irregularly arranged clusters of spinose elements, including biform spines (see arrow).

d: Close up of TRE1/115, Assemblage 1. Naked, hilate unfused dyad. Distal wall sculptured with irregularly arranged clusters of spinose elements, with long axis running parallel to the exine surface.

e: TRE1/236, Assemblage 1. Two naked, unfused tetrads. Distal walls sculptured with irregularly arranged clusters of spinose elements.

f: Close up of TRE1/236, Assemblage 1. Distal walls sculptured with irregularly arranged clusters of spinose elements.

g* to *i*: *Cymbohilates horridus

g: TRE1/003, Assemblage 1. Naked, unfused dyad. Distal walls sculptured with long spinose elements. Spines are fused at the base, forming muri (see arrow).

h: Close up of TRE1/003, Assemblage 1. Naked, unfused dyad, distal walls sculptured with spinose elements. Spines fused at the base, forming muri.

i: TQBH1-1(Ox1)-054, Assemblage 2. Partial naked, unfused dyad. Distal walls are sculptured with long spinose elements.

Plate 5.13: Apiculate sculptured hilates, dyads and tetrad

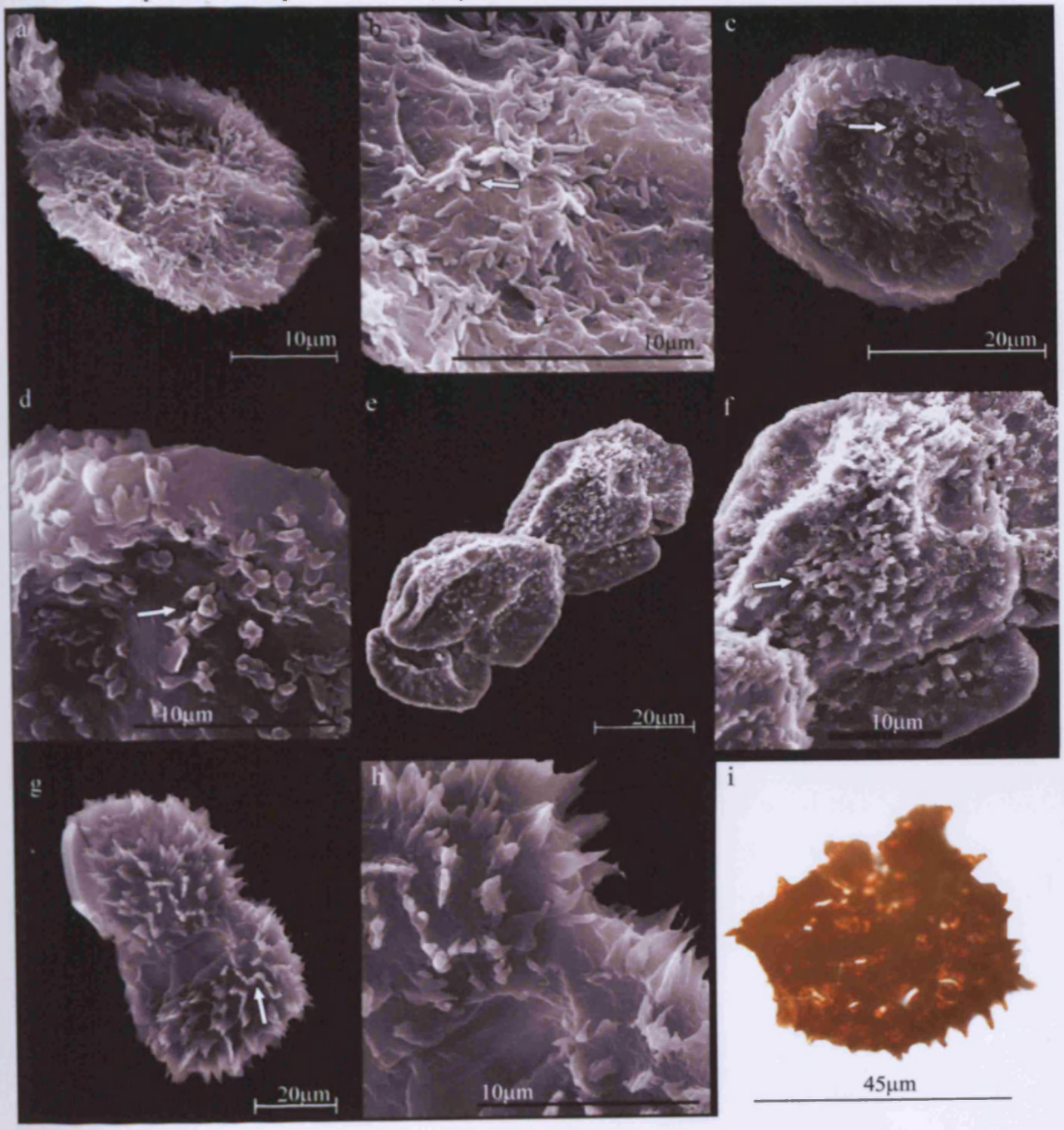

Plate 5.14: Spinose sculptured hilates and dyads.

***a* to *j*: *Cymbohilates horridus* var. A (var. nov.)**

a: TRE1/147, Assemblage 1. Naked hilate monad. Proximal surface is laevigate. Distal wall sculptured with small, evenly spaced spines (see arrow). Spine tips are rounded.

b: TQBH1-1(StubT1-2)-066, Assemblage 2. Naked hilate monad. Distal wall sculptured with small, evenly spaced spines. Spine tips are pointed.

c: Close up of TQBH1-1(StubT1-2)-066, Assemblage 2. Distal wall sculptured with small, evenly spaced spines (see arrow). Spine tips are pointed.

d: TQBH1-PB1(StubPB1-2008)-020, Assemblage 3. Naked hilate monad. Proximal surface laevigate. Distal walls sculptured with small, evenly spaced spines or coni. Spine tips are pointed.

e: TQBH2-1(Stub T(2)2-1)-015, Assemblage 4. Naked hilate monad (?). Distal walls sculptured with small spines or coni. Spine tips pointed (see arrow).

f: Close up of TQBH2-1(Stub T(2)2-1)-015, Assemblage 4. Spines small and pointed (see arrow). One element large and bulbous (see arrow).

g: TQBH1-1(StubT1-1)-002, Assemblage 2. Naked, unfused dyad. Distal walls sculptured with small, closely spaced spines or coni (see arrow).

h: Close up of TQBH1-1(StubT1-1)-002, Assemblage 2. Distal wall sculptured with small, irregularly, closely spaced spines or coni. Elements perpendicular to contact line in the junction area (see arrow).

i: TQBH1-PB1(StubPB1-2008)-133, Assemblage 3. Naked, unfused dyad (?). Distal wall sculptured with small, irregularly spaced spines or coni (see arrow).

j: Close up of TQBH1-PB1(StubPB1-2008)-133, Assemblage 3. Distal wall sculptured with irregularly arranged small spines or coni (see arrow).

k* and *l*: *Cymbohilates* cf. *horridus

k: TQBH1-3(Stub T1-3(2008)-125, Assemblage 5. Naked, hilate monad. Distal wall sculptured with sparsely distributed slender spines to bacula or pila. Distal walls broadly folded.

l: Close up of TQBH1-3(Stub T1-3(2008)-125, Assemblage 5. Distal wall sculptured with sparsely distributed slender spines (see arrow).

Plate 5.14: Spinose sculptured hilates and dyads

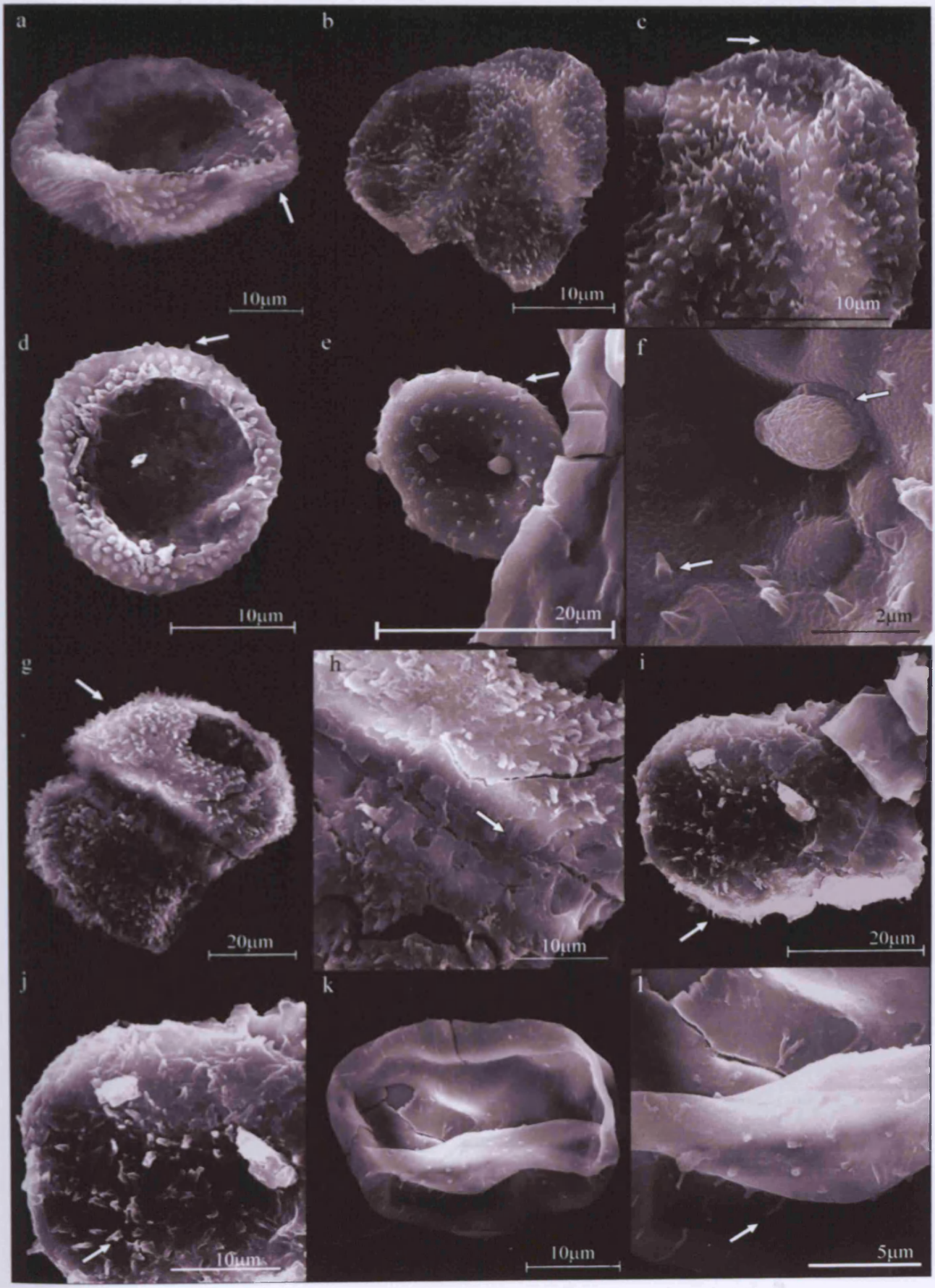

Plate 5.15: Murornate sculptured hilates, dyads and tetrads.

***a* to *g*: *Chelinohilates erraticus* – thick muri**

a: TRE1/109, Assemblage 1. Naked hilate monad. Distal wall sculptured with thick broad muri (see arrow). Muri connected forming a reticulate pattern, forming rectangular lumina.

b: TRE1/087, Assemblage 1. Naked, hilate monad. Distal wall sculptured with thick muri (see arrow). Muri connected forming a reticulate pattern, forming triangular lumina.

c: TRE1/204, Assemblage 1. Naked, hilate monad. Distal wall sculptured with thick muri (see arrow). Muri connected forming reticulate pattern, forming rectangular lumina.

d: TQBH2-1-203. Assemblage 4. Naked, unfused dyad. Distal walls sculptured with thick muri (see arrow). Muri connected forming a reticulate pattern, forming triangular lumina.

e: Close up of TQBH2-1-203. Assemblage 4. Distal wall sculptured with thick, sinuous muri. Muri connected forming a reticulate pattern, forming triangular lumina.

f: TRE1/073, Assemblage 1. Naked, unfused dyad. Distal wall sculptured with thick, sinuous muri. Muri connected forming a reticulate pattern, forming rectangular lumina.

g: TRE1/094, Assemblage 1. Naked, unfused tetrad. Distal wall sculptured with thick sinuous muri. Muri connected forming a reticulate pattern, forming rectangular lumina.

***h* to *l*: *Chelinohilates erraticus* – thin muri**

h: TRE1/107, Assemblage 1. Naked hilate monad with distal walls sculptured with thin muri (see arrow).

i: TQBH1-PB1-057, Assemblage 3. Naked hilate monad with distal walls sculptured with thin, closely spaced muri (see arrow).

j: Close up of TQBH1-PB1-057, Assemblage 3.

k: TQBH2-1-054, Assemblage 4. Naked hilate monad with distal walls sculptured with thin, closely spaced muri (see arrow).

l: Close up of TQBH2-1-054, Assemblage 4. Proximal surface is laevigate. Hilum has a lip (see arrow).

Plate 5.15: Murornate sculptured hilates, dyads and tetrad

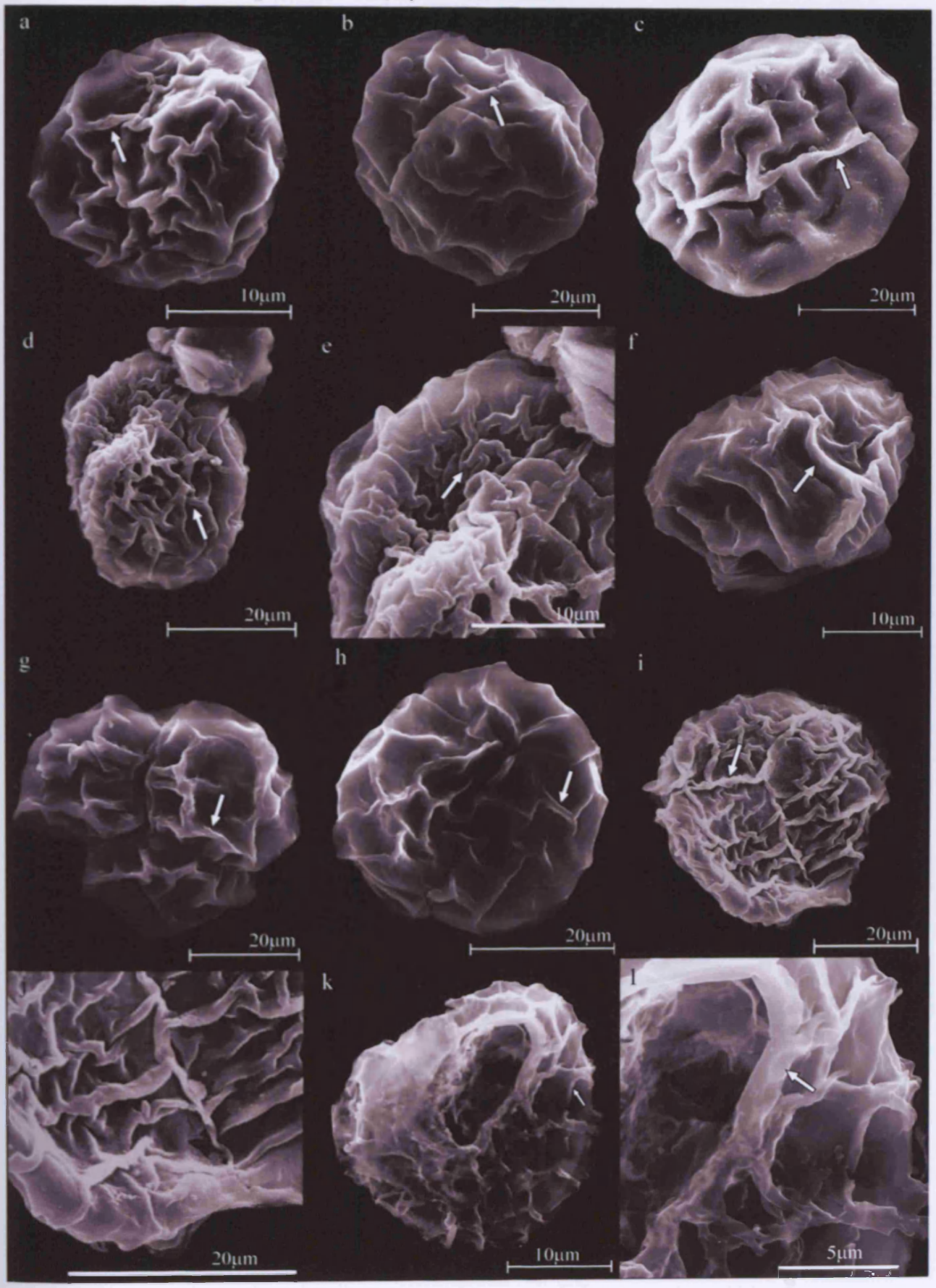

Plate 5.16: Murornate sculptured hilates, dyads and tetrads.

***a* to *f*: *Chelinohilates erraticus* – thin muri (continued)**

a: TQBH2-1-209, Assemblage 4. Naked, unfused dyad, with clear contact line (see arrow). Distal walls sculptured with thin, low flexuous muri and large lumina.

b: Close up of TQBH2-1-209, Assemblage 4. Distal walls sculptured with flexuous, thin muri, and large lumina.

c: TQBH1-PB1-143, Assemblage 3. Partial naked, unfused dyad. Distal walls sculptured with thin, sinuous muri, forming an irregular reticulate pattern.

d: Close up of TQBH1-PB1-143, Assemblage 3. Distal wall sculptured with thin, closely spaced sinuous muri and small lumina (see arrow).

e: TRE1/125, Assemblage 1. Naked, unfused tetrad. Distal walls sculptured with thin, sinuous muri (see arrow), forming irregular reticulate, and small lumina.

f: Close up of TRE1/125, Assemblage 1. Distal walls sculptured with thin, sinuous muri (see arrow), forming an irregular reticulate, and small lumina.

g* to *j*: *Chelinohilates* cf. *lornensis

g: TQBH1-1-161, Assemblage 2. Naked, hilate monad. Distal wall sculptured with broad, low muri (see arrow), forming a regular polygonal reticulum pattern. Lumina are six-sided. Exine has a blotchy appearance.

h: Close up of TQBH1-1-161, Assemblage 2. Distal wall sculptured with broad, low muri, forming a regular polygonal reticulum pattern. Lumina are six sided (see arrow), and exine has a blotchy appearance.

i: TQBH1-3-025, Assemblage 5. Naked, hilate monad (?). Distal wall sculptured with low, broad closely spaced muri, forming a regular polygonal reticulum pattern and six sided lumina.

j: Close up of TQBH1-3-025, Assemblage 5. Distal walls sculptured with low, broad muri, forming regular polygonal reticulum pattern.

k* and *l*: *Chelinohilates sinuosus* var. *sinuosus

k: TRE1/228, Assemblage 1. Naked, hilate monad. Distal walls sculptured with thick, bifurcating, irregularly arranged muri (see arrow). Lumina are small and irregular.

l: Close up of TRE1/228, Assemblage 1. Distal walls sculptured with thick bifurcating irregularly arranged muri (see arrow).

Plate 5.16: Murornate sculptured hilates, dyads and tetrad

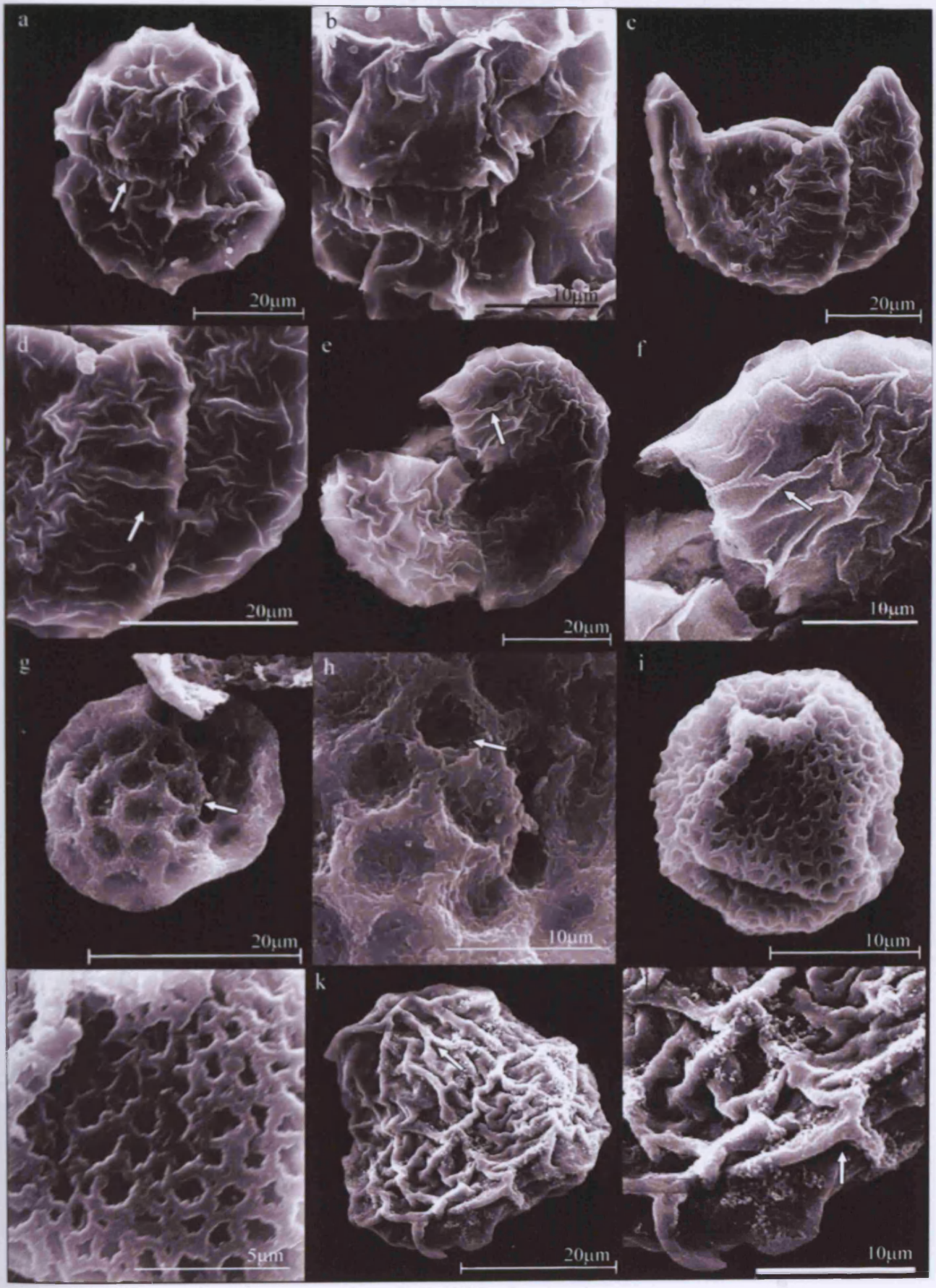

Plate 5.17: Murornate sculptured hilates and dyads.

***a* to *d*: *Chelinohilates sinuosus* var. *sinuosus* (continued)**

a: TQBH2-1-130, Assemblage 4. Naked, hilate monad (?). Distal walls sculptured with low, broad, bifurcating, irregularly arranged muri (see arrow), with small irregular lumina.

b: Close up of TQBH2-1-130, Assemblage 4. Distal walls sculptured with low, broad bifurcating irregularly arranged muri (see arrow).

c: TRE1/213, Assemblage 1. Naked, unfused dyad. Distal walls sculptured with low, broad, bifurcating muri, irregularly arranged, forming small lumina.

d: Close up of TRE1/213, Assemblage 1. Unfused dyad, contact line visible (see arrow). Distal walls sculptured with low, broad bifurcating irregularly arranged, forming small lumina.

e* and *f*: *Chelinohilates sinuosus* var. *angustus

e: TQBH2-1-006, Assemblage 4. Naked, hilate monad. Distal walls sculptured with low, narrow, convoluted, closely spaced muri.

f: Close up of TQBH2-1-006, Assemblage 4. Distal wall sculptured with low, narrow, convoluted, closely spaced muri (see arrow), forming small irregular lumina.

***g* to *l*: *?Chelinohilates* sp. A**

g: TRE1/217, Assemblage 1. Naked, hilate monad. Distal walls sculptured with distinctive murornate-apiculate sculpture. A dense, web-like network of convoluted muri, superimposed with apiculate elements.

h: Close up of TRE1/217, Assemblage 1. Distal walls sculptured with convoluted muri (see arrow), superimposed with apiculate elements (see arrow).

i: TRE1/089, Assemblage 1. Naked, hilate monad. Distal walls sculptured with a dense network of convoluted muri, superimposed with apiculate elements (see arrow).

j: Close up of TRE1/089, Assemblage 1. Distal walls sculptured with convoluted muri, superimposed with apiculate elements, including pila and bacula (see arrow).

k: TQBH2-1-012 Assemblage 4. Naked, hilate monad. Distal walls sculptured with convoluted, superimposed with apiculate elements.

l: Close up of TQBH2-1-012 Assemblage 4. Distal walls sculptured with convoluted, superimposed with apiculate elements.

Plate 5.17: Murornate sculptured hilates and dyad

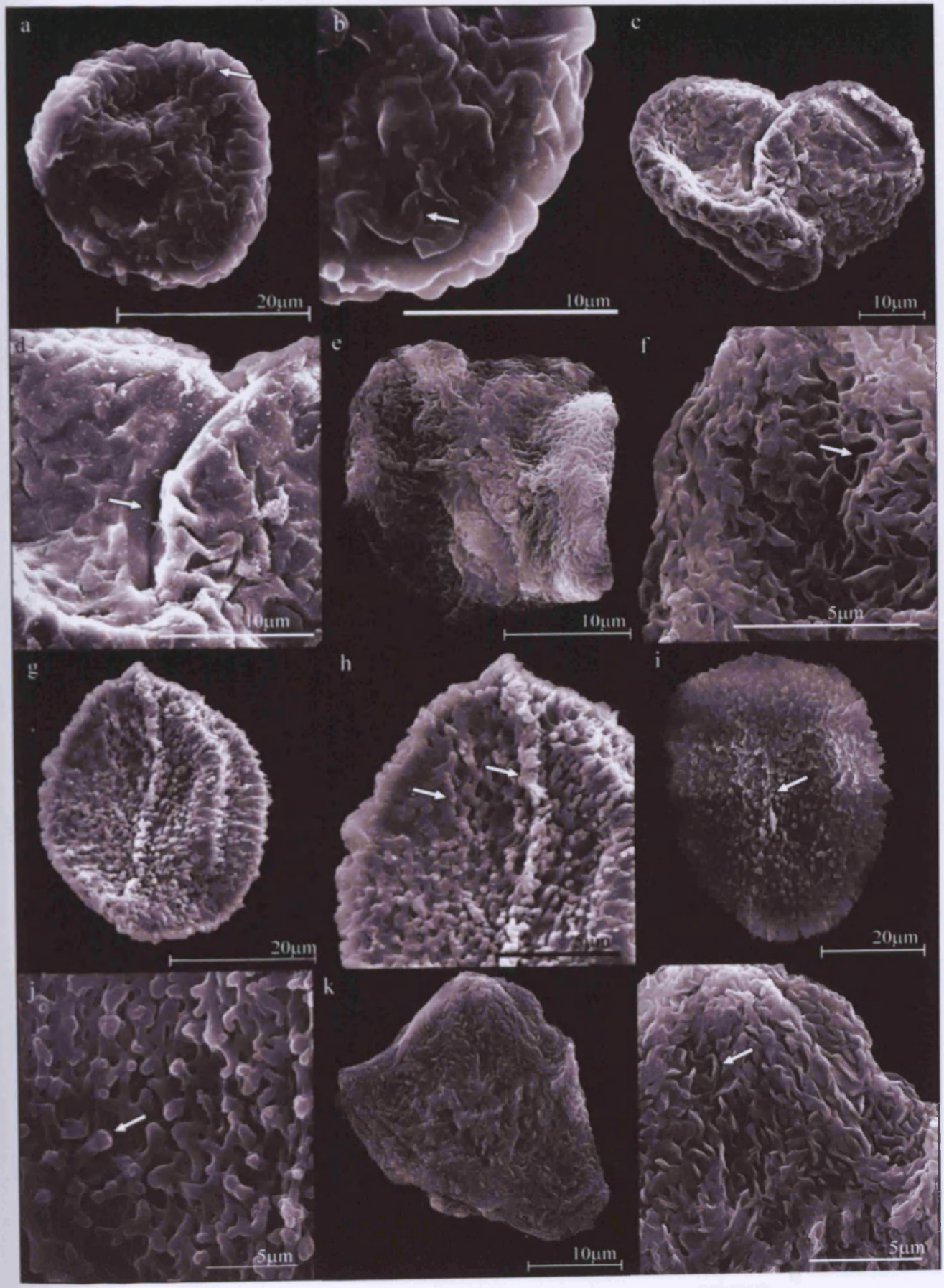

Plate 5.18: Verrucate sculptured hilates, dyads and tetrads.

a* and *b*: *Hispanaediscus major

a: TQBH1-1-141, Assemblage 2. Naked, hilate monad. Distal walls sculptured with low, broad, widely spaced verrucae (see arrow).

b: Close up of TQBH1-1-141, Assemblage 2. Distal walls sculptured with low, broad, widely spaced verrucae. Some fuse together to form rugulae (see arrow).

c* and *d*: *Hispanaediscus* cf. *major

c: TQBH1-1-187, Assemblage 2. Naked, hilate monad. Distal walls sculptured with small, irregularly sized verrucae (see arrow).

d: Close up of TQBH1-1-187, Assemblage 2. Distal walls sculptured with small, irregularly sized verrucae (see arrow). Some verrucae fused to form rugulae.

e* to *l*: *Hispanaediscus verrucatus

e: TQBH1-1-070, Assemblage 2. Naked, hilate monad (?). Distal walls sculptured with low, broad, closely spaced verrucae with rounded tips. In some places verrucae are fused to form rugulae.

f: TQBH1-PB1-159, Assemblage 3. Naked, hilate monad (?). Distal wall sculptured with low, broad, closely spaced verrucae with rounded tips. In some places verrucae are fused to form rugulae.

g: TQBH1-PB1-030, Assemblage 3. Naked, hilate monad (?). Distal walls sculptured with low, broad, closely spaced verrucae with rounded tips. In places verrucae are fused to form rugulae (see arrow).

h: T1-6/PB0-247, Assemblage 1. Naked, unfused dyad. Distal walls sculptured with low, broad, closely spaced verrucae, some with pointed tips (see arrow).

i: Close up of T1-6/PB0-247, Assemblage 1. Sub-equatorial contact area with perpendicular muri to contact line (see arrow). Proximal hilum is laevigate.

j: T1-6/PB0-264, Assemblage 1. Naked, unfused dyad. Distal walls sculptured with low, broad, closely spaced verrucae, some with rounded tips. Some verrucae fused to form rugulae.

k: TRE1/081, Assemblage 1. Naked, unfused tetrad, with contact line visible (see arrow). Distal walls sculptured with closely spaced verrucae of different sizes, some fused to form rugulae (see arrow).

l: TQBH1-3-198, Assemblage 5. Naked, unfused tetrad. Distal walls sculptured with closely spaced, variably sized verrucae. Some verrucae fused to form rugulae.

Plate 5.18: Verrucate sculptured hilates, dyads and tetrads

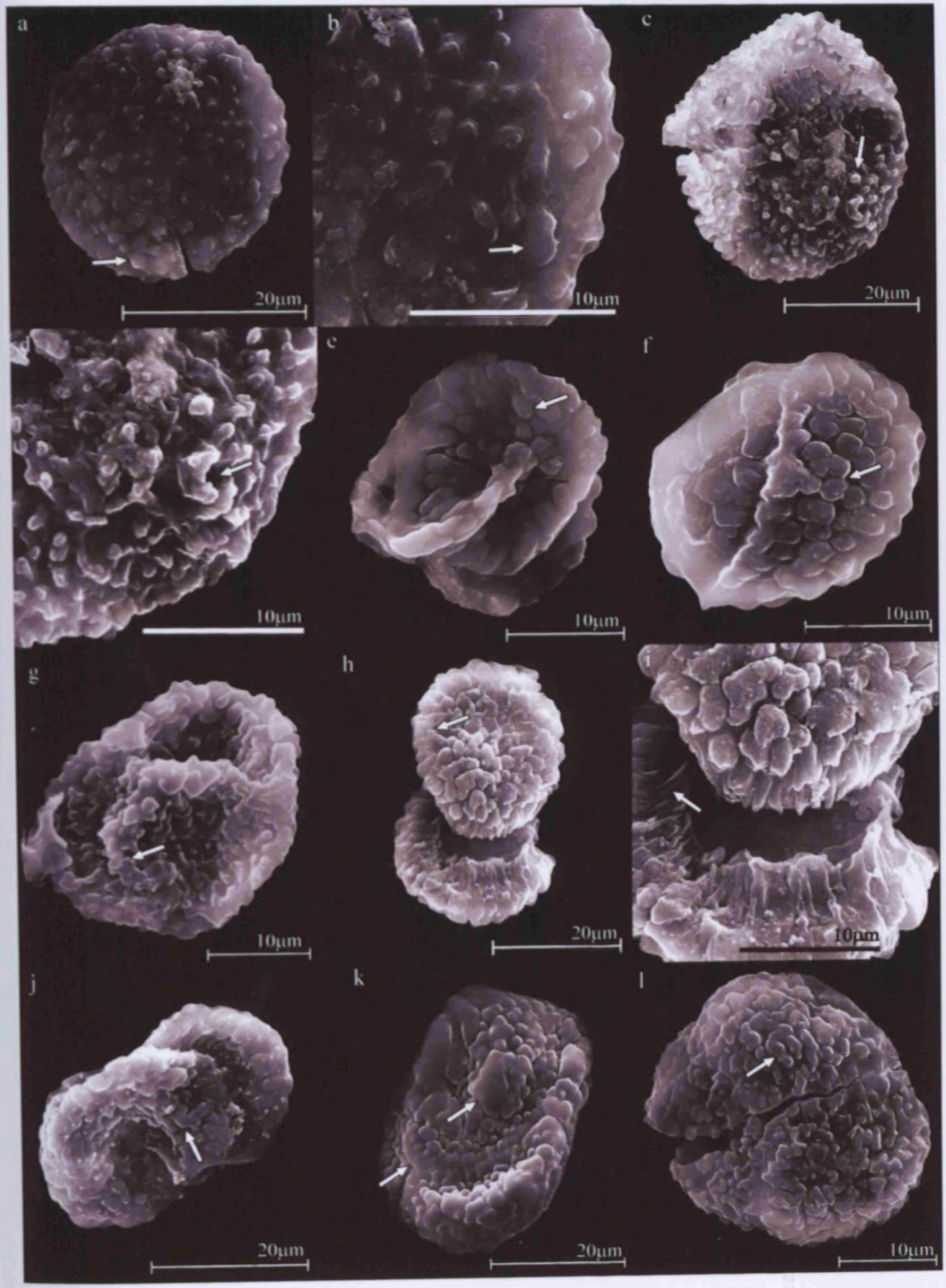

Plate 5.19: Verrucate sculptured hilates and tetrads.

a* and *b*: *Hispanaediscus* cf. *verrucatus

a: TQBH2-1-131, Assemblage 4. Naked, hilate monad. Distal walls sculptured with low, broad, closely spaced verrucae, which are nearly all fused to form rugulae or low, broad muri (see arrow).

b: Close up to TQBH2-1-131, Assemblage 4. Distal walls sculptured with low, broad, closely spaced verrucae, which are fused to form rugulae to low muri (see arrow).

c* to *f*: *Hispanaediscus wenlockensis

c: TQBH1-PB1-158, Assemblage 3. Naked, hilate monad (?). Distal walls sculptured with closely spaced, equally sized verrucae with rounded tips. Only a few verrucae are fused to form rugulae.

d: Close up to TQBH1-PB1-158, Assemblage 3. Distal walls sculptured with closely spaced, equally sized verrucae with rounded tips. Only a few verrucae are fused to form rugulae (see arrow).

e: TRE1/223, Assemblage 1. Naked, unfused tetrad, with visible contact lines (see arrow). Distal walls sculptured with closely spaced, equally sized verrucae with rounded tips. Few verrucae fuse to form rugulae.

f: Close up of TRE1/223, Assemblage 1. Distal walls are sculptured with closely spaced verrucae with rounded tips (see arrow).

Plate 5.19: Verrucate sculptured hilates and tetrad.

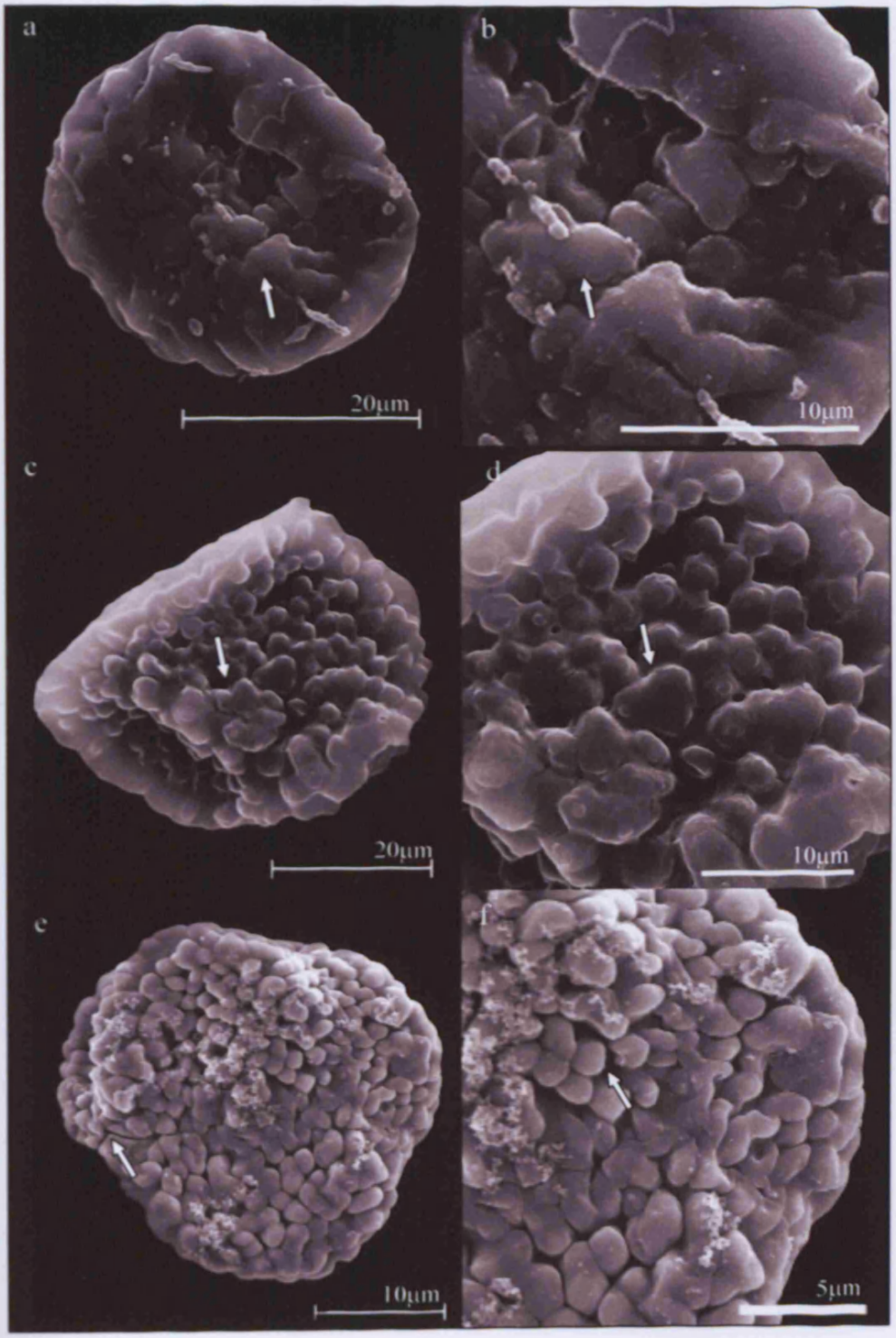

Plate 5.20: Laevigate alete monads.

***a* to *l*: Laevigate alete monads.**

a: TRE1/105, Assemblage 1.

b: TRE1/130, Assemblage 1.

c: TQBH1-1(StubT1-1)-003, Assemblage 2.

d: TQBH1-1(StubT1-2)-057, Assemblage 2.

e: TQBH1-PB1(StubPB1-2008)-193, Assemblage 3.

f: TQBH2-1(StubT2-1(2008)-071, Assemblage 3.

g: TQBH2-1(StubT2-1(2008)-149, Assemblage 4.

h: TQBH2-1(StubT2-1(2008)-158, Assemblage 4.

i: TQBH1-3(StubT3-1)-026, Assemblage 5.

j: TQBH1-3(StubT3-2)-043, Assemblage 5.

k: TQBH1-3(StubT3-2)-054, Assemblage 5.

l: TQBH1-3(StubT3-2)-084, Assemblage 5.

Plate 5.20: Laevigate alete monads

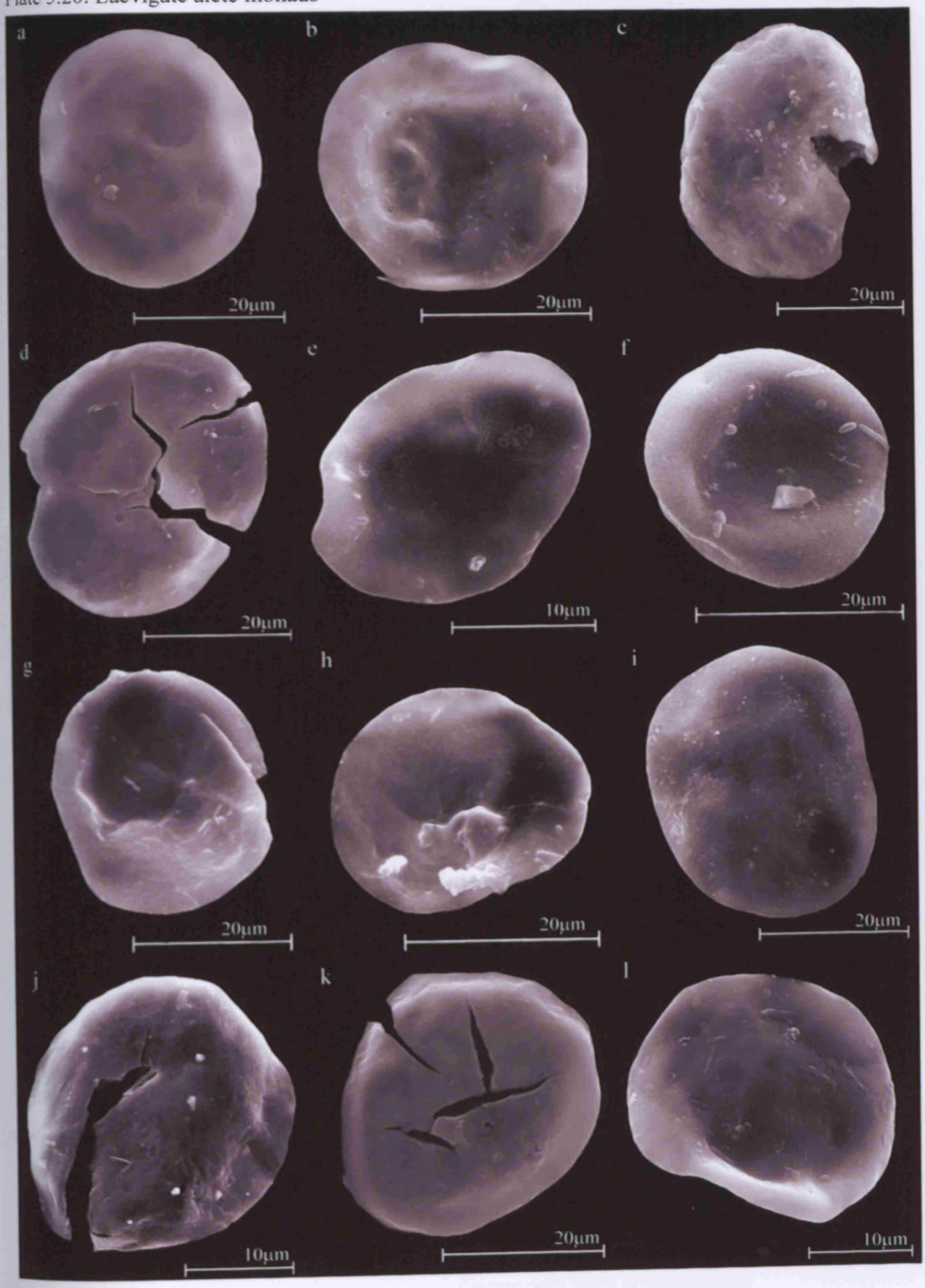

Plate 5.21: Enveloped tetrads

a* to *d*: *Velatitetras* cf. *reticulata

a: TRE1/206, Assemblage 1. Enveloped, permanent tetrahedral tetrad. Envelope sculptured with, narrow sinuous muri (see arrow), with irregular shaped reticulum.

b: TQBH1-PB1-053, Assemblage 3. Enveloped, permanent tetrahedral tetrad. Envelope sculptured with low, narrow sinuous muri (see arrow), with irregular shaped reticulum.

c: Close up of TQBH1-PB1-053, Assemblage 3. Envelope sculptured with low, narrow sinuous muri forming an irregular shaped reticulum.

d: TQBH2-1-146, Assemblage 4. Enveloped, permanent tetrahedral tetrad with one aborted spore unit (see arrow). Envelope sculptured with low, sinuous narrow muri forming an irregular shaped reticulum.

e* to *h*: *Velatitetras rugulata

e: TQBH1-1-124, Assemblage 2. Enveloped, permanent tetrahedral tetrad (?). Enveloped sculptured with low, irregularly spaced verrucae. Some verrucae fused to form rugulae (see arrow).

f: Close up of TQBH1-1-124, Assemblage 2. Envelope sculptured with low, irregularly spaced verrucae (see arrow).

g: TQBH2-1-002, Assemblage 4. Enveloped, permanent tetrahedral tetrad. Envelope sculptured with irregularly spaced verrucae (see arrow).

h: Close up of TQBH2-1-002, Assemblage 4. Envelope sculptured with irregularly spaced verrucae and rugulae (see arrow).

i* to *l*: *Velatitetras* cf. *cristata

i: TQBH1-1-081, Assemblage 2. Enveloped, permanent tetrahedral tetrad. Envelope sculptured with anastomosing muri, forming an irregular shaped and projecting reticulum (see arrow).

j: Close up of TQBH1-1-081, Assemblage 2. Envelope sculptured with anastomosing muri (see arrow).

k: TQBH1-3-037, Assemblage 5. Enveloped, tetrahedral tetrad, with visible contact lines (see arrow). Envelope sculptured with narrow, ill-defined anastomosing muri, forming an irregular shaped and projecting reticulum.

l: Close up of TQBH1-3-037, Assemblage 5. Envelope sculptured with narrow, anastomosing muri (see arrow).

Plate 5.21: Enveloped tetrads

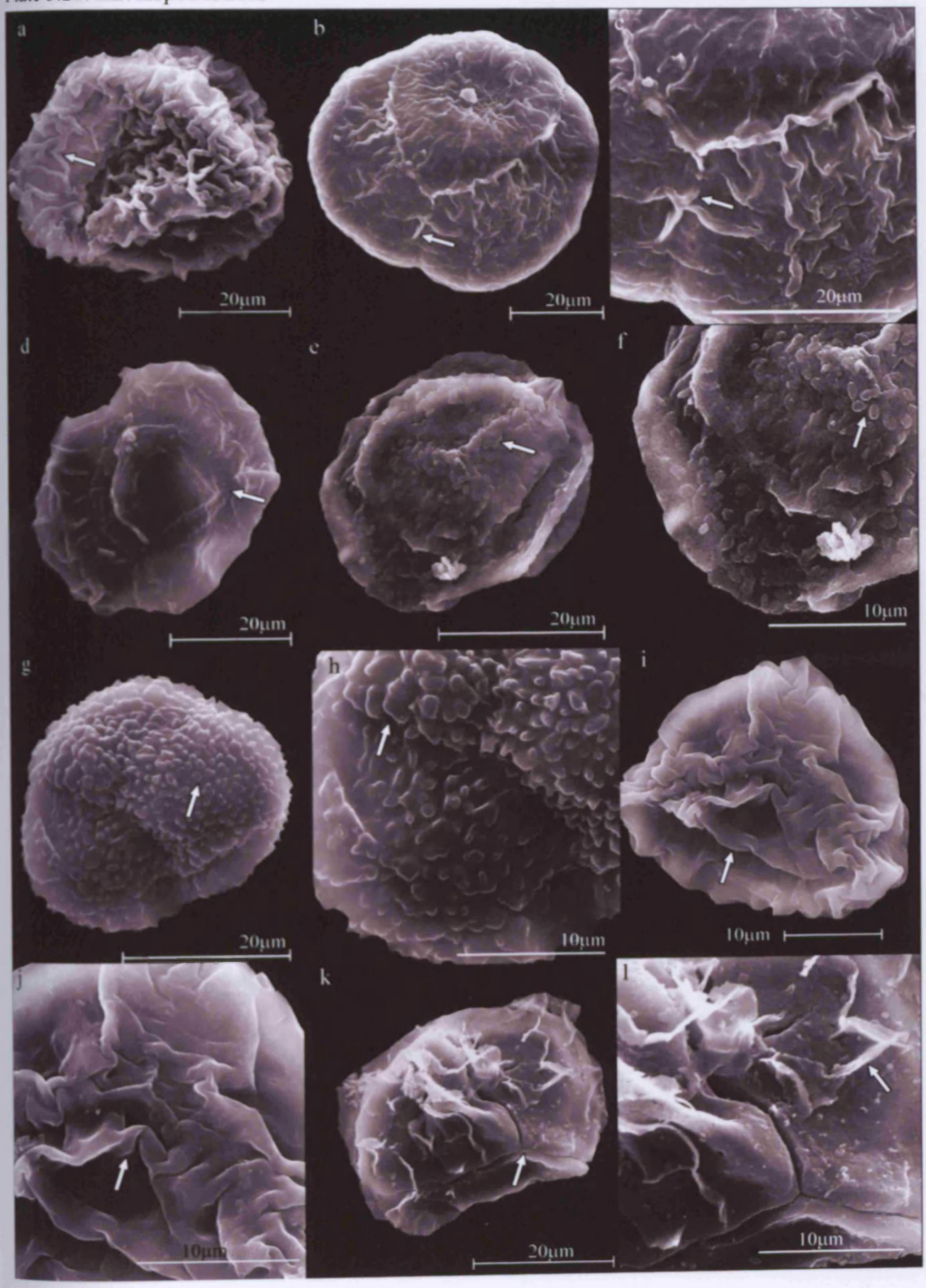

Plate 5.22: Enveloped tetrads

***a* to *f*: *Velatitetras* sp. B**

a: TQBH2-1-010, Assemblage 4. Enveloped, permanent tetrahedral tetrad. Envelope sculptured with evenly spaced, regularly arranged apiculate elements, including grana (see arrow).

b: Close up of TQBH2-1-010, Assemblage 4. Envelope sculptured with evenly spaced, regularly arranged, grana to spatulate elements (see arrow).

c: TQBH2-1-151, Assemblage 4. Enveloped, permanent tetrad, sculptured with irregularly and closely spaced apiculate elements, including micrograna (see arrow).

d: Close up of TQBH2-1-151, Assemblage 4. Envelope sculptured with irregularly, closely spaced micrograna (see arrow).

e: TQBH2-1-162, Assemblage 4. Enveloped, permanent tetrad, sculptured with evenly, regularly spaced apiculate elements, including microconi (see arrow).

f: Close up of TQBH2-1-162, Assemblage 4. Envelope sculptured with evenly, regularly spaced apiculate elements, including microconi (see arrow).

***g* to *j*: *Velatitetras* sp. C**

g: TRE1/169, Assemblage 1. Enveloped, permanent tetrad. Envelope sculptured with evenly, regularly spaced, low broad verrucae (see arrow).

h: Close up of TRE1/169, Assemblage 1. Enveloped sculptured with low, evenly spaced verrucae (see arrow).

i: TRE1/173, Assemblage 1.Enveloped, permanent tetrad. Envelope sculptured with evenly, closely spaced verrucae. Some verrucae fused to form rugulae (see arrow).

j: Close up of TRE1/173, Assemblage 1. Enveloped sculptured with closely spaced verrucae (see arrow).

Plate 5.22: Enveloped tetrads (continued)

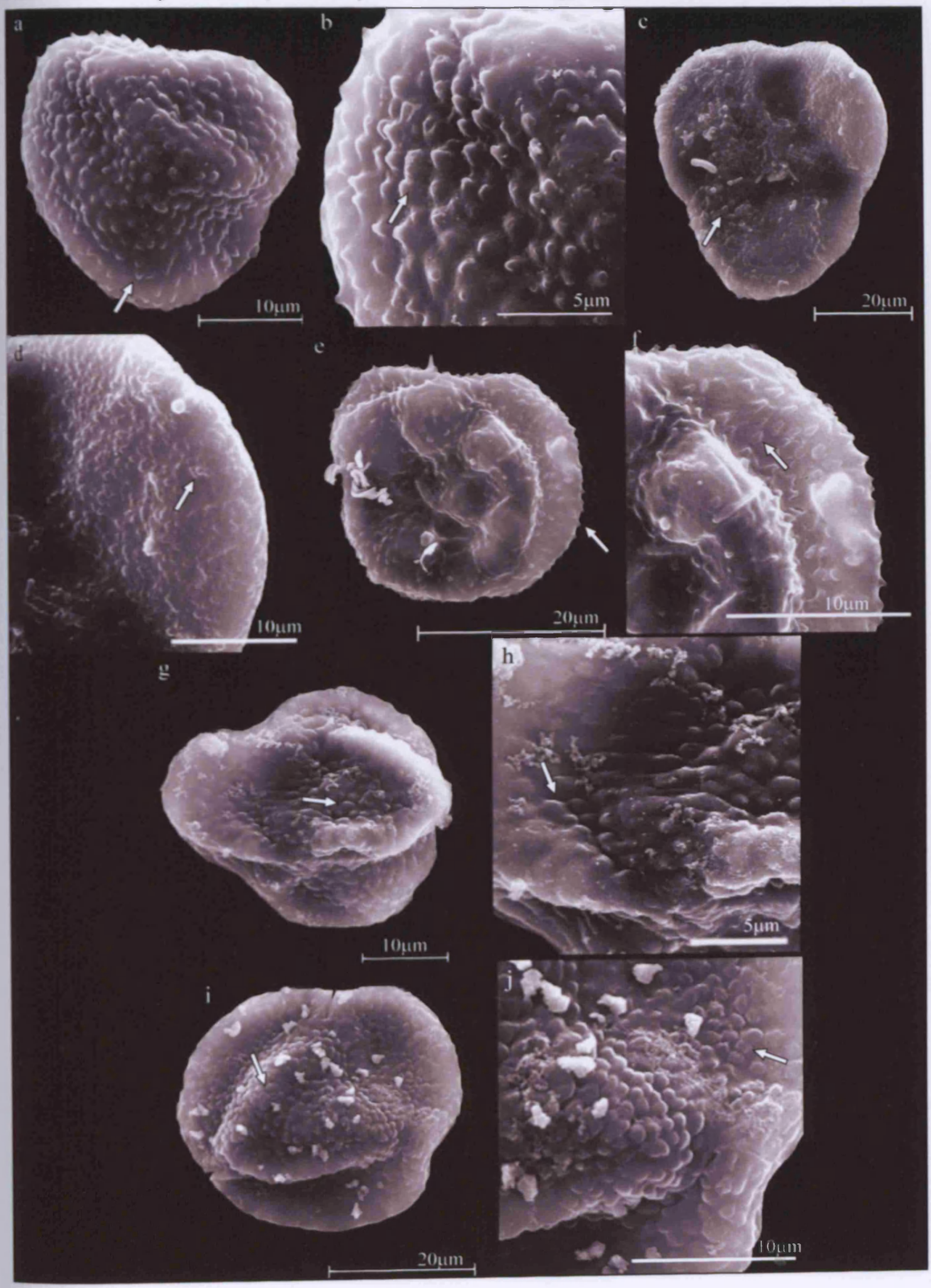

Plate 5.23: Enveloped dyads and hilates

a* to *d*: *Abditusdyadus histosus

a: TRE1/209, Assemblage 1. Enveloped, unfused elliptical dyad (?). Envelope sculptured with low, narrow muri, forming a regular reticulate pattern.

b: Close up of TRE1/209, Assemblage 1. Envelope sculptured with low, narrow muri, forming a regular reticulate pattern, forming small polygonal lumina (see arrow).

c: TRE1/144, Assemblage 1. Enveloped, unfused elliptical dyad. Envelope sculptured with low, narrow muri, forming a regular, polygonal reticulate pattern (see arrow).

d: Close up of TRE1/144, Assemblage 1. Envelope sculptured with low, narrow, muri, forming a regular, polygonal reticulate pattern (see arrow).

e* and *f*: *Segestrespora* cf. *membranifera

e: TRE1/049, Assemblage 1. Enveloped fused dyad. Envelope sculptured with narrow sinuous projecting muri (see arrow), forming irregular reticulate pattern.

f: Close up of TRE1/049, Assemblage 1. Envelope covering dyad contact area (see arrow). Sculptured with narrow, sinuous muri.

g* and *h*: *Qualisaspora sinuata

g: TRE1/121, Assemblage 1. Enveloped non-hilate monads. Envelope sculptured with regularly spaced straight to slightly sinuous muri (see arrow), which are radially arranged from the equator to the central pole. Muri are coni-shaped in profile (see arrow).

h: Close up of TRE1/121, Assemblage 1. Radially arranged muri coalesce at the central pole (see arrow).

Plate 5.23: Enveloped hilates and dyads

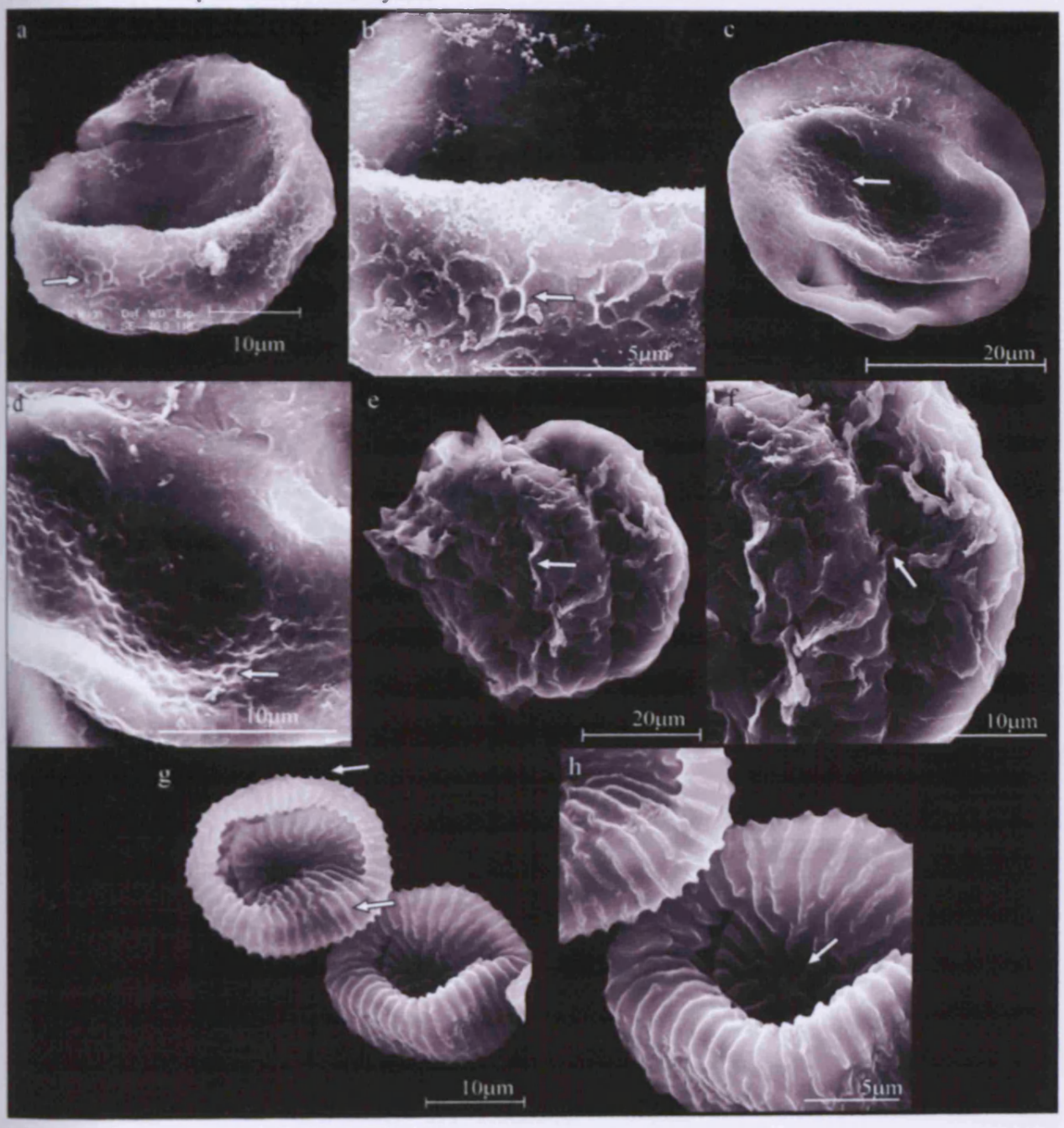

Plate 5.24: ***Incertae sedis***

***a* to *c*: ?Enveloped murornate monad and tetrad with broad muri**

a: TQBH2-1-094, Assemblage 4. Enveloped enclosed monad (?), sculptured with broad muri (see arrow), forming a broad reticulate pattern, with triangular to rectangular lumina. Superimposed with apiculate elements (grana) (see arrow).

b: TQBH1-3-209, Assemblage 5. Envelope enclosed tetrad (?) with visible contact lines (see arrow). Envelope sculptured with broad muri (see arrow), forming rectangular lumina. Lumina superimposed with closely spaced micrograna.

c: Close up of TQBH1-3-209, Assemblage 5. Envelope sculptured with broad muri, forming reticulate pattern, with rectangular lumina, superimposed with closely spaced micrograna (see arrow)

***d* to *e*: ?Enveloped murornate monad with sinuous muri**

d: TQBH2-1-041, Assemblage 4. Naked (?) non-hilate monad. Distal and proximal (?) walls sculptured with highly irregular, closely spaced, low, sinuous muri (see arrow). Muri are often fused together and separated by small lumina.

e: Close up of TQBH2-1-041, Assemblage 4. Distal and proximal (?) walls sculptured with highly irregular, closely spaced, low, sinuous muri, forming irregular reticulate pattern and small lumina (see arrow).

***f* to *i*: ?Enveloped verrucate monads**

f: TQBH2-1-007, Assemblage 4. Naked, sub-circular monad (?) Distal surface sculptured with densely packed, irregularly shaped verrucae, rugulae and muri (see arrow).

g: Close up of TQBH2-1-007, Assemblage 4. Densely packed, irregular, verrucae, rugulae and small muri elements (see arrow).

h: TQBH2-1-047, Assemblage 4. Naked, sub-circular monad (?). Distal surface sculptured with densely packed, irregularly shaped verrucae, rugulae and muri.

i: Close up of TQBH2-1-047, Assemblage 4. Distal surface sculptured with densely packed, irregularly shaped verrucae, rugulae and muri (see arrow).

***j* and *k*: ?Enveloped apiculate monad**

j: TRE1/187, Assemblage 1. Enveloped (?) sub-circular hilate monad (see arrow). Distal and proximal surface sculptured with evenly spaced apiculate elements (microconi).

k: Close up of TRE1/187, Assemblage 1. Enveloped (?) hilate monad, distal and proximal surfaces sculptured with evenly spaced microconi (see arrow).

Plate 5.24: *Incertae sedis*

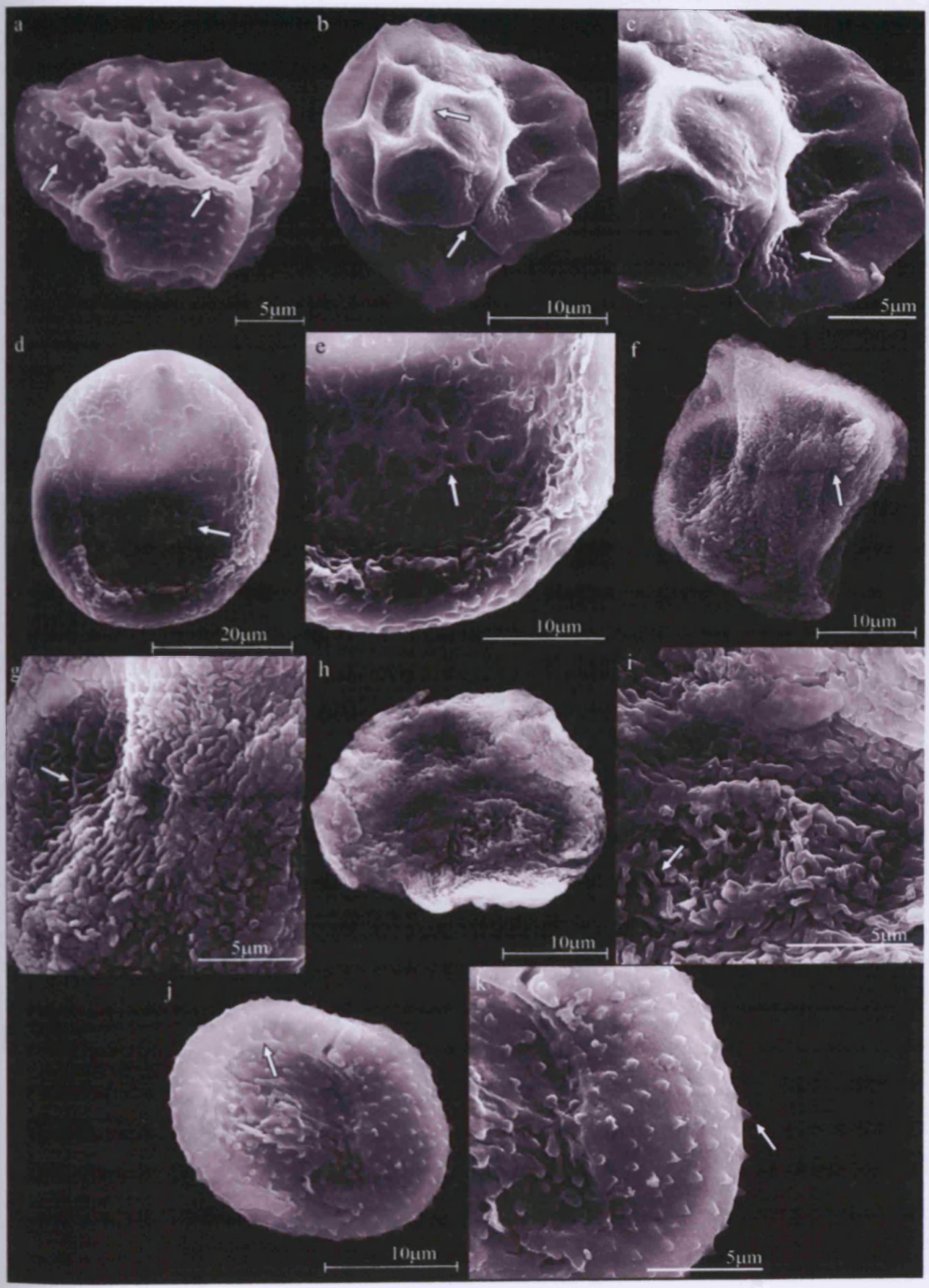

Plate 5.25: *Incertae sedis* (continued)

***a* to *h*: ?Enveloped spatulate monads and dyad**

a: TRE1/136, Assemblage 1. Enveloped (?) monad, sculptured with closely spaced irregular, blunt to pointed spatulate elements (see arrow), some fused to form narrow muri.

b: Close up of TRE1/136, Assemblage 1. Envelope sculptured with irregular blunt to pointed spatulate elements (see arrow).

c: TQBH2-1-053, Assemblage 4. Sub-circular enveloped (?) monad, sculptured with irregular, blunt to spatulate elements. Some fused to form rugulae.

d: Close up of TQBH2-1-053, Assemblage 4. Envelope sculptured with irregularly spaced, blunt to spatulate elements, some fused to form rugulae (see arrow).

e: TRE1/158, Assemblage 1. Enveloped sub-circular monad (?). Sculptured with closely spaced irregular spatulate elements, some fused to form rugulae or small muri.

f: Close up of TRE1/158, Assemblage 1. Envelope sculptured with closely spaced, irregular spatulate elements, some fused to form rugulae or small muri (see arrow).

g: TRE1/004, Assemblage 1. Enveloped dyad (?) Envelope sculptured with closely spaced, irregular spatulate elements, some fused to form rugulae or small muri.

h: Close up of TRE1/004, Assemblage 1. Envelope sculptured with closely spaced, irregular spatulate elements, some fused to form rugulae or small muri (see arrow).

***i* to *l*: ?Enveloped spinose monads with clustered spines**

i: TRE1/018, Assemblage 1. Enveloped monad (?). Envelope sculptured with closely spaced, irregular arranged spinose elements (see arrow). Some spines are fused at the base.

j: Close up of TRE1/018, Assemblage 1. Envelope sculptured with short spines, irregularly or radially arranged (see arrow). Spines are fused at the base, some fused to form rugulae or small muri.

k: TQBH1-1-156, Assemblage 2. Enveloped monad (?) Envelope sculptured with irregular closely spaced elements, including radially arranged short spines, grana or muri.

l: Close up of TQBH1-1-156, Assemblage 2. Envelope sculptured with irregular, closely spaced elements, including radially arranged, short spines (see arrow).

Plate 5.25: *Incertae sedis*

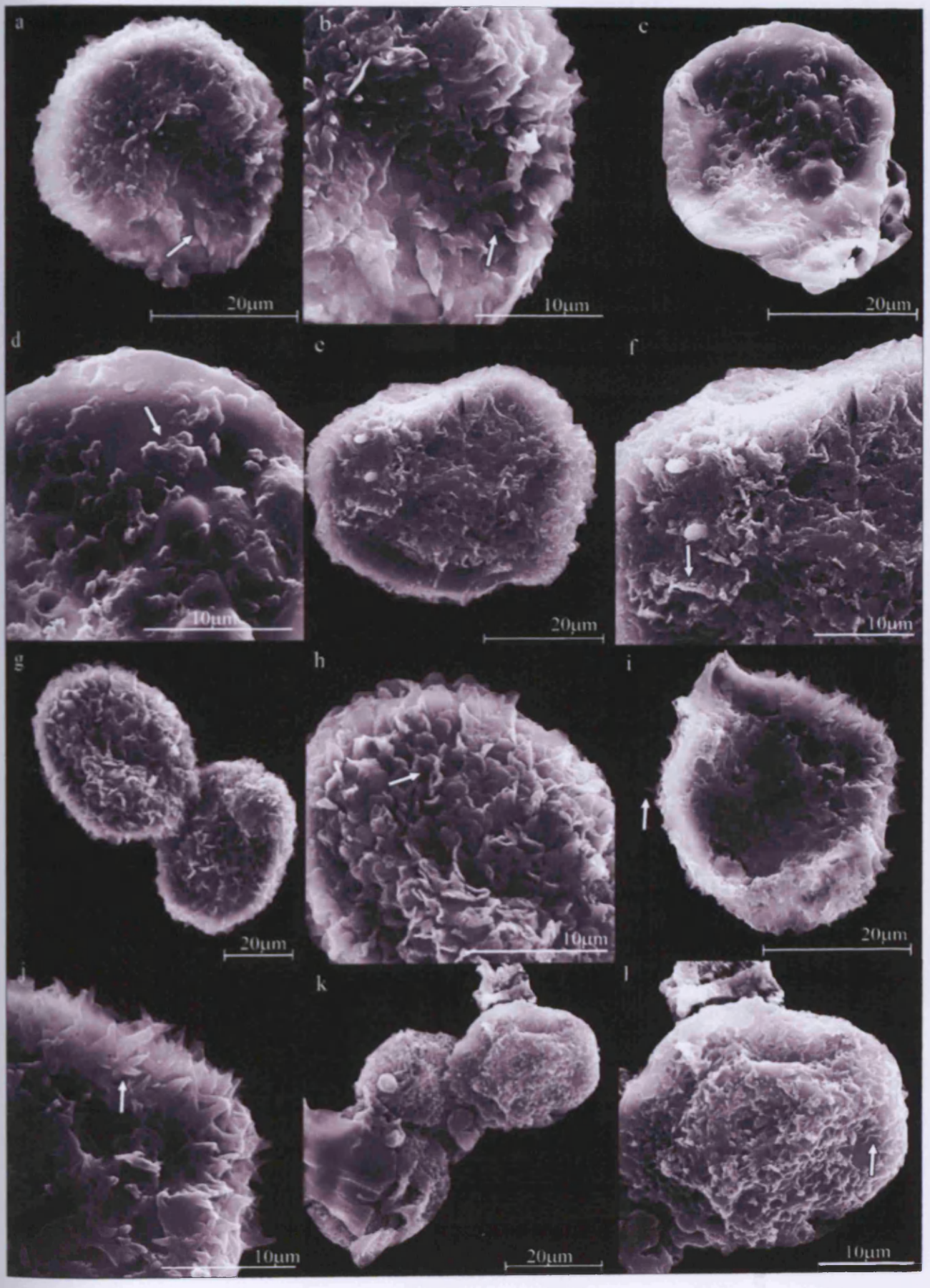

Plate 5.26: *Incertae sedis* (continued)

***a* to *d*: ?Enveloped spinose dyad and tetrad with clustered spines**

a: T1-6/PB0-255, Assemblage 1. Enveloped unfused dyad, with visible contact line (see arrow). Envelope sculptured with closely spaced, irregular spinose elements, some fused to form rugulae or muri.

b: Close up of T1-6/PB0-255, Assemblage 1. Envelope sculptured with closely spaced, irregular spinose elements (see arrow), some fused to form rugulae or muri.

c: TRE1/005, Assemblage 1. Enveloped tetrad. Envelope sculptured with closely spaced, irregular radially arranged, spinose elements, some fused to form rugulae (see arrow).

d: Close up of TRE1/005, Assemblage 1. Enveloped sculptured with closely spaced, irregular radially arranged, spinose elements (see arrow), some fused to form rugulae.

***e* to *h*: ?Enveloped spinose tetrads with slender spines**

e: TRE1/035b, Assemblage 1. Enveloped tetrad (?). Envelope sculptured with small evenly spaced spines with pointed tips. Some spines fused to form rugulae or muri.

f: Close up of TRE1/035b, Assemblage 1. Envelope sculptured with small evenly spaced spines with pointed tips (see arrow).

g: TRE1/128, Assemblage 1. Enveloped tetrad (?). Envelope sculptured with small irregularly spaced spines with pointed tips. Some spines are fused or biform (see arrow).

h: Close up of TRE1/128, Assemblage 1. Envelope sculptured with small, irregularly spaced spines, some fused at the base to form biform spines (see arrow).

Plate 5.26: *Incertae sedis*

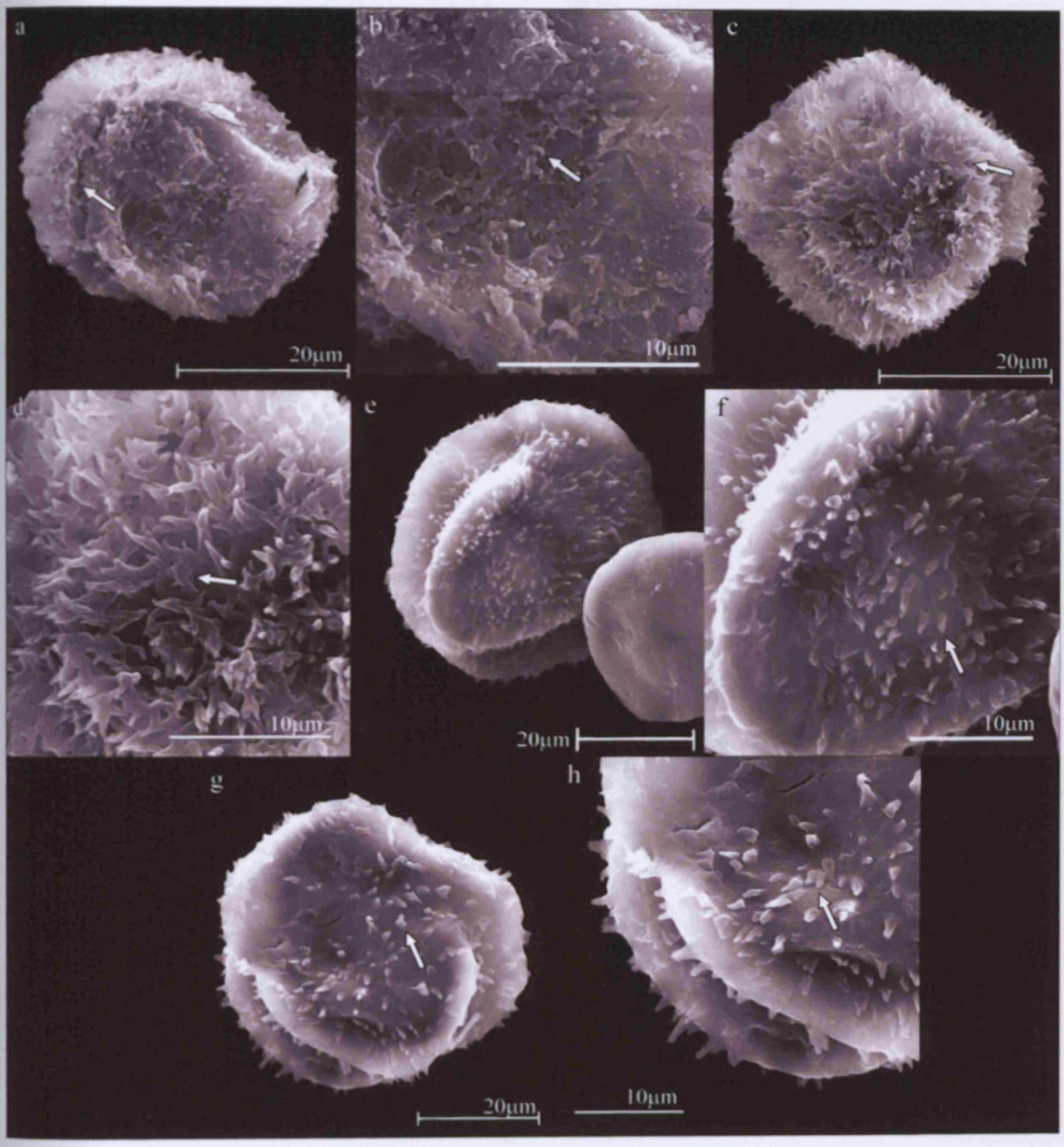

Plate 5.27: Laevigate retusoid triletes

a* to *d*: *Retusotriletes dittonensis

a: TQBH1-1(Ox1)-002, Assemblage 2. Retusoid, sub-circular trilete spore, with laevigate exine. Curvature perfectae is distinctive (see arrow).

b: TQBH1-PB1-006, Assemblage 3. Retusoid, sub-circular trilete spore, with laevigate exine. Small indentations where each laesurae meet the curvature (see arrow).

c: TQBH1-3-137, Assemblage 5. Retusoid, sub-circular trilete spore, with laevigate exine. Curvature perfectae is distinctive.

d: TQBH1-3-179, Assemblage 5. Retusoid, sub-circular trilete spore, with laevigate exine. Curvature perfectae is distinctive. Laesurae thickened into lips (see arrow).

e* to *j*: *Retusotriletes* cf. *dittonensis

e: TRE1/008, Assemblage 1. Retusoid, sub-circular trilete spore, with laevigate distal exine. Proximal surface ornamented with apiculate elements, microconi or grana. Laesurae are thin, but thicken towards the curvature perfectae (see arrow).

f: Close up of TRE1/008, Assemblage 1. Apiculate elements on proximal surface (see arrow).

g: TRE1/070, Assemblage 1. Retusoid, sub-circular trilete spore, with laevigate distal exine. Proximal surface ornamented with small apiculate elements (micrograna). Laesurae are thin, and thicken towards the curvature perfectae, with indentations where each laesurae meets the curvature (see arrow).

h: Close up of TRE1/070, Assemblage 1. Proximal surface ornamented with apiculate elements (micrograna).

i: TQBH1-1-115, Assemblage 2. Retusoid, sub-circular trilete spore, with laevigate exine. Distal walls are laevigate. Curvature perfectae distinctive. Laesurae thin, but thicken towards the curvature (see arrow). Proximal surface ornamented with micrograna.

j: TQBH1-3-035, Assemblage 5. Retusoid, sub-circular trilete spore. Distal wall laevigate. Proximal wall ornamented with micrograna. Laesurae thin, but thicken towards the curvature (see arrow).

Plate 5.27: Laevigate retusoid triletes

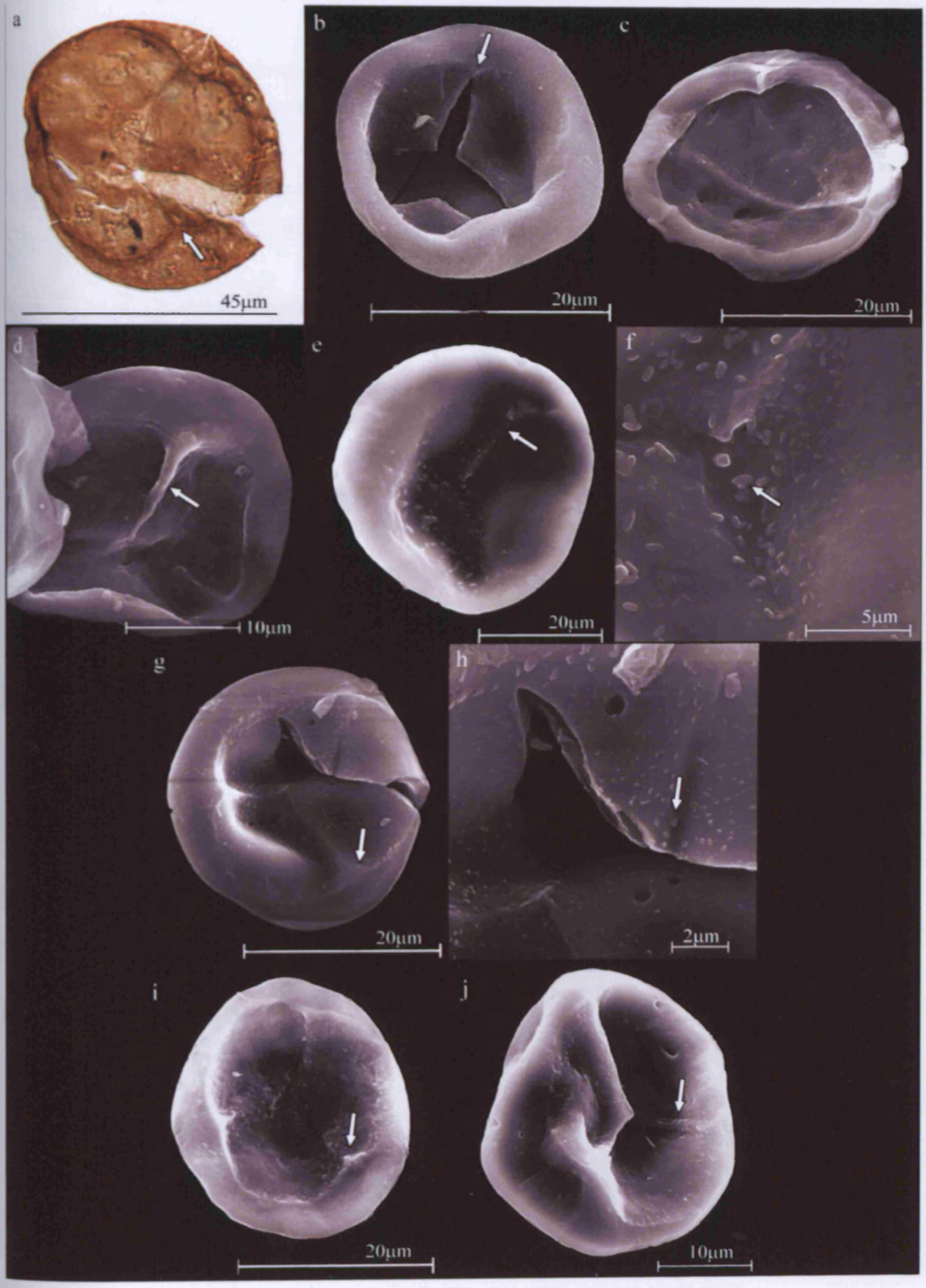

Plate 5.28: Laevigate retusoid triletes and tetrads of laevigate triletes.

a* and *b*: *Retusotriletes* cf. *triangulatus

a: TQBH1-1-020, Assemblage 2. Retusoid, sub-circular trilete spore, with laevigate distal and proximal surfaces. Trilete mark surrounded by distinctive thick darkened triangular area (see arrow).

b: TQBH1-1-024, Assemblage 2. Retusoid, sub-circular trilete spore, with laevigate distal and proximal surfaces. Laesurae are sutured (see arrow).

c* to *j*: *Retusotriletes* cf. *triangulatus* var. *minor

c: TQBH1-1-031, Assemblage 2. Retusoid, sub-circular trilete spore with laevigate surfaces. Laesurae surrounded by dark, thickened triangular area (see arrow).

d: TQBH1-1-035, Assemblage 2. Retusoid, sub-circular trilete spore with laevigate surfaces. Laesurae surrounded by a dark, thickened triangular area (see arrow).

e: TQBH1-1-040, Assemblage 2. Retusoid, sub-circular trilete spore with laevigate distal and proximal surfaces. Laesurae are surrounded by a dark, thickened triangular area (see arrow).

f: TQBH1-1-066, Assemblage 2. Retusoid, sub-circular trilete spore with laevigate surfaces. Laesurae surrounded by a dark, thickened triangular area (see arrow).

g: TQBH1-1-073, Assemblage 2. Retusoid, sub-circular trilete spore with laevigate distal and proximal surfaces. Laesurae surrounded by a dark, thickened triangular area (see arrow).

h: TQBH1-3-003, Assemblage 5. Retusoid, sub-circular trilete spore with laevigate distal and proximal surfaces. Laesurae surrounded by a dark, thickened triangular area (see arrow).

i: TQBH1-3-088, Assemblage 5. Retusoid, sub-circular trilete spore with laevigate surfaces. Curvature perfectae coincident with the equatorial margin, except where the trilete laesurae meets the margin (see arrow).

j: TQBH1-3-105, Assemblage 5. Retusoid, sub-circular trilete spore with laevigate surfaces. Curvature perfectae coincident with the equatorial margin, except where the trilete laesurae meets the margin (see arrow).

***k* and *l*: Tetrads of laevigate triletes (*Retusotriletes* or *Ambitisporites*)**

k: TRE1/022, Assemblage 1. Laevigate tetrad of inflated sub-triangular spore units, with clear contact lines (see arrow). Each unit has a slight equatorial crassitude.

l: TRE1/137, Assemblage 1. Laevigate tetrad of inflated sub-triangular spore units, with clear contact lines (see arrow). Each unit has a slight equatorial crassitude.

Plate 5.28: Laevigate retusoid triletes and tetrads of laevigate triletes

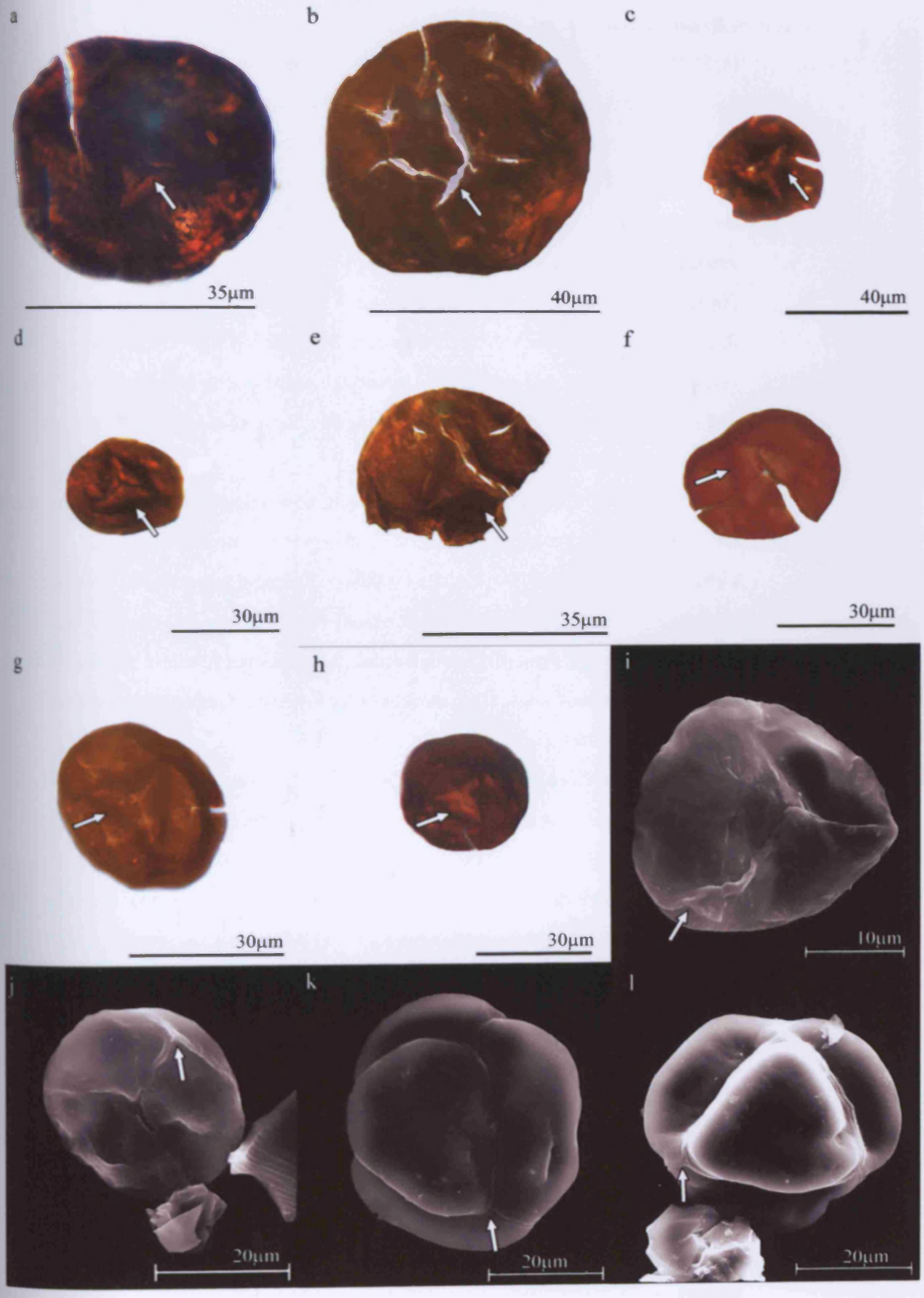

Plate 5.29: Apiculate retusoid triletes.

***a* to *l*: *Apiculiretusispora* sp.**

a: TRE1/194, Assemblage 1. Retusoid, sub-circular trilete spores. Distal and proximal surfaces are sculptured with apiculate elements (grana) (see arrow). Curvature perfectae is coincident with the equator (see arrow).

b: TQBH1-1-098, Assemblage 2. Retusoid, sub-triangular trilete spore, with thick laesurae (see arrow). Proximal surface sculptured with apiculate elements, including micrograna (see arrow).

c: Close up to TQBH1-1-098, Assemblage 2. Proximal surface sculptured with apiculate elements, including micrograna (see arrow).

d: TQBH1-PB1-031, Assemblage 3. Retusoid, sub-circular trilete spore. Proximal surface sculptured with irregularly arranged apiculate elements (grana and micrograna) (see arrow).

e: TQBH1-PB1-061, Assemblage 3. Retusoid, sub-triangular trilete spore. Proximal surface sculptured with apiculate elements (grana) (see arrow).

f: Close up of TQBH1-PB1-061, Assemblage 3. Thick laesurae are sculptured with apiculate elements (grana and micrograna) (see arrow).

g: TQBH1-PB1-094, Assemblage 3.Retusoid, sub-circular trilete spore. Proximal wall sculptured with apiculate elements (see arrow). Curvature perfectae is coincident with the equator.

h: Close up of TQBH1-PB1-094, Assemblage 3. Curvature perfectae is coincident with the equator (see arrow).

i: TQBH1-PB1-096, Assemblage 3. Retusoid, sub-circular trilete spore. Proximal wall sculptured with apiculate elements (grana and micrograna). Curvature perfectae is coincident with the equator where the laesurae reach the equator, but is closer to the centre in between laesurae, forming muri like features (see arrow).

j: Close up of TQBH1-PB1-096, Assemblage 3. Proximal surface sculptured with apiculate elements (grana and micrograna) (see arrow).

k: TQBH1-PB1-100, Assemblage 3. Retusoid, sub-triangular trilete spore. Proximal surface sculptured with apiculate elements (grana) (see arrow). Laesurae are thick forming lips.

l: Close up of TQBH1-PB1-100, Assemblage 3. Laesurae form thick lips (see arrow).

Plate 5.29: Apiculate sculptured retusoid triletes

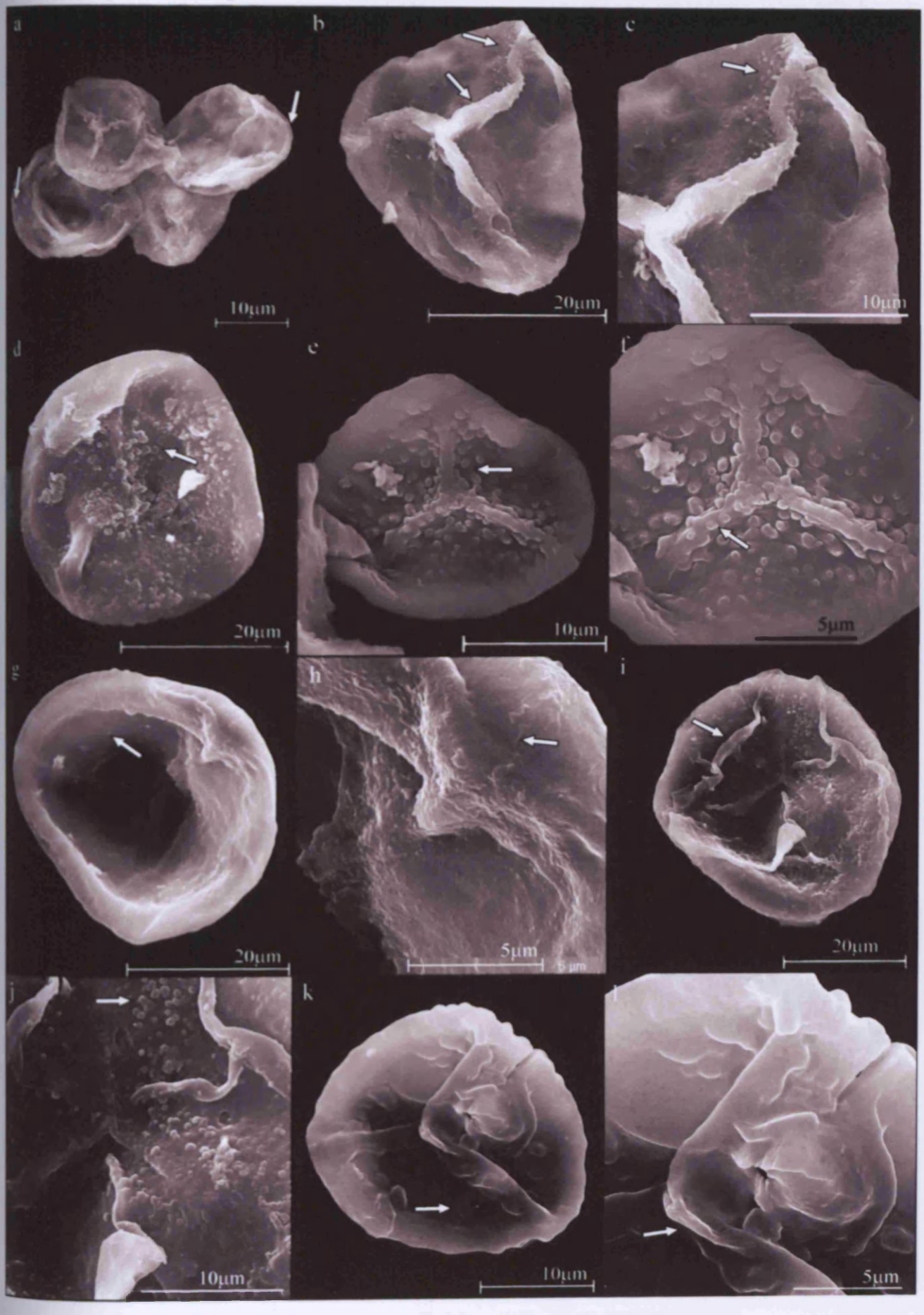

Plate 5.30: Murornate sculptured retusoid triletes.

a* to *c*: *Emphanisporites protophanus

a: TQBH1-1-107, Assemblage 1. Sub-circular, retusoid trilete spore. Proximal surface sculptured with closely spaced radial muri (see arrow). Laesurae thin (see arrow), reaching the curvature perfectae (see arrow). Distal surface laevigate.

b: TQBH1-1-179, Assemblage 2. Retusoid, sub-circular trilete spore. Proximal surface is sculptured with closely spaced inconspicuous radial muri. Laesurae are thin, reaching the curvature perfectae (see arrow). Distal surface is laevigate.

c: Close up of TQBH1-1-179, Assemblage 2. Proximal surface sculptured with closely spaced radial muri (see arrow). Laesurae are thin (see arrow).

***d* to *f*: *Emphanisporites* sp. B**

d: TQBH1-PB1-044, Assemblage 3. Retusoid, sub-circular trilete spore. Proximal surface sculptured with closely spaced distinctive radial muri (see arrow), with thin laesurae (see arrow). Distal surface sculptured with evenly spaced large verrucae (see arrow).

e: TQBH1-3-124, Assemblage 5. Retusoid, sub-circular trilete. Proximal surface sculptured with closely spaced sinuous radial muri, and distinctive laesurae (see arrow). Distal surface sculptured with evenly spaced verrucae (see arrow).

f: Close up of TQBH1-3-124, Assemblage 5. Proximal surface sculptured with sinuous radial muri (see arrow).

***g* to *l*: *Emphanisporites* sp.**

g: TQBH1-1-103, Assemblage 2. Retusoid, sub-circular trilete spore. Proximal surface sculptured with low-lying inconspicuous radial muri. Laesurae are thin (see arrow), reaching the curvature perfectae.

h: Close up of TQBH1-1-103, Assemblage 2. Proximal surface sculptured with low-lying inconspicuous radial muri (see arrow).

i: TQBH1-1-112, Assemblage 2. Retusoid, sub-circular trilete spore. Proximal surface sculptured with inconspicuous radial muri. Laesurae are thin (see arrow).

j: Close up of TQBH1-1-112, Assemblage 2. Proximal surface sculptured with inconspicuous radial muri (see arrow).

k: TQBH1-3-134, Assemblage 5. Retusoid, sub-triangular trilete spore. Proximal surface sculptured with inconspicuous radial muri.

l: Close up of TQBH1-3-134, Assemblage 5. Proximal surface sculptured with inconspicuous radial muri (see arrow).

Plate 5.30: Murornate sculptured retusoid triletes.

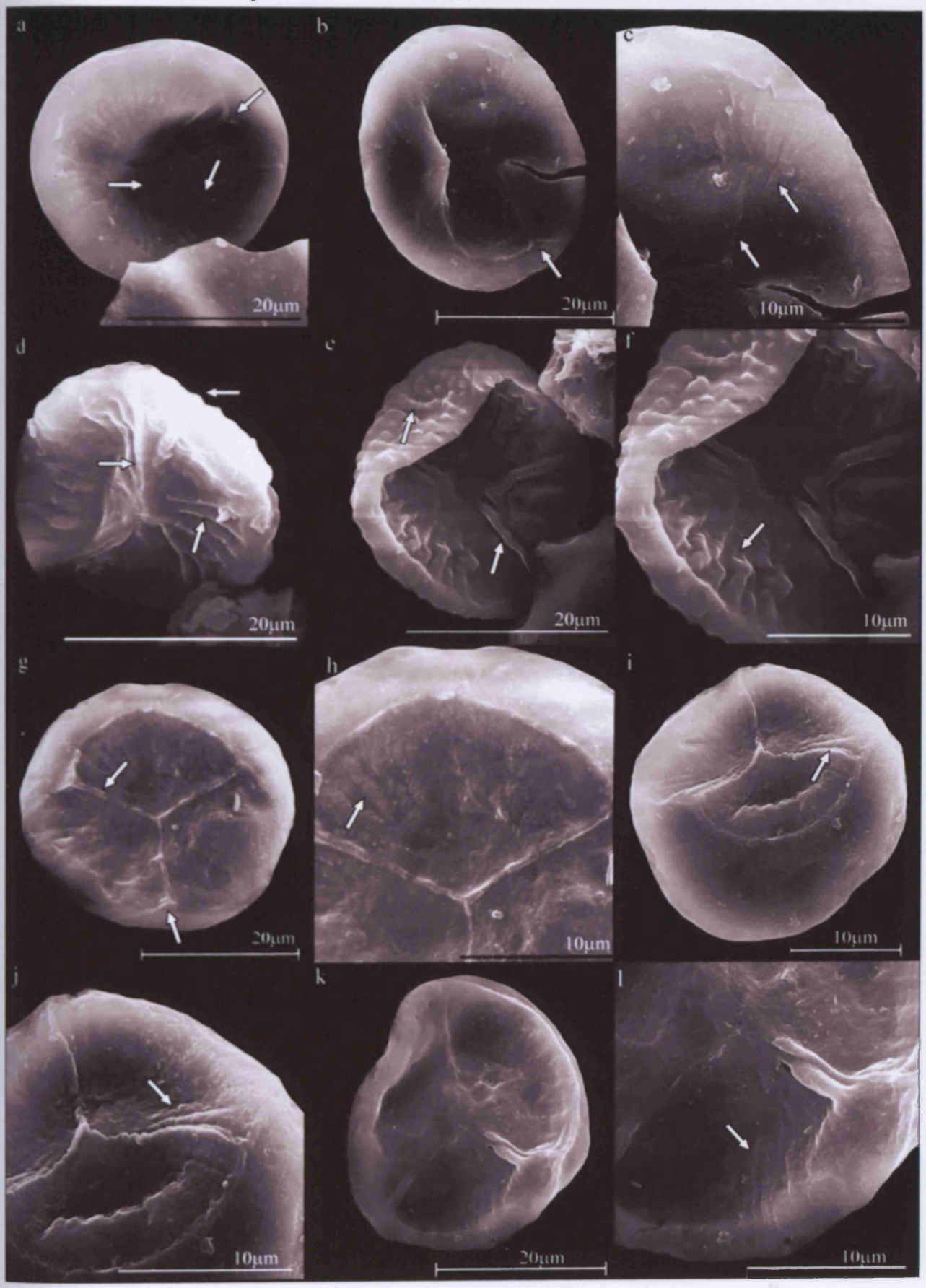

Plate 5.31: Laevigate crassitate triletes

a* to *d*: *Ambitisporites avitus

a: TRE1/142, Assemblage 1. Crassitate, sub-triangular trilete spore. Distal and proximal surfaces laevigate. Laesurae thick and raised (see arrow), reaching the inside of the equatorial crassitude (see arrow).

b: Close up of TRE1/142, Assemblage 1. Proximal surface sculptured with microgranular ornamentation (see arrow).

c: TQBH1-1-065, Assemblage 3. Crassitate, sub-triangular trilete spore. Distal and proximal surfaces laevigate. Laesurae is thick and slightly raised (see arrow).

d: TQBH1-1-113, Assemblage 3.Crassitate, sub-triangular trilete spore. Distal and proximal surfaces laevigate. Laesurae is thick and slightly raised, reaching the inside of the equatorial crassitude (see arrow).

e* to *l*: *Ambitisporites avitus* var. *minor

e: T1-6/PB0-274, Assemblage 1. Crassitate, sub-triangular trilete spore. Distal and proximal surfaces are laevigate. Laesurae are thick, and reach the equatorial crassitude (see arrow).

f: TRE1/044, Assemblage 1. Crassitate, sub-circular trilete spore. Distal and proximal surfaces are laevigate. Laesurae are thin, reaching the equatorial crassitude (see arrow).

g: TQBH1-1-134, Assemblage 2. Crassitate, sub-triangular trilete spore. Distal and proximal surfaces are laevigate. Laesurae are thin and inconspicuous (see arrow), reaching the equatorial crassitude.

h: TQBH1-1(Ox1)-036, Assemblage 2. Crassitate, sub-triangular trilete spore. Distal and proximal surfaces are laevigate Laesurae are thick (see arrow), reaching the equatorial crassitude.

i: TQBH1-PB1-011, Assemblage 3. Crassitate, sub-circular trilete spore. Distal and proximal surfaces are laevigate. Laesurae are thick (see arrow).

j: TQBH1-PB1-149, Assemblage 3. Crassitate, sub-triangular trilete spore. Distal and proximal surfaces are laevigate. Laesurae are thick, forming lips (see arrow), and reach the equatorial crassitude.

k: TQBH2-1-030, Assemblage 4. Crassitate, sub-circular trilete spore. Distal and proximal surfaces laevigate. Laesurae (see arrow) reach the equatorial crassitude.

l: TQBH2-1-155, Assemblage 5. Crassitate, sub-triangular trilete spore. Laesurae are thick, forming lips (see arrow) and reach the equatorial crassitude.

Plate 5.31: Laevigate crassitate triletes.

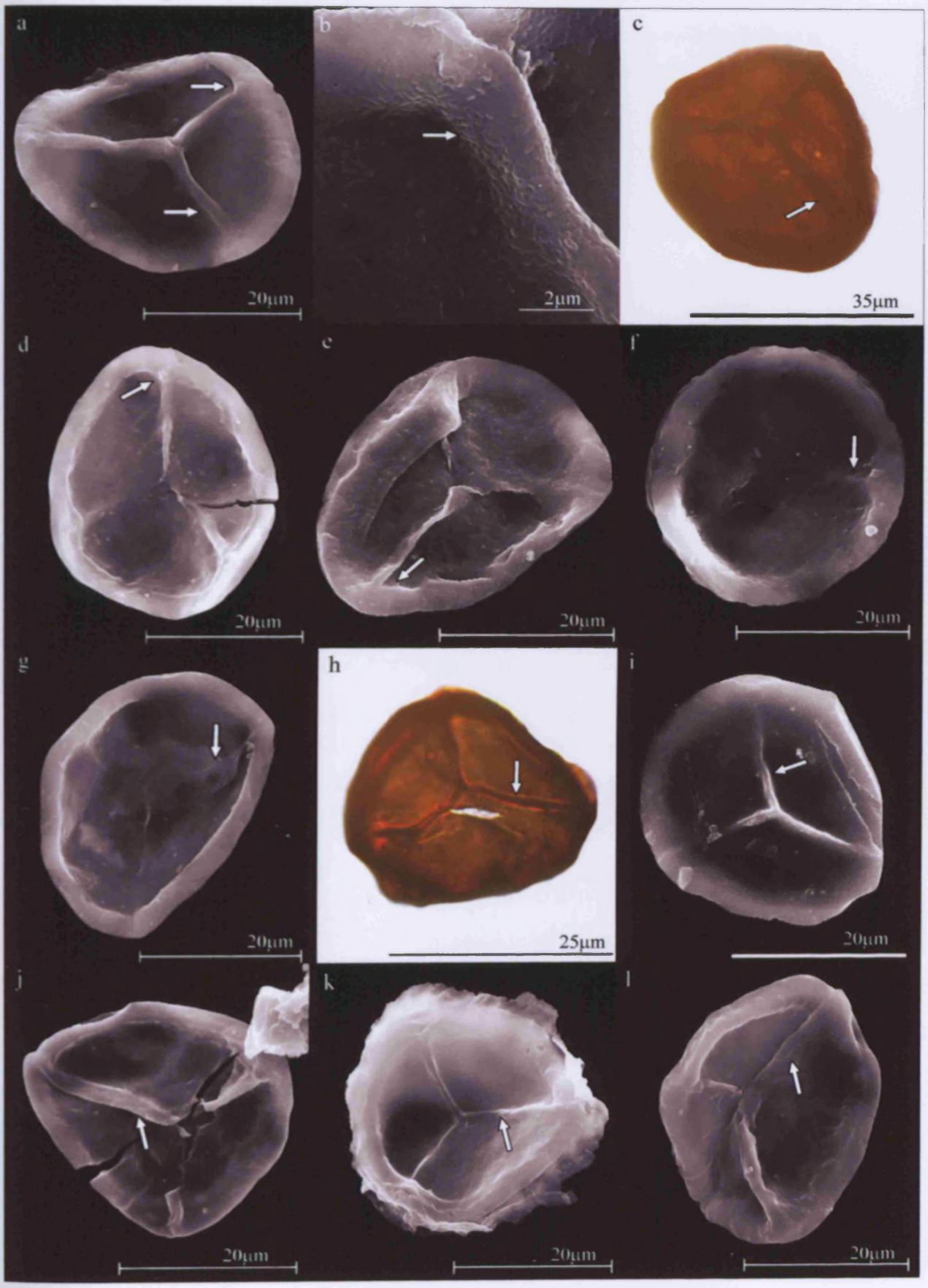

Plate 5.32: Laevigate crassitate triletes

a* to *f*: *Ambitisporites dilutus

a: TRE1/009, Assemblage 1. Crassitate, sub-triangular trilete spore. Distal and proximal surfaces laevigate. Laesurae are thick, forming lips (see arrow), reaching the thin equatorial crassitude.

b: TQBH1-1-027, Assemblage 2. Partial crassitate sib-circular trilete spore. Distal and proximal surfaces are laevigate. Laesurae are sutured (see arrow), reaching the equatorial crassitude.

c: TQBH1-PB1-025, Assemblage 3. Crassitate sub-circular trilete spore. Distal and proximal surfaces laevigate. Laesurae are thin (see arrow), reaching a thin equatorial crassitude.

d: TQBH2-1-055, Assemblage 4. Crassitate sub-circular trilete spore. Distal and proximal surfaces laevigate. Laesurae are sutured (see arrow), reaching the equatorial crassitude.

e: TQBH1-3-217, Assemblage 5. Crassitate sub-triangular trilete spore. Distal and proximal surfaces laevigate. Laesurae are thick and folded, reaching the equatorial crassitude (see arrow).

f: Close up of TQBH1-3-217, Assemblage 5. Laesurae are thick and folded (see arrow).

g* to *k*: *Ambitisporites warringtonii

g: TRE1/102, Assemblage 1. Crassitate, sub-circular trilete spore. Distal and proximal surfaces laevigate. Equatorial crassitude is thick, which thins out in the inter-radial areas. Laesurae are thick, but taper to the apical zone (see arrow).

h: Close up of TRE1/102, Assemblage 1. Proximal surface laevigate. Equatorial crassitude is thick, which thins out in the inter-radial areas (see arrow).

i: TQBH1-1-131, Assemblage 2. Crassitate sub-circular trilete spore. Laesurae are thin (see arrow), reaching a thick equatorial crassitude.

j: TQBH1-PB1-113, Assemblage 3. Crassitate sub-circular trilete spore. Laesurae are thin and sutured reaching a thick equatorial crassitude (see arrow).

k: TQBH1-PB1-043, Assemblage 3. Crassitate sub-triangular trilete spore. Laesurae are thin and sutured, reaching a thick equatorial crassitude (see arrow).

***l*: *Ambitisporites* sp. A**

l: TQBH1-1(Ox1)-079, Assemblage 2. Crassitate, sub-circular trilete spore. Distal and proximal surfaces laevigate. Central dark apex at the apical pole.

Plate 5.32: Laevigate crassitate triletes (continued)

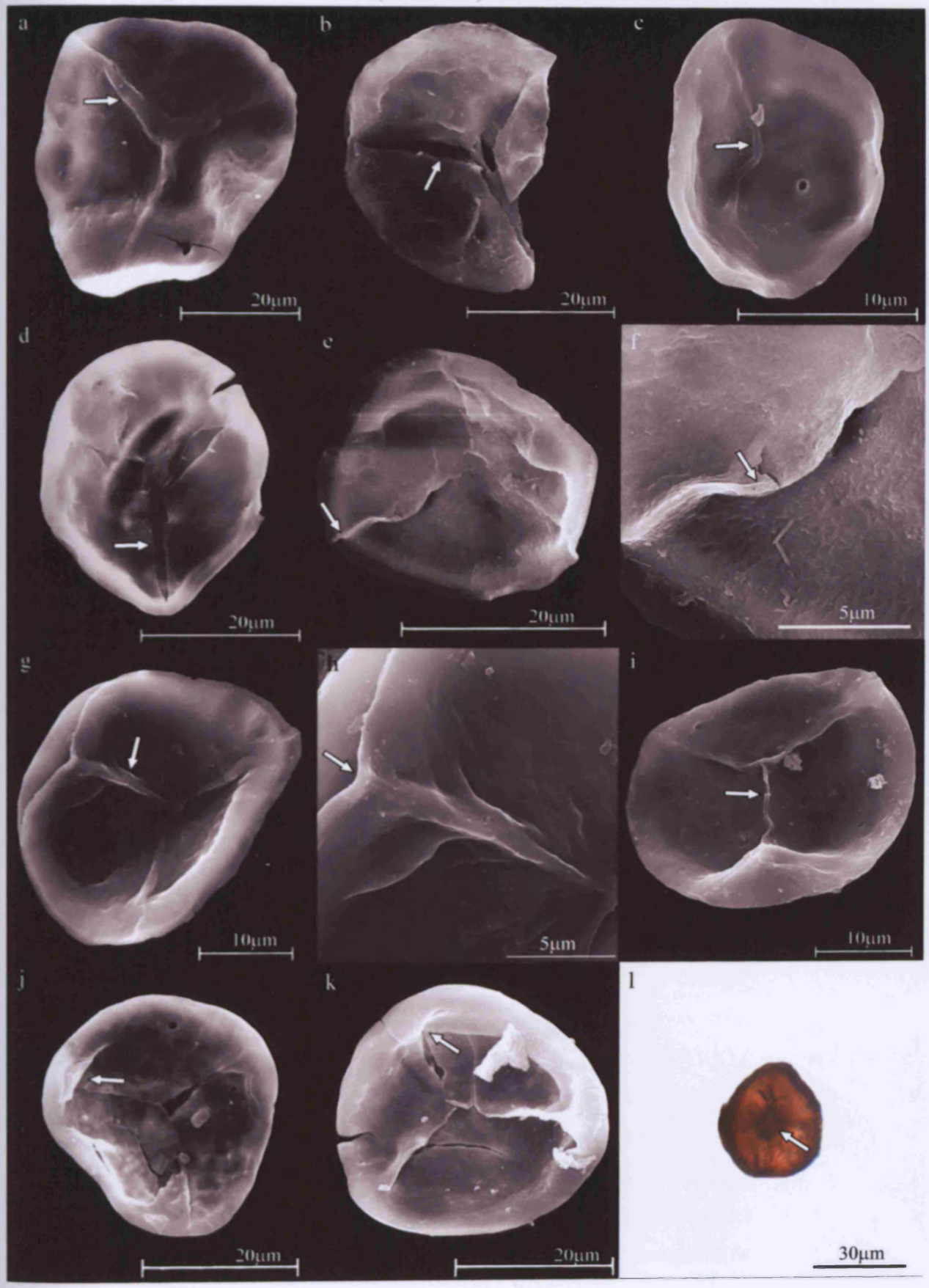

Plate 5.33: Apiculate sculptured crassitate triletes.

a* to *d*: *Streelispora newportensis

a: TRE1/172, Assemblage 1. Crassitate, sub-circular trilete spore. Proximal surface sculptured with three inter-radial rounded papillae. Papillae are attached to equator and laesurae by small folds. Laesurae are thick (see arrow). Distal wall sculptured with broad coni (see arrow).

b: Close up of TRE1/172, Assemblage 1. Proximal wall sculptured with inter-radial rounded papillae (see arrow), attached to the equator and laesurae by small folds (see arrow).

c: TQBH2-1-021, Assemblage 4. Crassitate, sub-circular trilete spore. Proximal surface sculptured with inter-radial rounded papillae (see arrow). Distal wall sculptured with small apiculate elements (coni) (see arrow).

d: Close up of TQBH2-1-021, Assemblage 4. Proximal surface sculptured with inter-radial papillae, attached to laesurae and equator by small folds (see arrow).

***e* to *l*: *Aneurospora* sp.**

e: TRE1/093, Assemblage 1. Crassitate, sub-circular trilete spores. Proximal surface laevigate, with simple laesurae (see arrow). Distal surface sculptured with apiculate elements (grana) (see arrow).

f: TQBH1-PB1-009, Assemblage 3. Crassitate, sub-triangular trilete spores. Proximal surface laevigate, with simple laesurae (see arrow). Distal surface sculptured with apiculate elements (grana and coni) (see arrow).

g: Close up of TQBH1-PB1-009, Assemblage 3. Distal surface sculptured with apiculate elements (grana and coni) (see arrow).

h: TRE1/019, Assemblage 1.Crassitate, sub-circular trilete spore. Distal wall sculptured with evenly spaced grana and microconi (see arrow).

i: TQBH1-PB1-049, Assemblage 3. Crassitate, sub-circular trilete spore. Distal wall sculptured with evenly spaced grana and microconi (see arrow).

j: TQBH1-PB1-088, Assemblage 3. Crassitate, sub-circular trilete spore. Distal wall sculptured with evenly spaced grana and microconi (see arrow).

k: TQBH2-1-139, Assemblage 4. Tetrad of crassitate sub-circular trilete spores. Distal walls sculptured with evenly spaced grana and microconi (see arrow).

l: Close up of TQBH2-1-139, Assemblage 4. Tetrad of crassitate sub-circular trilete spores. Proximal surface is laevigate. Distal surface sculptured with evenly spaced grana (see arrow).

Plate 5.33: Apiculate sculptured crassitate triletes

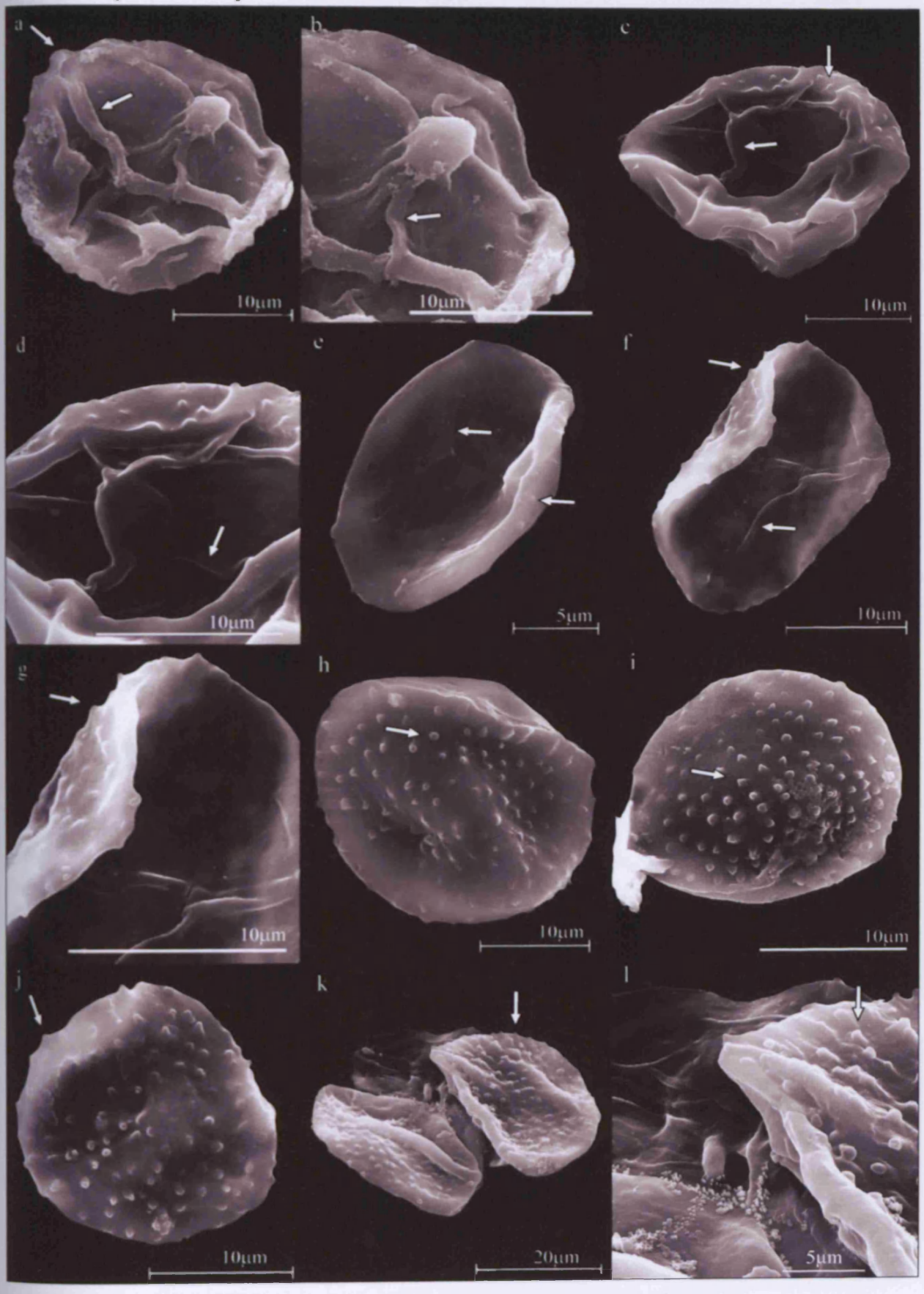

Plate 5.34: Murornate sculptured crassitate triletes.

a* and *b*: *Scylaspora* cf. *scripta

a: TQBH1-3-067, Assemblage 5. Crassitate, sub-circular trilete spore. Proximal surface sculptured with irregular arranged, low convoluted muri and rugulae. Laesurae are sutured, with laevigate lips (see arrow).

b: Close up of TQBH1-3-067, Assemblage 5. Proximal surface sculptured with low convoluted muri and rugulae (see arrow).

c* to *h*: *Scylaspora downiei

c: TQBH1-1-109, Assemblage 2. Crassitate, sub-circular trilete spore. Laesurae are thin and slightly sinuous (see arrow). Proximal surface is sculptured with closely spaced, irregularly arranged large verrucae to rugulae.

d: Close up of TQBH1-1-109, Assemblage 2. Proximal surface is sculptured with closely spaced, irregularly arranged large verrucae to rugulae (see arrow).

e: TQBH1-1-092, Assemblage 2. Crassitate, sub-circular trilete spore. Laesurae thin and sinuous (see arrow). Proximal surface sculptured with closely spaced, irregular verrucae to rugulae (see arrow).

f: Close up of TQBH1-1-092, Assemblage 2. Proximal surface sculptured with closely spaced, irregular verrucae to rugulae (see arrow).

g: TQBH1-PB1-071, Assemblage 3. Crassitate, sub-circular trilete spore. Laesurae are thin (see arrow). Proximal surface sculptured with low, inconspicuous verrucae and rugulae.

h: Close up of TQBH1-PB1-071, Assemblage 3. Proximal surface sculptured with low, inconspicuous verrucae and rugulae (see arrow).

i*: *Scylaspora* cf. *kozlica

i: TQBH1-3(Ox1)-034, Assemblage 5. Crassitate, sub-triangular trilete spore. Trilete mark simple, reaching equatorial crassitude. Proximal surface sculptured with micrograna.

***j* to *l*: *Scylaspora* sp.**

j: TQBH2-1-229, Assemblage 4. Crassitate (see arrow), sub-circular trilete spore. Proximal surface sculptured with irregular verrucae and rugulae.

k: Close up of TQBH2-1-229, Assemblage 4. Proximal surface sculptured with irregular verrucae and rugulae (see arrow).

l: TQBH1-3-188, Assemblage 5. Crassitate, sub-triangular trilete spore. Verrucae or rugulae elements ornamented apical zone of proximal surface (see arrow).

Plate 5.34: Murornate sculptured crassitate triletes

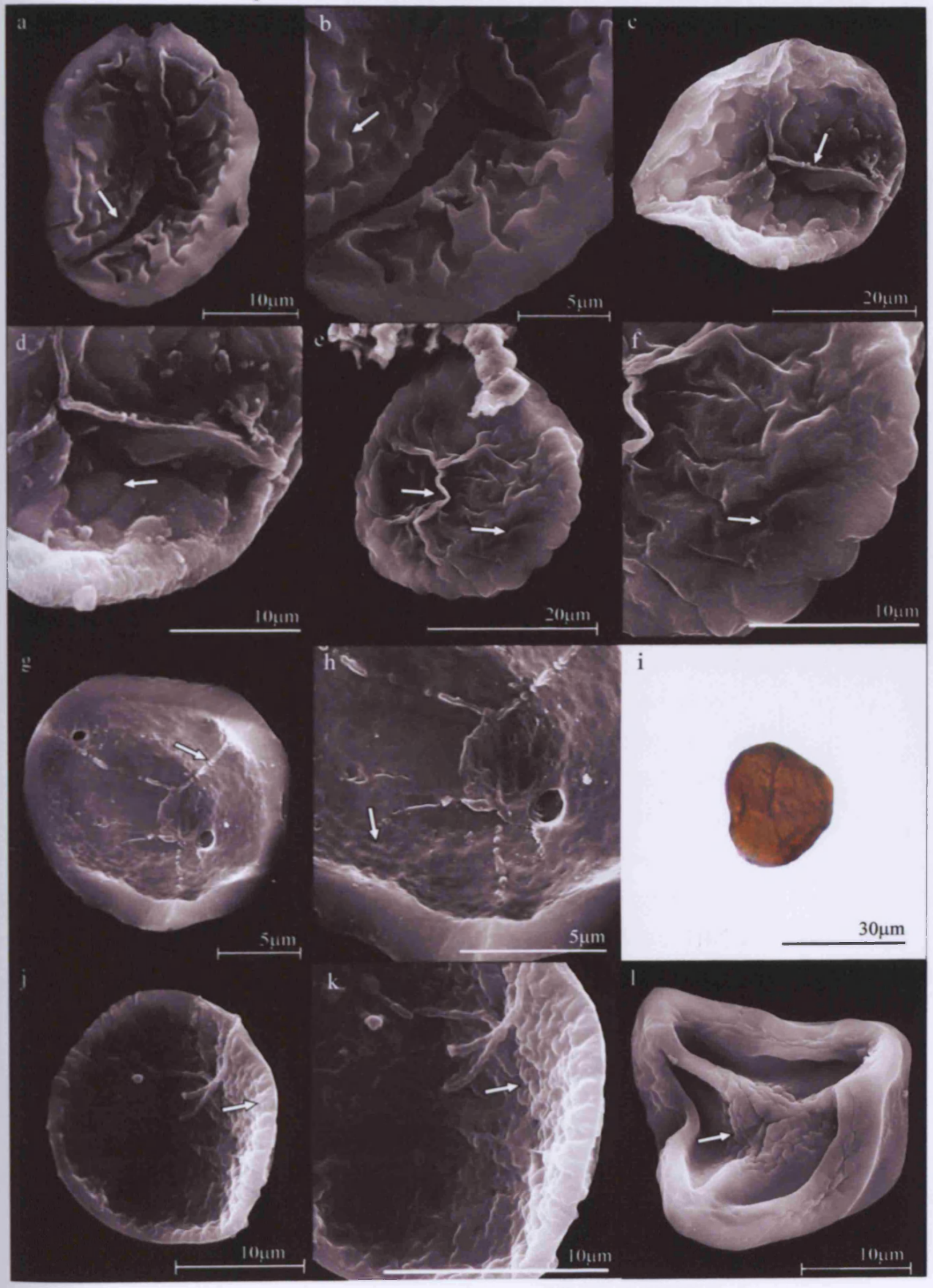

Plate 5.35: Verrucate sculptured crassitate triletes.

***a* to *d*: *Synorisporites* sp. A.**

a: T1-6/PB0 (Stub 1-6)-268, Assemblage 1. Crassitate, sub-circular trilete spore. Proximal surface sculptured with inter-radial papillae. Laesurae are narrow, surrounded by thick lips. Distal surface sculptured with verrucae (see arrow).

b: Close up of T1-6/PB0 (Stub 1-6)-268, Assemblage 1. Proximal surface sculptured with rounded inter-radial papillae (see arrow).

c: TQBH2-1(StubT(2)2-1)-051, Assemblage 4. Crassitate, sub-triangular trilete spore. Proximal surface sculptured with rounded inter-radial papillae. Distal surface sculptured with verrucae to coni elements (see arrow).

d: Close up of TQBH2-1(StubT(2)2-1)-051, Assemblage 4. Proximal surface sculptured rounded inter-radial papillae (see arrow).

***e* to *j*: *Synorisporites* sp.**

e: TQBH1-PB1(StubPB1-2008)-166, Assemblage 3. Crassitate, sub-circular trilete spore. Proximal surface sculptured with broad rugulae and convoluted muri. Distal surface sculptured with irregular broad verrucae or rugulae (see arrow).

f: Close up of TQBH1-PB1(StubPB1-2008)-166, Assemblage 3. Proximal surface sculptured with broad rugulae and convoluted muri (see arrow).

g: TQBH1-PB1(StubPB1-2008)-152, Assemblage 3. Crassitate, sub-circular trilete spore. Distal surface sculptured with closely spaced, irregular verrucae (see arrow). Proximal surface sculptured with low, convoluted verrucae or rugulae (see arrow).

h: Close up of TQBH1-PB1(StubPB1-2008)-152, Assemblage 3. Proximal surface sculptured with low, convoluted verrucae or rugulae (see arrow).

i: TQBH1-PB1(StubPB1-2008)-085, Assemblage 3.Crassitate, sub-triangular trilete spore. Proximal surface sculptured with irregular verrucae or rugulae. Distal surface sculptured with closely spaced verrucae (see arrow).

j: Close up of TQBH1-PB1(StubPB1-2008)-085, Assemblage 3. Proximal surface sculptured with irregular verrucae or rugulae. Laesurae are thin, surrounded by thick lips (see arrow).

Plate 5.35: Verrucate sculptured crassitate triletes

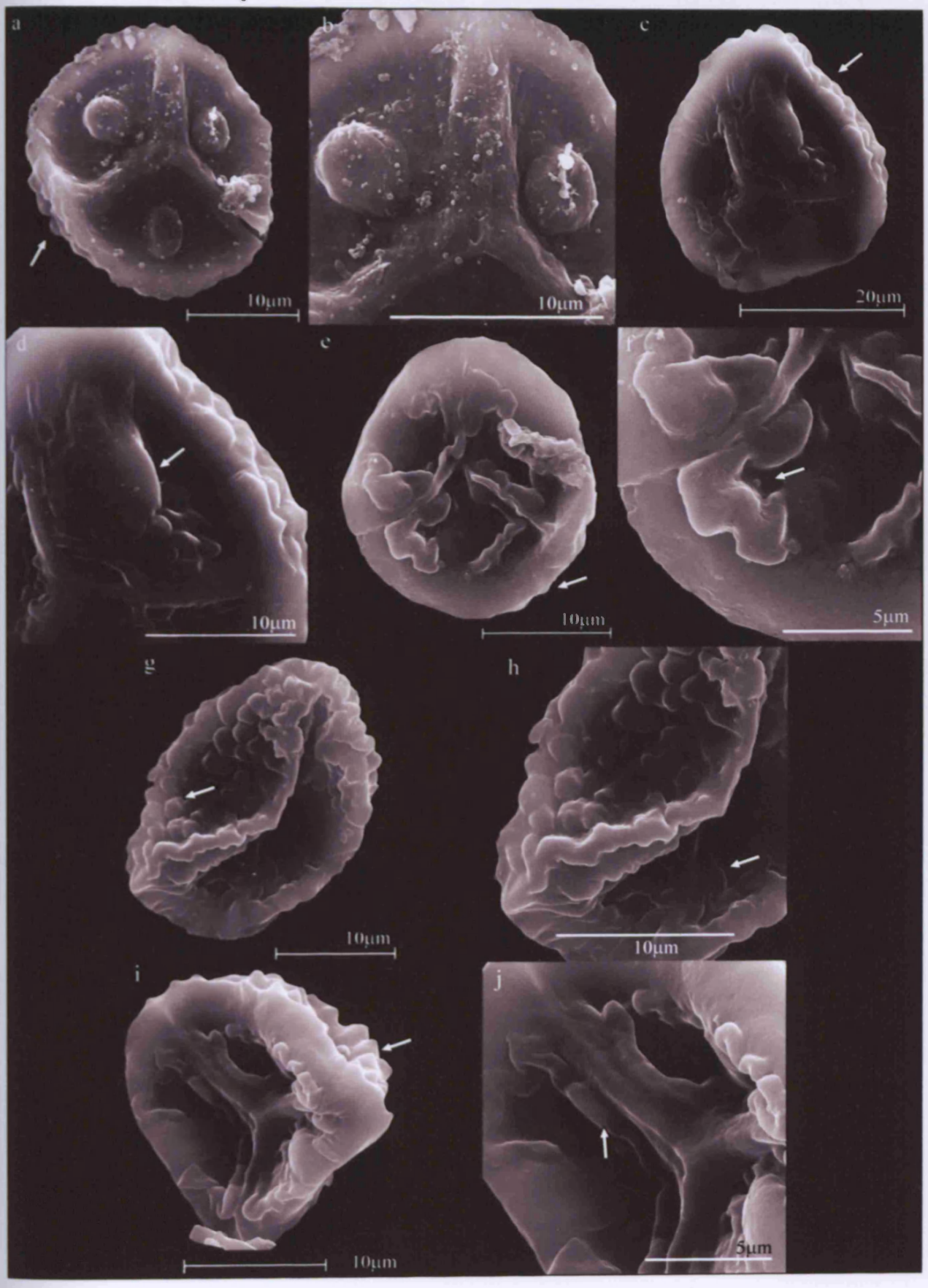

Plate 5.36: Laevigate patinate triletes.

a*: *Archaeozonotriletes chulus* var. *nanus

a: TRE1/200, Assemblage 1. Patinate, sub-triangular trilete spore. Exine thickened in equatorial regions (see arrow). Distal and proximal surfaces are laevigate.

b* to *e*: *Archaeozonotriletes chulus* var. *chulus

b: TQBH2-1(StubT2-1(2008)-096, Assemblage 4. Patinate, sub-triangular trilete spore. Proximal and distal surfaces laevigate. Laesurae thin and simple (see arrow). Exine thickened in equatorial region.

c: Close up of TQBH2-1(StubT2-1(2008)-096, Assemblage 4. Exine thickened in equatorial region (see arrow).

d: TQBH2-1(StubT2-1(2008)-136, Assemblage 4. Patinate, sub-circular trilete spore. Proximal and distal surfaces laevigate. Exine thickened in equatorial region (see arrow).

e: Close up of TQBH2-1(StubT2-1(2008)-136, Assemblage 4. Proximal surface laevigate. Laesurae thin or sutured (see arrow).

f* and *g*: *Archaeozonotriletes chulus* var. *inframurinatus

f: TRE1/024, Assemblage 1. Patinate, sub-triangular trilete spore. Proximal surface sculptured with inconspicuous radial muri. Central apical zone is thickened (see arrow).

g: Close up of TRE1/024, Assemblage 1. Proximal sculptured with inconspicuous radial muri (see arrow).

Plate 5.36: Laevigate patinate triletes

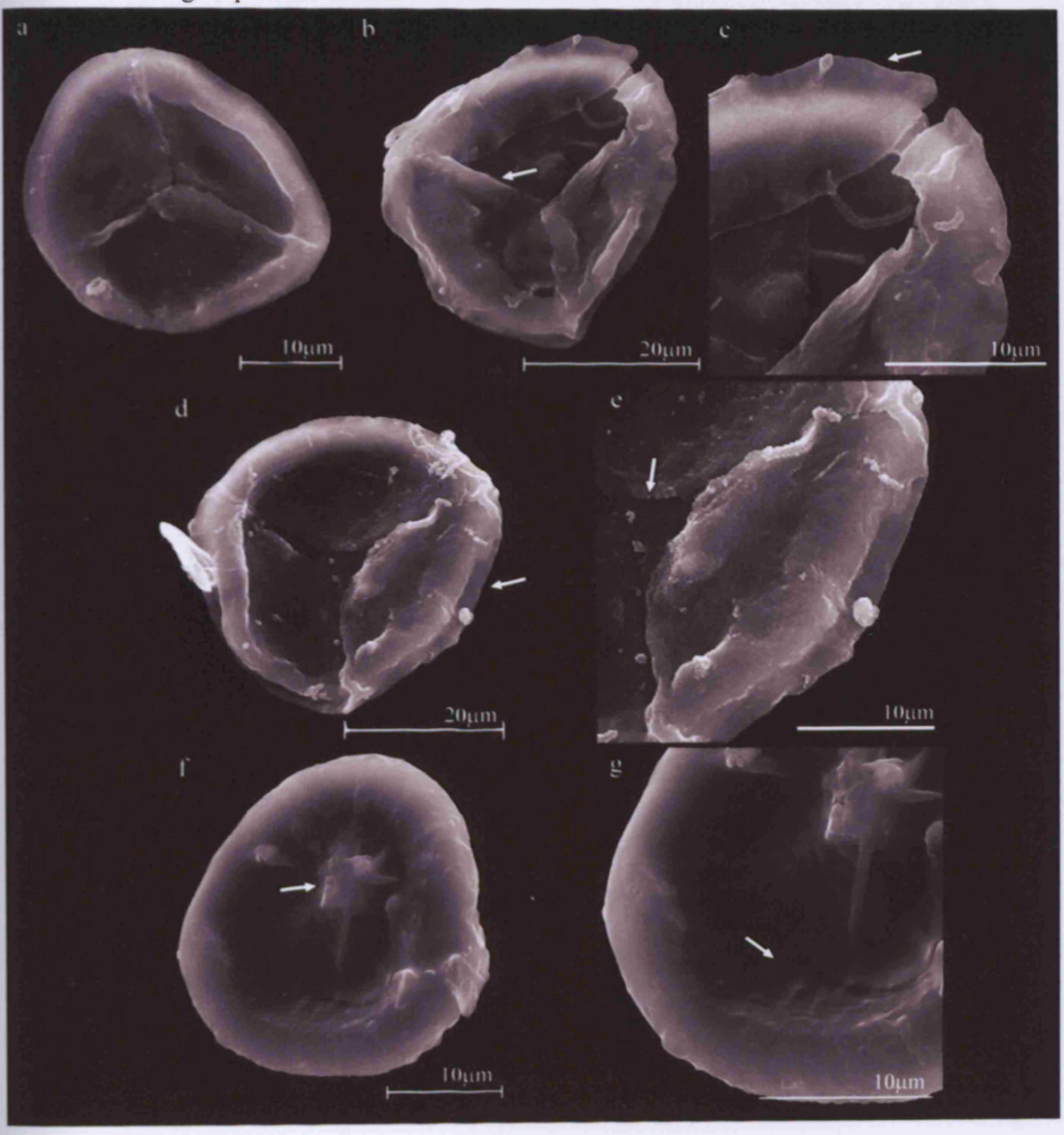

Plate 5.37: Murornate sculptured patinate triletes.

***a* to *g*: *Chelinospora* sp.**

a: TRE1/097, Assemblage 1. Patinate, sub-circular trilete spore. Proximal surface sculptured with irregular, sinuous muri forming a reticulate pattern (see arrow). Trilete mark is raised and slightly sinuous (see arrow).

b: Close up of TRE1/097, Assemblage 1. Proximal surface sculptured with sinuous muri forming a reticulate pattern. Laesurae slightly sinuous (see arrow).

c: TRE1/229, Assemblage 1. Patinate, sub-triangular trilete spore. Proximal surface sculptured with irregular, sinuous muri, forming a reticulate pattern (see arrow). Laesurae slightly sinuous (see arrow).

d: TQBH2-1(StubT2-1(2008)-189, Assemblage 4. Patinate, sub-triangular trilete spore. Proximal surface sculptured with irregular rugulae to muri. Laesurae highly sinuous (see arrow).

e: Close up of TQBH2-1(StubT2-1(2008)-189, Assemblage 4. Proximal surface sculptured with irregular, bifurcating rugulae to muri (see arrow).

f: TQBH1-3(StubT3-2)-042, Assemblage 5. Patinate, sub-triangular trilete spore. Distal and proximal surfaces sculptured with irregular verrucae, rugulae and muri. Laesurae highly sinuous (see arrow).

g: Close up of TQBH1-3(StubT3-2)-042, Assemblage 5. Proximal surfaces sculptured with irregular verrucae and rugulae (see arrow).

h* to *l*: *Perotrilites microbaculatus

h: TRE1/183, Assemblage 1. Sub-triangular trilete spore with thin perine (see arrow). Exine laevigate with equatorial crassitude. Perine sculptured with micrograna.

i: TRE1/170, Assemblage 1.Sub-circular trilete spore with thin perine (see arrow). Exine laevigate with equatorial crassitude. Perine sculptured with micrograna.

j: TQBH1-1(StubT1-1(2008)-101, Assemblage 2. Sub-circular trilete spore with thin perine, sculptured with micrograna. Contact area laevigate. Laesurae sinuous and folded (see arrow).

k: Close up of TQBH1-1-101, Assemblage 2. Perine sculptured with micrograna (see arrow).

l: TQBH1-1-132, Assemblage 2. Sub-circular trilete spore, with perine. Perine sculptured with micrograna (see arrow).

Plate 5.37: Murornate sculptured patinate triletes, and triletes with perispores

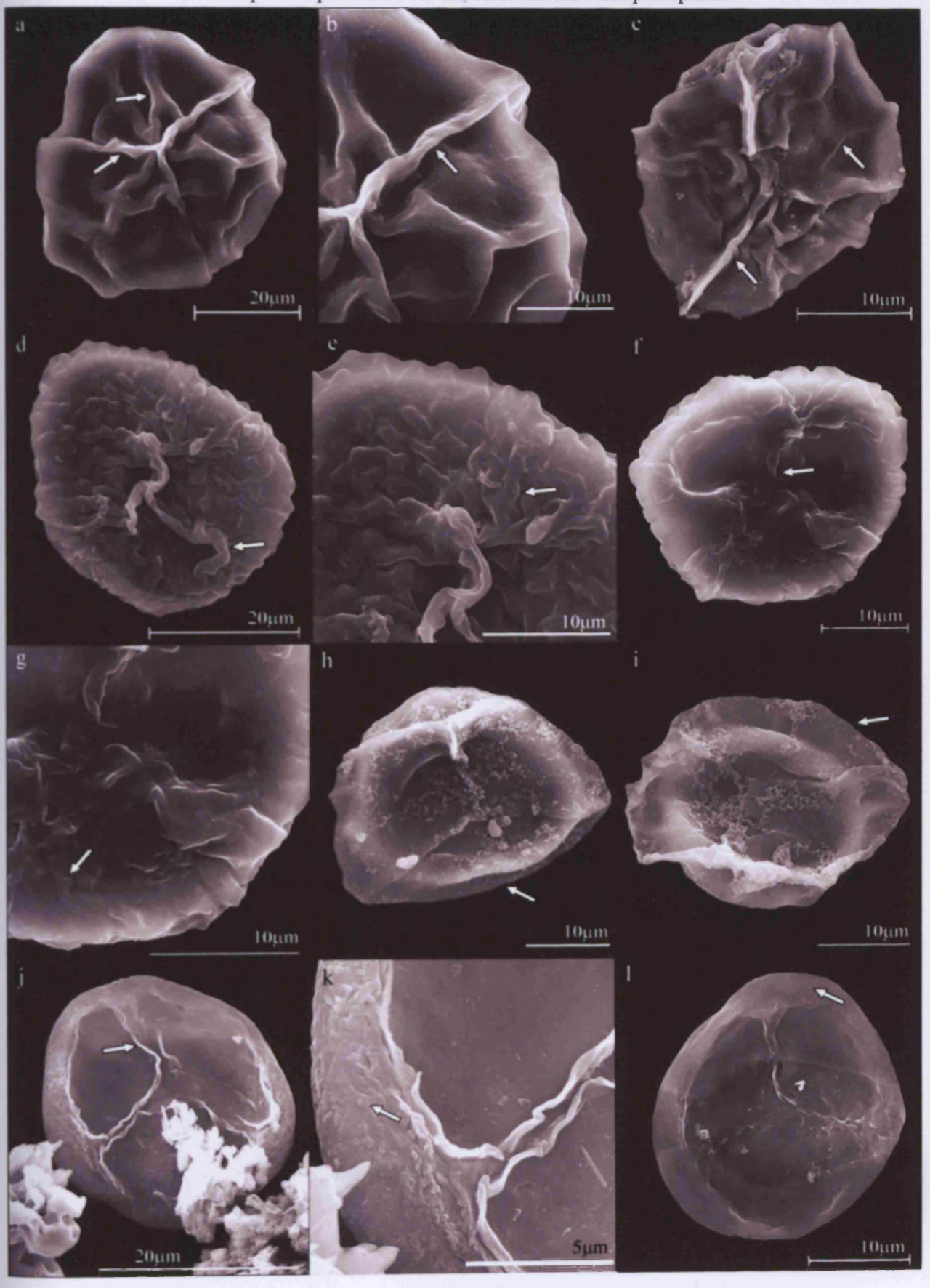

Plate 6.1: Intraformational conglomerates from Tredomen Quarry

***a* and *b*: Green intraformational conglomerates**

a: Green intraformational conglomerate with white calcareous nodule clasts, green argillaceous clasts, and a few red mudstone clasts, in a medium-grained green sandstone matrix. Bed 1, borehole 1, 0.8m below the surface.

b: Intraformational conglomerate with green argillaceous clasts in a sparry calcite matrix. Bed 1, borehole 1, 1.2m below the surface.

***c* to *e*: Red intraformational conglomerates**

c: Red intraformational conglomerate, with red argillaceous clasts and calcareous nodule clasts. Bed 62, borehole 2, 19.80m below the surface.

d: Red intraformational conglomerate with an argillaceous matrix. Bed 62, borehole 2, 20.10m below the surface.

e: Normal grading of red intraformational conglomerates. Bed 62, borehole 2, 19.40m below the surface.

Plate 6.1: Intraformational conglomerates from Tredomen Quarry

Plate 6.2: Green-grey sandstones from Tredomen Quarry

***a* to *f*: Medium-grained green to grey sandstones**

a: Medium-grained green sandstone with angular, red argillaceous gravel-sized clast horizons. Bed 6, borehole 1, 4.0m below the surface.

b: Planar-bedded medium-grained green sandstone. Bed 36, borehole 1, 29.5m below the surface.

c: Green, planar-bedded medium-grained sandstone in outcrop (1) (appears red on outer surface due to quarry workings), overlain by planar-cross-bedded medium-grained sandstone (2). Dotted line = boundary between 1 and 2.

d: Parting lineations on weathered bedding plane of medium-grained green sandstone.

e: Planar-cross-bedding of green medium-grained sandstone. Bed 2, borehole 1, 2.0m below the surface.

f: Trough-cross-bedding of green medium-grained sandstone. Bed 24, borehole 2, 8.0m below the surface.

***g* and *i*: Fine-grained green sandstones**

g: Field outcrop of fine-grained green sandstone units (1) in outcrop, with concave bases, pinching out into, and interbedded with dark green siltstones (2). Plant bed 1 indicated.

h: Planar-bedding and trough-cross-bedding of fine-grained green sandstone. Bed 45, borehole 2, 14.7m below the surface.

i: Small-scaled cross-ripple-laminations of green fine-grained sandstones. Bed 25, borehole 1, 20.5m below the surface.

Plate 6.2: Green-grey sandstones from Tredomen Quarry

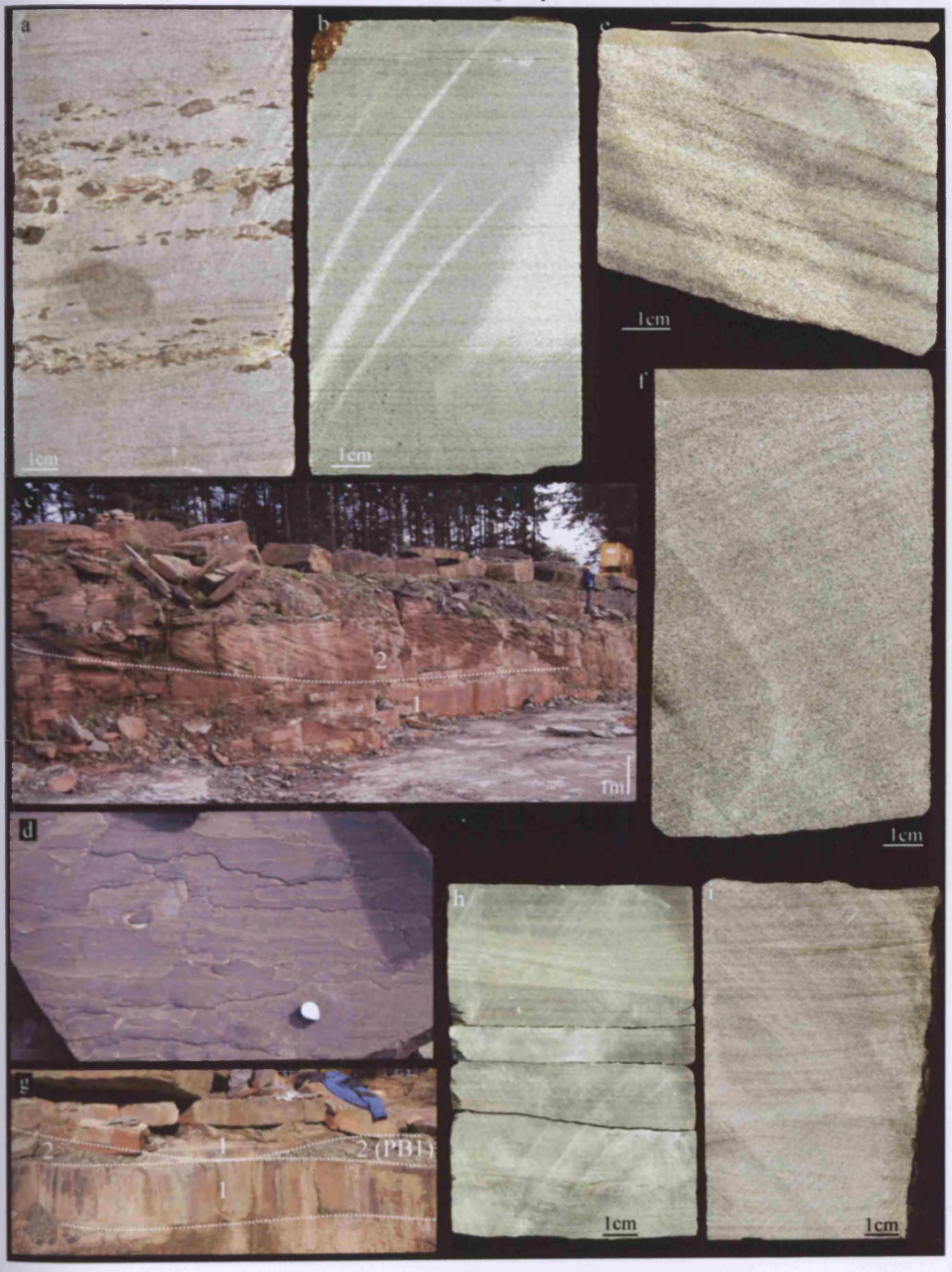

Plate 6.3: Siltstones from Tredomen Quarry

***a* to *d*: Green to grey siltstones**

a: Field outcrop of green to grey siltstones (2), interbedded with red siltstones (1).

b: Planar and wavy-ripple-laminated green to grey siltstones. Bed 41, borehole 2, 14.0m below the surface.

c: Wavy and cross-ripple-laminated green to grey siltstones. Bed 77, borehole 2, 27.5m below the surface.

d: Field outcrop of grey-green siltstones (1) overlain by red siltstones (2). Arrow points to iron-oxide spots within grey-green siltstones. Beds 7 to 6, quarry log A, 6.5m.

e: Iron - oxide spots occurring within horizons of weathered green siltstones. Bed 15, borehole 2, 5.0m below the surface.

***f* and *g*: Red siltstones**

f: Planar-laminated red siltstones. Bed 2, borehole 2, 1.4m below the surface.

g: Wavy and cross-ripple-laminated red siltstones. Bed 13, borehole 2, 4.4m below the surface.

Plate 6.3: Siltstones from Tredomen Quarry

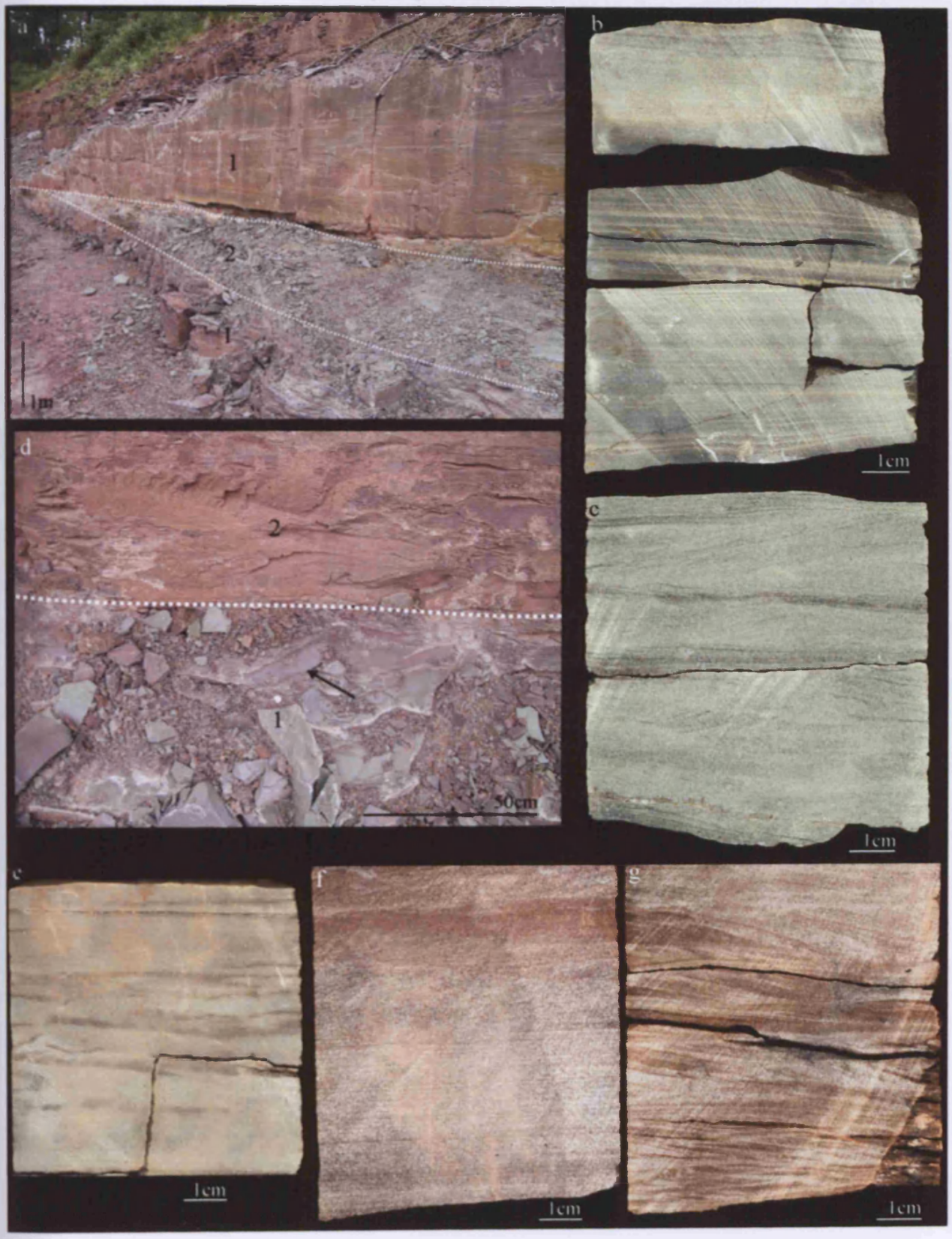

Plate 6.4: Siltstones from Tredomen Quarry (continued)

***a* to *g*: Red siltstones**

a: Cephalaspid trails (*Undichna*) on the bedding plane of red siltstones (pound coin 2.25cm in diameter). Approximately bed 6, quarry log A, ~6.3m.

b: Arthropod trackways (*Diplithnites gouldi*) on bedding plane of red siltstones (pound 2.25cm in diameter). Approximately bed 6, quarry log A, ~6.3m.

c: Iron-oxide spots within red siltstone horizons (Camera lens cap 52mm in diameter). Approximately base of bed 6, quarry log A, ~6.5m.

d: Bedding plane of red siltstone, with irregular, undulating surface (pound coin 2.25cm in diameter). Approximately bed 5, quarry log A, ~5.5m.

e: Vertical bifurcating feature surrounded by drab halo in red-grey siltstone. Base of bed 6, borehole 1, 4.2m below the surface.

f: Polygonal cracking on the bedding plane of red siltstones. (Handlens 25mm in diameter).Bed 10, quarry log A, 9.2m.

g: *Beaconites barretti* burrows on the bedding plane of red siltstones. Bed 11, quarry log A, ~9.9m.

Plate 6.4 : Siltstones from Tredomen Quarry (continued)

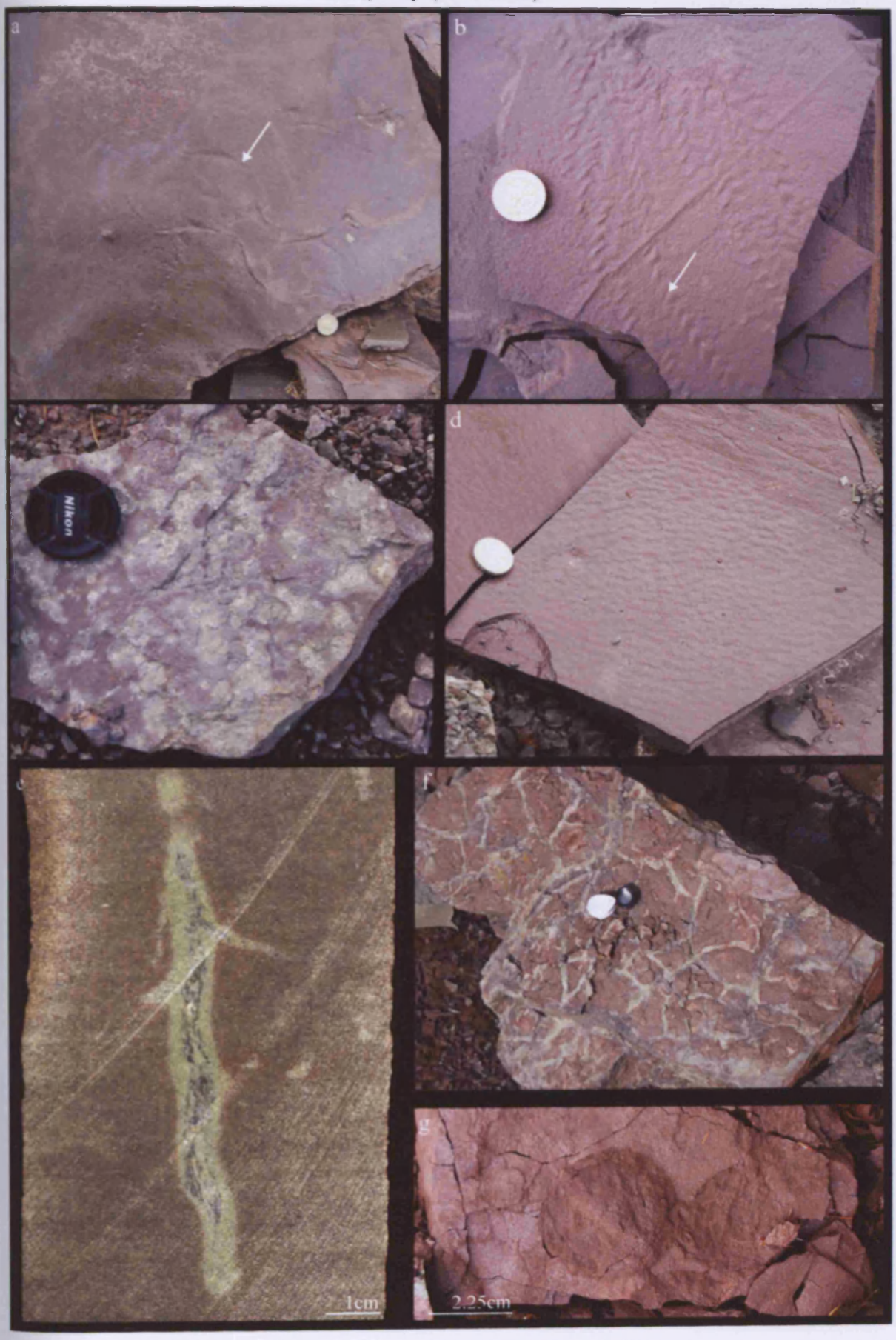

Plate 6.5: Heterolithics from Tredomen Quarry

***a* to *e*: Heterolithics**

a: Basal beds: Gravel lens (see arrow) within heterolithic unit. Bed 5, borehole 2, 2.2m below the surface.

b: Basal beds: Field outcrop of gravel lens (see arrow) composed of carbonate nodules within heterolithic unit.

c: Basal beds: Field outcrop of heterolithic units with internal inclined bedding (1), interbedded with structureless mudstones (2). Approximately beds 2,3 and 4 in quarry log A, ~1 to 4m.

d: Basal beds: Planar-cross and trough-cross-bedded heterolithic unit. Sparsely distributed small carbonate nodules are also visible (see arrow). Bed 21, borehole 1, 16.7m below the surface.

e: Basal beds: Planar-bedded heterolithic unit. Bed 21, borehole 1, 16.0m below the surface.

f: Upper beds: Wavy and cross-ripple-laminated fine-grained heterolithic unit. Bed 57, borehole 2, 18.0m below the surface.

g: Upper beds: Green-grey mottles within fine-grained heterolithic unit. Bed 8, borehole 1, 4.6m.

Plate 6.5: Heterolithics from Tredomen Quarry

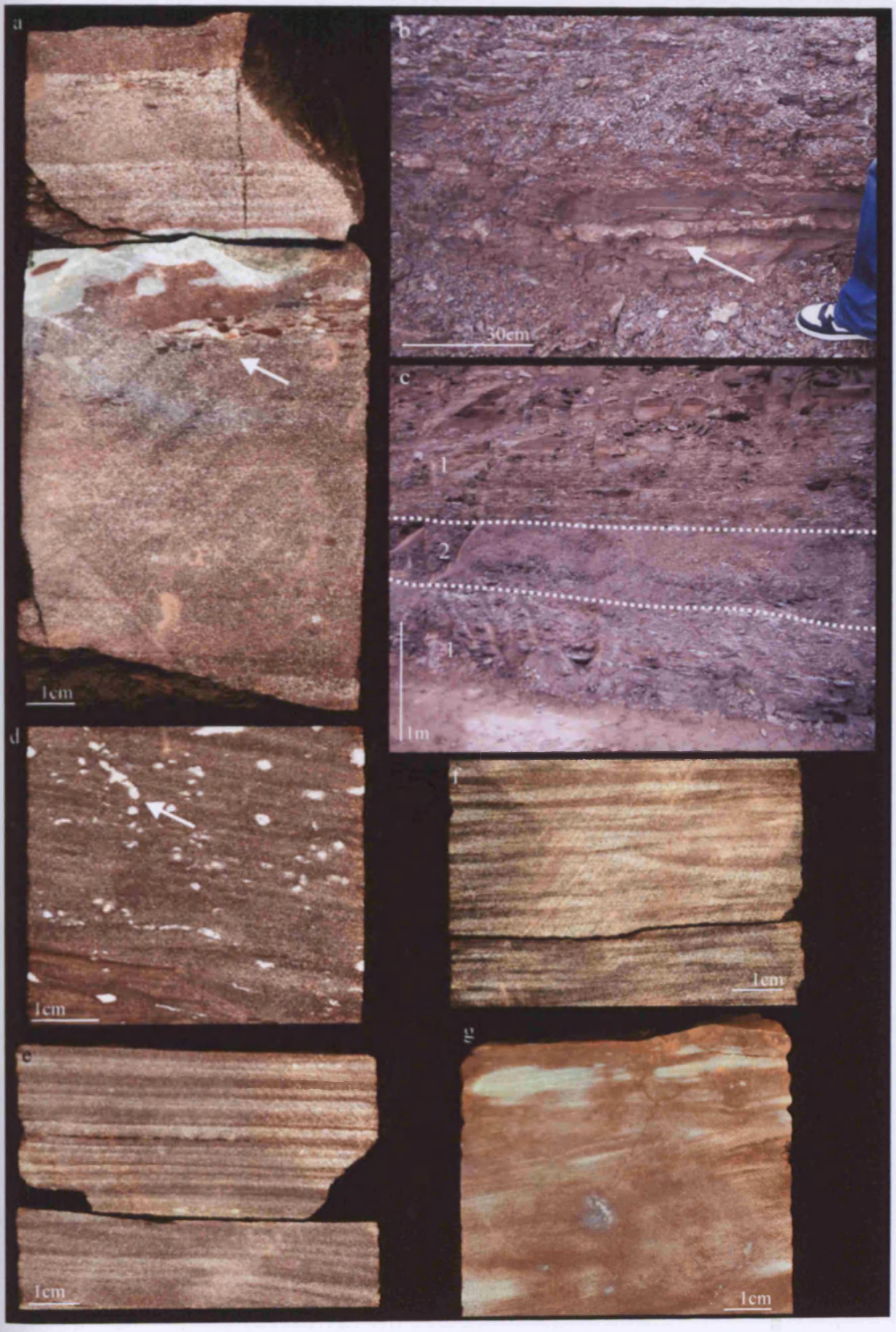

Plate 6.6: Mudstones from Tredomen Quarry

***a* to *e*: Massive, mud-pellet aggregate mudstones**

a: Massive structure of red mudstones. Bed 199, borehole 2, 101m below the surface.

b: Small carbonate nodules associated with drab haloes within massive red mudstones. Bed 193, borehole 2, 90.5m from surface.

c: Linear feature surrounded by drab halo (see arrow), within massive red mudstones. Mud aggregate visible (circled), surrounded by slightly coarser grained mud.

d: Mud aggregates visible within structureless red mudstone (circled). Linear feature surrounded by drab halo (see arrow).

e: Carbonate clasts 'floating' within red mudstone (see arrow), that is interbedded with heterolithic units.

Plate 6.6: Mudstones from Tredomen Quarry

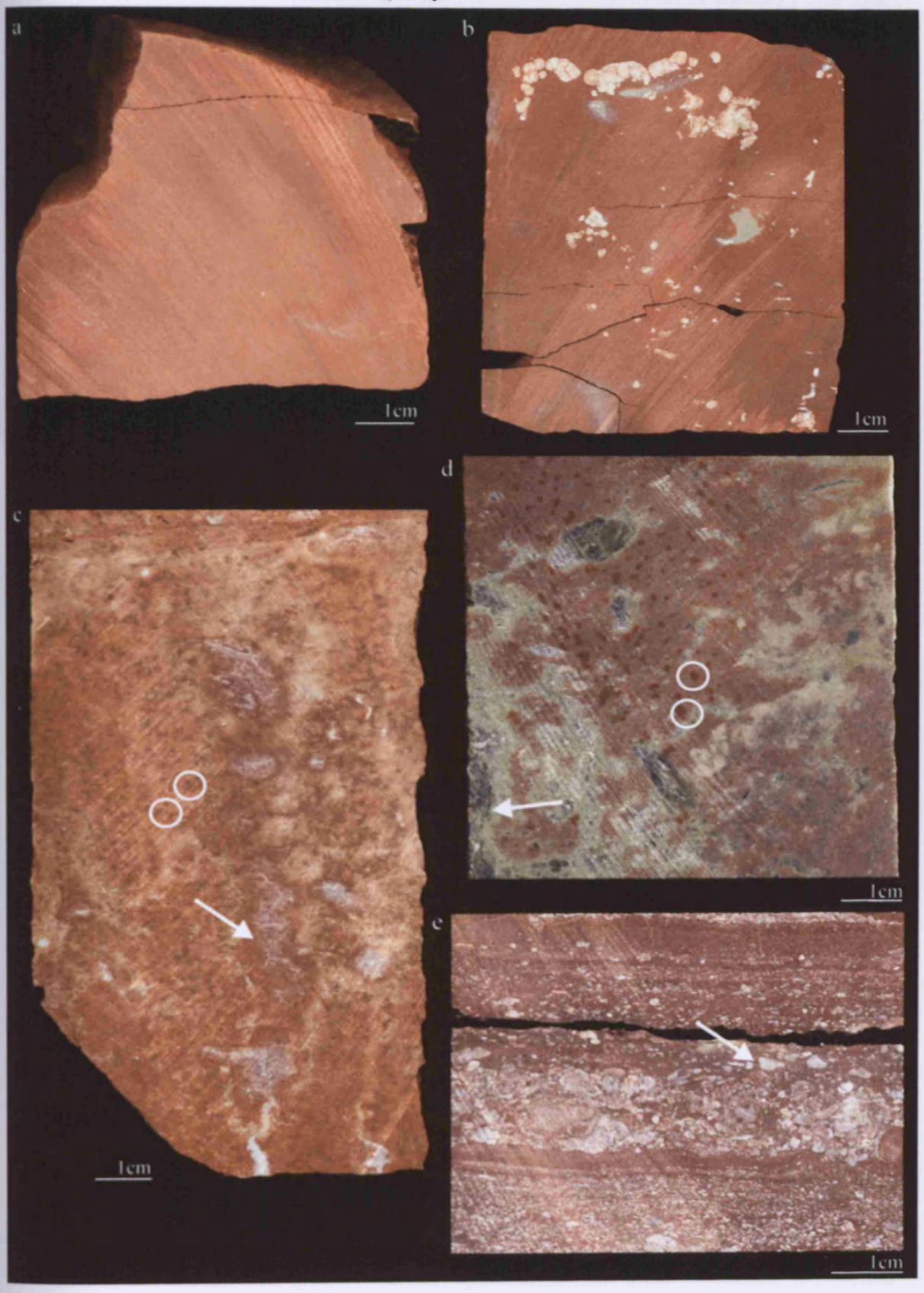

Plate 6.7: Pedified mudstones from Tredomen Quarry

***a* to *f*: Pedified profile type 1**

a: Dark, vertically linear features of the upper horizon (see arrow). Bed 173, borehole 2, 75m below the surface.

b: Field outcrop of curved slickensided, pseudo-anticlinal slip-plane surfaces (see arrow) of the middle horizon (see text). Here the middle horizon is superimposed by dark, vertically linear features (indicated by dashed line). Approximately bed 10, quarry log A, ~9.5m.

c: Lower horizon (see text). Sparsely distributed and individual small sub-spherical carbonate nodules within red mudstones. Fractures are non-pedogenic.

d: Lower horizon (see text). Elongate carbonate rods within red mudstones.

e: Lower horizon (see text). Large, partially coalesced carbonate nodules and rods within red mudstones. Bed 169, borehole 2, 68.5m below the surface.

f: Lower horizon (see text). Almost full replacement of parent red mudstone by coalescing carbonate nodules. Calcite spar cement is visible, forming the infill of non-pedogenic horizontal and vertical fractures (see arrows). Bed 82, borehole 1, 66.1m below the surface.

***g* and *h*: Pedified profile type 2**

g: Weak vertical features and carbonate nodules surrounded by drab haloes with red mudstones. Fracture is non-pedogenic. Bed 74, borehole 2, 25.8m below the surface.

h: Lower horizon (see text). Coalescing carbonate nodules within red mudstones. Calcite spar cement is visible, forming the infill of non-pedogenic horizontal and vertical fractures (see arrows). Bed 172, borehole 2, 74.5m below the surface.

Plate 6.7: Pedified mudstones from Tredomen Quarry

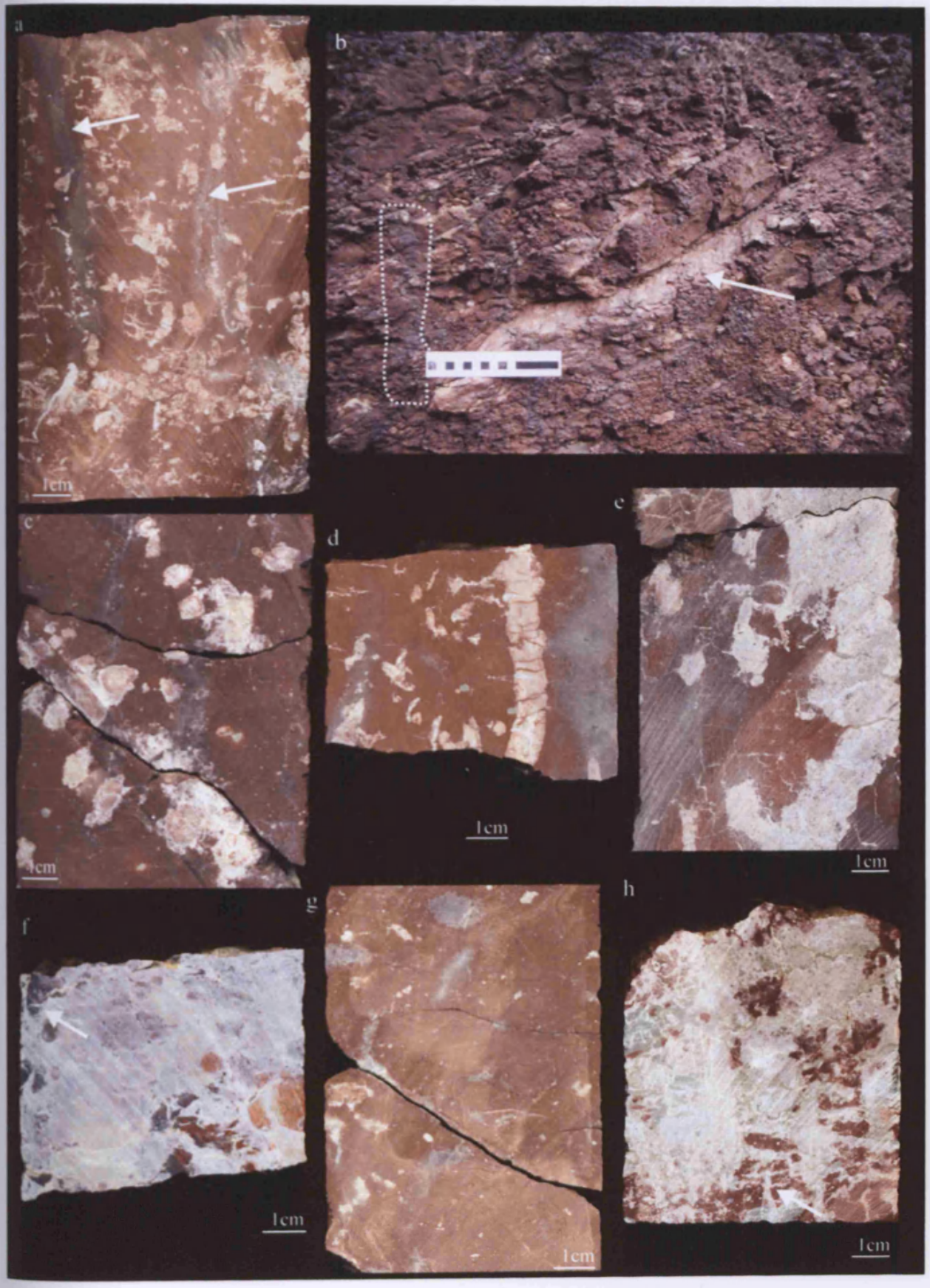

Plate 6.8: Intraformational conglomerates and sandstones from Targrove Quarry

***a*: Red to yellowish-brown intraformational conglomerates**

a: Red intraformational conglomerate (1) incising into red sandstone unit (2), incision marked by dashed line. Beds 25 and 26, Targrove Quarry log, ~1m.

***b* to *d*: Red sandstones**

b: Red medium-grained sandstone (1) grading normally into fine-grained sandstone (2). Basal beds are planar-bedded; upper units trough-cross-bedded fine-grained sandstone. Beds 24 and 25, Targrove Quarry log, ~2.6m.

c: Fissure infilled with carbonate (marked by dashed line), at the top of a medium-grained sandstone unit, truncated by intraformational conglomerates. Bed 1, Targrove Quarry log, ~13.0m.

d: Lower quarry profile at Targrove Quarry, showing red medium-grained sandstones (1), interbedded with siltstone-mudstone sequences (2). Beds 1 to 15, Targrove Quarry log.

Plate 6.8: Intraformational conglomerates and sandstones from Targrove Quarry

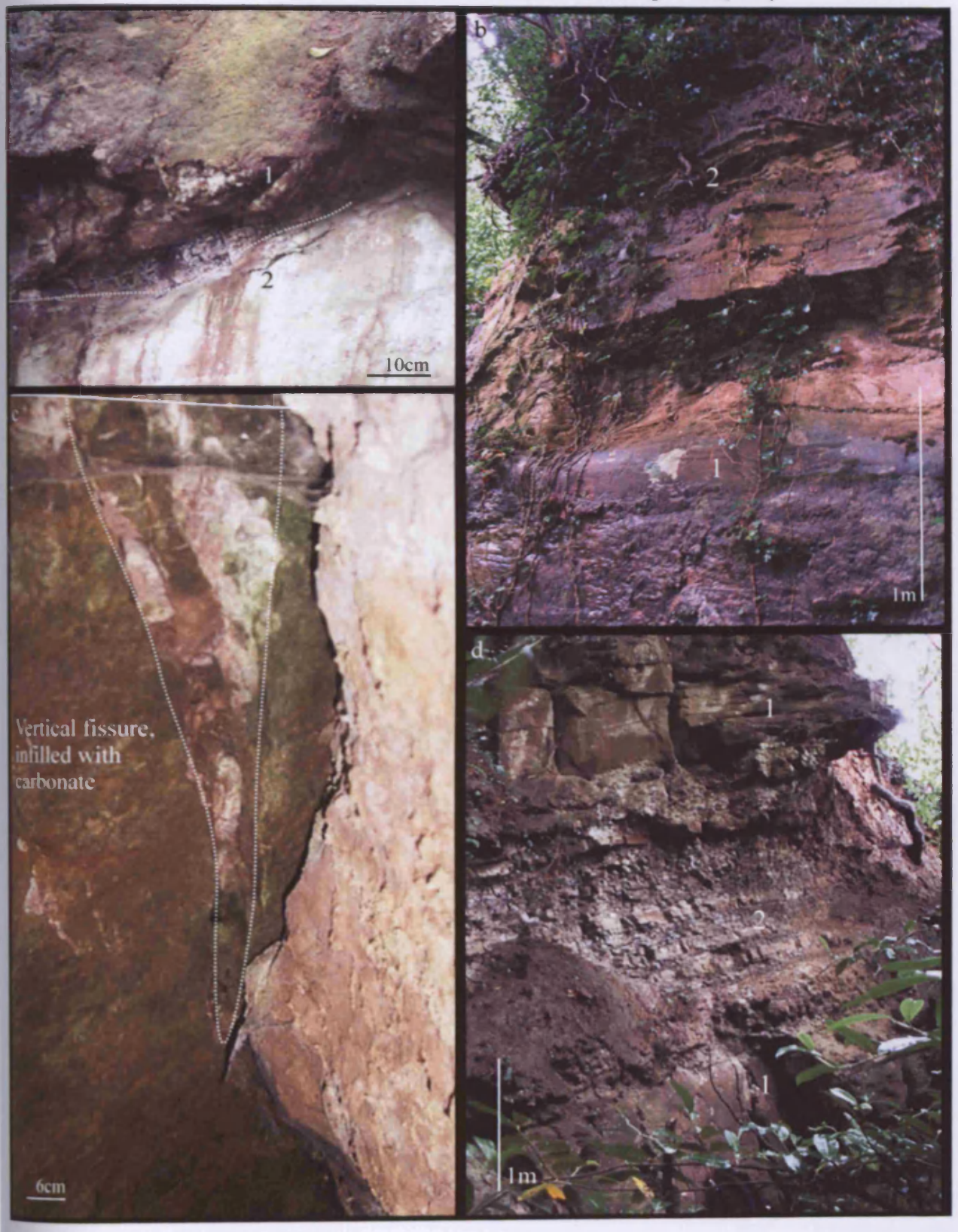

Plate 6.9: Siltstones and mudstones from Targrove Quarry

***a* to *c*: Interbedded siltstones and mudstones**

a: Close up of yellow-brown siltstone units (1) with sharp planar boundaries, interbedded with dark grey mudstones (2). Beds 4 to 7, Targrove Quarry log.

b: Interbedded siltstone (1) – mudstone (2) sequence. Beds 4 to 9, Targrove Quarry log.

c: Interbedded siltstone (1) – mudstone (2) sequence, showing lateral extent of beds, and slight wedging/ pinching out of mudstone beds. Beds 5 to 9, Targrove Quarry log.

***d* and *e*: Chapel Point Calcrete at Llansteffan**

d: Chapel Point Calcrete at Llansteffan. Stage III to stage IV stacked calcrete horizons (1), each approximately 1 to 1.5m in height.

e: Strata just above the Chapel Point Calcrete at Llansteffan: massive mudstones (1); palaeo-Vertisols, with pseudo-anticlinal slip planes overprinted with carbonate nodules (2); heterolithics (3), followed by more massive mudstones (4).

Plate 6.9: a to c: Siltstones and mudstones from Targrove Quarry.
d and e: Chapel Point Calcrete at Llansteffan

Plate 7.1: Taphofacies 1 and 2

Taphofacies 1

a: Fragment of *Prototaxites* under light microscopy, extracted from intraformational conglomerate.

b: Fragment of *Prototaxites* under SEM, extracted from intraformational conglomerate. Surface texture striated, with parallel-aligned tubes (see arrow).

c: Cross section of *Prototaxites* under SEM, showing tube internal wall with secondary thickenings (see arrow).

d: Cross section of *Prototaxites* under SEM, showing cell homogenisation as a result of charcoalification.

e: Cross section of *Pachytheca* under SEM, extracted from intraformational conglomerate.

Taphofacies 2

f: Bedding plane of medium-grained green sandstone, with coalified and charcoalified compressions of thalloid, non-embyrophytes (see arrow).

g: Coalified compression of *Cooksonia hemisphaerica* within medium-grained green sandstone.

h: Coalified compression of thalloid, non-embryophyte fragment on bedding plane of medium-grained green sandstone. Fragment is elongate and axial-like, tapering towards the end, with a rounded tip.

i: Thalloid, non-embryophyte charcoalified fragment, with irregular morphology and internal anatomy preserved, of parallel-aligned tubes (see arrow).

j: Cephalaspid fish remains within medium-grained green sandstone.

k: Disseminated vegetative debris occurring along the bedding plane surfaces of planar cross-bedded medium-grained green sandstone (see arrows).

l: Disseminated vegetative debris occurring along the bedding plane surfaces of planar cross-laminated fine-grained green sandstone (see arrow).

Plate 7.1: Taphofacies 1 and 2.

Plate 7.2: Taphofacies 3 and 4

Taphofacies 3

a: Vegetative debris along the bedding planes of horizontal and wavy-ripple laminated fine-grained sandstones to siltstones (see arrows).

b: cf. *Cooksonia caledonica* specimen within fine-grained horizontally bedded fine-grained green sandstones.

c: *Cooksonia hemisphaerica* specimen within fine-grained horizontally bedded fine-grained green sandstones.

d: Coalified compression fossil of *Salopella allenii*, with corresponding impression within fine-grained hydrated-iron-oxide rich coating (see arrow).

e: Three-dimensional preservation of cf. *Cooksonia caledonica* sporangia within fine-grained green sandstone. Three-dimensional preservation is a result of pyritisation, now converted to hydrated iron-oxide (see arrow).

f: Specimen of cf. *Cooksonia caledonica* arranged slightly oblique to bedding plane of fine-grained green sandstone (see arrow).

g: Disseminated vegetative debris along the foresets of trough-cross laminated fine-grained sandstone (see arrow).

Taphofacies 4

h: Bedding plane of green siltstone, with disseminated vegetative debris, including thalloid, non-embryophyte fragments (see arrow) and narrow branching and non-branching axial fragments (see arrow).

i: Mesofossil specimen lying parallel to the bedding plane of green siltstone (see arrow).

j: Mesofossil specimen lying parallel to the bedding plane of green siltstone (see arrow).

k: Mesofossil specimen lying parallel to the bedding plane of green siltstone (see arrow). Associated with limonite covering.

l: Irregular thalloid, non-embryophyte coalified fragment lying parallel to the bedding plane of green siltstone.

Plate 7.2: Taphofacies 3 and 4.

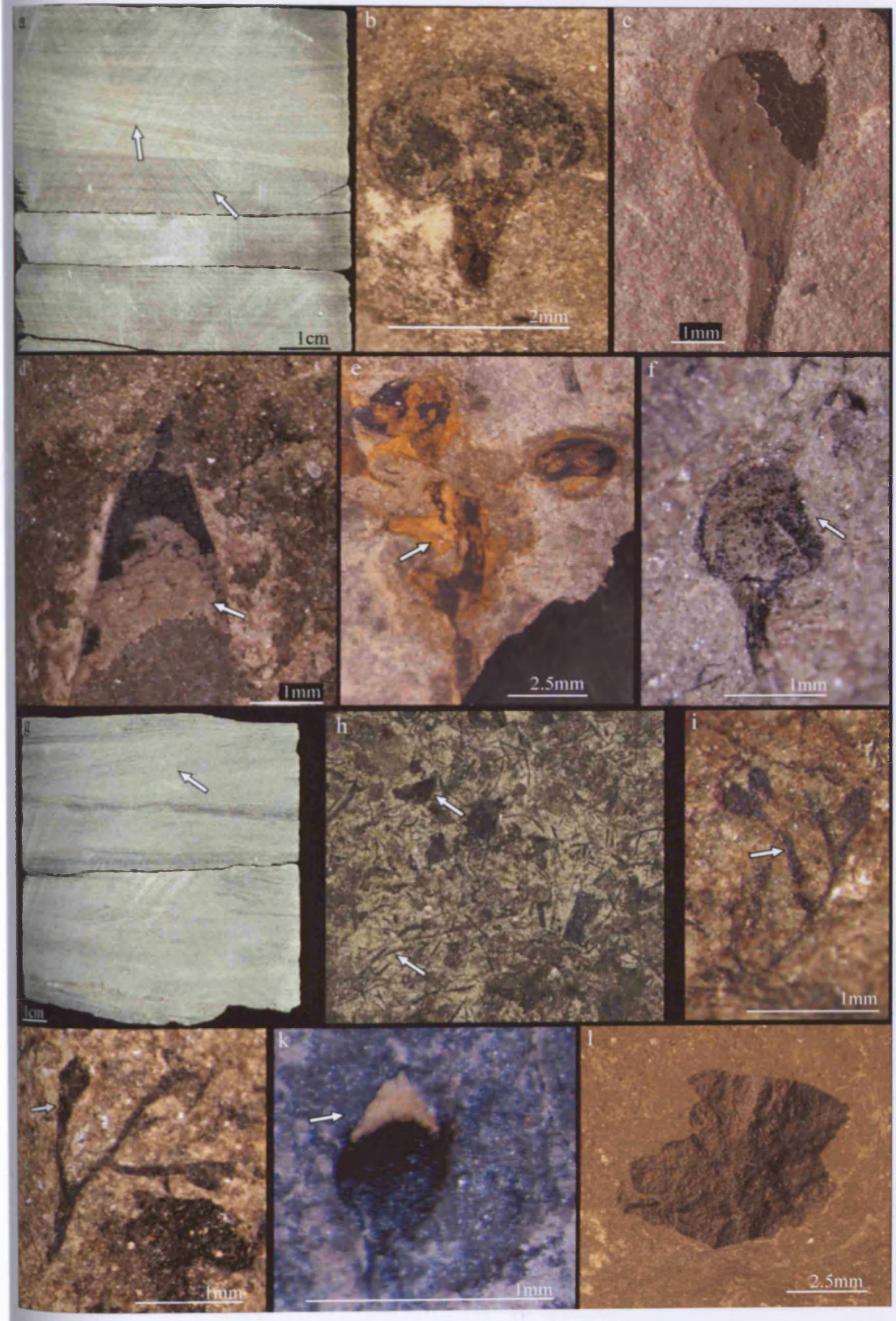

Plate 7.3: Taphofacies 5 and 6

Taphofacies 5

a: Minute, hyphal-like tubes occurring as part of a network (see arrow). Tubes parallel-aligned, and appear to intertwine and /or bifurcate across the top surface of siltstone bedding plane.

b: Minute, hyphal-like tubes occurring as part of a network (see arrow). Tubes are randomly arranged, and appear to intertwine.

c: SEM image of internal mould of one hyphal-like tube, showing banded character of internal surface (see arrow). Preserved in limonite.

Taphofacies 6

d: Horizontally-laminated, yellowish-brown, very-fine-grained sandstone collected from Targrove Quarry, packed with vegetative debris, including coalified compressions of non-embryophytes (see arrow).

e: Poorly preserved fragments of non-embryophytes, possibly *Nematothallus* cuticle (see arrows).

f: Coalified compression of non-embryophyte, with striation running parallel to the fragment long axis (see arrow). Possible fragment of *Prototaxites* sp./ *Nemataskетum*.

g: Cross section of poorly preserved *Pachytheca* sphere. Internal portions replaced by limonite. Coalified outer portions covered with iron-oxide coating.

h: Coalified compression of small, fertile dichotomously branched axis, possibly *Cooksonia hemisphaerica*.

Plate 7.3: Taphofacies 5 and 6.

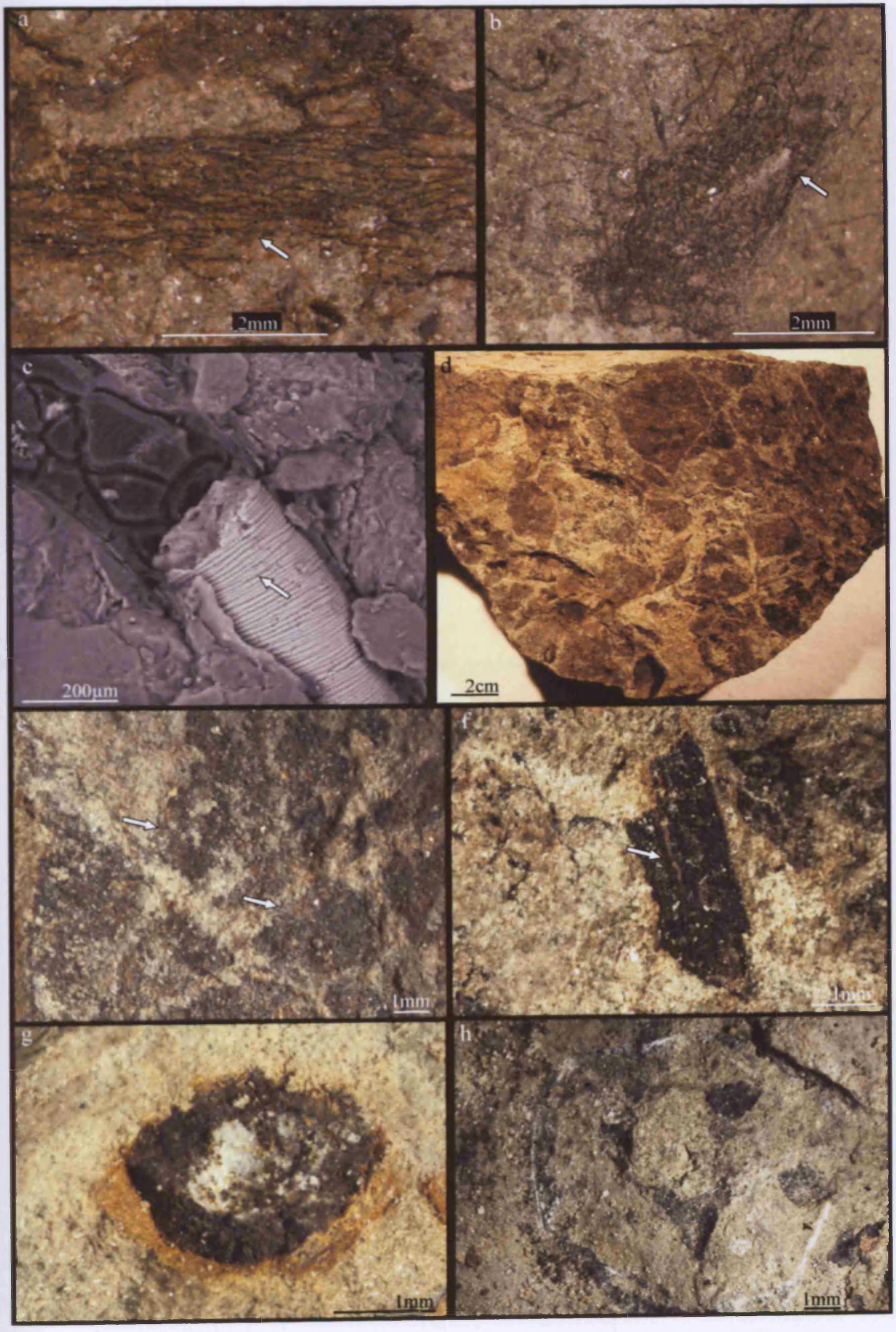

Plate 7.4: Taphofacies 7, 8 and 9

Taphofacies 7

a: Horizontally-laminated, yellow-brown siltstones at Targrove Quarry.

b: Coalified compression of sterile, dichotomously branched, naked axis (see arrow); early embryophyte.

c: Coalified compression of *Salopella allenii* sporangium, an early embryophyte.

d: Poorly preserved coalified compression of thalloid non-embryophyte, possibly *Nematothallus* cuticle.

Taphofacies 8

e: Coalified compression of thalloid non-embryophyte, possibly *Nematothallus* cuticle.

Taphofacies 9

f: Equivocal bifurcating, axial-like features that occur on the bedding planes of wavy or horizontally laminated red siltstone. In places, preserved in three dimensions, with a striated appearance (see arrow). Possibly *Prototaxites* sp. / *Nematasketum*.

g: Equivocal bifurcating, axial-like features that occur on the bedding planes of wavy or horizontally laminated red siltstone. Possibly *Prototaxites* sp. / *Nematasketum*.

Plate 7.4: Taphofacies 7, 8 and 9.

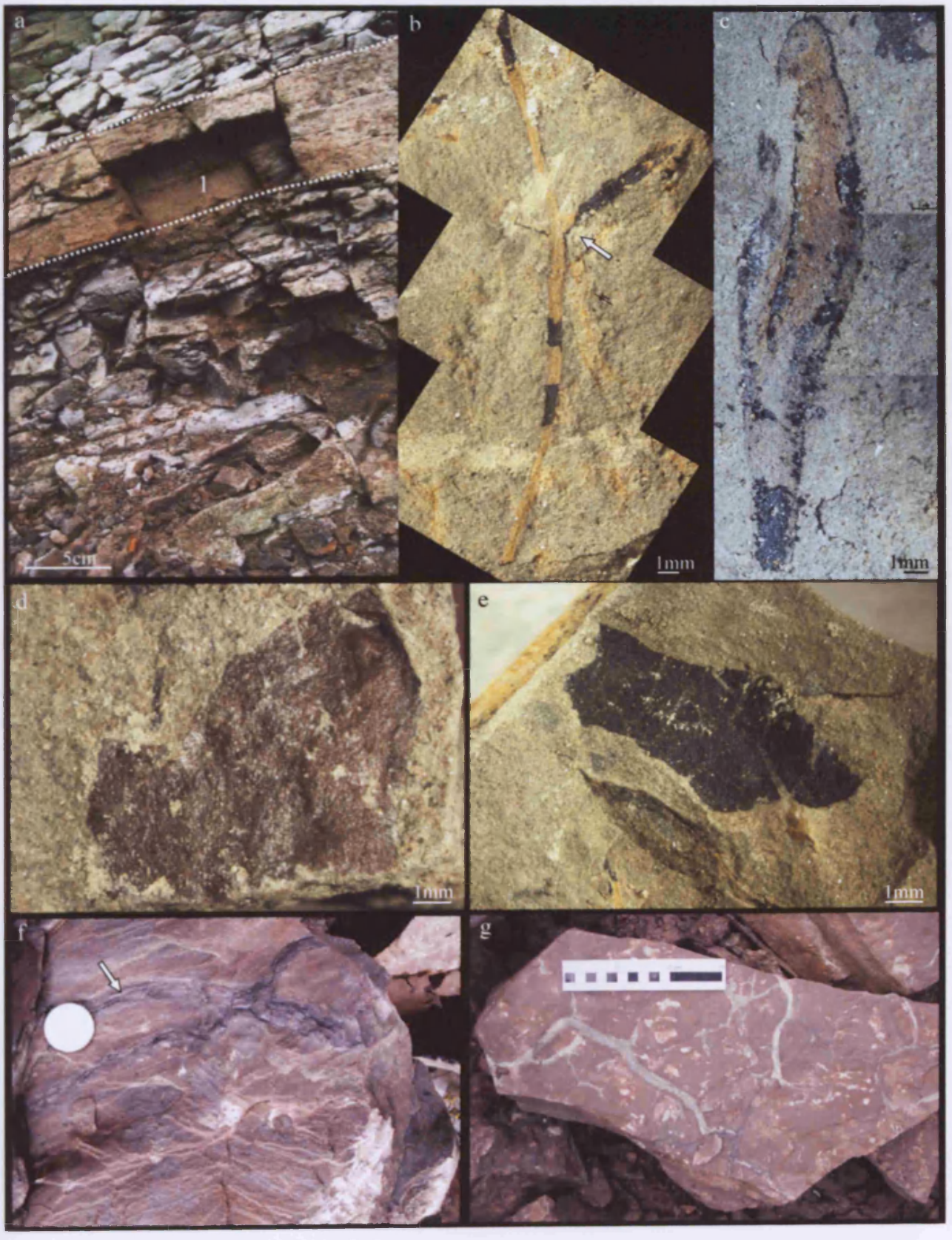

Plate 8.1: Carbonate nodules from Tredomen Quarry, selected for isotopic analysis

***a* to *d*: Nodule 1**

a: Nodule 1, within a stage I to II palaeo-Vertisol, from at a depth of 2.4m from the top of borehole 2 (approximately 17.4m from the quarry surface). Semi-spherical to slightly elongate, medium-sized nodule. The nodule has a sharp boundary and surrounded by radial cracks (see arrow).

b: Thin section of nodule 1. Groundmass is composed of microcrystalline calcite, being a light pink colour where stained. Small patches of segregated iron are distributed throughout the nodule (see arrow).

c: Thin section of nodule 1. Crack within carbonate nodule infilled with sparry calcite up to 0.5mm in diameter.

d: Thin section of nodule 1. Crack within carbonate nodule infilled with sparry calcite and lined with iron (see arrow).

***e* and *f*: Nodule 4**

e: Nodule 4, within a stage I to II palaeo-Vertisol, from at a depth of 18.95m from the top of borehole 2 (approximately 33.05m from the quarry surface). Elongate or cylindrical, medium-sized nodule. This nodule is actually composed of several coalesced nodules (see arrows) in a matrix of larger-sized calcite crystals.

f: Thin section of nodule 4. Groundmass of microcrystalline calcite, stained light pink to slightly purple, suggesting that the presence of some ferroan calcite. Patches of iron segregation (see arrow).

***g* and *h*: Nodule 8**

g: Nodule 8, within a stage II palaeo-Vertisol from at a depth of 40.10m from the top of borehole 2 (approximately 55.1m from the quarry surface). Large-sized spherical nodule, with the appearance of several smaller coalesced nodules (see arrows), separated by larger calcite grains.

h: Thin section of nodule 8. Groundmass is composed of microcrystalline calcite, staining light pink in colour. Iron segregation occurs throughout the nodule.

Plate 8.1: Carbonate nodules from Tredomen Quarry, selected for isotopic analysis

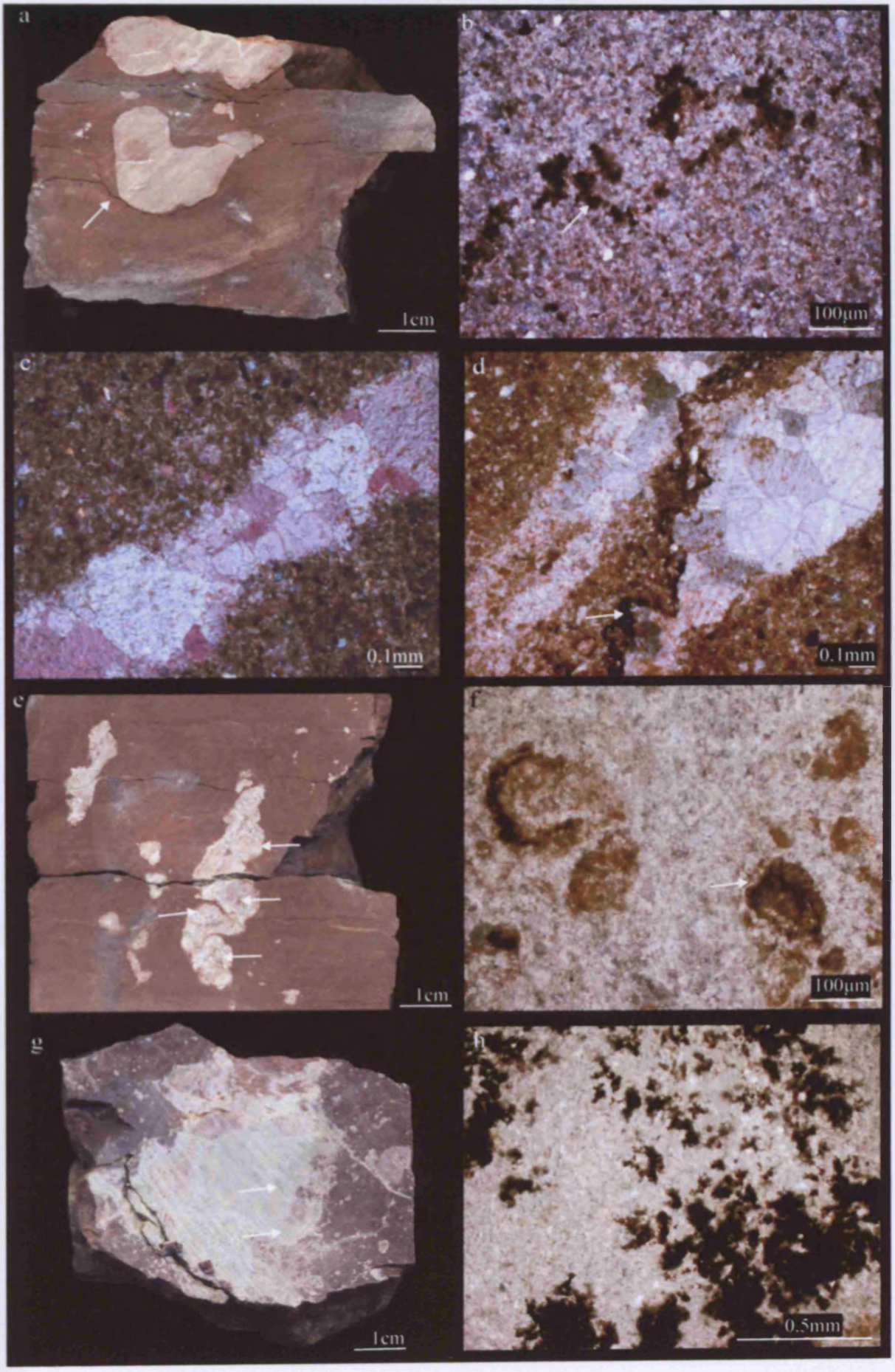

Plate 8.2: Carbonate nodules from Tredomen Quarry, selected for isotopic analysis (continued)

a: Nodule 8

a: Thin section of nodule 8. Iron segregation at the centre of a small nodule (see arrow), coalesced with other small nodule to form nodule 8.

***b* to *d*: Nodule 9**

b: Nodule 9, within a stage II to III palaeo-Vertisol, from a depth of 48.40m from the top of borehole 2 (approximately 63.4m from the quarry surface). C-horizon consists almost completely coalesced spherical carbonate nodules (see arrow), with some displaced angular-edged mudstone fragments (see arrow).

c: Thin section of nodule 9. Each small nodule is composed of microcrystalline calcite, stained a light pink colour. Calcite grains increase in size slightly from the centre of the nodule, up to a maximum of 0.05mm in diameter towards the edge of the nodule. Iron segregation is also present, particularly in the nodule centre.

d: Thin section of nodule 9. Angular-edged displaced mudstones are surrounded by radially arranged sparry calcite (see arrow), which also occurs between coalesced nodules.

***e* to *h*: Nodule 12**

e: Nodule 12, within a stage I to II non-Vertic palaeosol, from a depth of 58.70m from the top of borehole 2 (approximately 73.7m from the quarry surface). Large spherical nodule, composed of smaller coalesced spherical nodules, with a sharp boundary, surrounded by radial cracks (see arrow).

f: Thin section of nodule 12. Individual nodules are composed of microcrystalline calcite, stained light pink, with some degree of iron segregation (see arrow). Secondary sparry calcite can be found between some coalesced nodules (see arrow).

g: Thin section of nodule 12. Individual nodule composed of microcrystalline calcite, with iron segregation in the nodule centre (see arrow).

h: Thin section of nodule 12. Individual nodule surrounded by a thin layer of secondary sparry calcite (see arrow) where coalesced to another nodule.

APPENDIX I : TREDOMEN PALAEOBOTANY COLLECTION DATABASE

a: *Mega- and mesofossil collection*.....on DVD

b: *Palynological collection*.....on DVD

APPENDIX II: MEGAFOSSIL MEASUREMENTS

pII-1 to pII-10

APPENDIX II: MEGAFOSSIL MEASUREMENTS

A CF. COOKSONIA CALEDONICA/ RENALIA SP.

	Box / Sample ID	Sporangium max height mm	Sporangium max width mm	Length-width ratio	Sporangial area (mm2)	Axis length mm	Axis width mm	Width of subtending axis mm	Max width to junction width ratio	Length of axis taper mm	Distance between sporangia mm	Axes angle	Axes thickness before branching mm	Axes thickness after branching mm	Identification
1	JM004	1.6	2.2	0.72	3.52	13	0.2	0.8	2.75	0.20	/	70	/	/	C. cf.caledonica
2	JM008a	1.9	2.9	0.65	5.51	11	0.8	1	2.90	0.30	4	70	0.8	0.8	C. cf.caledonica
	JM008a c.p.	1.8	2.6	0.69	4.68			1.1	2.36	0.50					C. cf.caledonica
3	JM010a	1.9	2.4	0.79	4.56	3	0.7	1	2.40	0.60	/	/	/	/	C. cf.caledonica
4	JM010c	1.2	1.7	0.7	2.04	0.5	0.5	0.5	3.40	0.40	/	/	/	/	C. cf.caledonica
5	JM011a	1.9	2.4	0.79	4.56	20	0.8	1	2.40	0.40	0.7	75	0.8	0.8	C. cf.caledonica
	JM011a c.p	1.7	2.5	0.68	4.25	20	0.8	1	2.50	0.50	0.5	60	0.8	1	C. cf.caledonica
6	JM012b	2.2	2.4	0.91	5.28	2.4	0.5	0.8	3.00	0.40	/	/	/	/	C. cf.caledonica
7	JM020a	1.2	1.7	0.7	2.04	/	/	/			/	/	/	/	C. cf.caledonica
8	JM034c	1.9	2.9	0.65	5.51	10.25	0.46	0.88	3.30	0.30		20.56	0.77	0.46	C. cf.caledonica
9	JM034d	1.5	2.8	0.53	4.2			1.54	1.82						C. cf.caledonica
10	JM035a	1.3	1.8	0.72	2.34	/	/	/			/	/	/	/	C. cf.caledonica
11	JM052	1.4	1.8	0.77	2.52	0.95	0.39	0.78	2.31	0.10	/	/	/	/	C. cf.caledonica
12	JM053a	0.8	1.4	0.57	1.12	/	/	/		0.50	/	/	/	/	C. cf.caledonica
13	JM109	1.6	2.4	0.66	3.84	1.33	0.5	0.97	2.47	0.60	/	/	/	/	C. cf.caledonica
14	JM118	2.4	2.8	0.85	6.72	21	0.97	1.4	2.00	0.30		/	/	/	C. cf.caledonica
15	JM221 + c.p.	0.9	1.6	0.56	1.44	0.8	0.6	1	1.60	0.50	/	/	/	/	C. cf.caledonica
16	JM222 + c.p.	1.5	1.9	0.78	2.85	/	/	/			/	/	/	/	C. cf.caledonica
17	JM232 + c.p.	1.5	2.2	0.68	3.3	1.2	0.4	0.6	3.67	0.30	/	/	/	/	C. cf.caledonica
18	JM234c	1.4	2.4	0.58	3.36	2	0.8	1.5	1.60	0.60	/	/	/	/	C. cf.caledonica
19	JM234d	1.7	2.4	0.7	4.08					0.30	/	/	/	/	C. cf.caledonica
20	JM260 + c.p.	1.9	2.4	0.79	4.56	12	0.8	1	2.40	0.10	/	/	/	/	C. cf.caledonica
21	JM279	1.2	2	0.6	2.4	15	1	0.8	2.50	0.30	/	90	1.2	0.8	C. cf.caledonica
22	JM368	1.5	1.9	0.78	2.85	11.5	0.7	1	1.90	0.80	6	30	0.6	0.5	C. cf.caledonica
	JM368 c.p.	1.3	1.8	0.72	2.34					0.80					C. cf.caledonica
23	JM375	1.4	2.1	0.66	2.94	1.6	0.3	0.82	2.56	1.00	/	/	/	/	C. cf.caledonica
24	JM385	1.5	2.5	0.6	3.75	9.8	0.5	1	2.50	0.80	/	/	/	/	C. cf.caledonica
25	RHSp145_2	1.2	1.22	0.98	1.46	1.74	0.23	0.64	1.91	0.40	/	/	/	/	C. cf.caledonica
26	RH0157	1.53	2.31	/	3.5343	/	/	/	/	/	/	/	/	/	C. cf.caledonica
27	RH_1	1.55	1.97	/	3.0535	/	/	/	/	/	/	/	/	/	C. cf.caledonica
28	RHJM04	2.25	2.87	0.78397	6.4575	3.8	0.68	1.32	2.17	/	/	/	/	/	C. cf.caledonica

Min	0.80	1.22	0.53	1.12	0.50	0.20	0.50	1.60	0.10	0.50	20.56	0.60	0.46	
Max	2.40	2.90	0.98	6.72	21.00	1.00	1.54	3.67	1.00	6.00	90.00	1.20	1.00	
Averages	1.57	2.20	0.71	3.58	7.76	0.60	0.98	2.45	0.46	2.80	59.37	0.83	0.73	

B COOKSONIA HEMISPHAERICA

	Box / Sample ID	Sporangium max height mm	Sporangium max width mm	Length-width ratio	Sporangial area (mm2)	Axis length mm	Axis width mm	Width of subtending axis mm	Max width to junction width ratio	Length of axis taper mm	Distance between sporangia mm	Axes angle	Axes thickness before branching mm	Axes thickness after branching mm	Identification
1	JM001	1.2	1.1	1.09	1.32	3.4	0.6	0.9	1.22	1.20	/	100	0.6	0.3	*C.hemisphaerica*
2	JM002	2	2.2	0.9	4.4	1.8	0.6	1.4	1.57	1.80	/	/	/	/	*C.hemisphaerica*
3	JM003a	1.8	1.7	1.06	3.06	2.2	0.3	1.6	1.21	0.90	/	/	/	/	*C.hemisphaerica*
4	JM005a	1.4	1.4	1	1.96	2.5	0.3	1	1.40	1.50	/	45	0.3	0.15	*C.hemisphaerica*
5	JM010 b	1	0.8	1.25	0.8	2	0.6	0.4	2.00	0.70	/	45	0.6	0.2	*C.hemisphaerica*
6	JM012a	2.1	2.1	1	4.41	5.4	1	0.8	2.63	1.80	3	60	1	0.5	*C.hemisphaerica*
	JM012a c.p.	2.2	2.1	1.1	4.62	/	/	/	/	1.90	/	/	/		*C.hemisphaerica*
7	JM012b	2	2.1	0.95	4.2	2.8	0.4	1	2.10	1.60	2	60	0.4	0.2	*C.hemisphaerica*
	JM012b c.p.	2	2.1	0.95	4.2			1	2.10	1.80					*C.hemisphaerica*
8	JM014a	2.2	2	1.1	4.4	9	1	1.5	1.33	2.40	8	65	1	0.6	*C.hemisphaerica*
9	JM015	2.3	2.2	1.05	5.06	2.4	0.3	1.2	1.83	1.50	/	/	/	/	*C.hemisphaerica*
10	JM022a	1.5	1.6	0.93	2.4	0.4	0.4	1.4	1.14	0.80	/	/	/	/	*C.hemisphaerica*
11	JM025	1.8	2	0.9	3.6	2.2	0.6	1.5	1.33	1.20	/	/	/	/	*C.hemisphaerica*
12	JM032	1.9	1.5	1.26	2.85	0.9	0.5	0.55	2.73	1.00	/	/	/	/	*C.hemisphaerica*
13	JM048	2	1.8	1.1	3.6	2.1	0.2	1.4	1.29	0.60	/	/	/	/	*C.hemisphaerica*
14	JM058	2	1.8	1.1	3.6	0.4	0.4	0.4	4.50	0.40	/	/	/		*C.hemisphaerica*
15	JM060a	1.7	1.9	0.89	3.23	1.5	0.5	1.2	1.58	1.50	/	/	/	/	*C.hemisphaerica*
16	JM060b	1.6	1.6	1	2.56	3.6	0.5	1	1.60	1.00	/	45	0.5	0.5	*C.hemisphaerica*
17	JM065	2.8	2.8	1	7.84	4.2	0.7	0.8	3.50	1.20	/	80	0.7	0.4	*C.hemisphaerica*
18	JM068	2.2	2.1	1.04	4.62	2.1	0.8	1	2.10	1.20	/	/	/	/	*C.hemisphaerica*
19	JM077	1.5	1.2	1.25	1.8	16	1.4	1.1	1.09	2.00	/	100	1.4	0.5	*C.hemisphaerica*
20	JM078	1.6	1.5	1.06	2.4	0.8	1	1	1.50	0.20	/	/	/	/	*C.hemisphaerica*
21	JM081b	1.7	1.2	1.42	2.04	4.8	0.8	1	1.20	1.20	/	93	0.8	0.2	*C.hemisphaerica*
22	JM081c	1.8	1.7	1.05	3.06	2.8	0.3	1.3	1.31	1.20	/	/	/	/	*C.hemisphaerica*
23	JM093b	1	1	1	1	6.6	0.6	0.8	1.25	0.70	/	100	0.6	0.5	*C.hemisphaerica*
24	JM097a	1.3	1.5	0.86	1.95	0.6	0.8	1	1.50	0.60	/	/	/	/	*C.hemisphaerica*
25	JM097b	1.8	1.5	1.2	2.7	2	0.6	1	1.50	0.80	/	/	/	/	*C.hemisphaerica*
26	JM097c	2	1.8	1.1	3.6	/	/	/	/	/	/	/	/	/	*C.hemisphaerica*
27	JM098a	1.4	1.6	0.875	2.24	2.6	0.3	1.2	1.33	0.90	/	/	/	/	*C.hemisphaerica*
28	JM103	1.9	1.7	1.11	3.23	2.8	0.15	0.9	1.89	1.60	/	/	/	/	*C.hemisphaerica*
29	JM104	1.6	1.7	0.94	2.72	2.9	0.4	1	1.70	0.40	/	/	/	/	*C.hemisphaerica*
30	JM112	1.7	1.6	1.06	2.72	1	0.4	0.7	2.29	1.00	/	/	/	/	*C.hemisphaerica*
31	JM115	1.5	1.5	1	2.25	2	0.5	0.8	1.88	1.60	/	/	/	/	*C.hemisphaerica*
32	JM119	1.1	1.4	0.78	1.54	2.2	0.5	1	1.40	1.40	/	/	/	/	*C.hemisphaerica*
33	JM121a	1.5	1.3	1.15	1.95	6.8	0.8	1	1.30	0.90	3	100	0.8	0.2	*C.hemisphaerica*
	JM121a c.p.	1.6	1.4	1.14	2.24			0.8	1.75	0.90		/			*C.hemisphaerica*
34	JM121b	2.4	2.2	1.09	5.28	1	0.4	0.8	2.75	1.00	/	/	/	/	*C.hemisphaerica*

73	JM386a	2.4	2.2	1.09	3.28	2.2	0.8	1.2	1.83	1.00	/	/	/	/	*C.hemisphaerica*
74	JM386b	2	1.8	1.1	3.6	3	0.6	1.2	1.50	0.90					*C.hemisphaerica*
75	JM387b	2.3	2.4	0.95	5.52	3.5	0.6	1.2	2.00	1.80	/	/	/	/	*C.hemisphaerica*
76	JM388a	2	1.6	1.25	3.2	2	0.6	0.6	2.67	0.70	/	/	/	/	*C.hemisphaerica*
77	JM388b	2.1	1.8	1.16	3.78			0.6	3.00	1.20					*C.hemisphaerica*
78	JM393	1.3	1.5	0.86	1.95	0.6	0.6	0.8	1.88	0.80	/	/	/	/	*C.hemisphaerica*
79	JM396	2.2	1.8	1.22	3.96	3	0.8	1	1.80	0.80	/	/	/	/	*C.hemisphaerica*
80	RH008_1	1.15	1.10	1.05	1.27	1.72	0.13	0.81	1.36	1.50	/	89	0.27	0.13	*C.hemisphaerica*
81	RH118	1.06	1.00	1.06	1.06	2.73	0.61	0.57	1.75	0.40	/	51	0.61	0.47	*C.hemisphaerica*
82	RH109	2.36	2.26	1.04	5.33	2.63	0.88	1.56	1.45	0.40	/	/	/	/	*C.hemisphaerica*
83	RH117_1	1.51	1.52	0.99	2.30	1.53	0.53	1.19	1.28	1.53	/	/	/	/	*C.hemisphaerica*
84	RH117_2	0.89	0.96	0.93	0.85	2.63	0.51	0.81	1.19	0.20	/	/	/	/	*C.hemisphaerica*
85	RH001_1	2.03	1.99	1.02	4.04	0.60	0.73	1	1.99	0.60	/	/	/	/	*C.hemisphaerica*
86	RH001_2	1.75	1.69	1.02	2.92	/	0.54	1.03	1.64	/	/	/	/	/	*C.hemisphaerica*
87	RH015	1.74	1.87	0.93	3.25	4.41	0.57	1.21	1.55	1.40	/	/	/	/	*C.hemisphaerica*
88	RH020_2	1.49	1.48	1.01	2.21	3.53	0.41	0.94	1.57	3.53	/	/	/	/	*C.hemisphaerica*
89	RH153	1.80	1.51	1.19	2.72	12.72	0.57	1.05	1.44	2.20	/	/	/	/	*C.hemisphaerica*
90	RH150_1	1.53	1.63	0.94	2.49	2.77	0.34	1.11	1.47	2.77	/	/	/	/	*C.hemisphaerica*
91	RH150_2	2.34	1.92	1.22	4.49	12.26	0.47	1.2	1.60	0.60	/	73	0.88	0.47	*C.hemisphaerica*
92	RH025_1	1.65	1.49	1.11	2.46	0.88	0.75	1.02	1.46	0.30	/	/	/	/	*C.hemisphaerica*
93	RH025_2	1.18	1.17	1.01	1.38	4.01	0.45	0.83	1.41	0.00	/	/	/	/	*C.hemisphaerica*
94	RH033_1	1.72	1.94	0.89	3.34	1.14	0.43	1.03	1.88	1.14	/	/	/	/	*C.hemisphaerica*
95	RH0108_1	2.42	1.99	1.22	4.82	0.97	0.97	1.03	1.93	0.97	/	/	/	/	*C.hemisphaerica*
96	RH151_3	2.23	1.73	1.29	3.86	2.01	0.34	1.04	1.66	1.20	/	/	/	/	*C.hemisphaerica*
97	RH151_4	1.52	1.43	1.06	2.17	2.88	0.47	1.06	1.35	1.80	/	/	/	/	*C.hemisphaerica*
98	RH074_1	1.39	1.56	0.89	2.17	2.22	0.44	1.29	1.21	1.60	/	/	/	/	*C.hemisphaerica*
99	RH(01)_1	1.64	1.68	0.98	2.76	1.99	0.42	0.91	1.85	1.99	/	/	/	/	*C.hemisphaerica*
100	RH028_1	1.66	1.79	0.93	2.97	1.22	0.76	1.14	1.57	1.20	/	/	/	/	*C.hemisphaerica*
101	RH028_2	2.51	2.01	1.25	5.05	5.24	0.52	1.54	1.31	1.00	/	/	/	/	*C.hemisphaerica*
102	RH031_1	2.18	2.20	0.99	4.80	7.02	0.61	1.32	1.67	1.20	/	/	/	/	*C.hemisphaerica*
103	RH136_1	2.28	1.74	1.31	3.97	/	0.73	1.12	1.55	0.40	/	/	/	/	*C.hemisphaerica*
104	RH166_1	2.49	1.80	1.38	4.48	/	/	0.78	2.31	/	/	/	/	/	*C.hemisphaerica*
105	RH160_1	1.59	1.48	1.07	2.35	/	/	/			/	/	/	/	*C.hemisphaerica*
106	RH(02)_1	2.52	2.13	1.18	5.37	4.84	0.36	1.35	1.58	1.20	/	/	/	/	*C.hemisphaerica*

107	RH216_1	2.72	2.37	1.15	6.45	2.84	0.64	1.42	1.67	1.40	/	/	/	/	*C.hemisphaerica*
108	RH200_1	1.80	1.51	1.19	2.72	1.34	0.34	0.85	1.78	1.00	/	/	/	/	*C.hemisphaerica*
109	RH200_2	1.95	2.19	0.89	4.27	2.15	0.43	1.25	1.75	1.00	/	/	/	/	*C.hemisphaerica*
110	RH2_2	1.97	2.09	0.94	4.12	2.99	0.33	1.33	1.57	2.99	/	/	/	/	*C.hemisphaerica*
111	RH2_3_2	1.73	1.67	1.04	2.89	4	0.43	1.28	1.30	0.80	/	/	/	/	*C.hemisphaerica*
112	RH2_5	1.82	1.64	1.11	2.98	3.06	0.28	1.02	1.61	0.80	/	/	/	/	*C.hemisphaerica*
113	RHSp102a	2.70	2.30	1.17	6.21	1	0.5	0.7	3.29	1.00	/	/	/	/	*C.hemisphaerica*
114	RHSp99_2	1.10	1.10	1.00	1.21	0.8	0.4	0.8	1.38	0.80	/	/	/	/	*C.hemisphaerica*
115	RHSp116	1.50	1.20	1.25	1.80	3.4	0.6	0.8	1.50	0.80	/	30	0.6	0.4	*C.hemisphaerica*
116	RH0097b	1.48	1.67	0.89	2.47	4.67	0.53	1.43	1.17	/	3	85	0.72	0.53	*C.hemisphaerica*
117	RH0158	1.81	1.87	0.96791	3.3847	1.94	0.4	1.37	1.36	/	/	/	/	/	*C.hemisphaerica*
118	RH0054	1.25	1.49	0.83893	1.8625	3.57	0.33	1.26	1.18	/	/	/	/	/	*C.hemisphaerica*
119	RH0044	1.63	1.64	0.9939	2.6732	4.6	0.7	1.43	1.15	/	/	/	/	/	*C.hemisphaerica*
120	RH049	1.81	1.51	1.19868	2.7331	4.53	0.98	1.18	1.28	/	/	/	/	/	*C.hemisphaerica*
121	RHJM01	1.56	1.15	1.35652	1.794	8.38	0.3	0.9	1.28	/	6.61	66	0.76	0.3	*C.hemisphaerica*
122	RHJM02	1.8	1.85	0.97297	3.33	12	0.5	1.19	1.55	/	15	63	0.8	0.5	*C.hemisphaerica*
123	RHJM03	1.89	1.72	1.09884	3.2508	1.34	0.47	1.13	1.52	/	/	/	/	/	*C.hemisphaerica*

MIN	0.89	0.70	0.75	0.70	0.40	0.13	0.40	1.04	0.00	2.00	30.00	0.27	0.13
MAX	2.80	3.10	1.50	7.84	16.00	1.40	2.50	4.50	3.53	15.00	100.00	1.40	0.60
AVERAGE	1.85	1.78	1.05	3.46	2.96	0.57	1.08	1.76	1.17	5.80	70.50	0.69	0.37

D CF. USKIELLA RETICULATA/ TARRANTIA SALOPENSIS

	Box / Sample ID	Sporangium max height mm	Sporangium max width mm	Length-width ratio	Sporangial area mm2	Axis length mm	Axis width mm	Width of subtending axis mm	Max width to junction width ratio	Length of axis taper mm	Distance between sporangia mm	Axes angle	Axes thickness before branching	Axes thickness after branching	Identification
1	JM006a	2.2	1.8	1.2	3.96	2	0.6	1	1.80		/	/	/	/	cf. *U. reticulata*
2	JM013a	2.2	2.2	1	4.84	7	0.4	1			/	/	/	/	cf. *U. reticulata*
3	JM013b	2.4	2.7	0.88	6.48	1.2	0.6	0.6			/	/	/	/	cf. *U. reticulata*
4	JM013c	2.4	2.2	1.09	5.28	2	0.2	0.2			/				cf. *U. reticulata*
5	JM013d	2.8	2.6	1.07	7.28	9.5	0.8	0.6			/	45	0.8	0.6	cf. *U. reticulata*
6	JM047	2.3	1.65	1.39	3.795	2.2	0.6	1.5	1.10		/	/	/		cf. *U. reticulata*
7	JM092	2	1	2	2	1.4	0.3	0.45	2.22		/	/	/	/	cf. *U. reticulata*
8	JM111	2.3	1.6	1.25	3.68	5.9	0.47	0.79	2.03		/	/	/	/	cf. *U. reticulata*
9	JM113a	2	1.4	1.42	2.8	1.8	0.6	0.6	2.33		/	/	/	/	cf. *U. reticulata*
10	JM143	2.5	1.3	1.92	3.25	2.5	0.6	0.6	2.17		/	/	/	/	cf. *U. reticulata*
11	JM144	3	2	1.5	6	0.6	0.6	0.6	3.33		/	/	/	/	cf. *U. reticulata*
12	JM279a	2.4	1.5	1.6	3.6	2.5	0.2	0.5	3.00		1	60	0.2	0.2	cf. *U. reticulata*
	JM279a ii	2.2	1.4	1.57	3.08	2.5	0.2	0.5							cf. *U. reticulata*
13	JM328	3	2.2	1.36	6.6	/	/	/	/		/	/	/	/	cf. *U. reticulata*
14	JM353	1.9	1.4	1.3	2.66	2.8	0.4	0.6	2.33		/	/	/	/	cf. *U. reticulata*
15	JM354	1.9	1.3	1.46	2.47	0.5	0.4	0.6	2.17		/	/	/	/	cf. *U. reticulata*
16	JM369	3	1.5	2	4.5	1	0.2	0.2	7.50		/	/	/	/	cf. *U. reticulata*
17	JM390	2.8	1	2.8	2.80	1.4	0.3	0.5	2.00		/	/	/	/	cf. *U. reticulata*
18	RH008-2	2.85	2.44	1.17	6.95	0.82	0.6	1.03	2.37		/	/	/	/	cf. *U. reticulata*
19	RH079	1.8	1.28	1.41	2.30	3.34	0.33	0.4	3.20		/	/	/	/	cf. *U. reticulata*
20	RH019	1.13	1.08	1.05	1.22	1.51	0.59	0.9	1.20		/	/	/	/	cf. *U. reticulata*
21	RH154	2.87	2	1.44	5.74	1.99	0.55	0.91	2.20		/	/	/	/	cf. *U. reticulata*
22	RH125_2	2.2	1.29	1.71	2.84	/	/	/	/		/	/	/	/	cf. *U. reticulata*
23	RH125_3	1.4	1.09	1.28	1.53	1.57	0.44	0.7	1.56		/	/	/	/	cf. *U. reticulata*
24	RH198_1	2.35	1.81	1.31	4.31	2.17	1.3	1.3	1.39		/	/	/	/	cf. *U. reticulata*
25	RH187_1	1.97	1.52	1.30	2.99	9.23	0.42	0.82	1.85		/	/	/	/	cf. *U. reticulata*
26	RH266_1	2.59	2.08	1.25	5.39	2.1	0.63	1.04	2.00		/	/	/	/	cf. *U. reticulata*
27	RH291_1	1.69	1.33	1.27	2.25	2.11	0.79	0.97	1.37		/	/	/	/	cf. *U. reticulata*
28	RH2_3_1	1.63	1.35	1.21	2.20	2.57	0.61	1.07	1.26		/	/	/	/	cf. *U. reticulata*
29	RH2_6	2.43	1.74	1.40	4.23	/	/	/	/		/	/	/	/	cf. *U. reticulata*
30	RH2_7	2.51	2.63	0.95	6.60	10.09	1.04	1.23	2.14		/	/	/	/	cf. *U. reticulata*
31	RHSp110	3.6	2.6	1.38	9.36	4.75	1	1.2	2.17		/	80	1	0.9	cf. *U. reticulata*

	1.13	1.00	0.88	1.22	0.50	0.20	0.20	1.10		1.00	45.00	0.20	0.20	
MAX	3.60	2.70	2.80	9.36	10.09	1.30	1.50	7.50		1.00	80.00	1.00	0.90	
AVERAGE	2.32	1.72	1.40	4.16	3.07	0.54	0.77	2.28		1.00	61.67	0.67	0.57	

E SALOPELLA ALLENII

	Box / Sample ID	Sporangium max height mm	Sporangium max width mm	Length-width ratio	Sporangial area mm2	Axis length mm	Axis width mm	Width of subtending axis mm	Max width to junction width ratio	Length of axis taper mm	Distance between sporangia mm	Axes angle	Axes thickness before branching	Axes thickness after branching	Identification
1	JM005a	10.5	3.1	3.38	32.55	1	1.6	1.5	2.07		/	/	/	/	*Salopella allenii*
	JM005b	10.5	3.1	3.38	32.55	1	2	1.2	2.58		/	/	/	/	*Salopella allenii*
2	JM006a	11	2.8	3.92	30.8	2.3	1.4	0.8	3.50		/	/	/	/	*Salopella allenii*
	JM006b	10.6	2.5	4.24	26.5	2.7	1.6	0.8	3.13		/	/	/	/	*Salopella allenii*
3	JM007	10	2.4	4.2	24	30	1.3	0.8	3.00		/	/	/	/	*Salopella allenii*
	JM007b	9.6	2.4	4	23.04	30	1.1								*Salopella allenii*
4	JM009	9.9	2.4	4.125	23.76	9.2	0.9	1.1	2.18		/	/	/	/	*Salopella allenii*
5	JM081 + c.p.	7.4	2.2	3.36	16.28	11.7	1.5	1.5	1.47		/	/	/	/	*Salopella allenii*
6	JM377	8.4	2.3	3.6	19.32	/	/	/			/	/	/	/	*Salopella allenii*
7	JM289b	5.9	1.3	4.5	7.67	17.7	1.8	1	1.30		/	15	1.4	1	*Salopella allenii*
8	JM060c	4	1	4	4	3	0.5	0.3	3.33		1	15	0.5	0.2	*Salopella allenii*
9	RHSp127	10.22	2.49	4.1	25.4478	20.5	1.57	1.23	2.02		/	/	/	/	*Salopella allenii*
10	RHSp151_1	11.19	3.14	3.56	35.1366	/	/	/	/		/	/	/	/	*Salopella allenii*
11	RHSp034_1	8.42	2.01	4.18	16.9242	30	1.64	0.82	2.45		/	/	/	/	*Salopella allenii*
12	RHSp141_1	8.3	2.64	3.14	21.912	48	1.79	1.79	1.47486034		1	10	1.75	1.25	*Salopella allenii*
	RHSp141_1	10.3	3	3.43	30.9	/	/	/	/		/	/	/	/	*Salopella allenii*
13	RHSp181_1	9.85	2.36	4.17	23.246	30	2	2	1.18		/	/	/	/	*Salopella allenii*
14	RHSp99	9.81	2.41	4.07	23.6421	30	1.59	1.39	1.73381295		/	/	/	/	*Salopella allenii*
15	RHSp125b	9.69	3.04	3.1875	29.4576	/	/	/	/		/	/	/	/	*Salopella allenii*
16	RHJM07	8.93	2.5	3.572	22.325	4	1.4	1.59	/		/	/	/	/	*Salopella allenii*

MIN	4.00	1.00	3.14	4.00	1.00	0.50	0.30	1.18		1.00	10.00	0.50	0.20	
MAX	11.19	3.14	4.50	35.14	48.00	2.00	2.00	3.50		1.00	15.00	1.75	1.25	
AVERAGE	9.23	2.45	3.81	23.47	16.94	1.48	1.19	2.24		1.00	13.33	1.22	0.82	

17	JM106	3.72	1.38	2.6	5.1336	0.75	0.56	0.56			/	/	/	/	*Salopella allenii*
18	JM069	8.1	3	2.7	24.3	45.3	2.7	2			/	39	2.7	2	*Salopella allenii*

F SALOPELLA CF. MARCENSIS

	Box / Sample ID	Sporangium max height mm	Sporangium max width mm	Length-width ratio	Sporangial area mm2	Axis length mm	Axis width mm	Width of subtending axis mm	Max width to junction width ratio	Length of axis taper mm	Distance between sporangia mm	Axes angle	Axes thickness before branching	Axes thickness after branching	Identification
1	JM021	3.38	1.50	2.25	5.06	6.95	0.63	0.63	2.40		3.75	85.00	0.63	0.50	*S* cf *marcensis*
	JM021b	2.75	1.00	2.75	2.75										*S* cf *marcensis*
2	JM266 + c.p.	1.60	0.50	3.20	0.80	2.30	0.20	0.20	2.50		/	35.00	0.20	0.20	*S* cf *marcensis*
3	JM346a	1.70	0.60	2.80	1.02	/	/	/			/	/	/	/	*S* cf *marcensis*
4	JM346b	2.60	0.65	4.00	1.69	2.80	0.15	0.15	4.33		/	/	/	/	*S* cf *marcensis*
5	JM394	2.50	0.80	3.13	2.00	19.80	0.60	0.30	2.67		6.50	90.00	0.80	0.60	*S* cf *marcensis*
	JM394 b	3.10	0.80	3.88	2.48										*S* cf *marcensis*
6	RHSp120	2.36	0.92	2.56	2.17	1.19	0.24	0.23	4.00						*S* cf *marcensis*
7	RHSp302_1	2.21	0.71	3.11	1.57	9.61	0.55	0.20	3.55			90.00	0.70	0.50	*S* cf *marcensis*
8	RH040	2.52	1.44	1.75	3.63	2.68	0.51	1.03	1.40		/	/	/	/	*S* cf *marcensis*

MIN	1.60	0.50	1.75	0.80	1.19	0.15	0.15	1.40		3.75	35.00	0.20	0.20	
MAX	3.38	1.50	4.00	5.06	19.80	0.63	1.03	4.33		6.50	90.00	0.80	0.60	
Averages	2.47	0.89	2.94	2.32	6.48	0.41	0.39	2.98		5.13	75.00	0.58	0.45	

G ELONGATE CLUB-SHAPED SPORANGIA

	Box / Sample ID	Sporangium max height mm	Sporangium max width mm	Length-width ratio	Sporangial area mm2	Axis length mm	Axis width mm	Width of subtending axis mm	Max width to junction width ratio	Length of axis taper mm	Distance between sporangia mm	Axes angle	Axes thickness before branching	Axes thickness after branching	Identification
1	JM016	5.20	1.70	8.84	3.05	3.00	0.50	0.50	3.40		/	50.00	1.20	0.50	Elongate club
2	JM262a	4	1.3	5.20	3.07	/	/	/	/		/	/	/	/	Elongate club
	JM262b	5.00	1.20	6.00	4.10	/	/	/	/		/	/	/	/	Elongate club
3	JM287	4.30	1.50	6.45	2.86	8.50	0.80	0.80	1.88		/	90.00	0.80	0.80	Elongate club
4	JM371	5.60	2.30	12.88	2.40	/	/	/	/		/	/	/	/	Elongate club
5	RH117_4	2.16	1.42	3.07	1.52	/	/	/			/	/	/	/	Elongate club
6	RH020_1	1.52	1.43	2.17	1.06	4.79	0.4	1.36			/	/	/	/	Elongate club
7	RH034_1	2.06	1.73	3.56	1.19	/	/	/			/	/	/	/	Elongate club
8	RH2_1_1	2.42	1.76	4.26	1.38	0.9	/	1.24			/	/	/	/	Elongate club
9	RHSp102b	2	1.5	3.00	1.33	5.2	0.6	1			/	/	/	/	Elongate club
10	RHSp156	4	2.5	10.00	1.60	/	/	/			/	/	/	/	Elongate club
11	RHPB	3.65	1.75	6.39	2.09	4.77	0.56	0.74				73.00	0.56	0.37	Elongate club

MIN	1.52	1.20	2.17	1.06	0.90	0.40	0.50	1.88		0.00	50.00	0.80	0.50	
MAX	5.60	2.50	12.88	4.10	8.50	0.80	1.36	3.40		0.00	90.00	1.20	0.80	
AVERAGE	3.49	1.67	5.99	2.14	4.53	0.57	0.94	2.64		0.00	70.00	1.00	0.65	

APPENDIX III : MESOFOSSIL MEASUREMENTS

pIII-1 to pIII-11

APPENDIX III: MESOFOSSIL MEASUREMENTS

MESOFOSSILS : TYPE A

	Box / Sample ID	Sporangium max height mm	Sporangium max width mm	Length-width ratio	Sporangial area (mm2)	Axis length mm	Axis width mm	Width of subtending axis mm	Max width to junction width ratio	Distance between sporangia	Axes angle	Axes thickness before branching mm	Axes thickness after branching mm	Identification
1	JM010e	0.4	0.3	1.33	0.12	0.7	0.1	0.1	3.00	0	0	0.1	0.1	mesofossil type A
	JM10eii	0.4	0.3	1.33	0.12			0.1	3.00					mesofossil type A
2	JM079a	0.6	0.5	1.20	0.3	0.8	0.1	0.2	2.50	/	/	/	/	mesofossil type A
	JM079aii	0.6	0.5	1.20	0.3			0.2	2.50					mesofossil type A
3	JM086c	0.2	0.15	1.30	0.03	0.6	0.15	0.15	1.00	0.05	10	0.15	0.15	mesofossil type A
	JM086cii	0.2	0.2	1.00	0.04			0.15	1.33					mesofossil type A
4	JM095c	0.4	0.3	1.30	0.12	0.2	0.1	0.1	3.00	0.05	10	0.1	0.1	mesofossil type A
	JM095cii	0.3	0.3	1.00	0.09			0.1	3.00					mesofossil type A
5	JM095d	0.4	0.3	1.14	0.12	0.7	0.1	0.1	3.00	0.1	30	0.1	0.1	mesofossil type A
	JM095dii	0.5	0.4	1.25	0.2			0.1	4.00					mesofossil type A
6	JM123a	0.3	0.2	1.50	0.06	4.5	0.1	/		/	/	/	/	mesofossil type A
	JM123aii	0.4	0.25	1.60	0.1			/						mesofossil type A
7	JM123b	0.4	0.3	1.33	0.12	1.5	0.11	0.15	2.00	0.5	45	0.1	0.1	mesofossil type A
	JM123bii	0.3	0.2	1.50	0.06			0.15	1.33					mesofossil type A
8	JM125b	0.55	0.6	0.91	0.33	1.2	0.2	0.2	3.00	/	/	/	/	mesofossil type A
9	JM153a	0.65	0.45	1.44	0.2925	/	/	/		/	/	/	/	mesofossil type A
	JM153aii	0.65	0.45	1.44	0.2925			/						mesofossil type A
10	JM153b	0.35	0.3	1.16	0.105	1	0.1	0.1	3.00	/	/	/	/	mesofossil type A
	JM153bii	0.35	0.3	1.16	0.105			0.1	3.00					mesofossil type A
11	JM153c	0.3	0.4	0.75	0.12	0.3	0.1	0.1	4.00	/	/	/	/	mesofossil type A
12	JM162a	0.35	0.3	1.16	0.105	0.65	0.15	0.1	3.00	0.15	40	0.15	0.1	mesofossil type A
13	JM162b	0.45	0.3	1.50	0.135	0.8	0.1	0.1	3.00	0.5	50	0.1	0.1	mesofossil type A
14	JM164a	0.3	0.3	1.00	0.09	0.6	0.1	0.1	3.00	0	0	/	/	mesofossil type A
	JM164aii	0.35	0.25	1.40	0.0875			0.1	2.50					mesofossil type A
15	JM175	0.75	0.5	1.50	0.375	0.7	0.15	0.15	3.33	0	30	/	/	mesofossil type A
	JM175ii	0.55	0.5	1.10	0.275			0.15	3.33					mesofossil type A
16	JM180b	0.33	0.25	1.32	0.0825	0.5	0.15	0.07	3.57	/	50	/	/	mesofossil type A
17	JM185	0.5	0.33	1.51	0.165	0.35	0.1	0.1	3.30	0	~10	/	/	mesofossil type A
	JM185ii	0.25	0.3	0.83	0.075			0.1	3.00					mesofossil type A
18	JM186	0.4	0.2	2.00	0.08	1.4	0.15	0.15	1.33	/	42	/	/	mesofossil type A
19	JM187a	0.23	0.2	1.15	0.046	1.4	0.1	0.07	2.86	/	70	/	/	mesofossil type A
20	JM188a	0.28	0.3	0.93	0.084	1.3	0.1	0.1	3.00	0.15	35	/	/	mesofossil type A

	JM188aii	0.3	0.3	1.00	0.09			0.1	3.00					mesofossil type A
21	JM190b	0.3	0.19	1.57	0.057	0.7	0.1	0.07	2.71	0	35	0.1	0.07	mesofossil type A
	JM190bii	0.3	0.2	1.50	0.06			0.07	2.86					mesofossil type A
22	JM191a	0.25	0.2	1.25	0.05	0.6	0.1	0.1	2.00	/	/	/	/	mesofossil type A
23	JM191b	0.4	0.2	2.00	0.08	0.15	0.15	0.07	2.86	/	35	0.15	0.07	mesofossil type A
24	JM194a	0.35	0.25	1.40	0.0875	.	0.2	0.1	2.50	1.5	70	0.2	0.1	mesofossil type A
	JM194aii	0.35	0.25	1.40	0.0875			0.1	2.50					mesofossil type A
	JM194aiii	0.2	0.15	1.33	0.03			0.1	1.50					mesofossil type A
25	JM194d	0.4	0.4	1.00	0.16	0.7	0.15	0.15	2.67	0.2	65	0.15	0.15	mesofossil type A
26	JM197b	0.9	0.5	1.80	0.45	1.8	0.15	0.1	5.00	1.5	105	0.2	0.1	mesofossil type A
	JM197bii	0.8	0.6	1.33	0.48			0.1	6.00					mesofossil type A
27	JM202a	0.2	0.15	1.33	0.03	0.35	0.1	0.05	3.00	0.1	30	0.1	0.05	mesofossil type A
	JM202aii	0.2	0.15	1.33	0.03			0.05	3.00					mesofossil type A
	JM202aiii	0.2	0.13	1.54	0.026			0.05	2.60					mesofossil type A
28	JM202b	0.8	0.5	1.60	0.4	2.7	0.25	0.15	3.33	0.1	65, 60	0.25	0.15	mesofossil type A
	JM202bii	0.5	0.4	1.25	0.2			0.15	2.67					mesofossil type A
29	JM202e	0.18	0.12	1.50	0.0216	0.2	0.08	0.05	2.40	/	60	0.08	0.05	mesofossil type A
30	JM204b	0.3	0.15	2.00	0.045	0.35	0.1	0.07	2.14	0	40	0.1	0.07	mesofossil type A
	JM204bii	0.3	0.15	2.00	0.045			0.07	2.14					mesofossil type A
31	JM211a	0.2	0.15	1.33	0.03	0.45	0.1	0.1	1.50	0.1	20	0.1	0.1	mesofossil type A
	JM211aii	0.2	0.15	1.33	0.03			0.1	1.50					mesofossil type A
	JM211aiii	0.2	0.15	1.33	0.03			0.1	1.50					mesofossil type A
32	JM323a	0.6	0.4	1.50	0.24	4.8	0.1	0.1	4.00	0.1	40	0.1	0.1	mesofossil type A
	JM323aii	0.65	0.45	1.44	0.2925			0.1	4.50					mesofossil type A
	JM323aiii	0.45	0.3	1.50	0.135			0.1	3.00					mesofossil type A
33	JM323b	0.2	0.15	1.33	0.03			0.1	1.50					mesofossil type A
	JM323bii	0.2	0.15	1.33	0.03			0.1	1.50					mesofossil type A
	JM323biii	0.3	0.2	1.50	0.06			0.1	2.00					mesofossil type A
34	JM363a	0.4	0.3	1.30	0.12	2.4	0.1	0.1	3.00	0	65, 58	0.1	0.1	mesofossil type A
	JM363aii	0.3	0.3	1.00	0.09			0.1	3.00					mesofossil type A
35	JM363b	0.3	0.2	1.50	0.06	0.5	0.15	0.1	2.00	0	30	0.15	0.1	mesofossil type A
	JM363bii	0.25	0.2	1.25	0.05			0.1	2.00					mesofossil type A
36	JM365a	0.2	0.2	1.00	0.04	3.8	0.15	0.1	2.00	0	15	0.15	0.1	mesofossil type A

MESOFOSSILS : TYPE B

	Box / Sample ID	Sporangium max height mm	Sporangium max width mm	Length-width ratio	Sporangial area (mm2)	Axis length mm	Axis width mm	Width of subtending axis mm	Max width to junction width ratio	Distance between sporangia	Axes angle	Axes thickness before branching mm	Axes thickness after branching mm	Identification
1	JM074a	0.4	0.2	2.00	0.08	2	0.1	0.15	1.33	0.5	40	/	/	mesofossil type B
	JM074aii	0.5	0.2	2.50	0.1			0.15	1.33					mesofossil type B
2	JM086d	0.5	0.4	1.25	0.2	4.5	0.15	0.15	2.67	/	40	/	/	mesofossil type B
	JM086dii	0.5	0.35	1.43	0.175			0.15	2.33					mesofossil type B
3	JM124a	0.55	0.4	1.38	0.22	0.3	0.05	0.05	8.00	/	/	/	/	mesofossil type B
4	JM157b	0.5	0.3	1.67	0.15	0.7	0.1	0.1	3.00	/	/	/	/	mesofossil type B
5	JM164b	0.45	0.32	1.41	0.144	2.7	0.25	0.1	3.20	/	/	0.25	0.15	mesofossil type B
6	JM164c	0.33	0.19	1.74	0.0627	2	0.1	0.07	2.71	0.6	45	0.1	0.1	mesofossil type B
	JM164cii	0.3	0.2	1.50	0.06			0.07	2.86					mesofossil type B
7	JM164d	0.7	0.55	1.27	0.385	0.25	0.1	0.1	5.50	/	/	/	/	mesofossil type B
8	JM174	0.55	0.33	1.67	0.1815	2.9	0.2	0.05	6.60	/	70	0.2	0.1	mesofossil type B
9	JM178a	0.35	0.2	1.75	0.07	2	0.1	0.07	2.86	/	45	0.1	0.07	mesofossil type B
10	JM180a	0.6	0.3	2.00	0.18	2.2	0.1	0.1	3.00	/	40	/	/	mesofossil type B
11	JM184	0.5	0.4	1.25	0.2	0.5	0.05	0.05	8.00	/	/	/	/	mesofossil type B
12	JM187b	0.4	0.25	1.60	0.1	3	0.2	0.1	2.50	/	50	0.2	0.1	mesofossil type B
13	JM189	0.45	0.35	1.29	0.1575	2	0.2	0.1	3.50	0.1	35	/	/	mesofossil type B
	JM189ii	0.48	0.4	1.20	0.192			0.1	4.00					mesofossil type B
14	JM190c	0.4	0.2	2.00	0.08	1	0.1	0.1	2.00	/	85	0.1	0.1	mesofossil type B
15	JM194b	0.55	0.3	1.83	0.165	3	0.1	0.1	3.00	/	/	/	/	mesofossil type B
16	JM195a	0.5	0.4	1.25	0.2	0.6	0.1	0.1	4.00	/	/	/	/	mesofossil type B
17	JM195b	0.45	0.45	1.00	0.2025	0.5	0.1	0.15	3.00	/	/	/	/	mesofossil type B
18	JM195c	0.5	0.45	1.11	0.225	0.4	0.1	0.1	4.50	/	/	/	/	mesofossil type B
19	JM197e	0.5	0.35	1.43	0.175	0.3	0.1	0.12	2.92	/	/	/	/	mesofossil type B
20	JM197f	0.6	0.4	1.50	0.24	0.6	0.1	0.1	4.00	/	/	/	/	mesofossil type B
	JM197fii	0.6	0.4	1.50	0.24			0.1	4.00					mesofossil type B
21	JM204a	0.35	0.25	1.40	0.0875	0.4	0.1	0.12	2.08	0.1	/	/	/	mesofossil type B
	JM204aii	0.3	0.3	1.00	0.09			0.12	2.50					mesofossil type B
22	JM205a	0.45	0.5	0.90	0.225	4	0.45	0.3	1.67	1.7	50	0.4	0.25	mesofossil type B
	JM205aii	0.6	0.4	1.50	0.24			0.3	1.33					mesofossil type B

	JM205aiii	0.4	0.3	1.33	0.12			0.3	1.00					mesofossil type B
	JM205aiv	0.4	0.35	1.14	0.14			0.3	1.17					mesofossil type B
23	JM205b	0.5	0.4	1.25	0.2	4.2	0.15	0.15	2.67	0.6	40	0.15	0.1	mesofossil type B
	JM205bii	0.6	0.22	2.73	0.132			0.15	1.47					mesofossil type B
	JM205biii	0.6	0.25	2.40	0.15			0.15	1.67					mesofossil type B
24	JM206a	0.7	0.4	1.75	0.28	2.1	0.15	0.1	4.00	0.1	25	0.1	0.1	mesofossil type B
	JM206aii	0.65	0.35	1.86	0.2275			0.1	3.50					mesofossil type B
25	JM206b	0.3	0.2	1.50	0.06	3.4	0.1	0.1	2.00	0.2	50	0.1	0.1	mesofossil type B
	JM206bii	0.28	0.2	1.40	0.056			0.1	2.00					mesofossil type B
26	JM208	0.5	0.3	1.67	0.15	0.4	0.1	0.1	3.00	/	/	/	/	mesofossil type B
27	JM211b	0.5	0.25	2.00	0.125	2.5	0.2	0.2	1.25	0.2	60	0.2	0.2	mesofossil type B
	JM211bii	0.5	0.25	2.00	0.125			0.2	1.25					mesofossil type B
28	JM213b	0.35	0.2	1.75	0.07	2.3	0.2	0.18	1.11	0.2	50	0.2	0.15	mesofossil type B
	JM213bii	0.35	0.2	1.75	0.07			0.18	1.11					mesofossil type B
29	JM214a	0.68	0.45	1.51	0.306	3.4	0.15	0.25	1.80	1	80	0.1	0.1	mesofossil type B
30	JM214b	0.5	0.35	1.43	0.175	1	0.1	0.12	2.92	0.05	15	0.15	0.1	mesofossil type B
	JM214bii	0.65	0.3	2.17	0.195			0.12	2.50					mesofossil type B
31	JM220a	0.48	0.3	1.60	0.144	0.8	0.2	0.07	4.29	/	32	0.2	0.1	mesofossil type B
32	JM230a	0.6	0.45	1.33	0.27	2.2	0.15	0.1	4.50	0.8	40	0.15	0.1	mesofossil type B
	JM230aii	0.55	0.3	1.83	0.165			0.1	3.00					mesofossil type B
33	JM242a	0.4	0.3	1.33	0.12	1.5	0.2	0.2	1.50	0.2	45	0.2	0.2	mesofossil type B
34	JM251	0.4	0.3	1.33	0.12	1.3	0.1	0.15	2.00	/	/	/	/	mesofossil type B
35	JM268	0.3	0.25	1.20	0.075	1.8	0.1	0.12	2.08	/	55	0.15	0.15	mesofossil type B
36	JM317a	0.5	0.2	2.50	0.1	2	0.15	0.1	2.00	/	75	0.15	0.1	mesofossil type B
37	JM317c	0.45	0.35	1.29	0.1575	0.4	0.1	0.12	2.92	/	/	/	/	mesofossil type B
38	JM317b	0.8	0.3	2.67	0.24	1.8	0.25	0.25	1.20	0.5	70	0.25	0.1	mesofossil type B
	JM317bii	0.7	0.3	2.33	0.21			0.25	1.20					mesofossil type B
39	JM323c	0.4	0.35	1.14	0.14	1.5	0.1	0.15	2.33	0	80	0.15	0.1	mesofossil type B
	JM323cii	0.4	0.25	1.60	0.1			0.15	1.67					mesofossil type B
40	JM336	0.5	0.39	1.28	0.195	3	0.1	0.15	2.60	1.2	40	0.15	0.1	mesofossil type B
	JM336ii	0.48	0.35	1.37	0.168			0.15	2.33					mesofossil type B
41	JM357	0.4	0.25	1.60	0.1	1.3	0.1	0.1	2.50	/	50	0.1	0.1	mesofossil type B
	JM364a	0.7	0.45	1.56	0.315	3	0.15	0.1	4.50	1	95, 55	0.15	0.1	mesofossil type B
42	JM364aii	0.55	0.4	1.38	0.22			0.1	4.00					mesofossil type B
43	JM364b	0.6	0.35	1.71	0.21	1.3	0.2	0.1	3.50	0.6	40	0.2	0.1	mesofossil type B

	JM364bii	0.5	0.3	1.67	0.15			0.1	3.00					mesofossil type B
44	JM365b	0.5	0.35	1.43	0.175	0.8	0.15	0.1	3.50	/	50	0.1	0.1	mesofossil type B
45	RH2_4	0.53	0.36	1.47	0.1908	1.44	0.12	0.121	2.98	/	/	/	/	mesofossil type B
46	RH77a	0.41	0.33	1.24	0.1353	1.37	0.08	0.11	3.00	0.45	70	0.13	0.08	mesofossil type B

MIN	0.28	0.19	0.90	0.06	0.25	0.05	0.05	1.00	0.00	15.00	0.10	0.07
MAX	0.80	0.55	2.73	0.39	4.50	0.45	0.30	8.00	1.70	85.00	0.40	0.25
AVERAGE	0.49	0.32	1.59	0.16	1.75	0.14	0.13	2.84	0.51	50.59	0.16	0.12

MESOFOSSILS : TYPE C

	Box / Sample ID	Sporangium max height mm	Sporangium max width mm	Length-width ratio	Sporangial area (mm2)	Axis length mm	Axis width mm	Width of subtending axis mm	Max width to junction width ratio	Distance between sporangia	Axes angle	Axes thickness before branching mm	Axes thickness after branching mm	Identification
1	JM030a	0.6	0.4	1.50	0.24	1	0.05	0.05	8.00	/	100	0.05	0.05	mesofossil type C
2	JM075a	0.8	0.55	1.45	0.44	1.2	0.2	0.2	2.75	/	/	/	/	mesofossil type C
3	JM085a	0.4	0.3	1.33	0.12	1.33	0.1	0.1	3.00	/	/	/	/	mesofossil type C
4	JM085b	0.25	0.2	1.25	0.05	1.25	0.1	0.1	2.00	/	/	/	/	mesofossil type C
5	JM086a	0.5	0.3	1.67	0.15	0.8	0.1	0.2	1.50	/	50	0.1	0.1	mesofossil type C
6	JM086b	0.5	0.3	1.67	0.15	0.6	0.15	0.15	2.00	/	/	/	/	mesofossil type C
7	JM095a	0.5	0.5	1.00	0.25	0.2	0.3	0.3	1.67	/	/	/	/	mesofossil type C
8	JM098b	0.7	0.5	1.40	0.35	1.6	0.2	0.3	1.67	/	/	/	/	mesofossil type C
9	JM100a	0.7	0.6	1.17	0.42	0.8	0.2	0.2	3.00	/	/	/	/	mesofossil type C
10	JM100b	0.8	0.7	1.14	0.56	0.6	0.15	0.2	3.50	/	/	/	/	mesofossil type C
11	JM114a	1.1	0.8	1.38	0.88	1	0.2	0.3	2.67	/	/	/	/	mesofossil type C
12	JM114d	0.8	0.6	1.33	0.48	1.2	0.2	/		/	/	/	/	mesofossil type C
13	JM124b	0.6	0.4	1.50	0.24	0.4	0.1	0.1	4.00	/	/	/	/	mesofossil type C
14	JM124c	0.4	0.35	1.14	0.14	0.6	0.1	0.1	3.50	/	/	/	/	mesofossil type C
15	JM125a	0.7	0.6	1.17	0.42	1.8	0.1	0.2	3.00	/	/	/	/	mesofossil type C
16	JM125c	0.65	0.45	1.44	0.2925	1.29	0.33	0.33	1.36	/	92	0.33	0.21	mesofossil type C
17	JM125d	0.75	0.65	1.15	0.4875	1.2	0.15	0.15	4.33	/	124	0.15	0.06	mesofossil type C
18	JM152b	0.7	0.6	1.17	0.42	1.5	0.2	0.2	3.00	0.5	60	0.2	0.2	mesofossil type C
	JM152bii	0.7	0.6	1.17	0.42			0.2	3.00					mesofossil type C
19	JM154	0.7	0.65	1.08	0.455	1.7	0.15	0.15	4.33	/	/	/	/	mesofossil type C
20	JM157a	0.6	0.55	1.09	0.33	0.5	0.1	0.1	5.50	/	/	/	/	mesofossil type C
21	JM160 + c.p.	0.55	0.55	1.00	0.3025	2.2	0.1	0.1	5.50	/	/	0.1	0.1	mesofossil type C
22	JM166a	0.47	0.47	1.00	0.2209	0.85	0.1	0.1	4.70	/	/	/	/	mesofossil type C
23	JM178b	0.47	0.4	1.18	0.188	0.6	0.05	0.1	4.00	/	/	/	/	mesofossil type C
	JM178bii	0.3	0.3	1.00	0.09			0.1	3.00					mesofossil type C
24	JM178c	0.45	0.42	1.07	0.189	0.8	0.05	0.1	4.20	/	/	/	/	mesofossil type C
25	JM178d	0.55	0.42	1.31	0.231	0.8	0.05	0.1	4.20	/	/	/	/	mesofossil type C
26	JM178e	0.5	0.45	1.11	0.225	0.4	0.1	0.1	4.50	/	/	/	/	mesofossil type C
27	JM179a	0.65	0.7	0.93	0.455	1.3	0.15	0.15	4.67	/	/	/	/	mesofossil type C
28	JM181	0.45	0.42	1.07	0.189	0.45	0.1	0.1	4.20	/	/	/	/	mesofossil type C
29	JM188b	0.55	0.45	1.22	0.2475	1.8	0.15	0.15	3.00	/	/	/	/	mesofossil type C
30	JM190a	0.4	0.3	1.33	0.12	1.5	0.2	0.1	3.00	0.5	52	0.3	0.1	mesofossil type C

	JM190aii	0.35	0.4	0.88	0.14			0.1	4.00					mesofossil type C
	JM190aiii	0.5	0.25	2.00	0.125			0.1	2.50					mesofossil type C
31	JM197a	0.7	0.45	1.56	0.315	1.5	0.15	0.15	3.00	/	/	/	/	mesofossil type C
32	JM197c	0.9	0.85	1.06	0.765	3.5	0.15	0.3	2.83	1.9	50	0.15	0.1	mesofossil type C
33	JM197d	0.5	0.38	1.32	0.19	1	0.15	0.15	2.53	/	110	0.15	0.15	mesofossil type C
34	JM198a	0.7	0.55	1.27	0.385			0.15	3.67					mesofossil type C
	JM198aii	0.55	0.55	1.00	0.3025	1.3	0.2	0.15	3.67	0.7	60	0.2	0.15	mesofossil type C
35	JM198b	0.5	0.4	1.25	0.2	0.5	0.1	0.12	3.33	0.5	65	0.3	0.1	mesofossil type C
	JM198bii	0.5	0.45	1.11	0.225			0.12	3.75					mesofossil type C
36	JM202c	0.35	0.25	1.40	0.0875	1.8	0.1	0.07	3.57	0.2	55	0.1	0.1	mesofossil type C
	JM202cii	0.4	0.25	1.60	0.1			0.07	3.57					mesofossil type C
37	JM202d	0.37	0.35	1.06	0.1295	0.65	0.1	0.12	2.92	0.2	60	0.1	0.1	mesofossil type C
38	JM209	0.55	0.45	1.22	0.2475	0.65	0.15	0.15	3.00	/	/	/	/	mesofossil type C
39	JM210b	0.85	0.7	1.21	0.595	1.4	0.1	0.1	7.00	/	/	/	/	mesofossil type C
40	JM211c	0.3	0.25	1.20	0.075	0.5	0.05	0.05	5.00	/	/	/	/	mesofossil type C
41	JM212	0.4	0.3	1.33	0.12	0.2	0.1	0.1	3.00	/	/	/	/	mesofossil type C
42	JM213a	0.4	0.3	1.33	0.12	0.4	0.07	0.07	4.29	/	/	/	/	mesofossil type C
43	JM220b	0.5	0.55	0.91	0.275	1.8	0.1	0.12	4.58	/	30	0.1	0.1	mesofossil type C
44	JM230b	0.5	0.4	1.25	0.2	2	0.2	0.1	4.00	/	75	0.2	0.1	mesofossil type C
45	JM289a	0.2	0.2	1.00	0.04	2.3	0.2	0.2	1.00	/	85	0.2	0.2	mesofossil type C
46	JM290a	0.5	0.4	1.25	0.2	0.3	0.05	0.05	8.00	/	/	/	/	mesofossil type C
47	JM304	0.6	0.65	0.92	0.39	4	0.2	0.3	2.17	0.8	60	0.2	0.2	mesofossil type C
	JM304ii	0.55	0.6	0.92	0.33			0.3	2.00					mesofossil type C
48	JM344	0.6	0.4	1.50	0.24	1.7	0.15	0.1	4.00	/	90, 60	0.15	0.1	mesofossil type C
49	JM379b	0.7	0.5	1.40	0.35	1	0.1	0.1	5.00	/	100	0.1	0.1	mesofossil type C
50	JM401a	0.35	0.32	1.09	0.112	1.2	0.1	0.1	3.20	/	55	0.1	0.1	mesofossil type C
51	JM402a	0.6	0.6	1.00	0.36	3	0.4	0.2	3.00	/	60	0.4	0.2	mesofossil type C
52	RHSp036	0.1	0.1	1.00	0.01	0.5	0.08	0.08	1.25	/	80	/	/	mesofossil type C
53	RHSp77c	0.43	0.38	1.13	0.1634	0.37	0.13	0.16	2.38	/	/	/	/	mesofossil type C
54	RHSp87c	0.75	0.6	1.25	0.45	1.1	0.35	0.45	1.33	/	/	/	/	mesofossil type C
55	RH169_2	0.3	0.24	1.25	0.072	0.61	0.08	0.08	3.00	/	/	/	/	mesofossil type C
56	RH029	0.35	0.27	1.30	0.0945	0.38	0.05	0.05	5.40	/	/	/	/	mesofossil type C
57	RH087d	0.51	0.54	0.94	0.2754	2.1	0.2	0.2	2.70	/	87	/	/	mesofossil type C

MIN	0.10	0.10	0.88	0.01	0.20	0.05	0.05	1.00	0.20	30.00	0.05	0.05
MAX	1.10	0.85	2.00	0.88	4.00	0.40	0.45	8.00	1.90	124.00	0.40	0.21
AVERAGE	0.54	0.45	1.22	0.27	1.18	0.14	0.15	3.49	0.66	71.90	0.18	0.12

MESOFOSSILS: TYPE D

	Box / Sample ID	Sporangium max height mm	Sporangium max width mm	Length-width ratio	Sporangial area (mm2)	Axis length mm	Axis width mm	Width of subtending axis mm	Max width to junction width ratio	Distance between sporangia	Axes angle	Axes thickness before branching mm	Axes thickness after branching mm	Identification
1	JM010f	0.20	0.30	0.67	0.06	1.40	0.15	0.15	2.00	0.00	10.00	0.15	0.15	mesofossil type D
	JM010fii	0.15	0.25	0.60	0.04			0.15	1.67					mesofossil type D
2	JM029a	0.20	0.25	0.80	0.05	0.50	0.10	0.10	2.50	/	/	/	/	mesofossil type D
3	JM075b	0.30	0.30	1.00	0.09	0.75	0.10	0.10	3.00	/	/	/	/	mesofossil type D
4	JM083a	0.20	0.20	1.00	0.04	0.30	0.10	0.10	2.00	/				mesofossil type D
5	JM083b	0.25	0.20	1.25	0.05	0.70	0.10	0.10	2.00	/				mesofossil type D
6	JM110a	0.18	0.15	1.20	0.03	1.20	0.13	0.11	1.36	0.05	40.00	0.13	0.11	mesofossil type D
7	JM114c	0.30	0.20	1.50	0.06	3.00	0.10	0.10	2.00	/	/	/	/	mesofossil type D
8	JM157c	0.22	0.20	1.10	0.04	0.70	0.30	0.10	2.00	0.60	90.00	0.30	0.10	mesofossil type D
	JM157cii	0.20	0.20	1.00	0.04			0.10	2.00					mesofossil type D
9	JM187c	0.20	0.15	1.33	0.03	0.62	0.10	0.08	1.88	0.15	25.00	/	/	mesofossil type D
	JM187cii	0.17	0.15	1.13	0.03			0.08	1.88					mesofossil type D
10	JM194c	0.18	0.18	1.00	0.03	0.50	0.07	0.07	2.57	/	/	/	/	mesofossil type D
11	JM339	0.25	0.20	1.25	0.05	0.70	0.10	0.10	2.00	/	/	/	/	mesofossil type D
12	RH128_2	0.25	0.29	0.86	0.07	0.09	0.09	0.10	0.19		33	0.09	0.09	mesofossil type D
	RH128_2	0.23	0.26	0.88	0.06	/		/	/	/	/	/		mesofossil type D
13	RH050_2	0.15	0.18	0.83	0.03	0.07	0.07	0.10	/		83	0.07	0.07	mesofossil type D
14	JM290b	0.4	0.3	1.33	0.12	1.6	0.1	0.1	3.00	1	80	0.1	0.1	mesofossil type D
	JM290bii	0.4	0.3	1.33	0.12			0.1	3.00					mesofossil type D

MIN	0.15	0.15	0.60	0.03	0.07	0.07	0.07	0.19	0.00	10.00	0.07	0.07
MAX	0.40	0.30	1.50	0.12	3.00	0.30	0.15	3.00	1.00	90.00	0.30	0.15
AVERAGE	0.23	0.22	1.06	0.05	0.87	0.12	0.10	2.06	0.36	51.57	0.14	0.10

TORTILICAULIS CF. OFFAEUS

	Box / Sample ID	Sporangium max height mm	Sporangium max width mm	Length-width ratio	Sporangial area (mm2)	Axis length mm	Axis width mm	Width of subtending axis mm	Max width to junction width ratio	Distance between sporangia	Axes angle	Axes thickness before branching mm	Axes thickness after branching mm	Identification
1	JM397a	0.95	0.45	2.10	0.43	2.00	0.20	0.10	4.50	1.50	60.00	0.30	0.15	Tortilicaulis
	JM397aii	0.80	0.40	2.00	0.32	2.00	0.20	0.10	4.00	1.50	60.00	0.30	0.20	Tortilicaulis
2	RHSp012_1	0.83	0.37	2.24	0.31	0.62	0.18	0.18	2.06	/	/	/	/	Tortilicaulis

MIN	0.80	0.37	2.00	0.31	0.62	0.18	0.10	2.06	1.50	60.00	0.30	0.15
MAX	0.95	0.45	2.24	0.43	2.00	0.20	0.18	4.50	1.50	60.00	0.30	0.20
AVERAGE	0.86	0.41	2.11	0.35	1.54	0.19	0.13	3.52	1.50	60.00	0.30	0.18

OTHER ELONGATE SPORANGIA

	Box / Sample ID	Sporangium max height mm	Sporangium max width mm	Length-width ratio	Sporangial area (mm2)	Axis length mm	Axis width mm	Width of subtending axis mm	Max width to junction width ratio	Distance between sporangia	Axes angle	Axes thickness before branching mm	Axes thickness after branching mm	Identification
1	JM037iii	0.94	0.51	1.84	0.48	1.36	0.12	0.12	4.25	/	/	/	/	elongate
2	JM074b	0.9	0.4	2.25	0.36	1	0.1	0.1	4.00	/	/	/	/	elongate
3	JM095b	0.6	0.31	1.94	0.19	0.34	0.1	0.1	3.10	/	/	/	/	elongate
4	JM280a	0.9	0.45	2.00	0.41	0.45	0.1	0.13	3.46	/	/	/	/	elongate
5	RH005_1	0.35	0.21	1.67	0.07	0.86	0.07	0.07	3.00	/	/	/	/	elongate
6	RH2_8	0.46	0.34	1.35	0.16	1.04	0.07	0.12	2.83	/	/	/	/	elongate
7	RHSp53b	0.9	0.4	2.25	0.36	0.5	0.15	0.18	2.22	/	/	/	/	elongate
8	RH248_1	0.69	0.45	1.53	0.31	/	/	/	/	/	/	/	/	elongate

MIN	0.35	0.21	1.35	0.07	0.34	0.07	0.07	2.22	0.00	0.00	0.00	0.00
MAX	0.94	0.51	2.25	0.48	1.36	0.15	0.18	4.25	0.00	0.00	0.00	0.00
AVERAGE	0.72	0.38	1.85	0.29	0.79	0.10	0.12	3.27	/	/	/	/

APPENDIX IV: SHAPES USED IN GEOMETRIC MODELS

pIV-1 to pIV-6

APPENDIX IV: SHAPES USED IN GEOMETRIC MODELS

cf. *Cooksonia caledonica / Renalia* sp.

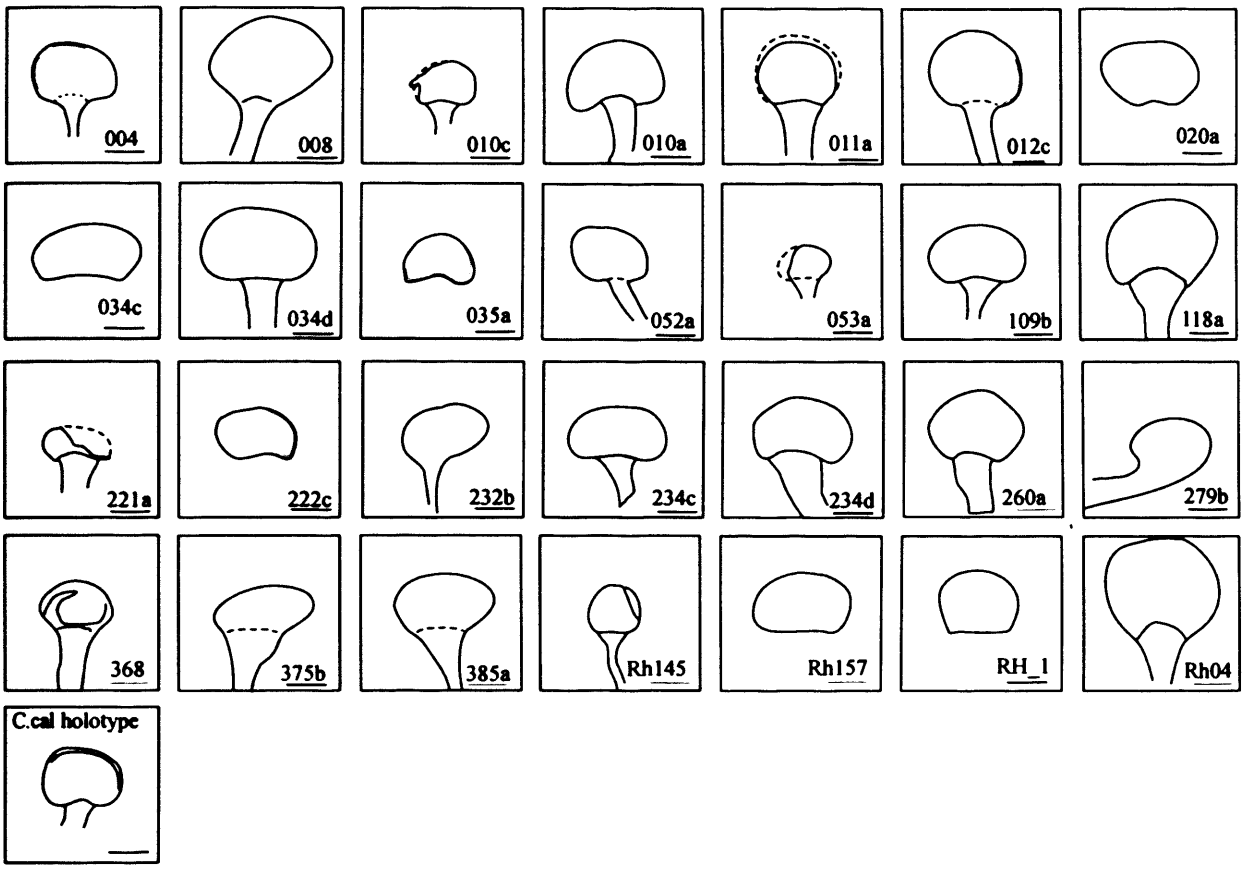

Cooksonia cf. *cambrensis*

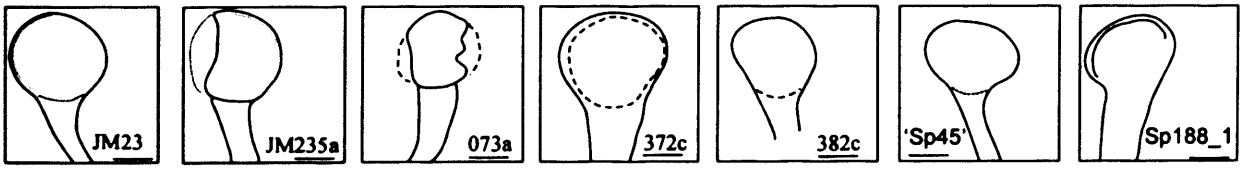

Cooksonia hemisphaerica

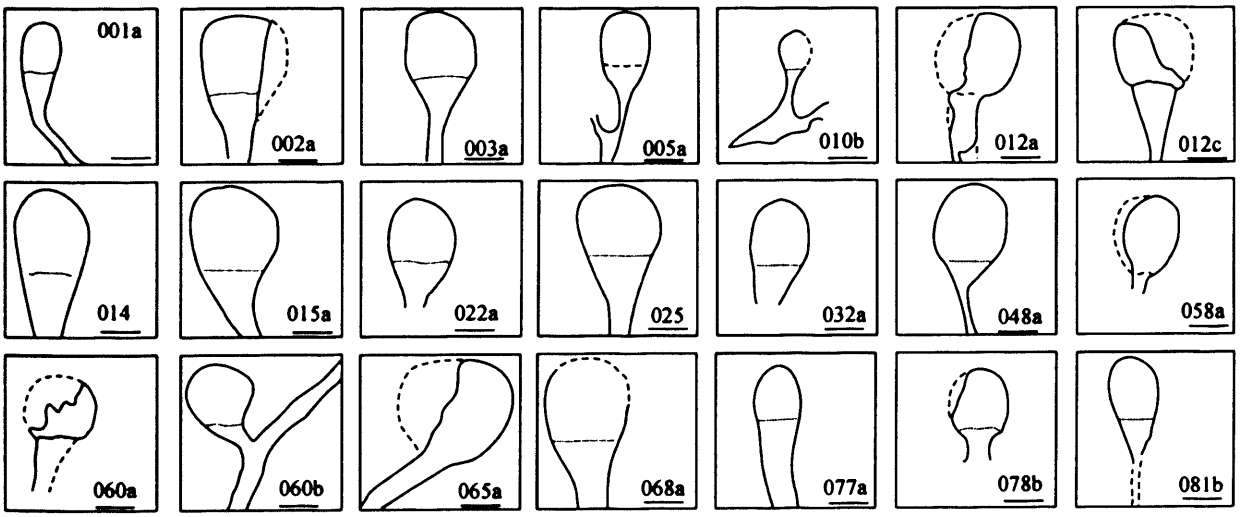

APPENDIX IV: SHAPES USED IN GEOMETRIC MODELS (continued)

Cooksonia hemisphaerica (continued)

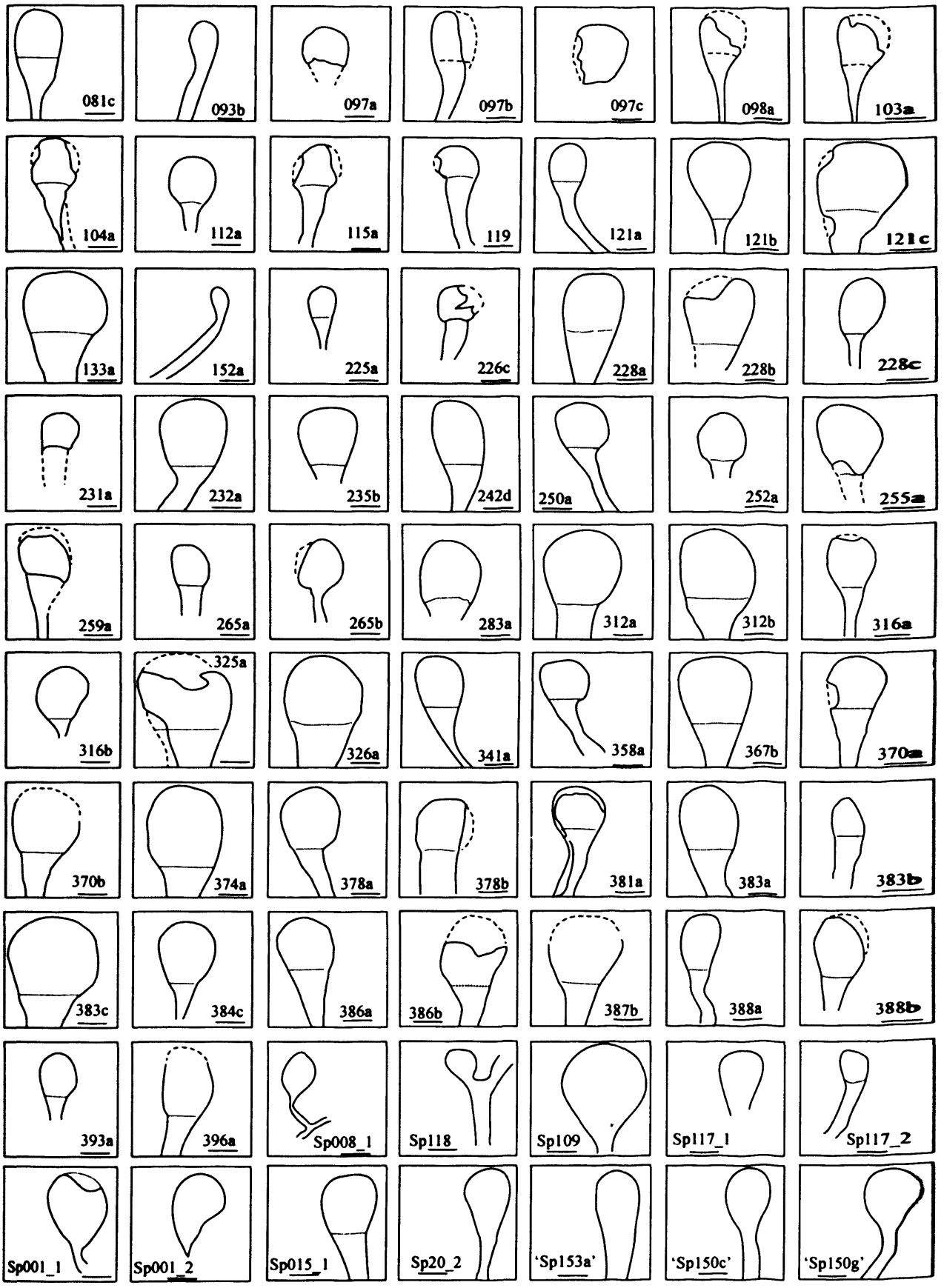

Cooksonia hemisphaerica (continued)

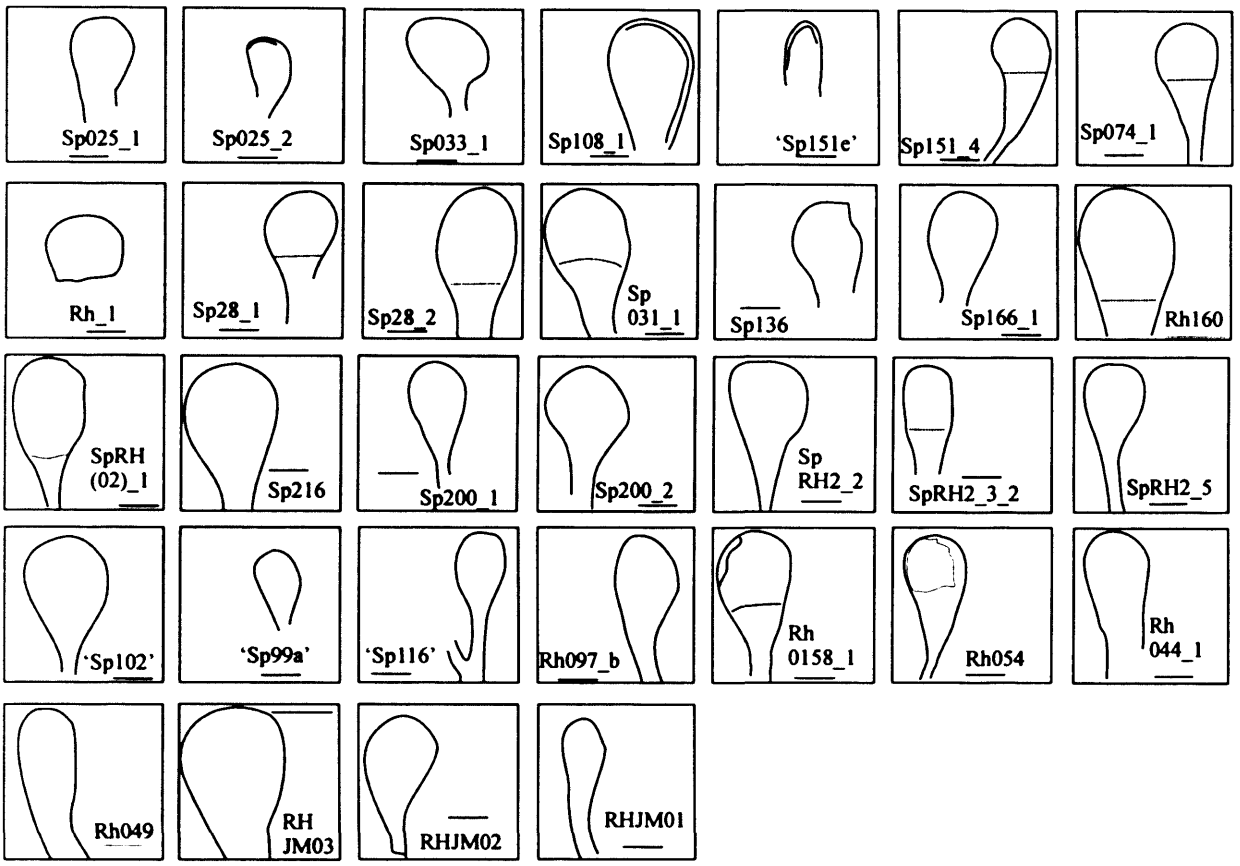

cf. *Uskiella reticulata / Tarrantia salopensis*

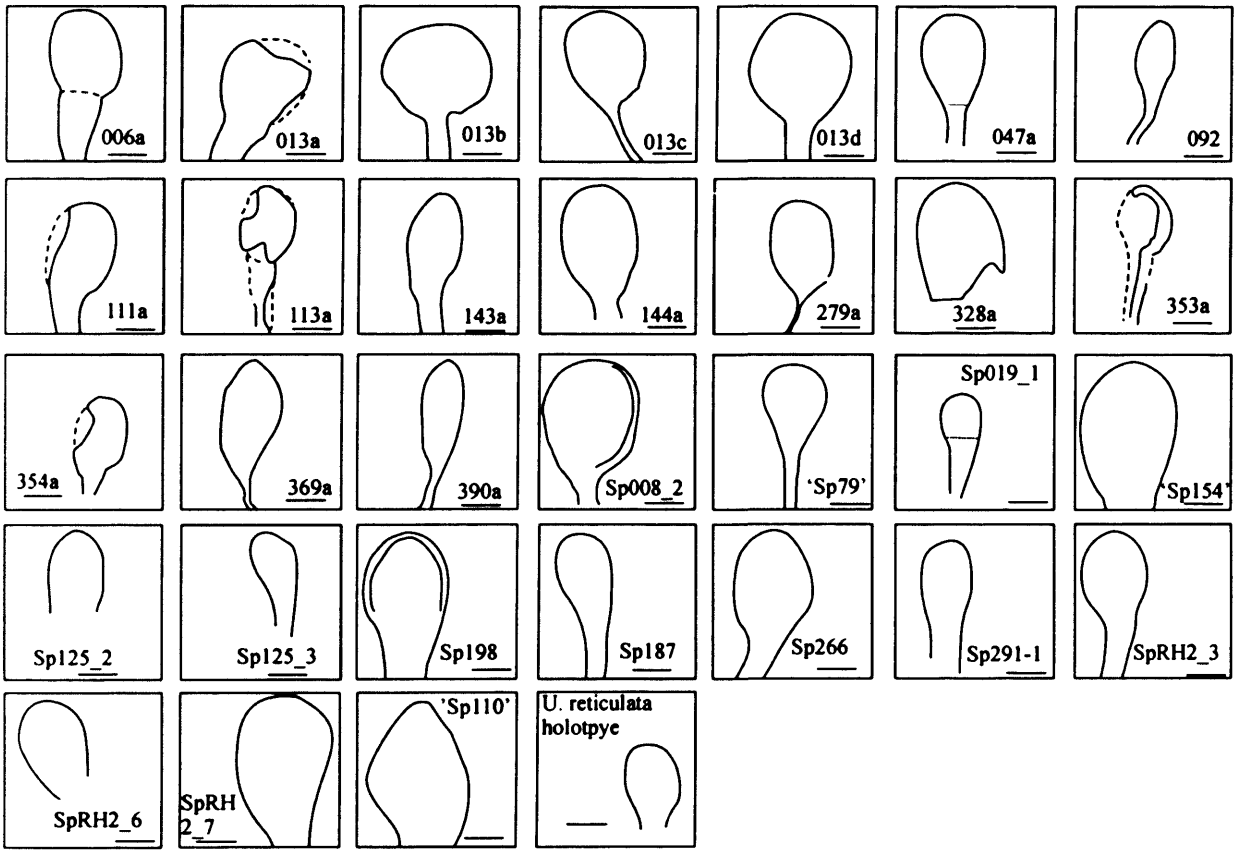

Elongate club-shaped sporangia

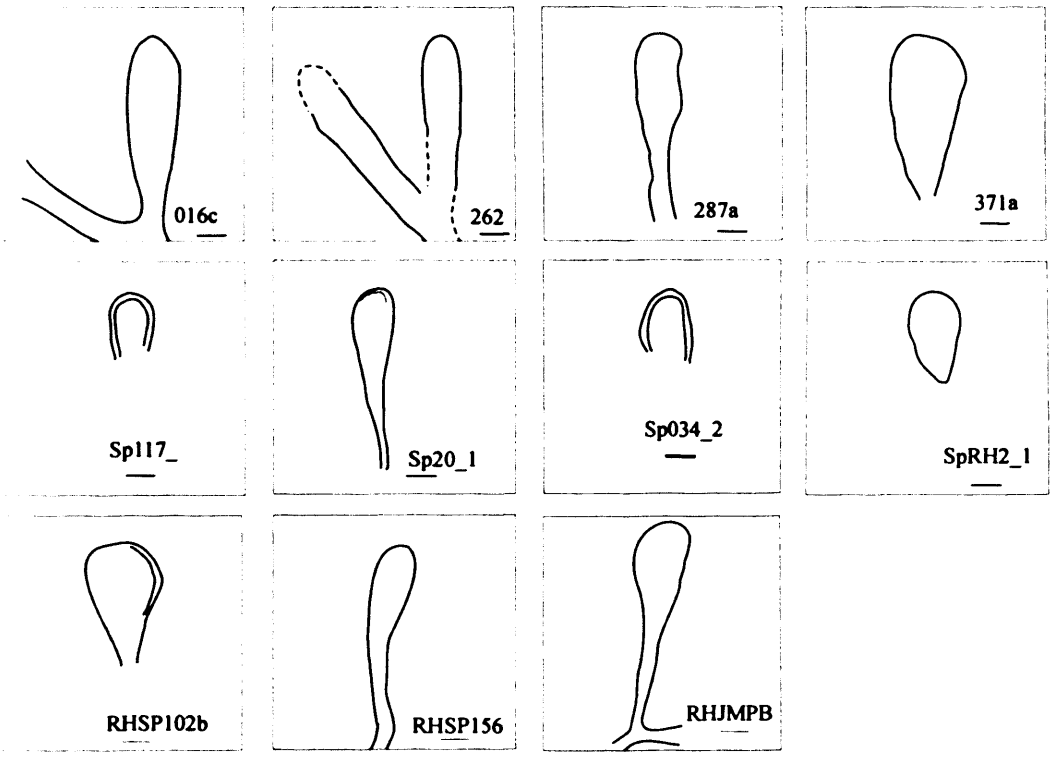

Salopella allenii

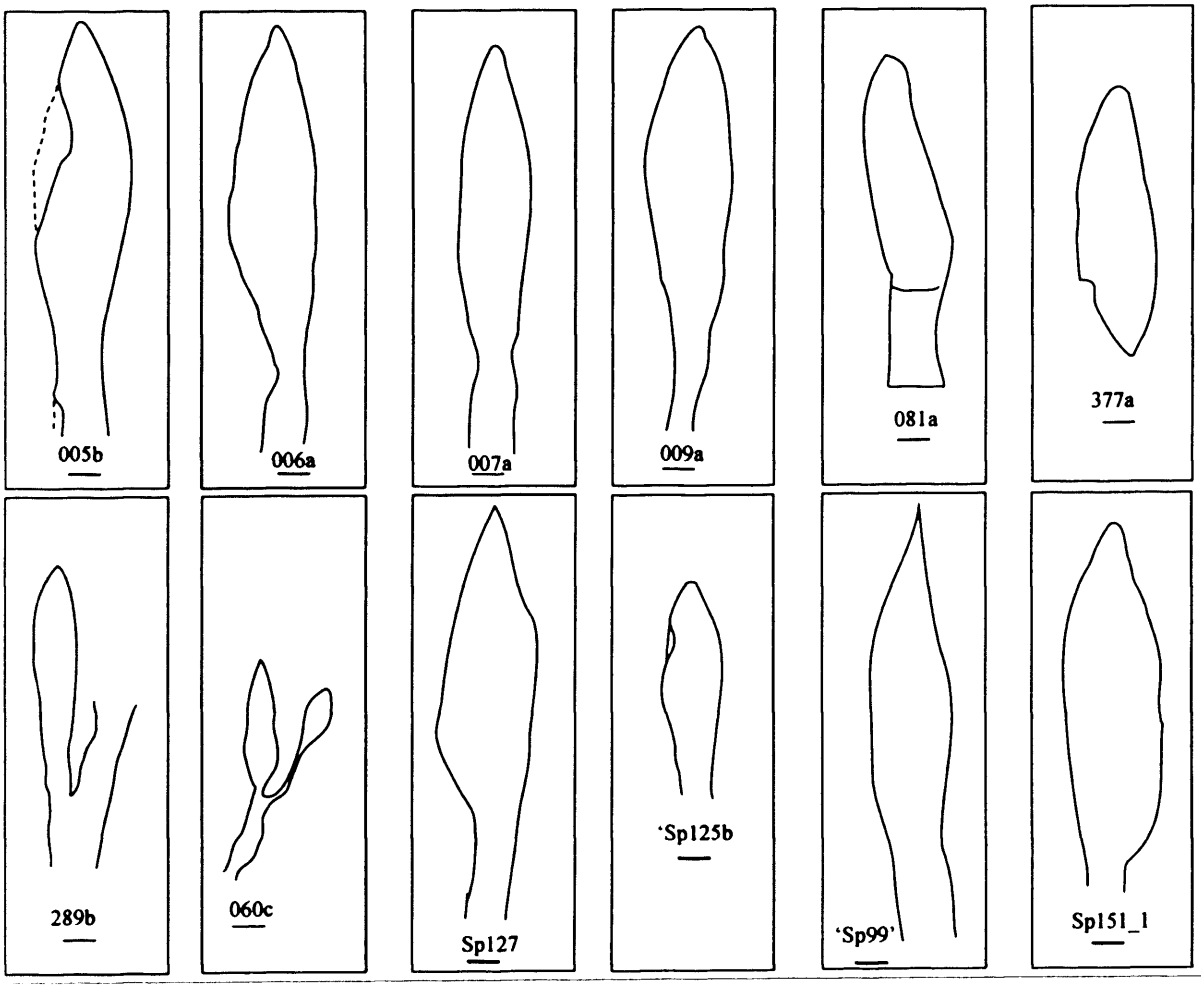

Salopella allenii (continued)

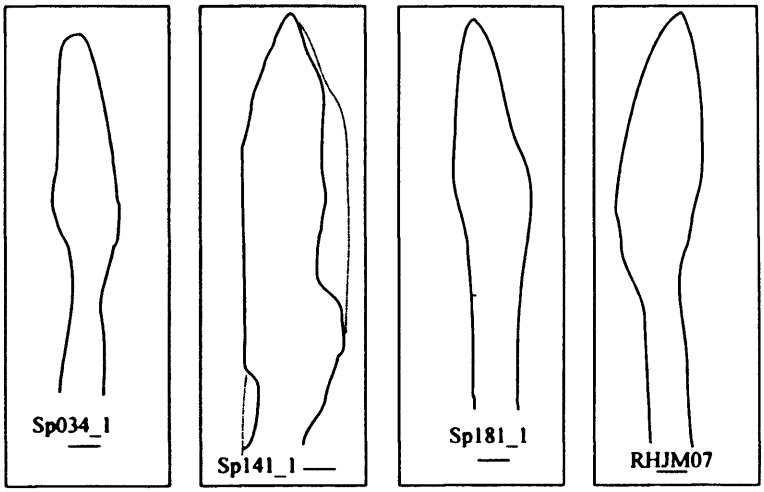

Salopella cf. *marcensis*

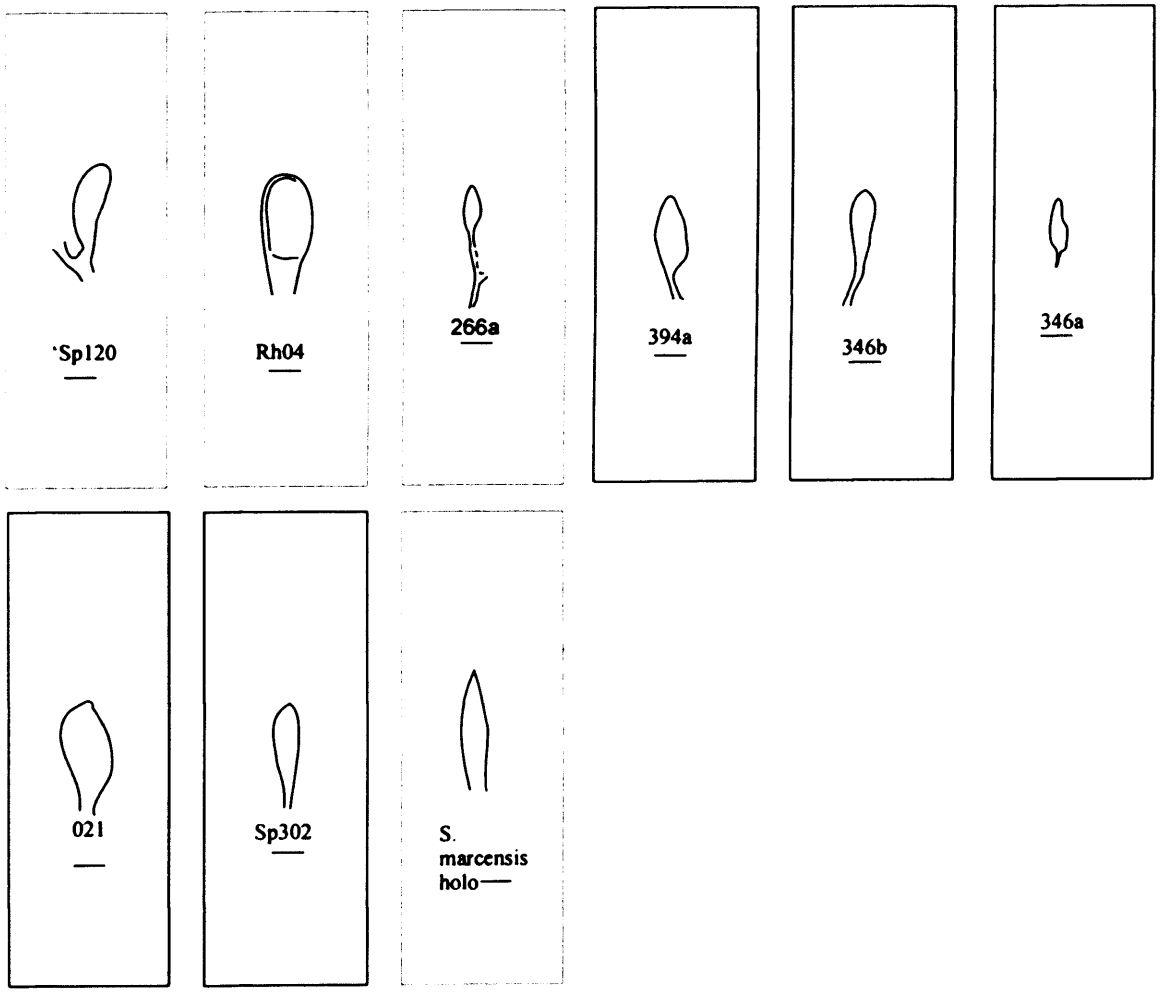

APPENDIX V: PALYNOLOGICAL COUNTS AND MEASUREMENTS

a: *Palynological assemblages collected from Tredomen Quarry surface and core* pV-2

b: *Palynological counts of each assemblage* pV-3

c: *Spore morphotypes* pV-27

d: *Spore size ranges* ..... on DVD

References numbered:

1. Wellman and Richardson 1993
2. Wellman 1996
3. Strother and Traverse 1979
4. Burgess 1991
5. Richardson 1996
6. Johnson 1985
7. Burgess and Richardson 1991
8. Wellman and Richardson 1996
9. Burgess and Richardson 1995
10. Richardson and Lister 1969
11. Streel 1967
12. Hoffmeister 1959

APPENDIX V*a*: PALYNOLOGICAL ASSEMBLAGES COLLECTED FROM TREDOMEN QUARRY SURFACE AND CORE

Location	Sample number	Assemblage	Depth from surface in m	Lithofacies		Productive sporomorph assemblage?	Date
Quarry Surface	BH1-6	1	0.00	Green fine-grained sandstone and siltstones	2b, 3a	Yes	Spring 2006
Quarry Surface	PB0	/	0.00	Green intraformational conglomerates	1a	No	Autumn 2006
Borehole 1	BH1-1	2	11.28	Green fine-grained trough-cross-bedded sandstones	2b	Yes	Spring 2006
Borehole 1	PB1	3	11.80	Green medium-grained planar-bedded sandstones	2a	Yes	Autumn 2006
Borehole 2	PB4	/	21.30 (7.30)	Green medium grained cross-bedded sandstone	2a	No	Autumn 2006
Borehole 2	BH2-1	4	21.60 (7.60)	Green planar-laminated mudstone	3a	Yes	Autumn 2006
Borehole 1	PB2	/	22.50	Green medium grained planar-bedded sandstones	2a	No	Autumn 2006
Borehole 2	PB5		22.70 (8.70)	Green medium grained planar-bedded sandstones	2a	No	Autumn 2006
Borehole 1	BH1-2	/	23.20	Green mudstone to siltstone - no bedding	3a	No	Spring 2006
Borehole 1	BH1-3	5	28.20	Green planar-laminated siltstones	3a	Yes	Spring 2006
Borehole 2	BH2-2	/	28.45 (14.45)	Green planar-laminated siltstones	3a	No	Autumn 2006
Borehole 2	PB6	/	28.80 (14.80)	Green fine-grained trough-cross-bedded sandstones	2b	No	Autumn 2006
Borehole 1	BH1-4	/	30.30	Green intraformational conglomerates	1a	No	Spring 2006
Borehole 1	PB3	/	30.80	Green intraformational conglomerates	1a	No	Autumn 2006
Borehole 1	BH1-5	/	30.90	Green intraformational conglomerates (gravel clasts)	1a	No	Spring 2006
Borehole 2	BH2-3	/	51.20 (37.20)	Green cross-ripple and wavy -laminated siltstones	3a	No	Autumn 2006
Borehole 2	BH2-4	/	51.40 (37.40)	Green cross-ripple and wavy -laminated siltstones	3a	No	Autumn 2006
Borehole 2	PB7	/	51.70 (37.70)	Green intraformational conglomerate	1a	No	Autumn 2006

APPENDIX V*b*: PALYNOLOGICAL COUNTS

BOREHOLE 1 - SAMPLE 6 (0m - QUARRY SURFACE)

		n	
Cryptospores			
Naked			
Permanent fused tetrads			
Laevigati	*Cheilotetras caledonica*	9	
	Cheilotetras sp.	5	
Sculptured	Fused apiculate tetrad	0	
	Fused verrucate tetrad	4	
	Fused murornate tetrad	3	
Permanent unfused tetrads			
Laevigati	*Tetrahedraletes medinensis* var. *medinensis*	12	
	Tetrahedraletes medinensis var. *parvus*	13	
	Rimosotetras problematica	1	
Apiculati	*Acontotetras inconspicus*	0	
	Tetrad of *Cymbohilates cymosus*	1	
Synorati	Tetrad of *Chelinohilates erraticus*	4	
	Tetrad of *Hispanaediscus verrucatus*	2	
	Tetrad of *Hispanaediscus wenlockensis*	1	
		Total	**55**
Triads			
Apiculati	Apiculate triad	2	
Synorati	Murornate triad	1	
	Verrucate triad	1	
		Total	**4**
Pseudodyads			
Laevigati	*Pseudodyadospora* cf. *laevigata*	2	
	Pseudodyadospora petasus	9	
		Total	**11**
True dyads			
Laevigati	*Dyadospora murusattenuata*	4	
	Dyadospora murusdensa	10	
Apiculati	Dyads of *Cymbohilates allenii* var. *magnus*	0	
	Dyads of *Cymbohilates cymosus*	2	
	Dyads of *Cymbohilates disponerus*	2	
	Dyads of *Cymbohilates horridus*	1	
	Dyads of *Cymbohilates horridus* var. A	0	
	Dyads of *Cymbohilates* cf. *microgranulatus*	0	
	Dyads of *Cymbohilates variabilis* var. *variabilis*	0	
	Dyads of *Cymbohilates variabilis* var. B	2	
Synorati	Dyads of *Chelinohilates erraticus*	2	
	Dyads of *Chelinohilates sinuosus* var. *sinuosus*	1	
	Dyads of *Hispanaediscus verrucatus*	3	
		Total	**27**

APPENDIX V*b*: PALYNOLOGICAL COUNTS

BOREHOLE 1 - SAMPLE 6 (0m - QUARRY SURFACE) (CONTINUED)			
Hilates			
Laevigati	*Artemopyra* sp. A (?sp. nov.)	0	
	Artemopyra cf. *robusta*	0	
	Laevolancis divellomedia	25	
	Laevolancis plicata	2	
Apiculati	*Cymbohilates allenii* var. *allenii*	4	
	Cymbohilates allenii var. *magnus*	4	
	Cymbohilates cf. *amplus*	2	
	Cymbohilates cymosus	1	
	Cymbohilates disponerus	0	
	Cymbohilates horridus var. A (?sp. nov.)	5	
	Cymbohilates cf. *horridus*	0	
	Cymbohilates cf. *microgranulatus*	0	
	Cymbohilates variabils var. *parvidecus*	3	
	Cymbohilates variabilis var. *variabilis*	2	
	Cymbohilates variabilis var. B (?sp. nov.)	1	
	Cymbohilates spp.	0	
Synorati	*Chelinohilates erraticus*	26	
	Chelinohilates cf. *lornensis*	0	
	Chelinohilates sinuosus var. *angustus*	0	
	Chelinohilates sinuosus var. *sinuosus*	1	
	Chelinohilates spp.	1	
	Chelinohilates sp. A (?sp. nov.)	2	
	Hispanaediscus verrucatus	0	
	Hispanaediscus cf. *verrucatus*	0	
	Hispanaediscus wenlockensis	0	
	Hispanaediscus major	0	
	Hispanaediscus cf. *major*	0	
		Total	**79**
Non-hilates			
Laevigati	Laevigate alete monads	9	
		Total	**9**
Enveloped			
Permanent unfused tetrads			
Apiculati	*Velatitetras* sp B. (?sp. nov.)	0	
Synorati	*Velatitetras* cf. *cristata*	0	
	Velatitetras cf. *reticulata*	4	
	Velatitetras rugulata	0	
	Velatitetras sp. C (?sp. nov.)	2	
		Total	**6**
Permanent unfused dyads			
Synorati	*Abditusdyadus histosus*	2	
		Total	**2**
Permanent fused dyads			
Synorati	*Segestrespora* cf. *membranifera*	1	
		Total	**1**
Non-hilates			
Synorati	*Qualisaspora sinuata*	2	
		Total	**2**

APPENDIX V*b*: PALYNOLOGICAL COUNTS

BOREHOLE 1 - SAMPLE 6 (0m - QUARRY SURFACE) (CONTINUED)			
Incertae sedis			
?Enveloped spactulate cryptospores			
	Monads	2	
	Dyads	2	
?Enveloped cluster spinose cryptospores			
	Monads	1	
	Dyads	1	
	Tetrads	1	
?Enveloped slender spinose cryptospores			
	Monads	2	
?Enveloped apiculate cryptospores			
	Monads	1	
?Enveloped murornate cryptospores			
	Monads with broad muri	0	
	Monads with sinuous muri	0	
?Enveloped verrucate cryptospores			
	Monads	0	
		Total	**10**
Unidentified cryptospores		7	
Cryptospore total			**213**
Trilete spores			
Laevigate			
Retusoid	*Retusotriletes dittonensis*	0	
	Retusotriletes cf. *dittonensis*	2	
	Retusotriletes cf. *triangulatus*	0	
	Retusotriletes cf. *triangulatus* var. *minor* (var. nov.)	0	
	Retusotriletes spp.	2	
Crassitate	*Ambitisporites avitus*	3	
	Ambitisporites avitus var. *minor* (var. nov.)	3	
	Ambitisporites dilutus	5	
	Ambitisporites spp.	1	
	Ambitisporites sp. A (?sp. nov.)	0	
	Ambitisporites warringtonii	6	
Patinate	*Archaeozonotriletes chulus* var. *inframurinatus*	1	
	Archaeozonotriletes chulus var. *chulus*	0	
	Archaeozonotriletes chulus var. *nanus*	2	
	Archaeozonotriletes spp.	1	
Tetrad	Laevigate tetrad (?*Ambitisporites* spp.)	2	
		Total	**28**

APPENDIX V*b*: PALYNOLOGICAL COUNTS

BOREHOLE 1 - SAMPLE 6 (0m - QUARRY SURFACE) (CONTINUED)			
Sculptured			
Retusoid	*Apiculiretusispora* spp.	1	
	Emphanisporites spp.	0	
	Emphanisporites protophanus	0	
	Emphanisporites sp. B	0	
Crassitate	*Streelispora* spp./ *Aneurospora* spp.	2	
	Aneurospora sp.	6	
	Streelispora newportensis	1	
	Scylaspora sp.	0	
	Scylaspora cf. *scripta*	0	
	Scylaspora downiei	0	
	Scylaspora cf. *kozlica*	0	
	Synorisporites sp.	0	
	Synorisporites tripapillatus	1	
Patinate	*Chelinospora* spp.	4	
Perispore	?*Perotrilites microbaculatus*	2	
Tetrad	Tetrad of *Aneurospora/ Streelispora*	2	
		Total	**19**
Unidentified triletes		7	
Trilete total			**54**
Acritarch		5	
Cuticle		2	
Tube		4	
Modern pollen grain		3	
Unidentified		1	
Sediment grain		1	
		TOTAL	**283**
		SUB TOTAL (- others and unidentified)	**258**

APPENDIX V*b*: PALYNOLOGICAL COUNTS

BOREHOLE 1 - SAMPLE 1 (11.28m - BH1-1)

		n	
Cryptospores			
Naked			
Permanent fused tetrads			
Laevigati	*Cheilotetras caledonica*	6	
	Cheilotetras sp.	0	
Sculptured	Fused apiculate tetrad	0	
	Fused verrucate tetrad	2	
	Fused murornate tetrad	0	
Permanent unfused tetrads			
Laevigati	*Tetrahedraletes medinensis* var. *medinensis*	15	
	Tetrahedraletes medinensis var. *parvus*	15	
	Rimosotetras problematica	0	
Apiculati	*Acontotetras inconspicus*	0	
	Tetrad of *Cymbohilates cymosus*	0	
Synorati	Tetrad of *Chelinohilates erraticus*	1	
	Tetrad of *Hispanaediscus verrucatus*	4	
	Tetrad of *Hispanaediscus wenlockensis*	0	
		Total	**43**
Triads			
Apiculati	Apiculate triad	0	
Synorati	Murornate triad	0	
	Verrucate triad	0	
		Total	**0**
Pseudodyads			
Laevigati	*Pseudodyadospora* cf. *laevigata*	2	
	Pseudodyadospora petasus	5	
		Total	**7**
True dyads			
Laevigati	*Dyadospora murusattenuata*	6	
	Dyadospora murusdensa	14	
Apiculati	Dyads of *Cymbohilates allenii* var. *magnus*	0	
	Dyads of *Cymbohilates cymosus*	0	
	Dyads of *Cymbohilates disponerus*	0	
	Dyads of *Cymbohilates horridus*	1	
	Dyads of *Cymbohilates horridus* var. A	1	
	Dyads of *Cymbohilates* cf. *microgranulatus*	0	
	Dyads of *Cymbohilates variabilis* var. *variabilis*	0	
	Dyads of *Cymbohilates variabilis* var. B	0	
Synorati	Dyads of *Chelinohilates erraticus*	1	
	Dyads of *Chelinohilates sinuosus* var. *sinuosus*	0	
	Dyads of *Hispanaediscus verrucatus*	0	
		Total	**23**

APPENDIX V*b*: PALYNOLOGICAL COUNTS

BOREHOLE 1 - SAMPLE 1 (11.28m - BH1-1) (CONTINUED)			
Hilates			
Laevigati	*Artemopyra* sp. A (?sp. nov.)	0	
	Artemopyra cf. *robusta*	0	
	Laevolancis divellomedia	59	
	Laevolancis plicata	9	
Apiculati	*Cymbohilates allenii* var. *allenii*	3	
	Cymbohilates allenii var. *magnus*	9	
	Cymbohilates cf. *amplus*	1	
	Cymbohilates cymosus	0	
	Cymbohilates disponerus	0	
	Cymbohilates horridus var. A (?sp. nov.)	1	
	Cymbohilates cf. *horridus*	0	
	Cymbohilates cf. *microgranulatus*	3	
	Cymbohilates variabilis var. *parvidecus*	1	
	Cymbohilates variabilis var. *variabilis*	1	
	Cymbohilates variabilis var. B (?sp. nov.)	0	
	Cymbohilates spp.	0	
Synorati	*Chelinohilates erraticus*	3	
	Chelinohilates cf. *lornensis*	1	
	Chelinohilates sinuosus var. *angustus*	0	
	Chelinohilates sinuosus var. *sinuosus*	0	
	Chelinohilates spp.	5	
	Chelinohilates sp. A (?sp. nov.)	0	
	Hispanaediscus verrucatus	2	
	Hispanaediscus cf. *verrucatus*	0	
	Hispanaediscus wenlockensis	0	
	Hispanaediscus major	1	
	Hispanaediscus cf. *major*	1	
		Total	**100**
Non-hilates			
Laevigati	Laevigate alete monads	20	
		Total	**20**
Enveloped			
Permanent unfused tetrads			
Apiculati	*Velatitetras* sp B. (?sp. nov.)	1	
Synorati	*Velatitetras* cf.*cristata*	1	
	Velatitetras cf. *reticulata*	0	
	Velatitetras rugulata	3	
	Velatitetras sp. C (?sp. nov.)	0	
		Total	**5**
Permanent unfused dyads			
Synorati	*Abditusdyadus histosus*	1	
		Total	**1**
Permanent fused dyads			
Synorati	*Segestrespora* cf. *membranifera*	0	
		Total	**0**
Non-hilates			
Synorati	*Qualisaspora sinuata*	0	
		Total	**0**

APPENDIX V*b*: PALYNOLOGICAL COUNTS

BOREHOLE 1 - SAMPLE 1 (11.28m - BH1-1) (CONTINUED)			
Incertae sedis			
?Enveloped spactulate cryptospores			
	Monads	0	
	Dyads	0	
?Enveloped cluster spinose cryptospores			
	Monads	3	
	Dyads	0	
	Tetrads	0	
?Enveloped slender spinose cryptospores			
	Monads	0	
?Enveloped apiculate cryptospores			
	Monads	0	
?Enveloped murornate cryptospores			
	Monads with broad muri	0	
	Monads with sinuous muri	0	
?Enveloped verrucate cryptospores			
	Monads	0	
		Total	**3**
Unidentifable cryptospores		7	
Cryptospore total			**209**
Trilete spores			
Laevigate			
Retusoid	*Retusotriletes dittonensis*	1	
	Retusotriletes cf. *dittonensis*	2	
	Retusotriletes cf. *triangulatus*	4	
	Retusotriletes cf. *triangulatus* var. *minor* (var. nov.)	11	
	Retusotriletes spp.	2	
Crassitate	*Ambitisporites avitus*	5	
	Ambitisporites avitus var. *minor* (var. nov.)	5	
	Ambitisporites dilutus	6	
	Ambitisporites spp.	4	
	Ambitisporites sp. A (?sp. nov.)	1	
	Ambitisporites warringtonii	4	
Patinate	*Archaeozonotriletes chulus* var. *inframurinatus*	0	
	Archaeozonotriletes chulus var. *chulus*	0	
	Archaeozonotriletes chulus var. *nanus*	0	
	Archaeozonotriletes spp.	0	
Tetrad	Laevigate tetrad (?*Ambitisporites* spp.)	0	
		Total	**45**

APPENDIX V*b*: PALYNOLOGICAL COUNTS

BOREHOLE 1 - SAMPLE 1 (11.28m - BH1-1) (CONTINUED)			
Sculptured			
Retusoid	*Apiculiretusispora* spp.	1	
	Emphanisporites spp.	2 ?	
	Emphanisporites protophanus	2	
	Emphanisporites sp. B	0	
Crassitate	*Streelispora* spp./ *Aneurospora* spp.	0	
	Aneurospora sp.	0	
	Streelispora newportensis	0	
	Scylaspora sp.	0	
	Scylaspora cf. *scripta*	0 ?	
	Scylaspora downiei	2	
	Scylaspora cf. *kozlica*	0	
	Synorisporites sp.	0	
	Synorisporites tripapillatus	0	
Patinate	*Chelinospora* spp.	0	
Perispore	*?Perotrilites microbaculatus*	2	
Tetrad	Tetrad of *Aneurospora/ Streelispora*	0	
		Total	**9**
Unidentified triletes		6	
Trilete total			**60**
Acritarch		4	
Cuticle		4	
Tube		6	
Modern pollen grain		0	
Unidentified/ Other		6	
Sediment grain		0	
	TOTAL		**289**
	SUB TOTAL (- others and unidentified)		**260**

APPENDIX V*b*: PALYNOLOGICAL COUNTS

BOREHOLE 1 - SAMPLE 2 (11.80m - PB1)

Cryptospores			
Naked			
Permanent fused tetrads			
Laevigati	*Cheilotetras caledonica*	1	
	Cheilotetras sp.	0	
Sculptured	Fused apiculate tetrad	0	
	Fused verrucate tetrad	6	
	Fused murornate tetrad	1	
Permanent unfused tetrads			
Laevigati	*Tetrahedraletes medinensis* var. *medinensis*	4	
	Tetrahedraletes medinensis var. *parvus*	5	
	Rimosotetras problematica	0	
Apiculati	*Acontotetras inconspicus*	1	
	Tetrad of *Cymbohilates disponerus*	1	
Synorati	Tetrad of *Chelinohilates erraticus*	1	
	Tetrad of *Hispanaediscus verrucatus*	0	
	Tetrad of *Hispanaediscus wenlockensis*	0	
		Total	**20**
Triads			
Apiculati	Apiculate triad	0	
Synorati	Murornate triad	0	
	Verrucate triad	0	
		Total	**0**
Pseudodyads			
Laevigati	*Pseudodyadospora* cf. *laevigata*	1	
	Pseudodyadospora petasus	7	
		Total	**8**
True dyads			
Laevigati	*Dyadospora murusattenuata*	2	
	Dyadospora murusdensa	12	
Apiculati	Dyads of *Cymbohilates allenii* var. *magnus*	0	
	Dyads of *Cymbohilates cymosus*	0	
	Dyads of *Cymbohilates disponerus*	4	
	Dyads of *Cymbohilates horridus*	0	
	Dyads of *Cymbohilates horridus var.* A	1	
	Dyads of *Cymbohilates* cf. *microgranulatus*	0	
	Dyads of *Cymbohilates variabilis* var. *variabilis*	0	
	Dyads of *Cymbohilates variabilis* var. B	0	
Synorati	Dyads of *Chelinohilates erraticus*	2	
	Dyads of *Chelinohilates sinuosus* var. *sinuosus*	0	
	Dyads of *Hispanaediscus verrucatus*	0	
		Total	**21**

APPENDIX V*b*: PALYNOLOGICAL COUNTS

BOREHOLE 1 - SAMPLE 2 (11.80m - PB1) (CONTINUED)			
Hilates			
Laevigati	*Artemopyra* sp. A (?sp. nov.)	0	
	Artemopyra cf. *robusta*	0	
	Laevolancis divellomedia	45	
	Laevolancis plicata	2	
Apiculati	*Cymbohilates allenii* var. *allenii*	2	
	Cymbohilates allenii var. *magnus*	6	
	Cymbohilates cf. *amplus*	0	
	Cymbohilates cymosus	0	
	Cymbohilates disponerus	13	
	Cymbohilates horridus var. A (?sp. nov.)	1	
	Cymbohilates cf. *horridus*	0	
	Cymbohilates cf. *microgranulatus*	2	
	Cymbohilates variabilis var. *parvidecus*	5	
	Cymbohilates variabilis var. *variabilis*	4	
	Cymbohilates variabilis var. B (?sp. nov.)	1	
	Cymbohilates spp.	3	
Synorati	*Chelinohilates erraticus*	3	
	Chelinohilates cf. *lornensis*	0	
	Chelinohilates sinuosus var. *angustus*	0	
	Chelinohilates sinuosus var. *sinuosus*	0	
	Chelinohilates spp.	0	
	Chelinohilates sp. A (?sp. nov.)	0	
	Hispanaediscus verrucatus	3	
	Hispanaediscus cf. *verrucatus*	0	
	Hispanaediscus wenlockensis	2	
	Hispanaediscus major	0	
	Hispanaediscus cf. *major*	0	
		Total	**92**
Non-hilates			
Laevigati	Laevigate alete monads	2	
		Total	**2**
Enveloped			
Permanent unfused tetrads			
Apiculati	*Velatitetras* sp B. (?sp. nov.)	0	
Synorati	*Velatitetras* cf.*cristata*	0	
	Velatitetras cf. *reticulata*	1	
	Velatitetras rugulata	0	
	Velatitetras sp. C (?sp. nov.)	0	
		Total	**1**
Permanent unfused dyads			
Synorati	*Abditusdyadus histosus*	0	
		Total	**0**
Permanent fused dyads			
Synorati	*Segestrespora* cf. *membranifera*	0	
		Total	**0**
Non-hilates			
Synorati	*Qualisaspora sinuata*	0	
		Total	**0**

APPENDIX V*b*: PALYNOLOGICAL COUNTS

BOREHOLE 1 - SAMPLE 2 (11.80m - PB1) (CONTINUED)			
Incertae sedis			
?Enveloped spactulate cryptospores			
	Monads	0	
	Dyads	0	
?Enveloped cluster spinose cryptospores			
	Monads	0	
	Dyads	0	
	Tetrads	0	
?Enveloped slender spinose cryptospores			
	Monads	0	
?Enveloped apiculate cryptospores			
	Monads	0	
?Enveloped murornate cryptospores			
	Monads with broad muri	1	
	Monads with sinuous muri	0	
?Enveloped verrucate cryptospores			
	Monads	0	
		Total	**1**
Unidentifable cryptospores		0	
Cryptospore total			**145**
Trilete spores			
Laevigate			
Retusoid	*Retusotriletes dittonensis*	2	
	Retusotriletes cf. *dittonensis*	1	
	Retusotriletes cf. *triangulatus*	0	
	Retusotriletes cf. *triangulatus* var. *minor* (var. nov.)	0	
	Retusotriletes spp.	2	
Crassitate	*Ambitisporites avitus*	2	
	Ambitisporites avitus var. *minor* (var. nov.)	6	
	Ambitisporites dilutus	2	
	Ambitisporites spp.	3	
	Ambitisporites sp. A (?sp. nov.)	0	
	Ambitisporites warringtonii	3	
Patinate	*Archaeozonotriletes chulus* var. *inframurinatus*	0	
	Archaeozonotriletes chulus var. *chulus*	0	
	Archaeozonotriletes chulus var. *nanus*	0	
	Archaeozonotriletes spp.	0	
Tetrad	Laevigate tetrad (?*Ambitisporites* spp.)	0	
		Total	**21**

APPENDIX V*b*: PALYNOLOGICAL COUNTS

BOREHOLE 1 - SAMPLE 2 (11.80m - PB1) (CONTINUED)				
Sculptured				
Retusoid	*Apiculiretusispora* spp.		6	
	Emphanisporites spp.		0	
	Emphanisporites protophanus		0	
	Emphanisporites sp. B		1	
Crassitate	*Streelispora* spp./ *Aneurospora* spp.		8	
	Aneurospora sp.		6	
	Streelispora newportensis		0	
	Scylaspora sp.		0 ?	
	Scylaspora cf. *scripta*		0	
	Scylaspora downiei		3	
	Scylaspora cf. *kozlica*		0	
	Synorisporites sp.		5	
	Synorisporites tripapillatus		0	
Patinate	*Chelinospora* spp.		0	
Perispore	*?Perotrilites microbaculatus*		0	
Tetrad	Tetrad of *Aneurospora/ Streelispora*		0	
			Total	**29**
Unidentified triletes		PB064	1	
Trilete total				**51**
Acritarch			4	
Cuticle			0	
Tube			0	
Modern pollen grain			0	
Unidentified/ Other			0	
Sediment grain			0	
	TOTAL			**200**
	SUB TOTAL (- others and unidentified)			**199**

APPENDIX V*b*: PALYNOLOGICAL COUNTS

BOREHOLE 2 - SAMPLE 1 (7.6m BH2 correlated with 21.6m in BH1)

Cryptospores			
Naked			
Permanent fused tetrads			
Laevigati	*Cheilotetras caledonica*	3	
	Cheilotetras sp.	1	
Sculptured	Fused apiculate tetrad	0	
	Fused verrucate tetrad	2	
	Fused murornate tetrad	0	
Permanent unfused tetrads			
Laevigati	*Tetrahedraletes medinensis* var. *medinensis*	8	
	Tetrahedraletes medinensis var. *parvus*	7	
	Rimosotetras problematica	0	
Apiculati	*Acontotetras inconspicus*	5	
	Tetrad of *Cymbohilates disponerus*	1	
Synorati	Tetrad of *Chelinohilates erraticus*	1	
	Tetrad of *Hispanaediscus verrucatus*	1	
	Tetrad of *Hispanaediscus wenlockensis*	0	
		Total	**29**
Triads			
Apiculati	Apiculate triad	0	
Synorati	Murornate triad	0	
	Verrucate triad	1	
		Total	**1**
Pseudodyads			
Laevigati	*Pseudodyadospora* cf. *laevigata*	3	
	Pseudodyadospora petasus	9	
		Total	**12**
True dyads			
Laevigati	*Dyadospora murusattenuata*	2	
	Dyadospora murusdensa	17	
Apiculati	Dyads of *Cymbohilates allenii* var. *magnus*	1	
	Dyads of *Cymbohilates cymosus*	0	
	Dyads of *Cymbohilates disponerus*	0	
	Dyads of *Cymbohilates horridus*	0	
	Dyads of *Cymbohilates horridus* var. A	0	
	Dyads of *Cymbohilates* cf. *microgranulatus*	1	
	Dyads of *Cymbohilates variabilis* var. *variabilis*	2	
	Dyads of *Cymbohilates variabilis* var. B	0	
Synorati	Dyads of *Chelinohilates erraticus*	9	
	Dyads of *Chelinohilates sinuosus* var. *sinuosus*	0	
	Dyads of *Hispanaediscus verrucatus*	1	
		Total	**33**

APPENDIX V*b*: PALYNOLOGICAL COUNTS

BOREHOLE 2 - SAMPLE 1 (7.6m BH2 correlated with 21.6m in BH1) (CONTINUED)			
Hilates			
Laevigati	*Artemopyra* sp. A (?sp. nov.)	1	
	Artemopyra cf. *robusta*	1	
	Laevolancis divellomedia	47	
	Laevolancis plicata	13	
Apiculati	*Cymbohilates allenii* var. *allenii*	2	
	Cymbohilates allenii var. *magnus*	2	
	Cymbohilates cf. *amplus*	2	
	Cymbohilates cymosus	0	
	Cymbohilates disponerus	6	
	Cymbohilates horridus var. A (?sp. nov.)	2	
	Cymbohilates cf. *horridus*	0	
	Cymbohilates cf. *microgranulatus*	3	
	Cymbohilates variabilis var. *parvidecus*	4	
	Cymbohilates variabilis var. *variabilis*	0	
	Cymbohilates variabilis var. B (?sp. nov.)	0	
	Cymbohilates spp.	0	
Synorati	*Chelinohilates erraticus*	8	
	Chelinohilates cf. *lornensis*	0	
	Chelinohilates sinuosus var. *angustus*	1	
	Chelinohilates sinuosus var. *sinuosus*	1	
	Chelinohilates spp.	3	
	Chelinohilates sp. A (?sp. nov.)	1	
	Hispanaediscus verrucatus	2	
	Hispanaediscus cf. *verrucatus*	1	
	Hispanaediscus wenlockensis	0	
	Hispanaediscus major	0	
	Hispanaediscus cf. *major*	0	
		Total	**100**
Non-hilates			
Laevigati	Laevigate alete monads	11	
		Total	**11**
Enveloped			
Permanent unfused tetrads			
Apiculati	*Velatitetras* sp B. (?sp. nov.)	4	
Synorati	*Velatitetras* cf.*cristata*	0	
	Velatitetras cf. *reticulata*	1	
	Velatitetras rugulata	3	
	Velatitetras sp. C (?sp. nov.)	0	
		Total	**8**
Permanent unfused dyads			
Synorati	*Abditusdyadus histosus*	0	
		Total	**0**
Permanent fused dyads			
Synorati	*Segestrespora* cf. *membranifera*	0	
		Total	**0**
Non-hilates			
Synorati	*Qualisaspora sinuata*	0	
		Total	**0**

APPENDIX V*b*: PALYNOLOGICAL COUNTS

BOREHOLE 2 - SAMPLE 1 (7.6m BH2 correlated with 21.6m in BH1) (CONTINUED)			
Incertae sedis			
?Enveloped spactulate cryptospores			
	Monads	2	
	Dyads	0	
?Enveloped cluster spinose cryptospores			
	Monads	0	
	Dyads	0	
	Tetrads	0	
?Enveloped slender spinose cryptospores			
	Monads	0	
?Enveloped apiculate cryptospores			
	Monads	0	
?Enveloped murornate cryptospores			
	Monads with broad muri	1	
	Monads with sinuous muri	1	
?Enveloped verrucate cryptospores			
	Monads	3	
		Total	**7**
Unidentified cryptospores		1	
Cryptospore total			**202**
Trilete spores			
Laevigate			
Retusoid	*Retusotriletes dittonensis*	1	
	Retusotriletes cf. *dittonensis*	0	
	Retusotriletes cf. *triangulatus*	0	
	Retusotriletes cf. *triangulatus* var. *minor* (var. nov.)	0	
	Retusotriletes spp.	1	
Crassitate	*Ambitisporites avitus*	0	
	Ambitisporites avitus var. *minor* (var. nov.)	3	
	Ambitisporites dilutus	4	
	Ambitisporites spp.	2	
	Ambitisporites sp. A (?sp. nov.)	0	
	Ambitisporites warringtonii	1	
Patinate	*Archaeozonotriletes chulus* var. *inframurinatus*	0	
	Archaeozonotriletes chulus var. *chulus*	2	
	Archaeozonotriletes chulus var. *nanus*	0	
	Archaeozonotriletes spp.	0	
Tetrad	Laevigate tetrad (?*Ambitisporites* spp.)	0	
		Total	**14**

APPENDIX V*b*: PALYNOLOGICAL COUNTS

BOREHOLE 1 - SAMPLE 3 (28.2m T1-3)

Cryptospores			
Naked			
Permanent fused tetrads			
Laevigati	*Cheilotetras caledonica*	0	
	Cheilotetras sp.	0	
Sculptured	Fused apiculate tetrad	1	
	Fused verrucate tetrad	0	
	Fused murornate tetrad	0	
Permanent unfused tetrads			
Laevigati	*Tetrahedraletes medinensis* var. *medinensis*	15	
	Tetrahedraletes medinensis var. *parvus*	22	
	Rimosotetras problematica	1	
Apiculati	*Acontotetras inconspicus*	1	
	Tetrad of *Cymbohilates cymosus*	0	
Synorati	Tetrad of *Chelinohilates erraticus*	1	
	Tetrad of *Hispanaediscus verrucatus*	2	
	Tetrad of *Hispanaediscus wenlockensis*	0	
		Total	**43**
Triads			
Apiculati	Apiculate triad	0	
Synorati	Murornate triad	1	
	Verrucate triad	1	
		Total	**2**
Pseudodyads			
Laevigati	*Pseudodyadospora* cf. *laevigata*	0	
	Pseudodyadospora petasus	16	
		Total	**16**
True dyads			
Laevigati	*Dyadospora murusattenuata*	8	
	Dyadospora murusdensa	17	
Apiculati	Dyads of *Cymbohilates allenii* var. *magnus*	0	
	Dyads of *Cymbohilates cymosus*	0	
	Dyads of *Cymbohilates disponerus*	0	
	Dyads of *Cymbohilates horridus*	0	
	Dyads of *Cymbohilates horridus* var. A	0	
	Dyads of *Cymbohilates* cf. *microgranulatus*	0	
	Dyads of *?Cymbohilates variabilis* var. *variabilis*	0	
	Dyads of *Cymbohilates variabilis* var. B	0	
Synorati	Dyads of *Chelinohilates erraticus*	0	
	Dyads of *Chelinohilates sinuosus* var. *sinuosus*	0	
	Dyads of *Hispanaediscus verrucatus*	0	
		Total	**25**

APPENDIX V*b*: PALYNOLOGICAL COUNTS

BOREHOLE 1 - SAMPLE 3 (28.2m T1-3) (CONTINUED)			
Hilates			
Laevigati	*Artemopyra* sp. A (?sp. nov.)	2	
	Artemopyra cf. *robusta*	0	
	Laevolancis divellomedia	72	
	Laevolancis plicata	14	
Apiculati	*Cymbohilates allenii* var. *allenii*	0	
	Cymbohilates allenii var. *magnus*	1	
	Cymbohilates cf. *amplus*	0	
	Cymbohilates cymosus	0	
	Cymbohilates disponerus	1	
	Cymbohilates horridus var. A (?sp. nov.)	0	
	Cymbohilates cf. *horridus*	1	
	Cymbohilates cf. *microgranulatus*	0	
	Cymbohilates variabilis var. *parvidecus*	0	
	Cymbohilates variabilis var. *variabilis*	1	
	Cymbohilates variabilis var. B (?sp. nov.)	0	
	Cymbohilates spp.	2	
Synorati	*Chelinohilates erraticus*	3	
	Chelinohilates cf. *lornensis*	2	
	Chelinohilates sinuosus var. *angustus*	0	
	Chelinohilates sinuosus var. *sinuosus*	0	
	Chelinohilates spp.	3	
	Chelinohilates sp. A (?sp. nov.)	0	
	Hispanaediscus verrucatus	0	
	Hispanaediscus cf. *verrucatus*	0	
	Hispanaediscus wenlockensis	0	
	Hispanaediscus major	0	
	Hispanaediscus cf. *major*	0	
		Total	**102**
Non-hilates			
Laevigati	Laevigate alete monads	22	
		Total	**22**
Enveloped			
Permanent unfused tetrads			
Apiculati	*Velatitetras* sp B. (?sp. nov.)	0	
Synorati	*Velatitetras* cf.*cristata*	1	
	Velatitetras cf. *reticulata*	0	
	Velatitetras rugulata	0	
	Velatitetras sp. C (?sp. nov.)	0	
		Total	**1**
Permanent unfused dyads			
Synorati	*Abditusdyadus histosus*	0	
		Total	**0**
Permanent fused dyads			
Synorati	*Segestrespora* cf. *membranifera*	0	
		Total	**0**
Non-hilates			
Synorati	*Qualisaspora sinuata*	0	
		Total	**0**

APPENDIX V*b*: PALYNOLOGICAL COUNTS

BOREHOLE 1 - SAMPLE 3 (28.2m T1-3) (CONTINUED)			
Incertae sedis			
?Enveloped spactulate cryptospores			
	Monads	0	
	Dyads	0	
?Enveloped cluster spinose cryptospores			
	Monads	0	
	Dyads	0	
	Tetrads	0	
?Enveloped slender spinose cryptospores			
	Monads	0	
?Enveloped apiculate cryptospores			
	Monads	0	
?Enveloped murornate cryptospores			
	Monads with broad muri	1	
	Monads with sinuous muri	0	
?Enveloped verrucate cryptospores			
	Monads	0	
		Total	**1**
Unidentifable cryptospores		4	
Cryptospore total			**216**
Trilete spores			
Laevigate			
Retusoid	*Retusotriletes dittonensis*	4	
	Retusotriletes cf. *dittonensis*	2	
	Retusotriletes cf. *triangulatus*	0	
	Retusotriletes cf. *triangulatus* var. *minor* (var. nov.)	6	
	Retusotriletes spp.	2	
Crassitate	*Ambitisporites avitus*	2	
	Ambitisporites avitus var. *minor* (var. nov.)	1	
	Ambitisporites dilutus	4	
	Ambitisporites spp.	5	
	Ambitisporites sp. A (?sp. nov.)	0	
	Ambitisporites warringtonii	3	
Patinate	*Archaeozonotriletes chulus* var. *inframurinatus*	0	
	Archaeozonotriletes chulus var. *chulus*	0	
	Archaeozonotriletes chulus var. *nanus*	0	
	Archaeozonotriletes spp.	0	
Tetrad	Laevigate tetrad (?*Ambitisporites* spp.)	0 ?	
		Total	**29**

APPENDIX V*b*: PALYNOLOGICAL COUNTS

BOREHOLE 1 - SAMPLE 3 (28.2m T1-3) (CONTINUED)			
Sculptured			
Retusoid	*Apiculiretusispora* spp.	0	
	Emphanisporites spp.	1	
	Emphanisporites protophanus	0	
	Emphanisporites sp. B	1	
Crassitate	*Streelispora* spp./ *Aneurospora* spp.	0	
	Aneurospora sp.	0	
	Streelispora newportensis	0	
	Scylaspora sp.	2	
	Scylaspora cf. *scripta*	1	
	Scylaspora downiei	0	
	Scylaspora cf. *kozlica*	1	
	Synorisporites sp.	1	
	Synorisporites tripapillatus	0	
Patinate	*Chelinospora* spp.	1	
Perispore	*?Perotrilites microbaculatus*	1	
Tetrad	Tetrad of *Aneurospora/ Streelispora*	0	
		Total	**9**
Unidentified triletes		6	
Trilete total			**44**
Acritarch		1	
Cuticle		3	
Tube		1	
Modern pollen grain		0	
Unidentified/ Other		2	
Sediment grain		0	
	TOTAL		**267**
	SUB TOTAL (- others and unidentified)		**251**

APPENDIX V*b*: PALYNOLOGICAL COUNTS

GRAND TOTAL

Cryptospores			
Naked			
Permanent fused tetrads			
Laevigati	*Cheilotetras caledonica*	19	
	Cheilotetras sp.	6	
Sculptured	Fused apiculate tetrad	1	
	Fused verrucate tetrad	14	
	Fused murornate tetrad	4	
Permanent unfused tetrad			
Laevigati	*Tetrahedraletes medinensis* var. *medinensis*	54	
	Tetrahedraletes medinensis var. *parvus*	62	
	Rimosotetras problematica	2	
Apiculati	*Acontotetras inconspicus*	7	
	Tetrad of *Cymbohilates* spp.	3	
Synorati	Tetrad of *Chelinohilates erraticus*	8	
	Tetrad of *Hispanaediscus verrucatus*	9	
	Tetrad of *Hispanaediscus wenlockensis*	1	
		Total	**190**
Triads			
Apiculati	Apiculate triad	2	
Synorati	Murornate triad	2	
	Verrucate triad	3	
		Total	**7**
Pseudodyads			
Laevigati	*Pseudodyadospora* cf. *laevigata*	8	
	Pseudodyadospora petasus	46	
		Total	**54**
True dyads			
Laevigati	*Dyadospora murusattenuata*	22	
	Dyadospora murusdensa	70	
Apiculati	Dyads of *Cymbohilates allenii* var. *magnus*	1	
	Dyads of *Cymbohilates cymosus*	2	
	Dyads of *Cymbohilates disponerus*	6	
	Dyads of *Cymbohilates horridus*	2	
	Dyads of *Cymbohilates horridus* var. A	2	
	Dyads of *Cymbohilates* cf. *microgranulatus*	1	
	Dyads of *Cymbohilates variabilis* var. *variabilis*	2	
	Dyads of *Cymbohilates variabilis* var. B	2	
Synorati	Dyads of *Chelinohilates erraticus*	14	
	Dyads of *Chelinohilates sinuosus* var. *sinuosus*	1	
	Dyads of *Hispanaediscus verrucatus*	4	
		Total	**129**

APPENDIX V*b*: PALYNOLOGICAL COUNTS

GRAND TOTAL (CONTINUED)			
Hilates			
Laevigati	*Artemopyra* sp. A (?sp. nov.)	3	
	Artemopyra cf. *robusta*	1	
	Laevolancis divellomedia	248	
	Laevolancis plicata	40	
Apiculati	*Cymbohilates allenii* var. *allenii*	11	
	Cymbohilates allenii var. *magnus*	22	
	Cymbohilates cf. *amplus*	5	
	Cymbohilates cymosus	1	
	Cymbohilates disponerus	20	
	Cymbohilates horridus var. A (?sp. nov.)	9	
	Cymbohilates cf. *horridus*	1	
	Cymbohilates cf. *microgranulatus*	8	
	Cymbohilates variabilis var. *parvidecus*	13	
	Cymbohilates variabilis var. *variabilis*	8	
	Cymbohilates variabilis var. B (?sp. nov.)	2	
	Cymbohilates spp.	5	
Synorati	*Chelinohilates erraticus*	43	
	Chelinohilates cf. *lornensis*	3	
	Chelinohilates sinuosus var. *angustus*	1	
	Chelinohilates sinuosus var. *sinuosus*	2	
	Chelinohilates spp.	12	
	Chelinohilates sp. A (?sp. nov.)	3	
	Hispanaediscus verrucatus	7	
	Hispanaediscus cf. *verrucatus*	1	
	Hispanaediscus wenlockensis	2	
	Hispanaediscus major	1	
	Hispanaediscus cf. *major*	1	
		Total	**473**
Non-hilates			
Laevigati	Laevigate alete monads	64	
		Total	**64**
Enveloped			
Permanent unfused tetrads			
Apiculati	*Velatitetras* sp B. (?sp. nov.)	5	
Synorati	*Velatitetras* cf.*cristata*	2	
	Velatitetras cf. *reticulata*	6	
	Velatitetras rugulata	6	
	Velatitetras sp. C (?sp. nov.)	2	
		Total	**21**
Permanent unfused dyads			
Synorati	*Abditusdyadus histosus*	3	
		Total	**3**
Permanent fused dyads			
Synorati	*Segestrespora* cf. *membranifera*	1	
		Total	**1**
Non-hilates			
Synorati	*Qualisaspora sinuata*	2	
		Total	**2**

APPENDIX V*b*: PALYNOLOGICAL COUNTS

GRAND TOTAL (CONTINUED)			
Incertae sedis			
?Enveloped spactulate cryptospores			
	Monads	4	
	Dyads	2	
?Enveloped cluster spinose cryptospores			
	Monads	4	
	Dyads	1	
	Tetrads	1	
?Enveloped slender spinose cryptospores			
	Monads	2	
?Enveloped apiculate cryptospores			
	Monads	1	
?Enveloped murornate cryptospores			
	Monads with broad muri	3	
	Monads with sinuous muri	1	
?Enveloped verrucate cryptospores			
	Monads	3	
		Total	**22**
Unidentifable cryptospores		19	
Cryptospore total			**966**
Trilete spores			
Laevigate			
Retusoid	*Retusotriletes dittonensis*	8	
	Retusotriletes cf. *dittonensis*	7	
	Retusotriletes cf. *triangulatus*	4	
	Retusotriletes cf. *triangulatus* var. *minor* (var. nov.)	17	
	Retusotriletes spp.	9	
Crassitate	*Ambitisporites avitus*	12	
	Ambitisporites avitus var. *minor* (var. nov.)	18	
	Ambitisporites dilutus	21	
	Ambitisporites spp.	15	
	Ambitisporites sp. A (?sp. nov.)	1	
	Ambitisporites warringtonii	17	
Patinate	*Archaeozonotriletes chulus* var. *inframurinatus*	1	
	Archaeozonotriletes chulus var. *chulus*	2	
	Archaeozonotriletes chulus var. *nanus*	2	
	Archaeozonotriletes spp.	1	
Tetrad	Laevigate tetrad (?*Ambitisporites* spp.)	2	
		Total	**137**

GRAND TOTAL (CONTINUED)			
Sculptured			
Retusoid	*Apiculiretusispora* spp.	8	
	Emphanisporites spp.	3	
	Emphanisporites protophanus	2	
	Emphanisporites sp. B	2	
Crassitate	*Streelispora* spp./ *Aneurospora* spp.	11	
	Aneurospora sp.	12	
	Streelispora newportensis	2	
	Scylaspora sp.	4	
	Scylaspora cf. *scripta*	1	
	Scylaspora downiei	5	
	Scylaspora cf. *kozlica*	1	
	Synorisporites sp.	8	
	Synorisporites tripapillatus	2	
Patinate	*Chelinospora* spp.	6	
Perispore	*?Perotrilites microbaculatus*	5	
Tetrad	Tetrad of *Aneurospora/ Streelispora*	4	
		Total	**76**
Unidentified triletes		20	
Trilete total			**233**
Acritarch		16	
Cuticle		9	
Tube		11	
Modern pollen grain		5	
Unidentified/ Other		9	
Sediment grain		1	
			1269
		SUB TOTAL (- others and unidentified)	**1195**

APPENDIX Vc: SPORE MORPHOTYPES

Tredomen quarry surface	0m	
Sporomorph	n	%
Cryptospores		
Permanent fused tetrads - laevigate	14	5.43%
Permanent fused tetrads - sculptured	7	2.71%
Permanent unfused tetrads- laevigate	26	10.08%
Permanent unfused tetrads- sculptured	8	3.10%
Triads- sculptured	4	1.55%
Pseudodyads - laevigate	11	4.26%
True dyads - laevigate	14	5.43%
True dyads - sculptured	13	5.04%
Hilates - laevigate	27	10.47%
Hilates - sculptured	52	20.16%
Non-hilates - laevigate	9	3.49%
Enveloped unfused tetrads - sculptured	6	2.33%
Enveloped unfused dyads - sculptured	2	0.78%
Enveloped fused dyads - sculptured	1	0.39%
Enveloped non-hilates -sculptured	2	0.78%
Sculptured ?enveloped cryptospores	10	3.88%
Triletes		
Laevigate triletes	28	10.85%
Sculptured triletes	17	6.59%
Perispore triletes	2	0.78%
Acritarchs	5	1.94%
Sub-total	**258**	**100.0%**
Unidentified/ others	25	
Total	**283**	

Tredomen borehole 1-1 palynology		11.28m
Sporomorph	n	%
Cryptospores		
Permanent fused tetrads - laevigate	6	2.31%
Permanent fused tetrads - sculptured	2	0.77%
Permanent unfused tetrads- laevigate	30	11.54%
Permanent unfused tetrads- sculptured	5	1.92%
Triads- sculptured	0	0.00%
Pseudodyads - laevigate	7	2.69%
True dyads - laevigate	20	7.69%
True dyads - sculptured	3	1.15%
Hilates - laevigate	68	26.15%
Hilates - sculptured	32	12.31%
Non-hilates - laevigate	20	7.69%
Enveloped unfused tetrads - sculptured	5	1.92%
Enveloped unfused dyads - sculptured	1	0.38%
Enveloped fused dyads - sculptured	0	0.00%
Enveloped non-hilates -sculptured	0	0.00%
Sculptured ?enveloped cryptospores	3	1.15%
Triletes		
Laevigate triletes	45	17.31%
Sculptured triletes	7	2.69%
Perispore triletes	2	0.77%
Acritarchs	4	1.54%
Sub-total	**260**	**100.0%**
Unidentified/ others	29	
Total	**289**	

APPENDIX Vc: SPORE MORPHOTYPES

Tredomen borehole plant bed 1 palynology		11.80m
Sporomorph	n	%
Cryptospores		
Permanent fused tetrads - laevigate	1	0.50%
Permanent fused tetrads - sculptured	7	3.52%
Permanent unfused tetrads- laevigate	9	4.52%
Permanent unfused tetrads- sculptured	3	1.51%
Triads- sculptured	0	0.00%
Pseudodyads - laevigate	8	4.02%
True dyads - laevigate	14	7.04%
True dyads - sculptured	7	3.52%
Hilates - laevigate	47	23.62%
Hilates - sculptured	45	22.61%
Non-hilates - laevigate	2	1.01%
Enveloped unfused tetrads - sculptured	1	0.50%
Enveloped unfused dyads - sculptured	0	0.00%
Enveloped fused dyads - sculptured	0	0.00%
Enveloped non-hilates -sculptured	0	0.00%
Sculptured ?enveloped cryptospores	1	0.50%
Triletes		
Laevigate triletes	21	10.55%
Sculptured triletes	29	14.57%
Perispore triletes	0	0.00%
Acritarchs	4	2.01%
Sub-total	**199**	**100.0%**
Unidentified/ others	1	
Total	**200**	

Tredomen borehole 2 sample 1		21.60m
Sporomorph	n	%
Cryptospores		
Permanent fused tetrads - laevigate	4	1.76%
Permanent fused tetrads - sculptured	2	0.88%
Permanent unfused tetrads- laevigate	15	6.61%
Permanent unfused tetrads- sculptured	8	3.52%
Triads- sculptured	1	0.44%
Pseudodyads - laevigate	12	5.29%
True dyads - laevigate	19	8.37%
True dyads - sculptured	14	6.17%
Hilates - laevigate	62	27.31%
Hilates - sculptured	38	16.74%
Non-hilates - laevigate	11	4.85%
Enveloped unfused tetrads - sculptured	8	3.52%
Enveloped unfused dyads - sculptured	0	0.00%
Enveloped fused dyads - sculptured	0	0.00%
Enveloped non-hilates -sculptured	0	0.00%
Sculptured ?enveloped cryptospores	7	3.08%
Triletes		
Laevigate triletes	14	6.17%
Sculptured triletes	10	4.41%
Perispore triletes	0	0.00%
Acritarchs	2	0.88%
Sub-total	**227**	**100.0%**
Unidentified/ others	3	
Total	**230**	

APPENDIX Vc: SPORE MORPHOTYPES

Tredomen borehole 1-3 palynology		28.20m
Sporomorph	n	%
Cryptospores		
Permanent fused tetrads - laevigate	0	0.00%
Permanent fused tetrads - sculptured	1	0.40%
Permanent unfused tetrads- laevigate	38	15.14%
Permanent unfused tetrads- sculptured	4	1.59%
Triads- sculptured	2	0.80%
Pseudodyads - laevigate	16	6.37%
True dyads - laevigate	25	9.96%
True dyads - sculptured	0	0.00%
Hilates - laevigate	88	35.06%
Hilates - sculptured	14	5.58%
Non-hilates - laevigate	22	8.76%
Enveloped unfused tetrads - sculptured	1	0.40%
Enveloped unfused dyads - sculptured	0	0.00%
Enveloped fused dyads - sculptured	0	0.00%
Enveloped non-hilates -sculptured	0	0.00%
Sculptured ?enveloped cryptospores	1	0.40%
Triletes		
Laevigate triletes	29	11.55%
Sculptured triletes	8	3.19%
Perispore triletes	1	0.40%
Acritarchs	1	0.40%
Sub-total	**251**	
Unidentified/ others	16	
Total	**267**	**100.0%**

	PB0	**BH1-1**	**PB1**	**BH2-1**	**BH1-3**	**Total**
	0m	11.28m	11.80m	21.60m	28.20m	
Miospores sculptured	17	9	29	8	9	72
Cryptospores sculptured	107	51	64	80	23	325
Cryptospores laevigate	101	151	81	123	189	645
Miospores laevigate	28	45	21	14	29	137
Acritarchs	5	4	4	2	1	16
	258	260	199	227	251	1195

APPENDIX VI: TREDOMEN QUARRY AND TARGROVE QUARRY

SEDIMENTOLOGICAL DATABASE

pVI-2 to pVI-8

ID	Log	Bed	facies	transition	Thickness m
1	Quarry A	1	3b	/	?
2	Quarry A	2	5b	3b-5b	0.7
3	Quarry A	3	1a	5b-1a	0.15
4	Quarry A	4	2a	1a-2a	1.4
5	Quarry A	5	2b	2a-2b	0.95
6	Quarry A	6	3a	2b-3a	0.85
7	Quarry A	7	3b	3a-3b	0.35
8	Quarry A	8	4	3b-4	2.4
9	Quarry A	9	5b	4-5b	1.95
10	Quarry A	10	4	5b-4	0.55
11	Quarry A	11	4	4-4	?
12	Quarry B	1	5b	/	?
13	Quarry B	2	1a	5b-1a	0.1
14	Quarry B	3	2a	1a-2a	2.15
15	Quarry B	4	3a	2a-3a	0.35
16	Quarry B	5	3a	3a-3a	0.5
17	Quarry B	6	4	3a-4	0.9
18	Quarry B	7	5b	4-5b	0.75
19	Quarry B	8	5b	5b-5b	0.05
20	Quarry B	9	5b	5b-5b	0.9
21	Quarry B	10	4	5b-4	0.4
22	Quarry B	11	4	4-4	0.6
23	Quarry B	12	4	4-4	0.55
24	Quarry B	13	4	4-4	1.05
25	Quarry B	14	5b	4-5b	1.75
26	Quarry B	15	5b	5b-5b	0.4
27	Quarry B	16	1a	5b-1a	0.1
28	Quarry B	17	2a	1a-2a	?
29	BH1	82	5b	/	0.75
30	BH1	81	5b	5b-5b	0.55
31	BH1	80	5b	5b-5b	0.5
32	BH1	79	5b	5b-5b	1.05
33	BH1	78	4	5b-4	0.55
34	BH1	77	4	4-4	0.5
35	BH1	75	4	4-4	0.6
36	BH1	76	4	4-4	1.2
37	BH1	74	5a	4-5a	0.9
38	BH1	73	5b	5a-5b	0.6
39	BH1	72	5b	5b-5b	0.75
40	BH1	71	5b	5b-5b	3.95
41	BH1	70	5b	5b-5b	0.65
42	BH1	69	5b	5b-5b	0.45
43	BH1	68	5b	5b-5b	0.45
44	BH1	67	5b	5b-5b	0.45
45	BH1	66	5b	5b-5b	0.6
46	BH1	65	5b	5b-5b	0.45
47	BH1	64	5b	5b-5b	0.45
48	BH1	63	4	5b-4	0.3
49	BH1	62	4	4-4	0.3
50	BH1	61	5b	4-5b	0.9

ID	Log	Bed	facies	transition	Thickness m
51	BH1	60	5b	5b-5b	1.6
52	BH1	59	5b	5b-5b	0.9
53	BH1	58	5b	5b-5b	0.35
54	BH1	57	5a	5b-5a	1.35
55	BH1	56	5a	5a-5a	1.45
56	BH1	55	5b	5a-5b	0.45
57	BH1	54	5b	5b-5b	0.45
58	BH1	53	5b	5b-5b	0.6
59	BH1	52	5b	5b-5b	0.6
60	BH1	51	5b	5b-5b	1.5
61	BH1	50	5b	5b-5b	0.3
62	BH1	49	4	5b-4	0.6
63	BH1	48	3b	4-3b	0.6
64	BH1	47	5a	3b-5a	1.2
65	BH1	46	3b	5a-3b	0.3
66	BH1	45	4	3b-4	0.3
67	BH1	44	5a	4-5a	0.45
68	BH1	43	4	5a-4	0.25
69	BH1	42	3b	4-3b	0.6
70	BH1	41	4	3b-4	0.45
71	BH1	40	3b	4-3b	1.00
72	BH1	39	5b	3b-5b	0.9
73	BH1	38	1b	5b-1b	0.6
74	BH1	37	1a	1b-1a	1.1
75	BH1	36	2a	1a-2a	0.85
76	BH1	35	3a	2a-3a	0.6
77	BH1	34	5b	3a-5b	0.3
78	BH1	33	1a	5b-1a	0.2
79	BH1	32	2a	1a-2a	0.7
80	BH1	31	3b	2a-3b	0.8
81	BH1	30	5a	3b-5a	1.1
82	BH1	29	5b	5a-5b	0.8
83	BH1	28	5b	5b-5b	0.6
84	BH1	27	5b	5b-5b	0.4
85	BH1	26	1a	5b-1a	0.4
86	BH1	25	2a	1a-2a	3.6
87	BH1	24	3a	2a-3a	5.5
88	BH1	23	3b	3a-3b	0.6
89	BH1	22	5b	3b-5b	0.6
90	BH1	21	4	5b-4	2.95
91	BH1	20	5b	4-5b	3.00
92	BH1	19	1a	5b-1a	0.15
93	BH1	18	2a	1a-2a	0.3
94	BH1	17	2b	2a-2b	1.45
95	BH1	16	5b	2b-5b	0.6
96	BH1	15	5b	5b-5b	0.5
97	BH1	14	1b	5b-1b	0.3
98	BH1	13	4	1b-4	1.1
99	BH1	12	5a	4-5a	0.3
100	BH1	11	5b	5a-5b	0.6

ID	Log	Bed	facies	transition	Thickness m
101	BH1	10	4	5b-4	1.2
102	BH1	9	3b	4-3b	0.55
103	BH1	8	4	3b-4	0.45
104	BH1	7	5b	4-5b	0.3
105	BH1	6	4	5b-4	1.1
106	BH1	5	1a	4-1a	0.15
107	BH1	4	3a	1a-3a	0.2
108	BH1	3	1a	3a-1a	0.15
109	BH1	2	2b	1a-2b	1.40
110	BH1	1	1a	2b-1a	?
111	BH2	199	5b	/	?
112	BH2	198	5b	5b-5b	0.45
113	BH2	197	5a	5b-5a	0.85
114	BH2	196	5b	5a-5b	0.8
115	BH2	195	5b	5b-5b	2.5
116	BH2	194	5b	5b-5b	3.1
117	BH2	193	5b	5b-5b	1.65
118	BH2	192	5b	5b-5b	1.35
119	BH2	191	5b	5b-5b	0.6
120	BH2	190	5b	5b-5b	0.8
121	BH2	189	5b	5b-5b	0.7
122	BH2	188	5b	5b-5b	0.6
123	BH2	187	5b	5b-5b	0.65
124	BH2	186	5b	5b-5b	0.7
125	BH2	185	5b	5b-5b	0.5
126	BH2	184	5b	5b-5b	1.05
127	BH2	183	5b	5b-5b	0.3
128	BH2	182	5b	5b-5b	0.5
129	BH2	181	5b	5b-5b	1.95
130	BH2	180	5b	5b-5b	1.1
131	BH2	179	5b	5b-5b	0.85
132	BH2	178	5a	5b-5a	0.65
133	BH2	177	1b	5a-1b	0.4
134	BH2	176	4	1b-4	0.7
135	BH2	175	4	4-4	0.5
136	BH2	174	5a	4-5a	0.45
137	BH2	173	5b	5a-5b	0.35
138	BH2	172	5a	5b-5a	1.5
139	BH2	171	5b	5a-5b	1.9
140	BH2	170	5b	5b-5b	0.65
141	BH2	169	5b	5b-5b	2.85
142	BH2	168	5b	5b-5b	0.75
143	BH2	167	5b	5b-5b	0.25
144	BH2	166	5b	5b-5b	0.2
145	BH2	165	5b	5b-5b	0.2
146	BH2	164	5b	5b-5b	0.2
147	BH2	163	5b	5b-5b	0.4
148	BH2	162	3b	5b-3b	1.9
149	BH2	161	5b	3b-5b	0.4
150	BH2	160	1b	5b-1b	0.05

ID	Log	Bed	facies	transition	Thickness m
151	BH2	159	3b	1b-3b	0.95
152	BH2	158	1b	3b-1b	0.01
153	BH2	157	3b	1b-3b	1.2
154	BH2	156	5b	3b-5b	0.05
155	BH2	155	3b	5b-3b	0.4
156	BH2	154	4	3b-4	0.45
157	BH2	153	5a	4-5a	0.55
158	BH2	152	5b	5a-5b	0.85
159	BH2	151	5b	5b-5b	0.75
160	BH2	150	5b	5b-5b	1.2
161	BH2	149	5b	5b-5b	0.2
162	BH2	148	5b	5b-5b	1.25
163	BH2	147	5b	5b-5b	1.3
164	BH2	146	5b	5b-5b	1.0
165	BH2	145	5b	5b-5b	0.2
166	BH2	144	5b	5b-5b	0.6
167	BH2	143	5b	5b-5b	0.6
168	BH2	142	5b	5b-5b	0.75
169	BH2	141	5b	5b-5b	0.65
170	BH2	140	5b	5b-5b	0.4
171	BH2	139	5b	5b-5b	0.2
172	BH2	138	5b	5b-5b	0.4
173	BH2	137	5b	5b-5b	2.4
174	BH2	136	5b	5b-5b	0.3
175	BH2	135	5b	5b-5b	0.25
176	BH2	134	2b	5b-2b	0.3
177	BH2	133	5b	2b-5b	0.05
178	BH2	132	5a	5b-5a	0.1
179	BH2	131	4	5a-4	0.3
180	BH2	130	4	4-4	0.55
181	BH2	129	5b	4-5b	0.25
182	BH2	128	4	5b-4	0.15
183	BH2	127	3b	4-3b	0.4
184	BH2	126	3b	3b-3b	0.3
185	BH2	125	4	3b-4	0.35
186	BH2	124	3b	4-3b	0.25
187	BH2	123	3b	3b-3b	0.2
188	BH2	122	3b	3b-3b	0.75
189	BH2	121	3b	3b-3b	0.4
190	BH2	120	5b	3b-5b	1.4
191	BH2	119	5b	5b-5b	0.2
192	BH2	118	5b	5b-5b	2.05
193	BH2	117	5b	5b-5b	1.40
194	BH2	116	1a	5b-1a	0.35
195	BH2	115	2b	1a-2b	0.25
196	BH2	114	3a	2b-3a	0.15
197	BH2	113	1a	3a-1a	0.05
198	BH2	112	2a	1a-2a	0.05
199	BH2	111	3a	2a-3a	0.05
200	BH2	110	3a	3a-3a	0.10

ID	Log	Bed	facies	transition	Thickness m
201	BH2	109	1a	3a-1a	0.15
202	BH2	108	2b	1a-2b	0.10
203	BH2	107	1a	2b-1a	0.13
204	BH2	106	3b	1a-3b	0.4
205	BH2	105	4	3b-4	0.5
206	BH2	104	4	4-4	0.05
207	BH2	103	4	4-4	0.05
208	BH2	102	4	4-4	0.15
209	BH2	101	3b	4-3b	0.4
210	BH2	100	5b	3b-5b	0.2
211	BH2	99	3b	5b-3b	0.3
212	BH2	98	4	3b-4	0.05
213	BH2	97	4	4-4	0.2
214	BH2	96	5b	4-5b	0.5
215	BH2	95	5b	5b-5b	0.2
216	BH2	94	5b	5b-5b	0.4
217	BH2	93	5b	5b-5b	0.55
218	BH2	92	4	5b-4	0.1
219	BH2	91	5b	4-5b	0.6
220	BH2	90	3b	5b-3b	0.05
221	BH2	89	5b	3b-5b	0.15
222	BH2	88	3b	5b-3b	0.05
223	BH2	87	3b	3b-3b	0.3
224	BH2	86	5b	3b-5b	0.85
225	BH2	85	3b	5b-3b	0.1
226	BH2	84	5b	3b-5b	0.55
227	BH2	83	3b	5b-3b	0.2
228	BH2	82	5b	3b-5b	0.4
229	BH2	81	5b	5b-5b	0.1
230	BH2	80	4	5b-4	0.2
231	BH2	79	4	4-4	0.3
232	BH2	78	4	4-4	0.6
233	BH2	77	3a	4-3a	0.35
234	BH2	76	3a	3a-3a	0.1
235	BH2	75	5b	3a-5b	1.05
236	BH2	74	5b	5b-5b	1.05
237	BH2	73	4	5b-4	0.2
238	BH2	72	5b	4-5b	0.1
239	BH2	71	5b	5b-5b	0.6
240	BH2	70	5b	5b-5b	0.75
241	BH2	69	5b	5b-5b	0.45
242	BH2	68	5b	5b-5b	0.25
243	BH2	67	5b	5b-5b	0.2
244	BH2	66	4	5b-4	0.1
245	BH2	65	5b	4-5b	0.95
246	BH2	64	5b	5b-5b	0.6
247	BH2	63	4	5b-4	0.2
248	BH2	62	1b	4-1b	0.8
249	BH2	61	4	1b-4	0.2
250	BH2	60	5b	4-5b	0.3

ID	Log	Bed	facies	transition	Thickness m
251	BH2	59	5b	5b-5b	0.3
252	BH2	58	4	5b-4	0.1
253	BH2	57	4	4-4	0.6
254	BH2	56	5b	4-5b	0.1
255	BH2	55	4	5b-4	0.3
256	BH2	54	5b	4-5b	0.1
257	BH2	53	4	5b-4	0.05
258	BH2	52	4	4-4	0.2
259	BH2	51	5b	4-5b	0.3
260	BH2	50	5b	5b-5b	0.25
261	BH2	49	1a	5b-1a	0.8
262	BH2	48	2a	1a-2a	0.12
263	BH2	47	1a	2a-1a	0.05
264	BH2	46	2a	1a-2a	0.15
265	BH2	45	2a	2a-2a	0.3
266	BH2	44	2b	2a-2b	0.6
267	BH2	43	3a	2b-3a	0.1
268	BH2	42	2a	3a-2a	0.3
269	BH2	41	3a	2a-3a	0.6
270	BH2	40	3a	3a-3a	0.1
271	BH2	39	2b	3a-2b	0.3
272	BH2	38	3b	2b-3b	0.35
273	BH2	37	3b	3b-3b	0.2
274	BH2	36	3b	3b-3b	0.9
275	BH2	35	3b	3b-3b	0.2
276	BH2	34	5b	3b-5b	0.45
277	BH2	33	4	5b-4	0.1
278	BH2	32	3b	4-3b	0.45
279	BH2	31	3b	3b-3b	0.55
280	BH2	30	5b	3b-5b	0.5
281	BH2	29	5b	5b-5b	0.15
282	BH2	28	3b	5b-3b	0.35
283	BH2	27	5b	3b-5b	0.25
284	BH2	26	1a	5b-1a	0.15
285	BH2	25	2a	1a-2a	0.2
286	BH2	24	2a	2a-2a	0.95
287	BH2	23	3a	2a-3a	0.05
288	BH2	22	2a	3a-2a	0.3
289	BH2	21	3a	2a-3a	0.15
290	BH2	20	2a	3a-2a	0.3
291	BH2	19	3a	2a-3a	0.1
292	BH2	18	3a	3a-3a	0.45
293	BH2	17	3a	3a-3a	0.45
294	BH2	16	3a	3a-3a	0.15
295	BH2	15	3a	3a-3a	0.65
296	BH2	14	3b	3a-3b	0.2
297	BH2	13	3b	3b-3b	0.1
298	BH2	12	3b	3b-3b	0.65
299	BH2	11	3b	3b-3b	0.2
300	BH2	10	3b	3b-3b	0.1

ID	Log	Bed	facies	transition	Thickness m
301	BH2	9	3b	3b-3b	0.15
302	BH2	8	3b	3b-3b	0.15
303	BH2	7	5b	3b-5b	0.45
304	BH2	6	3b	5b-3b	0.45
305	BH2	5	3b	3b-3b	0.35
306	BH2	4	3b	3b-3b	0.25
307	BH2	3	3b	3b-3b	0.15
308	BH2	2	3b	3b-3b	0.4
309	BH2	1	5b	3b-5b	?
310	Targrove	1	2c	/	(2.25)
311	Targrove	2	1a	2c-1a	0.4
312	Targrove	3	1c	1a-1c	0.2
313	Targrove	4	2d	1c-2d	0.1
314	Targrove	5	3c	2d-3c	0.2
315	Targrove	6	2d	3c-2d	0.1
316	Targrove	7	3c	2d-3c	0.2
317	Targrove	8	2d	3c-2d	0.1
318	Targrove	9	3c	2d-3c	0.2
319	Targrove	10	2d	3c-2d	0.1
320	Targrove	11	3c	2d-3c	0.2
321	Targrove	12	2d	3c-2d	0.2
322	Targrove	13	1a	2d-1a	0.5
323	Targrove	14	1b	1a-1b	0.5
324	Targrove	15	2c	1b-2c	2.5
325	Targrove	16	2c	2c-2c	0.7
326	Targrove	17	2d	2c-2d	0.1
327	Targrove	18	3c	2d-3c	0.2
328	Targrove	19	2d	3c-2d	0.15
329	Targrove	20	1b	2d-1b	0.6
330	Targrove	21	2d	1b-2d	0.1
331	Targrove	22	3c	2d-3c	0.15
332	Targrove	23	2d	3c-2d	0.1
333	Targrove	24	2c	2d-2c	0.24
334	Targrove	25	2c	2c-2c	0.16
335	Targrove	26	1b	2c-1b	0.25
336	Targrove	27	2c	1b-2c	? (0.8)

APPENDIX VII: TREDOMEN QUARRY AND TARGROVE QUARRY

SEDIMENTOLOGICAL ANALYSIS

a: *Sedimentary analysis of Tredomen Quarry* .....pVII-2 to pVII-12

b: *Sedimentary analysis of Targrove Quarry*.....pVII-13 to pVII-17

APPENDIX VII - SEDIMENTARY ANALYSIS OF TREDOMEN QUARRY SEQUENCE
LITHOFACIES OCCURRENCES

Lithofacies occurrence at Tredomen Quarry by number of beds (green = reduced green lithofacies, orange = oxidised red lithofacies).

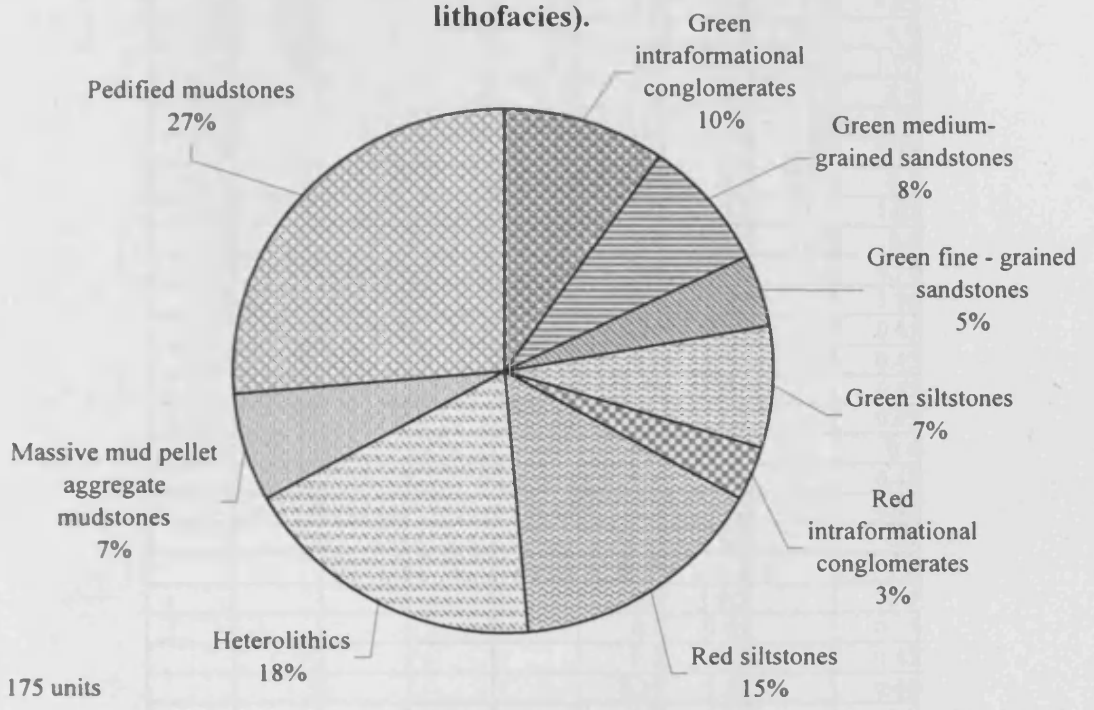

r	Green intraformational conglomerates	17
r	Green medium- grained sandstones	14
r	Green fine - grained sandstones	8
r	Green siltstones	13
o	Red intraformational conglomerates	6
o	Red siltstones	27
o	Heterolithics	32
o	Massive mud pellet aggregate mudstones	12
o	Pedified mudstones	46

(based on where lithology changes). 175

APPENDIX VII - SEDIMENTARY ANALYSIS OF TREDOMEN QUARRY SEQUENCE
LITHOFACIES OCCURRENCE BY THICKNESS (in m)

1a	1b	2a	2b	3a	3b	4	5a	5b
0.15	0.6	1.4	0.95	0.85	0.35	2.4	0.9	0.7
0.1	0.3	2.15	1.45	0.35	0.6	0.55	1.35	1.95
0.1	0.4	0.85	1.4	0.5	0.3	0.9	1.45	0.75
1.1	0.05	0.7	0.3	0.6	0.6	0.4	1.2	0.05
0.2	0.01	3.6	0.25	5.5	1	0.6	0.45	0.9
0.4	0.8	0.3	0.1	0.2	0.8	0.55	1.1	1.75
0.15		0.05	0.6	0.15	0.6	1.05	0.3	0.4
0.15		0.12	0.3	0.05	0.55	0.55	0.85	0.75
0.15		0.15		0.1	1.9	0.5	0.65	0.55
0.35		0.3		0.35	0.95	0.3	0.45	0.5
0.05		0.3		0.1	1.2	0.3	1.5	1.05
0.15		0.2		0.1	0.4	0.6	0.55	0.6
0.13		0.95		0.6	0.4	0.3	0.1	0.75
0.8		0.3		0.1	0.3	0.25		3.95
0.05		0.3		0.05	0.25	0.45		0.65
0.15				0.15	0.2	2.95		0.45
				0.1	0.75	1.1		0.45
				0.45	0.4	1.2		0.45
				0.45	0.4	0.45		0.6
				0.15	0.4	0.6		0.45
				0.65	0.3	1.2		0.45
					0.05	1.1		0.9
					0.05	0.7		1.6
					0.3	0.5		0.9
					0.1	0.45		0.35
					0.2	0.3		0.45
					0.35	0.55		0.45
					0.2	0.15		0.6
					0.9	0.35		0.6
					0.2	0.5		1.5
					0.45	0.05		0.3
					0.55	0.05		0.9
					0.35	0.15		0.3
					0.2	0.05		0.8
					0.1	0.2		0.6
					0.65	0.1		0.4
					0.2	0.2		0.6
					0.1	0.3		3
					0.15	0.6		0.6
					0.15	0.2		0.5
					0.45	0.1		0.6
					0.35	0.2		0.3
					0.25	0.2		0.45
					0.15	0.1		0.8
					0.4	0.6		2.5
						0.3		3.1
						0.05		1.65
						0.2		1.35
						0.1		0.6
								0.8
								0.7
								0.6
								0.65
								0.7
								0.5
								1.05
								0.3
								0.5

APPENDIX VII - SEDIMENTARY ANALYSIS OF TREDOMEN QUARRY SEQUENCE
LITHOFACIES OCCURRENCE BY THICKNESS (in m) (continued)

1a	1b	2a	2b	3a	3b	4	5a	5b
								1.95
								1.1
								0.85
								0.35
								1.9
								0.65
								2.85
								0.75
								0.25
								0.2
								0.2
								0.2
								0.4
								0.4
								0.05
								0.85
								0.75
								1.2
								0.2
								1.25
								1.3
								1
								0.2
								0.6
								0.6
								0.75
								0.65
								0.4
								0.2
								0.4
								2.4
								0.3
								0.25
								0.05
								0.25
								1.4
								0.2
								2.05
								1.4
								0.2
								0.5
								0.2
								0.4
								0.55
								0.6
								0.15
								0.85
								0.55
								0.4
								0.1
								1.05
								1.05
								0.1
								0.6
								0.75
								0.45
								0.25
								0.2

APPENDIX VII - SEDIMENTARY ANALYSIS OF TREDOMEN QUARRY SEQUENCE
LITHOFACIES OCCURRENCE BY THICKNESS (in m) (continued)

1a	1b	2a	2b	3a	3b	4	5a	5b
								0.95
								0.6
								0.3
								0.3
								0.1
								0.1
								0.3
								0.25
								0.45
								0.5
								0.15
								0.25
								0.45

Number of beds	16	6	15	8	21	45	49	13	129	Total 302
Thickness total	4.18	2.16	11.67	5.35	11.55	19.5	33.55	10.85	95.05	193.9
Average thickness	0.26	0.36	0.78	0.67	0.55	0.43	0.66	0.83	0.74	
Min	0.05	0.01	0.05	0.10	0.05	0.05	0.05	0.10	0.05	
Max	1.1	0.8	3.6	1.45	5.5	1.9	4	1.5	3.95	

(based on total number of beds minus the upper and lower unit thickness).

Lithofacies occurrence at Tredomen Quarry by bed thickness (green = reduced green lithofacies, orange = oxidised red lithofacies).

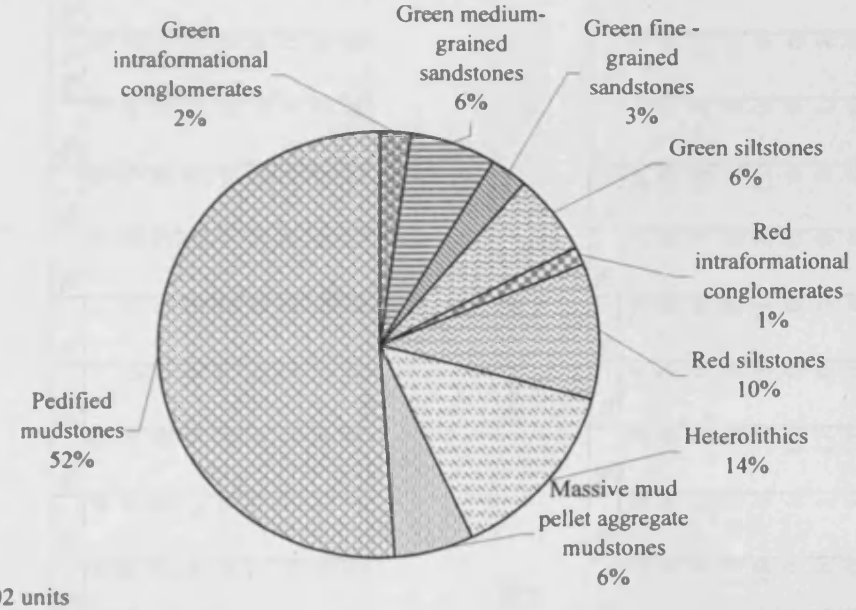

		Thickness in m
r	Green intraformational conglomerates	4.18
r	Green medium- grained sandstones	11.67
r	Green fine - grained sandstones	5.35
r	Green siltstones	11.55
o	Red intraformational conglomerates	2.16
o	Red siltstones	19.5
o	Heterolithics	25.55
o	Massive mud pellet aggregate mudstones	10.85
o	Pedified mudstones	95.05

APPENDIX VII - SEDIMENTARY ANALYSIS OF TREDOMEN QUARRY SEQUENCE
LITHOFACIES BOUNDARIES by percentage

UPPER BOUNDARIES (Facies 1a-?)

FROM \ TO	1a	%	1b	%	2a	%	2b	%	3a	%	3b	%	4	%	5a	%	5b	5b%	Row total	
1a	0	0	0	0	11	1	3	0	1	0	1	0	0	0	0	0	0	0	16	9
1b	1	0	0	0	0	0	0	0	0	0	2	0	3	1	0	0	0	0	6	4
2a	1	0	0	0	0	0	3	0	8	1	1	0	0	0	0	0	0	0	13	8
2b	2	0	0	0	0	0	0	0	3	0	1	0	0	0	0	0	2	0	8	5
3a	3	0	0	0	3	0	1	0	0	0	3	0	1	0	0	0	2	0	13	8
3b	0	0	1	0	0	0	0	0	0	0	0	0	8	0	2	0	16	1	27	16
4	1	0	1	0	0	0	0	0	1	0	8	0	0	0	5	0	15	0	31	18
5	0	0	1	0	0	0	0	0	0	0	1	0	2	0	0	0	8	1	12	7
5b	9	0	3	0	0	0	1	0	0	0	9	0	18	0	5	0	0	0	45	26
																			171	

(based on where lithologies change and removing the upper and lower boundaries)

LOWER BOUNDARIES (Facies ?-1a)

FROM \ TO	1a	%	1b	%	2a	%	2b	%	3a	%	3b	%	4	%	5a	%	5b	%	
1a	0	0	0	0	11	79	3	38	1	8	1	4	0	0	0	0	0	0	16
1b	1	6	0	0	0	0	0	0	0	0	2	8	3	94	0	0	0	0	6
2a	1	6	0	0	0	0	3	38	8	62	1	4	0	0	0	0	0	0	13
2b	2	12	0	0	0	0	0	0	3	23	1	4	0	0	0	0	2	5	8
3a	3	18	0	0	3	21	1	13	0	0	3	12	1	3	0	0	2	5	13
3b	0	0	1	17	0	0	0	0	0	0	0	0	8	25	2	17	16	37	27
4	1	6	1	17	0	0	0	0	1	8	8	31	0	0	5	42	15	35	31
5a	0	0	1	17	0	0	0	0	0	0	1	4	2	6	0	0	8	19	12
5b	9	53	3	50	0	0	1	13	0	0	9	35	18	56	5	42	0	0	45
Column total	17		6		14		8		13		26		32		12		43		
																	171		

(based on where lithologies change and removing the upper and lower boundaries

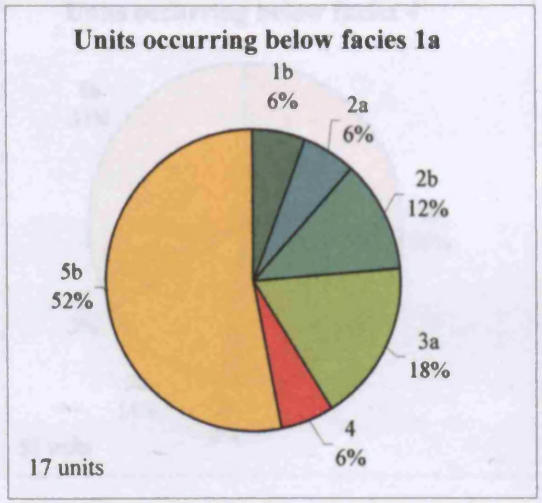
Units occurring below facies 1a
1b 6%
2a 6%
2b 12%
3a 18%
4 6%
5b 52%
17 units

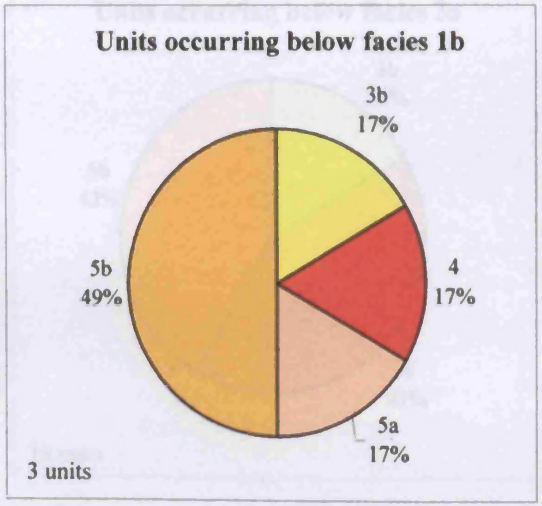
Units occurring below facies 1b
3b 17%
4 17%
5a 17%
5b 49%
3 units

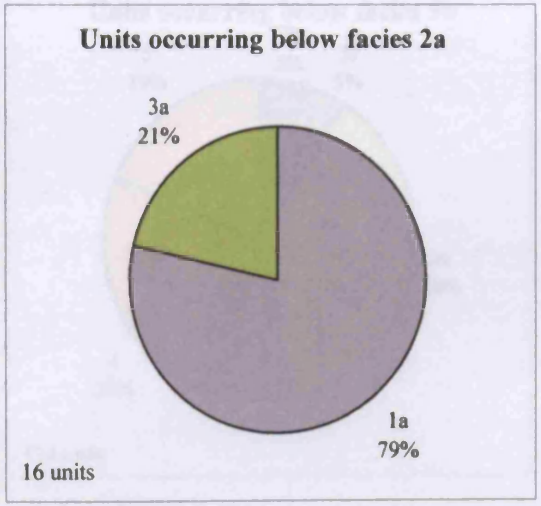
Units occurring below facies 2a
3a 21%
1a 79%
16 units

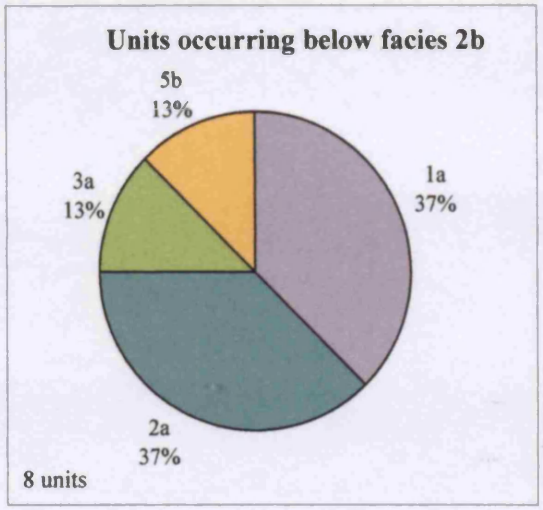
Units occurring below facies 2b
5b 13%
1a 37%
3a 13%
2a 37%
8 units

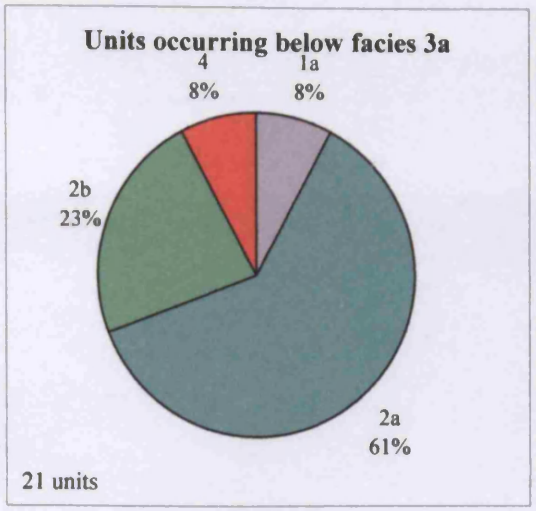
Units occurring below facies 3a
4 8%
1a 8%
2b 23%
2a 61%
21 units

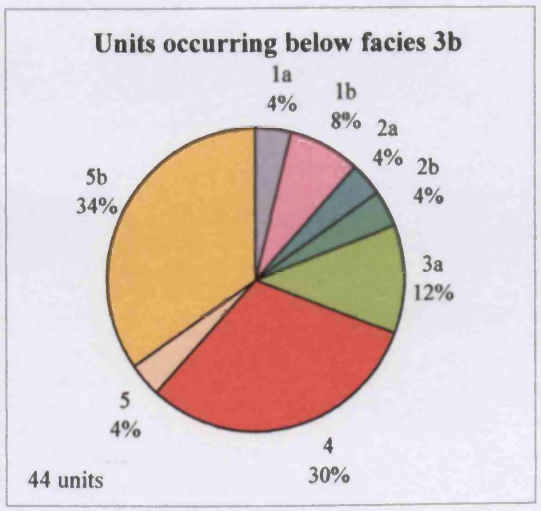
Units occurring below facies 3b
1a 4%
1b 8%
2a 4%
2b 4%
5b 34%
3a 12%
5 4%
4 30%
44 units

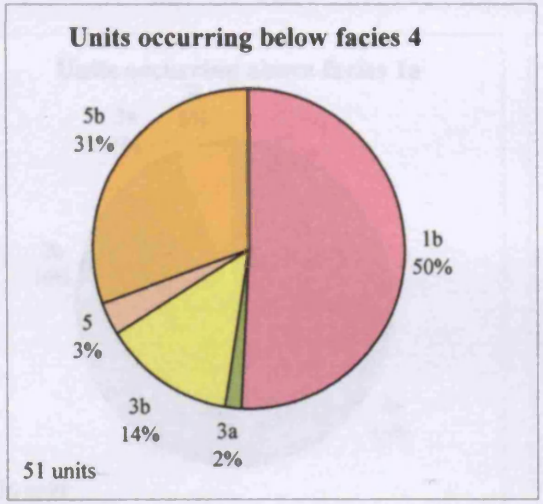
Units occurring below facies 4
5b
31%
1b
50%
5
3%
3b
14%
3a
2%
51 units

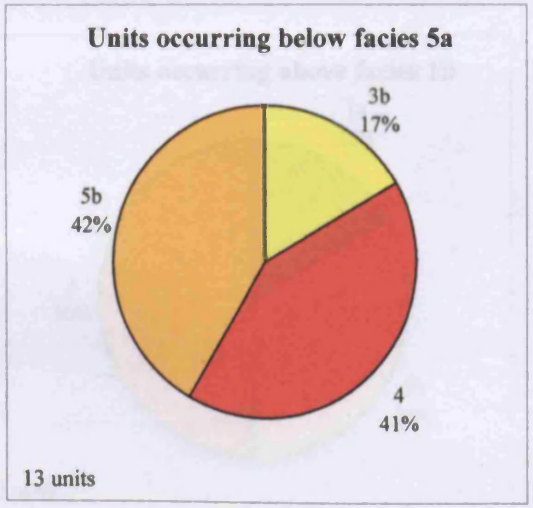
Units occurring below facies 5a
3b
17%
5b
42%
4
41%
13 units

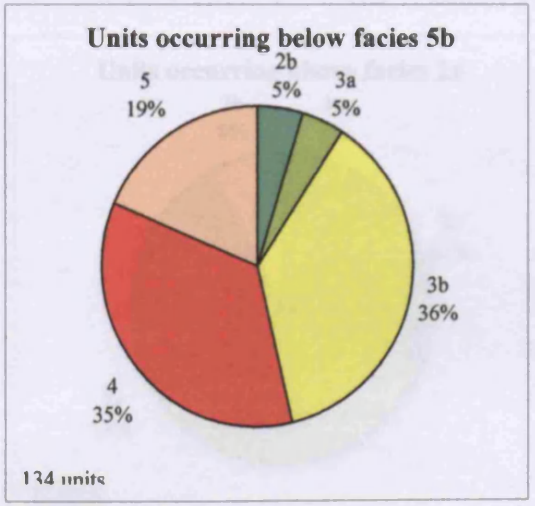
Units occurring below facies 5b
2b
5%
3a
5%
5
19%
3b
36%
4
35%
134 units

Units occurring above facies 1a

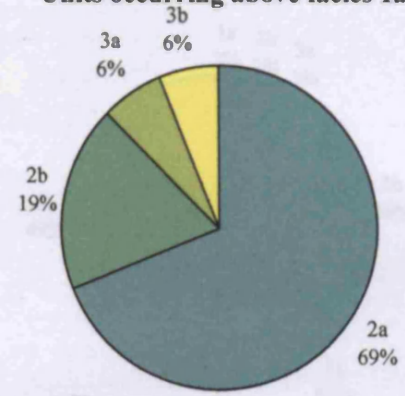

16 units

Units occurring above facies 1b

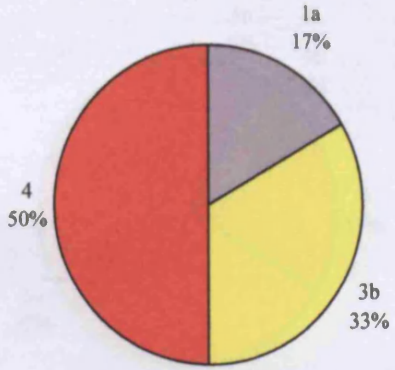

3 units

Units occurring above facies 2a

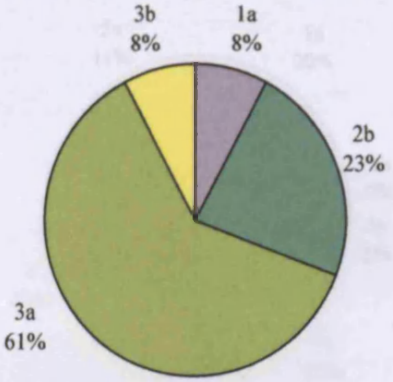

15 units

Units occurring above facies 2b

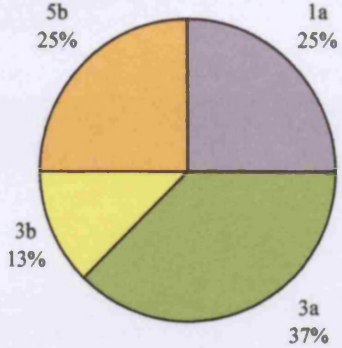

8 units

Units occurring above facies 3a

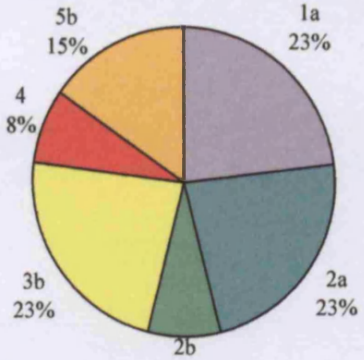

21 units

Units occurring above facies 3b

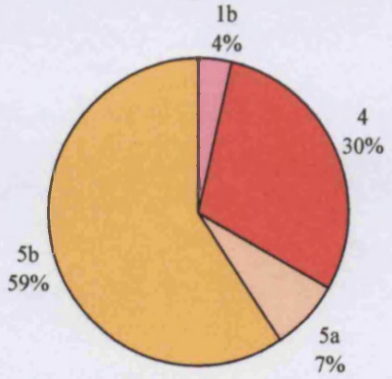

45 units

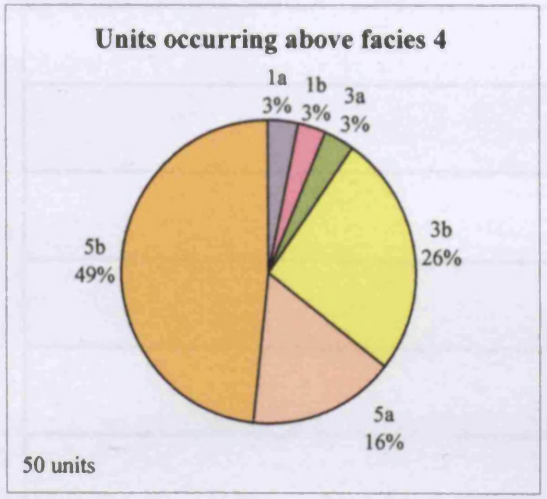
Units occurring above facies 4
1a 3%
1b 3%
3a 3%
3b 26%
5a 16%
5b 49%
50 units

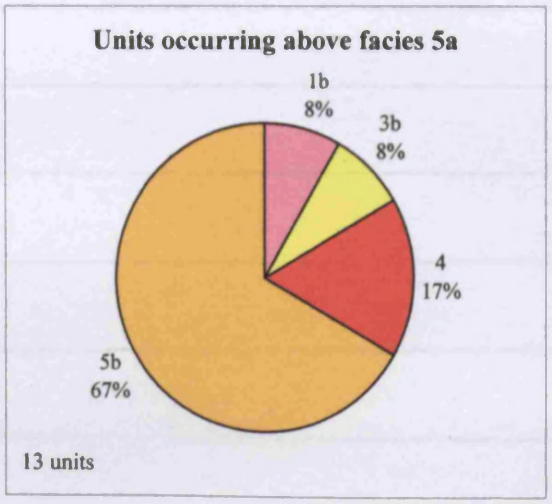
Units occurring above facies 5a
1b 8%
3b 8%
4 17%
5b 67%
13 units

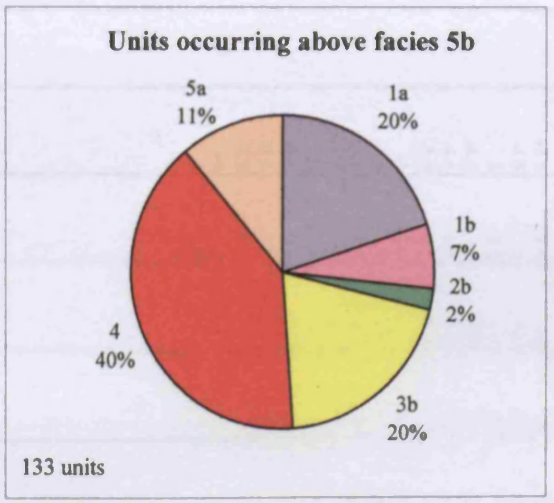
Units occurring above facies 5b
5a 11%
1a 20%
1b 7%
2b 2%
4 40%
3b 20%
133 units

APPENDIX VII - SEDIMENTARY ANALYSIS OF TREDOMEN QUARRY SEQUENCE
CLAST SIZE ANALYSIS

Facies	1a		1b		2a	2b	3a	3b	4	5a	5b	6
	clasts	matrix	clasts	matrix								
	-3.5	1.5	-4	2.5	0.5	1.5	1.5	2.5	2.5		8	6
	-4.5	2	-4	1.5	1.5	2.5	2	2.5	1.5		4.5	6
	-3	2.5	-4	1.5	2	1	2.5	4	3		4.5	-3.5
	-4.5	2	-3	1.5	1.5	2.5	4.5	2.5	2.5		4	6
	-4.5	2.5	-3	1.5	2	3.5	2.5	3.5	1.5		4	6
	-3.5	2.5	-2	1	2	0.5	4.5	2.5	0.5		6	6
	-4	1.5			1.5	4	6	4	1.5		8	-3.5
	-3.5	1.5			0.5	4	6	2.5	0.5		4.5	6
	-3.5	1.5			2.5		3.5	2.5	2.5		8	4
	-3.5	2			4		3.5	4	4.5		6	6
	-5	2			4		3.5	4	2.5		6	8
	-3.5	2.5			4		6	4	3		3.5	8
	-3.5	3.5			0		4	2.5	2		4.5	8
	-3.5	3.5			1		6	3.5	1.5			6
	-4	1.5			2		8	4	1.5			6
	-4	1.5			2		2.5	6	1			6
	-5	1.5					2	4	2			4.5
							3	6	4.5			6
							3.5	4.5	4			6
							3	3.5	2			6
							4	3.5	2			4.5
								4	1.5			4.5
								4	1			4.5
								4.5	1.5			4.5
								3.5	3			4.5
								3.5	6			4.5
								6	3			4.5
								6	6			4.5
								6	3.5			4.5
								6	3.5			4.5
								6	3.5			4.5
								6	3.5			4.5
								6	6			4.5
								4.5	6			4.5
								6	6			2.5
								6	0.5			4.5
								6	3.5			6
								4.5	3.5			6
								6	3.5			6
								4.5	3.5			3.5
								6	3.5			6
								4	4.5			3.5
								4	6			3.5
								4	0			6
								4	6			6
									0.5			4.5
									4			4.5
									4			4.5
									4			4.5
									6			4.5
									6			4.5
												4.5
												4.5
												4.5
												4.5
												4.5
												8
												8
												8
												8
												8
												8
												8
												8
												6
												6
												6
												6
												6
												6
												6

APPENDIX VII - SEDIMENTARY ANALYSIS OF TREDOMEN QUARRY SEQUENCE
CLAST SIZE ANALYSIS (CONTINUED)

Facies	1a		1b		2a	2b	3a	3b	4	5a	5b	6
	clasts	matrix	clasts	matrix								
												6
												6
												6
												4
												6
												6
												6
												6
												6
												6
												6
												8
												8
												8
												8
												4.5
												4.5
												4.5
												4.5
												4.5
												8
												8
												4.5
												3.5
												6
												6
												6
												6
												6
												6
												4
												4
												4
												4
												4.5
												4.5
												4.5
												4.5
												4.5
												4.5
												6
												6
												6
												6
												6
												6
												6
												6
												6
												6
												6
												6
												6
												6
												6
												6
												6
												6
												6
												6
												6
												4.5
No	17	17	6	6	16	8	21	45	52	0	13	135
Average	-3.91	2.09	-3.33	1.58	1.94	2.44	3.90	4.38	3.14		5.50	5.49
Mode	-3.5	1.5	-4	1.5	2	2.5	6	6	6		4.5	6

APPENDIX VII - SEDIMENTARY ANALYSIS OF TARGROVE QUARRY SEQUENCE
LITHOFACIES OCCURRENCES

Facies occurrence at Targrove Quarry (green = reduced lithofacies, orange = oxidised lithofacies).

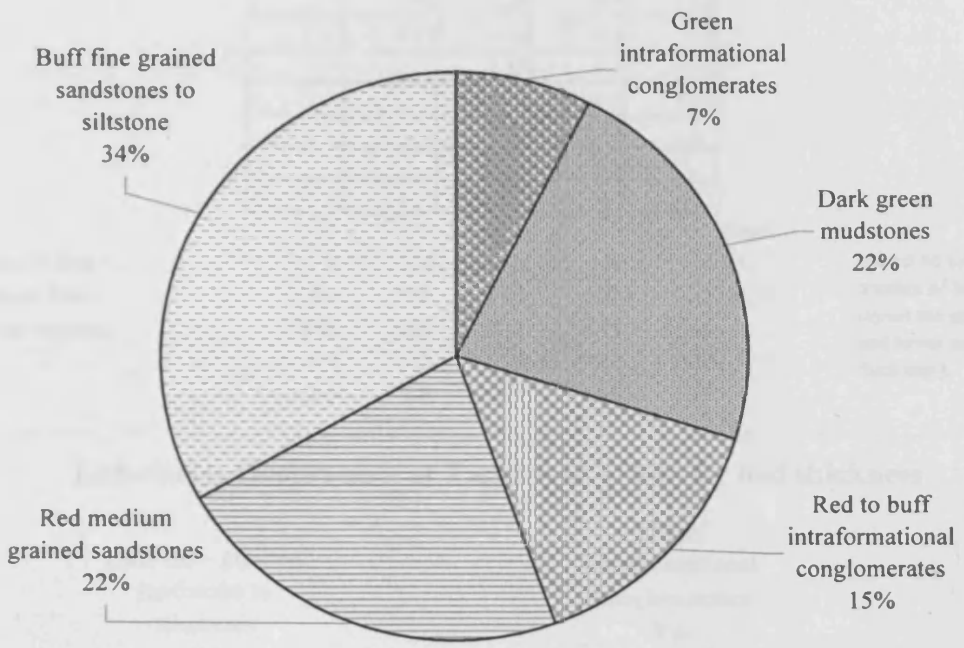

27 units

r	Green intraformational conglomerates	2
r	Dark green mudstones	6
o	Red to buff intraformational conglomerates	4
o	Red medium grained sandstones	6
o	Buff fine grained sandstones to siltstone	9

(based on where lithology changes) 27

APPENDIX VII - SEDIMENTARY ANALYSIS OF TARGROVE QUARRY SEQUENCE
LITHOFACIES OCCURRENCE BY THICKNESS (in m)

1a	1b	2c	3c	5c
0.4	0.2	2.5	0.1	0.2
0.5	0.5	0.7	0.1	0.2
	0.6	0.24	0.1	0.2
	0.25	0.16	0.1	0.2
		2.25	0.2	0.2
		0.8	0.1	0.15
			0.15	
			0.1	
			0.1	

					Total	
Number of beds	2	4	4	9	6	25
Thickness total	0.9	1.55	6.65	1.05	1.15	11.3
Average thickness	0.45	0.39	1.11	0.12	0.19	
Min	0.4	0.2	0.16	0.1	0.15	
Max	0.5	0.6	2.5	0.2	0.2	

(based on total number of beds minus the upper and lower unit thickness).

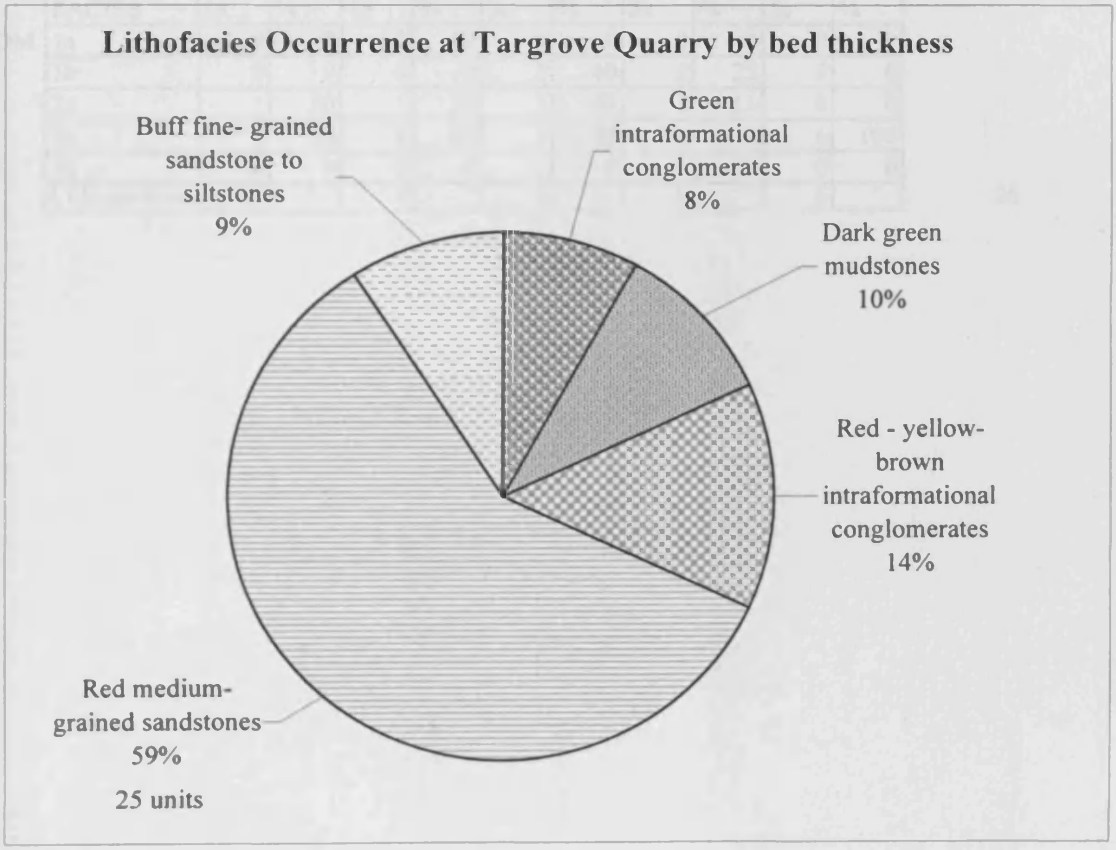

		Thickness in m
r	Green intraformational conglomerates	0.9
r	Dark green mudstones	1.15
o	Red - yellow-brown intraformational conglomerates	1.55
o	Red medium-grained sandstones	6.65
o	Buff fine- grained sandstone to siltstones	1.05

APPENDIX VII - SEDIMENTARY ANALYSIS OF TARGROVE QUARRY SEQUENCE
LITHOFACIES BOUNDARIES

UPPER BOUNDARIES (Facies 1a-?)

	TO											
	FACIES	1a	%	1b	%	2c	%	3c	%	5c	%	Row total
FROM	1a	0	0	2	100	0	0	0	0	0	0	2
	1b	0	0	0	0	2	50	2	50	0	0	4
	2c	1	20	1	20	2	40	1	20	0	0	5
	3c	1	11	1	11	1	11	0	0	6	67	9
	5c	0	0	0	0	0	0	6	100	0	0	6
												26

8
15
19
35
23

(based on where lithologies change and removing the upper and lower boundaries)

LOWER BOUNDARIES (Facies ?-1a)

	TO										
	FACIES	1a	%	1b	%	2c	%	3c	%	5c	%
FROM	1a	0	0	2	50	0	0	0	0	0	0
	1b	0	0	0	0	2	40	2	22	0	0
	2c	1	50	1	25	2	40	1	11	0	0
	3c	1	50	1	25	1	20	0	0	6	100
	5c	0	0	0	0	0	0	6	67	0	0
	Column total	2		4		5		9		6	

26

APPENDIX VII - SEDIMENTARY ANALYSIS OF TARGROVE QUARRY SEQUENCE
LITHOFACIES BOUNDARIES (CONTINUED)

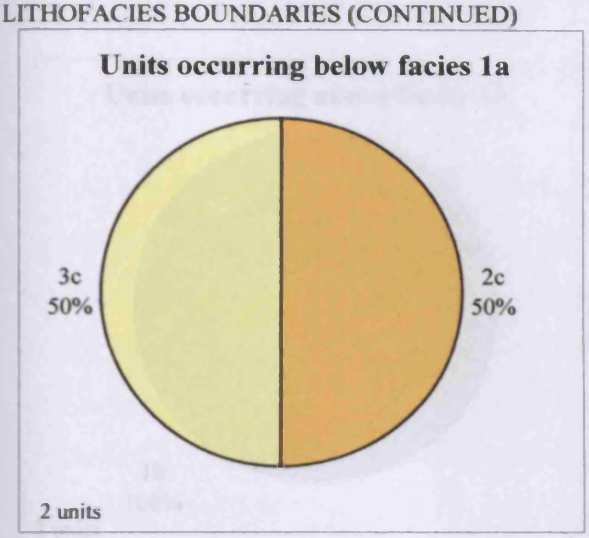

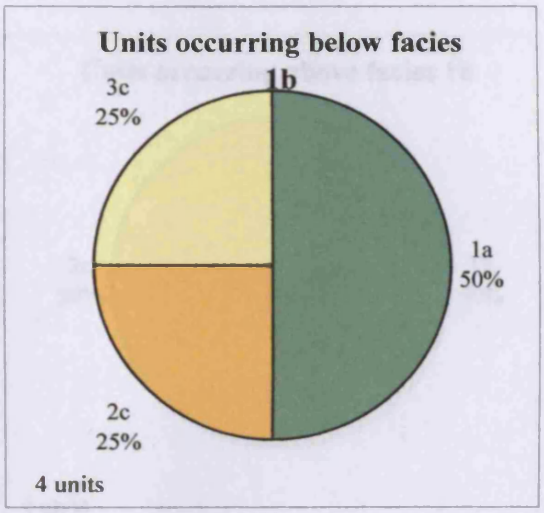

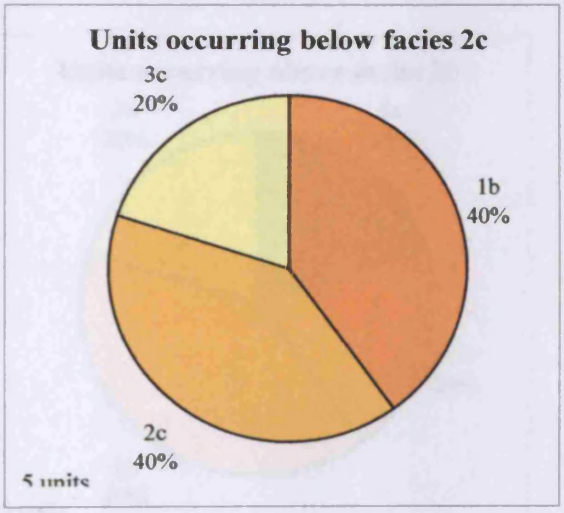

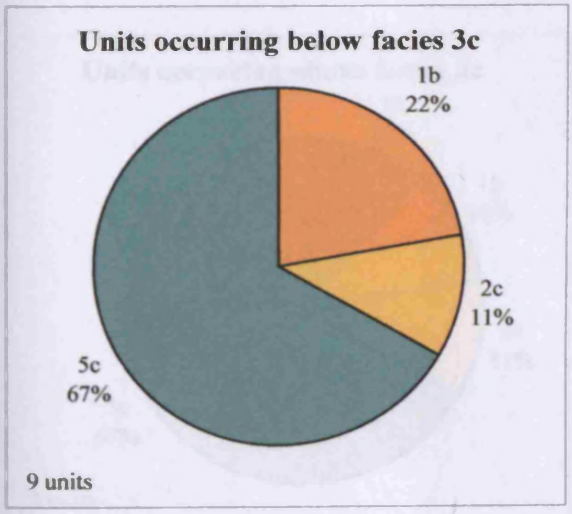

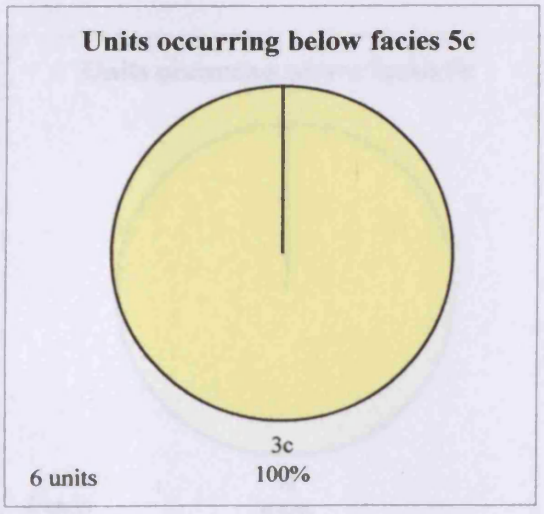

APPENDIX VII - SEDIMENTARY ANALYSIS OF TARGROVE QUARRY SEQUENCE
LITHOFACIES BOUNDARIES (CONTINUED)

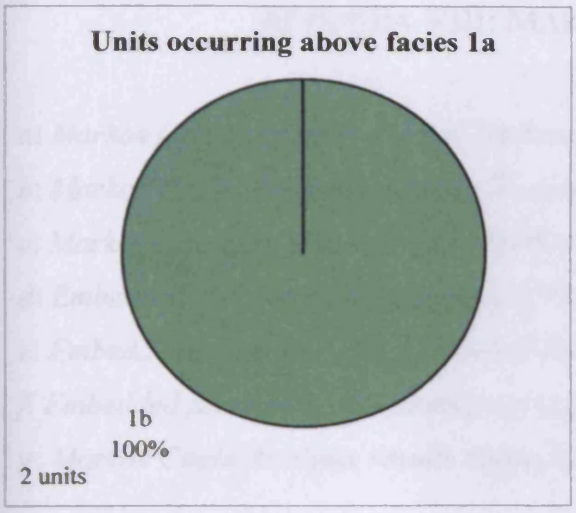

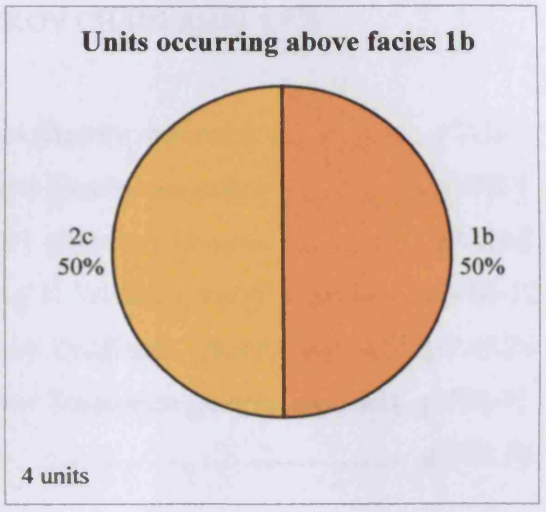

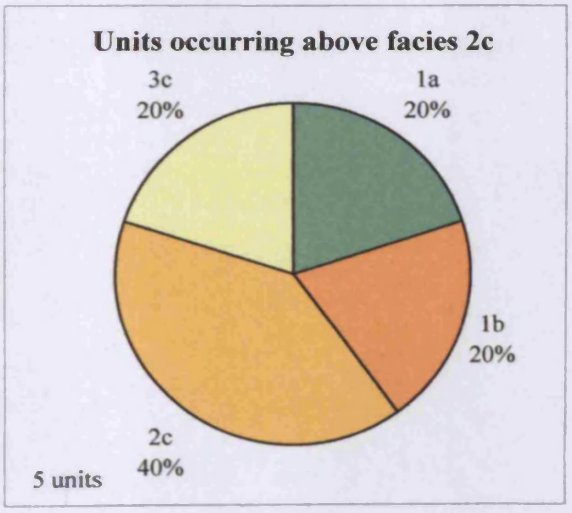

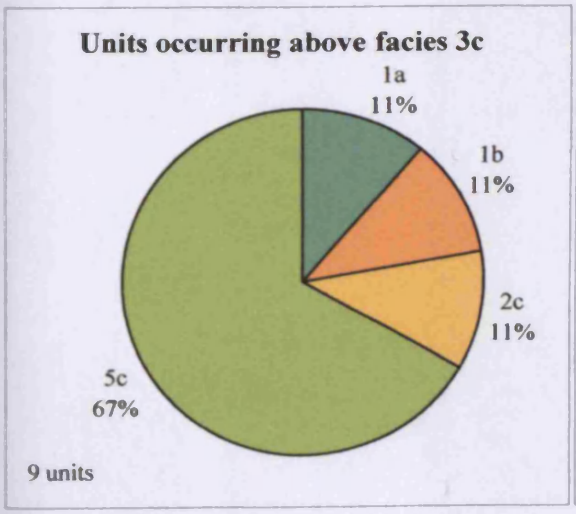

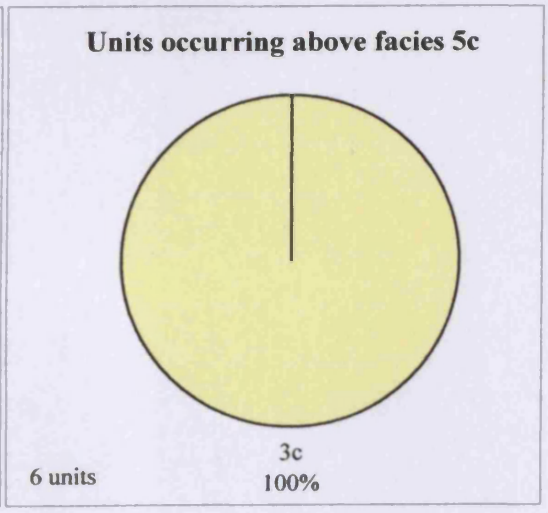

APPENDIX VIII: MARKOV CHAIN ANALYSIS

a: *Markov Chain Analysis of total Tredomen Quarry sequence*.....pVIII-2
b: *Markov Chain Analysis of lower Tredomen Quarry sequence*.....pVIII-5
c: *Markov Chain Analysis of upper Tredomen Quarry sequence*.....pVIII-8
d: *Embedded Markov Chain Analysis of total Tredomen Quarry sequence*...pVIII-12
e: *Embedded Markov Chain Analysis of lower Tredomen Quarry sequence*..pVIII-26
f: *Embedded Markov Chain Analysis of upper Tredomen Quarry sequence*..pVIII-41
g: *Markov Chain Analysis results summary*..... pVIII-53

APPENDIX VIII - MARKOV CHAIN ANALYSIS OF TREDOMEN QUARRY SEQUENCE

Markov Chain Analysis of total Tredomen Quarry sequence, using 10cm intervals

Observed transitions matrix

		TO									
		1a	*1b*	*2a*	*2b*	*3a*	*3b*	*4*	*5a*	*5b*	Row totals
FROM	*1a*	35	0	11	3	1	0	1	0	0	51
	1b	1	20	0	0	0	4	3	1	0	29
	2a	1	0	107	3	8	1	0	0	0	120
	2b	2	0	0	46	3	1	0	0	2	54
	3a	3	0	3	1	52	3	1	0	2	65
	3b	0	2	0	0	0	154	5	2	15	178
	4	1	1	0	0	1	6	225	4	15	253
	5a	0	2	0	0	0	1	1	90	6	100
	5b	9	3	0	1	0	8	18	3	994	1036
Column totals		52	28	121	54	65	178	254	100	1034	1886

Grand total 1886

Number of transitions 1885

Observed transitions matrix as fractions

		TO									
		1a	*1b*	*2a*	*2b*	*3a*	*3b*	*4*	*5a*	*5b*	
FROM	*1a*	0.69	0.00	0.22	0.06	0.02	0.00	0.02	0.00	0.00	1.00
	1b	0.03	0.69	0.00	0.00	0.00	0.14	0.10	0.03	0.00	1.00
	2a	0.01	0.00	0.89	0.03	0.07	0.01	0.00	0.00	0.00	1.00
	2b	0.04	0.00	0.00	0.85	0.06	0.02	0.00	0.00	0.04	1.00
	3a	0.05	0.00	0.05	0.02	0.80	0.05	0.02	0.00	0.03	1.00
	3b	0.00	0.01	0.00	0.00	0.00	0.87	0.03	0.01	0.08	1.00
	4	0.00	0.00	0.00	0.00	0.00	0.02	0.89	0.02	0.06	1.00
	5a	0.00	0.02	0.00	0.00	0.00	0.01	0.01	0.90	0.06	1.00
	5b	0.01	0.00	0.00	0.00	0.00	0.01	0.02	0.00	0.96	1.00

APPENDIX VIII - MARKOV CHAIN ANALYSIS OF TREDOMEN QUARRY SEQUENCE
Markov Chain Analysis of total Tredomen Quarry sequence, using 10cm intervals (continued)

Fixed probability vectors

1a	0.03
1b	0.02
2a	0.06
2b	0.03
3a	0.03
3b	0.09
4	0.13
5a	0.05
5b	0.55

Expected transitions probabilities matrix

		TO									
		1a	*1b*	*2a*	*2b*	*3a*	*3b*	*4*	*5a*	*5b*	Row totals
FROM	*1a*	0.03	0.02	0.06	0.03	0.03	0.09	0.13	0.05	0.55	51
	1b	0.03	0.02	0.06	0.03	0.03	0.09	0.13	0.05	0.55	29
	2a	0.03	0.02	0.06	0.03	0.03	0.09	0.13	0.05	0.55	120
	2b	0.03	0.02	0.06	0.03	0.03	0.09	0.13	0.05	0.55	54
	3a	0.03	0.02	0.06	0.03	0.03	0.09	0.13	0.05	0.55	65
	3b	0.03	0.02	0.06	0.03	0.03	0.09	0.13	0.05	0.55	178
	4	0.03	0.02	0.06	0.03	0.03	0.09	0.13	0.05	0.55	253
	5a	0.03	0.02	0.06	0.03	0.03	0.09	0.13	0.05	0.55	100
	5b	0.03	0.02	0.06	0.03	0.03	0.09	0.13	0.05	0.55	1036

Expected transitions matrix

		TO								
		1a	*1b*	*2a*	*2b*	*3a*	*3b*	*4*	*5a*	*5b*
FROM	*1a*	1.38	0.78	3.25	1.46	1.76	4.82	6.85	2.71	28.03
	1b	0.78	0.45	1.85	0.83	1.00	2.74	3.89	1.54	15.94
	2a	3.25	1.85	7.64	3.44	4.14	11.33	16.11	6.37	65.95
	2b	1.46	0.83	3.44	1.55	1.86	5.10	7.25	2.86	29.68
	3a	1.76	1.00	4.14	1.86	2.24	6.14	8.72	3.45	35.72
	3b	4.82	2.74	11.33	5.10	6.14	16.81	23.89	9.44	97.83
	4	6.85	3.89	16.11	7.25	8.72	23.89	33.96	13.42	139.05
	5a	2.71	1.54	6.37	2.86	3.45	9.44	13.42	5.31	54.96
	5b	28.03	15.94	65.95	29.68	35.72	97.83	139.05	54.96	569.39

APPENDIX VIII - MARKOV CHAIN ANALYSIS OF TREDOMEN QUARRY SEQUENCE

Markov Chain Analysis of total Tredomen Quarry sequence, using 10cm intervals (continued)

T	*O*	*E*	$((O-E)^2)/E$
1a-4	1	6.85	4.99
1a-5b	0	28.03	28.03
1b-5b	0	15.94	15.94
2a-2a	107	7.64	1292.35
2a-3b	1	11.33	9.42
2a-4	0	16.11	16.11
2a-5a	0	6.37	6.37
2a-5b	0	65.95	65.95
2b-3b	1	5.10	3.30
2b-4	0	7.25	7.25
2b-5b	2	29.68	25.81
3a-3b	3	6.14	1.60
3a-4	1	8.72	6.84
3a-5b	2	35.72	31.84
3b-2a	0	11.33	11.33
3b-2b	0	5.10	5.10
3b-3a	0	6.14	6.14
3b-3b	154	16.81	1119.76
3b-4	5	23.89	14.94
3b-5a	2	9.44	5.87
3b-5b	15	97.83	70.13
4-1a	1	6.85	4.99
4-2a	0	16.11	16.11
4-2b	0	7.25	7.25
4-3a	1	8.72	6.84
4-3b	6	23.89	13.40
4-4	225	33.96	1074.81
4-5a	4	13.42	6.61
4-5b	15	139.05	110.67
5a-2a	0	6.37	6.37
5a-3b	1	9.44	7.55
5a-4	1	13.42	11.50
5a-5a	90	5.31	1352.16
5a-5b	6	54.96	43.62
5b-1a	9	28.03	12.92
5b-1b	3	15.94	10.50
5b-2a	0	65.95	65.95
5b-2b	1	29.68	27.71
5b-3a	0	35.72	35.72
5b-3b	8	97.83	82.48
5b-4	18	139.05	105.38
5b-5a	3	54.96	49.12
5b-5b	994	569.39	316.65

$\chi^2 =$ **6117.35** with 64 degrees of freedom = (number of states -1)^2

critical value at 5% significance level for 64 degrees of freedom = 83.675

Therefore, the series of states are not independent of one another.

That is the series exhibits a first order Markovian property.

APPENDIX VIII - MARKOV CHAIN ANALYSIS OF TREDOMEN QUARRY SEQUENCE

Markov Chain Analysis of lower sequence of Tredomen Quarry sequence, using 10cm intervals

Observed transitions matrix

		TO									
		1a	*1b*	*2a*	*2b*	*3a*	*3b*	*4*	*5a*	*5b*	Row totals
FROM	*1a*	0	0	0	0	0	0	0	0	0	0
	1b	0	1	0	0	0	2	1	0	0	4
	2a	0	0	0	0	0	0	0	0	0	0
	2b	0	0	0	0	0	0	0	0	0	0
	3a	0	0	0	0	0	0	0	0	0	0
	3b	0	1	0	0	0	33	1	0	2	37
	4	0	0	0	0	0	0	18	2	0	20
	5a	0	1	0	0	0	0	0	35	4	40
	5b	0	1	0	0	0	2	1	3	481	488
Column totals		0	4	0	0	0	37	21	40	487	589

Grand total 589

Number of transitions 588

Observed transitions matrix as fractions

		TO									
		1a	*1b*	*2a*	*2b*	*3a*	*3b*	*4*	*5a*	*5b*	
FROM	*1a*	0.00	0.00	0.00	0.00	0.00	0.00	0.00	0.00	0.00	0.00
	1b	0.00	0.25	0.00	0.00	0.00	0.50	0.25	0.00	0.00	1.00
	2a	0.00	0.00	0.00	0.00	0.00	0.00	0.00	0.00	0.00	0.00
	2b	0.00	0.00	0.00	0.00	0.00	0.00	0.00	0.00	0.00	0.00
	3a	0.00	0.00	0.00	0.00	0.00	0.00	0.00	0.00	0.00	0.00
	3b	0.00	0.03	0.00	0.00	0.00	0.89	0.03	0.00	0.05	1.00
	4	0.00	0.00	0.00	0.00	0.00	0.00	0.90	0.10	0.00	1.00
	5a	0.00	0.03	0.00	0.00	0.00	0.00	0.00	0.88	0.10	1.00
	5b	0.00	0.00	0.00	0.00	0.00	0.00	0.00	0.01	0.99	1.00

APPENDIX VIII - MARKOV CHAIN ANALYSIS OF TREDOMEN QUARRY SEQUENCE
Markov Chain Analysis of lower sequence of Tredomen Quarry sequence, using 10cm intervals (continued)

Fixed probability vectors

1a	0.000
1b	0.007
2a	0.000
2b	0.000
3a	0.000
3b	0.063
4	0.034
5a	0.068
5b	0.830

Expected transitions probabilities matrix

		TO								
		1a	*1b*	*2a*	*2b*	*3a*	*3b*	*4*	*5a*	*5b*	Row totals
FROM	*1a*	0.000	0.007	0.000	0.000	0.000	0.063	0.034	0.068	0.830	0
	1b	0.000	0.007	0.000	0.000	0.000	0.063	0.034	0.068	0.830	4
	2a	0.000	0.007	0.000	0.000	0.000	0.063	0.034	0.068	0.830	0
	2b	0.000	0.007	0.000	0.000	0.000	0.063	0.034	0.068	0.830	0
	3a	0.000	0.007	0.000	0.000	0.000	0.063	0.034	0.068	0.830	0
	3b	0.000	0.007	0.000	0.000	0.000	0.063	0.034	0.068	0.830	37
	4	0.000	0.007	0.000	0.000	0.000	0.063	0.034	0.068	0.830	20
	5a	0.000	0.007	0.000	0.000	0.000	0.063	0.034	0.068	0.830	40
	5b	0.000	0.007	0.000	0.000	0.000	0.063	0.034	0.068	0.830	488

Expected transitions matrix

		TO								
		1a	*1b*	*2a*	*2b*	*3a*	*3b*	*4*	*5a*	*5b*
FROM	*1a*	0.00	0.00	0.00	0.00	0.00	0.00	0.00	0.00	0.00
	1b	0.00	0.03	0.00	0.00	0.00	0.25	0.14	0.27	3.32
	2a	0.00	0.00	0.00	0.00	0.00	0.00	0.00	0.00	0.00
	2b	0.00	0.00	0.00	0.00	0.00	0.00	0.00	0.00	0.00
	3a	0.00	0.00	0.00	0.00	0.00	0.00	0.00	0.00	0.00
	3b	0.00	0.25	0.00	0.00	0.00	2.33	1.26	2.52	30.71
	4	0.00	0.14	0.00	0.00	0.00	1.26	0.68	1.36	16.60
	5a	0.00	0.27	0.00	0.00	0.00	2.52	1.36	2.72	33.20
	5b	0.00	3.32	0.00	0.00	0.00	30.71	16.60	33.20	405.01

Markov Chain Analysis of lower sequence of Tredomen Quarry sequence, using 10cm intervals (continued)

T	*O*	*E*	$((O-E)^2)/E$
3b-5b	2	30.71	26.84
4-5b	0	16.60	16.60
5a-5b	4	33.20	25.68
5b-3b	2	30.71	26.84
5b-4	1	16.60	14.66
5b-5a	3	33.20	27.47
5b-5b	481	405.01	14.26

$\chi^2 =$ **152.34** with 64 degrees of freedom = (number of states -1)^2

critical value at 5% significance level for 64 degrees of freedom = 83.675

Therefore, the series of states are not independent of one another.

That is the series exhibits a first order Markovian property.

APPENDIX VIII - MARKOV CHAIN ANALYSIS OF TREDOMEN QUARRY SEQUENCE

Markov Chain Analysis of upper sequence of Tredomen Quarry sequence, using 10cm intervals

Observed transitions matrix

		TO								
		1a	*1b*	*2a*	*2b*	*3a*	*3b*	*4*	*5a*	*5b*	Row totals
FROM	*1a*	35	0	11	3	1	0	1	0	0	51
	1b	1	15	0	0	0	0	2	0	0	18
	2a	1	0	107	3	8	1	0	0	0	120
	2b	2	0	0	46	3	1	0	0	2	54
	3a	3	0	3	1	52	3	1	0	5	68
	3b	0	0	0	0	0	121	9	2	13	145
	4	1	1	0	0	1	8	207	3	15	236
	5a	0	0	0	0	0	1	1	62	3	67
	5b	9	2	0	1	0	6	18	0	502	538
Column totals		52	18	121	54	65	141	239	67	540	1297

Grand total 1297

Number of transitions 1296

Observed transitions matrix as fractions

		TO									
		1a	*1b*	*2a*	*2b*	*3a*	*3b*	*4*	*5a*	*5b*	
FROM	*1a*	0.69	0.00	0.22	0.06	0.02	0.00	0.02	0.00	0.00	1.00
	1b	0.06	0.83	0.00	0.00	0.00	0.00	0.11	0.00	0.00	1.00
	2a	0.01	0.00	0.89	0.03	0.07	0.01	0.00	0.00	0.00	1.00
	2b	0.04	0.00	0.00	0.85	0.06	0.02	0.00	0.00	0.04	1.00
	3a	0.04	0.00	0.04	0.01	0.76	0.04	0.01	0.00	0.07	1.00
	3b	0.00	0.00	0.00	0.00	0.00	0.83	0.06	0.01	0.09	1.00
	4	0.00	0.00	0.00	0.00	0.00	0.03	0.88	0.01	0.06	1.00
	5a	0.00	0.00	0.00	0.00	0.00	0.01	0.01	0.93	0.04	1.00
	5b	0.02	0.00	0.00	0.00	0.00	0.01	0.03	0.00	0.93	1.00

APPENDIX VIII - MARKOV CHAIN ANALYSIS OF TREDOMEN QUARRY SEQUENCE

Markov Chain Analysis of upper sequence of Tredomen Quarry sequence, using 10cm intervals (continued)

Fixed probability vectors

1a	0.039
1b	0.014
2a	0.093
2b	0.042
3a	0.052
3b	0.112
4	0.182
5a	0.052
5b	0.415

Expected transitions probabilities matrix

		TO								
		1a	*1b*	*2a*	*2b*	*3a*	*3b*	*4*	*5a*	*5b*	Row totals
FROM	*1a*	0.039	0.014	0.093	0.042	0.052	0.112	0.182	0.052	0.415	51
	1b	0.039	0.014	0.093	0.042	0.052	0.112	0.182	0.052	0.415	18
	2a	0.039	0.014	0.093	0.042	0.052	0.112	0.182	0.052	0.415	120
	2b	0.039	0.014	0.093	0.042	0.052	0.112	0.182	0.052	0.415	54
	3a	0.039	0.014	0.093	0.042	0.052	0.112	0.182	0.052	0.415	68
	3b	0.039	0.014	0.093	0.042	0.052	0.112	0.182	0.052	0.415	145
	4	0.039	0.014	0.093	0.042	0.052	0.112	0.182	0.052	0.415	236
	5a	0.039	0.014	0.093	0.042	0.052	0.112	0.182	0.052	0.415	67
	5b	0.039	0.014	0.093	0.042	0.052	0.112	0.182	0.052	0.415	538

Expected transitions matrix

		TO								
		1a	*1b*	*2a*	*2b*	*3a*	*3b*	*4*	*5a*	*5b*
FROM	*1a*	2.01	0.71	4.72	2.13	2.68	5.71	9.29	2.64	21.17
	1b	0.71	0.25	1.67	0.75	0.94	2.01	3.28	0.93	7.47
	2a	4.72	1.67	11.11	5.00	6.30	13.43	21.85	6.20	49.81
	2b	2.13	0.75	5.00	2.25	2.83	6.04	9.83	2.79	22.42
	3a	2.68	0.94	6.30	2.83	3.57	7.61	12.38	3.52	28.23
	3b	5.71	2.01	13.43	6.04	7.61	16.22	26.40	7.50	60.19
	4	9.29	3.28	21.85	9.83	12.38	26.40	42.98	12.20	97.97
	5a	2.64	0.93	6.20	2.79	3.52	7.50	12.20	3.46	27.81
	5b	21.17	7.47	49.81	22.42	28.23	60.19	97.97	27.81	223.34

APPENDIX VIII - MARKOV CHAIN ANALYSIS OF TREDOMEN QUARRY SEQUENCE

Markov Chain Analysis of upper sequence of Tredomen Quarry sequence, using 10cm intervals (continued)

T	*O*	*E*	*((O-E)2)/E*
1a-3b	0	5.71	5.71
1a-4	1	9.29	7.39
1a-5b	0	21.17	21.17
1b-5b	0	7.47	7.47
2a-2b	3	5.00	0.80
2a-3a	8	6.30	0.46
2a-3b	1	13.43	11.50
2a-4	0	21.85	21.85
2a-5a	0	6.20	6.20
2a-5b	0	49.81	49.81
2b-2a	0	5.00	5.00
2b-3b	1	6.04	4.21
2b-4	0	9.83	9.83
2b-5b	2	22.42	18.60
3a-2a	3	6.30	1.73
3a-3b	3	7.61	2.79
3a-4	1	12.38	10.46
3a-5b	5	28.23	19.11
3b-1a	0	5.71	5.71
3b-2a	0	13.43	13.43
3b-2b	0	6.04	6.04
3b-3a	0	7.61	7.61
3b-3b	121	16.22	676.71
3b-4	9	26.40	11.47
3b-5a	2	7.50	4.03
3b-5b	13	60.19	37.00
4-1a	1	9.29	7.39
4-2a	0	21.85	21.85
4-2b	0	9.83	9.83
4-3a	1	12.38	10.46
4-3b	8	26.40	12.83
4-4	207	42.98	626.04
4-5a	3	12.20	6.94
4-5b	15	97.97	70.27
5a-2a	0	6.20	6.20
5a-3b	1	7.50	5.63
5a-4	1	12.20	10.28
5a-5b	3	27.81	22.14
5b-1a	9	21.17	7.00
5b-1b	2	7.47	4.01
5b-2a	0	49.81	49.81

APPENDIX VIII - MARKOV CHAIN ANALYSIS OF TREDOMEN QUARRY SEQUENCE
Markov Chain Analysis of upper sequence of Tredomen Quarry sequence, using 10cm intervals (continued)

T	*O*	*E*	*((O-E)2)/E*
5b-2b	1	22.42	20.46
5b-3a	0	28.23	28.23
5b-3b	6	60.19	48.79
5b-4	18	97.97	65.28
5b-5a	0	27.81	27.81
5b-5b	502	223.34	347.70

$\chi^2 =$ **2375.05** with 64 degrees of freedom = (number of states -1)^2

critical value at 5% significance level for 64 degrees of freedom = 83.675

Therefore, the series of states are not independent of one another.

That is the series exhibits a first order Markovian property.

APPENDIX VIII - EMBEDDED MARKOV CHAIN ANALYSIS OF TREDOMEN QUARRY SEQUENCE

Embedded Markov Chain Analysis of total Tredomen Quarry sequence using 10cm intervals.

Observed Transitions matrix

		TO								
		1a	*1b*	*2a*	*2b*	*3a*	*3b*	*4*	*5a*	*5b*	Row totals
	1a		0	11	3	1	0	1	0	0	16
	1b	1		0	0	0	4	3	1	0	9
	2a	1	0		3	8	1	0	0	0	13
	2b	2	0	0		3	1	0	0	2	8
FROM	*3a*	3	0	3	1		3	1	0	2	13
	3b	0	2	0	0	0		5	2	15	24
	4	1	1	0	0	1	6		4	15	28
	5a	0	2	0	0	0	1	1		6	10
	5b	9	3	0	1	0	8	18	3		42
Column totals		17	8	14	8	13	24	29	10	40	163

Estimates of transition frequencies 1

		TO								
		1a	*1b*	*2a*	*2b*	*3a*	*3b*	*4*	*5a*	*5b*	Row totals
	1a	1000.00	0.00	11.00	3.00	1.00	0.00	1.00	0.00	0.00	1016.00
	1b	1.00	1000.00	0.00	0.00	0.00	4.00	3.00	1.00	0.00	1009.00
	2a	1.00	0.00	1000.00	3.00	8.00	1.00	0.00	0.00	0.00	1013.00
	2b	2.00	0.00	0.00	1000.00	3.00	1.00	0.00	0.00	2.00	1008.00
FROM	*3a*	3.00	0.00	3.00	1.00	1000.00	3.00	1.00	0.00	2.00	1013.00
	3b	0.00	2.00	0.00	0.00	0.00	1000.00	5.00	2.00	15.00	1024.00
	4	1.00	1.00	0.00	0.00	1.00	6.00	1000.00	4.00	15.00	1028.00
	5a	0.00	2.00	0.00	0.00	0.00	1.00	1.00	1000.00	6.00	1010.00
	5b	9.00	3.00	0.00	1.00	0.00	8.00	18.00	3.00	1000.00	1042.00
Column totals		1017.00	1008.00	1014.00	1008.00	1013.00	1024.00	1029.00	1010.00	1040.00	9163.00

Estimate of transition probabilities for diagonals 1

		TO								
		1a	*1b*	*2a*	*2b*	*3a*	*3b*	*4*	*5a*	*5b*
	1a	0.1109								
	1b		0.1101							
	2a			0.1106						
	2b				0.1100					
FROM	*3a*					0.1106				
	3b						0.1118			
	4							0.1122		
	5a								0.1102	
	5b									0.1137

APPENDIX VIII - EMBEDDED MARKOV CHAIN ANALYSIS OF TREDOMEN QUARRY SEQUENCE

Embedded Markov Chain Analysis of total Tredomen Quarry sequence using 10cm intervals (continued).

Estimates of transition frequencies 2

		TO								
		1a	*1b*	*2a*	*2b*	*3a*	*3b*	*4*	*5a*	*5b*	Row totals
FROM	*1a*	112.65	0.00	11.00	3.00	1.00	0.00	1.00	0.00	0.00	128.65
	1b	1.00	111.11	0.00	0.00	0.00	4.00	3.00	1.00	0.00	120.11
	2a	1.00	0.00	111.99	3.00	8.00	1.00	0.00	0.00	0.00	124.99
	2b	2.00	0.00	0.00	110.89	3.00	1.00	0.00	0.00	2.00	118.89
	3a	3.00	0.00	3.00	1.00	111.99	3.00	1.00	0.00	2.00	124.99
	3b	0.00	2.00	0.00	0.00	0.00	114.44	5.00	2.00	15.00	138.44
	4	1.00	1.00	0.00	0.00	1.00	6.00	115.33	4.00	15.00	143.33
	5a	0.00	2.00	0.00	0.00	0.00	1.00	1.00	111.33	6.00	121.33
	5b	9.00	3.00	0.00	1.00	0.00	8.00	18.00	3.00	118.49	160.49
Column totals		129.65	119.11	125.99	118.89	124.99	138.44	144.33	121.33	158.49	1181.22

Estimate of transition probabilities for diagonals 2

		TO								
		1a	*1b*	*2a*	*2b*	*3a*	*3b*	*4*	*5a*	*5b*
FROM	*1a*	0.1089								
	1b		0.1017							
	2a			0.1058						
	2b				0.1006					
	3a					0.1058				
	3b						0.1172			
	4							0.1213		
	5a								0.1027	
	5b									0.1359

Estimates of transition frequencies 3

		TO								
		1a	*1b*	*2a*	*2b*	*3a*	*3b*	*4*	*5a*	*5b*	Row totals
FROM	*1a*	14.01	0.00	11.00	3.00	1.00	0.00	1.00	0.00	0.00	30.01
	1b	1.00	12.21	0.00	0.00	0.00	4.00	3.00	1.00	0.00	21.21
	2a	1.00	0.00	13.23	3.00	8.00	1.00	0.00	0.00	0.00	26.23
	2b	2.00	0.00	0.00	11.97	3.00	1.00	0.00	0.00	2.00	19.97
	3a	3.00	0.00	3.00	1.00	13.23	3.00	1.00	0.00	2.00	26.23
	3b	0.00	2.00	0.00	0.00	0.00	16.22	5.00	2.00	15.00	40.22
	4	1.00	1.00	0.00	0.00	1.00	6.00	17.39	4.00	15.00	45.39
	5a	0.00	2.00	0.00	0.00	0.00	1.00	1.00	12.46	6.00	22.46
	5b	9.00	3.00	0.00	1.00	0.00	8.00	18.00	3.00	21.81	63.81
Column totals		31.01	20.21	27.23	19.97	26.23	40.22	46.39	22.46	61.81	295.53

APPENDIX VIII - EMBEDDED MARKOV CHAIN ANALYSIS OF TREDOMEN QUARRY SEQUENCE

Embedded Markov Chain Analysis of total Tredomen Quarry sequence using 10cm intervals (continued).

Estimate of transition probabilities for diagonals 3

TO

FROM	*1a*	*1b*	*2a*	*2b*	*3a*	*3b*	*4*	*5a*	*5b*
1a	0.1016								
1b		0.0718							
2a			0.0887						
2b				0.0676					
3a					0.0887				
3b						0.1361			
4							0.1536		
5a								0.076	
5b									0.2159

Estimates of transition frequencies 4

TO

FROM	*1a*	*1b*	*2a*	*2b*	*3a*	*3b*	*4*	*5a*	*5b*	Row totals
1a	3.05	0.00	11.00	3.00	1.00	0.00	1.00	0.00	0.00	19.05
1b	1.00	1.52	0.00	0.00	0.00	4.00	3.00	1.00	0.00	10.52
2a	1.00	0.00	2.33	3.00	8.00	1.00	0.00	0.00	0.00	15.33
2b	2.00	0.00	0.00	1.35	3.00	1.00	0.00	0.00	2.00	9.35
3a	3.00	0.00	3.00	1.00	2.33	3.00	1.00	0.00	2.00	15.33
3b	0.00	2.00	0.00	0.00	0.00	5.47	5.00	2.00	15.00	29.47
4	1.00	1.00	0.00	0.00	1.00	6.00	6.97	4.00	15.00	34.97
5a	0.00	2.00	0.00	0.00	0.00	1.00	1.00	1.71	6.00	11.71
5b	9.00	3.00	0.00	1.00	0.00	8.00	18.00	3.00	13.78	55.78
Column totals	20.05	9.52	16.33	9.35	15.33	29.47	35.97	11.71	53.78	201.50

Estimate of transition probabilities for diagonals 4

TO

FROM	*1a*	*1b*	*2a*	*2b*	*3a*	*3b*	*4*	*5a*	*5b*
1a	0.0945								
1b		0.0522							
2a			0.0761						
2b				0.0464					
3a					0.0761				
3b						0.1463			
4							0.1736		
5a								0.0581	
5b									0.2768

APPENDIX VIII - EMBEDDED MARKOV CHAIN ANALYSIS OF TREDOMEN QUARRY SEQUENCE

Embedded Markov Chain Analysis of total Tredomen Quarry sequence using 10cm intervals (continued).

Estimates of transition frequencies 5

		TO								
		1a	*1b*	*2a*	*2b*	*3a*	*3b*	*4*	*5a*	*5b*	Row totals
FROM	*1a*	1.80	0.00	11.00	3.00	1.00	0.00	1.00	0.00	0.00	17.80
	1b	1.00	0.55	0.00	0.00	0.00	4.00	3.00	1.00	0.00	9.55
	2a	1.00	0.00	1.17	3.00	8.00	1.00	0.00	0.00	0.00	14.17
	2b	2.00	0.00	0.00	0.43	3.00	1.00	0.00	0.00	2.00	8.43
	3a	3.00	0.00	3.00	1.00	1.17	3.00	1.00	0.00	2.00	14.17
	3b	0.00	2.00	0.00	0.00	0.00	4.31	5.00	2.00	15.00	28.31
	4	1.00	1.00	0.00	0.00	1.00	6.00	6.07	4.00	15.00	34.07
	5a	0.00	2.00	0.00	0.00	0.00	1.00	1.00	0.68	6.00	10.68
	5b	9.00	3.00	0.00	1.00	0.00	8.00	18.00	3.00	15.44	57.44
Column totals		18.80	8.55	15.17	8.43	14.17	28.31	35.07	10.68	55.44	194.62

Estimate of transition probabilities for diagonals 5

		TO								
		1a	*1b*	*2a*	*2b*	*3a*	*3b*	*4*	*5a*	*5b*
FROM	*1a*	0.0915								
	1b		0.0491							
	2a			0.0728						
	2b				0.0433					
	3a					0.0728				
	3b						0.1455			
	4							0.1751		
	5a								0.0549	
	5b									0.2951

Estimates of transition frequencies 6

		TO								
		1a	*1b*	*2a*	*2b*	*3a*	*3b*	*4*	*5a*	*5b*	Row totals
FROM	*1a*	1.63	0.00	11.00	3.00	1.00	0.00	1.00	0.00	0.00	17.63
	1b	1.00	0.47	0.00	0.00	0.00	4.00	3.00	1.00	0.00	9.47
	2a	1.00	0.00	1.03	3.00	8.00	1.00	0.00	0.00	0.00	14.03
	2b	2.00	0.00	0.00	0.37	3.00	1.00	0.00	0.00	2.00	8.37
	3a	3.00	0.00	3.00	1.00	1.03	3.00	1.00	0.00	2.00	14.03
	3b	0.00	2.00	0.00	0.00	0.00	4.12	5.00	2.00	15.00	28.12
	4	1.00	1.00	0.00	0.00	1.00	6.00	5.96	4.00	15.00	33.96
	5a	0.00	2.00	0.00	0.00	0.00	1.00	1.00	0.59	6.00	10.59
	5b	9.00	3.00	0.00	1.00	0.00	8.00	18.00	3.00	16.95	58.95
Column totals		18.63	8.47	15.03	8.37	14.03	28.12	34.96	10.59	56.95	195.15

APPENDIX VIII - EMBEDDED MARKOV CHAIN ANALYSIS OF TREDOMEN QUARRY SEQUENCE

Embedded Markov Chain Analysis of total Tredomen Quarry sequence using 10cm intervals (continued).

Estimate of transition probabilities for diagonals 6

TO

FROM	*1a*	*1b*	*2a*	*2b*	*3a*	*3b*	*4*	*5a*	*5b*
1a	0.0903								
1b		0.0485							
2a			0.0719						
2b				0.0429					
3a					0.0719				
3b						0.1441			
4							0.174		
5a								0.0542	
5b									0.3021

Estimates of transition frequencies 7

TO

FROM	*1a*	*1b*	*2a*	*2b*	*3a*	*3b*	*4*	*5a*	*5b*	Row totals
1a	1.59	0.00	11.00	3.00	1.00	0.00	1.00	0.00	0.00	17.59
1b	1.00	0.46	0.00	0.00	0.00	4.00	3.00	1.00	0.00	9.46
2a	1.00	0.00	1.01	3.00	8.00	1.00	0.00	0.00	0.00	14.01
2b	2.00	0.00	0.00	0.36	3.00	1.00	0.00	0.00	2.00	8.36
3a	3.00	0.00	3.00	1.00	1.01	3.00	1.00	0.00	2.00	14.01
3b	0.00	2.00	0.00	0.00	0.00	4.05	5.00	2.00	15.00	28.05
4	1.00	1.00	0.00	0.00	1.00	6.00	5.91	4.00	15.00	33.91
5a	0.00	2.00	0.00	0.00	0.00	1.00	1.00	0.57	6.00	10.57
5b	9.00	3.00	0.00	1.00	0.00	8.00	18.00	3.00	17.81	59.81
Column totals	18.59	8.46	15.01	8.36	14.01	28.05	34.91	10.57	57.81	195.77

APPENDIX VIII - EMBEDDED MARKOV CHAIN ANALYSIS OF TREDOMEN QUARRY SEQUENCE

Embedded Markov Chain Analysis of total Tredomen Quarry sequence using 10cm intervals (continued).

Estimate of transition probabilities for diagonals 7

		TO								
		1a	*1b*	*2a*	*2b*	*3a*	*3b*	*4*	*5a*	*5b*
FROM	*1a*	0.0899								
	1b		0.0483							
	2a			0.0716						
	2b				0.0427					
	3a					0.0716				
	3b						0.1433			
	4							0.1732		
	5a								0.054	
	5b									0.3055

Estimates of transition frequencies 8

		TO									
		1a	*1b*	*2a*	*2b*	*3a*	*3b*	*4*	*5a*	*5b*	Row totals
FROM	*1a*	1.58	0.00	11.00	3.00	1.00	0.00	1.00	0.00	0.00	17.58
	1b	1.00	0.46	0.00	0.00	0.00	4.00	3.00	1.00	0.00	9.46
	2a	1.00	0.00	1.00	3.00	8.00	1.00	0.00	0.00	0.00	14.00
	2b	2.00	0.00	0.00	0.36	3.00	1.00	0.00	0.00	2.00	8.36
	3a	3.00	0.00	3.00	1.00	1.00	3.00	1.00	0.00	2.00	14.00
	3b	0.00	2.00	0.00	0.00	0.00	4.02	5.00	2.00	15.00	28.02
	4	1.00	1.00	0.00	0.00	1.00	6.00	5.87	4.00	15.00	33.87
	5a	0.00	2.00	0.00	0.00	0.00	1.00	1.00	0.57	6.00	10.57
	5b	9.00	3.00	0.00	1.00	0.00	8.00	18.00	3.00	18.27	60.27
Column totals		18.58	8.46	15.00	8.36	14.00	28.02	34.87	10.57	58.27	196.14

Estimate of transition probabilities for diagonals 8

		TO								
		1a	*1b*	*2a*	*2b*	*3a*	*3b*	*4*	*5a*	*5b*
FROM	*1a*	0.0896								
	1b		0.0482							
	2a			0.0714						
	2b				0.0426					
	3a					0.0714				
	3b						0.1429			
	4							0.1727		
	5a								0.0539	
	5b									0.3073

APPENDIX VIII - EMBEDDED MARKOV CHAIN ANALYSIS OF TREDOMEN QUARRY SEQUENCE

Embedded Markov Chain Analysis of total Tredomen Quarry sequence using 10cm intervals (continued).

Estimates of transition frequencies 9

		TO									
		1a	*1b*	*2a*	*2b*	*3a*	*3b*	*4*	*5a*	*5b*	Row totals
	1a	1.58	0.00	11.00	3.00	1.00	0.00	1.00	0.00	0.00	17.58
	1b	1.00	0.46	0.00	0.00	0.00	4.00	3.00	1.00	0.00	9.46
	2a	1.00	0.00	1.00	3.00	8.00	1.00	0.00	0.00	0.00	14.00
	2b	2.00	0.00	0.00	0.36	3.00	1.00	0.00	0.00	2.00	8.36
FROM	*3a*	3.00	0.00	3.00	1.00	1.00	3.00	1.00	0.00	2.00	14.00
	3b	0.00	2.00	0.00	0.00	0.00	4.00	5.00	2.00	15.00	28.00
	4	1.00	1.00	0.00	0.00	1.00	6.00	5.85	4.00	15.00	33.85
	5a	0.00	2.00	0.00	0.00	0.00	1.00	1.00	0.57	6.00	10.57
	5b	9.00	3.00	0.00	1.00	0.00	8.00	18.00	3.00	18.52	60.52
Column totals		18.58	8.46	15.00	8.36	14.00	28.00	34.85	10.57	58.52	196.33

Estimate of transition probabilities for diagonals 9

		TO								
		1a	*1b*	*2a*	*2b*	*3a*	*3b*	*4*	*5a*	*5b*
	1a	0.0895								
	1b		0.0482							
	2a			0.0713						
	2b				0.0426					
FROM	*3a*					0.0713				
	3b						0.1426			
	4							0.1724		
	5a								0.0538	
	5b									0.3083

Estimates of transition frequencies 10

		TO									
		1a	*1b*	*2a*	*2b*	*3a*	*3b*	*4*	*5a*	*5b*	Row totals
	1a	1.57	0.00	11.00	3.00	1.00	0.00	1.00	0.00	0.00	17.57
	1b	1.00	0.46	0.00	0.00	0.00	4.00	3.00	1.00	0.00	9.46
	2a	1.00	0.00	1.00	3.00	8.00	1.00	0.00	0.00	0.00	14.00
	2b	2.00	0.00	0.00	0.36	3.00	1.00	0.00	0.00	2.00	8.36
FROM	*3a*	3.00	0.00	3.00	1.00	1.00	3.00	1.00	0.00	2.00	14.00
	3b	0.00	2.00	0.00	0.00	0.00	3.99	5.00	2.00	15.00	27.99
	4	1.00	1.00	0.00	0.00	1.00	6.00	5.84	4.00	15.00	33.84
	5a	0.00	2.00	0.00	0.00	0.00	1.00	1.00	0.57	6.00	10.57
	5b	9.00	3.00	0.00	1.00	0.00	8.00	18.00	3.00	18.66	60.66
Column totals		18.57	8.46	15.00	8.36	14.00	27.99	34.84	10.57	58.66	196.44

APPENDIX VIII - EMBEDDED MARKOV CHAIN ANALYSIS OF TREDOMEN QUARRY SEQUENCE

Embedded Markov Chain Analysis of total Tredomen Quarry sequence using 10cm intervals (continued).

Estimate of transition probabilities for diagonals 10

		TO								
		1a	*1b*	*2a*	*2b*	*3a*	*3b*	*4*	*5a*	*5b*
FROM	*1a*	0.0895								
	1b		0.0481							
	2a			0.0713						
	2b				0.0425					
	3a					0.0713				
	3b						0.1425			
	4							0.1723		
	5a								0.0538	
	5b									0.3088

Estimates of transition frequencies 11

		TO									
		1a	*1b*	*2a*	*2b*	*3a*	*3b*	*4*	*5a*	*5b*	Row totals
FROM	*1a*	1.57	0.00	11.00	3.00	1.00	0.00	1.00	0.00	0.00	17.57
	1b	1.00	0.46	0.00	0.00	0.00	4.00	3.00	1.00	0.00	9.46
	2a	1.00	0.00	1.00	3.00	8.00	1.00	0.00	0.00	0.00	14.00
	2b	2.00	0.00	0.00	0.36	3.00	1.00	0.00	0.00	2.00	8.36
	3a	3.00	0.00	3.00	1.00	1.00	3.00	1.00	0.00	2.00	14.00
	3b	0.00	2.00	0.00	0.00	0.00	3.99	5.00	2.00	15.00	27.99
	4	1.00	1.00	0.00	0.00	1.00	6.00	5.83	4.00	15.00	33.83
	5a	0.00	2.00	0.00	0.00	0.00	1.00	1.00	0.57	6.00	10.57
	5b	9.00	3.00	0.00	1.00	0.00	8.00	18.00	3.00	18.73	60.73
Column totals		18.57	8.46	15.00	8.36	14.00	27.99	34.83	10.57	58.73	196.49

Estimate of transition probabilities for diagonals 11

		TO								
		1a	*1b*	*2a*	*2b*	*3a*	*3b*	*4*	*5a*	*5b*
FROM	*1a*	0.0894								
	1b		0.0481							
	2a			0.0712						
	2b				0.0425					
	3a					0.0712				
	3b						0.1424			
	4							0.1722		
	5a								0.0538	
	5b									0.3091

APPENDIX VIII - EMBEDDED MARKOV CHAIN ANALYSIS OF TREDOMEN QUARRY SEQUENCE

Embedded Markov Chain Analysis of total Tredomen Quarry sequence using 10cm intervals (continued).

Estimates of transition frequencies 12

		TO									
		1a	*1b*	*2a*	*2b*	*3a*	*3b*	*4*	*5a*	*5b*	Row totals
	1a	1.57	0.00	11.00	3.00	1.00	0.00	1.00	0.00	0.00	17.57
	1b	1.00	0.45	0.00	0.00	0.00	4.00	3.00	1.00	0.00	9.45
	2a	1.00	0.00	1.00	3.00	8.00	1.00	0.00	0.00	0.00	14.00
	2b	2.00	0.00	0.00	0.36	3.00	1.00	0.00	0.00	2.00	8.36
FROM	*3a*	3.00	0.00	3.00	1.00	1.00	3.00	1.00	0.00	2.00	14.00
	3b	0.00	2.00	0.00	0.00	0.00	3.99	5.00	2.00	15.00	27.99
	4	1.00	1.00	0.00	0.00	1.00	6.00	5.82	4.00	15.00	33.82
	5a	0.00	2.00	0.00	0.00	0.00	1.00	1.00	0.57	6.00	10.57
	5b	9.00	3.00	0.00	1.00	0.00	8.00	18.00	3.00	18.77	60.77
Column totals		18.57	8.45	15.00	8.36	14.00	27.99	34.82	10.57	58.77	196.52

Estimate of transition probabilities for diagonals 12

		TO								
		1a	*1b*	*2a*	*2b*	*3a*	*3b*	*4*	*5a*	*5b*
	1a	0.0894								
	1b		0.0481							
	2a			0.0712						
	2b				0.0425					
FROM	*3a*					0.0712				
	3b						0.1424			
	4							0.1721		
	5a								0.0538	
	5b									0.3092

Estimates of transition frequencies 13

		TO									
		1a	*1b*	*2a*	*2b*	*3a*	*3b*	*4*	*5a*	*5b*	Row totals
	1a	1.57	0.00	11.00	3.00	1.00	0.00	1.00	0.00	0.00	17.57
	1b	1.00	0.45	0.00	0.00	0.00	4.00	3.00	1.00	0.00	9.45
	2a	1.00	0.00	1.00	3.00	8.00	1.00	0.00	0.00	0.00	14.00
	2b	2.00	0.00	0.00	0.36	3.00	1.00	0.00	0.00	2.00	8.36
FROM	*3a*	3.00	0.00	3.00	1.00	1.00	3.00	1.00	0.00	2.00	14.00
	3b	0.00	2.00	0.00	0.00	0.00	3.99	5.00	2.00	15.00	27.99
	4	1.00	1.00	0.00	0.00	1.00	6.00	5.82	4.00	15.00	33.82
	5a	0.00	2.00	0.00	0.00	0.00	1.00	1.00	0.57	6.00	10.57
	5n	9.00	3.00	0.00	1.00	0.00	8.00	18.00	3.00	18.79	60.79
Column totals		18.57	8.45	15.00	8.36	14.00	27.99	34.82	10.57	58.79	196.54

APPENDIX VIII - EMBEDDED MARKOV CHAIN ANALYSIS OF TREDOMEN QUARRY SEQUENCE

Embedded Markov Chain Analysis of total Tredomen Quarry sequence using 10cm intervals (continued).

Estimate of transition probabilities for diagonals 13

		TO								
		1a	*1b*	*2a*	*2b*	*3a*	*3b*	*4*	*5a*	*5b*
FROM	*1a*	0.0894								
	1b		0.0481							
	2a			0.0712						
	2b				0.0425					
	3a					0.0712				
	3b						0.1424			
	4							0.1721		
	5a								0.0538	
	5b									0.3093

Estimates of transition frequencies 14

		TO									
		1a	*1b*	*2a*	*2b*	*3a*	*3b*	*4*	*5a*	*5b*	Row totals
FROM	*1a*	1.57	0.00	11.00	3.00	1.00	0.00	1.00	0.00	0.00	17.57
	1b	1.00	0.45	0.00	0.00	0.00	4.00	3.00	1.00	0.00	9.45
	2a	1.00	0.00	1.00	3.00	8.00	1.00	0.00	0.00	0.00	14.00
	2b	2.00	0.00	0.00	0.36	3.00	1.00	0.00	0.00	2.00	8.36
	3a	3.00	0.00	3.00	1.00	1.00	3.00	1.00	0.00	2.00	14.00
	3b	0.00	2.00	0.00	0.00	0.00	3.98	5.00	2.00	15.00	27.98
	4	1.00	1.00	0.00	0.00	1.00	6.00	5.82	4.00	15.00	33.82
	5a	0.00	2.00	0.00	0.00	0.00	1.00	1.00	0.57	6.00	10.57
	5b	9.00	3.00	0.00	1.00	0.00	8.00	18.00	3.00	18.80	60.80
Column totals		18.57	8.45	15.00	8.36	14.00	27.98	34.82	10.57	58.80	196.55

Estimate of transition probabilities for diagonals 14

		TO								
		1a	*1b*	*2a*	*2b*	*3a*	*3b*	*4*	*5a*	*5b*
FROM	*1a*	0.0894								
	1b		0.0481							
	2a			0.0712						
	2b				0.0425					
	3a					0.0712				
	3b						0.1424			
	4							0.1721		
	5a								0.0538	
	5b									0.3094

APPENDIX VIII - EMBEDDED MARKOV CHAIN ANALYSIS OF TREDOMEN QUARRY SEQUENCE

Embedded Markov Chain Analysis of total Tredomen Quarry sequence using 10cm intervals (continued).

Estimates of transition frequencies 15

TO

FROM	*1a*	*1b*	*2a*	*2b*	*3a*	*3b*	*4*	*5a*	*5b*	Row totals
1a	1.57	0.00	11.00	3.00	1.00	0.00	1.00	0.00	0.00	17.57
1b	1.00	0.45	0.00	0.00	0.00	4.00	3.00	1.00	0.00	9.45
2a	1.00	0.00	1.00	3.00	8.00	1.00	0.00	0.00	0.00	14.00
2b	2.00	0.00	0.00	0.36	3.00	1.00	0.00	0.00	2.00	8.36
3a	3.00	0.00	3.00	1.00	1.00	3.00	1.00	0.00	2.00	14.00
3b	0.00	2.00	0.00	0.00	0.00	3.98	5.00	2.00	15.00	27.98
4	1.00	1.00	0.00	0.00	1.00	6.00	5.82	4.00	15.00	33.82
5a	0.00	2.00	0.00	0.00	0.00	1.00	1.00	0.57	6.00	10.57
5b	9.00	3.00	0.00	1.00	0.00	8.00	18.00	3.00	18.81	60.81
Column totals	18.57	8.45	15.00	8.36	14.00	27.98	34.82	10.57	58.81	196.56

Estimate of transition probabilities for diagonals 15

TO

FROM	*1a*	*1b*	*2a*	*2b*	*3a*	*3b*	*4*	*5a*	*5b*
1a	0.0894								
1b		0.0481							
2a			0.0712						
2b				0.0425					
3a					0.0712				
3b						0.1424			
4							0.1721		
5a								0.0538	
5b									0.3094

Estimates of transition frequencies 16

TO

FROM	*1a*	*1b*	*2a*	*2b*	*3a*	*3b*	*4*	*5a*	*5b*	Row totals
1a	1.57	0.00	11.00	3.00	1.00	0.00	1.00	0.00	0.00	17.57
1b	1.00	0.45	0.00	0.00	0.00	4.00	3.00	1.00	0.00	9.45
2a	1.00	0.00	1.00	3.00	8.00	1.00	0.00	0.00	0.00	14.00
2b	2.00	0.00	0.00	0.36	3.00	1.00	0.00	0.00	2.00	8.36
3a	3.00	0.00	3.00	1.00	1.00	3.00	1.00	0.00	2.00	14.00
3b	0.00	2.00	0.00	0.00	0.00	3.98	5.00	2.00	15.00	27.98
4	1.00	1.00	0.00	0.00	1.00	6.00	5.82	4.00	15.00	33.82
5a	0.00	2.00	0.00	0.00	0.00	1.00	1.00	0.57	6.00	10.57
5b	9.00	3.00	0.00	1.00	0.00	8.00	18.00	3.00	18.81	60.81
Column totals	18.57	8.45	15.00	8.36	14.00	27.98	34.82	10.57	58.81	196.56

APPENDIX VIII - EMBEDDED MARKOV CHAIN ANALYSIS OF TREDOMEN QUARRY SEQUENCE

Embedded Markov Chain Analysis of total Tredomen Quarry sequence using 10cm intervals (continued).

Fixed probability vectors

1a	0.0894
1b	0.0481
2a	0.0712
2b	0.0425
3a	0.0712
3b	0.1424
4	0.1721
5a	0.0538
5b	0.3094

Expected transitions probabilities matrix

		TO							
		1a	*1b*	*2a*	*2b*	*3a*	*3b*	*4*	*5a*	*5b*
FROM	*1a*	0.0080	0.0043	0.0064	0.0038	0.0064	0.0127	0.0154	0.0048	0.0277
	1b	0.0043	0.0023	0.0034	0.0020	0.0034	0.0068	0.0083	0.0026	0.0149
	2a	0.0064	0.0034	0.0051	0.0030	0.0051	0.0101	0.0123	0.0038	0.0220
	2b	0.0038	0.0020	0.0030	0.0018	0.0030	0.0061	0.0073	0.0023	0.0132
	3a	0.0064	0.0034	0.0051	0.0030	0.0051	0.0101	0.0123	0.0038	0.0220
	3b	0.0127	0.0068	0.0101	0.0061	0.0101	0.0203	0.0245	0.0077	0.0440
	4	0.0154	0.0083	0.0123	0.0073	0.0123	0.0245	0.0296	0.0093	0.0532
	5a	0.0048	0.0026	0.0038	0.0023	0.0038	0.0077	0.0093	0.0029	0.0166
	5b	0.0277	0.0149	0.0220	0.0132	0.0220	0.0440	0.0532	0.0166	0.0957

Expected transitions matrix

		TO							
		1a	*1b*	*2a*	*2b*	*3a*	*3b*	*4*	*5a*	*5b*
FROM	*1a*	1.57	0.85	1.25	0.75	1.25	2.50	3.02	0.94	5.44
	1b	0.85	0.45	0.67	0.40	0.67	1.35	1.63	0.51	2.93
	2a	1.25	0.67	1.00	0.59	1.00	1.99	2.41	0.75	4.33
	2b	0.75	0.40	0.59	0.36	0.59	1.19	1.44	0.45	2.58
	3a	1.25	0.67	1.00	0.59	1.00	1.99	2.41	0.75	4.33
	3b	2.50	1.35	1.99	1.19	1.99	3.98	4.81	1.50	8.66
	4	3.02	1.63	2.41	1.44	2.41	4.81	5.82	1.82	10.46
	5a	0.94	0.51	0.75	0.45	0.75	1.50	1.82	0.57	3.27
	5b	5.44	2.93	4.33	2.58	4.33	8.66	10.46	3.27	18.81

APPENDIX VIII - EMBEDDED MARKOV CHAIN ANALYSIS OF TREDOMEN QUARRY SEQUENCE

Embedded Markov Chain Analysis of total Tredomen Quarry sequence using 10cm intervals (continued).

Expected frequencies without estimates

		TO								
		1a	*1b*	*2a*	*2b*	*3a*	*3b*	*4*	*5a*	*5b*	Rows total
FROM	*1a*		0.85	1.25	0.75	1.25	2.50	3.02	0.94	5.44	16.00
	1b	0.85		0.67	0.40	0.67	1.35	1.63	0.51	2.93	9.00
	2a	1.25	0.67		0.59	1.00	1.99	2.41	0.75	4.33	13.00
	2b	0.75	0.40	0.59		0.59	1.19	1.44	0.45	2.58	8.00
	3a	1.25	0.67	1.00	0.59		1.99	2.41	0.75	4.33	13.00
	3b	2.50	1.35	1.99	1.19	1.99		4.81	1.50	8.66	24.00
	4	3.02	1.63	2.41	1.44	2.41	4.81		1.82	10.46	28.00
	5a	0.94	0.51	0.75	0.45	0.75	1.50	1.82		3.27	10.00
	5b	5.44	2.93	4.33	2.58	4.33	8.66	10.46	3.27		42.00
Column totals		16.00	9.00	13.00	8.00	13.00	24.00	28.00	10.00	42.00	163.00

Original Observed Transitions matrix

		TO								
		1a	*1b*	*2a*	*2b*	*3a*	*3b*	*4*	*5a*	*5b*	Row total
FROM	*1a*		0	11	3	1	0	1	0	0	16.00
	1b	1		0	0	0	4	3	1	0	9.00
	2a	1	0		3	8	1	0	0	0	13.00
	2b	2	0	0		3	1	0	0	2	8.00
	3a	3	0	3	1		3	1	0	2	13.00
	3b	0	2	0	0	0		5	2	15	24.00
	4	1	1	0	0	1	6		4	15	28.00
	5a	0	2	0	0	0	1	1		6	10.00
	5b	9	3	0	1	0	8	18	3		42.00
Column totals		17.00	8.00	14.00	8.00	13.00	24.00	29.00	10.00	40.00	163.00

APPENDIX VIII - EMBEDDED MARKOV CHAIN ANALYSIS OF TREDOMEN QUARRY SEQUENCE

Embedded Markov Chain Analysis of total Tredomen Quarry sequence using 10cm intervals (continued).

T	*O*	*E*	$((O-E)^2)/E$
1a-5b	0.00	5.44	5.44
3b-5b	15.00	8.66	4.65
4-5b	15.00	10.46	1.97
5b-1a	9.00	5.44	2.34
5b-3b	8.00	8.66	0.05
5b-4	18.00	10.46	5.43
orange	3	7.26	2.50
pink	1	6.92	5.06
light blue	4.00	6.73	1.11
red	9.00	6.54	0.93
light yellow	2.00	7.06	3.62
green	7.00	8.66	0.32
bright pink	7.00	6.60	0.02
turquiose	5.00	6.68	0.42
purple	18.00	5.76	25.97
aqua	1.00	5.52	3.71
lime	8.00	5.10	1.65
teal	9.00	5.91	1.61
tan	0.00	7.49	7.49
blue-grey	6.00	6.26	0.01
dark blue	5.00	8.98	1.76
grey	2.00	5.08	1.87
light green	4.00	5.00	0.20
marroon	7.00	6.32	0.07

$\chi^2 =$ **78.19** with 55 degrees of freedom = $(\text{number of states} - 1)^2$

critical value at 5% significance level for 55 degrees of freedom = 73.31

Therefore, the series of states are not independent of one another.

That is the series exhibits a first order Markovian property.

APPENDIX VIII - EMBEDDED MARKOV CHAIN ANALYSIS OF TREDOMEN QUARRY SEQUENCE

Embedded Markov Chain Analysis of lower Tredomen sequence using 10cm intervals.

Observed Transitions matrix

		TO									
		1a	*1b*	*2a*	*2b*	*3a*	*3b*	*4*	*5a*	*5b*	Row totals
FROM	*1a*		0	0	0	0	0	0	0	0	0.00
	1b	0		0	0	0	2	1	0	0	3.00
	2a	0	0		0	0	0	0	0	0	0.00
	2b	0	0	0		0	0	0	0	0	0.00
	3a	0	0	0	0		0	0	0	0	0.00
	3b	0	1	0	0	0		1	0	2	4.00
	4	0	0	0	0	0	0		2	0	2.00
	5a	0	1	0	0	0	0	0		4	5.00
	5b	0	1	0	0	0	2	1	3		7.00
Column totals		0.00	3.00	0.00	0.00	0.00	4.00	3.00	5.00	6.00	21.00

Estimates of transition frequencies 1

		TO									
		1a	*1b*	*2a*	*2b*	*3a*	*3b*	*4*	*5a*	*5b*	Row totals
FROM	*1a*	1000	0	0	0	0	0	0	0	0	1000.00
	1b	0	1000	0	0	0	2	1	0	0	1003.00
	2a	0	0	1000	0	0	0	0	0	0	1000.00
	2b	0	0	0	1000	0	0	0	0	0	1000.00
	3a	0	0	0	0	1000	0	0	0	0	1000.00
	3b	0	1	0	0	0	1000	1	0	2	1004.00
	4	0	0	0	0	0	0	1000	2	0	1002.00
	5a	0	1	0	0	0	0	0	1000	4	1005.00
	5b	0	1	0	0	0	2	1	3	1000	1007.00
Column totals		1000.00	1003.00	1000.00	1000.00	1000.00	1004.00	1003.00	1005.00	1006.00	9021.00

Estimate of transition probabilities for diagonals 1

		TO								
		1a	*1b*	*2a*	*2b*	*3a*	*3b*	*4*	*5a*	*5b*
FROM	*1a*	0.1109								
	1b		0.1112							
	2a			0.1109						
	2b				0.1109					
	3a					0.1109				
	3b						0.1113			
	4							0.1111		
	5a								0.1114	
	5b									0.1116

APPENDIX VIII - EMBEDDED MARKOV CHAIN ANALYSIS OF TREDOMEN QUARRY SEQUENCE

Embedded Markov Chain Analysis of lower Tredomen sequence using 10cm intervals (continued)

Estimates of transition frequencies 2

		TO								
		1a	*1b*	*2a*	*2b*	*3a*	*3b*	*4*	*5a*	*5b*	Row totals
FROM	*1a*	110.85	0	0	0	0	0	0	0	0	110.85
	1b	0	111.52	0	0	0	2	1	0	0	114.52
	2a	0	0	110.85	0	0	0	0	0	0	110.85
	2b	0	0	0	110.85	0	0	0	0	0	110.85
	3a	0	0	0	0	110.85	0	0	0	0	110.85
	3b	0	1	0	0	0	111.74	1	0	2	115.74
	4	0	0	0	0	0	0	111.30	2	0	113.30
	5a	0	1	0	0	0	0	0	111.96	4	116.96
	5b	0	1	0	0	0	2	1	3	112.41	119.41
Column totals		110.85	114.52	110.85	110.85	110.85	115.74	114.30	116.96	118.41	1023.34

Estimate of transition probabilities for diagonals 2

		TO								
		1a	*1b*	*2a*	*2b*	*3a*	*3b*	*4*	*5a*	*5b*
FROM	*1a*	0.1083								
	1b		0.1119							
	2a			0.1083						
	2b				0.1083					
	3a					0.1083				
	3b						0.1131			
	4							0.1107		
	5a								0.1143	
	5b									0.1167

Estimates of transition frequencies 3

		TO								
		1a	*1b*	*2a*	*2b*	*3a*	*3b*	*4*	*5a*	*5b*	Row totals
FROM	*1a*	12.01	0	0	0	0	0	0	0	0	12.01
	1b	0	12.82	0	0	0	2	1	0	0	15.82
	2a	0	0	12.01	0	0	0	0	0	0	12.01
	2b	0	0	0	12.01	0	0	0	0	0	12.01
	3a	0	0	0	0	12.01	0	0	0	0	12.01
	3b	0	1	0	0	0	13.09	1	0	2	17.09
	4	0	0	0	0	0	0	12.54	2	0	14.54
	5a	0	1	0	0	0	0	0	13.37	4	18.37
	5b	0	1	0	0	0	2	1	3	13.93	20.93
Column totals		12.01	15.82	12.01	12.01	12.01	17.09	15.54	18.37	19.93	134.78

APPENDIX VIII - EMBEDDED MARKOV CHAIN ANALYSIS OF TREDOMEN QUARRY SEQUENCE

Embedded Markov Chain Analysis of lower Tredomen sequence using 10cm intervals (continued)

Estimate of transition probabilities for diagonals 3

TO

FROM	*1a*	*1b*	*2a*	*2b*	*3a*	*3b*	*4*	*5a*	*5b*
1a	0.0891								
1b		0.1173							
2a			0.0891						
2b				0.0891					
3a					0.0891				
3b						0.1268			
4							0.1079		
5a								0.1363	
5b									0.1553

Estimates of transition frequencies 4

TO

FROM	*1a*	*1b*	*2a*	*2b*	*3a*	*3b*	*4*	*5a*	*5b*	Row totals
1a	1.07	0	0	0	0	0	0	0	0	1.07
1b	0	1.86	0	0	0	2	1	0	0	4.86
2a	0	0	1.07	0	0	0	0	0	0	1.07
2b	0	0	0	1.07	0	0	0	0	0	1.07
3a	0	0	0	0	1.07	0	0	0	0	1.07
3b	0	1	0	0	0	2.17	1	0	2	6.17
4	0	0	0	0	0	0	1.57	2	0	3.57
5a	0	1	0	0	0	0	0	2.50	4	7.50
5b	0	1	0	0	0	2	1	3	3.25	10.25
Column totals	1.07	4.86	1.07	1.07	1.07	6.17	4.57	7.50	9.25	36.63

Estimate of transition probabilities for diagonals 4

TO

FROM	*1a*	*1b*	*2a*	*2b*	*3a*	*3b*	*4*	*5a*	*5b*
1a	0.0292								
1b		0.1326							
2a			0.0292						
2b				0.0292					
3a					0.0292				
3b						0.1684			
4							0.0975		
5a								0.2049	
5b									0.2799

APPENDIX VIII - EMBEDDED MARKOV CHAIN ANALYSIS OF TREDOMEN QUARRY SEQUENCE

Embedded Markov Chain Analysis of lower Tredomen sequence using 10cm intervals (continued)

Estimates of transition frequencies 5

		TO								
		1a	*1b*	*2a*	*2b*	*3a*	*3b*	*4*	*5a*	*5b*	Row totals
FROM	*1a*	0.03	0	0	0	0	0	0	0	0	0.03
	1b	0	0.64	0	0	0	2	1	0	0	3.64
	2a	0	0	0.03	0	0	0	0	0	0	0.03
	2b	0	0	0	0.03	0	0	0	0	0	0.03
	3a	0	0	0	0	0.03	0	0	0	0	0.03
	3b	0	1	0	0	0	1.04	1	0	2	5.04
	4	0	0	0	0	0	0	0.35	2	0	2.35
	5a	0	1	0	0	0	0	0	1.54	4	6.54
	5b	0	1	0	0	0	2	1	3	2.87	9.87
Column totals		0.03	3.64	0.03	0.03	0.03	5.04	3.35	6.54	8.87	27.56

Estimate of transition probabilities for diagonals 5

		TO								
		1a	*1b*	*2a*	*2b*	*3a*	*3b*	*4*	*5a*	*5b*
FROM	*1a*	0.0011								
	1b		0.1322							
	2a			0.0011						
	2b				0.0011					
	3a					0.0011				
	3b						0.1828			
	4							0.0852		
	5a								0.2372	
	5b									0.3581

Estimates of transition frequencies 6

		TO								
		1a	*1b*	*2a*	*2b*	*3a*	*3b*	*4*	*5a*	*5b*	Row totals
FROM	*1a*	0.00	0	0	0	0	0	0	0	0	0.00
	1b	0	0.48	0	0	0	2	1	0	0	3.48
	2a	0	0	0.00	0	0	0	0	0	0	0.00
	2b	0	0	0	0.00	0	0	0	0	0	0.00
	3a	0	0	0	0	0.00	0	0	0	0	0.00
	3b	0	1	0	0	0	0.92	1	0	2	4.92
	4	0	0	0	0	0	0	0.20	2	0	2.20
	5a	0	1	0	0	0	0	0	1.55	4	6.55
	5b	0	1	0	0	0	2	1	3	3.53	10.53
Column totals		0.00	3.48	0.00	0.00	0.00	4.92	3.20	6.55	9.53	27.69

APPENDIX VIII - EMBEDDED MARKOV CHAIN ANALYSIS OF TREDOMEN QUARRY SEQUENCE

Embedded Markov Chain Analysis of lower Tredomen sequence using 10cm intervals (continued)

Estimate of transition probabilities for diagonals 6

TO

FROM	*1a*	*1b*	*2a*	*2b*	*3a*	*3b*	*4*	*5a*	*5b*
1a	1E-06								
1b		0.1258							
2a			1E-06						
2b				0.0000					
3a					1E-06				
3b						0.1777			
4							0.0795		
5a								0.2366	
5b									0.3805

Estimates of transition frequencies 7

TO

FROM	*1a*	*1b*	*2a*	*2b*	*3a*	*3b*	*4*	*5a*	*5b*	Row totals
1a	0.00	0	0	0	0	0	0	0	0	0.00
1b	0	0.44	0	0	0	2	1	0	0	3.44
2a	0	0	0.00	0	0	0	0	0	0	0.00
2b	0	0	0	0.00	0	0	0	0	0	0.00
3a	0	0	0	0	0.00	0	0	0	0	0.00
3b	0	1	0	0	0	0.87	1	0	2	4.87
4	0	0	0	0	0	0	0.17	2	0	2.17
5a	0	1	0	0	0	0	0	1.55	4	6.55
5b	0	1	0	0	0	2	1	3	4.01	11.01
Column totals	0.00	3.44	0.00	0.00	0.00	4.87	3.17	6.55	10.01	28.04

Estimate of transition probabilities for diagonals 7

TO

FROM	*1a*	*1b*	*2a*	*2b*	*3a*	*3b*	*4*	*5a*	*5b*
1a	2E-12								
1b		0.1226							
2a			2E-12						
2b				0.0000					
3a					2E-12				
3b						0.1738			
4							0.0775		
5a								0.2335	
5b									0.3925

APPENDIX VIII - EMBEDDED MARKOV CHAIN ANALYSIS OF TREDOMEN QUARRY SEQUENCE

Embedded Markov Chain Analysis of lower Tredomen sequence using 10cm intervals (continued)

Estimates of transition frequencies 8

		TO								
		1a	*1b*	*2a*	*2b*	*3a*	*3b*	*4*	*5a*	*5b*	Row totals
FROM	*1a*	0.00	0	0	0	0	0	0	0	0	0.00
	1b	0	0.42	0	0	0	2	1	0	0	3.42
	2a	0	0	0.00	0	0	0	0	0	0	0.00
	2b	0	0	0	0.00	0	0	0	0	0	0.00
	3a	0	0	0	0	0.00	0	0	0	0	0.00
	3b	0	1	0	0	0	0.85	1	0	2	4.85
	4	0	0	0	0	0	0	0.17	2	0	2.17
	5a	0	1	0	0	0	0	0	1.53	4	6.53
	5b	0	1	0	0	0	2	1	3	4.32	11.32
Column totals		0.00	3.42	0.00	0.00	0.00	4.85	3.17	6.53	10.32	28.29

Estimate of transition probabilities for diagonals 8

		TO								
		1a	*1b*	*2a*	*2b*	*3a*	*3b*	*4*	*5a*	*5b*
FROM	*1a*	3E-24								
	1b		0.121							
	2a			3E-24						
	2b				0.0000					
	3a					3E-24				
	3b						0.1714			
	4							0.0767		
	5a								0.2308	
	5b									0.4002

Estimates of transition frequencies 9

		TO								
		1a	*1b*	*2a*	*2b*	*3a*	*3b*	*4*	*5a*	*5b*	Row totals
FROM	*1a*	0.000	0	0	0	0	0	0	0	0	0.00
	1b	0	0.414	0	0	0	2	1	0	0	3.41
	2a	0	0	0.000	0	0	0	0	0	0	0.00
	2b	0	0	0	0.000	0	0	0	0	0	0.00
	3a	0	0	0	0	0.000	0	0	0	0	0.00
	3b	0	1	0	0	0	0.831	1	0	2	4.83
	4	0	0	0	0	0	0	0.166	2	0	2.17
	5a	0	1	0	0	0	0	0	1.507	4	6.51
	5b	0	1	0	0	0	2	1	3	4.530	11.53
Column totals		0.00	3.41	0.00	0.00	0.00	4.83	3.17	6.51	10.53	28.45

APPENDIX VIII - EMBEDDED MARKOV CHAIN ANALYSIS OF TREDOMEN QUARRY SEQUENCE

Embedded Markov Chain Analysis of lower Tredomen sequence using 10cm intervals (continued)

Estimate of transition probabilities for diagonals 9

		TO								
		1a	*1b*	*2a*	*2b*	*3a*	*3b*	*4*	*5a*	*5b*
FROM	*1a*	7E-48								
	1b		0.12							
	2a			7E-48						
	2b				0.0000					
	3a					7E-48				
	3b						0.1698			
	4							0.0761		
	5a								0.2287	
	5b									0.4053

Estimates of transition frequencies 10

		TO									
		1a	*1b*	*2a*	*2b*	*3a*	*3b*	*4*	*5a*	*5b*	Row totals
FROM	*1a*	0.000	0	0	0	0	0	0	0	0	0.00
	1b	0	0.410	0	0	0	2	1	0	0	3.41
	2a	0	0	0.000	0	0	0	0	0	0	0.00
	2b	0	0	0	0.000	0	0	0	0	0	0.00
	3a	0	0	0	0	0.000	0	0	0	0	0.00
	3b	0	1	0	0	0	0.820	1	0	2	4.82
	4	0	0	0	0	0	0	0.165	2	0	2.16
	5a	0	1	0	0	0	0	0	1.488	4	6.49
	5b	0	1	0	0	0	2	1	3	4.673	11.67
Column totals		0.00	3.41	0.00	0.00	0.00	4.82	3.16	6.49	10.67	28.56

Estimate of transition probabilities for diagonals 10

		TO								
		1a	*1b*	*2a*	*2b*	*3a*	*3b*	*4*	*5a*	*5b*
FROM	*1a*	4E-95								
	1b		0.1194							
	2a			4E-95						
	2b				0.0000					
	3a					4E-95				
	3b						0.1688			
	4							0.0758		
	5a								0.2272	
	5b									0.4088

APPENDIX VIII - EMBEDDED MARKOV CHAIN ANALYSIS OF TREDOMEN QUARRY SEQUENCE

Embedded Markov Chain Analysis of lower Tredomen sequence using 10cm intervals (continued)

Estimates of transition frequencies 11

		TO								
		1a	*1b*	*2a*	*2b*	*3a*	*3b*	*4*	*5a*	*5b*	Row totals
FROM	*1a*	0.000	0	0	0	0	0	0	0	0	0.00
	1b	0	0.407	0	0	0	2	1	0	0	3.41
	2a	0	0	0.000	0	0	0	0	0	0	0.00
	2b	0	0	0	0.000	0	0	0	0	0	0.00
	3a	0	0	0	0	0.000	0	0	0	0	0.00
	3b	0	1	0	0	0	0.814	1	0	2	4.81
	4	0	0	0	0	0	0	0.164	2	0	2.16
	5a	0	1	0	0	0	0	0	1.474	4	6.47
	5b	0	1	0	0	0	2	1	3	4.772	11.77
Column totals		0.00	3.41	0.00	0.00	0.00	4.81	3.16	6.47	10.77	28.63

Estimate of transition probabilities for diagonals 11

		TO								
		1a	*1b*	*2a*	*2b*	*3a*	*3b*	*4*	*5a*	*5b*
FROM	*1a*	2E-189								
	1b		0.119							
	2a			2E-189						
	2b				0.0000					
	3a					2E-189				
	3b						0.1681			
	4							0.0756		
	5a								0.2261	
	5b									0.4112

Estimates of transition frequencies 12

		TO								
		1a	*1b*	*2a*	*2b*	*3a*	*3b*	*4*	*5a*	*5b*	Row totals
FROM	*1a*	0.000	0	0	0	0	0	0	0	0	0.00
	1b	0	0.405	0	0	0	2	1	0	0	3.41
	2a	0	0	0.000	0	0	0	0	0	0	0.00
	2b	0	0	0	0.000	0	0	0	0	0	0.00
	3a	0	0	0	0	0.000	0	0	0	0	0.00
	3b	0	1	0	0	0	0.809	1	0	2	4.81
	4	0	0	0	0	0	0	0.164	2	0	2.16
	5a	0	1	0	0	0	0	0	1.464	4	6.46
	5b	0	1	0	0	0	2	1	3	4.840	11.84
Column totals		0.00	3.41	0.00	0.00	0.00	4.81	3.16	6.46	10.84	28.68

APPENDIX VIII - EMBEDDED MARKOV CHAIN ANALYSIS OF TREDOMEN QUARRY SEQUENCE

Embedded Markov Chain Analysis of lower Tredomen sequence using 10cm intervals (continued)

Estimate of transition probabilities for diagonals 12

TO

FROM	*1a*	*1b*	*2a*	*2b*	*3a*	*3b*	*4*	*5a*	*5b*
1a	0								
1b		0.1187							
2a			0						
2b				0.0000					
3a					0				
3b						0.1677			
4							0.0754		
5a								0.2254	
5b									0.4128

Estimates of transition frequencies 13

TO

FROM	*1a*	*1b*	*2a*	*2b*	*3a*	*3b*	*4*	*5a*	*5b*	Row totals
1a	0.00	0	0	0	0	0	0	0	0	0.00
1b	0	0.40	0	0	0	2	1	0	0	3.40
2a	0	0	0.00	0	0	0	0	0	0	0.00
2b	0	0	0	0.00	0	0	0	0	0	0.00
3a	0	0	0	0	0.00	0	0	0	0	0.00
3b	0	1	0	0	0	0.81	1	0	2	4.81
4	0	0	0	0	0	0	0.16	2	0	2.16
5a	0	1	0	0	0	0	0	1.46	4	6.46
5b	0	1	0	0	0	2	1	3	4.89	11.89
Column totals	0.00	3.40	0.00	0.00	0.00	4.81	3.16	6.46	10.89	28.72

Estimate of transition probabilities for diagonals 13

TO

FROM	*1a*	*1b*	*2a*	*2b*	*3a*	*3b*	*4*	*5a*	*5b*
1a	0								
1b		0.1185							
2a			0						
2b				0.0000					
3a					0				
3b						0.1674			
4							0.0753		
5a								0.2248	
5b									0.4139

APPENDIX VIII - EMBEDDED MARKOV CHAIN ANALYSIS OF TREDOMEN QUARRY SEQUENCE

Embedded Markov Chain Analysis of lower Tredomen sequence using 10cm intervals (continued)

Estimates of transition frequencies 14

		TO								
		1a	*1b*	*2a*	*2b*	*3a*	*3b*	*4*	*5a*	*5b*	Row totals
FROM	*1a*	0.00	0	0	0	0	0	0	0	0	0.00
	1b	0	0.40	0	0	0	2	1	0	0	3.40
	2a	0	0	0.00	0	0	0	0	0	0	0.00
	2b	0	0	0	0.00	0	0	0	0	0	0.00
	3a	0	0	0	0	0.00	0	0	0	0	0.00
	3b	0	1	0	0	0	0.80	1	0	2	4.80
	4	0	0	0	0	0	0	0.16	2	0	2.16
	5	0	1	0	0	0	0	0	1.45	4	6.45
	6	0	1	0	0	0	2	1	3	4.92	11.92
Column totals		0.00	3.40	0.00	0.00	0.00	4.80	3.16	6.45	10.92	28.74

Estimate of transition probabilities for diagonals 14

		TO								
		1a	*1b*	*2a*	*2b*	*3a*	*3b*	*4*	*5a*	*5b*
FROM	*1a*	0								
	1b		0.1184							
	2a			0						
	2b				0.0000					
	3a					0				
	3b						0.1671			
	4							0.0753		
	5a								0.2245	
	5b									0.4147

Estimates of transition frequencies 15

		TO								
		1a	*1b*	*2a*	*2b*	*3a*	*3b*	*4*	*5a*	*5b*	Row totals
FROM	*1a*	0.00	0	0	0	0	0	0	0	0	0.00
	1b	0	0.40	0	0	0	2	1	0	0	3.40
	2a	0	0	0.00	0	0	0	0	0	0	0.00
	2b	0	0	0	0.00	0	0	0	0	0	0.00
	3a	0	0	0	0	0.00	0	0	0	0	0.00
	3b	0	1	0	0	0	0.80	1	0	2	4.80
	4	0	0	0	0	0	0	0.16	2	0	2.16
	5a	0	1	0	0	0	0	0	1.45	4	6.45
	5b	0	1	0	0	0	2	1	3	4.94	11.94
Column totals		0.00	3.40	0.00	0.00	0.00	4.80	3.16	6.45	10.94	28.76

APPENDIX VIII - EMBEDDED MARKOV CHAIN ANALYSIS OF TREDOMEN QUARRY SEQUENCE

Embedded Markov Chain Analysis of lower Tredomen sequence using 10cm intervals (continued)

Estimate of transition probabilities for diagonals 15

FROM \ TO	*1a*	*1b*	*2a*	*2b*	*3a*	*3b*	*4*	*5a*	*5b*
1a	0								
1b		0.1183							
2a			0						
2b				0.0000					
3a					0				
3b						0.167			
4							0.0752		
5a								0.2242	
5b									0.4153

Estimates of transition frequencies 16

FROM \ TO	*1a*	*1b*	*2a*	*2b*	*3a*	*3b*	*4*	*5a*	*5b*	Row totals
1a	0.00	0	0	0	0	0	0	0	0	0.00
1b	0	0.40	0	0	0	2	1	0	0	3.40
2a	0	0	0.00	0	0	0	0	0	0	0.00
2b	0	0	0	0.00	0	0	0	0	0	0.00
3a	0	0	0	0	0.00	0	0	0	0	0.00
3b	0	1	0	0	0	0.80	1	0	2	4.80
4	0	0	0	0	0	0	0.16	2	0	2.16
5a	0	1	0	0	0	0	0	1.45	4	6.45
5b	0	1	0	0	0	2	1	3	4.96	11.96
Column totals	0.00	3.40	0.00	0.00	0.00	4.80	3.16	6.45	10.96	28.77

Estimate of transition probabilities for diagonals 16

FROM \ TO	*1a*	*1b*	*2a*	*2b*	*3a*	*3b*	*4*	*5a*	*5b*
1a	0								
1b		0.1183							
2a			0						
2b				0.0000					
3a					0				
3b						0.1669			
4							0.0752		
5a								0.224	
5b									0.4157

APPENDIX VIII - EMBEDDED MARKOV CHAIN ANALYSIS OF TREDOMEN QUARRY SEQUENCE

Embedded Markov Chain Analysis of lower Tredomen sequence using 10cm intervals (continued)

Estimates of transition frequencies 17

		TO								
		1a	*1b*	*2a*	*2b*	*3a*	*3b*	*4*	*5a*	*5b*	Row totals
FROM	*1a*	0.00	0	0	0	0	0	0	0	0	0.00
	1b	0	0.40	0	0	0	2	1	0	0	3.40
	2a	0	0	0.00	0	0	0	0	0	0	0.00
	2b	0	0	0	0.00	0	0	0	0	0	0.00
	3a	0	0	0	0	0.00	0	0	0	0	0.00
	3b	0	1	0	0	0	0.80	1	0	2	4.80
	4	0	0	0	0	0	0	0.16	2	0	2.16
	5a	0	1	0	0	0	0	0	1.44	4	6.44
	5b	0	1	0	0	0	2	1	3	4.97	11.97
Column totals		0.00	3.40	0.00	0.00	0.00	4.80	3.16	6.44	10.97	28.78

Estimate of transition probabilities for diagonals 17

		TO								
		1a	*1b*	*2a*	*2b*	*3a*	*3b*	*4*	*5a*	*5b*
FROM	*1a*	0								
	1b		0.1182							
	2a			0						
	2b				0.0000					
	3a					0				
	3b						0.1668			
	4							0.0751		
	5a								0.2239	
	5b									0.4159

Estimates of transition frequencies 18

		TO								
		1a	*1b*	*2a*	*2b*	*3a*	*3b*	*4*	*5a*	*5b*	Row totals
FROM	*1a*	0.00	0	0	0	0	0	0	0	0	0.00
	1b	0	0.40	0	0	0	2	1	0	0	3.40
	2a	0	0	0.00	0	0	0	0	0	0	0.00
	2b	0	0	0	0.00	0	0	0	0	0	0.00
	3a	0	0	0	0	0.00	0	0	0	0	0.00
	3b	0	1	0	0	0	0.80	1	0	2	4.80
	4	0	0	0	0	0	0	0.16	2	0	2.16
	5a	0	1	0	0	0	0	0	1.44	4	6.44
	5b	0	1	0	0	0	2	1	3	4.98	11.98
Column totals		0.00	3.40	0.00	0.00	0.00	4.80	3.16	6.44	10.98	28.79

APPENDIX VIII - EMBEDDED MARKOV CHAIN ANALYSIS OF TREDOMEN QUARRY SEQUENCE

Embedded Markov Chain Analysis of lower Tredomen sequence using 10cm intervals (continued)

Estimate of transition probabilities for diagonals 18

TO

FROM	*1a*	*1b*	*2a*	*2b*	*3a*	*3b*	*4*	*5a*	*5b*
1a	0								
1b		0.1182							
2a			0						
2b				0.0000					
3a					0				
3b						0.1668			
4							0.0751		
5a								0.2238	
5b									0.4161

Estimates of transition frequencies 19

TO

FROM	*1a*	*1b*	*2a*	*2b*	*3a*	*3b*	*4*	*5a*	*5b*	Row totals
1a	0.00	0	0	0	0	0	0	0	0	0.00
1b	0	0.40	0	0	0	2	1	0	0	3.40
2a	0	0	0.00	0	0	0	0	0	0	0.00
2b	0	0	0	0.00	0	0	0	0	0	0.00
3a	0	0	0	0	0.00	0	0	0	0	0.00
3b	0	1	0	0	0	0.80	1	0	2	4.80
4	0	0	0	0	0	0	0.16	2	0	2.16
5a	0	1	0	0	0	0	0	1.44	4	6.44
5b	0	1	0	0	0	2	1	3	4.98	11.98
Column totals	0.00	3.40	0.00	0.00	0.00	4.80	3.16	6.44	10.98	28.79

Fixed probability vectors

1a	0
1b	0.1182
2a	0
2b	0
3a	0
3b	0.1668
4	0.0751
5	0.2238
6	0.4161

APPENDIX VIII - EMBEDDED MARKOV CHAIN ANALYSIS OF TREDOMEN QUARRY SEQUENCE

Embedded Markov Chain Analysis of lower Tredomen sequence using 10cm intervals (continued)

Expected transitions probabilities matrix

		TO								
		1a	*1b*	*2a*	*2b*	*3a*	*3b*	*4*	*5a*	*5b*
FROM	*1a*	0.0000	0.0000	0.0000	0.0000	0.0000	0.0000	0.0000	0.0000	0.0000
	1b	0.0000	0.0140	0.0000	0.0000	0.0000	0.0197	0.0089	0.0264	0.0492
	2a	0.0000	0.0000	0.0000	0.0000	0.0000	0.0000	0.0000	0.0000	0.0000
	2b	0.0000	0.0000	0.0000	0.0000	0.0000	0.0000	0.0000	0.0000	0.0000
	3a	0.0000	0.0000	0.0000	0.0000	0.0000	0.0000	0.0000	0.0000	0.0000
	3b	0.0000	0.0197	0.0000	0.0000	0.0000	0.0278	0.0125	0.0373	0.0694
	4	0.0000	0.0089	0.0000	0.0000	0.0000	0.0125	0.0056	0.0168	0.0313
	5a	0.0000	0.0264	0.0000	0.0000	0.0000	0.0373	0.0168	0.0501	0.0931
	5b	0.0000	0.0492	0.0000	0.0000	0.0000	0.0694	0.0313	0.0931	0.1732

Expected transitions matrix

		TO								
		1a	*1b*	*2a*	*2b*	*3a*	*3b*	*4*	*5a*	*5b*
FROM	*1a*	0.00	0.00	0.00	0.00	0.00	0.00	0.00	0.00	0.00
	1b	0.00	0.40	0.00	0.00	0.00	0.57	0.26	0.76	1.42
	2a	0.00	0.00	0.00	0.00	0.00	0.00	0.00	0.00	0.00
	2b	0.00	0.00	0.00	0.00	0.00	0.00	0.00	0.00	0.00
	3a	0.00	0.00	0.00	0.00	0.00	0.00	0.00	0.00	0.00
	3b	0.00	0.57	0.00	0.00	0.00	0.80	0.36	1.07	2.00
	4	0.00	0.26	0.00	0.00	0.00	0.36	0.16	0.48	0.90
	5a	0.00	0.76	0.00	0.00	0.00	1.07	0.48	1.44	2.68
	5b	0.00	1.42	0.00	0.00	0.00	2.00	0.90	2.68	4.98

Expected frequencies without estimates

		TO									
		1a	*1b*	*2a*	*2b*	*3a*	*3b*	*4*	*5a*	*5b*	Rows total
FROM	*1a*		0.00	0.00	0.00	0.00	0.00	0.00	0.00	0.00	0.00
	1b	0.00		0.00	0.00	0.00	0.57	0.26	0.76	1.42	3.00
	2a	0.00	0.00		0.00	0.00	0.00	0.00	0.00	0.00	0.00
	2b	0.00	0.00	0.00		0.00	0.00	0.00	0.00	0.00	0.00
	3a	0.00	0.00	0.00	0.00		0.00	0.00	0.00	0.00	0.00
	3b	0.00	0.57	0.00	0.00	0.00		0.36	1.07	2.00	4.00
	4	0.00	0.26	0.00	0.00	0.00	0.36		0.48	0.90	2.00
	5a	0.00	0.76	0.00	0.00	0.00	1.07	0.48		2.68	5.00
	5b	0.00	1.42	0.00	0.00	0.00	2.00	0.90	2.68		6.99
Column totals		0.00	3.00	0.00	0.00	0.00	4.00	2.00	5.00	6.99	21.00

APPENDIX VIII - EMBEDDED MARKOV CHAIN ANALYSIS OF TREDOMEN QUARRY SEQUENCE

Embedded Markov Chain Analysis of lower Tredomen sequence using 10cm intervals (continued)

Original Observed Transitions matrix

		TO									
		1a	*1b*	*2a*	*2b*	*3a*	*3b*	*4*	*5a*	*5b*	Row totals
FROM	*1a*		0	0	0	0	0	0	0	0	0.00
	1b	0		0	0	0	2	1	0	0	3.00
	2a	0	0		0	0	0	0	0	0	0.00
	2b	0	0	0		0	0	0	0	0	0.00
	3a	0	0	0	0		0	0	0	0	0.00
	3b	0	1	0	0	0		1	0	2	4.00
	4	0	0	0	0	0	0		2	0	2.00
	5a	0	1	0	0	0	0	0		4	5.00
	5b	0	1	0	0	0	2	1	3		7.00
Column totals		0.00	3.00	0.00	0.00	0.00	4.00	3.00	5.00	6.00	21.00

T	*O*	*E*	$((O-E)^2)/E$
orange	5.00	5.00	0.00
purple	5.00	5.83	0.12
pink	11.00	10.16	0.07

$\chi^2 =$ **0.19** with 55 degrees of freedom = (number of states -1)^2

critical value at 5% significance level for 55 degrees of freedom = 73.31

Therefore, the series of states are independent of one another.

That is the series does not exhibits a first order Markovian property.

APPENDIX VIII - EMBEDDED MARKOV CHAIN ANALYSIS OF TREDOMEN QUARRY SEQUENCE

Embedded markov chain analysis of upper Tredomen sequence using 10cm intervals.

Observed Transitions matrix

		TO								
		1a	*1b*	*2a*	*2b*	*3a*	*3b*	*4*	*5a*	*5b*	Row totals
FROM	*1a*	0	0	11	3	1	1	0	0	0	16
	1b	1	0	0	0	0	0	2	0	0	3
	2a	1	0	0	3	8	1	0	0	0	13
	2b	2	0	0	0	3	1	0	0	2	8
	3a	3	0	3	1	0	3	1	0	2	13
	3b	0	0	0	0	0	0	7	2	14	23
	4	1	1	0	0	1	8	0	3	15	29
	5a	0	0	0	0	0	1	2	0	8	11
	5b	9	2	0	1	0	7	17	2	0	38
Column totals		17	3	14	8	13	22	29	7	41	154

Estimates of transition frequencies 1

		TO								
		1a	*1b*	*2a*	*2b*	*3a*	*3b*	*4*	*5a*	*5b*	Row totals
FROM	*1a*	1000	0	11	3	1	1	0	0	0	1016
	1b	1	1000	0	0	0	0	2	0	0	1003
	2a	1	0	1000	3	8	1	0	0	0	1013
	2b	2	0	0	1000	3	1	0	0	2	1008
	3a	3	0	3	1	1000	3	1	0	2	1013
	3b	0	0	0	0	0	1000	7	2	14	1023
	4	1	1	0	0	1	8	1000	3	15	1029
	5a	0	0	0	0	0	1	2	1000	8	1011
	5b	9	2	0	1	0	7	17	2	1000	1038
Column totals		1017	1003	1014	1008	1013	1022	1029	1007	1041	9154

Estimate of transition probabilities for diagonals 1

		TO								
		1a	*1b*	*2a*	*2b*	*3a*	*3b*	*4*	*5a*	*5b*
FROM	*1a*	0.111								
	1b		0.1096							
	2a			0.1107						
	2b				0.1101					
	3a					0.1107				
	3b						0.1118			
	4							0.1124		
	5a								0.1104	
	5b									0.1134

APPENDIX VIII - EMBEDDED MARKOV CHAIN ANALYSIS OF TREDOMEN QUARRY SEQUENCE

Embedded markov chain analysis of upper Tredomen sequence using 10cm intervals (continued)

Estimates of transition frequencies 2

		TO								
		1a	*1b*	*2a*	*2b*	*3a*	*3b*	*4*	*5a*	*5b*	Row totals
FROM	*1a*	112.77	0.00	11.00	3.00	1.00	1.00	0.00	0.00	0.00	129
	1b	1.00	109.90	0.00	0.00	0.00	0.00	2.00	0.00	0.00	113
	2a	1.00	0.00	112.10	3.00	8.00	1.00	0.00	0.00	0.00	125
	2b	2.00	0.00	0.00	111.00	3.00	1.00	0.00	0.00	2.00	119
	3a	3.00	0.00	3.00	1.00	112.10	3.00	1.00	0.00	2.00	125
	3b	0.00	0.00	0.00	0.00	0.00	114.32	7.00	2.00	14.00	137
	4	1.00	1.00	0.00	0.00	1.00	8.00	115.67	3.00	15.00	145
	5a	0.00	0.00	0.00	0.00	0.00	1.00	2.00	111.66	8.00	123
	5b	9.00	2.00	0.00	1.00	0.00	7.00	17.00	2.00	117.70	156
Column totals		129.77	112.90	126.10	119.00	125.10	136.32	144.67	118.66	158.70	1171

Estimate of transition probabilities for diagonals 2

		TO								
		1a	*1b*	*2a*	*2b*	*3a*	*3b*	*4*	*5a*	*5b*
FROM	*1a*	0.1099								
	1b		0.0964							
	2a			0.1068						
	2b				0.1016					
	3a					0.1068				
	3b						0.1172			
	4							0.1235		
	5a								0.1047	
	5b									0.1329

Estimates of transition frequencies 3

		TO								
		1a	*1b*	*2a*	*2b*	*3a*	*3b*	*4*	*5a*	*5b*	Row totals
FROM	*1a*	14.16	0.00	11.00	3.00	1.00	1.00	0.00	0.00	0.00	30
	1b	1.00	10.88	0.00	0.00	0.00	0.00	2.00	0.00	0.00	14
	2a	1.00	0.00	13.36	3.00	8.00	1.00	0.00	0.00	0.00	26
	2b	2.00	0.00	0.00	12.09	3.00	1.00	0.00	0.00	2.00	20
	3a	3.00	0.00	3.00	1.00	13.36	3.00	1.00	0.00	2.00	26
	3b	0.00	0.00	0.00	0.00	0.00	16.10	7.00	2.00	14.00	39
	4	1.00	1.00	0.00	0.00	1.00	8.00	17.87	3.00	15.00	47
	5a	0.00	0.00	0.00	0.00	0.00	1.00	2.00	12.85	8.00	24
	5b	9.00	2.00	0.00	1.00	0.00	7.00	17.00	2.00	20.70	59
Column totals		31.16	13.88	27.36	20.09	26.36	38.10	46.87	19.85	61.70	285

APPENDIX VIII - EMBEDDED MARKOV CHAIN ANALYSIS OF TREDOMEN QUARRY SEQUENCE

Embedded markov chain analysis of upper Tredomen sequence using 10cm intervals (continued)

Estimate of transition probabilities for diagonals 3

TO

FROM	*1a*	*1b*	*2a*	*2b*	*3a*	*3b*	*4*	*5a*	*5b*
1a	0.1057								
1b		0.0486							
2a			0.0924						
2b				0.0704					
3a					0.0924				
3b						0.137			
4							0.1642		
5a								0.0836	
5b									0.2057

Estimates of transition frequencies 4

TO

FROM	*1a*	*1b*	*2a*	*2b*	*3a*	*3b*	*4*	*5a*	*5b*	Row totals
1a	3.19	0.00	11.00	3.00	1.00	1.00	0.00	0.00	0.00	19
1b	1.00	0.68	0.00	0.00	0.00	0.00	2.00	0.00	0.00	4
2a	1.00	0.00	2.44	3.00	8.00	1.00	0.00	0.00	0.00	15
2b	2.00	0.00	0.00	1.41	3.00	1.00	0.00	0.00	2.00	9
3a	3.00	0.00	3.00	1.00	2.44	3.00	1.00	0.00	2.00	15
3b	0.00	0.00	0.00	0.00	0.00	5.36	7.00	2.00	14.00	28
4	1.00	1.00	0.00	0.00	1.00	8.00	7.70	3.00	15.00	37
5a	0.00	0.00	0.00	0.00	0.00	1.00	2.00	1.99	8.00	13
5b	9.00	2.00	0.00	1.00	0.00	7.00	17.00	2.00	12.07	50
Column totals	20.19	3.68	16.44	9.41	15.44	27.36	36.70	8.99	53.07	191

Estimate of transition probabilities for diagonals 4

TO

FROM	*1a*	*1b*	*2a*	*2b*	*3a*	*3b*	*4*	*5a*	*5b*
1a	0.1003								
1b		0.0192							
2a			0.0807						
2b				0.0492					
3a					0.0807				
3b						0.1483			
4							0.1919		
5a								0.0679	
5b									0.2618

APPENDIX VIII - EMBEDDED MARKOV CHAIN ANALYSIS OF TREDOMEN QUARRY SEQUENCE

Embedded markov chain analysis of upper Tredomen sequence using 10cm intervals (continued)

Estimates of transition frequencies 5

		TO									
		1a	*1b*	*2a*	*2b*	*3a*	*3b*	*4*	*5a*	*5b*	Row totals
FROM	*1a*	1.92	0.00	11.00	3.00	1.00	1.00	0.00	0.00	0.00	18
	1b	1.00	0.07	0.00	0.00	0.00	0.00	2.00	0.00	0.00	3
	2a	1.00	0.00	1.25	3.00	8.00	1.00	0.00	0.00	0.00	14
	2b	2.00	0.00	0.00	0.46	3.00	1.00	0.00	0.00	2.00	8
	3a	3.00	0.00	3.00	1.00	1.25	3.00	1.00	0.00	2.00	14
	3b	0.00	0.00	0.00	0.00	0.00	4.20	7.00	2.00	14.00	27
	4	1.00	1.00	0.00	0.00	1.00	8.00	7.04	3.00	15.00	36
	5a	0.00	0.00	0.00	0.00	0.00	1.00	2.00	0.88	8.00	12
	5b	9.00	2.00	0.00	1.00	0.00	7.00	17.00	2.00	13.11	51
Column totals		18.92	3.07	15.25	8.46	14.25	26.20	36.04	7.88	54.11	184

Estimate of transition probabilities for diagonals 5

		TO								
		1a	*1b*	*2a*	*2b*	*3a*	*3b*	*4*	*5a*	*5b*
FROM	*1a*	0.0973								
	1b		0.0167							
	2a			0.0773						
	2b				0.0459					
	3a					0.0773				
	3b						0.1477			
	4							0.1957		
	5a								0.0645	
	5b									0.2775

Estimates of transition frequencies 6

		TO									
		1a	*1b*	*2a*	*2b*	*3a*	*3b*	*4*	*5a*	*5b*	Row totals
FROM	*1a*	1.74	0.00	11.00	3.00	1.00	1.00	0.00	0.00	0.00	18
	1b	1.00	0.05	0.00	0.00	0.00	0.00	2.00	0.00	0.00	3
	2a	1.00	0.00	1.10	3.00	8.00	1.00	0.00	0.00	0.00	14
	2b	2.00	0.00	0.00	0.39	3.00	1.00	0.00	0.00	2.00	8
	3a	3.00	0.00	3.00	1.00	1.10	3.00	1.00	0.00	2.00	14
	3b	0.00	0.00	0.00	0.00	0.00	4.02	7.00	2.00	14.00	27
	4	1.00	1.00	0.00	0.00	1.00	8.00	7.05	3.00	15.00	36
	5a	0.00	0.00	0.00	0.00	0.00	1.00	2.00	0.77	8.00	12
	5b	9.00	2.00	0.00	1.00	0.00	7.00	17.00	2.00	14.18	52
Column totals		18.74	3.05	15.10	8.39	14.10	26.02	36.05	7.77	55.18	184

APPENDIX VIII - EMBEDDED MARKOV CHAIN ANALYSIS OF TREDOMEN QUARRY SEQUENCE

Embedded markov chain analysis of upper Tredomen sequence using 10cm intervals (continued)

Estimate of transition probabilities for diagonals 6

		TO								
		1a	*1b*	*2a*	*2b*	*3a*	*3b*	*4*	*5a*	*5b*
FROM	*1a*	0.0962								
	1b		0.0165							
	2a			0.0765						
	2b				0.0455					
	3a					0.0765				
	3b						0.1465			
	4							0.1955		
	5a								0.0638	
	5b									0.283

Estimates of transition frequencies 7

		TO									
		1a	*1b*	*2a*	*2b*	*3a*	*3b*	*4*	*5a*	*5b*	Row totals
FROM	*1a*	1.71	0.00	11.00	3.00	1.00	1.00	0.00	0.00	0.00	18
	1b	1.00	0.05	0.00	0.00	0.00	0.00	2.00	0.00	0.00	3
	2a	1.00	0.00	1.08	3.00	8.00	1.00	0.00	0.00	0.00	14
	2b	2.00	0.00	0.00	0.38	3.00	1.00	0.00	0.00	2.00	8
	3a	3.00	0.00	3.00	1.00	1.08	3.00	1.00	0.00	2.00	14
	3b	0.00	0.00	0.00	0.00	0.00	3.96	7.00	2.00	14.00	27
	4	1.00	1.00	0.00	0.00	1.00	8.00	7.05	3.00	15.00	36
	5a	0.00	0.00	0.00	0.00	0.00	1.00	2.00	0.75	8.00	12
	5b	9.00	2.00	0.00	1.00	0.00	7.00	17.00	2.00	14.77	53
Column totals		18.71	3.05	15.08	8.38	14.08	25.96	36.05	7.75	55.77	185

Estimate of transition probabilities for diagonals 7

		TO								
		1a	*1b*	*2a*	*2b*	*3a*	*3b*	*4*	*5a*	*5b*
FROM	*1a*	0.0958								
	1b		0.0165							
	2a			0.0762						
	2b				0.0454					
	3a					0.0762				
	3b						0.1459			
	4							0.195		
	5a								0.0636	
	5b									0.2855

APPENDIX VIII - EMBEDDED MARKOV CHAIN ANALYSIS OF TREDOMEN QUARRY SEQUENCE

Embedded markov chain analysis of upper Tredomen sequence using 10cm intervals (continued)

Estimates of transition frequencies 8

		TO								
		1a	*1b*	*2a*	*2b*	*3a*	*3b*	*4*	*5a*	*5b*	Row totals
FROM	*1a*	1.70	0.00	11.00	3.00	1.00	1.00	0.00	0.00	0.00	18
	1b	1.00	0.05	0.00	0.00	0.00	0.00	2.00	0.00	0.00	3
	2a	1.00	0.00	1.07	3.00	8.00	1.00	0.00	0.00	0.00	14
	2b	2.00	0.00	0.00	0.38	3.00	1.00	0.00	0.00	2.00	8
	3a	3.00	0.00	3.00	1.00	1.07	3.00	1.00	0.00	2.00	14
	3b	0.00	0.00	0.00	0.00	0.00	3.93	7.00	2.00	14.00	27
	4	1.00	1.00	0.00	0.00	1.00	8.00	7.03	3.00	15.00	36
	5a	0.00	0.00	0.00	0.00	0.00	1.00	2.00	0.75	8.00	12
	5b	9.00	2.00	0.00	1.00	0.00	7.00	17.00	2.00	15.06	53
Column totals		18.70	3.05	15.07	8.38	14.07	25.93	36.03	7.75	56.06	185

Estimate of transition probabilities for diagonals 8

		TO								
		1a	*1b*	*2a*	*2b*	*3a*	*3b*	*4*	*5a*	*5b*
FROM	*1a*	0.0956								
	1b		0.0165							
	2a			0.076						
	2b				0.0453					
	3a					0.076				
	3b						0.1455			
	4							0.1947		
	5a								0.0635	
	5b									0.2868

Estimates of transition frequencies 9

		TO								
		1a	*1b*	*2a*	*2b*	*3a*	*3b*	*4*	*5a*	*5b*	Row totals
FROM	*1a*	1.69	0.00	11.00	3.00	1.00	1.00	0.00	0.00	0.00	18
	1b	1.00	0.05	0.00	0.00	0.00	0.00	2.00	0.00	0.00	3
	2a	1.00	0.00	1.07	3.00	8.00	1.00	0.00	0.00	0.00	14
	2b	2.00	0.00	0.00	0.38	3.00	1.00	0.00	0.00	2.00	8
	3a	3.00	0.00	3.00	1.00	1.07	3.00	1.00	0.00	2.00	14
	3b	0.00	0.00	0.00	0.00	0.00	3.92	7.00	2.00	14.00	27
	4	1.00	1.00	0.00	0.00	1.00	8.00	7.02	3.00	15.00	36
	5a	0.00	0.00	0.00	0.00	0.00	1.00	2.00	0.75	8.00	12
	5b	9.00	2.00	0.00	1.00	0.00	7.00	17.00	2.00	15.22	53
Column totals		18.69	3.05	15.07	8.38	14.07	25.92	36.02	7.75	56.22	185

APPENDIX VIII - EMBEDDED MARKOV CHAIN ANALYSIS OF TREDOMEN QUARRY SEQUENCE

Embedded markov chain analysis of upper Tredomen sequence using 10cm intervals (continued)

Estimate of transition probabilities for diagonals 9

TO

FROM	*1a*	*1b*	*2a*	*2b*	*3a*	*3b*	*4*	*5a*	*5b*
1a	0.0956								
1b		0.0165							
2a			0.076						
2b				0.0453					
3a					0.076				
3b						0.1454			
4							0.1945		
5a								0.0634	
5b									0.2874

Estimates of transition frequencies 10

TO

FROM	*1a*	*1b*	*2a*	*2b*	*3a*	*3b*	*4*	*5a*	*5b*	Row totals
1a	1.69	0.00	11.00	3.00	1.00	1.00	0.00	0.00	0.00	18
1b	1.00	0.05	0.00	0.00	0.00	0.00	2.00	0.00	0.00	3
2a	1.00	0.00	1.07	3.00	8.00	1.00	0.00	0.00	0.00	14
2b	2.00	0.00	0.00	0.38	3.00	1.00	0.00	0.00	2.00	8
3a	3.00	0.00	3.00	1.00	1.07	3.00	1.00	0.00	2.00	14
3b	0.00	0.00	0.00	0.00	0.00	3.91	7.00	2.00	14.00	27
4	1.00	1.00	0.00	0.00	1.00	8.00	7.01	3.00	15.00	36
5a	0.00	0.00	0.00	0.00	0.00	1.00	2.00	0.75	8.00	12
5b	9.00	2.00	0.00	1.00	0.00	7.00	17.00	2.00	15.30	53
Column totals	18.69	3.05	15.07	8.38	14.07	25.91	36.01	7.75	56.30	185

Estimate of transition probabilities for diagonals 10

TO

FROM	*1a*	*1b*	*2a*	*2b*	*3a*	*3b*	*4*	*5a*	*5b*
1a	0.096								
1b		0.016							
2a			0.076						
2b				0.0452					
3a					0.076				
3b						0.145			
4							0.194		
5a								0.063	
5b									0.288

APPENDIX VIII - EMBEDDED MARKOV CHAIN ANALYSIS OF TREDOMEN QUARRY SEQUENCE

Embedded markov chain analysis of upper Tredomen sequence using 10cm intervals (continued)

Estimates of transition frequencies 11

		TO								
		1a	*1b*	*2a*	*2b*	*3a*	*3b*	*4*	*5a*	*5b*	Row totals
FROM	*1a*	1.69	0.00	11.00	3.00	1.00	1.00	0.00	0.00	0.00	18
	1b	1.00	0.05	0.00	0.00	0.00	0.00	2.00	0.00	0.00	3
	2a	1.00	0.00	1.07	3.00	8.00	1.00	0.00	0.00	0.00	14
	2b	2.00	0.00	0.00	0.38	3.00	1.00	0.00	0.00	2.00	8
	3a	3.00	0.00	3.00	1.00	1.07	3.00	1.00	0.00	2.00	14
	3b	0.00	0.00	0.00	0.00	0.00	3.91	7.00	2.00	14.00	27
	4	1.00	1.00	0.00	0.00	1.00	8.00	7.00	3.00	15.00	36
	5a	0.00	0.00	0.00	0.00	0.00	1.00	2.00	0.74	8.00	12
	5b	9.00	2.00	0.00	1.00	0.00	7.00	17.00	2.00	15.34	53
Column totals		18.69	3.05	15.07	8.38	14.07	25.91	36.00	7.74	56.34	185

Estimate of transition probabilities for diagonals 11

		TO								
		1a	*1b*	*2a*	*2b*	*3a*	*3b*	*4*	*5a*	*5b*
FROM	*1a*	0.0955								
	1b		0.0165							
	2a			0.0759						
	2b				0.0452					
	3a					0.0759				
	3b						0.1453			
	4							0.1943		
	5a								0.0634	
	5b									0.2879

Estimates of transition frequencies 12

		TO								
		1a	*1b*	*2a*	*2b*	*3a*	*3b*	*4*	*5a*	*5b*	Row totals
FROM	*1a*	1.69	0.00	11.00	3.00	1.00	1.00	0.00	0.00	0.00	18
	1b	1.00	0.05	0.00	0.00	0.00	0.00	2.00	0.00	0.00	3
	2a	1.00	0.00	1.07	3.00	8.00	1.00	0.00	0.00	0.00	14
	2b	2.00	0.00	0.00	0.38	3.00	1.00	0.00	0.00	2.00	8
	3a	3.00	0.00	3.00	1.00	1.07	3.00	1.00	0.00	2.00	14
	3b	0.00	0.00	0.00	0.00	0.00	3.91	7.00	2.00	14.00	27
	4	1.00	1.00	0.00	0.00	1.00	8.00	7.00	3.00	15.00	36
	5a	0.00	0.00	0.00	0.00	0.00	1.00	2.00	0.74	8.00	12
	5b	9.00	2.00	0.00	1.00	0.00	7.00	17.00	2.00	15.36	53
Column totals		18.69	3.05	15.07	8.38	14.07	25.91	36.00	7.74	56.36	185

APPENDIX VIII - EMBEDDED MARKOV CHAIN ANALYSIS OF TREDOMEN QUARRY SEQUENCE

Embedded markov chain analysis of upper Tredomen sequence using 10cm intervals (continued)

Estimate of transition probabilities for diagonals 12

TO

FROM	*1a*	*1b*	*2a*	*2b*	*3a*	*3b*	*4*	*5a*	*5b*
1a	0.0955								
1b		0.0165							
2a			0.0759						
2b				0.0452					
3a					0.0759				
3b						0.1453			
4							0.1943		
5a								0.0634	
5b									0.288

Estimates of transition frequencies 13

TO

FROM	*1a*	*1b*	*2a*	*2b*	*3a*	*3b*	*4*	*5a*	*5b*	Row totals
1a	1.69	0.00	11.00	3.00	1.00	1.00	0.00	0.00	0.00	18
1b	1.00	0.05	0.00	0.00	0.00	0.00	2.00	0.00	0.00	3
2a	1.00	0.00	1.07	3.00	8.00	1.00	0.00	0.00	0.00	14
2b	2.00	0.00	0.00	0.38	3.00	1.00	0.00	0.00	2.00	8
3a	3.00	0.00	3.00	1.00	1.07	3.00	1.00	0.00	2.00	14
3b	0.00	0.00	0.00	0.00	0.00	3.91	7.00	2.00	14.00	27
4	1.00	1.00	0.00	0.00	1.00	8.00	6.99	3.00	15.00	36
5a	0.00	0.00	0.00	0.00	0.00	1.00	2.00	0.74	8.00	12
5b	9.00	2.00	0.00	1.00	0.00	7.00	17.00	2.00	15.37	53
Column totals	18.69	3.05	15.07	8.38	14.07	25.91	35.99	7.74	56.37	185

Estimate of transition probabilities for diagonals 13

TO

FROM	*1a*	*1b*	*2a*	*2b*	*3a*	*3b*	*4*	*5a*	*5b*
1a	0.0955								
1b		0.0165							
2a			0.0759						
2b				0.0452					
3a					0.0759				
3b						0.1452			
4							0.1943		
5a								0.0634	
5b									0.2881

APPENDIX VIII - EMBEDDED MARKOV CHAIN ANALYSIS OF TREDOMEN QUARRY SEQUENCE

Embedded markov chain analysis of upper Tredomen sequence using 10cm intervals (continued)

Estimate of transition probabilities for diagonals 14

		TO								
		1a	*1b*	*2a*	*2b*	*3a*	*3b*	*4*	*5a*	*5b*	Row totals
FROM	*1a*	1.69	0.00	11.00	3.00	1.00	1.00	0.00	0.00	0.00	18
	1b	1.00	0.05	0.00	0.00	0.00	0.00	2.00	0.00	0.00	3
	2a	1.00	0.00	1.07	3.00	8.00	1.00	0.00	0.00	0.00	14
	2b	2.00	0.00	0.00	0.38	3.00	1.00	0.00	0.00	2.00	8
	3a	3.00	0.00	3.00	1.00	1.07	3.00	1.00	0.00	2.00	14
	3b	0.00	0.00	0.00	0.00	0.00	3.91	7.00	2.00	14.00	27
	4	1.00	1.00	0.00	0.00	1.00	8.00	6.99	3.00	15.00	36
	5a	0.00	0.00	0.00	0.00	0.00	1.00	2.00	0.74	8.00	12
	5b	9.00	2.00	0.00	1.00	0.00	7.00	17.00	2.00	15.37	53
Column totals		18.69	3.05	15.07	8.38	14.07	25.91	35.99	7.74	56.37	185

Fixed probability vectors

1a	0.0955
1b	0.0165
2a	0.0759
2b	0.0452
3a	0.0759
3b	0.1452
4	0.1943
5a	0.0634
5b	0.2881

Expected transitions probabilities matrix

		TO								
		1a	*1b*	*2a*	*2b*	*3a*	*3b*	*4*	*5a*	*5b*
FROM	*1a*	0.0091	0.0016	0.0072	0.0043	0.0072	0.0139	0.0185	0.0061	0.0275
	1b	0.0016	0.0003	0.0013	0.0007	0.0013	0.0024	0.0032	0.0010	0.0047
	2a	0.0072	0.0013	0.0058	0.0034	0.0058	0.0110	0.0148	0.0048	0.0219
	2b	0.0043	0.0007	0.0034	0.0020	0.0034	0.0066	0.0088	0.0029	0.0130
	3a	0.0072	0.0013	0.0058	0.0034	0.0058	0.0110	0.0148	0.0048	0.0219
	3b	0.0139	0.0024	0.0110	0.0066	0.0110	0.0211	0.0282	0.0092	0.0418
	4	0.0185	0.0032	0.0148	0.0088	0.0148	0.0282	0.0377	0.0123	0.0560
	5a	0.0061	0.0010	0.0048	0.0029	0.0048	0.0092	0.0123	0.0040	0.0183
	5b	0.0275	0.0047	0.0219	0.0130	0.0219	0.0418	0.0560	0.0183	0.0830

APPENDIX VIII - EMBEDDED MARKOV CHAIN ANALYSIS OF TREDOMEN QUARRY SEQUENCE

Embedded markov chain analysis of upper Tredomen sequence using 10cm intervals (continued)

Expected transitions matrix

		TO								
		1a	*1b*	*2a*	*2b*	*3a*	*3b*	*4*	*5a*	*5b*
FROM	*1a*	1.69	0.29	1.34	0.80	1.34	2.57	3.44	1.12	5.10
	1b	0.29	0.05	0.23	0.14	0.23	0.44	0.59	0.19	0.88
	2a	1.34	0.23	1.07	0.64	1.07	2.04	2.73	0.89	4.05
	2b	0.80	0.14	0.64	0.38	0.64	1.22	1.63	0.53	2.41
	3a	1.34	0.23	1.07	0.64	1.07	2.04	2.73	0.89	4.05
	3b	2.57	0.44	2.04	1.22	2.04	3.91	5.23	1.71	7.75
	4	3.44	0.59	2.73	1.63	2.73	5.23	6.99	2.28	10.37
	5a	1.12	0.19	0.89	0.53	0.89	1.71	2.28	0.74	3.38
	5b	5.10	0.88	4.05	2.41	4.05	7.75	10.37	3.38	15.38

Expected frequencies without estimates

		TO									
		1a	*1b*	*2a*	*2b*	*3a*	*3b*	*4*	*5a*	*5b*	Rows total
FROM	*1a*		0.29	1.34	0.80	1.34	2.57	3.44	1.12	5.10	16
	1b	0.29		0.23	0.14	0.23	0.44	0.59	0.19	0.88	3
	2a	1.34	0.23		0.64	1.07	2.04	2.73	0.89	4.05	13
	2b	0.80	0.14	0.64		0.64	1.22	1.63	0.53	2.41	8
	3a	1.34	0.23	1.07	0.64		2.04	2.73	0.89	4.05	13
	3b	2.57	0.44	2.04	1.22	2.04		5.23	1.71	7.75	23
	4	3.44	0.59	2.73	1.63	2.73	5.23		2.28	10.37	29
	5a	1.12	0.19	0.89	0.53	0.89	1.71	2.28		3.38	11
	5b	5.10	0.88	4.05	2.41	4.05	7.75	10.37	3.38		38
Column total		16.00	3.00	13.00	8.00	13.00	23.00	29.00	11.00	38.00	154

Original Observed Transitions matrix

		TO									
		1a	*1b*	*2a*	*2b*	*3a*	*3b*	*4*	*5a*	*5b*	Row totals
FROM	*1a*		0	11	3	1	1	0	0	0	16
	1b	1		0	0	0	0	2	0	0	3
	2a	1	0		3	8	1	0	0	0	13
	2b	2	0	0		3	1	0	0	2	8
	3a	3	0	3	1		3	1	0	2	13
	3b	0	0	0	0	0		7	2	14	23
	4	1	1	0	0	1	8		3	15	29
	5a	0	0	0	0	0	1	2		8	11
	5b	9	2	0	1	0	7	17	2		38
Column totals		17.00	3.00	14.00	8.00	13.00	22.00	29.00	7.00	41.00	154

Embedded markov chain analysis of upper Tredomen sequence using 10cm intervals (continued)

T	*O*	*E*	$((O-E)^2)/E$
1a-5b	0.00	5.10	5.10
3b-4	7.00	5.23	0.60
3b-5b	14.00	7.75	5.04
4-3b	8.00	5.23	1.47
4-5b	15.00	10.37	2.07
5b-1a	9.00	5.10	2.99
5b-3b	7.00	7.75	0.07
5b-4	17.00	10.37	4.24
orange	3.00	7.35	2.57
purple	1.00	5.34	3.52
pink	10.00	5.66	3.32
light green	5.00	5.66	0.08
turquiose	1.00	6.79	4.93
grey	2.00	8.39	4.87
teal	0.00	8.32	8.32
dark blue	4.00	5.76	0.54
peach	4.00	5.67	0.49
red	11.00	6.72	2.73
lime	6.00	6.43	0.03
bright pink	0.00	5.82	5.82
yellow	9.00	5.84	1.70
grey-blue	18.00	5.01	33.62
marroon	3.00	8.36	3.43

$\chi^2 =$ **97.55** with 55 degrees of freedom = (number of states -1)^2

critical value at 5% significance level for 55 degrees of freedom = 73.31

Therefore, the series of states are not independent of one another.

That is the series exhibits a first order Markovian property.

APPENDIX VIII - MARKOV CHAIN AND EMBEDDED MARKOV CHAIN ANALYSIS OF TREDOMEN QUARRY SEQUENCE

Markov Chain Analysis Results

	Series	t	m	v	$\chi 2$	critical value $\alpha 0.05$	critical value $\alpha 0.01$
Markov Chain Analysis	Total	1885	9	64	6117.35	83.68	93.22
	Upper sequence	1296	9	64	2375.05	83.68	93.22
	Lower sequence	588	5	16	152.34	26.29	32.00
Embedded Markov Chain Analysis	Total	163	9	55	78.19	73.31	82.29
	Upper sequence	154	9	55	97.55	73.31	82.29
	Lower sequence	21	5	11	0.189	19.68	24.73

N.B.

Upper sequence	defined as above the mature calcrete bands, interpreted as the Bishops Frome Limestone Includes quarry series, BH1 beds 1-77, BH2 beds 1-135.
Lower sequence	defined as below the mature calcrete bands, interpreted as the Bishops Frome Limestone
t	number of transitions in the series (grand total -1 in Markov Chain Analysis)
m	number of states in the series
v	degrees of freedom. For Markov Analysis v = (m-1)2. For Embedded Markov Analysis v = (m-1)2 -m
x2	x2 statistic
α 0.05	5% significance level
α 0.01	1% significance level

APPENDIX IX

IS THE CHANNEL COUNTRY OF CENTRAL AUSTRALIA A SUITABLE ANALOGUE FOR THE OLD RED SANDSTONE?

In collaboration with the Lake Eyre Basin Analogues Research Group, Australian School of Petroleum, University of Adelaide.

INTRODUCTION

The river systems of the Channel Country, part of the Lake Eyre Basin of central Australia, have been described as mud-dominated braided or anabranching (specifically anastomosing) dryland rivers with complex floodplains (Rust 1981, Nanson et al. 1986, Rust and Nanson 1986, Gibling et al. 1998, Fagan and Nanson 2004). The mud-dominated fluvial and floodplain deposits of the Channel Country are often quoted as modern analogues for ancient dryland mudstone-dominated formations, in particular the Upper Silurian sequences of the Old Red Sandstone of the Anglo-Welsh Basin (Marriott and Wright 1993, 1996, Wright and Marriott 2007, Hillier et al. 2007).

The comparison between the Old Red Sandstone sequences and the Channel Country rivers was first made based on the presence of sand-sized, pedogenically-formed, mud aggregate pellets, found in both the modern Channel Country river channel deposits and the ancient mudstone sequences of the upper Přídolí of the Anglo-Welsh Basin (Ékes 1993, Marriott and Wright 1996, Wright and Marriott 2007). In both the Channel Country and the Old Red Sandstone sequences there is evidence of Vertisols (Gibling et al.1998) and palaeo-Vertisols (Allen 1986, Marriott and Wright 1993) development of the floodplain sequences, suggesting a similar climatic regime of an overall moisture deficient, semi-arid to arid climate, but with strong seasonality. The sand-sized mud aggregates are thought to originate from the pedogenically-altered floodplain muds, later to be reworked and transported as bedload in muddy ephemeral channels and deposited in various fluvial elements (Rust 1981, Gibling et et al. 1998, Wright and Marriott 2007). Inclined heterolithics units recognised from the ancient Moor Cliffs Formation (Marriott and Wright 2004) and the Conigar Pit Sandstone (Hillier et al. 2007) from the Anglo-Welsh Basin have been interpreted as lateral accretion on accretionary benches of sinuous, ephemeral shallow channels, analogous to those of the anastomosing mud-dominated channels of the Channel Country.

Despite these noted similarities in some sediment type and channel and floodplain elements, there are many differences between the ancient Old Red Sandstone sequences and the modern Channel Country rivers which need to be investigated e.g. differences in sediment size ranges, channel elements and inferred fluvial landforms, as well as potential influences from flora and fauna. This study aims to makes some direct comparisons between collected data from the Diamantina River, one of the largest rivers of the Channel Country and the Upper Silurian to Lower Devonian Old Red Sandstone sequences of the Anglo-Welsh Basin to test the suitability of the Channel Country as a modern analogue. This study also aims to better understand the geomorphology of the Channel Country, which if proved a suitable analogue, can be used to infer the geomorphology of the Old Red Sandstone Continent landscape.

LOCALITIES

Lake Eyre Basin

The Lake Eyre Basin covers approximately one fifth of the land area of Australia (Figure 1a), at 1.3 x 10^6 km^2, and can be separated into four main areas: the Channel Country, consisting of three major tributaries (Cooper Creek (the Barcoo-Thomoson in the northern headwaters), the Diamantina-Warburton and the Georgina); Lake Eyre, a salt pan around 15m below sea level; western Lake Eyre Basin; and the Simpson Desert, predominately aeolian dune systems (Gilbing et al. 1998) (Figure 1b). The low gradient rivers (0.1 to 0.2 m/km, Maroulis et al. 2007) of the Channel Country rise in the northern uplands of the basin, and flow over 1000km to the southwest to drain internally into Lake Eyre (Gibling et al. 1998). The rivers of the Channel Country are typically ephemeral, and form a complex network of anastomosing channels, braided channels and associated braid bars, waterholes and aeolian dunes, that have been aggregating slowly over the past 100ka (Rust and Nanson 1986, Nanson et al. 1986, Gibling et al. 1998).

The Lake Eyre Basin lies on the ancient Australian stable craton, and much of the alluvial plain of the Channel Country lies below 150m elevation, with very low gradients (Gibling et al. 1998). The fluvial patterns of the Channel Country rivers are mainly controlled by gentle anticlines and synclines, as a result of Tertiary tectonism (Rust 1981, Maroulis et al. 2007). Localised exposed bedrock include the Cretaceous Winton Formation (composed of grey mudstones and lithic sandstone) (Wopfner 1963), as well as Tertiary wind-abraded gravel

Figure 1a: Map of Australia, showing the location of Lake Eyre Basin

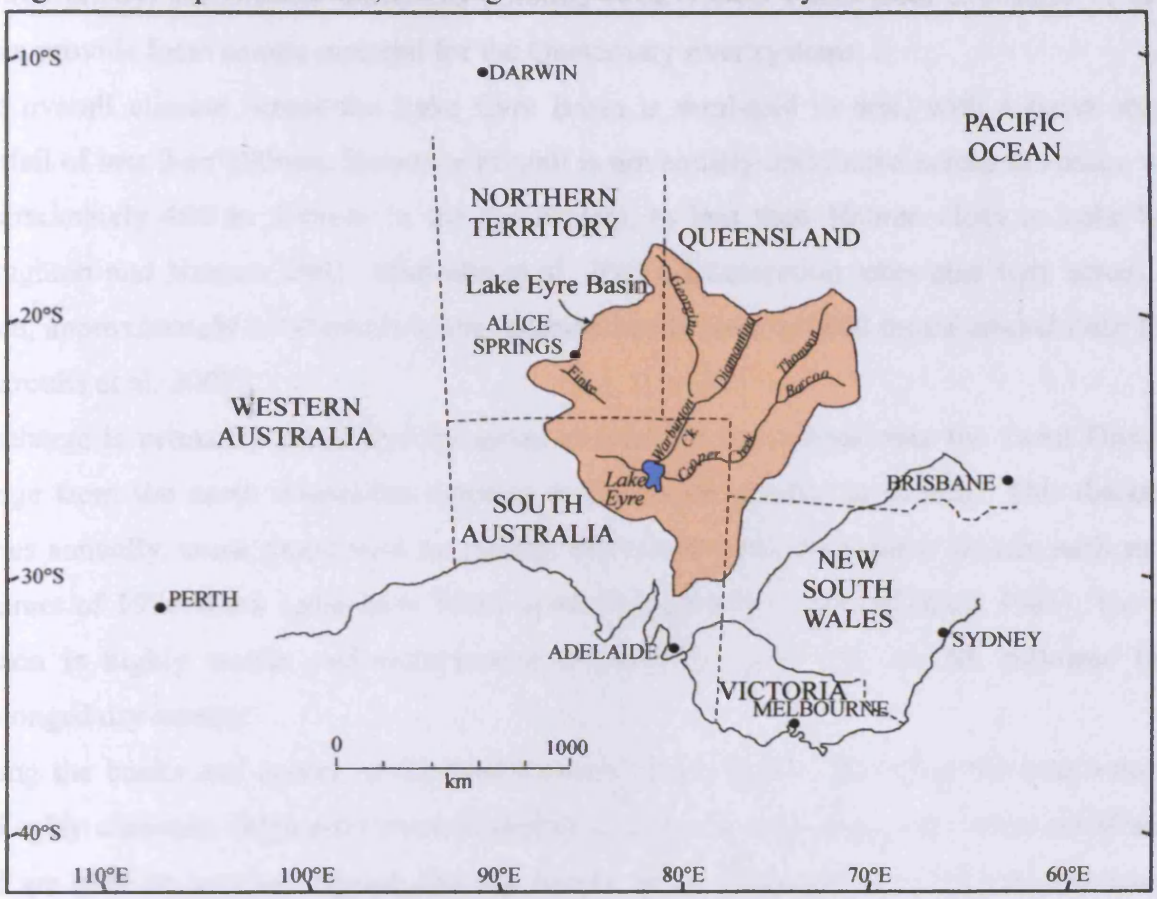

Figure 1b: Lake Eyre Basin

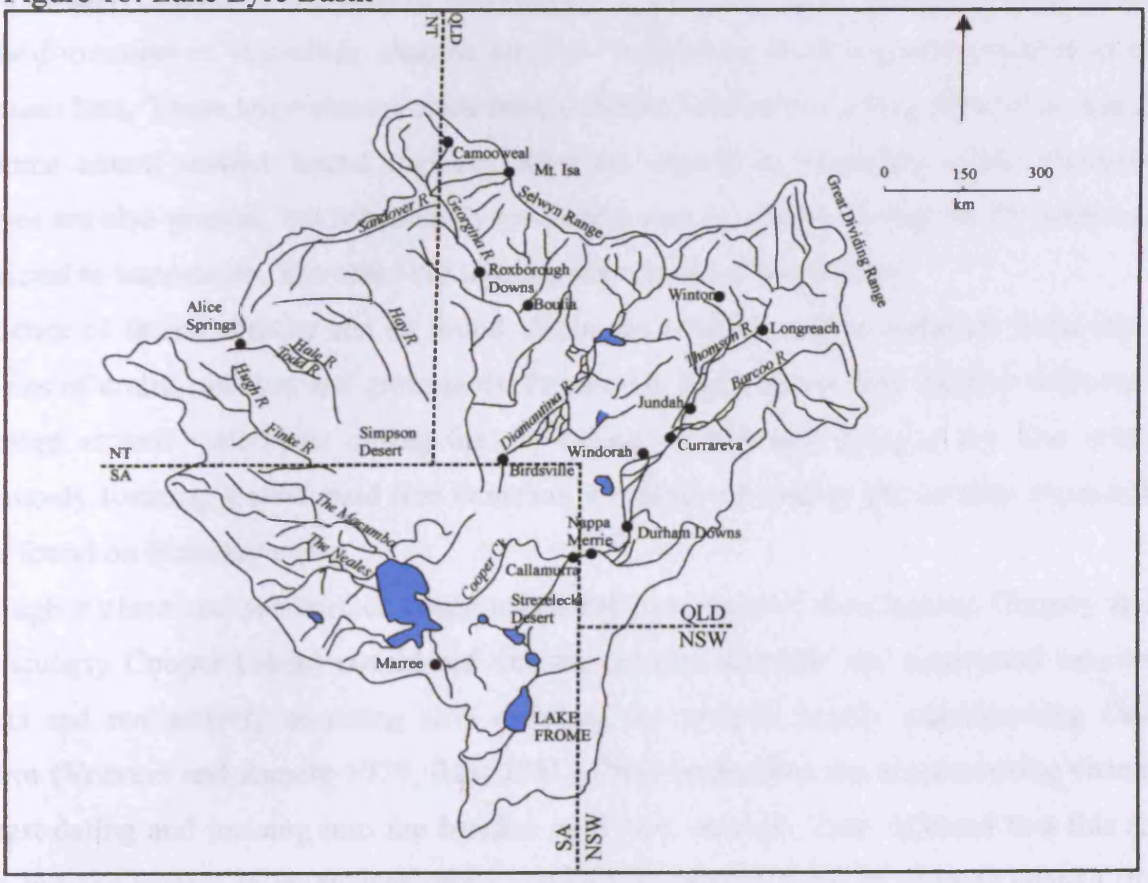

(gibber plains) and silcrete duricrusts (Gibling et al. 1998). These local exposures of older strata provide local source material for the Quaternary river systems.

The overall climate across the Lake Eyre Basin is semi-arid to arid, with a mean annual rainfall of less than 250mm. However rainfall is not equally distributed across the basin, with approximately 400 to 500mm in the headwaters, to less than 100mm close to Lake Eyre (Knighton and Nanson 2001, Maroulis et al. 2007). Evaporation rates also vary across the basin, approximately 2400 mm/a in the northern headwaters to 3600 mm/a around Lake Eyre (Maroulis et al. 2007).

Discharge is primarily controlled by moist tropical air that passes over the Great Dividing Range from the north Australian summer monsoon (November to March). This discharge varies annually, some years with no rainfall and others producing major floods, such as the summer of 1974 when Lake Eyre filled to the highest level recorded (Rust 1981). The wet season is highly erratic and occurs over a relatively short time period, followed by a prolonged dry season.

Along the banks and levees of Channel Country watercourses, including the anastomosing and splay channels, large gum trees (including *Eucalyptus microtheca*) are often established, and are able to survive through the dry season to be replenished during the wet season. Occasionally trees have established mid-channel, either causing sediment build up resulting in the formation of vegetation shadow bars or are growing on previously established mid-channels bars. These large trees provide bank cohesion with large rooting structures, and may to some extent restrict lateral incision. Riparian vegetation, including small shrubs and grasses are also present, but rely heavily on a water source, and so during the dry seasons are restricted to waterholes. The braid bar tops are very sparse of vegetation.

Evidence of faunal activity can be found within the channels and waterholes, including the remains of crabs, bivalves and gastropods. Fresh crab, beetle larvae and crayfish burrows are focussed around waterholes during the dry season. Freshwater sponges are also present, commonly forming around dead tree branches. Evidence of spiders and termite mounds has been found on braid bar tops.

Through surface and sub-surface observations early workers of the Channel Country rivers (particularly Cooper Creek) considered that the braided channels and associated bars were relicts and not actively accreting as a result of the modern muddy anastomosing fluvial system (Veevers and Rundle 1979, Rust 1981). They interpreted the anastomosing channels as post-dating and incising into the braided sand bars beneath. They inferred that this shift from braided system to an anastomosing system was primarily due to climate change (Rust

1981). Rust 1981 hypothesised that the relict braid bars represented a pluvial event, where as the modern muddy anastomosing channels represent fluvial adjustment to increased aridity, which began at least 5000 years ago.

Rust and co-workers reinvestigated Cooper Creek (Rust and Nanson 1986, Nanson et al. 1986) and colleted more subsurface data. They discovered that the muddy facies deposited by the modern anastomosing fluvial system was just a thin veneer, overlying a significant sand sheet body. They also determined that the braid bars of the Cooper Creek were in fact composed of clay in the form of sand-size mud aggregate pellets, and were not associated with the sand body beneath (Rust and Nanson 1986). Therefore the modern fluvial system produced co-exiting anastomosing channels and braided channels which are thought to operate at different flow levels, with braided channels active during flood events, whilst the anastomosing channels operate during moderate flows (Nanson et al. 1986). Trough cross ripple lamination and large-scale cross-bedded units within the significant underlying sand sheet body were interpreted as lateral accretion on a meander point bar, leading to interpretation that the sand sheet represents a meandering fluvial system, likely to have been formed in a wetter climate (Rust and Nanson 1986).

Using thermoluminence (TL) dating, Nanson et al. (1992) correlated the deposition of significant sand bodies with wetter interglacial periods, and dune building during drier glacial periods. The cross-bedded sand sheet discovered underlying the muddy veneer by Rust and Nanson (1986) represent pluvial events that have been linked to interglacials stage 7 and stage 5 in the marine isotope record (Nanson et al. 1992). Since the stage 5 pluvial event approximately 110ka B.P. aridity has gradually increased, and the meandering fluvial systems were replaced by anastomosing and braided systems, with oldest muds dated to about 85ka B.P. (Nanson et al. 1992).

More recently Maroulis et al. (2007) has studied the interaction between fluvial activity and sand-dominated dune building. As the dunefields around Cooper Creek have been rejuvenated, the dates obtained from TL may not be reliable, and therefore the dunes may be significantly older. Marloulis et al. (2007) hypothesised that instead of dune building occurring during periods of aridity, they were in fact formed during wetter periods by strong prevailing south-south-westerly winds (between stage 8-6 in the marine isotopic record) and sourced from sandy meandering channels.

This study focuses on two sites of the Diamantina River (Figures 1a and 1b). Site 1 is located approximately at the half way point of the river's course, near Davenport Downs (approximately 45km north east of Monkira Aerodrome), where an anastomosing to single

river channel is associated with a braid bar system with splays (Figures 2a and 2b). Site 2 is located approximately 250km further upstream in the headwaters, at Mt. Rourke Creek, approximately 8km NNW from Middleton on the Kennedy Development Road between Winton and Boulia (Figures 2c and 2d). Fieldwork was conducted during September 2008 and therefore during the dry season.

Anglo-Welsh Basin

The Anglo-Welsh Basin was one of several basins which formed on the edge of equatorial Laurussia (also known as the Old Red Sandstone Continent), an amalgamation of three separate landmasses: Laurentia, Baltica and Avalonia, brought together by the closure of the Iapetus Ocean between the Late Ordovician and the Early Devonian (Figure 3). Although models by Dewey and Strachan (2003) and Soper and Woodcock (2003) differ in collision nature and timing, both recognise a significant gap in time between the closure of the Iapetus Ocean by the Scandian Orogeny between 425Ma and 410Ma and the compressive regime of the Acadian Orogeny in 395Ma. During this time gap it is has been modelled that strike-slip and transtensional tectonics formed several basins across the Old Red Sandstone Continent, subsequently infilled with coarsening upwards sediments, with a marine to terrestrial transition (Soper and Woodcock 2003).

Palaeogeographic and palaeomagnetic reconstructions are in agreement that the Old Red Sandstone Continent lay from the equator to approximately 30° south, and that the Anglo-Welsh Basin lay on the margin at approximately 17° south (Scotese 2003, Channell et al.1992) (Figure 3). In today's climate this would place the basin into the sub-tropics, with distinct wet and dry seasons. Rainfall in these regions is between 500-2000mm and temperature ranges from 16-20°C. It is therefore likely that the Old Red Sandstone margin would have experienced a semi-arid to arid climate. This is confirmed by the presence of palaeo-Vertisols, a type of palaeosol that contains calcium carbonate horizons that are typically formed in semi-arid climates with distinct wet and dry seasons (Allen 1986, Marriott and Wright 1993).

The Anglo-Welsh Basin was an extramontane and coastal basin, distal to the older Caledonian mountain range to the northwest (Friend et al. 2000). Essentially the basin filled with post orogenic detritus, brought southward to the coastline by large river systems. During the Early Silurian, although progressively retreating, there was still a significant marine

Figure 2: Investigated sites of the Diamantina River

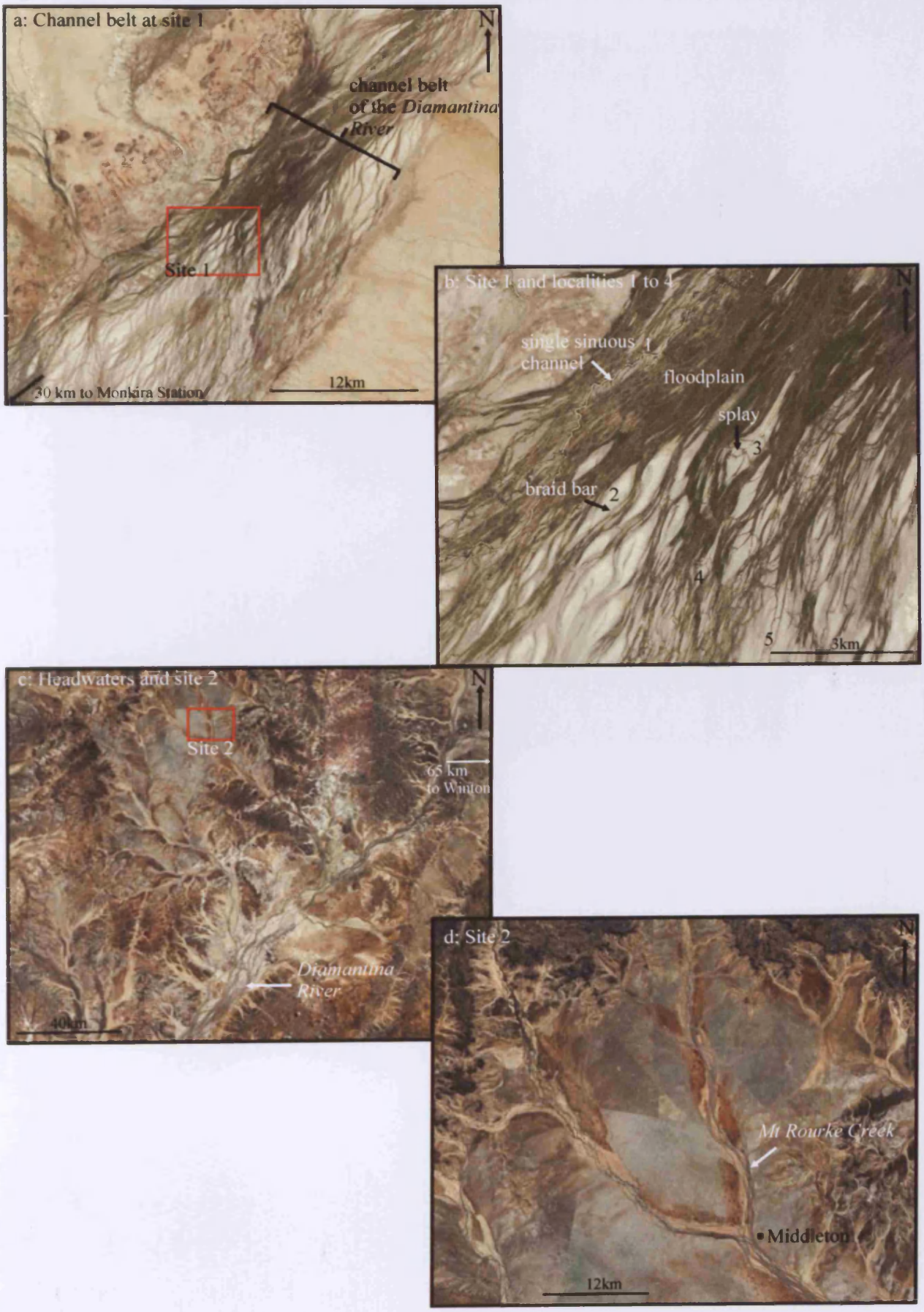

Figure 3: Reconstruction of the Old Red Sandstone Continent during the Early Devonian (modified after Ron Blakey).

influence. Strata of the Upper Silurian Old Red Sandstone contain plentiful mica grains, as well as staurolite and kyanite (Allen and Crowley 1983), sourced from weathered metamorphic strata. Simon and Bluck (1982) hypothesised that sediment was sourced from the newly-formed Caledonian mountains, and transported in a south-easterly direction by large fluvial systems to the coastal margins of the Old Red Sandstone Continent, infilling tectonically active basins. These rivers, approximately 500km in length, are thought to have connected the Anglo-Welsh Basin with other Lower Old Red Sandstone basins. A significant change in facies type and sedimentary style occurred in the Lower Devonian (Dittonian), from the Raglan Mudstone Formation to the St. Maughans Formation, and their equivalents. This may be due to local tectonic uplift (Allen and Crowley 1983). There is little evidence for any marine influence, and it has been hypothesised that broad fluvial channels occupied low-lying, muddy floodplains. Sediments are less micaceous, suggesting a halt to dispersal from the distant Caledonides (Allen and Crowley 1983). A greater proportion of igneous debris has been recorded, potentially transported from a more local source, such as the Irish Sea High or Bristol Landmass (Allen and Crowley 1983). There was also a higher degree of intra-basinal sediment re-working (Marriott and Wright 1996).

The first land plants evolved during the Late Ordovician and Early Silurian, although the earliest body fossils are not found until the Wenlock (Edwards and Feehan 1980). By the Early Devonian, small, dichotomosing branching vascular plants, such as *Cooksonia* (belonging to the rhyniophytes) would have inhabited the banks of the Anglo-Welsh Basin rivers (see Chapter 3, review by Edwards and Richardson 2004). Additionally, large fungal-like organisms, such as *Prototaxites* would likely to have dominated the Early Devonian landscape (Hueber 2001, Boyce et al. 2007).

OBSERVATIONS AT THE DIAMANTINA RIVER SITES

Site 1

1. Anastomosing to single sinuous channel

The wide channel belt at site 1 (approximately 12km wide, Figure 2a) is composed of a number of different components, the most obvious being a sinuous, single to anastomosing river channel (Figures 2b, 4a and 4b) which is typical of Lake Eyre Basin rivers. At locality 1 (Figure 2b), the main channel is approximately 4m deep, 39.9m in width, flat-based, with relatively steep sides (up to an angle of 52°) (Figure 4b). In straight sections, the downstream profiles are symmetrical (Figure 4b), whilst in sinuous sections the profiles are asymmetrical.

Figure 4: Main single sinuous channel of the Diamantina River at site 1

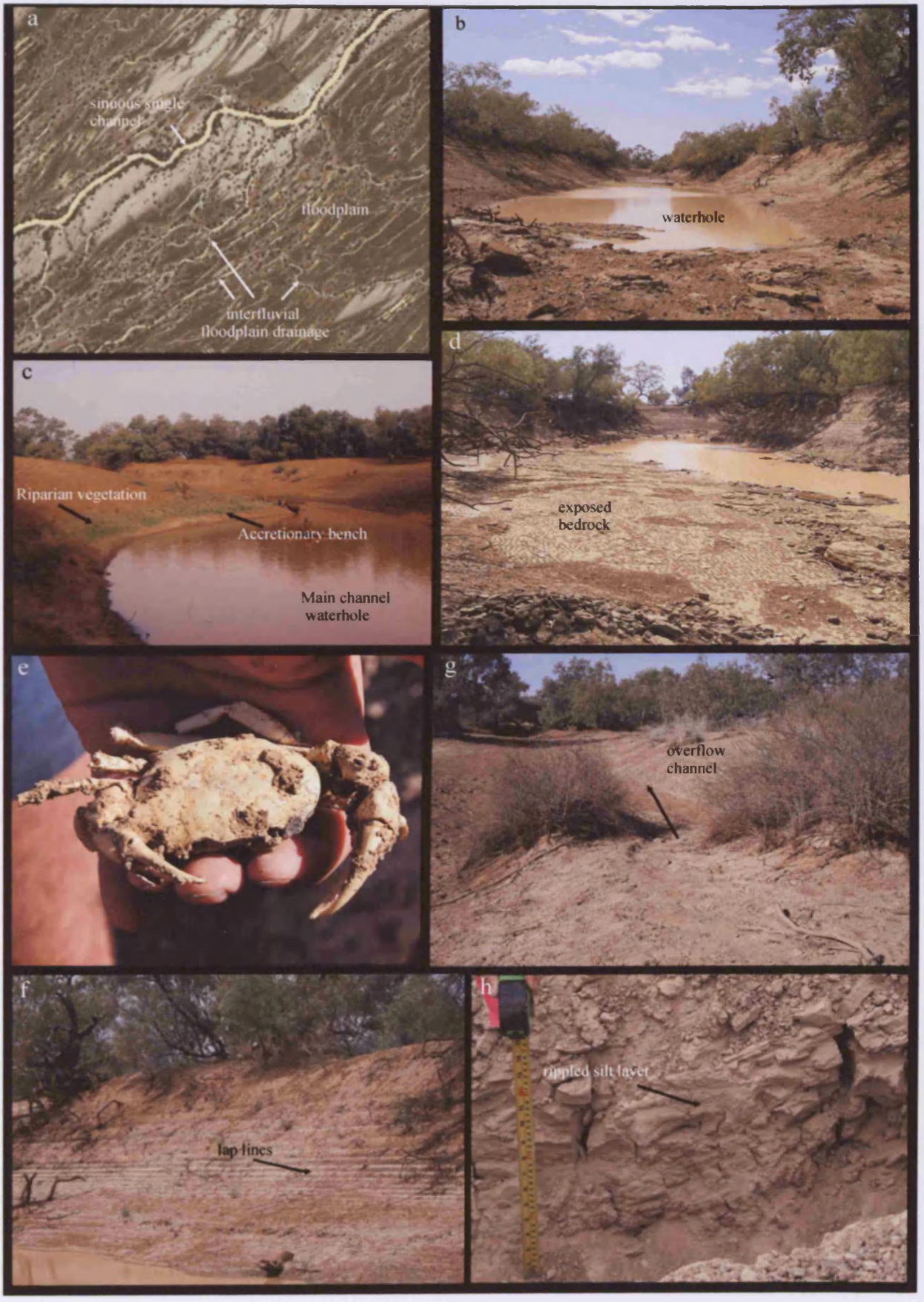

At sinuous points, shallow accretionary point bars have developed on the convex side (Figure 4c). Some accretionary bars are associated with a terrace (Figure 4c).

At locality 1 the channel base has been deepened further, and the underlying sandstone bedrock (the Winton Formation) has been exposed (Figure 4d). This section of the channel has been deepened enough to form a waterhole, an ephemeral standing body of water (Figure 4b) that provides a refuge of fauna such as crayfish and crabs (Figure 4e), and riparian vegetation (Figure 4c). Very distinctive lap lines can be seen on the channel sides (Figure 4f), indicating previous water levels of the waterhole.

Shallow, broad levees line the channels, and are inhabited by large gum trees (Figure 4b). Although the gum trees are restricted to the channel edge, smaller shrubs extend beyond the levees, on to a slight depression between the levees and the braid bar tops (area marked floodplain on Figure 4a). Networks of smaller, shallower secondary channels were found in this area (Figure 4a), acting as tributaries or overflow channels (Figure 4g) to the main channel, likely to operate only during flood events.

Two trenches were excavated through the channel at locality 1, one parallel and one perpendicular to flow. At the top of both trenches, thick units of blocky mud composed of sand-sized mud aggregates, with desiccation cracks and partially decayed organic material were exposed, interbedded with subordinate layers of ripple-laminated very-fine and fine-grained sand (Figure 4h). With increased depth, mud and sandy mud layers are platy, with remnant desiccation cracks and burrows infilled with sandy mud, with some evidence of mottling and manganese and carbonate nodules no bigger than a coarse sand grain. These features suggest incipient soil formation and therefore these sequences are likely to be older than the channel incising into them.

2. Braid bars

Shallow, broad braid bars are the second component of the wide channel belt of the Diamantina River at site 1 (Figures 2a and 2b). These lozenge-shaped bars (locality 2, Figure 2b) are generally the only highs in the landscape, but only by approximately a metre above the channels. Bar tops are sparse of vegetation, with few dead riparian vegetative remains (Figure 5a). The main features on the surface of the braid bars are desiccation cracks (Figure 5b), although excavation discovered that these cracks are only superficial. At location 2 (Figure 2b), the sediments of the braid bar tops are very hard, and excavation of only 35cm was possible. At the surface, a layer of silt to very fine-grained sand is powdery and easy to crumble. Although rare, small gravel-sized exotic clasts were found lying on top of these

Figure 5: Braid bars of the Diamantina River at site 1

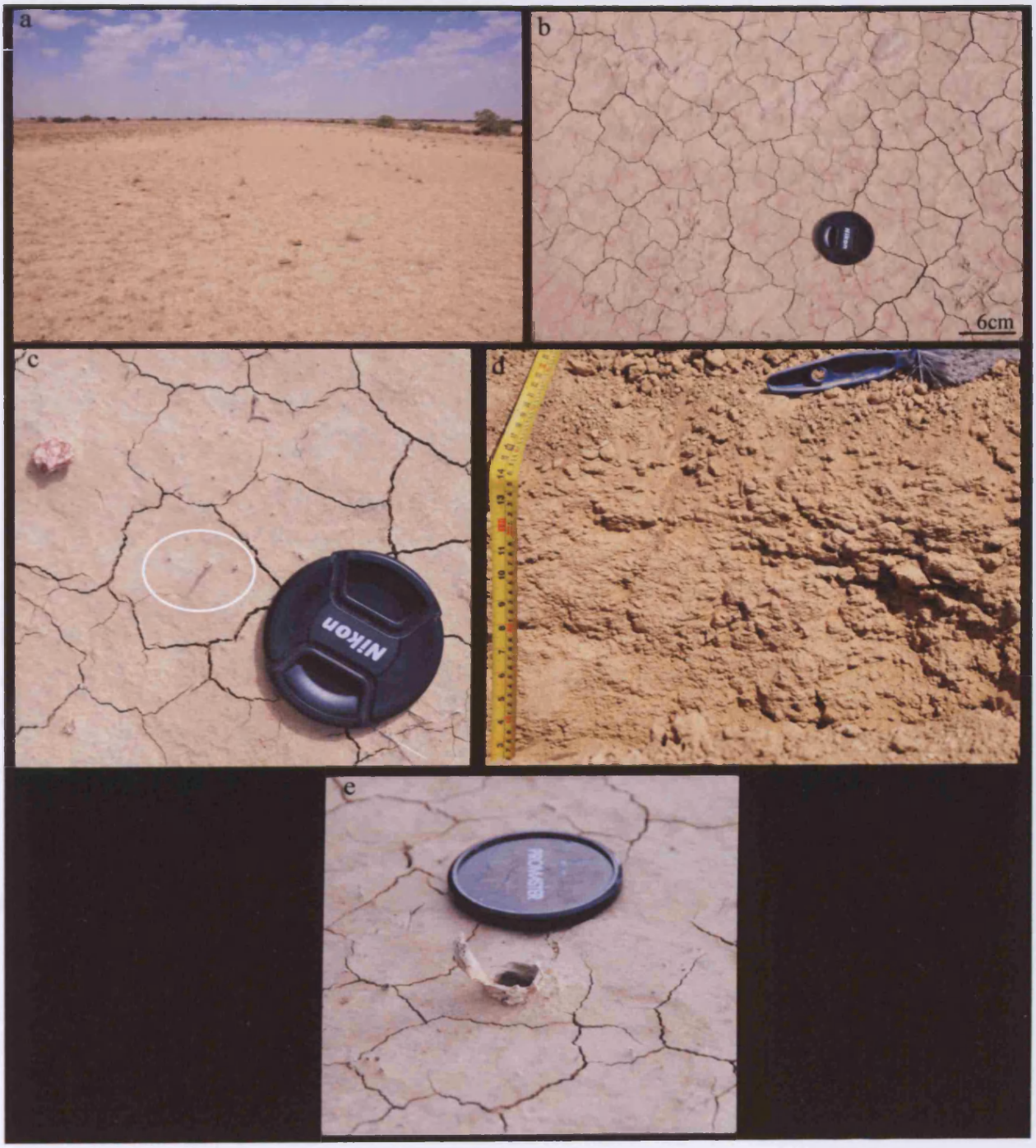

sediments (Figure 5c). Additionally, fine to medium-grained quartz grains appeared to be sticking out of the silt-sand layer (circled in Figure 5c), suggesting that this may be a deflation surface. Beneath this top layer of fine-grained sand and silt, harden silt and clay units were platy to angular and very hard to crumble. Partially decayed organic material (roots or fungal hyphae) as well as manganese nodules were found in the lowermost units. An old spider burrow was found cutting vertically down into the bar top (Figure 5d).

3. Splays

A number of braid bars are incised by splays (Figure 6a), which act as overflow from the main channels during flood events (localities 3, 4 and 5, Figure 2b). These distributary splay systems consist of a main splay channel, with several distributaries, becoming more frequent downstream (D1 to D5 in Figure 6c). At locality 4 (Figure 2b), at the upstream reaches of the splay, the main channel is approximately 2m deep, and 22.7m wide (measured between levees). The channel is highly sinuous and asymmetric in profile, with a narrow thalweg (Figure 6b). A large portion of the bank has been eroded away, and an associated bank-attached bar has developed beneath (Figure 6c). This feature could be a flood pathway from the main channel or the floodplain into the splay. The upper reaches of the splay is fed by an asymmetric tributary channel (T in Figure 6a), with a vegetated chute bar at the junction with the main splay channel (Figure 6d). Minor tributaries also flow into the upper reaches of the splay, and are generally a step up from the main splay channel (Figure 6e), and have been interpreted as interfluvial drainage channels (see section 4).

Further downstream, the main splay channel beings to widen out and become shallower, with a near flat base, although the asymmetric profile remains (Figure 6f). Along the mid-course straight section of the splay at locality 4 (Figure 6a), several in channel vegetated bars have developed (Figure 6g). Both living and dead gum trees inhabit these bars. These may be vegetative shadow bars or mid-channels bars that have been vegetated post –sedimentation. Excavation of one of these bars, parallel to flow direction, exposed interbedded layers of very fine to fine-grained sand with layers of sand-sized mud aggregates (Figure 6h). With further excavation the proportion of mud aggregates increased.

In the distal part of the splay, the main channel begins to dissipate into 5 distributaries. Some channels are shallower and narrower than the main splay channel (Figure 7a), whilst others appeared to deepen (Figure 7b). Lap lines on the banks of these distributaries suggest that these distal channels were once waterholes. Although evidence of faunal activity can be found along the full course of the main splay channel, there is an abundance of gastropod and

Figure 6: Splays of the Diamantina River at site 1

Figure 7: Distal splays and interfluvial floodplain drainage of the Diamantina River at site 1

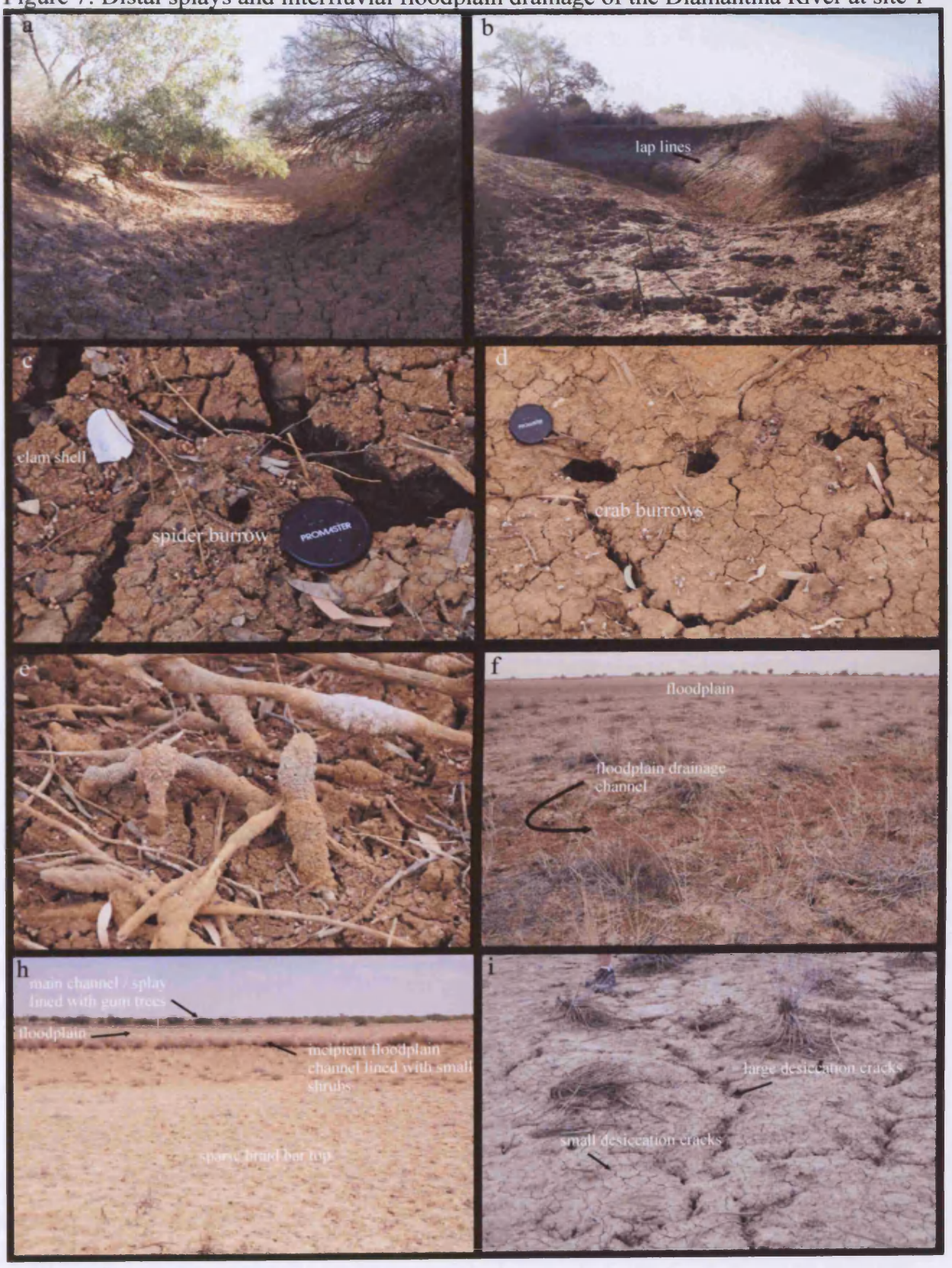

clam shells (Figure 7c), spider burrows (Figure 7c) crab and crayfish burrows (Figure 7d) and fresh water sponges (Figure 7e) found in these deeper parts of the distal splay.

4. Floodplain and interfluvial drainage

Between the levees of the main anastomosing to single channels and the highs of the braid bars and associated splays, there are areas of low-lying floodplain (Figures 4a and 6a). These floodplain areas are often partially vegetated, represented by the green-grey colour on the satellite images (Figures 4a and 6a). During the dry season the floodplains are covered in shrubs and small riparian plants (Figure 7f) that are either recently dead or dormant, to be revitalised during the wet season. Therefore the channel paths and floodplain areas can easily be recognised by the vegetation (Figure 7g). Desiccation cracks are more prominent on these floodplains than seen on the braid bar tops (Figure 7h). Small, shallow incipient drainage channels are also a key feature of the floodplain, forming a network across the floodplain, subsequently flowing into splays or the main channel (Figure 7i). These ephemeral channels would likely operate at small-scale flood or local rainfall events, draining the floodplain, transporting water into the waterholes.

Another feature of the floodplain area are rare cobble-sized clasts, lying on the floodplain surface, often caught up in the gum trees along the levees and banks of the main channels and splays (Figures 8a, 8band 8c). These cobbles could only have been transported by large, fast-flowing floodwaters, sweeping across the whole channel belt, depositing the cobbles where a tree provided some resistance. Mounds of dead gum tree branches and roots, as well as seeds and shells have also been transported the same way, only being deposited when against a resistant feature (Figures 8d, 8e, 8f and 8g). The large-scale floodwaters would have flowed into the main channels and splays via floodways, where large portions of the levee are washed away (Figure 6c).

Site 2

1. Anastomosing sinuous channels

Anastomosing sinuous rivers stretch over a channel belt approximately 0.78 km wide at site 2 (Mt. Rourke Creek, Figures 2a, 2b and 9a). This channel belt is much narrower than further downstream at site 1. The main channels are highly sinuous (Figure 9b) and anastomosing, although there are straight section (Figure 9c). At locality 1 (Figure 9a), the channel is approximately 3m deep and between 5 and 12m wide. Straight sections of river have symmetrical profiles with steep sides and flat bases (Figure 9b), whilst sinuous sections have

Figure 8: Evidence of large floods on the floodplains of the Diamantina River at site 1

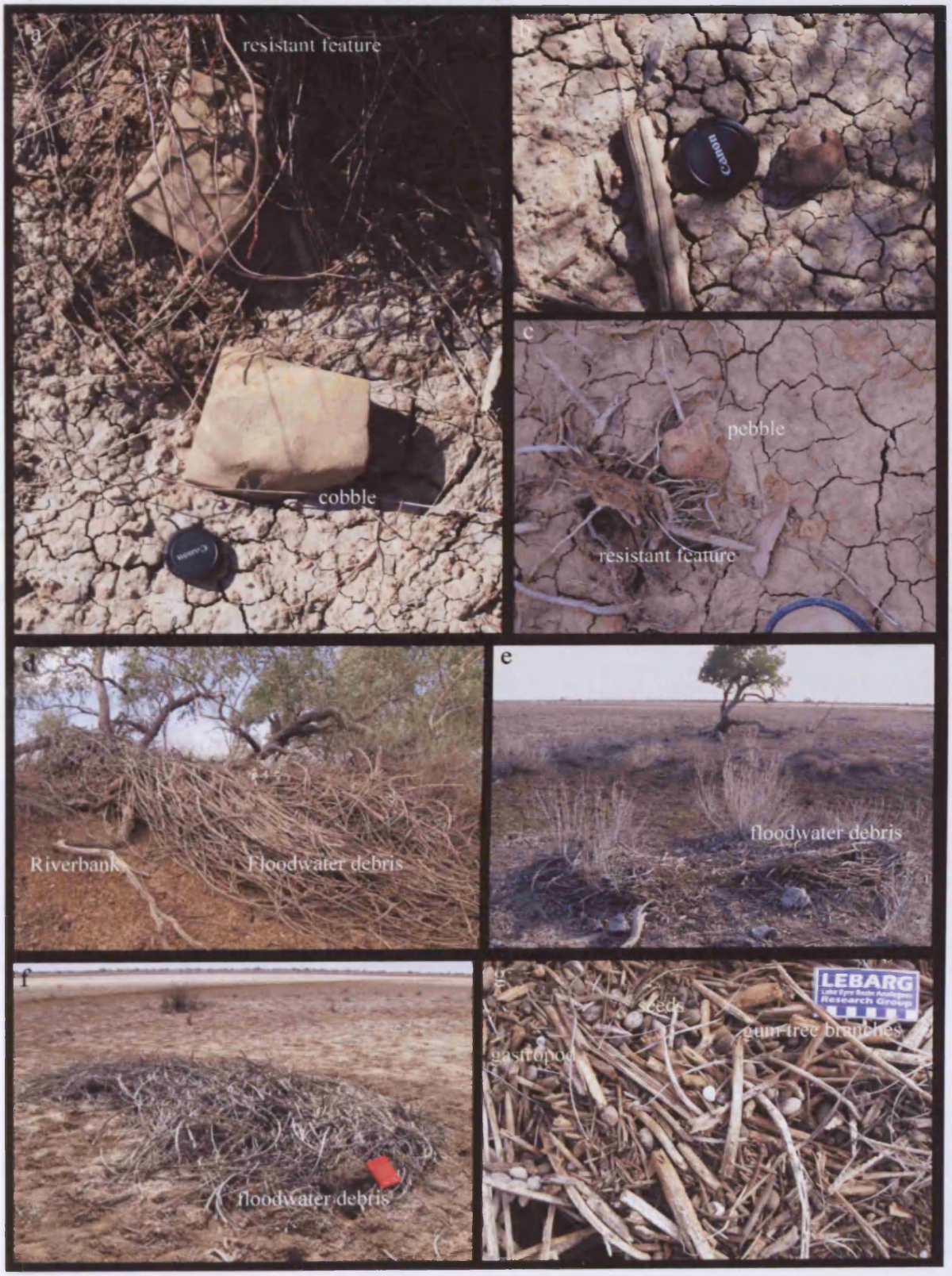

Figure 9: Anastomosing channels and braid bars of the headwaters of the Diamantina River, Mt. Rourke Creek, site 2.

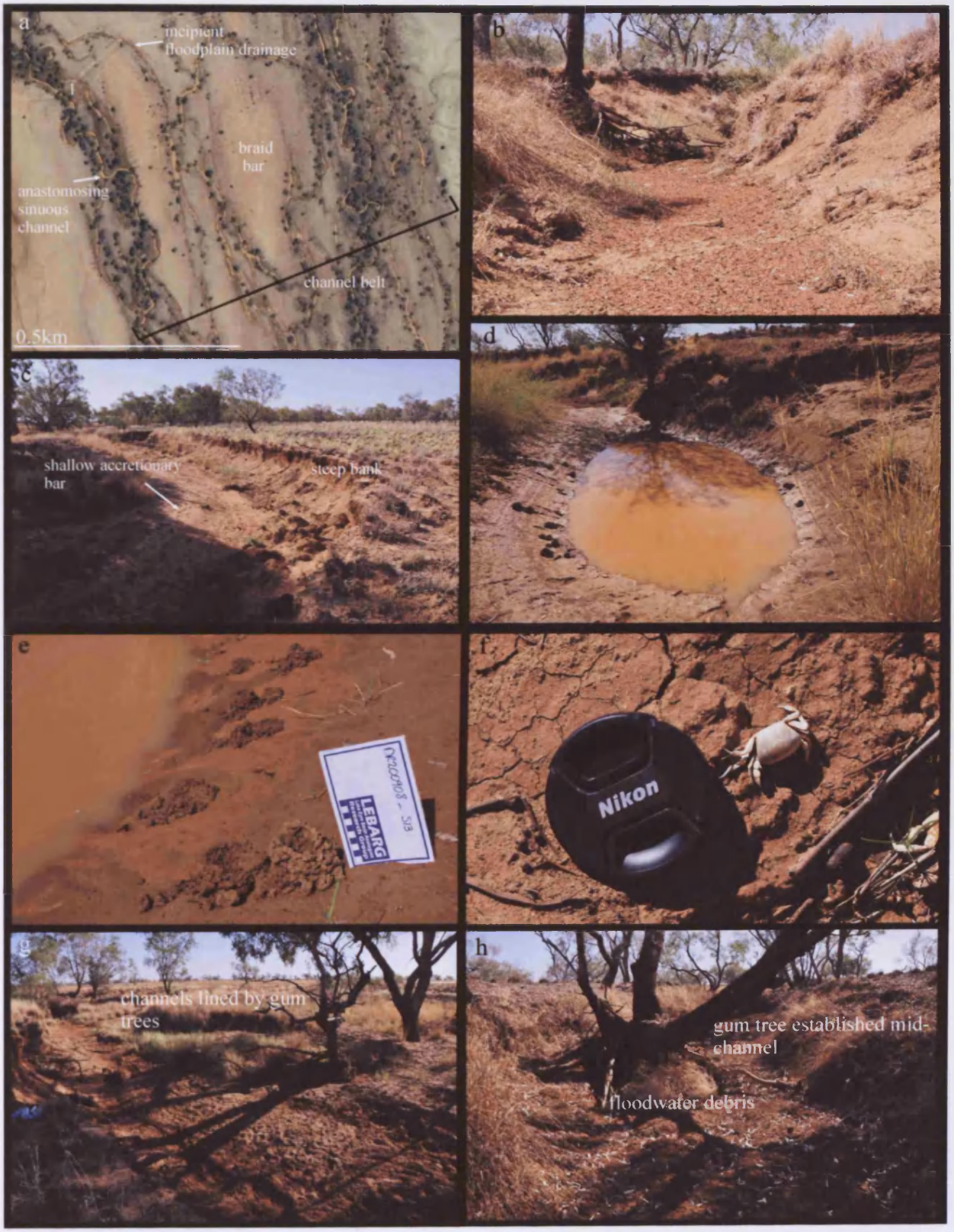

Figure 10: Mt Rourke Creek, headwaters of the Diamantina River, site 2.

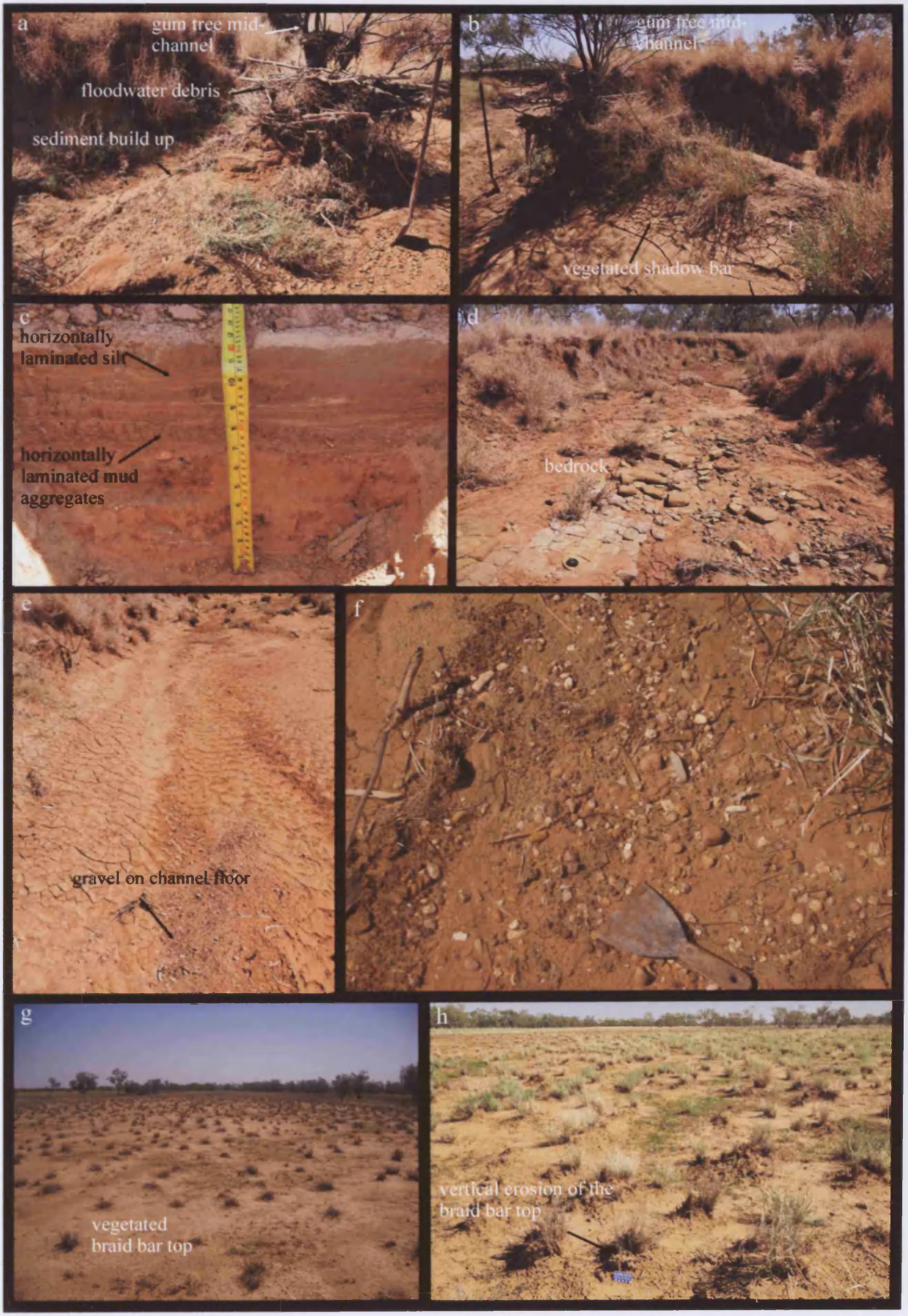

Figure 11: Mt Rourke Creek, headwaters of the Diamantina River, site 2.

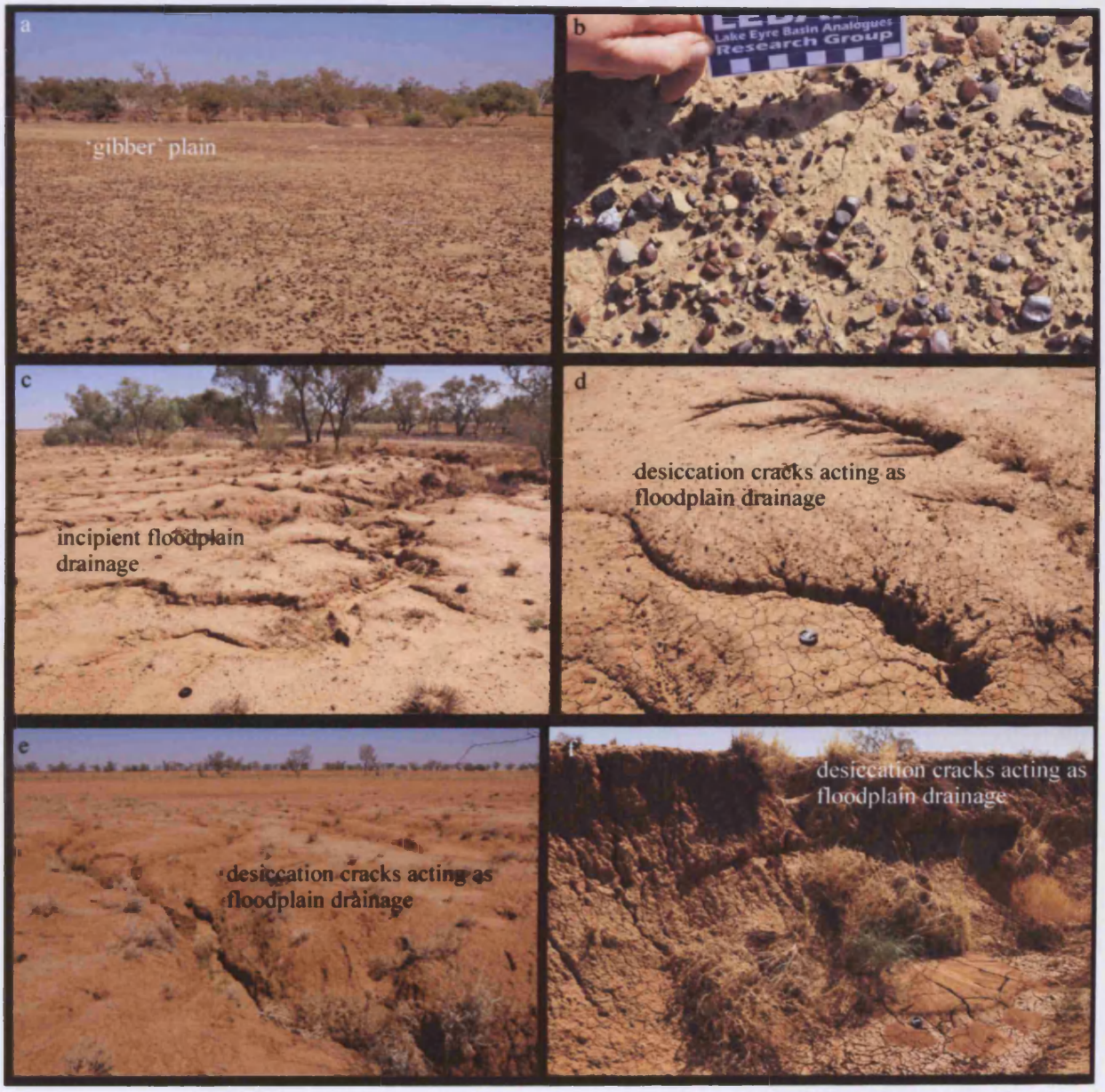

COMPARISONS WITH THE LOWER DEVONIAN OLD RED SANDSTONE LITHOFACIES

Raglan Mudstone Formation

The following lithofacies have been recognised from the uppermost Silurian Raglan Mudstone Formation from Tredomen Quarry cores (see Chapter 6 for complete descriptions and interpretations): red, thinly-bedded intraformational conglomerates (lithofacies 1b); red planar and wavy-laminated siltstones (lithofacies 3b); planar-bedded and cross-bedded heterolithics (lithofacies 4); massive mudstones, composed of pelleted mud aggregates (lithofacies 5a); and pedogenically-altered mudstones (lithofacies 5b, mostly pedified profile type 2).

Of the deposits observed from the Diamantina River, only the massive muds composed of mud aggregates and the planar-cross and cross-bedded heterolithics (interbedded mud aggregates and siltstone to very fine-grained sand layers) are similar to lithofacies 5a and 4 of the Raglan Mudstone Formation. These deposits were found in accretionary bars, bank-attached bars, shadow bars and channel bases of the Diamantina River. The heterolithics and mud aggregates found in the Raglan Mudstone Formation may have been deposited in similar channel elements of sinuous, possibly anastomosing, shallow ephemeral channels similar to those of the Diamantina River. Waterholes are one of the main components of the Diamantina River, and are the main refuge for fauna such as crayfish and crabs, leaving the sediment around the waterhole heavily bioturbated. Similarly, the bedding planes of wavy and planar-laminated siltstones of lithofacies 3b from the Raglan Mudstone Formation, interpreted as ephemeral lake deposits, are covered with arthropod tracks and burrows as well as fish trails.

Gravel or pebble clasts were found only in channel deposits in the headwaters of the Diamantina River, close to local sources, such as the 'gibber' plains. Compared to the intraformational conglomerates of the Raglan Mudstone Formation (lithofacies 1b), these are small, insignificant deposits. This may be due to a lack of source material for Lake Eyre Basin rivers. Source material is restricted to reworked muddy floodplain material and small local outcrops of the Winton Formation (sandstone) and silcretes (wind-abraded gravel and pebbles on 'gibber' plains). In addition, the intraformational conglomerates of the Raglan Mudstone Formation are predominantly composed of reworked floodplain material, in particular reworked carbonate nodules. Very small carbonate nodules grains were found in deposits of the Diamantina River, but only from very weakly pedified mudstones. The soils

of the Diamantina River floodplains / braid bars are too under-developed to produce carbonate nodules of the size seen in lithofacies 5b of the Raglan Mudstone Formation.

St. Maughans Formation

The following lithofacies have been observed from the Lower Devonian St. Maughans Formation of the Anglo-Welsh Basin (see Chapter 6 for complete descriptions and interpretations): green planar-bedded intraformational conglomerates (lithofacies 1a); medium-grained green-grey sandstones (lithofacies 2a); fine-grained green-grey sandstones (lithofacies 2b); green to grey planar and wavy-laminated siltstones (lithofacies 3a); red wavy to planar-laminated siltstones (lithofacies 3a); planar-bedded and cross-bedded heterolithics (lithofacies 4); massive mudstones composed of mud aggregates (lithofacies 5a); and pedogenically-altered mudstones (lithofacies 5b) (pedified profile type 1). Again the only similarities with the deposits of the Diamantina River are the massive mudstones composed of pelleted mud aggregates (lithofacies 5a), the heterolithics (interbedded muds and silt-sand layers) (lithofacies 4) and the wavy laminated siltstones (lithofacies 3a). Unlike the Raglan Mudstone Formation, the St. Maughans Formation is characterised by significant sandstone fining-upwards complexes (lithofacies 2a, 2b and 3a), with basal intraformational conglomerates (lithofacies 1a). Sand-sized grains are uncommon in the Diamantina River, occurring only within heterolithic units as thin laminations. Increases in the proportion of sand does occur where local outcrops of the Winton Formation occur, but appears to be transported short distances and deposited close by. Where sand deposits do occur along the Diamantina River, they are not in associated with gravel or pebble deposits beneath, as seen in the St. Maughans Formation sandstone complexes and basal intraformational conglomerates.

The pedogenically-altered mudstones of St. Maughans Formation are very distinctive of modern calcic-Vertisols, with pseudo-anticlinal slickensided slip-planes, representing the shrinking and swelling of clay during soil formation at depth. These slip-planes are represented on the surface by 'gilgai' structures (Wilding and Tessier 1988). These features are not present on the floodplains/ braid bars of the Diamantina River. Either calcic-Vertisols have not developed in this area due to prolonged aridity or the soils are too immature. Carbonate horizons from the St. Maughans Formation indicate palaeosols of at least stage II (lithofacies 5b).

CONCLUSIONS

The mud-dominated rivers of Lake Eyre Basin can be considered as a suitable analogue for the river systems of the uppermost Silurian of the Anglo-Welsh Basin, which deposited the Raglan Mudstone Formation, and an ephemeral, mud-dominated anastomosing river system model can be inferred. However, the deposits of the Diamantina River do not contain significant conglomerates, this may be explained by a lack of source material. The Lake Eyre Basin sits on the Austalian stable craton with no significant source area and very low gradient landscapes. In addition, the soils of the Diamantina River floodplains are immature and therefore have not developed significant carbonate nodule horizons as seen in the palaeosols of the Raglan Mudstone Formation.

With no evidence of any substantial sand deposition along the Diamantina River, it is less appropriate as an analogue for the St Maughans Formation of the Lower Devonian, which is characterised by fining upwards sandstone complexes with basal intraformational conglomerates typical of perennial meandering rivers. Palaeosols are typically stage II to III palaeo-calcic-Vertisols. There is no evidence of any significant calcic-Vertisol development on the floodplains of the Diamantina River. However, beneath the thin veneer of mud facies of the Lake Eyre Basin, a significant sand sheet has been reported (Rust and Nanson 1986, Nanson et al. 1986). It was found to consist of cross-bedded sandstones similar to point bar deposits of perennial, meandering rivers (Rust and Nanson 1986). This sand sheet has been linked with interglacial stages 7 and 5 from the marine isotope record, representing a wetter 'phase' than the present aridity. A similar switch from a dry 'phase' to a wet 'phase' as a result of global climate change may explain the shift in sedimentology from the muddy ephemeral channels of the Raglan Mudstone Formation to the sandier, perennial and meandering channels of the St. Maughans Formation across the Silurian-Devonian boundary.

ACKNOWLEDGEMENTS

This work was funded by and in collaboration with LEBARG (Lake Eyre Basin Analogues Research Group, Australian School of Petroleum, Adelaide University (Kathryn Amos, Carmen Krapf, Marianne Sandstrom, Rachel Nanson) and Steve Hasiotis (University of Kansas) and Joanna Morris (University of Durham).

REFERENCES

ALLEN J.R.L. 1986. Pedogenic calcretes in the Old Red Sandstone facies (Late Silurian-Early Carboniferous) of the Anglo-Welsh Area, southern Britain. In WRIGHT V.P. (ED). *Paleosols: their recognition and interpretation,* Blackwell Scientific, London: 58-86.

ALLEN J.R.L. AND CROWLEY S.J. 1983. Lower Old Red Sandstone fluvial dispersal systems in the British Isles. *Transactions of the Royal Society of Edinburgh* **74**: 61-68.

BOYCE K.C., HOTTON C.L., FOGEL M.L., CODY G.D., HAZEN R.M., KNOLL A.H. AND HUEBER F.M. 2007. Devonian landscape heterogeneity recorded by a giant fungus. *Geology* **35**: 399-402.

CHANNELL J.E.T., MCCABE C. AND WOODCOCK N.H. 1992. Early Devonian (pre-Acadian) magnetisation directions in the Lower Old Red Sandstone of South Wales (UK). *Geophyiscal Journal International* **108**: 883-894.

DEWEY J.F. AND STRACHAN R.A. 2003. Changing Silurian-Devonian relative plate motion in the Caledonides: sinistral transpression to sinistral transtension. *Journal of the Geological Society* **160**: 219- 299.

EDWARDS D. AND FEEHAN J. 1980. Records of *Cooksonia*-type sporangia from late Wenlock strata in Ireland. *Nature* **287**: 41-42.

ÉKES C. 1993. Bedload-transported pedogenic mud aggregates in Lower Old Red Sandstone in Southwest Wales. *Journal of the Geological Society, London* **150**: 469-471.

FAGAN S.D. AND NANSON G.C. 2004. The morphology and formation of floodplain surface channels, Cooper Creek Australia. *Geomorphology* **60**: 107-126.

FRIEND P.F., WILLIAMS B.P.J., FORD M. AND WILLIAMS E.A. 2000. Kinematics and dynamics of Old Red Sandstone basins. In FRIEND P.F. AND WILLIAMS B.P.J. (EDS.) *New Perspectives on the Old Red Sandstone*. London, Geological Society Special Publication **180**: 29-60.

GIBLING M.R., NANSON G.C. AND MAROULIS J.C. 1998. Anastomosing river sedimentation in the Channel Country of central Australia. *Sedimentology*, **45**: 595-619.

HILLIER R.D., MARRIOTT S.B., WILLIAMS B.P.J. AND WRIGHT V.P. 2007. Possible climate variability in the Lower Old Red Sandstone Conigar Pit Sandstone Member (Early Devonian), South Wales, UK. *Sedimentary Geology* **202** (1-2): 35-57.

HUEBER F.M. 2001. Rotted wood-alga-fungus: the history and life of *Prototaxites* Dawson 1859. *Review of Palaeobotany and Palynology* **116**: 123-158.

KNIGHTON A.D. AND NANSON G.C. 2001. An event-based approach to the hydrology of arid zone rivers in the Channel Country of Australia. *Journal of Hydrology* **254**: 102-123.

MAROULIS J.C., NANSON G.C., PRICE D.M. AND PIETSCH T. 2007. Aeolian–fluvial interaction and climate change: source-bordering dune development over the past ~100 ka on Cooper Creek, central Australia. *Quaternary Science Reviews* **26**: 386 - 404.

MARRIOTT S.B. AND WRIGHT V.P. 1993. Palaeosols as indicators of geomorphic stability in two Old Red Sandstone alluvial suites, South Wales. *Journal of the Geological Society, London* **150**: 1109-1120.

MARRIOTT S.B. AND WRIGHT V.P. 1996. Sediment recycling on Siluro-Devonian floodplains. *Journal of the Geological Society, London* **153**: 661-664.

MARRIOTT S.B. AND WRIGHT V.P. 2004. Mudrock deposition in an ancient dryland system: Moor Cliffs Formation, Lower Old Red Sandstone, southwest Wales, UK. *Geological Journal* **39**: 277-298.

NANSON G.C., RUST B.R. AND TAYLOR G. 1986. Coexistent mud braids and anastomosing channels in an arid-zone river: Cooper Creek, central Australia. *Geology*, **14**: 175-178.

NANSON G.C., PRICE D.M. AND SHORT S.A. 1992. Wetting and drying of Australia over the past 300 ka. *Geology* **20**: 791-794.

RUST B.R. 1981. Sedimentation in an arid-zone anastomosing fluvial system: Cooper's Creek, central Australia. *Journal of Sedimentary Petrology*, **51 (3)**: 745-755.

RUST B.R. AND NANSON G.C. 1986. Contemporary and paleo channel patterns and the Late Quaternary stratigraphy of Cooper Creek, southwest Queensland, Australia. *Earth Surface Processes and Landforms* **11**: 581-590.

SCOTESE C. 2003. Paleomap Project website. http://www.scotese.com.

SOPER N.J. AND WOODCOCK N.H. 2003. The lost Old Red Sandstone of England and Wales: a record of post-Iapetan flexure or Early Devonian transtension? *Geological Magazine* **140(6)**: 627-647.

SIMON J.B. AND BLUCK B.J. 1982. Palaeodrainage of the southern margin of the Caledonian mountain chain in the northern British Isles. *Transactions of the Royal Society of Edinburgh*: *Earth Sciences* **73**: 11-15.

VEEVERS J. J. AND RUNDLE A. S. 1979. Channel Country fluvial sands and associated facies of central-eastern Australia: modern analogues of Mesozoic desert sands of South America. *Palaeogeography, Palaeoclimatology, Palaeoecology* **26**: 1-16.

WOPFNER H. 1963. Post-Winton sediments of probable Upper Cretaceous age in the central Great Artesian Basin. *Trans. R. Soc. South Aust.* **86**: 247-253.

WRIGHT V.P. AND MARRIOTT S.B. 2007. The dangers of taking mud for granted: lessons from Lower Old Red Sandstone dryland river systems of South Wales. *Sedimentary Geology* **195**: 91-100.